Cover Picture

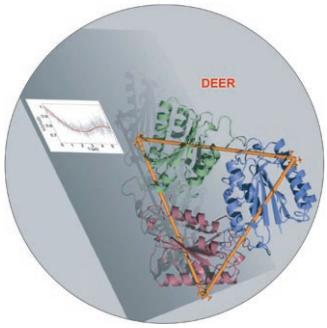


Ayyappanpillai Ajayaghosh,* Reji Varghese, Subi Jacob George, and Chakkooth Vijayakumar

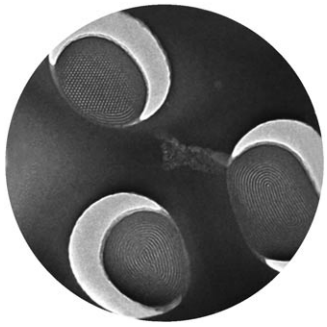
Inversion of helicity and the formation of unusual fused supercoiled left and right helices of gel-forming linear π-conjugated molecules by a "sergeants and soldiers" approach, in which the achiral molecules (soldiers) mistake orders from the chiral molecules (sergeants), is described by A. Ajayaghosh et al. on page 1141 ff. The cover picture shows Janus, the double-faced Greek God, holding a left-handed DNA helix and a right-handed conch which epitomize the marvels of natural creations.



Natural Products Synthesis
Natural polyynes have a broad spectrum of biological activities on account of their structural diversity. R. R. Tykwinski and A. L. K. Shi Shun report on the isolation and synthesis of polyynes in their Review on page 1034 ff.



Protein Structures
In their Communication on page 1058 ff., G. Jeschke and co-workers show how pulsed DEER methods are used to measure an intermolecular distance of 6.15 nm between noncovalently interacting proteins.



Circles or Columns
T. Bein and co-workers describe in their Communication on page 1134 ff. how the structure of mesoporous silica can be controlled by carefully tuning the reaction conditions during its synthesis.

Contents

VIP ***The following Communications have been judged by at least two referees to be "very important papers" and will be published online at www.angewandte.org soon:***

*H. Kiyohara, Y. Nakamura, R. Matsubara, S. Kobayashi**
Catalytic Asymmetric Allylation of Iminoesters and Iminophosphonates with a Variety of Allylsilanes Leading to Enantiomerically Enriched Allylglycine Derivatives

*J. J. La Clair**
Total Syntheses of Hexacyclinol, 5-epi-Hexacyclinol, and Desoxohexacyclinol Unveils an Antimalarial Prodrug Motif

H. Katagiri, T. Miyagawa, Y. Furusho, E. Yashima**
Synthesis and Optical Resolution of a Double Helicate Consisting of ortho-Linked Hexaphenol Strands Bridged by Spiroborates

D. Belder, M. Ludwig, Li-Wen Wang, M. T. Reetz**
Enantioselective Catalysis and Analysis on a Chip

*P. Cheung, A. Bhan, G. J. Sunley, E. Iglesia**
Selective Carbonylation of Dimethyl Ether to Methyl Acetate Catalyzed by Acidic Zeolites

W. Richtering, I. Berndt, J. S. Pedersen*
Temperature-Sensitive Core–Shell Microgel Particles with Dense Shells

Obituary

George S. Hammond (1921–2005) — *N. J. Turro, H. Gray* — **1018**

Books

Modern Physical Organic Chemistry — Eric V. Anslyn, Dennis A. Dougherty — *reviewed by C. Schmuck* — **1019**

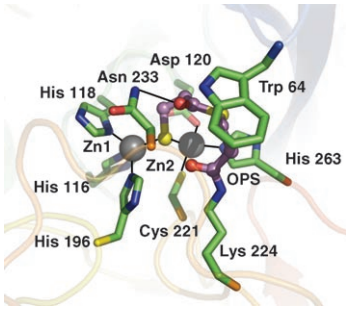
Posttranslational Modification of Proteins — Christopher T. Walsh — *reviewed by A. G. Beck-Sickinger, K. Mörl* — **1020**

Highlights

Bioorganic Chemistry

J. Spencer,* T. R. Walsh* — **1022 – 1026**

A New Approach to the Inhibition of Metallo-β-lactamases



Plan of attack: β-Lactam antibiotics remain at the forefront of the battle with pathogenic bacteria, particularly of Gram-negative strains that cause hospital-acquired infections. Metallo-β-lactamases, enzymes that confer resistance to almost all β-lactams, are spreading in these organisms. A new class of irreversible metallo-β-lactamase inhibitor (OPS; see picture) offers hope for the development of countermeasures to this growing clinical problem.

Essays

Philosophy behind Imaging

M. Hampe* — **1028 – 1031**

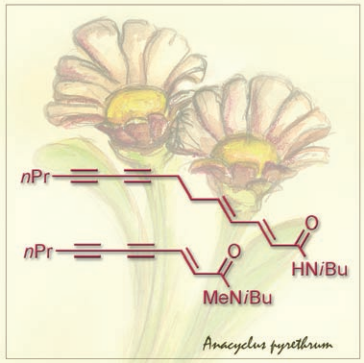
Visual Essences, Readable Signs, Means of Construction: On the Relevance of Images in Science

Seeing is believing, but images in science are often based on mathematical and philosophical presuppositions. Computation and imaging, which once seemed to be in conflict, have become interconvertible. It seems that pictures will become more and more important in science. This should not lead to new illusions about supposedly direct insights into the essence of things.

© 2006 Wiley-VCH Verlag GmbH & Co. KGaA, Weinheim

Reviews

Diverse structures and biological activities are shown by polyyne natural products (such as the compounds shown, isolated fron *Anacyclus pyrethrum*). Although some polyynes can be assembled with relative ease, most present a considerable synthetic challenge because of either a highly conjugated and unstable framework or stereochemical considerations. Recent strategies for the synthesis of these fascinating molecules are discussed.

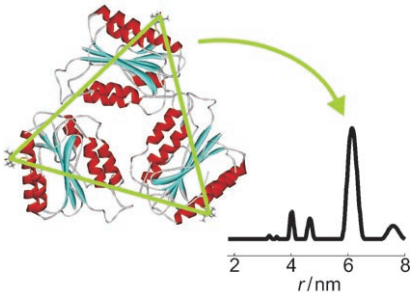


Natural Products Synthesis

A. L. K. Shi Shun,
R. R. Tykwinski* ——— **1034 – 1057**

Synthesis of Naturally Occurring Polyynes

Communications

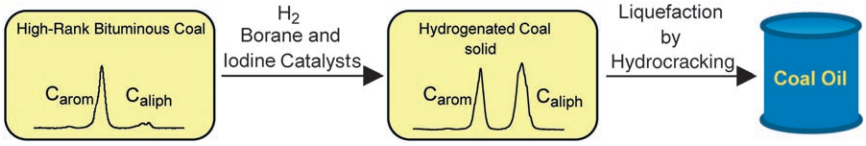


Distance determination: A double electron electron resonance (DEER) measurement of a distance of 6.1 nm (green lines) between singly nitroxide-labeled human von Willebrand Factor A domains demonstrates oligomerization of this domain in dilute solution (see structure); probably in an arrangement similar to that observed in the crystal structure. The DEER technique should be generally applicable for characterizing noncovalent interactions between macromolecules in solution.

EPR Spectroscopy

J. E. Banham, C. R. Timmel,
R. J. M. Abbott, S. M. Lea,
G. Jeschke* ——— **1058 – 1061**

The Characterization of Weak Protein–Protein Interactions: Evidence from DEER for the Trimerization of a von Willebrand Factor A Domain in Solution



In view of escalating oil prices, new processes are needed for the conversion of coal to liquid fuels. The first "real" coal hydrogenation in the sense of hydrogen addition to unsaturated C–C bonds enables the liquefaction of high-rank bituminous coals, which up to now could be processed only by combustion or gasification.

Coal Liquefaction

M. W. Haenel,* J. Narangerel,
U.-B. Richter, A. Rufińska ——— **1061 – 1066**

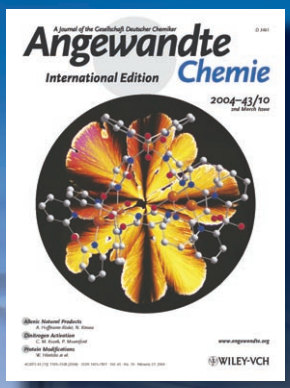
The First Liquefaction of High-Rank Bituminous Coals by Preceding Hydrogenation with Homogeneous Borane or Iodine Catalysts

For the USA and Canada:
ANGEWANDTE CHEMIE International Edition (ISSN 1433-7851) is published weekly by Wiley-VCH PO Box 191161, D 69451 Weinheim, Germany. Air freight and mailing in the USA by Publications Expediting Inc. 200 Meacham Ave., Elmont, NY 11003. Periodicals postage paid at Jamaica NY 11431. US POSTMASTER: send address changes to *Angewandte Chemie*, Wiley-VCH, 111 River Street, Hoboken, NJ 07030. Annual subscription price for institutions: US$ 5685/5168 (valid for print and electronic / print or electronic delivery); for individuals who are personal members of a national chemical society prices are available on request. Postage and handling charges included. All prices are subject to local VAT/sales tax.

© 2006 Wiley-VCH Verlag GmbH & Co. KGaA, Weinheim

The best in chemistry –

for more than a hundred years



A Journal of the Gesellschaft Deutscher Chemiker

Angewandte
International Edition **Chemie**

www.angewandte.org

1888: ***The beginning of a success story***

Constant Innovations

1962: *First issue of the International Edition*
1976: *Graphical abstracts*
1979: *Cover pictures*
1988: *Centenary of Angewandte*
1989: *Routine use of color*
1991: *New section: Highlights*
1992: *Computerized editorial tracking system*
1995: *Internet service for readers*
1998: *Regular press service; full-text online*
2000: *New section: Essays; EarlyView: Communications available online ahead of the printed version*
2001: *New section: Minireviews*
2002: *Online submission of manuscripts*
2003: *Weekly publication; new section: News; new layout*
2004: *Backfiles (1962-1997); ManuscriptXpress: Online system for authors and referees*



Angewandte's advisors...

Stefan Marcinowski
BASF AG
Ludwigshafen

» In our company ***Angewandte Chemie*** *is seen as an outstanding journal that combines first class performance in publishing innovative chemistry with a high international visibility. With its global recognition* ***Angewandte Chemie*** *functions as a seed cell for innovative technologies to be applied on a commercial basis in the future. «*

Angewandte Chemie International Edition *is a journal of the German Chemical Society (GDCh)*

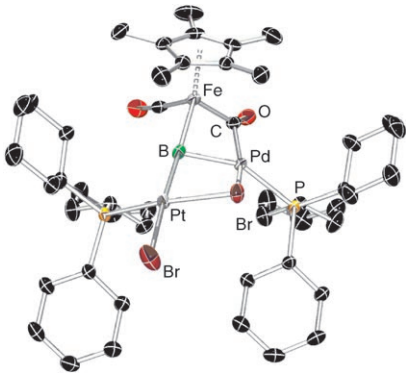
GDCh

WILEY InterScience® DISCOVER SOMETHING GREAT

WILEY-VCH

1186104_gu

Naked boron: Reaction of the bromoborylene complex $[(\eta^5\text{-}C_5Me_5)(OC)Fe(\mu\text{-}CO)(\mu\text{-}BBr)Pt(PCy_3)Br]$ with $[M(PCy_3)_2]$ (M = Pd, Pt) leads to complexes featuring the unprecedented coordination of one boron atom to three transition-metal centers (see picture). According to structural and DFT studies, the new compounds are best described as metalloborylene complexes stabilized by transition-metal bases.



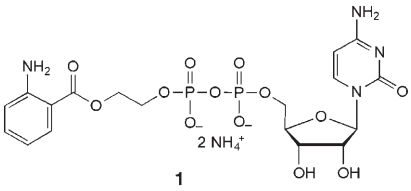
Borylene Complexes

H. Braunschweig,* K. Radacki, D. Rais, F. Seeler ——— 1066 – 1069

Boron in the Coordination Spheres of Three Transition-Metal Atoms: Syntheses and Structures of Metalloborylenes Stabilized by a Transition-Metal Base

---

Designed inhibitors (like **1**) of IspF, a key enzyme in the non-mevalonate pathway for terpene biosynthesis and a potential antimalarial target, were synthesized and evaluated. Since fluorescent probes were introduced in these ligands, their affinity towards IspF from *E. coli* could be determined by fluorescence titrations. The binding modes of two ligands in ternary complexes with IspF and a Zn^{II} ion were clarified by X-ray analysis.



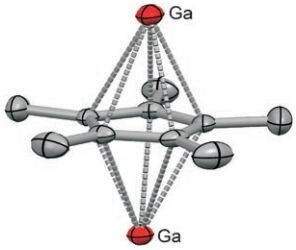
1

Inhibitors

C. M. Crane, J. Kaiser, N. L. Ramsden, S. Lauw, F. Rohdich, W. Eisenreich, W. N. Hunter,* A. Bacher,* F. Diederich* ——— 1069 – 1074

Fluorescent Inhibitors for IspF, an Enzyme in the Non-Mevalonate Pathway for Isoprenoid Biosynthesis and a Potential Target for Antimalarial Therapy

---

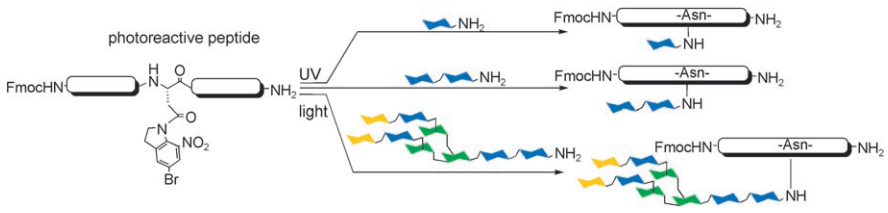


Partial protolysis of GaCp* with $[H(OEt_2)_2]^+[BAr^F]^-$ afforded the Ga^I compound $[Ga_2Cp^*]^+[BAr^F]^-$ (see structure). Experimental and computational studies confirm the mainly ionic structure of the cation, in which the Ga^+ ions are only weakly covalently stabilized by a bridging Cp* ligand. Initial experiments point to the interesting synthetic potential of this compound as a source for Ga^+ in solution.

Organogallium Complexes

B. Buchin, C. Gemel, T. Cadenbach, R. Schmid, R. A. Fischer* ——— 1074 – 1076

The $[Ga_2(C_5Me_5)]^+$ Ion: Bipyramidal Double-Cone Structure and Weakly Coordinated, Monovalent Ga^+



Two birds are killed with one stone when *N*-glycopeptides are synthesized by condensation of photoreactive peptides with glycosylamines. Firstly, the aspartic acid side chain is protected as an amide with a nitroindoline moiety, which is then converted into a powerful acylating agent by UV light. Secondly, photoacylation is carried out under base-free conditions, which minimizes an undesired side reaction, the formation of aspartimide.

Photochemical Syntheses

C. M. Kaneshiro, K. Michael* ——— 1077 – 1081

A Convergent Synthesis of *N*-Glycopeptides

© 2006 Wiley-VCH Verlag GmbH & Co. KGaA, Weinheim

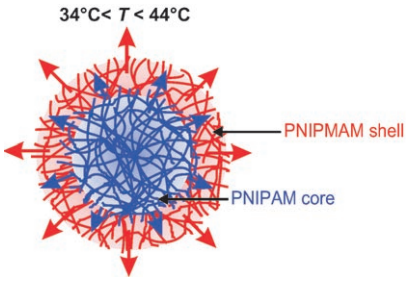
Contents

Core–Shell Particles

I. Berndt, C. Popescu, F.-J. Wortmann, W. Richtering* ——— **1081 – 1085**

Mechanics versus Thermodynamics: Swelling in Multiple-Temperature-Sensitive Core–Shell Microgels

The thermal transition of a thermoresponsive microgel of poly-*N*-isopropylacrylamide (PNIPAM; transition temperature = 34 °C) is shifted to higher temperatures when it is embedded in a shell of temperature-sensitive poly-*N*-isopropylmethacrylamide (PNIPMAM; transition temperature = 44 °C). The magnitude of the shift depends on the shell/core mass ratio. A thick shell induces a third transition arising from strong mechanical forces exerted on the core.

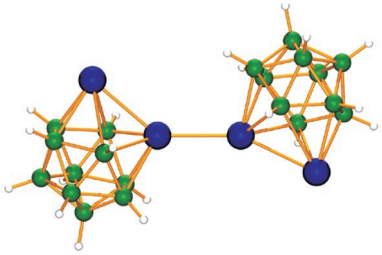


Borane Chemistry

D. Joosten, I. Pantenburg, L. Wesemann* ——— **1085 – 1087**

Distanna-*closo*-dodecaborate

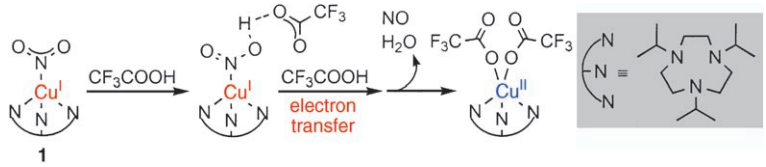
Hybrid clusters: Reductive cleavage of a novel dimeric *closo*-heteroborate (see picture; Sn blue, B green, H white), which was characterized by NMR spectroscopy and X-ray crystallography, provides a route to 1,2-distanna-*closo*-dodecaborate.



Enzyme Models

M. Kujime, H. Fujii* ——— **1089 – 1092**

Spectroscopic Characterization of Reaction Intermediates in a Model for Copper Nitrite Reductase

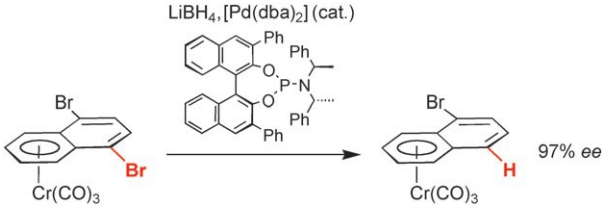


A nitrous acid complex was identified by spectroscopic and kinetic analyses under stopped-flow conditions as an intermediate in the reaction of copper(I) nitrite complex **1** with trifluoroacetic acid (see scheme). A reaction mechanism was proposed in which two protons are transferred in a stepwise manner to the nitrite anion. Intramolecular electron transfer from copper to the nitrite ligand occurs in the second protonation step.

Asymmetric Synthesis

E. P. Kündig,* P. D. Chaudhuri, D. House, G. Bernardinelli ——— **1092 – 1095**

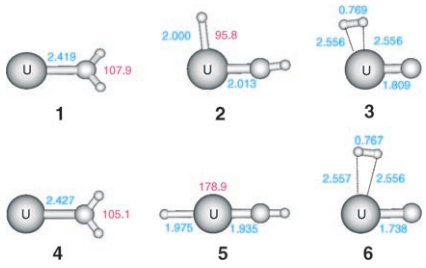
Catalytic Enantioselective Hydrogenolysis of [$Cr(CO)_3$(5,8-Dibromonaphthalene)]



Split and run: A study of the asymmetric hydrogenolysis of an aryl-carbon–bromine bond in a naphthalene chromiumtricarbonyl complex shows the use of a new bulky phosphoramidite ligand to yield the product in highly enantiomerically enriched form (see scheme).

© 2006 Wiley-VCH Verlag GmbH & Co. KGaA, Weinheim

Intermediates in theory and experiment: Different approaches of the density functional theory were used to obtain a close description of the reaction mechanisms of the title reactions. They supplied the minima **1**–**3** for U^+ and **4**–**6** for U^{2+}. The theoretical results are compared with experimental data.

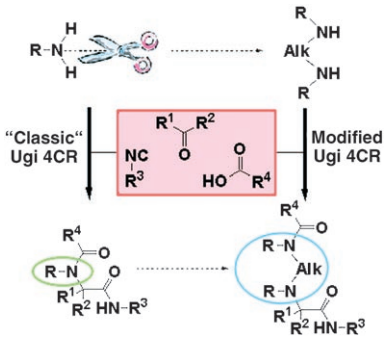


Actinide Chemistry

M. d. C. Michelini, N. Russo,* E. Sicilia ——— **1095 – 1099**

How Can Uranium Ions (U^+, U^{2+}) Activate the O—H Bond of Water in the Gas Phase?

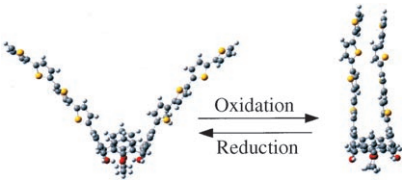
Splitting the amine! The Ugi four-component reaction (Ugi 4CR) relies on the presence of a component with a primary amino group. This protocol has been modified by "splitting" the primary amine into two secondary amines. The resulting variant of the Ugi 4CR proceeds with good to excellent yield and widens the versatility of the original multicomponent reaction by enabling variation of the molecular backbone.



Multicomponent Reactions

G. B. Giovenzana,* G. C. Tron,* S. Di Paola, I. G. Menegotto, T. Pirali ——— **1099 – 1102**

A Mimicry of Primary Amines by Bis-Secondary Diamines as Components in the Ugi Four-Component Reaction

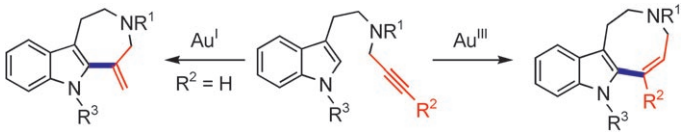


Contracted out: Quantum mechanical calculations and classical molecular dynamics simulations have been used to investigate the actuation mechanism of a substituted poly(calix[4]arene quaterthiophene). The results show that electrostatic repulsions between the charged atoms of the calix[4]arene scaffolds in the oxidized-deprotonated species induce a drastic contraction of the electrochemically activated polymer molecules.

Calculations

J. Casanovas,* D. Zanuy, C. Alemán* ——— **1103 – 1105**

Conducting Polymer Actuator Mechanism Based on the Conformational Flexibility of Calix[4]arene



Going for gold: Cationic gold(I) complexes favor formation of six- and seven-membered rings by 6-*endo*-dig, 6-*exo*-dig, and 7-*exo*-dig cyclizations of alkynyl indoles, whereas indoloazocines are favored with $AuCl_3$ as catalyst (see scheme). Allenes are also formed by a fragmentation process.

Cyclization

C. Ferrer, A. M. Echavarren* **1105 – 1109**

Gold-Catalyzed Intramolecular Reaction of Indoles with Alkynes: Facile Formation of Eight-Membered Rings and an Unexpected Allenylation

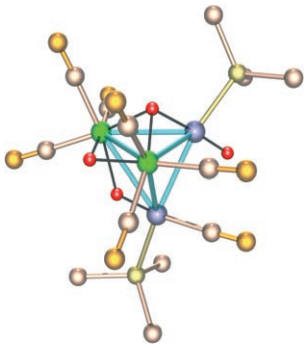
© 2006 Wiley-VCH Verlag GmbH & Co. KGaA, Weinheim

Contents

Cluster Chemistry

R. D. Adams,* B. Captain, M. D. Smith _____ **1109 – 1112**

A Highly Unsaturated Platinum–Rhenium Cluster Complex Activates Hydrogen Reversibly

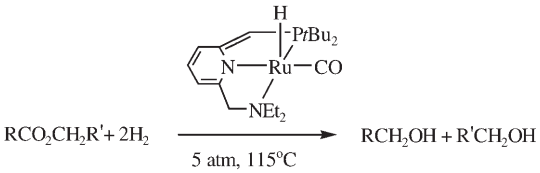


Give and take: The compounds $[PtRe_2(CO)_9(PtBu_3)(\mu\text{-}H)_2]$ and $[Pt_2Re_2(CO)_7(PtBu_3)_2(\mu\text{-}H)_2]$ (**1**) are obtained from the reaction of $[Pt(PtBu_3)_2]$ with $[Re_3(CO)_{12}(\mu\text{-}H)_3]$. Compound **1** adds hydrogen at 25 °C to yield the tetrahydrido complex $[Pt_2Re_2(CO)_7(PtBu_3)_2(\mu\text{-}H)_4]$ (**2**; see structure, red H, blue Pt, green Re, silver C, gold O, yellow P). When heated and also when irradiated, compound **2** eliminates one equivalent of H_2 to regenerate **1** in high yield.

Catalytic Hydrogenation

J. Zhang, G. Leitus, Y. Ben-David, D. Milstein* _____ **1113 – 1115**

Efficient Homogeneous Catalytic Hydrogenation of Esters to Alcohols

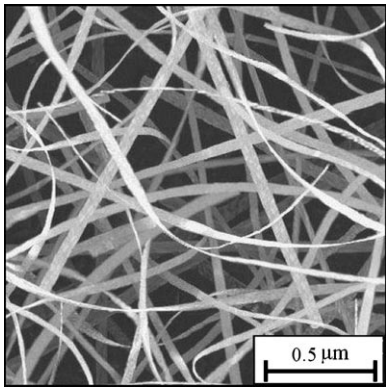


With open arms: A ruthenium PNN complex (see scheme) catalyzes the hydrogenation of esters in high yields under neutral conditions. The analogous PNP complex is less active. A mechanism is proposed based on the hemilabile nature of the PNN ligand which allows a vacant site to be created by decoordination of the $-CH_2NEt_2$ arm.

Nanostructures

J. Zhang, J. Du, B. Han,* Z. Liu, T. Jiang, Z. Zhang _____ **1116 – 1119**

Sonochemical Formation of Single-Crystalline Gold Nanobelts

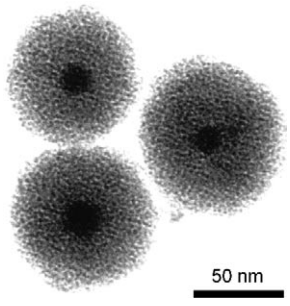


Benign belts: Single-crystalline gold nanobelts (see SEM image) can be synthesized by ultrasound irradiation of an aqueous solution of $HAuCl_4$ containing α-D-glucose as a biological directing agent. The gold nanobelts are typically 30–50 nm wide and several micrometers long. The method is simple, rapid, and avoids hazardous substances.

Nanoparticles

E. Ye, H. Tan, S. Li, W. Y. Fan* _____ **1120 – 1123**

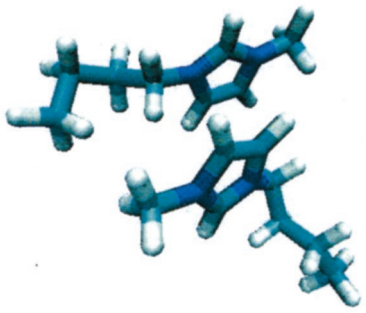
Self-Organization of Spherical, Core–Shell Palladium Aggregates by Laser-Induced and Thermal Decomposition of $[Pd(PPh_3)_4]$



Metal in the middle: Uniform, spherical, core–shell aggregates (100 ± 20 nm; see picture) are obtained by photodecomposition of $[Pd(PPh_3)_4]$ to form the metal core, followed by aggregation of smaller Pd nanocrystals and free phosphanes, produced by thermal decomposition of the remaining precursor, around this core. Prolonged irradiation or thermal decomposition alone yields only the core structure or the shell structure, respectively. This enables the nanoparticle structure to be tuned.

© 2006 Wiley-VCH Verlag GmbH & Co. KGaA, Weinheim

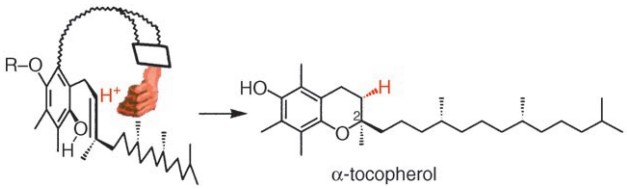
The polar domains within model ionic liquids are assessed by intermolecular NOE interaction studies. The cation–cation distances in pure ionic liquids 1-butyl-3-methylimidazolium (see picture) and 1-butyl-2,3-dimethylimidazolium tetrafluoroborate are obtained and used to provide models of the local structure of the liquids.



Ionic Liquids

A. Mele,* G. Romanò, M. Giannone, E. Ragg, G. Fronza, G. Raos, V. Marcon _____ **1123 – 1126**

The Local Structure of Ionic Liquids: Cation–Cation NOE Interactions and Internuclear Distances in Neat [BMIM][BF_4] and [BDMIM][BF_4]

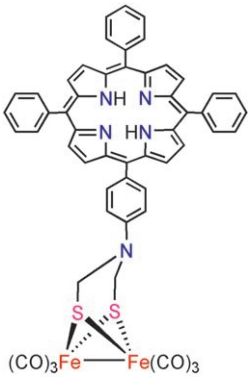


Vitamin E synthesis: Covalently linked dipeptides serve as readily removable and recyclable chiral auxiliaries in the diastereoselective cyclization of phytylhydroquinones. Depending on the chirality of the handle, (2*R*)- or (2*S*)-α-tocopherol (vitamin E) can be produced with a diastereomeric excess of up to 80% (see scheme).

Vitamin E

C. Grütter, E. Alonso, A. Chougnet, W.-D. Woggon* _____ **1126 – 1130**

A Biomimetic Chromanol Cyclization Leading to α-Tocopherol



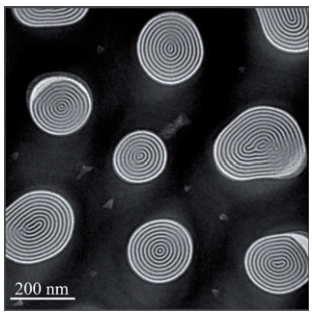
Efficient communication: The first porphyrin-photosensitizer-containing biomimetic model for the active site of Fe-only hydrogenases has been synthesized and structurally characterized (see picture). Its fluorescence spectrum reveals that an efficient electronic communication occurs between the porphyrin unit and the covalently linked diiron–azadithiolate moiety.

Enzyme Models

L.-C. Song,* M.-Y. Tang, F.-H. Su, Q.-M. Hu _____ **1130 – 1133**

A Biomimetic Model for the Active Site of Iron-Only Hydrogenases Covalently Bonded to a Porphyrin Photosensitizer

Circular or columnar orientations of mesoporous silica can be selectively prepared by tuning the silica-to-surfactant ratio and the humidity during the synthesis of the mesoporous material within the regular larger channels of anodic alumina membranes. The transmission electron microscopy image shows the circular orientation of these highly ordered hexagonal mesostructures.



Mesoporous Materials

VIP

B. Platschek, N. Petkov, T. Bein* _____ **1134 – 1138**

Tuning the Structure and Orientation of Hexagonally Ordered Mesoporous Channels in Anodic Alumina Membrane Hosts: A 2D Small-Angle X-ray Scattering Study

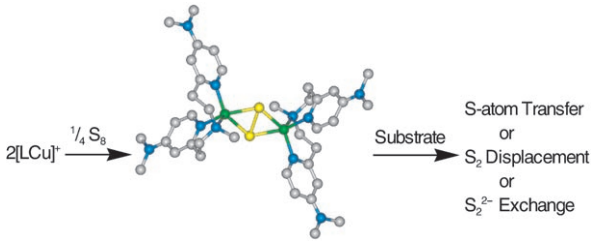
© 2006 Wiley-VCH Verlag GmbH & Co. KGaA, Weinheim

Contents

Bioinorganic Chemistry

M. E. Helton, D. Maiti, L. N. Zakharov, A. L. Rheingold, J. A. Porco, Jr., K. D. Karlin* _____ **1138 – 1141**

A μ-η²:η²-Disulfide Dicopper(II) Complex from Reaction of S_8 with a Copper(I) Precursor: Reactivity of the Bound Disulfur Moiety

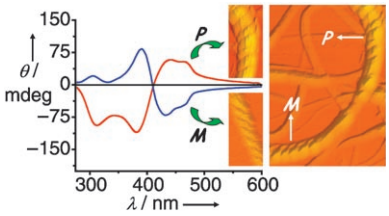


Side on: Elemental sulfur (S_8) reacts with a tridentate chelate $(MePY2)^{Me_2N}$ copper(I) compound, generating a side on μ-η²:η²-disulfido bridged complex $[\{Cu^{II}(MePY2)^{Me_2N}\}_2(S_2^{2-})]^{2+}$ (see structure: yellow S, green Cu, blue N, gray C); its reactivity towards PPh_3, RNC, CO, O_2, $PhCH_2Br$, and a tetradentate chelating ligand are described.

Helical Structures

A. Ajayaghosh,* R. Varghese, S. J. George, C. Vijayakumar _____ **1141 – 1144**

Transcription and Amplification of Molecular Chirality to Oppositely Biased Supramolecular π Helices

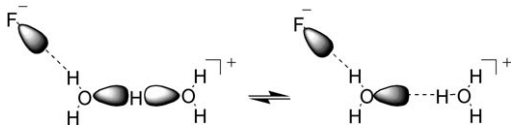


Let's twist again: Transcription of molecular chirality from common stereogenic centers to amplified supramolecular chirality during the coassembly of gel-forming π-conjugated molecules by inverted helicity results in the formation of longitudinally fused *M* and *P* helices. This "sergeants and soldiers" approach to coassembly under stereomutation has been confirmed by CD and AFM techniques (see picture).

Computational Chemistry

R. Iftimie,* M. E. Tuckerman* _____ **1144 – 1147**

The Molecular Origin of the "Continuous" Infrared Absorption in Aqueous Solutions of Acids: A Computational Approach



The origin of the continuum region ($\tilde{\nu}$ = 1000–3000 cm^{-1}) in the IR absorption spectra of solutions of strong acids is well understood, but in weak acids, it has remained a mystery until now. An ab initio molecular dynamics approach is used to explain the molecular origin of this continuum for aqueous solutions of the weak acid HF and identify the structure and chemical nature of the dominant species (see picture).

Organocatalysis

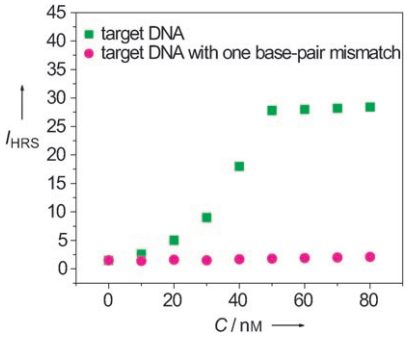
S. Brandes, M. Bella,* A. Kjærsgaard, K. A. Jørgensen* _____ **1147 – 1151**

Chirally Aminated 2-Naphthols—Organocatalytic Synthesis of Non-Biaryl Atropisomers by Asymmetric Friedel–Crafts Amination



Cinchona alkaloids are employed in an organocatalyzed asymmetric Friedel–Crafts amination reaction of 2-naphthols. These amination reactions proceed in high yields with up to 98% *ee* and have led to a new class of non-biaryl atropisomer. The rotation barriers of the chiral aminated 2-naphthols have been investigated by experimental and computational methods.

© 2006 Wiley-VCH Verlag GmbH & Co. KGaA, Weinheim



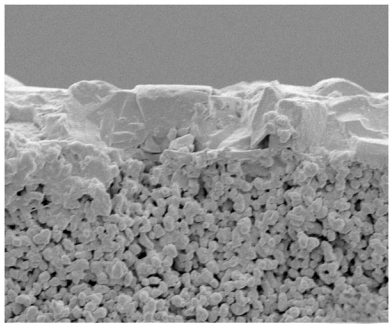
Highly sensitive: The hyper-Rayleigh Scattering (HRS) technique has been used to achieve the ultrasensitive detection of single base-pair mismatches in oligonucleotide strands without any modification of DNA. A very distinct HRS intensity change is observed after hybridization even at the concentration of 10-nanomolar probe single-stranded DNA.

DNA Structures

P. C. Ray* ——— 1151 – 1154

Diagnostics of Single Base-Mismatch DNA Hybridization on Gold Nanoparticles by Using the Hyper-Rayleigh Scattering Technique

Oriented assembly of zeolite crystals on a porous support followed by secondary growth leads to continuous, thin, uniformly oriented zeolite films (see picture for a cross-sectional SEM image) of MFI with the 5.1 × 5.5-Å zigzag channels perpendicular to the support. These *a*-oriented films along with their previously reported *b*-oriented counterparts are the first set of thin molecular-sieve membranes with uniform but drastically different orientations.



Zeolite Films

J. Choi, S. Ghosh, Z. Lai, M. Tsapatsis* ——— 1154 – 1158

Uniformly *a*-Oriented MFI Zeolite Films by Secondary Growth

Looking for outstanding employees?

Do you need another expert for your excellent team?
... Chemists, PhD Students, Managers, Professors, Sales Representatives...

Place an advert in the printed version and have it made available online for 1 month, free of charge!

Angewandte Chemie International Edition
Advertising Sales Department: Marion Schulz
Phone: 0 62 01 - 60 65 65
Fax: 0 62 01 - 60 65 50
E-Mail: MSchulz@wiley-vch.de

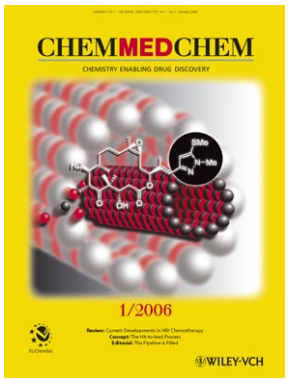
Service

Keywords ——— *1160*

Authors ——— *1161*

Angewandte's Sister Journals ——— *1162 – 1163*

Preview ——— *1165*

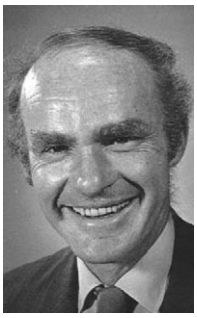


For more information on ChemMedChem see www.chemmedchem.org

© 2006 Wiley-VCH Verlag GmbH & Co. KGaA, Weinheim

George S. Hammond (1921–2005)

George Simms Hammond, a major figure in the fields of physical organic chemistry and mechanistic photochemistry, passed away on October 5, 2005, at the age of 84.



Hammond was born on a dairy farm outside of Auburn, Maine (USA). He received his BS degree from Bates College and his PhD from Harvard under the supervision of Paul D. Bartlett, and spent a postdoctoral year with Saul Winstein at UCLA. In 1948, he launched his academic career at Iowa State University, where he investigated the kinetics and mechanisms of many important organic reactions and made a major intellectual contribution to chemistry with the Hammond postulate:[1] when a high-energy reactive intermediate and transition state occur close to one another on a reaction coordinate, their energies and structures will be very similar. Chemists have found the postulate particularly useful when applied to elementary chemical steps that are either highly exothermic or highly endothermic: in highly exothermic steps the transition state is postulated to resemble the reactants, and in highly endothermic steps the products are postulated to be good models for transition states.

In 1958, Hammond moved to Caltech and published the first of a classic series of papers on mechanistic organic photochemistry.[2] He convincingly described a mechanism for the photoreduction of benzophenone by benzhydrol in which the role of the triplet state was unambiguously established. Hammond also made a major discovery: the ability to produce triplet states through electronic energy transfer.[3] At that time, the triplet state was a rather gossamer-like species, and Hammond's triplet energy transfer studies eventually put the triplet state on the same mechanistic footing as classical reactive intermediates such as carbocations and free radicals. Triplet energy transfer was shown to be a means of effecting a range of organic photoreactions such as intra- and intermolecular cycloadditions and *cis–trans* isomerizations. Perhaps of greater importance from his standpoint was the demonstration of the critical role of molecular dynamics in determining photochemical outcomes, as well as the development of methods to measure accurate rate constants for primary photochemical processes and for the deactivation of electronic excited states.

Starting in the late 1960s, in collaborations with Gray's group at Caltech, Hammond applied the lessons of mechanistic organic photochemistry to inorganic and organometallic systems. He worked out the mechanisms of the photoreactions of metal carbonyls,[4] once again by applying molecular orbital theory to rationalize reaction pathways, and investigated the photochemistry of metal–metal and metal–hydride bonds.[5,6] Hammond also collaborated on experiments[7] on rhodium isocyanide complexes that led to the discovery of visible-light-driven photoreactions that store solar energy through the production of high-energy molecules such as hydrogen.

In 1972, Hammond accepted the post of vice-chancellor for natural sciences at the University of California at Santa Cruz. In 1978, he accepted a position as Associate Director of Corporate Research for the Allied Chemical Corporation, where he remained until his retirement in 1988. Following formal retirement from Allied, Hammond returned to teaching and research as an adjunct faculty member at Bowling Green State University, Georgetown University, the University of Hawaii, and Portland State University, where he worked closely with both students and faculty for many years.

Hammond's research style, by his own admission, was "loose". He viewed the mentor–student relationship as a partnership. The student was working *with* the mentor not *for* the mentor. This style proved to be very effective and a model for many of his students who have later filled academic positions in the USA and all over the world.

Hammond was an innovator in chemical education and a gadfly urging serious reflection of the way chemists taught their discipline and in their attitude of the way chemical research was performed. His textbook with Cram, "*Organic Chemistry*",[8] totally abandoned the traditional functional group approach to teaching organic chemistry in favor of a mechanistic approach. The book was far ahead of its time and is still a valuable resource for pedagogical approaches to the subject.

Hammond's towering accomplishments were widely recognized by the scientific community. He was elected to the National Academy of Sciences (1963) and the American Academy of Arts and Sciences (1965). He received awards from the American Chemical Society in Petroleum Chemistry (1961), the James Flack Norris Award in Physical Organic Chemistry (1967), the Award in Chemical Education (1972), and the Priestley Medal (1976). He received the National Medal of Science in 1994.

It was a thrill and a great honor for both of us to work with George Hammond. His brilliance, profound chemical insight, and delight in grappling with all things chemical were a wonder to behold. He will be sorely missed, but his legacy continues in the students and colleagues who had the privilege of working with him.

Nicholas J. Turro
Columbia University
Harry Gray
California Institute of Technology

[1] G. S. Hammond, *J. Am. Chem. Soc.* **1955**, *77*, 334.
[2] G. S. Hammond, W. M. Moore, *J. Am. Chem. Soc.* **1959**, *81*, 6334.
[3] G. S. Hammond, N. J. Turro, P. A. Leermakers, *J. Phys. Chem.* **1962**, *66*, 1144.
[4] M. Wrighton, G. S. Hammond, H. B. Gray, *J. Mol. Photochem.* **1973**, *5*, 179.
[5] G. L. Geoffroy, H. B. Gray, G. S. Hammond, *J. Am. Chem. Soc.* **1974**, *96*, 5565.
[6] G. L. Geoffroy, G. S. Hammond, H. B. Gray, *J. Am. Chem. Soc.* **1975**, *97*, 3933.
[7] K. R. Mann, N. S. Lewis, V. M. Miskowski, D. K. Erwin, G. S. Hammond, H. B. Gray, *J. Am. Chem. Soc.* **1977**, *99*, 5525.
[8] D. J. Cram, G. S. Hammond, *Organic Chemistry*, McGraw-Hill, New York, **1959**.

DOI: 10.1002/anie.200600079

InterScience
© 2006 Wiley-VCH Verlag GmbH & Co. KGaA, Weinheim

Bioorganic Chemistry

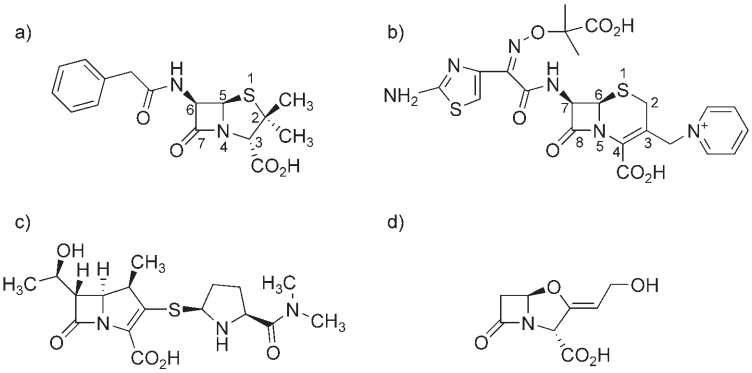
DOI: 10.1002/anie.200502984

A New Approach to the Inhibition of Metallo-β-lactamases**

James Spencer and Timothy R. Walsh**

Keywords:
antibiotics · bioorganic chemistry · inhibitors · lactams · metalloenzymes

It is more than 60 years since β-lactams were first used in patients and more than 20 since carbapenems were introduced into clinical practice (Scheme 1). Nevertheless the therapeutic importance of β-lactams remains extremely high—surveys show them to account for around half of the total prescriptions for antibiotics.[1] In the face of this intense selective pressure it is unsurprising that mechanisms of resistance continue to evolve and disseminate amongst pathogenic bacteria. Whilst β-lactam resistance can arise by a variety of mechanisms, including modification of the target (penicillin binding proteins), reduction in permeability, and efflux of the antibiotic, antibiotic inactivation through the action of β-lactamases represents a major mechanism of resistance for a large number of clinically important pathogens.[2] The number of known β-lactamase enzymes is currently approaching 500.[*] Medicinal chemistry has claimed some notable successes in counteracting the effects of β-lactamases: combination therapies such as augmentin that comprise β-lactamase-susceptible penicillins and β-lactamase inhibitors such as clavulanic acid, sulbactam, or tazobactam (Scheme 1) are effective against many β-lactamase-producing bacteria and are amongst the most profitable of all pharmaceuticals. However, clinically available inhibitors were never effective against all classes of β-lactamase, and inhibitor-resistant enzymes are continuing to emerge in a number of pathogenic bacteria.



Scheme 1. Representative β-lactam substrates of metallo-β-lactamases: a) benzylpenicillin (penicillin); b) ceftazidime (cephalosporin); c) meropenem (carbapenem); d) clavulanic acid (clavam; serine β-lactamase inhibitor).

The majority of β-lactamases employ an activated serine nucleophile to attack the carbonyl carbon atom of the scissile β-lactam amide bond. However, a second unrelated class of zinc metalloenzymes represents a new challenge to the efficacy of β-lactams. Metallo-β-lactamases (mβls) are notable for their broad spectrum of activity—they not only hydrolyze penicillins, cephalosporins, and carbapenems but also serine-β-lactamase inhibitors such as clavulanic acid.[3] Metallo-β-lactamases pose a particular threat in the case of pan-resistant Gram-negative bacteria such as *Pseudomonas aeruginosa* and *Acinetobacter* spp. that have acquired resistance to most, if not all, other antibiotic classes and against which carbapenems now represent the primary treatment option.[4] Whilst more than 20 mβl types are known, 4 mβl genes, bla_{IMP}, bla_{VIM}, bla_{SPM-1}, and bla_{GIM-1}, have now been mobilized on genetic elements such as plasmids, transposons, and integrons, and may be readily disseminated across geographic and species boundaries.[5]

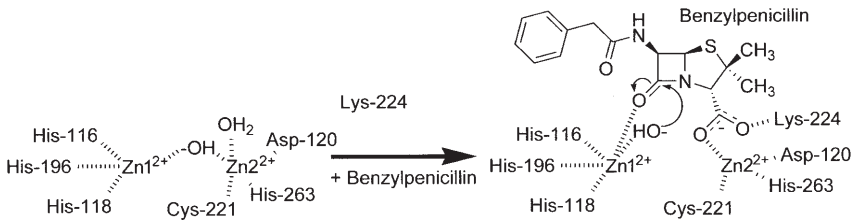
The mβl active site comprises a binuclear zinc center in which one tetrahedral (Zn1) and one trigonal bipyramidally coordinated (Zn2) zinc ion are positioned some 3.6 Å apart and connected by a μ-bridging hydroxide group (Scheme 2; Figure 1). Although exceptions are known—the enzymes of *Aeromonas* spp. that act as specific carbapenemases function with one Zn^{2+} ion equivalent bound, the *Bacillus*

[*] Dr. J. Spencer, Dr. T. R. Walsh
Department of Cellular and Molecular Medicine
School of Medical Sciences
University of Bristol
University Walk, Bristol BS8 1TD (UK)
Fax: (+44) 117-928-7896
E-mail: jim.spencer@bristol.ac.uk
t.r.walsh@bristol.ac.uk

[**] We thank Richard Sessions, Jackie Martin, Andrea Hadfield, and Dek Woolfson for their careful reading of the manuscript. J.S. acknowledges funding from the Beit Memorial Fellowships for Medical Research and the U.K. Biotechnology and Biological Sciences Research Council.

[*] http://www.lahey.org/studies.

WILEY InterScience DISCOVER SOMETHING GREAT
© 2006 Wiley-VCH Verlag GmbH & Co. KGaA, Weinheim



Scheme 2. β-Lactam binding by metallo-β-lactamases. Putative mode of binding of benzylpenicillin by IMP-1 shows ligation of Zn1 by the β-lactam amide and Zn2 and Lys224 by the C3 carboxylate group. The substrate is oriented for nucleophilic attack of the (formerly μ-bridging) hydroxide group upon the β-lactam carbonyl carbon atom. Coordination bonds are shown as broken lines. Note that standard BBL numbering[34] is applied throughout this Highlight.

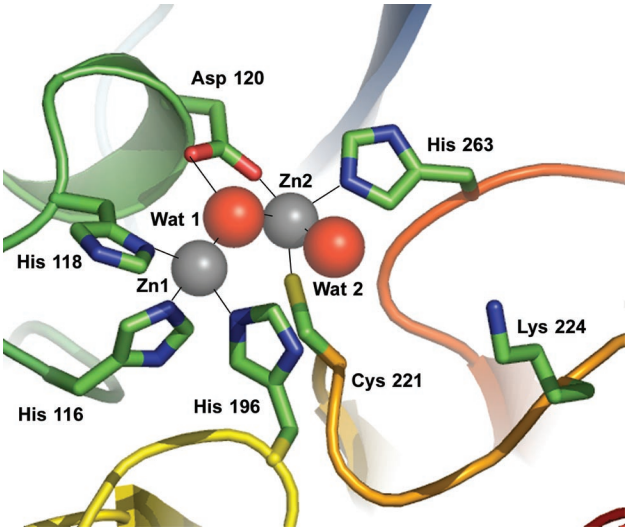


Figure 1. Dinuclear active site of metallo-β-lactamases. The figure shows the active site of the CcrA enzyme[35] (note that the available structure of free IMP-1[8] is of low resolution and the μ-bridging water is not resolved). Zinc ions are shown as gray spheres and water molecules as red spheres. The μ-bridging hydroxide group is labeled as Wat1 and Zn2-bound "apical" water as Wat2. Fine gray lines show coordination and hydrogen bonds.

cereus BcII enzyme appears to be active in the mono- or dizinc forms, and the issue of Zn^{2+} stoichiometry in vivo remains controversial—in most cases occupation of both sites is required for maximal activity.[6] Such an arrangement is common in biology; many hydrolytic enzymes employ similar dinuclear metal centers and the mβls themselves are now recognized as exemplars of a large and ancient enzyme superfamily with a wide range of hydrolytic and other functions.[7] In the mβls, however, this geometry enables efficient hydrolysis of a wide range of alternatively substituted β-lactams by utilizing the metal center not only for catalysis but also for recognition of a limited subset of substrate functional groups. Accumulating evidence suggests that the amide and C3/C4 carboxylate moieties of the β-lactam skeleton are bound by the Zn1 and Zn2 centers, respectively.[8,9] The importance of the metal center to substrate binding is illustrated by the striking observation that, whilst the crystal structure of the *B. cereus* BcII apoenzyme closely resembles that of the holoprotein, the apoenzyme is unable to bind β-lactams,[10] a result that contrasts with other metalloenzyme systems.[11] The surrounding protein environment, an open shallow groove, can provide productive hydrophobic and/or hydrogen-bonding interactions with the C6/C7 and C2/C3 substituents of the substrate (as evidenced by the alternative conformations of the Trp64 bearing loop in the various IMP-1 inhibitor complexes; Figure 2) but appears to be of secondary importance to substrate binding and differs significantly between family members.[12] Inhibiting mβls thus presents a significant challenge in that the metal center resembles many that are found in other enzyme systems, and there is an absence of conserved protein specificity pockets that may be readily exploited in drug design.

A variety of approaches has been employed in the search for effective mβl inhibitors. Several different chemical classes, including biphenyl tetrazoles, β-lactams, trifluoromethyl ketones, succinic acids, and various thiol compounds, have been investigated (reviewed in references [5,13]). Whilst only limited structural information is available, some common themes are apparent in the interactions of these disparate reagents with target enzymes. Firstly, the sulfur atom of thiol reagents such as D-captopril or thiomandelic acid, or the carboxylate oxygen of disuccinic acid inhibitors displaces the μ-bridging hydroxide group at the metal center that is generally believed to act as the nucleophile in the hydrolytic reaction.[14,15] Interestingly, electron paramagnetic resonance studies of the interaction of Co^{2+}-substituted *Stenotrophomonas maltophilia* L1 enzyme with β-lactams suggest that μ-bridged species are not a feature of productive enzyme–substrate complexes.[16] Secondly, the N_ε nitrogen atom of Lys224, a residue that mutagenic and structural data reveal contributes to binding and orientation of substrates by hydrogen bonding to the invariant C3/C4 carboxylate group of β-lactam substrates (Scheme 2),[17,18] makes similar contacts with inhibitor carboxylate or tetrazole substituents (Figure 2).

Kurosaki et al. have now exploited these common features of substrate and inhibitor binding to mβls to generate a new class of irreversible thiol inhibitor.[19] Irreversible inhibition of mβls by thiols is not a new observation—formation of disulfides with the Zn2 ligand Cys221 of BcII has been demonstrated for mercaptoacetic thiol esters and postulated for thiols formed when the cephalosporin dihydrothiazine ring opens subsequent to cleavage of the β-lactam amide bond.[20,21] Similarly, Lippard and co-workers showed that diaryl disulfides could covalently attach to the

 © 2006 Wiley-VCH Verlag GmbH & Co. KGaA, Weinheim

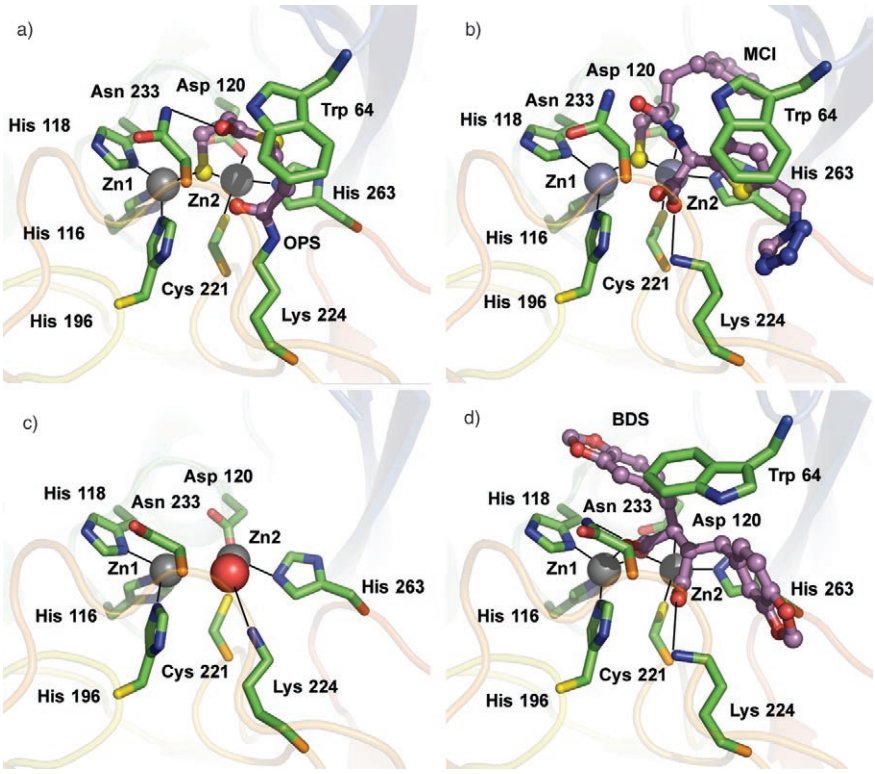


Figure 2. Crystal structures of IMP-1 metallo-β-lactamase and inhibitor complexes: a) 3-(3-mercaptopropionylsulfanyl)propionic acid (OPS; pdb accession 1vgn[19]); b) 2-[5-(1-tetrazolylmethyl)thien-3-yl]-*N*-[2-(mercaptomethyl)-4-(phenylbutyryl)glycine] (MCI; pdb 1ddk[8]); c) uncomplexed protein (pdb 1dd6)[8]); d) 2,3-bis-benzo[1,3]dioxol-5-ylmethylsuccinic acid (BDS; pdb 1jjt[15]). Protein main chains are color-ramped from the N to the C termini with secondary structural elements shown in the background. Side-chain and inhibitor atom colors are as standard except for inhibitor carbon atoms (shown in magenta). Zinc ions are shown as gray spheres and water molecules as red spheres. Fine gray lines show coordination and hydrogen bonds.

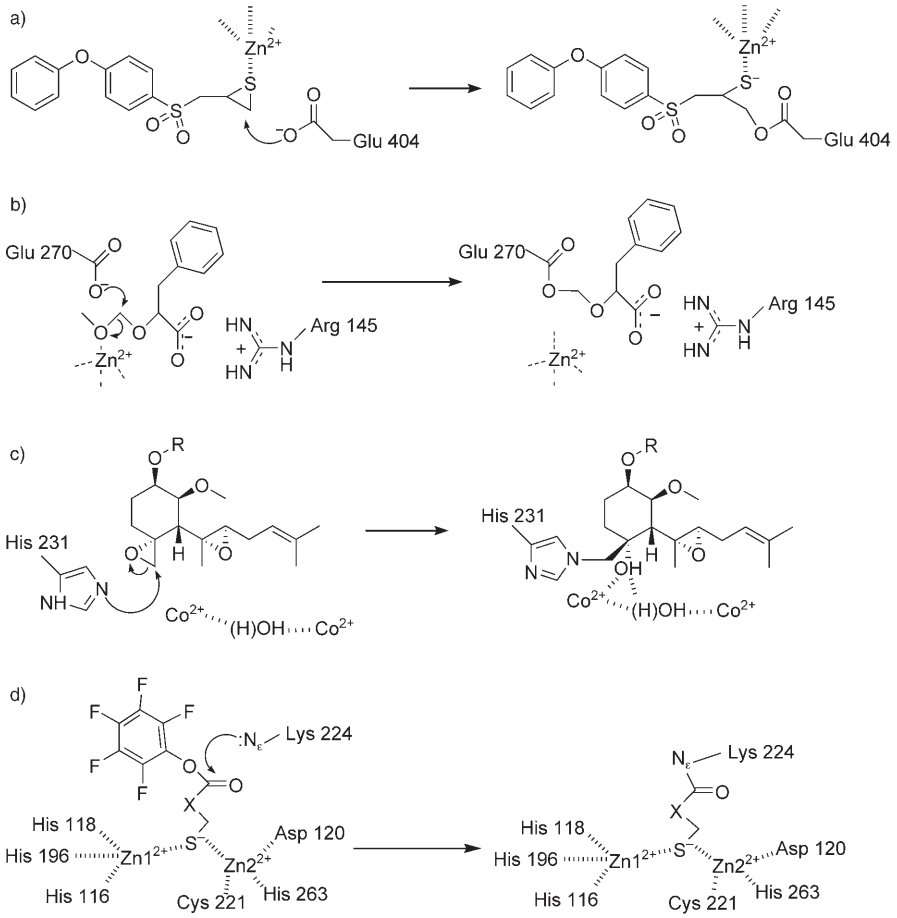
Bacteroides fragilis CcrA enzyme through a process of thiolate disulfide exchange.[22] Where this new strategy differs from those above is in the combination of a thiol group, which is able to form a stable μ-bridged complex with the dinuclear zinc center, with an ester that is activated sufficiently to enable complexation with the substrate-binding Lys224 residue. Kurosaki et al. showed that pentafluorophenyl esters of 3-mercapto- and 3-(3-mercaptopropionylsulfanyl)propionic acid indeed exhibit inhibition kinetics that are consistent with a mechanism comprising an initial reversible association step followed by irreversible inactivation involving displacement of the pentafluorophenolate leaving group (Scheme 3). Mass spectrometric analysis and crystallographic structure determination of the enzyme complex showed that the desired mode of binding had been achieved (Figure 2).

Whilst irreversible inactivators of several Zn^{2+} metalloenzymes have been reported, the study by Kurosaki et al. differs from these in one important respect. In cases such as the inactivation of carboxypeptidase A (CPA) by epoxides, acetals, or oxazolidinones,[23,24] of matrix metalloproteases (MMPs) by thiiranes,[25] or of the dinuclear cobalt enzyme methionine aminopeptidase (MetAP) by the epoxide angiogenesis inhibitor fumagillin,[26,27] mechanism-based inhibition is achieved using the metal center to activate a precursor to facilitate covalent attachment to a protein nucleophile such as Glu270 (CPA), Glu404 (MMP-2), or His231 (MetAP; Scheme 3). Inhibition thus proceeds by modification of catalytically essential residues. In contrast, it is the zinc ions that are primarily responsible for both substrate binding and catalysis in mβls, and the role of essential amino acids is, with the possible exception of Asp120,[28] to ligate zinc rather than to participate directly in the reaction mechanism. Irreversible inactivation of mβls by modification of Lys224 necessitates a more reactive agent to enable modification of a residue whose role in the hydrolytic reaction is in molecular recognition rather than catalysis and that is not significantly activated by the adjacent protein environment. Although it could be argued that these new agents might be described as affinity labels rather than true mechanism-based inhibitors,[29] these new data demonstrate that such an approach to mβl inhibition is feasible and can generate compounds with a potency approaching that of the best reversible inhibitors presently in the public domain.

The challenges involved in progressing to clinically effective mβl inhibitors nevertheless remain considerable. Previous studies reveal that, as would be expected for a diverse group of enzymes of comparatively distant sequence relationship, potency against even the more closely related targets can differ by several orders of magnitude for a given compound.[20,30] In the case of mobilized mβls, proliferation has led to the emergence of multiple variants of the bla_{IMP} and bla_{VIM} gene products, some of which differ substantially in their reactivity against different substrate classes.[31,32] Although interaction of protein side chains with the β-lactam C3/C4 carboxylate group is most likely functionally conserved across the entire mβl family, the means by which this is achieved varies and can involve Tyr, His, Arg, or Ser residues in place of Lys224.[8,9,18,32]

Both the extremely wide distribution of dinuclear metal centers and the necessary reactivity of the inhibitor pentafluorophenyl ester raise questions of specificity—such highly activated compounds with numerous potential targets are unlikely to be of use in their current form in a clinical or in vivo setting. One might however envisage improving selectivity of future compounds by exploiting interactions with the metal ion at the mβl Zn2 site to both more closely mimic the binding of the substrate carboxylate group and utilize such specific contacts with the Zn^{2+} ion to activate less intrinsically reactive agents. In pan-resistant Gram-negative opportunist bacterial pathogens such as

 © 2006 Wiley-VCH Verlag GmbH & Co. KGaA, Weinheim



Scheme 3. Irreversible inhibitors of metalloenzymes. a) Inhibition of gelatinase (MMP-2) by 2-(4-phenoxyphenylsulfonylmethyl)thiirane (from reference [25]). b) Inhibition of carboxypeptidase A by 2-benzyl-3,5-dioxahexanoic acid[24]. c) Inhibition of methionine aminopeptidase by fumagillin (from reference [27]). d) Inhibition of IMP-1 metallo-β-lactamase by 3-mercapto- and 3-(3-mercaptopropionylsulfanyl)propionic acid pentafluorophenyl esters (X = $COSCH_2CH_2$).[19]

P. aeruginosa, resistance to all therapeutic agents, including β-lactams, frequently involves multiple mechanisms that include modifications to porin and efflux pump expression that reduce the ability of antibiotics to reach their target. The requirement to penetrate such impermeable organisms thus places further constraints upon the chemistry of potential new agents.

Metallo-β-lactamases look set to increase significantly in terms of clinical importance over the coming years. Whilst several new antibiotic classes are now at or close to the marketplace, none is effective against all of the Gram-negative host species in which mβls are likely to be found.[33] Accordingly, β-lactams look set to remain in the front line of defense against these organisms for years to come. In this context, the new avenue of exploration in the search for effective mβl inhibitors that Kurosaki et al. have opened is very much to be welcomed.

Published online: January 11, 2006

[1] S. Molstad, C. S. Lundborg, A. K. Karlsson, O. Cars, *Scand. J. Infect. Dis.* **2002**, *34*, 366.

[2] K. Poole, *Cell. Mol. Life Sci.* **2004**, *61*, 2200; J. F. Fisher, S. O. Meroueh, S. Mobashery, *Chem. Rev.* **2005**, *105*, 395; G. A. Jacoby, L. S. Munoz-Price, *N. Engl. J. Med.* **2005**, *352*, 380.

[3] A. Felici, G. Amicosante, A. Oratore, R. Strom, P. Ledent, B. Joris, L. Fanuel, J. M. Frere, *Biochem. J.* **1993**, *291*, 151; C. Prosperi-Meys, G. Llabres, D. de Seny, R. P. Soto, M. H. Valladares, N. Laraki, J. M. Frere, M. Galleni, *FEBS Lett.* **1999**, *443*, 109.

[4] D. M. Livermore, *Ann. Med.* **2003**, *35*, 226.

[5] T. R. Walsh, M. A. Toleman, L. Poirel, P. Nordmann, *Clin. Microbiol. Rev.* **2005**, *18*, 306.

[6] M. Hernandez Valladares, A. Felici, G. Weber, H. W. Adolph, M. Zeppezauer, G. M. Rossolini, G. Amicosante, J. M. Frere, M. Galleni, *Biochemistry* **1997**, *36*, 11534; R. M. Rasia, A. J. Vila, *Biochemistry* **2002**, *41*, 1853; S. Wommer, S. Rival, U. Heinz, M. Galleni, J. M. Frere, N. Franceschini, G. Amicosante, B. Rasmussen, R. Bauer, H. W. Adolph, *J. Biol. Chem.* **2002**, *277*, 24142.

[7] H. Daiyasu, K. Osaka, Y. Ishino, H. Toh, *FEBS Lett.* **2001**, *503*, 1; D. S. Auld, *Biometals* **2001**, *14*, 271.

[8] N. O. Concha, C. A. Janson, P. Rowling, S. Pearson, C. A. Cheever, B. P. Clarke, C. Lewis, M. Galleni, J. M. Frere, D. J. Payne, J. H. Bateson, S. S. Abdel-Meguid, *Biochemistry* **2000**, *39*, 4288.

[9] J. Spencer, J. Read, R. B. Sessions, S. Howell, G. M. Blackburn, S. J. Gamblin, *J. Am. Chem. Soc.* **2005**, *127*, 14439.

[10] A. Carfi, E. Duee, M. Galleni, J. M. Frere, O. Dideberg, *Acta Crystallogr. Sect. D* **1998**, *54*(Pt3), 313; R. M. Rasia, A. J. Vila, *J. Biol. Chem.* **2004**, *279*, 26046.

[11] B. F. Cooper, V. Sideraki, D. K. Wilson, D. Y. Dominguez, S. W. Clark, F. A. Quiocho, F. B. Rudolph, *Protein Sci.* **1997**, *6*, 1031; J. G. Krum, H. Ellsworth, R. R. Sargeant, G. Rich, S. A. Ensign, *Biochemistry* **2002**, *41*, 5005; D. S. Auld, B. Holmquist, *Biochemistry* **1974**, *13*, 4355.

[12] C. Moali, C. Anne, J. Lamotte-Brasseur, S. Groslambert, B. Devreese, J. Van Beeumen, M. Galleni, J. M. Frere, *Chem. Biol.* **2003**, *10*, 319; J. J. Huntley, W. Fast, S. J. Benkovic, P. E. Wright, H. J. Dyson, *Protein Sci.* **2003**, *12*, 1368; J. D. Garrity, J. M. Pauff, M. W. Crowder, *J. Biol. Chem.* **2004**, *279*, 39663.

[13] J. H. Toney, J. G. Moloughney, *Curr. Opin. Invest. Drugs* **2004**, *5*, 823.

[14] I. Garcia-Saez, J. Hopkins, C. Papamicael, N. Franceschini, G. Amicosante, G. M. Rossolini, M. Galleni, J. M. Frere, O. Dideberg, *J. Biol. Chem.* **2003**, *278*, 23868; C. Damblon, M. Jensen, A. Ababou, I. Barsukov, C. Papamicael, C. J. Schofield, L. Olsen, R. Bauer, G. C. Roberts, *J. Biol. Chem.* **2003**, *278*, 29240.

[15] J. H. Toney, G. G. Hammond, P. M. Fitzgerald, N. Sharma, J. M. Balkovec, G. P. Rouen, S. H. Olson, M. L. Hammond, M. L. Greenlee, Y. D. Gao, *J. Biol. Chem.* **2001**, *276*, 31913.

[16] J. D. Garrity, B. Bennett, M. W. Crowder, *Biochemistry* **2005**, *44*, 1078.

[17] M. P. Yanchak, R. A. Taylor, M. W. Crowder, *Biochemistry* **2000**, *39*, 11330; S. Haruta, E. T. Yamamoto, Y. Eriguchi, T. Sawai, *FEMS Microbiol. Lett.* **2001**, *197*, 85; I. C. Materon, Z. Beharry, W.

 © 2006 Wiley-VCH Verlag GmbH & Co. KGaA, Weinheim

Huang, C. Perez, T. Palzkill, *J. Mol. Biol.* **2004**, *344*, 653.
[18] G. Garau, C. Bebrone, C. Anne, M. Galleni, J. M. Frere, O. Dideberg, *J. Mol. Biol.* **2005**, *345*, 785.
[19] H. Kurosaki, Y. Yamaguchi, T. Higashi, K. Soga, S. Matsueda, H. Yumoto, S. Misumi, Y. Yamagata, Y. Arakawa, M. Goto, *Angew. Chem.* **2005**, *117*, 3929; *Angew. Chem. Int. Ed.* **2005**, *44*, 3861.
[20] D. J. Payne, J. H. Bateson, B. C. Gasson, D. Proctor, T. Khushi, T. H. Farmer, D. A. Tolson, D. Bell, P. W. Skett, A. C. Marshall, R. Reid, L. Ghosez, Y. Combret, J. Marchand-Brynaert, *Antimicrob. Agents Chemother.* **1997**, *41*, 135.
[21] A. Badarau, A. Llinas, A. P. Laws, C. Damblon, M. I. Page, *Biochemistry* **2005**, *44*, 8578.
[22] H. Boerzel, M. Koeckert, W. Bu, B. Spingler, S. J. Lippard, *Inorg. Chem.* **2003**, *42*, 1604.
[23] M. Lee, D. H. Kim, *Bioorg. Med. Chem.* **2002**, *10*, 913; S. J. Chung, S. Chung, H. S. Lee, E. J. Kim, K. S. Oh, H. S. Choi, K. S. Kim, Y. J. Kim, J. H. Hahn, D. H. Kim, *J. Org. Chem.* **2001**, *66*, 6462.
[24] M. S. Han, C. H. Ryu, S. J. Chung, D. H. Kim, *Org. Lett.* **2000**, *2*, 3149.
[25] M. Ikejiri, M. M. Bernardo, R. D. Bonfil, M. Toth, M. Chang, R. Fridman, S. Mobashery, *J. Biol. Chem.* **2005**, *280*, 33992.
[26] S. Liu, J. Widom, C. W. Kemp, C. M. Crews, J. Clardy, *Science* **1998**, *282*, 1324; S. G. Bernier, D. D. Lazarus, E. Clark, B. Doyle, M. T. Labenski, C. D. Thompson, W. F. Westlin, G. Hannig, *Proc. Natl. Acad. Sci. USA* **2004**, *101*, 10768.
[27] E. C. Griffith, Z. Su, S. Niwayama, C. A. Ramsay, Y. H. Chang, J. O. Liu, *Proc. Natl. Acad. Sci. USA* **1998**, *95*, 15183.
[28] J. D. Garrity, A. L. Carenbauer, L. R. Herron, M. W. Crowder, *J. Biol. Chem.* **2004**, *279*, 920; Y. Yamaguchi, T. Kuroki, H. Yasuzawa, T. Higashi, W. Jin, A. Kawanami, Y. Yamagata, Y. Arakawa, M. Goto, H. Kurosaki, *J. Biol. Chem.* **2005**, *280*, 20824.
[29] M. J. Mueller, M. Andberg, J. Z. Haeggstrom, *J. Biol. Chem.* **1998**, *273*, 11570.
[30] M. L. Greenlee, J. B. Laub, J. M. Balkovec, M. L. Hammond, G. G. Hammond, D. L. Pompliano, J. H. Epstein-Toney, *Bioorg. Med. Chem. Lett.* **1999**, *9*, 2549; G. G. Hammond, J. L. Huber, M. L. Greenlee, J. B. Laub, K. Young, L. L. Silver, J. M. Balkovec, K. D. Pryor, J. K. Wu, B. Leiting, D. L. Pompliano, J. H. Toney, *FEMS Microbiol. Lett.* **1999**, *179*, 289; D. J. Payne, J. H. Bateson, B. C. Gasson, T. Khushi, D. Proctor, S. C. Pearson, R. Reid, *FEMS Microbiol. Lett.* **1997**, *157*, 171.
[31] S. Iyobe, H. Kusadokoro, J. Ozaki, N. Matsumura, S. Minami, S. Haruta, T. Sawai, K. O'Hara, *Antimicrob. Agents Chemother.* **2000**, *44*, 2023; S. Iyobe, H. Kusadokoro, A. Takahashi, S. Yomoda, T. Okubo, A. Nakamura, K. O'Hara, *Antimicrob. Agents Chemother.* **2002**, *46*, 2014; P. Oelschlaeger, R. D. Schmid, J. Pleiss, *Biochemistry* **2003**, *42*, 8945.
[32] J. D. Docquier, J. Lamotte-Brasseur, M. Galleni, G. Amicosante, J. M. Frere, G. M. Rossolini, *J. Antimicrob. Chemother.* **2003**, *51*, 257.
[33] D. M. Livermore, *Clin. Microbiol. Infect.* **2004**, *10(Suppl 4)*, 1.
[34] M. Galleni, J. Lamotte-Brasseur, G. M. Rossolini, J. Spencer, O. Dideberg, J. M. Frere, *Antimicrob. Agents Chemother.* **2001**, *45*, 660.
[35] N. O. Concha, B. A. Rasmussen, K. Bush, O. Herzberg, *Structure* **1996**, *4*, 823.

 © 2006 Wiley-VCH Verlag GmbH & Co. KGaA, Weinheim

Philosophy behind Imaging

DOI: 10.1002/anie.200502407

Visual Essences, Readable Signs, Means of Construction: On the Relevance of Images in Science**

*Michael Hampe**

Keywords:
computer chemistry · imaging · immediacy · new essentialism

Images are playing an increasingly important role in scientific journals and lectures. The visual aspect of a research project seems to have become a quality in itself. There are two possible reasons for this. Firstly, the authority of visual evidence is enormous. Someone who has seen something for himself or herself is a *privileged witness*. The presentation of images seems to put those who see them in a position similar to that of the researchers themselves. The scientists saw what the audience now sees; both seem to have become eyewitnesses. Thus, the gap separating persons who *acquire* scientific knowledge from the public who receives it appears to be diminished. It would seem that images are making a valuable contribution to public education. Secondly, an image is *entertaining*. It isn't associated with the unpleasant memories that may surround formulae that were already difficult to understand in school. So, a further barrier between science and the public seems to have been broken down. It no longer seems necessary to master the "secret language" of higher mathematics in order to be initiated into the results of scientific research. It now seems possible to understand complex connections with less effort. However, both reasons for the employment and enthusiastic reception of images are deceiving.

For the old dichotomy between numbers and images doesn't exist. For Platonists, "true being" was the *invisible* number, and the *visual* image was mere appearance (as for example in the "cave cinema" in Plato's "Republic"). The "initiated" had access to knowledge about the numbers and their interrelation, the unknowing abandoned themselves to the play of shadows on the wall. But since Descartes, in his analytical geometry, defined every point in space as a numerical triplet and every number as a possible geometrical representation, images and numbers have become interconvertible. Computers have become providers of images that represent nothing but complex numerical relationships. They convert columns of numbers into just those images they are *supposed* to produce according to a previously created program. As a rule, this program remains hidden from the recipients of scientific results. Because of the modern division of labor among scientists, it is often enough also unknown to the researchers who push the "enter" key for the PowerPoint presentations, because they cannot be computer scientists as well as experts on flow mechanics, or physicists, chemists, and neurologists all rolled into one. Being able to show and to see images does not mean, therefore, that it is possible to dispense with computing altogether. Even today, someone has to do the calculating and does it according to a theory that is generally quite complicated. But the theory remains hidden behind the image, and the image doesn't explicate the theoretical assumptions on the basis of which it was constructed. Thus someone hearing a scientific lecture often wrongly assumes himself or herself to be in the same situation as the scientists who created or are presenting the images. Still, that doesn't change the fact that there is no room any longer for the Platonic difference between the hidden numerical meaning and the visual appearance of things.

The new prevalence of images and the concomitant problem of what seems to be a new immediacy correspond to an academic development that has been called the "pictorial turn". W. T. Mitchell[1] coined this term in 1992,[2] and Gottfried Boehm employed the term "iconic turn" for this development in his 1994 article "Die Wiederkehr der Bilder" (The Return of the Images).[3] The coinages "pictorial" and "iconic turn" refer to the "linguistic turn" diagnosed by the American philosopher Richard Rorty in 1967.[4] At that time, Rorty was referring to the relevance that linguistic analysis had acquired in Anglo-American philosophy in the first half of the 20th century. Instead of arguing about the "essence" of things, philosophers deliberated about the meanings of the words with which such an argument might possibly be conducted. In a "semantic ascent", discussions about the meaning of linguistic signs took the place of theories about things. Anglo-American linguistic philosophy was not the only philosophical tradition marked by a concentration on language. The Hermeneutics and Deconstructionism[6] that originated in Heideggerian philosophy[5] considered language (Gadamer) or writing (Derrida) to be the true focus of man's being and of philosophical reflection. This "fixation on language" has not been received kindly by all

[*] Prof. Dr. M. Hampe
Professor of Philosophy
Center for the History of Knowledge
ETH Zürich
Rämistrasse 36, 8092 Zürich (Switzerland)
Fax: (+41) 44-632-1561
E-mail: hampe@phil.gess.ethz.ch

[**] I thank Dr. Peter Geimer of the Center for the History of Knowledge, ETH Zurich, for his valuable comments on the subject matter of this Essay.

InterScience
© 2006 Wiley-VCH Verlag GmbH & Co. KGaA, Weinheim

observers of philosophical developments. Some have seen in it a removal of philosophy from what is "real", the height of the estrangement of philosophical inquiry from the reality of the senses. From this point of view, the talk of a "pictorial turn" could be taken to refer to a *countermovement* back to essences and things given to the senses. But images are of course no more the things themselves than their linguistic descriptions are. Gottfried Boehm's hermeneutics of images, for instance, is not an investigation of immediately given essences, in which he doesn't believe any more than anyone else in hermeneutics. The notion that the turn to images somehow reverses or goes back on the linguistic turn is superficial and wrong. Rather, this development takes images seriously as media and forms of knowledge *alongside of* linguistic utterances; that has nothing to do with a perception of essences. Scientific images, too, *convey* something and need to be *deciphered*; they don't display essences. What the prevalence of images in the sciences has challenged is the notion that the analysis of language and arguments need to constitute the heart of reflection about scientific knowledge. It has quickly become clear that, for instance, the concept of scientific objectivity does not only have something to do with its moral origin (in the idea of unprejudiced observation), but also with the history of the use of a camera lens, that is, with the use of photography in research.[7] Art historians like Bredekamp therefore claim that their professional competence in analyzing pictures is relevant also for the examination of scientific images. In this connection, there doesn't always seem to be a clear understanding of the fact that scientists in general produce two kinds of images: the impressive ones for public appearances and for journals like *Nature*, and those that are *useful* for their findings.[8] The impressive ones can certainly be subjected to a stylistic analysis using the methods of art history. As for the useful ones, it would also be necessary to examine the theories and the computations on the basis of which they are produced, something that is hardly the case in an art historical analysis of scientific images. Even an analysis of images as independent phenomena (and not as results of theories) clearly shows that these don't represent essences that are objects of passive contemplation. This is not a shortcoming of scientific images. For modern science already bid farewell to the essence of things when Galileo Galilei wrote to Marco Velseri on December 1, 1612: *"I consider penetrating into the essence of things to be an impossible endeavor and lost labor."*[9]

Images are of course no more the things themselves than their linguistic descriptions are.

"I consider penetrating into the essence of things to be an impossible endeavor and lost labor."

Since then, it would have seemed that the knowledge of essences no longer has a role to play in science, at least not in the natural sciences. But meanwhile, with the flood of images appearing in journals and public lectures, the sciences are not always maintaining this modest position of sticking strictly to the phenomena. In some cases, the "iconic turn" in the natural sciences is associated with a *new essentialism*. Particularly in the biological sciences, in genetics and neurology, one comes across the explicit or implicit claim that a certain discovery about the brain or a deciphering of the human genome constitutes an *essential insight*.

In some cases, the "iconic turn" in the natural sciences is associated with a new essentialism.

This could have something to do with the enormous cost of the research involved. The more expensive the material for a research project becomes, the more difficult it is to show modesty in the claims of what insights are possible. Are public organizations supposed to spend billions just for insights into the order of phenomena? If someone promises essential knowledge as a research result, they have better chances to get funding. Sceptics on the other hand are bad fundraisers.

If, instead of just *asserting* the alleged essence of an object as something hidden, one can point to it *in an image*, all the better. Maybe that is the reason why, especially in neurology, one sees so many pictures—of the metabolic brain activity of a person in the act of making music, for instance, and even MRI scans of a copulating couple. The physics that made imaging techniques based on nuclear magnetic resonance possible has justly been honored with the Nobel Prize. The scientific and diagnostic insights that have been attained thanks to these methods can hardly be overestimated. And the outlook for further advances in knowledge is promising. For example, the ETH Zurich is planning to open an "Imaging Center" at its location on the Hönggerberg, in which mainly preclinical research is to be conducted using the imaging technique of Positron Emission Tomography (PET). The fact that it is also possible to make a fuss with these images, and—when these are accompanied by claims of ostensibly essentialist breakthroughs in knowledge—to do scientific and biological politics at best, is a different matter.

The "new biological essentialism" is neither a result nor a goal of imaging techniques; it is just a side effect. The public impact of the images may sometimes lead those who show them to make grandiose claims. But with or without images, essentialism remains implausible. Is the nature or the essence of man supposed to be located in his genome or his brain and, insofar as both are made visible by means of a computer, be perceptible in an image? Without genes there is no brain and without a brain no thinking. And it certainly is amazing that chromosomes and nerve tissue can be seen nowadays without a skull being opened and tissue damaged. Nevertheless, thinking is not and will never be seen. As the British philosopher Gilbert Ryle argued already in the 1950s: it is impossible to

© 2006 Wiley-VCH Verlag GmbH & Co. KGaA, Weinheim

Thinking is not and will never be seen.

play the violin without an index finger. Does that mean that the essence and the "actual location" of playing the violin lies in the index finger? One can see the index finger: for that, one doesn't need computed tomography. Yet the location and the essence of the competency of playing the violin cannot be seen any more than one can see thinking. Not because we are dealing with esoteric phenomena and hidden essences here, but because there is no such thing as a location or an essence of such a competency.[10] In the neurological sciences, one doesn't always talk about the "essence" of things in this connection, one refers rather to the "foundation" that lies "at the basis" of a surface phenomenon, or upon which it "rests", namely, brain activity.[11] At the same time, one emphasizes that imaging techniques exhibit the *plasticity* and variability of the brain. How is one supposed to decide whether a brain structure made visible in an image constitutes the foundation of a behavioral pattern or its expression? Not by looking at the image, which doesn't offer any information in this regard. Finding an answer to this question requires costly longitudinal section studies of brain development in relation to certain behavioral environments. The architectural metaphor of a foundation betrays a particular understanding of science. Commentaries on the image of a brain such as: and here you see what lies at the basis of hearing music, or of understanding texts, don't tell us what we see; rather, they tell us what the image that we see is *supposed* to be taken as a sign for.

In spite of these easily grasped insights, there is no shortage of neurologists wanting to show pictures of a brain in the act of thinking of a Mozart symphony. Also, there are researchers like Adolf Heschl of the Konrad Lorenz Institute for Research in Evolution and Cognition who think that "the entire knowledge of the (multicellular) individual must already preexist in its genome".[12] In other words, they don't differentiate between the *conditions* of a competency, the *location* of its realization and the "nature" of an *ability*. There is no doubt that insights into the human genome and the anatomy and function of the human brain, and pictorial representations of the same, are spectacular achievements of the *causal analysis* of biological processes. But they are no more than that. They disclose the necessary conditions for certain functions and performances, and that is all Galilean research sets out to do. Confusing necessary conditions with knowledge of essences is not only a mistake in argument but also, sadly, a betrayal of the Galilean spirit of modern science, that has long given up the search for essences. Perhaps it is because of the new possibilities in imaging techniques that the visualization of causal complexity has become associated with the localization of competencies, so that the "new essentialism" is joined by a "new locationism". Perhaps it is the evidence of a visible location that brings forth the enthusiasm leading some scientists to assert that here one has to do with a special kind of knowledge, that is, with an essential insight into thinking, consciousness, or whatever. Applied to man, this is particularly problematic. The only people in science who were still speaking about essences, whether of a particular individual or of "man as such" (whoever that may be), were backwardly oriented anthropologists, graphologists, skull interpreters, and other "researchers" who from the point of view of modern science were considered to be obscurantist. Allying the most modern technology with argumentatively untenable genetic or neurological essentialism may make it possible to secure research funds and win conceptual ground in the medium term. But it hardly promotes a differentiated understanding of the human situation.

If one wishes to interpret the contemplation of images as the intuition of essences, one needs to understand them *phenomenologically*, as the presence of something that is immediately given. A phenomenological understanding of images can be contrasted with an understanding based on the *theory of signs*, in which images and other nonpictorial traces are *indications* of something not present in the image (cf. Boehm on the difference and connection between the phenomenological and the semiotic understanding of images[13]). In principle, it is perfectly clear to the scientists creating images that this is a process of mediation involving data acquired from measurements, behind which in turn are theories of measurement and of the objects that are being measured. Gérard Crelier and Thomas Järmann, for example, write about the technique of magnetic resonance imaging as follows: *"MRI is an imaging technique, and the importance accorded to the preparation of the image is correspondingly high. As we have … indicated, an MRI scan is generated from large amounts of data. It does not directly represent an object; rather, it represents the data obtained from measurements performed upon the object. A different weighting of the data can influence contrast, brightness or colour."*[14] The Zurich chemist Reinhard Nesper writes about visual models and images of water molecules and ice crystals as follows: *"Of course, no chemist believes that the water molecule or the ice look like that, for the measurements show that there is no real boundary separating the water molecule from what is outside it, nor does the molecule contain atoms that are separable from each other; they don't have their own colour, and the particles are in constant motion—resonance, rotation and translation."* According to Nesper, atoms and molecules appear differently *"according to the way one looks at them, or better, according to the method of measurement one uses to look at them. Each of these methods of measurement is … indirect. In the end, the chemical symbolism is supposed to convey the essential results of such measurements."*[15] Here, Nesper is quite naturally treating images in chemistry as *signs*, and the generation and recognition of images as a semiotic process that has nothing to do with the witnessing and contemplation of something that is given. Every process of measurement refers to *certain, never* to *all* characteristics of an object; it is a procedure by means of which complexity is reduced. In this respect, measurement is no different from perception by means of instruments: in both cases patterns of recognition are "*followed*", "meanings are *extracted*" and, in order to establish these patterns and mean-

 © 2006 Wiley-VCH Verlag GmbH & Co. KGaA, Weinheim

ings, complexities are *suppressed*.[16] (This observation is elementary, and has nothing to do with the complications that have arisen in the theory of measurement in connection with quantum mechanics.)

In chemistry, one can observe a striking continuity between two-dimensional representations of the spatial structure of molecules that are clearly recognizable as *signs*, for example, a benzene ring, and images that at first glance seem to be not semiotic but rather iconic in nature, based on a relation of similarity, about which one can ask how "realistic" they are.[17] But even images that are produced, for instance, by means of X-ray crystallography refer to measurable relationships. When these images are processed, only those aspects of the object that can be described in terms of numbers, for instance the distances between the atomic components of a molecule, are taken into consideration. If all such images are based on measurements, then all scientific images refer to numerical relations. Let us call these images metrical images. What is not expressible in terms of numerical relationships in an object cannot be represented in a metrical image. In contrast to the sketch a traditional botanist or zoologist makes of a plant or an animal, which does not originate in a conscious calculation, the metrical image produced in magnetic resonance imaging, for instance, has its origin in measurable magnetic relations and effects in the subatomic realm, and in algorithms that convert these relations and effects to a pixel picture, which in the last analysis is a Cartesian coordinate system. According to Nesper: *"In chemistry we know from the start that we have to make rough estimations and that many potentially important aspects of the actually examined systems cannot be included in our formal descriptions of them. But that, too, can be advantageous. Just as a photographic image lacks the strong three-dimensional presence of many paintings, an overly detailed representation can hinder perception and channel it in undesired directions."*[15]

Something can be done with a metrical image that is impossible with an image taken as a qualitative phenomenon: it can be used as a model of the measured object that can be manipulated by varying the data of measurement on which it is based. Many movements in the microrealm, for instance in chemical reactions, take place at such great speed that the amount of data gathered per unit of time is hardly manageable. Compressing data into visual images seems to be a way to bring this fundamental problem of modern science, the management of streams of data, at least partially under control. If algorithms are available for the manipulation of large bundles of data, an image can be manipulated and transformed in a simulation. In this way, it is possible to gain insights into the spatial structure and the dynamics of an object that could not be obtained otherwise, certainly not from the object itself, and not from the data sets alone without the aid of visualization either. Metrical images thus become tools for constructing hypotheses about developments in the objects of study. As such, their relevance in sciences like chemistry will likely continue to increase.

Published online: December 28, 2005

[1] W. T. Mitchell, *Artforum* **1992**, 89 – 94.

[2] "Drehmomente – Merkmale und Ansprüche des Iconic Turn": H. Bredekamp in *Iconic Turn. Die neue Macht der Bilder* (Eds.: C. Maar, H. Burda), DuMont, Cologne, **2004**.

[3] "Die Wiederkehr der Bilder": G. Boehm in *Was ist ein Bild* (Ed.: G. Boehm), Wilhelm Fink Verlag, Munich, **1994**, p. 12.

[4] *The Linguistic Turn* (Ed.: R. Rorty), The Chicago University Press, Chicago, **1967**.

[5] H. G. Gadamer, *Wahrheit und Methode. Grundzüge einer philosophischen Hermeneutik*, Mohr Siebeck Verlag, Tübingen, **1960**.

[6] J. Derrida, *De la grammatologie*, Les Édition de Minuit, Paris, **1967**.

[7] "Die Kultur der wissenschaftlichen Objektivität": L. Daston in *Ansichten der Wissenschaftsgeschichte* (Ed.: M. Hagner), S. Fischer Verlag, Frankfurt am Main, **2001**, pp. 137 – 160; "Das Bild der Objektivität": L. Daston, P. Galison in *Ordnungen der Sichtbarkeit. Fotografie in Wissenschaft, Kunst und Technologie* (Ed.: P. Geimer), Suhrkamp, Frankfurt am Main, **2002**, pp. 29 – 99.

[8] J. Elkins, *The Domain of Images*, Cornell University Press, Ithaca, **1999**; P. Galison, *Picturing Science, Producing Art*, Routledge, London, **1998**.

[9] A. Ros, *Begründung und Begriff. Wandlungen des Verständnisses begrifflicher Argumentation*, Felix Meiner Verlag, Hamburg, **1990**, p. 8.

[10] "The World of Science and the Everyday World": G. Ryle in *Dilemmas* (Ed.: G. Ryle), Cambridge University Press, London, **1954**, pp. 68 – 81.

[11] W. Singer, *Ein neues Menschenbild? Gespräche über Hirnforschung*, Suhrkamp, Frankfurt am Main, **2003**, p. 11 and pp. 97 – 109.

[12] A. Heschl, *The Intelligent Genome*, Springer, Berlin, **2002**, p. 17.

[13] "Das Bild in der Kunstwissenschaft": G. Boehm in *Wege zur Bildwissenschaft* (Ed.: K. Sachs-Hombach), Herbert von Halem Verlag, Cologne, **2004**, pp. 11 – 21.

[14] "Abbildung von Wahrnehmung und Denken. Die funktionelle Magnetresonanz-Bildgebung in der Hirnforschung": G. Crelier, T. Järmann in *Mit dem Auge denken. Strategien der Sichtbarmachung in wissenschaftlichen und virtuellen Welten* (Eds.: B. Heintz, J. Huber), Springer, Vienna, **2001**, p. 107.

[15] "Die chemische Symbolik": R. Nesper in *Mit dem Auge denken. Strategien der Sichtbarmachung in wissenschaftlichen und virtuellen Welten* (Eds.: B. Heintz, J. Huber), Springer, Vienna, **2001**, p. 174.

[16] J. J. Gibson, *The Ecological Approach to Visual Perception*, Lawrence Erlbaum Associates, Neww Jersey, **1976**; E. H. Gombrich, *Art and Illusion. A Study in the Psychology of Pictorial Representation*, Princeton University Press, London, **1976**; M. Kemp, *Visualizations. The Nature Book of Art and Science*, Oxford University Press, Oxford, **2000**, p. 2 and p. 129; U. Neisser, *Cognition and Reality*, W. H. Freeman, San Francisco, **1976**, chap. II.

[17] R. Hoffmann, P. Laszlo, *Angew. Chem.* **1991**, *103*, 1 – 16; *Angew. Chem. Int. Ed. Engl.* **1991**, *30*, 1 – 16.

 © 2006 Wiley-VCH Verlag GmbH & Co. KGaA, Weinheim

R. R. Tykwinski and A. L. K. Shi Shun

DOI: 10.1002/anie.200502071

Natural Products Synthesis

Synthesis of Naturally Occurring Polyynes

*Annabelle L. K. Shi Shun and Rik R. Tykwinski**

Keywords:
synthesis design · alkynes · natural products · polyacetylenes · polyynes

Dedicated to Ferdinand Bohlmann



© 2006 Wiley-VCH Verlag GmbH & Co. KGaA, Weinheim

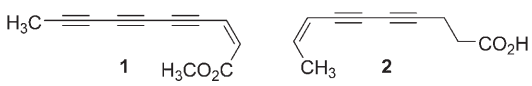
Over the past fifty years, hundreds of polyyne compounds have been isolated from nature. These often unstable molecules are found in sources as common as garden vegetables and as obscure as bacterial cultures. Naturally occurring polyynes feature a wide range of structural diversity and display an equally broad array of biological properties. Early synthetic efforts relied primarily on Cu-catalyzed, oxidative acetylenic homo- and heterocoupling reactions to assemble the polyyne framework. The past 25 years, however, have witnessed a renaissance in the field of polyyne natural product synthesis: transition-metal-catalyzed alkynylation reactions and asymmetric transformations have combined to substantially expand access to natural polyynes. This Review recounts these synthetic achievements and also highlights both the natural source(s) and biological relevance for many of these compounds.

From the Contents

1. Introduction	1035
2. Diynes from Plants	1035
3. Diynes from Marine Organisms	1045
4. Diynes from Fungi	1047
5. Triynes from Plants	1049
6. Triynes from Fungi	1051
7. Triynes from Bacteria	1051
8. Tetraynes from Plants	1052
9. Tetraynes from Bacteria	1052
10. Conclusions	1053

1. Introduction

According to Ferdinand Bohlmann, the first naturally occurring acetylenic compound, dehydromatricaria ester (**1**), was isolated from an *Artemisia* species in 1826.[1a] In the nearly two centuries that have followed, well over a thousand naturally occurring acetylenes have been discovered and reported.[1–3] Polyynes,[4] a subset of this class of natural products, have been isolated from a wide variety of plant species,[1,3] cultures of higher fungi,[2] bacteria, marine sponges, and corals.[5] In addition, dihydromatricaria acid (**2**)



is the solitary example of a polyyne obtained from an insect, the soldier beetle.[6] At present over 1000 compounds with two or more conjugated C≡C bonds have been isolated.[7] These compounds represent a unique class of compounds with an interesting array of biological activities, such as antibacterial, antimicrobial, antifungal, antitumor, anticancer, anti-HIV, and pesticidal properties.[8] Extensive reviews on the subject of naturally occurring polyacetylenes have been published over the past 40 years,[1–3,8,9] and it would be remiss not to acknowledge the tremendous contributions by both Bohlmann[1] and Jones[2] in the field of naturally occurring acetylenes. Excellent reviews on the biosynthesis and biological activity of acetylenes have also been written by Bu'Lock,[3a] Towers et al.,[8e] as well as Christensen and Lam.[9] The most recent review describing the synthesis of polyyne natural products was by Diederich and co-workers in 2000, but dealt only with selected examples that involved acetylenic coupling reactions.[10] The limited scope of recent reports, coupled with a broad range of research efforts currently being conducted on naturally occurring acetylenes, led us to compile a review focusing on, and restricted to, the latest developments in the area of naturally occurring polyynes since approximately 1980.

The Review has been ordered on the basis of the origin of the natural product. This approach was utilized in an attempt to highlight the presence of polyyne natural products in everyday sources such as carrots and common fungi, as well as more obscure media such as bacterial cultures.[11]

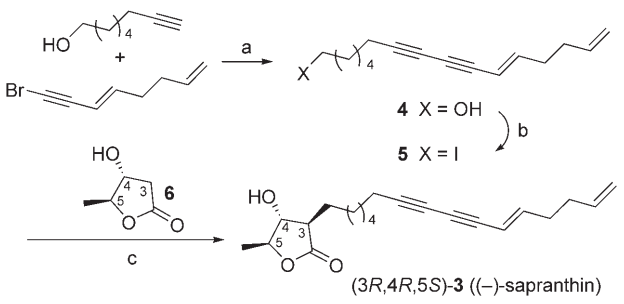
2. Diynes from Plants

2.1. Family Annonaceae (Custard-Apple Family)

The butenolide diyne (−)-sapranthin (**3**) was isolated from the bark of *Sapranthus palanga*, a Costa Rican tree of the custard-apple family.[12] The initial structure of (−)-sapranthin was proposed with the absolute configuration of (3*S*,4*S*,5*S*)-**3**.[12] Diyne (3*S*,4*S*,5*S*)-**3** was subsequently synthesized by Brückner and co-workers,[13] but a comparison of the NMR data of this synthetic sample with that of the authentic material revealed a number of discrepancies. It was deduced that the true structure of natural sapranthin was likely (3*R*,4*R*,5*S*)-**3**, and this premise was confirmed by the synthesis of this isomer (Scheme 1). A Cadiot–Chodkiewicz reaction under conditions developed by Cai and Vasella[14] was a key

[*] A. L. K. Shi Shun, Prof. R. R. Tykwinski
Department of Chemistry
University of Alberta
Edmonton, Alberta, T6G 2G2 (Canada)
Fax: (+1) 780-492-8231
E-mail: rik.tykwinski@ualberta.ca

 © 2006 Wiley-VCH Verlag GmbH & Co. KGaA, Weinheim

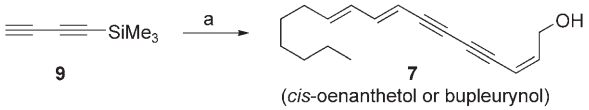


Scheme 1. Synthesis of sapranthin according to Brückner and co-workers.[13] a) $[Pd(dba)_2]$, CuI, LiI, DMSO, 10 min, then pentamethylpiperidine, 2 h, 60%; b) PPh_3, imidazole, I_2, THF, 0°C, 88%; c) **6**, LDA, THF, −78°C, 2 h, then addition of **5** in THF/DMPU (1:1), −45°C, 69%.

step that gave alcohol **4**, which was then converted into iodide **5**. A *trans*-selective alkylation of **5** with the dilithio derivative of **6** gave (3*R*,4*R*,5*S*)-**3**, which showed NMR spectral data and optical rotation consistent with that of the natural sample.[13]

2.2. Family Apiaceae (Carrot Family)

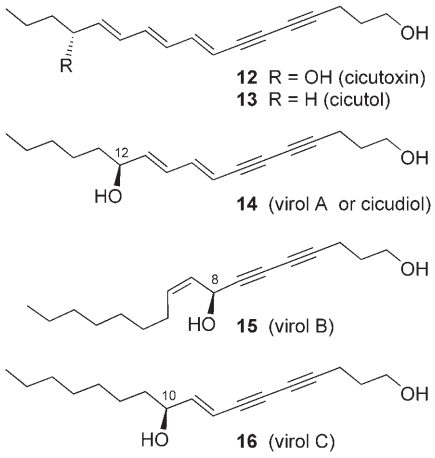
Bupleurynol (**7**, also called *cis*-oenanthetol) has been found in the Chinese perennial plant *Bupleurum longiradiatum*[15] and in *B. acutifolium*, a plant used in Spanish folk medicine.[16] Organ and co-workers have reported two syntheses of **7**,[17] the most recent being a single multireaction sequence (Scheme 2).[17b] Much like Negishi's synthesis of



Scheme 2. "One-pot" synthesis of bupleurynol according to Organ and co-workers.[17] a) 1. BuLi, THF, 2. $ZnCl_2$, 3. $[Pd(PPh_3)_4]$, (*E*)-BrCH=CHI (**8**), 4. $[C_6H_{13}CH{=}CHZrCp_2Cl]$ (**10**), THF, $[PdCl_2(PhCN)_2]$, 5. TBAF, 6. (*Z*)-BrCH=CHCH$_2$OH (**11**), CuI, iPr_2NH, PhH, 60°C, 43%.

xerulin (Scheme 40), (*E*)-1-bromo-2-iodoethylene (**8**) forms the core building block for a sequence of Pd-catalyzed coupling reactions. Negishi coupling of **8** with the zinc acetylide of diyne **9** and then with the zirconium intermediate **10** was followed by in situ desilylation. A final cross-coupling with (Z)-BrCH=CHCH$_2$OH ((*Z*)-**11**) gave bupleurynol. An analogous coupling with (*E*)-**11** in the final step gave the other isomer (not shown), a natural product called oenanthetol that has been isolated from species of *Bupleurum* and from *Oenanthe crocata* (hemlock water-dropwort).[18]

Water hemlock (genus *Cicuta*) is a well-known toxic plant in both Europe and North America.[19] Common acetylenic components isolated from water hemlock include cicutoxin (**12**) and cicutol (**13**), both C_{17}-polyacetylenes identified by



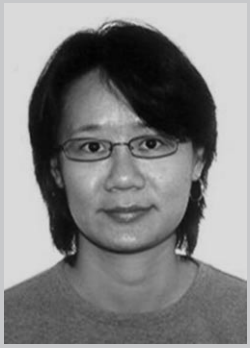
Anet et al. from *C. virosa*.[18a,20] Cicutoxin (**12**) has been found to affect the central nervous system directly, leading to convulsions and respiratory paralysis.[19b] Other diyne constituents isolated from *C. virosa* include the C_{17}-polyacetylenic analogues virols A–C (**14**–**16**),[21] which are chemically more stable than cicutoxin—a factor which enables the study of their mode of pharmacological action.[22]

The first stereoselective synthesis of virols A–C was reported by Oshima and co-workers, who used the Cadiot–Chodkiewicz protocol between suitably functionalized terminal alkynes and iodoalkyne **17** to give the diyne segment (Scheme 3).[22a] The *S* configuration of these toxic alcohols could be proposed from a comparison of the synthetic and natural samples.

Several other syntheses of virol C (**16**) have been described. Stefani et al. used a chiral sulfoxide for asymmetric induction to set the stereochemistry at C10 and a Cadiot–

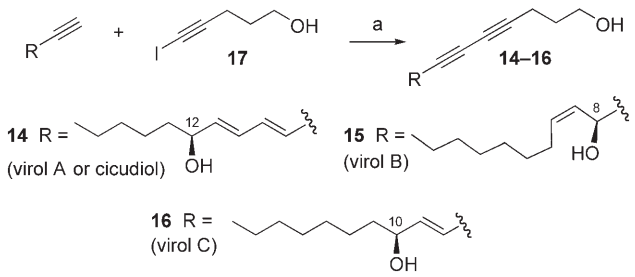


Rik R. Tykwinski was born in Marshall, MN. He completed his BS in 1987 at the University of Minnesota–Duluth, where he worked with Prof. Ron Caple and developed his interest in organic chemistry. He completed his PhD in 1994 with Prof. Peter J. Stang at the University of Utah, and then moved to ETH Zürich (1994–1997) to work with Prof. François Diederich as an ONR post-doctoral fellow. He joined the faculty at the University of Alberta in 1997, where he is now Professor of Chemistry. His research focuses on polyynes and polyenynes as well as photonic applications of organic molecules.



Annabelle L. K. Shi Shun was born in Mauritius. She received her BSc from the University of Mauritius in 1999. She completed her MSc in 2003 under the supervision of Prof. Rik Tykwinski at the University of Alberta, where her studies focused on the synthesis of naturally occurring and synthetic polyynes through alkylidene carbenoid rearrangements. She currently works for an Edmonton-based chemical company.

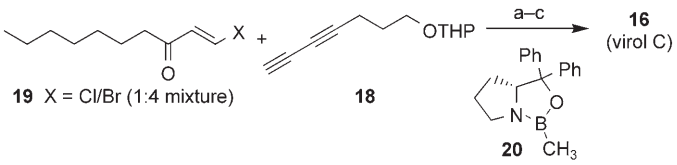
 © 2006 Wiley-VCH Verlag GmbH & Co. KGaA, Weinheim



Scheme 3. Synthesis of virols A–C according to Oshima and co-workers.[22a] a) CuI, pyrrolidine, RT, 91% (**14**), 91% (**15**), 65% (**16**).

Chodkiewicz coupling reaction to construct the diyne core.[23] Sabitha et al. have described two different routes.[24] In both cases, a Sharpless asymmetric epoxidation set the configuration at C10, while the enediyne core was then constructed by using either a Cadiot–Chodkiewicz or Sonogashira reaction.

The most recent stereoselective synthesis of virol C comes from Fiandanese et al. Substitution of bis(trimethylsilyl)butadiyne followed by desilylation gave diyne **18** (Scheme 4),[25]

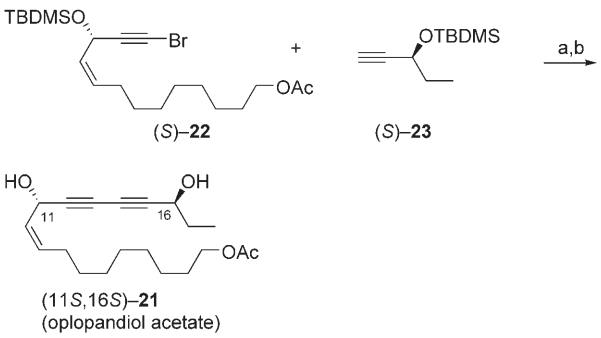


Scheme 4. Syntheses of virol C according to Fiandanese et al.[25] a) $[PdCl_2(PPh_3)_2]$, CuI, NEt_3, RT, 64%; b) **20**, BH_3·THF, THF, RT; c) *p*-TsOH, MeOH, RT, 52% (2 steps, 83% *ee*).

and the carbon framework was completed by Sonogashira coupling of the terminal alkyne with chloro/bromoalkene **19** (produced and used as a mixture). The configuration at C10 was then set in the final step by the enantioselective reduction of the ketone with borane in the presence of the catalyst (*R*)-**20** to give (*S*)-**16**.

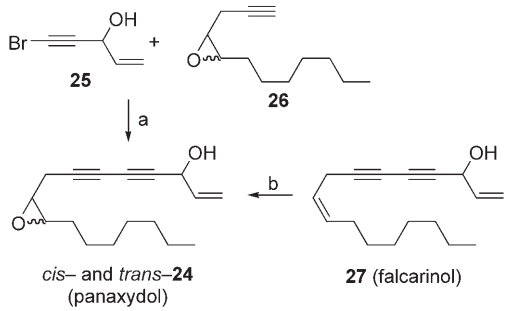
2.3. Family Araliaceae (Ginseng Family)

Oplopanax horridus, commonly known as Devil's club, is a shrub of western North American forests, and native Americans have made use of the inner bark and roots to treat a variety of ailments.[26] Several polyacetylenes isolated from *O. horridus* by Kobaisy et al. displayed antimycobacterial and antifungal activity.[27] Of these compounds, oplopandiol acetate (**21**) was recently synthesized by Cai and co-workers (Scheme 5).[28] The acetate segment (*S*)-**22** was available in ten steps from a known derivative of L-(+)-tartaric acid,[29] while the other segment (*S*)-**23** was formed from a known derivative of D-gluconolactone in five steps. A Cadiot–Chodkiewicz coupling of these two precursors, followed by removal of the TBDMS protecting groups, gave the product **21**.



Scheme 5. Synthesis of optically active oplopandiol acetate according to Cai and co-workers.[28] a) CuCl, NH_2OH·HCl, $EtNH_2$, H_2O, MeOH, 0°C; b) TBAF, THF/H_2O, 0°C, 52% (2 steps).

Red ginseng, the steamed and dried root of *Panax ginseng*, has been used extensively in oriental traditional medicine.[30] A host of polyacetylenes have been identified from this and other ginseng plants.[31] The epoxide panaxydol (**24**) was isolated in 1980[32] and was subsequently shown to possess significant cytotoxic activity toward L1210 cells.[33] Poplawski et al. first synthesized panaxydol to establish its structure, by using a Cadiot–Chodkiewicz coupling of **25** and **26** to construct the diyne core (Scheme 6).[32] An alternative route



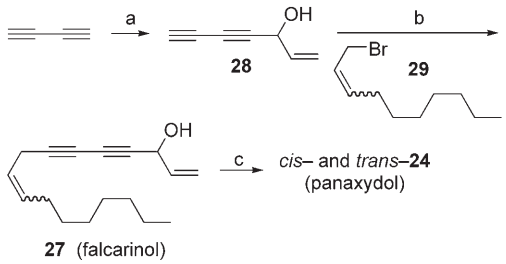
Scheme 6. Synthesis of panaxydol according to Poplawski et al.[32] a) CuCl, $EtNH_2$, NH_2OH·HCl, MeOH, H_2O, dioxane, 30°C, 35%; b) *m*CPBA, $CHCl_3$, RT, 41%.

relied on epoxidation of falcarinol (**27**, also called panaxynol), itself a natural product found in species of *Panax*.[34] Ultimately, it was suggested that natural panaxydol exists as a mixture of *cis* and *trans* isomers with respect to the epoxide moiety, although a ratio was not given.[32]

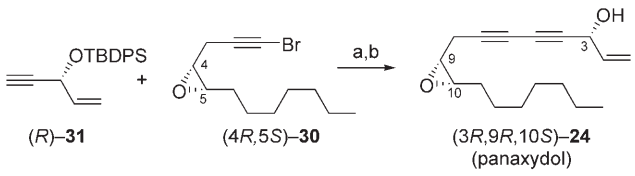
Ahn and coworkers synthesized panaxydol as part of a recent exploration of its antiproliferative activity toward L1210 cells (Scheme 7).[35] Deprotonation of butadiyne with EtMgBr and reaction with acrolein gave diynol segment **28**. Deprotonation at the other terminus of the diyne and reaction with allyl bromide **29** completed the carbon framework and gave a separable mixture of (*Z*)- and (*E*)-**27** (falcarinol). Regioselective epoxidation then afforded the products, *cis*- and *trans*-**24**.

Optically active panaxydol was first synthesized by Cai and coworkers (Scheme 8).[36] Chiral epoxide (4*R*,5*S*)-**30**, constructed from L-(+)-diethyl tartrate, was subjected to Cadiot–Chodkiewicz coupling with alkyne (*R*)-**31**. Removal

 © 2006 Wiley-VCH Verlag GmbH & Co. KGaA, Weinheim



Scheme 7. Synthesis of panaxydol according to Ahn and co-workers.[35] a) EtMgBr, Et_2O, RT, then CH_2=CHCHO, Et_2O, 0 °C; b) EtMgBr, Et_2O, 0 °C→reflux, then **29**, $CuCl_2$, 0 °C→reflux, 17% ((*Z*)-**27**) and 15% ((*E*)-**27**); c) *m*CPBA, $CHCl_3$, RT, 42% (*cis*-**24**) and 36% (*trans*-**24**).



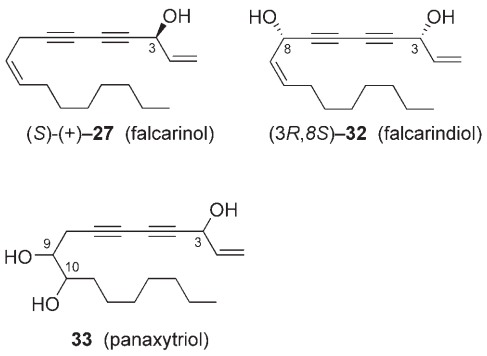
Scheme 8. Synthesis of optically active panaxydol according to Cai and co-workers.[36] a) CuCl, $EtNH_2$,NH_2OH·HCl, MeOH, 0 °C, 69%; b) TBAF, THF, RT, 66%.

of the *tert*-butyldiphenylsilyl (TBDPS) group provided (3*R*,9*R*,10*S*)-**24**, and, overall, this represented a 10% overall yield in 14 steps from a known derivative of L-(+)-diethyl tartrate.

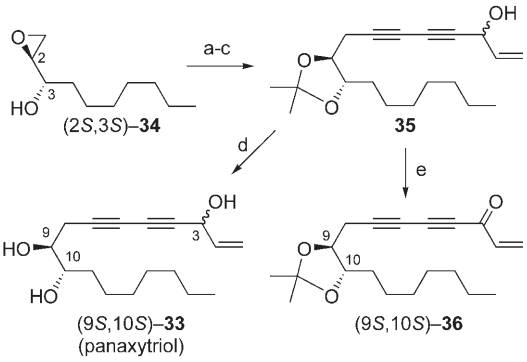
Shen and co-workers have also reported the synthesis of optically active **24** (not shown).[37] In their approach, an asymmetric reduction using the borane·dimethyl sulfide complex in the presence of the (*R*)-MeCBS reagent (**20**) set the configuration at C3 (as reported by Yun and Danishefsky[38]), while Sharpless asymmetric dihydroxylation was used to set the configuration of the epoxide moiety. A concluding Cadiot–Chodkiewicz completed the carbon framework.

Both (+)- and (−)-falcarinol (**27**) have been isolated from *P. ginseng* and show selective in vitro cytotoxicity toward several cancer cell lines.[39] A related compound, falcarindiol (**32**), has been found in many species of *Araliaceae* and other families, such as *Apiaceae*.[31,40b] It shows a range of biological activity, including growth inhibitory activity against bacteria such as *E. coli* and *Staphylococcus aureus*.[40] Cai and co-workers have reported the stereoselective synthesis of both falcarinol[41] and falcarindiol (**32**)[42,43] by using a Cadiot–Chodkiewicz coupling.

Panaxytriol (**33**) is believed to be a major constituent responsible for the biological activity of red ginseng.[44] Panaxytriol has been found to inhibit MK-1 cells[45] and to suppress the growth of B16 melanoma cells transplanted into mice.[46] In addition, its effectiveness at inhibiting cellular respiration and energy balance of a human breast carcinoma cell line (M25-SF) has been reported.[47] Few, if any, polyyne natural products have garnished as much interest synthetically as panaxytriol. The chemical structure of panaxytriol was proposed by Kitagawa et al., following their initial isolation of the substance.[44,48] In 1995, Kobayashi et al. proposed the absolute configuration of panaxytriol to be



3*R*,9*R*,10*R* by the CD exciton chirality method and the modified Mosher ester method.[49] Since this report, however, the issue of the relative and absolute configuration of panaxytriol has been a matter of controversy because of conflicting data.[50] In 1997, Fujimoto and co-workers proposed the 3*R*,9*S*,10*S* configuration for **33**[50] on the basis of the synthesis of panaxytriol derivatives and a comparison of optical rotations and NMR spectra with corresponding derivatives of panaxytriol from natural sources. In their synthesis (Scheme 9), L-(+)-tartrate was transformed in



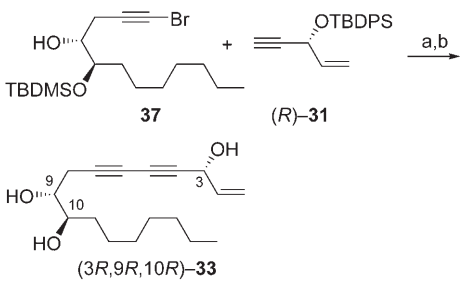
Scheme 9. Synthesis of panaxytriol according to Fujimoto and co-workers.[50] a) LiC≡CC≡CH, HMPA, THF, −30 °C 94%; b) 2,2-dimethoxypropane, CSA, RT, 89%; c) BuLi, THF, −30 °C, then acrolein, 18%; d) MeOH, HCl, RT, 91%; e) $(COCl)_2$, DMSO, NEt_3, CH_2Cl_2, RT, 40%.

several steps to epoxide (2*S*,3*S*)-**34**, which was converted into acetonide **35** in three steps. Deprotection of the diol produced a diastereomeric mixture of C3 epimers of (9*S*,10*S*)-**33**. Their subsequent stereochemical assignment was consistent with the fact that **35** could be oxidized to (9*S*,10*S*)-**36**, and the optical rotation of this synthetic compound was identical to that of the analogous ketone derived directly from naturally occurring panaxytriol.

However, the debate over the configuration at C9 and C10 continued. Kobayashi et al. reported an extensive spectroscopic and chemical study on the absolute configuration of **33**, and their results reaffirmed the initial assignment of 3*R*,9*R*,10*R*.[51] A synthetic study by Cai and co-workers also supported this result.[52] The diastereomers (3*R*,9*R*,10*R*)-**33** and (3*R*,9*S*,10*S*)-**33** were synthesized, and by comparing the optical rotation of these isomers and authentic panaxytriol

 © 2006 Wiley-VCH Verlag GmbH & Co. KGaA, Weinheim

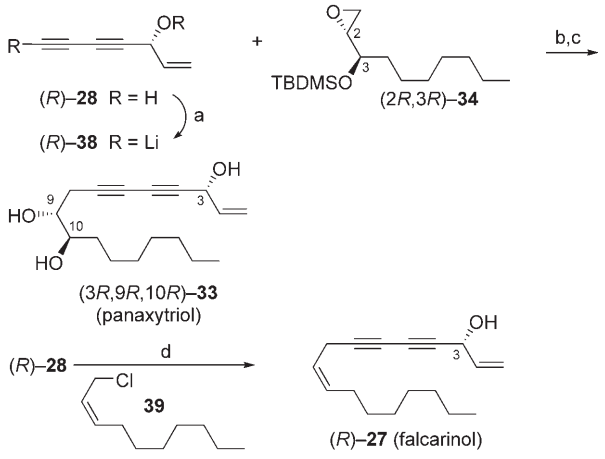
they concluded that the absolute configuration of the natural product was indeed 3*R*,9*R*,10*R*.[52] The synthesis of the 3*R*,9*R*,10*R* isomer is summarized in Scheme 10. Optically active bromoalkyne **37** was available in nine steps from D-arabinose, and a Cadiot–Chodkiewicz coupling with (*R*)-**31** (derived from D-xylose) gave panaxytriol.



Scheme 10. Synthesis of panaxytriol according to Cai and co-workers.[52] a) CuCl, $EtNH_2$, $NH_2OH{\cdot}HCl$, MeOH, H_2O, 0 °C, 75 %; b) TBAF, THF, RT, 83 %.

At the same time, Gurjar et al. came to an opposite conclusion; their synthesis of four diastereomers of panaxytriol led to them being proponents of the 3*R*,9*S*,10*S* assignment.[53] Of the four synthetic isomers they produced, they concluded that the optical rotation of the isomer assigned (3*R*,9*S*,10*S*)-**33** most closely matched that of the natural product.

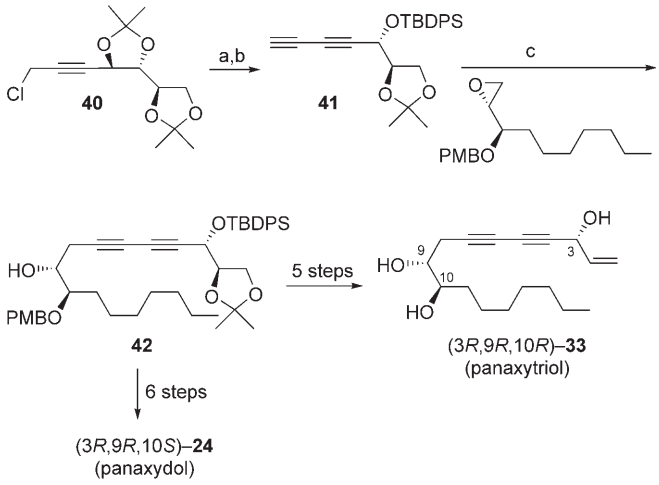
Three additional syntheses of **33** have subsequently been reported, and all three have come out in favor of the 3*R*,9*R*,10*R* configuration. Faber and co-workers used two main building blocks: alcohol **28** and epoxy-alcohol **34** (Scheme 11).[54] Both (*R*)- and (*S*)-**28** could be obtained enantioselectively (>98 % *ee*) by a *Candida antarctica* lipase B catalyzed kinetic resolution of either alcohol **28** or the corresponding acetate, and both C3 epimers of **33** were therefore accessible. As shown in Scheme 11, the 3*R*,9*R*,10*R* diastereomer was assembled by addition of the



Scheme 11. Synthesis of panaxytriol and falcarinol according to Faber and co-workers.[54] a) BuLi, THF, −78 °C; b) **34** + **38**, HMPA, 80 °C; c) TBAF, THF, RT, 68 % (over 3 steps); d) Bu_4NCl, K_2CO_3, CuI, DMF, RT, then **39**, 69 %.

corresponding lithium acetylide (*R*)-**38** to epoxide **34**. The analogous sequence with (*S*)-**28** and **34** gave (3*S*,9*R*,10*R*)-**33** in 59 % yield (not shown). The two enantiomers of falcarinol (**27**) were also readily formed from (*R*)- and (*S*)-**28** by coupling with allyl chloride **39**.

Yadav and Maiti have synthesized (3*R*,9*R*,10*R*)-panaxytriol from D-arabinose by using a base-induced double elimination of the 4,5-*O*-isopropylidene propargyl chloride **40** as a key step to introduce the diyne moiety of **41** (Scheme 12).[55,56] The advanced intermediate **42** was then



Scheme 12. Synthesis of panaxytriol and panaxydol according to Yadav and Maiti.[55] a) $LiNH_2$, NH_3(l), 85 %; b) TBDPSCl, imidazole, CH_2Cl_2, 88 %; c) BuLi, $BF_3{\cdot}OEt_2$, −78 °C, 75 %.

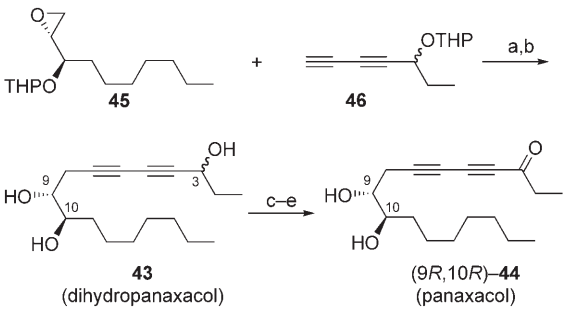
assembled through deprotonation of the terminal diyne **41** and opening of the epoxide ring under the conditions described by Yamaguchi and Hirao.[57] Five straightforward steps from **42** gave (3*R*,9*R*,10*R*)-**33**. The intermediate **42** was also elaborated to (3*R*,9*R*,10*S*)-**24** (panaxydol) in six steps.

The most recent synthesis of panaxytriol has been accomplished by Danishefsky and Yun.[38] A successful Cadiot–Chodkiewicz cross-coupling in the presence of three unprotected hydroxy groups to give (3*R*,9*R*,10*R*)-**33** constituted a key step in this synthesis.

Closely related to panaxytriol are dihydropanaxacol (**43**) and panaxacol (**44**),[58] and these were also the first of the panax polyynes to be synthesized in optically pure form (Scheme 13). In 1989, Fujimoto and Satoh established the 9*R*,10*R* configuration of panaxacol by stereoselective synthesis of both enantiomers starting from either D-(−)- or L-(+)-DET.[59] Epoxide **45**, derived from D-(−)-tartrate, was condensed with the lithium acetylide formed from **46** to give a diastereomeric mixture of C3 epimers of (9*R*,10*R*)-dihydropanaxacol (**43**). After protection of the glycol moiety as the acetonide, Swern oxidation gave the C3 ketone, and deprotection of the diol with CSA gave (9*R*,10*R*)-**44**. The configuration of natural dihydropanaxacol was also tentatively assigned as (3*S*,9*R*,10*R*)-**43** on the basis of this study.

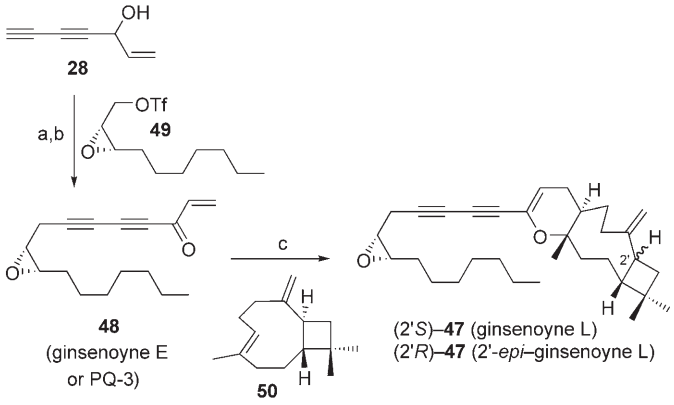
Ginsenoyne L (2′*S*-**47**) was isolated by Hirakura et al., who proposed its structure on the basis of 2D NMR experiments (Scheme 14).[60] Biogenetic consideration of compound

© 2006 Wiley-VCH Verlag GmbH & Co. KGaA, Weinheim



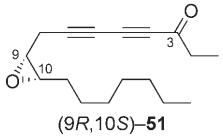
Scheme 13. Synthesis of dihydropanaxacol and panaxacol according to Fujimoto et al.[59] a) BuLi, HMPA, −30 °C; b) MeOH, CSA, RT, 65% (2 steps); c) 2,2-dimethoxypropane, CSA, RT; d) $(COCl)_2$, DMSO, CH_2Cl_2, RT; e) MeOH, CSA, RT (58% 3 steps).

47 suggested that it may be a Diels–Alder-type adduct derived from ginsenoyne E (**48**, also called PQ-3[61]) and 9-*epi*-caryophyllene. To probe this hypothesis, and to shed light on the original stereochemical assignment for (2′*S*)-**47**, Baldwin et al.[62] constructed enediynone **48** by the lithiation of diyne **28** and reaction with optically pure triflate **49** (Scheme 14), followed by oxidation under the conditions described by Bolm et al..[63] The hetero-Diels–Alder reaction with *trans*-β-caryophyllene **50** gave (2′*R*)-**47** (2′-*epi*-ginsenoyne L).

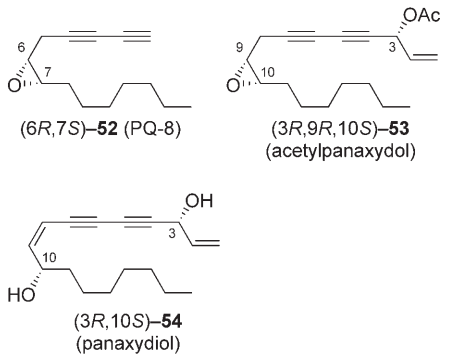


Scheme 14. Synthesis of PQ-3 and 2′-*epi*-ginsenoyne L according to Baldwin et al.[62] a) BuLi (2 equiv), THF/DMPU, −78 °C then **49** 47%; b) TEMPO, nBu_4NBr, oxone, toluene, 67%; c) toluene, 80 °C, 36%.

Related to PQ-3 (**48**) is the saturated analogue (9*S*,10*R*)-**51**, which has also been isolated from *P. ginseng*, and shown to be an effective diacylglycerol acyltransferase inhibitor.[64] By using a protocol similar to that described for **48** (Scheme 14), Lee and co-workers have synthesized all four stereoisomers of **51** using TPAP/NMO oxidation of the C3 alcohol to form the ketone product.[65]



Fujimoto et al. have also isolated several polyacetylenes from the American White ginseng plant (*P. quinquefolius*), including PQ-8 (**52**),[66] acetylpanaxydol (**53**),[66,67] PQ-3



(ginsenoyne E, **48**),[61] and panaxydiol (**54**).[61] The initial synthesis of PQ-8 by this research group[68] led subsequently to the synthesis of the latter three derivatives.[69]

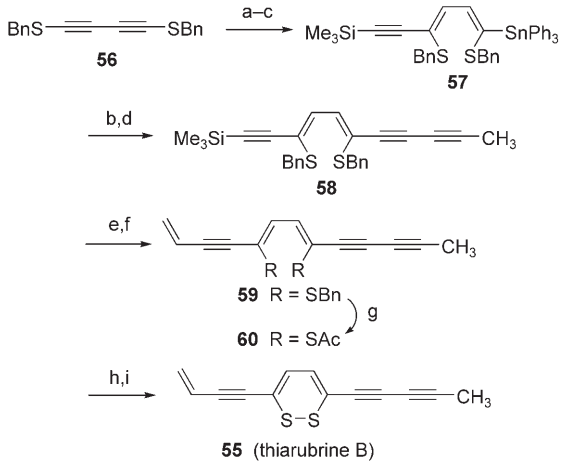
2.4. Family Asteraceae (Aster Family)

Thiarubrines are naturally occurring pigments containing a 1,2-dithiin moiety and have been isolated from about 50 species of the family *Asteraceae.* Thiarubrines were first identified in 1964/1965,[70] and these deeply colored natural products have been found in a range of plants used to treat skin infections and intestinal parasites by native people in Africa and Canada.[71] Surprisingly high quantities (ca. 0.003 wt%) of thiarubrine B (**55**) can be isolated from giant ragweed (*Ambrosia trifida*).[72] The synthesis of **55** was reported in 1994 by Block et al. and was necessarily designed around the chemical instability of the 1,2-dithiin ring system—which was ultimately introduced in the final step (Scheme 15).[73] Starting with diyne **56**, a double stannylation, tin–iodine exchange, and Sonogashira cross-coupling with trimethylsilylacetylene produced **57**. A second sequence of tin–iodine exchange and cross-coupling was used to append the pentadiyne moiety to give **58**. Finally, desilylation followed by cross-coupling with bromoethene completed the conjugated skeleton of **59**. Reaction of **59** with lithium 1-(*N*,*N*-dimethylamino)naphthalenide (LDMAN) followed by addition of acetyl chloride gave thioacetate **60**, which on treatment with KOH/MeOH and oxidation with iodine at low temperature ultimately gave thiarubrine B (**55**).

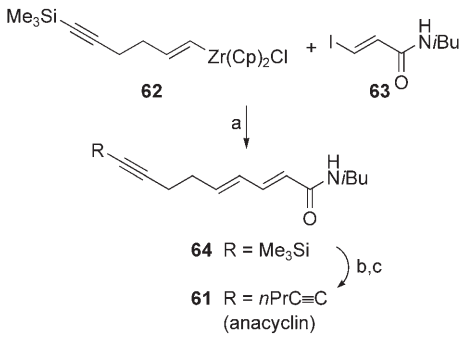
The insecticidal isobutylamide anacyclin (**61**) has been isolated from the Mount Atlas daisy *(Anacyclus pyrethrum*).[74] Crombie et al. used a Pd-catalyzed cross-coupling between vinylzirconium intermediate **62** and vinyl iodide **63** to construct the diene moiety of **64** (Scheme 16).[75] Protiodesilylation of **64**, followed by a Cadiot–Chodkiewicz coupling completed the structure of anacyclin.

Isolation of the isobutylamide **65** from *Anacyclus pyrethrum* was reported by Bohlmann and co-workers, but the stereochemistry was undefined.[76] Carpita et al. established the *E* configuration through synthesis of **65** by a Pd-catalyzed cross-coupling reaction. The diyne core of **66** was constructed by using a Cadiot–Chodkiewicz coupling (Scheme 17).[77] Liberation of the terminal diyne through reaction with base and subsequent Sonogashira coupling with (*E*)-ICH=

 © 2006 Wiley-VCH Verlag GmbH & Co. KGaA, Weinheim

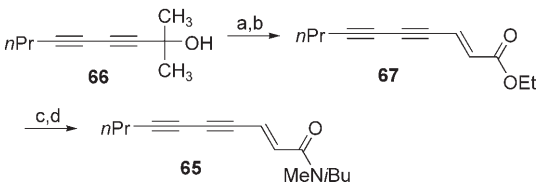


Scheme 15. Synthesis of thiarubrine B according to Block et al.[73] a) Ph_3SnH (2 equiv), $[Pd(PPh_3)_4]$, Et_3B, PhMe, −30→0 °C, 56%; b) I_2, CH_2Cl_2, 0 °C, 95–97%; c) $Me_3SiC{\equiv}CH$, CuI, $[PdCl_2(PPh_3)_2]$, Et_2NH, PhH, 86%; d) $MeC{\equiv}CC{\equiv}CH$, CuI, $[PdCl_2(PPh_3)_2]$, Et_2NH, PhH, 57%; e) TBAF, 86%; f) $H_2C{=}CHBr$, CuI, $[PdCl_2(PPh_3)_2]$, Et_2NH, PhH, 70%; g) LDMAN, THF, −80 °C, 1.5 h, then AcCl; h) KOH, MeOH; i) I_2, −30 °C (17% from **59**).



Scheme 16. Synthesis of anacyclin according to Crombie et al.[75] a) $[Pd(PPh_3)_4]$, THF, PhH, 42%; b) TBAF, THF, 90%; c) *n*PrC≡CBr, CuCl, Et_2NH, $NH_2OH{\cdot}HCl$, MeOH, H_2O, 65%.

$CHCO_2Et$ gave **67**. A sequence of hydrolysis, acid chloride formation, and reaction with isobutylmethylamine ultimately gave the amide product **65**.

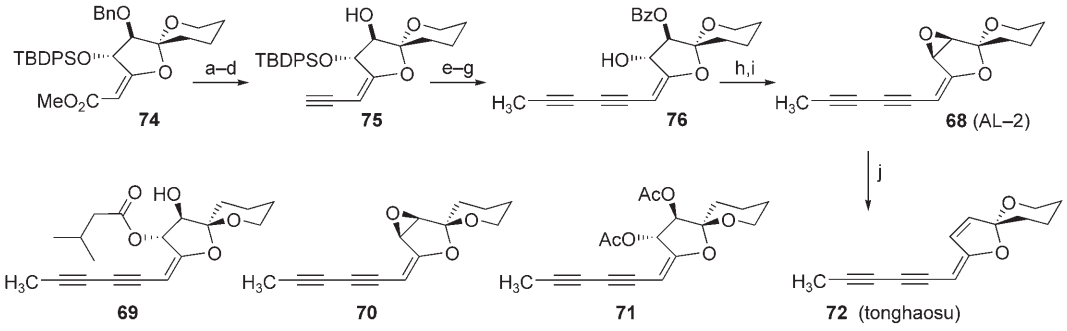


Scheme 17. Synthesis of **65** according to Carpita et al.[77] a) NaOH, PhMe; b) (*E*)-IHC=$CHCO_2Et$, $[Pd(PPh_3)_4]$, CuI, NEt_3, C_6H_6, 67% (2 steps); c) NaOH, MeOH, then H_2SO_4, 89%; d) $(COCl)_2$, toluene, reflux, then *i*BuNHMe, Et_2O, 0 °C, 63%.

Diacetylenic spiroacetal enol ether derivatives such as **68**–**73** (see Schemes 18 and 19) have been isolated from a range of plants from the *Asteraceae* family, including sage brush (*Artemisia*)[78a] and daisies (*Chrysanthemum*).[78b] Many have biological and pharmacological activities: for example **68** (AL-2) showed antitumor properties[79] and **72** (tonghaosu)[80] displayed antifeedant activity.[81] Mukai and co-workers have reported the first stereoselective synthesis of (−)-AL-2 (**68**),[82,83] starting from diethyl L-tartrate to provide advanced intermediate **74**, in which all of the stereogenic centers of the natural product are in place (Scheme 18). A four-step sequence culminating in reaction with lithium trimethylsilyldiazomethylide and formation of an alkyne unit gave **75**. Manipulation of the protecting groups, followed by a modified Cadiot–Chodkiewicz coupling with 1-iodo-1-propyne gave diyne **76**, and subsequent epoxide formation gave (−)-AL-2. Deoxygenation of the epoxy functionality with dimethyldiazomalonate in the presence of $[Rh_2(OAc)_4]{\cdot}2H_2O$ gave **72**. Adaptation of this general approach using a stereoisomer of **75** derived from diethyl D-tartrate led to synthesis of the analogues **69**–**71**.

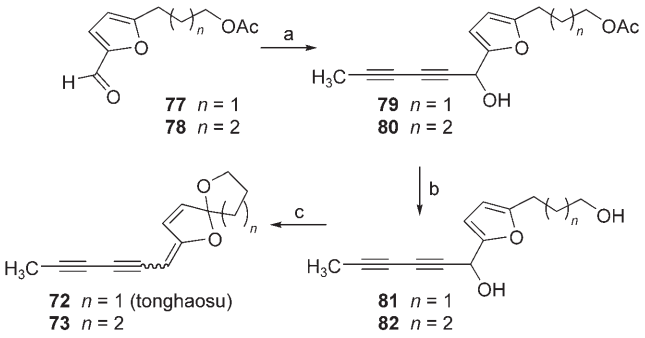
Wu and co-workers have developed a general approach to the formation of spiroketal enol ethers such as **72** and **73** (Scheme 19).[80] Furaldehyde derivative **77** or **78** was treated with 1-lithio-1,3-pentadiyne to give **79** or **80**, and removal of the acetate group produced diol **81** or **82**. Treatment of the diol **81** with $CuSO_4{\cdot}5H_2O$ in dry toluene gave tonghaosu as a 1.5:1 (*Z*/*E*) mixture, while the same conditions effected on **82** gave **73** as a 2:1 (*Z*/*E*) mixture.

The shrub Yin Chen Hao (*Artemisia capillaris*) is well-known in Chinese folk medicine.[15] One of the compounds,



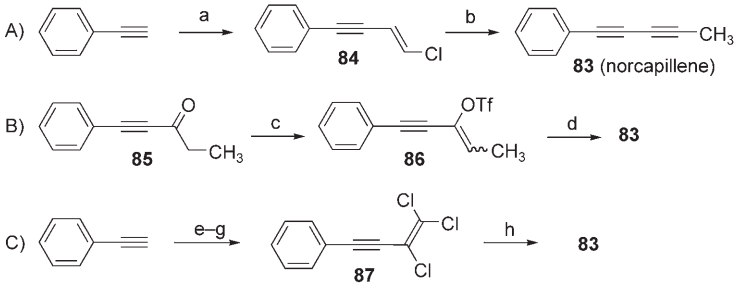
Scheme 18. Synthesis of (−)-AL-2 according to Mukai and co-workers.[82] a) DIBAH, CH_2Cl_2, −78 °C; b) LiDBB, THF, −78 °C, 72% (2 steps); c) MnO_2, CH_2Cl_2, RT; d) $TMSCHN_2$, BuLi, THF, −78 °C, 84% (2 steps); e) BzCl, pyridine, RT; f) TBAF, THF, RT, 95% (2 steps); g) MeC≡Cl, CuI, pyrrolidine, RT, 60%; h) MsCl, NEt_3, CH_2Cl_2, 0 °C; i) K_2CO_3, MeOH, RT, 79% (2 steps); j) $N_2C(CO_2Me)_2$, $[Rh_2(OAc)_4{\cdot}2H_2O]$, toluene, reflux, 86%.

 © 2006 Wiley-VCH Verlag GmbH & Co. KGaA, Weinheim



Scheme 19. Synthesis of tonghaosu and **73** according to Wu and coworkers.[80] a) MeC≡CC≡CLi, THF, −78 °C→RT, 75% (**79**) and 69% (**80**); b) $KHCO_3$, $MeOH/H_2O$, 92% (**81**) and 90% (**82**); c) $CuSO_4 \cdot 5H_2O$, toluene, 70 °C, 94% (**72**) and 92% (**73**).

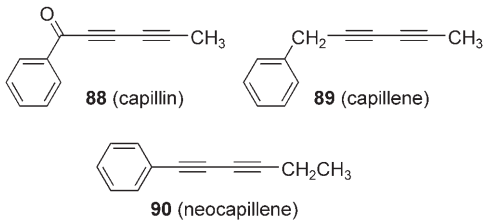
norcapillene (**83**),[84] isolated from this plant has been synthesized by a number of different routes (Scheme 20).



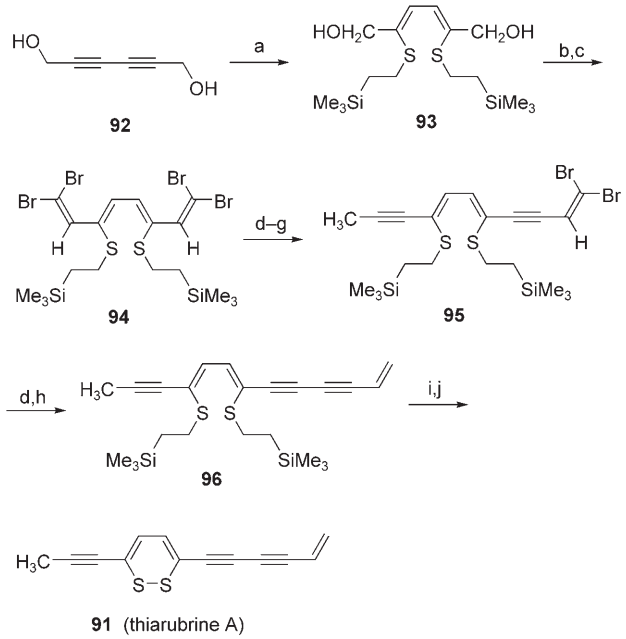
Scheme 20. Syntheses of norcapillene.[85–87] a) 1. BuLi, 2. $ZnCl_2$, 3. (*E*)-ICH=CHCl, $[Pd(PPh_3)_4]$, 91%; b) 1. $NaNH_2$, NH_3(l), 2. MeI, HMPA, THF, −78 °C, 89%; c) Tf_2O, 2,6-di-*tert*-butyl-4-methylpyridine, CH_2Cl_2, ca. 80%; d) potassium 2,6-di-*tert*-butylphenoxide, glyme, 50–55 °C, 85%; e) 1. EtMgBr, Et_2O, 0 °C, 2. CCl_3CHO, 3. H_2O; 77%; f) PCl_5, Et_2O, 0 °C; g) NEt_3, petroleum ether, 0 °C; h) 1. BuLi, Et_2O, −70 °C, 2. MeI, HMPA, 67%.

Negishi et al. used a Pd-catalyzed coupling to form enyne **84**, followed by elimination and trapping with MeI to give **83** (Scheme 20A).[85] Stang and Dixit reported that ynone **85** was readily converted into vinyl triflate **86**, and elimination then gave **83** in excellent yield (Scheme 20B).[86] Himbert et al. formed trichloroenyne **87** in three steps from phenylacetylene (Scheme 20C), and elimination with BuLi followed by trapping with MeI in the presence of HMPA gave **83**.[87]

Also isolated from *A. capillaris* were the diynone capillin (**88**)[88a,b] and the saturated, isomeric analogues capillene (**89**)[88c] and neocapillene (**90**).[88c] All three have been synthesized by standard methods.[89]



Wild chimpanzees have been observed picking the leaves of several species of *Aspilia* (wild sunflower) and swallowing them without chewing, which suggests that they consumed the leaves for a pharmacological effect rather than for nutrition.[90] Thiarubrine A (**91**) was subsequently found to be a major phytochemical in the leaves of one of these trees (*A. pluriseta*).[91] Shortly after the reported synthesis of thiarubrine B (Scheme 15), Koreeda and Yang described the synthesis of thiarubrine A (Scheme 21).[92] As previously

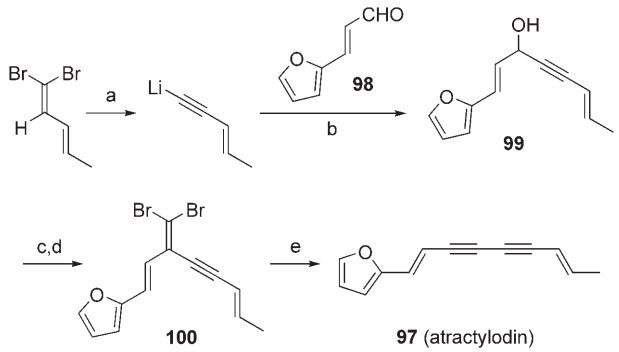


Scheme 21. Synthesis of thiarubrine A according to Koreeda and Yang.[92] a) $TMSCH_2CH_2SH$, KOH, DMF, RT, 87%; b) Dess–Martin periodinane, CH_2Cl_2, RT, 91%, or $(COCl)_2$/DMSO then NEt_3, CH_2Cl_2, −78 °C→RT, 81%; c) PPh_3, CBr_4, CH_2Cl_2, 0 °C, 89% (from **93**); d) BuLi, −78 °C→RT; e) MeI, −78 °C→RT; f) DMF, $BF_3 \cdot Et_2O$, −78 °C; g) PPh_3, CBr_4, CH_2Cl_2, 0 °C, 34% (from **94**); h) CH_2=CHBr, PhMe, $[Pd(PPh_3)_4]$, CuI, NEt_3, RT, 22% (from **95**); i) TBAF, 3-Å MS, THF, RT; j) I_2, RT, 53% (from **96**).

discussed in the synthesis of thiarubrine B, they too postponed assembly of the labile dithiin ring to the last step. Thus, diyne **92** was converted into the protected dithiol **93**, and a series of oxidation and dibromoolefination steps provided **94**. The acetylenic side groups were introduced by a one-pot sequence of elimination/alkylation and elimination/formylation/dibromo-olefination to give an impressive 34% yield of **95** (from **94**). Elimination to the terminal alkyne, followed by Sonogashira cross-coupling with bromoethene gave **96**, which was transformed into thiarubrine A through deprotection of the thiol group and oxidation with I_2.

The rhizomes of *Atractylodes lancea* have been used in Chinese traditional medicine,[15] and from this plant several acetylenes have been identified, such as atractylodin (**97**).[93] Atractylodin has recently been synthesized by us through a four-step sequence (Scheme 22).[94] The initial transformation was a one-pot reaction consisting of elimination to an acetylide, followed by addition to aldehyde **98** to give alcohol **99**. Oxidation and dibromo-olefination then gave **100**, and a

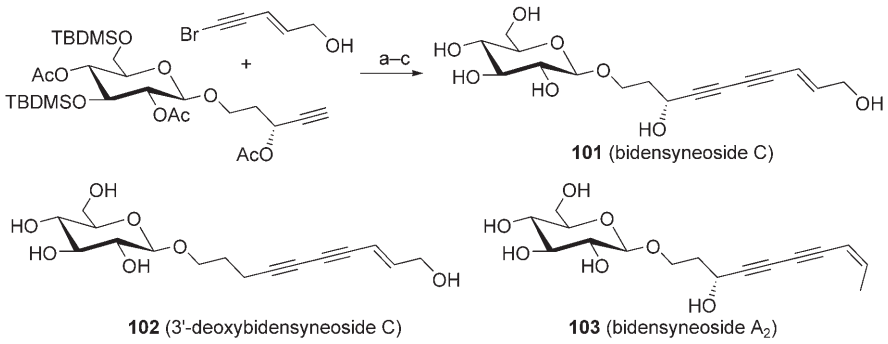
 © 2006 Wiley-VCH Verlag GmbH & Co. KGaA, Weinheim



Scheme 22. Synthesis of atractylodin according to Shi Shun and Tykwinski.[94] a) BuLi, THF, −78 °C→RT; b) THF, −78 °C→RT, 54%; c) MnO_2, CH_2Cl_2, RT, 59%; d) PPh_3, CBr_4, CH_2Cl_2, RT, 58%; e) BuLi, hexanes, −78→−40 °C, 72%.

Fritsch–Buttenberg–Wiechell rearrangement ultimately provided diyne **97**.

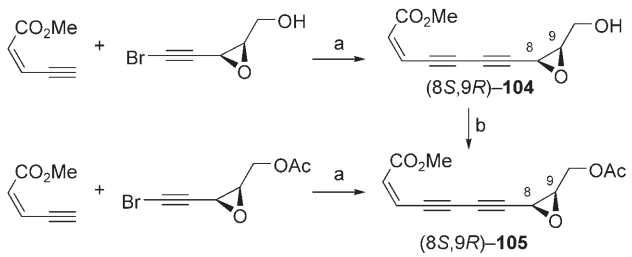
Species of the genus *Bidens* (beggarticks) have also long been used as traditional Chinese medicinal plants. Five polyacetylenic glucosides were isolated from *B. parviflora* and shown to inhibit both histamine release and production of nitric oxide.[95] The stereoselective synthesis of the three glucosides **101**–**103** has been reported by Gung and Fox (Scheme 23).[96] Although the pattern of protecting groups employed for the coupling partners varied among the three individual syntheses, the overall approach remained consistent. In each case, the diyne segment of each bidensyneoside was formed through a Cadiot–Chodkiewicz coupling and



Scheme 23. Bidensyneoside syntheses according to Gung and Fox.[96] a) CuCl, Et_2NH, $NH_2OH{\cdot}HCl$, MeOH, H_2O, 0 °C, 56%; b) HF·pyridine, THF, 0 °C, 58%; c) MeOH, K_2CO_3, RT, 50%.

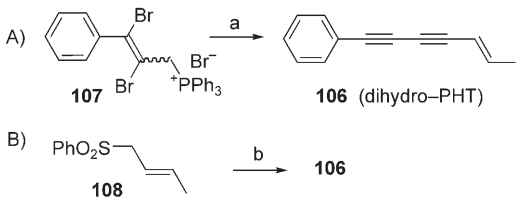
global deprotection then afforded the desired target (as shown in Scheme 23 for **101**).

Epoxypolyynes such as **104** and **105** have been isolated from *Chrysothamnus nauseosus* and *C. parryi* (rabbitbrush) and both show antifeedant activity (Scheme 24).[97] Pale and co-workers have reported asymmetric syntheses for both targets.[98] Their convergent approach to **104** and acetate **105** relied on a Cadiot–Chodkiewicz coupling in both cases, using mild conditions designed to minimize side reactions such as rearrangement and oxirane opening. Alcohol **104** can also be acylated to give **105** quantitatively.



Scheme 24. Synthesis of polyyne epoxides according to Pale and co-workers.[98] a) CuCl, $NH_2OH{\cdot}HCl$, $EtNH_2$, MeOH, 0 °C, 93% (**104**) and 91% (**105**); b) Ac_2O, DMAP, Et_2O, quant.

The enediyne dihydrophenylheptatriyne (**106**, dihydro-PHT) has been isolated from tickseed plants (*Coreopsis capillacea*).[99] Recent interest in methods of conjugated diyne synthesis has resulted in several syntheses being reported (Scheme 25). For example, Ziegler et al. used the phospha-

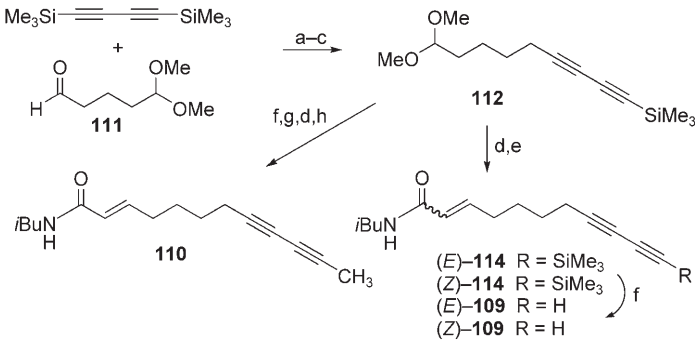


Scheme 25. Synthetic routes to dihydro-PHT.[100,101] a) $Bn(Me)_3N^+{}^-OMe$, MeCH=CHCHO, MeOH, −60 to 0 °C, 72%; b) 1. BuLi, THF, −78 °C, then TMSCl −78 °C→RT, 2. BuLi, −78 °C, then PhC≡CCHO, −78→0 °C, 3. TMS_2NLi, RT, 66%.

cumulene ylide derived from **107** to form **106** on reaction with acrolein (Scheme 25 A),[100] while Otera and co-workers[101] developed a one-pot double elimination protocol with sulfone **108** that gave **106** in good yield (Scheme 25 B).[102]

A mixture that contains at least 12 different acetylenic amides, including diacetylenic amides (*E*/*Z*)-**109** and **110**, can be extracted from the roots of the purple coneflower (*Echinacea angustifolia*).[103] Studies have shown that **109** is active against mosquito larvae (*Aedes aegypti*) and cornworm neonates (*Helicoverpa zea*).[104] Kraus and co-workers have synthesized (*E*)- and (*Z*)-**109** as well as **110** (Scheme 26).[105] The central diyne core of both targets was derived from bis(trimethylsilyl)butadiyne, which was subjected to silicon–lithium exchange and subsequently added to aldehyde **111**. Deoxygenation to the common intermediate **112**, followed by liberation of the aldehyde with *p*-TsOH and reaction with Ph_3P=CHCONH*i*Bu (**113**) gave a separable mixture of (*E*)- and (*Z*)-**114**. Desilylation with TBAF gave the products (*E*)- and (*Z*)-**109**, respectively. Alternatively, desilylation of **112** to give the terminal alkyne,

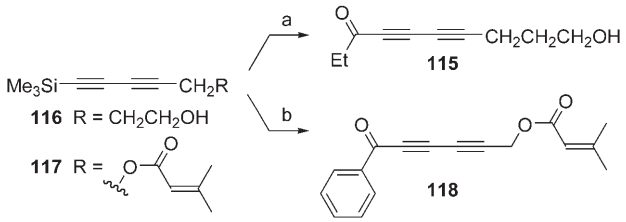
 © 2006 Wiley-VCH Verlag GmbH & Co. KGaA, Weinheim



Scheme 26. Synthesis of amides **109** and **110** according to Kraus and co-workers.[105] a) 1. MeLi·LiBr, THF, 0 °C, 2. then **111**, 88%; b) 1,1′-thiocarbonyldiimidazole, CH_2Cl_2, RT, 86%; c) $HSnBu_3$, AIBN, toluene, 80 °C, 69%; d) *p*-TsOH, acetone/H_2O, RT; e) $Ph_3P{=}CHCONHiBu$ (**113**), 73% ((*E*)-**114**) and 10% ((*Z*)-**114**); f) TBAF, THF, 0 °C, 95% ((*E*)-**109**) and 97% ((*Z*)-**109**); g) BuLi, MeI, THF, −78 °C; h) $Ph_3P{=}CHCONHiBu$ (**113**), 45% (from **112**).

deprotonation with BuLi, methylation, deprotection of the aldehyde, and a Wittig reaction with **113** gave **110**.

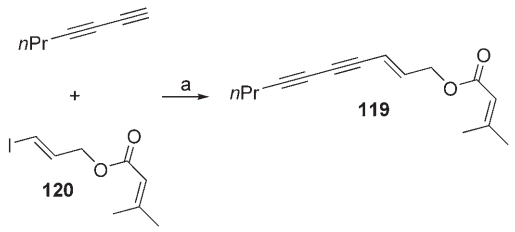
Diynone **115** was isolated from the Koonamore Daisy (*Erodiophyllum elderi)*, an endangered Australian species.[106] An efficient synthesis of **115** was achieved by Jones and Holmes using a $TiCl_4$-mediated acylation of trimethylsilyldiyne **116** with propanoyl chloride (Scheme 27).[89a] A similar



Scheme 27. Synthesis of **115** and **118** according to Jones and Holmes[89a] a) **116**, propanoyl chloride, $TiCl_4$, CH_2Cl_2, −78 °C, 56%; b) **117**, benzoyl chloride, $TiCl_4$, CH_2Cl_2, −78 °C, 47%.

strategy using diyne **117** gave ester **118**,[89a] which has been isolated from *Lonas annua*,[107] a shrub originating from the southwestern Mediterranean region.

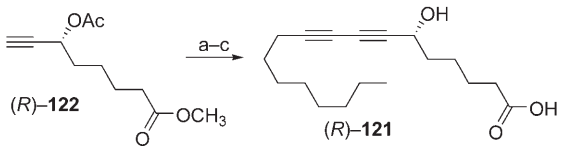
The enediyne lactone **119** was isolated from the Great Valley gumweed plant (*Grindelia camporum*) by Bohlmann et al.[108] Carpita et al. have assembled the enediyne structure through a Sonogashira reaction of 1,3-heptadiyne and vinyl iodide **120** (Scheme 28).[77]



Scheme 28. Synthesis of ester **119** according to Carpita et al.[77] a) $[Pd(PPh_3)_4]$, CuI, NEt_3, toluene, 77%.

2.5. Family Fabaceae (Pea Family)

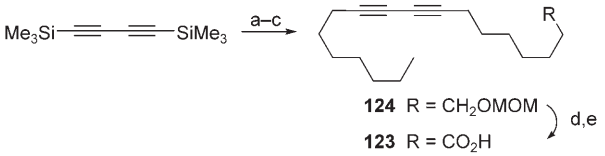
Several acetylenic fatty acids, such as **121**, have been isolated from the root bark of the legume *Paramacrolobium caeruleum* and shown to inhibit the activity of a HMG-CoA reductase.[109] The enantiospecific synthesis of diyne alcohol **121** has been reported by Mhaskar and Lakshminarayana,[110] who used a Sharpless epoxidation to introduce the stereogenic center in (*R*)-**122** (Scheme 29). A Pd-catalyzed coupling with 1-bromodec-1-yne and hydrolysis gave **121**.[111]



Scheme 29. Synthesis of acetylenic fatty acid **121** according to Mhaskar and Lakshminarayana.[110] a) 1-Bromodec-1-yne, Et_2NH, $[PdCl_2(PPh_3)_2]$, CuCl, PhH, RT, 33%; b) K_2CO_3, MeOH, RT, 54% (from **122**); c) KOH, EtOH, H_2O, RT, 95%.

2.6. Family Loranthaceae (Showy Mistletoe Family)

Stems and leaves of the oriental shrub *Scurrula atropurpurea* have been used for the treatment of cancer in Java and Indonesia. The fatty acid diyne **123** has been identified as one of several polyyne constituents of this plant.[112] Bittman and co-workers have synthesized **123** by using bis(trimethylsilyl)-butadiyne as the source of the diyne core (Scheme 30). A



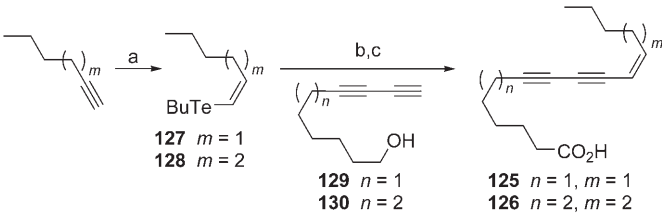
Scheme 30. Synthesis of acetylenic fatty acid **123** according to Bittman and co-workers.[113] a) MeLi·LiBr, THF, −78 °C, then $Br(CH_2)_7OMOM$, HMPA, −78 °C, 88%; b) KF·H_2O, DMF, RT, 91%; c) BuLi, THF, −23 °C, then $I(CH_2)_6CH_3$, −23 °C→RT, 78%; d) HCl, MeOH, RT, 92%; e) PDC, DMF, RT, 75%.

sequence of silicon–lithium exchange and derivatization was repeated twice to provide the unsymmetrical framework of **124**.[113] Final deprotection of the alcohol and oxidation with PDC gave **123**.

2.7. Family Olacaceae (Olax Family)

Diynes **125** and **126** have been isolated from the bark of *Heisteria acuminata*,[114] which has been used in Ecuadorian folk medicine.[115] These fatty acids are strong inhibitors of cyclooxygenase (COX) and also show potent inhibition of 5-lipoxygenase (5-LO).[115] Diynes **125** and **126** have been synthesized by Zeni et al. by using a rather interesting twist to the Pd-catalyzed cross-coupling methodology (Scheme 31).[116] (*Z*)-Vinyltellurides **127** and **128** were

 © 2006 Wiley-VCH Verlag GmbH & Co. KGaA, Weinheim



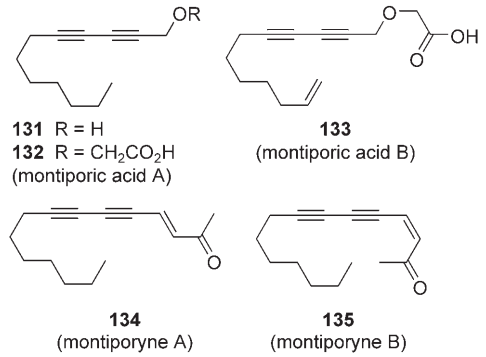
Scheme 31. Fatty acid syntheses according to Zeni et al.[116] a) [BuTeLi], EtOH, reflux, 48% in both cases; b) $PdCl_2$, CuI, MeOH, NEt_3; b) CrO_3/H_2SO_4, −10°C, 24% overall (**125**) and 22% overall (**126**).

formed as separable mixtures of regioisomers by hydrotelluration of the appropriate alkyne. Pd-catalyzed coupling of **127** and **128** with terminal diynes **129** and **130**, respectively, followed by chromate oxidation of the alcohol to the acid completed the syntheses of **125** and **126**.

3. Diynes from Marine Organisms

3.1. Family Acroporidae

A range of interesting bioactive compounds, including numerous acetylenes, has been isolated from stony corals.[117] The genus *Montipora* (velvet coral) has been a rich source of acetylenic natural products that possess antifungal, antibacterial, and cytotoxic properties.[118] Examples include diyne **131**, synthesized by several research groups,[119,120] as well as

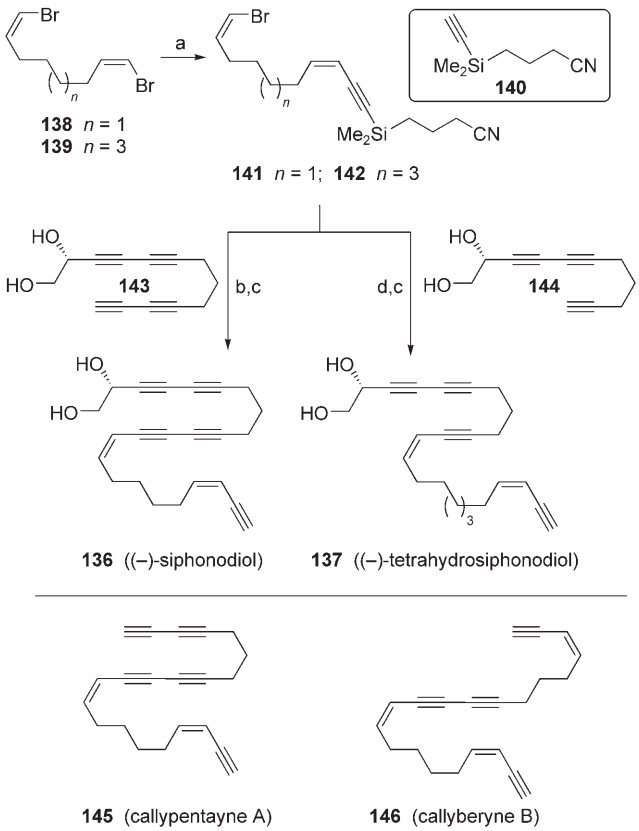


montiporic acids A (**132**) and B (**133**), synthesized by Stefani et al.[121] All three syntheses used a Cadiot–Chodkiewicz coupling to form the diyne framework.[122]

Montiporynes A (**134**) and B (**135**) have also been isolated from *Montipora* and exhibit in vitro cytotoxic activity against numerous human solid tumor cell lines.[123] Speed and Thamattoor synthesized diacetylenic ketones **134** and **135**, in three steps from commercially available starting materials.[124] They also determined that ketone **134** isomerizes to **135** within hours upon standing at room temperature, leading to an approximate ratio of 3:1 in favor of **134**.

3.2. Family Callyspongiidae

The C_{23} hydrocarbons (−)-siphonodiol (**136**) and (−)-tetrahydrosiphonodiol (**137**) were isolated from sponges of the family Callyspongiidae and show potent metamorphosis-inducing activity in sea squirt larvae (*Halocynthia roretzi*) and antifouling activity against barnacles (*Balanus amphitrite*).[126] The only synthesis of **136** and **137** was reported in 2005 by López et al.[125a] Vinyl bromides **138** and **139** can be assembled in three steps from commercially available *trans*-cyclohexane-1,2-diol, and Sonogashira cross-coupling with **140** gave **141** and **142**, respectively (Scheme 32). A second Pd-catalyzed



Scheme 32. Synthesis of (−)-siphonodiol and (−)-tetrahydrosiphonodiol according to López et al.[125] a) **140**, [$PdCl_2(PPh_3)_2$], CuI, piperidine, 75% (**141**) and 70% (**142**); b) [$PdCl_2(PPh_3)_2$], CuI, pyrrolidine, 68%; c) TBAF, THF, RT, 74% (**136**) and 70% (**137**); d) [$PdCl_2(PPh_3)_2$], CuI, piperidine, 71%.

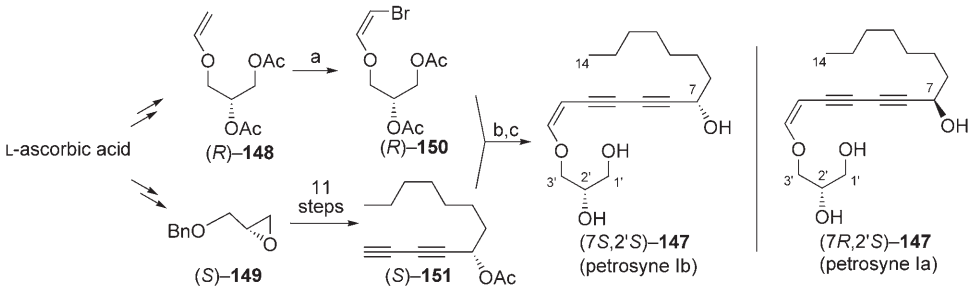
cross-coupling with either terminal diyne **143** or **144**, respectively, completed the carbon frameworks, and desilylation with TBAF gave the targets **136** and **137**. The C_{21} hydrocarbons callypentayne (**145**, also called callyberyne A) and callyberyne B (**146**) have also been isolated from sponges of Callyspongiidae,[126] and both have been synthesized by the same research group by using an analogous approach.[125b]

3.3. Family Petrosiidae

A collection of long-chain acetylenic natural products has been found in Okinawan sponges of the genus *Petrosia*, and many have biological activity.[127] Enol ether glycerides **147** are representative of these compounds, and while the

 © 2006 Wiley-VCH Verlag GmbH & Co. KGaA, Weinheim

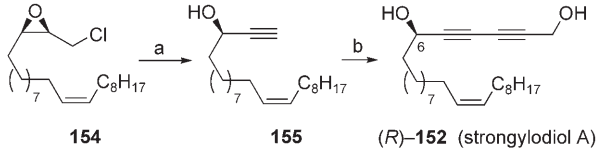
chemical structure of these and related diynes could be established from the isolated natural products, the absolute stereochemistry was unknown as a result of insufficient quantities of material. Iguchi et al. assigned the stereochemistry through the synthesis of all four possible stereoisomers of **147** (Scheme 33) by using D-mannitol or L-ascorbic acid as



Scheme 33. Synthesis of petrosyne Ib according to Iguchi et al.[127] a) Br_2, CH_2Cl_2, −78 °C then NEt_3, −78 °C→RT, 45 %; b) **150** + **151**, [$Pd(PPh_3)_4$], CuI, $BuNH_2$, DMF, RT, 11 %; c) Li_2CO_3, MeOH, RT, 93 %.

chiral building blocks for (7*R*)- and (7*S*)-**147**, respectively. As shown for the synthesis of (7*S*)-**147**, L-ascorbic acid provided both optically pure advanced intermediates (*R*)-**148** and (*S*)-**149**, and an additional 11 steps ultimately provided diyne (*S*)-**151** from (*S*)-**149**. Bromination of (*R*)-**148** gave (*R*)-**150**, and a Pd-catalyzed cross-coupling with (*S*)-**151** followed by alcohol deprotection gave petrosyne Ib. It was concluded on the basis of their syntheses that the isolated natural material was actually composed of a mixture of petrosyne Ia and Ib.

Strongylodiols A (**152**) and B (**153**) are long-chain acetylenic alcohols isolated from an Okinawan marine sponge of the genus *Strongylophora* and show potent cytotoxic activity against human T-lymphocyte leukemia (MOLT-4) cells.[128] Iguchi and co-workers determined the configuration at C6 and found that these acetylenic alcohols occur naturally as enantiomeric mixtures with ratios of 91:9 for **152** and 97:3 for **153**.[128] Yadav and Mishra reported the first enantioselective synthesis of (*R*)-strongylodiol A (Scheme 34).[129] Two sequential β-eliminations effected on epoxychloride **154** gave alcohol **155**, and a Cadiot–Chodkiewicz coupling finished the diyne structure of **152**.



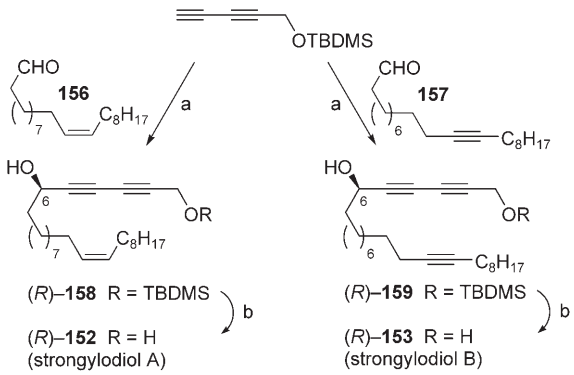
Scheme 34. Synthesis of strongylodiol A according to Yadav and Mishra.[129] a) $LiNH_2$, NH_3, 95 %; b) CuCl, $EtNH_2$, $NH_2OH{\cdot}HCl$, MeOH, H_2O, $BrC{\equiv}CCH_2OH$, 85 %.

Carreira and co-workers have reported the synthesis of (*R*)-strongylodiols A and B (Scheme 35),[130] based on the enantioselective addition of the TBDMS-protected pentadiynol to long-chain aliphatic aldehyde **156** or **157** in the presence of $Zn(OTf)_2$, NEt_3, and *N*-methylephedrine. This method gave alcohols **158** and **159** in good yield and reasonable enantiomeric excess. Removal of the protecting groups with TBAF provided the diols (*R*)-**152** and (*R*)-**153**.

The most recent synthesis of strongylodiols A and B has been reported by Baldwin and co-workers,[131] by using Noyori asymmetric reduction of an ynone[132] to set the stereochemistry at C6 and Cadiot–Chodkiewicz coupling to form the diyne moiety.

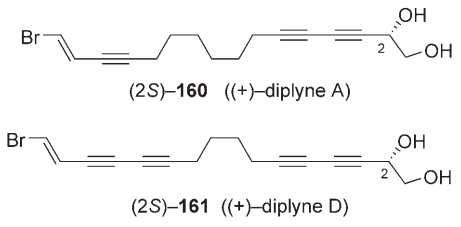
3.4. Family Spirastrellidae

As part of their effort to identify bioactive marine natural products, Lerch et al. screened the crude extract of the Philippines sponge *Diplastrella* and found that several fractions showed inhibitory activity against



Scheme 35. Synthesis of strongylodiol A and B according to Carreira and co-workers.[130] a) $Zn(OTf)_2$, NEt_3, (+)-*N*-methylephedrine, 23 °C, toluene, 62 % (**158**, 82 % *ee*) and 68 % (**159**, 80 % *ee*); b) TBAF, THF, 23 °C, 85 % (**152**) and 90 % (**153**).

HIV-1 integrase.[133] From these fractions, they isolated a number of brominated polyacetylenic diols, including diplynes A (**160**) and D (**161**). Gung et al. have demonstrated



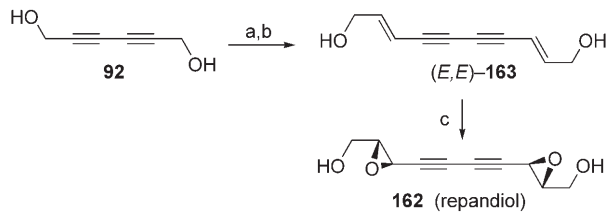
the synthesis of both (2*S*)-diplyne A and D, with the stereocenter at C2 derived from D-mannitol and a Cadiot–Chodkiewicz coupling used to construct the diyne segment of each molecule.[134] Their study concluded that the natural sample in both cases had the *R* configuration at C2.

 © 2006 Wiley-VCH Verlag GmbH & Co. KGaA, Weinheim

4. Diynes from Fungi

4.1. Family Hydnaceae

The symmetrical diyne diepoxide repandiol (**162**) was isolated from the tasty hedgehog mushroom (*Hydnum repandum*) and displays cytotoxic activity against several types of tumor cells.[135] The proposed structure was confirmed by comparison to a synthetic sample that was stereoselectively prepared by Nozoe and co-workers from diyne **92** (Scheme 36).[135] Swern oxidation, a Wittig reaction,

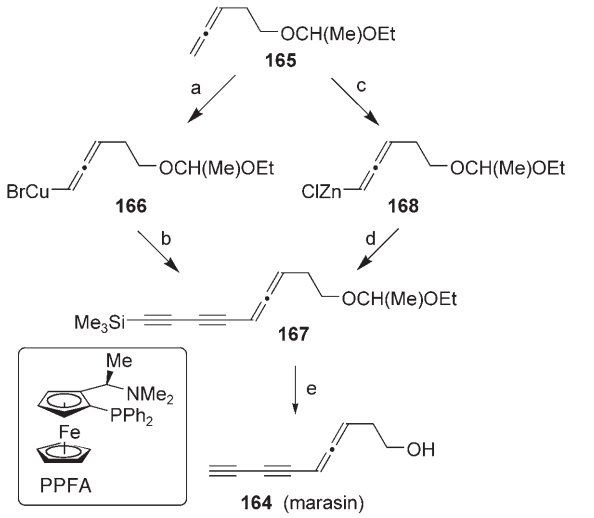


Scheme 36. Synthesis of repandiol according to Nozoe and co-workers.[135] a) 1. $(COCl)_2$, DMSO, CH_2Cl_2, 2. NEt_3, 3. Ph_3PCHCO_2Et, −78 °C→−20 °C, 54%; b) DIBAH, C_6H_6, −78 °C, 79%; c) $Ti(OiPr)_4$, D-(−)-DET, CH_2Cl_2, *t*BuOOH, −20 °C, 37%.

and reduction gave the diene–diyne core of (*E*,*E*)-**163**. Asymmetric epoxidation with either D-(−)- or L-(+)-DET gave the targeted product **162** or its enantiomer, respectively. The diol (*E*,*E*)-**163** is also a natural product isolated from the aerial parts of the ornamental knapweed (*Centaurea ruthenica*).[136]

4.2. Family Marasmiaceae

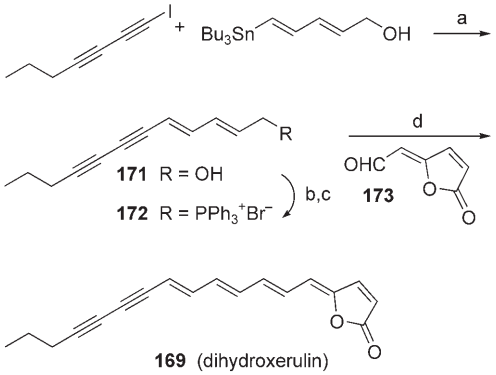
The allenediyne (−)-marasin ((−)-**164**) was the first naturally occurring allene to be isolated, and was extracted from the culture fluid of *Marasmius ramealis* in 1959 by Bendz as the active antibiotic component against *Staphylococcus aureus*.[137] The other enantiomer, (+)-marasin, was later isolated from a different fungal source (*Aleurodiscus roseus*) and appeared to have similar antibiotic activity.[138] The highly unsaturated and reactive framework of **164** made it a challenging synthetic target. Boersma and co-workers reported the synthesis of both racemic and (−)-marasin, although the stereoselective route gave a very low enantioselectivity (0.5% *ee*) and the absolute configuration was not determined.[139] Two different metal-mediated routes were explored (Scheme 37): both routes involved initial lithiation of allene **165** at low temperature and afforded a mixture of regioisomers that was carried on to the subsequent step. Treatment of lithiated **165** with $LiCuBr_2$ gave cuprate **166** and subsequent treatment with IC≡CC≡CTMS gave the protected diyne **167**. Alternatively, lithiation and treatment with $ZnCl_2$ gave **168**, which was then cross-coupled with BrC≡CC≡CTMS under Pd catalysis to give **167**. Protiodesilylation of **167** with $AgNO_3$ in MeOH also effected removal of the acetal protecting group, and provided marasin as a very unstable oil in 20% overall yield from cuprate **166**, or 13% overall



Scheme 37. Synthesis of marasin according to Boersma and co-workers.[139] a) BuLi, THF, −60 °C, then $LiCuBr_2$; b) $Me_3SiC{\equiv}CC{\equiv}CI$, −50→0 °C, 95% from **166**; c) BuLi, THF, −60 °C, then $ZnCl_2$; d) $Me_3SiC{\equiv}CC{\equiv}CBr$, Pd(0), −55 °C→RT, 75% from **168**; e) $AgNO_3$, MeOH, H_2O, 0 °C, then NaCN, then CSA.

yield from zincate **168**. Pd-catalyzed coupling of intermediate **168** with BrC≡CC≡CTMS in the presence of the enantiomerically pure ligand PPFA, followed by deprotection as before, gave (−)-marasin (0.5% *ee*).

Several unique γ-alkylidenebutenolides, including dihydroxerulin (**169**) and xerulin (**170**), have been isolated from the mushroom *Xerula melanotricha*, and both inhibited the biosynthesis of cholesterol in HeLa S3 cells without cytotoxicity.[140] Dihydroxerulin and xerulin have both been synthesized by Siegel and Brückner.[141] A key step for the formation of **169** involved a Stille coupling to assemble the conjugated diyne–diene segment **171**, which was subsequently converted into phosphonium salt **172** (Scheme 38). A Wittig reaction of **172** with aldehyde **173** gave a mixture of stereoisomers, from which the desired isomer **169** was isolated in 30% yield. A more recent synthesis of dihydroxerulin by this same research group has also been reported, in which a Stille coupling

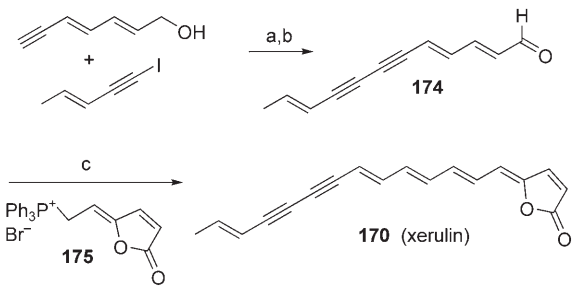


Scheme 38. Synthesis of dihydroxerulin according to Siegel and Brückner.[141a] a) LiCl, $[PdCl_2(PPh_3)_2]$, THF, RT, 81%; b) NaBr, $BF_3{\cdot}OEt_2$, MeCN, RT, 61%; c) PPh_3, MeCN, RT, 99%; d) BuLi, THF, then **173**, −83 °C→RT, 30% (other stereoisomers 25%).

© 2006 Wiley-VCH Verlag GmbH & Co. KGaA, Weinheim

analogous to that shown in their synthesis of xerulinic acid (see Scheme 41) was used.[142b]

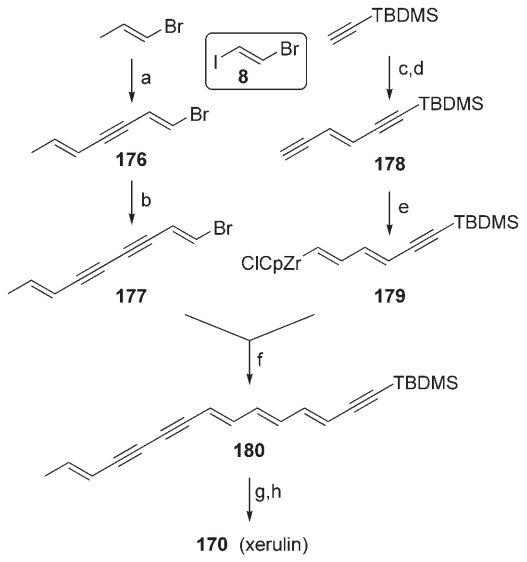
A similar strategy based on a Wittig reaction was used to synthesize xerulin (Scheme 39).[141b] In this case, the roles of



Scheme 39. Synthesis of xerulin according to Siegel and Brückner.[141b] a) $[Pd(dba)_2]$, CuI, iPr_2NH, THF, RT, 55%; b) Dess–Martin periodinane, CH_2Cl_2, RT, 81%; c) K_2CO_3, CH_2Cl_2, 50°C, 28% (other stereoisomers 27%).

the coupling partners were reversed, such that aldehyde **174**, available through a Cadiot–Chodkiewicz coupling and Dess–Martin oxidation, was treated with the ylide from **175** to give a mixture of isomers, including 28% of the intended product **170**.

Negishi et al. have assembled xerulin using (*E*)-ICH=CHBr (**8**) as a C_2 synthon and Pd-catalyzed cross-coupling reactions to form all seven C–C single bonds (Scheme 40).[143] 1-Bromo-1-propene was elaborated to bromoolefin **176** through two successive Pd-catalyzed couplings, first with BrZnC≡CH, then with **8**. LDA-induced elimination and a second coupling with **8** gave the left portion (**177**) of xerulin.

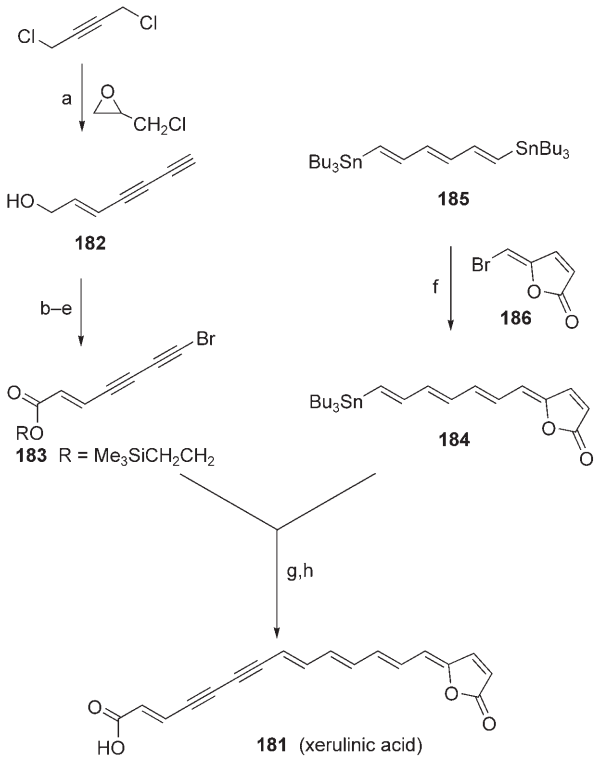


Scheme 40. Synthesis of xerulin according to Negishi et al.[143] a) 1. [BrZnC≡CH], $[Pd(PPh_3)_4]$, THF, 2. BuLi, 3. **8**, $[Pd(PPh_3)_4]$, 72%; b) 1. LDA, THF, 2. $ZnBr_2$, 3. **8**, $[Pd(PPh_3)_4]$, 65%; c) 1. BuLi, THF, 2. $ZnBr_2$, 3. **8**, $[Pd(PPh_3)_4]$, 70%; d) [BrZnC≡CH], $[Pd(PPh_3)_4]$, THF, 77%; e) $[ClCp_2ZrH]$; f) $ZnCl_2$, $[PdCl_2(PPh_3)_2]$, DIBAH, 95%; g) TBAF, 96%; h) (*Z*)-ICH=$CHCO_2H$, $[Pd(PPh_3)_4]$, CuI, NEt_3, BHT, 70%.

The other half of the conjugated core was derived from TBDMSC≡CH in a sequence of a Pd-catalyzed coupling with **8** and alkynylation with BrZnC≡CH to give **178**. Hydrozirconation gave intermediate **179**, which was directly cross-coupled with **177** to give **180**. Desilylation, cross-coupling with 3-iodopropenoic acid, and in situ lactonization gave xerulin in 30% overall yield and >96% stereoselectivity.

Dihydroxerulin was also synthesized in 2000 by Rossi et al. (not shown).[144] This approach also relied on a Stille coupling to introduce the diyne segment. A Wittig reaction completed the conjugated skeleton and provided the desired product in >90% stereoselectivity about the newly formed double bond. Both dihydroxerulin and xerulin were synthesized stereoselectively very recently by Fiandanese et al.[145] Their route relied on Sonogashira cross-coupling reactions to assemble the conjugated framework and afforded dihydroxerulin and xerulin in 97% and 98% *de*, respectively.

Xerulinic acid (**181**) was also isolated from *X. melanotricha*,[140] and recently synthesized by Sorg and Brückner.[142] Lithiobutadiyne was formed in situ from 1,4-dichloro-2-butyne and treated with epichlorohydrin to give **182** (Scheme 41). Bromination of diyne **182** at the terminal C atom, Dess–Martin oxidation to the aldehyde, Lindgren's oxidation to the acid, and esterification with 2-trimethylsilylethanol gave ester **183**. The tetraene section **184** was



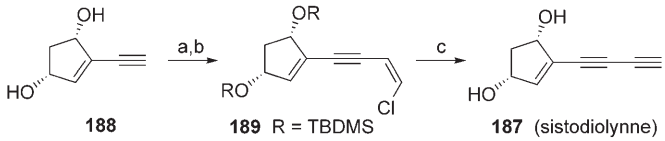
Scheme 41. Synthesis of xerulinic acid according to Sorg and Brückner.[142] a) $LiNH_2$, NH_3(l), −35°C then addition of epichlorohydrin, 17%; b) NBS, $AgNO_3$, acetone, RT, 79%; c) Dess–Martin periodinane, CH_2Cl_2, 0°C→RT, 79%; d) $NaClO_2$, KH_2PO_4, 2-methyl-2-butene, acetone/H_2O, 0°C, 89%; e) $HOCH_2CH_2SiMe_3$, DCC, DMAP, ethyl acetate, 0°C→RT, 83%; f) BuLi (1.3 equiv), THF, −78°C→RT, then $ZnCl_2$, then **186**, $[Pd(PPh_3)_4]$, 0°C, 63%; g) **184**, $[Pd(dba)_2]$, $AsPh_3$, THF, RT, 73%; h) TBAF, THF, 0°C→RT, 61%.

 © 2006 Wiley-VCH Verlag GmbH & Co. KGaA, Weinheim

assembled by the Stille coupling of **185** and **186**. A subsequent Stille coupling of **183** and **184**, followed by desilylation with TBAF gave **181**, which was spectroscopically identical to the natural product.

4.3. Family Sistotremataceae

Sistodiolynne (**187**), a polyketide metabolite of the wood rot decay fungus *Sistotrema raduloides*, was first isolated by Ayer and co-workers.[146] Sugahara and Ogasawara[147] constructed the 1,3-butadiyne unit of sistodiolynne by using a mild protocol developed by Kende and Smith.[148] Coupling of terminal alkyne **188** with (*Z*)-dichloroethene followed by formation of a silyl ether gave **189**. Treating **189** with TBAF induced concurrent desilylation and dehydrochlorination to give the highly unstable product **187** (Scheme 42).



Scheme 42. Synthesis of sistodiolynne according to Sugahara and Ogasawara.[147] a) (*Z*)-ClHC=CHCl, $[Pd(PPh_3)_4]$, CuI, $BuNH_2$, C_6H_6; b) TBDMSCl, imidazole, DMF, 71% (from **188**); c) TBAF, THF, RT.

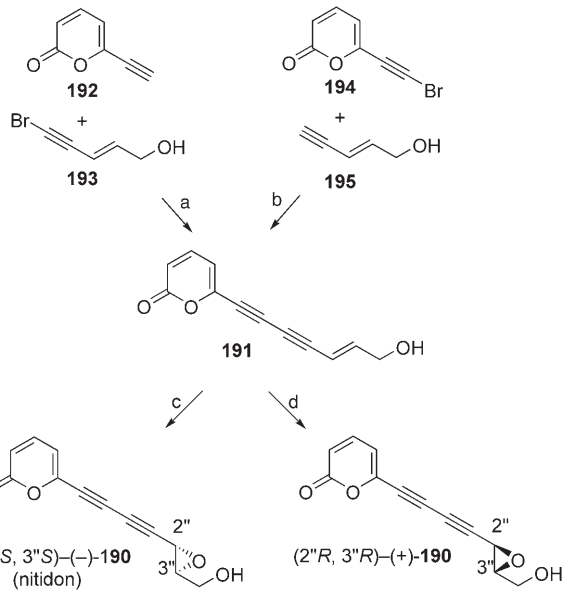
4.4. Family Steccherinaceae

The pyranone derivative (−)-nitidon (**190**) was isolated in 1998 by Gehrt et al. from the basidiomycete *Junghuhnia nitida* and found to induce morphological and physiological differentiation against HL-60 and U-937 tumor cell lines (Scheme 43).[149] Rossi and co-workers have synthesized both (+)- and (−)-nitidon stereoselectively.[150] The enediyne core of **191** was assembled by a Cadiot–Chodkiewicz coupling, and the yield was comparable when either a combination of **192**/**193** or **194**/**195** was used. Sharpless asymmetric epoxidation then gave (−)-**190** or (+)-**190**. The naturally occurring compound (−)-**190** was assigned the 2″*S*,3″*S* configuration on the basis of their syntheses.

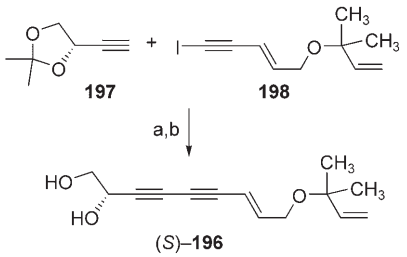
4.5. Family Tricholomataceae

The isoprenyl ether **196** has been isolated from cultures of the fungus *Fayodia bisphaerigera* and synthesized by Thaller and co-workers (Scheme 44).[151] Cadiot–Chodkiewicz coupling of the (*S*)-ethynyl acetonide **197**, which was readily available from D-glyceraldehyde acetonide, with **198** completed the enediyne moiety, and deprotection with *p*-TsOH gave the diol (*S*)-**196**.[152]

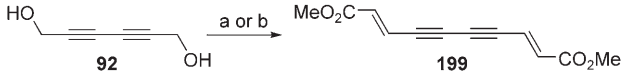
The *E*,*E* ester **199** (and the *E*,*Z* analogue) has been isolated from the edible snowy waxcap mushroom (*Hygrophorus virgineus*).[153] Two recent syntheses of this ester have appeared (Scheme 45), both relying on an in situ oxidation/Wittig reaction of **92** using either Dess–Martin periodinane[154] or MnO_2[155] as the oxidant. The stereochemical outcome of the two approaches was comparable.



Scheme 43. Synthesis of nitidon according to Rossi and co-workers.[150] a) CuCl, TMP, $NH_2OH{\cdot}HCl$, DMF, 0°C→RT, 50%; b) CuCl, $NH_2OH{\cdot}HCl$, TMP, DMF, 0°C, 41%; c) L-(+)-DET, $Ti(OiPr)_4$, CH_2Cl_2, 4-Å MS, *t*BuOOH, −20°C, then 10% aq tartaric acid, RT, 71% (>99% *ee*); d) D-(−)-DET, $Ti(OiPr)_4$, CH_2Cl_2, 4-Å MS, *t*BuOOH, −20°C, then 10% aq tartaric acid, RT, 76% (98% *ee*).



Scheme 44. Synthesis of **196** according to Thaller and co-workers.[151] a) CuCl, $EtNH_2$, $NH_2OH{\cdot}HCl$, MeOH, 60%; b) *p*-TsOH, EtOH, 40%.



Scheme 45. Syntheses of diester **199**.[154,155] a) $PhCO_2H$; $Ph_3P{=}CHCO_2Me$, Dess–Martin periodinane, DMSO, CH_2Cl_2, then $NaHCO_3$, H_2O, Et_2O, 94% ((*E*,*E*):(*Z*,*E*) 2.2:1); b) $Ph_3P{=}CHCO_2Me$, MnO_2, CH_2Cl_2, 55% ((*E*,*E*):(*Z*,*E*) 2:1).

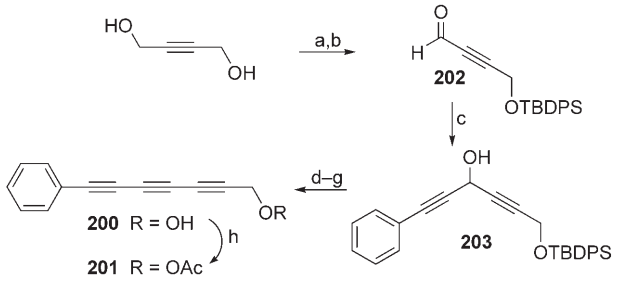
5. Triynes from Plants

5.1. Family Asteraceae (Aster Family)

The triynol **200** and acetate **201** were isolated from several species of *Bidens* (beggarticks), including *B. pilosus* and *B. leucanthus*.[156] Our research group has reported the syn-

 © 2006 Wiley-VCH Verlag GmbH & Co. KGaA, Weinheim

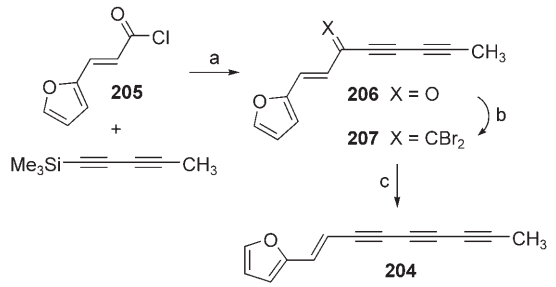
thesis of **200** and **201** starting from 1,4-butynediol (Scheme 46).[157] Monoprotection with TBDPS chloride followed by oxidation gave aldehyde **202**, which was then treated with lithiated phenylacetylene to provide **203**. A sequence of



Scheme 46. Synthesis of **200**–**201** according to Luu, Tykwinski, and coworkers.[157] a) TBDPSCl, DMAP, THF, RT, 84%; b) $BaMnO_4$, CH_2Cl_2, RT, 58%; c) PhC≡CLi, THF, −78°C, 85%; d) $BaMnO_4$, CH_2Cl_2, RT, 89%; e) PPh_3, CBr_4, NEt_3, CH_2Cl_2, 0°C, 53%; f) BuLi, hexanes, −78→10°C, 90%; g) TBAF, THF, RT 96%; h) Ac_2O, DMAP, NEt_3, CH_2Cl_2, RT, 81%.

oxidation, dibromo-olefination, and carbenoid Fritsch–Buttenberg–Wiechell rearrangement gave the triyne core. Deprotection of the alcohol with TBAF gave **200**, which was acylated to give **201**. A similar approach has been used by us to synthesize the structurally related species 1-phenylhepta-1,3,5-triyne (PHT, not shown), also isolated from species of *Bidens*.[94]

The enetriyne **204** was first isolated from plants of the genus *Chrysanthemum* (daisy),[158] and has been found to be highly phototoxic toward *Aedes atropalpus* and *A. aegypti* larvae.[159] Enetriyne **204** has been synthesized in three steps from acid chloride **205** (Scheme 47).[94] A Friedel–Crafts

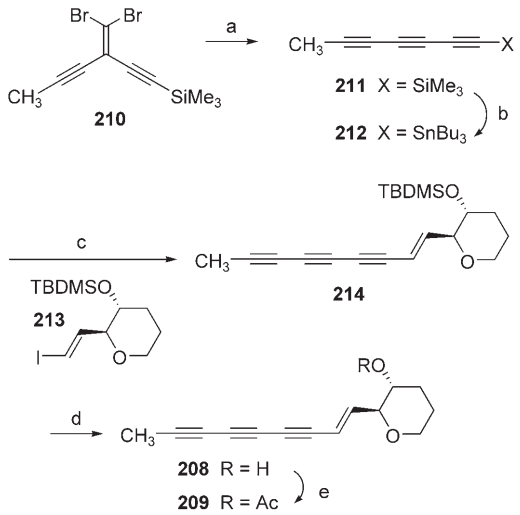


Scheme 47. Synthesis of enetriyne **204** according to Shi Shun and Tykwinski.[94] a) $AlCl_3$, CH_2Cl_2, 0°C, 56%; b) PPh_3, CBr_4, CH_2Cl_2, RT, 44%; c) BuLi, hexanes, −78→−40°C, 84%.

reaction gave **206** and dibromo-olefination provided the necessary precursor **207**. Finally, a Fritsch–Buttenberg–Wiechell rearrangement gave **204** in 84% yield.

5.2. Family Olacaceae

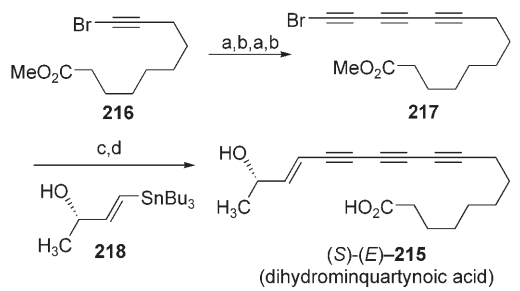
In 1965 (−)-ichthyothereol **208** and its acetate **209** were isolated from *Dahlia coccinea* and *Ichthyothere terminalis*.[160,161] The latter has been used by natives of the Lower Amazon Basin as a fish poison but has also been found to be poisonous to mammals.[160,161] The first synthesis of **208** and **209** was published in 2001 by Mukai et al. (Scheme 48).[162]



Scheme 48. Synthesis of ichthyothereol according to Mukai et al.[162] a) BuLi, hexane, −78°C, 76%; b) $(Bu_3Sn)_2O$, TBAF (cat.), THF, 60°C; c) $[PdCl_2(PPh_3)_2]$, THF, RT, 95%; d) TBAF, THF, RT, 100%; e) Ac_2O, DMAP, CH_2Cl_2, RT, 88%.

This synthesis relies on the carbenoid rearrangement of **210** to assemble the triyne portion. Following conversion of the alkynylsilane **211** into stannane **212**, a Stille coupling between **212** and vinyl iodide **213** completed the conjugated framework of **214**. Finally, removal of the TBDMS protecting group with TBAF quantitatively yielded **208**, and acetylation gave **209**.

Triyne **215** (along with two tetraynes, see Section 8) was isolated from the twigs of *Ochanostachys amentacea*, a tree indigenous to Malaysia and Indonesia, and showed a range of anticancer activity.[163] Gung and Kumi reported the first synthesis of **215**,[164] by using Cadiot–Chodkiewicz chemistry to build the triyne core (not shown). Kim et al. have recently reported an alternative strategy for the synthesis of **215** (Scheme 49).[165] Their approach employed a twofold sequence of acetylene homologation of bromoalkyne **216**



Scheme 49. Synthesis of dihydrominquartynoic acid according to Kim et al.[165] a) $iPr_3SiC{\equiv}CH$, $[PdCl_2(PPh_3)_2]$, CuI, iPr_2NH, THF, RT; b) NBS, AgF, MeCN, RT (47% overall); c) **218**, $[Pd(PPh_3)_4]$, CuI, DMF, RT, 69%; d) LiOH, THF, H_2O, 90%.

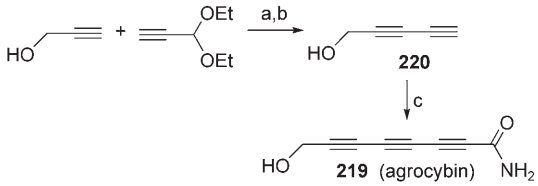
 © 2006 Wiley-VCH Verlag GmbH & Co. KGaA, Weinheim

through Pd-catalyzed Cadiot–Chodkiewicz coupling with triisopropylsilylacetylene followed by desilylation/bromination to form triyne **217** in a one-pot reaction. A final Pd-catalyzed cross-coupling with vinylstannane **218** and ester hydrolysis gave the triyne product **215**.

6. Triynes from Fungi

Triynes have been isolated from a number of fungi, although not nearly to the extent that they have been found in plants. By and large, these molecules have been synthesized by using methodology already described in detail earlier in this Review. Thus, only an abbreviated description will be provided here.

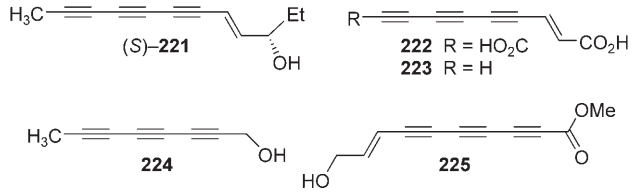
Agrocybin **219** (family Bolbitiaceae) is a triyne amide found in several species of higher fungi including the little lawn mushroom *Agrocybe dura*.[166] Bäuerle, Anke, and co-workers used a rather nontraditional route toward constructing the diynol segment **220**,[167] with a Glaser coupling of propargyl alcohol and 3,3-diethoxypropyne used to form the diyne bond (Scheme 50). Acid-catalyzed liberation of the



Scheme 50. Synthesis of agrocybin according to Bäuerle, Anke, and co-workers.[167] a) CuCl, NH_4Cl, MeOH, H_2O, 0 °C; b) HCl, 50 °C, then NaOH, MeOH, 50 °C; c) $HC{\equiv}CCONH_2$, CuCl, NH_4Cl, MeOH, H_2O, 0 °C.

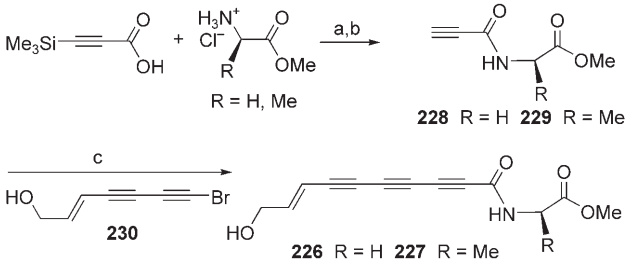
aldehyde and base-induced decarboxylation gave the terminal diyne, and a second Glaser coupling of **220** with propiolamide produced agrocybin (**219**).

The C_{12} triynenol **221** has been isolated from the fungus *Peniophora resinosa* (family Peniophoraceae).[168] The structure and tentative stereochemistry of the natural product



were confirmed by Thaller and co-workers through a stereoselective synthesis involving a Cadiot–Chodkiewicz coupling.[169] Triynes **222** and **223** were isolated from the fungus *Poria sinuosa* (family Polyporaceae) by Cambie et al.[170] Despite their unstable structures, Thaller and co-workers have successfully synthesized the methyl ester analogues of both **222** and **223** through a Cadiot–Chodkiewicz coupling.[171] Jones and co-workers have isolated the triynol **224** from the sheathed woodtuft *Kuehneromyces mutabilis* (family Strophariaceae), a commonly encountered edible mushroom.[172] We have constructed the triyne core of **224** in a similar manner as that of **200** (Scheme 46) by using a Fritsch–Buttenberg–Wiechell rearrangement.[157] The triyne ester **225** has been isolated from the esterified acid extract obtained from the fungus *Fayodia bisphaerigera* (family Tricholomataceae) and was synthesized by Thaller and co-workers by using a Cadiot–Chodkiewicz coupling.[173]

The rather unique amide esters **226** and **227** were also found in an esterified fraction extracted from cultures of *F. bisphaerigera* and synthesized by Thaller and co-workers (Scheme 51).[173] Reaction of the respective HCl salt with



Scheme 51. Synthesis of amide esters **226** and **227** according to Thaller and co-workers.[173] a) NEt_3, DCC, NHS, DMF/CH_2Cl_2, 0 °C, 25% (R = H) and 30% (R = Me); b) $AgNO_3$, KCN, MeOH, H_2O, 0 °C, 30% (**228**) and 63% (**229**); c) **230**, CuCl, $NH_2OH{\cdot}HCl$, $EtNH_2$, MeOH, H_2O, 34% (**226**) and 34% (**227**).

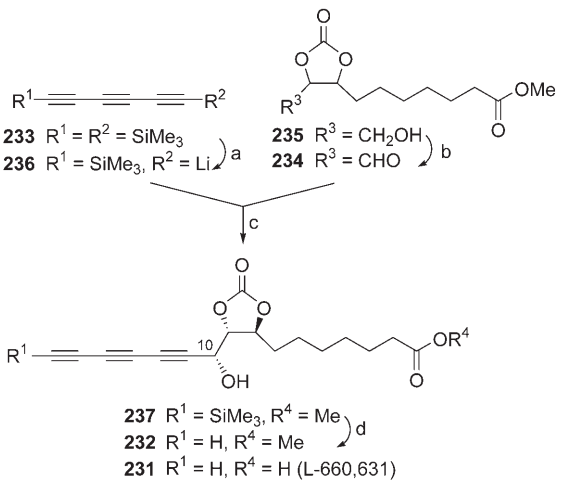
NEt_3 gave the methyl esters of either L-glycine or L-alanine, which were then treated with trimethylsilylpropiolic acid in the presence of DCC and *N*-hydroxysuccinimide (NHS) as an accelerator. Desilylation with $AgNO_3$/KCN gave **228** and **229**, respectively, and a Cadiot–Chodkiewicz coupling with bromodiyne **230** then afforded the products **226** and **227** without racemization.

7. Triynes from Bacteria

An unusual polyyne natural product L-660,631 (**231**) was initially isolated from *Actinomycetes* fermentation[174] and later from *Microbisporia*.[175] It was subsequently shown to be a potent inhibitor of cytosolic β-ketothiolase, the initial enzyme of cholesterol biosynthesis.[176] A stabilized derivative of

L-660,631, methyl ester **232**, has been assembled by Lewis et al. (Scheme 52).[177] Their approach sought to avoid the instability of both the monodesilylated triyne derived from **233** and the aldehyde **234**, and a clever in situ approach was thus devised. Alcohol **235** was converted into aldehyde **234** by a Swern oxidation in THF. The lithium acetylide **236**, formed by Li/Si exchange with triyne **233**, was then added directly to the oxidation reaction mixture of **234**, and this straightforward approach gave the product **237** in 39% yield as a 1:1.8 (α:β) ratio of C10 epimers. Protiodesilylation gave the terminal triyne **232**, which was identical to the naturally

© 2006 Wiley-VCH Verlag GmbH & Co. KGaA, Weinheim



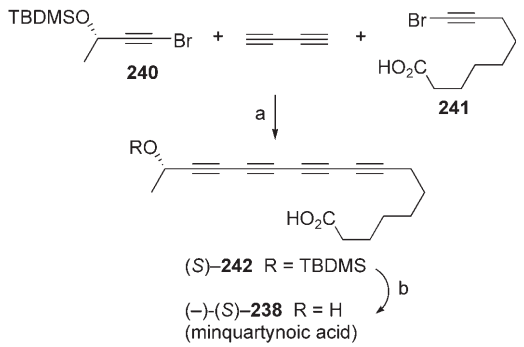
Scheme 52. Synthesis of L-660,631 methyl ester according to Lewis et al.[177] a) MeLi/LiBr, THF −78→0°C; b) $(COCl)_2$, DMSO, THF, NEt_3, −60→−35°C; c) **234** + **236**, THF, −78°C, 39%; d) TBAF, AcOH, THF, 80%.

derived material in all respects. An alternative route to L-660,631 methyl ester was subsequently reported by Yadav and Rajagopal, who used a Cadiot–Chodkiewicz coupling to complete the triyne framework.[178]

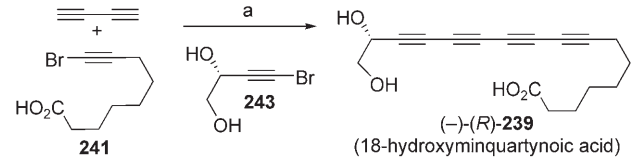
8. Tetraynes from Plants

In 1989 the tetrayne minquartynoic acid (**238**, see Scheme 53) was isolated from the bark of *Minquartia guianensis* (family Olacaceae), a traditional anthelmintic used by the Quijos Quichua people of Ecuador.[179] In 2001, minquartynoic acid was isolated, along with triyne **215** (Scheme 49) and tetrayne **239** (see Scheme 54), from the twigs of *Ochanostachys amentacea*, a tree indigenous to Malaysia and Indonesia.[163] Minquartynoic acid was reported to be highly cytotoxic against ten different tumor cell lines[163] and to have anti-HIV properties.[180]

Minquartynoic acid was synthesized by Gung and Dickson in a one-pot three-component Cadiot–Chodkiewicz reaction using butadiyne and bromoalkynes **240** and **241** (Scheme 53).[181] A lack of selectivity in this reaction resulted in a mixture of the three tetraynes that were, however, separable by column chromatography. The desired product **242** was then desilylated to give (−)-(*S*)-**238**.



Scheme 53. Synthesis of minquartynoic acid according to Gung and Dickson.[181] a) CuCl, $EtNH_2$, $NH_2OH{\cdot}HCl$, MeOH, H_2O, 0°C, 30% (other tetraynes: 29%); b) HF·pyridine, THF, 0°C→RT, 72%.

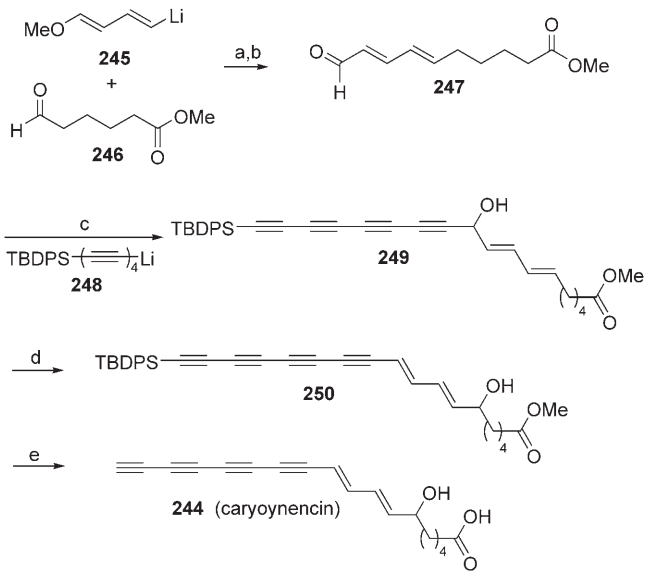


Scheme 54. Synthesis of (*R*)-18-hydroxyminquartynoic acid according to Gung and Kumi.[182] a) CuCl, $EtNH_2$, $NH_2OH{\cdot}HCl$, MeOH, H_2O, 1 h, then addition of **243**, 31%.

Gung and Kumi also exploited this one-pot three-component Cadiot–Chodkiewicz protocol for the synthesis of (*R*)-18-hydroxyminquartynoic acid (**239**, Scheme 54).[182] In this case, the less-reactive bromoalkyne **241** was allowed to react with butadiyne for one hour prior to the addition of **243**. From this reaction, **239** could be separated from two other tetrayne by-products by column chromatography and afforded the desired product in 31% yield.

9. Tetraynes from Bacteria

The extremely unstable terminal tetrayne caryoynencin (**244**, Scheme 55) has been isolated from liquid cultures of the plant pathogen *Pseudomonas caryophylli*, and has demonstrated antimicrobial activity against both Gram-positive and Gram-negative bacteria.[183] Yamaguchi et al. have reported the synthesis of **244**, as well as a number of tetrayne analogues



Scheme 55. Synthesis of caryoynencin according to Yamaguchi et al.[184] a) THF, −60°C, 56%; b) CSA, THF, 85%; c) **248**, THF/hexane (1:1), −78°C, 61%; d) HF, THF, RT, 59%; e) Bu_4NBr, NaOH, THF, 0°C.

 © 2006 Wiley-VCH Verlag GmbH & Co. KGaA, Weinheim

(not shown).[184] Addition of vinyllithium derivative **245** to aldehyde **246**, followed by treatment with acid to both effect elimination as well as liberation of the protected aldehyde gave **247**. Lithiated tetrayne **248** was prepared in situ and added to aldehyde **247** to give alcohol **249**, which was rearranged to the fully conjugated core of **250** with HF, ultimately affording a 2:1 ratio of 7*E*,9*E* and 7*E*,9*Z* isomers, respectively. Deprotection of the terminal alkyne and hydrolysis of the methyl ester moieties was then effected to give the unstable tetrayne caryoynencin, which was spectroscopically consistent with a natural sample.

10. Conclusions

Polyynes constitute a very structurally diverse and useful class of compounds with important biological activities such as antifungal, antibiotic, anticancer, antitumor, anti-HIV, anti-inflammatory, pesticidal, and antimicrobial properties. For polyynes, as with nearly all natural products, there exists a dynamic and symbiotic relationship between the intensive efforts to isolate new compounds, followed by the efforts of others who attempt to reproduce nature's elegance in the laboratory. As this Review shows, the Cadiot–Chodkiewicz coupling reaction remains a popular method for assembling natural acetylenic compounds. There is, however, no shortage of naturally occurring polyynes that cannot be assembled by this strategy, and numerous clever alternative methods have been and continue to be explored and developed.

List of Abbreviations

AIBN	azoisobutyronitrile
BHT	*tert*-butylhydroxytoluene
Bn	benzyl
Bz	benzoyl
CD	circular dichroism
Cp	cyclopentadienyl
CPDMS	(3-cyanopropyl)dimethylsilyl
CSA	camphorsulfonic acid
dba	dibenzylideneacetone
DCC	1,3-dicyclohexylcarbodiimide
DET	diethyl tartrate
DIBAH	diisobutylaluminum hydride
DMAP	4-dimethylaminopyridine
DMPU	1,3-dimethyl-3,4,5,6-tetrahydro-2(1*H*)-pyrimidone
DMSO	dimethylsulfoxide
HMPA	hexamethylphosphoramide
LDA	lithium diisopropylamide
LDMAN	lithium 1-(*N*,*N*-dimethylamino)naphthalenide
LiDBB	lithium di-*tert*-butylbiphenylide
*m*CPBA	*m*-chloroperoxybenzoic acid
MOM	methoxymethyl
Ms	methanesulfonyl
MS	molecular sieves
NBS	*N*-bromosuccinimide
NHS	*N*-hydroxysuccinimide
NMO	*N*-methylmorpholine *N*-oxide
PDC	pyridinium dichlorochromate
PHT	1-phenylhepta-1,3,5-triyne
PMB	*p*-methoxybenzyl
PPFA	(*R*)-l-*N*,*N*-dimethylamino-l-[(*S*)-2-diphenylphosphanylferrocenyl]ethane
*p*TsOH	*p*-toluenesulfonic acid
TBAF	tetrabutylammonium fluoride
TBDMS	*tert*-butyldimethylsilyl
TBDPS	*tert*-butyldiphenylsilyl
TEMPO	2,2,6,6-tetramethylpiperidine-1-oxyl
Tf	trifluoromethanesulfonyl
THP	tetrahydropyranyl
TMEDA	*N*,*N*,*N*′,*N*′-tetramethylethylenediamine
TMS	trimethylsilyl
TMP	2,2,6,6-tetramethylpiperidine
TPAP	tetra-*n*-propylammonium perruthenate
Ts	*para*-toluenesulfonyl

*This work was supported by the Natural Sciences and Engineering Research Council of Canada (NSERC) and the University of Alberta. We thank Annie Tykwinski for the artwork and design of the frontispiece. The picture of Ferdinand Bohlmann was used with permission (Liebigs Annalen der Chemie **1994**, 1).*

Received: June 15, 2005

[1] a) Ref. [1b], p. 1; b) F. Bohlmann, H. Burkhardt, C. Zdero, *Naturally Occurring Acetylenes*, Academic Press, New York, **1973**; c) F. Bohlmann, H. Bornowski, C. Arndt, *Fortschr. Chem. Forsch.* **1962**, *4*, 138–272; d) F. Bohlmann, *Fortschr. Chem. Forsch.* **1966**, *6*, 65–100; e) F. Bohlmann in *Chemistry of Acetylenes* (Ed.: H. G. Viehe), Dekker, New York, **1969**, chap. 14, pp. 977–986; f) F. Bohlmann, *Angew. Chem.* **1955**, *67*, 389–394.

[2] a) E. R. H. Jones, V. Thaller in *The Chemistry of the Carbon-Carbon Triple Bond*, *Part 2* (Ed.: S. Patai), Wiley, New York, **1978**, chap. 14, pp. 621–633; b) E. R. H. Jones, V. Thaller, *Handbook of Microbiology, Vol. 3* (Eds.: A. I. Laskin, H. A. Lechevalier), CRC, Cleveland, **1973**, pp. 63–74; c) E. R. H. Jones, *Proc. Chem. Soc. Lond.* **1960**, 199–210.

[3] a) J. D. Bu'Lock, *Prog. Org. Chem.* **1964**, *6*, 86–134; b) N. A. Sörensen, *Proc. Chem. Soc. Lond.* **1961**, 98–110.

[4] The term polyyne is meant to denote compounds with a structural sequence of two or more consecutive (conjugated) acetylene units. The term polyacetylene has often been used in this context as well, but can be ambiguous because of its more common use in reference to polymerized acetylene, $-[CH=CH]_n-$.

[5] a) J. W. Blunt, B. R. Copp, M. H. G. Munro, P. T. Northcote, M. R. Prinsep, *Nat. Prod. Rep.* **2003**, *20*, 1–48; b) D. J. Faulkner, *Nat. Prod. Rep.* **2002**, *19*, 1–48; c) D. J. Faulkner, *Nat. Prod. Rep.* **2001**, *18*, 1–49; d) D. J. Faulkner, *Nat. Prod. Rep.* **2000**, *17*, 7–55.

[6] J. Meinwald, Y. C. Meinwald, A. M. Chalmers, T. Eisner, *Science* **1968**, *160*, 890–892. It should be noted, however, that this compound likely derives from the plants composing the diet of the beetle, see Ref. [2a].

 © 2006 Wiley-VCH Verlag GmbH & Co. KGaA, Weinheim

[7] Beilstein database lists 1328 hits (as of September 12th, 2005) when searching for the "C≡CC≡C" substructure *and* "INP" (isolated natural product).

[8] a) G. H. N. Towers, J. T. Arnason, C.-K. Wat, J. D. H. Lambert, *Can. Pat.* 1173743, **1984** [*Chem. Abstr.* **1985**, *102*, 41602r]; b) *Biologically Active Natural Products—Potential Use in Agriculture*, *ACS Symposium Series Vol. 380* (Ed.: H. Cutler), American Chemical Society, Washington, DC, **1988**; c) *Chemistry and Biology of Naturally-Occurring Acetylenes and Related Compounds [NOARC]*, *Bioactive Molecules, Vol. 7* (Eds.: J. Lam, H. Breteler, T. Arnason, L. Hansen), Elsevier, New York, **1988**; d) D. J. Chitwood in *Pest Control with Enhanced Environmental Safety*, *ACS Symposium Series Vol. 524* (Eds.: S. Duke, J. Menn, J. Plimmer), American Chemical Society, Washington, DC, **1993**, pp. 300–315; e) G. H. N. Towers, J. E. Page, J. B. Hudson, *Curr. Org. Chem.* **1997**, *1*, 395–414; f) J. B. Hudson, E. A. Graham, R. Rossi, A. Carpita, D. Neri, G. H. N. Towers, *Planta Med.* **1993**, *59*, 447–450; g) G. H. N. Towers, C.-K. Wat, *Rev. Latinoam. Quim.* **1978**, *9*, 162–170.

[9] a) L. P. Christensen, *Phytochemistry* **1992**, *31*, 7–49; b) L. P. Christensen, J. Lam, *Phytochemistry* **1991**, *30*, 2453–2476; c) L. P. Christensen, J. Lam, *Phytochemistry* **1991**, *30*, 11–49; d) L. P. Christensen, J. Lam, *Phytochemistry* **1990**, *29*, 2753–2785.

[10] P. Siemsen, R. C. Livingston, F. Diederich, *Angew. Chem.* **2000**, *112*, 2740–2767; *Angew. Chem. Int. Ed.* **2000**, *39*, 2633–2657.

[11] Taxonomy was assigned on the basis of primary literature as well as the following sources: Plants: the *USDA PLANTS Classification Report* (http://plants.usda.gov/classification.html) and *The Flowering Plant Gateway* (http://www.csdl.tamu.edu/FLORA/newgate/cronang.htm); fungi: *Ainsworth and Bisby's Dictionary of Fungi, 9th ed.* (Eds.: G. C. Ainsworth, P. M. Kirk, G. R. Bisby, P. F. Cannon, J. C. David, J. A. Stalpers), Cabi Bioscience, Oxon, UK, **2001**; sponges: *Systema Porifera: A Guide to the Classification of Sponges* (Eds.: J. N. A. Hooper, R. W. M. Van Soest), Kluwer, New York, **2002**.

[12] J. T. Etse, P. G. Waterman, *Phytochemistry* **1986**, *25*, 1903–1905.

[13] C. Harcken, R. Brückner, E. Rank, *Chem. Eur. J.* **1998**, *4*, 2342–2352; corrigendum *Chem. Eur. J.* **1998**, *4*, 2390–2390.

[14] C. Cai, A. Vasella, *Helv. Chim. Acta* **1995**, *78*, 2053–2064.

[15] W. Tang, G. Eisenbrand, *Chinese Drugs of Plant Origin*, Springer, Berlin, **1992**.

[16] A. F. Barrero, M. M. Herrador, M. Akssira, P. Arteaga, J. L. Romera, *J. Nat. Prod.* **1999**, *62*, 946–948.

[17] a) L. M. Antunes, M. G. Organ, *Tetrahedron Lett.* **2003**, *44*, 6805–6808; b) H. Ghasemi, L. M. Antunes, M. G. Organ, *Org. Lett.* **2004**, *6*, 2913–2916.

[18] a) E. F. L. J. Anet, B. Lythgoe, M. H. Silk, S. Trippett, *J. Chem. Soc.* **1953**, 309–322; b) F. Bohlmann, K.-M. Rode, *Chem. Ber.* **1968**, *101*, 1163–1175.

[19] a) C. A. Jacobson, *J. Am. Chem. Soc.* **1915**, *37*, 916–934; b) E. Starreveld, Ch. E. Hope, *Neurology* **1975**, *25*, 730–734.

[20] E. Anet, B. Lythgoe, M. H. Silk, S. Trippett, *Chem. Ind.* **1952**, 757–758.

[21] a) U. Wittstock, F. Hadacek, G. Wurz, E. Teuscher, H. Greger, *Planta Med.* **1995**, *61*, 439–445; b) F. Bohlmann, P. Hänel, *Chem. Ber.* **1969**, *102*, 3293–3297.

[22] a) T. Ohta, K. Uwai, R. Kikuchi, S. Nozoe, Y. Oshima, K. Sasaki, F. Yoshizaki, *Tetrahedron* **1999**, *55*, 12087–12098; b) K. Uwai, Y. Oshima, T. Sugihara, T. Ohta, *Tetrahedron* **1999**, *55*, 9469–9480; c) K. Uwai, K. Ohashi, Y. Takaya, T. Ohta, T. Tadano, K. Kisara, K. Shibusawa, R. Sakakibara, Y. Oshima, *J. Med. Chem.* **2000**, *43*, 4508–4515.

[23] H. A. Stefani, P. H. Menezes, I. M. Costa, D. O. Silva, N. Petragnani, *Synlett* **2002**, 1335–1337.

[24] G. Sabitha, Ch. S. Reddy, P. Srihari, J. S. Yadav, *Synthesis* **2003**, 2699–2704.

[25] V. Fiandanese, D. Bottalico, C. Cardellicchio, G. Marchese, A. Punzi, *Tetrahedron* **2005**, *61*, 4551–4556.

[26] N. J. Turner, *J. Ethnobiol.* **1982**, *2*, 17–38.

[27] M. Kobaisy, Z. Abramowski, L. Lermer, G. Saxena, R. E. W. Hancock, G. H. N. Towers, D. Doxsee, R. W. Stokes, *J. Nat. Prod.* **1997**, *60*, 1210–1213.

[28] L. Xu, X. H. Wu, G. R. Zheng, J. C. Cai, *Chin. Chem. Lett.* **2000**, *11*, 213–216.

[29] For a review of the use of tartrates in the synthesis of biomolecules, including polyyne natural products, see: A. K. Ghosh, E. S. Koltun, G. Bilcer, *Synthesis* **2001**, 1281–1301.

[30] T. Saita, H. Matsunaga, H. Yamamoto, F. Nagumo, H. Fujito, M. Mori, M. Katano, *Biol. Pharm. Bull.* **1994**, *17*, 798–802.

[31] L. Hansen, P. M. Boll, *Phytochemistry* **1986**, *25*, 285–293.

[32] J. Poplawski, J. T. Wrobel, T. Glinka, *Phytochemistry* **1980**, *19*, 1539–1541.

[33] B.-Z. Ahn, S.-I. Kim, *Arch. Pharm.* **1988**, *321*, 61–63.

[34] For the initial synthesis of panaxynol, see: F. Bohlmann, C. Arndt, H. Bornowski, K.-M. Kleine, *Chem. Ber.* **1961**, *94*, 958–967.

[35] S.-I. Kim, Y.-H. Lee, B.-Z. Ahn, *Arch. Pharm.* **1999**, *332*, 133–136.

[36] W. Lu, G. Zheng, H. A. Aisa, J. Cai, *Tetrahedron Lett.* **1998**, *39*, 9521–9522.

[37] H.-J. Yu, C.-M. Sun, C.-C. Chen, T.-C. Wu, C.-L. Wei, C.-C. Shen, *Heterocycles* **2004**, *62*, 857–868.

[38] H. Yun, S. J. Danishefsky, *J. Org. Chem.* **2003**, *68*, 4519–4522.

[39] a) H. Matsunaga, M. Katano, H. Yamamoto, H. Fujito, M. Mori, K. Takata, *Chem. Pharm. Bull.* **1990**, *38*, 3480–3482; b) Y. S. Kim, S. H. Jin, S. I. Kim, D. R. Hahn, *Arch. Pharmacal Res.* **1989**, *12*, 207–213.

[40] a) D. Lechner, M. Stavri, M. Oluwatuyi, R. Pereda-Miranda, S. Gibbons, *Phytochemistry* **2004**, *65*, 331–335; b) H. Matsuura, G. Saxena, S. W. Farmer, R. E. W. Hancock, G. H. N. Towers, *Planta Med.* **1996**, *62*, 256–259.

[41] G. Zheng, W. Lu, H. A. Aisa, J. Cai, *Tetrahedron Lett.* **1999**, *40*, 2181–2182.

[42] G. Zheng, W. Lu, J. Cai, *J. Nat. Prod.* **1999**, *62*, 626–628.

[43] The stereochemical assignment of falcarindiol has been confirmed by others: A. S. Ratnayake, T. Hemscheidt, *Org. Lett.* **2002**, *4*, 4667–4669; erratum, A. S. Ratnayake, T. Hemscheidt, *Org. Lett.* **2003**, *5*, 381.

[44] I. Kitagawa, M. Yoshikawa, M. Yoshihara, T. Hayashi, T. Taniyama, *Yakugaku Zasshi* **1983**, *103*, 612–622; I. Kitagawa, M. Yoshikawa, M. Yoshihara, T. Hayashi, T. Taniyama, *Chem. Abstr.* **1983**, *99*, 128194c.

[45] H. Matsunaga, M. Katano, T. Saita, H. Yamamoto, M. Mori, *Cancer Chemother. Pharmacol.* **1994**, *33*, 291–297.

[46] M. Katano, H. Yamamoto, H. Matsunaga, M. Mori, K. Takata, M. Nakamura, *Jpn. J. Cancer Chemother.* **1990**, *17*, 1045–1049; M. Katano, H. Yamamoto, H. Matsunaga, M. Mori, K. Takata, M. Nakamura, *Chem. Abstr.* **1990**, *113*, 144987b.

[47] H. Matsunaga, T. Saita, F. Nagumo, M. Mori, M. Katano, *Cancer Chemother. Pharmacol.* **1995**, *35*, 291–296.

[48] I. Kitagawa, T. Taniyama, H. Shibuya, T. Noda, M. Yoshikawa, *Yakugaku Zasshi* **1987**, *107*, 495–505; I. Kitagawa, T. Taniyama, H. Shibuya, T. Noda, M. Yoshikawa, *Chem. Abstr.* **1987**, *107*, 205003c.

[49] M. Kobayashi, T. Mahmud, T. Umezome, I. Kitagawa, *Chem. Pharm. Bull.* **1995**, *43*, 1595–1597.

[50] M. Satoh, N. Takeuchi, Y. Fujimoto, *Chem. Pharm. Bull.* **1997**, *45*, 1114–1116.

[51] M. Kobayashi, T. Mahmud, T. Umezome, W. Wang, N. Murakami, I. Kitagawa, *Tetrahedron* **1997**, *53*, 15691–15700.

 © 2006 Wiley-VCH Verlag GmbH & Co. KGaA, Weinheim

[52] W. Lu, G. Zheng, D. Gao, J. Cai, *Tetrahedron* **1999**, *55*, 7157 – 7168.
[53] M. K. Gurjar, V. S. Kumar, B. V. Rao, *Tetrahedron* **1999**, *55*, 12563 – 12576.
[54] S. F. Mayer, A. Steinreiber, R. V. A. Orru, K. Faber, *J. Org. Chem.* **2002**, *67*, 9115 – 9121.
[55] J. S. Yadav, A. Maiti, *Tetrahedron* **2002**, *58*, 4955 – 4961.
[56] For the synthesis of enantiomerically pure polyhydroxy diacetylenic alcohols from precursors from the chiral pool, see: J. S. Yadav, A. Maiti, *Tetrahedron Lett.* **2001**, *42*, 3909 – 3912.
[57] M. Yamaguchi, I. Hirao, *Tetrahedron Lett.* **1983**, *24*, 391 – 394.
[58] Y. Fujimoto, M. Satoh, *Phytochemistry* **1987**, *26*, 2850 – 2852.
[59] a) Y. Fujimoto, M. Satoh, N. Takeuchi, M. Kirisawa, *Chem. Lett.* **1989**, 1619 – 1622; b) Y. Fujimoto, M. Satoh, N. Takeuchi, M. Kirisawa, *Chem. Pharm. Bull.* **1990**, *38*, 1447 – 1450.
[60] K. Hirakura, K. Sugama, M. Morita, K. Nakajima, H. Sasaki, M. Okada, H. Sato, *Heterocycles* **2000**, *53*, 2451 – 2457.
[61] Y. Fujimoto, M. Satoh, N. Takeuchi, M. Kirisawa, *Chem. Pharm. Bull.* **1991**, *39*, 521 – 523.
[62] J. E. Baldwin, R. M. Adlington, P. J. Wilkinson, R. Marquez, M. F. A. Adamo, *Heterocycles* **2003**, *59*, 81 – 85.
[63] C. Bolm, A. S. Magnus, J. P. Hildebrand, *Org. Lett.* **2000**, *2*, 1173 – 1175.
[64] S. W. Lee, K. Kim, M.-C. Rho, M. Y. Chung, Y. H. Kim, S. Lee, H. S. Lee, Y. K. Kim, *Planta Med.* **2004**, *70*, 197 – 200.
[65] J. H. Oh, H. S. Lee, M.-C. Rho, Y. K. Kim, H. K. Lee, W. S. Lee, J. N. Kim, S. Lee, S. H. Jung, *Tetrahedron Lett.* **2004**, *45*, 7077 – 7079.
[66] Y. Fujimoto, H. Wang, M. Satoh, N. Takeuchi, *Phytochemistry* **1994**, *35*, 1255 – 1257.
[67] B. Z. Ahn, S. I. Kim, Y. H. Lee, *Arch. Pharm.* **1989**, *322*, 223 – 226.
[68] M. Satoh, N. Takeuchi, Y. Fujimoto, *Heterocycles* **1997**, *45*, 177 – 180.
[69] M. Satoh, M. Watanabe, M. Kawahata, K. Mohri, Y. Yoshida, K. Isobe, Y. Fujimoto, *Chem. Pharm. Bull.* **2004**, *52*, 418 – 421.
[70] a) J. T. Mortensen, J. S. Sørensen, N. A. Sørensen, *Acta Chem. Scand.* **1964**, *18*, 2392 – 2394; b) F. Bohlmann, K.-M. Kleine, *Chem. Ber.* **1965**, *98*, 3081 – 3086.
[71] E. Rodriguez, M. Aregullin, T. Nishida, S. Uehara, R. Wrangham, Z. Abramowski, A. Finlayson, G. H. N. Towers, *Experientia* **1985**, *41*, 419 – 420.
[72] T. Lu, F. J. Parodi, D. Vargas, L. Quijano, E. R. Mertooetomo, M. A. Hjortso, N. H. Fischer, *Phytochemistry* **1993**, *32*, 113 – 116.
[73] E. Block, C. Guo, M. Thiruvazhi, P. J. Toscano, *J. Am. Chem. Soc.* **1994**, *116*, 9403 – 9404.
[74] a) L. Crombie, *J. Chem. Soc.* **1955**, 999 – 1006; b) L. Crombie, M. Manzoor-i-Khuda, *J. Chem. Soc.* **1955**, 2767 – 2777.
[75] L. Crombie, A. J. W. Hobbs, M. A. Horsham, R. J. Blade, *Tetrahedron Lett.* **1987**, *28*, 4875 – 4878.
[76] R. Jente, P.-H. Bonnet, F. Bohlmann, *Chem. Ber.* **1972**, *105*, 1694 – 1700.
[77] A. Carpita, D. Neri, R. Rossi, *Gazz. Chim. Ital.* **1987**, *117*, 481 – 489.
[78] a) F. Bohlmann, N. Ates, J. Jakupovic, R. M. King, H. Robinson, *Phytochemistry* **1982**, *21*, 2691 – 2697; b) J. A. Marco, J. F. Sanz, J. Jakupovic, S. Huneck, *Tetrahedron* **1990**, *46*, 6931 – 6938.
[79] Y. Nakamura, N. Kawamoto, Y. Ohto, K. Torikai, A. Murakami, H. Ohigashi, *Cancer Lett.* **1999**, *140*, 37 – 45.
[80] Y. Gao, W.-L. Wu, Y.-L. Wu, B. Ye, R. Zhou, *Tetrahedron* **1998**, *54*, 12523 – 12538.
[81] M. Tada, K. Chiba, *Agric. Biol. Chem.* **1984**, *48*, 1367 – 1369.
[82] N. Miyakoshi, D. Aburano, C. Mukai, *J. Org. Chem.* **2005**, *70*, 6045 – 6052.
[83] For previous synthetic studies, see: H. Toshima, H. Aramaki, Y. Furumoto, S. Inamura, A. Ichihara, *Tetrahedron* **1998**, *54*, 5531 – 5544, and references therein.
[84] M. Miyazawa, H. Kameoka, *Phytochemistry* **1976**, *15*, 223 – 224.
[85] E. Negishi, N. Okukado, S. F. Lovich, F.-T. Luo, *J. Org. Chem.* **1984**, *49*, 2629 – 2632.
[86] P. J. Stang, V. Dixit, *Synthesis* **1985**, 962 – 963.
[87] G. Himbert, H. Umbach, M. Barz, *Z. Naturforsch. B* **1984**, *39*, 661 – 667.
[88] a) F. Bohlmann, K.-M. Kleine, *Chem. Ber.* **1962**, *95*, 39 – 46; b) T.-S. Wu, Z.-J. Tsang, P.-L. Wu, M.-J. Liou, Y.-L. Leu, Y.-Y. Chan, F.-W. Lin, L.-S. Shi, *Phytochemistry* **1998**, *47*, 1645 – 1648; c) M. Miyazawa, H. Kameoka, *Phytochemistry* **1976**, *15*, 1987 – 1988.
[89] a) Capillin: G. E. Jones, A. B. Holmes, *Tetrahedron Lett.* **1982**, *23*, 3203 – 3206; b) capillene: Y. Hori, K. Ito, Y. Arima, H. Tanigushi, *Chem. Exp.* **1987**, *2*, 491 – 494; Y. Hori, K. Ito, Y. Arima, H. Tanigushi, *Chem. Abstr.* **1988**, *109*, 37545b; c) neocapillene: Refs. [87], [89b], and S. F. Vasilevskii, M. Fossatelli, A. H. T. M. van der Kork, L. Brandsma, *Russ. Chem. Bull.* **1993**, *42*, 307 – 309.
[90] R. W. Wrangham, T. Nishida, *Primates* **1983**, *24*, 276 – 282.
[91] F. Bohlmann, J. Jakupovic, N. Ates, A. Schuster, J. Pickardt, R. M. King, H. Robinson, *Liebigs Ann. Chem.* **1983**, 962 – 973.
[92] M. Koreeda, W. Yang, *J. Am. Chem. Soc.* **1994**, *116*, 10793 – 10794.
[93] I. Yosioka, H. Hikino, Y. Sasaki, *Chem. Pharm. Bull.* **1960**, *8*, 957 – 959.
[94] A. L. K. Shi Shun, R. R. Tykwinski, *J. Org. Chem.* **2003**, *68*, 6810 – 6813.
[95] N. Wang, X. Yao, R. Ishii, S. Kitanaka, *Chem. Pharm. Bull.* **2001**, *49*, 938 – 942.
[96] B. W. Gung, R. M. Fox, *Tetrahedron* **2004**, *60*, 9405 – 9415.
[97] a) A. F. Rose, B. A. Butt, T. Jermy, *Phytochemistry* **1980**, *19*, 563 – 566; b) F. Bohlmann, C. Zdero, H. Robinson, R. M. King, *Phytochemistry* **1979**, *18*, 1519 – 1521.
[98] D. Grandjean, P. Pale, J. Chuche, *Tetrahedron* **1993**, *49*, 5225 – 5236.
[99] F. Bohlmann, M. Ahmed, M. Grenz, R. M. King, H. Robinson, *Phytochemistry* **1983**, *22*, 2858 – 2859.
[100] C. B. Ziegler, Jr., S. M. Harris, J. E. Baldwin, *J. Org. Chem.* **1987**, *52*, 443 – 446.
[101] A. Orita, N. Yoshioka, P. Struwe, A. Braier, A. Beckmann, J. Otera, *Chem. Eur. J.* **1999**, *5*, 1355 – 1363.
[102] Negishi et al. have reported a synthesis of **106** by using an approach analogous to his synthesis of xerulin (**170**), see: E. Negishi, M. Hata, C. Xu, *Org. Lett.* **2000**, *2*, 3687 – 3689.
[103] R. Bauer, P. Remiger, *Planta Med.* **1989**, *55*, 367 – 371, and references therein.
[104] R. S. Ramsewak, A. J. Erickson, M. G. Nair, *Phytochemistry* **1999**, *51*, 729 – 732.
[105] L. Wu, J. Bae, G. A. Kraus, E. S. Wurtele, *Phytochemistry* **2004**, *65*, 2477 – 2484.
[106] F. Bohlmann, C. Zdero, U. Niedballa, *Chem. Ber.* **1968**, *101*, 2987 – 2994.
[107] F. Bohlmann, C. Zdero, *Chem. Ber.* **1966**, *99*, 2413 – 2415.
[108] F. Bohlmann, W. Thefeld, C. Zdero, *Chem. Ber.* **1970**, *103*, 2245 – 2251.
[109] A. D. Patil, J. A. Chan, P. Lois-Flamberg, R. J. Mayer, J. W. Westley, *J. Nat. Prod.* **1989**, *52*, 153 – 161.
[110] S. Y. Mhaskar, G. Lakshminarayana, *Tetrahedron Lett.* **1990**, *31*, 7227 – 7228.
[111] An unsaturated analogue has also been synthesized, see: S. Y. Mhaskar, G. Lakshminarayana, *Synth. Commun.* **1990**, *20*, 2001 – 2009.

 © 2006 Wiley-VCH Verlag GmbH & Co. KGaA, Weinheim

[112] K. Ohashi, H. Winarno, M. Mukai, M. Inoue, M. S. Prana, P. Simanjuntak, H. Shibuya, *Chem. Pharm. Bull.* **2003**, *51*, 343 – 345.
[113] Z. Xu, H.-S. Byun, R. Bittman, *J. Org. Chem.* **1991**, *56*, 7183 – 7186.
[114] L. P. Kvist, L. B. Holm-Nielsen, *Opera Bot.* **1987**, *92*, 83 – 107.
[115] C. M. Kraus, A. Neszmélyi, S. Holly, B. Wiedemann, A. Nenninger, K. B. G. Torssell, L. Bohlin, H. Wagner, *J. Nat. Prod.* **1998**, *61*, 422 – 427.
[116] G. Zeni, R. B. Panatieri, E. Lissner, P. H. Menezes, A. L. Braga, H. A. Stefani, *Org. Lett.* **2001**, *3*, 819 – 821.
[117] a) N. Alam, B. H. Bae, J. Hong, C. O. Lee, K. S. Im, J. H. Jung, *J. Nat. Prod.* **2001**, *64*, 1059 – 1063, and references therein; b) N. Alam, J. Hong, C.-O. Lee, J. S. Choi, K. S. Im, J. H. Jung, *Chem. Pharm. Bull.* **2002**, *50*, 661 – 662.
[118] N. Fusetani, T. Toyoda, N. Asai, S. Matsunaga, T. Maruyama, *J. Nat. Prod.* **1996**, *59*, 796 – 797.
[119] J. C. Coll, B. F. Bowden, G. V. Meehan, G. M. Konig, A. R. Carroll, D. M. Tapiolas, P. M. Aliño, A. Heaton, R. De Nys, P. A. Leone, M. Maida, T. L. Aceret, R. H. Willis, R. C. Babcock, B. L. Willis, Z. Florian, M. N. Clayton, R. L. Miller, *Mar. Biol.* **1994**, *118*, 177 – 182.
[120] See also: R. E. Doolittle, *Synthesis* **1984**, 730 – 732; J. Wityak, J. B. Chan, *Synth. Commun.* **1991**, *21*, 977 – 979.
[121] H. A. Stefani, I. M. Costa, G. Zeni, *Tetrahedron Lett.* **1999**, *40*, 9215 – 9217.
[122] A recent synthesis of **132** and **133** has also been reported: V. Fiandanese, D. Bottalico, G. Marchese, A. Punzi, *J. Organomet. Chem.* **2005**, *690*, 3004 – 3008.
[123] B. H. Bae, K. S. Im, W. C. Choi, J. Hong, C.-O. Lee, J. S. Choi, B. W. Son, J.-I. Song, J. H. Jung, *J. Nat. Prod.* **2000**, *63*, 1511 – 1514.
[124] T. J. Speed, D. M. Thamattoor, *Tetrahedron Lett.* **2002**, *43*, 367 – 369.
[125] a) S. López, F. Fernández-Trillo, P. Midon, L. Castedo, C. Saá, *J. Org. Chem.* **2005**, *70*, 6346 – 6352; b) S. López, F. Fernández-Trillo, L. Castedo, C. Saá, *Org. Lett.* **2003**, *5*, 3725 – 3728.
[126] a) A. Umeyama, C. Nagano, S. Arihara, *J. Nat. Prod.* **1997**, *60*, 131 – 133; b) S. Tsukamoto, H. Kato, H. Hirota, N. Fusetani, *J. Nat. Prod.* **1997**, *60*, 126 – 130.
[127] K. Iguchi, M. Kitade, T. Kashiwagi, Y. Yamada, *J. Org. Chem.* **1993**, *58*, 5690 – 5698.
[128] K. Watanabe, Y. Tsuda, Y. Yamane, H. Takahashi, K. Iguchi, H. Naoki, T. Fujita, R. W. M. Van Soest, *Tetrahedron Lett.* **2000**, *41*, 9271 – 9276.
[129] J. S. Yadav, R. K. Mishra, *Tetrahedron Lett.* **2002**, *43*, 1739 – 1741.
[130] S. Reber, T. F. Knöpfel, E. M. Carreira, *Tetrahedron* **2003**, *59*, 6813 – 6817.
[131] J. E. D. Kirkham, T. D. L. Courtney, V. Lee, J. E. Baldwin, *Tetrahedron* **2005**, *61*, 7219 – 7232.
[132] K. Matsumura, S. Hashiguchi, T. Ikariya, R. Noyori, *J. Am. Chem. Soc.* **1997**, *119*, 8738 – 8739.
[133] M. L. Lerch, M. K. Harper, D. J. Faulkner, *J. Nat. Prod.* **2003**, *66*, 667 – 670.
[134] B. W. Gung, C. Gibeau, A. Jones, *Tetrahedron: Asymmetry* **2004**, *15*, 3973 – 3977.
[135] A. Takahashi, T. Endo, S. Nozoe, *Chem. Pharm. Bull.* **1992**, *40*, 3181 – 3184.
[136] R. Jente, F. Bohlmann, S. Schöneweiss, *Phytochemistry* **1979**, *18*, 829 – 837.
[137] G. Bendz, *Ark. Kemi* **1959**, *14*, 305 – 321.
[138] R. C. Cambie, A. Hirschberg, E. R. H. Jones, G. Lowe, *J. Chem. Soc.* **1963**, 4120 – 4130.
[139] W. de Graaf, A. Smits, J. Boersma, G. van Koten, W. P. M. Hoekstra, *Tetrahedron* **1988**, *44*, 6699 – 6704.
[140] D. Kuhnt, T. Anke, H. Besl, M. Bross, R. Herrmann, U. Mocek, B. Steffan, W. Steglich, *J. Antibiot.* **1990**, *43*, 1413 – 1420.
[141] a) K. Siegel, R. Brückner, *Chem. Eur. J.* **1998**, *4*, 1116 – 1122; b) K. Siegel, R. Brückner, *Synlett* **1999**, 1227 – 1230.
[142] a) A. Sorg, R. Brückner, *Angew. Chem.* **2004**, *116*, 4623 – 4626; *Angew. Chem. Int. Ed.* **2004**, *43*, 4523 – 4526; ; b) A. Sorg, K. Siegel, R. Brückner, *Chem. Eur. J.* **2005**, *11*, 1610 – 1624.
[143] E. Negishi, A. Alimardanov, C. Xu, *Org. Lett.* **2000**, *2*, 65 – 67.
[144] R. Rossi, F. Bellina, A. Catanese, L. Mannina, D. Valensin, *Tetrahedron* **2000**, *56*, 479 – 487.
[145] V. Fiandanese, D. Bottalico, G. Marchese, A. Punzi, *Tetrahedron* **2004**, *60*, 11 421 – 11 425.
[146] A. K. Amegadzie, W. A. Ayer, L. Sigler, *Can. J. Chem.* **1995**, *73*, 2119 – 2125.
[147] T. Sugahara, K. Ogasawara, *Chem. Commun.* **1997**, 767 – 768.
[148] A. S. Kende, C. A. Smith, *J. Org. Chem.* **1988**, *53*, 2655 – 2657.
[149] A. Gehrt, G. Erkel, T. Anke, O. Sterner, *Z. Naturforsch. C* **1998**, *53*, 89 – 92.
[150] F. Bellina, A. Carpita, L. Mannocci, R. Rossi, *Eur. J. Org. Chem.* **2004**, 2610 – 2619.
[151] M. Ahmed, G. J. Broad, E. R. H. Jones, A. A. Taha, V. Thaller, *J. Chem. Res. Synop.* **1982**, 199; M. Ahmed, G. J. Broad, E. R. H. Jones, A. A. Taha, V. Thaller, *J. Chem. Res. Miniprint* **1982**, 2055 – 2071.
[152] The optical rotation of the synthetic sample was positive, while that of the natural product was negative, thus indicating a 2*R* configuration for the naturally occurring diyne.
[153] I. W. Farrell, V. Thaller, J. L. Turner, *J. Chem. Soc. Perkin Trans. 1* **1977**, 1886 – 1888.
[154] A. G. M. Barrett, D. Hamprecht, M. Ohkubo, *J. Org. Chem.* **1997**, *62*, 9376 – 9378.
[155] X. Wei, R. J. K. Taylor, *Tetrahedron Lett.* **1998**, *39*, 3815 – 3818.
[156] a) F. Bohlmann, H. Bornowski, K.-M. Kleine, *Chem. Ber.* **1964**, *97*, 2135 – 2138; b) F. Bohlmann, C. Arndt, K.-M. Kleine, M. Wotschokowsky, *Chem. Ber.* **1965**, *98*, 1228 – 1232.
[157] T. Luu, W. Shi, T. L. Lowary, R. R. Tykwinski, *Synthesis* **2005**, 3167 – 3178.
[158] F. Bohlmann, W. von Kap-Herr, L. Fanghänel, C. Arndt, *Chem. Ber.* **1965**, *98*, 1411 – 1415.
[159] J. T. Arnason, B. J. R. Philogène, C. Berg, A. MacEachern, J. Kaminski, L. C. Leitch, P. Morand, J. Lam, *Phytochemistry* **1986**, *25*, 1609 – 1611.
[160] C. Chin, E. R. H. Jones, V. Thaller, R. T. Aplin, L. J. Durham, S. C. Cascon, W. B. Mors, B. M. Tursch, *J. Chem. Soc. Chem. Commun.* **1965**, 152 – 154.
[161] S. C. Cascon, W. B. Mors, B. M. Tursch, R. T. Aplin, L. J. Durham, *J. Am. Chem. Soc.* **1965**, *87*, 5237 – 5241.
[162] C. Mukai, N. Miyakoshi, M. Hanaoka, *J. Org. Chem.* **2001**, *66*, 5875 – 5880.
[163] A. Ito, B. Cui, D. Chávez, H.-B. Chai, Y. G. Shin, K. Kawanishi, L. B. S. Kardono, S. Riswan, N. R. Farnsworth, G. A. Cordell, J. M. Pezzuto, A. D. Kinghorn, *J. Nat. Prod.* **2001**, *64*, 246 – 248.
[164] B. W. Gung, G. Kumi, *J. Org. Chem.* **2004**, *69*, 3488 – 3492.
[165] S. Kim, S. Kim, T. Lee, H. Ko, D. Kim, *Org. Lett.* **2004**, *6*, 3601 – 3604.
[166] E. R. H. Jones, J. D. Bu'Lock, *J. Chem. Soc.* **1953**, 3719 – 3720.
[167] R. Jente, F. Bosold, J. Bäuerle, T. Anke, *Phytochemistry* **1985**, *24*, 553 – 559.
[168] M. Ahmed, J. W. Keeping, T. A. Macrides, V. Thaller, *J. Chem. Soc. Perkin Trans. 1* **1978**, 1487 – 1489.
[169] K. Green, J. W. Keeping, V. Thaller, *J. Chem. Res. Synop.* **1985**, 103 – 103; K. Green, J. W. Keeping, V. Thaller, *J. Chem. Res. Miniprint* **1985**, 1260 – 1267.
[170] R. C. Cambie, J. N. Gardner, E. R. H. Jones, G. Lowe, G. Read, *J. Chem. Soc.* **1963**, 2056 – 2064.

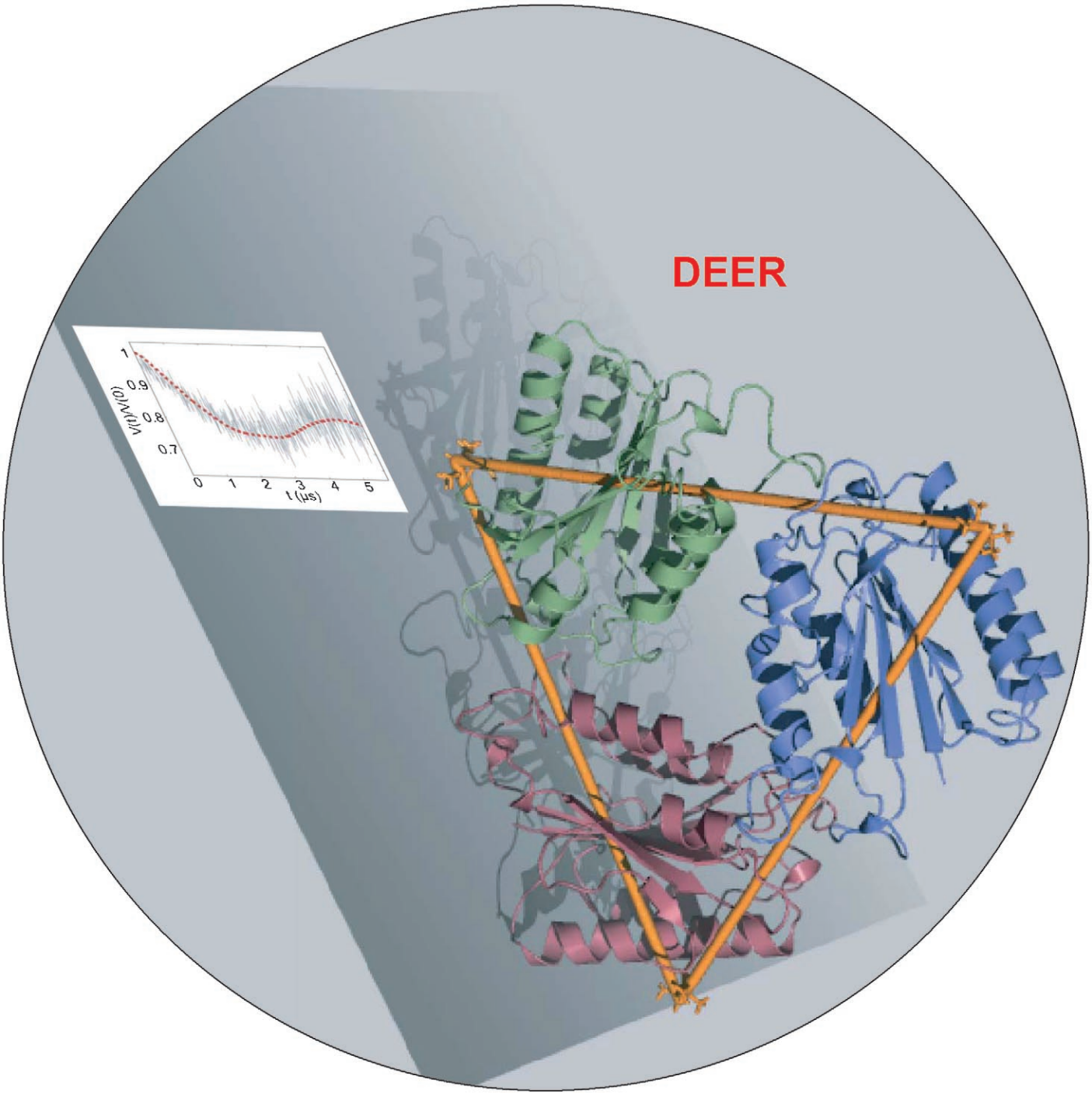
 © 2006 Wiley-VCH Verlag GmbH & Co. KGaA, Weinheim

[171] E. R. H. Jones, T. A. Macrides, V. Thaller, *J. Chem. Res. Synop.* **1981**, 157; E. R. H. Jones, T. A. Macrides, V. Thaller, *J. Chem. Res. Miniprint* **1981**, 2017 – 2030.
[172] M. T. W. Hearn, E. R. H. Jones, M. G. Pellatt, V. Thaller, J. L. Turner, *J. Chem. Soc. Perkin Trans. 1* **1973**, 2785 – 2788.
[173] M. Ahmed, M. Y. Jarrah, E. R. H. Jones, A. F. Magalhães, M. G. Roberts, V. Thaller, *J. Chem. Res. Synop.* **1981**, 262 – 263; M. Ahmed, M. Y. Jarrah, E. R. H. Jones, A. F. Magalhães, M. G. Roberts, V. Thaller, *J. Chem. Res. Miniprint* **1981**, 3261 – 3278.
[174] M. D. Lewis, R. Menes, *Tetrahedron Lett.* **1987**, *28*, 5129 – 5132.
[175] J. J. Wright, M. S. Puar, B. Pramanik, A. Fishman, *J. Chem. Soc. Chem. Commun.* **1988**, 413 – 414.
[176] M. D. Greenspan, J. B. Yudkovitz, J. S. Chen, D. P. Hanf, M. N. Chang, P. Y. C. Chiang, J. C. Chabala, A. W. Alberts, *Biochem. Biophys. Res. Commun.* **1989**, *163*, 548 – 553.
[177] M. D. Lewis, J. P. Duffy, J. V. Heck, R. Menes, *Tetrahedron Lett.* **1988**, *29*, 2279 – 2282.
[178] J. S. Yadav, D. Rajagopal, *Tetrahedron Lett.* **1990**, *31*, 5077 – 5080.
[179] Isolation, see: R. J. Marles, N. R. Farnsworth, D. A. Neill, *J. Nat. Prod.* **1989**, *52*, 261 – 266; for the determination of the absolute configuration, see: H. B. Rasmussen, S. B. Christensen, L. P. Kvist, A. Kharazmi, A. G. Huansi, *J. Nat. Prod.* **2000**, *63*, 1295 – 1296.
[180] M. A. Rashid, K. R. Gustafson, J. H. Cardellina II, M. R. Boyd, *Nat. Prod. Lett.* **2001**, *13*, 21 – 26.
[181] B. W. Gung, H. Dickson, *Org. Lett.* **2002**, *4*, 2517 – 2519.
[182] B. W. Gung, G. Kumi, *J. Org. Chem.* **2003**, *68*, 5956 – 5960.
[183] T. Kusumi, I. Ohtani, K. Nishiyama, H. Kakisawa, *Tetrahedron Lett.* **1987**, *28*, 3981 – 3984.
[184] a) M. Yamaguchi, H.-J. Park, M. Hirama, K. Torisu, S. Nakamura, T. Minami, H. Nishihara, T. Hiraoka, *Bull. Chem. Soc. Jpn.* **1994**, *67*, 1717 – 1725; b) M. Yamaguchi, H.-J. Park, S. Ishizuka, K. Omata, M. Hirama, *J. Med. Chem.* **1995**, *38*, 5015 – 5022.

 © 2006 Wiley-VCH Verlag GmbH & Co. KGaA, Weinheim

Communications

DOI: 10.1002/anie.200503720



Using double electron electron resonance (DEER) spectroscopy, a distance of 6.15 nm is measured between the nitroxide labels of von Willebrand Factor A domains. The picture shows the DEER spectrum and the trimeric structure of the protein that is deduced from the DEER results. For more information see the Communication by G. Jeschke and co-workers on the following pages.

WILEY InterScience DISCOVER SOMETHING GREAT
© 2006 Wiley-VCH Verlag GmbH & Co. KGaA, Weinheim

EPR Spectroscopy

DOI: 10.1002/anie.200503720

The Characterization of Weak Protein–Protein Interactions: Evidence from DEER for the Trimerization of a von Willebrand Factor A Domain in Solution**

*Janet E. Banham, Christiane R. Timmel, Rachel J. M. Abbott, Susan M. Lea, and Gunnar Jeschke**

Noncovalent ("weak") interactions between biological or synthetic macromolecules in solution are difficult to characterize with established techniques. On the other hand, noncovalent protein–protein interactions are increasingly recognized to be very important with many functional processes relying upon them, additionally such interactions between synthetic macromolecules are the basis of self-assembly.[1,2] Herein we extend the current toolbox of methods for studying weakly interacting macromolecules in dilute solutions to include the pulsed electron paramagnetic resonance (EPR) method of double electron electron resonance (DEER). DEER is a complementary technique to Förster resonant energy transfer (FRET), which is widely used for studying protein–protein interactions.[3] Both methods follow a similar strategy of labeling the target molecules (with fluorescence or paramagnetic labels, for FRET or DEER, respectively), but while FRET requires two different relatively large chromophores, which must be chosen according to the expected distance, DEER distance measurements can be performed between two identical much smaller (nitroxide) labels and are precise over a broader range of distances.[4,5] However, EPR spectroscopy is less sensitive than FRET. The sensitivity limitation translates into a limitation to shorter distances, as longer distances correspond to weaker couplings between the two probes. Consequently generally shorter distances have been measured by EPR techniques than are accessible by FRET. Herein we demonstrate a DEER measurement of a distance of 6.15 nm in nitroxide spin-labeled human von Willebrand Factor A domain (vWF-A) from the complement component Factor B. The distance is the longest measured to date by an EPR method with proteins and is consistent with the trimerization of the isolated Factor B vWF-A in dilute solution, such a trimerization normally occurs when this protein is crystallized.[6]

The DEER experiment measures the dipolar coupling between paramagnetic centers as a modulation of the electron spin echo decay.[7] If the paramagnetic centers can be approximated as point dipoles (as is the case for nitroxide radicals) the distance between the spin centers, r (in nm), can be related to the signal's modulation frequency, ν (in MHz), using Equation (1).[4]

$$r = \left[\frac{52.04}{\nu}\right]^{1/3} \quad (1)$$

The maximum distance that can be measured using DEER and other pulsed EPR techniques (such as, double quantum coherence (DQC))[8] is determined by the maximum dipolar evolution time at which a signal can still be observed and thus by the phase memory time, T_m of the electron spins. To date, the longest distances measured by pulsed EPR techniques have been 7.5 nm for DEER of a rigid biradical[5] and 7.0 nm for the DQC of a rigid RNA sample.[9] These were unique experiments on model systems to test the scope of the techniques. Other DEER measurements on biomacromolecules provided distances of up to 5.25 nm for DNA model systems[10] and a distance estimate of roughly 6.1 nm for a trimer of singly spin-labeled plant light-harvesting complex IIb (LHCIIb).[11] For the LHCIIb case, no precise distance could be given because T_m was too short to allow for the measurement of a full dipolar oscillation. At low temperatures (relaxation is dominated by proton spin diffusion) T_m, and therefore the maximum dipolar evolution time, can be increased by up to seven times upon total deuteration of the solvent matrix and sample.[5]

vWF-A domains are found in many extracellular or cell-surface proteins and are used to mediate protein–protein interactions. Protein–protein interactions of the Factor B vWF-A domain are important in regulation of the innate immune system. We have therefore expressed and spin-labeled Factor B vWF-A with a methane thiosulfonate nitroxide spin label (MTSSL). The nitroxide label will react specifically with cysteine 267 to provide one single label per molecule. The protein was transferred into a mixture of 60% D_2O (with 50 mM tris(hydroxymethyl)aminomethane (Tris) buffer) and 40% deuterated glycerol which led to a doubling of T_m compared to the value in protonated buffers and thus allowed the dipolar evolution time to be extended to 6 μs. This time is long enough to see a complete oscillation for distances up to about 6.8 nm. The protein concentration was varied between 45 and 180 μM and measurements were repeated with 250 and 500 mM NaCl added to the buffer.

[*] Dr. G. Jeschke
Max Planck Institut für Polymerforschung
Postfach 3148, 55021 Mainz (Germany)
Fax: (+49) 6131-379-100
E-mail: jeschke@mpip-mainz.mpg.de
R. J. M. Abbott, Dr. S. M. Lea
Laboratory of Molecular Biophysics
Department of Biochemistry
University of Oxford, Oxford, OX1 3QU (UK)
Dr. C. R. Timmel
Inorganic Chemistry Laboratory
University of Oxford, Oxford, OX1 3QR (UK)
J. E. Banham
Physical and Theoretical Chemistry Laboratory
University of Oxford, Oxford, OX1 3QZ (UK)

[**] J.E.B. is supported by a studentship from the Engineering and Physical Science Research Council and RJMA by a studentship from the Medical Research Council. C.R.T. would like to thank the Royal Society for a University Research Fellowship. C. Bauer is thanked for technical support. DEER = double electron electron resonance.

 © 2006 Wiley-VCH Verlag GmbH & Co. KGaA, Weinheim

Figure 1a shows the typical result from the DEER experiment. A modulation of the detected echo can be seen and this is evidence that the vWF-A is forming an aggregate. Inspection of the data with the home-written program

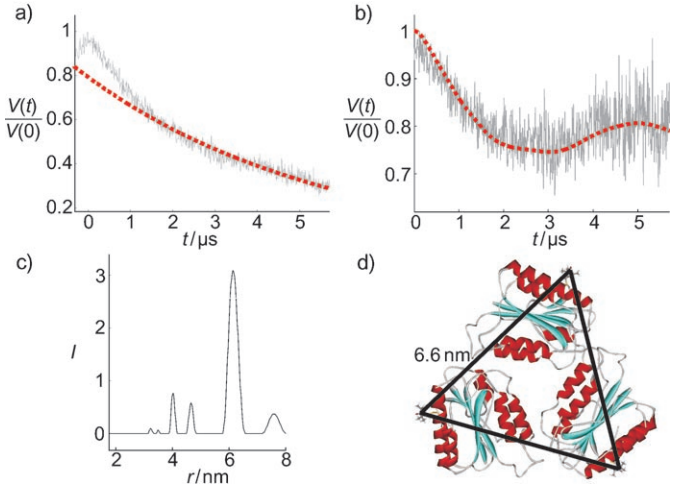


Figure 1. The DEER measurement (180 μM protein in deuterated water and glycerol, as described in the text), analysis and proposed structure of vWF-A. a) Experimental data (gray) and the exponentially decaying background arising from remote spins, as fitted by DeerAnalysis 2004 (red). b) Background corrected experimental data (gray) and fit by the Tikhonov regularization (red). c) Distance distribution. d) The structure of a trimer which contains spin labels. The distance shown (black lines) between spin labels is one contribution to the anticipated distribution: there is expected to be considerable flexibility of the label and protein structure.

DeerAnalysis2004,[12] using Tikhonov regularization in the distance domain with a regularization parameter of 10, gives the same main distance between spin centers of (6.15 ± 0.14) nm for all the protein and salt concentrations studied, irrespective of whether the constant-time or variable-time DEER experiment is used.[5,13] The background corrected data and distance distribution are shown in Figure 1b and Figure 1c. Smaller peaks corresponding to shorter and longer distances are due to noise and limitations of the background correction and differ between different measurements.

Expanding the symmetry of the X-ray structure of Factor B vWF-A (1Q0P.pdb) shows that the crystal is formed by stacking trimers of the protein.[6] The crystal structure was obtained for the Cys267Ser mutant to avoid interprotein disulfide bridges. Deep View–spdbv3.7 was used to change the Ser back to a Cys and to add MTSSL to it in the structural model.[14] The distance between the C_α sites of the labeling positions is 5.77 nm. When the nitroxide spin label was added, the C_β–S bond torsion angle was optimized such that interactions with the protein structure were minimized. This approach gave a distance of 6.6 nm between the centers of N–O bonds in the nitroxide (Figure 1d). As the spin label is flexible and the temperature factor in the X-ray structure for the C_β atom of the Ser267 side-chain is as large as 51 Å^2, the deviation between this prediction and our measured data can be easily reconciled with the notion that the same type of trimer found in the crystal structure is also formed in solution. Note however that formation of a trimer rather than a dimer could not be demonstrated unequivocally by the DEER modulation depth as there is an equilibrium between monomer and oligomer.

In conclusion, four-pulse DEER in its constant- and variable-time versions has been used to measure a distance of (6.15 ± 0.14) nm in a frozen solution of Factor B vWF-A. This is the longest distance measured in a solution of a non-covalently bound protein–protein complex with EPR. The measurement is consistent with formation of vWF-A trimers in solution, as also happens during crystallization. Despite the observation of this interaction in relatively dilute solution there is no evidence to date that trimerization of this domain has any physiological role (presumably this domain is not free to associate in this way in the context of intact Factor B) nor has there been any prior detection of trimers of this isolated domain in solution. We envisage that the technique will be useful for detecting a diverse range of molecular interactions from proteins to the self-assembly of synthetic macromolecules in solution.

Experimental Section

Protein preparation: Recombinant vWF-A domain of human Factor B was expressed in *E. coli* as a fusion protein with glutathione *S*-transferase using published methods.[15] The purification procedure was modified to enable the protein to be labeled (for example, the iodoacetamide was omitted from the cell lysis buffer to leave the cysteine residue free to react with the nitroxide label). The methanethiosulfonate (Toronto Research Chemicals) spin label and protein were left to react for two hours at room temperature before adding 400 U of human thrombin in phosphate buffered saline (PBS; 5 mL) and leaving for a further 16 h. The excess spin label and unwanted proteins were removed by washing through GSTrap and HiTrap Benzamidine FF columns with 20 mM sodium phosphate, 0.15 M NaCl, pH 7.5. After this procedure came a second wash step with a high-salt buffer (20 mM sodium phosphate, 1.0 M NaCl, pH 7.5). The collected fractions, containing vWF-A, were then concentrated and further purified with gel filtration on a S75 column (Amersham Biosciences).

DEER experiments: Four-pulse DEER experiments with the sequence $\pi/2(\nu_{obs})$-τ_1-$\pi(\nu_{obs})$-t'-$\pi(\nu_{pump})$-$(\tau_1+\tau_2-t')$-$\pi(\nu_{obs})$-τ_2-*echo* at X-band frequencies (≈9.5 GHz) were performed at 50 K with observer frequency pulses of 32 ns, the pump pulse was at 65 MHz lower frequency with a π pulse length of 12 ns.[13] The resonator was overcoupled ($Q \approx 100$) and the pump pulse coincided with both the center of the microwave mode of the resonator and the maximum of the nitroxide spectrum. Proton and deuterium modulations were minimized by adding eight data sets with variable delay τ_1, starting at 400 ns and using an increment $\Delta\tau_1 = 16$ ns. The delay τ_2 between the first Hahn echo and the final observer pulse was 6 μs, data traces had 755 points with an increment $\Delta t = 8$ ns. The spectrum shown in Figure 1a was accumulated overnight. In data processing with the home-written program DeerAnalysis 2004 an exponential background correction was used.[16]

Received: October 20, 2005
Published online: January 10, 2006

Keywords: DEER · EPR spectroscopy · noncovalent interactions · proteins · structure elucidation

 © 2006 Wiley-VCH Verlag GmbH & Co. KGaA, Weinheim

[1] S. J. Davis, S. Ikemizu, E. J. Evans, L. Fugger, T. Bakker, A. P. van der Merwe, *Nat. Immunol.* **2003**, *4*, 217.
[2] H. M. Keizer, R. P. Sijbesma, *Chem. Soc. Rev.* **2005**, *34*, 226.
[3] Y. Yan, G. Marriott, *Curr. Opin. Chem. Biol.* **2003**, *7*, 635.
[4] G. Jeschke, *ChemPhysChem* **2002**, *3*, 927.
[5] G. Jeschke, A. Bender, H. Paulsen, H. Zimmermann, A. Godt, *J. Magn. Reson.* **2004**, *169*, 1.
[6] A. A. Bhattacharya, M. L. Lupher, D. E. Staunton, R. C. Liddington, *Structure* **2004**, *12*, 371.
[7] A. D. Milov, K. M. Salikhov, M. D. Shirov, *Fiz. Tverd. Tela* **1981**, *23*, 975.
[8] P. P. Borbat, J. H. Freed, *Chem. Phys. Lett.* **1999**, *313*, 145.
[9] P. P. Borbat, J. H. Davis, S. E. Butcher, J. H. Freed, *J. Am. Chem. Soc.* **2004**, *126*, 7746.
[10] O. Schiemann, N. Piton, Y. Mu, G. Stock, J. W. Engels, T. F. Prisner, *J. Am. Chem. Soc.* **2004**, *126*, 5724.
[11] G. Jeschke, A. Bender, T. Schweikardt, G. Panek, H. Decker, H. Paulsen, *J. Biol. Chem.* **2005**, *280*, 18623.
[12] G. Jeschke, G. Panek, A. Godt, A. Bender, H. Paulsen, *Appl. Magn. Reson.* **2004**, *26*, 223.
[13] M. Pannier, S. Veit, A. Godt, G. Jeschke, H. W. Spiess, *J. Magn. Reson.* **2000**, *142*, 331.
[14] N. Guex, M. C. Peitsch, *Electrophoresis* **1997**, *18*, 2714.
[15] S. C. Williams, J. Hinshelwood, S. J. Perkins, R. B. Sim, *Biochem. J.* **1999**, *342*, 625.
[16] See: http://www.mpip-mainz.mpg.de/~jeschke/distance.html.

 © 2006 Wiley-VCH Verlag GmbH & Co. KGaA, Weinheim

Coal Liquefaction

DOI: 10.1002/anie.200502614

The First Liquefaction of High-Rank Bituminous Coals by Preceding Hydrogenation with Homogeneous Borane or Iodine Catalysts**

Matthias W. Haenel, Janchig Narangerel, Udo-Burckhard Richter, and Anna Rufińska*

Dedicated to Professor Günther Wilke on the occasion of his 80th birthday

The prospect that the world's petroleum reserves will be depleted within a few decades has caused the price of oil to escalate. Hence the more abundant coal might become economically competitive as a source for liquid fuels and chemicals. The Bergius direct coal liquefaction and the indirect liquefaction consisting of coal gasification and Fischer–Tropsch synthesis are two fundamental Coal-To-Liquid technologies that have been available since the first half of the last century.[1] Direct liquefaction is a hydrocracking process by which coal is converted at 450 °C under hydrogen pressures of >30 MPa in the presence of a process-derived solvent and a heterogeneous catalyst (mainly iron oxides and sulfides).[1,2] For the thermal C–C bond breaking and the transfer of hydrogen to carbon radicals, the solvent plays a main role ("hydrogen shuttling" and "hydrogen donation").[3] On the other hand, in the initial liquefaction stage the efficiency of the catalyst is low, mainly because a heterogeneous inorganic solid cannot penetrate the macromolecular network structure of insoluble coal.[4] The expectation that a homogeneous catalyst would be more suitable in this regard[5] prompted us some time ago to investigate the hydrogenation/hydrogenolysis of coals with borane catalysts.[6] This led to the first example of an effective homogeneous hydrogenation of coal and opened a route for the subsequent liquefaction of high-rank bituminous coals, which up to now can be processed only by combustion or gasification.

At $T>200$ °C trialkylboranes and tetraalkyldiboranes can be used as homogeneous catalysts for the hydrogenation of olefins[7] and polycyclic aromatic hydrocarbons[8,9] including coal tar pitch[10] and for the hydrogenolytic cleavage of C–C bonds, in particular the C_{arom}–C_{aliph} bonds of diarylmethanes and 1,2-diarylethanes.[8,11] But whereas a cross-linked insoluble polystyrene was degraded with hydrogen in presence of triethylborane forming benzene and various alkylbenzenes, no reaction occurred with bituminous coal.[8,12] However, by using iododi-*n*-propylborane (nPr$_2$BI, DPIB)[13] we observed the hydrogenation/hydrogenolysis of bituminous coals under non-liquefaction conditions ($T<350$ °C, no hydrogen-donor solvent). The product obtained by stirring a suspension of a medium-volatile bituminous coal [mvb coal, German Fettkohle (coking coal)] in toluene together with DPIB for 48 h at 280 °C under hydrogen (15 MPa initial pressure at RT) was still a solid, but its solubility in pyridine, relative to that of the original coal, had changed from 13 % to 91 % and the C/H ratio from $C_{100}H_{63}$ to $C_{100}H_{99}$ (Table 1, entries 1 and 4). The dramatically increased solubility is attributed to hydrogenolytic cleavage of C_{arom}–C_{aliph} bonds disrupting the network structure of coal as well as to partial hydrogenation of polycyclic aromatic units. The latter leads to an increase of aliphatic carbon atoms at the expense of aromatic carbon atoms, as shown by the solid-state ^{13}C CP/MAS NMR spectra (Figure 1 a,d; CP = cross polarization, MAS = magic angle spinning). The C_{aliph}/C_{arom} ratio increased from 20:80 in the original mvb coal to 40:60 in the product.

The ^{13}C CP/MAS NMR spectra of the products from control experiments without any catalyst or with iodine (50 mol % compared to DPIB) as catalyst showed only a very low or modest increase of the C_{aliph}/C_{arom} ratio from 20:80 to 22:78 or 27:73, respectively (Figure 1 b,c and Table 1, entries 2 and 3). It has been known for a long time that iodine in various forms promotes coal liquefaction,[14] but comparison of spectra (c) and (d) clearly shows that the activity of DPIB

[*] Prof. Dr. M. W. Haenel, Dr. J. Narangerel, Ing. grad. U.-B. Richter, Dr. A. Rufińska
Max-Planck-Institut für Kohlenforschung
Kaiser-Wilhelm-Platz 1, 45470 Mülheim an der Ruhr (Germany)
Fax: (+49) 208 306–2980
E-mail: haenel@mpi-muelheim.mpg.de

[**] The work was supported by the German Academic Exchange Service and the German Research Foundation (scholarships to J.N.).

Supporting information for this article is available on the WWW under http://www.angewandte.org or from the author.

 © 2006 Wiley-VCH Verlag GmbH & Co. KGaA, Weinheim

Table 1: Conditions and results for the hydrogenation/hydrogenolysis of bituminous coals.[a]

Entry	Coal[b]	Cat. (mmol)	Pressure[c] H_2 [MPa]	T [°C]	t [h]	Sol.[d] [%]	C_{al}/C_{ar}[e]	C/H[f]
1	mvb coal[g]	–	–	–	–	13	20:80	$C_{100}H_{63}$
2	mvb coal	–	15	280	48	25	22:78	$C_{100}H_{81}$
3	mvb coal	I_2 (15)	15	280	48	64	27:73	$C_{100}H_{86}$
4	mvb coal	nPr_2BI (29.6)	15	280	48	91	40:60	$C_{100}H_{99}$
5	mvb coal	$NaBH_4/I_2$ (30/30)	15	280	12	86	35:65	$C_{100}H_{85}$
6	mvb coal	$NaBH_4/I_2$ (30/30)	15	280	48	92	40:60	$C_{100}H_{102}$
7	lvb coal[g]	–	–	–	–	<1	11:89	$C_{100}H_{51}$
8	lvb coal	–	25	350	6	5	12:88	$C_{100}H_{52}$
9	lvb coal	$NaBH_4/I_2$ (30/30)	25	350	3	55	41:59	$C_{100}H_{82}$
10	lvb coal	$NaBH_4/I_2$ (30/30)	25	350	6	69	46:54	$C_{100}H_{87}$
11	lvb coal	$NaBH_4/I_2$ (30/30)	25	350	12	80	51:49	$C_{100}H_{96}$
12	lvb coal	$NaBH_4/I_2$ (30/30)	25	350	24	86	60:40	$C_{100}H_{104}$
13	lvb coal	I_2 (30)	25	350	6	61	44:56	$C_{100}H_{86}$
14	lvb coal	I_2/TiI_4 (30/5)	25	350	6	76	58:42	$C_{100}H_{101}$
16	lvb coal	BI_3 (20)	25	350	6	89	59:41	$C_{100}H_{99}$
17	anthracite[g]	–	–	–	–	<1	<5:95	$C_{100}H_{40}$
18	anthracite	$NaBH_4/I_2$ (30/30)	25	350	12	27	39:61	$C_{100}H_{80}$
19	anthracite	$NaBH_4/I_2$ (30/30)	25	350	24	40	45:55	$C_{100}H_{82}$
20	anthracite	I_2 (30)	25	350	24	41	51:49	$C_{100}H_{90}$
21	anthracite	I_2/TiI_4 (30/5)	25	350	24	44	58:42	$C_{100}H_{90}$
22	anthracite	BI_3 (20)	25	350	24	52	62:38	$C_{100}H_{94}$

[a] Suspension of 40 g of coal in 150 mL of toluene, stirring autoclave with a volume of 500 mL. [b] Medium-volatile bituminous coal (mvb coal, Fettkohle), Westerholt Mine, Robert Seam: 23.6% volatile matter (daf), 89.4% C (daf), 4.5% ash (wf). Low-volatile bituminous coal (lvb coal, Magerkohle), Niederberg Mine: 11.2% volatile matter (daf), 91.2% C (daf), 7.1% ash (wf). Anthracite, Sophia Jacoba Mine: 7.4% volatile matter, 91.9% C (daf), 6.5% ash (wf). daf: dry and ash-free; wf: water-free. [c] Pressure of hydrogen at room temperature. [d] Solubility in pyridine as determined by Soxhlet extraction. [e] Ratio of aliphatic to aromatic carbon atoms from ^{13}C CP/MAS NMR solid-state spectra. [f] Carbon/hydrogen ratio from elemental analysis. [g] Untreated original coal.

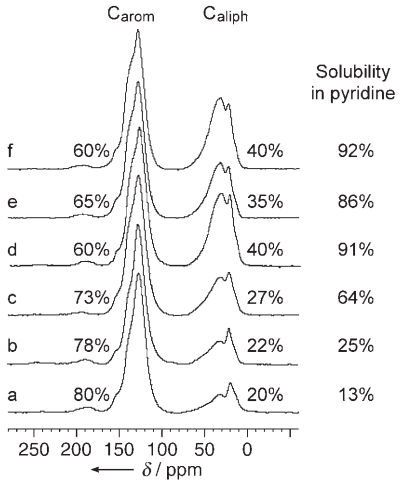


Figure 1. ^{13}C CP/MAS NMR spectra (solid state, 75 MHz) and solubility in pyridine of a) the original mvb coal (German Fettkohle, Westerholt Mine, Robert Seam, Table 1) and b–f) the products obtained by hydrogenation (15 MPa H_2, 280°C, toluene): b) without a catalyst, 48 h; c) with I_2, 48 h; d) with DPIB, 48 h; e) with $NaBH_4/I_2$, 12 h; f) with $NaBH_4/I_2$, 48 h. The spectra were calibrated to equal intensities of the signals for C_{arom}.

cannot be attributed solely to its iodine.[15] An equimolar mixture of sodium borohydride and iodine can be used conveniently to generate an iodoborane catalyst in situ, which was found to be as active as DPIB (Figure 1e,f and Table 1, entries 5 and 6).[16]

The IR spectrum (KBr) of the coal product obtained by hydrogenation with DPIB showed, in comparison to the original mvb coal, the relative decrease of the aromatic C–H stretching (3040 cm^{-1}) vibration and the increase of the symmetrical and asymmetrical aliphatic C–H stretching vibrations (2950–2850 cm^{-1}). But there was also a notable decrease of the broad, weakly structured bands of C–O stretching vibrations between 1300 and 1000 cm^{-1}.[17] In the course of the hydrogenation apparently some oxygen-containing functional groups in the coal, mainly phenolic ether links,[4,15a] were removed by stoichiometric reactions with the borane catalyst, which is thus consumed and converted into borates.[18] Since during geochemical coalification, the number of oxygen-containing functional groups in coals decreases, high-rank bituminous coals have the lowest oxygen content.[4] Hence one could assume that the high-rank bituminous coals in particular, even though they are generally considered to be less reactive, might be the most appropriate for the borane-catalyzed hydrogenation.

Indeed, a low-volatile bituminous coal (lvb coal, German Magerkohle) suspended in toluene was hydrogenated under more drastic conditions (350°C, 25 MPa H_2). Whereas the control reaction (no catalyst, 6 h) resulted in only small changes of C_{aliph}/C_{arom} ratio and the solubility (Figure 2a,b, Table 1, entries 7 and 8), extensive hydrogenation/hydrogenolysis was observed in the presence of equimolar $NaBH_4/I_2$. With increasing reaction times (3, 6, 12, and 24 h) the C_{aliph}/C_{arom} ratio increased from 11:89 in the original lvb coal to 60:40 in the product obtained from the hydrogenation after 24 h, and concomitantly the solubility in pyridine increased

 © 2006 Wiley-VCH Verlag GmbH & Co. KGaA, Weinheim

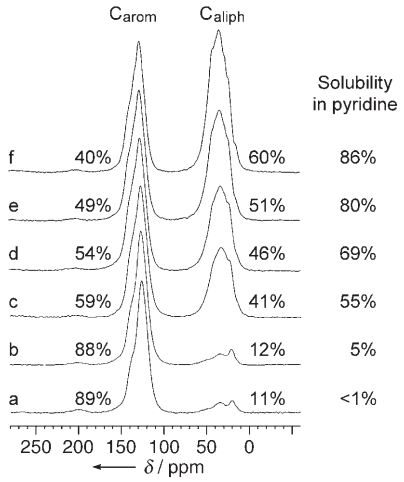


Figure 2. ^{13}C CP/MAS NMR spectra (solid state, 75 MHz) and solubility in pyridine of a) the original lvb coal (German Magerkohle, Niederberg Mine, Table 1) and b–f) the products obtained by hydrogenation (25 MPa H_2, 350 °C, toluene): b) without a catalyst, 6 h; c–f) with $NaBH_4/I_2$ for 3, 6, 12, and 24 h, respectively. The spectra were calibrated to equal intensities of the signals for C_{arom}.

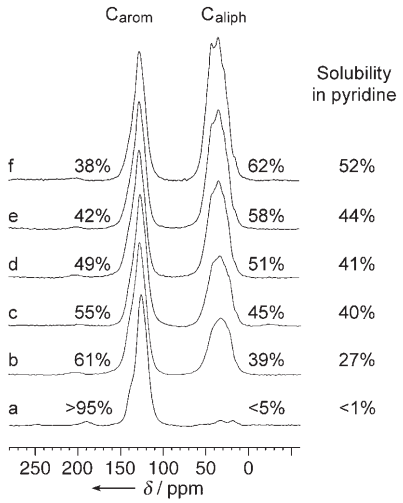


Figure 3. ^{13}C CP/MAS NMR spectra (solid state, 75 MHz) and solubility in pyridine of a) the original German anthracite (Sophia Jacoba Mine, Table 1) and b–f) the products obtained by hydrogenation (25 MPa H_2, 350 °C, toluene): b) with $NaBH_4/I_2$, 12 h; c) with $NaBH_4/I_2$, 24 h; d) with I_2, 24 h; e) with I_2/TiI_4, 24 h; f) with BI_3, 24 h. The spectra were calibrated to equal intensities of the signals for C_{arom}.

from $<1\%$ to 86% (Figure 2a,c–f, Table 1, entries 7 and 9–12). Surprisingly, under the more drastic conditions (25 MPa H_2, 350 °C) iodine alone showed almost the same catalytic activity as equimolar $NaBH_4/I_2$ in the hydrogenation of lvb coal for 6 h (Table 1, entries 13 and 10).[19] The addition of titanium tetraiodide (17 mol% relative to I_2) raised the activity of iodine to such an extent that this boron-free catalyst became more active than equimolar $NaBH_4/I_2$ (cf. entries 14 and 12 keeping the reaction times of 6 and 24 h in mind). However, the best catalyst so far was found to be boron triiodide, which after a hydrogenation time of 6 h gave a product that was highly aliphatic ($C_{aliph}/C_{arom} = 59:41$) and 89% soluble in pyridine (entry 16).[19]

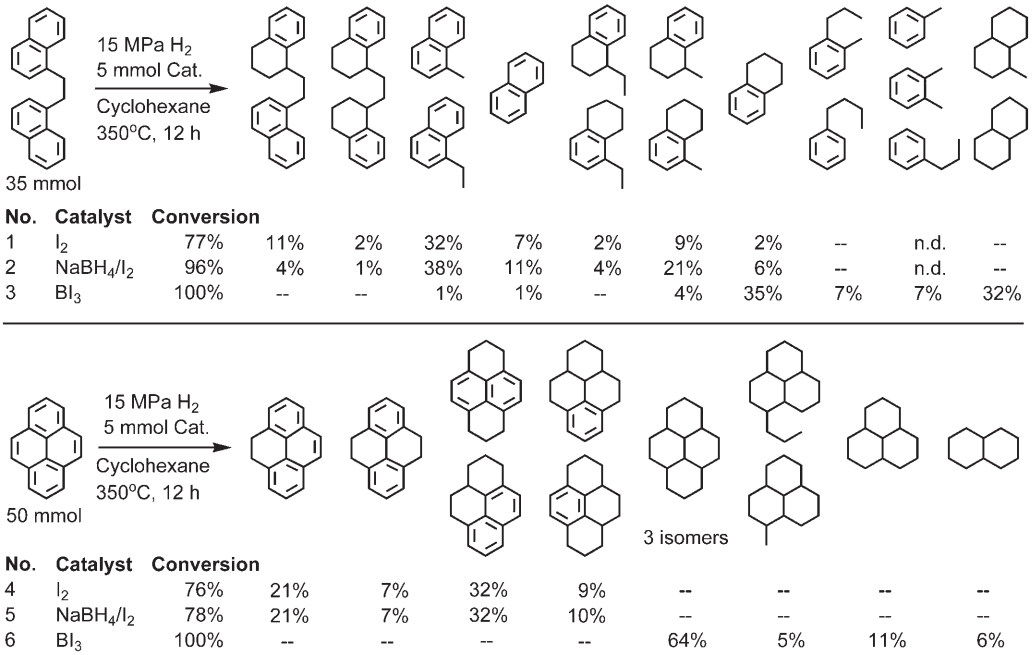
A special challenge is the hydrogenation of anthracites, which represent the high end of the rank range and are distinguished by having the highest C/H and lowest C_{aliph}/C_{arom} ratios of all coals.[4,20] In comparison to the lvb coal the hydrogenation of a German anthracite (toluene, 25 MPa H_2, 350 °C) required considerably longer reaction times but still resulted in the strong increase of aliphatic structures. With equimolar $NaBH_4/I_2$ as the catalyst, the C_{aliph}/C_{arom} ratio increased from $<5:95$ in the original anthracite to 39:61 and 45:55 after reaction times of 12 h and 24 h, respectively (Figure 3a–c, Table 1, entries 17–19). For the hydrogenation of anthracite, iodine alone was even somewhat more active than equimolar $NaBH_4/I_2$ (24 h: $C_{aliph}/C_{arom} = 51:49$; entry 20, Figure 3d), and the activity also increased further by addition of TiI_4 ($C_{aliph}/C_{arom} = 58:42$; entry 21, Figure 3e). However, as in the case of the lvb coal, BI_3 was the best catalyst and led to $C_{aliph}/C_{arom} = 62:38$ in 24 h (entry 22, Figure 3f).[19] This product, despite of the high aliphatic portion, was only 52% soluble in pyridine, and generally the solubility of the hydrogenated products of anthracite was lower than those of the lvb coal.

The number of catalytic cycles for the hydrogen uptake of the coals can be calculated from the change in the C/H ratios determined by elemental analysis (Table 1, last column) and the amount of catalyst. The number of catalytic cycles is about 20 in the case mvb coal and 28–43 in the case of lvb coal or anthracite. The pressure drop of 4–6 MPa observed during the coal hydrogenations corresponds surprisingly well to the amount of hydrogen calculated from the elemental analysis for the hydrogen uptake of the coals. This indicated a sufficient stability of the solvent, and accordingly the toluene recovered from the hydrogenations also contained only traces of methylcyclohexane, benzene, and cyclohexane.

In investigations of model compounds, the three catalysts iodine, equimolar $NaBH_4/I_2$, and boron triiodide showed remarkable differences in yields and product distributions (Scheme 1). The catalytic reactions of 1,2-di(1-naphthyl)-ethane with hydrogen (15 MPa, cyclohexane,[17] 350 °C, 12 h) resulted in hydrogenolytic C–C bond cleavages at the aliphatic link and hydrogenation of naphthalene units. With iodine or equimolar $NaBH_4/I_2$ as the catalyst, naphthalene was hydrogenated only partially to tetralin leaving one intact benzene ring.[8,9] In contrast, the reactions with the boron triiodide catalyst led not only to a higher conversion and extent of cleavage but also to the hydrogenation and hydrogenolytic degradation of tetralin units forming decalins and alkylbenzenes, respectively. This difference was even more pronounced in the case of the polycyclic aromatic hydrocarbon pyrene. The hydrogenation with iodine or equimolar $NaBH_4/I_2$ gave mixtures of di-, tetra-, hexa-, and decahydropyrenes, but with boron triiodide the pyrene was completely converted into aliphatic compounds, mainly perhydropyrenes and compounds formed by subsequent hydrogenolytic degradation (Scheme 1).[17]

The Bergius process for direct coal liquefaction and all new related processes give liquids in satisfactory yields only for lignites (brown coals), subbituminous coals, and low-rank bituminous coals such as high-volatile bituminous (hvb) coals.

 © 2006 Wiley-VCH Verlag GmbH & Co. KGaA, Weinheim

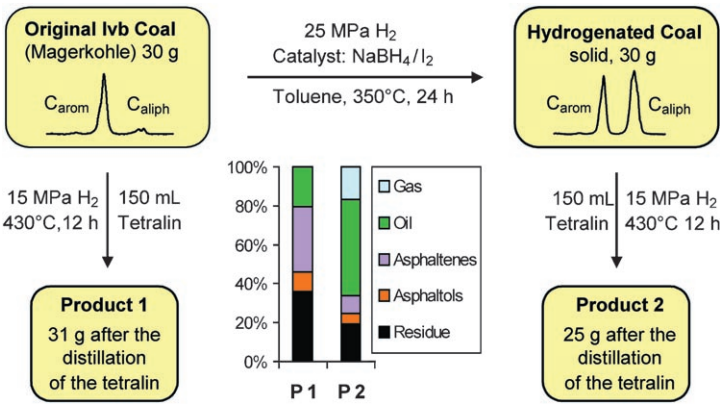


No.	Catalyst	Conversion										
1	I_2	77%	11%	2%	32%	7%	2%	9%	2%	--	n.d.	--
2	$NaBH_4/I_2$	96%	4%	1%	38%	11%	4%	21%	6%	--	n.d.	--
3	BI_3	100%	--	--	1%	1%	--	4%	35%	7%	7%	32%

No.	Catalyst	Conversion								
4	I_2	76%	21%	7%	32%	9%	--	--	--	--
5	$NaBH_4/I_2$	78%	21%	7%	32%	10%	--	--	--	--
6	BI_3	100%	--	--	--	--	64%	5%	11%	6%

Scheme 1. Hydrogenation/hydrogenolysis of 1,2-di(1-naphthyl)ethane and pyrene using I_2, $NaBH_4/I_2$, and BI_3 as the catalysts (15 MPa H_2, cyclohexane, 350 °C, 12 h). Product analysis by GC and GC/MS. If two or three products are listed in a column, the sum of the yields are given. n.d.: not determined.

In contrast, high-rank bituminous coals (from mvb or coking coals to lvb coals), semi-anthracite, and anthracite are not reactive enough for such hydrocracking processes.[1,21] On the other hand, exactly these high-rank bituminous coals are, as shown, most suitable for the hydrogenation with homogeneous borane and iodine catalysts. As a result, the aliphatic portion of these coals is increased to such an extent that the subsequent conventional hydrocracking into liquid products might become possible. The feasibility of such a two-stage liquefaction process for high-rank coals was demonstrated on the example of the lvb coal (Magerkohle). For this purpose the original lvb coal having 11 % C_{aliph} and its hydrogenation product having 60 % C_{aliph} (obtained from the hydrogenation with equimolar $NaBH_4/I_2$, Table 1, entry 12) were compared with respect their reactivity towards a hydrocracking process (Scheme 2). The suspension of the coal or the hydrogenation product in tetralin, which is generally used to simulate a hydroaromatic recycling oil as the hydrogen-donor solvent in coal-liquefaction processes, was stirred without a catalyst under hydrogen (15 MPa initial pressure at RT) at 430 °C for 12 h.[17] After the tetralin had been distilled off, the product 1 of the original coal showed an increase in mass of 3 %, but product 2 of the hydrogenated coal showed a loss in mass of 17 %. Whereas the former is attributed to tetralin being adsorbed and/or bonded chemically as a result of radical reactions, in the latter case a conversion of coal into low-molecular-weight compounds, gas and volatile compounds, has taken place. Both products 1 and 2 were characterized by solvent fractionation, that is, consecutive extractions with pentane, toluene, and pyridine (Scheme 2).[22] Whereas the one-stage liquefaction of the lvb coal in tetralin gave oil, that is, compounds soluble in pentane, in only 20 % yield, the two-stage process produced gas and oil in 66 % yield (17 % gas and 49 % oil).[17]



Scheme 2. Comparison of the products obtained from the one-stage and the two-stage liquefaction of the lvb coal (German Magerkohle, Niederberg Mine, Table 1). "Gas": gas and volatile compounds that co-distilled with tetralin; "oil": soluble in pentane; "asphaltenes": insoluble in pentane but soluble in toluene; "asphaltols" (preasphaltenes): insoluble in toluene but soluble in pyridine; residue: insoluble in pyridine.[17] The ^{13}C CP/MAS NMR signals indicate C_{aliph}/C_{arom}.

In summary, it was shown that iodoboranes and iodine can be used as homogeneous catalysts to hydrogenate high-rank bituminous coals, including anthracite, resulting in a strong increase of the aliphatic at the expense of the aromatic structures of these coals. In our view this represents a first

 © 2006 Wiley-VCH Verlag GmbH & Co. KGaA, Weinheim

case of an extensive homogeneous and "real" coal hydrogenation in the sense of hydrogen addition to unsaturates of coal, and hence contrasts with coal liquefaction by hydrocracking. An iodoborane catalyst could simply be generated in situ from the equimolar mixture of sodium borohydride and iodine. Iodine itself, which is known for a long time to promote the liquefaction of low-rank coals,[14] was shown to be also useful as a homogeneous catalyst for hydrogenating high-rank bituminous coals under non-liquefaction conditions. By adding titanium tetraiodide the catalytic activity of iodine could be increased, but remained still lower than that of boron triiodide, the best catalyst so far. The hydrogenation of simple model compounds with different catalysts revealed remarkable differences in yields and product distributions, which to these details are unobtainable with coal. In view of the progress recently made in the transition and rare earth metal catalyzed hydroboration of alkenes[23] and borylation of C–H bonds,[24] combinations of boranes, iodine and various metal compounds appear to have good prospects to develop catalysts having activities high enough for applications. The homogeneous coal hydrogenation presented for the first time also enables high-rank bituminous coals to be liquefied in subsequent conventional hydrocracking processes, and thus might help to strengthen our potentialities of Coal-To-Liquid technologies.

Received: July 26, 2005
Published online: January 3, 2006

Keywords: boranes · coal liquefaction · homogeneous catalysis · hydrogenation · iodine

[1] F. Derbyshire, D. Gray in *Ullmann's Encyclopedia of Industrial Chemistry, 5th ed*, *Vol. A7*, VCH, Weinheim, **1986**, pp. 197–243.
[2] D. D. Whitehurst, M. L. Gorbaty in *Handbook of Heterogeneous Catalysis, Vol. 3* (Eds.: G. Ertl, H. Knözinger, J. Weitkamp), VCH, Weinheim, **1997**, pp. 2078–2090.
[3] J. R. Pullen in *Coal Science, Vol. 2* (Eds.: M. L. Gorbaty, J. W. Larsen, I. Wender), Academic Press, Orlando, **1983**, pp. 173–288; M. W. Haenel, G. Collin, M. Zander, *Erdoel Erdgas Kohle* **1989**, *105*, 131–138; M. L. Poutsma, *Energy Fuels* **1990**, *4*, 113–131; R. Malhotra, D. F. McMillen, *Energy Fuels* **1993**, *7*, 227–233; T. Autrey, E. A. Alborn, J. A. Franz, D. M. Camaioni, *Energy Fuels* **1995**, *9*, 420–428; P. E. Savage, *Energy Fuels* **1995**, *9*, 590–598, and references therein.
[4] For coal structure see for instance: J. C. Crelling, D. H. Sauter, R. V. Ramani, D. Leininger, B. Bonn, U. Bertmann, R. Reimert, W. Gatzka in *Ullmann's Encyclopedia of Industrial Chemistry, 5th ed.*, *Vol. A7*, VCH, Weinheim, **1986**, pp. 153–196; H. Given in *Coal Science, Vol. 3* (Eds.: M. L. Gorbaty, J. W. Larsen, I. Wender), Academic Press, Orlando, **1984**, pp. 63–252; M. W. Haenel, *Fuel* **1992**, *71*, 1211–1223; M. L. Gorbaty, *Fuel* **1994**, *73*, 1819–1828; K. H. van Heek, *Fuel* **2000**, *79*, 1–26.
[5] a) J. P. Collman, K. M. Kosydar, M. Bressan, W. Lamanna, T. Garret, *J. Am. Chem. Soc.* **1984**, *106*, 2569–2579; b) R. K. Hessley, J. W. Reasoner, J. T. Tiley, *Coal Science, An Introduction to Chemistry, Technology, and Utilization*, Wiley, New York, **1986**, pp. 143–145.
[6] Attempts of using homogeneous transition metal catalysts for coal hydrogenation were reported: N. Holy, T. Nalesnik, S. McClanahan, *Fuel* **1977**, *56*, 47–48; J. W. Larsen, L. W. Chang, *Fuel* **1978**, *57*, 57–58; "Organic Chemistry of Coal": J. L. Cox, W. A. Wilcox, G. L. Roberts, *ACS Symp. Ser.* **1978**, *71*, 187–206. Impregnation of coal with soluble transition-metal compounds was used to form highly dispersed heterogeneous catalyst particles during the liquefaction process: S. W. Weller, *Energy Fuels* **1994**, *8*, 415–420, and references therein.
[7] a) R. Köster, G. Bruno, P. Binger, *Justus Liebigs Ann. Chem.* **1961**, *644*, 1–22; E. J. DeWitt, F. L. Ramp, L. E. Trapasso, *J. Am. Chem. Soc.* **1961**, *83*, 4672; b) F. L. Ramp, E. J. DeWitt, L. E. Trapasso, *J. Org. Chem.* **1962**, *27*, 4368–4372.
[8] a) E. Osthaus, M. W. Haenel in *Coal Science and Technology*, *Vol. 11* (Eds.: J. A. Moulijn, K. A. Nater, H. A. G. Chermin), Elsevier, Amsterdam, **1987**, pp. 765–768 (Proc. 1987 Intern. Conf. Coal Sci.); b) E. Osthaus, Dissertation, Ruhr-Universität Bochum, **1986**.
[9] M. Yalpani, T. Lunow, R. Köster, *Chem. Ber.* **1989**, *122*, 687–693; M. Yalpani, R. Köster, *Chem. Ber.* **1990**, *123*, 719–724.
[10] M. Yalpani, R. Köster, M. W. Haenel, *Erdoel Kohle Erdgas Petrochem.* **1990**, *43*, 344–347.
[11] M. Yalpani, R. Köster, *Erdoel Kohle Erdgas Petrochem.* **1990**, *43*, 486–489.
[12] The hydrogenolytic cleavage of an insoluble cross-linked polystyrene indicates the homogeneous nature of the borane catalysts.[5a]
[13] Prepared according to the reaction: $(n\mathrm{Pr_2BH})_2 + I_2 \rightarrow 2\,n\mathrm{Pr_2BI} + H_2$; R. Köster, M. A. Grassberger, *Justus Liebigs Ann. Chem.* **1968**, *719*, 169–186.
[14] Ausgewählte Arbeiten: a) M. Berthelot, *Bull. Soc. Chim. Fr.* **1869**, *11*, 278–286; b) J. J. Th. M. Geerards, H. I. Waterman, D. W. van Krevelen, *Brennst.-Chem.* **1958**, *39*, 332–336; c) A. M. Vassallo, M. A. Wilson, M. I. Attalla, *Energy Fuels* **1988**, *2*, 539–547; d) P. S. Maa, L. W. Vernon, W. E. Winter, G. H. Singhal (Exxon Company), US 4824558, **1989** [*Chem. Abstr.* **1989**, *111*, 118070]; e) D. Fraenkel, V. R. Pradhan, J. W. Tierney, I. Wender, *Fuel* **1991**, *70*, 64–73; f) J. T. Joseph, J. E. Duffield, M. G. Davidson, *Energy Fuels* **1992**, *6*, 764–770, and references therein.
[15] a) The mvb coal used contains ca. 3 O atoms per 100 C atoms mainly in phenolic ether links. b) The increase of the solubility in pyridine from 13% to 64% (Table 1, entry 3) can be explained by acidic (HI) cleavage of ether links and/or hydrogenolytic cleavage of C_{arom}–C_{aliph} bonds (compare the studies of model compounds).
[16] The aim was the generation of H_2BI in analogy to the preparation of DPIB:[13] $NaBH_4 + I_2 \rightarrow NaI + H_2BI + H_2$. However, the reaction might be more complex: a) H. Nöth, H. Beyer, *Chem. Ber.* **1960**, *93*, 2251–2263; b) F. Klanberg, H. W. Kohlschütter, *Chem. Ber.* **1961**, *94*, 786–789; c) G. F. Freeguard, L. H. Long, *Chem. Ind.* **1965**, 471; d) R. W. Jotham, L. H. Long, *Chem. Commun.* **1967**, 1288–1289; e) K. Kinberger, W. Siebert, *Z. Naturforsch. B* **1975**, *30*, 55–59; f) C. Narayana, M. Periasamy, *J. Organomet. Chem.* **1987**, *323*, 145–147.
[17] See the Supporting Information for the IR spectrum (Figure S1), discussions on the mechanisms and solvents, and experimental details.
[18] L. H. Long, G. F. Freeguard, *Nature* **1965**, *207*, 403.
[19] I_2 and equimolar $NaBH_4/I_2$ were used in30 mmol, but BI_3 in only 20 mmol, in order to keep the amount of iodine consistently. On the other hand, molecular iodine can generate two equivalents of catalytically active species ($H_2 + I_2 = 2\,HI$),[14] whereas in the case of equimolar $NaBH_4/I_2$ one iodide is consumed to form NaI.[16] The question, whether the boron and iodine used in the present once-through catalysts can be recycled, needs to be investigated in detail.
[20] A recent report describes the conversion of anthracite into a pitch-like material by a hydrotreatment (6.89 MPa H_2) in presence of hydrogen donor solvents (tetralin, 9,10-dihydroanthracene) and molybdenum catalysts at 300–400 °C, which,

 © 2006 Wiley-VCH Verlag GmbH & Co. KGaA, Weinheim

however, does not imply hydrogenation to aliphatic structures: J. M. Andrésen, Y. Zhang, C. E. Burgess, H. H. Schobert, *Fuel Process. Technol.* **2004**, *85*, 1361 – 1372.

[21] K. H. van Heek, B. O. Strobel, W. Wanzl, *Fuel* **1994**, *73*, 1135 – 1143; P. Redlich, W. R. Jackson, F. P. Larkins, *Fuel* **1985**, *64*, 1383 – 1390.

[22] It is common practice to characterize the products of such liquefaction studies by the solubility in various solvents (solvent fractionation): R. K. Hessley, J. W. Reasoner, J. T. Tiley, *Coal Science, An Introduction to Chemistry, Technology, and Utilization*, Wiley, New York, **1986**, pp. 98 – 105. See also references [1, 14e,f].

[23] D. Männig, H. Nöth, *Angew. Chem.* **1985**, *97*, 854 – 855; *Angew. Chem. Int. Ed. Engl.* **1985**, *24*, 878 – 879; H. Braunschweig, *Angew. Chem.* **1998**, *110*, 1882 – 1898; *Angew. Chem. Int. Ed.* **1998**, *37*, 1786 – 1801; J. F. Hartwig, C. N. Muhoro, *Organometallics* **2000**, *19*, 30 – 38; C. M. Vogels, S. A. Westcott, *Curr. Org. Chem.* **2005**, *9*, 687 – 699, and references therein.

[24] H. Chen, S. Schlecht, T. C. Semple, J. F. Hartwig, *Science* **2000**, *287*, 1995 – 1997; J.-Y. Cho, M. K. Tse, D. Holmes, R. E. Maleczka, Jr., M. R. Smith III, *Science* **2002**, *295*, 305 – 308; T. Ishiyama, J. Takagi, J. F. Hartwig, N. Miyaura, *Angew. Chem.* **2002**, *114*, 3182 – 3184; *Angew. Chem. Int. Ed.* **2002**, *41*, 3056 – 3058; T. Ishiyama, N. Miyaura, *J. Organomet. Chem.* **2003**, *680*, 3 – 11; D. N. Coventry, A. S. Batsanov, A. E. Goeta, J. A. K. Howard, T. B. Marder, R. N. Perutz, *Chem. Commun.* **2005**, 2172 – 2174, and references therein.

 © 2006 Wiley-VCH Verlag GmbH & Co. KGaA, Weinheim

Borylene Complexes

DOI: 10.1002/anie.200503807

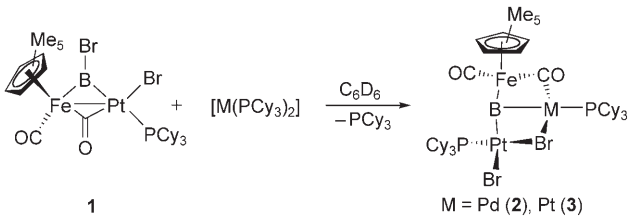
Boron in the Coordination Spheres of Three Transition-Metal Atoms: Syntheses and Structures of Metalloborylenes Stabilized by a Transition-Metal Base**

Holger Braunschweig, Krzysztof Radacki, Daniela Rais, and Fabian Seeler*

The study of transition-metal complexes of boron has become an area of widespread interest over the past 15 years.[1] Boryl complexes [$L_xM{-}BR_2$] are most prominent, and the development of various synthetic strategies for these species and subsequent elucidation of their electronic and structural properties by experimental[2] and quantum-chemical[3] methods has led to important applications.[4] Far less common are terminal [$L_xM{=}B{-}R$][5] and homodinuclear [$L_xM{-}B(R){-}ML_x$][6] borylene complexes, which owe much of their importance to the fact that they are boron-based counterparts of pivotal organometallic compounds, such as carbonyl or vinylidene complexes.

In addition to these two classes of compounds, a number of systems have very recently been described in which boron-based ligands adopt unusual coordination modes, for example, boryl-bridged species [$L_xM{-}B(R_2){-}M'L_x$],[7] heterodinuclear complexes with bridging[8] and semibridging[9] borylene ligands [$L_xM{-}B(R){-}M'L_x$], and metalloborylenes [$L_xM{=}B{-}ML_x$] with a bridging "naked" boron atom.[10] This series of molecules comprises two different metal fragments, which are linked by boron atoms bearing a decreasing number of main-group-element substituents. We recently turned our attention to the possibility of increasing the number of metal fragments linked to boron to three, without leaving the scenario of classical bonding and passing into the regime of electron-deficient bonding, where boron can accommodate a much higher degree of metal "substitution", as is the case for interstitial metallaboranes.[11] Herein, we report the full characterization of [(η^5-C_5Me_5)(OC)Fe(μ-CO)M(PCy_3)(μ-Br)Pt(PCy_3)Br(μ^3-B)] (M = Pd (**2**), Pt (**3**); Cy = cyclohexyl), which feature the unprecedented coordination of one boron atom to three transition-metal centers.

The reaction of the dibromoboryl complex [(η^5-C_5Me_5)$(OC)_2$Fe(BBr_2)] with one equivalent of [$Pt(PCy_3)_2$] in toluene yielded, in analogy to the previously reported reaction with [$Pd(PCy_3)_2$],[8] the heterodinuclear bridging bromoborylene complex [(η^5-C_5Me_5)$(OC)_2$Fe(μ-BBr)Pt(PCy_3)Br] (**1**). Subsequently, **1** was treated with one equivalent of [$Pd(PCy_3)_2$] in C_6D_6, and the multinuclear NMR spectra of the reaction mixture indicated the quantitative formation of the new species **2** within minutes, with liberation of PCy_3 (Scheme 1). The $^{11}B\{^1H\}$ NMR spectrum of **2** shows



Scheme 1. Synthesis of compounds **2** and **3**.

one broad singlet at $\delta = 144$ ppm ($\omega_{1/2} = 1990$ Hz), which is downfield shifted with respect to that of the precursor **1** ($\delta =$ 108 ppm). The $^{31}P\{^1H\}$ NMR spectrum displays two sharp resonances, one at $\delta = 31.9$ ppm and one for a platinum-bound PCy_3 ligand at $\delta = 32.5$ ppm ($^1J(Pt,P) = 4559$ Hz).

To investigate the generality of the synthesis, the reaction of [(η^5-C_5Me_5)$(OC)_2$Fe(BBr_2)] with two equivalents of [Pt(PCy_3)$_2$] in C_6D_6 was performed. Multinuclear NMR spectroscopy revealed the initial formation of the bridging bromoborylene complex **1**, as expected. After 2 h, however, the formation of another compound, **3**, was observed; the conversion of **1** into **3** was complete after 24 h. Similar to the

[*] Prof. Dr. H. Braunschweig, Dr. K. Radacki, Dr. D. Rais, F. Seeler
Institut für Anorganische Chemie
Bayerische Julius-Maximilians-Universität Würzburg
Am Hubland, 97074 Würzburg (Germany)
Fax: (+49) 931-888-4623
E-mail: h.braunschweig@mail.uni-wuerzburg.de

[**] This work was supported by the Deutsche Forschungsgemeinschaft. D.R. thanks the Alexander von Humboldt-Foundation for a postdoctoral fellowship. The authors are grateful to Prof. Dr. M. Kaupp for assistance with the theoretical calculations.

Supporting information for this article is available on the WWW under http://www.angewandte.org or from the author.

InterScience
© 2006 Wiley-VCH Verlag GmbH & Co. KGaA, Weinheim

case of **2**, the $^{11}B\{^1H\}$ NMR spectrum of **3** displays one broad singlet at $\delta = 130$ ppm ($\omega_{1/2} = 1320$ Hz), while the $^{31}P\{^1H\}$ NMR spectrum displays two sharp resonances for platinum-bound PCy_3 ligands at $\delta = 31.1$ ppm ($^1J(Pt,P) = 4703$ Hz) and $\delta = 57.3$ ppm ($^1J(Pt,P) = 4626$ Hz).

The structures of the new compounds **2** and **3**, determined by single-crystal X-ray diffraction (Figure 1).[12] In both compounds, the boron atom is surrounded by three transition-metal atoms and lies only 0.175 (**2**) or 0.186 Å (**3**) out of the Fe1-Pt1-Pd1 or Fe1-Pt1-Pt2 plane, respectively. The Fe1–B1 distances (**2**: 1.910(4); **3**: 1.903(4) Å) are rather short, and are equivalent, within experimental error, to that in $[(\eta^5\text{-}C_5Me_5)(OC)Fe(\mu\text{-}CO)(\mu\text{-}BFc)Pd(PCy_3)Br]$ (Fc = ferrocenyl; 1.903(3) Å).[8] The coordination geometry at Pt1 is slightly distorted square planar in both **2** and **3**, with one PCy_3 ligand *cis* and one bromide ligand *trans* to the boron atom. The Pt1–B1 distances (**2**: 1.923(4); **3**: 1.938(4) Å) are also short, particularly in comparison to that in *trans*-$[(Cy_3P)_2Pt\{B(Fc)Br\}][B(Ar^f{}_4)]$ ($Ar^f = 3,5\text{-}(CF_3)_2C_6H_3$; 1.966(4) Å), where the platinum center is, however, only three-coordinate.[13] The most remarkable feature of the structures is the nearly linear arrangement of the iron, boron, and platinum centers (**2**: Fe1-B1-Pt1 168.7(2); **3**: 167.1(2)°), which is similar to that observed in the metalloborylene complexes $[(\eta^5\text{-}C_5Me_5)(OC)_2Fe(\mu\text{-}B)Cr(CO)_5]$ (Fe-B-Cr 177.75(11)°) and $[(\eta^5\text{-}C_5Me_5)(OC)_2Fe(\mu\text{-}B)Fe(CO)_4]$ (Fe-B-Fe 175.38(12)°).[10] This arrangement indicates an sp hybridization of the boron atom; however, in **2** and **3** an additional boron–metal interaction is present. Rather long Pd1–B1 (2.150(4) Å) and Pt2–B1 (2.158(4) Å) bonds occur in **2** and **3**, respectively, which are supported by a bridging carbonyl ligand and a bridging bromide ligand that connect Pd1 in **2** and Pt2 in **3** with Fe1 and Pt1, respectively. The resulting coordination environments of Pd1 in **2** and Pt2 in **3** are distorted tetrahedral. On the basis of this structural information, the bonding situation in **2** and **3** can be described in terms of a central metalloborylene moiety, Fe-B=Pt, in which the boron center is additionally stabilized through interaction with a transition-metal base of the type $\{M(PCy_3)\}$ (M = Pd, Pt). A similar interaction between a $\{Pd(PCy_3)\}$ fragment and the boron atom of a terminal aminoborylene complex was recently reported.[9]

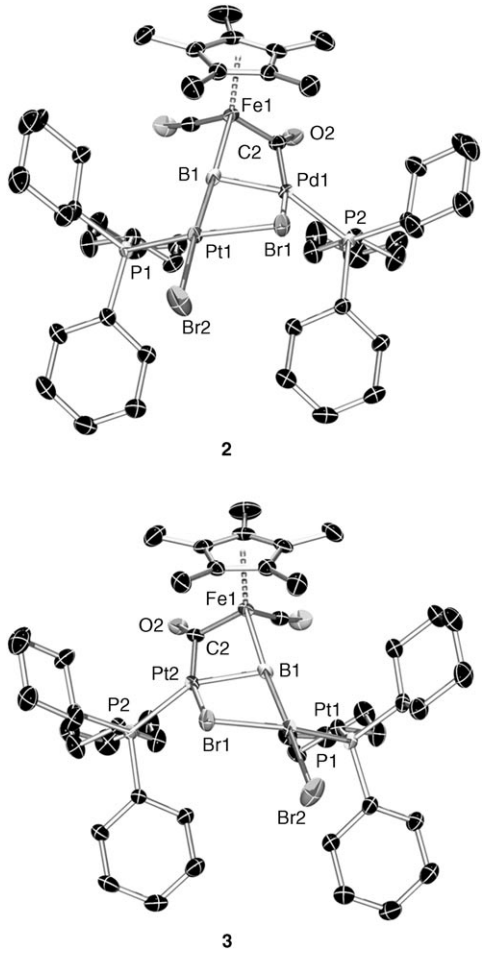


Figure 1. Molecular structures of **2** and **3**. Selected bond lengths [Å] and angles [°]. **2**: Pt1–B1 1.923(4), Fe1–B1 1.910(4), Pd1–B1 2.150(4); Fe1-B1-Pt1 168.7(2), Fe1-B1-Pd1 78.46(15), Pt1-B1-Pd1 104.96(17). **3**: Pt1–B1 1.938(4), Fe1–B1 1.903(4), Pt2–B1 2.158(4); Fe1-B1-Pt1 167.1(2), Fe1-B1-Pt2 77.98(15), Pt1-B1-Pt2 107.22(17). Hydrogen atoms are omitted for clarity. Thermal ellipsoids are set at 50% probability.

To elucidate the bonding situation in this unprecedented BM_3 system, density functional theory (DFT) calculations on a model system for complex **2** were performed.[14] To reduce the computation time, PMe_3 was used in place of PCy_3, and C_5H_5 in place of C_5Me_5. The optimization at the B3LYP level of theory reproduced the experimental structure of **2** well, but all computed distances were slightly longer than those observed in the crystal structure.

The BM_3 core of the model is highly unsymmetrical. The four atoms do not lie on the same plane (the boron atom deviates 0.175 Å from the Pt-Fe-Pd plane), and the ligands at all three transition-metal centers have no symmetry plane in common. Hence, the molecular orbitals that are involved in bonding with the boron center are composed of rather complicated mixtures of boron s and p orbitals (Figure 2).

Since the $\{Pd(PMe_3)\}$ fragment has a d_{z^2}-type HOMO pointing along the Pd–P bond, it was of interest to search for a suitable acceptor orbital localized on the hypothetical metalloborylene molecule $[(\eta^5\text{-}C_5H_5)(OC)_2Fe\text{-}B{=}PtBr_2(PMe_3)]$. Indeed, the first six unoccupied orbitals on this unit are partially localized on the Lewis acidic boron atom, thus allowing an interaction with the $\{Pd(PMe_3)\}$ fragment. Additional stabilization is provided by the bridging carbonyl and bromide ligands, as indicated by the presence of the corresponding bonding orbitals.

Electron localization function (ELF) calculations on the hypothetical borylene complex $[(\eta^5\text{-}C_5H_5)(OC)_2Fe\text{-}B{=}PtBr_2(PMe_3)]$ show the presence of a ring attractor between the boron and platinum atoms, thus emphasizing the significance of both orthogonal π components for the B–Pt bond, and possibly indicating a partial triple-bond character. Addition of the $\{Pd(PMe_3)\}$ moiety changes the electronic situation: the ring attractor between the platinum and boron atoms becomes unsymmetrical and converts into a point attractor. The basin of the B–Fe bond now also affects the palladium center and effectively represents a three-centre two-electron (3c,2e) Fe-B-Pd bond (Figure 2).[15]

 © 2006 Wiley-VCH Verlag GmbH & Co. KGaA, Weinheim

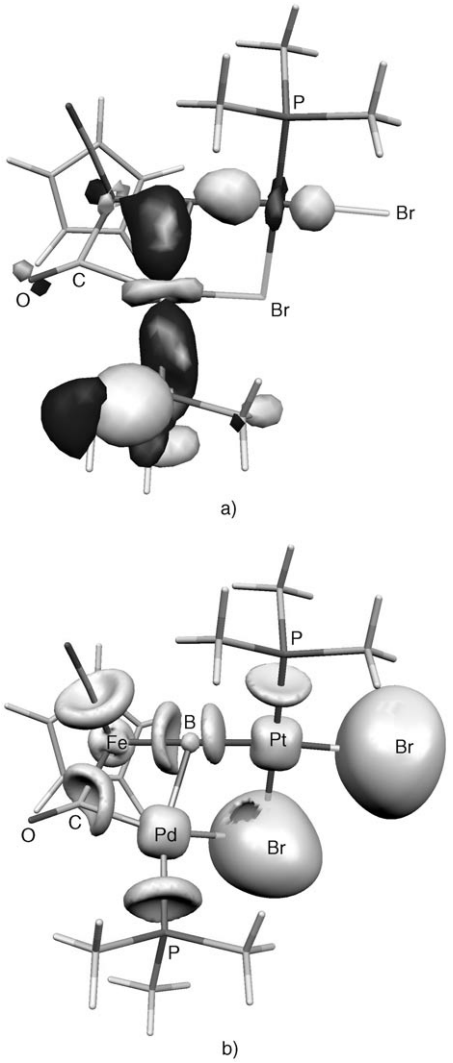


Figure 2. a) Kohn–Sham orbital of the σ component of the Pd→B bond and b) ELF = 0.7 plot, for the model of complex **2**. The ELF contributions of some ligands are omitted for clarity.

Earlier DFT studies revealed that classical transition-metal–boron compounds usually feature a positively charged boron atom, while the transition-metal atom carries a partial negative charge.[16] In the model system for **2**, however, the electronegative halogen ligands bound to the platinum and palladium atoms induce partial positive charges on both transition-metal centers (+0.16 and +0.21, respectively). The boron atom is, as expected, positively charged (+0.12), while the iron center is slightly negatively charged (−0.25). Such a modest ionic contribution to the bonding is expected to increase the covalent character of all the transition-metal–boron bonds. Nonetheless, relatively low values of the corresponding Wiberg bond indices are calculated (Pt−B: 0.90, Fe−B: 0.71, Pd−B: 0.37), which indicates the importance of the bridging carbonyl and bromide ligands for the stability of the molecule.

In conclusion, by binding boron to three transition-metal atoms, an unprecedented coordination mode for a "naked" boron atom was realized. According to structural and DFT studies, the new compounds are best described as metalloborylene complexes stabilized by a transition-metal base.

Experimental Section

All manipulations were performed under an atmosphere of dry argon, using standard Schlenk-line and glove-box techniques.

2: Solid **1** (0.035 g, 0.039 mmol) was added to a solution of $[Pd(PCy_3)_2]$ (0.026 g, 0.039 mmol) in C_6D_6 (0.6 mL). After 10 min, hexane (1 mL) was added. The resulting yellow precipitate was washed with hexane (2 × 0.5 mL) and dried in vacuo, yielding **2** as a yellow solid (0.028 g, 56%). IR(toluene): $\tilde{\nu}$ = 1950 (s, CO), 1798 cm^{-1} (s, CO); ^1H NMR (500 MHz, C_6D_6, 17 °C, TMS): δ = 1.82 (s, 15H, C_5Me_5), 2.26–1.49 ppm (m, 66H, Cy); $^{13}C\{^1H\}$ NMR (125.8 MHz, C_6D_6, 17 °C, TMS): δ = 245.1 (s, CO), 218.1 (s, CO), 97.4 (s, C_5Me_5), 33.5–26.7 (multiple overlapping signals, Cy), 10.8 ppm (s, C_5Me_5); $^{31}P\{^1H\}$ NMR (202.5 MHz, C_6D_6, 17 °C, H_3PO_4): δ = 32.5 (^1J(Pt,P) = 4559 Hz, Pt-PCy_3), 31.9 ppm (Pd-PCy_3); ^{11}B NMR (160.5 MHz, C_6D_6, 17 °C, $Et_2O{\cdot}BF_3$): δ = 144 ($\omega_{1/2}$ = 1990 Hz); elemental analysis (%) calcd for $C_{48}H_{81}BBr_2FeP_2PdPtO_2{\cdot}0.5\,C_6D_6$: C 46.33, H 6.63; found: C 46.12, H 6.92.

3: Solid $[(\eta^5\text{-}C_5Me_5)(OC)_2Fe(BBr_2)]$ (0.028 g, 0.065 mmol) was added to a solution of $[Pt(PCy_3)_2]$ (0.100 g, 0.132 mmol) in C_6D_6 (0.5 mL). After 24 h, all volatiles were removed in vacuo. The residue was washed with hexane (3 × 0.5 mL) to remove the liberated PCy_3 and dried in vacuo, yielding **3** as an orange solid (0.045 g, 50%). IR(toluene): $\tilde{\nu}$ = 1940 (s, CO), 1771 cm^{-1} (s, CO); ^1H NMR (500 MHz, CD_2Cl_2, 17 °C, TMS): δ = 1.93 (s, 15H, C_5Me_5), 2.42–1.20 ppm (m, 66H, Cy); $^{13}C\{^1H\}$ NMR (125.8 MHz, CD_2Cl_2, 17 °C, TMS): δ = 248.2 (s, CO), 217.1 (s, CO), 97.8 (s, C_5Me_5), 35.2–26.5 (multiple overlapping signals, Cy), 10.8 ppm (s, C_5Me_5); $^{31}P\{^1H\}$ NMR (202.5 MHz, CD_2Cl_2, 17 °C, H_3PO_4): δ = 57.3 (^1J(Pt,P) = 4626 Hz), 31.1 ppm (^1J(Pt,P) = 4703 Hz); ^{11}B NMR (160.5 MHz, CD_2Cl_2, 17 °C, $Et_2O{\cdot}BF_3$): δ = 130 ppm ($\omega_{1/2}$ = 1320 Hz); elemental analysis (%) calcd for $C_{48}H_{81}BBr_2FeP_2Pt_2O_2{\cdot}0.5\,C_6D_6$: C 43.42, H 6.22; found: C 44.07, H 6.25.

Received: October 27, 2005
Published online: January 3, 2006

Keywords: boron · coordination chemistry · density functional calculations · structure elucidation · transition metals

[1] a) H. Braunschweig, *Angew. Chem.* **1998**, *110*, 1882–1898; *Angew. Chem. Int. Ed.* **1998**, *37*, 1786–1801; b) H. Braunschweig, M. Colling, *Coord. Chem. Rev.* **2001**, *223*, 1–51.

[2] a) G. J. Irvine, M. G. J. Lesley, T. B. Marder, N. C. Norman, C. R. Rice, E. G. Robins, W. R. Roper, G. R. Whittell, L. J. Wright, *Chem. Rev.* **1998**, *98*, 2685–2722; b) S. Aldridge, D. L. Coombs, *Coord. Chem. Rev.* **2004**, *248*, 535–559.

[3] a) G. Frenking, N. Fröhlich, *Chem. Rev.* **2000**, *100*, 717–774; b) K. T. Giju, F. M. Bickelhaupt, G. Frenking, *Inorg. Chem.* **2000**, *39*, 4776–4785; c) A. A. Dickinson, D. J. Willock, R. J. Calder, S. Aldridge, *Organometallics* **2002**, *21*, 1146–1157.

[4] Transition-metal–catalyzed hydroboration: I. Beletskaya, A. Pelter, *Tetrahedron* **1997**, *53*, 4957–5026; diboration: T. B. Marder, N. C. Norman, *Top. Catal.* **1998**, *5*, 63–73; C−H-bond functionalization: T. Ishiyama, N. Miyaura, *J. Organomet. Chem.* **2003**, *680*, 3–11.

[5] a) H. Braunschweig, C. Kollann, U. Englert, *Angew. Chem.* **1998**, *110*, 3355–3357; *Angew. Chem. Int. Ed.* **1998**, *37*, 3179–3180; b) G. J. Irvine, C. E. F. Rickard, W. R. Roper, A. Williamson, L. G. Wright, *Angew. Chem.* **2000**, *112*, 978–980; *Angew. Chem. Int. Ed.* **2000**, *39*, 948–950; c) H. Braunschweig, C. Kollann, U. Englert, *Angew. Chem.* **2001**, *113*, 4327–4329; *Angew. Chem.*

 © 2006 Wiley-VCH Verlag GmbH & Co. KGaA, Weinheim

Int. Ed. **2001**, *40*, 4198 – 4200; d) H. Braunschweig, M. Colling, C. Kollann, H. G. Stammler, B. Neumann, *Angew. Chem.* **2001**, *113*, 2359 – 2361; *Angew. Chem. Int. Ed.* **2001**, *40*, 2298 – 2300; e) C. E. F. Rickard, W. R. Roper, A. Williamson, J. L. Wright, *Organometallics* **2002**, *21*, 4862 – 4872; f) H. Braunschweig, M. Colling, C. Hu, K. Radacki, *Angew. Chem.* **2003**, *115*, 215 – 218; *Angew. Chem. Int. Ed.* **2003**, *42*, 205 – 208; g) D. L. Coombs, S. Aldridge, C. Jones, D. J. Willock, *J. Am. Chem. Soc.* **2003**, *125*, 6356 – 6357.

[6] a) H. Braunschweig, T. Wagner, *Angew. Chem.* **1995**, *107*, 904 – 905; *Angew. Chem. Int. Ed. Engl.* **1995**, *34*, 825 – 826; b) H. Braunschweig, B. Ganter, *J. Organomet. Chem.* **1997**, *545–546*, 163 – 167; c) H. Braunschweig, M. Müller, *Chem. Ber./Recl.* **1997**, *130*, 1295 – 1298; d) H. Braunschweig, C. Kollann, U. Englert, *Eur. J. Inorg. Chem.* **1998**, 465 – 468; e) M. Shimoi, S. Ikubo, Y. Kawano, K. Yasuro, K. Katoh, H. Ogino, *J. Am. Chem. Soc.* **1998**, *120*, 4222 – 4223; f) H. Braunschweig, C. Kollann, W. Klinkhammer, *Eur. J. Inorg. Chem.* **1999**, 1523 – 1529; g) S. Aldridge, D. L. Coombs, C. Jones, *Chem. Commun.* **2002**, 856 – 857; h) D. L. Coombs, S. Aldridge, S. J. Coles, M. B. Hursthouse, *Organometallics* **2003**, *22*, 4213 – 4217.

[7] H. Braunschweig, K. Radacki, D. Rais, G. R. Whittell, *Angew. Chem.* **2005**, *117*, 1217 – 1219; *Angew. Chem. Int. Ed.* **2005**, *44*, 1192 – 1194.

[8] H. Braunschweig, K. Radacki, D. Rais, F. Seeler, K. Uttinger, *J. Am. Chem. Soc.* **2005**, *127*, 1386 – 1387.

[9] H. Braunschweig, D. Rais, K. Uttinger, *Angew. Chem.* **2005**, *117*, 3829 – 3832; *Angew. Chem. Int. Ed.* **2005**, *44*, 3763 – 3766.

[10] H. Braunschweig, K. Radacki, D. Scheschkewitz, G. R. Whittell, *Angew. Chem.* **2005**, *117*, 1685 – 1688; *Angew. Chem. Int. Ed.* **2005**, *44*, 1658 – 1661.

[11] a) A. K. Bandyopadhyay, R. Khattar, J. Pugar, T. P. Fehlner, A. L. Rheingold, *Inorg. Chem.* **1992**, *31*, 465 – 472; b) C. E. Housecroft, *Coord. Chem. Rev.* **1995**, *143*, 297 – 330.

[12] The X-ray diffraction data for **2** and **3** were collected on a Bruker APEX diffractometer with a CCD area detector, using graphite-monochromated $Mo_{K\alpha}$ radiation. The structure was solved by using direct methods, refined, and expanded by using Fourier techniques with the SHELX software package (G. M. Sheldrick, SHELX-97, Universität Göttingen, **1997**). All non-hydrogen atoms were refined anisotropically. Hydrogen atoms were placed in idealized positions and included in structure factor calculations. Crystal data for **2**: $C_{48}H_{81}BBr_2FeP_2PdPtO_2\cdot 0.5\,C_6D_6$, $M_r = 1319.09$, orange blocks, $0.34\times0.29\times0.21$ mm, triclinic, space group $P\bar{1}$, $a = 10.5758(8)$, $b = 14.5329(11)$, $c = 19.3246(14)$ Å, $\alpha = 69.1460(10)$, $\beta = 86.5450(10)$, $\gamma = 73.7620(10)°$, $V = 2662.3(3)$ Å^3, $Z = 2$, $\rho_{calcd} = 1.646$ g cm^{-3}, $\mu = 4.821$ cm^{-1}, $F(000) = 1322$, $T = 173(2)$ K, $R_1 = 0.0345$, $wR_2 = 0.0756$, 10563 independent reflections [$2\theta \le 52.34°$] and 555 parameters. Crystal data for **3**: $C_{48}H_{81}BBr_2FeP_2Pt_2O_2\cdot 0.5\,C_6D_6$, $M_r = 1407.78$, orange blocks, $0.22\times0.21\times0.16$ mm, triclinic, space group $P\bar{1}$, $a = 10.5663(8)$, $b = 14.5257(11)$, $c = 19.3244(14)$ Å, $\alpha = 68.9980(10)$, $\beta = 86.6100(10)$, $\gamma = 73.6760(10)°$, $V = 2654.4(3)$ Å^3, $Z = 2$, $\rho_{calcd} = 1.761$ g cm^{-3}, $\mu = 7.129$ cm^{-1}, $F(000) = 1386$, $T = 173(2)$ K, $R_1 = 0.0276$, $wR_2 = 0.0672$, 10521 independent reflections [$2\theta \le 52.28°$] and 555 parameters. CCDC-287178 (**2**) and CCDC-287179 (**3**) contain the supplementary crystallographic data for this paper. These data can be obtained free of charge from The Cambridge Crystallographic Data Centre via www.ccdc.cam.ac.uk/data_request/cif.

[13] H. Braunschweig, K. Radacki, D. Rais, D. Scheschkewitz, *Angew. Chem.* **2005**, *117*, 5796 – 5799; *Angew. Chem. Int. Ed.* **2005**, *44*, 5651 – 5654.

[14] Electronic structure calculations were performed with the program Gaussian 03 (Gaussian 03, Revision B.04, M. J. Frisch et al., Gaussian, Inc., Wallingford CT, **2004**). The ELFs were computed with the TopMoD package (S. Noury, X. Krokidis, F. Fuster, B. Silvi, TopMoD, Université Pierre et Marie Curie, **1997**). The natural bond orbital (NBO) analysis was performed with the program NBO (E. D. Glendening, A. E. Reed, J. E. Carpenter, F. Weinhold, NBO Version 3.1, University of Wisconsin. See Supporting Information for details.

[15] The hole visible in the ELF surface of the μ-Br ligand is a result of the Pauli repulsion that is characteristic for electronegative halogen ions. The shape of the high-ELF region on the carbonyl ligand is typical for bridging ligands.

[16] a) G. Frenking, N. Froehlich, *Chem. Rev.* **2000**, *100*, 717 – 774; b) Y. Chen, G. Frenking, *J. Chem. Soc. Dalton Trans.* **2001**, 434 – 440.

 © 2006 Wiley-VCH Verlag GmbH & Co. KGaA, Weinheim

Inhibitors

DOI: 10.1002/anie.200503003

Fluorescent Inhibitors for IspF, an Enzyme in the Non-Mevalonate Pathway for Isoprenoid Biosynthesis and a Potential Target for Antimalarial Therapy**

Christine M. Crane, Johannes Kaiser, Nicola L. Ramsden, Susan Lauw, Felix Rohdich, Wolfgang Eisenreich, William N. Hunter, Adelbert Bacher,* and François Diederich**

Malaria remains a leading cause of illness and death in endemic areas, infecting 300–500 million and killing 2.5–5 million people annually. As a result of rapidly emerging

[*] N. L. Ramsden, Prof. Dr. W. N. Hunter
Division of Biological Chemistry and Molecular Microbiology
School of Life Sciences
MSI/WTB Complex
University of Dundee
Dow Street, Dundee DD1 5EH (UK)
Fax: (+44) 138-232-2558
E-mail: w.n.hunter@dundee.ac.uk

Dr. J. Kaiser, S. Lauw, Dr. F. Rohdich, Dr. W. Eisenreich, Prof. Dr. A. Bacher
Lehrstuhl für Organische Chemie und Biochemie
Technische Universität München
Lichtenbergstrasse 4, 85748 Garching (Germany)
Fax: (+49) 89-289-13363
E-mail: adelbert.bacher@ch.tum.de

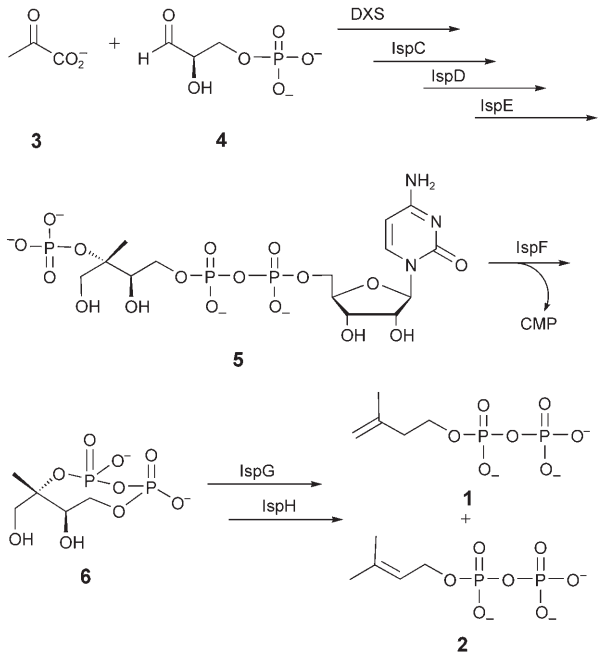
C. M. Crane, Prof. Dr. F. Diederich
Laboratorium für Organische Chemie
ETH Hönggerberg
HCI, 8093 Zürich (Switzerland)
Fax: (+41) 44-632-1109
E-mail: diederich@org.chem.ethz.ch

[**] We gratefully acknowledge financial support for this work from the following agencies: the Hans-Fischer Gesellschaft e.V. (to J.K.), The Wellcome Trust (to W.N.H.), the Biotechnology and Biological Sciences Research Council (UK) (to W.N.H.), and InPharmatica (to W.N.H.). The authors also thank Prof. D. Arigoni and Dr. L. Kemp for help and advice. IspF = 2*C*-Methyl-D-erythritol 2,4-cyclodiphosphate synthase.

Supporting information for this article is available on the WWW under http://www.angewandte.org or from the author.

© 2006 Wiley-VCH Verlag GmbH & Co. KGaA, Weinheim

multiple-drug-resistant strains of the various *Plasmodium* parasites, the search for new therapies with novel modes of action is of urgent necessity.[1] Enzymes in the non-mevalonate pathway, utilized for assembling the C_5 precursors to terpenes, isopentenyl diphosphate (IPP) **1** and dimethylallyl diphosphate (DMAPP) **2**, were recently identified as targets for antimalarial and antimicrobial drugs.[2,3] The non-mevalonate pathway[4] is characterized by the condensation of pyruvate **3** and glyceraldehyde 3-phosphate **4** (Scheme 1) and



Scheme 1. The non-mevalonate pathway for the biosynthesis of the C_5 precursors to terpenes, IPP **1** and DMAPP **2** (see the Supporting Information). DXS = 1-deoxy-D-xylulose-5-phosphate synthase, CMP = cytidine 5′-monophosphate.[4–8]

is the sole source for **1** and **2** in plastids of higher plants[5a–c] and in many bacteria[4b,5c,6] including some responsible for serious diseases such as *Mycobacterium tuberculosis*[6b] and the protozoan *Plasmodium* parasites (*Apicomplexa*).[3] Since mammals exclusively utilize the mevalonate pathway,[6] the development of small-molecule lead compounds inhibiting the enzymes of the non-mevalonate pathway may be a key step towards new antimalarial drugs.[1b,2,3]

We have chosen the enzyme IspF (2*C*-methyl-D-erythritol 2,4-cyclodiphosphate synthase, *ygbB*) as a target for structure-based lead generation.[7,8] IspF is the fifth enzyme in the non-mevalonate pathway and catalyzes the cyclization of 4-diphosphocytidyl-2*C*-methyl-D-erythritol 2-phosphate (**5**), to the key cyclic diphosphate intermediate, 2*C*-methyl-D-erythritol 2,4-cyclodiphosphate (**6**). Published crystal structures (Protein Data Bank (PDB)[8,9] codes 1GX1 and 1JY8) show IspF to be a C_3-symmetric homotrimer. The topologically equivalent active sites are located at the interfaces of adjacent subunits. The rigid, well-conserved "Pocket III" of one monomer binds the cytidine moiety of **5**, and the larger, more flexible "Pocket II" of an adjacent monomer binds the 2*C*-methyl-D-erythritol moieties of **5** and **6** (for the protein residues lining these pockets, see Figure 1b). The latter pocket also contains a tetrahedrally coordinated Zn^{II} ion.

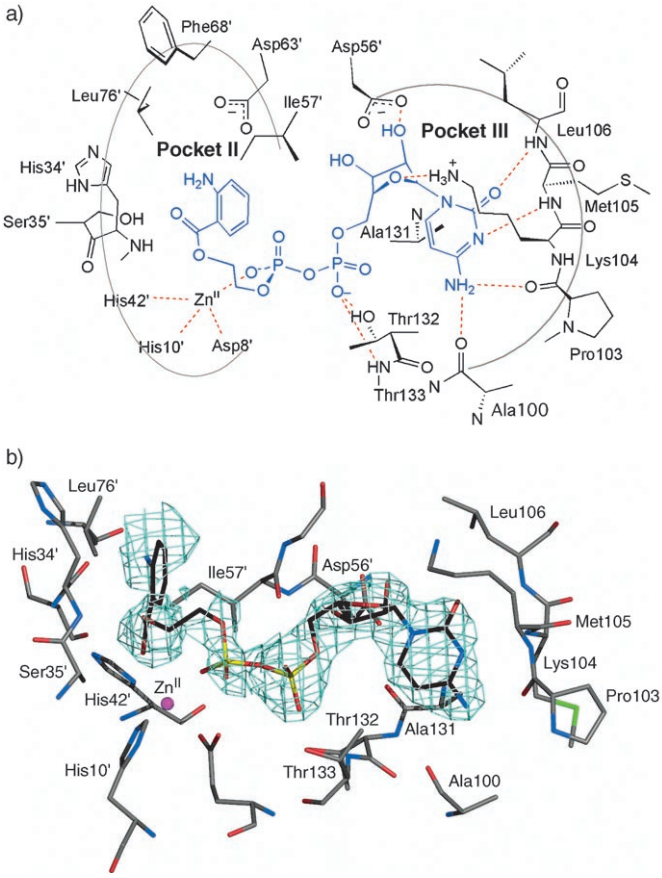
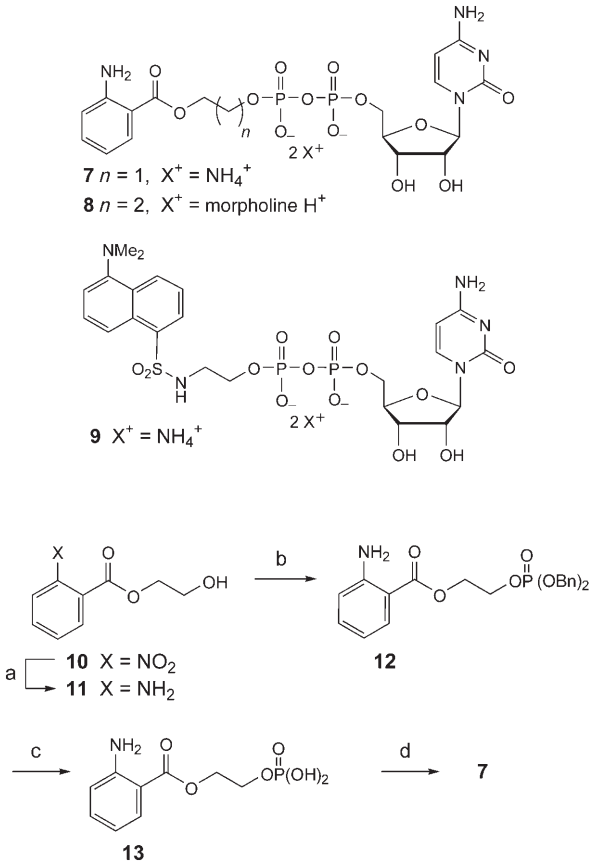


Figure 1. Binding mode of **7** in the ternary complex of IspF with Zn^{II} as determined by X-ray crystallography to 2.3-Å resolution.[17] Ligand binding shown occurs at the interface of subunits A and C (primes designate residues from an adjacent monomer). Five of the six independent active sites of IspF show the depicted binding conformation. a) Schematic representation of the binding mode of **7** (in blue) with potential hydrogen bonds depicted as red dashed lines. b) F_o-F_c omit electron density map surrounded by residues within 4 Å, contoured at the 2σ level. Color code: C gray, O red, N blue, S green, P yellow, Zn^{II} pink ball.

Inhibitors **7**–**9**, occupying both pockets, were designed with the help of the molecular modeling software MOLOC.[10,11] In the absence of known inhibitors, we chose in a first step to maintain the CDP moiety of the natural substrate to occupy Pocket III while connecting the diphosphate by means of an appropriately sized linker to an aromatic residue, for occupation of the hydrophobic cleft of Pocket II, defined by Leu 76′, Phe 61′, and Ile 57′ (Figure 1). Since at a first stage, we were also interested in developing a fluorescence-based enzyme inhibition assay, fluorescent anthranilate (2-aminobenzoate) and dansyl (5,5-dimethylaminonaphthalenesulfamoyl) residues were chosen as aromatic moieties reaching into Pocket II.[12]

The synthesis of target compound **7** is shown in Scheme 2 (for the synthesis of compounds **8** and **9**, see the Supporting Information). Reduction of nitro derivative **10** afforded

 © 2006 Wiley-VCH Verlag GmbH & Co. KGaA, Weinheim



Scheme 2. Synthesis of fluorescent ligand **7**. a) Zn, AcOH, MeOH, 0 °C→20 °C, 5 h, quant.; b) $HOPO(OBn)_2$, DIAD, Ph_3P, THF, 20 °C, 63 %; c) H_2, 10 % Pd/C, CH_2Cl_2/EtOH, 7 h, 20 °C, 98 %; d) Et_3N, cytidine 5′-monophosphomorpholidate 4-morpholine-*N*,*N*′-dicyclohexylcarboxamidine salt, 1*H*-tetrazole, pyridine, 20 °C, 48 h, then DOWEX ion-exchange (NH_4^+), 45 %. THF = tetrahydrofuran, Bn = benzyl, DIAD = diisopropyl azodicarboxylate.

anthranilate **11**, which was phosphorylated using a modified Mitsunobu reaction[13] to furnish phosphotriester **12**. Removal of the benzyl residues by hydrogenation provided the free phosphate **13**. The desired diphosphate was obtained using a modified Moffatt condensation of **13** with cytidine 5′-monophosphomorpholidate 4-morpholine-*N*,*N*′-dicyclohexylcarboxamidine salt, catalyzed by 1*H*-tetrazole.[14] Ion-exchange chromatography (DOWEX 50 WX8 (NH_4^+)) gave the diammonium salt of **7**, which was purified by column chromatography on cellulose and fully characterized (see the Supporting Information).

Fluorescence binding titrations were performed to determine the dissociation constants, K_d, for the complexes of IspF from *Escherichia coli* with ligands **7**–**9**.[15] In the presence of the enzyme, the emission of the fluorescent probes is shifted hypsochromically and increases in intensity (hyperchromism), which is most likely attributed to complexation in an environment of reduced polarity. Affinity data were found to depend substantially on the concentration of Zn^{II} ions present in solution; therefore $Zn(OAc)_2$ was added in a concentration sufficient to ensure saturation of the enzyme. Typical titration curves[15] are depicted in Figure 2. Dissoci-

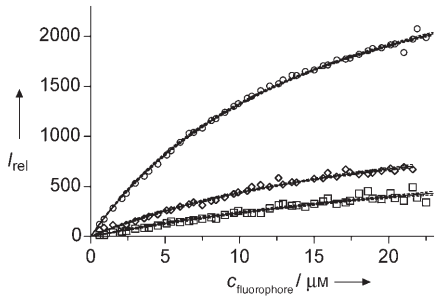


Figure 2. Typical fluorescence titration curves of *E. coli* IspF (6.25 μM) with inhibitors **7** (□), **8** (◇), and **9** (○), measured from 0–24 μM in 0.3-μM aliquots (0.6-μM steps shown for clarity).[15]

ation constants were obtained by nonlinear least-squares approximation and are given in Table 1. All three fluorescent probes show activities in the lower double-digit micromolar

Table 1: Affinities of ligands against *E. coli* IspF measured by fluorescence (**7**–**9**) and ^{13}C NMR assays (**9**, CMP, CDP).

Compound	K_d [μM][a]	IC_{50} [mM][b]
7	36 ± 5	
8	23 ± 2	
9	15 ± 0.3	3.0
CMP		15.0
CDP		7.3

[a] Determined at 25 °C; for details, see ref. [15]. [b] Determined at 37 °C; for details, see ref. [16] and the Supporting Information.

range. In parallel, the IC_{50} values (IC_{50} = concentration of inhibitor at which 50 % of the maximum initial velocity is observed) for **9**, cytidine 5′-diphosphate (CDP), and cytidine 5′-monophosphate (CMP) were determined in enzymatic assays monitored by ^{13}C NMR spectroscopy (see the Supporting Information).[16] These results show inhibitor **9** has a lower IC_{50} value (3.0 mM) than both CDP (7.3 mM) and CMP (15.0 mM), suggesting that binding free enthalpy is gained upon introduction of the aromatic fluorophore on inhibitor **9**. The participation of the fluorescent probes in the binding to the *E. coli* enzyme, as suggested by the fluorescence assays, was subsequently confirmed by X-ray crystal structure analyses of inhibitors **7** and **9** bound to IspF.

The structures of the ternary complexes of **7** (Figure 1) and **9** (see the Supporting Information) with tetrahedrally coordinated Zn^{II} in the active site of *E. coli* IspF were determined to 2.3-Å and to 2.5-Å resolution, respectively.[17] The complex of **7** consists of six subunits (two trimers) in the asymmetric unit, and the complex of **9** consists of one subunit. The crystal structures confirm that the cytidine moieties in both complexes are firmly anchored in Pocket III as predicted. There are four highly conserved hydrogen bonds between the nucleobase, π-stacked against Ala 131, and the backbone from Ala 100 to Leu 106 (see Figure 1a and the Supporting Information).[8,9] The ribose moiety is further held by hydrogen bonds between the ribose C(2′) and C(3′) hydroxyl groups and the carboxylate of Asp 56′. The catalytic Zn^{II} ions in both structures are tetrahedrally coordinated to

 © 2006 Wiley-VCH Verlag GmbH & Co. KGaA, Weinheim

the side chains of His10′, His42′, and Asp8′, the fourth coordination site being occupied by the β-phosphate of the inhibitors. The structures confirm our predicted binding mode with the anthranilate and dansyl fluorophores bound in Pocket II.

Two different conformations are observed for the six independent active sites (arbitrarily designated A–F) of IspF in the crystal of the ternary complex with ligand **7** and Zn^{II}. In active sites B–F, the ligand orientation and interactions with the protein are well conserved (see the Supporting Information). The CDP moiety of **7** takes a similar orientation in all six active sites A–F. The imidazole of His34′ in active site A is observed to be in a "closed" (into the active site) conformation, in contrast to the "open" one seen in active sites B–F.[18] Pocket II in structure A shows a higher degree of flexibility, which is mirrored in much larger thermal parameters (see the Supporting Information).

Figure 3 shows the superimposition of the X-ray crystal structures of the ternary complex of IspF-Zn^{II}-**7** (conformers B–F) with the previously reported structure of the quaternary complex of IspF with CMP, **6**, and Zn^{II} (PDB code 1JY8).[8a] In both structures, His34′ adopts the "open" conformation. The anthranilate nicely superimposes with the hydrophobic region of cyclodiphosphate **6**. The loop Leu60′–Phe68′, which shapes the hydrophobic cleft of Pocket II, shows substantial flexibility, approaching the ligands to varying degrees in the two complexes. Interestingly, this flexible loop adopts a nearly identical orientation in the superimposition of the crystal structures of the ternary complex IspF-Zn^{II}-**7** and the quaternary complex IspF-Zn^{II}-Mn^{II}-CDP (PDB code 1GX1).[8b] On the other hand, His34′ assumes the "closed" conformation in the latter complex to interact with the β-phosphate of CDP (see the Supporting Information).

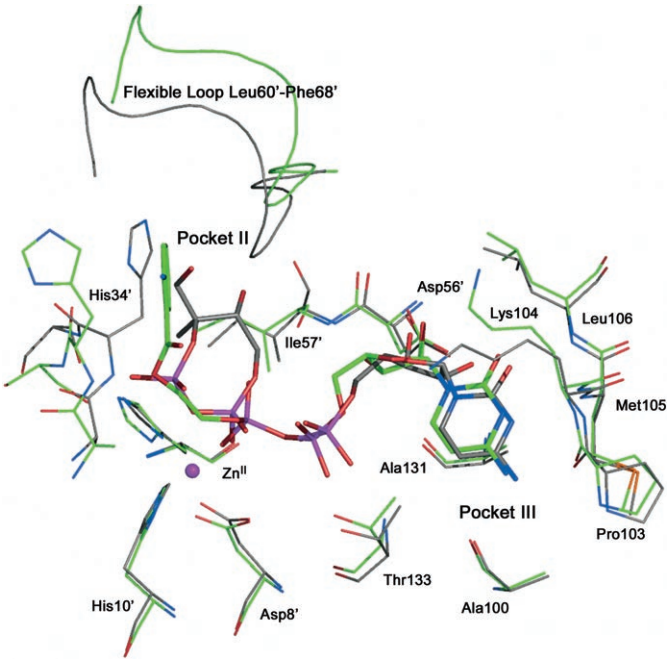


Figure 3. Superimposition of the X-ray crystal structures of the ternary complex of IspF-Zn^{II}-**7** (conformers B–F; C atoms: light-green) with the previously reported structure of the quaternary complex of IspF with CMP, 2C-methyl-D-erythritol 2,4-cyclodiphosphate (**6**), and Zn^{II} (PDB code 1JY8;[8a] C atoms: gray). Color code: O red, N blue, S red-orange, P purple, Zn^{II} ion: purple ball.[17]

The crystals of the ternary complex of IspF bound to **9** and Zn^{II} contain a single monomer in the asymmetric unit. Interactions in the cytidine pocket mirror those seen for the complex with **7** (see the Supporting Information). His34′ adopts an "open" conformation. A superimposition of the X-ray crystal structures of the enzyme bound to **7** and **9** (see the Supporting Information) provides additional evidence for the large conformational flexibility of the hydrophobic cleft of Pocket II. Compared to the complex of **7**, the lipophilic residues Ile56′, Phe61′, Phe68′, and Leu76′ interacting with **9** have undergone a considerable reorientation to accommodate the larger dansyl residue and engage in hydrophobic enzyme–ligand contacts. The F_o-F_c omit electron density map of bound **9** shows only weak electron density about the dansyl ring and elevated thermal parameters suggest a large degree of flexibility (see the Supporting Information).

In conclusion, we have reported the synthesis, biological evaluation, and co-crystal structures of the first designed inhibitors of IspF. By introducing fluorescent probes in inhibitors **7**–**9**, we could determine their affinity towards IspF by fluorescence binding titrations. Efforts to validate the utility of the fluorescent inhibitors as standards in rapid and economic affinity assays are ongoing. The predicted binding modes of **7** and **9** were largely confirmed by X-ray crystal structure analysis. Although the hydrophobic region in Pocket II apparently is very flexible, its occupation by aromatic rings leads to a measurable gain in binding free enthalpy. The results provide fruitful guidance for the future development of new inhibitors of the non-mevalonate pathway, by structure-based design, with the promise to ultimately generate new classes of antimalarials and other antimicrobials.

Received: August 23, 2005
Published online: January 3, 2005

Keywords: fluorescence · inhibitors · IspF · non-mevalonate pathway · protein crystal structure analysis

[1] a) U. Weiss (Ed.), "Malaria", in *Nature* **2002**, *415*, 669–715; b) L. Schofield, M. C. Hewitt, K. Evans, M.-A. Siomos, P. H. Seeberger, *Nature* **2002**, *418*, 785–789; c) J. K. Baird, *N. Engl. J. Med.* **2005**, *352*, 1565–1577.

[2] Fosmidomycin (OHC-N(OH)-$(CH_2)_3$-PO_3H_2) is a potent inhibitor of 1-deoxy-D-xylulose-5-phosphate reductoisomerase (IspC) in the non-mevalonate pathway. For some selected publications, see: a) J. Wiesner, R. Ortmann, H. Jomaa, M. Schlitzer, *Angew. Chem.* **2003**, *115*, 5432–5451; *Angew. Chem. Int. Ed.* **2003**, *42*, 5274–5293; b) T. Kuzuyama, T. Shimizu, S. Takahashi, H. Seto, *Tetrahedron Lett.* **1998**, *39*, 7913–7916; c) M. A. Missinou, S. Borrmann, A. Schindler, S. Issifou, A. A. Adegnika, P.-B. Matsiegui, R. Binder, B. Lell, J. Wiesner, T. Baranek, H. Jomaa, P. G. Kremsner, *Lancet* **2002**, *360*, 1941–1942; d) B. Lell, R. Ruangweerayut, J. Wiesner, M. A. Missinou, A. Schindler, T. Baranek, M. Hintz, D. Hutchinson, H. Jomaa,

 © 2006 Wiley-VCH Verlag GmbH & Co. KGaA, Weinheim

P. G. Kremsner, *Antimicrob. Agents Chemother.* **2003**, *47*, 735–738.

[3] H. Jomaa, J. Wiesner, S. Sanderbrand, B. Altincicek, C. Weidemeyer, M. Hintz, I. Türbachova, M. Eberl, J. Zeidler, H. K. Lichtenthaler, D. Soldati, E. Beck, *Science* **1999**, *285*, 1573–1576.

[4] a) W. Eisenreich, M. Schwarz, A. Cartayrade, D. Arigoni, M. H. Zenk, A. Bacher, *Chem. Biol.* **1998**, *5*, R221–R233; b) M. Rohmer, M. Knani, P. Simonin, B. Sutter, H. Sahm, *Biochem. J.* **1993**, *295*, 517–524.

[5] a) M. K. Schwarz, PhD Dissertation, ETH Zürich, No. 10951, **1994**; b) W. Eisenreich, B. Menhard, P. J. Hylands, M. H. Zenk, A. Bacher, *Proc. Natl. Acad. Sci. USA* **1996**, *93*, 6431–6436; c) S. T. J. Broers, PhD Dissertation, ETH Zürich, No. 10978, **1994**.

[6] a) F. Rohdich, S. Hecht, A. Bacher, W. Eisenreich, *Pure Appl. Chem.* **2003**, *75*, 2–3, 393–405; b) Y. Boucher, W. F. Doolittle, *Mol. Microbiol.* **2000**, *37*, 703–716; c) F. Rohdich, J. Wungsintaweekul, M. Fellermeier, S. Sanger, S. Herz, K. Kis, W. Eisenreich, A. Bacher, M. H. Zenk, *Proc. Natl. Acad. Sci. USA* **1999**, *96*, 11758–11763.

[7] For selected publications, see: a) F. Rohdich, W. Eisenreich, J. Wungsintaweekul, S. Hecht, C. A. Schuhr, A. Bacher, *Eur. J. Biochem.* **2001**, *268*, 3190–3197; b) S. B. Richard, J.-L. Ferrer, M. E. Bowman, A. M. Lillo, C. N. Tetzlaff, D. E. Cane, J. P. Noel, *J. Biol. Chem.* **2002**, *277*, 8667–8672; c) T. L. Campbell, E. D. Brown, *J. Bacteriol.* **2002**, *184*, 5609–5618.

[8] a) S. Steinbacher, J. Kaiser, J. Wungsintaweekul, S. Hecht, W. Eisenreich, S. Gerhardt, A. Bacher, F. Rohdich, *J. Mol. Biol.* **2002**, *316*, 79–88; b) L. E. Kemp, C. S. Bond, W. N. Hunter, *Proc. Natl. Acad. Sci. USA* **2002**, *99*, 6591–6596.

[9] Published crystal structures of IspF: a) H. Kishida, T. Wada, S. Unzai, T. Kuzuyama, M. Takagi, T. Terada, M. Shirouzu, S. Yokoyama, J. R. H. Tame, S.-Y. Park, *Acta Crystallogr. D* **2003**, *59*, 23–31; b) S. Ni, H. Robinson, G. C. Marsing, D. E. Bussiere, M. A. Kennedy, *Acta Crystallogr. D* **2004**, *60*, 1949–1957; c) C. Lehmann, K. Lim, J. Toedt, W. Krajewski, A. Howard, E. Eisenstein, O. Herzberg, *Proteins: Struct. Funct. Bioinf.* **2002**, *49*, 135–138; d) L. E. Kemp, M. S. Alphey, C. S. Bond, M. A. J. Ferguson, S. Hecht, A. Bacher, W. Eisenreich, F. Rohdich, W. N. Hunter, *Acta Crystallogr. D* **2005**, *61*, 45–52; e) T. Sgraja, L. E. Kemp, N. L. Ramsden, W. N. Hunter, *Acta Crystallogr. F* **2005**, *61*, 625–629.

[10] a) P. R. Gerber, K. Müller, *J. Comput.-Aided Mol. Des.* **1995**, *9*, 251–268; b) Gerber Molecular Design (http://www.moloc.ch).

[11] For structure-based design of inhibitors of plasmepsin II, another potential target in antimalarial therapy, see: D. Carcache, S. Hörtner, A. Bertogg, C. Bonkert, D. Bur, H. P. Märki, A. Dorn, F. Diederich, *ChemBioChem* **2002**, *3*, 1137–1141.

[12] a) Y.-H. Li, L.-M. Chan, L. Tyler, R. T. Moody, C. M. Himel, D. M. Hercules, *J. Am. Chem. Soc.* **1975**, *97*, 3118–3126; b) F. Diederich, K. Dick, D. Griebel, *Chem. Ber.* **1985**, *118*, 3588–3619.

[13] M. Saady, L. Lebeau, C. Mioskowski, *Tetrahedron Lett.* **1995**, *36*, 2239–2242.

[14] V. Wittmann, C.-H. Wong, *J. Org. Chem.* **1997**, *62*, 2144–2147.

[15] a) The fluorescent inhibitors **7–9** were titrated into a solution (2 mL) of IspF (17 kDa per subunit) from *E. coli* (6.25 μM) in 50 mM Tris hydrochloride, pH 8.2, containing 10 mM $MgSO_4$ and 2 mM $ZnO(Ac)_2$ in a total volume of 3 mL at 20 °C (Tris = tris(hydroxymethyl)aminomethane). Spectral data were recorded at $\lambda_{exc} = 320$ nm, $\lambda_{em} = 423$ nm for compounds **7** and **8**, and $\lambda_{exc} = 366$ nm, $\lambda_{em} = 532$ nm for **9**, using a Hitachi F-2000 fluorescence spectrophotometer (1-cm quartz cuvette, 3-mL volume). K_d values were derived using Equation (1):

$$I_{rel} = (I_{max} F_o)(K_d + F_o)^{-1} \quad (1),$$

where I_{rel} is the relative fluorescence intensity at the recorded emission wavelength, I_{max} the maximal fluorescence enhancement of bound inhibitor at saturation, and F_o is the concentration of the fluorophore. Background emissions of **7–9** (from 0–24 μM) as well as of IspF in 50 mM Tris hydrochloride, pH 8.2, containing 10 mM $MgSO_4$ and 2 mM $Zn(OAc)_2$, were subtracted to obtain the saturation curves shown in Figure 2. The relative fluorescence enhancements $(I_{max}-I)/I$, where I is the maximum fluorescence of the unbound inhibitor, were 20% (**7**), 30% (**8**), and 80% (**9**). Binding data were analyzed by nonlinear least-squares approximation (GraphPad Prism 4 Software, San Diego, CA, 2005). Uncertainties given are standard deviations, with R^2 for all fits ≥ 0.96); b) R. S. Sarfati, V. K. Kansal, H. Munier, P. Glaser, A.-M. Gilles, E. Labruyère, M. Mock, A. Danchin, O. Bârzu, *J. Biol. Chem.* **1990**, *265*, 18902–18906; c) W. O. McClure, G. M. Edelman, *Biochemistry* **1967**, *6*, 559–566.

[16] The IC_{50} values for CMP, CDP, and **9** were determined in enzymatic reactions catalyzed by the *E. coli* IspF enzyme using [1,3,4-$^{13}C_3$]-**5** (1 mM) as substrate. Product formation was monitored by ^{13}C NMR spectroscopy (see the Supporting Information).

[17] a) Crystals of *E. coli* IspF complexed with ligands **7** or **9** were grown by the vapor-diffusion method.[8b] The reservoir solution was 0.1 M ammonium sulfate and 0.1 M sodium acetate, pH 5, and 10% and 8% monomethylether polyethylene glycol 200 for compounds **7** and **9**, respectively. The hanging drops consisted of 1 μL of reservoir and 3 μL of a solution of IspF (5.5 mg mL^{-1}) in 50 mM Tris (tris(hydroxymethyl)aminomethane) hydrochloride, pH 7.7, containing 50 mM NaCl and 2 mM ligand. Crystals of the complex with **7** are monoclinic plates in the space group $P2_1$ with unit cell dimensions $a = 54.03$, $b = 115.27$, $c = 87.61$ Å, $\beta = 90.18°$. Crystals of the complex with **9** are cubic blocks in the space group $I2_13$ with $a = 145.1$ Å. Data were measured on beamline ID29 at the European Synchrotron Radiation Facility (Grenoble, France) and processed with MOSFLM (A. G. W. Leslie, H. R. Powell, G. Winter, O. Svensson, D. Spruce, S. McSweeney, D. Love, S. Kinder, E. Duke, C. Nave, *Acta Crystallogr. D* **2002**, *58*, 1924–1928). The dataset for the complex of **7** is 99.5% complete to 2.3-Å resolution with an R_{sym} value of 9.7%, 27.1% in the highest resolution bin. The dataset for the complex of **9** is 99% complete to 2.5-Å resolution with an R_{sym} value of 8%, 68.5% in the highest resolution bin. The starting model for both analyses was the structure of *E. coli* IspF in complex with CDP (PDB code 1GX1). Molecular replacement methods (Collaborative Computational Project Number 4, *Acta Crystallogr. D* **1994**, *50*, 760–763; J. Navaza, *Acta Crystallogr. Sect. D* **2001**, *57*, 1367–1372) were used to generate the starting models for refinement, which consisted of six subunits (two trimers) for the complex with **7** and a single subunit for the complex with **9**. The structures were refined using a combination of O (T. A. Jones, J. Y. Zou, S. W. Cowan, M. Kjeldgaard, *Acta Crystallogr. A* **1991**, *47*, 110–119) and refmac5 (G. N. Murshudov, A. A. Vagin, E. J. Dodson, *Acta Crystallogr. D* **1997**, *53*, 240–255) to an R factor of 24.3% and R-free of 27.9% for the complex with **7**; an R factor of 21.5% and R-free of 25.9% for the complex of **9**. The model for the complex of **7** includes 233 water molecules, six Zn^{II} ions, one in each active site and two molecules of geranyldiphosphate (GPP).[9d] A total of 92.1% of the residues are in the most favored regions of the Ramachandran plot with none in disallowed regions. The model for the complex of **9** includes 56 water molecules, a Zn^{II} ion, and one geranyldiphosphate; 90.8% of the residues are in the most favored regions of the Ramachandran plot with none in disallowed regions. Further details are included in the Protein Data Bank depositions PDB codes: 2AMT and 2AO4; b) It should be noted that a screen of crystallization conditions were

 © 2006 Wiley-VCH Verlag GmbH & Co. KGaA, Weinheim

explored to generate useful crystals, and the best conditions did not have Mg^{II} present for either ligands **7** and **9**. Crystals with other ligands in the presence and absence of Mg^{II} or Mn^{II} have been grown in the past; structural differences that can be attributed to the presence/absence of the divalent cations could not be observed (unpublished data).

[18] a) The imidazole ring of His34′ in active sites B–F is observed to varying degrees to be in an "open" (away from the active site) conformation. Distances from the anthranilate NH_2 to the imidazole ring range from 3.8 to 4.5 Å, thereby precluding the presence of any strong interaction. The "open" and "closed" conformations of His34′ have been observed in some of the previously reported crystal structures of IspF.[8,9] b) Deviation in active site A cannot be attributed to crystal-packing effects.

 © 2006 Wiley-VCH Verlag GmbH & Co. KGaA, Weinheim

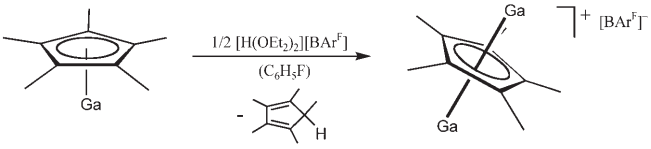
Organogallium Complexes

DOI: 10.1002/anie.200503028

The $[Ga_2(C_5Me_5)]^+$ Ion: Bipyramidal Double-Cone Structure and Weakly Coordinated, Monovalent Ga^+**

*Beatrice Buchin, Christian Gemel, Thomas Cadenbach, Rochus Schmid, and Roland A. Fischer**

Who understands how to play with weak interactions and metastable states can break new synthetic ground in organoelement chemistry. In this context, Al^I and Ga^I compounds and metalloid clusters of Group 13 investigated by Schnöckel and co-workers are considered as milestones.[1,2] The good accessibility of low-coordinate Ga^I organyls such as [GaCp*],[3,4] [Ga(ddp)] (Cp* = C_5Me_5; ddp = 2-{(2,6-diisopropylphenyl)amino}-4-{(2,6-diisopropylphenyl)imino}-2-pentene)[5] and GaR (R = $C(SiMe_3)_3$,[6] $Si(SiMe_3)$[7]) allows inter alia their use as exceptionally electron-rich carbenoid ligands in organometallic chemistry,[8,9] a field which we have been focusing on for quite some time.[10] Aiming at complex cations of the type $[M(ECp^*)_n]^{m+}$, we recently investigated the reaction of [GaCp*] with $[M(NCCH_3)_6][BAr^F]_2$ (M = V, Cr, Fe, Co, Ni; $BAr^F = [B\{C_6H_3(CF_3)_2\}_4]$.[11] Surprisingly, a redox-neutral Cp* transfer to the transition metal is observed in certain cases, which is accompanied by the formation of the title compound $[Ga_2Cp^*][BAr^F]$ (**1**) as a by-product. According to Scheme 1, **1** can be prepared quantitatively by controlled protolysis of [GaCp*].



1

Scheme 1. Reaction of [GaCp*] with $[H(OEt_2)_2][BAr^F]$.

Treatment of a solution of [GaCp*] in fluorobenzene with one half molar equivalent of $[H(OEt_2)_2][BAr^F]$ in fluorobenzene at 25 °C leads to an immediate color loss of the initial yellowish reaction mixture. Product **1** is precipitated by slow addition of *n*-hexane as small, colorless needles in reproducible good yields of around 85 %. The formation of **1** is similar to the synthesis of $[Cp^*Si][B(C_6F_5)_4]$ by protolysis of $[Cp^*_2Si]$ with $[Cp^*H_2][B(C_6F_5)_4]$ in dichloromethane recently reported by Jutzi and co-workers.[12] Compound **1** is very well soluble in fluorobenzene but almost insoluble in nonpolar solvents such as *n*-hexane or toluene. In the presence of strongly coordinating solvents such as THF, compound **1** decomposes immediately under formation of [GaCp*] and other unidentified side products. The ^1H NMR spectrum of **1** in fluorobenzene shows signals for the protons of the BAr^F group at $\delta = 7.64$ (4H) and 8.32 ppm (8H) as well as a singlet at $\delta =$ 1.69 ppm (15H) for the chemically equivalent methyl groups of the Cp* ring. The ^{71}Ga NMR signal for **1** at $\delta = -519$ ppm is distinctly downfield shifted compared to the respective signal for [GaCp*] ($\delta = -653$ ppm)[13] and those of the arene complexes $[Ga(arene)_2][GaX_4]$ ($\delta = -609$ to -675 ppm).[20] The ^1H NMR spectrum of a 1:1 mixture of **1** and [GaCp*] in fluorobenzene reveals a coalesced signal at $\delta = 1.80$ ppm. Obviously, a fast exchange of Ga^+ ions between [GaCp*] units is taking place, which points to a comparably weak Ga–Cp* interaction as well as a complete dissociation of **1** into ions in solution.

Compound **1** crystallizes in the triclinic space group $P\bar{1}$.[14] The cation shows an unusual, highly symmetric bipyramidal double-cone structure, in which both gallium atoms are almost exactly above and below the center of the C_5 ring, respectively (Figure 1). The ionic bonding situation is

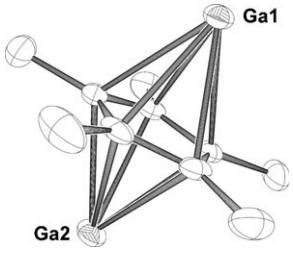


Figure 1. Structure of the $[Ga_2(C_5Me_5)]^+$ ion of **1** (ORTEP plot: 50% ellipsoids; hydrogen atoms have been omitted for clarity). Selected bond lengths [Å] and angles [°]: Ga1–$Cp^*_{centr.}$ 2.228, Ga2–$Cp^*_{centr.}$ 2.237; Ga1-$Cp^*_{centr.}$-Ga2 178.2.

[*] B. Buchin, Dr. C. Gemel, T. Cadenbach, Dr. R. Schmid, Prof. Dr. R. A. Fischer
Lehrstuhl für Anorganische Chemie II
Organometallics & Materials
Ruhr-Universität Bochum
44780 Bochum (Germany)
Fax: (+49) 234-321-4174
E-mail: roland.fischer@ruhr-uni-bochum.de

[**] Organometal Complexes of d-Block Elements, Part 41. Part 40: Ref. [10b].

Supporting information for this article is available on the WWW under http://www.angewandte.org or from the author.

InterScience
© 2006 Wiley-VCH Verlag GmbH & Co. KGaA, Weinheim

reflected by the Ga–Cp*$_{centr.}$ distances of 2.228 Å and 2.237 Å, which are significantly longer than that in [GaCp*] (2.081 Å) in the solid state as well as in the gas phase. The individual Ga–C distances of 2.505 to 2.562 Å hardly deviate from each other (cf. the solid-state structure of [GaCp*]: 2.380–2.421 Å).[15,16] The Ga1-Cp*$_{centr.}$-Ga2 arrangement is almost linear (178.2°).[17] Similar structures with Cp* as a symmetrically coordinated bridging ligand are very rare. One example is $[Cs_2Cp^*([18]crown\text{-}6)_2]^+[Cs_4Cp_3Cp^*_2([18]crown\text{-}6)_2]^-$, whose cation reveals the structural motif $[Cs_2Cp^*]^+$ analogous to **1**.[18,19]

The crystal packing (Figure 2) of the ions places each Ga atom between two of the four $[C_6H_3(CF_3)_2]$ groups of the anion. The distances of the Ga atoms to the individual C atoms of the [BAr^F] ion differ only slightly from each other (3.4–4.0 Å), but are too long to be considered as a directed bonding interaction. Similarly, the Ga–F contacts in **1** (>3.7 Å) are very long, and thus not comparable to the crown-ether cesium interaction in the above example.

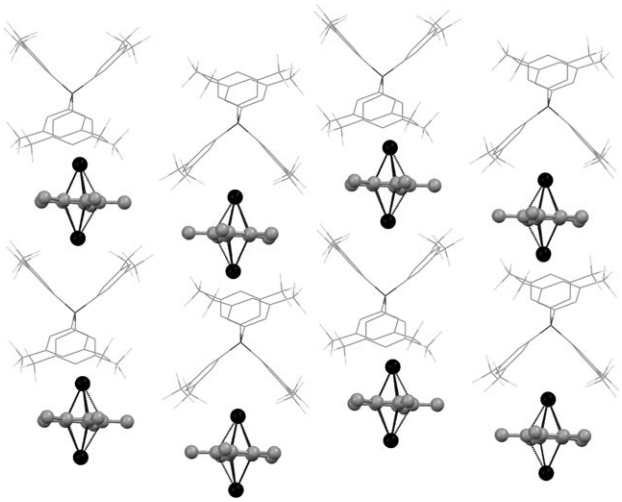


Figure 2. Mercury plot of the crystal packing of **1** (ball-and-stick model for the cation, wireframe-plot for the anion); hydrogen atoms and C_6H_5F are omitted for clarity.

The stabilization of Ga^I ions in solution by arene complexes is known, but only in halogeno-bridged complexes. A typical example for this is $[Ga(mesitylene)_2][GaX_4]$, which reveals distinctly shorter Ga–C$_{aryl}$ distances than **1** (ca. 3.0 Å).[20] Figure 3 shows the frontier orbital schemes of the model compounds $[Ga_2Cp]^+$ and $[Al_2Cp]^+$ (B3LYP/cc-pVDZ).[21] Cp adopts the role of a typical bridging ligand in an electron-deficient compound with multicenter bonds. The two free electron pairs of the E^I centers result from the interaction of the doubly occupied s(p$_z$) orbitals with the occupied a$_1$-symmetric ψ_1 orbital of the Cp ligand and are found in the nonbonding and the antibonding σ orbital, respectively. The elongated Ga–Cp$_{centr.}$ distances of **1** (ca. 0.2 Å longer than those in [GaCp*]) are very well reproduced in the optimized structures and are explained by a decrease of the covalent contribution. The π–π* splitting for the ionic compounds $[E_2Cp]^+$ is slightly larger than for [ECp] (7 eV in **1**, 6.1 eV in [GaCp]), which leads to a significant weakening of the π bond to each individual E.

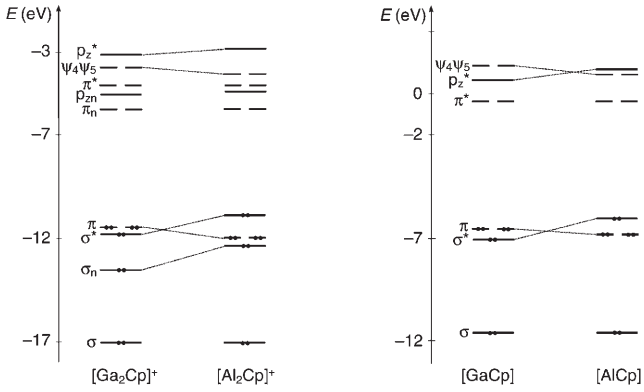
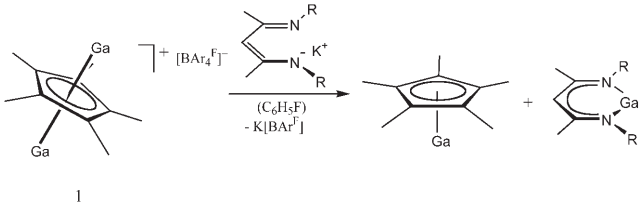


Figure 3. Frontier orbitals of $[Ga_2Cp]^+$ and $[Al_2Cp]^+$ (left) and the monomers [GaCp] and [AlCp] (right).

Thus, the $[Ga_2(C_5Me_5)]^+$ ion can be regarded as a stabilized, almost "naked" Ga$^+$ ion, which is not known in solution under ordinary conditions. Accordingly, **1** should serve as a selective source for highly reactive Ga$^+$. Co-crystallization of **1** with soft π donors such as HC≡C(SiMe$_3$), PhC≡CPh, divinyldisiloxane, t,t,t-1,5,9-cyclododecatriene, and ferrocene led to neither new isolable products nor a shift of the ^{1}H NMR signals. However, treatment with electron-rich decamethylferrocene resulted in a clean redox reaction under deposition of gallium metal and formation of [GaCp*] and the ferrocenium cation $[Cp^*_2Fe]^+$. Treatment of **1** with strong Lewis acids (B(C$_6$F$_5$)$_3$) or hard nucleophiles (LiCl) led to decomposition or disproportionation and Ga deposition. However, the salt **1** reacts cleanly as a source for Ga$^+$ with K[ddp] to give [GaCp*] and [Ga(ddp)] (Scheme 2).



Scheme 2. Reaction of **1** with K[ddp].

As shown by ^{1}H NMR spectroscopy, **1** also reacts cleanly with Li[N(SiMe$_3$)$_2$] in fluorobenzene under selective cleavage of [GaCp*] and formation of a new sepecies, which could be the so far unknown Ga^I amide $[Ga\{N(SiMe_3)_2\}]_n$. The isolation and characterization of this new species is still in progress. The high reactivity of **1**, in particular the reactions with soft anionic nucleophiles, point to the potential of the title compound as a source of Ga$^+$ for the synthesis of new Ga^I compounds. This applies similarly to the protonation of $[(Cp^*Al)_4]$ in fluorobenzene, which leads to a dark red solution, the characterization of which we are currently working on. In general it can be expected that analogous protonation of clusters of the type $[M_a(ECp^*)_b]$ with [H-

 © 2006 Wiley-VCH Verlag GmbH & Co. KGaA, Weinheim

$(OEt_2)_2][BAr^F]$ leads to cleavage of Cp*H and formation of interesting new and reactive products.

Experimental Section

1: A solution of $[H(EtO_2)_2][BAr^F]$ (200 mg, 0.197 mmol) in fluorobenzene (3 mL) was added slowly to a solution of [GaCp*] (85 mg, 0.415 mmol) in fluorobenzene (3 mL), whereupon the color changed immediately from yellow to colorless. The reaction mixture was stirred for a few minutes at room temperature, then the solvent was reduced in vacuo to about 2 mL, and the product was precipitated by addition of *n*-hexane to give a white crystalline solid. The solvent was removed by filtration, the residue washed with hexane (2 × 2 mL), and dried in vacuo. Yield: 188 mg (84%). Recrystallization of the crude product by slow diffusion of hexane into a solution of **1** in fluorobenzene at 25°C gave well-formed needle-shaped single crystals.

^{1}H NMR (fluorobenzene/C_6D_6, 20°C): $\delta = 8.30$ (8H, $[BAr^F]$), 7.63 (4H, $[BAr^F]$), 1.69 ppm (15H, C_5Me_5); ^{1}H NMR (CD_2Cl_2, 20°C): $\delta = 7.73$ (8H, $[BAr^F]$), 7.57 (4H, $[BAr^F]$), 2.24 ppm (15H, C_5Me_5); ^{13}C NMR (CD_2Cl_2, 20°C): $\delta = 162.2$ (q, $J = 50$ Hz, $[BAr^F]$), 135.2 ($[BAr^F]$), 129.2 (q, $J = 31.5$ Hz, $[BAr^F]$), 125.0 (q, $J = 272.4$ Hz, $[BAr^F]$), 123.5 (C_5Me_5), 117.9 ($[BAr^F]$), 10.1 ppm (C_5Me_5); ^{71}Ga NMR (CD_2Cl_2, 20°C): $\delta = -519$ ppm; elemental analysis calcd (%) for $C_{48}H_{32}BF_{25}Ga_2$ (**1**·C_6H_5F): C 46.72, H 2.61; found: C 46.27, H 2.85.

Quantum-chemical calculations: All calculations were performed by using the Gaussian 03 program package[22] with the hybrid exchange-correlation functional B3LYP[23,24] and the all-electron basis set cc-pVDZ.[25,26] All structures were fully optimized and characterized as stationary minima by inspection of the vibrational frequencies.

Received: August 25, 2005
Revised: September 28, 2005
Published online: December 15, 2005

Keywords: carbenoids · cyclopentadienyl compounds · gallium · Group 13 elements

[1] C. Dohmeier, D. Loos, H. Schnöckel, *Angew. Chem.* **1996**, *108*, 141–161; *Angew. Chem. Int. Ed. Engl.* **1996**, *35*, 129–149.
[2] A. Schnepf, H. Schnöckel, *Angew. Chem.* **2002**, *114*, 3682–3704; *Angew. Chem. Int. Ed.* **2002**, *41*, 3533–3552.
[3] P. Jutzi, B. Neumann, G. Reumann, H. G. Stammler, *Organometallics* **1998**, *17*, 1305–1314.
[4] P. Jutzi, L. O. Schebaum, *J. Organomet. Chem.* **2002**, *654*, 176–179.
[5] N. J. Hardman, B. E. Eichler, P. P. Power, *Chem. Commun.* **2000**, 1991–1992.
[6] W. Uhl, W. Hiller, M. Layh, W. Schwarz, *Angew. Chem.* **1992**, *104*, 1378–1380; *Angew. Chem. Int. Ed. Engl.* **1992**, *31*, 1364–1366.
[7] G. Linti, *J. Organomet. Chem.* **1996**, *520*, 107–113.
[8] R. A. Fischer, J. Weiss, *Angew. Chem.* **1999**, *111*, 3002–3022; *Angew. Chem. Int. Ed.* **1999**, *38*, 2830–2850.
[9] R. Murugavel, V. Chandrasekhar, *Angew. Chem.* **1999**, *111*, 1289–1293; *Angew. Chem. Int. Ed.* **1999**, *38*, 1211–1215.
[10] a) C. Gemel, T. Steinke, M. Cokoja, A. Kempter, R. A. Fischer, *Eur. J. Inorg. Chem.* **2004**, 4161–4176; b) B. Buchin, C. Gemel, T. Cadenbach, R. A. Fischer, *Inorg. Chem.* **2005**, submitted .
[11] B. Buchin, Diploma Thesis, Ruhr Universität Bochum (Bochum), **2005**.
[12] P. Jutzi, A. Mix, B. Rummel, W. W. Schoeller, B. Neumann, H.-G. Stammler, *Science* **2004**, *305*, 849–851.
[13] D. Loos, H. Schnöckel, *J. Organomet. Chem.* **1993**, *463*, 37–40.
[14] Crystal structure analysis of **1**·C_6H_5F: crystal size: 0.25 × 0.20 × 0.15 mm, triclinic, $P\bar{1}$, $a = 10.272(3)$, $b = 13.231(3)$, $c = 18.852(2)$ Å, $\alpha = 92.643(18)$, $\beta = 92.006(15)$, $\gamma = 112.327(19)°$, $V = 2363.8(10)$ Å^3, $Z = 2$, $\rho_{calcd} = 1.636$ mg m^{-3}, $2\Theta_{max} = 50.10°$, $\lambda(Mo_{K\alpha}) = 0.71073$ Å, $T = 105(2)$ K. A total of 28404 reflections (8322 unique) were measured on a Oxford Excalibur 2 diffractometer [R(int) = 0.0527]. The structural solution and refinement was done using the programs SHELXS-97 and SHELXL-97. The final values for $R1$ and $wR2(F^2)$ were 0.0518 and 0.0944 (all data). CCDC-281940 contains the supplementary crystallographic data for this paper. These data can be obtained free of charge from The Cambridge Crystallographic Data Centre via www.ccdc.cam.ac.uk/data_request/cif.
[15] D. Loos, E. Baum, A. Ecker, H. Schnöckel, *Angew. Chem.* **1997**, *109*, 894–896; *Angew. Chem. Int. Ed. Engl.* **1997**, *36*, 860–862.
[16] A. Haaland, K.-G. Martinsen, H. V. Volden, D. Loos, H. Schnöckel, *Acta Chem. Scand.* **1994**, *48*, 172–174.
[17] The structural motif Ga-X-Ga is reminiscent of the monomeric unit of the neutral gallium suboxide Ga_2O, see: a) T. R. Burkholder, J. T. Justein, L. Andrews, *J. Phys. Chem.* **1992**, *96*, 10189–10195; b) S. Gowtham, A. Costales, R. Pandey, *J. Phys. Chem. B* **2004**, *108*, 17295–17300.
[18] P. Jutzi, G. Reumann, *J. Chem. Soc. Dalton Trans.* **2000**, 2237–2244.
[19] F. Olbrich, unpublished results.
[20] H. Schmidbaur, *Angew. Chem.* **1985**, *97*, 893–904; *Angew. Chem. Int. Ed. Engl.* **1985**, *24*, 893–904.
[21] For information on M–ECp bonds, see: J. Uddin, G. Frenking, *J. Am. Chem. Soc.* **2001**, *123*, 1683–1693.
[22] Gaussian 03 (Revision B.04), M. J. Frisch, G. W. Trucks, H. B. Schlegel, G. E. Scuseria, M. A. Robb, J. R. Cheeseman, J. A. Montgomery, Jr., T. Vreven, K. N. Kudin, J. C. Burant, J. M. Millam, S. S. Iyengar, J. Tomasi, V. Barone, B. Mennucci, M. Cossi, G. Scalmani, N. Rega, G. A. Petersson, H. Nakatsuji, M. Hada, M. Ehara, K. Toyota, R. Fukuda, J. Hasegawa, M. Ishida, T. Nakajima, Y. Honda, O. Kitao, H. Nakai, M. Klene, X. Li, J. E. Knox, H. P. Hratchian, J. B. Cross, C. Adamo, J. Jaramillo, R. Gomperts, R. E. Stratmann, O. Yazyev, A. J. Austin, R. Cammi, C. Pomelli, J. W. Ochterski, P. Y. Ayala, K. Morokuma, G. A. Voth, P. Salvador, J. J. Dannenberg, V. G. Zakrzewski, S. Dapprich, A. D. Daniels, M. C. Strain, O. Farkas, D. K. Malick, A. D. Rabuck, K. Raghavachari, J. B. Foresman, J. V. Ortiz, Q. Cui, A. G. Baboul, S. Clifford, J. Cioslowski, B. B. Stefanov, G. Liu, A. Liashenko, P. Piskorz, I. Komaromi, R. L. Martin, D. J. Fox, T. Keith, M. A. Al-Laham, C. Y. Peng, A. Nanayakkara, M. Challacombe, P. M. W. Gill, B. Johnson, W. Chen, M. W. Wong, C. Gonzalez, J. A. Pople, Gaussian, Inc., Pittsburgh, PA, **2003**.
[23] A. D. Becke, *J. Chem. Phys.* **1993**, *98*, 5648–5652.
[24] R. G. Parr, W. Yang, C. Lee, *Phys. Rev. B* **1988**, *37*, 785–789.
[25] J. T. H. Dunning, *J. Chem. Phys.* **1989**, *90*, 1007–1023.
[26] A. K. Wilson, D. E. Woon, K. A. Peterson, J. T. H. Dunning, *J. Chem. Phys.* **1999**, *110*, 7667–7676.

 © 2006 Wiley-VCH Verlag GmbH & Co. KGaA, Weinheim

Photochemical Syntheses

DOI: 10.1002/anie.200502687

A Convergent Synthesis of *N*-Glycopeptides**

*Clyde M. Kaneshiro and Katja Michael**

Interest in glycopeptides has experienced a dramatic resurgence partly because of their importance as building blocks for the synthesis of large, structurally defined glycopeptides and glycoproteins by native chemical ligation.[1] The sequential solid-phase synthesis of *N*-glycopeptides by the Fmoc/*t*Bu strategy, which requires coupling of an Fmoc-protected *N*-glycosylasparagine building block to the peptide chain, is well established.[2] However, the Fmoc-protected amino acid building block is typically applied in large excess to drive coupling in the heterogeneous phase to completion, but glycosylated amino acids are precious materials. Another problem arises when the glycosyl moiety of the Fmoc-Asn(glycosyl)-OH building block has unprotected hydroxy groups, as *O*-acylation can occur in all following coupling steps.

A promising alternative to stepwise synthesis is convergent synthesis, in which an aspartic acid containing peptide is condensed with a glycosylamine.[3] The reactants can be utilized in equimolar amounts in solution or with one component in small excess. However, none of the known protocols are capable of avoiding the formation of persistent by-products, such as peptide aspartimides and peptide rearrangement products.[4] Not only are these by-products sometimes the major products, but they can also be difficult to separate.

Major factors influencing aspartimide formation upon activation of the aspartic acid β-carboxyl group are a) the neighboring amino acid located at the C terminus of the aspartic acid;[5] and b) the amount of base, for example, diisopropylethylamine (DIPEA), which is commonly employed as an additive in coupling reactions.[3a] Although the amino acid sequence is dictated by the target glycopeptide, we envisioned that the problem of aspartimide formation may be addressed by performing a photochemical coupling under neutral conditions. Several base-free methods exist, for example, coupling with *O*-(benzotriazol-1-yl)-*N*,*N*,*N*′,*N*′-tetramethyluronium hexafluorophosphate (HBTU)/1-hydroxybenzotriazole (HOBt) or 2-isobutyloxy-1-isobutyloxycarbonyl-1,2-dihydroquinoline (IIDQ).[3a–c] However, these methods require orthogonally protected peptides to allow the selective deprotection and activation of the carboxyl group to be condensed with a glycosylamine. Although orthogonal protecting groups for the aspartic acid side chain are available (e.g., the allyl or *p*-methoxybenzyl ester),[6] at least two synthetic steps are required for deprotection, activation, and coupling. We felt that the process could be simplified if the protecting group of the aspartic acid side chain could be easily converted into an activating group in situ, followed by immediate interception by a glycosylamine to form the desired amide bond.

Our solution to both challenges—the formation of aspartimide and single-step activation of an orthogonal protecting group—is the use of a photoreactive 7-nitroindoline amide of the aspartyl side chain. In 1976 Patchornik and co-workers discovered that *N*-acyl-7-nitroindolines undergo photosolvolysis in nucleophilic solvents.[7] The 5-bromo-7-nitroindoline moiety was subsequently used as a photocleavable protecting group generating peptidyl acids and esters,[8] and it has been applied in peptide segment condensation.[9] More recently, an *N*-acyl-7-nitroindoline moiety was incorporated into a photolabile linker for the solid-phase synthesis of linear and cyclic amides.[10] Aliphatic amines were also photochemically acylated with *N*-acyl-5,7-dinitroindolines.[11] We have explored the applicability of *N*-acyl-5-bromo-7-nitroindolines in the synthesis of *N*-glycosyl asparagines and glutamines through coupling of photoreactive amino acid derivatives with small glycosylamines.[12]

The acylation relies on the unique photochemical properties of *N*-acyl-7-nitroindolines ($\lambda_{max} \approx 350$ nm), which can be excited with UV light from a mercury lamp. Standard Pyrex glassware completely filters out destructive high-energy light at wavelengths below 310 nm. A number of aprotic organic solvents, such as dichloromethane, chloroform, tetrahydrofuran (THF), acetonitrile, tetramethylurea, *N*-methylpyrrolidone, and dimethyl sulfoxide (DMSO), can be used. The latent *N*-acyl-7-nitroindoline is believed to rearrange upon excitation in organic solvents to give a nitronic anhydride, the *anti* conformation[13] of which reacts with an amine to afford an amide and 7-nitroindoline.[14] In water, the nitronic anhydride generates a carboxylic acid and a 7-nitrosoindole (Scheme 1).[14b,15]

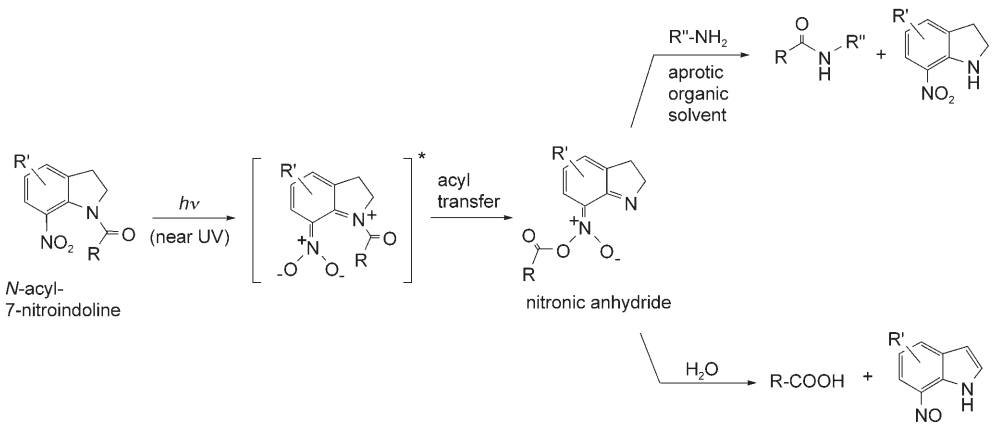
We demonstrate the photochemical convergent synthesis of *N*-glycopeptides on model sequences of human erythropoietin (hEpo), a glycoprotein hormone with *N*-glycosylation sites at positions 24, 38, and 83.[16] Four hEpo peptides were synthesized by solid-phase synthesis using the Fmoc/*t*Bu strategy and HBTU/HOBt/DIPEA coupling on Sieber amide resin.[17] The Fmoc-Asp(Bni)-OH building block is readily available by Pd-catalyzed deallylation of Fmoc-Asp(Bni)-OAll[12] with *N*-methylaniline.[18] Cleavage from the resin with dilute trifluoroacetic acid (TFA) produced the fully protected photoreactive peptide amides **1**–**4** (Figure 1), which were each purified by flash chromatography and characterized by mass spectrometry. The Fmoc chromophore present in each peptide allowed additional analysis of the peptides and

[*] Dr. C. M. Kaneshiro, Prof. Dr. K. Michael
Department of Chemistry
University of Hawaii
2545 McCarthy Mall, Honolulu, HI 96822 (USA)
Fax: (+1) 808-956-5908
E-mail: kmichael@hawaii.edu

[**] We thank Prof. Yasuhiro Kajihara (Yokohama City Univ.) for providing the oligosaccharide precursor of glycosylamine **9**, Wesley Yoshida and Mike Burger (Univ. of Hawaii) for the NMR and MS analyses, and the donors of the American Chemical Society Petroleum Research Fund for financial support (PRF Type 40279-G1).

Supporting information for this article is available on the WWW under http://www.angewandte.org or from the author.

 © 2006 Wiley-VCH Verlag GmbH & Co. KGaA, Weinheim



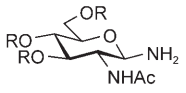
Scheme 1. Mechanism of the photolysis of *N*-acyl-7-nitroindolines.[13,14,15a]

1: Fmoc-Glu(OBn)-Asp(Bni)-Ile-Thr(*t*Bu)-Thr(*t*Bu)-Gly-Cys(Trt)-Ala-NH_2

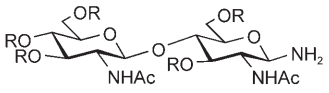
2: Fmoc-Glu(OtBu)-Asp(Bni)-Ile-Thr(*t*Bu)-Val-Pro-NH_2

3: Fmoc-Glu(OBn)-Asp(Bni)-Ile-Thr(*t*Bu)-Val-Pro-NH_2

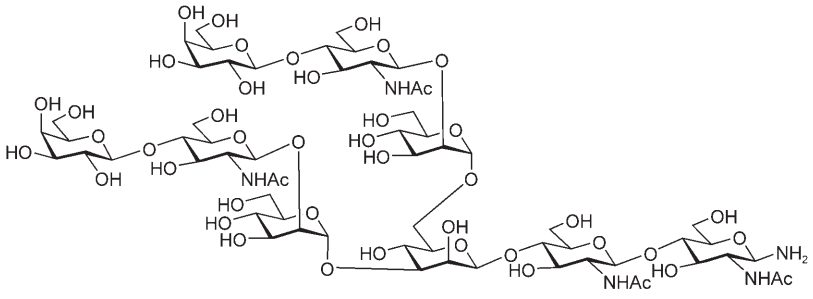
4: Fmoc-Ala-Leu-Leu-Val-Asp(Bni)-Ser(*t*Bu)-Ser(*t*Bu)-NH_2



5 (R = Ac)
6 (R = H)



7 (R = Ac)
8 (R = H)



9

Figure 1. Photoreactive hEpo peptides and glycosylamines used for *N*-glycopeptide synthesis. Bni = 5-bromo-7-nitroindoline; Fmoc = 9-fluorenylmethyloxycarbonyl.

monitoring of the photochemical coupling reactions by HPLC.

Whereas peptides **1**–**3** were synthesized by standard solid-phase synthesis, peptide **4** was prepared by coupling of the tripeptide H-Asp(Bni)-Ser(*t*Bu)-Ser(*t*Bu)-NH-resin with Fmoc-Ala-Leu-Leu-Val-OH to minimize exposure to basic conditions. This precaution stemmed from the observation that the crude peptides contain a small amount of aspartimide; for example, reverse-phase (RP) HPLC analysis of crude peptide **3** suggests the presence of 2% aspartimide.

The solubility of the peptides allowed us to test their ability to photoacylate glycosylamines in different solvents. Five protected and unprotected glycosylamines of different complexity (**5**–**9**, Figure 1) were prepared. The O-acetylated β-glycosylamines **5** and **7**, which are derived from GlcNAc and chitobiose, respectively, were synthesized by PtO_2-catalyzed hydrogenation of the peracetylated β-glycosyl azides.[19] Glycosylamine **8** was synthesized from the peracetylated β-chitobiosylazide by Zemplén deacetylation followed by PtO_2-catalyzed hydrogenation, and **6** and **9** were prepared by Kochetkov amination of the O-unprotected hemiacetals.[20]

Phototransamidation with all four peptides and glycosylamine **5** in dichloromethane or chloroform produced the glycopeptides in excellent yields of 82–88% (Table 1, entries 1–4). Only 1–5% yield of aspartimides, and 11–13% yield of aspartyl or isoaspartyl peptides resulted. The formation of peptide acids by the photoredox mechanism depicted in Scheme 1 can be excluded as no 5-bromo-7-nitrosoindole was formed.

When peptide **3** and glycosylamine **5** were irradiated in THF instead of dichloromethane, the yield of *N*-glycopeptide decreased to 22%, while the yields of the hydrolysis product and aspartimide increased to 56% and 22%, respectively (Table 1, entry 5). Interestingly, this unwanted solvent-dependent effect can be reversed by the addition of HOBt. The reaction of all four photoreactive peptides with glycosylamine **5** in THF/HOBt afforded the glycopeptides as major products in 57–80% yield (Table 1, entries 6–9). The somewhat lower yield of 57% obtained for the coupling with peptide **4**, which contains the aspartimide-prone sequence -Asp-Ser-,[5] was not unexpected (entry 9). On the basis of the results obtained with and without HOBt, we believe that the initially formed peptide nitronic anhydride is a highly reactive acylating species that is converted in situ into a less reactive activated ester, which reacts faster with the glycosylamine than with water or, intramolecularly, with a neighboring amide nitrogen atom.

To our surprise, comparable results could not be obtained for the reaction of the O-acetylated chitobiosylamine **7** with peptides **3** and **4** in dichloromethane or DMSO (Table 1, entries 10–14). None of the conditions tested gave satisfactory glycopeptide yields, even when the reactions were conducted in the presence of HOBt (Table 1, entry 12) or pentafluorophenol (entry 14). Instead, substantial hydrolysis was observed, and substantial aspartimide formation also took place in the reaction with pentafluorophenol. Evidently, the acetylated chitobiosylamine **7** is not reactive enough.

We reasoned that chitobiosyl peptide formation may be possible by using O-unprotected chitobiosylamine, which is

 © 2006 Wiley-VCH Verlag GmbH & Co. KGaA, Weinheim

Table 1: Influence of solvent, addition of an auxiliary nucleophile, and glycosylamine reactivity on *N*-glycopeptide production.

Entry	Peptide	Glycosylamine	Ratio[a]	Solvent	Additive[b]	Glycopeptide	Yields[c][25]
1	**1**	**5**	1:2	$CDCl_3$	–	Fmoc-E(Bn)-N-I-T(*t*Bu)-T(*t*Bu)-G-C(Trt)-A-NH_2 **10**	84:13:3
2	**2**	**5**	1:2	$CDCl_3$ or CH_2Cl_2	–	Fmoc-E(*t*Bu)-N-I-T(*t*Bu)-V-P-NH_2 **11** (70%)[d]	86:13:1
3	**3**	**5**	1:2	CH_2Cl_2	–	Fmoc-E(Bn)-N-I-T(*t*Bu)-V-P-NH_2 **12**	88:11:1
4	**4**	**5**	1:2	$CDCl_3$	–	Fmoc-A-L-L-V-N-S(*t*Bu-)S(*t*Bu)-NH_2 **13**	82:13:5
5	**3**	**5**	1:2	THF	–	**12**	22:56:22
6	**3**	**5**	1:2	THF	HOBt	**12**	68:16:16
7	**1**	**5**	1:1.8	THF	HOBt	**10**	77:23:0
8	**2**	**5**	1:2	THF	HOBt	**11**	80:10:10
9	**4**	**5**	1:2	THF	HOBt	**13**	57:27:16
10	**3**	**7**	1:1.4	DMSO	–	Fmoc-E(Bn)-N-I-T(*t*Bu)-V-P-NH_2 **14**	0:50:50
11	**3**	**7**	1:1.4	DMSO	HOBt	**14**	7:71:22
12	**4**	**7**	1:1.7	DMSO	HOBt	Fmoc-A-L-L-V-N-S(*t*Bu-)S(*t*Bu)-NH_2 **15**	0:75:25
13	**4**	**7**	1:1.7	CH_2Cl_2	–	**15**	26:67:7
14	**4**	**7**	1:1.7	CH_2Cl_2	Pfp-OH[e]	**15**	0:50:50
15	**3**	**6**	1:1.5	DMSO	–	Fmoc-E(Bn)-N-I-T(*t*Bu)-V-P-NH_2 **16**	29:14:57
16	**3**	**6**	1:1.5	DMSO	HOBt	**16**	66:12:22
17	**2**	**8**	1:2 (1.9:1)[f]	DMSO	HOBt	Fmoc-E(*t*Bu)-N-I-T(*t*Bu)-V-P-NH_2 **17** (45%)[d]	73:15:12

[a] Peptide/glycosylamine ratio. [b] Amount of additive: two molar equivalents. [c] Yields of glycopeptide/peptide acid(s)/aspartimide based on HPLC; reaction scale 5–10 μmol. [d] Yield of the isolated product, reaction scale 30–80 μmol, see the Supporting Information. [e] Pfp-OH = pentafluorophenol. [f] Ratio in parentheses refers to the larger-scale reaction.

expected to be more nucleophilic.[3a] The phototransamidation of peptide **2** with **8** in DMSO in the presence of HOBt afforded the desired glycopeptide in 73% yield, along with the hydrolysis product and aspartimide in yields of 15 and 12%, respectively (Table 1, entry 17, Figure 2). The addition of HOBt is essential, as the amidation of glycosylamine **6** with peptide **3** in DMSO in the absence of HOBt furnishes the glycopeptide in only 29% yield (Table 1, entry 15), whereas the same reaction with HOBt results in 66% yield (Table 1, entry 16).

We were interested in validating this convergent photochemical strategy with an oligosaccharide of the complex type to generate the corresponding *N*-glycopeptide.[21] Photoreactive peptide **2** and substoichiometric amounts of the valuable glycosylamine **9**, derived from a biantennary asialo-*N*-glycan,[21b,22] were irradiated in DMSO in the presence of HOBt

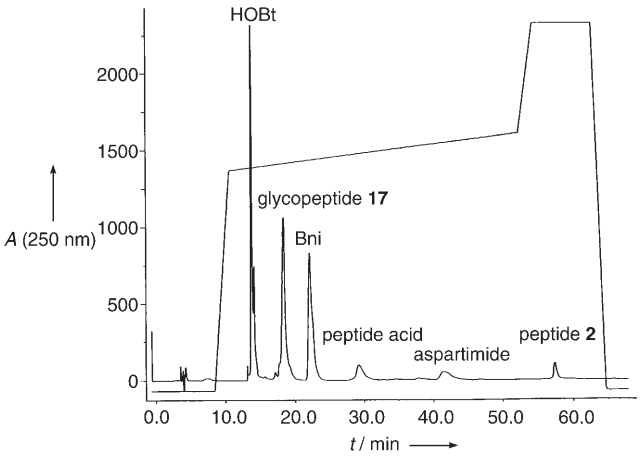
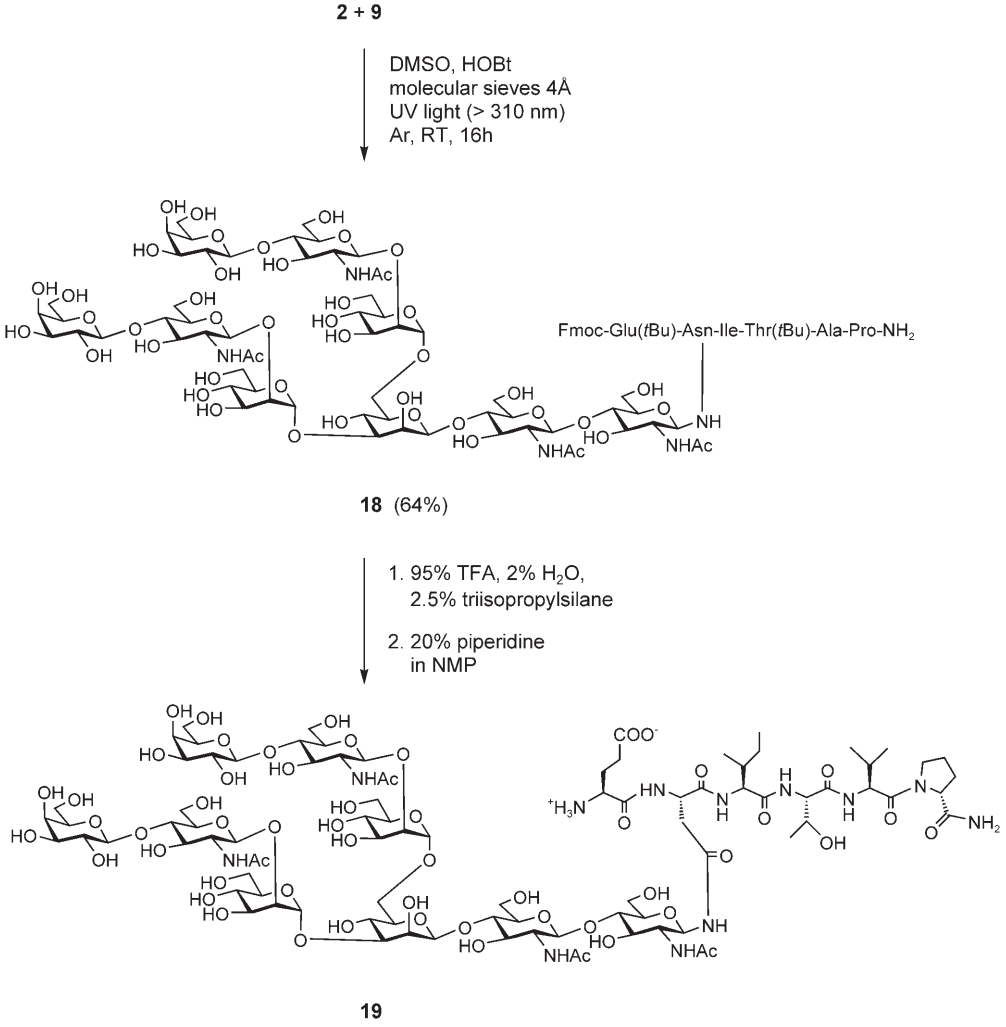


Figure 2. RP HPLC trace of the crude reaction mixture from the synthesis of glycopeptide **17** (Table 1, entry 17).

 © 2006 Wiley-VCH Verlag GmbH & Co. KGaA, Weinheim



Scheme 2. Convergent synthesis of an intricate *N*-glycopeptide.

(Scheme 2). The desired glycopeptide **18** was formed in 64% yield, and the excess peptide **2** was completely converted into peptide acids and aspartimide.[23] A portion of crude **18** was purified by HPLC followed by complete deprotection with TFA and piperidine to yield the unprotected glycopeptide **19** (Scheme 2), which was characterized by mass spectrometry.[24]

Glycopeptide **16** was analyzed by LC–MS (ESI–TOF) and ^{1}H NMR spectroscopy to confirm its structural integrity.[24] Ion extraction located a single signal of the correct mass (*m*/*z* 1242.63 $[M+H]^+$ and 1264.61 $[M+Na]^+$) in the total-ion current diagram. After purification by HPLC, **16** gave a ^{1}H NMR spectrum showing only a single set of signals. The β linkage is confirmed by the triplet for H-1 at $\delta = 4.78$ ppm ($^3J_{1,2} = {}^3J_{1,NH} = 9.3$ Hz). There is no evidence of an α-configured *N*-glycopeptide or a glycopeptide with an ester linkage.

The results show that orthogonally protected photoreactive peptides are particularly useful to acylate O-unprotected glycosylamines in the presence of HOBt. The photocoupling reaction is conducted under base-free conditions. This novel convergent synthesis offers a solution to the long-standing "aspartimide problem" and provides a shorter synthetic route to *N*-glycopeptides by light activation of the same group that serves as a protecting group for the aspartic acid side chain during peptide synthesis.

Received: July 31, 2005
Revised: November 25, 2005
Published online: January 10, 2006

Keywords: amides · aspartimides · convergent synthesis · glycopeptides · photochemistry

[1] a) Y. Shin, K. A. Winans, B. J. Backes, S. B. H. Kent, J. A. Ellman, C. R. Bertozzi, *J. Am. Chem. Soc.* **1999**, *121*, 11684; b) L. A. Marcaurelle, L. S. Mizoue, J. Wilken, L. Oldham, S. B. H. Kent, T. Handel, C. R. Bertozzi, *Chem. Eur. J.* **2001**, *7*, 1129; c) J. S. Miller, V. Y. Dudkin, G. J. Lyon, T. W. Muir, S. J. Danishefsky, *Angew. Chem.* **2003**, *115*, 447; *Angew. Chem. Int. Ed.* **2003**, *42*, 431; d) J. D. Warren, J. S. Miller, S. J. Keding, S. J. Danishefsky, *J. Am. Chem. Soc.* **2004**, *126*, 6576; S. Mezzato, M. Schaffrath, C. Unverzagt, *Angew. Chem.* **2005**, *117*, 1677; *Angew. Chem. Int. Ed.* **2005**, *44*, 1650.

[2] a) H. Kunz, M. Schultz in *Carbohydrates in Chemistry and Biology, Vol. 1* (Eds.: B. Ernst, G. W. Hart, P. Sinaÿ), Wiley-VCH, Weinheim, **2000**, pp. 267; b) J. Kihlberg in *Fmoc Solid*

 © 2006 Wiley-VCH Verlag GmbH & Co. KGaA, Weinheim

Phase Peptide Synthesis (Eds.: W. C. Chan, P. D. White), Oxford University Press, New York, **2000**, p. 195.
[3] a) S. T. Anisfeld, J. P. T. Lansbury, *J. Org. Chem.* **1990**, *55*, 5560; b) S. T. Cohen-Anisfeld, J. P. T. Lansbury, *J. Am. Chem. Soc.* **1993**, *115*, 10531; c) S. J. Danishefsky, S. Hu, P. F. Cirillo, M. Eckhardt, P. H. Seeberger, *Chem. Eur. J.* **1997**, *3*, 1617; d) H. Kunz, B. Liebe, O. Seitz, J. Habermann, K. Peilstocker, U. Sprengard, *Collect. Symp. Ser.* **1999**, *1*, 134; e) U. Sprengard, M. Schudok, W. Schmidt, G. Kretzschmar, H. Kunz, *Angew. Chem.* **1996**, *108*, 359; *Angew. Chem. Int. Ed. Engl.* **1996**, *35*, 321.
[4] M. Wagner, H. Kunz, *Angew. Chem.* **2002**, *114*, 315; *Angew. Chem. Int. Ed.* **2002**, *41*, 317.
[5] M. Bodanszky, J. Z. Kwei, *Int. J. Pept. Protein Res.* **1978**, *12*, 69.
[6] a) H. Kunz, H. Waldmann, C. Unverzagt, *Int. J. Pept. Protein Res.* **1985**, *26*, 493; b) D. Vetter, D. Tumelty, S. K. Singh, M. A. Gallop, *Angew. Chem.* **1995**, *107*, 94; *Angew. Chem. Int. Ed. Engl.* **1995**, *34*, 60; c) J. Y. Roberge, X. Beebe, S. J. Danishefsky, *J. Am. Chem. Soc.* **1998**, *120*, 3915.
[7] B. Amit, D. A. Ben-Efraim, A. Patchornik, *J. Am. Chem. Soc.* **1976**, *98*, 843.
[8] G. Goissis, B. W. Erickson, R. B. Merrifield, *Pept. Proc. Am. Pept. Symp.*, *5th* **1977**, 559.
[9] S. Pass, B. Amit, A. Patchornik, *J. Am. Chem. Soc.* **1981**, *103*, 7674.
[10] K. C. Nicolaou, B. S. Safina, N. Winssinger, *Synlett* **2001**, 900.
[11] a) C. Helgen, C. G. Bochet, *Synlett* **2001**, 1968; b) C. Helgen, C. G. Bochet, *J. Org. Chem.* **2003**, *68*, 2483.
[12] a) K. Vizvardi, C. Kreutz, A. S. Davis, V. P. Lee, B. J. Philmus, O. Simo, K. Michael, *Chem. Lett.* **2003**, *32*, 348; b) O. Simo, V. P. Lee, A. S. Davis, C. Kreutz, P. H. Gross, P. R. Jones, K. Michael, *Carbohydr. Res.* **2005**, *340*, 557.
[13] A. D. Cohen, C. Helgen, C. G. Bochet, J. P. Toscano, *Org. Lett.* **2005**, *7*, 2845.
[14] a) G. Papageorgiou, J. E. T. Corrie, *Tetrahedron* **2000**, *56*, 8197; b) J. Morrison, P. Wan, J. E. T. Corrie, G. Papageorgiou, *Photochem. Photobiol. Sci.* **2002**, *1*, 960.
[15] a) G. Papageorgiou, D. C. Ogden, A. Barth, E. E. T. Corrie, *J. Am. Chem. Soc.* **1999**, *121*, 6503; b) G. Papageorgiou, M. Lukeman, P. Wan, J. E. T. Corrie, *Photochem. Photobiol. Sci.* **2004**, *3*, 366.
[16] P.-H. Lai, R. Everett, F.-F. Wang, T. Arakawa, E. Goldwasser, *J. Biol. Chem.* **1986**, *261*, 3116.
[17] P. Sieber, *Tetrahedron Lett.* **1987**, *28*, 2107.
[18] H. Waldmann, H. Kunz, *Liebigs Ann. Chem.* **1983**, 1712.
[19] a) M. Spinola, R. W. Jeanloz, *J. Biol. Chem.* **1970**, *245*, 4158; b) L. Szilágyi, Z. Györgydeák, *Carbohydr. Res.* **1985**, *143*, 21; c) H. Kunz, H. Waldmann, J. März, *Liebigs Ann. Chem.* **1989**, 45.
[20] L. M. Likhosherstov, O. S. Novikova, V. A. Derevitskaja, N. K. Kochetkov, *Carbohydr. Res.* **1986**, *146*, C1.
[21] a) C. Unverzagt, *Tetrahedron Lett.* **1997**, *38*, 5627; b) E. Meinjohanns, M. Meldal, H. Paulsen, R. A. Dwek, K. Bock, *J. Chem. Soc. Perkin Trans. 1* **1998**, 549; c) N. Yamamoto, Y. Ohmori, T. Sakakibara, K. Sasaki, L. R. Juneja, Y. Kajihara, *Angew. Chem.* **2003**, *115*, 2641; *Angew. Chem. Int. Ed.* **2003**, *42*, 2537.
[22] a) A. Seko, M. Koketsu, M. Nishizono, Y. Enoki, H. R. Ibrahim, L. R. Juneja, M. Kim, T. Yamamoto, *Biochim. Biophys. Acta* **1997**, *1335*, 23; b) N. Yamamoto, T. Sakakibara, Y. Kajihara, *Tetrahedron Lett.* **2004**, *45*, 3287; c) Y. Kajihara, Y. Suzuki, N. Yamamoto, K. Sasaki, T. Sakakibara, L. R. Juneja, *Chem. Eur. J.* **2004**, *10*, 971.
[23] In this reaction the photoreactive peptide **2** was used in twofold excess. All of peptide **2** that was not converted into glycopeptide **18** was converted into the corresponding peptide acid and the aspartimide. The product distribution was **18**/peptide acid/aspartimide = 32:30:38.
[24] See the Supporting Information.
[25] As the photoreactive peptides were completely or nearly completely converted into three products with the same chromophores (glycopeptide, peptide acid, and aspartimide; see, for example, Figure 2), the reaction yields were calculated by using the following equation: $\text{Yield}_{\text{glycopeptide}}[\%] = A_{\text{glycopeptide}} / [0.01\,(A_{\text{glycopeptide}} + A_{\text{peptide acid}} + A_{\text{aspartimide}})]$; A is the area of the integrated HPLC absorption signal detected at 250 or 260 nm.

 © 2006 Wiley-VCH Verlag GmbH & Co. KGaA, Weinheim

Core–Shell Particles

DOI: 10.1002/anie.200502893

Mechanics versus Thermodynamics: Swelling in Multiple-Temperature-Sensitive Core–Shell Microgels**

*Ingo Berndt, Crisan Popescu, Franz-Josef Wortmann, and Walter Richtering**

In the past few years the synthesis of multifunctional nanomaterials has been the focus of various synthetic approaches in which different chemical functionalities are incorporated at different positions within the molecule. In this work compounds such as dendrimers, hyperbranched polymers, and cross-linked micelles have been employed.[1] A second field of research concerns stimuli-responsive nanomaterials. Here thermosensitive microgels, often based on poly-*N*-isopropylacrylamide (PNIPAM), which exhibits a lower critical solution temperature (LCST) of ca. 32 °C in H_2O (and ca. 34 °C in D_2O), have been investigated intensively in the past years and found application in numerous fields.[2] More advanced polymer architectures can lead to materials with superior properties, and, for example, core–shell microgels responsive to two external stimuli (temperature and pH) have been introduced by Lyon and co-workers.[3]

Multiresponsive core–shell microgels can display unique behavior since the two domains, core and shell, are mechanically linked. Indeed it has been observed that the degree of swelling of the core and shell regions is mutally influenced.[4] However, it is not clear whether such a mechanical connection can lead to qualitatively different properties.

[*] Dipl.-Chem. I. Berndt, Prof. W. Richtering
Institute of Physical Chemistry
RWTH Aachen University
Landoltweg 2, 52074 Aachen (Germany)
Fax: (+49) 241-809-2327
E-mail: richtering@rwth-aachen.de
Prof. C. Popescu, Prof. F.-J. Wortmann
Deutsches Wollforschungsinstitut (DWI)
RWTH Aachen University
Pauwelstrasse 8, 52056 Aachen (Germany)

[**] Financial support by the Deutsche Forschungsgemeinschaft is gratefully acknowledged. The authors thank Heiko Huth, Institute of Physics, University of Rostock, for his support during the DSC experiments.

 © 2006 Wiley-VCH Verlag GmbH & Co. KGaA, Weinheim

Herein we report on the thermal behavior of aqueous (D_2O) solutions of core–shell microgels composed of a temperature-sensitive PNIPAM core and a temperature-sensitive shell of poly-*N*-isopropylmethacrylamide (PNIPMAM); the latter exhibits an LCST of ca. 44 °C. These particles combine the two above-mentioned concepts: two polymers with different temperature sensitivity are combined in spherical core–shell morphology. The mutual influences can be controlled by adjusting the core/shell mass ratio, and in this study a wide range of mass ratios were investigated. In aqueous solution these particles show a two-step shrinking behavior corresponding to the LCSTs of core and shell polymer.

Figure 1 shows the baseline-corrected and normalized differential scanning calorimetry (DSC) thermograms of four PNIPAM core/PNIPMAM shell microgels with core/shell

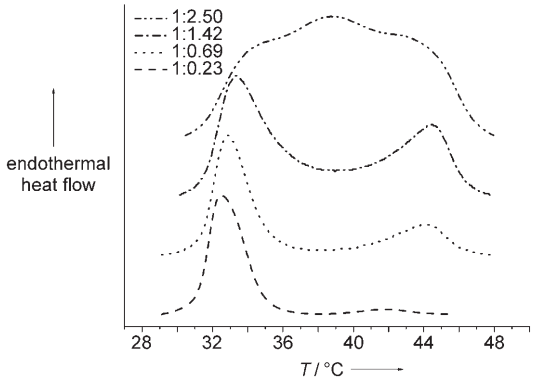


Figure 1. Normalized DSC thermograms of PNIPAM core/PNIPMAM shell microgels with core/shell mass ratios of 1:0.23, 1:0.69, 1:1.42, and 1:2.50 recorded at a heating rate of 2 K min^{-1}.

mass ratios of 1:0.23, 1:0.69, 1:1.42, and 1:2.50. All core–shell samples are based on the same PNIPAM core. The core–shell microgels exhibit, generally, two peaks, which correspond to the shrinking processes of the core at low and shell at high temperatures.

With increased amounts of PNIPMAM in the shell, in other words, with increased shell thickness, the transition peak of the core shifts towards higher temperatures from 32.5 to 33.9. The peak temperatures of the shell transition stay fairly constant at 44.5 °C, except for the case of a very thin shell where the peak transition is reduced to 41.8 °C. This observation will be explained further below.

A general kinetic function was employed to deconvolute the DSC signals and allowed characterizing each peak by its enthalpy and peak temperature assuming a weighted superposition of each thermal process. Peak temperatures and calorimetric heats of the thermal transitions of the core–shell particles as well as of the pure core and shell materials are listed in Table 1.

The enthalpy values of the different transitions correlate very well with the variation in the samples' composition. For three samples the transition enthalpy of the PNIPAM core component was found to be 4.8–5.3 kJ mol^{-1} (per mol of the NIPAM repeating unit), which is in good agreement with data

Table 1: Peak temperatures and calorimetric heats of core–shell microgels and pure core and shell material.

Sample	m_{core}/m_{shell}	Core transition T [°C]	Core transition ΔH_{PNIPAM} [kJ mol^{-1}]	Shell transition T [°C]	Shell transition $\Delta H_{PNIPMAM}$ [kJ mol^{-1}]
1[a]	1:0	32.5	5.38	–	–
2	1:0.23	32.5	5.32	41.8	1.20
3	1:0.69	32.8	4.94	44.3	2.61
4	1:1.42	33.3	4.82	44.5	2.12
5	1:2.50	33.9	2.47	44.5	2.01
5[b]	1:2.50	38.7	9.23	–	–
6[c]	0:1	–	–	43.0	5.04

[a] Pure core. [b] Additional third transition. [c] Pure shell material.

reported for similar systems.[5] This indicates that the thermal transition of the PNIPAM component in these core–shell microgels, as measured by DSC, is not altered qualitatively by the presence of the other component. On the other hand, the transition enthalpy of the PNIPMAM shell in these core–shell microgels is always significantly smaller than that obtained for a pure PNIPMAM microgel with the same cross-linker content. Apparently the swelling behavior in a shell is different; this will be discussed further below.

Most important, however, is the case of the core–shell microgel with the greatest amount of shell component, that is, with the thickest shell: Here a third peak appears at an intermediate temperature without any evident relation to the two polymer components. All three peaks were also observed upon cooling (Figure 2). All transitions were fully reversible

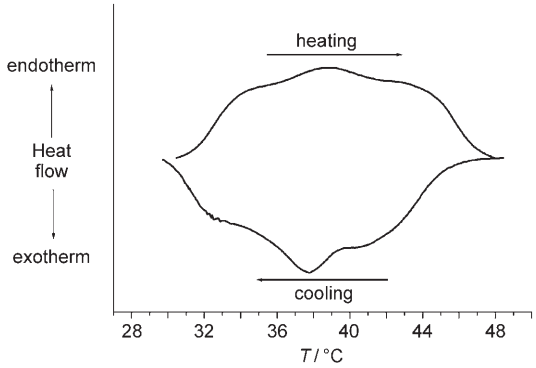


Figure 2. DSC heating and cooling curve for PNIPAM core/PNIPMAM shell microgel sample 5 with a core/shell mass ratio of 1:2.50 recorded at 2 K min^{-1}.

and appeared in each heating–cooling cycle. Because of the above-mentioned peaks shifts, the third thermal transition cannot be considered to be an overlap of two distinct peaks of core and shell.

The influence of the composition on the core transition can be interpreted with a rather simple mechanical model. The core–shell microgels are considered as spherical particles with a total radius R. Each particle is composed of a PNIPAM core of radius r and a PNIPMAM shell of thickness d. We can assume that the densities of PNIPAM and PNIPMAM are very similar, so that one can express the core-shell mass ratio as Equation (1), where a is the relative amount of the

 © 2006 Wiley-VCH Verlag GmbH & Co. KGaA, Weinheim

PNIPMAM shell. The radius r of the PNIPAM core is thus given as Equation (2).

$$\frac{m_{core}}{m_{shell}} = \frac{r^3}{R^3 - r^3} = \frac{1}{a} \quad (1)$$

$$r = \frac{R}{\sqrt{1+a}} \quad (2)$$

Upon heating from a temperature below the core LCST, the core shrinks and expells water through the water-permeable PNIPMAM shell. The heat signal recorded by DSC is directly proportional to the reduction in the radius of the core $x = r_0 - r$, where r_0 is the core radius at 25 °C. Core and shell are connected by an interpenetrating network layer. Assuming this interaction of core and shell, the temperature shift may be understood as being caused by an elastic force developed in the shell, which balances the thermodynamic force and thus decreases the shrinking force in the core.

The total shrinking force F_{core} acting in the core is temperature dependent and can be expressed by Equation (3), where k_C is a material constant of the core. This force

$$F_C = k_C T \quad (3)$$

drives the shrinking process in the core at elevated temperatures and is related to the elastic properties of the PNIPAM network. Since it is an elastic force one may apply Hook's law for the core sphere of radius r_0 [Eq. (4)]. Here, $S_C = 4\pi(r_0 - x)^2$

$$\frac{F_C}{S_C} = \frac{k_C T}{4\pi(r_0 - x)^2} = -E_C \frac{x}{r_0} \quad (4)$$

is the surface on which the force is applied. When a PNIPMAM shell, which prevents the core from collapsing, is present, one may describe the same shrinkage by Equation (5).

$$\frac{F_{CS}}{S_{CS}} = \frac{k_{CS} T'}{4\pi(r - x)^2} = -E_{CS} \frac{x}{r} \quad (5)$$

The subscript CS denotes a material constant for the core–shell microgel and T' is the peak temperature shifted due to the shell. The peak-temperature shift caused by the elastic force of the shell is now readily inferred as the difference of the two temperatures above [Eq. (6)], calculated at x_p the core shrinkage at the peak temperature.

$$\Delta T_P = 4\pi x_p \left(\frac{E_{CS}}{k_{CS}} \frac{(r_0 - x_p)^2}{r_0} - \frac{E_{CS}}{k_{CS}} \frac{(r - x_p)^2}{r} \right) \quad (6)$$

In Figure 3 the experimental and calculated shifts ΔT_P of the core (PNIPAM) peak temperature are shown, and very good agreement is observed. The thicker the shell, the stronger the elastic force and the higher the transition temperature of the core. The simple elastic model also accounts for the second peak. For microgels with a very thin shell, the shell cannot sustain itself against the shrinking force of the core. When the core collapses, the shell shrinks at lower temperatures as a result of the confined geometry. Consequently, the temperature of this peak is lowered to 41.7 °C. For all other samples, the shell resists the collapse of the core, and the temperature of the shell-shrinking process stays fairly constant at 44.5 °C.

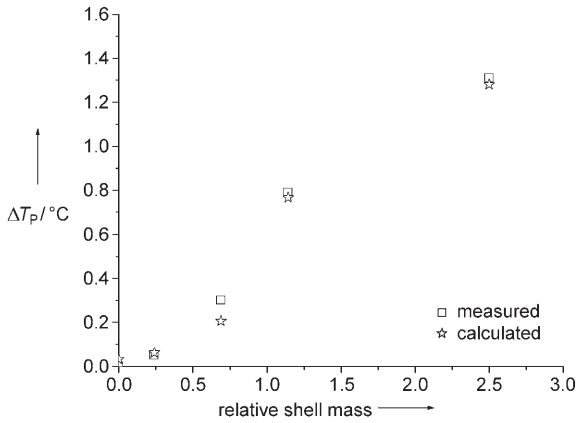


Figure 3. Shifts of the core (PNIPAM) peak temperatures as measured by DSC and calculated from the elastic model compared to data for the pure core. Thicker shells lead to stronger elastic forces and higher transition temperatures.

The sample with the thin shell can be compared with systems where a thermosensitive polymer is attached to a rigid particle.[6] In such a case the rigid substrate reduces the mobility of the chains in the shell, and the transition is shifted to higher temperatures. In our case the core can be considered as an "active" substrate and the shrinking core shifts the transition of the shell material to lower temperatures. However, the model *cannot* explain the appearance of a third peak in case of a very thick shell.

Our group recently established a form factor to analyze small-angle neutron scattering data (SANS) from such core–shell microgels.[4d] This model provides the polymer volume fraction in the core and shell as well as the core size and the shell thickness. The analysis of SANS data recorded at 39 °C, where the third peak is found, provides the radial density profiles shown in Figure 4. The SANS data give additional information on the swelling behavior of core and shell.

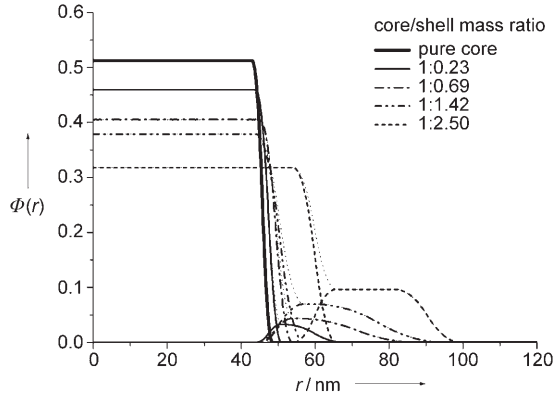


Figure 4. Profiles of the radial polymer volume fraction $\phi(r)$ of the PNIPAM core/PNIPMAM shell microgels and of pure PNIPAM core microgel at 39 °C obtained from SANS.

 © 2006 Wiley-VCH Verlag GmbH & Co. KGaA, Weinheim

The swelling properties of the shell material can be discussed in terms of the volume change when the temperature is reduced from 50 to 39 °C. The form factor model described in reference [4d] enables one to calculate the shell volume at different temperatures, taking into account the decay of the density profile at the particle surface. We find that the volume change in the PNIPMAM shell when the temperature is decreased from 50 to 39 °C is much smaller than the volume change in a pure PNIPMAM microgel. If we take the volume change and enthalpy of the pure PNIPMAM microgel as a reference, we can compare the ratio of experimental enthalpy values (i.e., ΔH per repeating unit in the shell normalized by ΔH per repeating unit in the pure microgel) with the ratio of volume changes in the shell and the pure microgel, respectively. These data are plotted in Figure 5

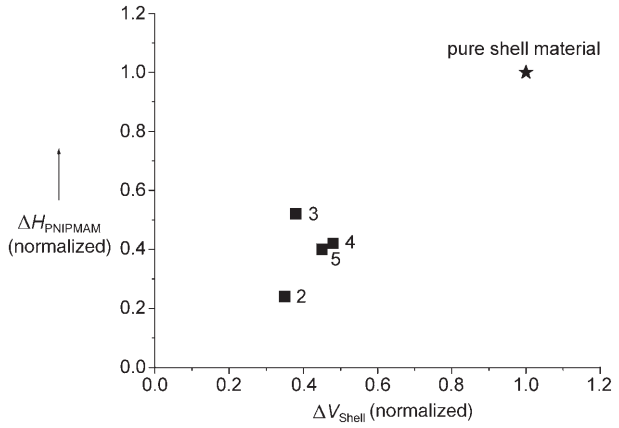


Figure 5. Plot of the normalized enthalpy of the transition of the shell component $\Delta H_{PNIPMAM}$ in the core–shell microgels against the normalized volume change of shell component ΔV_{shell}. The experimental data of the pure PNIPMAM microgel were used for normalization.

and clearly show that the low enthalpy values found for the shell transition are correlated with the lower swelling ratio. Apparently the PNIPMAM shell cannot swell as much as a pure PNIPMAM microgel can and consequently the heat flow is reduced.

The analysis of the SANS data also provides important information on the dimensions of the core in the core–shell microgel. Compared to the particles in the pure PNIPAM microgel (bold line in Figure 4), the core dimensions in the core–shell microgels with mass ratios up to 1:1.42 are only slightly increased. In agreement with the above model, the core expands more, the stronger the elastic force from the shell is, in other words, the thicker the shell is. The sample with the thickest shell has the largest, most expanded core.

The DSC analysis clearly shows that the third peak at intermediate temperature must be caused by additional molecular interactions. In principle these could come from the interpenetrating network at the core–shell interface. However, Lyon et al. demonstrated that the thickness of the interpenetrating network is rather limited[7] and furthermore should be identical for all samples. Thus the third peak should be observed with all samples if it were caused simply by the interfacial region. The experimental finding that the third peak in the DSC is observed only with the sample where the thick shell leads to a significant stretching of the core at intermediate temperature leads us to suggest that the additional thermal transition is caused by the breaking of hydrogen bonds between mechanically stretched chain segments. In other words, the conformations of the chains in the microgel network near the core–shell interface are altered when the elastic force in the shell overcompensates the thermodynamic force during the PNIPAM transition. These altered chain conformations lead to the formation of different hydrogen bonds, the breaking of which leads to the addition thermal transition.

In conclusion, thermal characteristics of PNIPAM core/PNIPMAM shell microgels in D_2O have been investigated by DSC. DSC thermograms reveal two transitions assigned to the thermal transitions of core and shell material. With increased shell thickness a shift of the core transition towards higher temperatures is observed, which is interpreted in terms of an elastic model. In contrast, the collapse of the core can shift the transition of a thin shell to lower temperatures. An additional thermal transition is found in case of a very thick shell, suggesting that the balance between the thermodynamic forces developed in the core material upon heating and the elastic force resisting a volume change of the shell leads to stretching of chain segments which allows additional hydrogen bonds to be formed. Thus an additional "chemomechanical" process is generated. Apparently the competition between thermodynamic and elastic forces gives rise to *qualitatively* different behaviors thus demonstrating the unique properties of cross-linked, multiresponsive core–shell nanomaterials.

Experimental Section

Thermal measurements were carried out with a Perkin-Elmer Pyris 1 DSC. Stainless-steel pans with silicon rubber gaskets were used as sample holders, and a pan with 30 mg of D_2O was used as a reference. The sample environment was rinsed with a nitrogen flow during measurement. Approximately 30 mg of a 6-wt % microgel dispersion in D_2O was used per measurement. D_2O was used as the solvent so that the data could be compared with results from small-angle neutron-scattering experiments. The study was carried out over a temperature range from 25 to 55 °C with a constant heating rate of 2 K min^{-1}. For all samples at least two heating runs and one cooling run were performed; all transitions were fully reversible and appeared in each heating–cooling cycle. Several heating–cooling rates (0.5, 1, 2, 5, 10, and 20 K min^{-1}) were employed for sample 3, and only rates ≥ 10 K min^{-1} had an influence on the transitions. The errors in calculating the enthalpies were determined from the peaks in repeated cycles and were $< 5\,\%$, in most cases $< 1\,\%$. The core–shell samples were all based on the same PNIPAM core with a molar cross-linker content of 1.4 %. The pure PNIPMAM microgel and the PNIPMAM shell have a cross-linker content of 5 mol %. Synthesis, removal of soluble polymer chains by ultracentrifugation, and sample preparation are described elsewhere.[4c,d]

Received: August 15, 2005
Published online: January 10, 2006

Keywords: core–shell particles · gels · polymers · thermochemistry · thermodynamics

 © 2006 Wiley-VCH Verlag GmbH & Co. KGaA, Weinheim

[1] a) G. E. Oosterrom, J. N. H. Reek, P. C. J. Kamer, P. W. N. M. van Leeuwen, *Angew. Chem.* **2001**, *113*, 1878 – 1901; *Angew. Chem. Int. Ed.* **2001**, *40*, 1828 – 1849; b) S. E. Stiriba, H. Kautz, H. Frey, *J. Am. Chem. Soc.* **2002**, *124*, 9698 – 9699; c) R. Haag, *Angew. Chem.* **2004**, *116*, 280 – 284; *Angew. Chem. Int. Ed.* **2004**, *43*, 278 – 282; d) H. Huang, E. E. Remsen, T. Kowalewski, K. L. Wooley, *J. Am. Chem. Soc.* **1999**, *121*, 3805 – 3806; T. K. Bronich, P. A. Keifer, L. S. Shlyakhtenko, A. V. Kabanov, *J. Am. Chem. Soc.* **2005**, *127*, 8236 – 8237.
[2] R. Pelton, *Adv. Colloid Interface Sci.* **2000**, *85*, 1 – 33.
[3] a) C. D. Jones, L. A. Lyon, *Macromolecules*, **2000**, *33*, 8301 – 8306; b) S. Nayak, L. A. Lyon, *Angew. Chem.* **2004**, *116*, 6874 – 6877; *Angew. Chem. Int. Ed.* **2004**, *43*, 6706 – 6709.
[4] a) C. D. Jones, L. A. Lyon, *Macromolecules* **2003**, *36*, 1988 – 1993; b) C. D. Jones, L. A. Lyon, *Langmuir* **2003**, *19*, 4544 – 4547; c) I. Berndt, W. Richtering, *Macromolecules* **2003**, *36*, 8780 – 8785; d) I. Berndt, J. S. Pedersen, W. Richtering, *J. Am. Chem. Soc.* ***2005***, *127*, 9372 – 9373.
[5] H. Kawasaki, S. Sasaki, H. Maeda, *Langmuir* **2000**, *16*, 3195 – 3199.
[6] a) M. Schönhoff, A. Larsson, P. B. Welzel, D. Kuckling, *J. Phys. Chem. B* **2002**, *106*, 7800 – 7808; b) S. Seelenmeyer, I. Deike, S. Rosenfeldt, C. Norhausen, N. Dingenouts, M. Ballauff, T. Narayanan, P. Lindner, *J. Chem. Phys.* **2001**, *114*, 10471 – 10478.
[7] D. Gan, L. A. Lyon, *J. Am. Chem. Soc.* **2001**, *123*, 8203 – 8209.

 © 2006 Wiley-VCH Verlag GmbH & Co. KGaA, Weinheim

Borane Chemistry

DOI: 10.1002/anie.200503197

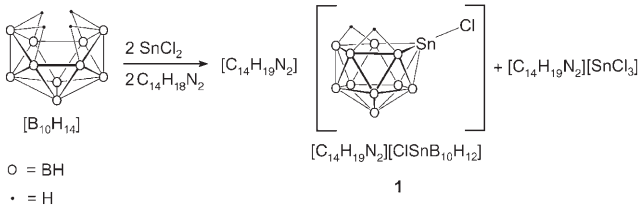
Distanna-*closo*-dodecaborate**

*Dominik Joosten, Ingo Pantenburg, and Lars Wesemann**

Dedicated to Professor Hansgeorg Schnöckel on the occasion of his 65th birthday

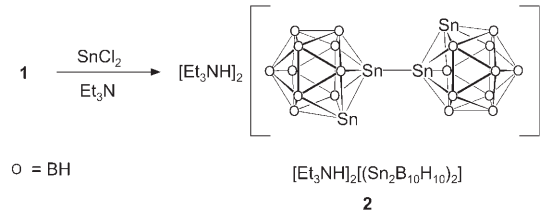
Dicarba-*closo*-dodecaborane ($[C_2B_{10}H_{12}]$) is by far the most prominent and best investigated heteroborane. The chemistry of this nearly icosahedral cluster has been a field of active research for more than forty years.[1] Fifteen years ago, the higher homologue of the *o*-carbaborane, disila-*closo*-dodecaborane ($[Me_2Si_2B_{10}H_{10}]$), was fortuitously isolated from a mixture of decaborane and bis(dimethylamino)methylsilane ($(Me_2N)_2SiHMe$).[2] The incorporation of tin atoms into the skeleton of boranes or carbaboranes is possible for a variety of clusters. The following heteroboranes with naked tin atoms as cluster vertices have been prepared through typical salt-elimination reactions between deprotonated *nido* clusters and tin(II) halides: *closo*-[1-Sn-2,3-$(SiMe_3)_2$-2,3-$C_2B_4H_4$],[3] *closo*-[1-Sn-2,4-$(SiMe_3)_2$-2,4-$C_2B_4H_4$],[3] *closo*-[1,2,3-$SnC_2B_8H_{10}$],[4] *closo*-[1,2,3-$SnC_2B_9H_{11}$],[5] *closo*-[4,1,6-$SnC_2B_{10}H_{12}$].[6] However, 1,2-distanna-*closo*-dodecaborate, a higher homologue of *o*-carbaborane and *o*-silaborane, was unknown prior to our investigation.

Herein, we present the first synthesis of a distanna-*closo*-dodecaborate with adjacent tin atoms. First, one tin vertex was incorporated into the decaborane cluster skeleton by applying an adaptation of the method published by Gaines et al.;[7] accordingly, stanna-*nido*-undecaborate $[C_{14}H_{19}N_2][7\text{-Cl-}7\text{-}SnB_{10}H_{12}]$ (**1**) was synthesized from a mixture of decaborane, proton sponge (1,8-bis(dimethylamino)naphthalene, $C_{14}H_{18}N_2$), and tin(II) chloride (Scheme 1).



Scheme 1. Formation of stanna-*nido*-undecaborate **1** with proton sponge ($C_{14}H_{18}N_2$) as base.

Reaction of the *nido*-borate **1** with additional equivalents of proton sponge and tin(II) chloride did not lead to the incorporation of a second tin atom into the cluster skeleton. However, use of a different base in the reaction was successful: the interesting derivative $[Et_3NH]_2[(Sn_2B_{10}H_{10})_2]$ (**2**) of the distanna-*closo*-dodecaborate was isolated from a mixture of the eleven-vertex cluster **1**, triethylamine, and tin(II) chloride. In **2**, two clusters are joined together by a Sn–Sn bond (Scheme 2).



Scheme 2. Formation of the dimeric *closo*-heteroborate **2**.

According to the $^{11}B\{^1H\}$ NMR spectra, this surprising reaction proceeds almost quantitatively. However, the fate of the chlorine substituent is unknown. A comparable intermolecular Sn–Sn bond formation occurs in the synthesis of $[7,7'\text{-}(SnB_{10}H_{12})_2]^{2-}$; this species was postulated by Gaines et al. to be formed after oxidative elimination of C_2H_6 from [7-Me-7-

[*] D. Joosten, Prof. Dr. L. Wesemann
Institut für Anorganische Chemie
Universität Tübingen
Auf der Morgenstelle 18, 72076 Tübingen (Germany)
Fax: (+49) 7071-295-306
E-mail: lars.wesemann@uni-tuebingen.de
Dr. I. Pantenburg
Institut für Anorganische Chemie
Universität zu Köln
Greinstrasse 6, 50939 Köln (Germany)

[**] This work was supported by the Deutsche Forschungsgemeinschaft.

 © 2006 Wiley-VCH Verlag GmbH & Co. KGaA, Weinheim

$SnB_{10}H_{12}]^-$.[7] The structure of the dimeric distannaborate salt **2** in the solid state was unequivocally determined by single-crystal X-ray structure analysis (Figure 1).[8] The Sn–Sn distances of 2.795(1) and 2.794(1) Å within the clusters are

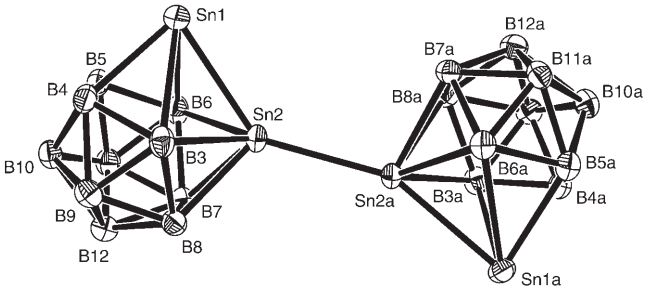


Figure 1. Structure of the dianion of **2** in the solid state (ORTEP plot, hydrogen atoms omitted, 50% probability ellipsoids). Selected distances [Å] and angles [°], standard deviations in parentheses: Sn1–Sn2 2.7945(4), Sn1–B3 2.673(4), Sn1–B4 2.379(4), Sn1–B5 2.383(4), Sn1–B6 2.686(4), Sn2–B3 2.375(4), Sn2–B6 2.373(4), Sn2–B7 2.319(4), Sn2–B8 2.321(4), Sn2–Sn2a 2.7240(4), Sn1a–Sn2a 2.7954(4), Sn1a–B3a 2.689(4), Sn1a–B4a 2.390(4), Sn1a–B5a 2.403(4), Sn1a–B6a 2.699(4), Sn2a–B3a 2.388(4), Sn2a–B6a 2.390(4), Sn2a–B7a 2.333(4), Sn2a–B8a 2.327(4); Sn1-Sn2-Sn2a 137.42(1), Sn1a-Sn2a-Sn2 153.57(1), Sn1-Sn2-Sn2a-Sn1a 145.12(2).

very similar to the Sn–Sn distance of 2.724(1) Å between the clusters, and are somewhat longer than the distance of 2.587(1) Å between the tin atoms in $[7,7'\text{-}(SnB_{10}H_{12})_2]^{2-}$. Interestingly, the Sn–B distances involving the substituted tin atoms (Sn2/Sn2a) are shorter than those involving the unsubstituted ones (Sn1/Sn1a).

In the $^{11}B\{^1H\}$ NMR spectrum of the C_s-symmetrical cluster units in solution, six signals with an intensity ratio of 1:1:2:2:2:2 are detected, as expected. However, even with a supplementary two-dimensional ^{11}B–^{11}B COSY NMR spectrum, only the resonance at $\delta = -14.4$ ppm with five cross peaks can unequivocally be assigned to boron atoms B9/B9a and B11/B11a.

The signals in the $^{119}Sn\{^1H\}$ NMR spectrum of **2** (Figure 2) can be assigned according to stannaborate chemistry: upon

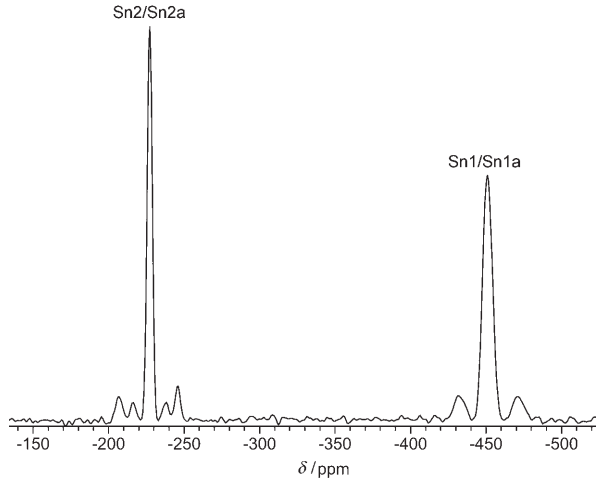
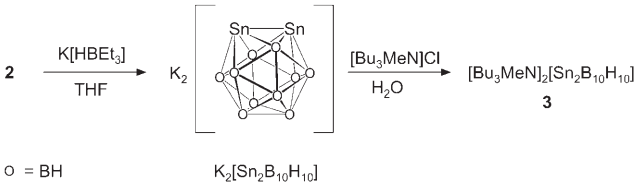


Figure 2. The $^{119}Sn\{^1H\}$ NMR spectrum of **2**.

substitution at the naked tin vertex in $[SnB_{11}H_{11}]^{2-}$, a downfield shift from $\delta = -546$ to between -350 to -150 ppm is observed.[12,13] Therefore, we conclude that in **2** the tin atoms Sn1/Sn1a and Sn2/Sn2a show signals at $\delta = -452$ and -228 ppm, respectively. Furthermore, a $^{119}Sn\{^1H\}$ NMR simulation[11] corroborates this assignment of the $^{119}Sn\{^1H\}$ NMR spectrum. The $^{117/119}Sn$ satellites of the unsubstituted atoms Sn1/Sn1a (at $\delta = -452$ ppm) show a coupling to Sn2/Sn2a ($^1J(^{119}Sn1, ^{119}Sn2/^{117}Sn2, \ ^{119}Sn1a, ^{119}Sn2a/^{117}Sn2a) = 3705$ Hz), whereas the $^{117/119}Sn$ satellites of the substituted atoms Sn2/Sn2a (at $\delta = -228$ ppm) show couplings to both Sn1/Sn1a and Sn2a/Sn2 ($^1J(^{119}Sn2, ^{117}Sn2a, \ ^{119}Sn2a, ^{117}Sn2) = 2190$ Hz, in addition to the former ones).

To cleave the Sn2–Sn2a bond we reacted the dimeric stannaborate salt **2** with an excess of the reducing agent $K[HBEt_3]$ (Scheme 3). $^{11}B\{^1H\}$ NMR spectroscopy reveals



Scheme 3. Formation of 1,2-distanna-*closo*-dodecaborate **3** by reductive cleavage of the dimeric *closo*-heteroborate **2**.

that this cleavage proceeds quantitatively. After cation exchange, the 1,2-distanna-*closo*-dodecaborate was isolated from an aqueous solution of the potassium salt as the tetraalkylammonium salt $[Bu_3MeN]_2[Sn_2B_{10}H_{10}]$ (**3**). The distannaborate dianion was characterized by NMR spectroscopy, mass spectrometry, and elemental analysis. The $^{11}B\{^1H\}$ NMR spectrum of **3**, which comprises four signals with an intensity ratio of 2:2:4:2, is consistent with the C_{2v} symmetry of the distannaborate cluster. On the basis of the two-dimensional ^{11}B–^{11}B COSY NMR spectrum, we were able to assign the four resonances to the respective boron atoms by taking into account that heteroatom-bridged B–B contacts usually show weak cross peaks. In the $^{119}Sn\{^1H\}$ NMR spectrum, one resonance was detected at $\delta = -349$ ppm for the two tin atoms in the distannaborate cluster, as expected. In conclusion, with the three-step procedure presented herein we are able to prepare the 1,2-distanna-*closo*-dodecaborate cluster from decaborane. The coordination chemistry of this dianion is now under investigation.

Experimental Section

All manipulations were carried out under a dry argon atmosphere in Schlenk glassware. Solvents were purified by standard methods and stored under an argon atmosphere. The mass spectrometry measurements were recorded in positive- and negative-ion mode using a Bruker esquire 3000^{plus} spectrometer equipped with an ESI interface. NMR spectra were recorded by using a Bruker DRX400 spectrometer. Elemental analyses were performed by the Institut für Anorganische Chemie, Universität Tübingen using a Vario EL analyzer.

2: Triethylamine (0.7 mL, $\rho = 0.726$ g cm^{-3}, 5.022 mmol) in dimethoxy ethane (DME; 20 mL) was added dropwise over 1.5 h to a solution of **1** (561.7 mg, 1.147 mmol) and tin(II) chloride (224.1 mg,

 © 2006 Wiley-VCH Verlag GmbH & Co. KGaA, Weinheim

1.182 mmol) in DME (40 mL). After stirring for 48 h, the yellow solution was filtered, and the solvent was evaporated in vacuo. The residue was washed with hexane (3 × 10 mL), water (3 × 10 mL), and diethyl ether (3 × 10 mL), and then dried in vacuo to give **2** (349.4 mg, ca. 67 %) as a yellow powder. $^{11}B\{^1H\}$ NMR ([D$_6$]acetone, 128 MHz): $\delta = 0.9$ (1 B), −1.1 (1 B), −1.9 (2 B), −7.1 (2 B), −8.1 (2 B), −14.4 ppm (2 B, B9/B9a, B11/11a); $^{119}Sn\{^1H\}$ NMR ([D$_6$]acetone, 149 MHz): $\delta = -232$ [$^1J(^{119}Sn1, ^{119/117}Sn2, ^{119}Sn1a, ^{119/117}Sn2a) = 3705$ Hz, $^1J(^{119}Sn2, ^{117}Sn2a, ^{119}Sn2a, ^{117}Sn2) = 2190$ Hz]; −448 ppm [$^1J(^{119}Sn1, ^{119/117}Sn2, ^{119}Sn1a, ^{119/117}Sn2a) = 3705$ Hz]; C,H,N analysis (%) calcd for $C_{12}H_{52}B_{20}N_2Sn_4$: C 15.74, H 5.72, N 3.06; found: C 13.56, H 3.70, N 2.42. Even after a series of elemental analyses from different samples, there was no better correspondence.

3: A potassium triethylhydridoborate solution (3.2 mL, 1 M in THF) was added dropwise to a suspension of **2** (723.3 mg, 0.790 mmol) in THF (40 mL) and stirred for 45 min. The mixture turned dark brown, and the hydrogen gas evolved was removed through an argon bubbler. The solvent was evaporated in vacuo. The dark gray residue was dissolved in water (30 mL) and filtered into a solution of [Bu$_3$MeN]Cl (slight excess) in water (20 mL). The precipitate was collected by filtration, washed with diethyl ether, and dried in vacuo to give **3** as a white powder (394.8 mg, 66 %). $^{11}B\{^1H\}$ NMR ([D$_8$]THF, 128 MHz): $\delta = 1.6$ (2 B, B3, B6), −0.1 (2 B, B10, B12), −6.1 (4 B, B4, B5, B7, B8), −11.7 ppm (2 B, B9, B11); $^{119}Sn\{^1H\}$ NMR ([D$_6$]acetone, 149 MHz): $\delta = -349$ ppm; MS (ESI): *m/z*: 956.7 $\{[Bu_3MeN]_3[Sn_2B_{10}H_{10}]\}^+$, 556.1 $\{[Bu_3MeN][Sn_2B_{10}H_{10}]\}^-$, 355.0 $[Sn_2B_{10}H_{10}]^{\bullet-}$; C,H,N analysis (%) calcd for $C_{26}H_{70}B_{10}N_2Sn_2$: C 41.29, H 9.33, N 3.70; found: C 41.01, H 8.92, N 3.62.

Received: September 8, 2005
Published online: December 28, 2005

Keywords: boranes · cluster compounds · tin

[1] a) V. I. Bregadze, *Chem. Rev.* **1992**, *92*, 209 – 223; b) R. A. Wiesboeck, M. F. Hawthorne, *J. Am. Chem. Soc.* **1964**, *86*, 1642 – 1643; c) Z. Zheng, C. B. Knobler, M. D. Mortimer, G. Kong, M. F. Hawthorne, *Inorg. Chem.* **1996**, *35*, 1235 – 1243.

[2] a) D. Seyferth, K. Büchner, W. S. Rees, Jr., W. M. Davis, *Angew. Chem.* **1990**, *102*, 911 – 913; *Angew. Chem. Int. Ed. Engl.* **1990**, *29*, 918 – 920; b) D. Seyferth, K. Büchner, W. S. Rees, Jr., L. Wesemann, W. M. Davis, S. S. Bukalov, L. A. Leites, H. Bock, B. Solouki, *J. Am. Chem. Soc.* **1993**, *115*, 3586 – 3594.

[3] a) N. S. Hosmane, L. Jia, H. Zhang, J. A. Maguire, *Organometallics* **1994**, *13*, 1411 – 1423; b) A. K. Saxena, J. A. Maguire, N. S. Hosmane, *Chem. Rev.* **1997**, *97*, 2421 – 2461; c) N. S. Hosmane, J. A. Maguire, *Organometallics* **2005**, *24*, 1356 – 1389.

[4] K. Nestor, B. Štíbr, T. Jelínek, J. D. Kennedy, *J. Chem. Soc. Dalton Trans.* **1993**, 1661 – 1663.

[5] a) A. H. Cowley, P. Galow, N. S. Hosmane, P. Jutzi, N. C. Norman, *J. Chem. Soc. Chem. Commun.* **1984**, 1564 – 1565; b) K. H. Wong, H.-S. Chan, Z. Xie, *Organometallics* **2003**, *22*, 1775 – 1778; c) P. Jutzi, P. Galow, *J. Organomet. Chem.* **1987**, *319*, 139 – 147.

[6] a) N. M. Wilson, D. Ellis, A. S. F. Boyd, B. T. Giles, S. A. Macgregor, G. M. Rosair, A. J. Welch, *Chem. Commun.* **2002**, 464 – 465; b) A. S. F. Boyd, A. Burke, D. Ellis, D. Ferrer, B. T. Giles, M. A. Laguna, R. McIntosh, S. A. Macgregor, D. L. Ormsby, G. M. Rosair, F. Schmidt, N. M. M. Wilson, A. J. Welch, *Pure Appl. Chem.* **2003**, *75*, 1325 – 1333; c) K.-H. Wong, H.-S. Chan, Z. Xie, *Organometallics* **2003**, *22*, 1775 – 1778.

[7] J. A. Dopke, D. R. Powell, R. K. Hayashi, D. F. Gaines, *Inorg. Chem.* **1998**, *37*, 4160 – 4161.

[8] a) Crystals of the proton sponge salt $[C_{14}H_{19}N_2]_2[(Sn_2B_{10}H_{10})_2]$ ($M_r = 1141.74$) suitable for X-ray structure analysis were obtained by slow diffusion of diethyl ether into the reaction mixture at room temperature; b) crystal-structure analysis: STOE IPDS II diffractometer: $Mo_{K\alpha}$ radiation, $T = 150$ K; yellow transparent needle, $0.45 \times 0.18 \times 0.12$ mm^3, monoclinic space group $P2_1/a$ (no. 14); $a = 14.2322(1)$, $b = 13.3667(1)$, $c = 24.685(2)$ Å, $\beta = 103.142(5)°$, $V = 4573.1(5)$ Å^3, $Z = 4$, $\rho_{calcd} = 1.658$ g cm^{-3}, $\mu(Mo_{K\alpha}) = 21.87$ cm^{-1}, $F(000) = 2216$; 67 103 reflections with $3.4 < 2\theta < 54.7°$, 10 207 independent in structure solution and refinement for 737 parameters;[9] $R_1 = 0.0460$, $wR_2 = 0.0716$, $w = 1/\{\sigma^2(F_o^2) + [0.0378(F_o^2 + 2F_c^2)/3]^2\}$; numerical absorption correction based on an optimized crystal shape;[10] all hydrogen atoms were found and isotropically refined; c) CCDC-283258 contains the supplementary crystallographic data for this paper. These data can be obtained free of charge from The Cambridge Crystallographic Data Centre via www.ccdc.cam.ac.uk/data_request/cif.

[9] a) WinGX, L. J. Farrugia, *J. Appl. Crystallogr.* **1999**, *32*, 837 – 838; b) G. M. Sheldrick, SHELXS-97, Program for the Solution of Crystal Structures, Göttingen, **1997**; c) G. M. Sheldrick, SHELXL-97, Program for Crystal Structure Refinement, Göttingen, **1997**.

[10] a) X-RED 1.26, Stoe Data Reduction Program, Stoe & Cie GmbH, Darmstadt, **2004**; b) X-Shape 2.05, Crystal Optimization for Numerical Absorption Correction, Stoe & Cie GmbH, Darmstadt, **1999**.

[11] Win-Daisy Version 4.0, Bruker-Franzen Analytik GmbH.

[12] R. W. Chapman, J. G. Kester, K. Folting, W. E. Streib, L. J. Todd, *Inorg. Chem.* **1992**, *31*, 979 – 983.

[13] T. Marx, B. Mosel, I. Pantenburg, S. Hagen, H. Schulze, L. Wesemann, *Chem. Eur. J.* **2003**, *9*, 4472 – 4478.

 © 2006 Wiley-VCH Verlag GmbH & Co. KGaA, Weinheim

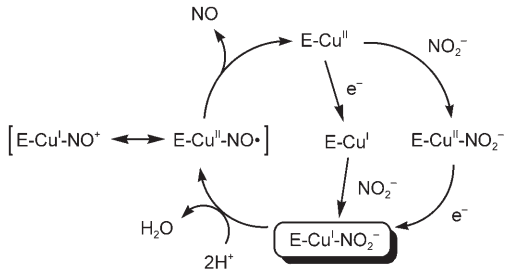
Enzyme Models

DOI: 10.1002/anie.200503555

Spectroscopic Characterization of Reaction Intermediates in a Model for Copper Nitrite Reductase**

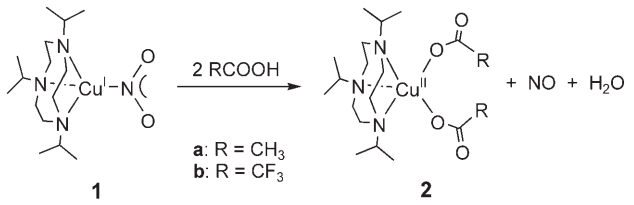
*Masato Kujime and Hiroshi Fujii**

The reduction of nitrite (NO_2^-) to gaseous nitric oxide (NO) is a key process in the global nitrogen cycle and is achieved catalytically by the copper-containing nitrite reductases (NiR) of certain types of bacteria.[1] The reaction mechanism of NiR has been proposed on the basis of the results of a number of biochemical, spectroscopic, and crystallographic studies.[1–4] The reaction involves the formation of a copper(I) nitrite complex by binding of nitrite to oxidized NiR followed by reduction, or by the reduction of oxidized NiR followed by nitrite binding. The copper-bound nitrite is then reduced to NO by protons from protein residues and by one electron from the copper(I) center via a copper nitrosyl intermediate (Scheme 1).[2–4] In this mechanism, the copper(I) nitrite



Scheme 1. Proposed mechanism for nitrite reduction by NiR. E = enzyme.

complex is a key intermediate in the reduction by NiR. While there are numerous reports of copper nitrite complexes,[5] the first and only structurally characterized model of the copper(I) nitrite complex of NiR, namely, [(*i*Pr$_3$tacn)Cu^{I}-(NO_2)] (**1**, *i*Pr$_3$tacn = 1,4,7-triisopropyl-1,4,7-triazacyclononane), was reported by Tolman et al.[6,7] Compound **1** is a good functional model of NiR and reacts with two equivalents of acetic acid to yield NO and a copper(II) acetate complex, [(*i*Pr$_3$tacn)Cu^{II}(O_2CCH_3)$_2$] (**2a**, Scheme 2). The structure of



Scheme 2. Reaction of **1** with acetic acid and trifluoroacetic acid (TFA).

the nitrite complex of reduced NiR was recently determined by incubating nitrite with crystals of reduced NiR at low temperature.[4] On the other hand, the mechanism of reduction of copper-bound nitrite has not yet been elucidated. While protonation of the copper(I) nitrite complex appears to be a key process in nitrite reduction, the protonation step has not been observed in either enzymatic or synthetic model systems. Herein, we report the first observation of reaction intermediates in the reduction of nitrite in a copper(I) nitrite complex by rapid mixing of **1** and trifluoroacetic acid (TFA) with stopped flow at low temperature. The characterization of the observed intermediate suggests the formation of a unique copper(I)/nitrous acid structure. It also suggests a reaction mechanism in which two protons are transferred in a stepwise manner to copper-bound nitrite, followed by intramolecular electron transfer from copper to the nitrite and cleavage of the N–O bond of the copper-bound nitrite ligand in the second protonation step.

The reaction of **1** with acetic acid is sufficiently slow that intermediates could be detectable, but none were observed (Figure 1a). The clear isosbestic points suggest that protonation of **1** is the rate-limiting step of the overall reaction. Therefore, it seems likely that a reaction intermediate might be detected if a much stronger acid were used. To examine this, we monitored the reaction of **1** with TFA, which is a stronger acid than acetic acid, at low temperature.[8] As shown in Figure 1b, the change in the absorption spectrum after mixing **1** with an excess of TFA at 203 K was completely different from that in the presence of acetic acid. The absorption spectrum of **1** immediately transformed into a new spectrum with absorption maxima at 350 and 423 nm during mixing (less than 10 ms) in stopped flow. The absorption band at 423 nm then rapidly decreased and those at 290 and 680 nm increased in intensity. Finally, the absorption spectrum corresponded to that of copper(II) trifluoroacetate complex [(*i*Pr$_3$tacn)Cu^{II}(O_2CCF_3)$_2$] (**2b**).[9] A previous study reported that the reaction of **1** with trimethylsilyl triflate ($Me_3SiO_3SCF_3$), a proton equivalent, initially yielded a mixed-valent dinuclear copper(I,II) nitrite complex as the result of a side reaction of **1** and the copper(II) reactant,[7] but the absorption spectrum of the new species is different from that of the dinuclear copper(I,II) nitrite complex. The time course for the reaction, monitored at 290, 423, and 680 nm, is poorly described by a single-exponential function, but better fitted by a biexponential function with k_{fast} and k_{slow} (Figure 1 and Supporting Information). These results indicate that at least two reaction intermediates are produced in this reaction [Eq. (1)]. From the absorbance coefficient of intermediate **B**, calculated from

[*] Dr. M. Kujime, Prof. Dr. H. Fujii
Institute for Molecular Science and
Okazaki Institute for Integrative Bioscience
National Institutes of Natural Sciences
Myodaiji, Okazaki 444-8787 (Japan)
Fax: (+81) 564-59-5600
E-mail: hiro@ims.ac.jp

[**] This work was supported by grants from the Ministry of Education, Science, Sport, and Culture, Japan and from the Japan Science and Technology Agency, CREST.

Supporting information for this article is available on the WWW under http://www.angewandte.org or from the author.

 © 2006 Wiley-VCH Verlag GmbH & Co. KGaA, Weinheim

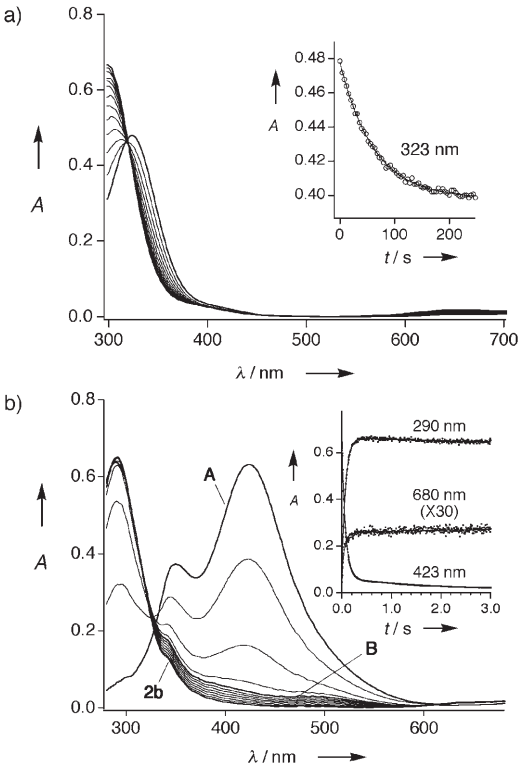


Figure 1. Change in the absorption spectrum after the rapid mixing of **1** (0.125 mM) in CH_2Cl_2 with a) acetic acid (12.5 mM) at 233 K, 0–250 s and b) with TFA (2.5 mM) at 203 K, 0–4.0 s. Typical spectra of intermediates **A** and **B** and of **2b** are shown in bold lines in (b). Insets: kinetic profiles for the reactions. a) Single-exponential curve fit at 323 nm, $k_{obs} = 1.62 \times 10^{-2}\ s^{-1}$. b) Biexponential curve fits at 290, 423, and 680 nm, $k_{fast} = 13.7\ s^{-1}$ and $k_{slow} = 0.67\ s^{-1}$.

the time-course curve fit, it is reasonable to assume that the second step (**A**→**B**) is a fast process and the third step (**B**→**2b**) slow.[10]

$$\mathbf{1} \rightarrow \text{intermediate } \mathbf{A} \rightarrow \text{intermediate } \mathbf{B} \rightarrow \mathbf{2b} \qquad (1)$$

To gain further understanding of the reaction mechanism, we examined the dependence of the rate constants k_{fast} and k_{slow} on the concentration of excess TFA. The rate constant for the second step k_{fast} is linearly dependent on the concentration of excess TFA (Figure 2 and Supporting Information). From the slope of k_{fast}, the second-order rate constant for the second step is $k_{second} = 6.54 \times 10^3\ M^{-1} s^{-1}$ at 203 K. This also indicates that one equivalent of TFA reacts in this step. On the other hand, the rate constant for the third step k_{slow} is independent of the concentration of TFA ($k_{third} = 6.82 \times 10^{-1}\ s^{-1}$). Since intermediate **A** is produced by the reaction of **1** and TFA, the rate constant for the first step (**1**→**A**) would be expected to be correlated with the concentration of TFA. However, the first step is too fast to permit the reaction rate constant to be estimated, even at a low concentration of TFA. All of these results support a scenario in which two equivalents of TFA react in the first and second steps.

To further investigate proton transfer in the reaction, the kinetic isotope effect was determined for each step. Even when deuterium-labeled TFA (CF_3COOD, [D]TFA) was

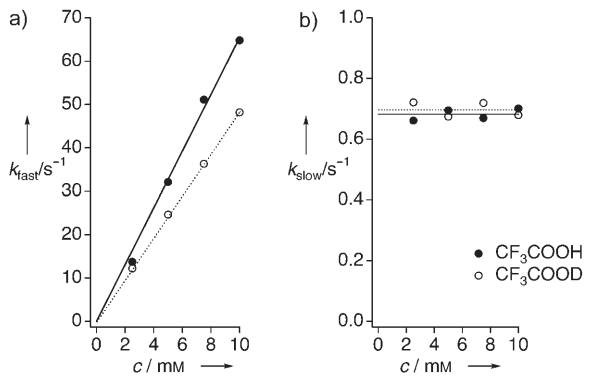


Figure 2. Plots of observed pseudo-first-order rate constants for a) the second step and b) the third step in the reaction of **1** (0.125 mM) in CH_2Cl_2 at 203 K at various TFA concentrations, *c*. Filled circles: TFA, empty circles: [D]TFA.

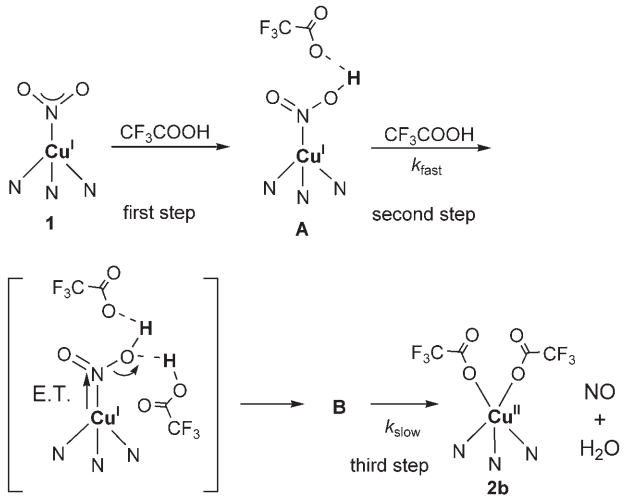
mixed with **1** at 203 K, the first step could not be observed, and the overall absorption spectral change after mixing **1** with [D]TFA was the same as that with TFA. On the other hand, the reaction rate for the second step with [D]TFA ($k_{second} = 4.84 \times 10^3\ M^{-1} s^{-1}$) was slightly smaller than that for TFA (Figure 2 and Supporting Information). The observed kinetic isotope effect for the second step was $k_H/k_D \approx 1.4$ at 203 K. As expected, no significant deuterium isotope effect could be observed for the third step ($k = 6.98 \times 10^{-1}\ s^{-1}$, $k_H/k_D = 1.0$).

To further characterize the reaction steps, we determined the activation parameters for the second and third steps from Eyring plots over the temperature range $T = 193$–223 K (Supporting Information). The enthalpy of activation $\Delta H^{\neq}$ and the entropy of activation $\Delta S^{\neq}$ for the second step were found to be $28.4 \pm 3.2\ kJ\,mol^{-1}$ and $-27.1 \pm 2.4\ J\,mol^{-1}\,K^{-1}$, and those for the third step were $18.9 \pm 1.5\ kJ\,mol^{-1}$ and $-151.0 \pm 24.7\ J\,mol^{-1}\,K^{-1}$, respectively. The negative $\Delta S^{\neq}$ values suggest associative transient states in the second and third steps.

To identify the oxidation state of copper in the intermediates, we examined the reaction with O_2 by means of a double-mixing stopped-flow technique (see Supporting Information). It has been reported that the copper(I) complex of *i*Pr_3tacn reacts with O_2 to form a μ-η_2:η_2-peroxo dicopper(II) complex which shows a strong absorption peak at 365 nm in CH_2Cl_2 at low temperature, but the copper(II) complex of *i*Pr_3tacn does not react with O_2.[11] When O_2 in CH_2Cl_2/10% THF was mixed with intermediate **A** in CH_2Cl_2 at 203 K, the absorption bands of intermediate **A** immediately disappeared within the mixing time, and the absorption band at 368 nm, resulting from the μ-η_2:η_2-peroxo dicopper(II) complex, then appeared within a few seconds.[12] However, when O_2 in CH_2Cl_2/10% THF was mixed with intermediate **B** in CH_2Cl_2 at 203 K, the μ-η_2:η_2-peroxo dicopper(II) complex was not detected. These results show that the intermediates **A** and **B** have copper(I) and copper(II) oxidation states, respectively, and that one electron from the copper(I) center is utilized for nitrite reduction in the second step.

A possible structure of intermediate **A** and a reaction mechanism are proposed, based on the above results (Scheme 3). Complex **1** rapidly reacts with one equivalent

 © 2006 Wiley-VCH Verlag GmbH & Co. KGaA, Weinheim



Scheme 3. Proposed mechanism for nitrite reduction of **1**. E.T. = electron transfer.

of TFA to give intermediate **A**. Intermediate **A** gives rise to strong absorption peaks at 350 and 423 nm (see Figure 1). The absence of a d–d transition band at 680 nm in the absorption spectrum and the double-mixing experiment clearly indicate an oxidation state +I of copper in intermediate **A**. Thus, the strong absorption band at 423 nm is assigned to the MLCT band of intermediate **A**, which shows a strong red shift from the MLCT band of **1** (308 nm). Intermediate **A** can not be regarded as a copper nitrosyl intermediate because it is still a copper(I) compound, and one additional proton is required for the subsequent reaction. Rather, intermediate **A** is a copper(I) nitrous acid complex formed by protonation of **1**. The red shift in the MLCT band is reasonable for protonation of the copper-bound nitrite, because the protonation of copper-bound nitrite stabilizes its π^* orbital. In fact, the MLCT band of **1** shifts to lower energy on binding of metal ions to the copper-bound nitrite.[6,7] To our knowledge this is the first example of a metal complex of nitrous acid. The strong MLCT band of intermediate **A** would be a useful marker for identifying a similar intermediate in the reaction of NiR. Intermediate **A** subsequently reacts with a second equivalent of TFA to form intermediate **B**. This is assisted by the first-order dependence of the reaction rate k_{fast} on the concentration of TFA. The appearance of a d–d transition band at 680 nm and the double-mixing experiment are consistent with intramolecular electron transfer from copper(I) to the copper-bound nitrite in this step. The significant deuterium isotope effect in the second step also supports the second protonation of the copper bound nitrite. The negative $\Delta S^{\neq}$ value in this step is also consistent with the associative transient state shown in Scheme 3. The second protonation of the copper-bound nitrite would further stabilize the energy level of its π^* orbital and result in intramolecular electron transfer. Donation of one electron and two protons to the copper-bound nitrite result in breakage of the N–O bond, and would lead to the copper nitrosyl intermediate Cu^{II}–$NO^{\bullet} \leftrightarrow Cu^{I}$–$NO^{+}$ and water. Finally, two trifluoroacetate counteranions bind to the copper(II) ion with release of NO to give **2b**. Although we were able to observe intermediate **B** after protonation of intermediate **A**, the structure of intermediate **B** is in doubt, because its absorption spectrum (see Figure 1, $\lambda_{max} = 290, 490$, ca. 680 nm) is close to that of **2b**, and the spectroscopic properties of the copper nitrosyl intermediate are not known with certainty. Intermediate **B** could be the copper nitrosyl intermediate or a copper(II) complex that has released NO. Further characterization will be required to identify intermediate **B**. More details of the reaction mechanism and the structures of the reaction intermediates are currently being investigated in our laboratory.

Received: October 7, 2005
Revised: November 14, 2005
Published online: January 3, 2006

Keywords: bioinorganic chemistry · copper · enzyme models · reaction mechanisms · reactive intermediates

[1] a) P. M. H. Kroneck, W. G. Zumft in *Denitrification in Soil and Sediment* (Eds.: N. P. Revsbech, J. Sorensen), Plenum, New York, **1990**, pp. 1–20; b) E. T. Adman, S. K. Turley in *Bioinorganic Chemistry of Copper* (Eds.: K. D. Karlin, Z. Tyeklár), Chapman & Hall, New York, **1993**, pp. 397–405; c) B. A. Averill, *Chem. Rev.* **1996**, *96*, 2951–2964; d) S. J. Ferguson, *Curr. Opin. Chem. Biol.* **1998**, *2*, 182–193; e) I. M. Wasser, S. de Vries, P. Moénne-Loccoz, I. Schröder, K. D. Karlin, *Chem. Rev.* **2002**, *102*, 1201–1234.

[2] a) C. L. Hulse, B. A. Averill, J. M. Tiedje, *J. Am. Chem. Soc.* **1989**, *111*, 2322–2323; b) R. W. Ye, I. Toro-Suarez, J. M. Tiedje, B. A. Averill, *J. Biol. Chem.* **1991**, *266*, 12848–12851; c) M. A. Jackson, J. M. Tiedje, B. A. Averill, *FEBS Lett.* **1991**, *291*, 41–44.

[3] a) M. J. Boulanger, M. Kukimoto, M. Nishiyama, S. Horiuchi, M. E. P. Murphy, *J. Biol. Chem.* **2000**, *275*, 23957–23964; b) K. Kataoka, K. Furusawa, H. Takagi, K. Yamaguchi, S. Suzuki, *J. Biochem.* **2002**, *197*, 345–350; c) Y. Zhao, D. A. Lukoyanov, Y. V. Toropov, K. Wu, J. P. Sharleigh, C. P. Scholes, *Biochemistry* **2002**, *41*, 7464–7474.

[4] a) M. E. P. Murphy, S. Turley, E. T. Adman, *J. Biol. Chem.* **1997**, *272*, 28455–28460; b) R. W. Strange, L. M. Murphy, F. E. Dodd, Z. H. Abraham, R. R. Eady, B. E. Smith, S. S. Hasnain, *J. Mol. Biol.* **1999**, *287*, 1001–1009; c) E. I. Tocheva, F. I. Rosell, A. G. Mauk, M. E. P. Murphy, *Science* **2004**, *304*, 867–870; d) S. V. Antonyuk, R. W. Strange, G. Sawers, R. R. Eady, S. Hasnain, *Proc. Natl. Acad. Sci. USA* **2005**, *102*, 12041–12046.

[5] a) F. Jiang, R. R. Conry, L. Bubacco, Z. Tyeklár, R. R. Jacobson, K. D. Karlin, J. Peisach, *J. Am. Chem. Soc.* **1993**, *115*, 2093–2102; b) N. Komeda, H. Nagao, G. Adachi, M. Suzuki, A. Uehara, K. Tanaka, *Chem. Lett.* **1993**, 1521–1524; c) C. E. Ruggiero, S. M. Carrier, W. B. Tolman, *Angew. Chem.* **1994**, *106*, 917; *Angew. Chem. Int. Ed. Engl.* **1994**, *33*, 895–897; d) R. T. Stibrany, J. A. Potenza, H. J. Schugar, *Inorg. Chim. Acta* **1996**, *243*, 33–37; e) E. Monzani, G. J. A. A. Koolhaas, A. Spandre, E. Leggieri, L. Casella, M. Gullotti, G. Nardim, L. Randaccio, M. Fontani, P. Zanello, J. Reedijk, *J. Biol. Inorg. Chem.* **2000**, *5*, 251–261.

[6] J. A. Halfen, W. B. Tolman, *J. Am. Chem. Soc.* **1994**, *116*, 5475–5476.

[7] J. A. Halfen, S. Mahapatra, E. C. Wilkinson, A. J. Gengenbach, V. G. Young, Jr., L. Que, Jr., W. B. Tolman, *J. Am. Chem. Soc.* **1996**, *118*, 763–776.

[8] The spectroscopic titration of **1** with TFA showed that, as in the case of acetic acid[6,7], 2 equivalents of TFA are required to complete the reaction. According to EPR analysis, about 70% of

 © 2006 Wiley-VCH Verlag GmbH & Co. KGaA, Weinheim

NO gas is trapped by iron(II) octaethylporphyrin complex in this reaction.

[9] Data for **2b** prepared from **1** and 2 equiv of TFA: ESI-MS: *m*/*z* (%): 431.2 (100) [**2b**−$CF_3CO_2^-$]$^+$; UV/Vis (CH_2Cl_2): λ_{max} (ε) = 289 (6000), 692 nm (110 $M^{-1}cm^{-1}$); EPR (CH_2Cl_2, 4 K): $g = 2.06$, $g_{\|} = 2.28$, $A_{\|} = 15.5$ mT. C,H,N analysis (%) calcd for $C_{19}H_{33}N_3O_4F_6Cu$: C 41.87, H 6.10, N 7.71; found: C 41.62, H 5.99, N 7.63.

[10] If the second step were the fast process, the absorption coefficient at 423 nm of intermediate **B** would be approximately 500 $M^{-1}cm^{-1}$. On the other hand, if the second step were the slow process, the absorption coefficient at 423 nm of intermediate **B** would have a large negative value (approximately −90 000 $M^{-1}cm^{-1}$).

[11] a) S. Mahapatra, J. A. Halfen, E. C. Wilkinson, L. Que, Jr., W. B. Tolman, *J. Am. Chem. Soc.* **1994**, *116*, 9785–9786; b) W. B. Tolman, *Acc. Chem. Res.* **1997**, *30*, 227–237.

[12] The small red shift (3 nm) of the absorption peak may be induced by THF or TFA in the solvent.

 © 2006 Wiley-VCH Verlag GmbH & Co. KGaA, Weinheim

Asymmetric Synthesis

DOI: 10.1002/anie.200502688

Catalytic Enantioselective Hydrogenolysis of [Cr(CO)$_3$(5,8-Dibromonaphthalene)]**

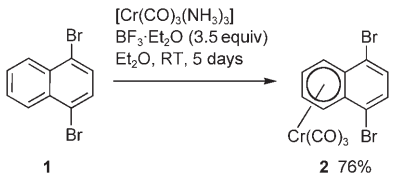
E. Peter Kündig, Piyali Datta Chaudhuri, David House, and Gérald Bernardinelli*

Highly enantiomerically enriched (η^6-arene)tricarbonylchromium(0) complexes whose chirality originates from the 1,2-disubstitution pattern of the arene and the coordination of the metal to one enantiotopic face of the arene are powerful chirons in asymmetric synthesis.[1] Robust, planar chiral arene complexes also increasingly find application as chiral ligands in asymmetric catalysis.[2]

Enantiomerically enriched arene complexes are accessible by both resolution and asymmetric synthesis. The latter method includes diastereoselective complexation, diastereoselective or enantioselective nucleophilic addition/hydride abstraction, and diastereoselective and enantioselective lithiation/electrophile addition.[1] While these approaches are potent methods that often give the target complexes in high enantiomeric purity, they rely on the use of stoichiometric quantities of chiral information and the diastereoselective methods often require additional steps for the introduction and the removal of chiral auxiliaries. A potentially very attractive catalytic route is the desymmetrization of *meso*-complexes by a chiral catalyst. In pioneering studies, Uemura, Mishimura, and Hayashi reported palladium-catalyzed asymmetric cross-coupling reactions of alkenyl metal and aryl metal compounds with [Cr(CO)$_3$(1,2-dichlorobenzene)].[3] A palladium-catalyzed Miyaura–Suzuki coupling reaction using a chiral bidentate ferrocene ligand ((*S*,*R*)-1-[1-(dimethylamino)ethyl]-2-(diphenylphosphino)ferrocene ((*S*,*R*)-PPFA) afforded the biaryl complex in 55% yield with 69% *ee*. More recently, a very similar level of induction and yield was reported for a methoxycarbonylation of the same substrate (47% yield, 63% *ee*).[4a] In this particular reaction, kinetic resolution in the second step allowed the isolation of the highly enantiomerically enriched product (95% *ee*) in 31% yield. Bidentate ferrocenyl ligands again were the best performers in this as well as in analogous reactions of [Cr(CO)$_3$(2,6-dichlorotoluene)].[4b] To complete the short list of precedents of asymmetric desymmetrizations, a report by Kamikawa et al. appeared during the preparation of this manuscript. It describes an asymmetric intramolecular Heck reaction of [Cr(CO)$_3$(2,6-bisbutenyl chlorobenzene)] with the best results reaching 78% yield and 73% *ee*.[5] We conclude that despite considerable efforts, a highly asymmetric, high-yield desymmetrization of a *meso* arene complex has not yet been realized. Herein, we present the results of our studies to carry out such a transformation and show that this goal can be realized by using a new bulky phosphoramidite ligand.

We selected [Cr(CO)$_3$($\eta^{(1-4,4a,8a)}$-5,8-dibromonaphthalene)] (**2**; see Scheme 1) as the substrate and asymmetric hydrogenolysis as the reaction. A highly enantiomerically enriched planar chiral bromonaphthalene complex could be a valuable precursor for asymmetric synthesis,[6] for planar chiral ligands,[2] and as a chiral {Cr(CO)$_3$}-transfer agent.[7] To our knowledge, desymmetrization of *meso* dihalides by asymmetric hydrogenolysis has not been reported. We were aware that by choosing a naphthalene complex we compounded the problem because of the lability of the metal–arene bond in this class of compounds.[1b]

Dibromonaphthalene complex **2** was obtained as a single regioisomer in 76% yield by treating [Cr(CO)$_3$(NH$_3$)$_3$] with $BF_3{\cdot}OEt_2$ in the presence of the arene **1** (Scheme 1). This mild and high-yielding procedure[8] avoids insertion of a zero-valent {Cr(CO)$_n$} fragment into the aryl–bromine bond, a process that results in the decomposition of the starting materials.



1 2 76%

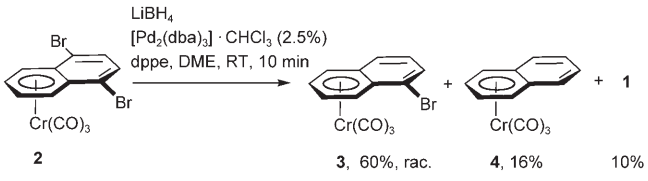
Scheme 1. Regioselective complexation of 1,4-dibromonaphthalene.

[*] Prof. Dr. E. P. Kündig, P. D. Chaudhuri, Dr. D. House
Department of Organic Chemistry
University of Geneva
30 Quai Ernest Ansermet, 1211 Geneva 4 (Switzerland)
Fax: (+41) 223-793-215
E-mail: Peter.Kundig@chiorg.unige.ch
Dr. G. Bernardinelli
Laboratory of Crystallography
University of Geneva
24 Quai Ernest Ansermet, 1211 Geneva 4 (Switzerland)

[**] We thank the Swiss National Science Foundation (SNF grant 200020-103851) for support.

WILEY InterScience DISCOVER SOMETHING GREAT
© 2006 Wiley-VCH Verlag GmbH & Co. KGaA, Weinheim

We next tested conditions for the palladium-catalyzed hydrogenolysis of one of the two C–Br bonds in complex **2**. Lewis bases readily cleave the naphthalene–chromium bond and this proved a major hurdle in this chemistry because it precluded the use of polar solvents or polar additives.[1b] We investigated sodium formiate and $NaBH_4$ as reducing agents in this reaction in combination with a number of palladium catalyst precursors ($Pd(OAc)_2/PPh_3$ or 1,2-ethanediylbis-(diphenyl)phosphine (dppe), $[Pd(PPh_3)_4]$) but found that in most of the solvents tested (DMF, acetonitrile, CH_2Cl_2, MeOH, toluene), decomplexation, induced by either the solvent or the formiate was faster than, or competitive with, arene–halide hydrogenolysis. Complex **2** is soluble and stable in toluene but hydrogenolysis with $NaBH_4$ in the presence of $[Pd(PPh_3)_4]$ was hampered by the low solubility of the reducing agent and resulted in an exceedingly slow reaction (2–3 days at 30 °C) even with 10–15 mol % catalyst. Worse, the yield of the sought after monobromonaphthalene complex **3** never exceeded 20 % of the final mixture, with 1,4-dibromonaphthalene (**1**) and starting complex **2** still present in 32 % and 47 %, respectively, after 62 h. After much experimentation, and after switching to the much more soluble $LiBH_4$ and using dimethoxyethane (DME) as solvent and $[Pd_2(dba)_3]\cdot CHCl_3$ (dba = dibenzylideneacetone) as catalyst, conditions were found that afforded the monobromonaphthalene complex **3** in reasonable yield as a racemic mixture (Scheme 2). While over reduction to give **4** was a

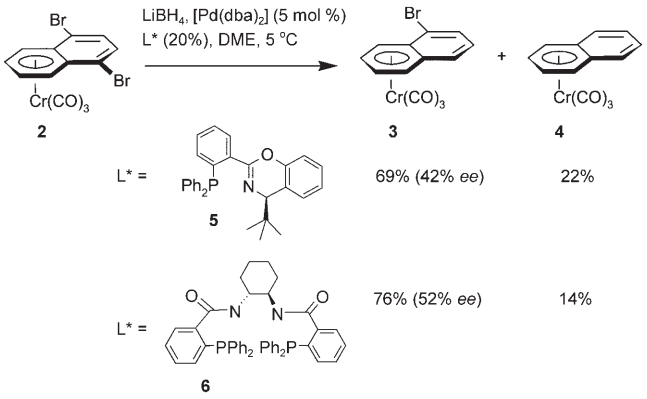


Scheme 2. Palladium-catalyzed hydrogenolysis of an aryl C–Br bond to give a racemic mixture of **3** in reasonable yield.

problem in this reaction, we hoped that with an efficient chiral catalyst the reaction would stop after one of the enantiotopic C–Br units had been converted into a C–H unit.

Initially asymmetric reactions were carried out by stirring $[Pd(dba)_2]$ (5 mol %), chiral ligand (2 equiv), and a small quantity of phenanthrene (HPLC calibration) in DME at 5 °C under N_2 for 10 min and subsequent sequential addition of complex **2** and $LiBH_4$ as solids. The reaction was monitored by chiral HPLC (Chiralcel ODH column). The ferrocenyl ligands that had worked best with $[Cr(CO)_3$(1,2-dichlorobenzene)$]$[3,4] afforded **3** with less than 20 % *ee*. Subsequently, a large number of chiral bidentate ligands were screened. These included ligands from the Solvias-kit,[9] Binap, DuPhos, Phox and analogues, and many others.[10] While it was satisfying to note that yields of **3** with some ligands reached 80 %, chiral induction remained low. Of all the ligands tested, only two, **5**[11] and **6**[12] afforded **3** with an enantioselectivity exceeding 40 % (Scheme 3).

Checking if incomplete dba dissociation in $[Pd(dba)_2]$ was part of the problem, we turned to [CpPd(allyl)][OTf] (Cp = C_5H_5, OTf = $CF_3SO_3^-$) as catalyst precursor.[13] Unfortunately this brought no improvement. Leaving the reaction to proceed further and to yield substantial amounts of the naphthalene complex **4** gave no improvement of the *ee* value of **3**, thereby indicating that the second hydogenolysis takes place without kinetic resolution.



Scheme 3. The two best results in palladium-catalyzed asymmetric hydrogenolysis of an aryl-Br bond using chiral bidentate ligands (L*) are obtained with **5** and **6**.

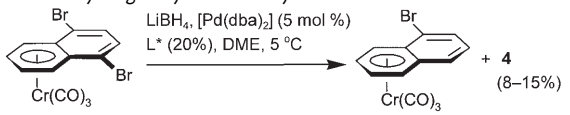
Although good yields were obtained, at this stage our work just reinforced the message of earlier work, that this transformation yields products with low to modest asymmetric induction.[3–5] We therefore decided to turn our attention to chiral monodentate phosphoramidite ligands.

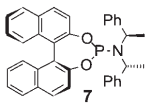
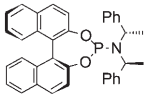
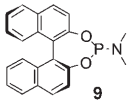
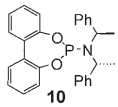
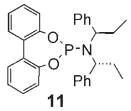
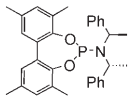
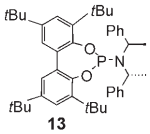
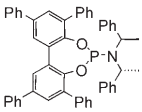
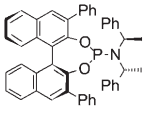
We were pleased to find that phosphoramidite ligand **7**[14] (Table 1, entry 1) afforded complex **3** in good yield and a better enantiomeric purity than achieved with the bidentate ligands. Increasing the ligand equivalents brought no improvement whereas reducing the amount of ligand led to a decrease in *ee* value. The diastereomeric ligand **8** made the reaction sluggish and also afforded **3** in racemic form (Table 1, entry 2). Ligands **9** (entry 3) and **10** (entry 4) showed that the absence of one of the two chiral elements of the ligands leads to a serious erosion of chiral induction. Ligand **11** was tested because it outperforms **10** in the copper-catalyzed conjugate addition of diethyl zinc to enones.[15] However, as the result in entry 5 shows, this is not the case in the reaction at hand. Substitution in the 3,3′ position of the biaryl portion of ligand **11** by alkyl groups brought an increase from 38 % *ee* (entry 4) to a respectable 64 % *ee* and 66 % *ee* (entries 6 and 7). The breakthrough came with the 3,3′-phenyl substituted ligand **14**[15] (entry 8) with which the reaction approached 90 % *ee* for the first time. Returning to the chiral binaphthyl motive with the new phosphoramidite ligand **15**,[16] chiral induction was raised to 92 % *ee*. Optimization, by lowering the temperature and by adding $LiBH_4$ dropwise as a solution, finally yielded the result given in entry 9.[17]

Racemic **3** was subjected to the same conditions and the reaction was followed by chiral HPLC analysis. As with the bidentate ligands, no kinetic resolution was observed, that is, the residual **3** remained racemic. The chiral induction in the reaction depicted in Table 1 thus arises entirely from the recognition of one of the enantiotopic C–Br units in complex **2**.

 © 2006 Wiley-VCH Verlag GmbH & Co. KGaA, Weinheim

Table 1: Chiral phosphoramidite ligands in the palladium-catalyzed asymmetric hydrogenolysis of an aryl-Br bond.[a]



Entry	Ligand	*pR*-**3** yield [%]	*ee* [%]
1	 **7**	78	62
2	 **8**	62	rac.
3	 **9**	60	22
4	 **10**	74	38
5	 **11**	78	18
6	 **12**	78	64
7	 **13**	80	66
8	 **14**	79	89
9	 **15**	80 78[b] (65)[c]	92 97[b]

[a] All yields determined by HPLC (calibration: phenanthrene). [b] Conditions: −10 °C, 35 min, $LiBH_4$ added as solution, see Experimental Section for full details. [c] Yield of *pR*-**3** isolated after chromatography.

All the reactions shown in Table 1 afforded the dextrorotatoy enantiomer as the major product (see Experimental Section). The absolute configuration (*pR*) was assigned by an X-ray structure determination (Figure 1).[18]

The final catalytic step in this reaction is likely to involve a reductive elimination of a *cis*-{Pd(aryl)(H)} moiety. Models show that it is unlikely that two of the very bulky chiral phosphoramidite units are coordinated to the metal in a *cis*-fashion at this stage. Further studies will be required to probe the mechanism and the scope of this reaction.

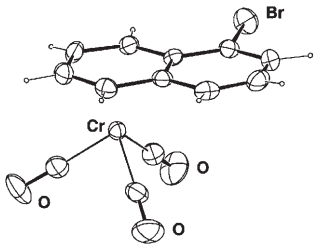


Figure 1. ORTEP view of the crystal structure of compound *pR*-**3**. Thermal ellipsoids are set at 40% probability.

Herein we show the dominant role that ligands play in governing both rates and selectivities of asymmetric reactions. The unusual application in asymmetric hydrogenolysis opens the door to a range of new applications of planar chiral arene complexes. Complex *pR*-**3** promises to be an attractive starting material for further transformations.

Experimental Section

2: $[Cr(CO)_3(NH_3)_3]$ (2.89 g, 15.5 mmol) and **1** (4.00 g, 15.5 mmol) were combined in a Schlenk tube. Dry diethyl ether (60 mL) was added followed by boron trifluoride etherate (6.9 mL, 6.11 g, 55 mmol) and the reagents were thoroughly degassed with four freeze-pump-thaw cycles. After approximately 1 h the yellow suspension began to turn red. Stirring was continued for five days at room temperature and the reaction mixture was then filtered through a pad of celite washing with small portions of toluene until all of the red material (filtrate) had been collected. The solid-liquid interface was stirred frequently with a glass rod to facilitate the filtration process. The solvent was removed under reduced pressure. The dark red solid was dried thoroughly under vacuum and transferred to a small flask. Residual **1** was removed by sublimation (heating to 60–70 °C at 0.2 mmHg). Compound **2** was obtained as a deep red solid (4.50 g, 76%), m.p. 128–132 °C (decomp); IR: $\tilde{\nu}=(CH_2Cl_2)$ 1969, 1898 cm^{-1}. ^1H NMR (400 MHz; C_6D_6): $\delta = 6.68$ (2H, s), 5.91–5.88 (2H, m, $H_{AA'}H_{BB'}$), 4.58–4.55 ppm (2H, m, $H_{AA'}H_{BB'}$); ^{13}C NMR (101 MHz; $CDCl_3$): $\delta = 230.2$ (CO), 130.7, 122.3 (C quaternary), 104.6 (C quat.), 91.7, 88.4 ppm; UV (λ_{max} nm; CH_2Cl_2) 358, 295, 234; MS *m*/*z* (EI) 424 (2%, $[M^+]$, $2\times{}^{81}Br$), 422 (3, $[M^+]$, $^{79}Br+{}^{81}Br$), 420 (2, $[M^+]$, $2\times{}^{79}Br$), 288 [3, $[M-Cr(CO)_3]$, $2\times{}^{81}Br$], 286 [6, $[M-Cr(CO)_3]$, $^{79}Br+{}^{81}Br$], 284 [3, $[M-Cr(CO)_3]$, $2\times{}^{79}Br$), 126 (62, $[C_{10}H_6^+]$), 52 (100, [Cr]); HRMS(EI) (Found: $[M^+]$, 423.8049. $C_{13}H_6CrO_3{}^{81}Br_2$ calcd: *M*, 423.8048).

pR-**3** (optimized, Table 1, entry9): Under N_2 (S_a*R*,*R*)-**15** (248 mg, 0.36 mmol) was added at room temperature to a solution of $[Pd(dba)_2]$ (54 mg, 0.09 mmol) in freshly distilled, dry and degassed DME (20 mL) in a Schlenk reaction vessel. The mixture was stirred for 30 min at room temperature and then cooled to −10 °C. Then **2** (750 mg, 1.8 mmol) was added at the same temperature. A freshly prepared solution of $LiBH_4$ in DME (5.5 M in DME, 0.66 mL, 3.6 mmol) was diluted with DME (6.0 mL) at room temperature and then added by cannula over 10 min to the stirred reaction mixture maintained at −10 °C. Stirring was continued at −10 °C under N_2. Formation of **3** was monitored by thin layer chromatography (TLC) (pentane/toluene 3/1, $R_f = 0.3$). The reaction was stopped after 35 min and the reaction mixture was filtered over celite under N_2, and washed with dry DME. HPLC indicated **3** to be formed in a yield of 78%. The *ee* value (97%) was determined by chiral HPLC (Chiralcel-ODH, 0.5 × 20 cm, hexane:*i*PrOH, 95:5, 1 mL min^{-1}, 17 min:(*pR*-**3**); 32 min:((1*S*)-**3**). To isolate the bulk product silica gel was added to the

 © 2006 Wiley-VCH Verlag GmbH & Co. KGaA, Weinheim

filtrate and solvent was evaporated. Chromatography (silica, pentane/toluene 3/1, column: OD 5 cm, length 15 cm) afforded p*R*-**3** as a bright red solid (395 mg, 1.15 mmol, 65%); m.p. 118–122 °C (decomp); $[\alpha]_D^{20} = (+)\ 401$ ($c = 0.12$ in $CHCl_3$); IR (methylcyclohexane): $\tilde{\nu} = 1969$, 1897 cm^{-1}; ^1H NMR (400 MHz, C_6D_6): $\delta = 6.96$ (dd, $J = 7.3$, 1.0 Hz, 1H), 6.66 (d, $J = 8.5$ Hz, 1H), 6.32 (dd, $J = 8.5$, 7.3 Hz, 1H), 5.93–5.91 (m, 1H), 5.05–5.03 (m, 1H), 4.53–4.51 ppm (m, 2H); ^{13}C NMR (100 MHz, C_6D_6): $\delta = 231.1$ (CO), 131.0, 127.9, 127.7, 123.2 (C quaternary), 106.0 (C quat.), 103.9 (C quat.), 91.8, 91.7, 89.4, 88.7 ppm; MS: *m*/*z* (%) 342 (4, $[M^+]$, ^{79}Br), 258 (21), 208 (5, $[M-Cr(CO)_3]$, ^{79}Br), 127 (5, $[C_{10}H_6^+]$), 52 (100, [Cr]); HRMS(EI) calcd for $C_{13}H_7CrO_3{}^{81}Br$: *M* 341.8984; found: $[M^+]$ 341.9027. Elemental analysis (%) calcd for $C_{13}H_7O_3CrBr$: C 45.51, H 2.06; found: C 45.71, H 2.32.

Received: July 31, 2005
Published online: January 11, 2006

Keywords: asymmetric synthesis · chromium · hydrogenolysis · P ligands · palladium

[1] a) *Transition Metal Arene π-Complexes in Organic Synthesis and Catalysis, Topics in Organometallic Chemistry, Vol. 7.* (Ed.: E. P. Kündig), Springer, Heidelberg, **2004**; b) E. P. Kündig, S. H. Pache, *Sci. Synth.* **2003**, *2*, 155–228; c) A. R. Pape, K. P. Kaliappan, E. P. Kündig, *Chem. Rev.* **2000**, *100*, 2917.

[2] a) K. Muniz in *Topics in Organometallic Chemistry, Vol. 7* (Ed.: E. P. Kündig), Springer, Heidelberg, **2004**, p. 205; b) W. Braun, A. Salzer, F. Spindler, E. Alberico, *Appl. Cat. A* **2004**, *274*, 191; c) S. E. Gibson, H. Ibrahim, *Chem. Commun.* **2002**, 2465; d) C. Bolm, K. Muniz, *Chem. Soc. Rev.* **1999**, *28*, 51.

[3] a) M. Uemura, H. Nishimura, T. Hayashi, *Tetrahedron Lett.* **1993**, *34*, 107; b) M. Uemura, H. Nishimura, T. Hayashi, *J. Organomet. Chem.* **1994**, *473*, 129.

[4] a) B. Gotov, H. G. Schmalz, *Org Lett.* **2001**, *3*, 1753; b) A. Bottcher, H. G. Schmalz, *Synlett* **2003**, 1595.

[5] a) K. Kamikawa, K. Harada, M. Uemura, *Tetrahedron: Asymmetry* **2005**, *16*, 1419; b) For analogous, diastereoselective reactions see: E. P. Kündig, H. Ratni, B. Crousse, G. Bernardinelli, *J. Org. Chem.* **2001**, *66*, 1852.

[6] a) For a synthesis of the aklavinone AB ring system starting from *rac*-[$Cr(CO)_3$(5-methoxynaphthalene)] see: E. P. Kündig, M. Inage, G. Bernardinelli, *Organometallics* **1991**, *10*, 2921.

[7] a) There is no precedent for this transformation. For arene exchange reactions with [$Cr(CO)_3$(naphthalene)] see ref. [1b].

[8] a) J. A. Morley, N. F. Woolsey, *J. Org. Chem.* **1992**, *57*, 6487; b) D. Schinzer, U. Abel, P. G. Jones, *Synlett* **1997**, 632; c) E. P. Kündig, T. Lomberget, R. Bragg, C. Poulard, G. Bernardinelli, *Chem. Commun.* **2004**, 1548.

[9] http://www.solvias.com. We thank Drs. H. U. Blaser and F. Spindler for a gift of ligands.

[10] To be detailed in a forthcoming full paper.

[11] E. P. Kündig, P. Meier, A. Pfaltz, K. Radkowskic, N. Zimmermann, M. Neuburger-Zehnder, *Helv. Chim. Acta* **2001**, *84*, 3233.

[12] a) B. M. Trost, D. L. Van Vranken, C. Bingel, *J. Am. Chem. Soc.* **1992**, *114*, 9327; b) For a study of the coordination mode of this ligand to Pd^{II} centers see: G. C. Lloyd-Jones, S. C. Stephen, I. J. S. Fairlamb, A. Martorell, B. Dominguez, P. M. Tomlin, M. Murray, J. M. Fernandez, J. C. Jeffery, T. Riis-Johannessen, T. Guerziz, *Pure Appl. Chem.* **2004**, *76*, 589.

[13] We thank Prof. Guy Lloyd-Jones, Bristol, for a sample and for helpful discussions.

[14] L. A. Arnold, R. Imbos, A. Mandoli, A. H. Vries, R. Naasz, B. L. Feringa, *Tetrahedron* **2000**, *56*, 2865.

[15] A. Alexakis, D. Polet, S. Rosset, S. March, *J. Org. Chem.* **2004**, *69*, 5660. We thank Prof. Alexakis for a gift by of a sample of **11**.

[16] Ligand **15** was readily prepared from 3,3′diphenyl binaphthol, Whitesell amine, and PCl_3.

[17] The reaction is clean and affords the product in 78% yield and 97% *ee* as indicated by chiral HPLC. The major contaminants are **1** and **4**. On small scale reactions, column chromatography is the best way to purify **3**. The lability of naphthalene complexes causes a drop in yield to 65% of isolated **3** after chromatography. Efforts to scale up and use crystallization to overcome this problem are underway.

[18] Crystallographic data: Cell dimensions and intensities were measured at 200 K on a Stoe IPDS diffractometer with graphite-monochromated $Mo_{K\alpha}$ radiation. ($\lambda = 0.71073$ Å). Data were corrected for Lorentz and polarization effects and for absorption. The structures were solved by direct methods (SIR97),[19] all other calculations were performed with XTAL system.[20] $C_{13}H_7BrCrO_3$, $M_r = 343.1$, Orthorhombic, $P2_12_12_1$, $a = 9.0686$ (4), $b = 10.1876(4)$, $c = 27.0683(13)$ Å, $V = 2500.8(2)$ Å^3, $Z = 8$, $\mu = 4.11$ mm^{-1}, $d_x = 1.823$ $g\,cm^{-3}$, Flack parameter $x = -0.01(2)$, $R = 0.025$, $\omega R = 0.027$. Both molecules of the asymmetric unit show the same *pR* configuration. CCDC-277480 contains the supplementary crystallographic data for this paper. These data can be obtained free of charge from The Cambridge Crystallographic Data Centre via www.ccdc.cam.ac.uk/data_request/cif.

[19] A. Altomare, M. C. Burla, M. Camalli, G. Cascarano, C. Giacovazzo, A. Guagliardi, A. G. G. Moliterni, G. Polidori, R. Spagna, *J. Appl. Crystallogr.* **1999**, *32*, 115.

[20] S. R. Hall, H. D. Flack, J. M. Stewart, XTAL3.2 (User's Manual), Eds. Universities of Western Australia and Maryland, **1992**.

 © 2006 Wiley-VCH Verlag GmbH & Co. KGaA, Weinheim

Actinide Chemistry

DOI: 10.1002/anie.200501931

How Can Uranium Ions (U^+, U^{2+}) Activate the O–H Bond of Water in the Gas Phase?**

Maria del Carmen Michelini, Nino Russo, and Emilia Sicilia*

Theoretical and experimental investigations of transition metal cations in the gas phase have attracted considerable attention, focusing mainly on the fundamental understanding of activation of prototypical bonds (e.g. C–H, N–H, O–H).[1] Most of these studies dealt with cations of the first and second transition metal rows. However, the heavier 5f-block elements are also of great interest, mainly because of their

[*] Dr. M. d. C. Michelini, Prof. N. Russo, Prof. E. Sicilia
Dipartimento di Chimica
Università della Calabria
Via P. Bucci, Cubo 14C, 87030 Arcavacata di Rende (Italy)
Fax: (+39) 0984-493-390
E-mail: nrusso@unical.it

[**] Financial support from the Università degli Studi della Calabria and MIUR is gratefully acknowledged.

Supporting information for this article is available on the WWW under http://www.angewandte.org or from the author.

© 2006 Wiley-VCH Verlag GmbH & Co. KGaA, Weinheim

unique ability to activate notoriously unreactive molecules such as CH_4 and CO_2.[2] In addition, there is an increasing interest in studying the gas-phase chemistry of actinides in order to obtain a better understanding of the particular character of the electronic structures and energetics of the early actinides, and especially the direct and indirect roles of the 5f electrons in their chemistry.[3] Moreover, the chemistry of uranium, particularly the hydrolysis reaction, is of fundamental importance.[4]

In a recent experimental study,[5] the pathways and rate constants of the reaction of gas-phase uranium cations with H_2O were investigated using a quadrupole ion-trap mass spectrometer (QIT-MS). In the case of the reaction between U^+ and H_2O the reaction products shown in Equations (1) and (2) were detected.

$$U^+ + H_2O \rightarrow UO^+ + H_2 \quad (1)$$

$$U^+ + H_2O \rightarrow UOH^+ + H \quad (2)$$

There is some disagreement in experimental data regarding the relative rates for reactions (1) and (2). In low-energy ion-beam experiments,[6] both reactions were shown to be exothermic with a branching ratio of about 10:1 in favor of the first one. Therefore, it was concluded that the formation of UO^+ is thermodynamically favored at low kinetic energies and the second reaction channel competes only at higher kinetic energies. In the QIT-MS experiments,[5] the minor product UOH^+ was also detected with a branching ratio close to 10:1, in agreement with the ion-beam experiments. In Fourier transform ion cyclotron mass spectrometry (FTICR-MS) experiments, on the other hand,[7,8] reaction (2) was not observed. UOH^+ was formed only under conditions where thermalization was not effective.[8]

The reaction of U^{2+} led to similar products, although reliable reaction rate constants were not determined for this reaction.[5] In contrast, recent experimental data (FTICR-MS) indicate that U^{2+} reacts with H_2O to produce only UOH^{2+}.[9]

We used three approaches of density functional theory (DFT) to analyze the reactions under study (see the Supporting Information for the method chosen and for computational details). First, B3LYP formulation was used together with the Stuttgart/Bonn (SDD) relativistic effective core potential (RECP, small core). The 6-311^{++}G(d,p) basis set of Pople and co-workers was employed for the rest of the atoms (B3LYP/SDD, hereafter, where SDD = Stuttgart/Bonn relativistic effective core potential). Second, the same RECP and basis sets were used together with the PW91 functionals for the exchange and correlation parts of the generalized gradient approximation (PW91/SDD). Additional calculations were performed by using the zero-order regular approximation together with the PW91 functionals (exchange and correlation) and the type TZ2P basis set as implemented in the ADF package (PW91/ZORA). Finally, we analyzed the effect of spin–orbit interaction by performing single-point calculations on the optimized geometries obtained at the PW91/ZORA level within the spin–orbit ZORA approximation (PW91/SO-ZORA).

In both reaction paths, more than one spin state was considered: for U^+ the quartet state (electronic configuration of the outer shells: $5f^37s^2$), which corresponds to the ground state (GS) of the bare cation, and the low-lying sextet ($5f^36d^17s^1$ and $5f^47s^1$) and doublet states ($5f^37s^2$); for U^{2+} the triplet and quintet (GS of the bare cation) states (the electronic configuration is $5f^4$ in both cases).

In Figure 1 we present the reaction pathway for the interaction of U^+ and H_2O.[10] Only in the case of the B3LYP/SDD approximation was possible to correctly determine the U^+ GS. As a consequence, the potential energy profiles were constructed based on the energy results obtained at that level of theory. The quartet state remained the GS for the whole reaction path. Therefore, we restrict our discussion of the $U^+ + H_2O$ reaction pathway to the results for this state.

The first step of the reaction involves the exothermic formation of a stable ion–dipole complex (**I**, Figure 2). The next step, that is, the O–H bond breaking, takes place through

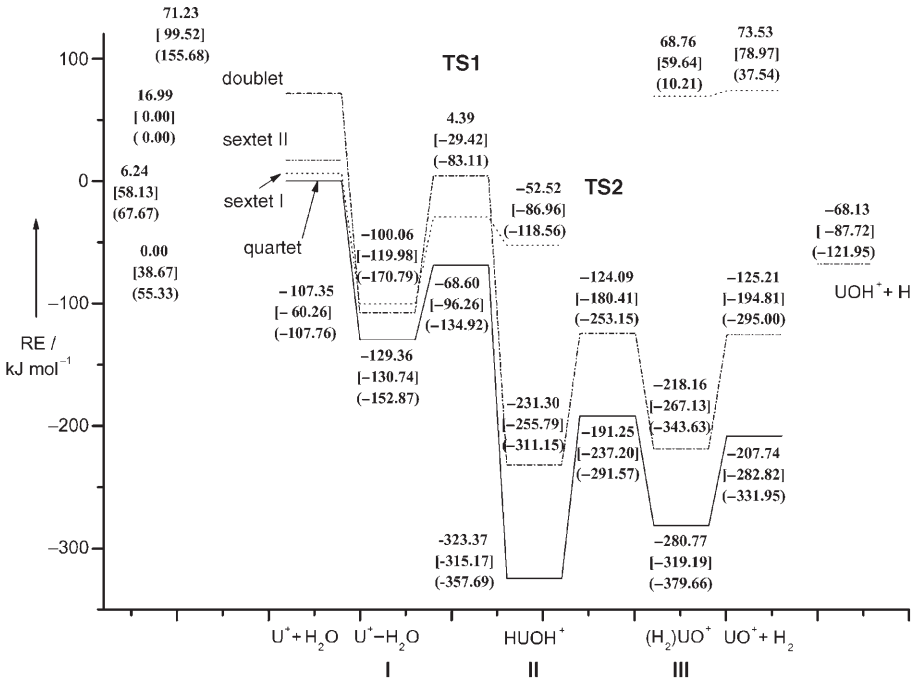


Figure 1. Potential energy profiles (RE: relative energy, in kJ mol^{-1}) for the reaction of U^+ with H_2O at the B3LYP/SDD, PW91/SDD (in square brackets), and PW91/ZORA (in parentheses) levels for the quartet (——), sextet (•••••, –·····), and doublet states (–•–•) of U^+.[10] The statistically averaged experimental data indicate the $5f^37s^2$ configuration (quartet) as the GS of U^+, followed by the $5f^36d^17s^1$ configuration (sextet I) at 3.73 kJ mol^{-1}, the $5f^47s^1$ configuration (sextet II) at 58.85 kJ mol^{-1}, and the $5f^37s^2$ configuration (doublet) at 115.95 kJ mol^{-1}.[10]

 © 2006 Wiley-VCH Verlag GmbH & Co. KGaA, Weinheim

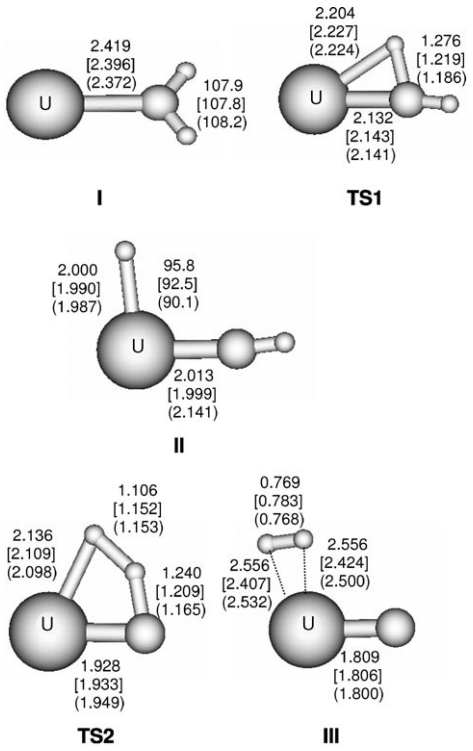


Figure 2. Geometrical parameters of minima and transition states at the B3LYP/SDD, PW91/SDD (in square brackets), and PW91/ZORA (in parentheses) levels for the reaction of U^+ (quartet state) with H_2O. Bond lengths are in Å and angles in deg.

the U^+ insertion into a O–H bond to form the $HUOH^+$ intermediate (**II**). The formation of this intermediate, which is a highly exothermic process, is possible after the system surpasses the first transition state (**TS1**). The reaction, then, can proceed toward the formation of the dehydrogenation products [Eq. (1)], through a concerted four-center elimination of H_2; or toward the formation of UOH^+, as the result of a simple cleavage of the U–H bond in the intermediate **II** [Eq. (2)]. The formation of the GS insertion complex is energetic enough so that the exit channel leading to the formation of the products could be kinetically reached. Activation barriers for all the TSs along the paths are reported in Table 1.

As can be seen in Figure 1, the second exit channel, namely the formation of UOH^+ (quintet state) with a loss of an H atom, is exothermic and has no barriers in excess of the reactant energy, in agreement with the ion-beam experiments.[6] The exothermicity of this process, however, is lower than that of the dehydrogenation reaction. These results agree with the experimental conclusion that the formation of UO^+ is thermodynamically favored.[5,6] The calculated exothermicity for the dehydrogenation reaction fairly agrees with the experimental estimation (about 315 kJ mol^{-1}).[7]

In addition to the previously mentioned dehydrogenation path, which involves the formation of the $(H_2)UO^+$ intermediate, we also considered the formation of a dihydride uranium oxo ion, $(H)_2UO^+$. However, in a quite large inspection of the potential energy surfaces, we could localize this species only for U^+ doublet states. In each case, the

Table 1: Activation barriers [kJ mol^{-1}] of the transition states (see Figures 1 and 3).

U^+–H_2O	B3LYP/ SDD	PW91/ SDD	PW91/ ZORA	PW91/SO-ZORA
TS1[a]	60.76	34.48	17.95	21.97
TS2[b]	132.12	77.97	66.12	65.83
dissociation barrier[c]	73.03	36.37	47.71	41.10
U^{2+}–H_2O	B3LYP/ SDD	PW91/ SDD	PW91/ ZORA	PW91/SO-ZORA
TS1′[a]	143.41	128.73	112.83	110.40
TS2′[b]	124.67	106.13	108.22	69.93
dissociation barrier[c]	55.63	61.85	86.13	52.35

[a] Calculated as the energy difference between the first transition state and the first complex (**I** or **IV**). [b] Calculated as the energy difference between the second transition state and the first intermediate (**II** or **V**). [c] Energy difference between the dissociated products ($UO^+ + H_2$ or $UO^{2+} + H_2$) and the last intermediate (**III** or **VI**).

$(H)_2UO^+$ isomer has been found to be higher in energy than the $(H_2)UO^+$ isomer.

We have ensured that every transition state had only one imaginary frequency and, by performing IRC (intrinsic reaction coordinate) calculations, that this frequency connects reactants and products. Therefore we are confident that the dehydrogenation pathway involves the $(H_2)UO^+$ intermediate. Geometrical parameters of all the stationary points along the dehydrogenation path are presented in Figure 2. All the structures are planar, with the exception of $HUOH^+$, in which there is a deviation from planarity by about 4 deg.

An analysis analogous to that for the U^+ reaction revealed a similar reaction mechanism for the interaction between U^{2+} and H_2O. The high-spin/low-spin splittings for the bare U^{2+} cation at all the studied levels of theory are given in Figure 3,[10] which also shows the reaction profile for the reaction. The situation is quite different from that of the reaction of U^+. Firstly, there is a crossing of the potential energy surfaces just after the first transition state. After this point, the reaction evolves along the triplet-state surface. We were not able to characterize the second transition state for the quintet state, independent of the level of theory employed. However, this structure is surely quite high in energy and it is not fundamental for the description of the pathway, which evolves at this stage along the triplet-state surface.

A comparison between the reaction pathways (Figures 1 and 3) and the barrier heights (Table 1) indicates that the reaction of U^{2+} has to surpass a higher barrier for the first transition state (around 85 kJ mol^{-1} higher than in the reaction of U^+). The second barrier height (TS2) is comparable for both reactions, whereas the dissociation barrier is 17.4 kJ mol^{-1} higher than for the reaction of U^+.

Experimental studies led to partly contrasting results regarding the reaction products for the reaction of U^{2+} with H_2O. FTICR-MS results[9] indicated that the only reaction product is UOH^{2+}, whereas QIT-MS studies[5] detected both reaction products, that is, UOH^{2+} and UO^{2+}. From our

 © 2006 Wiley-VCH Verlag GmbH & Co. KGaA, Weinheim

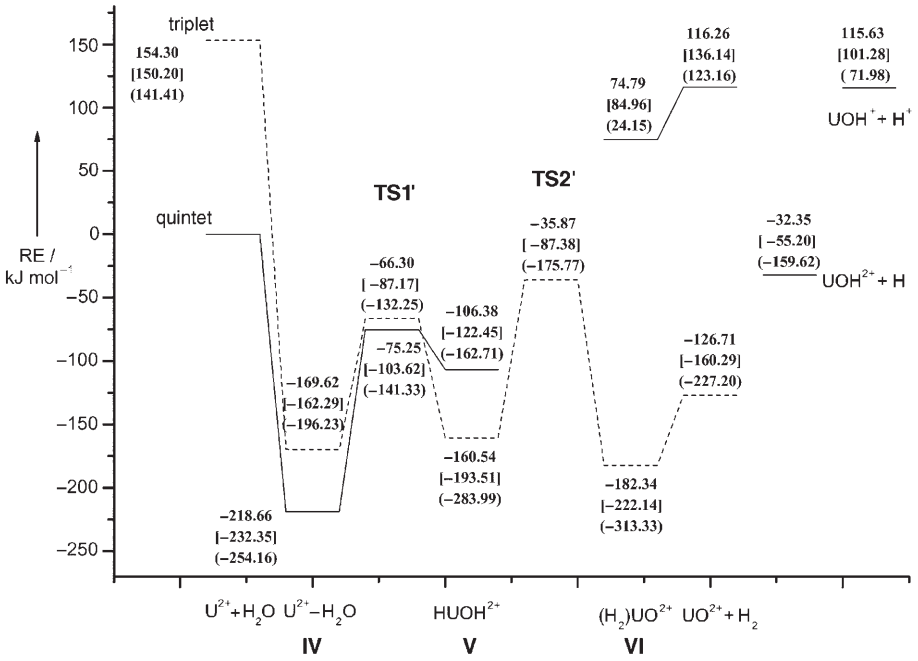


Figure 3. Potential energy profiles (RE: relative energy, in kJ mol^{-1}) for the reaction of U^{2+} with H_2O at the B3LYP/SDD, PW91/SDD (in square brackets), and PW91/ZORA (in parentheses) levels for the quintet (——) and triplet (-----) states of U^{2+}.[10] The lowest energy triplet state reported in the Blaise and Wyart tables[10] has the $5f^27s^2$ configuration and is 442 ± 72 kJ mol^{-1} higher in energy than the quintet GS. The $5f^4$ triplet state is not reported in these tables[10]. Our calculations indicated the $5f^4$ configuration to be the lowest-energy triplet state at 154.30 kJ mol^{-1}, whereas the $5f^27s^2$ triplet state is calculated to be at 419 kJ mol^{-1} from the quintet GS (B3LYP calculations).

theoretical results, we conclude that the thermodynamically favored reaction channel corresponds to the dehydrogenation process, whereas the products $UOH^{2+} + H$ have been found to be about 95 kJ mol^{-1} higher in energy (see Figure 3).

For the reaction of U^{2+}, we also considered the charge-separation asymptotes, that is, $UOH^+ + H^+$ and $UH^+ + OH^+$. The first one has been included in Figure 3. The $UH^+ + OH^+$ asymptote has been found to be much higher in energy; its endothermicity with respect to the $U^{2+} + H_2O$ asymptote was calculated to be 651.6 kJ mol^{-1} (B3LYP/SDD).

In Figure 4, we report the geometrical parameters for all the species involved in the reaction with U^{2+} (GS species). All the structures are planar, with the exception of the last insertion structure (**VI**), in which there is a deviation from planarity of about 6 deg (H_2 fragment with respect to UO).

Bonding was studied by means of natural bond orbital (NBO) and natural population analyses (NPA). The main conclusions obtained from these analyses can be summarized as follows. NPA analyses indicate that all the species involved in the reaction path have a highly ionic character, mainly from **TS1**/**TS1**′ to the products. This feature is particularly noticeable in the case of U^+, for which the charge on the metal center becomes +2.32 for $HUOH^+$. It is interesting to note, that the electronic configuration and the charge on the metal center corresponding to the same reaction species on the reaction paths of U^+ and U^{2+} seem to be quite close (e.g., NPA charge of U in $HUOH^+$: 2.32; of U in $HUOH^{2+}$: 2.87), which indicates more electron transfer from the metal center to the ligand in the case of U^+.

A detailed description of the NBO analysis is available as Supporting Information, which also offers some insight into the bonding evolution along the reaction paths and the direct role of 5f uranium electrons.

In summary, a DFT study of the reactions of U^+ and U^{2+} with H_2O had the following results: 1) for both reactions the dehydrogenation process is thermodynamically favored; 2) the exothermic formation of H_2 in the reaction between U^+ and H_2O takes place without changes in the spin state of the system; 3) the reaction of U^{2+} with water is less favored, both thermodynamically and kinetically, and involves a spin transition between a quintet and a triplet state; 4) no sharp differences between the theoretical approaches employed in this work have been found, which could permit us to decide which of them is the better one. The B3LYP functional seems to better reproduce the experimental data of bare uranium cations, whereas the PW91 functional shows a better agreement with experimental estimations of thermochemical data. The

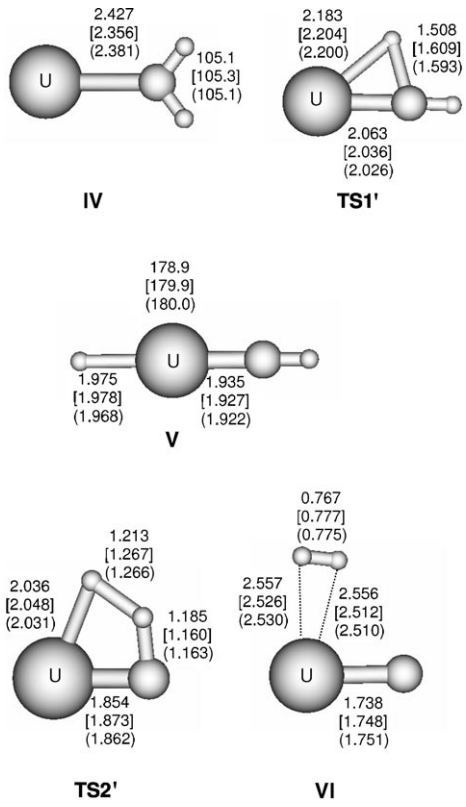


Figure 4. Geometrical parameters of minima and transition states at the B3LYP/SDD, PW91/SDD (in square brackets), and PW91/ZORA (in parentheses) levels for the reaction of U^{2+} with H_2O. Bond lengths are in Å and angles in deg.

 © 2006 Wiley-VCH Verlag GmbH & Co. KGaA, Weinheim

inclusion of spin–orbit corrections generally decreases the activation barriers by 1 to 38 kJ mol^{-1}.

Received: June 3, 2005
Revised: October 31, 2005
Published online: January 3, 2006

Keywords: actinides · density functional calculations · gas-phase chemistry · O–H activation

[1] a) P. B. Armentrout, *Annu. Rev. Phys. Chem.* **1990**, *41*, 313 – 344; b) K. Eller, H. Schwarz, *Chem. Rev.* **1991**, *91*, 1121 – 1177; c) J. C. Weisshaar, *Acc. Chem. Res.* **1993**, *26*, 213 – 219.
[2] C. Heinemann, H. H. Cornehl, H. Schwarz, *J. Org. Chem.* **1995**, *60*, 201 – 209.
[3] J. K. Gibson, *Int. J. Mass Spectrom.* **2002**, *214*, 1 – 21.
[4] B. Liang, R. D. Hunt, G. P. Kushto, L. Andrews, *Inorg. Chem.* **2005**, *44*, 2159 – 2168.
[5] G. P. Jackson, F. L. King, D. E. Goeringer, D. C. Duckworth, *J. Phys. Chem. A* **2002**, *106*, 7788 – 7794.
[6] P. B. Armentrout, J. L. Beauchamp, *Chem. Phys.* **1980**, *50*, 27 – 36.
[7] H. H. Cornehl, R. Wesendrup, M. Diefenbach, H. Schwarz, *Chem. Eur. J.* **1997**, *3*, 1083 – 1090.
[8] M. Santos, J. Marçalo, A. Pires de Matos, J. K. Gibson, R. G. Haire, *J. Phys. Chem. A* **2002**, *106*, 7190 – 7194.
[9] J. K. Gibson, R. G. Haire, M. Santos, J. Marçalo, A. Pires de Matos, *J. Phys. Chem. A* **2005**, *109*, 2768 – 2781.
[10] The calculated first and second adiabatic ionization energies (IE1, IE2; in eV) for a U atom are: B3LYP/SDD: 6.42, 11.58; PW91/SDD: 5.56, 11.18; PW91/ZORA: 5.91, 11.13; the experimental values are: IE1:6.19, IE2:11.59. The experimental energy levels and ionization energies have been taken from J. Blaise, J.-F. Wyart, *International Tables of Selected Constants, Energy Levels and Atomic Spectra of Actinides, Vol. 20*, Tables of Constants and Numerical Data, Paris, **1992**. The calculated relative energies for the lowest-energy PW91/SO-ZORA configurations (*jj* coupling) are: for U^+: $5f^3_{5/2}7s^2_{1/2}$ as GS, $5f^4_{5/2}7s^1_{1/2}$ at +36.76 kJ mol^{-1}, $5f^2_{5/2}5f^1_{7/2}7s^2_{1/2}$ at +65.27 kJ mol^{-1}, and $5f^3_{5/2}6d^1_{3/2}7s^1_{1/2}$ at +75.02 kJ mol^{-1}; for U^{2+}: $5f^4_{5/2}$ as GS and $5f^3_{5/2}5f^1_{7/2}$ at +58.72 kJ mol^{-1}. The calculated total energies (in atomic units) of the GS cations at the different levels of theory are: B3LYP/SDD: $U^+ = -476.6219577$, $U^{2+} = -476.19053$; PW91/SDD: U^+:−476.7041557, $U^{2+} = -476.2747229$; in the case of PW91/ZORA, the values ($U^+ = 0.14066495$, $U^{2+} = 0.57073732$) correspond to relative energies with respect to the fragments, as implemented in the ADF package.

 © 2006 Wiley-VCH Verlag GmbH & Co. KGaA, Weinheim

DOI: 10.1002/anie.200503095

A Mimicry of Primary Amines by Bis-Secondary Diamines as Components in the Ugi Four-Component Reaction**

Giovanni Battista Giovenzana, Gian Cesare Tron,* Stefano Di Paola, Ivan Guglielmo Menegotto, and Tracey Pirali*

In memory of Ivar Ugi

Recent years have witnessed a fast growing interest in multicomponent reactions (MCRs),[1] mainly because of their ability to assemble complicated structures in just a few steps. The Ugi four-component reaction (Ugi 4CR)[2] is one of the cornerstone MCRs and great efforts have been devoted to the exploration of the potential of this transformation.[3] In the archetypal Ugi 4CR, a primary amine, a carbonyl compound, a carboxylic acid, and an isocyanide react in methanol to give α-acylamino amides. Several modifications of the classic Ugi 4CR have been described; these modifications involve the variation of one of the components or the introduction of a linkage between two of them, which leads to interesting potential druglike derivatives of the original α-acylamino amide product.[4]

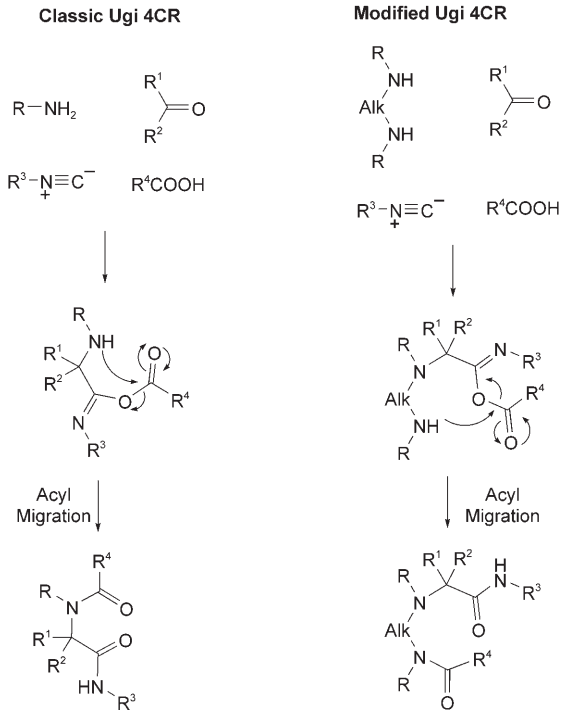
Although a large number of modifications of the carboxylic acid reactant have been successfully explored (for example, water,[5] alcohol and carbon dioxide,[6] hydrazoic acid[7]), the other components are less well suited to structural changes in view of the accepted mechanism of the Ugi 4CR. Isocyanide is the key reagent of the Ugi 4CR, and the carbonyl compound and the primary amine are required for the formation of the intermediate imine.[8]

Herein we focus our attention on the role of the primary amine (Scheme 1), which reacts first with the carbonyl compound to give an intermediate imine. Protonation by the carboxylic acid moiety to give an iminium ion followed by nucleophilic attack of the isocyanide leads to the formation of a nitrilium ion intermediate, which is subsequently intercepted by the corresponding carboxylate anion.[9] The resulting imino anhydride typically undergoes an irreversible transacylation (Mumm rearrangement)[10] to give the final Ugi 4CR product. The primary amine plays a dual role in this

[*] Prof. G. B. Giovenzana, Dr. G. C. Tron, Dr. S. Di Paola, Dr. I. G. Menegotto, Dr. T. Pirali
Di.S.C.A.F.F. and
Drug and Food Biotechnology Center
Università degli Studi del Piemonte Orientale "A. Avogadro"
Via Bovio 6, 28100 Novara (Italy)
Fax: (+39) 0321-375-821
E-mail: giovenza@pharm.unipmn.it
tron@pharm.unipmn.it

[**] We are grateful to Dr. Alberto Massarotti and Dr. Erika Del Grosso for technical assistance.

 © 2006 Wiley-VCH Verlag GmbH & Co. KGaA, Weinheim WILEY InterScience DISCOVER SOMETHING GREAT



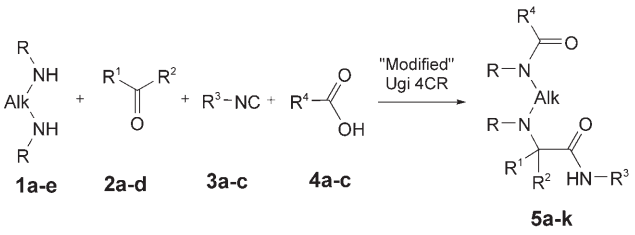
Scheme 1.

mechanism, being simultaneously alkylated, acylated, and losing both hydrogen atoms.

In contrast, when a secondary amine reacts in an Ugi-type reaction, the amine nitrogen atom cannot undergo transacylation. In this case, the isocyanide nitrogen atom usually captures the acyl moiety, to give an α,α′-diacyl amide in a nonnucleophilic solvent.[6a] However, if the stoichiometric amount of the secondary amine is twice that of the other components, the imino anydride intermediate or the α,α′-diacyl amide is promptly attacked by the other secondary amine to give a nearly equimolar mixture of an α-acyl amide and an amide, as was elegantly demonstrated by McFarland.[11]

We were thus prompted to verify whether two secondary amino groups, suitably contained within the same molecule, could take the place of the primary amino group. The "splitting" of the primary amine into two secondary amines could allow the expansion of the skeleton of the MCR product, thus increasing the versatility of the Ugi 4CR and leading to useful new building blocks for the construction of chemical libraries. In detail (Scheme 1), one of the two nitrogen atoms may react with the carbonyl group to afford an iminium ion (in place of the protonated imine), which then interacts with the isocyanide and the carboxylate moiety. The resulting intermediate may undergo a subsequent transacylation in which the acyl moiety migrates to the second nitrogen atom of the diamine (a "remote" Mumm rearrangement), as the first nitrogen atom has already become a tertiary amine and is unable to receive the acyl group.[12]

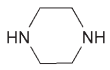
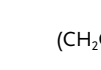
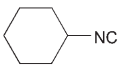
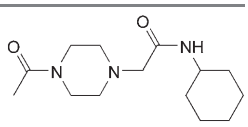
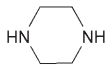
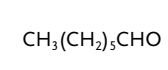
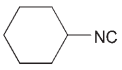
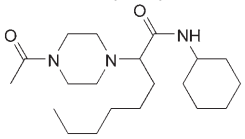
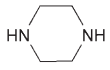
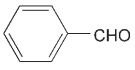
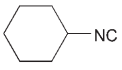
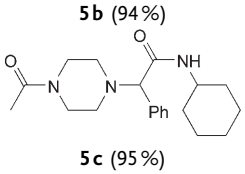
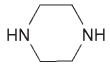
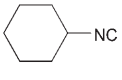
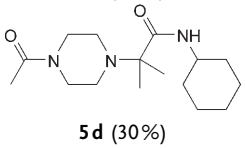
For this reason, we treated piperazine with equimolar amounts of paraformaldehyde, acetic acid, and cyclohexylisocyanide in refluxing methanol. Indeed, we observed a clean transformation, which enabled the isolation, after evaporation and recrystallization or column chromatography, of **5a–k** (Scheme 2).



Scheme 2.

The generality of the N-split Ugi 4CR was then checked by varying the single components. Besides the formaldehyde, alkanals (Table 1, entry 2), aryl aldehydes (Table 1, entry 3), and ketones (Table 1, entry 4) were successfully employed as the carbonyl compound. Good to excellent yields were observed with the exception of the ketone. Steric hindrance could be invoked to justify the modest yield in this case; although the Ugi 4CR is reported to be quite insensitive to steric hindrance,[3] the N-split Ugi 4CR relies on the forma-

Table 1: Compounds obtained by variation of the carbonyl component.

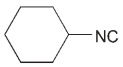
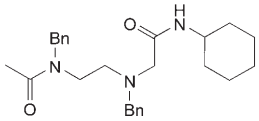
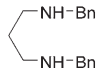
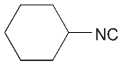
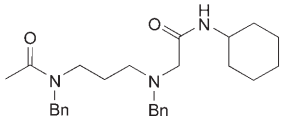
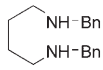
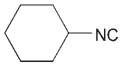
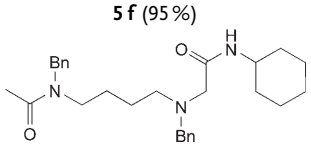
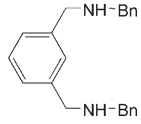
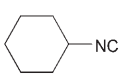
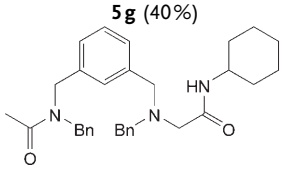
Entry	Diamine	Carbonyl compound	Isocyanide	Carboxylic acid	Product (yield)
1					
	1a	**2a**	**3a**	**4a**	**5a** (75%)
2					
	1a	**2b**	**3a**	**4a**	**5b** (94%)
3					
	1a	**2c**	**3a**	**4a**	**5c** (95%)
4					
	1a	**2d**	**3a**	**4a**	**5d** (30%)

 © 2006 Wiley-VCH Verlag GmbH & Co. KGaA, Weinheim

tion of a crowded, fully alkylated intermediate iminium ion (versus the less encumbered iminium ion derived from the protonation of an imine).

Table 2 reports the products obtained from the variation of the secondary diamine. As well as piperazine, *N*,*N*′-diaryl ethylenediamine **1b** (Table 2, entry 1), propanediamine **1c** (Table 2, entry 2), butanediamine **1d** (Table 2, entry 3), and *m*-xylylenediamine **1e** (Table 2, entry 4) were successfully subjected to the N-split Ugi 4CR protocol. As shown, although the desired conversion always takes place, the yields vary widely within the range 35–95%, with the best result being obtained with *N*,*N*′-dibenzyl-1,3-propanediamine. The length and the conformational mobility of the linking moiety connecting the two secondary amines evidently play a crucial role in the "remote" Mumm rearrangement step, although a precise rationalization cannot be given at this stage. The remarkable 56% yield for the reaction of *N*,*N*′-dibenzyl-1,3-xylylenediamine is quite unexpected, as the putative "remote" Mumm rearramgement involves an 11-membered metacyclophane. Preliminary data from molecular modeling studies of the tetrahedral intermediate in the formation of **5h** (MMFF, Spartan Package)[13] shows the absence of significant strain in the macrocyclic structure; similar 11-membered metacyclophanes are known to be stable.[14]

Table 2: Compounds obtained by variation of the secondary diamine.[a]

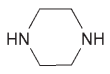
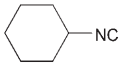
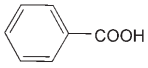
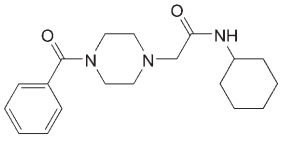
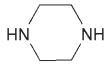
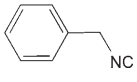
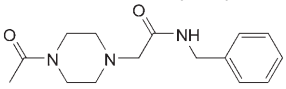
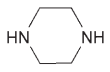
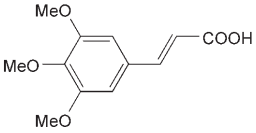
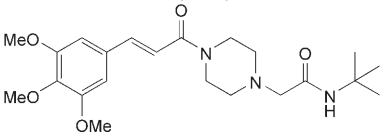
Entry	Diamine	Carbonyl compound	Isocyanide	Carboxylic acid	Product (yield)
1					
	1b	**2a**	**3a**	**4a**	**5e** (35%)
2					
	1c	**2a**	**3a**	**4a**	**5f** (95%)
3					
	1d	**2a**	**3a**	**4a**	**5g** (40%)
4					
	1e	**2a**	**3a**	**4a**	**5h** (56%)

[a] Bn = benzyl.

Furthermore, Table 3 (entry 3) exemplifies the extraordinary synthetic power of this transformation: the product **5k** is a known vasodilator and is usually synthesized in four steps starting from piperazine.[15] The N-split Ugi 4CR allows its one-pot preparation in higher yield from commercially available compounds and avoids the time- and chemical-consuming

Modification of the isocyanide and the carboxylic acid were similarly performed, and the results are listed in Table 3. As with the parent Ugi 4CR, structural modification of one or both components does not affect either the progress or the yield of the corresponding reactions, which are still characterized by good overall efficiency.

Table 3: Compounds obtained by variation of carboxylic acid and isocyanide.

Entry	Diamine	Carbonyl compound	Isocyanide	Carboxylic acid	Product (yield)
1					
	1a	**2a**	**3a**	**4b**	**5i** (80%)
2					
	1a	**2a**	**3b**	**4a**	**5j** (95%)
3					
	1a	**2a**	**3c**	**4c**	**5k** (77%)

 © 2006 Wiley-VCH Verlag GmbH & Co. KGaA, Weinheim

steps needed to discriminate the chemically equivalent nitrogen atoms of the diamine.[16] Additional advantages for the large-scale application of this protocol are its high atom economy (always approaching unity) and environmentally friendly nature (the only by-product is one water molecule per product molecule).[17]

In summary, we have described herein a novel and efficient multicomponent reaction that allows extension of the conventional Ugi 4CR product backbone and provides a new way to create molecular diversity. We have only scraped the surface of its potential in synthetic and medicinal chemistry within the text. Additional work is in progress to elucidate in detail the applicability and limitations of this new weapon in the synthetic chemist's arsenal.

Experimental Section

Typical procedure: Carbonyl compound **2a–d** (1 equiv), carboxylic acid **4a–c** (1 equiv), and isocyanide **3a–c** (1 equiv) were added sequentially to a solution of diamine **1a–e** (1 equiv) in methanol (0.5 M) at room temperature. The reaction mixture was heated at reflux for 2 h, cooled to room temperature, and the solvent was evaporated. The crude reaction mixture was purified by column chromatography or by recrystallization.

Physical data for selected compounds (all data correspond to the main rotamer): **5a**: white powder; m.p. 91–92 °C; ^{1}H NMR (300 MHz, $CDCl_3$, 50 °C) : $\delta = 6.92$ (brs, 1H), 3.80 (m, 1H), 3.64 (brs, 2H), 3.49 (brs, 2H), 3.02 (s, 2H), 2.53 (brs, 4H), 2.08 (s, 3H), 1.95–1.12 ppm (m, 10H); ^{13}C NMR (75.4 MHz, $CDCl_3$, 50 °C): $\delta = 168.8$, 168.2, 61.4, 53.2, 52.9, 47.3, 46.1, 41.3, 32.8, 25.3, 24.5, 20.9 ppm; MS (ESI): *m/z* (%) 268 (100) $[M+H]^+$. **5d**: yellowish powder; m.p. 108–109 °C; ^{1}H NMR (300 MHz, $CDCl_3$, 50 °C): $\delta = 7.04$ (brd, 1H), 3.63 (m, 1H), 3.51 (brs, 2H), 3.38 (brs, 2H), 2.29 (brs, 4H), 2.00 (s, 3H), 1.75–1.08 (m, 10H), 1.08 ppm (s, 6H); ^{13}C NMR (75.4 MHz, $CDCl_3$, 50 °C): $\delta =$ 175.3, 169.2, 63.5, 47.5, 47.1, 46.9, 46.4, 42.1, 33.1, 25.6, 24.6, 21.0, 20.6 ppm; MS (ESI): *m/z* (%) 296 (100) $[M+H]^+$. **5f**: pale yellow oil; ^{1}H NMR (300 MHz, $CDCl_3$, 50 °C): $\delta = 7.23$–7.15 (m, 10H), 6.78 (brd, 1H), 4.37 (s, 2H), 3.61 (m, 1H), 3.48 (s, 2H), 3.29 (t, $J = 7.4$ Hz, 2H), 2.93 (s, 2H), 2.39 (t, $J = 6.8$ Hz, 2H), 2.00 (s, 3H), 1.95–0.99 ppm (m, 12H); ^{13}C NMR (75.4 MHz, $CDCl_3$, 50 °C): $\delta = 170.9$, 170.0, 137.0, 136.8, 128.8, 128.4, 128.3, 128.2, 127.4, 125.9, 59.6, 58.1, 52.5, 52.1, 47.5, 44.1, 32.9, 26.4, 25.3, 24.7, 21.6 ppm; MS (ESI): *m/z* (%) 436 (100) $[M+H]^+$. **5i**: pale yellow solid; m.p. 141–142 °C; ^{1}H NMR (300 MHz, $CDCl_3$, 50 °C): $\delta = 7.34$ (brs 5H), 6.85 (brd, 1H), 3.74 (m, 1H), 3.57 (brs, 4H), 2.96 (s, 2H), 2.48 (brs, 4H), 1.81–1.11 ppm (m, 10H); ^{13}C NMR (75.4 MHz, $CDCl_3$, 50 °C): $\delta = 170.4$, 168.2, 135.7, 129.8, 128.5, 127.0, 61.6, 53.4 (×2), 47.5, 33.1, 25.6, 24.7 ppm; MS (ESI): *m/z* (%) 330 (100) $[M+H]^+$. **5k**: white solid; m.p. 184–185 °C; ^{1}H NMR (300 MHz, $CDCl_3$, 50 °C): $\delta = 7.56$ (d, $J = 15.4$ Hz, 1H), 6.90 (brs, 1H), 6.70 (s, 2H), 6.68 (d, $J = 15.4$ Hz, 1H), 3.86 (s, 6H), 3.85 (s, 3H), 3.72 (brs, 4H), 2.97 (s, 2H), 2.59 (brs, 4H), 1.35 ppm (s, 9H); ^{13}C NMR (75.4 MHz, $CDCl_3$, 50 °C): $\delta = 165.6$ (×2), 153.6, 143.3, 140.3, 130.8, 116.1, 105.6, 62.2, 60.9, 56.5, 53.3 (×2), 50.8, 28.9 ppm; MS (ESI): *m/z* (%) 420 (100) $[M+H]^+$.

Received: August 31, 2005
Revised: November 15, 2005
Published online: January 3, 2006

[1] a) *Multicomponent Reactions* (Eds.: J. Zhu, H. Bienaymé), Wiley-VCH, Weinheim **2005**, and references therein; b) J. Zhu, *Eur. J. Org. Chem.* **2003**, *7*, 1133-1144.
[2] I. Ugi, *Angew. Chem.* **1962**, *74*, 9–22; *Angew. Chem. Int. Ed. Engl.* **1962**, *1*, 8–21.
[3] A. Dömling, I. Ugi, *Angew. Chem.* **2000**, *112*, 3300–3344; *Angew. Chem. Int. Ed.* **2000**, *39*, 3168–3210.
[4] a) R. W. Armstrong, A. P. Combs, P. A. Tempest, S. D. Brown, T. A. Keating, *Acc. Chem. Res.* **1996**, *29*, 123–131; b) L. Weber, *Curr. Med. Chem.* **2002**, *9*, 1241–1253; c) C. Hulme, V. Gore, *Curr. Med. Chem.* **2003**, *10*, 51–80.
[5] I. Ugi, C. Steinbrückner, DE 1103337, **1959**.
[6] a) I. Ugi, C. Steinbrückner, *Chem. Ber.* **1961**, *94*, 2802–2814; b) T. A. Keating, R. W. Armstrong, *J. Org. Chem.* **1998**, *63*, 867; c) C. Hulme, L. Ma, J. J. Romano, G. Morton, S. Y. Tang, M. P. Cherrier, S. Choi, J. Salvino, R. Labaudiniere, *Tetrahedron Lett.* **2000**, *41*, 1889–1893.
[7] a) I. Ugi, R. Meyr, *Chem. Ber.* **1961**, *94*, 2229–2233; b) for an application using safer trimethylsilyl azide ($TMSN_3$), see: H. Bienaymé, K. Bouzid, *Tetrahedron Lett.* **1998**, *39*, 2735–2738.
[8] Several amine-like derivatives have been used in the Ugi 4CR (e.g. ammonia, hydroxylamines, hydrazines, hydrazides, ureas) but all can be considered as a particular type of primary amine.
[9] The exact nature of the Ugi 4CR mechanism is still under discussion and a competitive pathway involving the reaction between the activated iminium ion and the carboxylate may be operating; see "Asymmetric isocyanide-based MCR": L. Banfi, A. Basso, G. Guanti, R. Riva in *Multicomponent Reactions* (Eds.: J. Zhu, H. Bienaymé), Wiley-VCH, Weinheim **2005**, pp. 1–32.
[10] O. Mumm, *Ber. Dtsch. Chem. Ges.* **1910**, *43*, 886–893.
[11] J. W. McFarland, *J. Org. Chem.* **1963**, *28*, 2179–2181.
[12] Similar transacylation reactions are known to occur following MCRs, for example, acid-catalyzed macrolactonization as reported in: G. Zhao, X. Sun, H. Bienaymé, J. Zhu, *J. Am. Chem. Soc.* **2001**, *123*, 6700–6701.
[13] PcSpartan Pro, Wavefunction, Inc., Irvine, CA, **1999**.
[14] B. B. Smith, D. E. Hill, T. Ashton Cropp, R. D. Walsh, D. Cartrette, S. Hipps, A. M. Shachter, W. T. Pennington, W. R. Kwochka, *J. Org. Chem.* **2002**, *67*, 5333–5337.
[15] Y. Itho, H. Kato, E. Koshinaka, N. Ogawa, S. Kurata, K. Yamagishi, US 4478838, **1984**.
[16] For examples of selective protection of polyamine nitrogen atoms, see: a) M. C. O'Sullivan, D. M. Dalrymple, *Tetrahedron Lett.* **1995**, *36*, 3451–3452; b) D. Xu, K. Prasad, O. Repic, T. J. Blacklock, *Tetrahedron Lett.* **1995**, *36*, 7357–7360; c) S. H. Lee, C. S. Cheong, *Tetrahedron* **2001**, *57*, 4801–4815.
[17] a) J. Andraos, *Org. Process Res. Dev.* **2005**, *9*, 149–163; b) J. Andraos, *Org. Process Res. Dev.* **2005**, *9*, 404–431.

Keywords: amines · isocyanides · molecular diversity · multicomponent reactions

 © 2006 Wiley-VCH Verlag GmbH & Co. KGaA, Weinheim

Calculations

DOI: 10.1002/anie.200503304

Conducting Polymer Actuator Mechanism Based on the Conformational Flexibility of Calix[4]arene**

Jordi Casanovas, David Zanuy, and Carlos Alemán**

The reversible electrochemical mechanism typical of conducting polymer actuators is based on the addition or removal of charge from the polymer backbone and a flux of ions into or out of the material to balance the charge.[1] Despite their impressive performance, these conducting polymer actuators, which can be envisaged as potential artificial muscles, are limited by the small conformational changes of the molecules, since polymer chains are not able to alter their length. In recent studies a new class of conducting polymer actuators based on conformational changes of the molecular chains rather than on the exchange of ions was developed.[2,3] The actuation mechanism of this material, which was constructed from small thiophene oligomers (quaterthiophenes) separated by calix[4]arene scaffolds (25,27-dihydroxy-26,28-dimethoxycalix[4]arene), namely, poly(calix[4]arene quaterthiophene), was explained in terms of reversible conformational changes produced by variations in the electronic structure of electrochemically activated polymer molecules (Figure 1).

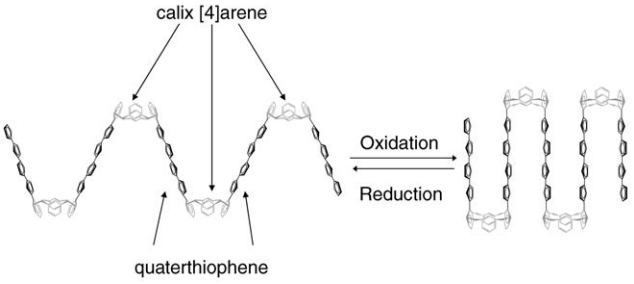


Figure 1. Schematic representation of the poly(calix[4]arene quaterthiophene) molecular actuator.

[*] Dr. J. Casanovas
Departament de Química
Escola Politècnica Superior
Universitat de Lleida
c/Jaume II No 69, 25001 Lleida (Spain)
Fax: (+34) 97-370-2783
E-mail: jcasanovas@quimica.udl.es
Dr. D. Zanuy, Dr. C. Alemán
Departament d'Enginyeria Química
E.T.S. d'Enginyeria Industrial de Barcelona
Universitat Politècnica de Catalunya
Diagonal 647, 08028 Barcelona (Spain)
Fax: (+34) 93-401-6600
E-mail: carlos.aleman@upc.edu

[**] This research was supported by MCYT and FEDER funds through grant no. MAT2003-00251. We are indebted to the CESCA and CEPBA for computational facilities.

Herein we prove that the molecular actuation mechanism of this material is driven by repulsive electrostatic interactions involving the calix[4]arene scaffolds rather than by attractive π–π stacking interactions between quaterthiophene units as was recently suggested.[3,4]

Computer studies based on different simulation techniques have been used to obtain accurate and detailed microscopic information. It should be noted that atomistic modeling is currently considered to be a powerful tool for studying the structure and properties of polymeric materials.[5] Both quantum mechanical calculations and classical molecular dynamics simulations reported in the current study support the flexibility of the calix[4]arene units being the main cause of the surprising ability of poly(calix[4]arene quaterthiophene) to be deformed.

Figure 2 shows one actuating unit of poly(calix[4]arene quaterthiophene) in the reduced, oxidized-nondeprotonated, and oxidized-deprotonated states (hereafter abbreviated Red., Ox-Ndep, and Ox-Dep, respectively) after full structural and electronic relaxation by using quantum mechanics analyses. Calculations were performed that allowed oxidation of the two quaterthiophene segments, while deprotonation occurred at the two hydroxy groups of the 25,27-dihydroxy-26,28-dimethoxycalix[4]arene scaffold. It should be emphasized that experimental evidence indicated the presence of nondeprotonated and deprotonated forms after oxidation of the fully reduced state,[3] which justifies the study of both the Ox-Ndep and Ox-Dep forms.

Oxidation produces an expansion of 9.03 Å. This is a very reasonable result since the main interaction in the Ox-Ndep species is the electrostatic repulsion between charged quaterthiophene units. Previous studies using bithiophene as a model compound indicated that the electrostatic repulsion of two radical cations is very high: about 50 kcal mol^{-1} at distances of 5 Å.[6] Thus, the conformational flexibility of the calix[4]arene scaffold, which arises mainly by the rotation of an oxygen atom through the annulus, alleviates the repulsive interaction between the charged quaterthiophene units by expanding the system. It should be noted that recent studies[7,8] proved the conformational flexibility of calix[4]arenes, in particular of 25,27-dihydroxy-26,28-dimethoxycalix[4]arene.[8]

On the other hand, deprotonation produces a dramatic contraction of 30.37 Å, which is in agreement with experimental observations.[2–4] It should be noted that no restriction was imposed during optimization of the geometry, the starting structure being that of the Ox-Ndep species. The origin of this drastic contraction is the electrostatic repulsive interaction between the charged atoms of the phenolate rings, which is partially reduced
by increasing the distance between them. This effect is illustrated in Table 1, which compares the O···O distances of the three states shown in Figure 1 with those obtained for 25,27-dihydroxy-26,28-dimethoxycalix[4]arene and its deprotonated form. As can be seen, the O···O distance increases by 2.705 Å when the two hydroxy protons of the oxidized actuating unit are removed. This expansion brings the two oxidized quaterthiophene units nearer, with the repulsion between the two radical cations being alleviated by the

 © 2006 Wiley-VCH Verlag GmbH & Co. KGaA, Weinheim

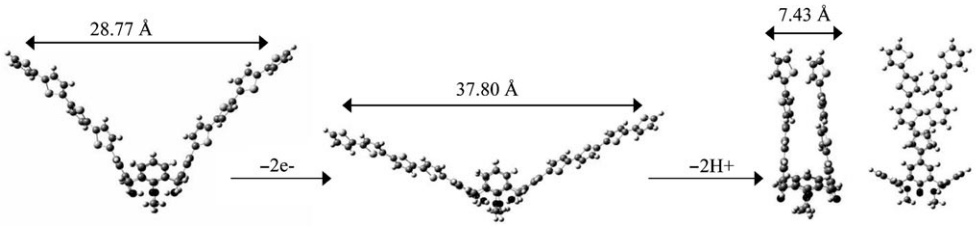
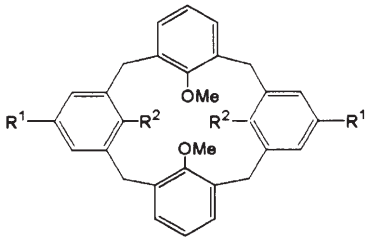


Figure 2. Optimized structure of one actuating unit in the Red. (left), Ox-Ndep (middle), and Ox-Dep (right) states. The distance between the ends of the two quaterthiophene oligomers is indicated. The deprotonated-oxidized form is displayed in two different orientations to illustrate the scissor-shaped arrangement of the quaterthiophene oligomers.

Table 1: Distance[a] between the oxygen atoms of R^2 for the actuating unit (Figure 1) and 25,27-dihydroxy-26,28-dimethoxycalix[4]arene in different states.



Compound	State	O···O [Å]
actuating unit		
R^1 = quaterthiophene, R^2 = OH	Red. (neutral)	4.276
R^1 = quaterthiophene$^{\bullet+}$, R^2 = OH	Ox-Ndep	3.196
R^1 = quaterthiophene$^{\bullet+}$, R^2 = O^-	Ox-Dep	5.901
25,27-dihydroxy-26,28-dimethoxy-calix[4]arene		
R^1 = H, R^2 = OH	nondeprotonated	4.357
R^1 = H, R^2 = O^-	deprotonated	5.575

[a] Results obtained from HF/6-31G(d) (non-oxidized species) and UHF/6-31G(d) (oxidized species) geometry optimizations.

adoption of a scissor-shaped arrangement (Figure 1). Furthermore, the O···O distance for the Ox-Dep actuating unit and the deprotonated 25,27-dihydroxy-26,28-dimethoxycalix[4]arene differ by only 0.326 Å. This similarity indicates that the repulsion between the two charged oxygen atoms of the calix[4]arene moiety is crucial for explaining the remarkable geometric changes observed upon deprotonation of the charged actuating unit (Figure 2).

Classical molecular dynamics (MD) simulations of a system consisting of six calix[4]arene scaffolds separated by five quaterthiophene units (Figure 3) were performed in both the gas phase and in CH_2Cl_2 solution for the Red, Ox-Ndep, and Ox-Dep states. Figure 3 shows snapshots of each simulated system at 10-ps intervals over the 10 ns of the MD simulation in solution, with the average distance calculated between the ends of the quaterthiophene oligomers belonging to the same actuating unit also displayed.

As can be seen, the results obtained using classical molecular dynamics calculations are fully consistent with those predicted by quantum mechanical calculations. Thus, oxidation of the quaterthiophene oligomers produced an expansion, while deprotonation of the oxidized species led to a dramatic contraction. It should be noted that the force-field parameters used in these simulations were derived explicitly for each species, taking into account the charge of the quaterthiophene oligomers and/or the deprotonation of the calix[4]arene unit. Despite this, the distance between the ends of the actuating unit derived from classical simulations differs quantitatively, although not qualitatively, from those obtained using quantum mechanics. This situation can be attributed to different reasons, the most important being: 1) the use of fixed force-field parameters in MD simulations, that is, electronic relaxation effects are neglected; 2) an isolated actuating unit is considered in quantum mechanical calculations whose conformational flexibility is expected to be higher than that of a unit linked to neighbors in a polymer; and 3) the omission of anionic counterions in quantum mechanical calculations, which are expected to mitigate the repulsive electrostatic interactions.

It was recently suggested that the π–π stacking between the thiophene oligomers is the driving force for molecular actuation of poly(calix[4]arene quaterthiophene).[4] Thus, the contraction of the material was attributed to the formation of stable dimers of oxidized quaterthiophenes in solution, while the conformational flexibility of the calix[4]arene was only used to explain the accordion-like molecular displacement. In this study we have analyzed both Ox-Ndep and Ox-Dep forms by using different theoretical methods in both gas-phase and solution environments. The overall results lead to the conclusion that the electrostatic repulsions between the charged atoms of the calix[4]arene scaffolds are responsible

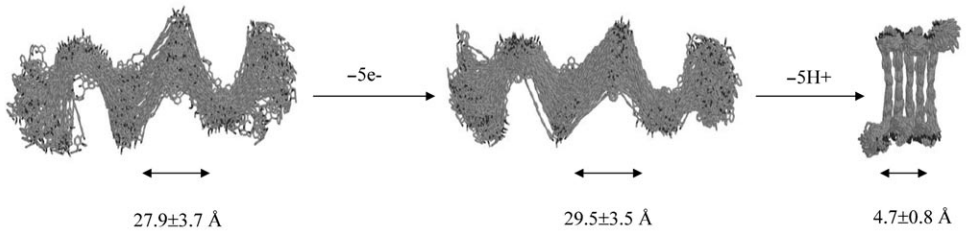


Figure 3. Superposition of snapshots recorded from classical molecular dynamics simulations of a system constituted by five actuating units in the Red. (left), Ox-Ndep (middle), and Ox-Dep (right) states in CH_2Cl_2 solution. The average distance between the ends of the two quaterthiophenes belonging to the actuating unit is indicated.

 © 2006 Wiley-VCH Verlag GmbH & Co. KGaA, Weinheim

for the reduction in the length of the poly(calix[4]arene quaterthiophene) chains. Thus, conjugated quaterthiophene segments should not be considered to be the main active elements in the molecular actuation mechanism, even though their electrochemical oxidation is essential to promote the deprotonation of the calix[4]arene unit and to control the conductivity of the polymer. It is hoped that the proposed actuation mechanism will help in the design of optimized molecular devices containing calix[4]arene scaffolds.

Experimental Section

Ab initio quantum mechanical calculations were performed on calix[4]arene, 25,27-dihydroxy-26,28-dimethoxycalix[4]arene, and one actuating unit formed from two quaterthiophene oligomers attached to a calix[4]arene scaffold. Full geometry optimizations were carried out at the Hartree–Fock level using a 6-31G(d) basis set.[9] Calculations on the oxidized actuating unit were performed considering the unrestricted quantum-chemical formalism with triplet spin multiplicity, that is, allowing oxidation of the two quaterthiophene oligomers.

Classical MD simulations were performed with the NAMD2.0 program,[10] with an integration step of 2 fs selected. The bond geometries that involved non-hydrogen atoms were kept at their equilibrium distances as obtained by using the SHAKE algorithm.[11] Electrostatic interactions were extensively computed by means of Ewald summations. The real space term was defined by the van der Waals cut-off (14.0 Å), while the reciprocal space was computed by interpolation into an infinite grid of points (Particle Mesh Ewald), with a grid density of 5.0 points $Å^{-3}$. Sets of partial atomic charges were derived explicitly for all the investigated species taking into account the electronic state of the thiophene oligomers. Equilibrium bond lengths and angles for the latter were derived from quantum mechanical geometry optimizations on one actuating unit. Simulations were performed with a fixed all-*anti* conformation of the quaterthiophene oligomers, independent of their electronic state. The force-field parameters required for the calix[4]arene scaffold[12] and the CH_2Cl_2 solvent[13] were taken from the literature. The counterion used in simulations of the Ox-Ndep form was PF_6^-, which was recently parametrized.[14]

Received: September 16, 2005
Published online: December 30, 2005

Keywords: ab initio calculations · calixarenes · polymers · redox chemistry · thiophenes

[1] a) R. H. Baughman, *Synth. Met.* **1996**, *78*, 339; b) T. F. Otero, J. M. Sansiñena, *Adv. Mater.* **1998**, *10*, 491; c) E. W. H. Jager, O. Inganäs, I. Lundström, *Science* **2000**, *288*, 2335; d) J. D. Madden, R. A. Cush, T. S. Kaningan, I. W. Hunter, *Synth. Met.* **2000**, *113*, 185; e) W. Lu, A. G, Fadeev, B. Qui, E. Smela, B. R. Mattes, J. Ding, G. M. Spinks, J. Mazurkiewicz, D. Zhou, G. G. Wallace, D. R. MacFarlane, S. A. Forsyth, M. Forsyth, *Science* **2002**, *297*, 983; f) T. F. Otero, M. Cortes, *Adv. Mater.* **2003**, *15*, 279; g) G. M. Spinks, B. Xi, D. Zhou, V. Truong, G. G. Wallace, *Synth. Met.* **2004**, *140*, 173.
[2] A. Vigalok, T. M. Swager, *Adv. Mater.* **2002**, *14*, 368.
[3] H.-h. Yu, B. Xu, T. M. Swager, *J. Am. Chem. Soc.* **2003**, *125*, 1142.
[4] D. A. Scherlis, N. Marzari, *J. Am. Chem. Soc.* **2005**, *127*, 3207.
[5] a) S. Muñoz-Guerra, F. López-Carrasquero, C. Alemán, M. Morillo, V. Castelletto, I. Hamley, *Adv. Mater.* **2002**, *14*, 203; b) C. Gatti, G. Frigerio, T. Benincori, E. Brenna, F. Sannicolò, G. Zotti, S. Zecchin, G Schiavon, *Chem. Mater.* **2000**, *12*, 1490.
[6] D. A. Scherlis, N. Marzari, *J. Phys. Chem. B* **2004**, *108*, 17791.
[7] a) A. Ikeda, S. Shinkai, *Chem. Rev.* **1997**, *97*, 1713; b) W. K. den Otter, W. J. Briels, *J. Am. Chem. Soc.* **1998**, *120*, 13167; c) C. Alemán, W. K. Otter, T. V. Topekina, W. J. Briels, *J. Org. Chem.* **2004**, *69*, 951.
[8] C. Alemán, J. Casanovas, *J. Phys. Chem. A* **2005**, *109*, 8049.
[9] P. C. Hariharan, J. A. Pople, *Theor. Chim. Acta* **1973**, *23*, 213.
[10] L. Kale, R. Skeel, M. Bhandarkar, R. Brunner, A. Gursoy, N. Krawetz, J. Phillips, A. Shinozaki, K. Varadarajan, K. Schulten, *J. Comput. Phys.* **1999**, *151*, 283.
[11] J.-P. Ryckaert, G. Ciccotti, H. J. C. Berendsen, *Comput. Phys.* **1990**, *94*, 1683.
[12] a) M. Baaden, G. Wipff, M. R. Yaftian, M. Burgard, D. Matt, *J. Chem. Soc. Perkin Trans. 2* **2000**, 1315; b) J. R. Blas, M. Marquez, J. L. Sessler, F. J. Luque, M. Orozco, *J. Am. Chem. Soc.* **2002**, *124*, 12796.
[13] W. L. Jorgensen, J. M. Briggs, M. L. Contrerast, *J. Phys. Chem.* **1990**, *94*, 1683.
[14] Z. Liu, S. Huang, W. Wang, *J. Phys. Chem. B* **2004**, *108*, 12978.

 © 2006 Wiley-VCH Verlag GmbH & Co. KGaA, Weinheim

Cyclization

DOI: 10.1002/anie.200503484

Gold-Catalyzed Intramolecular Reaction of Indoles with Alkynes: Facile Formation of Eight-Membered Rings and an Unexpected Allenylation**

*Catalina Ferrer and Antonio M. Echavarren**

The hydroarylation of alkynes (or alkenylation of arenes) catalyzed by electrophilic transition-metal complexes has emerged as a valuable method for the synthesis of alkenyl arenes and heteroarenes.[1] Reetz and Sommer[2] as well as Shi and He[3] found independently that gold complexes catalyze the intermolecular hydroarylation of alkynes. An intramolecular version was disclosed by Murai, Chatani, and co-workers, who used as catalysts Ru^{II} and Pt^{II} ions[4] as well as $GaCl_3$.[5,6] Fürstner et al. reported a similar reaction for the synthesis of phenanthrenes that is catalyzed by $PtCl_2$ and other metal halides.[7] Sames and co-workers developed an intramolecular hydroarylation catalyzed by $PtCl_4$ that proceeds under mild conditions.[8] Cycloisomerization of ω-aryl-

[*] C. Ferrer, Prof. Dr. A. M. Echavarren[+]
Institute of Chemical Research of Catalonia (ICIQ)
Av. Països Catalans 16, 43007 Tarragona (Spain)
Fax: (+34) 97-792-0225
E-mail: aechavarren@iciq.es

[+] Additional affiliation:
Departamento de Química Orgánica
Universidad Autónoma de Madrid
Cantoblanco, 28049 Madrid (Spain)

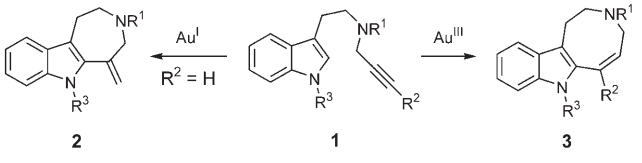
[**] This work was supported by the MEC (Project CTQ2004-02869), the AGAUR (predoctoral fellowship to C.F.), and the ICIQ Foundation.

© 2006 Wiley-VCH Verlag GmbH & Co. KGaA, Weinheim

1-alkynes has also been performed with Hg^{II} ions[9] or Tf_2NH.[10]

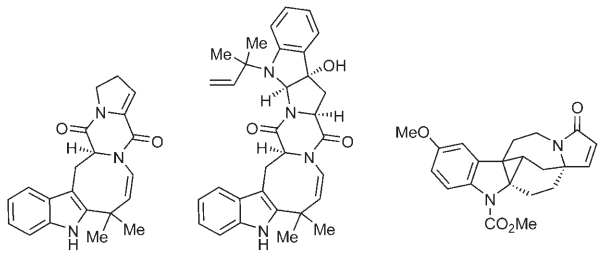
We have recently reported the cyclization of aryl alkynes with Pt^{II} or Au^{I} catalysts.[11,12] Computational studies[11] indicate that two pathways compete: a Friedel–Crafts alkenylation and a reaction proceeding through metal cyclopropyl carbenes which show very similar activation energies.

We have now found that, whereas substrates **1** cyclize readily with a cationic gold(I) complex to give azepino[4,5-*b*]indole derivatives **2**,[13,14] the more electrophilic $AuCl_3$[15] leads to indoloazocines **3** by an 8-*endo*-dig process (Scheme 1), a cyclization that has not been observed in



Scheme 1. 7-*exo*-dig versus 8-*endo*-dig cyclization of alkynyl indoles **1**.

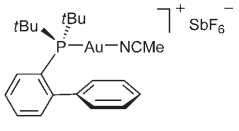
other hydroarylations of alkynes.[16] This type of regiochemical control by the oxidation state of the metal catalyst appears to be unprecedented.[17] Indoloazocine subunit **3** is present in indole alkaloids such as deoxyisoaustamide (**4**),[18,19] okaramine N,[20] and the lundurines (namely, lundurine A (**5**), Scheme 2).[21–23] We also report an unexpected



Scheme 2. Representative indoloazocine alkaloids.

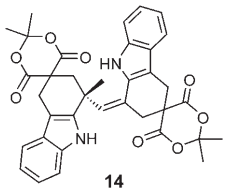
fragmentation reaction that results in the allenylation of the indole nucleus at C2. As predicted by our previous theoretical study,[11] indoles tethered to alkynes by two or three atoms undergo 6-*endo*-dig and 6-*exo*-dig cyclizations, respectively.

Several gold complexes and salts, including new Au^{I} complexes bearing bulky phosphanes or N-heterocyclic ligands,[24,25] were tested in the intramolecular reaction of indoles with alkynes. In general, the best catalyst for the formation of seven-membered rings **2** is cationic gold(I) complex **7**,[25,26] which allows the cyclizations to be performed in the absence of Ag^{I} salts (Table 1). This complex is readily prepared as an air-stable white solid from the corresponding gold chloride complex. Among the solvents screened ($MeNO_2$, acetone, DMF, CH_2Cl_2), the best results were



obtained in CH_2Cl_2. Thus, reaction of tryptophan derivative **8a** with complex **7** as catalyst at room temperature for 30 minutes gave azepino[4,5-*b*]indole **9a** cleanly (Table 1, entry 1). In contrast, the reaction of **8a** with $AuCl_3$ gave indoloazocine **10a** cleanly (Table 1, entry 2). Reaction with AuCl also provided **10a**, although significant amounts of depropargylated starting material were also obtained (Table 1, entry 3). Reaction of **8a** with a catalyst made in situ by chloride abstraction from $[AuCl(PPh_3)]$ with $AgSbF_6$ was less selective, and a 1.3:1 mixture of **9a** and **10a** was obtained (Table 1, entry 4). Similar results were obtained with **8b** and **8c** (Table 1, entries 5–9), although in these cases reaction with $AuCl_3$ gave indoloazocines **10b** and **10c** along with seven-membered-ring derivatives **11b** and **11c**, respectively (Table 1, entries 6 and 9). As expected, treatment of **9b** with 5 mol% $AuCl_3$ (CH_2Cl_2, room temperature, 16 h) led quantitatively to **11b**. *N*-Allylindole **8d** provided seven-membered-ring derivative **9d** when **7** was used as the catalyst (Table 1, entry 10). Protic acids do not promote the cyclization of these substrates. Thus, treatment of **8b** with *para*-toluenesulfonic acid (10 mol%) in CH_2Cl_2 at room temperature for 16 h led only to unchanged starting material.

Substrate **12**, with a tether of only three atoms, reacted satisfactorily with catalyst **7** in CH_2Cl_2 by a 6-*exo*-dig pathway to give **13** (Table 2, entry 1), whereas $[AuCl(PPh_3)]/AgSbF_6$ gave **13** in lower yield along with dimer **14** (Table 2, entry 2). The configuration of **14** at the exocyclic double bond was determined by a NOESY experiment. Decomposition was observed when $AuCl_3$ was used as the catalyst (Table 2, entry 3). Formation of **14** may involve a proton-catalyzed reaction via a tertiary, benzylic-type carbocation derived from **12**. Reaction of **15** with an unprotected propargyl alcohol moiety proceeded uneventfully with Au^{I} catalysts to give **16** (Table 2, entries 4 and 5). In contrast, reaction of **15** in the presence of $AuCl_3$ gave ketone **17**, as a result of isomerization of the exocyclic double bond (Table 2, entry 6).

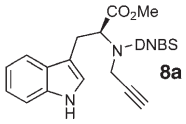
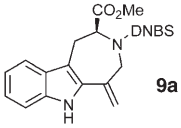
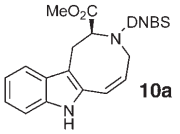
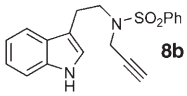
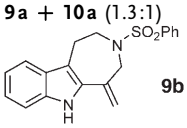
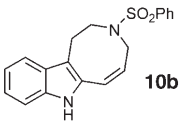
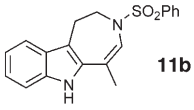
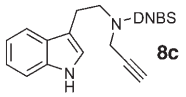
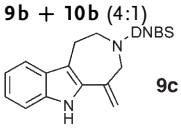
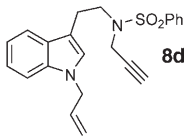
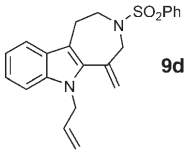


Amide **18** afforded 5-methylene-4,5-dihydrooxazole **19** under all the conditions examined (Table 2, entries 7–9), although the best results were obtained with catalyst **7**. This type of reactivity has been described recently by Hashmi et al.[27] using $AuCl_3$ as the catalyst. Dihydrooxazole **19** is remarkably stable and does not isomerize to the oxazole under the different reaction conditions. Derivative **20**, a substrate with a tether of only two atoms, reacted with Au^{I} catalysts through a 6-*endo*-dig pathway to give **21** (Table 2, entries 10 and 11). In this case, no cyclization was observed with $AuCl_3$ (Table 2, entry 12).

Surprisingly, when indole **8d** was treated with $AuCl_3$ (2 mol%) in CH_2Cl_2 at room temperature for 16 h, allene **22** was obtained as a result of an overall intramolecular allenylation at C-2 of the indole by the *N*-propargyl chain (Scheme 3). Tryptophan derivative **23a** provided indoloazocine **24** and allene **25a** (ca. 1:1 mixture) after being heated at

 © 2006 Wiley-VCH Verlag GmbH & Co. KGaA, Weinheim

Table 1: Formation of seven- or eight-membered-ring compounds by cyclization of indoles with alkynes catalyzed by gold complexes.

Entry	Indole	Catalyst[a]	*t* [h]	Product(s)	Yield [%]
1	 **8a**	**7**	0.5	 **9a**	82
2	**8a**	$AuCl_3$	0.5	 **10a**	75
3	**8a**	AuCl	1	**10a**	70[b]
4	**8a**	$[AuCl(PPh_3)]/AgSbF_6$	0.5	**9a** + **10a** (1.3:1)	80
5	 **8b**	**7**	16	 **9b**	65
6	**8b**	$AuCl_3$	24	 **10b** +  **11b**	71
7	**8b**	$[AuCl(PPh_3)]/AgSbF_6$	16	**9b** + **10b** (4:1)	65
8	 **8c**	**7**	16	 **9c**	77
9	**8c**	$AuCl_3$	16	**10c** + **11c** (2.8:1)	87
10	 **8d**	**7**	0.5	 **9d**	68

[a] Reactions carried out with 5 mol% of the catalyst in CH_2Cl_2. [b] *N*-Depropargylated starting material was also obtained in 23% yield. DNBS = 2,4-dinitrobenzenesulfonyl.

90 °C in toluene with catalyst **7**. Allene **25b** was also obtained as the major compound from **23b**.

A rationale for the formation of the allene derivatives is provided in Scheme 4. Eight-membered-ring compound **24** may arise from a 1,2-shift of the initially formed iminium cation **I** to give **II** (Scheme 4),[28] which would lose a proton to form **III**, and then form **24** by protodemetalation. An alternative elimination, facilitated by the electron-withdrawing sulfonyl group R^2, would yield allenes **25**. A similar mechanism is probably followed in the formation of allene **22** from **8d** by fragmentation of an Au^{III} intermediate similar to **III**. Fragmentation does not occur with the final indoloazocines. Thus, no reaction was observed on treatment of **24** with **7** (5 mol%) in CH_2Cl_2 at room temperature for 16 h or in toluene at 90 °C for 5 h.

Intermediates **I** and **II** might also be involved in the formation of indoloazocines **10a–c** (Table 1). A related 1,2-shift could also be involved in the formation of six- and seven-membered-ring compounds by exocyclic pathways, although this seems rather unlikely in the 6-*endo*-dig cyclization of **20** to form **21** (Table 1, entries 20–21) which would require a 5-*endo*-dig reaction to form the first spiro intermediate. The different regiochemical outcomes observed in reactions catalyzed by Au^I complex **7** and $AuCl_3$ suggests that different mechanisms are involved in these reactions. It is noteworthy that the most electrophilic Au^{III} catalyst leads to indoloazocines, which according to PM3 calculations are about 2–5 kcal mol^{-1} less stable than their seven-membered-ring isomers **9**.

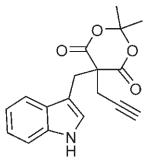
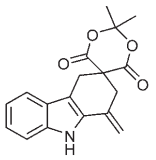
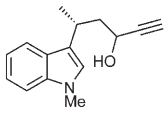
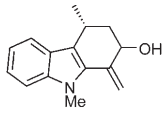
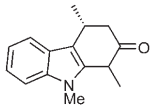
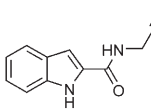
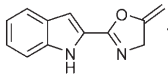
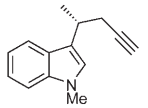
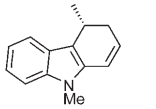
In summary, we have found a facile annulation of six–eight-membered rings on indoles by cyclization with alkynes catalyzed by Au^I or Au^{III} species. Cationic Au^I complex **7** is the best catalyst for the formation of six- and seven-membered rings through 6-*endo*-dig, 6-*exo*-dig, and 7-*exo*-dig cyclizations. Indoloazocines are obtained with $AuCl_3$ as catalyst through a rare 8-*endo*-dig process. Surprisingly, allenes are formed by a fragmentation reaction. This allenylation provides a simple entry into functionalized indole derivatives such as **22** and **25a–b**, which could be used as scaffolds for additional annulation processes.[29]

Received: October 2, 2005
Published online: January 3, 2006

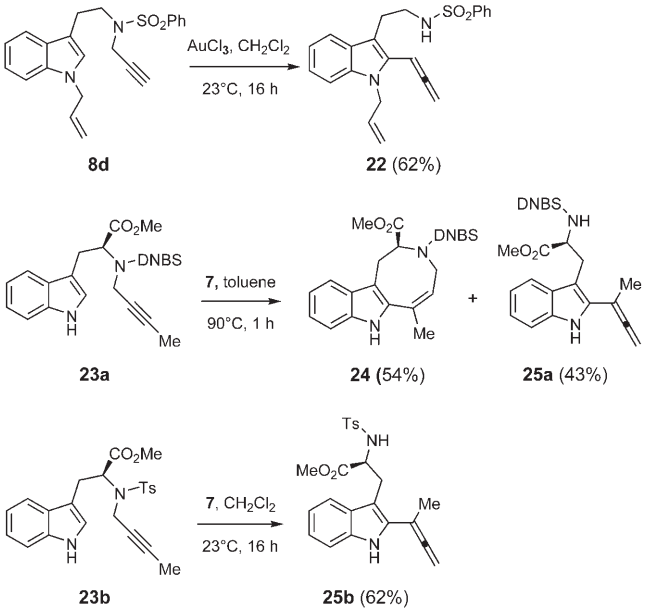
Keywords: alkynes · allenes · cyclization · gold · indoles

 © 2006 Wiley-VCH Verlag GmbH & Co. KGaA, Weinheim

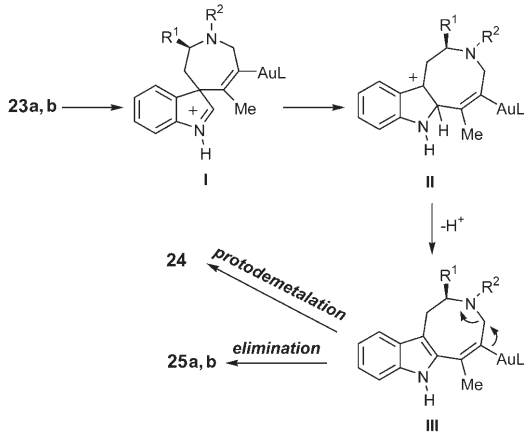
Table 2: Formation of six-membered-ring compounds by cyclization of indoles with alkynes catalyzed by gold complexes.

Entry	Indole	Catalyst[a]	*t* [h]	Product(s)	Yield [%]
1	 **12**	**7**	0.2	 **13**	68
2	**12**	$[AuCl(PPh_3)]/AgSbF_6$	0.5	**13**	54[a]
3	**12**	$AuCl_3$	2	–[b]	–
4	 **15**	**7**	0.2	 **16**	72
5	**15**	$[AuCl(PPh_3)]/AgSbF_6$	0.2	**16**	60
6	**15**	$AuCl_3$	0.2	 **17**	100
7	 **18**	**7**	16	 **19**	77
8[c]	**18**	$[AuCl(PPh_3)]/AgSbF_6$	16	**19**	56
9	**18**	$AuCl_3$	16	**19**	57
10	 **20**	**7**	1	 **21**	92
11	**20**	$[AuCl(PPh_3)]/AgSbF_6$	16	**21**	63
12	**20**	$AuCl_3$	24	–[d]	–

[a] Dimer **14** (25%) was also obtained. [b] Decomposition was observed. [c] Starting material was recovered. [d] Reaction carried out in DMF.



Scheme 3. Formation of allenyl indoles.



Scheme 4. Proposed mechanism for the formation of eight-membered-ring compounds **24** and allenes **25**.

[1] Review: C. Nevado, A. M. Echavarren, *Synthesis* **2005**, 167 – 182.
[2] M. Reetz, K. Sommer, *Eur. J. Org. Chem.* **2003**, 3485 – 3496.
[3] Z. Shi, C. He, *J. Org. Chem.* **2004**, *69*, 3669 – 3671.
[4] N. Chatani, H. Inoue, T. Ikeda, S. Murai, *J. Org. Chem.* **2000**, *65*, 4913 – 4918.
[5] H. Inoue, N. Chatani, S. Murai, *J. Org. Chem.* **2002**, *67*, 1414 – 1417.
[6] The intermolecular reaction of indoles catalyzed by $GaCl_3$ only takes place with phenylacetylene to give 1,1-bis(1*H*-3-indolyl)-1-phenylethanes: J. S. Yadav, B. V. S. Reddy, B. Padmavani, M. K. Gupta, *Tetrahedron Lett.* **2004**, *45*, 7577 – 7579.
[7] a) A. Fürstner, V. Mamane, *J. Org. Chem.* **2002**, *67*, 6264 – 6267; b) A. Fürstner, V. Mamane, *Chem. Commun.* **2003**, 2112 – 2113;

 © 2006 Wiley-VCH Verlag GmbH & Co. KGaA, Weinheim

c) V. Mamane, P. Hannen, A. Fürstner, *Chem. Eur. J.* **2004**, *10*, 4556 – 4575.
[8] a) S. J. Pastine, S. W. Youn, D. Sames, *Org. Lett.* **2003**, *5*, 1055 – 1058; b) S. J. Pastine, S. W. Youn, D. Sames, *Tetrahedron* **2003**, *59*, 8859 – 8868.
[9] M. Nishizawa, H. Takao, V. K. Yadav, H. Imagawa, T. Sugihara, *Org. Lett.* **2003**, *5*, 4563 – 4565.
[10] L. Zhang, S. A. Kozmin, *J. Am. Chem. Soc.* **2004**, *126*, 10204 – 10205.
[11] C. Nevado, A. M. Echavarren, *Chem. Eur. J.* **2005**, *11*, 3155 – 3164.
[12] C. Nieto-Oberhuber, M. P. Muñoz, E. Buñuel, C. Nevado, D. J. Cárdenas, A. M. Echavarren, *Angew. Chem.* **2004**, *116*, 2456 – 2460; *Angew. Chem. Int. Ed.* **2004**, *43*, 2402 – 2406.
[13] For recent transition-metal-catalyzed annulations of indoles, see: a) E. M. Beccalli, C. Broggini, *Tetrahedron Lett.* **2003**, *44*, 1919 – 1921; b) E. M. Ferreira, B. M. Stoltz, *J. Am. Chem. Soc.* **2003**, *125*, 9578 – 9579; c) C. Liu, X. Han, X. Wang, R. A. Widenhoefer, *J. Am. Chem. Soc.* **2004**, *126*, 3700 – 3701; d) C. Liu, R. A. Widenhoefer, *J. Am. Chem. Soc.* **2004**, *126*, 10250 – 10251; e) C. Bressy, D. Alberico, M. Lautens, *J. Am. Chem. Soc.* **2005**, *127*, 13148 – 13149; f) B. A. Bhanu Prasad, F. K. Yoshimoto, R. Sarpong, *J. Am. Chem. Soc.* **2005**, *127*, 12468 – 12469; g) for a review on palladium-catalyzed synthesis and functionalization of indoles, see: S. Cacchi, G. Fabrizi, *Chem. Rev.* **2005**, *105*, 2873 – 2920.
[14] For a recent review on indolic natural products, see: M. Somei, F. Yamada, *Nat. Prod. Rep.* **2005**, *22*, 73 – 103.
[15] For lead references on the formation of C–C bonds by activation of alkynes with $AuCl_3$, see: a) A. S. K. Hashmi, T. M. Frost, J. W. Bats, *J. Am. Chem. Soc.* **2000**, *122*, 11553 – 11554; b) A. S. K. Hashmi, T. M. Frost, J. W. Bats, *Org. Lett.* **2001**, *3*, 3769 – 3771; c) C. Nevado, D. J. Cárdenas, A. M. Echavarren, *Chem. Eur. J.* **2003**, *9*, 2627 – 2635; d) A. S. K. Hashmi, L. Ding, J. W. Bats, P. Fischer, W. Frey, *Chem. Eur. J.* **2003**, *9*, 4339 – 4345; e) A. S. K. Hashmi, J. P. Weyrauch, M. Rudolph, E. Kurpejovic, *Angew. Chem.* **2004**, *116*, 6707 – 6709; *Angew. Chem. Int. Ed.* **2004**, *43*, 6545 – 6547; f) A. S. K. Hashmi, M. Rudolph, J. P. Weyrauch, M. Wölfle, W. Frey, J. W. Bats, *Angew. Chem.* **2005**, *117*, 2858 – 2861; *Angew. Chem. Int. Ed.* **2005**, *44*, 2798 – 2801.
[16] For a rare cycloisomerization of 1,7-enynes with a stoichiometric amount of $[Co_2(CO)_8]$ to give 1,3-cyclooctadienes, see: H. Kagoshima, M. Hayashi, Y. Hashimoto, K. Saigo, *Organometallics* **1996**, *15*, 5439 – 5441.
[17] We have observed a different stereochemical outcome depending on the oxidation state of the palladium catalyst in the cyclization of allylstannanes with alkynes: B. Martín-Matute, E. Buñuel, D. J. Cárdenas, M. Méndez, C. Nieto-Oberhuber, A. M. Echavarren, *J. Organomet. Chem.* **2003**, *687*, 410 – 419.
[18] a) P. S. Steyn, *Tetrahedron Lett.* **1971**, 3331 – 3334; b) P. S. Steyn, *Tetrahedron* **1973**, 107 – 120; c) P. G. Sames, *Fortschr. Chem. Org. Naturst.* **1975**, *32*, 51 – 117.
[19] Synthesis of **4** and related alkaloids: P. S. Baran, E. J. Corey, *J. Am. Chem. Soc.* **2002**, *124*, 7904 – 7905.
[20] Synthesis of **5**: P. S. Baran, C. A. Guerrero, E. J. Corey, *J. Am. Chem. Soc.* **2003**, *125*, 5628 – 5629.
[21] T.-S. Kam, K.-H. Lim, K. Yoganathan, M. Hayashi, K. Komiyama, *Tetrahedron* **2004**, *60*, 10739 – 10745.
[22] For indoloazocines as intermediates in the synthesis of other indole alkaloids, see: M. E. Kuehne, S. D. Cowen, F. Xu, L. S. Borman, *J. Org. Chem.* **2001**, *66*, 5303 – 5316.
[23] Synthesis of indoloazocines: L. G. Voskressensky, T. N. Borisova, L. N. Kulikova, A. V. Varlamov, M. Catto, C. Altomare, A. Carotti, *Eur. J. Org. Chem.* **2004**, 3128 – 3135, and references therein.
[24] C. Nieto-Oberhuber, S. López, A. M. Echavarren, *J. Am. Chem. Soc.* **2005**, *127*, 6178 – 6179.
[25] C. Nieto-Oberhuber, S. López, M. P. Muñoz, D. J. Cárdenas, E. Buñuel, C. Nevado, A. M. Echavarren, *Angew. Chem.* **2005**, *117*, 6302 – 6304; *Angew. Chem. Int. Ed.* **2005**, *44*, 6146 – 6148.
[26] The structure of **7** has been confirmed by X-ray diffraction studies. Details of this structure and those of related Au^I complexes will be reported separately.
[27] S. K. Hashmi, J. P. Weyrauch, W. Frey, J. W. Bats, *Org. Lett.* **2004**, *6*, 4391 – 4394.
[28] Involvement of 3,3-disubstituted indolenines in 1,2-migrations to form indoles: a) A. H. Jackson, P. Smith, *Chem. Commun.* **1967**, 264 – 266; b) A. H. Jackson, P. Smith, *Tetrahedron* **1968**, *24*, 403 – 413; c) A. H. Jackson, P. Smith, *Tetrahedron* **1968**, *24*, 2227 – 2239; d) A. Ganesan, C. H. Heathcock, *Tetrahedron Lett.* **1993**, *34*, 439 – 440.
[29] For a recent review on synthetic applications of allenes, see: S.-M. Ma, *Chem. Rev.* **2005**, *105*, 2829 – 2872.

 © 2006 Wiley-VCH Verlag GmbH & Co. KGaA, Weinheim

Cluster Chemistry

DOI: 10.1002/anie.200503736

A Highly Unsaturated Platinum–Rhenium Cluster Complex Activates Hydrogen Reversibly**

Richard D. Adams, Burjor Captain, and Mark D. Smith*

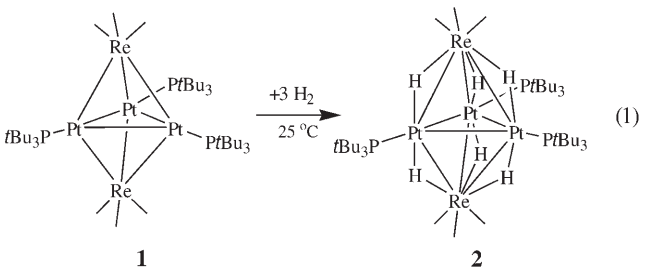
We have recently shown that electron-deficient bimetallic carbonyl cluster complexes containing palladium and platinum can be readily obtained from the reactions of metal carbonyl complexes with $[Pd(PtBu_3)_2]$ and $[Pt(PtBu_3)_2]$.[1] The success of this reaction is, undoubtedly, due in part to ligand deficiencies caused by steric effects of the very bulky tri-*tert*-butylphosphine ligand. Metal complexes of the noble metals are also of interest for their ability to activate and store large quantities of hydrogen.[2] Hydrogen-storage applications require the hydrogen additions to be reversible. We have recently shown that the highly electron-deficient platinum–rhenium complex $[Pt_3Re_2(CO)_6(PtBu_3)_3]$ (**1**) is capable of adding three equivalents of hydrogen at room temperature to form the hexahydrido complex $[Pt_3Re_2(CO)_6(PtBu_3)_3(\mu\text{-}H)_6]$ (**2**) which contains a bridging hydrido ligand on each of its six Pt–Re bonds [Eq. (1)].[3] This addition reaction is thermally

[*] Prof. Dr. R. D. Adams, Dr. B. Captain, Dr. M. D. Smith
Department of Chemistry and Biochemistry
University of South Carolina
Columbia, SC 29208 (USA)
Fax: (+1) 803-777-6781
E-mail: adams@mail.chem.sc.edu

[**] This research was supported by the Office of Basic Energy Sciences of the US Department of Energy under Grant No. DE-FG02-00ER14980 and USC Nanocenter. We wish to thank Dr. Perry J. Pellechia for his assistance with the VT NMR spectroscopy experiments.

Supporting information for this article is available on the WWW under http://www.angewandte.org or from the author.

© 2006 Wiley-VCH Verlag GmbH & Co. KGaA, Weinheim



(1)

1 **2**

irreversible. Herein we report a new member of this family of unsaturated platinum–rhenium cluster complexes that not only exhibits an unusual ability to activate hydrogen under mild conditions, but also does it reversibly.

Two new compounds: $[PtRe_2(CO)_9(PtBu_3)(\mu\text{-}H)_2]$ (**3**; 35% yield) and $[Pt_2Re_2(CO)_7(PtBu_3)_2(\mu\text{-}H)_2]$ (**4**; 24% yield), were obtained from the reaction of $[Pt(PtBu_3)_2]$ with $[Re_3(CO)_{12}(\mu\text{-}H)_3]$ in hexane heated to reflux for 2 h. Compound **3** contains a simple $PtRe_2$ triangular cluster with two bridging hydrido ligands (see Supporting Information for ORTEP diagram). It is related to a number of similar compounds that have been reported.[4]

Compound **4** contains four metal atoms: two of platinum and two of rhenium. The molecular structure of **4** was established crystallographically. The compound crystallizes with three independent molecules in the crystallographic asymmetric unit. Due to molecular disorder (see Supporting Information), the quality of this structural analysis is not high. All three molecules are structurally similar and an ORTEP diagram of the molecular structure of one of them is shown in Figure 1. The four metal atoms are arranged in the shape of a tetrahedron. There are seven carbonyl ligands: each rhenium atom is bound to three of them and one is bonded to one of the two platinum atoms. Each platinum atom has one $PtBu_3$ ligand. The compound contains two hydrido ligands as confirmed by its mass and variable temperature (VT) ^{1}H NMR spectra. The hydrido ligands were not located in the structural analysis, but the ^{1}H NMR spectrum recorded at −40 °C exhibits two highly shielded resonances at $\delta = -0.87$ (s, 1H, hydride), −2.05 (dd, $^2J(P,H) = 6$ Hz, $^2J(P,H) = 11$ Hz, $^1J(Pt,H) = 621$ Hz, 1H, hydride) that can be attributed to them. The first resonance exhibits no couplings to ^{195}Pt or ^{31}P of the phosphine ligands. This ligand probably bridges the Re–Re bond. The second resonance is coupled to both phosphine ligands and ^{195}Pt. This hydrido ligand may bridge the Pt–Pt bond; however, we can not rule out that it could be a terminal ligand as found in compound **5**, see below. The hydrido ligands in **4** are dynamically active as shown by the VT ^{1}H NMR spectra shown in Figure 2. The ^{31}P{^{1}H} NMR

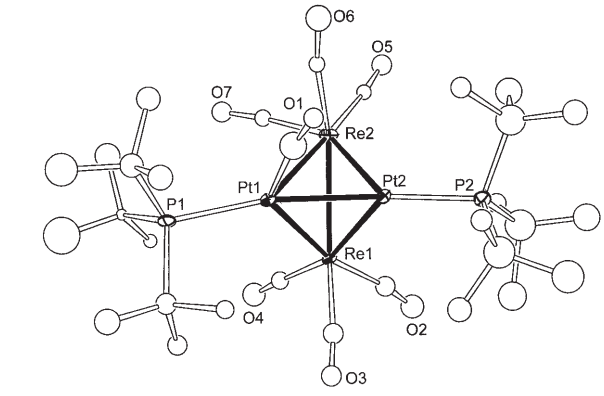


Figure 1. An ORTEP diagram of the molecular structure of one of the three independent molecules in the unit cell of the crystal of **4**, thermal ellipsoids set at 40% probability. Hydrogen atoms are not shown. The hydrido ligands were not located in the structural analysis. Selected interatomic distances [Å]: Molecule 1: Pt1-Pt2 2.6665(16), Pt1-Re1 2.9100(15), Pt1-Re2 2.8648(16), Pt2-Re1 2.7259(15), Pt2-Re2 2.6119(15), Re1-Re2 2.9419(13), Molecule 2: Pt3-Pt4 2.6738(16), Pt3-Re3 2.8662(15), Pt3-Re4 2.9152(16), Pt4-Re3 2.6144(15), Pt4-Re4 2.7019(16), Re3-Re4 2.9388(14), Molecule 3: Pt5-Pt6 2.6646(17), Pt5-Re5 2.8972(18), Pt5-Re6 2.8674(18), Pt6-Re5 2.7116(18), Pt6-Re6 2.6139(18), Re5-Re6 2.921(2).

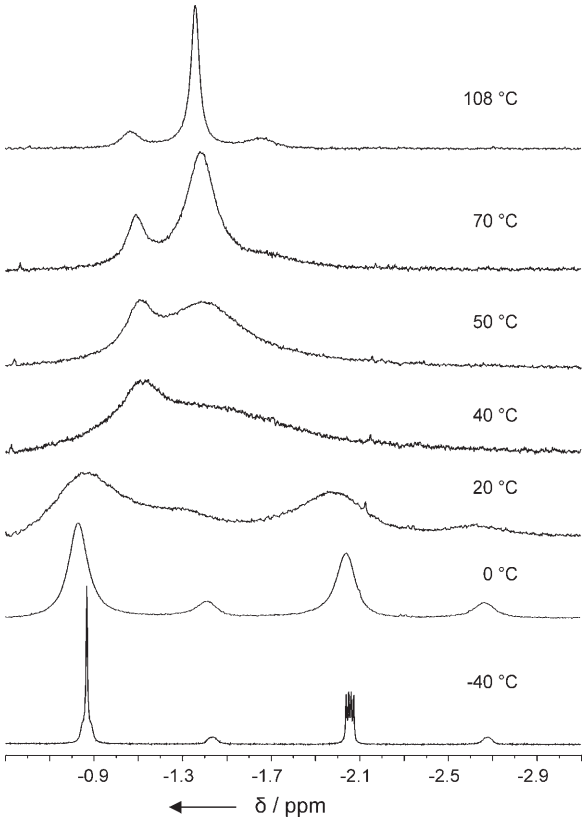
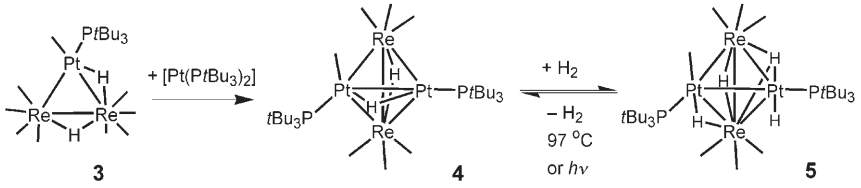


Figure 2. ^{1}H NMR spectra at 500 MHz of compound **4** in the hydride region at various temperatures in $[D_8]$toluene solvent.

spectrum of **4** at −25 °C shows two resonances of equal intensity with mutual couplings and couplings to ^{195}Pt, $\delta =$ 85.5 (d, $^3J(P,P) = 82$ Hz, $^1J(Pt,P) = 3880$ Hz, 1P), 112.7 ppm (d, $^3J(P\text{-}P) = 82$ Hz, $^1J(Pt,P) = 2435$ Hz, 1P) consistent with the structure as found in the solid state. The ^{31}P resonances are broad at room temperature and the ^{31}P couplings between the two resonances are not observed. This situation is suggestive of yet another dynamic exchange process, and these resonances do broaden still further at higher temperatures, but the averaged spectrum was not attained at 108 °C and the compound decomposed significantly at higher

 © 2006 Wiley-VCH Verlag GmbH & Co. KGaA, Weinheim

temperatures. A simple exchange of the terminal carbonyl ligand on atom Pt1 between the two platinum atoms could account for the broadening effects observed in these ^{31}P resonances. Significantly, the cluster of **4** contains only 54 valence electrons. This number is six less than the 60 required for a tetrahedral cluster in which all the metal atoms obey the 18 electron rule. Although there are other $\{Pt_2M_2\}$ compounds with less than 60 electrons,[5] having as few as 54 electrons is very unusual. Compound **4** can also be obtained from **3** by further treatment with $[Pt(PtBu_3)_2]$, see Scheme 1.



3 4 5

Scheme 1.

It was found that **4** adds one equivalent of H_2 (1 atm/25 °C) to yield the new tetrahydrido compound $[Pt_2Re_2(CO)_7(PtBu_3)_2(\mu\text{-}H)_4]$ (**5**) in 71% yield. Compound **5** was also characterized crystallographically. This compound has only one formula equivalent in the asymmetric crystal unit and a very high quality structural analysis was obtained which included the location and refinement of all four of the hydrido ligands (Figure 3). The structure of **5** is very similar to that of **4** except that it has four hydrido ligands. One of the hydrido ligands H1 bridges the Re–Re bond (as similarly proposed for **4**). H2 is a triple bridge on the Pt2-Re1-Re2 triangle. H3 bridges the Pt1–Re1 bond and H4 is a terminal ligand on Pt2. As expected, the addition of hydrido ligands to the bonds Pt1–Re1 and Pt2–Re2 leads to an increase in the metal–metal bond distances compared to those in **4**.[6]

The ^1H NMR spectrum of **5** exhibits only three resonances for the four hydrido ligands, $\delta = -2.13$ (s, $^2J(Pt,H) = 37$ Hz, 1H), -2.34 (d, $^1J(Pt,H) = 588$ Hz, $^2J(P,H) = 12$ Hz, 1H), -6.10 (dd, $^1J(Pt,H) = 801$ Hz, $^2J(Pt,H) = 43$ Hz, $^2J(P,H) = 10$ Hz, $^3J(P,H) = 3$ Hz, 2H). The resonance at $\delta = -6.10$ (2H) indicates that two of the hydrido ligands are selectively averaged. These remain averaged throughout the temperature range -90 °C to 110 °C.

When solutions of **5** in heptane were heated to reflux for 3 h in the presence of a slow purge of nitrogen, compound **4** was regenerated in high yield (90% isolated) by loss of H_2 (confirmed by ^1H NMR spectroscopy). Most interestingly, however when solutions of **5** were irradiated (UV/Vis) at room temperature in the presence of a slow purge of nitrogen for 4 h, compound **4** was also formed in high yield (83% isolated) by loss of H_2 (also confirmed by ^1H NMR spectroscopy).

The photochemical elimination of hydrogen from mononuclear metal complexes is well known,[7] but we are unaware of any reports of the photoelimination of hydrogen from polynuclear metal cluster complexes. Goodfellow et al. have described the addition of hydrogen to some highly unsaturated tetraplatinum compounds containing $PtBu_3$ ligands under mild conditions; the hydrogen could be removed from them by treatment with ethylene.[8]

Bimetallic materials have attracted attention for hydrogen-storage applications.[9] Bimetallic nanoclusters have attracted considerable attention because of their ability to function as highly active hydrogenation catalysts when placed on supports.[10] Platinum–rhenium bimetallic catalysts are widely used by the petroleum industry because of their superior properties for the important process known as reforming.[11] Unusual electronic and reactivity properties of these new electron-deficient platinum–rhenium cluster complexes[3] suggest that this combination of metals has special features that could be important for future applications to the hydrogen industry and hydrogenation catalysis. Further studies of the mechanism of this unusual reversible reaction with hydrogen are in progress.

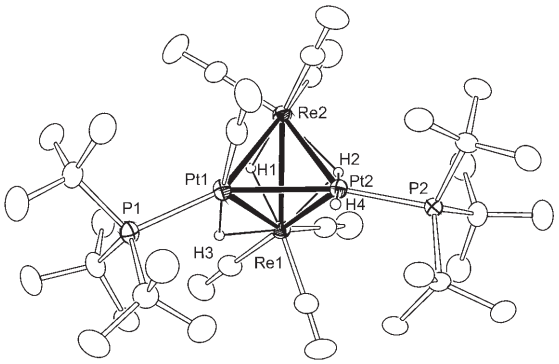


Figure 3. An ORTEP diagram of the molecular structure of **5**, thermal ellipsoids set at 40% probability. Selected interatomic distances [Å]: Pt1-Pt2 2.7025(2), Pt1-Re1 2.9732(2), Pt1-Re2 2.8805(2), Pt2-Re1 2.9182(2), Pt2-Re2 2.7866(2), Re1-Re2 2.8303(3), Pt1-H3 1.50(7), Pt2-H2 1.78(6), Pt2-H4 1.51(5), Re1-H1 1.74(4), Re1-H2 2.03(6), Re1-H3 2.02(7), Re2-H1 1.89(4), Re2-H2 1.95(6), Pt1-P1 2.3909(10), Pt2-P2 2.2729(9).

Experimental Section

Reaction of $[Re_3(CO)_{12}(\mu\text{-}H)_3]$ with $[Pt(PtBu_3)_2]$: $[Pt(PtBu_3)_2]$ (30.0 mg, 0.050 mmol) and $[Re_3(CO)_{12}(\mu\text{-}H)_3]$ (23.0 mg, 0.026 mmol) were dissolved in hexane (40 mL) and then heated to reflux for 2 h. After cooling, the solvent was removed in vacuo, and the products were separated by thin-layer chromatography (TLC; on silica gel) using a 3:1 hexane/CH_2Cl_2 solvent mixture to yield, in order of elution: 9.2 mg (35% yield) of yellow $[PtRe_2(CO)_9(PtBu_3)(\mu\text{-}H)_2]$ (**3**), 1.8 mg of an uncharacterized purple band, and 8.4 mg (24% yield) of red $[Pt_2Re_2(CO)_7(PtBu_3)_2(\mu\text{-}H)_2]$ (**4**). Spectral data for **3**: IR ν_{CO} (in hexane): $\tilde{\nu} = 2101$ (m), 2070 (s), 2008 (vs), 1991 (m), 1982 (m), 1972 (m), 1958 (s), 1950 cm^{-1} (m). ^1H NMR (400 MHz, $CDCl_3$, 25 °C, TMS): $\delta = 1.53$ (d, $^3J(P,H) = 13$ Hz, 27H, CH_3), -7.19 (d, $^2J(P,H) = 14$ Hz, $^1J(Pt,H) = 538$ Hz, 1H, hydride), -15.41 ppm (s, $^2J(Pt,H) = 31$ Hz, 1H, hydride); $^{31}P\{^1H\}$ NMR (400 MHz, $CDCl_3$, 25 °C, 85% *ortho*-H_3PO_4): $\delta = 110.6$ ppm (s, $^1J(Pt,P) = 2936$ Hz, 1P). Elemental analysis (%) calcd: C 24.63, H 2.76; found: C 25.31, H 2.72. Crystal data for **3**: $PtRe_2PO_9C_{21}H_{29}$, M_r=1023.90, monoclinic, space group $C2/c$, $a = 27.395(3)$, $b = 14.3333(16)$, $c = 19.087(2)$ Å, $\beta = 130.348(2)°$, $V =$

 © 2006 Wiley-VCH Verlag GmbH & Co. KGaA, Weinheim

5711.9(11) Å^3, $Z=8$, $T=294$ K, $Mo_{K\alpha}=0.71073$ Å. The final $R1(F^2)$ was 0.0385 for 6066 reflections $I>2\sigma(I)$. Spectral data for **4**: IR ν_{CO} (in CH_2Cl_2): $\tilde{\nu}=2035$ (w), 2015 (m), 1994 (vs), 1916 (m, sh), 1900 cm^{-1} (s, br). ^{1}H NMR (500 MHz, [D$_8$]toluene, −40 °C, TMS): $\delta=1.20$ (broad, 27 H, CH_3), −0.87 (s, 1 H, hydride), −2.05 ppm (dd, ^2J(P,H) = 6 Hz, ^2J(P,H) = 11 Hz, ^1J(Pt,H) = 621 Hz, 1 H, hydride). ^{31}P{^{1}H} NMR (202.5 MHz, [D$_8$]toluene, −25 °C, 85 % *ortho*-H_3PO_4): $\delta=85.5$ (d, ^3J(P,P) = 82 Hz, ^1J(Pt,P) = 3880 Hz, 1 P), 112.7 ppm (d, ^3J(P-P) = 82 Hz, ^1J(Pt,P) = 2435 Hz, 1 P). Mass Spectrometry: ES$^+$/MS calcd for M^+, $[Pt_2Re_2(CO)_7(PtBu_3)_2(\mu\text{-}H)_2]^+$, 1365, found 1365. Elemental analysis (%) calcd: C 27.27, H 4.14; found: C 27.27, H 3.90. Crystal data for **4**: $Pt_2Re_2P_2O_7C_{31}H_{54}$, $M_r=1363.26$, orthorhombic, space group $P2_12_12_1$, $a=15.2359(14)$, $b=15.2464(14)$, $c=50.847(5)$ Å, $V=11811.3$ (19) Å^3, $Z=12$, $T=100$ K, $Mo_{K\alpha}=0.71073$ Å. The final $R_1(F^2)$ was 0.0734 for 17760 reflections $I>2\sigma(I)$.

Reaction of **3** with $Pt(PtBu_3)_2$: $[Pt(PtBu_3)_2]$ (30.0 mg, 0.050 mmol) was added to a solution of **3** (10.4 mg, 0.010 mmol) in hexane (25 mL). The reaction mixture was heated to reflux for 8 h, after which the solvent was removed in vacuo. The products were separated by TLC (silica gel) using a 3:1 hexane/CH_2Cl_2 solvent mixture to yield, in order of elution: 6.0 mg (58 % yield) of starting yellow **3**, and 3.0 mg (22 % yield) of red $[Pt_2Re_2(CO)_7(PtBu_3)_2(\mu\text{-}H)_2]$ (**4**).

Addition of H_2 to **4**: Compound **4** (16.1 mg, 0.012 mmol) was dissolved in heptane (30 mL). With stirring, hydrogen gas was passed through the solution at room temperature for 12 h. The heptane solvent was then removed in vacuo and the product was isolated by TLC (silica gel) using a 3:1 hexane/ CH_2Cl_2 solvent mixture to yield 11.5 mg (71 %) of bright-orange $[Pt_2Re_2(CO)_7(PtBu_3)_2(\mu\text{-}H)_4]$ (**5**) as the major product. Spectral data for **5**: IR ν_{CO} (in Hexane): $\tilde{\nu}=2041$ (m), 2028 (s), 2006 (vs), 1936 (s), 1927 (vs), 1918 cm^{-1} (m, sh). ^{1}H NMR (400 MHz, [D$_8$]toluene, 25 °C, TMS): $\delta=1.29$ ppm (d, ^3J(P,H) = 13 Hz, 27 H, CH_3), 1.27 ppm (d, ^3J(P,H) = 13 Hz, 27 H, CH_3), −2.13 (s, ^2J(Pt,H) = 37 Hz, 1 H, hydride), −2.34 (d, ^1J(Pt,H) = 588 Hz, ^2J(P,H) = 12 Hz, 1 H, hydride), −6.10 ppm (dd, ^1J(Pt,H) = 801 Hz, ^2J(Pt,H) = 43 Hz, ^2J(P,H) = 10 Hz, ^3J(P,H) = 3 Hz, 2 H, hydride). ^{31}P{^{1}H} NMR (162 MHz, [D$_8$]toluene, 25 °C, 85 % *ortho*-H_3PO_4): 95.75 ppm (d, ^3J(P,P) = 62 Hz, ^1J(Pt,P) = 3388 Hz, ^2J(Pt,P) = 197 Hz, 1 P), 108.14 ppm (d, ^3J(P,P) = 62 Hz, ^1J(Pt,P) = 2720 Hz, ^2J(Pt,P) = 296 Hz, 1 P). Mass Spectrometry ES$^+$/MS calcd for M^+, $[Pt_2Re_2(CO)_7(PtBu_3)_2(\mu\text{-}H)_4]^+$, 1367, found 1367. Elemental analysis (%) calcd: C 27.23, H 4.28; found: C 27.64, H 3.99. Crystal data for **5**: $Pt_2Re_2P_2O_7C_{31}H_{58}\cdot 1/2\,CH_2Cl_2$, $M_r=1409.76$, monoclinic, space group $P2_1/c$, $a=14.7121(9)$, $b=17.2332(11)$, $c=17.1146(11)$ Å, $\beta=105.0020(10)°$, $V=4191.3(5)$ Å^3, $Z=4$, $T=294$ K, $Mo_{K\alpha}=0.71073$ Å. The final $R_1(F^2)$ was 0.0198 for 9236 reflections $I>2\sigma(I)$. CCDC 286932–286934 (**3**–**5**) contain the supplementary crystallographic data for this paper. These data can be obtained free of charge from The Cambridge Crystallographic Data Centre via www.ccdc.cam.ac.uk/data_request/cif.

Thermal elimination of hydrogen from **5**: Compound **5** (12.8 mg, 0.009 mmol) was dissolved in heptane (60 mL) in a 100 mL three-neck flask equipped with a reflux condenser and a gas inlet. A slow stream of nitrogen (flow rate ≈27 mL min^{-1}) was allowed to flow through the flask while refluxing this solution for 3 h. The heptane solvent was then removed in vacuo and the products were separated by TLC (silica gel) using a 3:1 hexane/CH_2Cl_2 solvent mixture to yield, in order of elution: 0.7 mg (5 % yield) of unchanged **5**, and 11.5 mg (90 % yield) of **4**.

Photoelimination of hydrogen from **5**: Compound **5** (12.8 mg, 0.009 mmol) was dissolved in hexane (60 mL) in a 100 mL three-neck flask equipped with a reflux condenser and a gas inlet. A slow stream of nitrogen (flow rate ≈27 mL min^{-1}) was allowed to flow through the flask while irradiating this solution for 4 h. The progress of this reaction can be monitored by IR. The hexane solvent was then removed in vacuo and the products were separated by TLC (silica gel) using a 3:1 hexane/CH_2Cl_2 solvent mixture to yield, in order of elution: 1.0 mg (8 % yield) of unchanged **5**, and 10.6 mg (83 % yield) of **4**. There were a few uncharacterized bands present on the TLC plate in trace amounts (< 1 mg).

Received: October 21, 2005
Published online: January 3, 2006

Keywords: cluster compounds · hydrogen addition · hydrogen elimination · platinum · rhenium

[1] a) R. D. Adams, B. Captain, W. Fu, M. B. Hall, J. Manson, M. D. Smith, C. E. Webster, *J. Am. Chem. Soc.* **2004**, *126*, 5253; b) R. D. Adams, B. Captain, W. Fu, M. D. Smith, *J. Am. Chem. Soc.* **2002**, *124*, 5628; c) R. D. Adams, B. Captain, W. Fu, P. J. Pellechia, M. D. Smith, *Angew. Chem.* **2002**, *114*, 2031; *Angew. Chem. Int. Ed.* **2002**, *41*, 1951; d) R. D. Adams, B. Captain, W. Fu, P. J. Pellechia, M. D. Smith, *Inorg. Chem.* **2003**, *42*, 2094; e) R. D. Adams, B. Captain, M. B. Hall, J. L. Smith, Jr., C. E. Webster, *J. Am. Chem. Soc.* **2005**, *127*, 1007.

[2] a) S. K. Brayshaw, M. J. Ingleson, J. C. Green, P. R. Raithby, G. Kociok-Köhn, J. S. McIndoe, A. S. Weller, *Angew. Chem.* **2005**, *117*, 7035; *Angew. Chem. Int. Ed.* **2005**, *44*, 6875; b) P. J. Dyson, J. S. McIndoe, *Angew. Chem.* **2005**, *117*, 5918; *Angew. Chem. Int. Ed.* **2005**, *44*, 5772; c) P. J. Dyson, J. S. McIndoe, *Angew. Chem.* **2004**, *116*, 6152; *Angew. Chem. Int. Ed.* **2004**, *43*, 6028; d) J. M. Thomas, R. Raja, B. F. G. Johnson, S. Hermans, M. D. Jones, T. Khimyak, *Ind. Eng. Chem. Res.* **2003**, *42*, 1563.

[3] R. D. Adams, B. Captain, *Angew. Chem.* **2005**, *117*, 2587; *Angew. Chem. Int. Ed.* **2005**, *44*, 2531.

[4] a) T. Beringhelli, A. Ceriotti, G. D'Alfonso, R. Della Pergola, *Organometallics* **1990**, *9*, 1053; b) P. Antognazza, T. Beringhelli, G. D'Alfonso, A. Minoja, G. Ciani, M. Moret, A. Sironi, *Organometallics* **1992**, *11*, 1777.

[5] a) J. Powell, J. C. Brewer, G. Gulia, J. F. Sawyer *J. Chem. Soc. Dalton Trans.* **1992**, 2503; b) G. Ciani, .M. Moret, A. Sironi, T. Beringhelli, G. D'Alfonso, R. Della Pergola, *J. Chem. Soc. Chem. Commun.* **1990**, 1668; c) R. D. Adams, B. Captain, W. Fu, M. B. Hall, M. D. Smith, C. E. Webster, *Inorg. Chem.* **2004**, *43*, 3921; d) D. G. Evans, D. M. P. Mingos, *J. Organomet. Chem.* **1982**, *240*, 321.

[6] R. G. Teller, R. Bau, *Struct. Bonding (Berlin)* **1981**, *41*, 1.

[7] a) R. Perutz, *Pure Appl. Chem.* **1998**, *70*, 2211; b) G. L. Geoffroy, M. S. Wrighton, *Organometallic Photochemistry*, Academic Press, New York, **1979**, chap. 7; c) G. L. Geoffroy, *Prog. Inorg. Chem.* **1980**, *27*, 123; d) C. Daniel, *J. Phys. Chem.* **1991**, *95*, 2394; e) G. L. Geoffroy, M. G. Bradley, *Inorg. Chem.* **1978**, *17*, 2410.

[8] R. J. Goodfellow, E. M. Hamon, J. A. K. Howard, J. L. Spencer, D. G. Turner, *J. Chem. Soc. Chem. Commun.* **1984**, 1604.

[9] a) L. Schapbach, A. Züttel, *Nature* **2001**, *414*, 353; b) G. D. Berry, S. M. Aceves, *Energy Fuels* **1998**, *12*, 49.

[10] a) J. M. Thomas, B. F. G. Johnson, R. Raja, G. Sankar, P. A. Midgley, *Acc. Chem. Res.* **2003**, *36*, 20; b) "Catalysis and Related Reactions with Compounds Containing Heteronuclear Metal–Metal Bonds": P. Braunstein, J. Rosé, *Comprehensive Organometallic Chemistry II, Vol. 10* (Eds.: G. Wilkinson, F. G. A. Stone, E. Abel), Elsevier, Dordrecht, **1995**, chap. 7.

[11] a) J. Xiao, R. J. Puddephatt, *Coord. Chem. Rev.* **1995**, *143*, 457; b) S. M. Augustine, W. M. H. Sachtler, *J. Catal.* **1989**, *116*, 184; c) M. S. Nacheff, L. S. Kraus, M. Ichikawa, B. M. Hoffman, J. Butt, W. M. H. Sachtler, *J. Catal.* **1987**, *106*, 263.

 © 2006 Wiley-VCH Verlag GmbH & Co. KGaA, Weinheim

Catalytic Hydrogenation

DOI: 10.1002/anie.200503771

Efficient Homogeneous Catalytic Hydrogenation of Esters to Alcohols**

*Jing Zhang, Gregory Leitus, Yehoshoa Ben-David, and David Milstein**

The reduction of esters to the corresponding alcohols is an important reaction in organic synthesis. Compared with traditional procedures using stoichiometric amounts of metal hydride reagents (e.g. $LiAlH_4$),[1] the catalytic hydrogenation of esters to alcohols, which generates no waste, is attractive environmentally and economically [Eq. (1)]. Het-

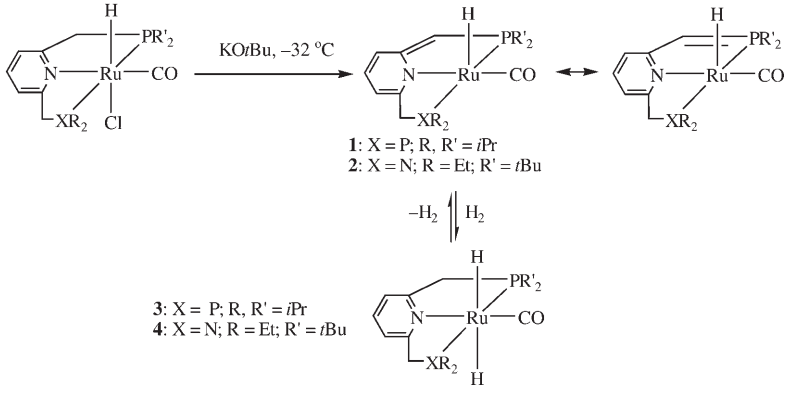
$$RCOOR' + 2\,H_2 \xrightarrow{\text{catalyst}} RCH_2OH + R'OH \qquad (1)$$

erogeneous hydrogenation of some fatty esters is practiced industrially at relatively high temperatures (200–300 °C) and high hydrogen pressures (200–300 atm) using transition-metal catalysts,[2] while homogeneous systems capable of hydrogenation of esters are very scarce[3–7] and mostly limited to activated esters. In these systems, large amounts of additives, such as an organic base,[3] inorganic acids,[3] salts,[5,6] zinc,[7] and fluorinated alcoholic solvents[3] were needed to obtain high conversion of esters into alcohols. Grey and coworkers[4] reported that the anionic ruthenium hydride complex $K_2[(PPh_3)_3(PPh_2)Ru_2H_4]\cdot(C_6H_{14}O_3)_2$, catalyzed the hydrogenation of activated esters, while ethyl acetate was hydrogenated to ethanol in only 8% yield and aromatic esters (e.g. methyl benzoate) were not hydrogenated with this catalyst.

We are aware of only two homogeneously catalyzed systems that are effective for the hydrogenation of nonactivated esters (i.e. esters in which there is no electron-withdrawing group adjacent to the carbalkoxy group).[3,7] Elsevier and Teunissen[3] reported a system of $[Ru(acac)_3]$ (acac = acetylacetonate) with $MeC(CH_2PPh_2)_3$, which effectively catalyzed the hydrogenation of benzyl benzoate to benzyl alcohol at 120 °C under 84 atm of H_2; this system required fluorinated alcohols (CF_3CH_2OH or $CF_3CH(OH)CF_3$) as solvents and an excess of triethylamine. Nomura et al.[7] reported that using $[Ru(acac)_3]$ with excess $P(n\text{-}C_8H_{17})_3$ in the presence of zinc in polar solvents at 200 °C and 10 atm H_2, methyl phenylacetate underwent hydrogenation and transesterification, the latter often being the major process.

Herein we report the hydrogenation of non-activated esters to the corresponding alcohols under relatively mild, neutral conditions, with no additives being required. The reaction is catalyzed by a ruthenium hydride complex based on the pincer ligand PNN (2-(di-*tert*-butylphosphinomethyl)-6-(diethylaminomethyl)pyridine). A comparison with the analogous PNP system reveals a major ligand effect, attributable to ligand hemilability.

The new PNP complex **1** was prepared by deprotonation of the chloro hydride complex [(PNP)RuHCl(CO)][8] with KO*t*Bu at −32 °C in 85% yield (Scheme 1).[9,10] The $^{31}P\{^1H\}$ NMR spectrum of **1** shows two groups of doublets at $\delta = 67.0$ and 66.3 ppm with $J_{PP} = 256.0$ Hz, corresponding to the two magnetically different phosphorus atoms of the *i*Pr-PNP ligand. The hydride ligand exhibits a triplet at $\delta = -13.02$ ppm ($J_{PH} = 24.0$ Hz) in the ^1H NMR spectrum. A one-proton doublet at $\delta = 3.85$ ppm ($J_{PH} = 12.0$ Hz) in the ^1H NMR spectrum and a broad singlet at $\delta = 39.0$ ppm in the $^{13}C\{^1H\}$ NMR spectrum indicate formation of an anionic PNP system (also confirmed by ^{13}C-DEPT and J_1-HMQC NMR spectra). The CO ligand gives a band at 1888 cm^{-1} in the IR spectrum.



Scheme 1.

A single-crystal X-ray diffraction study of **1** (Figure 1) indicates a distorted square-pyramidal geometry around the Ru^{II} center, with the CO ligand coordinated *trans* to the pyridinic nitrogen atom and the hydride located in the apical position (Ru-H1r 1.48(11) Å). It is noted that the bond length of C1–C2 (1.450(9) Å) is significantly shorter than that of C7–C6 (1.552(9) Å) while the bond length of C1–P1 (1.803(6) Å) is shorter to a smaller extent than that of P2–C7 (1.843(7) Å), indicating that the dearomatic configuration of **1** contributes much more than that of the aromatic phosphor–ylide configuration in the solid state (see Scheme 1 for resonance forms).

[*] Dr. J. Zhang, Y. Ben-David, Prof. D. Milstein
Department of Organic Chemistry
Weizmann Institute of Science
76100 Rehovot (Israel)
Fax: (+972) 8-934-4142
E-mail: david.milstein@weizmann.ac.il
Dr. G. Leitus
Chemical Research Support, Weizmann Institute of Science
76100 Rehovot (Israel)

[**] This research was supported by the German Federal Ministry of Education and Research (BMBF) within the framework of the German–Israeli cooperation (DIP). J.Z. is the recipient of the Aron Zandman Postdoctoral Fellowship. D.M. holds the Israel Matz Professorial Chair of Organic Chemistry.

Supporting information for this article is available on the WWW under http://www.angewandte.org or from the author.

 © 2006 Wiley-VCH Verlag GmbH & Co. KGaA, Weinheim

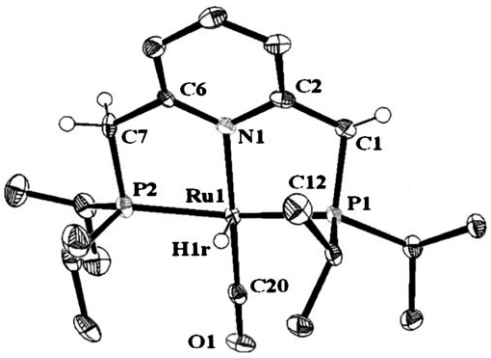


Figure 1. ORTEP diagram of a molecule of complex **1** with the thermal ellipsoids set at 50% probability. Selected bond lengths [Å] and angles [°]: Ru1–C20 1.844(7), Ru1–N1 2.163(5), Ru1–P1 2.350(2), Ru1–P2 2.291(2), Ru1–H1r 1.48(11), C1–C2 1.450(9), P1–C1 1.803(6), P2–C7 1.843(7), C6–C7 1.552(9); C20-Ru1-N1 171.4(2), P1-Ru1-P2 153.1(1), H1r-Ru1-P1 72(4), H1r-Ru-P2 85(4).

Upon treatment of complex **1** with dihydrogen, the *trans* dihydride complex **3** is quantitatively formed (see Scheme 1). This complex can also be prepared by treatment of the corresponding hydridochloride complex with $NaHBEt_3$.[9] Complex **3** slowly looses H_2 at room temperature to regenerate complex **1**. The PNN complex **2** was recently reported by us,[8] although crystals suitable for a single-crystal X-ray diffraction study could not be obtained. This complex shows analogous reactivity with dihydrogen, and it catalyzes the dehydrogenation of primary alcohols to esters.[8,11]

Complexes **1** and **2** were studied as catalysts for the hydrogenation of esters. Upon treatment of ethyl benzoate with dihydrogen (5.3 atm) at 115°C for 16 h with a catalytic amount of **3** (1 mol%), 7.5% conversion of the ester to yield 7% of benzyl alcohol and 7.5% of ethanol were obtained. Performing the reaction at 140°C resulted in 12% conversion to these alcohols. A trace amount of the transesterification product benzyl benzoate was also formed (Table 1, entries 1 and 2).

Remarkably, using complex **2** (1 mol%) as catalyst under the same conditions (115°C) for 4 h resulted in 99.2% conversion of ethyl benzoate into benzyl alcohol and ethanol (Table 1, entry 3). Hydrogenation of hexyl hexanoate resulted in formation of 1-hexanol in 82% yield after 5 h (entry 4). Ethyl acetate was hydrogenated to ethanol under similar conditions in almost 86% yield (entry 8). Reaction of benzyl benzoate with dihydrogen resulted in almost quantitative yield of benzyl alcohol after 7 h (entry 5); Reaction at room temperature led to quantitative formation of the *trans* dihydride ruthenium complex **4**, although no alcohol was formed. The aromatic methyl benzoate is quantitatively hydrogenated to benzyl alcohol and methanol (entry 6) in a relatively short time (4 h). As expected, the activated ester dimethyl terephthalate is converted into the corresponding dialcohol, 1,4-dimethanolbenzene, in high yield (97%) under our conditions (Table 1, entry 10). In a previous report, dimethyl phthalate was hydrogenated to phthalide using a ruthenium hydride complex in a yield of 11.5% after 144 h at 180°C under a hydrogen pressure of 128 atm.[5a] The bulky ester, *tert*-butyl acetate, was not effectively hydrogenated (10.5% conversion after 24 h; Table 1, entry 9), probably because of steric reasons.

A possible cycle for catalysis of ester hydrogenation by **2** is presented in Scheme 2. Initially, dihydrogen addition to complex **2** results in aromatization, to form the coordinatively saturated, *trans* dihydride complexes **4**, as experimentally observed. Dissociation of the amine "arm" can provide a site for ester coordination to the ruthenium center, to give the intermediate **A**. A hydride ligand subsequently transfers to the carbonyl group of the ester, followed by O–H elimination of a hemiacetal and regeneration of complex **2**. The hemiacetal is in equilibrium with the aldehyde, which is readily hydrogenated following a similar catalytic cycle via intermediate **B** to form the corresponding alcohol.[12] The much lower catalytic activity of complex **1** is attributable to the difficulty in opening the chelate ring to provide a coordination site for ester coordination, to generate an intermediate analogous to **A**, possibly indicating the importance of ligand hemilability for ester hydrogenation. This mechanism differs significantly from the ones outlined for ruthenium-catalyzed ketone hydrogenation, in which binding of the ketone to the metal is not required and hydrogenation takes place by a concerted hydride/proton transfer.[13]

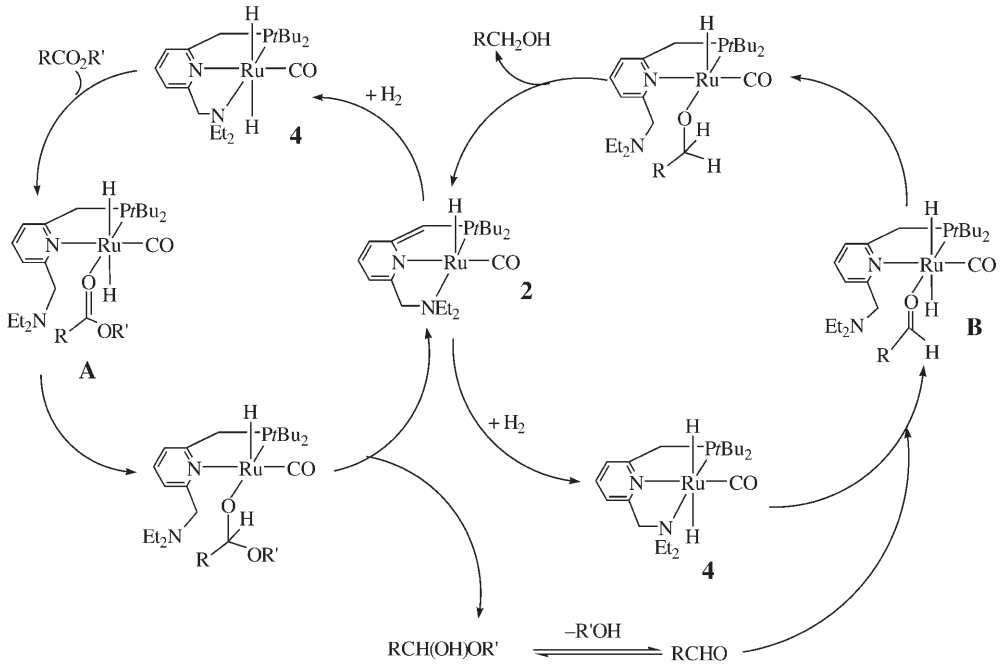
In conclusion, non-activated aromatic and aliphatic esters can be effectively hydrogenated to the corresponding alcohols under relatively mild, neutral conditions using a (PNN)ruthenium hydride complex as catalyst. This reaction involves an unusual aromatization/dearomatization sequence. The analogous PNP complex is much less active, suggesting that

Table 1: Hydrogenation of esters catalyzed by **1** and **2**.[a]

Entry	Ester	cat.	*t* [h]	*T* [°C]	Conversion [%]	Products (yield [%])[b]
1	ethyl benzoate	**1**	16	115	7.5	benzyl alcohol (7); ethanol (7.5)[c]
2	ethyl benzoate	**1**	16	140	12	benzyl alcohol (11.5); ethanol (12)[c]
3	ethyl benzoate	**2**	4	115	99.2	benzyl alcohol (96); ethanol (99)[c]
4	hexyl hexanoate	**2**	5	115	82.2	1-hexanol (82.2)
5	benzyl benzoate	**2**	7	115	98.5	benzyl alcohol (98)
6	methyl benzoate	**2**	4	115	100	benzyl alcohol (97); methanol (100)[c]
7	ethyl butyrate	**2**	4	115	100	1-butanol (98); ethanol (98.6)
8	ethyl acetate	**2**	12	115	86	ethanol (85.6)
9	*tert*-butyl acetate	**2**	24	115	10.5	ethanol (10.5); *tert*-butanol (10.5)
10	dimethyl terephthalate	**2**	5	115	100	1,4-dimethanolbenzene (97); methanol (100)

[a] Reaction conditions: ester (2 mmol); catalyst (0.02 mmol); H_2 (5.3 atm); dioxane (2 mL). [b] Percentage of maximum possible amount of each of the product alcohols; determined by GC. [c] A trace of benzyl benzoate was also formed: 0.3% (entries 1 and 2); 1% (entries 3 and 6).

 © 2006 Wiley-VCH Verlag GmbH & Co. KGaA, Weinheim



Scheme 2.

pincer ligand hemilability[14] and ester coordination are part of the reaction mechanism, although other mechanisms might also be possible. The mechanism and scope of this reaction are being investigated.

Received: October 24, 2005
Published online: January 3, 2006

Keywords: alcohols · esters · homogeneous catalysis · hydrogenation · ruthenium

[1] S. N. Ege, *Organic Chemistry*, D. C. Heath and Company, Lexington, **1989**, p. 596.
[2] Y. Pouilloux, F. Autin, J. Barrault, *Catal. Today* **2000**, *63*, 87, and references therein.
[3] H. T. Teunissen, C. J. Elsevier, *Chem. Commun.* **1998**, 1367.
[4] a) R. A. Grey, G. P. Pez, A. Wallo, *J. Am. Chem. Soc.* **1981**, *103*, 7536; b) mechanistic studies revealed that the actual catalyst in this process is $[RuH_4(PPh_3)_3]$: D. E. Linn, J. Halpern, *J. Am. Chem. Soc.* **1987**, *109*, 2969.
[5] a) U. Matteoi, M. Bianchi, G. Menchi, P. Frediani, F. Piacenti, *J. Mol. Catal.* **1984**, *22*, 353; b) U. Matteoi, G. Menchi, M. Bianchi, P. Frediani, F. Piacenti, *J. Organomet. Chem.* **1986**, *299*, 233; c) U. Matteoi, G. Menchi, M. Bianchi, P. Frediani, F. Piacenti, *J. Organomet. Chem.* **1995**, *498*, 177, and references therein.
[6] a) Y. Hara, H. Inagaki, S. Nishimura, K. Wada, *Chem. Lett.* **1992**, 1983; b) H. T. Teunissen, C. J. Elsevier, *Chem. Commun.* **1997**, 667.
[7] K. Nomura, H. Ogura, Y. Imanishi, *J. Mol. Catal. A* **2002**, *178*, 105.
[8] J. Zhang, G. Leitus, Y. Ben-David, D. Milstein, *J. Am. Chem. Soc.* **2005**, *127*, 10840.
[9] See Supporting Information.
[10] Transition-metal complexes with an anionic PNP ligand $(C_5H_3N\text{-}(CHPPh_2)(CH_2PPh_2))$ were reported: M. Sacco, G. Vasapollo, C. F. Nobile, A. Piergiovanni, *J. Organomet. Chem.* **1988**, *356*, 397.
[11] Catalytic dehydrogenation of secondary alcohols to ketones with PNP–Ru complexes: J. Zhang, M. Gandelman, L. J. W. Shimon, H. Rozenberg, D. Milstein, *Organometallics* **2004**, *23*, 4026.
[12] As expected, complex **2** readily catalyzes the hydrogenation of aldehydes: J. Zhang, D. Milstein, unpublished results.
[13] a) M. Yamakawa, H. Ito, R. Noyori, *J. Am. Chem. Soc.* **2000**, *122*, 1466; b) C. P. Casey, S. W. Singer, D. R. Powel, R. K. Hayashi, M. Kavanah, *J. Am. Chem. Soc.* **2001**, *123*, 1090; c) R. Noyori, M. Koizumi, D. Ishii, T. Ohkuma, *Pure Appl. Chem.* **2001**, *73*, 227; d) K. Abdur-Rashid, M. Faatz, A. J. Lough, R. H. Morris, *J. Am. Chem. Soc.* **2001**, *123*, 7473; e) K. Abdur-Rashid, S. E. Clapham, A. Hadzovic, J. N. Harvey, A. J. Lough, R. H. Morris, *J. Am. Chem. Soc.* **2002**, *124*, 15104; f) J. Wu, J.-X. Ji, R. Guo, C-H. Yeung, A. S. C. Chan, *Chem. Eur. J.* **2003**, *9*, 2963; g) C. P. Casey, J. B. Johnson, *J. Org. Chem.* **2003**, *68*, 1998 h) R. M. Bullock, *Chem. Eur. J.* **2004**, *10*, 2366; i) R. Abbel, K. Abdur-Rashid, M. Faatz, A. Hadzovic, A. J. Lough, R. H. Morris, *J. Am. Chem. Soc.* **2005**, *127*, 1870.
[14] Hemilability of PCN-type pincer complexes: a) E. Poverenov, M. Gandelman, L. J. W. Shimon, H. Rozenberg, Y. Ben-David, D. Milstein, *Chem. Eur. J.* **2004**, *10*, 4673; b) E. Poverenov, M. Gandelman, L. J. W. Shimon, H. Rozenberg, Y. Ben-David, D. Milstein, *Organometallics* **2005**, *24*, 1082.

 © 2006 Wiley-VCH Verlag GmbH & Co. KGaA, Weinheim

Nanostructures

DOI: 10.1002/anie.200503762

Sonochemical Formation of Single-Crystalline Gold Nanobelts**

Jianling Zhang, Jimin Du, Buxing Han, Zhimin Liu, Tao Jiang, and Zhaofu Zhang*

In recent years, metal nanostructures with specific size and morphology have been the focus of intensive research owing to their potential applications in the fabrication of electronic, optical, optoelectronic, and magnetic devices. The intrinsic properties of a metal nanostructure can be tuned by controlling its size, shape, and crystallinity.[1] One-dimensional (1D) nanostructures such as nanowires, nanotubes, and nanobelts (or nanoribbons) have attracted much attention on account of their numerous potential applications in science and engineering.[2] In particular, the planar nanostructures of nanobelts have been intensively studied because the nanobelts may represent a good system for examining dimensionally confined transport phenomena.[3] However, there are very few reports on the synthesis of metal nanobelts (or nanoribbons), although many processes have been successfully applied to the synthesis of oxide,[4] sulfide,[5] and carbon[6] nanobelts. Xia et al. reported the synthesis of silver nanobelts by heating an aqueous dispersion of spherical colloids of silver with a diameter of 3.5 nm under reflux.[7] Qian and coworkers prepared ultrathin nickel[8] and tellurium nanobelts[9] by a hydrothermal method.

Ultrasound has become an important tool for the synthesis of metal nanoparticles in recent years.[10] It is well known that ultrasonic irradiation of liquids has a variety of physical and chemical effects derived from acoustic cavitation, and can provide a unique method for driving chemical reactions under extreme conditions.[11] The sonochemical method is advantageous as it is nonhazardous, rapid in reaction rate, and produces very small metal particles. Unfortunately, metal nanoparticles prepared by sonochemical reduction generally have multiple shapes and wide size distributions. To solve these problems, surfactants and coexisting alcohols are usually used in the sonochemical process to control the particle shape and size.[12]

More recently, with the advent of green chemistry, the biosynthesis of nanostructures has attracted much interest in materials science because of the minimized adverse environmental effects.[13] The biomaterial templating technique has been demonstrated to be an efficient method for directing the synthesis and manufacture/assembly of artificial nanostructures of crystalline inorganic materials under environmentally benign conditions.[14] Many biomaterials, such as DNA, viruses, and sugars, have been used as biological templates to grow nanostructures of noble metals,[15] oxides,[16] sulfides,[17] and metal alloys.[18]

It is interesting to fabricate various gold nanostructures, which may find practical applications in nanodevices, and the syntheses of nanorods,[19] nanowires,[20] nanorings,[21] nanocubes,[22] and nanoplates[23] have been reported. Herein, we report a method for synthesizing single-crystalline gold nanobelts through the combination of ultrasound irradiation and a biological directing agent. In this route, an aqueous solution of $HAuCl_4$ containing α-D-glucose was ultrasonically irradiated to produce gold nanobelts. This method has some clear advantages: it is green, simple, rapid, and can be performed under ambient conditions.

The major reactions that occur in the sonolysis of an aqueous solution containing $HAuCl_4$ and α-D-glucose can be summarized by the following steps [Eq. (1)–(4)]:[24]

$$H_2O \rightarrow H^{\cdot} + {}^{\cdot}OH \quad (1)$$

$$\text{sugar} \rightarrow \text{pyrolysis radicals} \quad (2)$$

$$Au^{III} + \text{reducing radicals} \rightarrow Au^0 \quad (3)$$

$$n\,Au^0 \rightarrow Au_n \quad (4)$$

The two reducing radicals, generated from the reaction of α-D-glucose with primary radicals such as the hydroxyl radical and the hydrogen radical originating from water molecules [Eq. (1)], and from the direct decomposition of glucose at the interfacial region between the collapsing cavities and the bulk water [Eq. (2)], are effective for the reduction of $AuCl_4^-$ [Eq. (3)] followed by particle growth [Eq. (4)].

Figure 1a and b show representative scanning electron microscopy (SEM) images of the as-synthesized gold prod-

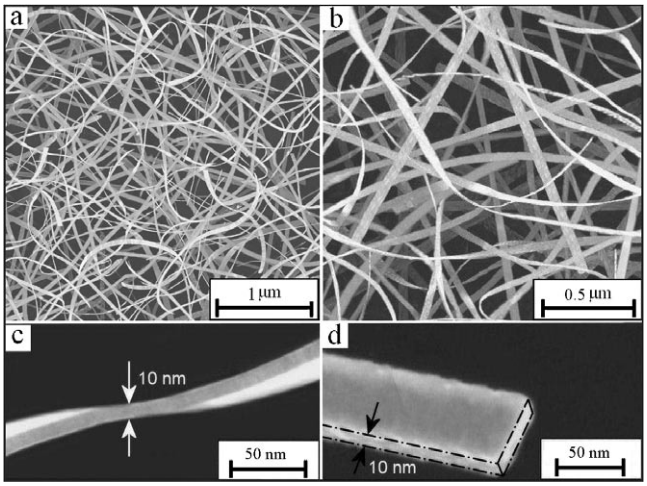


Figure 1. a,b) SEM images and c,d) high-magnification SEM images of as-synthesized gold nanobelts; $[HAuCl_4] = 50\ mg\,mL^{-1}$, [α-D-glucose] = 0.2 M, ultrasound time = 1 h.

[*] Dr. J. Zhang, J. Du, Prof. B. Han, Dr. Z. Liu, Dr. T. Jiang, Dr. Z. Zhang
Center for Molecular Sciences, Institute of Chemistry
Chinese Academy of Sciences
Beijing 100080 (P.R. China)
Fax: (+86) 106-255-9373
E-mail: Hanbx@iccas.ac.cn

[**] This work was supported by the National Natural Science Foundation of China (20403021).

Supporting information for this article is available on the WWW under http://www.angewandte.org or from the author.

InterScience
© 2006 Wiley-VCH Verlag GmbH & Co. KGaA, Weinheim

ucts. The initial concentrations of $HAuCl_4$ and α-D-glucose were 50 mg mL^{-1} and 0.2 M, respectively, and the ultrasound irradiation time was 1 h. The geometrical configuration of the nanobelts is clearly displayed in the SEM images. The gold nanobelts typically have a width of 30–50 nm and a length of several micrometers. They are highly flexible and can bend > 90° without breaking. To further analyze the characteristics of the nanobelts, high-magnification SEM images are given in Figure 1c and d. Typical nanobelts have smooth side edges and an even thickness of approximately 10 nm. Figure 1d shows the tip surface of a typical nanobelt, in which a rectangular-shaped cross section is observed, similar to those of semiconducting oxide nanobelts.[4f]

The detailed microstructure of the gold nanobelts was further characterized by transmission electron microscopy (TEM; see Figure 2a). The TEM images also reveal that the

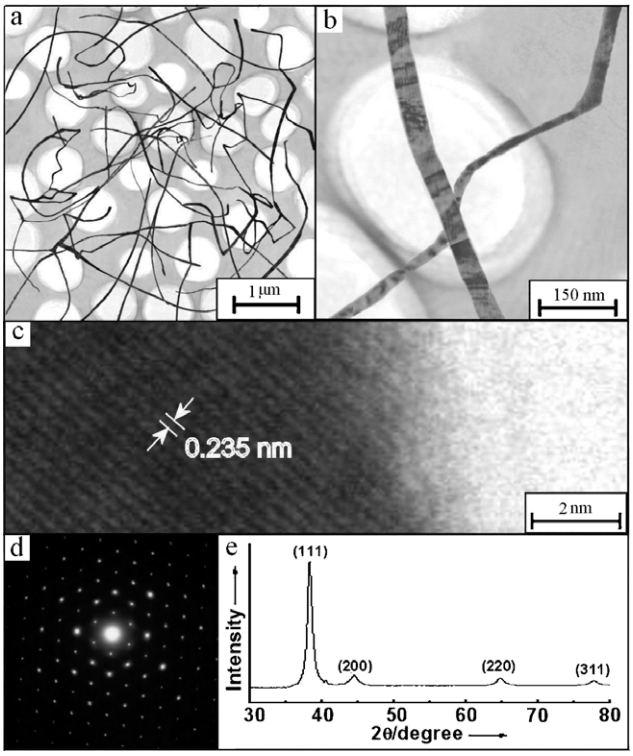


Figure 2. TEM images with a) lower and b) higher magnification, c) HRTEM image, d) SAED pattern, and e) XRD pattern of gold nanobelts; [$HAuCl_4$] = 50 mg mL^{-1}, [α-D-glucose] = 0.2 M, ultrasound time = 1 h.

width of the gold products is in the range 30–50 nm and that the length can reach several micrometers. The characteristic variation in lateral dimension associated with a belt is clearly observed from the bending in the middle of a 1D nanostructure (see Figure 2b). A high-resolution TEM (HRTEM) image of typical nanobelts is shown in Figure 2c, which was obtained with the incident electron beam perpendicular to the wide surface of the nanobelt. The measured interplanar spacing for all the lattice fringes is 0.235 nm, which corresponds to the (111) lattice plane of face-centered-cubic (fcc) gold. Figure 2d presents the selected-area electron diffraction (SAED) pattern of the gold nanobelts, which was obtained by focusing the electron beam on a nanobelt lying flat on the TEM grid. A diffraction pattern with hexagonal symmetry is generated, which demonstrates that the gold nanobelt is a single crystal with preferential growth along the Au[111] direction.[23a,25] The SAED patterns are essentially identical over the entire belt, thus revealing the single-crystalline and structurally uniform nature of the nanobelts. X-ray diffraction (XRD) gives further support to the phase structure of the gold nanobelts. The four diffraction peaks shown in Figure 2e correspond to the (111), (200), (220), and (311) diffraction peaks of metallic gold, which indicates that the products are composed of pure crystalline gold. The gold nanobelts were additionally characterized by energy-dispersive X-ray spectroscopy (EDS) and X-ray photoelectron spectroscopy (XPS), which confirmed that the nanobelts are pure gold (see Supporting Information).

To investigate the details of the sonochemical formation of gold nanobelts, we studied the different stages in the growth of gold by changing the reaction time (see Figure 3).

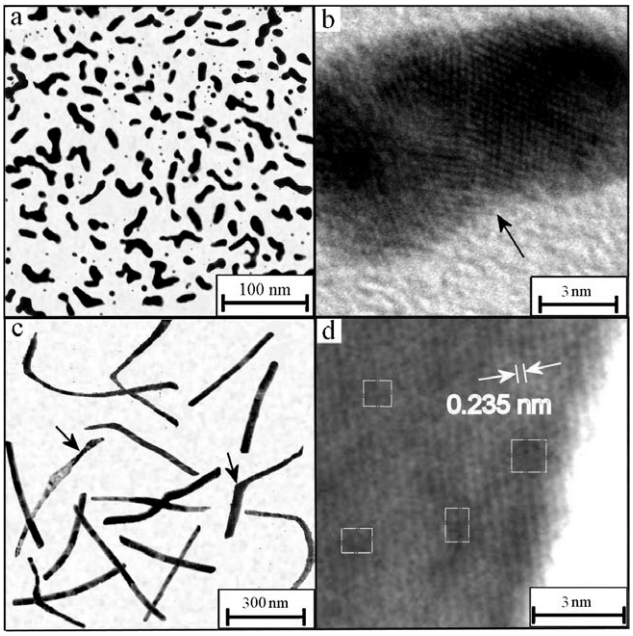


Figure 3. TEM images of gold after ultrasound irradiation for a) 10 and c) 30 min, and the corresponding HRTEM images (b,d); [$HAuCl_4$] = 50 mg mL^{-1}, [α-D-glucose] = 0.2 M. The arrow in (b) marks the junction of two neighboring gold particles; the arrows in (c) reveal characteristic variations in lateral dimensions associated with a beltlike shape; the rectangles in (d) show structures that are not fully crystallized.

When the irradiation time was as short as 10 min, directional aggregates of gold were formed (8 nm average width; Figure 3a). The HRTEM image of the same sample (Figure 3b) shows that two neighboring gold particles are fused at their junction and exhibit a polycrystalline structure. When the ultrasound time was prolonged to 30 min, short 1D nanostructures of gold with an average width and length of 20 nm and 0.5 μm, respectively, were obtained. The beltlike shape is clearly observed from the curving and bending in the

 © 2006 Wiley-VCH Verlag GmbH & Co. KGaA, Weinheim

middle of these short 1D nanostructures (marked with arrows in Figure 3c). Figure 3d is the corresponding HRTEM image. By comparison with Figure 2c, it is noted that the structure of these short nanobelts is the same as that of the nanobelts obtained after ultrasound irradiation for 1 h. However, these short nanobelts are not fully crystallized and are somewhat disordered (see rectangles marked in Figure 3d). The longer ultrasound irradiation time gives rise to high-quality single-crystalline nanobelts (see Figure 2). It can therefore be concluded that the nanobelts grow from the merged particles. We reasonably speculate that the nanobelt formation process has following steps: 1) gold nuclei are formed and grow into nanoparticles; 2) the gold nanoparticles are directionally aggregated, melted, and then bound to each other (actually a recrystallization process); and 3) growth along the Au[111] direction and further crystallization result in the single-crystalline nanobelt structure. Note that some spherical particles with smaller sizes (2–3 nm) were observed in the early stage of the reaction (10 min, see Figure 3a). We suggest that the anisotropic growth of gold nanobelts follows the Ostwald ripening process at the expense of the small gold nanoparticles.[1a,26]

The above formation process of the gold nanobelts is similar to that of single-crystalline selenium nanowires prepared by the sonication method.[27] As for the reason for the formation of nanobelts, we believe that α-D-glucose can selectively adsorb onto the crystallographic planes of gold,[28] thus serving as a directing agent and kinetically controlling the anisotropic growth of gold. To understand the function of α-D-glucose, we conducted a contrast experiment with β-cyclodextrin, which is a cyclic oligomer containing seven α-D-glucose units. The other conditions were the same as those for preparing the gold nanobelts with α-D-glucose. The results showed that only spherical particles with a diameter of approximately 30 nm were obtained in the presence of β-cyclodextrin (see Supporting Information). This finding indicates that α-D-glucose plays a key role in the formation of gold nanobelts. We also found that the formation of gold nanobelts depends on the concentration of α-D-glucose. When its concentration was as low as 0.05 M, only gold particles with a size of approximately 40 nm were obtained (see Supporting Information). The reason may be that the capping effect of the glucose in the dilute solution is not sufficient for the effective coverage or passivation of gold facets, thus resulting in the formation of nanoparticles instead of nanobelts. In addition, cavitations and shock waves created by ultrasound irradiation can not only accelerate solid particles to high velocities and drive them together to induce effective melting at the point of interparticle collision,[27,29] but may also enhance the entanglement and rearrangement of the α-D-glucose molecules on gold crystals. All these effects induced by ultrasound may partly contribute to the final formation of single-crystalline gold nanobelts.

Gold nanomaterials show unique optical properties as a result of surface plasmon resonance. It is well known that spherical gold nanoparticles exhibit a single absorption band at 520 nm, whereas anisotropic gold particles show two surface plasmon resonance absorption peaks that are characteristic of the short (transverse band) and long (longitudinal band) axes of these systems.[30] Spectrum a in Figure 4 shows the UV/Vis absorption spectrum of gold nanobelts suspended in water. One peak corresponding to the short axes of the nanobelts appears at about 544 nm; the other peak increases into the IR region with no indication of leveling off, as also observed for gold nanowires,[31] and can be attributed to the long aspect ratio of the gold nanobelts. For gold particles with a diameter of approximately 30 nm synthesized in the presence of β-cyclodextrin, the characteristic surface plasmon band is observed at $\lambda_{max} = 530$ nm (spectrum b in Figure 4). Thus, the appearance of the absorption band actually mirrors the appearance of the different nanostructures of gold.

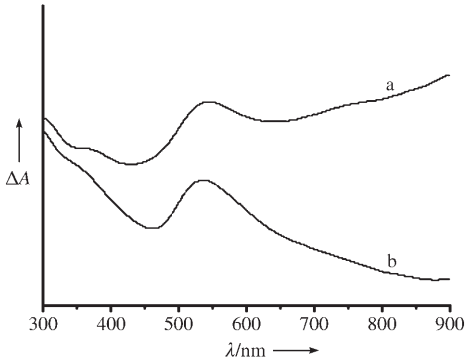


Figure 4. UV/Vis spectra of a) gold nanobelts and b) gold nanospheres synthesized in the presence of α-D-glucose (a) and β-cyclodextrin (b), respectively; $[HAuCl_4] = 50\ mg\,mL^{-1}$, [α-D-glucose] = 0.2 M, [β-cyclodextrin] = 0.2 M, ultrasound time = 1 h.

In conclusion, we have successfully synthesized single-crystalline gold nanobelts by a sonochemical route in the presence of α-D-glucose. This method is simple, convenient, economical, and environmentally benign, and can be performed under ambient conditions. The gold nanobelts have potential for incorporation into functional electronic, optoelectronic, or sensing devices, which could lead to extreme miniaturization and enhanced performance. In addition, such gold nanobelts can be used as building blocks to form a variety of functional nanostructures with special physical and chemical properties. This method may be applied to the synthesis of other nanosized metal materials.

Experimental Section

$HAuCl_4 \cdot 4H_2O$, α-D-glucose, and β-cyclodextrin were provided by the Beijing Analytical Instrument Factory. Deionized water was used. In a typical experiment, an aqueous solution of $HAuCl_4$ ($50\ mg\,mL^{-1}$) was placed in a sonication vessel, and then mixed with the desired amount of α-D-glucose (or β-cyclodextrin). The solution was exposed to high-intensity ultrasound irradiation (40 kHz, 100 W) for 10–60 min. The products were collected after deposition and aging, and then washed with deionized water.

The morphologies of the products were characterized by SEM (Hitachi-530) and TEM (Tecnai 20, Philips). The HRTEM images and SAED patterns were recorded on a JEOL JEM-2010 transmission electron microscope operating at 200 kV. XRD analysis of the samples was carried out by using an X-ray diffractometer (Model D/MAX2500, Rigaku) with $Cu_{K\alpha}$ radiation. X-ray photoelectron spectra

 © 2006 Wiley-VCH Verlag GmbH & Co. KGaA, Weinheim

were collected by an ESCALab220i-XL spectrometer operating at 15 kV and 20 mA, at a pressure of 3×10^{-9} mbar with $Al_{K\alpha}$ as the exciting source ($h\nu = 1486.6$ eV). UV/Vis absorption spectra of gold particles suspended in water were collected by a TU-1201 Model spectrophotometer (Beijing General Instrument Company).

Received: October 24, 2005
Published online: January 3, 2006

Keywords: crystal growth · gold · nanostructures · ultrasound

[1] a) R. Jin, Y. Cao, C. A. Mirkin, K. L. Kelly, G. C. Schatz, J. G. Zheng, *Science* **2001**, *294*, 1901; b) M. A. El-Sayed, *Acc. Chem. Res.* **2001**, *34*, 257.

[2] a) Z. L. Wang, R. P. Gao, Z. W. Pan, Z. R. Dai, *Adv. Eng. Mater.* **2001**, *3*, 657; b) Y. Xia, P. Yang, Y. Sun, Y. Wu, B. Mayers, B. Gates, Y. Yin, F. Kim, H. Yan, *Adv. Mater.* **2003**, *15*, 353; c) Z. L. Wang, *Adv. Mater.* **2003**, *15*, 432; d) G. A. Baker, *Adv. Mater.* **2005**, *17*, 639.

[3] a) Z. W. Pan, Z. R. Dai, Z. L. Wang, *Science* **2001**, *291*, 1947; b) W. Shi, H. Peng, N. Wang, C. P. Li, L. Xu, C. S. Lee, R. Kalish, S.-T. Lee, *J. Am. Chem. Soc.* **2001**, *123*, 11095.

[4] a) X. Y. Kong, Y. Ding, R. Yang, Z. L. Wang, *Science* **2004**, *303*, 1348; b) X. G. Wen, S. H. Wang, Y. Ding, Z. L. Wang, S. H. Yang, *J. Phys. Chem. B* **2005**, *109*, 215; c) Z. L. Wang, *Annu. Rev. Phys. Chem.* **2004**, *55*, 159; d) J. Liu, Q. Li, T. Wang, D. Yu, Y. Li, *Angew. Chem.* **2004**, *116*, 5158; *Angew. Chem. Int. Ed.* **2004**, *43*, 5048; e) Z. R. Dai, Z. W. Pan, Z. L. Wang, *Adv. Funct. Mater.* **2003**, *13*, 9; f) B. C. Cheng, Y. H. Xiao, G. S. Wu, L. D. Zhang, *Adv. Funct. Mater.* **2004**, *14*, 913; g) X.-S. Fang, C.-H. Ye, L.-D. Zhang, T. Xie, *Adv. Mater.* **2005**, *17*, 1661; h) R. Ma, Y. Bando, L. Zhang, T. Sasaki, *Adv. Mater.* **2004**, *16*, 918.

[5] a) X. S. Fang, C. H. Ye, L. D. Zhang, Y. H. Wang, Y. C. Wu, *Adv. Funct. Mater.* **2005**, *15*, 63; b) C. Ma, D. Moore, J. Li, Z. L. Wang, *Adv. Mater.* **2003**, *15*, 228; c) W. Zhang, L. Xu, K. Tang, F. Li, Y. Qian, *Eur. J. Inorg. Chem.* **2005**, 653; d) W.-T. Yao, S.-H. Yu, L. Pan, J. Li, Q.-S. Wu, L. Zhang, J. Jiang, *Small* **2005**, *1*, 320.

[6] a) Z. Kang, E. Wang, B. Mao, Z. Su, L. Gao, S. Lian, L. Xu, *J. Am. Chem. Soc.* **2005**, *127*, 6534; b) J. Liu, M. Shao, Q. Tang, S. Zhang, Y. Qian, *J. Phys. Chem. B* **2003**, *107*, 6329.

[7] Y. Sun, B. Mayers, Y. Xia, *Nano Lett.* **2003**, *3*, 675.

[8] Z. Liu, S. Li, Y. Yang, S. Peng, Z. Hu, Y. Qian, *Adv. Mater.* **2003**, *15*, 1946.

[9] M. Mo, J. Zeng, X. Liu, W. Yu, S. Zhang, Y. Qian, *Adv. Mater.* **2002**, *14*, 1658.

[10] a) M. Ashokkumar, F. Grieser, *Rev. Chem. Eng.* **1999**, *15*, 41; b) S. Zhu, H. Zhou, M. Hibino, I. Honma, M. Ichihara, *Adv. Funct. Mater.* **2005**, *15*, 381; c) T. Gao, T. H. Wang, *Chem. Commun.* **2004**, 2558; d) T. Gao, T. H. Wang, *Chem. Mater.* **2005**, *17*, 887; e) H. S. Xia, Q. Wang, *Chem. Mater.* **2002**, *14*, 2158; f) A. Gedanken, X. Tang, Y. Wang, N. Perkas, Y. Koltypin, M. V. Landau, L. Vradman, M. Herskowitz, *Chem. Eur. J.* **2001**, *7*, 4546.

[11] K. S. Suslick, G. J. Price, *Annu. Rev. Mater. Sci.* **1999**, *29*, 295.

[12] a) K. Barbour, M. Ashokkumar, R. A. Caruso, F. Grieser, *J. Phys. Chem. B* **1999**, *103*, 9231; b) X.-F. Qiu, J.-J. Zhu, H.-Y. Chen, *J. Cryst. Growth* **2003**, *257*, 37; c) K. Okitsu, A. Yue, S. Tanabe, H. Matsumoto, Y. Yobiko, *Langmuir* **2001**, *17*, 7717.

[13] S. Mann, *Nature* **1993**, *365*, 499.

[14] a) J. Aizenberg, D. A. Muller, J. L. Grazul, D. R. Hamann, *Science* **2003**, *299*, 1205; b) C. B. Mao, D. J. Solis, B. D. Reiss, S. T. Kottmann, R. Y. Sweeney, A. Hayhurst, G. Georgiou, B. Iverson, A. M. Belcher, *Science* **2004**, *303*, 213; c) H. Liang, T. E. Angelini, P. V. Braun, G. C. L. Wong, *J. Am. Chem. Soc.* **2004**, *126*, 14157.

[15] a) J. L. Gardea-Torresdey, J. G. Parsons, E. Gomez, J. Peralta-Videa, H. E. Troiani, P. Santiago, M. Jose Yacaman, *Nano Lett.* **2002**, *2*, 397; b) P. Mukherjee, A. Ahmad, D. Mandal, S. Senapati, S. R. Sainkar, M. I. Khan, R. Parishcha, P. V. Ajaykumar, M. Alam, R. Kumar, M. Sastry, *Nano Lett.* **2001**, *1*, 515; c) Z. M. Qi, H. S. Zhou, N. Matsuda, I. Honma, K. Shimada, A. Takatsu, K. Kato, *J. Phys. Chem. B* **2004**, *108*, 7006; d) Y. Liu, K. B. Male, P. Bouvrette, J. H. T. Luong, *Chem. Mater.* **2003**, *15*, 4172.

[16] a) C. E. Fowler, W. Shenton, G. Stubbs, S. Mann, *Adv. Mater.* **2001**, *13*, 1266; b) W. Shenton, S. Mann, H. Cölfen, A. Bacher, M. Fischer, *Adv. Mater.* **2001**, *13*, 442; c) T. Douglas, V. T. Stark, *Inorg. Chem.* **2000**, *39*, 1828.

[17] a) C. T. Dameron, R. N. Reese, R. K. Mehra, A. R. Kortan, P. J. Carroll, M. L. Steigerwald, L. E. Brus, D. R. Winge, *Nature* **1989**, *338*, 596; b) M. Kowshik, W. Vogel, J. Urban, S. K. Kulkarni, K. M. Paknikar, *Adv. Mater.* **2002**, *14*, 815; c) K. K. W. Wong, S. Mann, *Adv. Mater.* **1996**, *8*, 928.

[18] B. D. Reiss, C. Mao, D. J. Solis, K. S. Ryan, T. Thomson, A. M. Belcher, *Nano Lett.* **2004**, *4*, 1127.

[19] a) F. Kim, J. H. Song, P. Yang, *J. Am. Chem. Soc.* **2002**, *124*, 14316; b) D. A. Zweifel, A. Wei, *Chem. Mater.* **2005**, *17*, 4256; c) J. Y. Chang, H. M. Wu, H. Chen, Y. C. Liang, W. H. Tan, *Chem. Commun.* **2005**, 1092; d) J. H. Song, F. Kim, D. Kim, P. D. Yang, *Chem. Eur. J.* **2005**, *11*, 910.

[20] a) E. Tosatti, S. Prestipino, *Science* **2000**, *289*, 561; b) T. Sainsbury, D. Fitzmaurice, *Chem. Mater.* **2004**, *16*, 2174; c) T. O. Hutchinson, Y. P. Liu, C. Kiely, C. J. Kiely, M. Brust, *Adv. Mater.* **2001**, *13*, 1800.

[21] a) Q. Sun, Q. Wang, P. Jena, R. Note, J. Z. Yu, Y. Kawazoe, *Phys. Rev. B* **2004**, *70*, 245411; b) Y. Sun, Y. Xia, *Adv. Mater.* **2003**, *15*, 695.

[22] a) Y. Sun, Y. Xia, *Science* **2002**, *298*, 2176; b) J. Chen, B. Wiley, Z.-Y. Li, D. Campbell, F. Saeki, H. Cang, L. Au, J. Lee, X. Li, Y. Xia, *Adv. Mater.* **2005**, *17*, 2255.

[23] a) X. Sun, S. Dong, E. Wang, *Angew. Chem.* **2004**, *116*, 6520; *Angew. Chem. Int. Ed.* **2004**, *43*, 6360; b) D. Brohm, S. Metzger, A. Bhargava, O. Müller, F. Lieb, H. Waldmann, *Angew. Chem.* **2002**, *114*, 203; *Angew. Chem. Int. Ed.* **2002**, *41*, 195.

[24] a) K. Okitsu, Y. Mizukoshi, H. Bandow, A. T. Yamamoto, Y. Nagata, Y. Maeda, *J. Phys. Chem. B* **1997**, *101*, 5470; b) Y. Mizukoshi, E. Takagi, H. Okuno, R. Oshima, Y. Maeda, Y. Nagata, *Ultrason. Sonochem.* **2001**, *8*, 1.

[25] Y. Zhou, C. Y. Wang, Y. R. Zhu, Z. Y. Chen, *Chem. Mater.* **1999**, *11*, 2310.

[26] a) A. R. Roosen, W. C. Carter, *Physica A* **1998**, *261*, 232; b) Y. Sun, Y. Yin, B. Mayers, T. Herricks, Y. Xia, *Chem. Mater.* **2002**, *14*, 4736.

[27] H. Zhang, D. Yang, Y. Ji, X. Ma, J. Xu, D. Que, *J. Phys. Chem. B* **2004**, *108*, 1179.

[28] a) R. Holze, M. Beltowska-Brzezinska, *Electrochim. Acta* **1985**, *30*, 937; b) P. S. Vukusic, G. W. Bradberry, J. R. Sambles, *Surf. Sci.* **1992**, *277*, L34; c) R. A. Caruso, M. Ashokkumar, F. Grieser, *Langmuir* **2002**, *18*, 7831.

[29] a) S. J. Doktycz, K. S. Suslick, *Science* **1990**, *247*, 1067; b) H. Wang, Y.-N. Lu, J.-J. Zhu, H.-Y. Chen, *Inorg. Chem.* **2003**, *42*, 6404.

[30] a) N. Malikova, I. Pastoriza-Santos, M. Schierhorn, N. A. Kotov, L. M. Liz-Marzán, *Langmuir* **2002**, *18*, 3694; b) T. K. Sau, C. J. Murphy, *Langmuir* **2004**, *20*, 6414; c) Z. Zhong, J. Luo, T. P. Ang, J. Highfield, J. Lin, A. Gedanken, *J. Phys. Chem. B* **2004**, *108*, 18119.

[31] a) C. D. Chen, Y. T. Yeh, C. R. C. Wang, *J. Phys. Chem. Solids* **2001**, *62*, 1587; b) S. S. Chang, C. W. Shih, C. D. Chen, W. C. Lai, C. R. C. Wang, *Langmuir* **1999**, *15*, 701; c) L. Pei, K. Mori, M. Adachi, *Langmuir* **2004**, *20*, 7837.

 © 2006 Wiley-VCH Verlag GmbH & Co. KGaA, Weinheim

Nanoparticles

DOI: 10.1002/anie.200503408

Self-Organization of Spherical, Core–Shell Palladium Aggregates by Laser-Induced and Thermal Decomposition of $[Pd(PPh_3)_4]$**

*Enyi Ye, Hua Tan, Shuping Li, and Wai Yip Fan**

Metallic nanoparticles serve many functions. For example, palladium and platinum metal nanoparticles stabilized by surfactants and solvents can act as catalysts for hydrogenation[1,2] and Heck, Suzuki, and Stille cross-coupling reactions.[3–5] Nanoparticles are also potential building blocks for designing larger organized structures for chemical sensing applications and magnetic and electronic devices.[6] This is fundamentally important because these structures display properties that are distinct from those of the individual constituent particles.[7] Several methods have been applied to obtain 3D aggregates of metal nanoparticles,[8–11] one of the more efficient being the "brick-and-mortar" ("BM") strategy, which involves the use of multifunctional organic ligands, polymers, or biomolecules as the cohesion "mortar".[12,13] Naka et al. have also used cubic silsesquioxanes as the cross-linker for generating spherical palladium aggregates.[14]

Recently we have embarked on a project to assemble metal nanoparticles by the laser decomposition of transition metal carbonyls or phosphanes, with particular interest in understanding the reaction pathways that lead to nanoparticle formation. We chose the photolysis of organometallic species in which the metal is already present in the zero oxidation state, thereby eliminating the need for reducing agents and possibly high temperatures. Herein a facile method for assembling palladium nanoparticles into spherical, core–shell aggregates by visible laser decomposition of commercially available tetrakis(triphenylphosphane)palladium is presented. In this two-step procedure, palladium nanocores (15–25 nm) are first generated by laser decomposition and then smaller palladium nanocrystals (<5 nm) are formed by the thermal decomposition of the remaining $[Pd(PPh_3)_4]$ aggregated around the Pd core.

In a typical experiment, $[Pd(PPh_3)_4]$ (11.5 mg, 0.01 mmol; 99% Sigma-Aldrich) was dissolved in 5 mL of DMF (HPLC grade, Aldrich) and 5 mL of ethanol (AR grade, Aldrich) to form an orange solution. The UV/Vis absorption spectrum of the solution was recorded with a Shimadzu UV-2550 spectrometer to check its absorptivity around 532 nm, which is the pulsed-laser wavelength available in our laboratory (Figure 1). The broad absorption spectrum (from <300 to 650 nm) obtained showed that it should be possible to induce changes in $[Pd(PPh_3)_4]$ by irradiation with the laser. The solution was then irradiated with a 532-nm pulsed YAG laser (Continuum Surelite III-10, 80–100 mJ per 10-ns pulse), with vigorous stirring, for 30 min. A change of color from orange to black occurred in around 10 minutes, thereby indicating the decomposition of the precursor and formation of palladium nanoparticles. This could also be seen from the changes in the UV/Vis spectrum (Figure 1). An aliquot of this solution (labeled as product **A**) was removed immediately for characterization, while the remainder (labeled as product **B**) was kept in the dark and maintained under ambient conditions for 24 h without shaking or stirring. This allowed the precursor to decompose thermally in the dark and generate more Pd particles. Both **A** and **B** were centrifuged and rinsed with DMF and ethanol several times to remove the free PPh_3. The remaining black solids were then collected and redispersed in ethanol for further investigation. The UV/Vis absorption spectrum of **B** dispersed in ethanol is essentially the same as that of **A**.

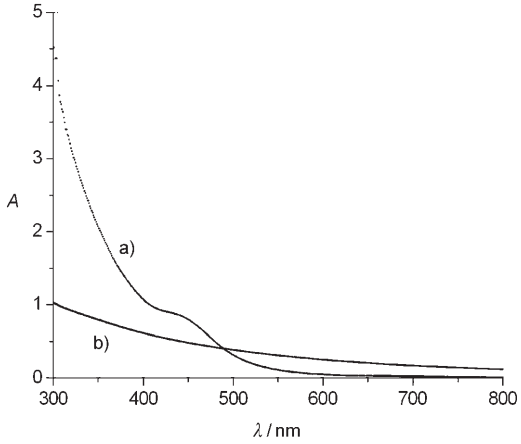


Figure 1. The absorption spectrum of the precursor $[Pd(PPh_3)_4]$ (a) and the as-prepared core and core–shell palladium nanoparticles (b).

Figure 2 shows a scheme for the formation of our core–shell palladium spheres. The first step requires the laser photodecomposition of $[Pd(PPh_3)_4]$ into Pd atoms and free PPh_3. We monitored the progress of the photodecomposition by ^{31}P NMR spectroscopy and, indeed, the signals of the precursor ($\delta = 29.8$ ppm) decrease in intensity with a concomitant increase of the signal for free PPh_3 ($\delta = -4.75$ ppm).

A TEM image taken of the Pd nanocores (**A**) with a JEOL TEM-2010F instrument (field emission, 200 keV) is shown in Figure 3. A narrow distribution of core sizes, with diameters ranging from 15 to 25 nm, is achieved upon laser photodecomposition of $[Pd(PPh_3)_4]$. The selective area electron diffraction (SAED) pattern obtained during the acquisition of the TEM image shows the cores to be polycrystalline palladium corresponding to a face-centered cubic (fcc)

[*] E. Ye, H. Tan, S. Li, Dr. W. Y. Fan
Department of Chemistry
National University of Singapore
3 Science Drive 3, Singapore 117543 (Singapore)
Fax: (+65) 6779-1691
E-mail: chmfanwy@nus.edu.sg

[**] We thank Binghai Liu for the TEM imaging and the electron diffraction data analysis, and Shuhua Wang for the XRD measurements. This work was carried out under an ASTAR nanoscience grant (143-000-198-305).

Supporting information for this article is available on the WWW under http://www.angewandte.org or from the author.

InterScience
© 2006 Wiley-VCH Verlag GmbH & Co. KGaA, Weinheim

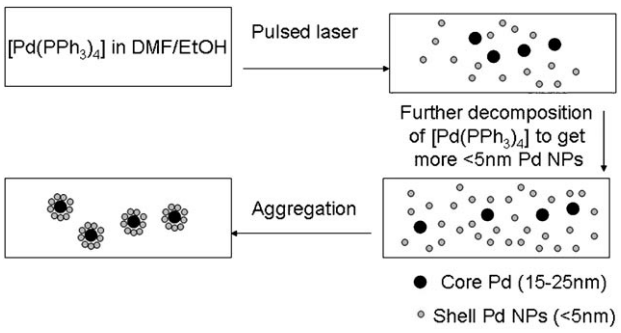


Figure 2. Formation of the core–shell palladium nanostructures. NP = nanoparticle.

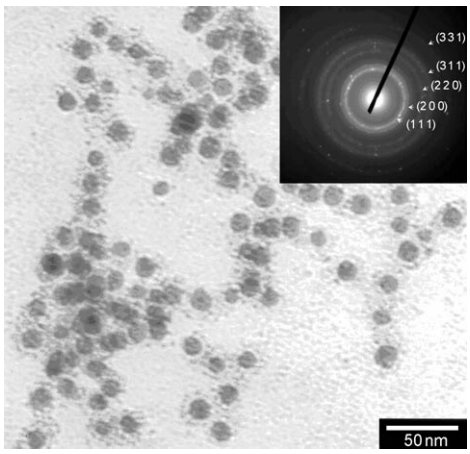


Figure 3. TEM image showing the cores formed during the laser-induced decomposition of [Pd(PPh$_3$)$_4$]; the insert shows the SAED pattern of these core Pd particles.

structure. Smaller palladium nanoparticles of the order of 5 nm can also be seen individually or as aggregates on the surface of the larger core particles upon closer inspection.

Further thermal decomposition of the remaining [Pd(PPh$_3$)$_4$], in the absence of irradiation, produces many more of these small Pd nanoparticles (< 5 nm) and, in turn, induces even more aggregation on the surface of the core Pd nanoparticles. This results in the formation of spherical core–shell palladium structures (**B**; Figure 4a). These TEM images of product **B** show that the overall core–shell spheres are larger but maintain a fairly narrow size distribution of 100 ± 20 nm. Incidentally, the core diameters remain unchanged at about 20 nm. With the higher magnification provided by a JEOL TEM-3010 (300 keV) instrument, the shells were seen to be composed of dark spots (Figure 4b,c). These dark spots were determined to be individual Pd nanocrystals whose lattice spacing of 0.23 nm corresponds to the (111) distance of fcc Pd (Figure 4d). Almost every nanoparticle smaller than about 5 nm appears to be a discrete entity in the nanoshell of the core–shell structure, although some merging of the particles could also be observed upon closer inspection.

An X-ray diffraction (XRD) analysis with a Siemens Powder XRD D5005 diffractometer also confirmed the

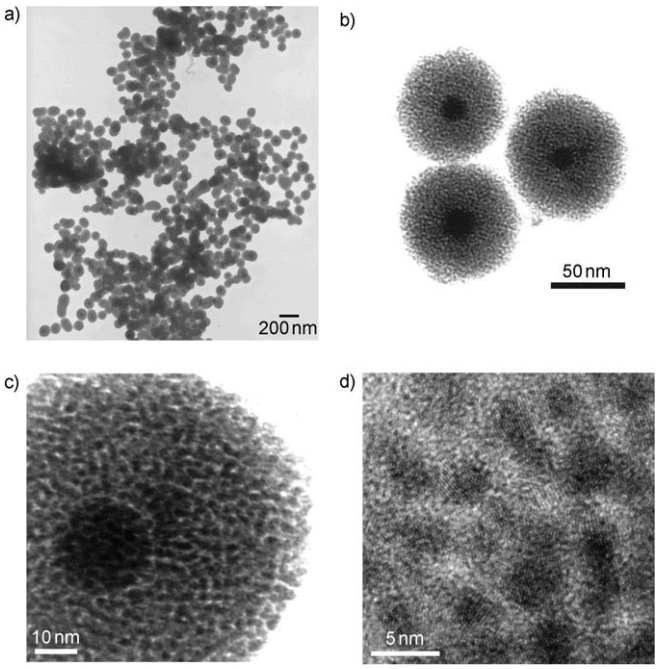


Figure 4. a) TEM image of the core–shell structure; b) and c) high-magnification TEM images showing the core–shell structure clearly; d) an HRTEM image of the shell showing that it is composed of palladium nanoparticles.

formation of the Pd nanoparticles by revealing the characteristic diffraction peaks of the palladium fcc phase (Figure 5).[15]

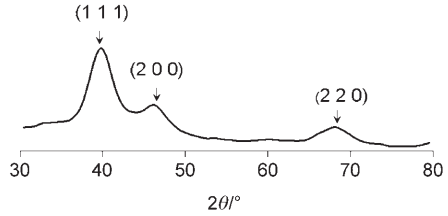


Figure 5. The XRD pattern of the core–shell palladium spheres (product **B**).

An energy-dispersive X-ray (EDX) analysis of the core–shell structure revealed the presence of phosphorus within the shell with a P/Pd ratio of around 0.06. Therefore, the shell most likely consists of at least two types of PPh$_3$, namely free PPh$_3$ in the space surrounding the small Pd nanoparticles and PPh$_3$ adsorbed on the nanoparticle surface. Both these types of PPh$_3$ play a key role in the aggregation process during formation of the core–shell structure. Unfortunately we did not obtain an NMR signal for the adsorbed PPh$_3$ because of the low concentration of the core–shell nanoparticles. Although it is likely that [Pd(PPh$_3$)$_4$] would also be trapped upon Pd nanoparticle formation, this species would decompose within the nanoparticle in a manner similar to the thermal decomposition in solution. Hence, [Pd(PPh$_3$)$_4$] represents, at most, a minor contribution to the composition of the core–shell Pd structure, especially if the nanoparticles have been left in the dark for a few days.

 © 2006 Wiley-VCH Verlag GmbH & Co. KGaA, Weinheim

When the EDX beam was directed towards the center of the core–shell structure, the P/Pd ratio was found to decrease to 0.02. We believe that the detected phosphorus, albeit in lower amounts, originates from the shell, since the beam still has to sample this region around the core. A simple calculation shows that for a core thickness of about 20% of the whole structure (as estimated from Figure 4b), the P/Pd ratio should decrease slightly to about 0.05 assuming that the core consists of only Pd atoms of the same density as the shell. However, a larger decrease is seen, which strongly suggests that the packing of Pd atoms within the core is denser, closely resembling that of the pure metal, and that phosphorus species are absent. Hence, EDX analysis supports the formation of an almost pure Pd core, or at least one with a much higher Pd density, surrounded by aggregates of smaller Pd nanoparticles interspersed with phosphanes.

We also found that when the solution of $[Pd(PPh_3)_4]$ was irradiated with the pulsed laser for a longer time (>2 h), no core–shell structures could be obtained even after the solution had been stored in the dark for a few days. During such a prolonged irradiation period the precursor would have decomposed completely to give only the core palladium nanoparticles. If the duration of the photolysis is shortened not all of the precursor decomposes, thus allowing the remainder to undergo gradual thermal decomposition to form the smaller palladium nanoparticles, which then aggregate on the core surface. In another experiment, $[Pd(PPh_3)_4]$ was allowed to decompose slowly in the absence of any laser or light irradiation under ambient conditions and without any heating, shaking, or stirring. The solution gradually became turbid and within 24 to 40 h turned from orange to black. After performing the required workup to isolate the nanoparticles, we found that they were spherical aggregates with no Pd core. These spherical aggregates are larger, with diameters of up to 400 nm.

The formation of larger aggregates of Pd nanoparticles in the absence of irradiation is due to the smaller number of "seed" nuclei in the solution. The precursor can only decompose slowly in the dark to form smaller Pd nanoparticles (<5 nm), which, in turn, are adsorbed by the free PPh_3 released during the decomposition process. These individual nanoparticles aggregate, perhaps through intermolecular π–π interactions, and their growth may be diffusion-controlled.[16] Laser photolysis greatly influences the size of the Pd aggregates formed. In the initial step, efficient decomposition of $[Pd(PPh_3)_4]$ accelerated by the intense laser pulse releases more palladium atoms during each pulse and causes the aggregation into larger palladium nanoparticles (20 ± 5 nm). Since no further triphenylphosphane is added, there is insufficient adsorbate to prevent the formation of these large nanocores. However, once the irradiation is stopped, and providing some Pd precursors remain, slower thermal decomposition can take place instead to form much smaller nanoparticles. Interestingly, these smaller particles tend to move towards the larger, laser-generated Pd cores to form core–shell assemblies. We are not aware of any previous work that reports the formation of such a core–shell structure for palladium, although aggregates resembling the shell structure have been observed previously.[14]

It is worth pointing out that the outer-shell aggregates of palladium nanoparticles are formed spontaneously without the influence of any external forces. As seen in Figure 4b, the core–shell structures are spherical. According to the diffusion-controlled-growth theory, every nucleus gathers the neighboring primary particles within its individual field of attraction, which extends as a circular arc around a spherical particle to a defined distance from the center of the particle. It is therefore not surprising that the nanostructures obtained here are spherical when this formation process is considered[17] as the particles tend to grow into a spherical shape in order to minimize their surface energy.[18] In the present case, the shape of the spontaneously formed core–shell aggregates also becomes spherical in order to minimize their surface energy.

In summary, stable core–shell palladium nanoparticles (100 ± 20 nm) are formed by laser decomposition followed by thermal decomposition of a solution containing $[Pd(PPh_3)_4]$. The core (20 ± 5 nm) consists of pure, metallic palladium while the shell is an aggregate of smaller Pd particles (<5 nm) interspersed with phosphanes. If the palladium precursor is allowed to decompose thermally only the shell structure is formed, whereas if the laser irradiation is prolonged only the core structure is observed. This provides a convenient method for tuning the structure of palladium nanoparticles by making use of both photochemical and thermal decomposition pathways.

Received: September 27, 2005
Published online: December 30, 2005

Keywords: aggregation · nanostructures · palladium · photochemistry · self-assembly

[1] A. Henglein, B. G. Ershov, M. Malow, *J. Phys. Chem.* **1995**, *99*, 14129.
[2] G. Schmid, M. Harms, J. O. Malm, J. O. Bovin, J. V. Ruitenbeck, H. W. Zandbergen, T. W. Fu, *J. Am. Chem. Soc.* **1993**, *115*, 2046.
[3] M. Beller, H. Fischer, K. Kuhlein, C. P. Reisinger, W. A. Herrmann, *J. Organomet. Chem.* **1996**, *520*, 257.
[4] M. T. Reetz, G. Lohmer, *Chem. Commun.* **1996**, 1921.
[5] R. Narayanan, M. A. El-Sayed, *J. Am. Chem. Soc.* **2004**, *126*, 8340.
[6] R. P. Andres, J. D. Bielefeld, J. I. Henderson, D. B. Janes, V. R. Kolagunta, C. P. Kubiak, W. J. Mahoney, R. G. Osifchin, *Science* **1996**, *273*, 1690.
[7] D. Feldheim, *The Electrochemical Society Interface Fall Meeting*, **2001**, pp. 22–25.
[8] A. K. Boal, F. Ilhan, J. E. DeRouchey, T. Thurn-Albrecht, T. P. Russell, V. M. Rotello, *Nature* **2000**, *404*, 746.
[9] X. G. Peng, T. E. Wilson, A. P. Alivisatos, P. G. Schultz, *Angew. Chem.* **1997**, *109*, 113; *Angew. Chem. Int. Ed. Engl.* **1997**, *36*, 145.
[10] S. Y. Chang, L. Liu, S. A. Asher, *J. Am. Chem. Soc.* **1994**, *116*, 6739.
[11] Z. Zhong, A. S. Subramanian, J. Highfield, K. Carpenter, A. Gedanken, *Chem. Eur. J.* **2005**, *11*, 1473.
[12] C. A. Mirkin, R. L. Letsinger, R. C. Mucic, J. J. Storhoff, *Nature* **1996**, *382*, 607.
[13] R. Elghanian, J. J. Storhoff, R. C. Mucic, R. L. Letsinger, C. A. Mirkin, *Science* **1997**, *277*, 1078.
[14] K. Naka, H. Itoh, Y. Chujo, *Nano Lett.* **2002**, *2*, 1183.

 © 2006 Wiley-VCH Verlag GmbH & Co. KGaA, Weinheim

[15] Joint Committee on Standards, Powder Diffraction, *Diffraction Data File, JCPDS Instrumental Center for Diffraction Data*, Pennsylvania, **1991**.
[16] T. Sugimoto, *Monodispersed Particles*, Elsevier, New York, **2001**.
[17] T. Sugimoto, E. J. J. Matijevic, *J. Colloid Interface Sci.* **1980**, *74*, 227.
[18] X. Peng, J. Wickham, A. P. Alivisatos, *J. Am. Chem. Soc.* **1998**, *120*, 5343.

 © 2006 Wiley-VCH Verlag GmbH & Co. KGaA, Weinheim

Ionic Liquids

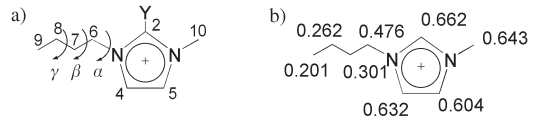
DOI: 10.1002/anie.200503745

The Local Structure of Ionic Liquids: Cation–Cation NOE Interactions and Internuclear Distances in Neat [BMIM][BF_4] and [BDMIM][BF_4]**

Andrea Mele, Greta Romanò, Matteo Giannone, Enzio Ragg, Giovanni Fronza, Guido Raos, and Valentina Marcon*

The increasing interest in room-temperature ionic liquids (RTILs) is related to their possible exploitation as environmentally friendly neoteric solvents because of their vanishing vapor pressure, thermal and chemical stability, air and moisture stability, wide liquidus range, solvent capability. Suitable applications of RTILs in synthesis, catalysis, biocatalysis, material science, and chemical engineering have been reported.[1] The rapidly increasing number and relevance of applications stimulated deeper understanding of the structure of RTILs in terms of intermolecular interactions that take place in the bulk liquid at the atomic level.[2] In such a context, the nuclear overhauser effect (NOE) is a powerful investigative tool, as it originates from dipolar interaction between pairs of nuclei and thus provides information on the molecular sites involved in the interactions. A pioneering study by Osteryoung and co-workers[3] demonstrated the existence of intermolecular NOE interactions between ring protons in 1-ethyl-2-methylimidazolium [EMIM]Cl·$AlCl_3$. The cation–cation contacts suggested a local or short-range structure of the liquid. The concept of a local structure in liquid methylimidazolium salts that resembles those found in the solid state has been stressed by some authors on the basis of X-ray diffraction,[4] neutron scattering,[5] and NMR spectroscopy.[6]

Herein, we present the first attempt to provide cation–cation distances in neat liquid 1-butyl-3-methylimidazolium tetrafluoroborate ([BMIM]$^+$[BF_4]$^-$ (**1a**)) and 1-butyl-2,3-dimethylimidazolium tetrafluoroborate ([BDMIM]$^+$[BF_4]$^-$ (**2a**); Scheme 1) by NMR spectroscopy. Two-dimensional



1a: Y= H $X^- = BF_4^-$
1b: Y=H $X^- = Cl^-$
1c: Y=H $X^- = Br^-$
1d: Y=H $X^- = [Tf_2]N^-$
2a: Y= Me $X^- = BF_4^-$
2b: Y= Me $X^- = Cl^-$
2c: Y= Me $X^- = PF_6^-$
2d: Y= Me $X^- = SbF_6^-$
2e: Y= Me $X^- = HSO_4^-$
2f: Y= Me X^- = Chloroferrate (II,III)
2g: Y= Me $X^- = [Tf_2]N^-$

Scheme 1. a) chemical structure and atom numbering of [BMIM]$^+$[X]$^-$ (**1**) and [BDMIM]$^+$[X]$^-$ (**2**). Curved arrows and Greek letters refer to the torsion angles of the butyl chain. b) Effective correlation times τ_{eff} (ns) at 305 K for **1a** and 315 K for **2a**. Tf = triflate.

NOE experiments (NOESY) on neat **1a** and **2a** showed both intra- and intermolecular contacts. Interestingly, no intermolecular contacts were detected in neat BMIM bis(trifluoromethylsulfonylimide) ([BMIM]$^+$[Tf_2N]$^-$ (**1d**)) and [BDMIM]$^+$[Tf_2N]$^-$ (**2g**), which bear a bulky and non-coordinating anion, possibly because of the effect of increased intercation distance rather than unfavorable correlation times. The methodology for the assessment of distances in the liquid relies upon the distance dependence of the cross-relaxation rate σ obtained by intermolecular NOE build-up rates.[7]

The cations **1a** and **2a** can be depicted as a polar head (the charged imidazolium ring) and an apolar tail (the *n*-butyl chain). NOESY spectra showed both head-to-head and head-to-tail cation–cation contacts. Herein, we assume that a) the tumbling of the system is isotropic and can be described by a single correlation time and b) the contact time of the cation–cation association is long enough to contribute to dipolar relaxation. These are reasonable hypotheses for head-to-head contacts and could be verified if individual correlation times

[*] Prof. A. Mele, G. Romanò, M. Giannone, Dr. G. Raos, V. Marcon
Dipartimento di Chimica
Materiali e Ingegneria Chimica "Giulio Natta" Politecnico di Milano
Via L. Mancinelli, 7, 20131 Milano (Italy)
Fax: (+39) 022-399-3080
E-mail: andrea.mele@polimi.it
Prof. E. Ragg
Dipartimento di Scienze Molecolari Agroalimentari
Università di Milano
Via Celoria, 2, 20133 Milano (Italy)
Prof. G. Fronza
CNR—Istituto di Chimica del Riconoscimento Molecolare
Via L. Mancinelli, 7
20131 Milano (Italy)

[**] We thank Dr. Luciana Malpezzi (Politecnico di Milano) for helpful discussions, Prof. Chieu D. Tran (Marquette University, Milwaukee (USA)) for a generous gift of ionic liquids, and Mr. Walter Panzeri (CNR-ICRM) for technical assistance. BMIM = 1-butyl-3-methyl imidazolium, BDMIM = 1-butyl-2,3-dimethylimidazolium.

Supporting information for this article is available on the WWW under http://www.angewandte.org or from the author.

 © 2006 Wiley-VCH Verlag GmbH & Co. KGaA, Weinheim

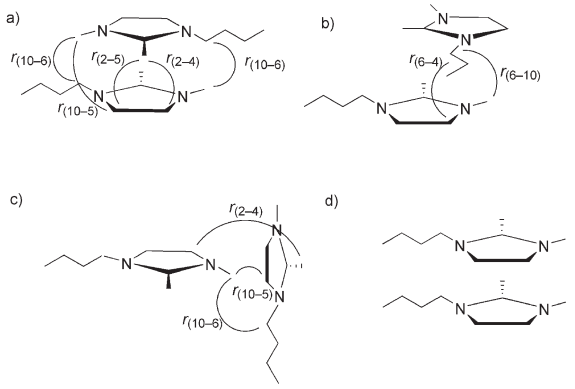
of the component of the noncovalent association could be experimentally assessed, as in the case of cation–anion association.[8] In the present case, such an approach cannot be applied as the individual components are chemically identical cations and therefore cannot be distinguished.

Quantitative NOE interaction data and average internuclear distances of the head-to-head interactions are presented in Tables 1 and 2. The rather short distances H5–H10, H2–H4, and H2–H5 are consistent with the presence of some type of aromatic-ring association, either stacking, as previously postulated for structurally related [EMIM] halides,[9] or perpendicular T-shaped assembly. Moreover, the short distances of H6–H4 and H6–H10 rule out the aggregation of imidazolium rings with parallel and eclipsed butyl chains as a dominant aggregation motif. Simple sketches of the aggregation motives of cations in **1a** and **2a** are depicted in Scheme 2.

Table 1: Corrected[17] cross-relaxation rate constant σ_{ij} (s^{-1}, absolute value) and average internuclear distances $\langle r_{ij}\rangle$ (Å) in **1a** (liquid) and **1b** and **1c** (single crystal).

Distance (type)	σ_{ij} [s^{-1}]	R^2 [a]	**1a**[b]	**1b**[c]	**1b**[d]	**1c**[e]
H2–H10 (H–Me)	0.2880	0.997	3.03[f]	2.82[g]	2.91[g]	2.75[g]
H5–H10 (H–Me)	0.1055	0.998	3.5(8)	3.47	–	3.44
H6–H4 (CH_2–H)	0.0545	0.914	4.0(0)	3.27	–	3.22

[a] Correlation coefficient for linear regression of NOE interaction intensity versus mixing time τ_m; only the regressions that afford $R^2 \geq 0.900$ are reported. [b] Average intermolecular distance (Å) of a given H-atom pair in liquid **1a** from NOE interactions (this work). [c] Average intermolecular distance (Å) of a given H-atom pair in single crystal of orthorhombic $[BMIM]^+Cl^-$; atomic coordinates taken from ref. [21]. [d] As in [c] but for monoclinic $[BMIM]^+Cl^-$, from ref. [4c]. [e] As in [c] but for monoclinic $[BMIM]^+Br^-$; from ref. [22]. [f] Reference proton–proton distance (intramolecular) calculated ab initio [average value from Equation (3)]; the distance is in good agreement with the equivalent in 1-methyl-3-ethylimidazolum tetrafluoroborate, as calculated from atomic coordinates of ab initio calculations reported by Tsuzuki et al.[23] [g] Intramolecular distance reported for the sake of comparison with [f].



Scheme 2. Sketch of the head-to-head aggregation motives of $[BMIM]^+$ and $[BDMIM]^+$ which are consistent with the displayed experimental intermolecular distances r_{ij}: a), b) sandwich, c) T-shaped, d) arrangement is not consistent with experimental data; for the sake of simplicity only $[BDMIM]^+$ ions are depicted.

Distance restraints alone, however, do not allow a conclusion about the parallelism of the imidazolium rings or the existence of π–π interactions to be drawn. It is interesting to note that a similar sketch for molecular arrangements have been recently reported for $[BMIM]^+[PF_6]^-$ by X-ray reflectivity study.[10] The distance values corresponding to head-to-head aggregation in liquids **1a** and **2a** can be compared to the values of the corresponding contacts in the solid state. To this end, the full set of intermolecular contacts of the type reported in the first column of Tables 1 and 2 was generated from the atomic coordinates of various $[BMIM]^+[X]^-$ ionic liquids taken from the literature, and the distances in the range for detectable NOE interactions ($r_{ij} \leq 4$ Å) were selected along with the average value (see the Experimental Section). The results are reported in the right-hand side of Tables 1 and 2. The comparison between the data obtained from the liquid and the solid state points out that the cation–cation distances obtained in this investigation are in the range of the homologous short contacts observed in the crystals of $[BMIM]^+$ and $[BDMIM]^+$ with miscellaneous anions. Indeed, the imidazolium cations in the liquid are close in space despite coulombic repulsion, and show, at short range, the

Table 2: Corrected[17] cross-relaxation rate constant σ_{ij} (s^{-1}, absolute value) and average internuclear distances $\langle r_{ij}\rangle$ (Å) in **2a** (liquid) and **2a**–**2f** (single crystal).

Distance (type)	σ_{ij} [s^{-1}]	R^2 [a]	**2a** (liquid)[b]	**2a**[c]	**2b**[d]	**2c**[c]	**2d**[c]	**2e**[d]	**2f**[d]
H4–H10 (H–Me)	0.2627	0.987	3.00[e]	2.97[f]	3.03[f]	2.99[f]	3.02[f]	3.00[f]	2.99[f]
H5–H10 (H–Me)	0.1807	0.999	3.1(9)	–	3.33	3.10	–	–	–
H5–H2 (H–Me)	0.1888	0.995	3.1(7)	–	⟨3.14⟩	3.59	3.24	–	3.17
					3.14				
					2.89				
					3.48				
					3.31				
					3.00				
H4–H2 (H–Me)	0.1435	0.967	3.3(2)	–	3.37	3.04	⟨3.19⟩	⟨3.41⟩	⟨3.35⟩
							3.23	3.50	3.27
							3.15	3.34	3.44
H6–H4 (CH_2–H)	0.1518	0.951	3.2(9)	⟨2.90⟩	⟨3.09⟩	–	–	⟨2.84⟩	–
				2.56	2.98			3.26	
				3.04	3.56			2.58	
				3.60					
				2.78					
H6–H10 (CH_2–Me)	0.2218	0.977	3.0(9)	–	⟨3.19⟩	⟨3.14⟩	⟨3.30⟩	–	⟨3.02⟩
					3.52	3.44	3.13		2.71
					3.22	3.05	3.51		3.54
					3.13	3.48			3.04
					2.90	2.55			
					3.31	3.55			
						3.29			

[a] As in note [a] in Table 1. [b] As in note [b] in Table 1. [c] As in note [c] in Table 1; atomic coordinates taken from ref. [11]]. [d] As in note [c]; from ref. [24]. [e] Reference proton–proton distance (intramolecular) calculated ab initio (this work) [average calculated by using Equation (3)]. [f] Intramolecular distance reported for the sake of comparison with [e].

 © 2006 Wiley-VCH Verlag GmbH & Co. KGaA, Weinheim

same attitude to "close packing" demonstrated in all the quoted single crystal structures, with the unique exception of the bulky $[SbF_6]^-$ ion. In particular, the close packing of **2a** observed in the solid state is described as the result of "maximizing non-directional interactions".[11] It seems that also for liquid **1a** and **2a** the same principle could be invoked to provide a rationale for the observed short intermolecular contacts. These findings provide quantitative foundation to the general idea of local structure in ionic liquids, direct evidence of the existence of polar domains in the pure liquid (in close analogy to that reported for the single crystal), and quantitative distance parameters to characterize such domains.

NOE interaction data at a mixing time of 50 ms for the head-to-tail contacts are reported in Table 3. The assessment of distances in this case is hampered by the internal motion and conformational flexibility of the butyl chain (Scheme 1, right) and will not be attempted herein.[12] Nevertheless, the data of Table 3 show that the butyl chain points toward the polar head of adjacent cations, as evidenced by NOE interactions H10–H9 and H5–H9 for both **1a** and **2a** and H2–H9 for **2a**. The NOE interactions that involve H8 and the polar head groups H2, H5, and H4 suggest that the apolar chain significantly penetrates the polar domain of surrounding cations. Consequently, the possibility of micellar aggregates is ruled out. In a similar way, the formation of extended nonpolar domains because of aggregation of the alkyl chains seems not to be consistent with the observed NOE interactions (the direct observation of intermolecular tail-to-tail contacts is not possible due to difficulty in separating intra- and intermolecular contributions to cross relaxation). However, the issue of alkyl-chain aggregation in $[BMIM]^+$ ions is still open to debate, as opposite conclusions have been reported by experimental[10] and theoretical methods.[13]

Table 3: Head-to-tail intermolecular NOE interactions [a] in liquid **1a** and **2a**.

NOE interactions [%]	H4–H7	H5–H7	H2–H7	H10–H7	H4–H8	H5–H8	H2–H8	H10–H8	H4–H9	H5–H9	H2–H9	H10–H9
1a	[b]	[b]	0.62	[b]	0.27	0.41	0.40	[b]	[b]	0.66	[b]	0.84
2a	0.48	0.79	0.99	[b]	[b]	0.49	[b]	0.64	[b]	0.57	0.86	0.73

[a] NOE (%) interactions are scaled to the number of equivalent spins and are thus directly comparable; only the NOE interactions that belong to linear regression with $R^2 \geq 0.900$ are reported. [b] Data not fulfilling the criterion reported above.

In conclusion, we have reported our attempt to use quantitative intermolecular NOE interaction studies for the assessment of the polar domains within bulk model RTILs. Cation–cation distances and sites of interaction thus obtained show significant correlation with data taken from X-ray diffraction studies of similar compounds. Moreover, semi-quantitative intermolecular NOE interactions point out significant interactions of the butyl chains with the polar domains. A detailed knowledge of the structural features of polar domains in RTILs is a requisite for a rational understanding of solute–solvent interactions. Indeed, recent neutron-scattering studies on a RTIL–benzene mixture demonstrated that the cation–cation first shell plays a key role in the mechanism of dissolution of benzene in 1,3-dimethylimidazolium hexafluorophosphate.[14] From this viewpoint, NOE interaction data can be complementary to partial radial distribution functions obtained from neutron scattering and contribute to a deeper understanding of the structure of the liquid.

Experimental Section

Compounds **1a**, **1d**, **2a**, and **2g** were synthesized as reported previously,[15] dried under vacuum at 70 °C overnight, and kept either under nitrogen or in a vacuum desiccator.

Routine NMR experiments and sample preparations were carried out on a Bruker Avance 500 instrument as previously described.[6a] Gradient-selected NOESY experiments were carried out using standard library sequences with mixing times τ_m of 10, 20, 30, 40, and 50 ms; longer mixing times gave spectra affected by spin diffusion.[16] All NOE interactions (intra- and intermolecular) were negative. The volumes of intermolecular cross peaks plotted versus τ_m provided the NOE interaction build-up curve; all the experimental points fell in the linear region. The cross-relaxation rates σ_{ij} were extracted from the slope of the linear fitting of the experimental points (initial rate approximation). Spin equivalence was accounted for.[17] Distances r_{ij} were calculated from Equation (1):

$$r_{ij} = r_{ref}\left[\frac{\sigma_{ref}}{\sigma_{ij}}\frac{\zeta_{ref}}{\zeta_{ij}}\right]^{1/6} \quad (1)$$

where r_{ref} is a "reference distance" (e.g., from X-ray diffraction, ab initio calculations, etc.) and ζ_{ij} is defined as:

$$\zeta_{ij} = K\,\tau_c\left(\frac{6}{1+4\omega^2\,\tau_c^2}\right) \quad (2)$$

Overall (effective) correlation times τ_{eff} (Scheme 1) were estimated through $^{13}C\{^1H\}$ NOE factors η measured at the same temperature of NOESY experiments, assuming only dipole–dipole relaxation. The values thus obtained should be considered as a first approximation as other mechanisms can be effective.[18] The measurements were carried out in quintuplicate.

Crystallographic data were processed using SHELXL-97.[19] Average distance values reported in Table 1 are calculated as in Equation (3):

$$\langle r_{ij}\rangle = \left(\frac{1}{n}\sum_{k=1}^{n}\frac{1}{r_{ij,k}^3}\right)^{-1/3} \quad (3)$$

Ab initio calculations on **1a** and **2a** were based on hybrid density functional theory (DFT). The geometries were optimized at the B3LYP/6-31G** level, with the GAMESS-USA program.[20] NOESY spectra of **1a** and **2a** are available in the Supporting Information.

Received: October 21, 2005
Published online: January 13, 2006

Keywords: ionic liquids · local structure · molten salts · NMR spectroscopy · NOE interactions

 © 2006 Wiley-VCH Verlag GmbH & Co. KGaA, Weinheim

[1] *Ionic Liquids IIIB: Fundamentals, Progress, Challenges and Opportunities* (Eds.: R. Rogers, K. R. Seddon), ACS Symposium Series 902, American Chemical Society, Washington, DC, **2005**.
[2] C. Chiappe, D. Pieraccini, *J. Phys. Org. Chem.* **2005**, *18*, 275 – 297.
[3] R. A. Mantz, P. C. Trulove, R. T. Carlin, R. A. Osteryoung, *Inorg. Chem.* **1995**, *34*, 3846 – 3847.
[4] a) J. Fuller, R. T. Carlin, H. C. De Long, D. Haworth, *J. Chem. Soc. Chem. Commum.* **1994**, 299 – 300; b) S. Hayashi, R. Ozawa, H. Hamaguchi, *Chem. Lett.* **2003**, *32*, 498 – 499; c) S. Saha, S. Hayashi, A. Kobayashi, H. Hamaguchi, *Chem. Lett.* **2003**, *32*, 740 – 741.
[5] C. Hardacre, J. D. Holbrey, S. E. J. McMath, D. T. Bowron, A. K. Soper, *J. Chem. Phys.* **2003**, *118*, 273 – 278.
[6] a) J. Dupont, P. A. Z. Suarez, R. F. de Souza, R. A. Burrow, J. P. Kintzinger, *Chem. Eur. J.* **2000**, *6*, 2377 – 2381; b) A. Mele, C. Tran, S. H. De Paoli Lacerda, *Angew. Chem.* **2003**, *115*, 4500 – 4502; *Angew. Chem. Int. Ed.* **2003**, *42*, 4364 – 4366; c) A. Mele in *Ionic Liquids IIIA: Fundamentals, Progress, Challenges and Opportunities* (Eds.: R. Rogers, K. R. Seddon), ACS Symposium Series 901, American Chemical Society, Washington DC. **2005**, pp. 2–17; d) C. S. Consorti, P. A. Z. Suarez, R. F. de Souza, R. A. Burrow, D. H. Farrar, A. J. Lough, W. Loh, L. H. M. de Silva, J. Dupont, *J. Phys. Chem. B* **2005**, *109*, 4341 – 4349; e) J. Dupont, *J. Braz. Chem. Soc.* **2004**, *15*, 341 – 350.
[7] D. Neuhaus, M. P. Williamson, *The Nuclear Overhauser Effect in Structural and Conformational Analysis*, Wiley-VCH, New York, **2000**, pp. 98 – 128.
[8] C. Zuccaccia, G. Bellachioma, G. Cardaci, A. Macchioni, *J. Am. Chem. Soc.* **2001**, *123*, 11020 – 11028.
[9] A. G. Avent, P. A. Chaloner, M. P. Day, K. R. Seddon, T. Welton, *J. Chem. Soc. Dalton Trans.* **1994**, 3405 – 3413.
[10] E. Soluskin, B. M. Ocko, L. Taman, I. Kuzmenko, T. Gog, M. Deutsch, *J. Am. Chem. Soc.* **2005**, *127*, 7796 – 7804.
[11] P. Kölle, R. Dronskowski, *Eur. J. Inorg. Chem.* **2004**, 2313 – 2320.
[12] The effective correlation times of nonquaternary carbon atoms displayed in Scheme 1 clearly show that the butyl chain undergoes unrestricted motion. The conformational flexibility of the chain is documented by the analysis of the *J*(H6,H7) and *J*(H7,H8) coupling constants and is in turn connected to the β and γ torsion angles (see Scheme 1). Indeed, the *trans t* population for β and γ is 49 and 59% for **1a** and 54 and 59% for **2a** (both liquid, this work). Conversely, in the solid state the β angle assumes either a pure $\pm g$ (orthorombic: **1b**, **1c**, **2b**, **2c**, **2e**) or pure *t* conformation (monoclinic: **1b**, **2a**). The dihedral angle corresponding to the γ torsion angle is reported as *t* in all the reported X-ray structures. Only **2f** showed disordered butyl chains.
[13] Y. Wang, G. A. Voth, *J. Am. Chem. Soc.* **2005**, *127*, 12192 – 12193.
[14] M. Deetlefs, C. Hardacre, M. Nieuwenhuyzen, O. Sheppard, A. K. Soper, *J. Phys. Chem. B* **2005**, *109*, 1593 – 1598.
[15] a) J. D. Holbrey, K. R. Seddon, *J. Chem. Soc. Dalton Trans.* **1999**, 2133 – 2140; b) J. G. Huddleston, H. D. Willauer, R. P. Swatloski, A. E. Visser, R. D. Rogers, *Chem. Commun.* **1998**, 1765 – 1766; c) P. Bonhote, A. P. Dias, N. Papageourgiou, K. Kalyanasundaram, M. Gratzel, *Inorg. Chem.* **1996**, *35*, 1168 – 1178.
[16] N. E. Heimer, R. E. Del Sesto, W. R. Carper, *Magn. Reson. Chem.* **2004**, *42*, 71 – 75.
[17] S. Macura, R. R. Ernst, *Mol. Phys.* **1980**, *41*, 95.
[18] J. H. Antony, A. Dolle, D. Mertens, P. Wasserscheid, W. R. Carper, P. G. Wahlbeck, *J. Phys. Chem. A* **2005**, *109*, 6676 – 6682.
[19] G. M. Sheldrick, SHELXL-97, Program for the Refinement of Crystal Structures, University of Göttingen (Germany) **1997**.
[20] M. W. Schmidt, K. K. Baldridge, J. A. Boatz, S. T. Elbert, M. S. Gordon, J. H. Jensen, S. Koseki, N. Matsunaga, K. A. Nguyen, S. J. Su, T. L. Windus, M. Dupuis, J. A. Montgomery, *J. Comput. Chem.* **1993**, *14*, 1347 – 1363.
[21] J. D. Holbrey, W. M. Reichert, M. Nieuwenhuyzen, S. Johnson, K. R. Seddon, R. D. Rogers, *Chem. Commun.* **2003**, 1636 – 1637.
[22] D. G. Golovanov, K. A. Lyssenko, M. Y. Antipin, Y. S. Vygodskii, E. I. Lozinskaya, A. S. Shaplow, *Cryst. Growth Des.* **2005**, *5*, 337 – 340.
[23] S. Tsuzuki, H. Tokuda, H. Hayamizu, M. Watanabe, *J. Phys. Chem. B* **2005**, *109*, 16474 – 16481.
[24] P. Kölle, R. Dronskowski, *Inorg. Chem.* **2004**, *43*, 2803 – 2809.

 © 2006 Wiley-VCH Verlag GmbH & Co. KGaA, Weinheim

Vitamin E

DOI: 10.1002/anie.200503123

A Biomimetic Chromanol Cyclization Leading to α-Tocopherol**

*Christian Grütter, Emma Alonso, Antoinette Chougnet, and Wolf-D. Woggon**

The diastereoselective formation of the chromanol ring is one of the most challenging reactions during the biosynthesis of tocopherols in photosynthetic organisms. We discovered the enzyme that catalyzes this transformation in the cyanobacteria *Anabaena variabilis*[1] and subsequently determined its substrate specificity[2] and recently cloned the tocopherol cyclase from the related *Anabaena* sp. into *E. coli*.[3] The enzymatic reaction mechanism was determined by isotopic labeling experiments,[4] which revealed that the reaction proceeds by *si* protonation of the double bond of **1** followed by *re* attack of the phenolic oxygen to yield γ-tocopherol (**2**; Scheme 1).

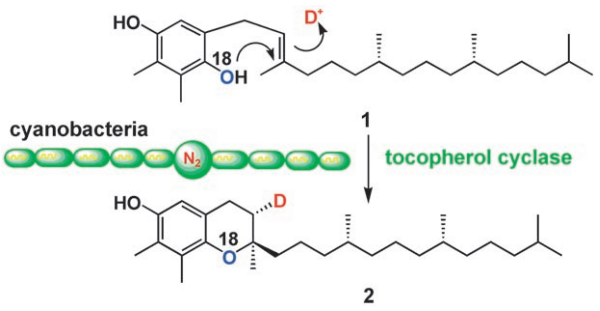
Two further observations suggest a concerted nonsynchronous cyclization, during which positive charge develops at the carbon atom that is trapped by the phenol (see **3**, Scheme 2): 1) the tetrahydroisoquinolinium terpenoid **4** as a transition-state analogue is an excellent inhibitor (IC_{50} = 1.4 nM) of tocopherol cyclase,[5] and 2) the epoxide of **1** cyclizes under acidic conditions yielding two compounds, the five-membered-ring "Baldwin" product and the six-membered ring analogue of the enzymatic product (4:6 ratio).[3,4]

[*] C. Grütter, Dr. E. Alonso, Prof. Dr. A. Chougnet, Prof. Dr. W.-D. Woggon
Department of Chemistry
University of Basel
St. Johanns-Ring 19, 4056 Basel (Switzerland)
Fax: (+41) 61-267-1109
E-mail: wolf-d.woggon@unibas.ch

[**] We thank DSM, F. Hoffmann–La Roche, and the Swiss National Science Foundation for generous financial support, and Dr. Daniel Häussinger for NMR spectra.

Supporting information for this article, including spectroscopic data of **5**, **6**, **13**, **18**, and **22**-*p*TsOH, is available on the WWW under http://www.angewandte.org or from the author.

WILEY InterScience DISCOVER SOMETHING GREAT
© 2006 Wiley-VCH Verlag GmbH & Co. KGaA, Weinheim



Scheme 1. Chromanol ring closure catalyzed by tocopherol cyclase.

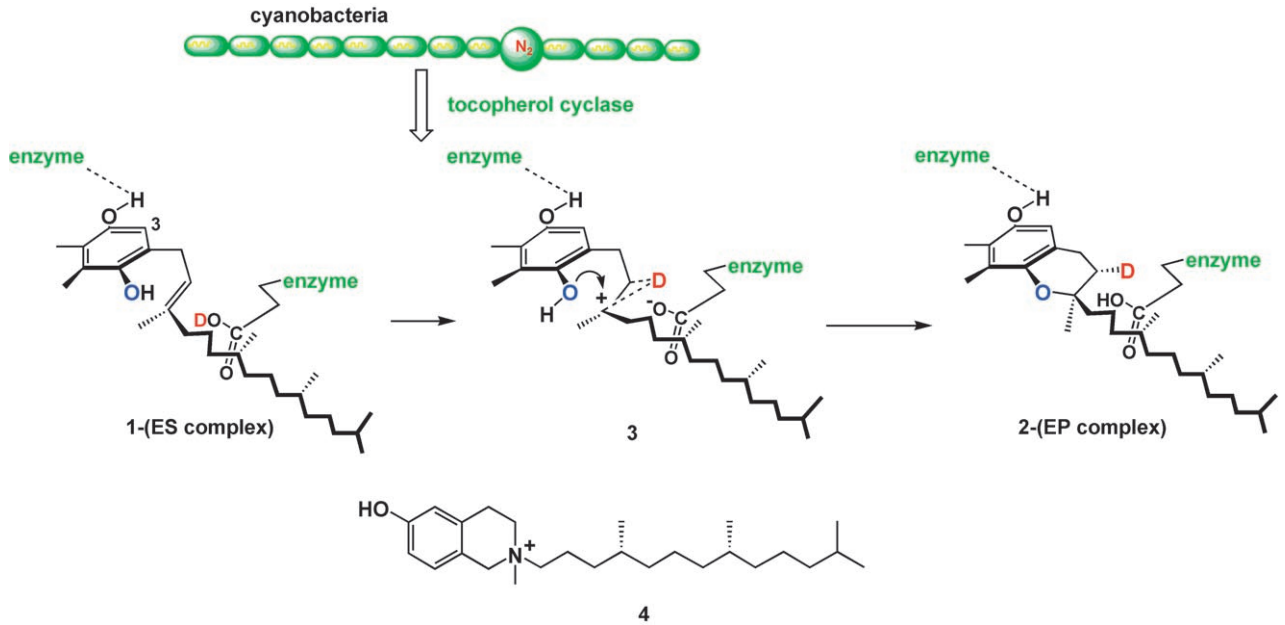
The structure of the enzyme–substrate (ES) complex of **1** is tentatively drawn in a conformation that positions the double bond in between the phenolic oxygen atom and an acid group from the protein.[3] It appears that the enzyme enforces this activated conformation in the enzyme–substrate complex; computer modeling studies show that **1**, in solution or in the gas phase, adopts a conformation in which the phytyl side chain is bent down such that the double bond is 6–7 Å apart from the phenol.

Herein, we report on a new biomimetic approach that leads to enantiomerically enriched α-tocopherol. (For earlier syntheses of tocopherols[6,7] and for two recent reports regarding access to the chromanol unit of tocopherols, see references [8,9] and references cited therein.) Our concept comprises 1) the modification of structure **1** by attaching a chiral acid at C3, b) restriction of the conformational freedom of this acid through derivatization of the phenolic OH group at C4 using a bulky substitutent, 3) the choice of a suitable chiral acid, and 4) removal/recovery of the chiral unit after cyclization and determination of the product on an α-tocopherol derivative.

First, the target prolinyl phytylhydroquinone derivatives **5** and **6** were prepared from the monoprotected hydroquinone **7** by addition of the Mannich reagents **8** or **9** and followed by protecting group manipulations (Scheme 3). Exploratory experiments with **5** and **6** in the presence of either Lewis or Brønsted acids gave cyclized **10** and **11**, respectively, which were subsequently converted into the α-tocopheryl camphanate **12** (Scheme 4). The diastereomeric excess (*de*) was determined by HPLC, and a maximum value of 35–40% *de* was obtained in favor of the *S* configuration at C2. As the acidity of the chiral unit had no profound effect on the reaction rate, yield, and *de* value, it was concluded that systems **5** and **6** were too flexible and the distances between the acids and the double bonds were too large.

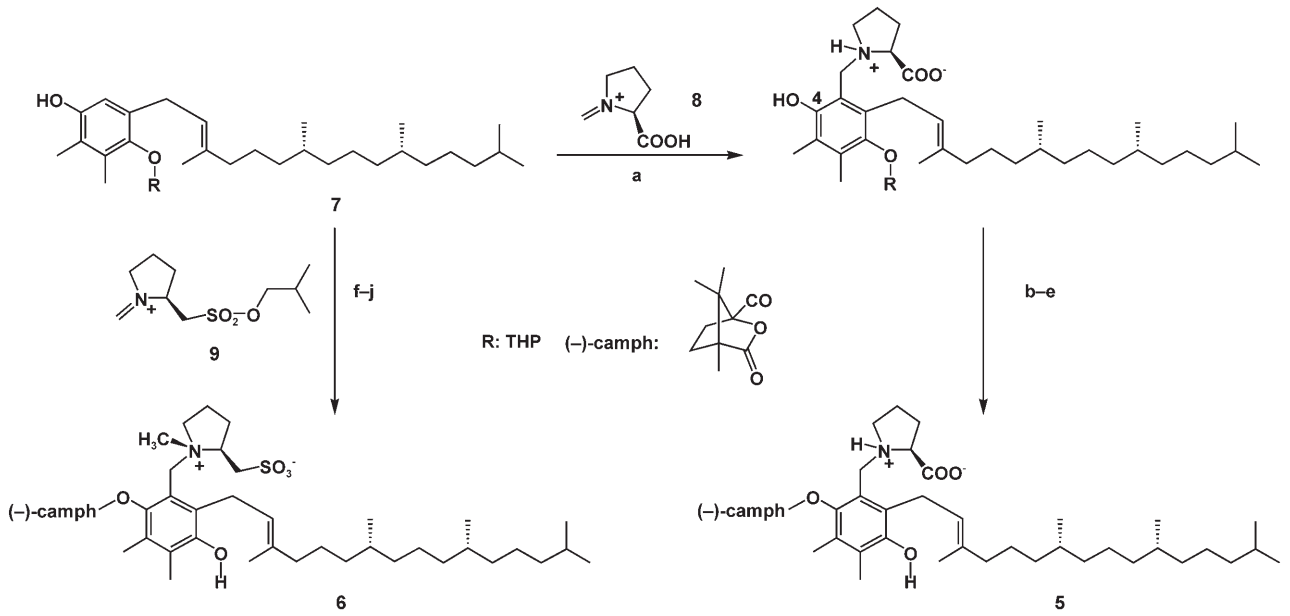
Accordingly, we thought a more-rigid acidic spacer would be advantageous to accomplish higher diasteromeric excesses and hence we prepared compound **13** (Scheme 5). Cyclization of **13** in the presence of *p*TsOH indeed confirmed the idea, as **12** was obtained with a *de* value of 80% and (2*S*)-**14** was obtained as the dominant diastereoisomer (80% overall yield). In contrast to **13**, the monoesters **15** and **16** (Figure 1) were less efficient, yielding a maximum diastereomeric excess of 47%, which indicates cooperativity of the two aspartate COOH groups in the presence of *p*TsOH. When the aspartate residue of **13** was replaced by serine or threonine to give **17** and **18**, respectively, the Lewis acid $SnCl_4$ was the additive of choice rather than *p*TsOH. For example, with (−)-(*S*,*S*)-**18** and $SnCl_4$ a *de* value of 77% for the final product **12** (80% overall yield) was observed; that is, the same value was observed, within experimental error, as that for the cyclization of **13** with *p*TsOH.

The proposed mechanism of this reaction (Figure 2) resembles the formalism described by Yamamoto and coworkers[10,11] for a binol/$SnCl_4$ system and apparently belongs to the category of "Lewis acid assisted, Brønsted acid



Scheme 2. The reaction mechanism of ring closure catalyzed by tocopherol cyclase. ES = enzyme–substrate; EP = enzyme–product.

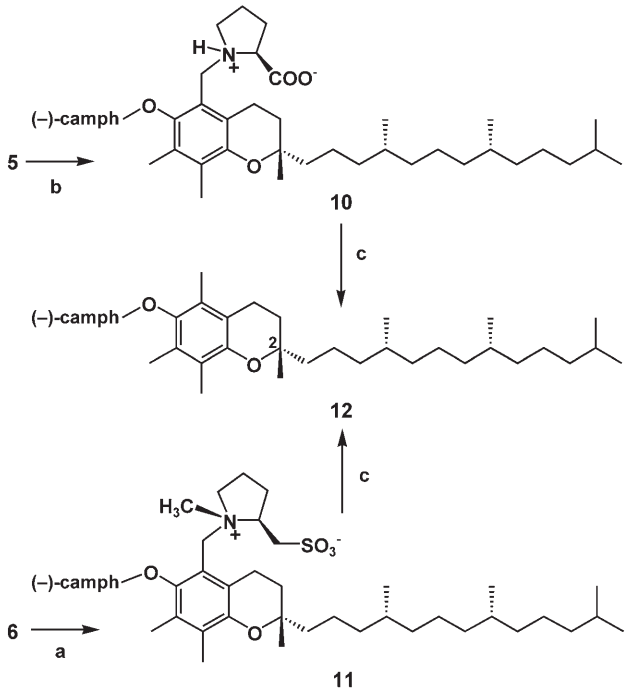
 © 2006 Wiley-VCH Verlag GmbH & Co. KGaA, Weinheim



Scheme 3. Synthesis of cyclization precursors **5** and **6**. Reagents and conditions: a) 1) (*S*)-proline, HCHO (35% in water), 40°C, 10 min; 2) **8** (in MeOH), **7**, 40°C, 8 h, 87%; b) $(Me)_3SiCHN_2$, MeOH, room temperature, 30 min, 98%; c) (−)-camphanoyl chloride, DMAP, CH_2Cl_2, room temperature, 2 h, 96%; d) LiI, EtOAc, 70°C, under N_2, 13 h, 70%; e) 1 N HCl, THF, room temperature, 1 h, 95%; f) **9** added to **7** in MeOH, 50°C, 2 days, 80%; g) (−)-camphanoyl chloride, DMAP, CH_2Cl_2, room temperature, 1 h, 98%; h) MeOTf, DMAP, room temperature, 4 h, 83%; i) LiI, EtOAc, 40°C, 16 h, 65%; j) 1 N HCl, THF, room temperature, 1 h, 89%. THP = tetrahydropyranyl; DMAP = (4-dimethyl)aminopyridine; Tf = trifluoromethanesulfonyl.

supported reactions" (see compound **19**; binol = 1,1′-bi-2-naphthol).

When the *S*-configured amino acids and the (−)-camphanate in **13** were replaced by their enantiomers to give



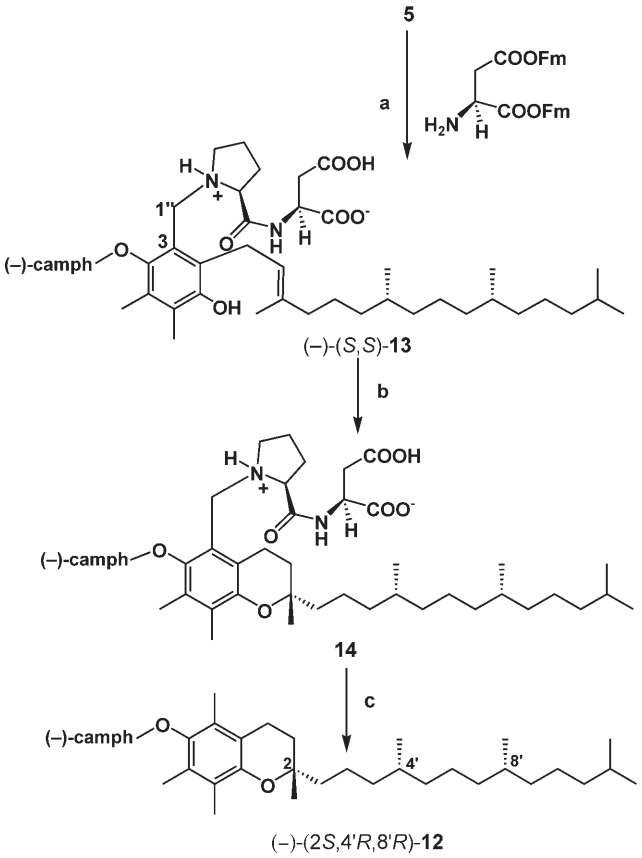
Scheme 4. Chromanol cyclization of **5** and **6**. Reagents and conditions: a) *p*TsOH (2.5 equiv), propylene carbonate, 50°C, 17 h, 70%, 38% *de*; b) $AlCl_3$ (0.7 equiv), CH_2Cl_2, room temperature, 2 days, 65%, 35% *de*; c) Pd/C (15–20%), HCOOH, MeOH, H_2 (85 bar, room temperature) 2 days, 92%. *p*TsOH = *p*-toluenesulfonic acid.

(+)-(*R*,*R*)-**20**, cyclization of the latter occurred in the presence of *p*TsOH to yield the natural (2*R*,4′*R*,8′*R*)-α-tocopherol (**21**) as the dominant diastereoisomer (70% *de*) of the reaction (Scheme 6).[12]

The superior results with the proline–aspartate phytylhydroquinone **13** relative to the monoesters **15** and **16** suggest cooperativity of the two "free" COOH units. Furthermore, as more than one equivalent of *p*TsOH is required for cyclization a Brønsted acid assisted, Brønsted acid supported reaction may be operative.[10] The structure of the reactive supramolecular assembly could be tentatively assigned from ^{1}H NMR spectroscopy of the precursor (−)-(*R*,*R*)-**22** in CH_2Cl_2 at 5°C. In the absence of *p*TsOH a slightly resolved NMR spectrum was obtained that showed the presence of two conformations in 6:4 ratio. After addition of two equivalents of *p*TsOH the system converged to one conformation that displayed a well-resolved signal pattern. From these spectra a significant NOE between a benzylic proton (at C7, in green) and the proton at the stereogenic center of the proline moiety (at C2′, in green) was observed which indicated that the proline--aspartate unit of **22** lies below the double bond (Scheme 7), ready to add the proton from the *si* face in an enzyme-like fashion.

Interestingly a further significant NOE was detected between the *meta*-positioned hydrogen atom of *p*TsOH (in red) and the allylic methyl group of the phytyl side chain. These results suggest that the second *p*TsOH molecule forms the fairly stable complex **22**-*p*TsOH through hydrogen bonding of the two S=O bonds to aspartate COOH groups to enhance the acidity of *p*TsOH. Accordingly, the proton required to initiate cyclization appears to be delivered from the second *p*TsOH moiety.

 © 2006 Wiley-VCH Verlag GmbH & Co. KGaA, Weinheim



Scheme 5. Synthesis of the proline–aspartate phytylhydroquinone **13**, and its cyclization to the chromanol. Reagents and conditions: a) 1) HATU (1.4 equiv), DIPEA (6 equiv), di-Fm-aspartate (3 equiv), CH_2Cl_2, room temperature, 2 h; 2) 20% Et_2NH in CH_2Cl_2, 1 h, room temperature; iii) $KHSO_4$, 59%; b) *p*TsOH (2 equiv), CH_2Cl_2, room temperature, 2 days, 85%; c) Pd/C (15–20%), HCOOH, MeOH, H_2 (85 bar, room temperature) 2 days, 92%. HATU = *N*,*N*,*N*,*N*-tetramethyluronium hexafluorophosphate; DIPEA = diisopropylethylamine; Fm = 9-fluorenylmethyl.

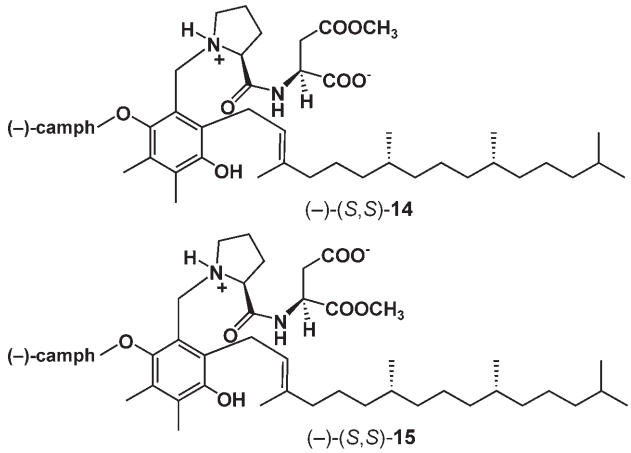


Figure 1. Aspartate monoesters for cyclization.

In conclusion, through attachment of a proline–aspartate unit to a phytylhydroquinone an enzyme-like conformation of the cyclization precursor is created that allows for diastereoface-selective preferential protonation of the double bond and concomitant attack of the phenolic oxygen atom. Similar results are obtained with a proline–threonine moiety in the presence of $SnCl_4$. To the bets of our knowledge, this is the first biomimetic cyclization that leads to the chromane structure of tocopherols with high diastereoselectivity.

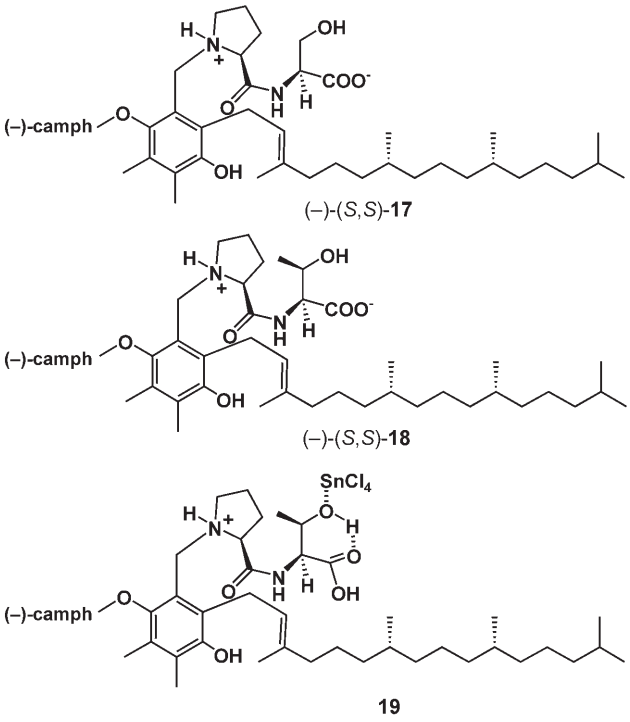
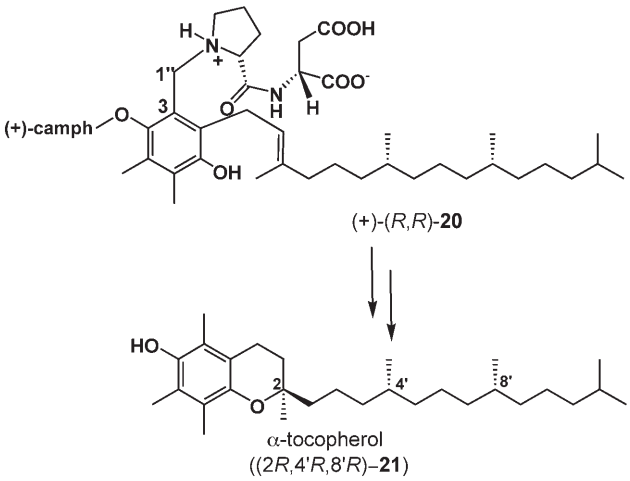


Figure 2. Proline–serine and proline–threonine cyclization precursors **16** and **17**, respectively.

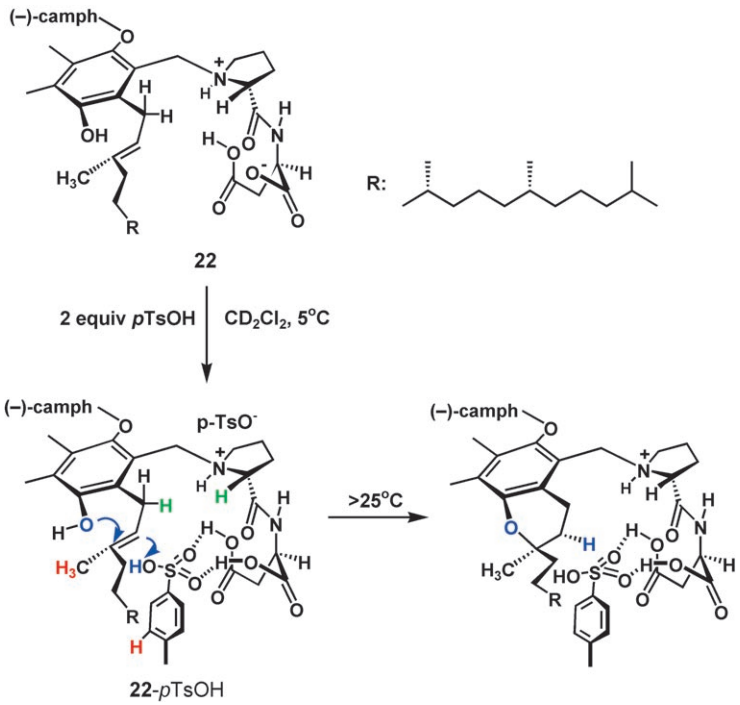


Scheme 6. Cyclization of (+)-(*R*,*R*)-**20** to give natural α-tocopherol.

Experimental Section

General procedure for the acid-supported cyclization of phytylhydroquinones: Anhydrous *p*-toluenesulfonic acid (0.0715 mmol, 2 equiv; 1.23 mL of a 0.058 M solution (10 mg mL^{-1}) in CH_3CN) was added to a round-bottomed flask containing **13** (30.0 mg, 0.0358 mmol) in CH_2Cl_2 (40 mL) at room temperature under argon,

 © 2006 Wiley-VCH Verlag GmbH & Co. KGaA, Weinheim



Scheme 7. Proposed mechanism for the diastereoselective protonation of a phytylhydroquinone. Colored protons show significant NOE interactions (see text for details).

and the solution was stirred for 48 h at this temperature. Saturated $NaHCO_3$ solution (10 mL) was added, and the mixture was extracted with CH_2Cl_2 (3 × 10 mL). The organic layers were combined, dried (Na_2SO_4), and filtered. Evaporation of the solvents provided the crude product, which was taken up in CH_2Cl_2/MeOH (4:1) and filtered through celite to give **14** as a colorless solid (28 mg, 93 %). This material was used directly in the reduction step.

General procedure for reductive debenzylation: Formic acid (99 %; 15 μL) and palladium hydroxide (6 mg) on activated charcoal (15–20 % Pd, moistened with water ≈ 50 %) were added to a solution of **14** (3.0 mg, 3.58 μmol) in a mixture of MeOH (2.5 mL) and CH_2Cl_2 (0.1 mL). The reaction was stirred at room temperature under a hydrogen pressure of 85 bar for 2 days. The reaction mixture was filtered through a cotton plug, quenched with a saturated solution of $NaHCO_3$, and extracted with CH_2Cl_2 (2 × 10 mL). The combined organic layers were dried (Na_2SO_4) and filtered, and the solvents were removed under vacuum. The resulting crude product was filtered, first through celite and then through silica gel (CH_2Cl_2/MeOH 95:5) to give **12** (2.3 mg, 92 %). The diastereomeric excess (*de*) was determined by HPLC (DAICEL Chiralpac AD-H, 1 % 2-propanol in heptane; 0.5 mL min^{-1}); retention time: 28.9 min for (–)-(*S*,*R*,*R*)-**12** and 30.9 min for (–)-(*R*,*R*,*R*)-**12**, ratio 9:1). Correlations were made by admixing the camphanate of authentic all-(*R*)-α-tocopherol.

Received: September 2, 2005

Keywords: biomimetic synthesis · cyclization · diastereoselectivity · enzyme catalysis · peptides

[1] A. Stocker, A. Rüttimann, W.-D. Woggon, *Helv. Chim. Acta* **1993**, *76*, 1729.
[2] A. Stocker, H. Fretz, H. Frick, A. Rüttimann, W.-D. Woggon, *Bioorg. Med. Chem.* **1996**, *4*, 1129.
[3] M. Christen, A. Chougnet, R. Manetsch, J. Chapelat, B. Christen U. Jenal, W.-D. Woggon, unpublished results.
[4] A. Stocker, T. Netscher, A. Rüttimann, R. K. Müller, H. Schneider, L. J. Todaro, G. Derungs, W.-D. Woggon, *Helv. Chim. Acta* **1994**, *77*, 1721.
[5] R. Manetsch, L. Zheng, M. T. Reymond, W.-D. Woggon, J.-L. Reymond, *Chem. Eur. J.* **2004**, *10*, 2487.
[6] T. Netscher, *Chimia* **1996**, *50*, 563.
[7] T. Netscher, M. Scalone, R. Schmid in *Asymmetric Catalysis on an Industrial Scale* (Eds.: H. U. Blaser, E. Schmidt), Wiley-VCH, Weinheim, **2004**, p. 71.
[8] L. F. Tietze, K. M. Sommer, J. Zinngrebe, F. Stecker, *Angew. Chem.* **2005**, *117*, 262; *Angew. Chem. Int. Ed.* **2005**, *44*, 257.
[9] B. M. Trost, H. C. Shen, L. Dong, J.-P. Surivet, C. Sylvain, *J. Am. Chem. Soc.* **2004**, *126*, 11966.
[10] H. Yamamoto, K. Futatsugi, *Angew. Chem.* **2005**, *117*, 1958; *Angew. Chem. Int. Ed.* **2005**, *44*, 1924.
[11] M. Uyanik, H. Ishibashi, K. Ishihara, H. Yamamoto, *Org. Lett.* **2005**, *7*, 1601.
[12] The diastereo-face-selectivity depends on the configurations of the dipeptide, whereas the influence of the camphanoyl unit is negligible. The use of (–)-camphanate is purely for convenience, as tocopherols that are epimeric at C2 can be separated by HPLC and hence the *de* of the cyclization can be easily determined (C. Grütter, E. Alonso, A. Chougnet, W.-D. Woggon, unpublished results).

 © 2006 Wiley-VCH Verlag GmbH & Co. KGaA, Weinheim

Enzyme Models

DOI: 10.1002/anie.200503602

A Biomimetic Model for the Active Site of Iron-Only Hydrogenases Covalently Bonded to a Porphyrin Photosensitizer**

Li-Cheng Song, Ming-Yi Tang, Fu-Hai Su, and Qing-Mei Hu*

Hydrogenases are highly efficient enzymes that catalyze the production and consumption of hydrogen reversibly in a wide variety of microorganisms.[1–3] Hydrogenases are generally classified into two major groups depending on their metal content, namely NiFe hydrogenases and Fe-only hydrogenases.[4] Although both groups of hydrogenases catalyze the consumption and production of hydrogen, the Fe-only hydrogenases have much greater reaction rates for H_2 production than NiFe hydrogenases.[5] Therefore, Fe-only hydrogenases (hereafter referred to as FeHases) have received much more attention than NiFe hydrogenases in biomimetic studies

[*] Prof. L.-C. Song, Dr. M.-Y. Tang, Dr. F.-H. Su, Prof. Q.-M. Hu
Department of Chemistry and
The State Key Laboratory of Elemento-Organic Chemistry
Nankai University
Tianjin 300071 (China)
Fax: (+86) 22-2350-4853
E-mail: lcsong@nankai.edu.cn

[**] The authors are grateful to the NSF of China for financial support of this work.

WILEY InterScience DISCOVER SOMETHING GREAT
© 2006 Wiley-VCH Verlag GmbH & Co. KGaA, Weinheim

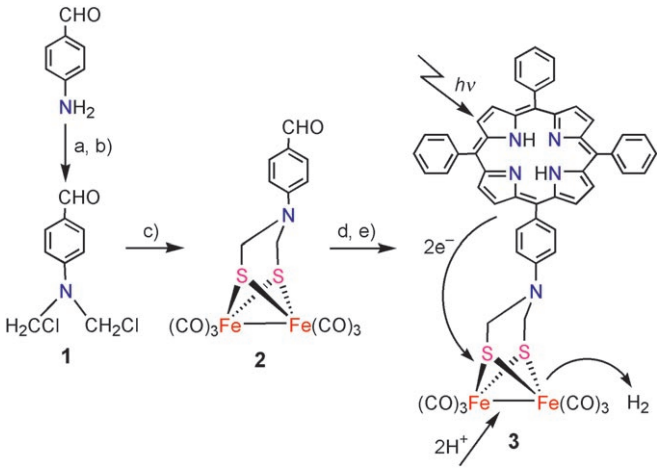
aimed at synthesizing model compounds that can act as H_2 production catalysts that are as effective as those found in the natural systems.[6,7]

Recent X-ray crystallographic[8] and IR spectroscopic[9] studies have indicated that the active site of FeHases, the H-cluster, consists of two iron atoms that are within bonding distance of each other and bridged by a dithiolate ligand. These studies also indicated that there are three other ligands, namely CO, CN^-, and a cysteine-*S*-linked cubic 4Fe4S cluster, coordinated to the two dithiolate-bridged iron atoms; the cubic 4Fe4S cluster is actually the part of the electron transfer chain that links the active site of FeHases. Numerous model compounds have been successfully synthesized and structurally characterized based on the above-mentioned structural studies regarding the active site.[10]

We recently initiated a study on the possibility of linking a porphyrin-type photosensitizer to this simple biomimetic model in order to prepare a new type of light-driven model compounds. Fortunately, we were able to synthesize one such model compound, namely **3** (see Scheme 1), in which a photosensitizing tetraphenylporphyrin group (TPP) is covalently linked to the N atom of the diiron azadithiolate (ADT) moiety $[\{(\mu\text{-}SCH_2)_2N\}Fe_2(CO)_6]$. It follows that our light-driven model compound **3** is different from the previously reported cationic model in which a Ru^{II} complex $[Ru(terpy)_2]^{2+}$ is the photosensitizer (terpy = terpyridyl).[11] We chose TPP as the photosensitizer because: 1) TPP can absorb as much as 46% of the energy of sunlight;[12] 2) the lifetime of the excited state of TPP is much longer than those of common Ru^{II}-based photosensitizers;[12] 3) $[Ru(terpy)_2]^{2+}$ is cationic, while TPP is neutral; and 4) as a result of the above three points, the expected photoinduced electron transfer in **3** should be easier than in the previously reported cationic model. The ADT-bridged diiron moiety was selected to constitute this model, because it has recently been suggested that the ADT bridge plays an important role in H_2 production in the natural system.[13] In fact, diiron–ADT complexes have proved to be some of the best simple models for the active site of FeHases.[10c,f]

The synthetic route to **3** and its expected light-driven process are briefly illustrated in Scheme 1. First, *N*,*N*-di(chloromethyl)-4-formylaniline (**1**) is prepared by treatment of *p*-aminobenzaldehyde with paraformaldehyde and then with $SOCl_2$.[14] Second, compound **1** was treated with di-μ-sulfanylbis(tricarbonyliron)[15] to afford the simple *p*-benzaldehyde-substituted model **2**. Finally, the target model **3** was synthesized by treatment of **2** with pyrrole and benzaldehyde in a 1:4:3 molar ratio followed by the oxidant *p*-chloranil.[16] In the expected light-driven process, model **3** should first absorb a photon at the photosensitizer TPP. This photoexcited TPP is then oxidatively quenched by the diiron unit to give a reduced iron species. After regeneration of the TPP by transfer of an electron from an external donor, this process is repeated to produce a doubly reduced diiron species that should be able to drive the reduction of protons to hydrogen (Scheme 1).

The new compounds **1**–**3** were characterized by elemental analysis and various spectroscopic techniques. The IR spectrum of **3** shows three absorption bands at 1558, 1472, and 1350 cm^{-1}, assigned to the skeletal vibrations of the pyrrole



Scheme 1. a) $(CH_2O)_n$, CH_2Cl_2, room temperature, 5 h; b) $SOCl_2$, room temperature, 1 h; c) $[(\mu\text{-}HS)_2Fe_2(CO)_6]$, THF, room temperature, 12 h; d) PhCHO, pyrrole, CF_3CO_2H, CH_2Cl_2, room temperature, 15 h; e) *p*-chloranil, reflux, 1 h.

rings in the porphyrin unit,[17] and strong absorption bands at 2073, 2033, and 1996 cm^{-1} due to the terminal CO groups in the diiron–ADT moiety. The ^1H NMR spectrum of **3** displays a singlet at $\delta = 4.55$ ppm for the CH_2 groups in the diiron–ADT moiety and another singlet at $\delta = -2.76$ ppm for the NH groups of the porphyrin unit.[18] The electronic absorption spectra of **3** and TPP were also recorded. As shown in Figure 1, there is one Soret band at 419 nm in the near-UV

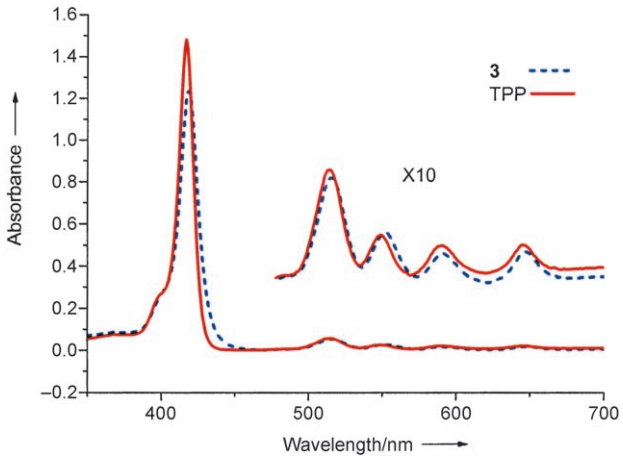


Figure 1. UV/Vis spectra of **3** and TPP in CH_2Cl_2 (3×10^{-6} M). The Soret band absorptions have been normalized and the spectra amplified 10-fold in the Q band region.

region and four Q bands at 516, 552, 592, and 647 nm in the visible region.[19] These Soret and Q bands are red-shifted by only 1–3 nm relative to the corresponding bands of TPP under the same conditions.

The fluorescence emission spectrum of **3**, along with those of TPP and an equimolar mixture of TPP and $[\{(\mu\text{-}SCH_2)_2NH\}Fe_2(CO)_6]$, were also recorded. As shown in Figure 2, the two fluorescence emission bands at 655 and 719 nm displayed by **3** are red-shifted by about 3 nm relative

 © 2006 Wiley-VCH Verlag GmbH & Co. KGaA, Weinheim

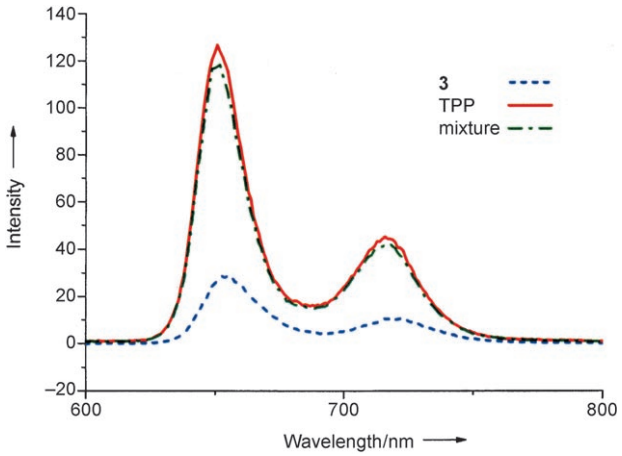


Figure 2. Fluorescence emission spectra (λ_{ex} = 425 nm) of **3**, TPP, and an equimolar mixture of TPP and [{(μ-SCH_2)$_2$NH}$Fe_2(CO)_6$] in CH_2Cl_2 (3×10^{-5} M).

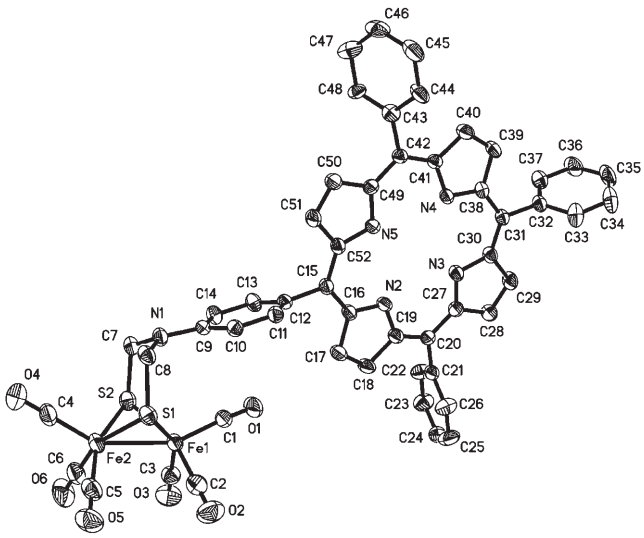


Figure 3. Structure of **3**. Selected bond lengths [Å]: Fe1–Fe2 2.5000(9), Fe1–S1 2.2630(13), Fe1–S2 2.2607(15), N1–C7 1.428(6), N1–C8 1.413(6), C12–C15 1.503(6), C16–N2 1.367(5), C27–N3 1.375(5), C38–N4 1.373(5), C49–N5 1.370(6).

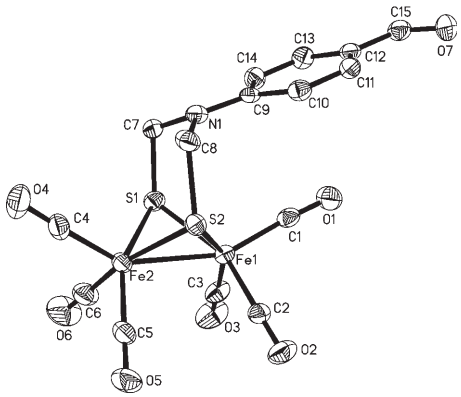


Figure 4. Structure of **2**. Selected bond lengths [Å]: Fe1–Fe2 2.4956(9), Fe1–S1 2.2542(12), Fe1–S2 2.2417(11), Fe2–S1 2.2486(11), N1–C7 1.424(4), N1–C8 1.431(4), N1–C9 1.387(4), O7–C15 1.193(4).

to the corresponding bands of TPP under the same conditions, although their intensities are strongly quenched relative to those of the TPP bands, with a quenching efficiency, *Q*, of 86.4 %. Since the intensities of the two bands of the equimolar mixture of TPP and [{(μ-SCH_2)$_2$NH}$Fe_2(CO)_6$] are almost the same as those of the corresponding TPP bands, we believe that the remarkably decreased intensities of the two fluorescence bands of **3** relative to those of TPP are most likely due to strong intramolecular electron transfer from the photoexcited state of the porphyrin macrocycle of TPP to the covalently bonded diiron–ADT moiety and not by an intermolecular collision process between molecules of **3**.[20] It is interesting to note that such an intramolecular electron transfer is one of the important steps required for the proton reduction performed by biomimetic models.

The molecular structures of model **3** and its precursor **2** were confirmed by X-ray crystallography (Figures 3 and 4, respectively).[21] Both **2** and **3** contain a diiron–ADT moiety in which the six-membered ring Fe1-S1-C7-N1-C8-S2 has a boat conformation and the other six-membered ring Fe2-S1-C7-N1-C8-S2 adopts a chair conformation. The bond between the disubstituted benzene ring and the N1 atom is axially oriented in both **2** and **3**, and all the iron nuclei in **2** and **3** have the expected square-pyramidal coordination sphere. The Fe–Fe bond lengths of 2.4956(9) Å for **2** and 2.5000(9) Å for **3** are in good agreement with the corresponding lengths in similar complexes.[10] The sum of the C-N-C angles around N1 is 356.8° for **2** and 355.3° for **3**, which implies somewhat interrupted π conjugation between the disubstituted benzene ring and the p orbital of the nitrogen atom.

While **2** is a simple model compound where the nitrogen atom is linked to an aromatic aldehyde system, the target compound **3** is a novel light-driven-type model with a porphyrin photosensitizer. The C–N bond lengths in the pyrrole rings of the porphyrin unit of **3** are nearly the same (1.364(5)–1.378(5) Å) and lie between those of normal single and double C–N bonds.[22] The four benzene rings attached to the porphyrin unit of **3** are planar and twisted relative to the porphyrin plane in order to reduce the steric interactions between the phenyl hydrogen atoms proximal to the porphyrin unit and the pyrrole rings. The twist angles between the porphyrin plane and the benzene rings involving C12, C21, C32, and C43 are 75.9°, 99.1°, 77.4°, and 63.1°, respectively.

In conclusion, we have synthesized and crystallographically characterized a novel light-driven-type model compound (**3**) that contains a TPP photosensitizer covalently bonded to the N atom of a diiron–ADT moiety. In view of the strong coordination ability of porphyrin macrocycles with a wide variety of metal ions[12] and the facile substitution of the Fe-bound CO by other ligands,[23] we expect that we will be able to further modify **3** in order to facilitate the electron transfer from the photoexcited TPP to the diiron–ADT moiety and thus finally accomplish the light-driven reduction of protons to hydrogen. Further investigations in this area are in progress.

 © 2006 Wiley-VCH Verlag GmbH & Co. KGaA, Weinheim

Experimental Section

1: A mixture of *p*-$NH_2C_6H_4CHO$ (1.265 g, 10.4 mmol), paraformaldehyde (1.14 g), and CH_2Cl_2 (20 mL) was stirred at room temperature for 5 h. After addition of $SOCl_2$ (3.0 mL, 41.2 mmol), the new mixture was stirred for an additional hour. The solvent and unreacted $SOCl_2$ were then removed under vacuum. The residue was extracted with Et_2O and recrystallized to give 1.383 g (61%) of **1** as a yellow solid. $C_9H_9Cl_2NO$: calcd. C 49.57, H 4.16, N 6.42; found C 49.67, H 4.37, N 6.37; ^{1}H NMR (300 MHz, $CDCl_3$): $\delta = 5.54$ (s, 4H; $2CH_2$), 7.31, 7.91 (2d, $J = 8.7$ Hz, 4H; C_6H_4), 9.94 ppm (s, 1H; CHO); IR (KBr disk): $\tilde{\nu} = 1694\ cm^{-1}$ (CHO).

2: A solution of $Li(Et_3BH)$ in THF (1M, 17.0 mL, 17.0 mmol) was added to a solution of $[(\mu\text{-}S_2)Fe_2(CO)_6]$ (2.924 g, 8.5 mmol) in THF (40 mL) at −78°C. At the midpoint of the addition, the reaction mixture turned from red to dark green; for the rest of addition it remained green. CF_3CO_2H (1.3 mL, 17.0 mmol) was then added to give a red solution of $[(\mu\text{-}HS)_2Fe_2(CO)_6]$.[15] Compound **1** (1.845 g, 8.5 mmol) was added to this solution and the mixture was stirred at −78°C for 0.5 h and at room temperature for 12 h. The volatiles were removed under vacuum and the residue was separated by TLC using CH_2Cl_2/petroleum ether (2:1, v/v) as eluent. Complex **2** was obtained as a red solid from the major, red band (1.320 g, 32%). $C_{15}H_9Fe_2NO_7S_2$: calcd. C 36.69, H 1.85, N 2.85; found C 36.75, H 1.80, N 3.02; ^{1}H NMR (300 MHz, $CDCl_3$): $\delta = 4.36$ (s, 4H; $2CH_2$), 6.83, 7.85 (2d, $J = 8.4$ Hz, 4H; C_6H_4), 9.86 ppm (s, 1H; CHO); IR (KBr disk): $\tilde{\nu} = 2084$, 2034, 2007, 1987, 1966 (C≡O), 1666 cm^{-1} (CHO).

3: A mixture of benzaldehyde (0.182 mL, 1.8 mmol), **2** (0.295 g, 0.6 mmol), pyrrole (0.166 mL, 2.4 mmol), CF_3CO_2H (0.184 mL, 2.4 mmol), and CH_2Cl_2 (240 mL) was stirred at room temperature in the dark for 15 h to give a purple-red solution. 2,3,5,6-Tetrachlorobenzoquinone (*p*-chloranil; 0.443 g, 1.8 mmol) was added to this solution and the new mixture was refluxed for 1 h to give a brown-green solution. The solvent was removed under reduced pressure and the residue was subjected to flash column chromatography (Al_2O_3, CH_2Cl_2). The eluate was reduced to a suitable volume for TLC separation with CH_2Cl_2/petroleum ether (1:1, v/v) as eluent. Tetraphenylporphyrin (0.052 g, 19%) was obtained from the first band as a purple solid that was identified by comparison of its IR and ^{1}H NMR spectra with those of an authentic sample.[17,18] Complex **3** (0.138 g, 23%) was obtained as a purple-red solid from the second band. $C_{52}H_{33}Fe_2N_5O_6S_2$: calcd. C 62.48, H 3.37, N 7.01; found C 62.39, H 3.32, N 7.04; ^{1}H NMR (300 MHz, $CDCl_3$): $\delta = -2.76$ (s, 2H; 2NH), 4.55 (s, 4H; $2CH_2$), 7.04, 7.07 (2s, 2H; 2*m*-H of C_6H_4), 7.74, 7.76 (2s, 9H; 6*m*-H of C_6H_5 and 3*p*-H of C_6H_5), 8.11, 8.14 (2s, 2H; 2*o*-H of C_6H_4), 8.20, 8.23 (2s, 6H; 6*o*-H of C_6H_5), 8.85, 8.86 ppm (2s, 8H; pyrrole rings); IR (KBr disk): $\tilde{\nu} = 3317$ (NH), 2073, 2033, 1996 (C≡O), 1558 (pyrrole C=C), 1472 (pyrrole C=N), 1350 cm^{-1} (pyrrole C–N); ESI-MS: m/z 999.85 [M^+]; UV/Vis (CH_2Cl_2) : λ_{max} ($\log\varepsilon$) = 419 (5.61), 516 (4.24), 552 (3.93), 592 (3.72), 647 nm (3.74).

Received: October 12, 2005
Published online: January 3, 2006

Keywords: bioinorganic chemistry · enzyme models · hydrogenases · iron · porphyrinoids

[1] R. Cammack, *Nature* **1999**, *397*, 214–215.
[2] M. W. W. Adams, E. I. Stiefel, *Science* **1998**, *282*, 1842–1843.
[3] M. Y. Darensbourg, E. J. Lyon, J. J. Smee, *Coord. Chem. Rev.* **2000**, *206–207*, 533–561.
[4] M. Frey, *ChemBioChem* **2002**, *3*, 153–160.
[5] M. W. W. Adams, *Biochim. Biophys. Acta* **1990**, *1020*, 115–145.
[6] J. Alper, *Science* **2003**, *299*, 1686–1687.
[7] D. J. Evans, C. J. Pickett, *Chem. Soc. Rev.* **2003**, *32*, 268–275.
[8] a) J. W. Peters, W. N. Lanzilotta, B. J. Lemon, L. C. Seefeldt, *Science* **1998**, *282*, 1853–1858; b) Y. Nicolet, C. Piras, P. Legrand, C. E. Hatchikian, J. C. Fontecilla-Camps, *Structure* **1999**, *7*, 13–23.
[9] a) A. L. de Lacey, C. Stadler, C. Cavazza, E. C. Hatchikian, V. M. Fernandez, *J. Am. Chem. Soc.* **2000**, *122*, 11232–11233; b) Z. Chen, B. J. Lemon, S. Huang, D. J. Swartz, J. W. Peters, K. A. Bagley, *Biochemistry* **2002**, *41*, 2036–2043.
[10] See, for example: a) F. Gloaguen, J. D. Lawrence, M. Schmidt, S. R. Wilson, T. B. Rauchfuss, *J. Am. Chem. Soc.* **2001**, *123*, 12518–12527; b) M. Razavet, S. C. Davies, D. L. Hughes, J. E. Barclay, D. J. Evans, S. A. Fairhurst, X. Liu, C. J. Pickett, *Dalton Trans.* **2003**, 586–595; c) J. D. Lawrence, H. Li, T. B. Rauchfuss, M. Bénard, M.-M. Rohmer, *Angew. Chem.* **2001**, *113*, 1818–1821; *Angew. Chem. Int. Ed.* **2001**, *40*, 1768–1771; d) H. Li, T. B. Rauchfuss, *J. Am. Chem. Soc.* **2002**, *124*, 726–727; e) L.-C. Song, Z.-Y. Yang, H.-Z. Bian, Q.-M. Hu, *Organometallics* **2004**, *23*, 3082–3084; f) S. Ott, M. Kritikos, B. Åkermark, L. Sun, R. Lomoth, *Angew. Chem.* **2004**, *116*, 1024–1027; *Angew. Chem. Int. Ed.* **2004**, *43*, 1006–1009.
[11] S. Ott, M. Kritikos, B. Åkermark, L. Sun, *Angew. Chem.* **2003**, *115*, 3407–3410; *Angew. Chem. Int. Ed.* **2003**, *42*, 3285–3288.
[12] a) J. R. Darwent, P. Douglas, A. Harriman, G. Porter, M.-C. Richoux, *Coord. Chem. Rev.* **1982**, *44*, 83–126; b) I. Okura, *Coord. Chem. Rev.* **1985**, *68*, 53–99.
[13] a) Y. Nicolet, A. L. de Lacey, X. Vernède, V. M. Fernandez, E. C. Hatchikian, J. C. Fontecilla-Camps, *J. Am. Chem. Soc.* **2001**, *123*, 1596–1601; b) H.-J. Fan, M. B. Hall, *J. Am. Chem. Soc.* **2001**, *123*, 3828–3829.
[14] J. D. Lawrence, H. Li, T. B. Rauchfuss, *Chem. Commun.* **2001**, 1482–1483.
[15] D. Seyferth, R. S. Henderson, L.-C. Song, *J. Organomet. Chem.* **1980**, *192*, C1–C5.
[16] J. S. Lindsey, I. C. Schreiman, H. C. Hsu, P. C. Kearney, A. M. Marguerettaz, *J. Org. Chem.* **1987**, *52*, 827–836.
[17] D. W. Thomas, A. E. Martell, *J. Am. Chem. Soc.* **1959**, *81*, 5111–5119.
[18] B. C. Bookser, T. C. Bruice, *J. Am. Chem. Soc.* **1991**, *113*, 4208–4218.
[19] J. L. Shaw, S. A. Garrison, E. A. Alemán, C. J. Ziegler, D. A. Modarelli, *J. Org. Chem.* **2004**, *69*, 7423–7427.
[20] a) M. Dudiè, P. Lhoták, V. Král, K. Lang, I. Stibor, *Tetrahedron Lett.* **1999**, *40*, 5949–5952; b) D. Baskaran, J. W. Mays, X. P. Zhang, M. S. Bratcher, *J. Am. Chem. Soc.* **2005**, *127*, 6916–6917.
[21] CCDC-284275 (**2**) and -284276 (**3**) contain the supplementary crystallographic data for this paper. These data can be obtained free of charge from The Cambridge Crystallographic Data Centre via www.ccdc.cam.ac.uk/data_request/cif..
[22] a) S. J. Silvers, A. Tulinsky, *J. Am. Chem. Soc.* **1967**, *89*, 3331–3337; b) J. L. Sessler, M. R. Johnson, S. E. Creager, J. C. Fettinger, J. A. Ibers, *J. Am. Chem. Soc.* **1990**, *112*, 9310–9329.
[23] L.-C. Song, *Acc. Chem. Res.* **2005**, *38*, 21–28.

 © 2006 Wiley-VCH Verlag GmbH & Co. KGaA, Weinheim

Mesoporous Materials

DOI: 10.1002/anie.200503301

Tuning the Structure and Orientation of Hexagonally Ordered Mesoporous Channels in Anodic Alumina Membrane Hosts: A 2D Small-Angle X-ray Scattering Study**

*Barbara Platschek, Nikolay Petkov, and Thomas Bein**

Periodic mesoporous materials have attracted considerable attention during the last decade because of their promising applications as catalyst supports and nanoreactors, or as hosts for nanostructured materials with appealing optoelectronic properties.[1,2] Many of these applications will benefit from arrangements of preferentially aligned, ordered arrays of certain mesostructures. The evaporation-induced self-assembly (EISA) method has been established as an efficient process for the preparation of thin films with mono-oriented mesostructured domains.[3,4] However, the most frequently obtained films display hexagonally ordered channels that are aligned parallel to the surface of the substrate.[5]

Recently, the synthesis of mesoporous materials within the regular, larger channels of anodic alumina membranes (AAMs) has been explored, with the aim of attaining greater control over the morphology of the mesoporous system.[6] A first approach, through a sol–gel synthesis route using the triblock copolymer poly(ethylene oxide)$_{100}$-b-poly(propylene oxide)$_{65}$-b-poly(ethylene oxide)$_{100}$ ($PEO_{100}PPO_{65}PEO_{100}$ or Pluronic F-127) as a structure-directing agent, resulted in 2D hexagonal mesostructures with two different orientations that were found to coexist at different ratios depending on the concentration of the surfactant.[7] In one case, the long axes of the mesopores were aligned with the long axes of the AAM channels (columnar orientation). In another case, a circular orientation of the mesostructure was observed. Similar (free-standing) unusual mesophase structures are known to exist in cetyltrimethylammonium bromide (CTAB)-templated materials prepared by solvothermal methods and have been named "circulites" or circular crystals.[8,9]

The efficient EISA method can also be used to prepare AAM mesoporous composite materials by applying coating solutions that are typically used for the deposition of mesoporous silica films. When using cationic CTAB as a template, partially ordered mesoporous materials with aligned, columnar mesopores only in the vicinity of the alumina walls were obtained that showed promising behavior as molecular separators.[10] Use of the triblock copolymer $PEO_{20}PPO_{70}PEO_{20}$ (Pluronic123 or P123) as a template resulted in striking mesostructures with concentric or helical mesopores and single chains of spherical mesopores, depending on the confinement conditions imposed by alumina nanochannels with diameters of less than 100 nm.[11] In contrast, columnar mesopores were reported when the same template (P123) was used in the sol–gel approach in larger Anopore channels.[12] However, when a slightly different protocol at the same surfactant/silica ratio was used in the sol–gel synthesis route, hexagonal mesophases with mixed orientations resulted.[13] The presence of water vapor in the ageing process was investigated in a related study using the P123 template.[14,15] In this case, the circular orientation was favored over the columnar one at higher water pressure; this selectivity was attributed to the increased rate of gelation. Multiple mesoporous silica phases have also been included in AAM channels through sequential loading techniques.[16]

From the studies discussed above, it is clear that subtle changes in stoichiometry and reaction conditions can lead to striking changes in the order and morphology of the mesopores. With an aim to better understand the mechanism and the ability to tune these intriguing structures at will, we present herein a combined 2D small-angle X-ray scattering (SAXS) and transmission electron microscopy (TEM) study, which shows that highly ordered hexagonal mesoporous structures with adjustable orientation can be formed with the templates CTAB, P123, and decaethylene glycol hexadecyl ether (Brij56) under the conditions of the EISA method. We demonstrate that when using the ionic surfactant CTAB, the hexagonally structured mesopores are solely oriented along the AAM channels. With the non-ionic surfactants P123 or Brij56, it was possible to control the formation of either orientation (circular or columnar) by tuning the silica-to-surfactant ratio of the initial synthetic mixtures as well as the humidity level during the EISA process.

The method used here for the self-assembly of the ordered silica/surfactant nanocomposites in the channels of the anodic alumina membranes is depicted in Figure 1. The AAMs used in this study showed almost hexagonal packing of vertical pores, with diameters in the range of 120–200 nm, through the entire thickness of the membrane (Figure 2a). The synthetic mixtures containing the silica precursor and either CTAB, P123, or Brij56 as structure-directing agents were introduced into the pores of the AAM by soaking the membranes at room temperature in a flat pool of liquid. As a result of evaporation of the solvent, which progressively increases the concentration of the surfactant and other nonvolatile components of the synthetic mixtures, the self-assembly process is driven towards the formation of micelles and the condensation of silica, followed by a disorder-to-order transition to provide the final, extended mesophase structure.

Figure 2a and b show side-view scanning electron microscopy (SEM) images of the AAM before and after loading with P123-templated mesoporous silica, respectively. As expected, pure AAMs show well-aligned, almost regularly arranged nanochannels (Figure 2a). After the assembly of the mesoporous silica structures using CTAB or P123 as structure-directing agents, well-shaped nanoscopic filaments that

[*] B. Platschek, Dr. N. Petkov, Prof. Dr. T. Bein
Department of Chemistry and Biochemistry
University of Munich (LMU)
Butenandtstrasse 11, 81377 Munich (Germany)
Fax: (+49) 89-2180-77622
E-mail: bein@lmu.de

[**] This work was supported by the SFB486 of the German Research Foundation (DFG).

InterScience
© 2006 Wiley-VCH Verlag GmbH & Co. KGaA, Weinheim

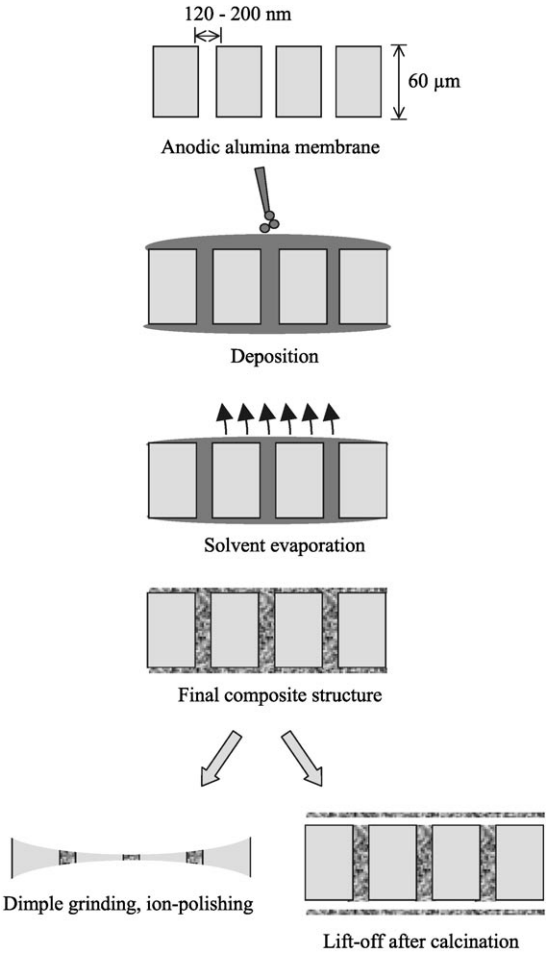


Figure 1. Schematic representation of the synthetic route to obtain mesostructured silica–surfactant nanocomposites in the AAMs.

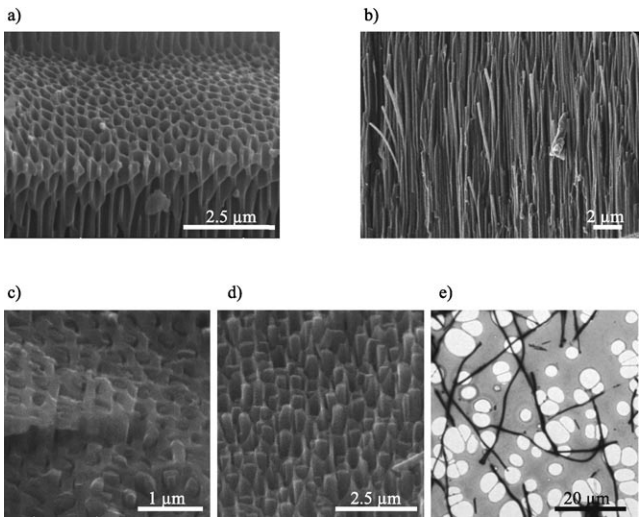


Figure 2. a, b) Side-view SEM images of sample D1 (with P123) showing the morphology of the AAMs before (a) and after (b) inclusion of mesoporous silica. c, d) SEM images of the silica filaments encapsulated within pores of AAMs, templated with CTAB (c) and P123 (d). e) TEM image of the isolated silica filaments imaged on a holey carbon grid (sample CTAB1).

protrude from the openings of the AAM channels were observed (Figure 2c, d). Figure 2b depicts the uniformity and continuity of the as-deposited nanostructures, viewed normal to the direction of the channel of the membrane, while Figure 2e shows the isolated mesoporous 1D nanofibers obtained by dissolution of the AAM matrix in phosphoric acid. Energy-dispersive X-ray (EDX) measurements taken along the whole thickness of the membrane showed similar Al/Si atomic ratios, demonstrating the continuous and homogeneous filling of the membrane with the silica–surfactant nanocomposites.

The geometry of the SAXS experiments, performed close to the grazing angle, and the proposed mesophase structures are shown in Figure 3. Both out-of-plane and in-plane

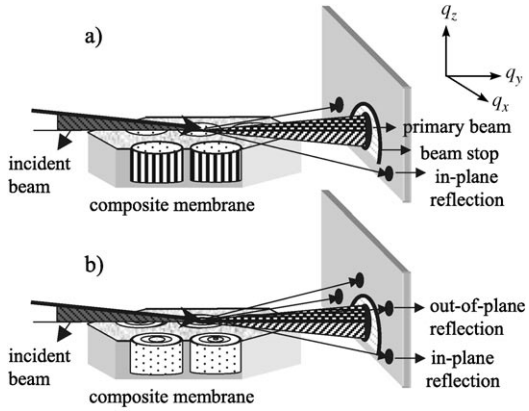


Figure 3. Geometry of the grazing incidence (GI)-SAXS experiment for the mesophase structures with a) hexagonally ordered mesopores fully aligned along the channels of the AAMs (columnar orientation) and b) circular mesopores with local hexagonal order parallel to the surface of the AAMs.

diffracted beams were recorded simultaneously. Full alignment of the mesoporous channels in the direction perpendicular to the membrane surface (parallel to the channels of the AAMs) will result in only two reflections in the direction of the q_x vector and the absence of out-of-plane reflections (Figure 3a). This distinct case was observed for the two CTAB-templated samples that were prepared at different concentrations of surfactant (see Figure 4 and Experimental Section). The indexing of the diffraction spots is given in Figure 4a. These highly structured mesophases are directly observed in the representative plan-view TEM images shown in Figure 5a. For the sample CTAB2, almost all of the pores of the alumina membrane (about 90%) were filled with fully mesostructured material. The power spectrum (inset in Figure 5a) calculated from the corresponding TEM image showed a well-ordered hexagonal mesophase structure with a d spacing of about 4.5 nm, which corresponds to the spacing observed for CTAB-templated mesoporous powders (e.g. MCM-41-type materials).[17] We observe that with a decrease in the concentration of the surfactant in the deposition mixtures (sample CTAB1, Figure 4a), the intensity of the diffraction spots in the SAXS patterns also decreases (Table 1). This behavior is due to the decreased density of the ordered mesostructured domains in the alumina matrix.

 © 2006 Wiley-VCH Verlag GmbH & Co. KGaA, Weinheim

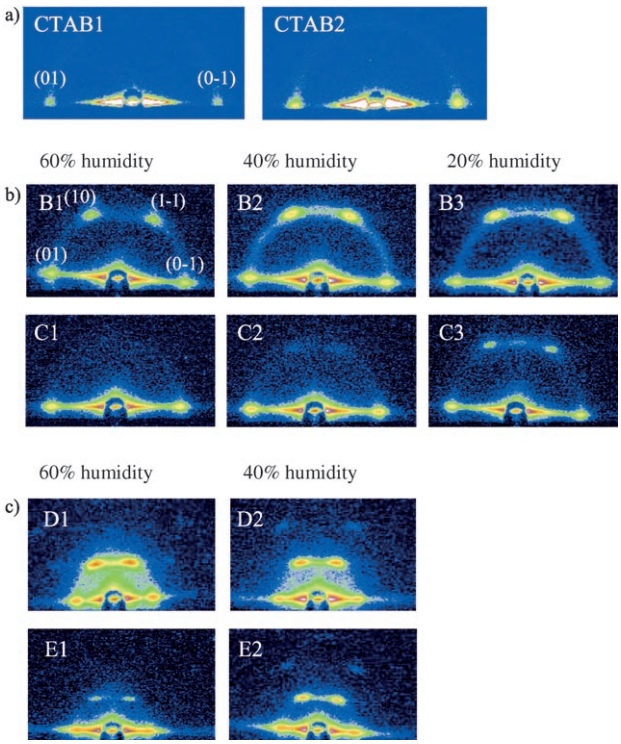


Figure 4. GI-SAXS patterns of the samples: a) CTAB1 and CTAB2 (templated with different concentrations of CTAB), b) B1–B3 and C1–C3 (templated with Brij56 but at different surfactant concentrations (B, C) and humidities (1–3)), and c) D1, D2, E1, and E2 (templated with P123 but at different surfactant concentrations (D, E) and humidities (1, 2)). All images are shown with the same spatial and intensity scale. See text and Experimental Section for details. For the circular structure, a system of rings is found in reciprocal space.[8] Indexation is given as for the normal hexagonal lattice.

Table 1: Summary of SAXS data of CTAB-templated mesoporous channel systems.

Sample	Surfactant/silica molar ratio	Diffraction spots detected	Relative intensity[a]	*d* spacing[b]
CTAB1	0.18	(01); (0-1)	0.14	4.5
CTAB2	0.26	(01); (0-1)	0.19	4.3

[a] The intensity of the reflections was normalized to the intensity of the primary beam after the semitransparent beam stop. [b] The *d* spacings were calculated from the position of the diffraction spots according to $q = 2\pi/d$.

The corresponding TEM images from this sample show that almost 30% of the alumina pores are either empty or show inferior hexagonal order. The results suggest that the ordering process (formation of the lyotropic liquid-crystalline mesophase) can be directly controlled by varying the concentrations of surfactant in the deposition mixtures.

The second mesophase configuration (circular mesopores) that was studied here by using P123 or Brij56 as structure-directing agents is schematically shown in Figure 3b. With these samples, four well-resolved diffraction spots from both out-of-plane and in-plane reflections were recorded (see Figure 4b for indexing). This diffraction pattern can be identified as one that arises from the local hexagonal

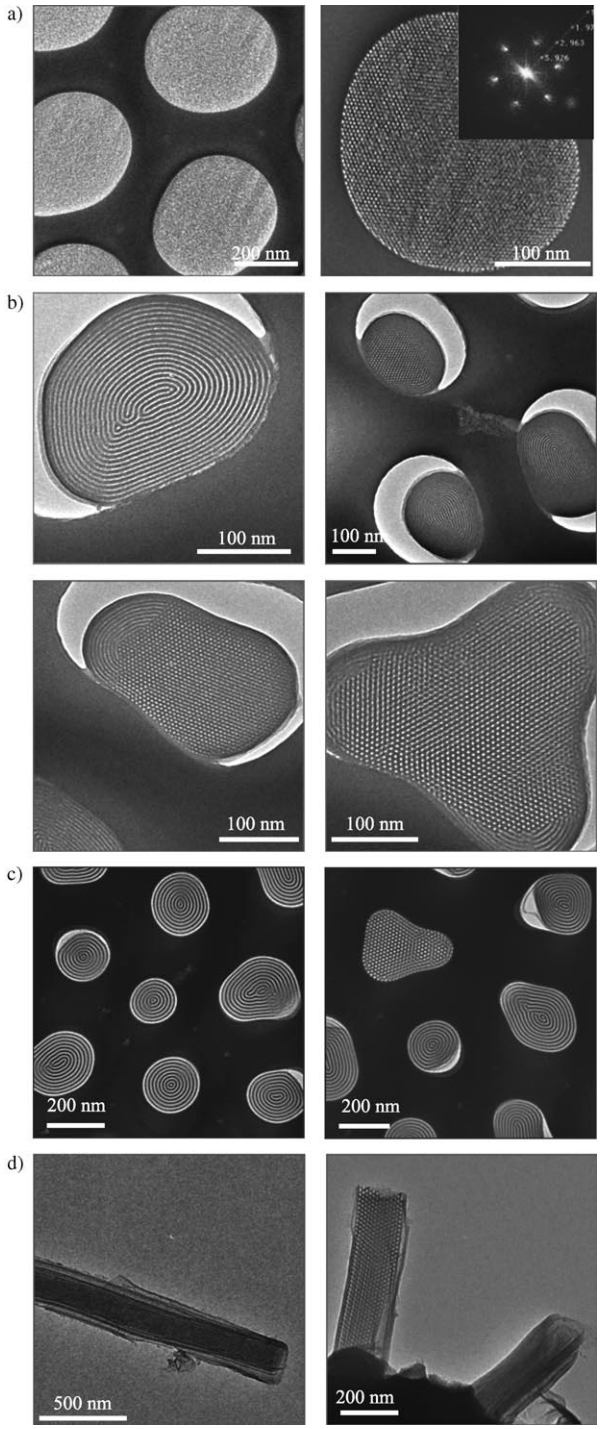


Figure 5. a)–c) Plan-view TEM images of samples a) CTAB2 showing the columnar oriented hexagonal mesostructure (insert: 2D power spectrum), b) B1 (templated with Brij56 at 60% humidity) with approximately equal distribution of columnar and circular mesophases, showing AAM pores with columnar or circular orientation as well as an AAM pore with a hybrid structure, and c) D1 (templated with P123 at 60% humidity; predominantly circular orientation). d) Cross-section TEM image of sample E1 (templated with P123 at 60% humidity; predominantly columnar orientation) showing mesoporous fibers protruding from the AAM channels at a site of fracture.

 © 2006 Wiley-VCH Verlag GmbH & Co. KGaA, Weinheim

arrangement of mesopores with the (100) lattice plane (i.e. the close packing of mesopore channels) parallel to the curved AAM channel surface (the two missing diffraction spots, below the membrane surface, are shadowed by the beam stop). To record plan-view TEM images the structure was imaged in the direction perpendicular to the membrane surface, and circular, concentric mesophase channels as well as some columnar channels were observed (see Figure 5b and c for the Brij56- and P123-templated structures, respectively).

We observed that the mesophase structure of the AAM-embedded P123- and Brij56-templated materials (columnar or circular pore orientation) could be tuned by varying the amount of surfactant in the deposition mixtures or by adjusting the humidity during the drying process. Note that this behavior was not observed if CTAB was used as the structure-directing agent; this might be due to the fact that CTAB is an ionic template and therefore interacts differently with the silica precursors and the AAM surface. The corresponding SAXS patterns of the mesophase structures that were prepared in the channels of the AAMs with deposition solutions that contained increasing amounts of template and synthesized at different humidities are shown in Figure 4b and c, respectively. All the patterns can be described as superpositions of the patterns typical for the structures that exhibit a columnar orientation (Figure 3a) and those with the circular mesophase structure (Figure 3b). This implies that the in-plane reflections will be preserved in any case, whereas both out-of-plane reflections should appear with decreased intensity in the case of mixed structures. The intensity ratios (10)/(01) for the P123- and Brij56-templated silica material in the AAMs are shown in Table 2. It is striking that by increasing the concentration of surfactant in the deposition mixtures and by carrying out the synthesis at high humidity, a drastic shift in population towards the columnar mesostructures results. It was observed in both cases that the drying of the composite material, which usually took between three to five hours, takes longer than at lower humidity or with a lower concentration of surfactant. We therefore suggest that there is a small energy difference between both orientations and that with a longer reaction time the reaction is driven towards the thermodynamically more stable state which results in the vertical, columnar mesopore alignment.

Table 2: Summary of SAXS data of block-copolymer-templated mesoporous channel systems.

Sample	Surfactant/silica molar ratio	Relative integrated intensities of diffraction spots, (10)/(01)[a]			*d* spacings[b]
		60% humidity	40% humidity	20% humidity	
B1–B3	Brij56/Si = 0.133	0.5	0.75	0.96	6.2 (B1) 6.0 (B2) 5.8 (B3)
C1–C3	Brij56/Si = 0.265	0	0.03	0.3	6.4
D1, D2	P123/Si = 0.013	1.1	1.0	[c]	11.0
E1, E2	P123/Si = 0.017	0.03	0.3	[c]	11.5

[a] The intensity of the reflections was normalized to the intensity of the primary beam after the semitransparent beam stop. [b] The *d* spacings were calculated from the position of the diffraction spots according to $q = 2\pi/d$. [c] No structure detected.

When P123 was used as structure-directing agent, the reflections corresponding to the circular mesopore orientation did not completely vanish. This effect may be related to the larger pore diameter of these structures, which implies that the ratio of the diameter of the mesopore to the diameter of the AAM channel differs significantly from the analogous ratios for samples synthesized with CTAB or Brij56. Thus the curvature of the AAM channel wall may drive the micelles towards the circular orientation.

The corresponding plan-view TEM images (Figure 5b and c for the Brij56- and P123-templated structures, respectively) show the circular orientation as well as highly ordered hexagonal structures arising from the columnar mesopore orientation that are present in different relative populations. The cross-sectional images shown in Figure 5d (P123-templated structure E1) illustrate the predominantly columnar alignment of the embedded mesoporous channels within the AAM channels, as well as the hexagonal structure that becomes visible when the cross-section of the circular mesopore orientation is viewed. The plan-view TEM images also show the coexistence of the circular and columnar mesopores in different channels of the AAMs or, in some cases, "twinned" structures that show both configurations.

The embedded silica–surfactant nanocomposite mesophases obtained here differ significantly from those reported previously for confined polymer systems[18] in that the mesostructures discussed in the present study form a rigid silica framework upon removal of the template, to leave solid supports with ordered porosity that can, for example, offer a matrix for the guided growth of a variety of conductive materials. Recent research on the 1D confinement of conductive nanostructures has shown that extended control over the morphology and size of such structures is important for their potential application in integrated electronic circuits.[19,20]

To summarize, this study of the 1D confinement of silica–surfactant composites in the vertical channels of anodic alumina membranes showed that new, mesoscopic structures with intriguing arrangements of the mesoporous channels are possible. We demonstrated that three of the most commonly used structure-directing agents (CTAB, P123, and Brij56) can be employed for the synthesis of hexagonally ordered mesoporous silica embedded in AAM channels. The formation of both circular and columnar phases can take place, and with the non-ionic surfactants the occurrence of these phases can be tuned by changing the concentration of the surfactant and the humidity in the adjacent gas phase. The structural features of the CTAB-, Brij56-, and P123-templated mesoporous filaments in the AAMs will allow the fast and effective inclusion of a variety of interesting 1D nanostructures, which range from metallic nanowires, semiconductor nanoparticles and nanowires, to carbon nanotubes.

 © 2006 Wiley-VCH Verlag GmbH & Co. KGaA, Weinheim

Experimental Section

Preparation of the samples: The deposition mixtures were prepared by applying a two-step synthesis procedure: First, tetraethyl orthosilicate (Aldrich; 2.08 g, 0.01 mol) was mixed with 0.2 M HCl (3 g), H_2O (1.8 g), and EtOH (5 mL), and the mixture was heated at 60 °C for 1 h to carry out acid-catalyzed hydrolysis–condensation of the silica precursor. For the preparation of CTAB-containing deposition mixtures, this solution was mixed with CTAB (0.644 g, 1.77 mmol for sample CTAB1; or 0.947 g, 2.6 mmol for CTAB2) dissolved in EtOH (10 mL). The Brij56-containing samples were prepared using Brij56 (0.906 g, 1.33 mmol dissolved in ethanol (15 mL) or 1.81 g, 2.65 mmol dissolved in ethanol (30 mL) for samples B1–B3 and C1–C3, respectively). For the preparation of the P123-containing solutions, the prehydrolyzed silica was mixed with 5 wt % solutions of P123 in ethanol: 15 mL (0.13 mmol P123 for sample D1–D3) or 20 mL (0.17 mmol P123 for sample E1–E3). The AAMs (47 mm, Anodisc, Whatman) with average pore diameters of 120–200 nm and a thickness of approximately 60 μm were soaked with the prepared mixtures of the precursor by distributing 0.75 mL of the solutions over the whole membrane surface. After 3–5 h at room temperature and under controlled humidity, the membrane appeared dry and homogeneously filled with the mixture.

Characterization of the embedded silica mesostructures: GI-SAXS measurements were performed with a SAXSess small-angle X-ray scattering system by Anton Paar after alignment of the X-ray beam with the surface of the sample as shown in Figure 3. The incident beam was shadowed with a circular beam stop, and the signal was recorded on image plates after collecting the pattern for 1 h. The TEM images were obtained with a JEOL 2010 transmission electron microscope operating at 200 kV. Samples for electron microscopy were prepared by the following method: 1) the alumina matrix was dissolved in phosphoric acid to release the embedded mesoporous silica; 2) plan views and cross-sections were prepared by dimple grinding followed by Ar ion polishing. The elemental composition and surface morphology of the samples were determined by SEM using a JEOL JSM 6500F field emission scanning electron microscope equipped with an Oxford EDX detector.

Received: September 16, 2005
Published online: January 3, 2006

Keywords: host–guest systems · membranes · mesoporous materials · surfactants · template synthesis

[1] A. P. Wight, M. E. Davis, *Chem. Rev.* **2002**, *102*, 3589.
[2] B. J. Scott, G. Wirnsberger, G. D. Stucky, *Chem. Mater.* **2001**, *13*, 3140.
[3] C. J. Brinker, Y. Lu, A. Sellinger, H. Fan, *Adv. Mater.* **1999**, *11*, 579.
[4] D. Grosso, F. Babonneau, P.-A. Albouy, H. Amenitsch, A. R. Balkenende, A. Brunet-Bruneau, J. Rivory, *Chem. Mater.* **2002**, *14*, 931.
[5] M. Klotz, P.-A. Albouy, A. Ayral, C. Menager, D. Grosso, A. van der Lee, V. Cabuil, F. Babonneau, C. Guizard, *Chem. Mater.* **2000**, *12*, 1721.
[6] G. Kickelbick, *Small* **2005**, *1*, 168 – 170.
[7] Z. Yang, Z. Niu, X. Cao, Z. Yang, Y. Lu, Z. Hu, C. C. Han, *Angew. Chem.* **2003**, *115*, 4333 – 4335; *Angew. Chem. Int. Ed.* **2003**, *42*, 4201 – 4203.
[8] F. Marlow, I. Leike, C. Weidenthaler, C. W. Lehmann, U. Wilczok, *Adv. Mater.* **2001**, *13*, 307 – 310.
[9] F. Kleitz, F. Marlow, G. D. Stucky, F. Schüth, *Chem. Mater.* **2001**, *13*, 3587.
[10] A. Yamaguchi, F. Uejo, T. Yoda, T. Uchida, Y. Tanamura, T. Yamashita, N. Teramae, *Nat. Mater.* **2004**, *3*, 337.
[11] Y. Wu, G. Cheng, K. Katsov, S. W. Sides, J. Wang, J. Tang, G. H. Fredrickson, M. Moskovits, G. D. Stucky, *Nat. Mater.* **2004**, *3*, 816.
[12] Q. Lu, F. Gao, S. Komarneni, T. E. Mallouk, *J. Am. Chem. Soc.* **2004**, *126*, 8650.
[13] D. Wang, R. Kou, Z. Yang, J. He, Z. Yang, Y. Lu, *Chem. Commun.* **2005**, 166.
[14] B. Yao, D. Fleming, M. A. Morris, S. E. Lawrence, *Chem. Mater.* **2004**, *16*, 4851.
[15] K. Jin, B. Yao, N. Wang, *Chem. Phys. Lett.* **2005**, *409*, 172.
[16] A. Y. Ku, S. T. Taylor, S. M. Loureiro, *J. Am. Chem. Soc.* **2005**, *127*, 6934.
[17] A. Monnier, F. Schüth, Q. Huo, D. Kumar, D. Margolese, R. S. Maxwell, G. D. Stucky, M. Krishnamurty, P. Petroff, A. Firouzi, M. Janicke, B. F. Chmelka, *Science*, **1993**, *261*, 1299.
[18] J. Y. Cheng, A. M. Mayes, C. A. Ross, *Nat. Mater.* **2004**, *3*, 823.
[19] M. L. Cohen, *Mater. Sci. Eng. C* **2001**, *15*, 1.
[20] Y. Xia, P. Yang, Y. Sun, Y. Wu, B. Mayers, B. Gates, Y. Yin, F. Kim, H. Yan, *Adv. Mater.* **2003**, *15*, 353.

 © 2006 Wiley-VCH Verlag GmbH & Co. KGaA, Weinheim

Bioinorganic Chemistry

DOI: 10.1002/anie.200503216

A μ-η²:η²-Disulfide Dicopper(II) Complex from Reaction of S_8 with a Copper(I) Precursor: Reactivity of the Bound Disulfur Moiety**

*Matthew E. Helton, Debabrata Maiti, Lev N. Zakharov, Arnold L. Rheingold, John A. Porco, Jr., and Kenneth D. Karlin**

Copper chalcogenide compounds including clusters are of continuing interest in structural, synthetic, and materials chemistry,[1,2] while examples of copper/inorganic-sulfur

[*] Dr. M. E. Helton, D. Maiti, Prof. K. D. Karlin
Department of Chemistry
Johns Hopkins University
3400 North Charles Street, Baltimore, MD 21218 (USA)
Fax: (+1) 410-516-7044
E-mail: karlin@jhu.edu

L. N. Zakharov,[+] Prof. A. L. Rheingold[+]
Department of Chemistry and Biochemistry
University of Delaware
Newark, DE 19716 (USA)

Prof. J. A. Porco, Jr.
Department of Chemistry and
Center for Chemical Methodology and
Library Development
Boston University
Boston, MA 02215 (USA)

[+] Current address:
Department of Chemistry and Biochemistry
University of California San Diego
La Jolla, CA 92093 (USA)

[**] K. D. Karlin is grateful to the US National Institute of Health (NIH, GM 28962) for financial support of the research. M. E. Helton acknowledges support from the NIH for a postdoctoral fellowship. We also acknowledge Dr. Andreas Heutling (Boston University) for carrying out preliminary studies.

WILEY InterScience DISCOVER SOMETHING GREAT
© 2006 Wiley-VCH Verlag GmbH & Co. KGaA, Weinheim

active-site entities in biology were recently discovered in the case of two metalloenzymes.[3,4,5] Nitrous oxide reductase (N_2OR) has an active-site {(histidine)$_7$Cu$_4$S} cluster (called Cu_Z), where nitrous oxide binds and is reduced in the terminal step in bacterial denitrification ($N_2O + 2e^- + 2H^+ \rightarrow H_2O + N_2$).[3,4] The other case occurs in the active site of aerobic organism carbon monoxide dehydrogenase ($CO + H_2O \rightleftarrows CO_2 + 2H^+ + 2e^-$), with a molybdopterin and copper containing Mo-S-Cu^I-S$_{cysteine}$ moiety.[5] With these findings, there has been a surge of interest in relevant copper coordination chemistry, with goals including 1) the generation of discreet and tractable copper sulfide complexes, 2) the elucidation of their structure and spectroscopy, and 3) determination of copper sulfide compound chemistry, that is, redox and/or atom-transfer reactivity patterns.

Our own interests are focused towards chemistry potentially relevant to N_2OR. We previously reported the use of elemental sulfur as a reagent to generate new copper sulfide complexes with nitrogen containing co-ligands. In the reaction of a copper(I) complex of tris(2-pyridylmethyl)amine (TMPA) with S_8, the first example of an end-on bound μ-1,2-disulfido dicopper(II) complex was discovered.[6,7] Herein, we report rather that, with a tridentate ligand, *N*,*N*-bis{2-[2-(*N*′,*N*′-4-dimethylamino)pyridyl]ethyl} methylamine ((MePY2)^{Me_2N}), and S_8 a side-on bound μ-η^2:η^2-disulfido dicopper(II) compound is formed, [{Cu^{II}(MePY2)^{Me_2N}}$_2$-(S_2^{2-})]$^{2+}$ (**1**). It is notable that the pattern of structures, end-on versus side-on binding with a tetradentate versus tridentate ligand for copper, exactly follows that already known for peroxo dicopper(II) complexes formed in ligand–Cu^I/O_2 reactivity investigations.[8,9] We also report the reactivity of **1** towards exogenous substrates; (reversible) displacement of bound sulfur can be effected by a number of reagents, and substrate-sulfur-atom transfer can also be demonstrated. Kitajima, Fujisawa, and co-workers have also generated a side-on bound analogue of **1** using a tridentate hydrotris(3,5-diisopropyl-1-pyrazolyl)borate (HB(3,5-*i*Pr$_2$pz)$_3$) ligand; the disulfide moiety formed through thermal decomposition (through C–S bond cleavage and follow-up chemistry) of a thiolate copper(II) complex.[10] More recently, Tolman, Alvarez, and co-workers employed bidentate β-diketiminate and anilido imine supporting ligands and ligand–copper(I) reactions with either trimethylsilylsulfide or S_8 to form μ-η^2:η^2-disulfido dicopper(II) compounds.[11] The study presented herein complements this investigation, but **1** shows a considerably more diverse reactivity than has been previously known.

The X-ray crystal structure of **1**-[B(C$_6$F$_5$)$_4$]$_2$·2 CH$_2$Cl$_2$ (Figure 1) reveals that the copper ions in the centrosymmetric binuclear complex are pentacoordinate, in slightly distorted square-pyramidal environments ($\tau = 0.06$);[12] both pyridyl nitrogen atoms (N(1) and N(4)) and the disulfur unit are equatorial ligands. The remaining alkylamino nitrogen N(3) is in the axial position. The nonbonding Cu···Cu (3.9336(10) Å) distance and the S–S (2.117(2) Å) bond in **1** fall in the middle of a relatively narrow range of values seen for the other known disulfido dicopper(II) complexes.[6,10,11]

The UV/Vis absorption spectrum of **1**-[B(C$_6$F$_5$)$_4$]$_2$·CH$_2$Cl$_2$ in acetone at reduced temperature contains multiple features

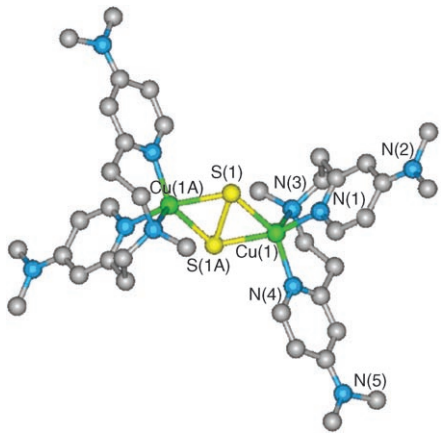
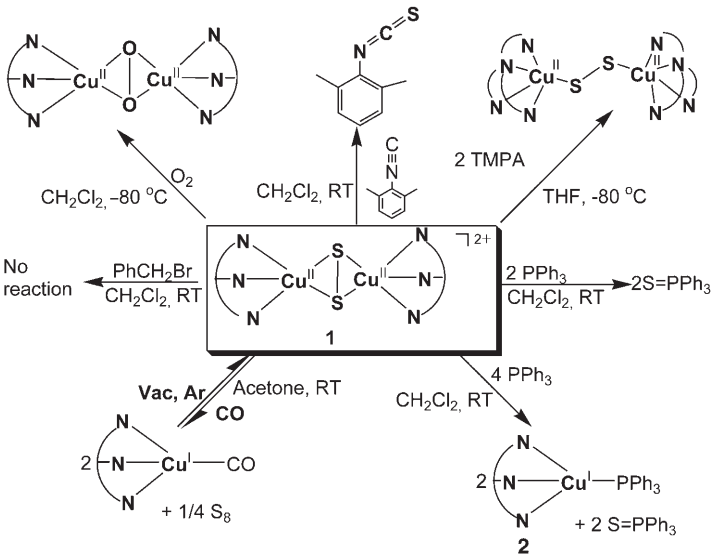


Figure 1. X-ray structure of the cation of **1**-[B(C$_6$F$_5$)$_4$]$_2$·2 CH$_2$Cl$_2$ (hydrogen atoms are omitted for clarity; yellow S, green Cu, blue N, gray C). Selected bond lengths [Å] and angles [°]: S(1)–S(1A) 2.117(2), Cu(1)–S(1) 2.2249(12), Cu(1)–S(1A) 2.2420(12), Cu(1)–N(1) 1.978(4), Cu(1)–N(3) 2.225(4), Cu(1)–N(4) 1.978(4). Cu(1A)···Cu(1) 3.9336(10); N(1)-Cu(1)-S(1) 96.53(12), N(3)-Cu(1)-S(1) 105.18(10), N(4)-Cu(1)-S(1) 151.30(11), N(1)-Cu(1)-S(1A) 147.50(12), N(3)-Cu(1)-S(1A) 104.59(10), N(4)-Cu(1)-S(1A) 98.93(11), S(1A)-S(1)-Cu(1) 62.12(5), S(1)-Cu(1)-S(1A) 56.57(5), S(1A)-S(1)-Cu(1A) 61.31(6), Cu(1)-S(1)-Cu(1A) 123.43(5).

λmax [nm] (ε, M^{-1}cm^{-1}) at 315 (13900), 395 (3700), 460 (1850), and 630 (460). There is a noticeable difference in the charge-transfer energy and intensity for these transitions of complex **1** relative to Kitajima's[10] and Tolman's[11] complexes, most likely because the (MePY2)^{Me_2N} ligand is neutral whereas the other systems have ligands with a −1 charge.

As mentioned above, an understanding of the reactivity of copper sulfur (disulfide in this case) complexes is of considerable interest, but almost no information is yet available. Preliminary studies, the first of their kind, are described below. The reaction of **1** with PPh_3 leads to nearly quantitative yields of triphenylphosphine sulfide (S=PPh$_3$; Scheme 1), assuming the reaction leads to formal "release" of zero-valent



Scheme 1. Reactivity of the {Cu$_2$S$_2$} core in **1** towards exogenous substrates.

 © 2006 Wiley-VCH Verlag GmbH & Co. KGaA, Weinheim

sulfur and reduction of copper ion to give $[Cu^{I}(MePY2)^{Me_2N}]^{+}$. With excess (4 equiv) PPh_3, the copper(I) is trapped as the phosphine complex $[Cu^{I}(MePY2)^{Me_2N}(PPh_3)]^{+}$ (**2**; Scheme 1). Sulfur atom transfer from **1** also occurs in a near quantitiative manner (GC and GC/MS analysis) when treated with 2,6-dimethylphenylisocyanide, leading to the corresponding isothiocyanate (Scheme 1). Such chemistry is known for other metal sulfur compounds.[13]

Interestingly, there is no reaction of **1** with benzyl bromide (Scheme 1). This observation, combined with the results of the PPh_3 and isocyanide reactivity, indicates that the disulfur moiety in **1** is electrophilic. In fact, this reactivity directly contrasts with what we otherwise observe for an end-on μ-1,2-disulfido complex where nucleophilic chemistry occurs; with a modified TMPA ligand, $TMPA^{R}$, we observe that $[\{Cu^{II}(TMPA^{R})\}_2(S_2)]^{2+} + 2\,PhCH_2Br \rightarrow 2\,[Cu^{II}(TMPA^{R})Br]^{+} + PhCH_2SSCH_2Ph$. Thus, our findings with ligand–Cu^{I}/S_8 reactivity appear to parallel those for ligand–Cu^{I}/O_2 chemistry, as side-on bound peroxo dicopper(II) complexes are generally electrophilic compared to end-on bound peroxides (e.g., as with TMPA) which are nucleophilic towards exogenous substrates.[8,14]

Other reactions also provide insight concerning the nature of the Cu^{II} disulfide moiety in **1**. Dioxygen displaces the disulfur moiety in **1**, leading to the already well established μ-η^2:η^2-peroxo complex $[\{Cu^{II}(MePY2)^{Me_2N}\}_2(O_2^{2-})]^{2+}$ (λ_{max} = 360 nm; Scheme 1).[15] When CO is bubbled through an acetone solution of **1**, the reddish color is bleached as a result of the formation of the previously reported[15] carbonyl complex, $[Cu^{I}(MePY2)^{Me_2N}(CO)]^{+}$ ($\nu_{CO} = 2077\ cm^{-1}$) (Scheme 1). That elemental sulfur is reformed in the reaction of **1** with CO is indicated by the reversible nature of the reaction. Application of a vacuum/Ar purge to the solution (which removes the carbon monoxide) leads to a change from colorless back to reddish as concomitant growth in the absorption features arising to **1** occurs. This carbonylation/sulfur-release/CO-removal cycle can be repeated several times.

Addition of the tetradentate ligand TMPA to a THF solution of **1** causes an immediate color change to purple, the solution exhibiting a UV/Vis feature at 568 nm ascribed to the known complex $[\{Cu^{II}(TMPA)\}_2(S_2^{2-})]^{2+}$ (Scheme 1).[6,7] This result implies the greater thermodynamic stability of $[\{Cu^{II}(TMPA)\}_2(S_2^{2-})]^{2+}$ compared to $[\{Cu^{II}(MePY2)^{Me_2N}\}_2(S_2^{2-})]^{2+}$ (**1**) and may reside with the tetradentate (versus tridentate) nature of the ligand. Tolman and co-workers have also demonstrated related disulfide exchange reactions.[11]

In conclusion, a $\{Cu_2S_2\}$ core with bound side-on μ-η^2:η^2-S_2^{2-} moiety has been synthesized and characterized and the reactivity with exogenous substrates has been explored. This represents the first example of a sulfur atom-transfer reaction from a copper sulfur moiety to substrates. Striking analogies between copper dioxygen and copper sulfur chemistry appear to be emerging. The use of elemental sulfur in reactions with ligand–copper(I) complexes seems to be a lucrative avenue for future generation of copper sulfur entities. Future investigations will include further structural–spectroscopic interrogations and elaboration of the scope of sulfur atom-transfer reactivity of this and other dicopper disulfide moieties. Redox chemistry, including reduction of **1** or analogues, could lead to new copper sulfide species capable of N_2O reduction chemistry.[3,16]

Experimental Section

Preparation of **1**-$[B(C_6F_5)_4]_2\cdot CH_2Cl_2$: Solid elemental sulfur (0.0045 g, 1.75×10^{-5} mol) was added to a stirred solution of $[\{Cu^{I}((MePY2)^{Me_2N}\}][B(C_6F_5)_4]$ (0.150 g, 1.40×10^{-4} mol) prepared in dry/deoxygenated CH_2Cl_2 (5 mL). The color of the solution changed from near-colorless to dark red-brown over the course of a few hours; this solution was allowed to stir for at least 1 day. Addition of dry/deoxygenated pentane (75 mL) precipitated dark colored solid **1** which was collected by filtration through a coarse porosity Schlenk filter-frit. The solid was redissolved in CH_2Cl_2 and filtered through a KimWipe plugged pipette and then the solvent was removed under vacuum, and this process was repeated 5 times to confirm the removal of all residual S_8. The product was finally precipitated out with pentane. After collection by filtration, the solid product $[\{Cu^{II}(MePY2)^{Me_2N}\}_2(S_2^{2-})][B(C_6F_5)_4]_2\cdot CH_2Cl_2$ (0.080 g; 50%) was dried under vacuum. Elemental analysis (%) calcd for $C_{87}H_{60}B_2Cl_2Cu_2F_{40}N_{10}S_2$: C 45.65, H 2.64, N 6.12; found: C 45.97, H 2.72, N 6.11.

X-ray crystal structure analysis of **1**-$[B(C_6F_5)_4]_2\cdot 2\,CH_2Cl_2$: A red crystal suitable for X-ray diffraction was obtained from dichloromethane layered with pentane. Crystal data: $C_{88}H_{62}B_2Cl_4Cu_2F_{40}N_{10}S_2$, $M_r = 2374.10$, triclinic, space group $P\bar{1}$ (no. 2), $a = 11.3778(7)$, $b = 14.9669(9)$, $c = 15.8101(9)$ Å, $\alpha = 106.7870(10)$, $\beta = 103.6420(10)$, $\gamma = 107.3320(10)°$, $V = 2302.9(2)C^3$, $Z = 1$, $\rho_{calcd} = 1.712\ g\,cm^{-3}$, $\mu = 0.758\ mm^{-1}$, $Mo_{K\alpha}$ radiation ($\lambda = 0.71070$ Å), $T = 173$ K, $R_1 = 0.074$, $R_w = 0.088$. CCDC-283434 contains the supplementary crystallographic data for this paper. These data can be obtained free of charge from The Cambridge Crystallographic Data Centre via www.ccdc.cam.ac.uk/data_request/cif.

PPh_3 reactions: ^{31}P NMR spectroscopy of the reaction mixture of **1**-$[B(C_6F_5)_4]_2\cdot 2\,CH_2Cl_2$ with 4 equiv PPh_3 in $CDCl_3$ with $P(Mes)_3$ as reference: (400 MHz); $\delta = 43.92$ ($S{=}PPh_3$), −1.69 (**2**), −4.62 (PPh_3), −35.91 ppm ($P(Mes)_3$). On the basis of integration, the ratio of $S{=}PPh_3/[\mathbf{2}{+}PPh_3] \approx 1{:}1.2$ showed the reaction yield was 91%. ^{31}P NMR, **2** in $CDCl_3$ with $P(Mes)_3$ as reference (400 MHz): $\delta = -1.72$(**2**), −35.92 ppm ($P(Mes)_3$). ^{1}H NMR, **2** in $CDCl_3$ (400 MHz): $\delta = 7.8$ (2H, d, $J = 6.0$ Hz), 7.41–7.34 (15H, m, PPh_3), 6.29 (2H, d, $J = 2.8$ Hz), 6.25 (2H, d, $J = 6.4$ Hz), 2.97 (8H, m), 2.57 (8H, m), 2.26 ppm (3H, s). Elemental analysis (%) calcd for $[Cu^{I}(MePY2)^{Me_2N}(PPh_3)]\cdot(B(C_6F_5)_4)\cdot(C_5H_{12})_{0.9}$: C 56.30, H 3.95, N 5.01; found: 56.24, H 3.82, N 4.89.

Received: September 9, 2005
Published online: December 30, 2005

Keywords: atom transfer · bioinorganic chemistry · copper · N ligands · sulfur

[1] I. Dance, K. Fisher, *Prog. Inorg. Chem.* **1994**, *41*, 637–803.
[2] S. Dehnen, A. Eichhöfer, D. Fenske, *Eur. J. Inorg. Chem.* **2002**, *2*, 279–317.
[3] P. Chen, S. I. Gorelsky, S. Ghosh, E. I. Solomon, *Angew. Chem.* **2004**, *116*, 4224–4233; *Angew. Chem. Int. Ed.* **2004**, *43*, 4132–4140.
[4] T. Haltia, K. Brown, M. Tegoni, C. Cambillau, M. Saraste, K. Mattila, K. Djinovic-Carugo, *Biochem. J.* **2003**, *369*, 77–88.
[5] H. Dobbek, L. Gremer, R. Kiefersauer, R. Huber, O. Meyer, *Proc. Natl. Acad. Sci. USA* **2002**, *99*, 15971–15976.

 © 2006 Wiley-VCH Verlag GmbH & Co. KGaA, Weinheim

[6] M. E. Helton, P. Chen, P. P. Paul, Z. Tyeklár, R. D. Sommer, L. N. Zakharov, A. L. Rheingold, E. I. Solomon, K. D. Karlin, *J. Am. Chem. Soc.* **2003**, *125*, 1160 – 1161.
[7] P. Chen, K. Fujisawa, M. E. Helton, K. D. Karlin, E. I. Solomon, *J. Am. Chem. Soc.* **2003**, *125*, 6394 – 6408.
[8] L. Q. Hatcher, K. D. Karlin, *J. Biol. Inorg. Chem.* **2004**, *9*, 669 – 683.
[9] L. M. Mirica, X. Ottenwaelder, T. D. P. Stack, *Chem. Rev.* **2004**, *104*, 1013 – 1045.
[10] K. Fujisawa, Y. Moro-oka, N. Kitajima, *J. Chem. Soc. Chem. Commun.* **1994**, 623 – 624.
[11] E. C. Brown, N. W. Aboelella, A. M. Reynolds, G. Aullon, S. Alvarez, W. B. Tolman, *Inorg. Chem.* **2004**, *43*, 3335 – 3337.
[12] A. W. Addison, T. N. Rao, J. Reedijk, J. v. Rijn, G. C. Verschoor, *J. Chem. Soc. Dalton Trans.* **1984**, 1349 – 1356.
[13] M. Arisawa, M. Ashikawa, A. Suwa, M. Yamaguchi, *Tetrahedron Lett.* **2005**, *46*, 1727 – 1729.
[14] P. P. Paul, Z. Tyeklar, R. R. Jacobson, K. D. Karlin, *J. Am. Chem. Soc.* **1991**, *113*, 5322 – 5332.
[15] C. X. Zhang, H.-C. Liang, E.-i. Kim, J. Shearer, M. E. Helton, E. Kim, S. Kaderli, C. D. Incarvito, A. D. Zuberbuehler, A. L. Rheingold, K. D. Karlin, *J. Am. Chem. Soc.* **2003**, *125*, 634 – 635.
[16] J. M. Chan, J. A. Bollinger, C. L. Grewell, D. M. Dooley, *J. Am. Chem. Soc.* **2004**, *126*, 3030 – 3031.

 © 2006 Wiley-VCH Verlag GmbH & Co. KGaA, Weinheim

Helical Structures

DOI: 10.1002/anie.200503142

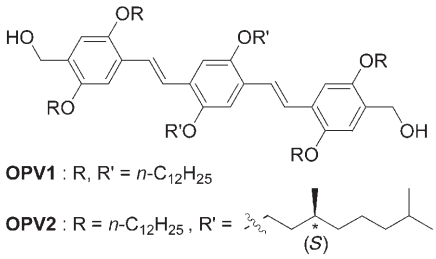
Transcription and Amplification of Molecular Chirality to Oppositely Biased Supramolecular π Helices**

Ayyappanpillai Ajayaghosh, Reji Varghese, Subi Jacob George, and Chakkooth Vijayakumar*

Nature has the amazing ability to create functional architectures with a preferred helicity over a wide range of scales: from nanoscopic DNA to macroscopic seashells. For example, the helical sense of biomacromolecules such as the DNA double helix and the collagen triple helix is determined by the configuration of the chiral centers present in their nucleotide or peptide backbone that bias the long-range overall order to a single handedness in a well-defined self-assembled architecture. The elegance and complexity of natural homochiral architectures has inspired chemists to explore noncovalent interactions, such as H bonding, π stacking, and van der Waals forces, between chiral building blocks to form a variety of aesthetically appealing helical supramolecular assemblies.[1–4] However, the control and prediction of the supramolecular chirality of artificial systems on the nano- to micrometer length scale continues to elude scientists.[5]

The amplification of chirality in polyisocyanates by Green et al. through the "sergeants and soldiers" approach was a clever step toward achieving macromolecular chirality in synthetic polymers.[6] The same principle was later independently applied by the research groups of Meijer and Reinhoudt to induce chirality in dynamic hydrogen-bonded assemblies.[7,8] These observations have prompted us to explore the viability of the "sergeants and soldiers" approach in organogel systems based on oligo(*p*-phenylenevinylene) (OPV).[9] Herein we show spectroscopic and microscopy evidence for the transcription and amplification of molecular chirality to supramolecular helicity through the unprecedented formation of right-handed (*P*) and left-handed (*M*) helices. These oppositely biased structures originate from the same stereogenic centers during the coassembly processes. Most surprisingly, we observed the formation of longitudinally fused *M* and *P* helices, which is a unique phenomenon.

We chose to use an achiral molecule **OPV1**[9a] and a chiral analogue **OPV2** with two remote chiral handles[9c] (Scheme 1). **OPV2** tends to aggregate above a concentration



Scheme 1. Structures of the achiral and chiral molecules under investigation.

of 1.8×10^{-4} M in dodecane and leads to an exciton-coupled bisignate CD signal in the region of the π-π* transition which is characteristic of a left-handed helical assembly. However, it does not show any CD signal below this concentration, thus confirming that it is not possible to transfer chiral information from the stereogenic centers to the chromophore. In contrast, **OPV1** is inherently CD silent, although it forms aggregates and gels in dodecane.[9e] Mixing **OPV2** and **OPV1** together in dodecane (1.67 mol% of **OPV2**) at a total concentration of 7.5×10^{-4} M results in a CD signal with positive and negative Cotton effects, with the intensity of the signal increasing as the composition of **OPV2** increases up to 22 mol% (Figure 1a). The inversion of the CD spectrum with a near mirror image relationship at low compositions of **OPV2** indicates the formation of helices with opposite handedness, which was quite surprising (Figure 1a, inset). Increasing the mol% of **OPV2** further results in a decrease in the intensity of the CD

[*] Dr. A. Ajayaghosh, R. Varghese, S. J. George, C. Vijayakumar
Photosciences and Photonics Unit
Chemical Sciences Division
Regional Research Laboratory, CSIR
Trivandrum 695 019 (India)
Fax: (+91) 471-490186
E-mail: aajayaghosh@rediffmail.com

[**] This work was supported by the Department of Science and Technology (DST), Government of India, New Delhi, and the Council of Scientific and Industrial Research (CSIR, Task Force Program, CMM 10). R.V., S.J.G., and C.V. thank the CSIR, Government of India, for research fellowships. This is contribution No. RRLT-PPU-211.

 © 2006 Wiley-VCH Verlag GmbH & Co. KGaA, Weinheim

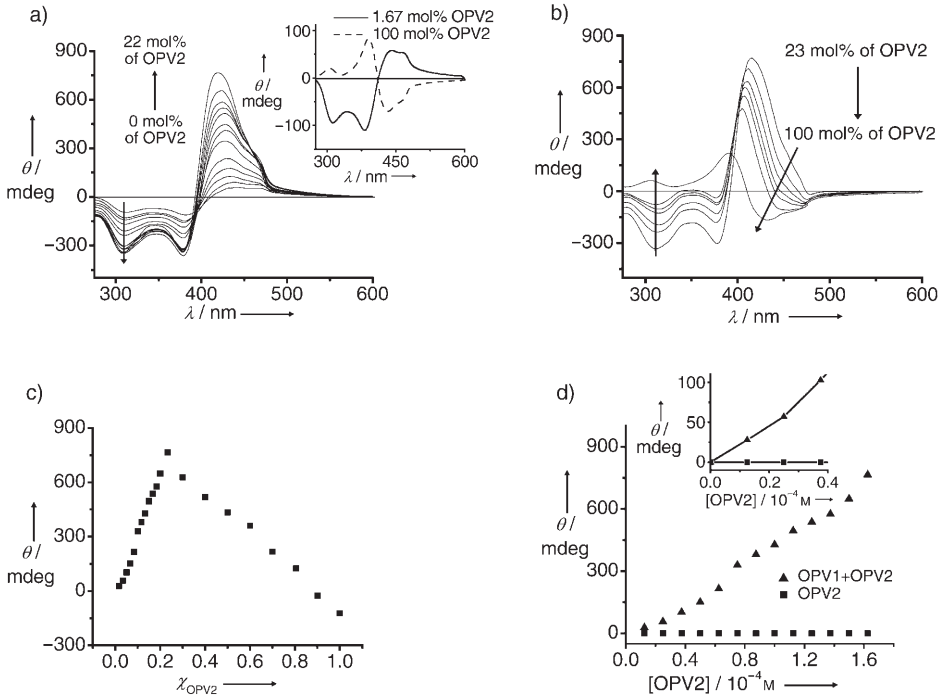


Figure 1. Changes in the CD spectrum during the coassembly of **OPV1**–**OPV2** in dodecane (7.5×10^{-4} M) at different compositions: a) 0–22 mol% of **OPV2**; the inset shows the mirror-image relationship of the CD spectra of **OPV2** and the **OPV1**–**OPV2** coassembly at 1.67 mol% of **OPV2**; b) 23–100 mol% of **OPV2**; c) variation of CD intensity at 420 nm with increasing mole fraction (χ) of **OPV2** at a total concentration of 7.5×10^{-4} M in dodecane; d) plots of CD intensity at 420 nm against the concentrations of **OPV2** in the homoassembly and coassembly; the inset shows the CD intensity variation up to 0.4×10^{-4} M. All measurements were carried out in a 1-mm cuvette at 278 K.

signal. A gradual blue-shift of the positive Cotton effect with concomitant weak growth of a negative signal is observed which tend to merge with the CD spectrum of pure **OPV2** (Figure 1b). This situation is clear from the plot of the CD intensity at 420 nm against the mole fraction of **OPV2** in the coassembly (Figure 1c). It is important to remember that **OPV2** on its own failed to give a CD signal up to a concentration of 1.6×10^{-4} M (Figure 1d). The observed CD spectrum, therefore, is the direct result of the formation of a coassembly and not the intrinsic property of the individual components. CD signals are observed even at very low concentrations (1.25×10^{-5} M, 1.67 mol%) of **OPV2** (Figure 1d, inset) during coassembly. This concentration is nearly 14 times less than that of pure **OPV2** which results in the onset of a CD signal, and reveals a remarkable induction and amplification of chirality as a result of the "sergeants and soldiers" effect during the coassembly process.

A temperature-dependent CD signal and the changes in the UV spectra (not shown) indicate a sharp transition above 45 °C for compositions up to 22 mol% of **OPV2**. However, at least two transitions are observed over a wide range of temperatures with greater than 22 mol% of **OPV2**. The composition-dependent variation of the CD spectra and the plots of the temperature-dependent changes in the CD intensity transition are complementary, and reveal the formation of helical aggregates that differ in stability at higher mole ratios of **OPV2** (>22 mol%). The observations from the CD studies are unequivocally confirmed by AFM analysis of the coassembly.

The tapping mode AFM height image (Figure 2a) of the **OPV2** homoassembly showed left-handed helical tapes, in agreement with the observed CD spectrum. The width of the tapes varies from 78 ± 1 to 176 ± 1 nm and they are several micrometers in length, with an average helical pitch length of 156 ± 1 nm. The thickness of these tapes varied from 9 ± 1 to 20 ± 1 nm. The AFM image of the coassembly of **OPV1** with 9 mol% of **OPV2** showed the presence of *P*-helical tapes along with a few oppositely biased *M*-helical tapes (Figure 2b). The width of the smallest fiber obtained in this case is 106 ± 1 nm and the thickness is 4 ± 1 nm. The number of *M* helices increase as the mol% of **OPV2** in the coassembly is increased. The AFM image of the coassembly of **OPV1** with 60 mol% **OPV2** shows the presence of mainly *M* helices along with a few *P* helices (Figure 2c), which is in agreement with the CD spectral changes.

Surprisingly, in addition to the oppositely biased individual helices, longitudinally fused *M* and *P* helices were also observed (Figure 3). These unusual structures are formed in large numbers at around 20 mol% of **OPV2** (Figure 3a, $c=9\times10^{-5}$ M). This observation supports the initial formation of individual nonhelical stacks of **OPV1**, left-handed stacks of **OPV2**, and a right-handed coassembly of **OPV1** and **OPV2**,

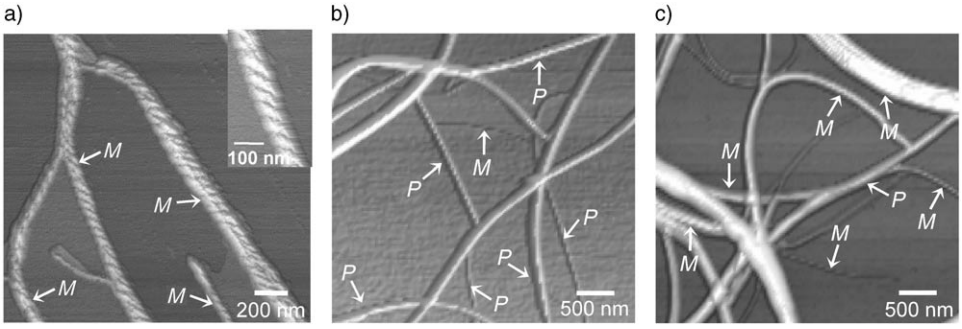


Figure 2. AFM height images of: a) **OPV2** homoassembly, b) coassembly of **OPV1** with 9 mol% of **OPV2**, and c) coassembly of **OPV1** with 60 mol% of **OPV2**. Samples were prepared in dodecane ($c=9\times10^{-5}$ M) and transferred to freshly cleaved mica by drop-casting under ambient conditions.

 © 2006 Wiley-VCH Verlag GmbH & Co. KGaA, Weinheim

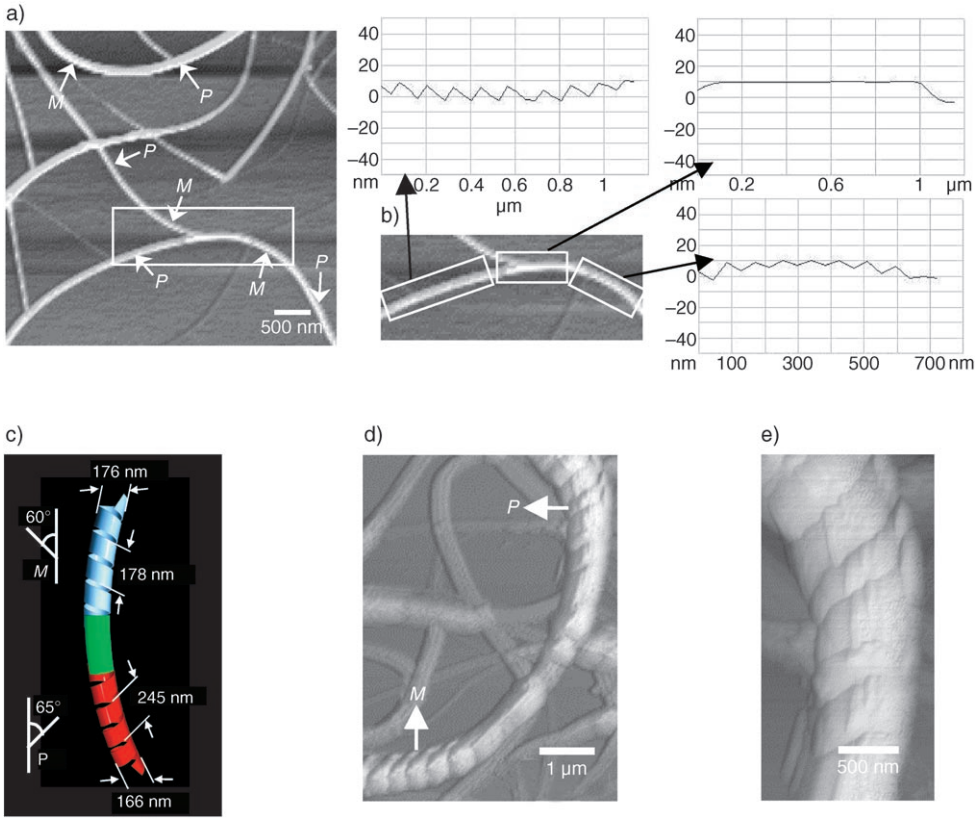


Figure 3. a) AFM image of fused helices at 20 mol% **OPV2**. b) Cross-sectional analysis of *P*-, *M*-, and nonhelical zones. c) A schematic representation of the fused helical tape showing the morphological parameters. d) An enlarged image of the coassembly showing the *M*- and *P*-supercoiled segments. e) A right-handed coiled-coil super structure formed from left-handed coiled tapes.

which at a later stage self-associate, thus resulting in fused superstructures. *M* helices predominate above 20 mol% of **OPV2**. The sign of the CD signal changes dramatically at these compositions (Figure 1b). Detailed section analysis of a fused helix showed a thickness of 13 ± 2 nm and a width of 166–176 nm. Cross-sectional analysis along the length of a fused assembly showed a uniform corrugated height profile for the *P*- and *M*-helical portions. The nonhelicity of the fused zone is clear from the linear profile (Figure 3b). AFM analysis of dried gels of the coassembly formed in dodecane (20 mol% of **OPV2**) showed micrometer-sized fused helices (Figure 3d). The enlarged image of the *P*-helical zone shows right-handed coiled-coil superstructures formed from the winding of left-handed helical tapes in the opposite screw sense (Figure 3e). Such artificial helical assemblies are reminiscent of the collagen triple helix in which three left-handed helices are wound to form a right-handed supercoil, but are rarely found in artificial assemblies.[5a]

Insights from the CD and AFM studies reveal that a helical bias of supramolecular chirality is possible within OPV coassemblies without changing the chiral handle attached to the chromophore. This result is in analogy to some of the previous reports on chirality inversion[10] and stereomutation[11] in polymers and in molecular excitons.[12] In these studies, other than CD spectral evidence, no morphological support of inverted or stereomutated helicity was reported. However, Würthner and coworkers have recently shown inversion of helicity in merocyanine dye aggregates, as evidenced by the changes in the exciton-coupled Cotton effect. However, AFM studies did not show the formation of opposite supramolecular helices.[13] In our case, $M \rightarrow P$ helix inversion and the associated changes could be unambiguously proved by CD and AFM techniques. It is interesting to note that in the "sergeants and soldiers" approach reported previously, the soldiers strictly follow the chiral instructions of the sergeants. In the present case, however, the soldiers mistake orders from the sergeants and behave in an opposite sense, which is a unique phenomenon in coassembled supramolecular architectures.

In conclusion, shown here is the hitherto unknown phenomenon of transcription of molecular chirality by inverted helicity. This process leads to supramolecular π helices with longitudinally fused *M* and *P* helices (originating from common stereogenic centers) during the coassembly of linearly π-conjugated organogelators. Apart from the exotic appeal, helical assemblies of such molecules may have implications in the emerging field of supramolecular electronics.[14]

Received: September 5, 2005
Published online: December 6, 2005

Keywords: chirality · gels · helical structures · scanning probe microscopy · self-assembly

[1] a) J.-M. Lehn, *Supramolecular Chemistry, Concepts and Perspectives*, VCH, Weinheim, **1995**.
[2] For recent reviews, see a) A. E. Rowan, R. J. M. Nolte, *Angew. Chem.* **1998**, *110*, 65–71; *Angew. Chem. Int. Ed.* **1998**, *37*, 63–68; b) J. J. L. M. Cornelissen, A. E. Rowan, R. J. M. Nolte, N. A. J. M. Sommerdijk, *Chem. Rev.* **2001**, *101*, 4039–4070; c) L. Brunsveld, B. J. B. Folmer, E. W. Meijer, R. P. Sijbesma, *Chem. Rev.* **2001**, *101*, 4071–4097; d) C. Schmuck, *Angew. Chem.* **2003**, *115*, 2552–2556; *Angew. Chem. Int. Ed.* **2003**, *42*, 2448–2452.
[3] See, for example, a) M. de Loos, J. van Esch, R. M. Kellogg, B. L. Feringa, *Angew. Chem.* **2001**, *113*, 633–636; *Angew. Chem. Int. Ed.* **2001**, *40*, 613–616; b) F. Würthner, S. Yao, U. Beginn, *Angew. Chem.* **2003**, *115*, 3368–3371; *Angew. Chem. Int. Ed.*

 © 2006 Wiley-VCH Verlag GmbH & Co. KGaA, Weinheim

2003, *42*, 3247 – 3250; c) M. Kimura, T. Kuroda, K. Ohta, K. Hanabusa, H. Shirai, N. Kobayashi, *Langmuir* **2003**, *19*, 4825 – 4830; d) J. P. Hill, W. Jin, A. Kosaka, T. Fukushima, H. Ichihara, T. Shimomura, K. Ito, T. Hashizume, N. Ishii, T. Aida, *Science* **2004**, *304*, 1481 – 1483.

[4] a) A. P. H. J. Schenning, P. Jonkheijm, E. Peeters, E. W. Meijer, *J. Am. Chem. Soc.* **2001**, *123*, 409 – 416; b) P. Jonkheijm, A. Miura, M. Zdanowska, F. J. M. Hoeben, S. De Feyter, A. P. H. J. Schenning, F. C. De Schryver, E. W. Meijer, *Angew. Chem.* **2004**, *116*, 76 – 80; *Angew. Chem. Int. Ed.* **2004**, *43*, 74 – 78.

[5] See, for example: a) H. Engelkamp, S. Middelbeek, R. J. M. Nolte, *Science* **1999**, *284*, 785 – 788; b) J. J. D. de Jong, L. N. Lucas, R. M. Kellogg, J. H. van Esch, B. L. Feringa, *Science* **2004**, *304*, 278 – 281; c) A. Petitjean, H. Nierengarten, A. van Dorsselaer, J.-M. Lehn, *Angew. Chem.* **2004**, *116*, 3781 – 3785; *Angew. Chem. Int. Ed.* **2004**, *43*, 3695 – 3699; d) T. Yamaguchi, T. Kimura, H. Matsuda, T. Aida, *Angew. Chem.* **2004**, *116*, 6510 – 6515; *Angew. Chem. Int. Ed.* **2004**, *43*, 6350 – 6355; e) B. W. Messmore, P. A. Sukerkar, S. I. Stupp, *J. Am. Chem. Soc.* **2005**, *127*, 7992 – 7993.

[6] a) M. M. Green, M. P. Reidy, *J. Am. Chem. Soc.* **1989**, *111*, 6452 – 6454; b) M. M. Green, J.-W. Park, T. Sato, A. Teramoto, S. Lifson, R. L. B. Selinger, J. V. Selinger, *Angew. Chem.* **1999**, *111*, 3328 – 3345; *Angew. Chem. Int. Ed.* **1999**, *38*, 3138 – 3154.

[7] a) A. R. A. Palmans, J. A. J. M. Vekemans, E. E. Havinga, E. W. Meijer, *Angew. Chem.* **1997**, *109*, 2763 – 2765; *Angew. Chem. Int. Ed. Engl.* **1997**, *36*, 2648 – 2651; b) R. B. Prince, J. S. Moore, L. Brunsveld, E. W. Meijer, *Chem. Eur. J.* **2001**, *7*, 4150 – 4154; c) A. P. H. J. Schenning, A. F. M. Kilbinger, F. Biscarini, M. Cavallini, H. J. Cooper, P. J. Derrick, W. J. Feast, R. Lazzaroni, Ph. Leclère, L. A. McDonel, E. W. Meijer, S. C. J. Meskers, *J. Am. Chem. Soc.* **2002**, *124*, 1269 – 1275; d) A. J. Wilson, M. Masuda, R. P. Sijbesma, E. W. Meijer, *Angew. Chem.* **2005**, *117*, 2315 – 2319; *Angew. Chem. Int. Ed.* **2005**, *44*, 2275 – 2279.

[8] a) L. J. Prins, J. Huskens, F. de Jong, P. Timmerman, D. N. Reinhoudt, *Nature* **1999**, *398*, 498 – 502; b) L. J. Prins, P. Timmerman, D. N. Reinhoudt, *J. Am. Chem. Soc.* **2001**, *123*, 10153 – 10163.

[9] a) A. Ajayaghosh, S. J. George, *J. Am. Chem. Soc.* **2001**, *123*, 5148 – 5149; b) A. Ajayaghosh, S. J. George, V. K. Praveen, *Angew. Chem.* **2003**, *115*, 346 – 349; *Angew. Chem. Int. Ed.* **2003**, *42*, 332 – 335; c) S. J. George, A. Ajayaghosh, P. Jonkheijm, A. P. H. J. Schenning, E. W. Meijer, *Angew. Chem.* **2004**, *116*, 3504 – 3507; *Angew. Chem. Int. Ed.* **2004**, *43*, 3422 – 3425; d) R. Varghese, S. J. George, A. Ajayaghosh, *Chem. Commun.* **2005**, 593 – 595; e) S. J. George, A. Ajayaghosh, *Chem. Eur. J.* **2005**, *11*, 3217 – 3227.

[10] a) M. Fujiki, *J. Am. Chem. Soc.* **2000**, *122*, 3336 – 3343; b) W. Peng, M. Motonaga, J. R. Koe, *J. Am. Chem. Soc.* **2004**, *126*, 13822 – 13826.

[11] M. M. Bouman, E. W. Meijer, *Adv. Mater.* **1995**, *7*, 385 – 387.

[12] a) S. E. Boiadjiev, D. A. Lightner, *J. Am. Chem. Soc.* **2000**, *122*, 378 – 383; b) S.-J. Su, M. Takeishi, N. Kuramoto, *Macromolecules* **2002**, *35*, 5752 – 5757.

[13] A. Lohr, M. Lysetska, F. Würthner, *Angew. Chem.* **2005**, *117*, 5199 – 5202; *Angew. Chem. Int. Ed.* **2005**, *44*, 5071 – 5074.

[14] a) E. W. Meijer, A. P. H. J. Schenning, *Nature* **2002**, *419*, 353 – 354; b) M. V. D. Auweraer, F. C. De Schryver, *Nat. Mater.* **2004**, *3*, 507 – 508; c) H. John, R. Bauer, P. Espindola, P. Sonar, J. Heinze, K. Müllen, *Angew. Chem.* **2005**, *117*, 2501 – 2505; *Angew. Chem. Int. Ed.* **2005**, *44*, 2447 – 2451; d) A. P. H. J. Schenning, E. W. Meijer, *Chem. Commun.* **2005**, 3245 – 3258.

 © 2006 Wiley-VCH Verlag GmbH & Co. KGaA, Weinheim

Computational Chemistry

DOI: 10.1002/anie.200502259

The Molecular Origin of the "Continuous" Infrared Absorption in Aqueous Solutions of Acids: A Computational Approach**

Radu Iftimie and Mark E. Tuckerman**

The dissociation of weak acids in water is a process of fundamental importance in chemistry and biochemistry. The familiar reaction shown in [Eq. (1)] that describes the

$$HA_{(aq)} + H_2O \rightarrow A^-_{(aq)} + H_3O^+_{(aq)} \quad (1)$$

dissociation process of the weak acid HA has been the object of numerous experimental and theoretical investigations, which have focused on the chemical nature of the solvated reactants and products[1] and stable or transient intermediate structures.[2]

However, the deceptive simplicity of reaction (1) masks a wealth of microscopic behavior that remains largely unexplained. Important insights into the dissociation mechanism can be gleaned from infrared (IR) spectra of aqueous solutions of weak acids.[3] In particular, the IR spectra of these acids exhibit a broad absorption band extending from the lower range of the OH stretch band of water at $\tilde{\nu} = 3000\ cm^{-1}$ to the HOH bending peak at $\tilde{\nu} = 1500\ cm^{-1}$ and in some instances all the way down to the onset of the water libration band at $\tilde{\nu} = 1000\ cm^{-1}$. This "continuum of absorption" is reminiscent of that seen for solutions of strong acids, where its origin can be explained in terms of frequent proton-transfer events between H_3O^+ and H_2O units. In the case of weak acids, however, the early transmission spectroscopy investigations of Leuchs and Zundel[3] as well as the more recent attenuated total reflection measurements of Max and Chapados[4] strongly suggest that it is either the unionized hydrated acid $HA_{(aq)}$ or some relatively stable supramolecular

[*] Prof. Dr. R. Iftimie
Département de Chimie
Université de Montréal
Montréal, H3T1J4 (Canada)
Fax: (+1) 514-343-7586
E-mail: radu.ion.iftimie@umontreal.ca
Prof. Dr. M. E. Tuckerman
Department of Chemistry and
Courant Institute for Mathematical Sciences
New York University
New York, NY 10003 (USA)
Fax: (+1) 212-260-7905
E-mail: mark.tuckerman@nyu.edu

[**] This work was supported by the NSF (CHE-0121375 and CHE-0310107) and by an NSERC PDF of Canada.

Supporting information for this article, containing analysis of statistical errors, is available on the WWW under http://www.angewandte.org or from the author.

WILEY InterScience DISCOVER SOMETHING GREAT
© 2006 Wiley-VCH Verlag GmbH & Co. KGaA, Weinheim

ionic assembly of A^- with a protonated cluster of water molecules that is directly responsible for the observed continuous absorption.

Herein, we employ Car–Parrinello ab initio molecular dynamics[5] to investigate the ability of IR spectroscopy to differentiate between unionized molecules and the solvent-separated, solvent-shared, and contact ion pair supramolecular intermediates that appear in theoretical treatments of the dissociation of weak acids (see Figure 1).[6,7] The conclusion

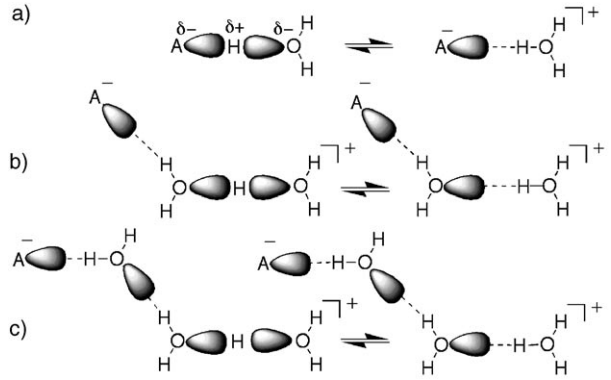


Figure 1. A schematic representation of some of the possible stable and transient intermediates in reaction 1: a) contact ion pairs, b) solvent-shared ion pairs, and c) solvent-separated ion pairs. If the oppositely charged ions are separated by more than 8 Å (roughly two intervening water molecules), they tend to diffuse away from each other[6] to form the products of dissociation shown in reaction (1). The structures on the left-hand side of the equilibria correspond to ideal "Zundel" structures, in which a proton can move freely between two electronegative atoms. The structures on the right-hand side correspond to ideal "Eigen" structures in which a distinct hydronium ion H_3O^+ is formed.

that emerges from the present investigation is that the concentration of the ion pairs is proportional to the intensity of the continuous IR absorption between $\tilde{\nu}=1500$ and $1000\,cm^{-1}$. In contrast, we find that the intensity of the absorption between $\tilde{\nu}=3000$ and $1800\,cm^{-1}$ depends essentially as much on the concentration of the ion pairs as on that of the unionized molecules. These results complement and enhance the utility of existing IR spectra decomposition approaches[4] and suggest new ways in which these experiments can be used to elucidate the nature of the chemical species that exist in weakly acidic media.

The theoretical investigation consists of simulating the absolute IR dielectric spectra of two systems containing 0.85 M aqueous solutions of either unionized or ionized (but not dissociated) forms of the weak acid HF. The nature of the chemical species in the two systems was predetermined by the choice of the starting configuration. The initial configuration for the first system was generated by replacing a molecule of H_2O by a molecule of HF from an equilibrated system that contained 65 water molecules. The initial configuration of the second system was prepared by first equilibrating an aqueous solution of dissociated HCl and then replacing Cl^- with F^-. The HF molecule maintained its identity throughout the equilibration and the production stages of the simulation in the first system. In contrast, a Zundel-like contact ion pair (see Figure 1a) was formed during the equilibration period in the second system. This contact ion pair remained stable for most of the production run, except for a period of 1.5 ps in the middle of the trajectory when an Eigen-like contact ion pair and a Zundel-like solvent-shared ion pair were transiently formed.

The short 10 ps timescale accessed in our simulations and the limitations of the density functional theory (DFT) for investigating hydrogen-bonded systems precludes us from computing the concentration of the ion pairs with adequate confidence. Nevertheless, these limitations are most likely unimportant for calculations of the continua of absorption in IR spectra. Indeed, the timescale of the vibrations responsible for the continua of absorption is significantly shorter than our simulation timescale, while the performance of the exchange correlation functional employed is reasonably accurate in the prediction of vibrational frequencies for stable structures.[8]

With $\alpha(\tilde{\nu})$ denoting the Beer–Lambert absorptivity $(-1/l\ln(I/I_0))$ and $n(\tilde{\nu})$ representing the index of refraction, difference spectra $\Delta(\tilde{\nu})$ as a function of wavenumber $\tilde{\nu}$ between the absorption $[\alpha(\tilde{\nu})n(\tilde{\nu})]_c$ of an aqueous solution of HF of concentration "c" ($mol\,L^{-1}$) and the absorption $[\alpha(\tilde{\nu})n(\tilde{\nu})]_0$ of pure water were computed (see Equation (2)) using an approach recently developed by us.[10]

$$\Delta(\tilde{\nu}) = [\alpha(\tilde{\nu})n(\tilde{\nu})]_c - [\alpha(\tilde{\nu})n(\tilde{\nu})]_0 \qquad (2)$$

The new methodology allows both terms on the right-hand side of Equation (2) to be obtained from the simulation of the aqueous solution. Specifically, we employed on-the-fly Wannier orbital dynamics[11] to compute the trajectories of the dipole moments of those water molecules that were not hydrogen-bonded to HF or to its products of ionization. The "bulk" water spectrum was then computed from the cross-correlation of the solution dipole moment with the dipole moments of these selected water molecules by means of linear response theory. We have recently demonstrated[10] that this procedure dramatically improves the statistical accuracy of the reported difference spectra $\Delta(\tilde{\nu})$ thanks to substantial error cancellation in Equation (2).

After subtracting the contribution of the bulk water from the total absorption as illustrated in Equation (2), one is left with the continuous absorption generated by the presence of the various forms of HF. The difference spectra depicted in Figure 2 suggest that unionized species can be differentiated from ionized and dissociated acids because the presence of the former in an aqueous solution does not lead to significant absorption enhancements between $\tilde{\nu}=1000$ and $1500\,cm^{-1}$. The present results suggest that an analytical investigation of the aqueous solutions of weak acids in terms of unionized, ion pairs, and dissociated species should be possible by quantitative IR spectroscopic methods. The key aspect of such an analysis is the decomposition of the absorption spectrum (after the contributions of bulk water and free hydronium ions have been removed) into a sum of two elementary spectra. One such spectrum should exhibit a continuous absorption pattern similar to that found in strong acids which is attributable to ion pairs. The remaining spectrum should

 © 2006 Wiley-VCH Verlag GmbH & Co. KGaA, Weinheim

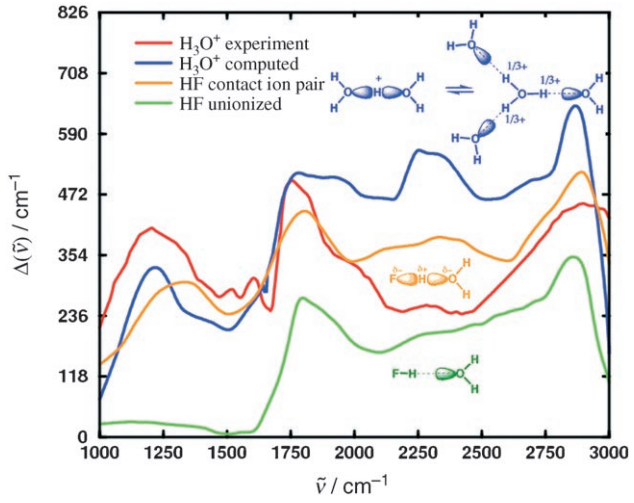


Figure 2. Comparison between difference spectra $\Delta(\tilde{\nu})$ as a function of wavenumber $\tilde{\nu}$ as defined in Equation (2) for different chemical species. Experimental results for a solution of HBr are taken from the study by Downing and Williams[9] and are scaled to a concentration $c = 0.85$ M. Although not directly comparable to the HF system studied here, Downing and Williams[9] provide values for $\alpha(\tilde{\nu})$ and $n(\tilde{\nu})$ separately so that direct comparison of the difference spectrum [see Eq. (2)] for H_3O^+ can be made. Note that theory[10] is able to describe quantitatively the "continuous absorption" in solutions of strong acids. Absorption in the region between $\tilde{\nu} = 1000$ and 1500 cm^{-1} is due to structural vibrations of Zundel-like symmetric structures. The absorption between $\tilde{\nu} = 1700$ and 3000 cm^{-1} is due to overextended FH and OH bonds as well as to transitions between Zundel and Eigen structures (see text).

exhibit a continuous absorption only between $\tilde{\nu} = 1800$ and 3000 cm^{-1} attributable to the unionized acid.

The present results are consistent with the recent interpretation of Asmis et al.[12] and Headrick et al.[13] regarding the assignment of spectra of liquid-phase acids. On the basis of the spectra of the bare protonated water dimer[12] and the Ar-tagged protonated multimers,[13] and of our computed difference spectra, we can confidently conclude that the broad absorption between $\tilde{\nu} = 1000$ and 1500 cm^{-1} in acid solutions can be attributed to the asymmetric stretch and the two bending modes of the $O\cdots H^{+}\cdots O$ and of the $F^{\delta-}\cdots H^{\delta+}\cdots O^{\delta-}$ Zundel-like moieties. This band appears as three broad peaks in the gas-phase spectrum of the dimer[12] but is almost nonexistent in the difference spectrum of the unionized HF or in the argon matrix spectra of the trimer and tetramer, respectively.[13]

The broad band between $\tilde{\nu} = 1800$ and 3000 cm^{-1}, on the other hand, cannot be attributed to any structural vibration of an isolated Zundel-like ion because such vibrations do not appear in the spectra of the protonated water dimer in the gas phase[12] or in an argon matrix.[13] Several interpretations exist as to the molecular origin of this band in aqueous solutions of strong acids that emphasize the electronic changes associated with transitions between Zundel and Eigen structures.[14] Complementary to these interpretations, the present difference spectra of the unionized HF molecule suggest that one of the most important contributions to the intensity of the continuum of absorption between $\tilde{\nu} = 1800$ and 3000 cm^{-1} in solutions of weak acids is due to the anharmonic character of the HA bond stretch in the unionized acid and to the OH bond stretch modes in the water molecule whose oxygen atom acts as a Lewis donor to HA.

Interestingly, the computed spectra in Figure 2 suggest that the dissociation of the contact ion pair (spectrum in yellow) followed by formation of the bulk (solvated) hydronium ions (blue) is characterized by relatively minor changes in the continuum absorption in the $\tilde{\nu} = 1000$–1700 cm^{-1} region but involves more significant changes at larger wavenumbers. Similar patterns have been observed in recent IR experimental studies of the proton-pumping step in bacteriorhodopsin.[15] The possibility that contact ion pairs are involved as stable intermediates in the mechanism of the dissociation of weak aqueous acids cannot be readily dismissed in light of the present results and of previous experimental studies.[3,4] It is intriguing to consider the possibility that such molecular species play a role in the mechanism of proton-release pathways through intramolecular single-file water channels in bacteriorhodopsin and other biomolecules, a hypothesis that is supplementary to other theoretical investigations that have appeared recently.[16]

Our spectra can neither confirm nor affirm Giguère's interpretation of the IR spectra of concentrated HF solutions as containing a large fraction of contact ion pairs.[17] As can be seen from Figure 2, both the contact ion pair and the unionized acid shift the maximum of the HOH bending absorption from $\tilde{\nu} = 1730$ cm^{-1} in aqueous solutions of strong acids (blue curve) to approximately $\tilde{\nu} = 1800$ cm^{-1}. Therefore, we conclude that the question of the nature of the majority chemical species present in solutions of hydrofluoric acid should be resolved by carefully determining the difference spectra experimentally in the region of $\tilde{\nu} = 1000$ to 1500 cm^{-1}.

Experimental Section

Methods: Trajectories of the dipole moments were obtained using the Berry phase approach[18] and were utilized to compute the Beer–Lambert absorptivity $\alpha(\tilde{\nu})$ and refractive index $n(\tilde{\nu})$ spectra for wavenumbers $\tilde{\nu}$ varying between 40 and 4000 cm^{-1} by means of the time-correlation formalism of linear response theory[19] and the Kramers–Kronig relations.[19] The simulations were performed using Car–Parrinello molecular dynamics, density functional theory (DFT),[8] the B-LYP generalized gradient exchange-correlation functional,[20] plane-wave basis sets, and Troullier–Martin pseudopotentials.[21] The plane-wave basis set cut-off was taken to be 80 Ry, and a fictitious electron mass $\mu = 400$ a.u. in conjunction with an integration time-step of $\delta = 0.1$ fs were utilized. The Car–Parrinello molecular dynamics with localized orbitals was performed by employing multiple time-step integration algorithms in which the total dipole moment and the centers of the maximally localized Wannier orbitals were computed every 10 steps as described in reference [11]. The simulated systems consist of primitive cubic boxes containing 64 water molecules and one molecule of HF or HCl. All systems were equilibrated for a period of 10 ps using a Nosé–Hoover chain thermostat on each degree of freedom, after which the thermostats were removed and dynamical trajectories were collected for another 10 ps. The average temperature during the production runs was approximately 300 K in

 © 2006 Wiley-VCH Verlag GmbH & Co. KGaA, Weinheim

all simulations. All the calculations were carried out using the PINY MD package.[22]

Received: June 28, 2005
Revised: November 23, 2005
Published online: January 3, 2006

Keywords: ab initio calculations · density functional calculations · hydrogen bonds · IR spectroscopy · proton transport

[1] a) G. Zundel, *Hydrogen Bonds with Large Proton Polarizabilities* (Eds.: S. Rice, I. Prigogine), Wiley, New York, **2000**; b) M. Eigen, *Angew. Chem.* **1963**, *75*, 489 – 508; *Angew. Chem. Int. Ed. Engl.* **1964**, *3*, 1 – 19; c) M. Tuckerman, D. Marx, M. Parrinello, *Science* **1997**, *275*, 817 – 820.
[2] a) P. L. Geissler, C. Dellago, D. Chandler, J. Hutter, M. Parrinello, *Science* **2001**, *291*, 2121 – 2124; b) H. J. Bakker, H.-K. Nienhuys, *Science* **2002**, *297*, 587 – 590; c) K. Ando, J. T. Hynes, *J. Phys. Chem. A* **1999**, *103*, 10398 – 10408.
[3] a) M. Leuchs, G. Zundel, *Can. J. Chem.* **1980**, *58*, 311 – 322; b) M. Leuchs, G. Zundel, *Can. J. Chem.* **1980**, *58*, 2118 – 2131.
[4] a) J. J. Max, C. Chapados, *J. Phys. Chem. A* **2004**, *108*, 3324 – 3337; b) J. J. Max, C. Chapados, *J. Phys. Chem. A* **2002**, *106*, 6452 – 6461.
[5] R. Car, M. Parrinello, *Phys. Rev. Lett.* **1985**, *55*, 2471 – 2474.
[6] a) M. Eigen, W. Kruse, L. DeMayer, *Prog. React. Kinet.* **1964**, *2*, 287 – 318; b) A. Weller, *Prog. React. Kinet.* **1961**, 1, 187 – 214.
[7] M. Rini, B.-Z. Magnes, E. Pines, E. T. J. Nibbering, *Science* **2003**, *301*, 349 – 352.
[8] W. Koch, M. C. Holthausen, *A Chemist's Guide to Density Functional Theory*, VCH, New York, **2000**.
[9] H. D. Downing, D. Williams, *J. Phys. Chem.* **1976**, *80*, 1640 – 1641.
[10] R. Iftimie, M. Tuckerman, *J. Chem. Phys.* **2005**, *122*, 214508.
[11] a) R. Iftimie, J. W. Thomas, M. E. Tuckerman, *J. Chem. Phys.* **2004**, *120*, 2169 – 2181; b) J. W. Thomas, R. Iftimie, M. E. Tuckerman, *Phys. Rev. B* **2004**, *69*, 125105.
[12] K. R. Asmis, N. L. Pivonka, G. Santambrogio, M. Brümmer, C. Kaposta, D. M. Neumark, *Science* **2003**, *299*, 1375 – 1377.
[13] J. M. Headrick, E. G. Diken, R. S. Walters, N. I. Hammer, R. A. Christie, J. Cui, E. M. Myshakin, M. A. Duncan, M. A. Johnson, K. D. Jordan, *Science* **2005**, *308*, 1765 – 1769.
[14] R. Vuilleumier, D. Borgis, *J. Chem. Phys.* **1999**, *111*, 4251 – 4266.
[15] J. Wang, M. A. El-Sayed, *Biophys. J.* **2001**, *80*, 961 – 971.
[16] R. Rousseau, V. Kleinschmidt, U. W. Schmitt, D. Marx, *Angew. Chem.* **2004**, *116*, 4908 – 4911; *Angew. Chem. Int. Ed.* **2004**, *43*, 4804 – 4807.
[17] P. A. Giguère, S. Turrell, *J. Am. Chem. Soc.* **1980**, *102*, 5473 – 5477.
[18] a) R. D. King-Smith, D. Vanderbilt, *Phys. Rev. B* **1993**, *47*, 1651 – 1661; b) D. Vanderbilt, R. D. King-Smith, *Phys. Rev. B* **1993**, *48*, 4442 – 4452; R. Resta, *Rev. Mod. Phys.* **1994**, *66*, 899 – 915; R. Resta, *Phys. Rev. Lett.* **1998**, *80*, 1800 – 1803.
[19] R. Kubo, M. Toda, N. Hashitsume, *Statistical Physics II, 2nd ed.*, Springer, New York, **1991**.
[20] a) A. Becke, *Phys. Rev. A* **1998**, *38*, 3098 – 4000; b) C. Lee, W. Yang, R. G. Parr, *Phys. Rev. B* **1998**, *37*, 785 – 795.
[21] N. Trouillier, J. L. Martins, *Phys. Rev. B* **1991**, *43*, 1993 – 2003.
[22] M. E. Tuckerman, D. A. Yarne, S. O. Samuelson, A. L. Hughes, G. J. Martyna, *Comput. Phys. Commun.* **2000**, *128*, 333 – 343.

 © 2006 Wiley-VCH Verlag GmbH & Co. KGaA, Weinheim

Organocatalysis

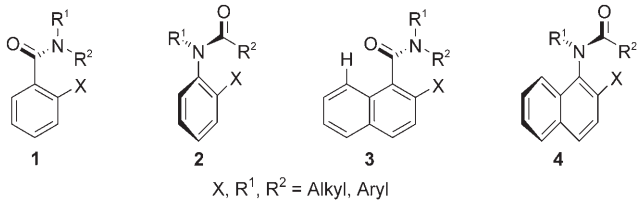
DOI: 10.1002/anie.200503042

Chirally Aminated 2-Naphthols—Organocatalytic Synthesis of Non-Biaryl Atropisomers by Asymmetric Friedel–Crafts Amination**

Sebastian Brandes, Marco Bella, Anne Kjærsgaard, and Karl Anker Jørgensen**

Atropisomers, compounds in which the chirality originates from restricted rotation along a chiral axis rather than a stereogenic center, have received much attention, since they are among the most useful ligands in asymmetric catalysis.[1] In most of the known structures, the chiral axis is between two aromatic moieties, but there are examples of non-biaryl atropisomers.

Several reports followed the pioneering work by Curran et al. disclosed in 1994 on atropisomeric anilides.[2] Two classes of compounds emerged afterwards, namely atropisomeric amides **1** and anilides **2** (Scheme 1), and both have been



Scheme 1. Non-biaryl atropisomers.

employed in asymmetric catalysis.[3] The rotation along the chiral axis in structures of type **1** and **2** is hindered by a substituent in the aromatic *ortho* position of the aryl group. Compounds of class **3** with *peri* substitution have also been investigated. The hydrogen atom in the 8-position of the naphthyl moiety causes a rotational barrier of sufficient magnitude to generate optical antipodes, although these compounds readily racemize ($t_{1/2}{}^{25}{}_{rac}$ less than 1 s).[4] There is no reported data on the chiral properties of the corresponding compounds of class **4**, in which the nitrogen atom is directly attached to the aromatic ring, such as *N*,*N*-disubstituted 1-naphthamides or carbamates.

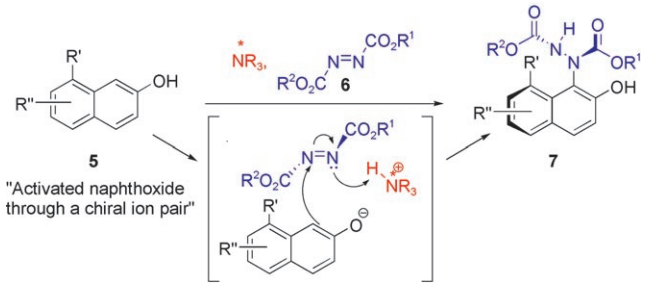
[*] Dr. S. Brandes, Dr. M. Bella, A. Kjærsgaard, Prof. Dr. K. A. Jørgensen
The Danish National Research Foundation
Center for Catalysis, Department of Chemistry
Aarhus University, 8000 Aarhus C (Denmark)
Fax: (+45) 8919-6199
E-mail: kaj@chem.au.dk

[**] This work was made possible by a grant from the Danish National Research Foundation. Thanks are expressed to Dr. Jacob Overgaard for X-ray analysis.

Supporting information for this article is available on the WWW under http://www.angewandte.org or from the authors.

© 2006 Wiley-VCH Verlag GmbH & Co. KGaA, Weinheim

The preparation of compounds **1**–**3** is usually a tedious multistep sequence, and in most cases a resolution of the racemate is required to obtain enantiopure material.[5] Only recently Taguchi and co-workers reported a highly enantioselective catalytic synthesis of atropisomeric anilides **2**.[6] It is of no doubt that efficient and enantioselective methods to access these compounds can trigger the discovery of new applications. Herein, we report the properties and the easy asymmetric organocatalytic synthesis of atropisomers of class **4**. The strategy of the formation of this new class of atropisomer is based on the organocatalytic asymmetric amination of 2-naphthols (Scheme 2).

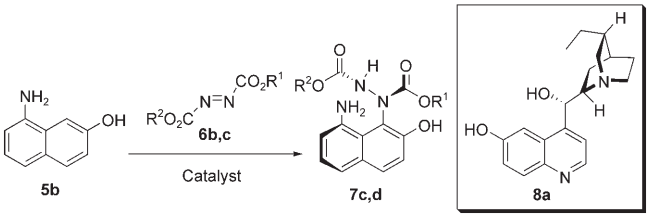


Scheme 2. Organocatalytic asymmetric amination of 2-naphthols.

The reaction of activated naphthalenes and azodicarboxylates was described by Diels and Back in 1921,[7] and it was later shown that it can be catalyzed by metals.[8] Although aminated naphthalenes have been known for nearly a century, they have not been recognized as chiral compounds. By employing tertiary amines as catalysts, 2-naphthol **5a** (R′, R″ = H) is activated through deprotonation of the hydroxy group, and the addition of diethyl azodicarboxylate (**6a**) ($R^1 = R^2 = Et$) is completed within minutes at room temperature or overnight at −20 °C. The aminated naphthol **7a** ($R^1 = R^2 = Et$, R′, R″ = H) is indeed a chiral compound, since the two enantiomers can be readily separated by chiral HPLC and one of the two CH_2 groups of the carbamate moiety turned out to be diastereotopic.[9] We then employed a chiral amine to access these compounds by an asymmetric catalyzed reaction (Scheme 2). In the first screening of the reaction of **5a** with di-*tert*-butyl azodicarboxylate (**6b**) ($R^1 = R^2 = t$Bu), we succeeded in achieving a modest level of enantiomeric excess (15 % *ee*) by using cinchonine as the chiral catalyst. Unfortunately, products **7a**,**b** are not configurationally stable at room temperature. We measured the half life ($t_{1/2}{}^{29}{}_{rac}$ = 26 min) for **7b** ($R^1 = R^2 = t$Bu, R′, R″ = H) and determined the energy barrier for the rotation along the C(aryl)–N axis to be $\Delta G_{rac} = 84\ kJ\,mol^{-1}$ (see the Supporting Information). We then employed 8-amino-2-naphthol (**5b**), as the substrate and were able to generate more stable atropisomers.[10]

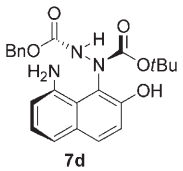
A screening of azodicarboxylates **6b**,**c** and different solvents, concentrations, and catalysts[11] (see Table 1) showed that the symmetric azodicarboxylate **6b** in combination with catalyst **8a** (dihydrocupreidine)[12] gave **7c** in high yield with up to 88 % *ee* (entry 8). The enantiomeric excess of **7c** does not appreciably change when kept at −20 °C, and we measured a decrease of only 3 % *ee* after 10 days at room temperature. In the reaction with the nonsymmetric azodicarboxylate **6c**, only a single regioisomer was isolated (up to 87 % *ee*; entry 9); the other regioisomer yielded a cyclized compound (see the Supporting Information). The HPLC traces of the racemate and the optically active compound **7d** are shown in Figure 1.

Table 1: Screening of catalysts and conditions for the organocatalyzed (20 mol %) asymmetric Friedel–Crafts reaction of **5b** with azodicarboxylates **6b**,**c**.[a]



Entry	Catalyst	(*T* [°C])	Solvent	R^1, R^2	Yield [%][b]	*ee* [%][c]
1	quinine	(RT)	toluene	*t*Bu, *t*Bu (**6b**)	85, **7c**	16
2	**8a**	(RT)	toluene	*t*Bu, *t*Bu (**6b**)	91, **7c**	58
3	**8a**	(−20)	toluene	*t*Bu, *t*Bu (**6b**)	95, **7c**	71
4	**8a**	(RT)	DCE	*t*Bu, *t*Bu (**6b**)	95, **7c**	82
5	**8a**	(−20)	DCE	*t*Bu, *t*Bu (**6b**)	92, **7c**	84
6	**8b**[d]	(RT)	DCE	*t*Bu, *t*Bu (**6b**)	85, **7c**	−61[e]
7	**8b**[d]	(−20)	DCE	*t*Bu, *t*Bu (**6b**)	85, **7c**	−22[e]
8[f]	**8a**	(−20)	DCE	*t*Bu, *t*Bu (**6b**)	90, **7c**	88
9	**8a**	(−20)	DCE	*t*Bu, Bn (**6c**)	62, **7d**	87

[a] Reaction performed with 0.20 mmol of **5b** and 0.20 mmol of **6b**,**c** in 0.4 mL of solvent [0.5 M]; 99 % conversion in all reactions. [b] Yield of isolated product after flash chromatography. [c] *ee* determined by HPLC. [d] Catalyst: dihydrocupreine, a pseudoenantiomer of **8a**. [e] The atropisomer with the opposite sign of optical rotation is formed. [f] The concentration of **5b** was [0.05 M], instead of [0.5 M]. DCE = dichloroethane.



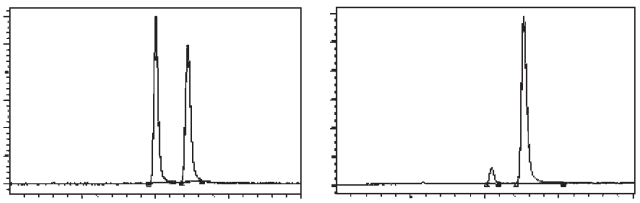


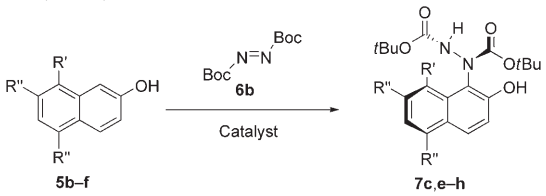
Figure 1. HPLC traces (Chiralpak AD, hexane/*i*PrOH 80:20) of **7d** as a racemate (left) and with 87 % *ee* (right).

At this stage, we realized and observed that the catalyst can also act as a substrate for the Friedel–Crafts reaction. However, it is obvious that the quinoline-6-ol system is deactivated towards electrophilic aromatic substitution relative to the 2-naphthol system. As expected, catalysts **8a**,**b** do not appreciably react under the asymmetric catalytic exper-

 © 2006 Wiley-VCH Verlag GmbH & Co. KGaA, Weinheim

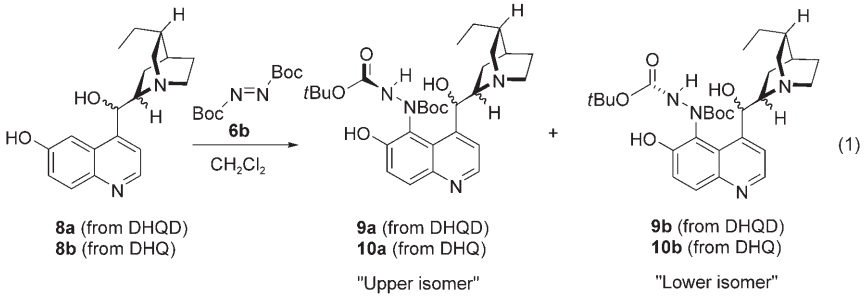
imental conditions (see the Supporting Information). On the other hand, the phenol group of **8a**,**b** is more acidic with respect to a simple 2-naphthol unit, and these catalysts can be seen as a zwitterionic species. Therefore a considerable portion of the molecules might be in an activated form. By forcing the reaction conditions, we could isolate two diastereoisomers (herein named "upper" and "lower" according to their respective TLC R_f values) in good yield from the treatment of **8a**,**b** with **6b** [Eq. (1); DHQD = dihydroquinidine, DHQ = dihydroquinine]. The **9a**/**9b** and **10a**/**10b** ratios were 3.5:1 and 1:2.3, respectively. This notable example of quinoline-core functionalization gives access to a new class of cinchona-alkaloid catalyst. These compounds are stable toward racemization when stored as solids at room temperature.

Table 2: Asymmetric Friedel–Crafts reaction of different 2-hydroxy-8-amino naphthols **5b–f** with azodicarboxylate **6b** catalyzed by **8a**, **9b**, and **10b**.[a]



Entry	Substrate R′, R″	Product	Catalyst **8a** *ee* [%]	Catalyst **8a** (yield [%])[b,c]	Catalyst **9b** *ee* [%]	Catalyst **9b** (yield [%])[b,c]	Catalyst **10b** *ee* [%]	Catalyst **10b** (yield [%])[b,c]
1	NH_2, H (**5b**)	**7c**	88	(90)	87	(87)	−96	(91)[d]
2	NHMe, H (**5c**)	**7e**	33	(95)	93	(91)	−96	(94)[d]
3	NHBn, H (**5d**)	**7f**	48	(98)	98	(92)	−98	(80)[d]
4	NHC_5H_{11}, H (**5e**)	**7g**	78	(98)	94	(95)	−94	(98)[d]
5	NH_2, Br (**5f**)	**7h**	80	(96)	98	(85)	−96	(95)[d]

[a] Reaction performed with 0.20 mmol of **5b–f**, 0.20 mmol of **6b**, and 0.04 mmol of catalyst in 4 mL of DCE [0.05 M]; 99% conversion in all reactions. [b] *ee* determined by HPLC. [c] Yield of isolated product after flash chromatography. [d] The atropisomer with the opposite sign of optical rotation is formed.



After screening a large number of different cinchona-alkaloid derivatives as catalysts for the asymmetric Friedel–Crafts amination, we decided to test these four new compounds also in the hope of finally increasing the enantioselectivity. To our delight, catalyst **10b** increased the enantiomeric excess of **7c** from 22% *ee* (see Table 1, entry 7) to 96% *ee*. This very promising result prompted us to investigate the generality of the asymmetric Friedel–Crafts amination.

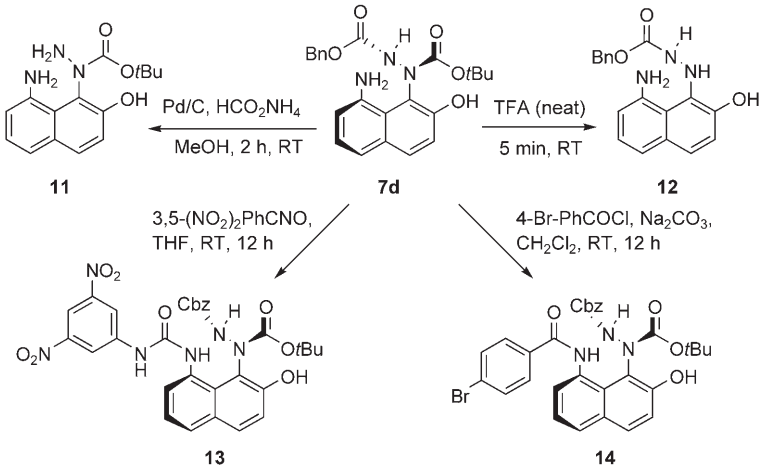
A significant improvement in enantioselectivity takes place when using the new cinchona-alkaloid catalysts **9b** and **10b** compared with **8a**. The results obtained for a variety of different substrates with these catalysts are shown and compared in Table 2.[13]

For 8-amino-2-naphthol (**5b**), the enantiomeric excess of **7c** was improved (up to 96% *ee*; Table 2, entry 1). An even larger improvement was observed for the *N*-substituted naphthols **5c–e**; from these substrates, the optically active aminated naphthols **7e–g** are obtained in high yields and with excellent enantioselectivities (93–98% *ee*; Table 2, entries 2–4). The introduction of further substituents in the naphthol ring (**5f**) gave also excellent results, as **7h** was obtained with 98% *ee* (Table 2, entry 5).

This organocatalytic asymmetric Friedel–Crafts amination reaction represents easy access to a novel class of chiral compounds which can undergo various transformations. The carbamate protective groups of **7d** can be orthogonally deprotected to afford **11** or **12** (see Scheme 3); however, the products were found to be non-chiral.

The presence of both a hydroxy and an amino group in the product offers several possibilities for further elaborations. As an example, **7d** was converted in good yields and without racemization into both chiral ureas and anilides, such as **13** or **14**, respectively.

The latter compound was recrystallized to be enantiopure, and a crystal suitable for X-ray diffraction analysis was obtained.[14] The absolute configuration and regiochemistry of **14** were thereby determined. The crystal belongs to the chiral space group $P2_12_12_1$. The crystal structure shows intramolecular hydrogen bonding between the amide NH moiety and the



Scheme 3. Chemical transformation of **7d**. TFA = trifluoroacetic acid, Cbz = carbonylbenzyloxy.

© 2006 Wiley-VCH Verlag GmbH & Co. KGaA, Weinheim

carbonyl oxygen atom of the carbonylbenzyloxy (Cbz) group (Figure 2). The value of the torsion angle between the two carbamate carbonyl functions bound to the hydrazine is 92°.

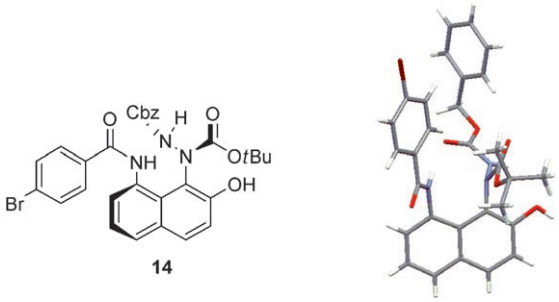
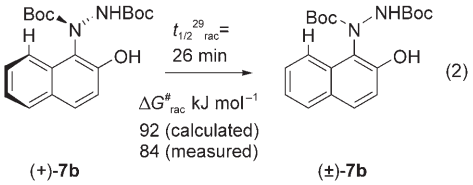


Figure 2. X-ray structure of **14**.

Based on the measured $t_{1/2}{}^{29}{}_{rac} = 26$ min for **7b** and the experimentally calculated energy barrier for rotation along the C–N axis ($\Delta G_{rac} = 84\ kJ\,mol^{-1}$), we performed a series of quantum-chemical calculations. The rotation along the C–N axis for **7b** has been estimated (see the Supporting Information) at the HF/6-31G level of theory[15] to be $\Delta G_{rac} = 92\ kJ\,mol^{-1}$ in the gas phase [Eq. (2)], which is in good



agreement with the experimental value. Furthermore, the experimental and computational values also fit with, for example, the barriers of rotation of compounds related to class **3**.[4a]

In conclusion, we have reported an unprecedented example of a cinchona-alkaloid organocatalyzed Friedel–Crafts amination of 2-naphthols.[16] The reaction represents easy access to a novel class of non-biaryl atropisomers, which can be further elaborated to several new chiral molecules. The use of new aminated cinchona alkaloids for the Friedel–Crafts amination reaction leads to a general reaction that proceeds for a series of different 2-naphthol derivatives with excellent enantioselectivities. Further work is in progress to clearly define the scope of this reaction, as well as employing these optically active aminated 2-naphthol derivatives and aminated cinchona alkaloids as, for example, chiral catalysts.

Received: August 26, 2005
Revised: October 28, 2005
Published online: January 3, 2006

Keywords: amination · asymmetric synthesis · Friedel–Crafts reaction · naphthols · organocatalysis

[1] a) E. L. Eliel, S. H. Wilen, *Stereochemistry of Organic Compounds*, Wiley, New York, **1994**; b) C. Rosini, L. Franzini, A. Raffaelli, P. Salvadori, *Synthesis* **1992**, 503 – 517; G. Bringmann, A. J. Price Mortimer, P. A. Keller, M. J. Gresser, J. Garner, M. Breuning, *Angew. Chem.* **2005**, *117*, 5518 – 5563; *Angew. Chem. Int. Ed.* **2005**, *44*, 5384 – 5427.

[2] D. P. Curran, H. Qi, S. J. Geib, N. C. DeMello, *J. Am. Chem. Soc.* **1994**, *116*, 3131 – 3132.

[3] Tetrahedron symposium-in-print on atropisomerism (Ed.: J. Clayden), *Tetrahedron* **2004**, *60*, 4325 – 4558; see also: J. Clayden, *Angew. Chem.* **1997**, *109*, 986 – 988; *Angew. Chem. Int. Ed. Engl.* **1997**, *36*, 949 – 951.

[4] a) A. Ahmed, R. A. Bragg, J. Clayden, L. W. Lai, C. McCarthy, J. H. Pink, N. Westlund, S. A. Yasin, *Tetrahedron* **1998**, *54*, 13277 – 13294; the term atropisomers is generally used for conformers that have a half-life that is arbitrarily defined as longer than 1000 s, see: b) M. Oki, *Top. Stereochem.* **1983**, *14*, 1 – 81.

[5] For example, see: a) O. Kitagawa, H. Izawa, K. Sato, A. Dobashi, T. Taguchi, M. Shiro, *J. Org. Chem.* **1998**, *63*, 2634 – 2640; b) A. D. Hughes, D. A. Price, N. S. Simpkins, *J. Chem. Soc. Perkin Trans. 1* **1999**, 1295 – 1304; c) K. Kondo, H. Fujita, T. Suzuki, Y. Murakami, *Tetrahedron Lett.* **1999**, *40*, 5577 – 5580; d) T. Hata, H. Koide, N. Taniguchi, M. Uemura, *Org. Lett.* **2000**, *2*, 1907 – 1910; e) A. Ates, D. P. Curran, *J. Am. Chem. Soc.* **2001**, *123*, 5130 – 5131; f) J. Clayden, D. Mitjans, L. H. Youssef, *J. Am. Chem. Soc.* **2002**, *124*, 5266 – 5267; g) D. J. Bennett, P. L. Pickering, N. S. Simpkins, *Chem. Commun.* **2004**, 1392 – 1393; h) V. Chan, J. G. Kim, C. Jimeno, P. J. Carroll, P. J. Walsh, *Org. Lett.* **2004**, *6*, 2051 – 2053.

[6] O. Kitagawa, M. Takahashi, M. Yoshikawa, T. Taguchi, *J. Am. Chem. Soc.* **2005**, *127*, 3676 – 3677.

[7] O. Diels, I. Back, *Chem. Ber.* **1921**, *54*, 213 – 226.

[8] a) H. Mitchell, Y. Leblanc, *J. Org. Chem.* **1994**, *59*, 682 – 687; b) Y. Leblanc, N. Boudreault, *J. Org. Chem.* **1995**, *60*, 4268 – 4271; c) W. J. Kinart, C. M. Kinart, *J. Organomet. Chem.* **2003**, *665*, 233 – 236.

[9] The splitting of the methylene group into two quartets in the ^{1}H NMR spectra (400 MHz) was reported in ref. [8c] without apparently recognizing that **7a** is a chiral compound; this splitting is not due to the presence of rotamers.

[10] A substituent in the 8-position of the binaphthyl moiety does not always correspond to a higher rotational barrier; for example, see: A. S. Cooke, M. M. Harris, *J. Chem. Soc.* **1963**, 2365 – 2373; A. S. Cooke, M. M. Harris, *J. Chem. Soc. C* **1967**, 988 – 992; K. Fuji, M. Sakurai, N. Tohkai, A. Kuroda, T. Kawabata, Y. Fukazawa, T. Kinoshita, T. Tada, *Chem. Commun.* **1996**, 1609 – 1610.

[11] Besides the catalysts mentioned in Table 1, a variety of other catalysts were tested (**6b**, toluene, −20 °C, [0.5 M]); among these were (*ee* (%) given in parentheses, +/− refers to the opposite stereochemistry): quinidine (0), cinchonine (0), cinchonidine (8), dihydroquinine (18), $[DHQ]_2PYR$ (−70), $[DHQD]_2PYR$ (28), $[DHQ]_2PHAL$ (−12), $[DHQD]_2PHAL$ (10); PYR = 2,5-diphenyl-4,6-pyrimidinediyl diether, PHAL = 1,4-phthalazinediyl diether.

[12] Preparation of **8a**,**b**: M. Heidelberger, W. A. Jacobs, *J. Am. Chem. Soc.* **1919**, *41*, 817 – 833.

[13] The isomers **9a** and **10a** with the higher R_f values afforded lower conversions (15–50 % after 4 days) and enantioselectivities (48–69 % *ee*).

[14] CCDC-288198 contains the supplementary crystallographic data for this paper. These data can be obtained free of charge from The Cambridge Crystallographic Data Centre via www.ccdc.cam.ac.uk/data_request/cif.

 © 2006 Wiley-VCH Verlag GmbH & Co. KGaA, Weinheim

[15] Gaussian 03 (Revision B.05): M. J. Frisch et al. (see the Supporting Information).
[16] Very recently, a cinchona-alkaloid-mediated organocatalytic Friedel–Crafts-type reaction was reported: B. Török, M. Abid, G. London, J. Esquibel, M. Török, S. C. Mhadgut, P. Yan, G. K. Surya Prakash, *Angew. Chem.* **2005**, *117*, 3146 – 3149; *Angew. Chem. Int. Ed.* **2005**, *44*, 3086 – 3089.

 © 2006 Wiley-VCH Verlag GmbH & Co. KGaA, Weinheim

DNA Structures

DOI: 10.1002/anie.200503114

Diagnostics of Single Base-Mismatch DNA Hybridization on Gold Nanoparticles by Using the Hyper-Rayleigh Scattering Technique**

*Paresh Chandra Ray**

The integration of nanotechnology with biology and medicine is expected to produce major advances in molecular diagnostics, therapeutics, and bioengineering.[1a–p] Detection of specific DNA sequences has important applications in clinical diagnosis, the food and drug industry, pathology, genetics, and environmental monitoring. The increasing availability of nanostructures with highly controlled optical properties in the nanometer-size range has created widespread interest in their use in biotechnological systems for diagnostic applications and biological imaging. Most assays identify specific sequences through the hybridization of an immobilized probe to the target analyte after the latter has been modified with a fluorescent or Raman tag. Diagnostics of oligonucleotide sequences by using unmodified DNA remains attractive owing to simplified sample preparation, decreased assay costs, and the elimination of potential artifacts from modification. Herein, we demonstrate for the first time that the hyper-Rayleigh scattering (HRS) technique,[2a–e,3a–e,4a–c] which has emerged over the past decade as a powerful method to determine the microscopic nonlinear optical (NLO) properties of species in solution, can be used to achieve the ultrasensitive detection of single base-pair mismatches in oligonucleotide strands without any modification of DNA. The HRS or nonlinear light scattering can be observed from fluctuations in symmetry, caused by rotational fluctuations. A solution is only centrosymmetric on average in time and space. Locally, deviations from centrosymmetry occur and give rise to a second-order NLO response. Hence, scattering by a fundamental laser beam can be detected at the second harmonic wavelength. The HRS technique can be easily applied to study a very wide range of materials because electrostatic fields and phase matching are not required. The HRS technique is 1–2 orders of magnitude more sensitive than the usual colorimetric technique. Vance et al.[2a] have shown that the HRS intensity was enhanced by a factor of up to 10^5 in suspensions of nanocrystalline gold particles. Although HRS spectroscopy has been shown[2a–e] to be capable for the ultrasensitive detection of nanoparticle aggregation, second-order nonlinear spectroscopy remains unexplored for DNA-detection purposes.

Oligonucleotides with different chain lengths, for example, 1) GGCCCCAAACCTTTTGAAAGGACCC-3′, 2) GGCCAAAACCTGGAGG-3′, 3) GGCAACCT-3′ and their complement and noncomplements (one base-pair mismatch) were purchased from MWG Biotech. Hydrogen tetrachloroaurate ($HAuCl_4 \cdot 3H_2O$), phosphate-buffered solution (PBS), sodium chloride, and sodium citrate were purchased from Sigma–Aldrich and used without further purification. The HRS technique[3a–e] is based on light scattering—linear light scattering is caused by refractive-index variations—and the typical HRS experimental setup that was used in this project has been described previously.[3a–e] In brief, a Q-switched Nd:YAG laser (Spectra Physics) that delivers 8 ns pulses and up to 800 mJ per pulse at 1064 nm was used as a laser source. To avoid multiphoton photoluminescence contribution, an optical parametric oscillator was used to generate the 1300 nm fundamental wavelength so that the second harmonic is out of an absorption band for the gold-coated DNA. Figure 1 shows the output signal intensities

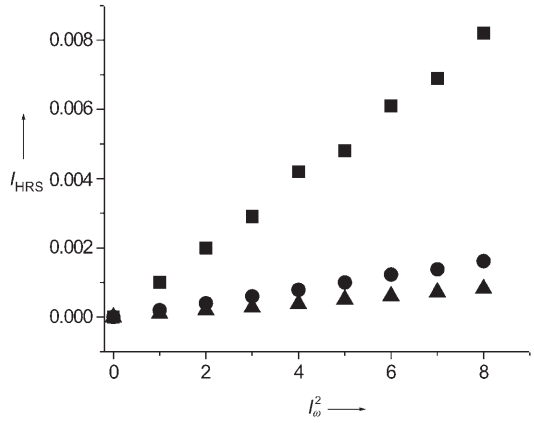


Figure 1. Power dependence of HRS intensity at different concentrations of ss-DNA (GGCAACCTGAGGACCC-3′) adsorbed on gold nanoparticles. Squares: 3×10^{16} cm^{-3}; circles: 6×10^{15} cm^{-3}; triangles: 4×10^{15} cm^{-3}.

at 650 nm from single-stranded DNA (ss-DNA) adsorbed onto gold nanoparticles at different powers of 1300 nm incident light. The linear nature of the plot implies that the doubled light is indeed due to the HRS signal. The intensity (I_{HRS}) of the hyper-Rayleigh signal from an aqueous solution

[*] Prof. Dr. P. C. Ray
Department of Chemistry
Jackson State University
1400 J. R. Lynch Street, Jackson, MS 39217 (USA)
Fax: (+1) 601-979-3674
E-mail: paresh.c.ray@jsums.edu

[**] P.C.R. thanks the NSF-CRIF:MU (grant number 0443547) and the NIH-RCMI (grant number G12RR13459) for their generous funding, and the reviewers whose valuable suggestions improved the quality of this manuscript.

 © 2006 Wiley-VCH Verlag GmbH & Co. KGaA, Weinheim

of gold nanoparticles can be expressed as shown in [Eq. (1)],

$$I_{HRS} = G\langle N_w \beta_w^2 + N_{nano} \beta_{nano}^2 \rangle I_w^2 \, e^{-N_{nano} \varepsilon 2\omega l} \quad (1)$$

where G is a geometric factor, N_w and N_{nano} are the number of water molecules and gold nanoparticles per unit volume, respectively, β_w and β_{nano} are the quadratic hyperpolarizabilities of a single water molecule and a single gold nanoparticle, respectively, $\varepsilon_{2\omega}$ is the molar extinction coefficient of the gold nanoparticle at 2ω, l is the path length, and I_w the fundamental intensity. The exponential factor accounts for the losses through absorption at the harmonic frequency.

The HRS signal intensities were normalized to the square of the fundamental beam power. To extract absolute values for the hyperpolarizabilities, the intensities were normalized again with *para*-nitroaniline (pNA) in methanol. The measured hyperpolarizability for pNA was 34.6×10^{-30} esu at 1064 nm excitation, which is in complete agreement with the reported values[3b–c] and 25.6×10^{-30} esu at 1300 nm excitation. Through the use of $\beta_w = 0.56 \times 10^{-30}$ esu, as reported in the literature, we have found that $\beta_{nano} = 4.5 \times 10^{-26}$ esu for 13-nm gold nanoparticles and 4.8×10^{-26} esu for DNA-adsorbed gold nanoparticles, which is much higher than the β values reported for the best available molecular chromophores.

The HRS response from spherical particles has two origins. The first one is a surface contribution that arises from the breaking of centrosymmetry at the particle surface. Because the particle diameter is much smaller than the wavelength of incident light, it is always possible to find a surface element opposite to the surface element of consideration with an inverted orientation of its nonlinear polarization. The second-harmonic light emitted from the surface of the sphere only originates from a nonlocally excited effective electric dipole and a locally excited effective electric quadrupole. As a result, the SH signal intensity scales with the sixth power of the particle radius and may be resonantly enhanced when the dipolar or the quadrupolar mode of the local field is excited at either the fundamental or the harmonic frequency. The second contribution is owing to the bulk contribution that arises from the electromagnetic-field gradients due to the presence of the interface. This contribution extends to over several nanometers away from the interface. Figure 2 shows how the HRS intensity varies after the addition of target DNA into probe DNA (GGCAACCTGAGGACCC-3′; 50 nM). We observed a very distinct HRS intensity change after hybridization even at the concentration of 10 nM probe ss-DNA. The HRS intensity did not change when we added the target DNA with one base-pair mismatch with respect to the probe DNA. One can note that although the visible color changes (as shown in Scheme 1) can be observed only after addition of 250 nM complementary DNA, the HRS signal change can be observed even after addition of complementary DNA (10 nM).

The HRS intensity change is mainly owing to two factors. First, when target DNA with a complementary sequence is added to the probe DNA, a clear colorimetric change from red to blue-gray is observed as shown in Scheme 1. This is owing to the fact that in the presence of ss-DNA, the oligonucleotides adsorb onto the gold colloid through van der

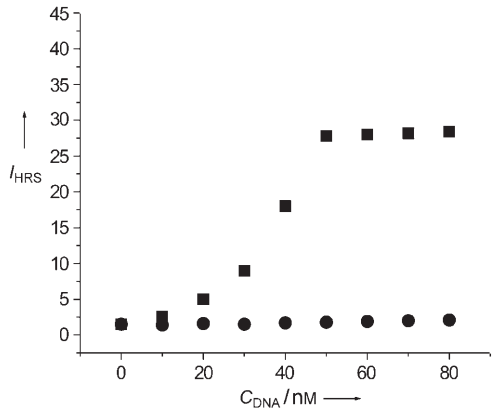
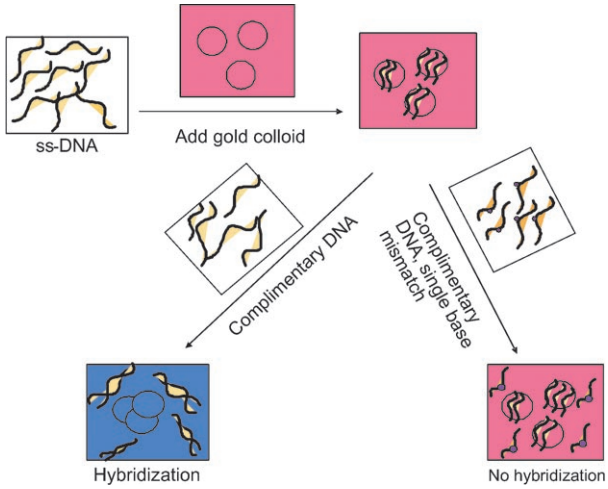


Figure 2. Plot of HRS intensity versus concentration of target DNA, Squares: target DNA; circles: target DNA with one base-pair mismatch.



Scheme 1. Schematic representation of the DNA-hybridization process. The circles represent colloidal gold nanoparticles. Dots in ss-DNA represent one base-pair mismatch

Waals electrostatic forces and provide negative charges that enhance the repulsion between the gold nanoparticles. The electrostatic forces are due to dipolar interactions and depend on the configuration and orientation of the ss-DNA. As transient structural fluctuations permit short segments of the ss-DNA to uncoil, the bases face the gold nanoparticle. Attractive electrostatic forces between the gold nanoparticles and nucleotides cause the ss-DNA to adsorb onto the gold colloid. After hybridization, ss-DNA forms ds-DNA (double-stranded DNA) that has double-helix geometry. As a result, the ds-DNA cannot uncoil sufficiently (unlike ss-DNA) to expose its bases toward the gold nanoparticle. Repulsion between the charged phosphate backbone of ds-DNA and the citrate ions from the gold nanoparticle dominates the electrostatic interaction and does not allow the ds-DNA to adsorb onto the gold nanoparticle. As a result, gold nanoparticles undergo aggregation owing to the presence of NaCl (as shown in Scheme 1).

A two-level model that has been extensively used for donor–acceptor NLO chromophores can be used to explain

 © 2006 Wiley-VCH Verlag GmbH & Co. KGaA, Weinheim

the difference in first-order nonlinearity owing to the change in color of nanoparticles. According to the two-state model [Eq. (2)],[5] where μ_{eg} is the transition dipole moment between

$$\beta^{\text{two state}} = \underbrace{\frac{3\mu_{eg}^2\,\delta\mu_{eg}}{E_{eg}^2}}_{\text{static factor}}\ \underbrace{\frac{\omega_{eg}^2}{(1-4\omega^2/\omega_{eg}^2)\,(\omega_{eg}^2-\omega^2)}}_{\text{dispersion factor}} \qquad (2)$$

the ground state $|g\rangle$ and the charge-transfer excited state $|e\rangle$, $\Delta\mu_{eg}$ is the difference in dipole moment, and E_{10} is the transition energy.

As the color changed from red to blue-gray, the λ_{max} changed from 520 nm to 640 nm and β changed tremendously. This is owing to the fact that at the laser wavelength of 1300 nm and a λ_{max} of 520 nm, there is a small two-photon resonance enhancement (factor of 3.31). For the λ_{max} at 640 nm, however, this resonance enhancement factor is much larger (factor of 43) owing to the closeness of λ_{max} with the second-harmonic wavelength at 650 nm.

Second, after hybridization, the gold nanoparticles undergo aggregation and the HRS intensity increases tremendously with the increase in particle size. Figure 3 shows

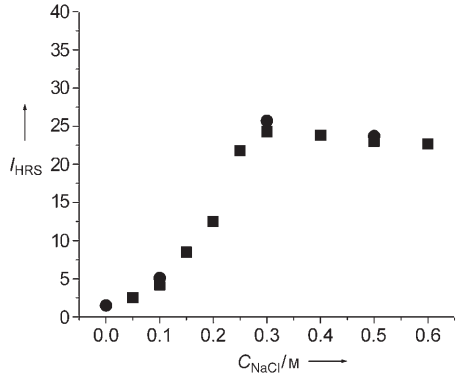


Figure 3. Plot of HRS intensity from gold nanoparticles versus different concentrations of NaCl. Squares: gold nanoparticles; circles: probe DNA adsorbed gold nanoparticles after hybridization.

how the HRS intensity increases with the particle size of gold aggregates by varying NaCl concentration. The HRS intensity was enhanced by a factor of 20 as compared to the HRS signal of the pure gold solution which was decreased slightly and then finally saturated at higher NaCl concentrations. The enhancement factor after hybridization is about the same for pure and DNA-adsorbed gold nanoparticles. To understand the limitation of HRS assays on long target DNA sequences, we have performed our experiment by using 8-, 16-, 25-, 45-, 65-, and 75-base oligonucleotides. Our results indicate that the HRS assay can be easily used to probe longer oligonucleotides (<75 bases), with the only limitation being that the hybridization process is slow owing to the adsorption process of long ss-DNA sequences on gold nanoparticles.

In summary, we have demonstrated that the HRS assay for ss-DNA sequence recognition at the 10-nanomolar level is based on the differences in electrostatic properties between ss-DNA and ds-DNA. Our experimental results reported herein open up the new possibility of rapid, easy, and reliable diagnosis of single base-mismatch DNA by measuring the HRS intensity from DNA-modified gold nanoparticles. This method has several advantages: 1) unmodified protein and DNA can be used to probe single base-mismatch DNA in solution by the HRS technique, 2) it can be 1–2 orders of magnitude more sensitive than the usual colorimetric technique, and 3) single base-pair mismatches are easily detected. For the development of practical bioassays, much more research needs to be done on the improvement of the HRS experimental system and the variation of the HRS intensity with the shape and size of metal nanoparticles should also be investigated. It is probably possible to improve the HRS intensity by several orders of magnitude by choosing proper materials and detection systems. We believe that the HRS method has enormous potential for the application of pathogen detection, clinical analysis, and biomedical research.

Experimental Section

Gold nanoparticles with 15 nm diameter were synthesized by using a reported method.[1a–d,q] In brief, aqueous solutions of $HAuCl_4{\cdot}3H_2O$ (0.01 %) and sodium citrate (1 wt %) were prepared. A solution of $HAuCl_4{\cdot}3H_2O$ (100 mL) was heated to reflux while being stirred. A solution of sodium citrate (3 mL, 1 %) was added to the boiling solution. The solution then underwent a series of color changes and finally turned wine red after which it was boiled for a further 30 min. After cooling to room temperature, the gold nanoparticle solution was diluted to 100 mL with deionized water. The gold nanoparticles were characterized by TEM (as shown in Figure 4) and were found to

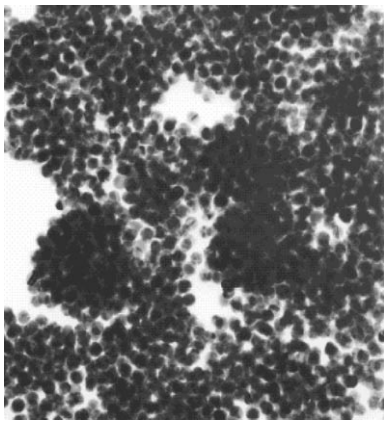


Figure 4. TEM image of aggregate gold nanoparticles after the addition of target DNA in probe DNA

be mostly spherical with the average diameter of 15 ± 3 nm. The UV/Vis absorption spectrum shows a well-developed surface plasmon absorption peak at 512 nm. Hybridization of the probe and the target was conducted for 5 minutes in PBS with NaCl (0.3 M) for a few minutes at room temperature. An aliquot of the hybridization solution was added to the gold colloid solution (1 mL), and PBS (1 mL) was then added immediately to the same solution. To estimate the number of DNA probes adsorbed on the gold nanoparticle surface, dithiothreitol was added to release the probes from the nanoparticles into solution. By using the ss-DNA quantification kit, we measured the concentration of the released DNA to be about

 © 2006 Wiley-VCH Verlag GmbH & Co. KGaA, Weinheim

220 DNA probes per nanoparticle. To remove non-adsorbed probes, the solution was centrifuged at 13000 rpm for 20 min and the supernatant was replaced by buffer solution (2 mL). After another centrifugation under the same conditions, the precipitate was redispersed into the same buffer solution (1 mL) to make a stock solution, which was then used for the HRS experiments.

Received: September 2, 2005
Revised: November 24, 2005
Published online: January 11, 2006

Keywords: base pairs · DNA structures · hyper-Rayleigh scattering · nanostructures

[1] a) N. L. Rosi, C. A. Mirkin, *Chem. Rev.* **2005**, *105*, 1547; b) P. Alivisatos, *Nat. Biotechnol.* **2004**, *22*, 47; c) M. Christine, D. Astruc, *Chem. Rev.* **2004**, *104*, 293; d) K. Kinbara, T. Aida, *Chem. Rev.* **2005**, *105*, 1377; e) I. Bontidean, A. Kumar, E. Csoregi, I. Yu, G. B. Mattiason, *Angew. Chem.* **2001**, *113*, 2748–2750; *Angew. Chem. Int. Ed.* **2001**, *40*, 2676; ; f) C. Dueymes, J. L. Decout, P. Peltie, M. Fontecav, *Angew. Chem.* **2002**, *114*, 504; *Angew. Chem. Int. Ed.* **2002**, *41*, 486; g) D. J. Maxwell, J. R. Taylor, S. Nie, *J. Am. Chem. Soc.* **2002**, *124*, 9606; h) H. Li, L. J. Rothberg, *Anal. Chem.* **2004**, *76*, 5414; i) W. C. Cao, R. C. Jin, C. A. Mirkin, *Science* **2002**, *297*, 1536; j) R. Nitu, Y. Li, *Angew. Chem.* **2005**, *117*, 5600; *Angew. Chem. Int. Ed.* **2005**, *44*, 5464; k) H. Shiigi, S. Tokonami, H. Yakabe, T. Nagaoka, *J. Am. Chem. Soc.* **2005**, *127*, 3280; l) H. Li, J. Huang, J. Lv, H. An, X. Zhang, Z. Zhang, C. Fan, J. Hu, *Angew. Chem.*, **2005**, *117*, 5230; *Angew. Chem. Int. Ed.* **2005**, *44*, 5100; m) K. Sato, K. Hosokawa, M. Maeda, *J. Am. Chem. Soc.* **2003**, *125*, 8102; n) B. Dubertrel, M. Calame, A. J. Libchaber, *Nat. Biotechnol.* **2001**, *19*, 365; o) H. Li, L. Rothberg, *Anal. Chem.* **2005**, *77*, 6229; p) P. C. Ray, A. Fortner, J. Griffin, C. K. Kim, J. P. Singh, H. Yu, *Chem. Phys. Lett.* **2005**, *414*, 259.

[2] a) F. W. Vance, B. I. Lemon, J. T. Hupp, *J. Phys. Chem. B* **1998**, *102*, 10091; b) J. P. Novak, F. W. Vance, R. C. Johnson, B. I. Lemon, J. T. Hupp, D. L. Feldheium, *J. Am. Chem. Soc.* **2000**, *122*, 12029; c) P. Galleotto, P. F. Brevet, H. Girault, R. Antoine, M. Broyer, *J. Phys. Chem. B* **1999**, *103*, 8706; d) I. R. Antione, C. Jonin, J. Nappa, E. Benichou, P.-F. Brevt, *J. Chem. Phys.* **2004**, *120*, 10748; e) J. Nappa, G. Revillod, J. P. Abid, C. Jonin, E. Benichou, H. H. Girault, P. F. Brever, *Faraday Discuss.* **2004**, *125*, 145; f) C. Zhang, Y. Zhang, X. Wang, M. Tang, L.-Z. Hong, *Anal. Biochem.* **2003**, *320*, 136.

[3] a) R. W. Terhune, P. D. Maker, C. M. Savage, *Phys. Rev. Lett.* **1965**, *14*, 681; b) K. Clays, A. Persoons, *Phys. Rev. Lett.* **1991**, *66*, 2980; c) C. Sporer, I. Ratera, Y. Zho, J. V. Gancedo. K. Wurst, P. Jaitner, K. Clays, A. Persoons, C. Rovira, J. Veciana, *Angew. Chem.* **2004**, *116*, 5378; *Angew. Chem. Int. Ed.* **2004**, *43*, 5266; d) J. J. Wolff, F. Siegler, R. Matschiner, R. Wortmann, *Angew. Chem.* **2000**, *112*, 1494; *Angew. Chem. Int. Ed.* **2000**, *39*, 1436; e) P. C. Ray, P. K. Das, *J. Phys. Chem.* **1995**, *99*, 17891.

[4] a) B. J. Coe, L. A. Jones, J. A. Harris, B. S. Brunschwing, I. Asselberghs, K. Clays, A. Persoons, *J. Am. Chem. Soc.* **2004**, *126*, 3880; b) B. J. Coe, L. A. Jones, J. A. Harris, B. S. Brunschwig, I. Asselberghs, K. Clays, A. Persoons, *J. Am. Chem. Soc.* **2003**, *125*, 862; c) G. P. Bartholomew, I. Ledoux, S. Mukamel, G. C. Bazan, J. Zyss, *J. Am. Chem. Soc.* **2002**, *124*, 13480.

[5] J. L. Oudar, *J. Chem. Phys.* **1977**, *67*, 446.

 © 2006 Wiley-VCH Verlag GmbH & Co. KGaA, Weinheim

Zeolite Films

DOI: 10.1002/anie.200503011

Uniformly *a*-Oriented MFI Zeolite Films by Secondary Growth**

*Jungkyu Choi, Shubhajit Ghosh, Zhiping Lai, and Michael Tsapatsis**

Molecular-sieve thin films are attracting research interest because of emerging applications as membranes,[1–6] chemical sensors,[7–9] low-*k* dielectrics,[10] and hosts for supramolecular organization of guest molecules and/or stabilization of guest nanostructures.[11–14] Siliceous ZSM-5 ($Si_{98}O_{196}$-ZSM-5; structure type MFI) films, from now on referred to as MFI films, are studied widely because they serve as a model system and hold promise for practical applications.[15–19] For example, MFI membranes are ideally suited for separating xylene isomers, since the pore size of the MFI framework should allow *p*-xylene (kinetic diameter ca. 5.8 Å) to permeate relatively fast, while the bulkier *o*- and *m*-xylene (kinetic diameters ca. 6.8 Å) should permeate at a much lower rate. The separation of xylene isomers is important in the petrochemical industry, since they are widely used as industrial solvents and precursors. Separations based on MFI membranes could be a better alternative to current technology that is based on energy-intensive operations such as fractional crystallization, adsorption in a simulated moving bed, and distillation. Among other microstructural characteristics, the preferred orientation correlates strongly with film performance, and therefore controlling the preferred orientation is important.[20,21] Although continuous MFI films with certain types of preferred orientation have been reported,[22–39] a method that allows systematic manipulation of molecular-sieve pore orientation in supported, thin, continuous films has not been demonstrated.

Syntheses of MFI membranes described recently can be broadly classified into two categories: in situ and secondary (or seeded) growth. In the in situ technique, the support surface is directly contacted with an alkaline solution containing the zeolite precursors and subjected to hydrothermal conditions. Under appropriate conditions, zeolite crystals nucleate on the support and grow to form a

[*] J. Choi, S. Ghosh, Prof. M. Tsapatsis
Department of Chemical Engineering and Materials Science
University of Minnesota
421 Washington Ave. SE, Minneapolis, MN, 55455 (USA)
Fax: (+1) 612-626-7246
E-mail: tsapatsi@cems.umn.edu

Z. Lai
Division of Chemical and Biomolecular Engineering
Nanyang Technological University
Singapore 637722 (Singapore)

[**] Funding for this work was provided by NSF (CTS-05 22518). All characterizations were performed at the Minnesota Characterization Facility, which receives support from NSF through the National Nanotechnology Infrastructure Network (NNIN).

WILEY InterScience DISCOVER SOMETHING GREAT
© 2006 Wiley-VCH Verlag GmbH & Co. KGaA, Weinheim

continuous zeolite layer. At the same time, reactions occurring in the solution lead to deposition of nuclei and crystals on the surface followed by their incorporation into the membrane. MFI films grown in situ may exhibit a preferred orientation that depends on the synthetic protocol and associated interplay of nucleation and growth phenomena.[24] However, because of the insufficient understanding of nucleation and growth processes in hydrothermal systems, the success of in situ methods in yielding uniformly oriented MFI films is limited. In the secondary (or seeded) growth technique, zeolite nucleation is largely decoupled from zeolite growth by predepositing a seed layer of zeolite crystals on the support surface. The seed layer can be deposited with one of the crystallographic directions oriented perpendicular to the support.[20] The seeded surface is then exposed to hydrothermal growth conditions, whereupon the seed crystals grow into a continuous film. At the expense of additional processing steps, this method offers greater flexibility in controlling the orientation of the zeolite crystals and the microstructure of the zeolite membrane, since it decouples nucleation from growth. In principle, the orientation and morphology of the membrane can be manipulated by changing the morphology and orientation of the deposited seed layer and then performing secondary growth under appropriate conditions.

Recently,[20,40] we reported the formation of uniformly *b*-out-of-plane oriented (i.e., with the 5.6×5.4-Å straight pore of MFI perpendicular to the membrane surface) MFI films with by secondary growth of *b*-oriented seed layers. This was achieved by appropriate use of structure-directing agents (SDAs) that act as crystal-shape modifiers to enable the necessary orientation of the seed layer and the appropriate balance between in-plane and out-of-plane growth rates during secondary growth. Herein we present an extension of our approach that allowed the formation of the first continuous MFI films with uniform *a*-out-of-plane orientation, that is, with the 5.1×5.5-Å zigzag channels of MFI perpendicular to the support surface throughout the film thickness.

The procedure follows closely that used for the formation of *b*-oriented films,[20,40] with the main difference being the SDAs used for seed formation and secondary growth. More specifically, the SDA used for seed formation in the procedure leading to *b*-oriented films, that is, tetrapropylammonium hydroxide (TPA), was now used for secondary growth while the SDA that was used for secondary growth in the procedure leading to *b*-oriented films (*N*,*N*-bis(tripropylammonium-hexamethylene)-*N*,*N*-dipropylammonium cation, *trimer*-TPA) was now used for synthesis of the MFI seed crystals. The two processes are illustrated schematically in Figure 1. The procedure for the fabrication of *b*-oriented films has been described in detail before,[20,40] while that for *a*-oriented films is described below.

First, a mesoporous silica layer was prepared on the polished side of an α-alumina porous disk by slip-coating.[40,41] It has been suggested that the silica layer plays several important roles, which include: 1) providing a smooth surface for MFI seed deposition, 2) accommodating a higher density of OH groups than bare α-alumina for bonding the zeolite seed crystals to the substrate, and 3) preventing incorporation of Al from the support in the MFI film during secondary growth. The X-ray diffraction (XRD) patterns of bare porous α-alumina and silica-coated α-alumina are shown in Figure 2a and b, respectively.

To form the *a*-oriented seed layer, MFI crystals were produced in the presence of *trimer*-TPA as SDA.[42] The morphology of these MFI crystals is *b*-elongated leaf-shaped with the order of crystal dimensions $L_c \geq L_b > L_a$, where L_i denotes crystal length along the *i* axis[43,44] (Figure 3a and b). This shape is drastically different from the well-known coffin-shaped MFI crystals with $L_c \geq L_a > L_b$ obtained with TPA as SDA. The difference in crystal morphology is believed to be a direct result of the SDA used, on the basis of the findings of an earlier modeling study.[45] In this study[45] the distinct morphologies obtained with the different SDAs were attributed to the fitting of the SDAs in the straight (along the *b* axis) and sinusoidal channels (along the *a* axis), which correlate with the relative crystal dimensions along the *a* and *b* axes, respectively. More specifically, *trimer*-TPA appears to limit growth along the *a* axis due to the relative difficulty of fitting its long dimension along the *a* axis versus along the *b* axis.[43,44]

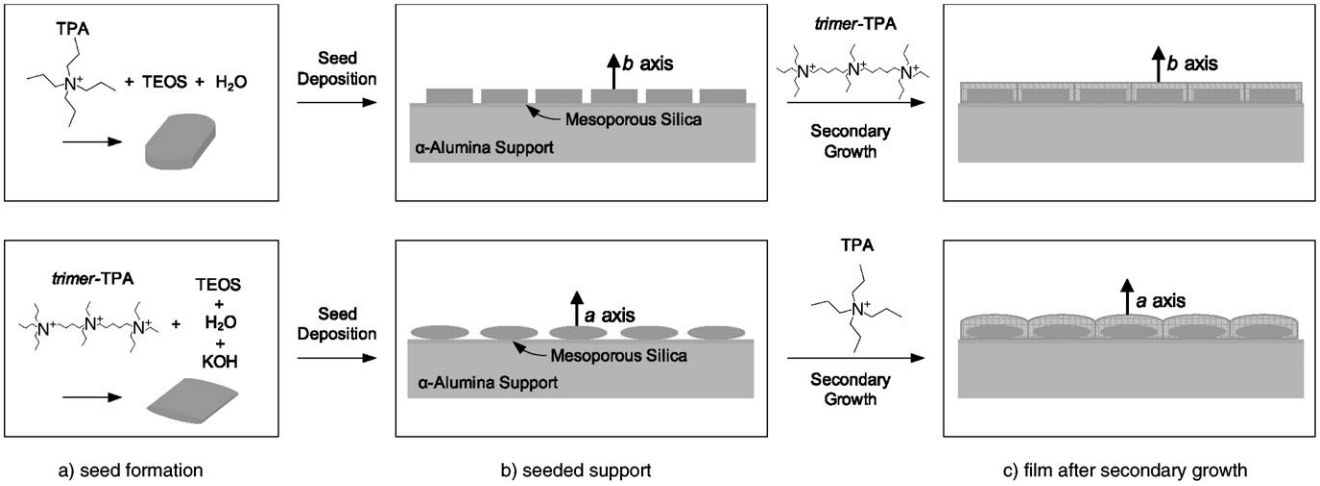


Figure 1. Schematic representation of the steps used to fabricate MFI films with *b*- and *a*-out-of-plane orientations are shown in the upper and lower panels, respectively.

 © 2006 Wiley-VCH Verlag GmbH & Co. KGaA, Weinheim

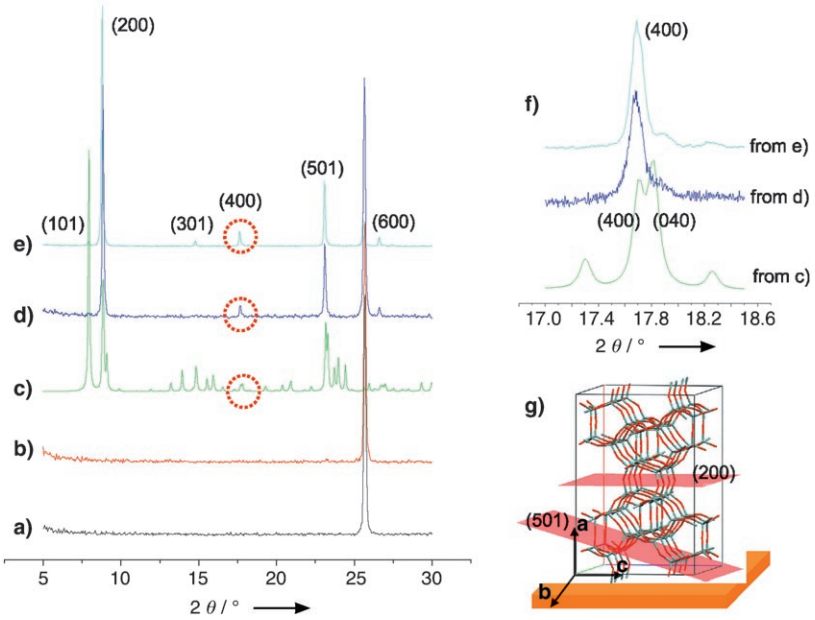


Figure 2. XRD patterns of a) bare porous α-alumina, b) silica-coated α-alumina, c) MFI powder, generated with Mercury Software (Cambridge Crystallographic Data Centre), d) MFI seed monolayer, and e) MFI films after secondary growth. XRD patterns in the 2θ region around the (400) and (040) MFI peaks, indicated by circles in c), d), and e), are shown in f). The MFI unit cell with representative crystallographic planes is shown in g).

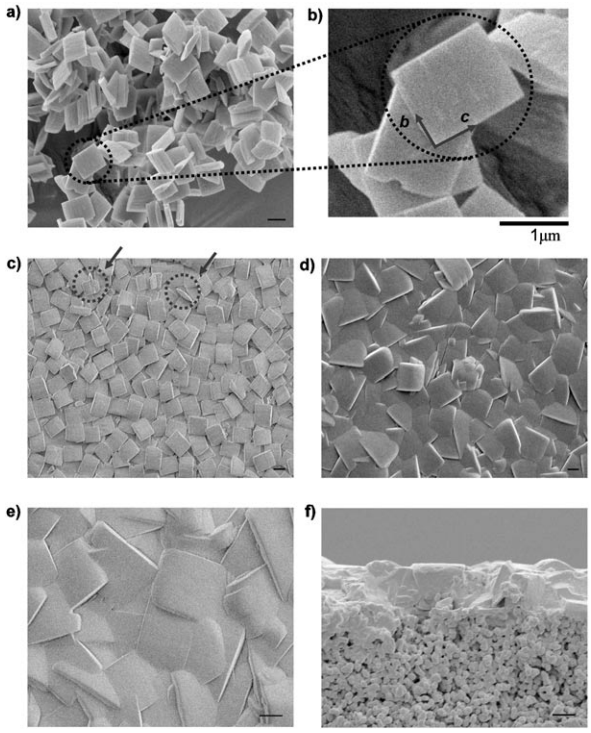


Figure 3. SEM images of a) zeolite MFI crystals obtained with *trimer*-TPA as SDA, b) magnified crystal with indication of *b* and *c* axes, and c) chemically bonded monolayer of MFI seeds after seed deposition with most of the MFI crystals lying flat on the support and few misoriented seeds indicated by arrows. Top-view SEM images of MFI films after secondary growth are shown in d) and e), with lower and higher magnification, respectively, and a cross-sectional view is shown in f). Scale bars are 1 μm.

Following the synthesis of seeds with short dimension along the *a* axis, a monolayer of MFI seeds was formed by bonding zeolite crystals and substrate by the procedure of Yoon and co-workers.[46] The formation of a close-packed nearly monolayer deposit of MFI seeds was evidenced by scanning electron microscopy (SEM, Figure 3c). The majority of MFI crystals rests with their short dimension (*a* axis) perpendicular to the support. A few exceptions of misoriented seed crystals can be found, and representative examples are indicated by arrows in Figure 3c. The *a*-out-of-plane orientation of the monolayer was verified by XRD (Figure 2c, d, and f). Apparently, the anisometric morphology of MFI crystals facilitated deposition with their short dimension (along the *a* axis) perpendicular to the support.

The starting point for the selection of secondary growth conditions was the criterion of comparable in-plane (parallel to the membrane surface) and out-of-plane (perpendicular to the membrane surface) rates.[40] If the out-of-plane growth rate is relatively high, it will lead to films with insufficient grain intergrowth, or large film thickness will be required to obtain intergrown columnar films. On the other hand, if the out-of-plane growth rate is very low then the relatively fast growth of misoriented seeds, twins with *b*-out-of-plane orientation, or randomly oriented nuclei will lead to loss of preferred orientation before a well-intergrown film is achieved. For this reason we selected TPA as SDA and secondary growth conditions of relatively high supersaturation and low temperature to obtain comparable growth rates along the *a* and *c* crystallographic axes of MFI. Screening experiments (not shown) led to selection of secondary growth at 90 °C with a composition of $60\,SiO_2$:9 TPAOH:9500 H_2O:240 EtOH. After hydrothermal secondary growth under the above conditions in the presence of TPA, a continuous MFI film was formed from the *a*-oriented seed layer. Representative SEM top views of a well-intergrown membrane after secondary growth are shown in Figure 3d and e. The thickness of the membrane was estimated to be around 2 μm from cross-sectional views (Figure 3f). The *a*-out-of-plane orientation achieved in seed deposition was preserved during secondary growth, as indicated by the XRD patterns in Figure 2c, e, and f. In these patterns, (*h*00), (301), and (501) MFI reflections (Figure 2g) are present along with the XRD peak from the α-alumina support. The peak of the α-alumina support is still detectable because of the thinness of the zeolite layer, as was the case for thin *b*-oriented film.[20,40] Although some degree of preferred *a*-out-of-plane orientation has been reported before,[39,40,47,48] to our knowledge this is the first time that a uniformly (throughout the membrane thickness) *a*-oriented intergrown MFI film has been fabricated.

In summary, the previously reported procedure for fabrication of *b*-oriented MFI membranes has been extended to acquire *a*-oriented MFI membranes by secondary growth from an *a*-oriented monolayer of MFI seeds. First, MFI crystals were synthesized by using *trimer*-TPA as SDA. The anisometric crystals (thin along the *a* axis) facilitated for-

 © 2006 Wiley-VCH Verlag GmbH & Co. KGaA, Weinheim

mation of a close-packed near-monolayer of MFI seeds by chemical bonding on a porous α-alumina substrate coated with mesoporous silica. As a result, an MFI seed layer with *a*-out-of-plane orientation was observed throughout the substrate. During secondary growth in the presence of TPA as SDA, comparable in-plane and out-of-plane growth rates were achieved to obtain well-intergrown *a*-oriented MFI membranes preserving the orientation of the seed layer. Thus, continuous and uniformly *a*-oriented MFI films were fabricated by the methodology of secondary growth and use of SDAs that act as crystal-shape modifiers. It is expected that the approach demonstrated here for siliceous ZSM-5 will also be applicable to other zeolites including cation-substituted ZSM-5. Along with the previously reported *b*-oriented membranes, they provide the first set of uniformly oriented zeolite films. We are currently comparing their permeation properties in an attempt to provide the first set of data for gas and vapor permeation through zeolite membranes of a given structure type with drastically different preferred orientations. Such a data set is expected to be valuable in revealing the relationship between microstructure and membrane performance.

Experimental Section

The synthesis, as well as elemental and NMR analyses, of *trimer*-TPA^{3+}-$3I^-$ were performed as described in reference [43].

Zeolite seeds: The synthesis sol was prepared by dissolving a specific amount of *trimer*-TPA^{3+}-$3I^-$ in deionized water and adding KOH solution (1N, Aldrich). Tetraethyl orthosilicate (TEOS, 98% Aldrich) was added as silica source. The final molar composition of the mixture was $40\,SiO_2$:5 (*trimer*-TPA^{3+}-$3I^-$):25 KOH:9500 H_2O:160 EtOH. The mixture was stirred at room temperature overnight and then filtered (qualitative P8, Fisher Scientific) into 45-mL teflon-lined stainless steel autoclaves (Parr). The autoclaves were placed in an oven, preheated to 175 °C. After 24 h, the autoclaves were removed from the oven and quenched in a cold water bath. Solid product was obtained after five repetitions of centrifugation and decantation. The recovered crystals were dried in an oven (ca. 70 °C) and calcined for 10 h at 525 °C with a ramp rate of 1 °C min^{-1}.

Seed deposition: A surfactant-templated silica layer was coated onto a 2-mm-thick α-alumina disk (∅ 22 mm) and calcined for 4 h at 450 °C with a ramp rate of 1 °C min^{-1} (For details on support preparation, see reference [40]). The silica-coated α-alumina was functionalized with (3-chloropropyl)trimethoxysilane (3CP-TMS, 4 mL, 97%, Aldrich) at reflux for 3 h at around 110 °C in dry toluene under argon flow. Calcined and dried MFI seeds (ca. 0.01 g) were dispersed in anhydrous toluene (40 mL) by sonication. The functionalized substrate was then immersed in the toluene/seeds suspension, which was heated to reflux for 3 h at about 110 °C under argon flow. The substrate was sonicated briefly in 30 mL of fresh toluene.

Secondary growth: The molar composition of the synthesis sol was $60\,SiO_2$:9 TPAOH:9500 H_2O:240 EtOH. The synthesis mixture was hydrolyzed for 6 h. The seeded substrate was secured in a 45-mL teflon liner with a slight tilt and the seeded side facing down. The synthesis mixture was then filtered into teflon-lined autoclaves. The autoclaves were placed in an oven preheated to 90 °C and left for 4 days. The films were calcined at 480 °C for 4 h with a ramp rate of 0.5 °C min^{-1}.

Received: August 23, 2005
Published online: December 30, 2005

Keywords: hydrothermal synthesis · monolayers · thin films · zeolites

[1] J. Caro, M. Noack, P. Kölsch, R. Schäfer, *Microporous Mesoporous Mater.* **2000**, *38*, 3.
[2] J. Coronas, J. Santamaria, *Catal. Today* **1999**, *51*, 377.
[3] Y. S. Lin, I. Kumakiri, B. N. Nair, H. Alsyouri, *Sep. Purif. Methods* **2002**, *31*, 229.
[4] T. C. Bowen, R. D. Noble, J. L. Falconer, *J. Membr. Sci.* **2004**, *245*, 1.
[5] T. Bein, *Chem. Mater.* **1996**, *8*, 1636.
[6] M. E. Davis, *Nature* **2002**, *417*, 813.
[7] M. Vilaseca, J. Coronas, A. Cirera, A. Cornet, J. R. Morante, J. Santamaria, *Catal. Today* **2003**, *82*, 179.
[8] J. Coronas, J. Santamaria, *Chem. Eng. Sci.* **2004**, *59*, 4879.
[9] J. Coronas, J. Santamaria, *Top. Catal.* **2004**, *29*, 29.
[10] Z. Wang, A. Mitra, H. Wang, L. Huang, Y. Yan, *Adv. Mater.* **2001**, *13*, 1463.
[11] S. Li, C. Demmelmaier, M. Itkis, Z. Liu, R. C. Haddon, Y. Yan, *Chem. Mater.* **2003**, *15*, 2687.
[12] K. Ha, Y.-J. Lee, D.-Y. Jung, J. H. Lee, K. B. Yoon, *Adv. Mater.* **2000**, *12*, 1614.
[13] a) D. Brühwiler, G. Calzaferri, *Microporous Mesoporous Mater.* **2004**, *72*, 1; b) G. Calzaferri, M. Pauchard, H. Maas, S. Huber, A. Khatyr, T. Schaafsma, *J. Mater. Chem.* **2002**, *12*, 1.
[14] J. Caro, F. Marlow, M. Wübbenhorst, *Adv. Mater.* **1994**, *6*, 413.
[15] A. I. Skoulidas, D. S. Sholl, R. Krishna, *Langmuir* **2003**, *19*, 7977.
[16] S. Sommer, T. Melin, J. L. Falconer, R. D. Noble, *J. Membr. Sci.* **2003**, *224*, 51.
[17] C. J. Gump, X. Lin, J. L. Falconer, R. D. Noble, *J. Membr. Sci.* **2000**, *173*, 35.
[18] K. Kusakabe, A. Murata, T. Kuroda, S. Morooka, *J. Chem. Eng. Jpn.* **1997**, *30*, 72.
[19] T. Matsufuji, N. Nishiyama, M. Matsukata, K. Ueyama, *J. Membr. Sci.* **2000**, *178*, 25.
[20] Z. Lai, G. Bonilla, I. Diaz, J. G. Nery, K. Sujaoti, M. A. Amat, E. Kokkoli, O. Terasaki, R. W. Thompson, M. Tsapatsis, D. G. Vlachos, *Science* **2003**, *300*, 456.
[21] J. L. H. Chau, Y. S. S. Wan, A. Gavriilidis, K. L. Yeung, *Chem. Eng. J.* **2002**, *88*, 187.
[22] Z. Wang, Y. Yan, *Microporous Mesoporous Mater.* **2001**, *48*, 229.
[23] Z. Wang, Y. Yan, *Chem. Mater.* **2001**, *13*, 1101.
[24] S. Li, Z. Li, K. N. Bozhilov, Z. Chen, Y. Yan, *J. Am. Chem. Soc.* **2004**, *126*, 10732.
[25] A. Gouzinis, M. Tsapatsis, *Chem. Mater.* **1998**, *10*, 2497.
[26] M. C. Lovallo, M. Tsapatsis, *AIChE J.* **1996**, *42*, 3020.
[27] G. Xomeritakis, A. Gouzinis, S. Nair, T. Okubo, M. He, R. M. Overney, M. Tsapatsis, *Chem. Eng. Sci.* **1999**, *54*, 3521.
[28] J. H. Koegler, H. van Bekkum, J. C. Jansen, *Zeolites* **1997**, *19*, 262.
[29] F.-Z. Zhang, M. Fuji, M. Takahashi, *Chem. Mater.* **2005**, *17*, 1167.
[30] T. Seike, M. Matsuda, M. Miyake, *J. Am. Ceram. Soc.* **2004**, *87*, 1585.
[31] W. C. Wong, L. T. Y. Au, C. T. Ariso, K. L. Yeung, *J. Membr. Sci.* **2001**, *191*, 143.
[32] L. T. Y. Au, K. L. Yeung, *J. Membr. Sci.* **2001**, *194*, 33.
[33] L. H. Chau, W. C. Wong, K. L. Yeung, *Fifth International Conference on Inorganic Membranes*, Nagoya, Japan, **1998**, pp. 432.
[34] J. Sun, G. Zhu, X. Yin, Y. Chen, Y. Cui, S. Qiu, *Chem. Commun.* **2005**, 1070.
[35] S. Mintova, V. Valtchev, V. Engström, B. J. Schoeman, J. Sterte, *Microporous Mater.* **1997**, *11*, 149.
[36] S. Mintova, J. Hedlund, V. Valtchev, B. J. Schoeman, J. Sterte, *J. Mater. Chem.* **1998**, *8*, 2217.
[37] S. Mintova, T. Bein, *Adv. Mater.* **2001**, *13*, 1880.

 © 2006 Wiley-VCH Verlag GmbH & Co. KGaA, Weinheim

[38] H. W. Deckman, E. W. Corcoran, Jr., J. A. Mchenry, W. F. Lai, L. R. Czarnetzki, W. E. Wales (Exxon Research and Engineering Company), WO 96/01686, **1996**, [*Chem. Abstr.* **1996**, *124*, 180384p].
[39] J. P. Verduijn, A.-J. Bons, M. H. C. Anthonis, L. R. Czarnetzki (Exxon Chemical Patents Inc.), WO 96/01683, **1996**, [*Chem. Abstr.* **1996**, *124*, 236420s].
[40] Z. Lai, M. Tsapatsis, J. P. Nicolich, *Adv. Funct. Mater.* **2004**, *14*, 716.
[41] Y. Lu, R. Ganguli, C. A. Drewien, M. T. Anderson, C. J. Brinker, W. Gong, Y. Guo, H. Soyez, B. Dunn, M. H. Huang, J. I. Zink, *Nature* **1997**, *389*, 364.
[42] L. W. Beck, M. E. Davis, *Microporous Mesoporous Mater.* **1998**, *22*, 107.
[43] G. Bonilla, I. Díaz, M. Tsapatsis, H.-K. Jeong, Y. Lee, D. G. Vlachos, *Chem. Mater.* **2004**, *16*, 5697.
[44] I. Díaz, E. Kokkoli, O. Terasaki, M. Tsapatsis, *Chem. Mater.* **2004**, *16*, 5226.
[45] E. de Vos Burchart, J. C. Jansen, B. van de Graaf, H. van Bekkum, *Zeolites* **1993**, *13*, 216.
[46] a) K. Ha, Y.-J. Lee, H. J. Lee, K. B. Yoon, *Adv. Mater.* **2000**, *12*, 1114; b) S. Y. Choi, Y. J. Lee, Y. S. Park, K. Ha, K. B. Yoon, *J. Am. Chem. Soc.* **2000**, *122*, 5201; c) A. Kulak, Y. J. Lee, Y. S. Park, K. B. Yoon, *Angew. Chem.* **2000**, *112*, 980; *Angew. Chem. Int. Ed.* **2000**, *39*, 950; d) G. S. Lee, Y. J. Lee, K. B. Yoon, *J. Am. Chem. Soc.* **2001**, *123*, 9769; e) J. S. Park, G. S. Lee, Y. J. Lee, Y. S. Park, K. B. Yoon, *J. Am. Chem. Soc.* **2002**, *124*, 13366; f) J. S. Park, Y. J. Lee, K. B. Yoon, *J. Am. Chem. Soc.* **2004**, *126*, 1934.
[47] J. Hedlund, S. Mintova, J. Sterte, *Microporous Mesoporous Mater.* **1999**, *28*, 185.
[48] J. S. Lee, Y.-J. Lee, E. L. Tae, Y. S. Park, K. B. Yoon, *Science* **2003**, *301*, 818.

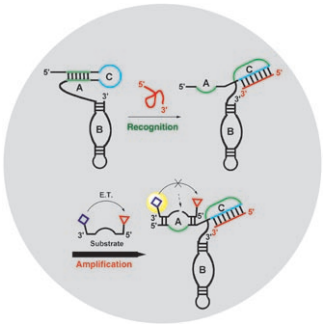
 © 2006 Wiley-VCH Verlag GmbH & Co. KGaA, Weinheim

Cover Picture



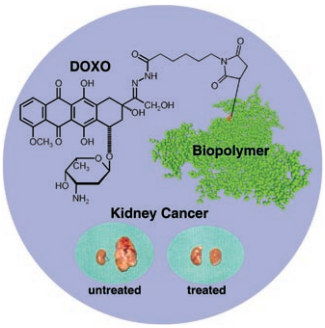
Aneta Oleksi, Alexandre G. Blanco, Roeland Boer, Isabel Usón, Joan Aymamí, Alison Rodger, Michael J. Hannon,* and Miquel Coll*

Metallosupramolecular helicates with trigonal-antiprismatic geometry thread through and fit perfectly into the central hydrophobic cavity of a three-way DNA junction. Six hydrophobic rings of the drug stack on six DNA bases, with three more sandwiched in the minor grooves. This work reveals and enables a new approach to targeting DNA and specifically DNA junctions. For more details, see the Communication by M. Coll, M. J. Hannon, and co-workers on page 1227 ff.



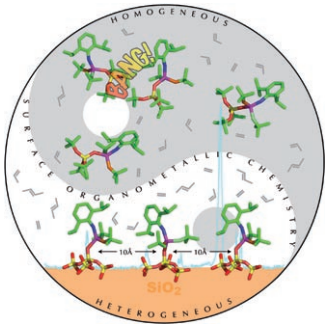
Sensors

The molecular recognition between an external signal and a receptor is transduced allosterically to catalytically amplified chemical information. E. V. Anslyn and L. Zhu outline this approach in their Minireview on page 1190 ff.



Medicinal Chemistry

Polymeric carrier systems enable the optimization and transport of low-molecular-weight drugs, proteins, and oligonucleotides. Current developments in polymer therapeutics are given by R. Haag and F. Kratz in their Review on page 1198 ff.



Metathesis Catalysts

In their Communication on page 1216 ff., C. Copéret and co-workers describe the preparation of a silica-supported Mo–carbene catalyst for olefin metathesis and how its performance compares relative to its molecular equivalent.

Contents

VIP ***The following Communications have been judged by at least two referees to be "very important papers" and will be published online at www.angewandte.org soon:***

*H. Kiyohara, Y. Nakamura, R. Matsubara, S. Kobayashi**
Catalytic Asymmetric Allylation of Iminoesters and Iminophosphonates with a Variety of Allylsilanes Leading to Enantiomerically Enriched Allylglycine Derivatives

*J. J. La Clair**
Total Syntheses of Hexacyclinol, 5-epi-Hexacyclinol, and Desoxohexacyclinol Unveils an Antimalarial Prodrug Motif

H. Katagiri, T. Miyagawa, Y. Furusho, E. Yashima**
Synthesis and Optical Resolution of a Double Helicate Consisting of ortho-Linked Hexaphenol Strands Bridged by Spiroborates

D. Belder, M. Ludwig, L.-W. Wang, M. T. Reetz**
Enantioselective Catalysis and Analysis on a Chip

*P. Cheung, A. Bhan, G. J. Sunley, E. Iglesia**
Selective Carbonylation of Dimethyl Ether to Methyl Acetate Catalyzed by Acidic Zeolites

W. Richtering, I. Berndt, J. S. Pedersen*
Temperature-Sensitive Core–Shell Microgel Particles with Dense Shells

News

Catalysis: K. Severin ____ **1182** Theoretical Chemistry: K. N. Houk **1182** Organic Chemistry: B. L. Feringa ____ **1182**

Books

Thermodynamics — John P. O'Connell, J. M. Haile — *reviewed by M.-O. Coppens* ____ **1183**

Protein–Lipid Interactions — Lukas K. Tamm — *reviewed by A. Janshoff* ____ **1184**

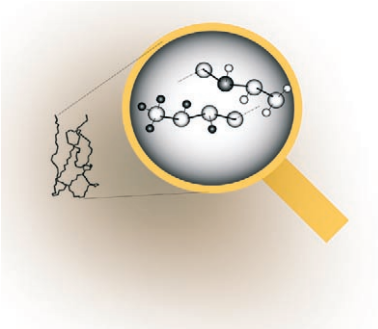
Highlights

Solid-State NMR Spectroscopy

M. Baldus* ____ **1186 – 1188**

Solid-State NMR Spectroscopy: Molecular Structure and Organization at the Atomic Level

Worth a closer look: Solid-state nuclear magnetic resonance spectroscopy (ssNMR) has led to significant progress in the study of three-dimensional molecular structures. Recent applications demonstrate the use of high-resolution ssNMR in research areas ranging from structural biology to nanotechnology as a complementary means to microscopic and crystallographic imaging techniques.

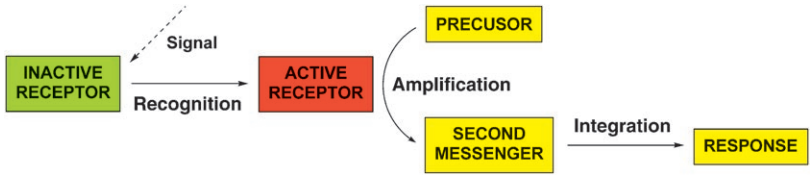


Minireviews

Sensors

L. Zhu, E. V. Anslyn* ____ **1190 – 1196**

Signal Amplification by Allosteric Catalysis

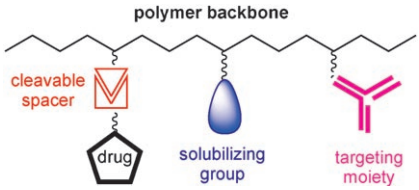


Strong signals: A series of recent studies are unified under a single concept: SAAC (signal amplification by allosteric catalysis). Addition of a signal leads to a recognition step, followed by amplification and integration steps (see scheme).

WILEY InterScience DISCOVER SOMETHING GREAT
© 2006 Wiley-VCH Verlag GmbH & Co. KGaA, Weinheim

Reviews

Thirty years ago polymeric carriers were first suggested as covalent drug-delivery vehicles. Polymer therapeutics has now emerged as an exciting field of research for improving the therapeutic potential of low-molecular-weight drugs, proteins, and oligonucleotides. Polymer-based therapeutics have enhanced stability as well as longer circulation in the blood, and several special effects, such as tumor selectivity and multivalent interactions, can now be tailored.



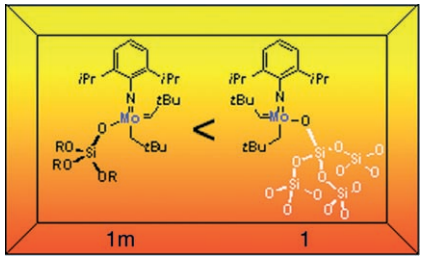
Medicinal Chemistry

R. Haag,* F. Kratz* ____ **1198 – 1215**

Polymer Therapeutics: Concepts and Applications

Communications

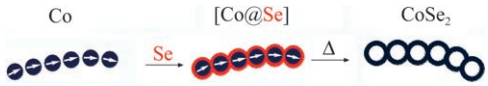
Surface organometallic chemistry: Similar electronic properties of molecular and surface siloxy ligands in **1m** and **1** were revealed by a structural investigation with solid-state NMR spectroscopy and a reactivity study in olefin metathesis. Despite similar initial turnover frequencies, the silica-supported catalyst **1** is more stable than **1m** and allows it to achieve higher turnovers, thus showing the advantage of site isolation on surfaces.



Alkene Metathesis

F. Blanc, C. Copéret,* J. Thivolle-Cazat, J.-M. Basset,* A. Lesage, L. Emsley,* A. Sinha, R. R. Schrock* ____ **1216 – 1220**

Surface versus Molecular Siloxy Ligands in Well-Defined Olefin Metathesis Catalysts: [{(RO)$_3$SiO}Mo(=NAr)(=CH*t*Bu)(CH$_2$*t*Bu)]



Giving cobalt some stick: A general strategy for the synthesis of 1D assemblies of hollow nanocrystals is presented. Cobalt nanostructures assembled through magnetic dipolar interactions (see scheme) are used as templates for the formation of wires of hollow nanocrystals of $CoSe_2$ (and Co_3S_4, CoTe). The wires of hollow $CoSe_2$ nanocrystals are ferromagnetic, with a Curie temperature of 570 K.

Magnetic Nanowires

J. Gao, B. Zhang, X. Zhang, B. Xu* ____ **1220 – 1223**

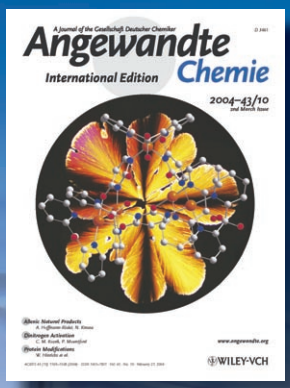
Magnetic-Dipolar-Interaction-Induced Self-Assembly Affords Wires of Hollow Nanocrystals of Cobalt Selenide

For the USA and Canada:
ANGEWANDTE CHEMIE International Edition (ISSN 1433-7851) is published weekly by Wiley-VCH PO Box 191161, D 69451 Weinheim, Germany. Air freight and mailing in the USA by Publications Expediting Inc. 200 Meacham Ave., Elmont, NY 11003. Periodicals postage paid at Jamaica NY 11431. US POSTMASTER: send address changes to *Angewandte Chemie*, Wiley-VCH, 111 River Street, Hoboken, NJ 07030. Annual subscription price for institutions: US$ 5685/5168 (valid for print and electronic / print or electronic delivery); for individuals who are personal members of a national chemical society prices are available on request. Postage and handling charges included. All prices are subject to local VAT/sales tax.

© 2006 Wiley-VCH Verlag GmbH & Co. KGaA, Weinheim

The best in chemistry –

for more than a hundred years



A Journal of the Gesellschaft Deutscher Chemiker

Angewandte
International Edition **Chemie**

www.angewandte.org

1888: ***The beginning of a success story***

Constant Innovations

1962: *First issue of the International Edition*
1976: *Graphical abstracts*
1979: *Cover pictures*
1988: *Centenary of Angewandte*
1989: *Routine use of color*
1991: *New section: Highlights*
1992: *Computerized editorial tracking system*
1995: *Internet service for readers*
1998: *Regular press service; full-text online*
2000: *New section: Essays; EarlyView: Communications available online ahead of the printed version*
2001: *New section: Minireviews*
2002: *Online submission of manuscripts*
2003: *Weekly publication; new section: News; new layout*
2004: *Backfiles (1962-1997); ManuscriptXpress: Online system for authors and referees*



Angewandte's advisors...

E. W. "Bert" Meijer
Technische Universiteit Eindhoven

» ***Angewandte Chemie,*** *in its way of publishing, is as original as the chemistry described in the journal. It serves our society in a superb and attractive way. Many leading communications and comprehensive reviews have been published through the years and many of them are used in my teaching and cited in my own papers. It is a privilege to publish in and to be connected to a journal that is the trendsetter in chemistry of the highest standards.* «

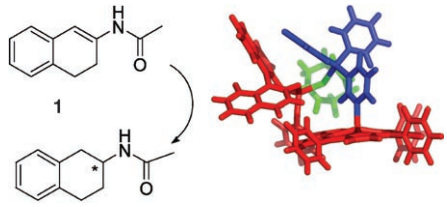
Angewandte Chemie International Edition *is a journal of the German Chemical Society (GDCh)*

GDCh

WILEY InterScience® DISCOVER SOMETHING GREAT

WILEY-VCH

12001404_gu

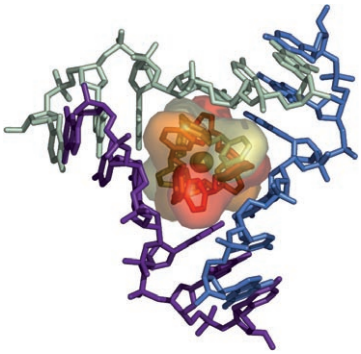


Bindings for libraries: Large numbers of bidentate ligands have been formed from two monodentate ligands (one based on zinc(II) porphyrin and the other on a substituted phosphane) by using high-throughput methods combined with self-assembly principles. The library provided a Rh catalyst that hydrogenates the enamide **1** with the highest enantioselectivity known to date.

Combinatorial Chemistry

X.-B. Jiang, L. Lefort, P. E. Goudriaan, A. H. M. de Vries, P. W. N. M. van Leeuwen, J. G. de Vries, J. N. H. Reek* _____ **1223 – 1227**

Screening of a Supramolecular Catalyst Library in the Search for Selective Catalysts for the Asymmetric Hydrogenation of a Difficult Enamide Substrate



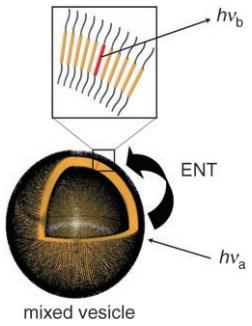
Three point turn: A metallosupramolecular helicate with trigonal-antiprismatic geometry fits perfectly into the central hydrophobic cavity of a three-way DNA junction allowing a new mode of DNA recognition.

DNA Recognition

A. Oleksi, A. G. Blanco, R. Boer, I. Usón, J. Aymamí, A. Rodger, M. J. Hannon,* M. Coll* _____ **1227 – 1231**

Molecular Recognition of a Three-Way DNA Junction by a Metallosupramolecular Helicate

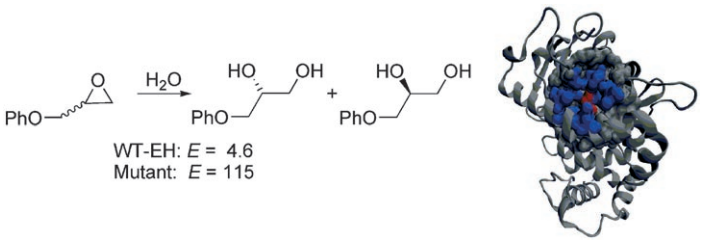
Monitoring self-assembled objects: Optical studies and scanning confocal microscopy have been used to monitor intermolecular energy transfer (ENT) in mixed vesicles of donor/acceptor oligo(*p*-phenylene vinylene)s (OPVs) in water (see picture) over time. This probing of the ongoing exchange process between separate donor and acceptor vesicles proved that the properties of individual vesicles were different from those of the bulk solution.



Supramolecular Chemistry

F. J. M. Hoeben, I. O. Shklyarevskiy, M. J. Pouderoijen, H. Engelkamp, A. P. H. J. Schenning,* P. C. M. Christianen, J. C. Maan, E. W. Meijer* _____ **1232 – 1236**

Direct Visualization of Efficient Energy Transfer in Single Oligo(*p*-phenylene vinylene) Vesicles



ReCASTing for success: The recently introduced method of combinatorial active-site saturation test (CAST) has been applied in iterative cycles in the directed evolution of enantioselective wild-type epoxide hydrolases (WT-EH).

Directed Evolution

M. T. Reetz,* L.-W. Wang, M. Bocola _____ **1236 – 1241**

Directed Evolution of Enantioselective Enzymes: Iterative Cycles of CASTing for Probing Protein-Sequence Space

© 2006 Wiley-VCH Verlag GmbH & Co. KGaA, Weinheim

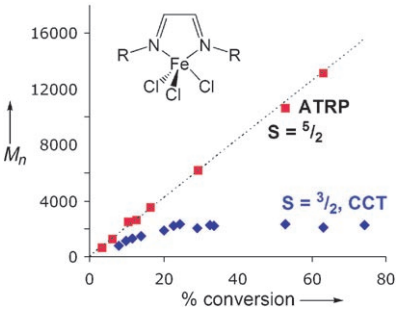
Contents

Homogeneous Catalysis

M. P. Shaver, L. E. N. Allan, H. S. Rzepa, V. C. Gibson* ——— **1241 – 1244**

Correlation of Metal Spin State with Catalytic Reactivity: Polymerizations Mediated by α-Diimine–Iron Complexes

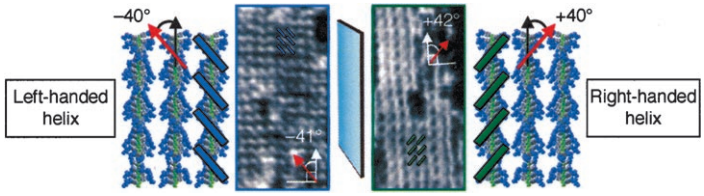
The mechanism of styrene polymerization by α-diimine iron complexes correlates with the metal spin state of the catalyst. Experimental and theoretical studies indicate that high-spin catalysts are halogenophilic, resulting in atom transfer radical polymerization (ATRP), while intermediate-spin complexes are carbophilic giving rise to catalytic chain transfer (CCT, see graph).



Helical Structures

S.-i. Sakurai, K. Okoshi, J. Kumaki,* E. Yashima* ——— **1245 – 1248**

Two-Dimensional Hierarchical Self-Assembly of One-Handed Helical Polymers on Graphite

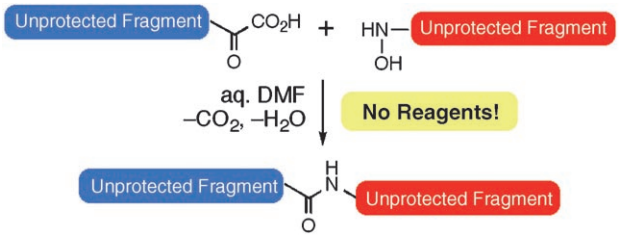


Rigid and rodlike, helical polyacetylene molecules self-assemble hierarchically on graphite upon exposure to solvent vapors. Flat polyacetylene monolayers form epitaxially on the basal plane of the graphite, on which helical polyacetylene molecules further self-assemble into chiral 2D bundles of helices with controlled helicity (see picture).

Ligation Reactions

J. W. Bode,* R. M. Fox, K. D. Baucom ——— **1248 – 1252**

Chemoselective Amide Ligations by Decarboxylative Condensations of *N*-Alkylhydroxylamines and α-Ketoacids



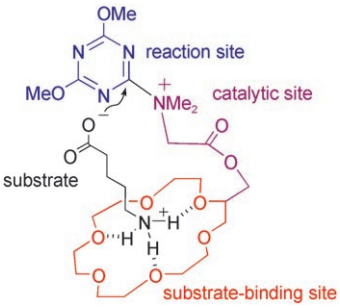
Additive-free: The chemoselective amide-bond-forming ligation between *N*-alkylhydroxylamines and α-ketoacids requires no reagents and the only by-products are water and carbon dioxide. This process proceeds on unprotected peptide substrates without epimerization, and as such, this process has the potential to serve as a novel chemoselective ligation for the synthesis of peptides and complex materials.

Enzyme Models

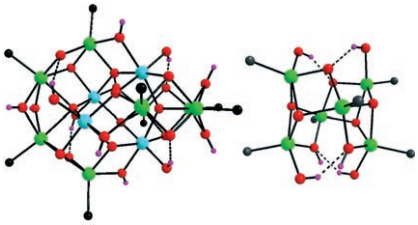
M. Kunishima,* K. Hioki, T. Moriya, J. Morita, T. Ikuta, S. Tani ——— **1252 – 1255**

Primary-Amine-Specific Lactamization of ω-Amino Acids by an Artificial Cyclotransferase Based on [18]Crown-6

Feet first: Carboxylic acids with a primary amino group in the farthest position from the carboxy group are specifically bound to an artificial cyclotransferase based on [18]crown-6. The amino group fits into the [18]crown-6 substrate-binding site to bring the carboxyl group close to the 2-ammonio-1,3,5-triazine reaction site for selective conversion into a lactam.



© 2006 Wiley-VCH Verlag GmbH & Co. KGaA, Weinheim



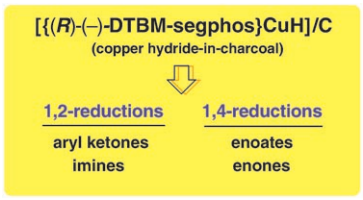
Organic meets inorganic: Hydrolysis of an aryl trialkynyl tin compound leads to an organic–inorganic tin oxide–hydroxide cluster, which consists of an inorganic tin oxide core surrounded by eight aryl tin fragments (see picture, left; Sn green, inorganic Sn blue, O red, C gray, H pink). Slightly modified reaction conditions produce a hexameric aryl tin oxide–hydroxide cage, which can be described as a double-twist Möbius band (see picture, right).

Tin Clusters

G. Prabusankar, B. Jousseaume,* T. Toupance, H. Allouchi — **1255 – 1258**

Organic–Inorganic Sn_{12} and Organic Sn_6 Oxide–Hydroxide Clusters

Asymmetric copper chemistry ... done heterogeneously? It's doable: Copper-in-charcoal (Cu/C) is introduced as an easily prepared catalyst that is readily converted in situ into a nonracemically ligated form of copper hydride that effects asymmetric hydrosilylations. DTBM = 3,5-di-*tert*-butyl-4-methoxydiphenylphosphinyl.

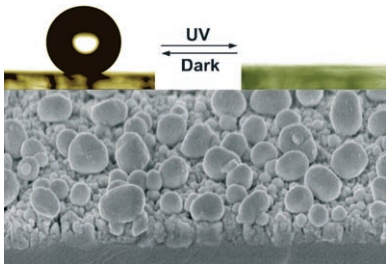


Heterogeneous Catalysis VIP

B. H. Lipshutz,* B. A. Frieman, A. E. Tomaso, Jr. — **1259 – 1264**

Copper-in-Charcoal (Cu/C): Heterogeneous, Copper-Catalyzed Asymmetric Hydrosilylations

A wet and dry paper! Tungsten oxide films prepared by a facile electrochemical deposition process provide the first example of a dual surface functionality. The reversible switch of wettability between superhydrophobicity and superhydrophilicity is realized by alternating irradiation with UV light and storage in the dark; this phenomenon is accompanied by photochromism (see picture).

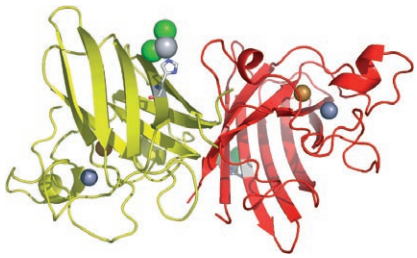


Tungsten Oxide Films

S. Wang, X. Feng, J. Yao, L. Jiang* — **1264 – 1267**

Controlling Wettability and Photochromism in a Dual-Responsive Tungsten Oxide Film

Drug adduct: The X-ray crystal structure of an adduct of cisplatin and bovine erythrocyte superoxide dismutase has been solved at 1.8-Å resolution. Selective platination of His19 occurs far away from the copper–zinc site. Remarkably, the protein-bound platinum center retains both chloro ligands (see picture, Cu orange, Zn dark gray, Pt light gray, Cl green).

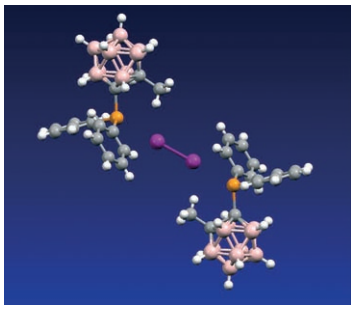


Drug–Protein Adducts

V. Calderone, A. Casini, S. Mangani,* L. Messori,* P. L. Orioli — **1267 – 1269**

Structural Investigation of Cisplatin–Protein Interactions: Selective Platination of His19 in a Cuprozinc Superoxide Dismutase

Seeing I to I: The reaction of a weakly coordinating carboranyl phosphane ligand with I_2 leads to the formation of an adduct containing the bridging P···I–I···P assembly in the solid state (see picture; I purple, P orange, C gray, B pink, H white). DFT calculations combined with a variety of experimental techniques suggest that this structural motif also exists in solution.



Phosphane–Diiodine Complexes

R. Núñez, P. Farràs, F. Teixidor, C. Viñas,* R. Sillanpää, R. Kivekäs — **1270 – 1272**

A Discrete P···I–I···P Assembly: The Large Influence of Weak Interactions on the ^{31}P NMR Spectra of Phosphane–Diiodine Complexes

© 2006 Wiley-VCH Verlag GmbH & Co. KGaA, Weinheim

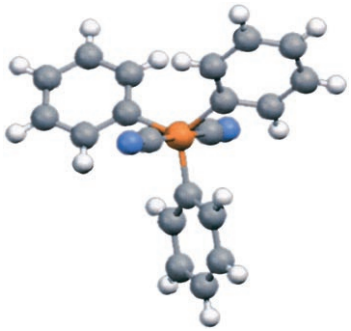
Contents

Phosphoranes

N. A. Barnes, S. M. Godfrey,*
R. T. A. Halton, S. Law,
R. G. Pritchard ——— **1272 – 1275**

Formation of a Dicyanotriorganophosphorane from the Reaction of Triphenylphosphane with Phenylselenocyanate

A glimpse of the elusive: A Group 15 triorganodicyanide has been prepared and crystallographically characterized for the first time. The reaction of phenylselenocyanate with triphenylphosphane affords a facile route to the elusive dicyanotriorganophosphorane $Ph_3P(CN)_2$. The complex reaction mechanism also results in formation of the diiminophosphorane $Ph_3PNC(CN)_2C(CN)_2NPPh_3$.



Coupling Reactions

Q. Cai, B. Zou, D. Ma* ——— **1276 – 1279**

Mild Ullmann-Type Biaryl Ether Formation Reaction by Combination of *ortho*-Substituent and Ligand Effects

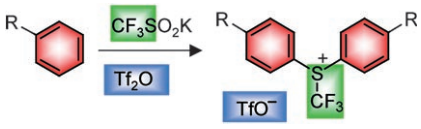


An important position: A strong *ortho*-substituent effect caused by NHCOR groups in 2-haloacetanilides in combination with the ligand effect greatly promotes an Ullmann-type biaryl formation reaction that takes place at room temperature.

Electrophilic Reagents

E. Magnier,* J.-C. Blazejewski,*
M. Tordeux, C. Wakselman ——— **1279 – 1282**

Straightforward One-Pot Synthesis of Trifluoromethyl Sulfonium Salts

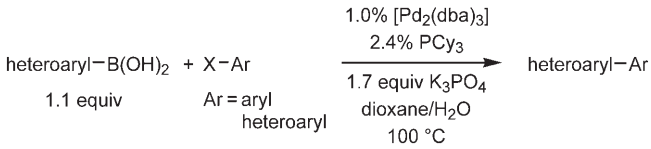


Mix and wait: Trifluoromethyl sulfonium salts that are able to react as reagents in the trifluoromethylation of various nucleophiles are formed in a multicomponent reaction. The desired electrophilic reagents are prepared from an aryl substrate, trifluoromethanesulfonic anhydride, and potassium trifluoromethanesulfinate in a one-pot procedure (see scheme).

Homogeneous Catalysis

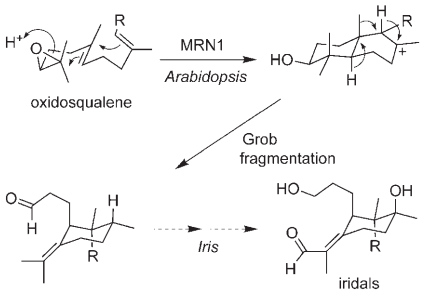
N. Kudo, M. Perseghini,
G. C. Fu* ——— **1282 – 1284**

A Versatile Method for Suzuki Cross-Coupling Reactions of Nitrogen Heterocycles



A wide-ranging study of Suzuki reactions which use nitrogen-containing heterocycles is described (see scheme; dba = dibenzylideneacetone, Cy = cyclohexyl). This method is highly versatile (a single procedure was used for all substrates, including boronate esters and trifluoroborates), compatible with a variety of unprotected functionalities (e.g., NH_2- and OH-substituted substrates), and efficient even with unactivated aryl chlorides.

© 2006 Wiley-VCH Verlag GmbH & Co. KGaA, Weinheim

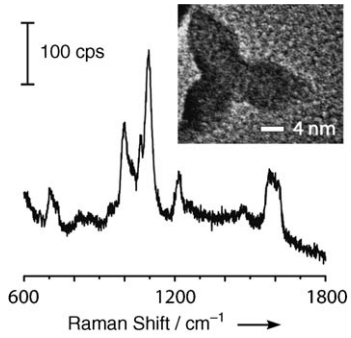


Mechanistic and phylogenetic surprises: A triterpene synthase (MRN1) from *Arabidopsis* invokes a Grob fragmentation in the cyclization of oxidosqualene. The enzymatic product is the elusive carbocyclic precursor of iridals, unusual triterpenoids known only in the distant *Iris* family. The results demonstrate the power of genome mining and exemplify the facile evolution of cyclases to generate diverse triterpene skeletons.

Enzymes

Q. Xiong, W. K. Wilson, S. P. T. Matsuda* ——— **1285 – 1288**

An *Arabidopsis* Oxidosqualene Cyclase Catalyzes Iridal Skeleton Formation by Grob Fragmentation

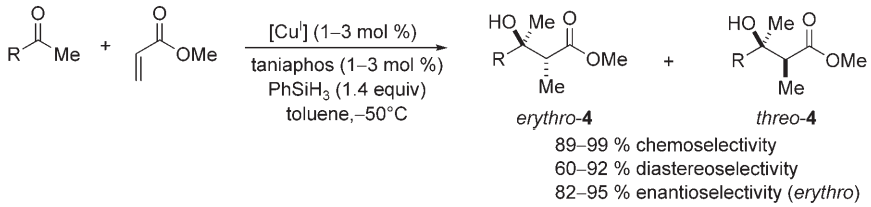


Multipodal Rh nanocrystals (see HRTEM image of a tripod) prepared through a polyol synthesis display surface plasmon resonance bands in the visible region. Surface-enhanced Raman scattering from 4-mercaptopyridine adsorbed on Rh multipods is 19-times stronger than that from Rh nanocubes.

Rhodium Nanoparticles

N. Zettsu, J. M. McLellan, B. Wiley, Y. Yin, Z.-Y. Li, Y. Xia* ——— **1288 – 1292**

Synthesis, Stability, and Surface Plasmonic Properties of Rhodium Multipods, and Their Use as Substrates for Surface-Enhanced Raman Scattering



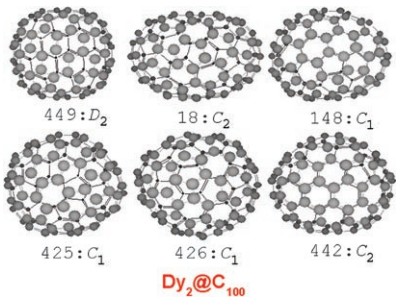
A good choice: A new catalytic method was found for the construction of stereogenic quaternary carbon centers through a copper-catalyzed domino conjugated reduction/aldol reaction of methyl acrylate with various alkyl aryl ketones. The proper choice of the chiral diphosphine ligand leads to high chemo-, diastereo-, and enantioselectivity.

Asymmetric Aldol Reactions

J. Deschamp, O. Chuzel, J. Hannedouche, O. Riant* ——— **1292 – 1297**

Highly Diastereo- and Enantioselective Copper-Catalyzed Domino Reduction/Aldol Reaction of Ketones with Methyl Acrylate

The largest isolated fullerene cage is found in a stable $Dy_2@C_{100}$ dimetallofullerene (probable structures are shown with Dy atoms omitted). In addition, a $Dy_3@C_{98}$ trimetallofullerene and two $Dy_2@C_{94}$ isomers were produced in high yields and separated by single-step HPLC. The new higher multimetallofullerenes are all classified as small band-gap fullerenes.



Fullerenes

S. Yang,* L. Dunsch* ——— **1299 – 1302**

Di- and Tridysprosium Endohedral Metallofullerenes with Cages from C_{94} to C_{100}

© 2006 Wiley-VCH Verlag GmbH & Co. KGaA, Weinheim

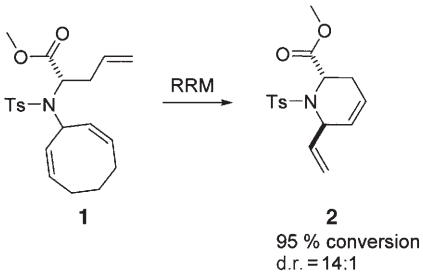
Contents

Metathesis

V. Böhrsch, J. Neidhöfer, S. Blechert* ——— **1302 – 1305**

Diastereoselective Ring-Rearrangement Metathesis

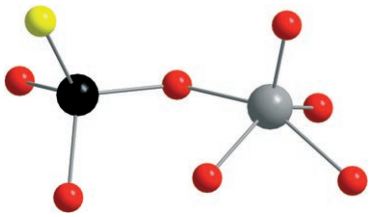
A new stereocenter is formed by ring-rearrangement metathesis (RRM), which has now been extended to diastereoselective processes. Selectivities are catalyst- and substrate-dependent. In these conversions yielding carbo- and heterocycles, d.r. values of up to 14:1 were obtained. For example, cyclooctadiene **1** was converted into piperideine **2** at room temperature and with high diastereoselectivity (Ts = toluene-4-sulfonyl).



Magnetic Properties

D. Pitzschke, J. Wang, R.-D. Hoffmann, R. Pöttgen, W. Bensch* —— **1305 – 1308**

Two Compounds Containing the Mixed Germanium–Vanadium Polyoxothioanion $[V_{14}Ge_8O_{42}S_8]^{12-}$



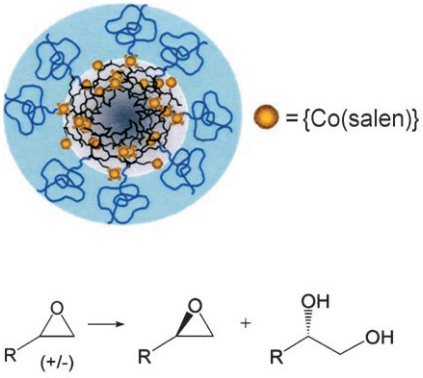
GeO_3S tetrahedra and square-pyramidal VO_5 units are primary building units of two new compounds containing the unusual anion $[V_{14}Ge_8O_{42}S_8]^{12-}$ (see section of the structure; Ge black, O red, S yellow, V gray). Both compounds were prepared under solvothermal conditions. Strong antiferromagnetic exchange interactions between V^{4+} centers dominate the magnetic properties.

Kinetic Resolution

B. M. Rossbach, K. Leopold, R. Weberskirch* ——— **1309 – 1312**

Self-Assembled Nanoreactors as Highly Active Catalysts in the Hydrolytic Kinetic Resolution (HKR) of Epoxides in Water

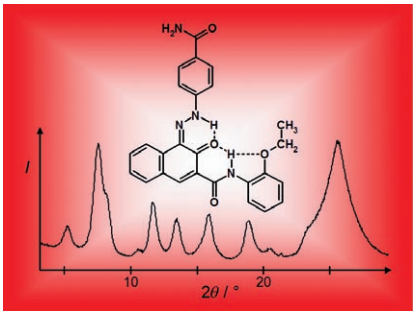
Co^{III}(salen) complexes have been immobilized on amphiphilic block copolymers, which self-assemble in water to give micellar aggregates with a hydrophobic Co(salen) core and a water-soluble shell (see picture). These aggregates were used to catalyze the hydrolytic kinetic resolution (HKR) of racemic aromatic epoxides over four consecutive cycles and gave the epoxides in up to 99% *ee*. H_2salen = *N*,*N*′-bis(salicylidene)ethylenediamine.



Crystal Engineering

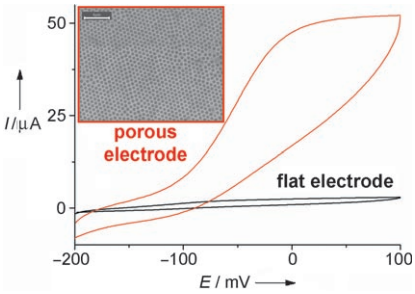
M. U. Schmidt,* D. W. M. Hofmann, C. Buchsbaum, H. J. Metz —— **1313 – 1317**

Crystal Structures of Pigment Red 170 and Derivatives, as Determined by X-Ray Powder Diffraction



Red automotive coatings fade over time possibly because of the insufficient photostability of Pigment Red 170. The crystal structures of the α and γ phases of this pigment were determined from X-ray powder diagrams, even without indexing (the α phase is shown). Subsequently, the weatherfastness could be improved by crystal engineering.

© 2006 Wiley-VCH Verlag GmbH & Co. KGaA, Weinheim



Porous golden interiors: Highly organized macroporous metal structures can be synthesized by the preparation of ordered colloidal crystals by the Langmuir–Blodgett technique and subsequent precision electrodeposition controlled by current oscillations. After the assembly of a bioelectrocatalytic chain in the pores, these tailored surfaces can be used as transducers with currents increased by more than one order of magnitude (see diagram).

Bioelectrochemistry

R. Szamocki, S. Reculusa, S. Ravaine, P. N. Bartlett, A. Kuhn, R. Hempelmann* ——— **1317 – 1321**

Tailored Mesostructuring and Biofunctionalization of Gold for Increased Electroactivity

WILEY InterScience® DISCOVER SOMETHING GREAT

"**Hot Papers**" are chosen by the Editors for their importance in a rapidly evolving field of high current interest. A preview with the graphical abstracts of these articles can be found on the *Angewandte Chemie* homepage in Wiley InterScience at www.angewandte.org.

All articles in *Angewandte Chemie* are published online several weeks ahead of print. They are found under the "**EarlyView**" link on the journal's homepage in Wiley InterScience.

Service

Keywords ——— ***1322***

Authors ——— ***1323***

Preview ——— ***1325***



For more information on ChemMedChem see www.chemmedchem.org

 © 2006 Wiley-VCH Verlag GmbH & Co. KGaA, Weinheim



Awarded...

K. Severin Receives Otto Roelen Medal

The German Society for Chemical Engineering and Biotechnology, DECHEMA, has awarded Kay Severin (Ecole Polytechnique Fédérale de Lausanne, EPFL, Switzerland) the Otto Roelen Medal 2005. Every two years, the society rewards outstanding achievements in homogeneous catalysis; Severin was honored in particular for his work on biomimetic catalysis and bimetallic homogeneous catalysts. His research group is also interested in supramolecular and organometallic chemistry. He recently reported on the use of dynamic combinatorial libraries of dye complexes as sensors in *Angewandte Chemie*, and in a cover contribution in *Chemistry—A European Journal* he described the use of self-sorting processes to generate dynamic combinatorial libraries with new network topologies.[1]



K. Severin

Severin obtained his PhD in 1995 from the University of Munich, where he worked in the group of W. Beck on the synthesis and reactivity of organometallic complexes with amino acids and peptides. Subsequently, he joined the group of M. R. Ghadiri at the Scripps Research Institute (La Jolla, CA), where he studied self-replicating peptides, autocatalytic networks, and artificial enzymes. During 1997–2001, he completed his habilitation at the University of Munich. Following a visiting professorship at the University of Vienna, he joined the EPFL as an assistant professor.

K. N. Houk Receives Ziegler Prize

Kendall N. Houk (University of California, Los Angeles; UCLA) gave the Karl Ziegler Lecture 2005 at the Max Planck Institute for Coal Research in Mülheim/Ruhr on the mechanism and dynamics of thermal reactions of hydrocarbons. The research work in his theoretically oriented group is focused on stereoselective organic reactions and catalysis, pericyclic reactions, molecular recognition in proteins and synthetic hosts, biological catalysis, reactive intermediates in biology and the atmosphere, as well as molecular organic materials. He recently reviewed the chemistry and biology of nitroxyl (HNO) in *ChemBioChem* and described the dynamic effects of [3,3] and [1,3] shifts of 6-methylenebicyclo-[3.2.0]hept-2-ene in *Angewandte Chemie*.[2]



K. N. Houk

Houk completed his PhD in 1968 at Harvard University (Cambridge, MA) in the group of R. B. Woodward, working on experimental tests of orbital symmetry selection rules. He then joined Louisiana State University (Baton Rouge) as assistant professor and was later promoted to full professor there. In 1980, he moved to the University of Pittsburgh, and in 1986, he joined UCLA. Houk serves as a member of the editorial board of, among others, *Chemistry—A European Journal* and the *Journal of Computational Chemistry*.

B. L. Feringa Receives Prelog Medal

Ben L. Feringa (University of Groningen, The Netherlands) recently gave the Prelog Medal Lecture at the ETH Zürich on the theme of the control of chirality. His research is focused on synthetic organic chemistry and uses principles of molecular aggregation, recognition, transport, and catalysis in this respect to create new structures and functions, such as molecular switches and motors. His group are interested also in the development of new methodology for stereoselective synthesis and recently reported on DNA-based asymmetric catalysis in *Angewandte Chemie*.[3a]

Feringa completed his PhD in 1978 in Groningen under the guidance of H. Wynberg on the topic of asymmetric phenol oxidation and then worked for Shell in Amsterdam and Sittingbourne (UK). In 1984, he returned as a lecturer to the University of Groningen and became full professor there in 1988. In 2003, he was appointed the Jacobus H. van't Hoff Professor of Molecular Sciences. Feringa is a member of the advisory boards of *Advanced Synthesis & Catalysis* and *Chemistry—An Asian Journal* and has written a book on molecular switches.[3b]



B. L. Feringa

[1] a) A. Buryak, K. Severin, *Angew. Chem.* **2005**, *116*, 8149; *Angew. Chem. Int. Ed.* **2005**, *44*, 7935; b) I. Saur, R. Scopelliti, K. Severin, *Chem. Eur. J.* **2006**, *12*, 1058.

[2] a) C. P. Suhrada, C. Selçuki, M. Nendel, C. Cannizzaro, K. N. Houk, P.-J. Rissing, D. Baumann, D. Hasselmann, *Angew. Chem.* **2005**, *117*, 3614; *Angew. Chem. Int. Ed.* **2005**, *44*, 3548; b) J. M. Fukuto, A. S. Dutton, K. N. Houk, *ChemBioChem* **2005**, *6*, 612.

[3] a) G. Roelfes, B. L. Feringa, *Angew. Chem.* **2005**, *117*, 3294; *Angew. Chem. Int. Ed.* **2005**, *44*, 3230; b) B. L. Feringa, *Molecular Switches*, Wiley-VCH, Weinheim, **2001**.

DOI: 10.1002/anie.200600148

WILEY InterScience DISCOVER SOMETHING GREAT
© 2006 Wiley-VCH Verlag GmbH & Co. KGaA, Weinheim

Solid-State NMR Spectroscopy

DOI: 10.1002/anie.200503223

Solid-State NMR Spectroscopy: Molecular Structure and Organization at the Atomic Level

*Marc Baldus**

Keywords:
fibers · NMR spectroscopy · polymorphism · X-ray diffraction · zeolites

Understanding structural organization in densely packed molecular assemblies is a central objective of current structural biology and nanotechnology. Solid-state nuclear magnetic resonance (ssNMR) spectroscopy is a spectroscopic method ideally suited to study structure and dynamics in such systems at the atomic level. For example, ssNMR has been extensively used to understand why compounds of low molecular weight can occur simultaneously in different solid forms. Such polymorphic systems often given rise to distinct solid-state NMR resonance frequencies.[1] In addition, ssNMR is a powerful tool to study ring-current effects and hydrogen-bond interactions that can be of crucial importance in supramolecular structure and organization.[2]

Access to high-field ssNMR instruments, advancements in solid-state NMR methodology, and novel sample preparation and isotope labeling techniques have significantly expanded the use of solid-state NMR spectroscopy. A principal challenge has been to assemble complete three-dimensional molecular structures from ssNMR data using a single sample or a small number of compounds under MAS (magic angle spinning[3]) conditions. These difficulties are intimately related to the dominant influence of nearest-neighbor dipole–dipole interactions that are usually of limited structural relevance and obscure the precise measurement of weak interactions that encode information about the 3D molecular arrangement.

Recently, complementary approaches to circumvent these problems have been proposed. Firstly, the spin network can be diluted by chemical-shift-selective pulse schemes[4] or by tailored chemical synthesis[5,6] (Figure 1a). In addition, the direct[6,7] or indirect[8] detection of proton–proton interactions (Figure 1b) has been shown to deliver structural constraints useful for the determination of complete 3D molecular structures. If the conformation of the monomer is known, these methods can also be used to characterize supramolecular organization.[9]

Ideally, ssNMR methods should provide simultaneously information about the local molecular conformation and the macromolecular arrangement of the system of interest. Levitt and co-workers[10] have now shown that both aspects can be addressed by monitoring dipolar interactions in a naturally diluted spin network (Figure 1c). For this purpose, zeolite frameworks were investigated by two-dimensional (2D) high-resolution ^{29}Si ssNMR spectroscopy. In general, dipolar-coupled spin pairs are conveniently detected in a double-quantum (2Q) filtered correlation experiment

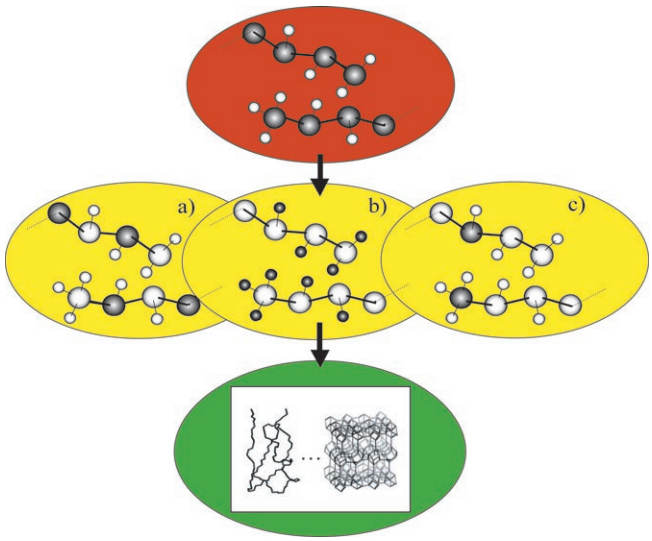


Figure 1. Three approaches to determine molecular structures by high-resolution solid-state NMR spectroscopy ranging from material-science applications to proteins. To overcome strong coupling conditions (top), a dilution of the spin network can be achieved by chemical-shift-selective pulse schemes or by tailored chemical synthesis (a); NMR-active nuclei are in gray. In addition, proton–proton interactions (b) report on 3D molecular structure. Levitt and co-workers[10] recently showed that structure and supramolecular organization can also be inferred from monitoring dipolar interactions in a naturally diluted spin network (c).

[*] Dr. M. Baldus
Max-Planck-Institut für Biophysikalische Chemie
Abteilung für NMR-Basierte Strukturbiologie
37077 Göttingen (Germany)
Fax: (+49) 551-201-2212
E-mail: maba@mpibpc.mpg.de

InterScience
© 2006 Wiley-VCH Verlag GmbH & Co. KGaA, Weinheim

that separates out ssNMR signals of spin pairs found in close spatial proximity.[11] Because of the natural abundance of ^{29}Si of 4.7%, a significant number of isolated ^{29}Si–^{29}Si spin pairs are distributed throughout the zeolite structure. Unlike the case of a densely coupled spin network where the spin dynamics are dominated by the strongest interaction, the intensity of a 2Q signal for a given mixing time directly reports on the distribution of Si–Si distances. While for short mixing times, 2Q signals arise primarily from ^{29}Si–^{29}Si spin pairs across the Si-O-Si linkages, longer distances (up to 8 Å according to Ref. [10]) contribute to 2Q intensities seen for mixing times between 10 and 32 ms. Using a series of two-dimensional double-quantum, single-quantum (2Q,1Q) correlation experiments, Si–Si distance distributions can be mapped out for each (2Q,1Q) correlation.

Firstly, Levitt et al.[10] showed that the ^{29}Si 2Q build-up curves are highly sensitive to the Si–Si internuclear distance and can be faithfully simulated if the supramolecular arrangement is known. On the basis of these findings, they more recently discussed how these correlations can be combined with knowledge about unit-cell parameters and space group to solve structural models that refine successfully against the powder X-ray diffraction (XRD) data (Figure 2a). Briefly, the corresponding algorithm is tailored to find a set of Si atomic coordinates in the asymmetric unit that minimizes the sum of the squares of the residuals between the experimental 2Q curves and the 2Q curves calculated from the set of Si–Si distances for a given arrangement of Si atoms. Candidate structures are built up by using one Si site at a time consistent with the atomic coordinates of the asymmetric unit. Final candidate structures that meet the occupancy and connectivity criteria are then subjected to a least-squares minimization against the set of experimental 2Q curves. This approach was successfully demonstrated for two test cases in which X-ray data were available. ^{29}Si ssNMR spectroscopy on zeolites can be performed under more favorable conditions than spectroscopic studies on other nuclei, for example, with enhanced spectral dispersion and the absence of a strongly coupled proton environment. It seems likely that adaptations of this method to other inorganic materials or isotopically enriched organic molecules are possible.

Understanding macromolecular organization also is of key relevance in the context of amyloid fibrils. These self-assembled molecular aggregates are formed by peptides and proteins with diverse amino acid sequences, and they are involved in protein misfolding dis-

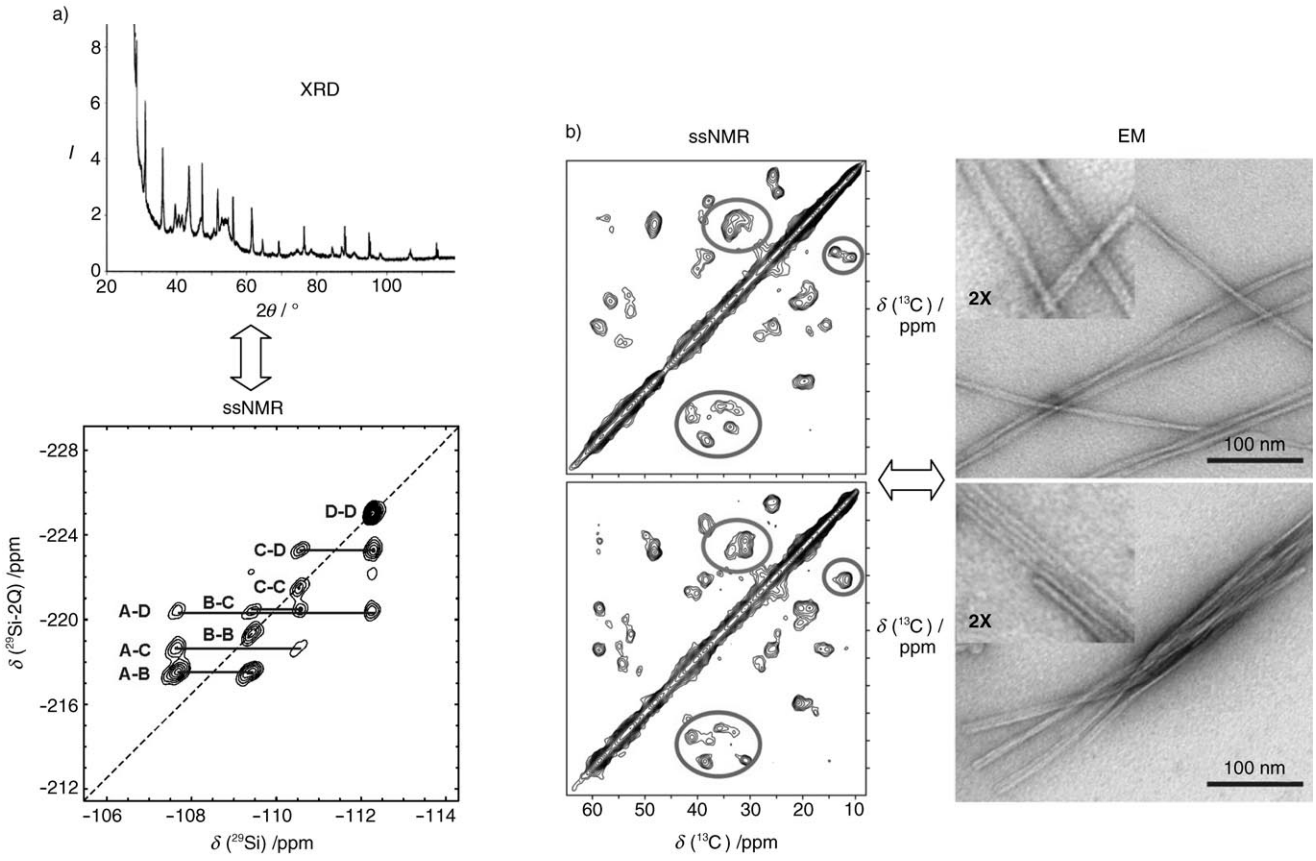


Figure 2. a) Complementary use of ^{29}Si double-quantum ssNMR spectroscopy and X-ray powder diffraction (XRD) data to solve structural models of zeolite frameworks.[10] Letters A–D refer to resonances that are detectable by the ssNMR experiment. b) Combination of high-resolution solid-state NMR spectroscopy and electron microscopy as described by Tycko et al.[12] These studies not only yielded a correlation between distinct fibril morphologies and molecular structures but may also have important implications in understanding the relationship between fibril structure and neurotoxicity. The figure was assembled using files kindly provided by M. H. Levitt (a) and R. Tycko (b).

 © 2006 Wiley-VCH Verlag GmbH & Co. KGaA, Weinheim

orders including Alzheimer's and Parkinson's diseases. Images obtained by transmission electron microscopy (TEM) and atomic force microscopy (AFM) have revealed that amyloid fibrils can exhibit multiple distinct morphologies. Are these morphologies related to different molecular structures? What about the relationship between molecular structure and biological activity?

High-resolution solid-state NMR was recently used to answer these questions in the case of the 40-residue β-amyloid peptide associated with Alzheimer's disease, $A\beta_{1-40}$. Firstly, Petkova et al.[12] prepared residue-specific labeled fibrils by two different growth conditions—so-called quiescent and agitated parent fibrils. These compounds were used as seeds to obtain daughter and granddaughter fibrils under comparable experimental conditions. TEM images of negatively stained $A\beta_{1-40}$ fibrils revealed that only for quiescent fibrils can the predominant morphology be described by a periodic twist and that the morphological difference is preserved in daughter and granddaughter fibrils.

To monitor molecular structure, a series of 2D high-resolution ^{13}C ssNMR spectra of parent, daughter, and granddaughter fibrils with uniform labeling of specific residues were recorded. The patterns of strong one-bond crosspeaks in these spectra are determined by isotropic ^{13}C chemical shifts that report on local structural and conformational environment. Remarkably, the 2D spectra of quiescent and agitated parent fibrils showed pronounced differences in crosspeak patterns (indicated in Figure 2b by circles) that are transmitted to the daughter and granddaughter fibrils. Additional ssNMR data indeed confirmed that different fibril morphologies have different underlying molecular conformation and supramolecular organization. Such molecular-level polymorphism and the correlation between molecular structure and fibril morphology has also been detected for other protein aggregates involved in neurodegenerative diseases.[13]

Both studies discussed here hence underline the complementary use of imaging, diffraction methods, and solid-state NMR techniques to study molecular complexes. Such information may not only help to optimize material-science applications, for example, in the context of self-assembled nanomaterials with novel electronic or optical properties, but also offers novel biological insight: In the case of $A\beta_{1-40}$, different fibril morphologies were shown to exhibit significantly different toxicities in neuronal cell cultures. Further evidence that biological activity may be closely related to the details of the fibril structure comes from a recent structural study on the HET-s prion protein.[14,15] Again, solid-state NMR spectroscopy provided crucial insights into the structure of prion protein aggregates. Mutations within the central β-sheet regions of these fibrils that were determined by high-resolution solid-state NMR spectroscopy seem to correlate with prion infectivity.[15] These examples demonstrate the growing potential of this method to provide an important link between microscopic and crystallographic imaging and molecular functionality.

[1] R. K. Harris in *Encyclopedia of Nuclear Magnetic Resonance* (Eds.: D. M. Grant, R. K. Harris), Wiley, Chichester, **1996**, pp. 3734–3740.

[2] J. S. Waugh, R. W. Fessenden, *J. Am. Chem. Soc.* **1957**, *79*, 846–849; B. Berglund, R. W. Vaughan, *J. Chem. Phys.* **1980**, *73*, 2037–2043; G. A. Jeffrey, Y. Yeon, *Acta Crystallogr. Sect. B* **1986**, *42*, 410–413; R. K. Harris, P. Jackson, L. H. Merwin, B. J. Say, G. Hagele, *J. Chem. Soc. Faraday Trans. 1* **1988**, *84*, 3649–3672.

[3] E. R. Andrew, A. Bradbury, R. G. Eades, *Nature* **1958**, *182*, 1659.

[4] K. Nomura, K. Takegoshi, T. Terao, K. Uchida, M. Kainosho, *J. Am. Chem. Soc.* **1999**, *121*, 4064–4065; C. P. Jaroniec, B. A. Tounge, J. Herzfeld, R. G. Griffin, *J. Am. Chem. Soc.* **2001**, *123*, 3507–3519.

[5] F. Castellani, B. van Rossum, A. Diehl, M. Schubert, K. Rehbein, H. Oschkinat, *Nature* **2002**, *420*, 98–102; S. G. Zech, A. J. Wand, A. E. McDermott, *J. Am. Chem. Soc.* **2005**, *127*, 8618–8626.

[6] B. Reif, C. P. Jaroniec, C. M. Rienstra, M. Hohwy, R. G. Griffin, *J. Magn. Reson.* **2001**, *151*, 320–327; E. K. Paulson, C. R. Morcombe, V. Gaponenko, B. Dancheck, R. A. Byrd, K. W. Zilm, *J. Am. Chem. Soc.* **2003**, *125*, 14222–14223.

[7] S. P. Brown, H. W. Spiess, *Chem. Rev.* **2001**, *101*, 4125–4155; B. Elena, L. Emsley, *J. Am. Chem. Soc.* **2005**, *127*, 9140–9146.

[8] A. Lange, S. Luca, M. Baldus, *J. Am. Chem. Soc.* **2002**, *124*, 9704–9705; A. Lange, S. Becker, K. Seidel, K. Giller, O. Pongs, M. Baldus, *Angew. Chem.* **2005**, *117*, 2125–2129; *Angew. Chem. Int. Ed.* **2005**, *44*, 2089–2092.

[9] V. Percec, M. Glodde, T. K. Bera, Y. Miura, I. Shiyanovskaya, K. D. Singer, V. S. K. Balagurusamy, P. A. Heiney, I. Schnell, A. Rapp, H.-W. Spiess, S. D. Hudson, H. Duan, *Nature* **2002**, *419*, 384–387; I. de Boer, J. Matysik, M. Amakawa, S. Yagai, H. Tamiaki, A. R. Holzwarth, H. J. M. de Groot, *J. Am. Chem. Soc.* **2003**, *125*, 13374–13375; R. Tycko, Y. Ishii, *J. Am. Chem. Soc.* **2003**, *125*, 6606–6607; M. Etzkorn, A. Böckmann, A. Lange, M. Baldus, *J. Am. Chem. Soc.* **2004**, *126*, 14746–14751.

[10] D. H. Brouwer, P. E. Kristiansen, C. A. Fyfe, M. H. Levitt, *J. Am. Chem. Soc.* **2005**, *127*, 542–543; D. H. Brouwer, R. J. Darton, R. E. Morris, M. H. Levitt, *J. Am. Chem. Soc.* **2005**, *127*, 10365–10370.

[11] A. Bax, R. Freeman, S. P. Kempsell, *J. Am. Chem. Soc.* **1980**, *102*, 4849–4851; M. Munowitz, A. Pines, *Adv. Chem. Phys.* **1987**, *66*, 1–152.

[12] A. T. Petkova, R. D. Leapman, Z. Guo, W.-M. Yau, M. P. Mattson, R. Tycko, *Science* **2005**, *307*, 262–265.

[13] P. Chien, J. S. Weissman, A. H. DePace, *Annu. Rev. Biochem.* **2004**, *73*, 617–656; S. B. Prusiner, M. R. Scott, S. J. DeArmond, F. E. Cohen, *Cell* **1998**, *93*, 337–348; H. Heise, W. Hoyer, S. Becker, O. C. Andronesi, D. Riedel, M. Baldus, *Proc. Natl. Acad. Sci. USA* **2005**, *102*, 15871–15876.

[14] A. B. Siemer, C. Ritter, M. Ernst, R. Riek, B. H. Meier, *Angew. Chem.* **2005**, *117*, 2494–2497; *Angew. Chem. Int. Ed.* **2005**, *44*, 2441–2444.

[15] C. Ritter, M.-L. Maddelein, A. B. Siemer, T. Luhrs, M. Ernst, B. H. Meier, S. J. Saupe, R. Riek, *Nature* **2005**, *435*, 844–848.

 © 2006 Wiley-VCH Verlag GmbH & Co. KGaA, Weinheim

DOI: 10.1002/anie.200501476

Sensors

Signal Amplification by Allosteric Catalysis

*Lei Zhu and Eric V. Anslyn**

Keywords:
allosterism · homogeneous catalysis · immunoassay · intrasteric regulation · signal amplification

In this article we unify a series of recent studies on bio- and chemosensors under a single signaling strategy: signal amplification by allosteric catalysis (SAAC). The SAAC strategy mimics biological signal transduction processes, where molecular recognition between an external signal and a protein receptor is allosterically transduced into catalytically amplified chemical information (usually second messengers). Several recent biosensing and chemosensing studies apply this nature-inspired strategy by using engineered allosteric enzymes, ribozymes, or regulatable organic catalysts. The factors pertinent to achieving high sensitivity and specificity in SAAC strategies are analyzed. The authors believe that these early studies from a variety of research groups have opened up a new venue for the development of sensing technologies where molecular recognition and catalysis can be coupled for practical purposes.

1. Introduction

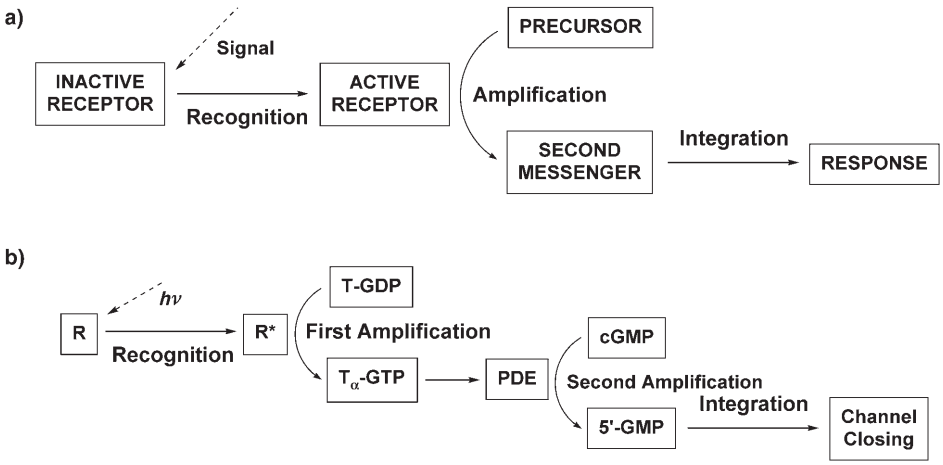
Sensing technologies broadly cover the endeavor of converting unknown information (identity, quantity, chirality, reactivity, etc.) in chemical or biological samples to measurable signals. The signals may be generated by means of a diverse set of transduction techniques, where the unknown information is converted to optical,[1–4] electrical,[5–7] or mechanical[8] readouts. In order to increase the sensitivity of an optical sensing protocol, for instance, classic procedures involve increasing the extinction coefficient (ε) in a colorimetric assay, or increasing the quantum yield (ϕ) in a fluorimetric assay.[9,10]

Alternatively, for devising sensing protocols with high sensitivity and selectivity, nature often serves as the ultimate source of inspiration.[11] Biological systems detect and respond to external signals (e.g. photons) or stimulants (e.g. hormone molecules) through a series of signal transduction events, where the original signal is transduced to amplified chemical information through well-organized catalytic processes. Such processes can be either allosteric, where the reception of the external signal takes place at a remote location from the active site, or intrasteric, where the interaction with an external signal directly alters the structure of the catalytic center.[12] In a typical biological sensing event (Scheme 1a), the external signal (first messenger) is recognized through its interaction with specific membrane-bound receptors. Subsequently, this recognition event is amplified by triggering a cascade of catalytic reactions that generate a great number of second messengers. Finally, the second messengers further communicate with other proteins (often also through catalytic reactions) to complete the integration of the original external signal, where the amplified chemical information is converted to signals (often electric) that are processable by the central nervous system. We refer to this sensing strategy as signal amplification by allosteric catalysis (SAAC).

As a specific example, let us consider the vertebrate visual response. Photons are detected by photoreceptor transmembrane proteins, such as rhodopsin (R) in retinal cells (Scheme 1b).[13] In a stepwise fashion, a photon is first absorbed by the cofactor of rhodopsin, 11-*cis*-retinal. Consequently, 11-*cis*-retinal is isomerized to all-*trans*-retinal. This isomerization event physically dislocates the rhodopsin structure, leading to the allosteric catalytic activation of the intracellular protein transducin (T-GDP), which completes the first stage of signal amplification. The activated transducin (T_α-GTP) turns on the enzyme phosphodiesterase (PDE) by removing inhibitory subunit of the latter. PDE continues the signal-amplification process by hydrolyzing cyclic guanosine monophosphate (cGMP) to create 5′-GMP with an extraordinary turnover (4200 s^{-1}). The hydrolysis of cGMP causes the closure of cation-specific channels gated by cGMP. Membrane hyperpolarization occurs when a sufficient num-

[*] L. Zhu, E. V. Anslyn
Department of Chemistry and Biochemistry
the University of Texas at Austin
Austin, TX 78712 (USA)
Fax: (+1) 512-471-7791
E-mail: anslyn@ccwf.cc.utexas.edu

InterScience
© 2006 Wiley-VCH Verlag GmbH & Co. KGaA, Weinheim



Scheme 1. a) General biological signal-transduction pathway. b) Typical vertebrate visual response. R: rhodopsin; R*: activated rhodopsin; T: transducin; PDE; phosphodiesterase; cGMP: cyclic guanosine monophosphate.

ber of channels are closed. A nerve signal is generated that propagates through the nervous system before eventually being processed and analyzed by the brain. In short, a single photon absorbed by a retinal cell can be amplified to a membrane hyperpolarization of about 1 mV through a cascade of catalytic reactions. This action potential is sensed by the synapses and processed by the nervous system.

Signal amplification using catalysis was first harnessed by biochemists and clinical chemists three decades ago for the detection and measurement of substances in biological fluids.[14] Enzyme immunoassays (EIAs) were developed where antigen or antibody was labeled by an enzyme for catalysis-driven signal-amplification purposes.[15–17] A notable example of EIA that has enjoyed wide clinical success is the enzyme-linked immunosorbent assay (ELISA, Figure 1).[18]

Although not allosteric in nature, ELISA certainly inspired many of the allosteric strategies discussed herein. In ELISA, the analyte (A) is first captured by an analyte-specific antibody (IgG) immobilized on a solid surface. A second enzyme-linked antibody binds with, or is recruited by, the now surface-bound analyte through another epitope. Finally, a chromogenic substrate (S) of the enzyme (E) is added so that the color of the product (CP) from the enzyme-catalyzed reaction, also called the indicator reaction,[19]

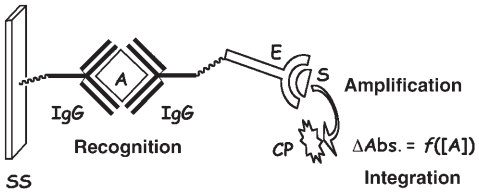


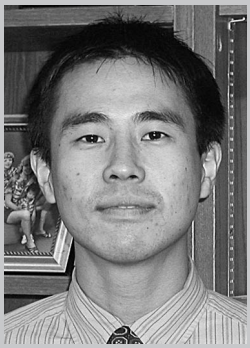
Figure 1. Representation of ELISA. SS: solid support; IgG: analyte-specific antibody; A: analyte; E: enzyme; S: substrate; CP: colorimetric product. The absorbance of CP (ΔAbs) is a function of analyte concentration ([A]).

correlates to the quantity of the analyte. Although the heterogeneous ELISA requires extensive washing steps between each binding event, and only multi-epitope analytes are compatible, it still is frequently employed because of its generality and independent detection and signal-amplification steps (favorable for modular design of sensing assays).

In ELISA, signal-recognition, amplification, and integration steps are separated by extensive washing steps. The stepwise protocol holds certain advantages. For example, the design is modular, since all the steps can be carried out independently. However, the often time-consuming and laborious analytical procedure undermines its scope of



Eric V. Anslyn received his PhD in Chemistry from the California Institute of Technology in 1987 for research with R. Grubbs and conducted postdoctoral research at Columbia University in the group led by R. Breslow. In 1989 he became an Assistant Professor of Chemistry at the University of Texas at Austin, in 1994 he was promoted to Associate Professor with tenure, and in 1997 he became a Full Professor. He has been an Associate Editor of the Journal of the American Chemical Society since 1998. His research encompasses physical organic and bioorganic chemistry. He explores the use of synthetic receptors for catalysis and sensing applications. For his research accomplishments, in 2004 he received the Norman Hackerman Professorship in Chemistry.



Lei Zhu was born in 1975 in Nanjing, China. In 1997 he earned his BSc in Chemistry from Peking University before moving to New York University for graduate studies with James Canary in organic chemistry. After defending his PhD dissertation in January 2003, he joined Eric Anslyn's group at the University of Texas at Austin as a postdoctoral fellow. During the past two years, he has focused on developing sensing technologies based on indicator-displacement assays and catalytic signal-amplification approaches. In August 2005 he started as an Assistant Professor in the Department of Chemistry and Biochemistry at Florida State University.

 © 2006 Wiley-VCH Verlag GmbH & Co. KGaA, Weinheim

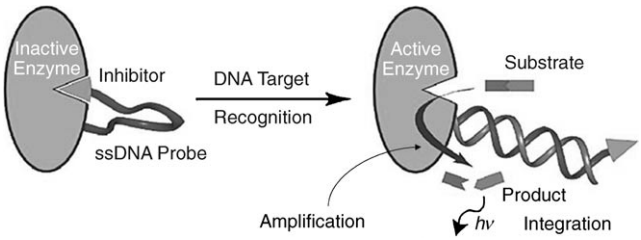
applications.[20] In contrast, the real-time detection scheme used by an organism through a delicate external signal-activated allosteric catalytic reaction cascade, that combines signal recognition, amplification, and integration into one homogenous, autonomous transduction event, is clearly superior technologically. Although homogeneous EIAs that resemble more closely the biological signal transduction processes with allosteric features indeed emerged shortly after the enzyme-immunosensing technology was formulated,[21] it was not until recently that the SAAC strategy was extended beyond the immunochemistry arena. Another boost to the SAAC strategy took place following the invention of the polymerase chain reaction (PCR) technology.[22] PCR and its variants are now the indispensable tools for the amplification and detection of specific DNA sequences.[23,24] Also, the development of EIA variants are still very active, as demonstrated by very recent examples,[25–31] including immuno-PCR, a technology that combines the power of both PCR and EIA.[32,33]

In addition to antibody–antigen interactions, other forms of molecular recognition patterns have been explored to couple with catalytic processes in the development of ultrasensitive detection assays. Several recent bio-[34] and chemosensing examples implementing the SAAC strategy are discussed in the following sections. It is noted that this article focuses on signal-amplification strategies based on analyte-activated, in another words, allosteric catalytic processes. Many other incredibly creative sensing applications where the analytes themselves serve as catalysts for signal-amplification purposes are not discussed.[35–38] These technologies conceptually belong to the traditional kinetic methods of chemical analysis.[19]

2. Signal Amplification by Biocatalysis

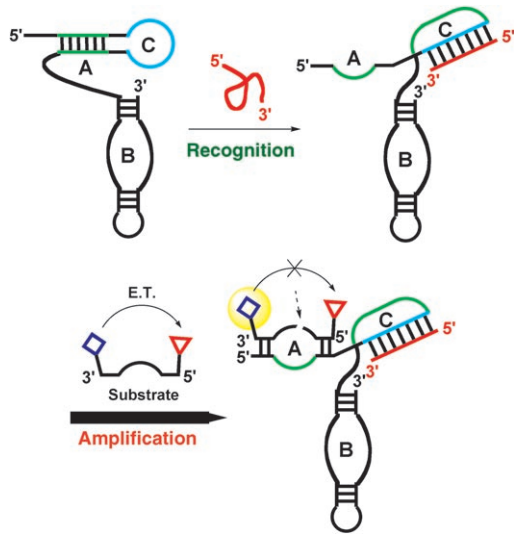
In 2003, Ghadiri's group reported that an intrasterically regulated protease[39] was engineered as a signal-amplification module for sequence-specific DNA detection.[40] A zinc metalloprotease—Cereus neural protease (CNP)—was chosen as the basis for the catalytic signal-amplification step. This enzyme can be effectively inactivated by treatment with a transition-state-analogue inhibitor based on phosphoramidate.[41] The allostery was engineered into this enzyme by the covalent attachment of a single-stranded DNA (ssDNA) probe and phosphoramidate inhibitor conjugate to a CNP mutant (Scheme 2), where the surface-exposed Glu151 residue in the native structure was mutated to a cysteine as a covalent attachment anchor.

When there was no complementary DNA sequence (the target) present, the inhibitor moiety was able to reach the active site of the engineered CNP because of the flexibility of the ssDNA probe.[42] Hence, the enzyme was rendered inactive (Scheme 2). When the DNA target was present and recognized during annealing to the complementary ssDNA probe, formation of a rigid duplex resulted in removal of the phosphoramidate inhibitor moiety from the enzyme active site. The enzyme was consequently "switched on" to convert a fluorogenic peptide substrate[43] to a fluorescent product. At this stage, the detection of a DNA analyte had been transduced into amplified chemical information resulting from catalysis by an allosteric enzyme effected by the analyte. As a result, 100 pM of the target DNA molecules can be readily detected within three minutes. The specificity of this assay was dictated by the sequence complementarity between the target and the probe.



Scheme 2. Detection scheme for sequence-specific DNA molecules utilizing an engineered allosteric protease as the catalytic signal amplification module. Adapted from reference [40].

In addition to allosteric enzymes, allosteric ribozymes ("aptazymes")[44–46] are examples of SAAC strategies in the biosensing arena. For example, an inducible hairpin ribozyme (iHP-let7), which is an allosteric ribozyme that cleaves a specific RNA substrate, was designed for the detection of the microRNA (miRNA) strand let-7 of *Drosophila melanogaster*.[47] In the absence of the miRNA analyte, the substrate recognition domain (A) of the ribozyme was physically blocked by forming a stem–loop structure with the allosteric C domain (Scheme 3). The loop sequence of the C domain was designed as a probe for the target miRNA sequence. Complementary association of the miRNA with the loop sequence (domain C) led to the disruption of the stem structure. Consequently, the A domain was available to recruit the fluorogenic substrates and cleave them with turnover. Because the substrate was modified with a fluo-



Scheme 3. Reaction of the hairpin ribozyme iHP-let7 responsive to miRNA let-7 (the red strand). Blue square: fluorophore; red triangle: quencher; E.T.: energy transfer. Adapted from reference [47].

© 2006 Wiley-VCH Verlag GmbH & Co. KGaA, Weinheim

rophore and a quencher at its 3′- and 5′-ends, respectively, cleavage resulted in fluorescent products as a result of the termination of fluorescence resonance energy transfer (FRET)[48] within the intact substrates. A fluorescent signal was generated whose intensity reflected the concentration of the target miRNA molecules. Because of its catalytic signal amplification capacity, this assay displayed superior sensitivity in detection of specific miRNA sequences over the traditional molecular beacon techniques[49,50] in a head to head competition.

3. Amplification Factor

In devising a SAAC strategy, one must consider several kinetic and thermodynamic issues. First and foremost, the rate of the indicator reaction should be negligible when the enzyme or catalyst is inactive in the absence of the analyte. Providing that, the SAAC strategy consists of two chemical steps: first, the production of an activated catalyst (Enz_A) triggered by an analyte (A) through a competitive equilibrium (Scheme 4a); second, the catalytic indicator reaction that generates an amplified, detectable signal ([P], Scheme 4b). The total catalyst concentration ($[Enz]_T$) should be significantly larger than the likely maximum analyte concentration ($[A]_T$), so that enzyme saturation would not be reached. The rate of establishing the equilibrium between the inactive (Enz_I) and active catalysts (Enz_A) should be much faster than the rate of the indicator reaction (k_{cat}/K_M, K_M is the Michaelis constant), so that the amplified transduced signal ([P]) can be correlated reliably to the analyte concentration ($[A]_T = f([P])$). In another words, the catalytic step should be rate-determining. In an ideal situation, the equilibrium (Scheme 4a) should greatly favor the generation of Enz_A ($k_a \gg k_d$). In such a case, the value of $1/K$ will be low. Because $[Enz_A]$ and $[Enz_I]$ have similar magnitude (by design), the amount of Enz_A ($[Enz_A]$) generated will be very close to the analyte concentration [($[A]_T$, Scheme 4, Eq. (2)]. Therefore, one molecule of the analyte will be converted to one molecule of the active catalyst through a rapid equilibrium. Such considerations are implicitly applied in the previous two biosensing examples, and they are also the recurring features of the sensing assays based on SAAC with supramolecular and organometallic catalysis (see Section 4).

a) $Enz_I + A \underset{k_d}{\overset{k_a}{\rightleftharpoons}} Enz_A \qquad K = k_a/k_d$

$$[Enz_A] = K[Enz_I][A] = K[Enz_I]([A]_T - [Enz_A]) \quad (1)$$

$$([A]_T - [Enz_A]) = ([Enz_A]/[Enz_I])(1/K) \approx 0 \quad (2)$$

b) $S \xrightarrow{Enz_A} P$

$$[P] = v_{max} \cdot \Delta t = k_{cat}[Enz_A]\Delta t \quad (3)$$

Scheme 4. Two chemical steps involved in the catalytic amplification strategy (see text). Enz_I: inactive enzyme; A: analyte; Enz_A: activated enzyme. $[Enz_I] + [Enz_A] = [Enz]_T$ (enzyme total concentration); K (k_a/k_d): equilibrium constant; $[A]_T$: total analyte concentration; S: substrate; P: product; v_{max}: maximum rate; Δt: reaction duration; k_{cat}: catalytic turnover.

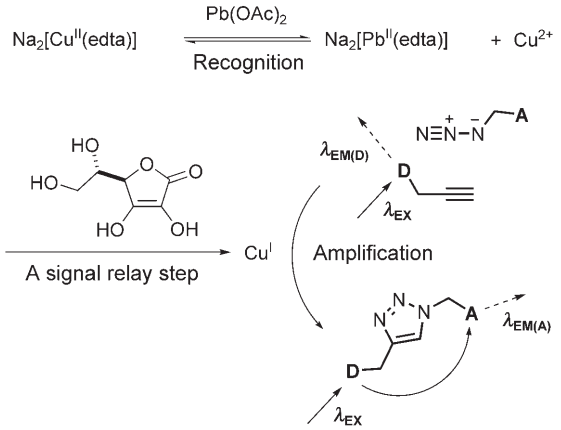
In the catalytic step (Scheme 4b), the amplified signal [P] is proportional to the concentration of activated catalyst ($[Enz_A]$) when the reaction follows Michaelis–Menten kinetics [Scheme 4, Eq. (3)]. When $[Enz_A] \approx [A]_T$, as in an ideal situation, [P] will be proportional to $[A]_T$ by an amplification factor of $k_{cat}\Delta t$—the product of catalytic turnover and reaction time ($[P] \approx k_{cat}\Delta t[A]_T$).

4. Signal Amplification by Supramolecular and Organometallic Catalysis

The development of biosensing protocols using SAAC strategies has been progressing very rapidly. However, they generally involve allosteric enzymes or ribozymes that are tailored for specific analytes. These bioassays have been limited to sensing nucleotide-related molecules such as DNA,[40,51–59] RNA,[47] or ATP.[60] In contrast to enzymatic reactions, supramolecular[61,62] and organometallic catalysis[63] is still an uncharted territory full of opportunities for devising sensing applications with catalytic amplification. A great number of synthetic receptors and ligands have been used to modulate a diverse group of catalytic reactions. The richness of the diversity provides ample opportunities for engineering "allosteric" supramolecular and organometallic catalytic systems[64] that can be used in the same manner as allosteric biocatalysts for sensing purposes. We describe several recent examples in that direction.

The first organometallic catalytic reaction reported for a SAAC purpose is the Cu^I-catalyzed Huisgen cycloaddition between a carbon azide and a terminal alkyne.[65,66] In a popular procedure, the catalytically active Cu^I species is generated in situ by reducing copper(II) sulfate with sodium ascorbate.[66] Therefore, this in situ method offers two ingredients—Cu^{2+} ion and sodium ascorbate—that may be engineered into allosteric handles. In a study from our group,[67] one equivalent of EDTA was introduced into the catalytic system so that it coordinated with Cu^{2+} to prevent it from being reduced to the catalytically active Cu^I state.[68,69] Starting from this inactive catalyst (Scheme 5), the addition of metal ion analytes, such as Pb^{2+}, shifted the equilibrium of $[Cu^{II}(edta)]^{2-}$ so that a certain amount of Cu^{2+} ion was released, and subsequently reduced by ascorbate to the Cu^I state, which was the active catalyst. This step is analogous to the recognition step in a biological signal-transduction event where the interaction between the first messenger (the external signal) and the dormant transmembrane protein is transduced proportionally into an active enzyme (see Scheme 1a). The Cu^I species catalyzed the Huisgen cycloaddition between the carbon azide and alkyne functionalized with fluorophores (anthracene and coumarin in this study) to form a product that can undergo efficient FRET. In this step, the original signal (the Pb^{2+} ion with a certain concentration) was catalytically amplified into another chemical species—the FRET product, which is analogous to a second messenger. The quantity of the FRET product as a function of time was monitored by fluorescence intensity, which can be related to the concentration of the analyte Pb^{2+} ion. This study demonstrated that, in principle, an analyte can be amplified

 © 2006 Wiley-VCH Verlag GmbH & Co. KGaA, Weinheim



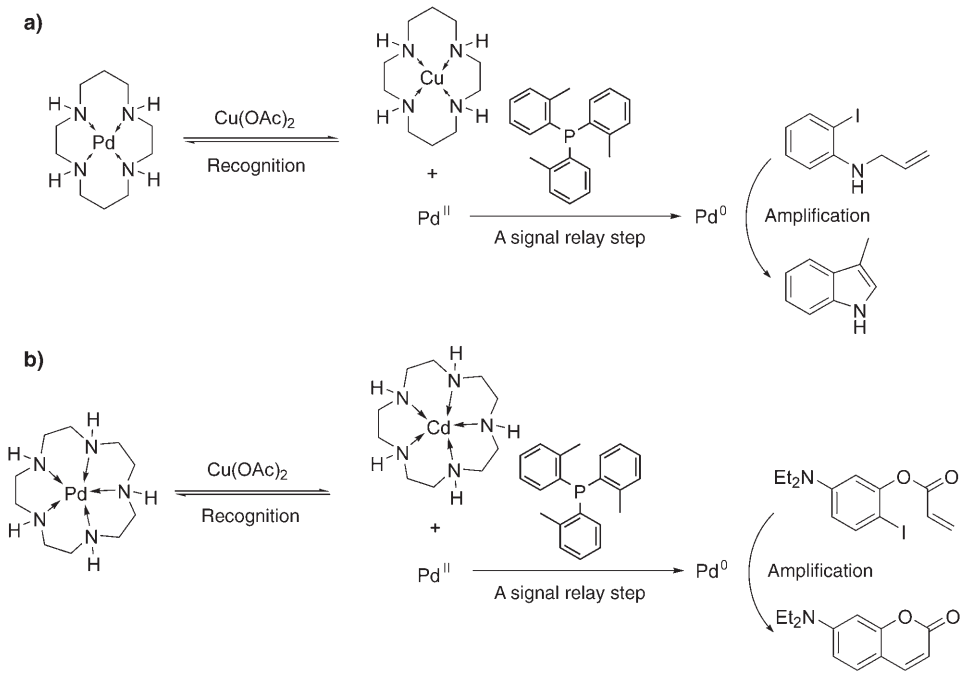
Scheme 5. An "allosteric" Huisgen cycloaddition effected by transition-metal ions. D: energy donor; A: energy acceptor; EX: excitation; EM: emission.

through an organometallic catalytic reaction to a greater number of secondary molecules with an optical readout.

In order to further demonstrate the utility of organometallic SAAC processes, the second study from our group aimed to develop a sensitive and specific assay for Cu^{2+} ions.[70] A Heck reaction to produce 3-methylindole, which is fluorescent, was inactivated by one equivalent of a cyclam ligand (Scheme 6a). When a sample of Cu^{2+} ion was introduced into this inactivated catalytic ensemble, the signal transduction was initiated by the Cu^{2+} ion sequestering the cyclam ligand to proportionally release Pd^{II} into the solution. In practice, the Cu^{2+} analyte was first mixed with the deactivating ligand before one equivalent of Pd^{II} was added to soak up the remaining ligand. The remaining Pd^{II} was rapidly reduced in situ to Pd^0, which turned on the Heck reaction to generate the fluorescent 3-methylindole product with turnover. As a function of time, the fluorescent signal characteristic of the product was read out to reveal the quantity of the Cu^{2+} analyte. Cu^{2+} ions at 30-nM concentration can be detected by this approach. Unlike other examples, the catalytic amplification of 3-methylindole has a linear relationship with the analyte (Cu^{2+}) concentration, as reflected by the linear increase of fluorescence intensity with increasing concentration of Cu^{2+}. Therefore, the turnover of 3-methylindole by each Cu^{2+} ion is independent of the concentration of Cu^{2+}. Furthermore, selectivity for Cu^{2+} ion was programmed by the choice of the cyclam deactivating ligand, which had higher affinity for Cu^{2+} over other metal ions.

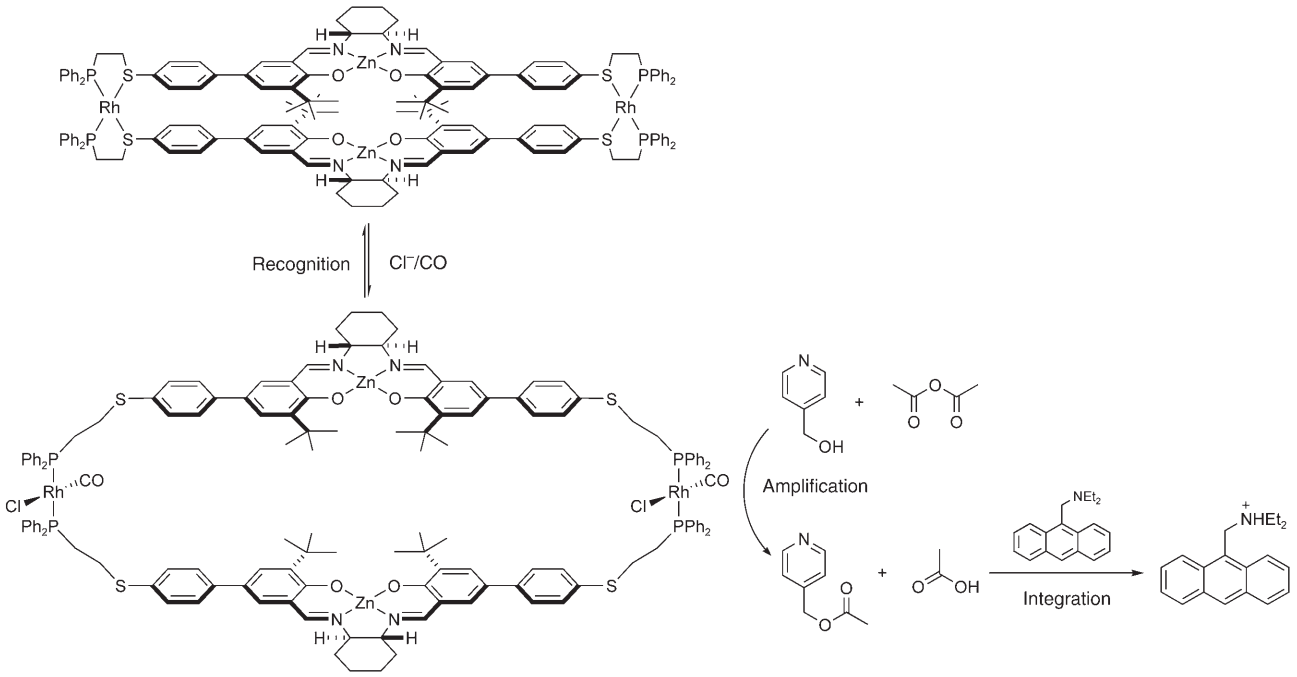
As a direct extension of this approach based on the Heck reaction, we engineered a Cd^{2+} ion-selective assay. Here, allostery was designed into another fluorogenic Heck reaction to afford 7-diethylaminocoumarin (Scheme 6b).[71] Ligand 1,4,7,10,13-pentaazacyclopentadecane, which is Cd^{2+}-selective, was chosen as the deactivating ligand in the catalytic ensemble. The Heck reaction was initiated by the introduction of a sample of Cd^{2+} to sequester a proportional amount of the deactivating ligand, as in the previous example. The fluorescent intensity of the 7-diethylaminocoumarin product after turnover amplification was successfully related to the concentration of the Cd^{2+} in the sample. This assay has higher sensitivity than the previous example because of the more advantageous optical parameters (ε and ϕ) of coumarin and the inherently faster rate of the indicator reaction (k_{cat}) compared to that for the formation of 3-methylindole. However, initiation of the Pd catalyst became rate-determining, thereby lowering the practical aspect of the system.[71]

Mirkin et al. recently converted a supramolecular allosteric catalytic system[72] into a chloride-sensing assay (Scheme 7).[73] The supramolecular allosteric catalyst is a zinc(II) salen dimer constructed by the "weak-link" approach[74] developed in Mirkin's group. In the absence of



Scheme 6. a) An engineered Heck reaction ensemble for the detection of Cu^{2+} ions; b) A different Heck ensemble tailored for Cd^{2+} sensing.

© 2006 Wiley-VCH Verlag GmbH & Co. KGaA, Weinheim



Scheme 7. A supramolecular allosteric catalytic signal amplifier (see text). The Rh—S bonds in the closed structure are the "weak-link" bonds, which are broken to yield the open structure upon treatment with Cl^- and CO.

allosteric effectors CO or Cl^-, the catalyst adopted a closed form which was unable to catalyze the acyl-transfer reaction[75] between pyridyl carbinol and acetic anhydride. The presence of both CO and Cl^- broke the relatively weak thioether–Rh^I bonds so that the catalyst shifted to an open form capable of catalyzing the acyl-transfer reaction in a bimetallic manner to afford 4-acetoxymethylpyridine and acetic acid (signal enhancement). Acetic acid protonated a pH-sensitive fluorophore—diethylaminomethylanthracene—so that the amplified chemical information was integrated into an optical signal readily analyzable by a fluorimeter to reveal the Cl^- concentration (with CO pressure as a fixed parameter). The sensitivity for Cl^- reached submicromolar levels after a running time of six hours.

5. Summary and Outlook

The development of SAAC strategies has created a new chapter in bio-/chemosensing research. It is especially exciting that chemists are just starting to explore the repertoire of catalytic reactions that have been used exclusively for synthetic purposes. The explosive growth of supramolecular[76,77] and organometallic catalyses in the past several decades provides us ample opportunities for converting regulatable catalytic reactions into sensing assays.

As for all sensing applications, sensitivity, specificity, and analyzing time have to be addressed. From our simple theoretical analysis (Scheme 4), the sensitivity and practicality of such assays are controlled primarily by the amplification factor ($k_{cat}\Delta t$) of the indicator reaction. In principle, sensitivity can always be increased by increasing the analyzing time Δt, but lengthy detection is not desirable for a practical sensing application. Clearly one desires rapid reactions with large turnovers. The magnitude of the catalytic turnover is not only dependent on the reaction itself, but also dependent on substrate structures. Therefore, in future studies, specific substrates should be sought for achieving facile indicator reactions. Furthermore, since many detection protocols rely on optical readout, catalytic reactions that afford fluorophores or luminophores with excellent optical parameters (ε and ϕ) are highly desirable.

In summary, molecular recognition studies have yielded a diverse list of specific small-molecule-based ligand–receptor interactions that can be tapped for sensing developments. Furthermore, supramolecular and organometallic catalysis have evolved into mature research areas, and may be considered two of the most important chemical accomplishments in the 20th century (as acknowledged by Nobel Prizes in Chemistry in 1987, 2001, and 2005). It is the perfect time to consolidate these areas to unleash their combined power for the advance of sensing technologies in the new millennium.

We thank Joy Wu and Ron Houk, who are actively creating new SAAC strategies in our group. Our research is supported by the National Institutes of Health (EB-00549-5).

Received: April 28, 2005
Published online: January 24, 2006

[1] A. P. de Silva, H. Q. N. Gunaratne, T. Gunnlaugsson, A. J. M. Huxley, C. P. McCoy, J. T. Rademacher, T. E. Rice, *Chem. Rev.* **1997**, *97*, 1515.
[2] L. Fabbrizzi, M. Licchelli, A. Taglietti, *Dalton Trans.* **2003**, 3471.
[3] T. M. Swager, T.-H. Kim, *Angew. Chem.* **2003**, *115*, 4951; *Angew. Chem. Int. Ed.* **2003**, *42*, 4803.

 © 2006 Wiley-VCH Verlag GmbH & Co. KGaA, Weinheim

[4] L. Zhu, E. V. Anslyn, *J. Am. Chem. Soc.* **2004**, *126*, 3676.
[5] J. Wang, D. Liu, B. Munge, L. Lin, Q. Zhu, *Angew. Chem.* **2004**, *116*, 2210; *Angew. Chem. Int. Ed.* **2004**, *43*, 2158.
[6] C. Fan, K. W. Plaxco, A. J. Heeger, *Proc. Natl. Acad. Sci. USA* **2003**, *100*, 9134.
[7] T. G. Drummond, M. G. Hill, J. K. Barton, *Nat. Biotechnol.* **2003**, *21*, 1192.
[8] J. Fritz, M. K. Baller, H. P. Lang, H. Rothuizen, P. Vettiger, E. Meyer, H.-J. Guntherodt, C. Gerber, J. K. Gimzewski, *Science* **2000**, *288*, 316.
[9] F. J. Green, *The Sigma-Aldrich Handbook of Stains, Dyes and Indicators*, Sigma-Aldrich Corporation, Milwaukee, WI, **1990**.
[10] R. P. Haugland, *Handbook of Fluorescent Probes and Research Products*, 9th ed., Molecular Probes, Eugene, OR, **2002**.
[11] P. Ball, *Nature* **2001**, *409*, 413.
[12] B. Kobe, B. E. Kemp, *Nature* **1999**, *402*, 373.
[13] L. Stryer, *Biochemistry*, 4th ed., W. H. Freeman, New York, **1995**.
[14] W. J. Blaedel, R. C. Boguslaski, *Anal. Chem.* **1978**, *50*, 1026.
[15] G. B. Wisdom, *Clin. Chem.* **1976**, *22*, 1243.
[16] J. P. Gosling, *Clin. Chem.* **1990**, *36*, 1408.
[17] T. Porstmann, S. T. Kiessig, *J. Immunol. Methods* **1992**, *150*, 5.
[18] J. R. Crowther, *ELISA: Theory and Practice*, Humana Press, Totowa, NJ, **1995**.
[19] D. Perez-Bendito, M. Silva, *Kinetic Methods in Analytical Chemistry*, Wiley, New York, **1988**.
[20] G. J. Kost, P. J. Vogelsang, B. L. Reeder, K. L. Omand, C. S. Leach, *Lab. Rob. Autom.* **1989**, *1*, 275. For example, Beckman Coulter now manufactures ELISA automation workstations.
[21] S. H. Jenkins, *J. Immunol. Methods* **1992**, *150*, 91.
[22] R. K. Saiki, S. Scharf, F. Faloona, K. B. Mullis, G. T. Horn, H. A. Erlich, N. Arnheim, *Science* **1985**, *230*, 1350.
[23] B. Schweitzer, S. Kingsmore, *Curr. Opin. Biotechnol.* **2001**, *12*, 21.
[24] M. P. Robertson, A. D. Ellington, *Nat. Biotechnol.* **1999**, *17*, 62.
[25] P. Geymayer, N. Bahr, J.-L. Reymond, *Chem. Eur. J.* **1999**, *5*, 1006.
[26] H. C. Hang, C. Yu, M. R. Pratt, C. R. Bertozzi, *J. Am. Chem. Soc.* **2004**, *126*, 6.
[27] G. MacBeath, D. Hilvert, *J. Am. Chem. Soc.* **1994**, *116*, 6101.
[28] H. Oguri, M. Hirama, T. Tsumuraya, I. Fujii, M. Maruyama, H. Uehara, Y. Nagumo, *J. Am. Chem. Soc.* **2003**, *125*, 7608.
[29] F. Taran, C. Gauchet, B. Mohar, S. Meunier, A. Valleix, P. Y. Renard, C. Créminon, J. Grassi, A. Wagner, C. Mioskowski, *Angew. Chem.* **2002**, *114*, 132; *Angew. Chem. Int. Ed.* **2002**, *41*, 124.
[30] H. Ueda, K. Tsumoto, K. Kubota, E. Suzuki, T. Nagamune, H. Nishimura, P. A. Schueler, G. Winter, I. Kumagai, W. C. Mohoney, *Nat. Biotechnol.* **1996**, *14*, 1714.
[31] Y. Weizmann, F. Patolsky, E. Katz, I. Willner, *J. Am. Chem. Soc.* **2003**, *125*, 3452.
[32] T. Sano, C. L. Smith, C. R. Cantor, *Science* **1992**, *258*, 120.
[33] C. M. Niemeyer, M. Adler, R. Wacker, *Trends Biotechnol.* **2005**, *23*, 208.
[34] A. Villaverde, *FEBS Lett.* **2003**, *554*, 169.
[35] Z. Ma, J.-S. Taylor, *Proc. Natl. Acad. Sci. USA* **2000**, *97*, 11159.
[36] J. Cai, X. Li, X. Yue, J.-S. Taylor, *J. Am. Chem. Soc.* **2004**, *126*, 16324.
[37] H. Abe, E. T. Kool, *J. Am. Chem. Soc.* **2004**, *126*, 13980.
[38] I. Boll, R. Krämer, J. Brunner, A. Mokhir, *J. Am. Chem. Soc.* **2005**, *127*, 7849.
[39] In their report, the authors still used the term "allosteric". In the following sections, we do not attempt to differentiate the terms "allosteric" and "intrasteric" either.
[40] A. Saghatelian, K. M. Guckian, D. A. Thayer, M. R. Ghadiri, *J. Am. Chem. Soc.* **2003**, *125*, 344.
[41] B. W. Matthews, *Acc. Chem. Res.* **1988**, *21*, 333.
[42] F. C. Simmel, W. U. Dittmer, *Small* **2005**, *1*, 284.
[43] E. D. Matayoshi, G. T. Wang, G. A. Krafft, J. Erickson, *Science* **1990**, *247*, 954.
[44] G. A. Soukup, R. R. Breaker, *Trends Biotechnol.* **1999**, *17*, 469.
[45] G. A. Soukup, R. R. Breaker, *Curr. Opin. Struct. Biol.* **2000**, *10*, 318.
[46] R. R. Breaker, *Curr. Opin. Biotechnol.* **2002**, *13*, 31.
[47] J. S. Hartig, I. Grüne, S. H. Najafi-Shoushtari, M. Famulok, *J. Am. Chem. Soc.* **2004**, *126*, 722.
[48] J. R. Lakowicz, *Principles of Fluorescence Spectroscopy*, Plenum, New York, **1999**.
[49] S. Tyagi, F. R. Kramer, *Nat. Biotechnol.* **1996**, *14*, 303.
[50] W. Tan, K. Wang, T. J. Drake, *Curr. Opin. Chem. Biol.* **2004**, *8*, 547.
[51] M. N. Stojanovic, P. de Prada, D. W. Landry, *ChemBioChem* **2001**, *2*, 411.
[52] S. Sando, A. Narita, K. Abe, Y. Aoyama, *J. Am. Chem. Soc.* **2005**, *127*, 5300.
[53] V. Pavlov, B. Shlyahovsky, I. Willner, *J. Am. Chem. Soc.* **2005**, *127*, 6522.
[54] F. Patolsky, E. Katz, I. Willner, *Angew. Chem.* **2002**, *114*, 3548; *Angew. Chem. Int. Ed.* **2002**, *41*, 3398.
[55] F. Patolsky, Y. Weizmann, I. Willner, *J. Am. Chem. Soc.* **2002**, *124*, 770.
[56] S. Sando, T. Sasaki, K. Kanatani, Y. Aoyama, *J. Am. Chem. Soc.* **2003**, *125*, 15720.
[57] P. Simon, C. Dueymes, M. Fontecave, J.-L. Decout, *Angew. Chem.* **2005**, *117*, 2824; *Angew. Chem. Int. Ed.* **2005**, *44*, 2764.
[58] F. Patolsky, R. Gill, Y. Weizmann, T. Mokari, U. Banin, I. Willner, *J. Am. Chem. Soc.* **2003**, *125*, 13918.
[59] Y. Xiao, V. Pavlov, R. Gill, T. Bourenko, I. Willner, *ChemBioChem* **2004**, *5*, 374.
[60] E. J. Cho, L. Yang, M. Levy, A. D. Ellington, *J. Am. Chem. Soc.* **2005**, *127*, 2022.
[61] J. W. Steed, J. L. Atwood, *Supramolecular Chemistry*, Wiley, Ltd., **2000**.
[62] J.-M. Lehn, *Supramolecular Chemistry: Concepts and Perspectives*, VCH, Weinheim, **1995**.
[63] J. P. Collman, L. S. Hegedus, J. R. Norton, R. G. Finke, *Principles and Applications of Organotransition Metal Chemistry*, University Science Books, Mill Valley, CA, **1987**.
[64] L. Kovbasyuk, R. Krämer, *Chem. Rev.* **2004**, *104*, 3161.
[65] C. W. Tornoe, C. Christensen, M. Meldal, *J. Org. Chem.* **2002**, *67*, 3057.
[66] V. V. Rostovtsev, L. G. Green, V. V. Fokin, K. B. Sharpless, *Angew. Chem.* **2002**, *114*, 2708; *Angew. Chem. Int. Ed.* **2002**, *41*, 2596.
[67] L. Zhu, V. M. Lynch, E. V. Anslyn, *Tetrahedron* **2004**, *60*, 7267.
[68] B. Beekman, J. W. Drijfhout, W. Bloemhoff, H. K. Ronday, P. P. Tak, J. M. te Koppele, *FEBS Lett.* **1996**, *390*, 221.
[69] J. Hirata, F. Ariese, C. Gooijer, H. Irth, *Anal. Chim. Acta* **2003**, *478*, 1.
[70] Q. Wu, E. V. Anslyn, *J. Am. Chem. Soc.* **2004**, *126*, 14682.
[71] Q. Wu, E. V. Anslyn, *J. Mater. Chem.* **2005**, *15*, 2815.
[72] N. C. Gianneschi, P. A. Bertin, S. T. Nguyen, C. A. Mirkin, L. N. Zakharov, A. L. Rheingold, *J. Am. Chem. Soc.* **2003**, *125*, 10508.
[73] N. C. Gianneschi, S. T. Nguyen, C. A. Mirkin, *J. Am. Chem. Soc.* **2005**, *127*.
[74] M. S. Khoshbin, M. V. Ovchinnikov, C. A. Mirkin, L. N. Zakharov, A. L. Rheingold, *Inorg. Chem.* **2005**, *44*, 496.
[75] L. G. Mackay, R. S. Wylie, J. K. M. Sanders, *J. Am. Chem. Soc.* **1994**, *116*, 3141.
[76] J. K. M. Sanders, *Chem. Eur. J.* **1998**, *4*, 1378.
[77] R. Cacciapaglia, S. D. Stefano, L. Mandolini, *Acc. Chem. Res.* **2004**, *37*, 113.

 © 2006 Wiley-VCH Verlag GmbH & Co. KGaA, Weinheim

DOI: 10.1002/anie.200502113

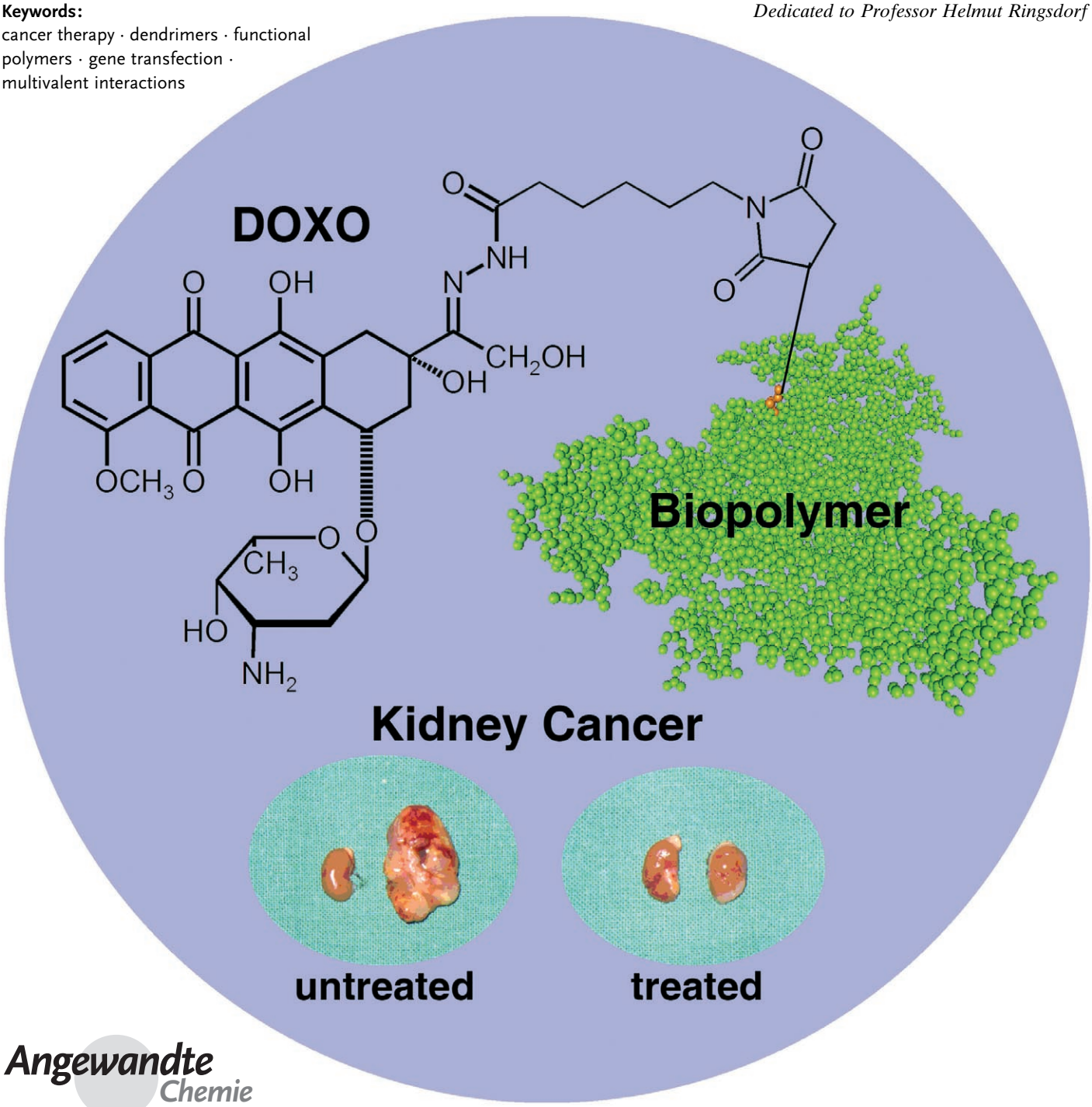
Medicinal Chemistry

Polymer Therapeutics: Concepts and Applications

Rainer Haag and Felix Kratz**

Keywords:
cancer therapy · dendrimers · functional polymers · gene transfection · multivalent interactions

Dedicated to Professor Helmut Ringsdorf



© 2006 Wiley-VCH Verlag GmbH & Co. KGaA, Weinheim

Polymer therapeutics encompass polymer–protein conjugates, drug–polymer conjugates, and supramolecular drug-delivery systems. Numerous polymer–protein conjugates with improved stability and pharmacokinetic properties have been developed, for example, by anchoring enzymes or biologically relevant proteins to polyethylene glycol components (PEGylation). Several polymer–protein conjugates have received market approval, for example the PEGylated form of adenosine deaminase. Coupling low-molecular-weight anticancer drugs to high-molecular-weight polymers through a cleavable linker is an effective method for improving the therapeutic index of clinically established agents, and the first candidates have been evaluated in clinical trials, including, N-(2-hydroxypropyl)methacrylamide conjugates of doxorubicin, camptothecin, paclitaxel, and platinum(II) complexes. Another class of polymer therapeutics are drug-delivery systems based on well-defined multivalent and dendritic polymers. These include polyanionic polymers for the inhibition of virus attachment, polycationic complexes with DNA or RNA (polyplexes), and dendritic core–shell architectures for the encapsulation of drugs. In this Review an overview of polymer therapeutics is presented with a focus on concepts and examples that characterize the salient features of the drug-delivery systems.

From the Contents

1. Introduction 1199
2. Macromolecules as Drug-Delivery Systems: Biological Rationale 1201
3. Approaches and Applications: "In Vivo Veritas" 1203
4. Summary and Conclusions 1213

1. Introduction

Improving the therapeutic index[1] of drugs is a major impetus for innovation in many therapeutic areas such as cancer, inflammatory, and infective diseases. The search for new drug-delivery concepts and new modes of action are the major driving force in polymer therapeutics.[2–5]

Today, the vast majority of clinically used drugs are low-molecular-weight compounds (typically under 500 $g\,mol^{-1}$) that exhibit a short half-life in the blood stream and a high overall clearance rate. These small-molecule drugs typically interact through a multiple but monovalent binding with a given receptor. Furthermore, they diffuse rapidly into healthy tissues and are distributed evenly within the body. As a consequence, relatively small amounts of the drug reach the target site, and therapy is associated with side effects. These disadvantages are especially pronounced with drugs that exhibit a narrow therapeutic index,[1] such as anticancer, antirheumatic, and immunosuppressive agents. Frequent side-effects associated with these drugs are nephrotoxicity, bone-marrow toxicity, neurotoxicity, cardiotoxicity, mucositis, and gastrointestinal toxicity, which are dose-limiting and thus prevent effective treatment.

A number of macromolecular delivery systems are under investigation to circumvent these limitations and improve the potential of the respective drug. Generally, these can be classified as nanoparticulate drug-delivery systems or as drug–polymer conjugates. Particulate delivery systems in which the drugs are physically incorporated into nanoparticles include emulsions, liposomes, and noncovalent polymeric carrier systems. In drug–polymer conjugates, however, a drug is covalently linked to polymers such as proteins, polysaccharides, or synthetic polymers.

The coupling of drugs to macromolecular carriers received an important impetus from 1975 onwards with the development of monoclonal antibodies by Milstein and Köhler,[6] and from Ringsdorf's notion of a general drug-delivery system based on synthetic polymers (Figure 1).[3,7] Initially,

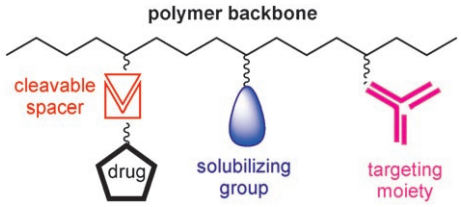


Figure 1. Ringsdorf's model for drug-delivery systems based on synthetic polymers.

research work has focused on realizing drug conjugates with antibodies to selectively target cell-specific antigens or receptors. This propagated the therapeutic concept of drug targeting that was founded on Paul Ehrlich's vision of "the magic bullet" which he proclaimed at the beginning of the last

[*] Prof. Dr. R. Haag
Organic and Macromolecular Chemistry
Department of Chemistry and Biochemistry
Freie Universität Berlin
Takustrasse 3, 14195 Berlin (Germany)
Fax: (+49) 30-838-53357
E-mail: haag@chemie.fu-berlin.de
Dr. F. Kratz
Macromolecular Prodrugs
Tumor Biology Center
Breisacher Strasse 117, 79106 Freiburg (Germany)
Fax: (+49) 761-2062905
E-mail: felix@tumorbio.uni-freiburg.de

© 2006 Wiley-VCH Verlag GmbH & Co. KGaA, Weinheim

century. However, it took many years for the dawning era of "polymer therapeutics" to "kick-off".[4]

In Ringsdorf's original model (Figure 1) a number of drug molecules are bound to a macromolecule through a spacer molecule, which can incorporate a predetermined breaking point to ensure release of the drug at the site of interest. The polymer conjugate can additionally contain moieties, for example, antibodies or sugar moieties, which target disease-related antigens or receptors. In addition, solubilizing groups can be attached to the polymer backbone to modify the bioavailability of the drug–polymer conjugate.

Macromolecules chosen for the preparation of drug–polymer conjugates should ideally be water-soluble, nontoxic, and nonimmunogenic, as well as degraded and/or eliminated from the organism.[8] Finally, the macromolecular carrier should exhibit suitable functional groups for attaching the respective drug or spacer. Initially, *N*-(2-hydroxypropyl)methacrylamide (HPMA) copolymers were intensively studied as linear polymers for therapeutic applications according to the Ringsdorf model.[9–11] However, a spectrum of other synthetic polymers with structural and architectural variations, including A) monofunctional linear, B) polyfunctional linear, C) starlike, and D) dendritic architectures are being investigated today (Figure 2).

Conjugates of drugs and polymers as well as other polymeric carrier systems have collectively been termed polymer therapeutics,[4,5] which primarily encompass polymer–protein conjugates, drug–polymer conjugates, and more recently supramolecular drug-delivery systems as well as other defined nanosized systems.[12–14] Anchoring of enzymes

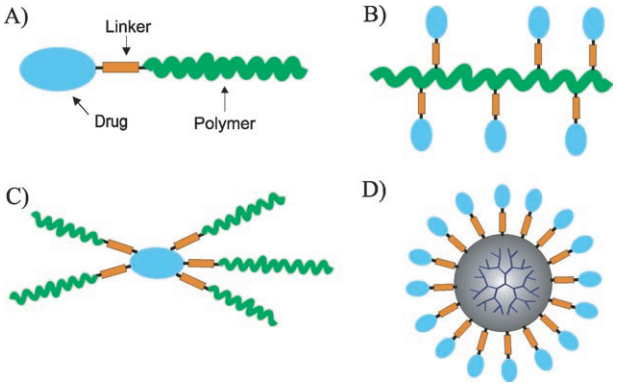


Figure 2. Selected structural and architectural types of drug–polymer conjugates.

or biological response modifiers to polyethylene glycol components (PEGylation) has led to numerous polymer–protein conjugates with improved stability and pharmacokinetic properties. Several polymer–protein conjugates have received market approval (Table 1).[4] The coupling of low-molecular-weight anticancer drugs to polymers through a cleavable linker has been an effective method for improving the therapeutic index of clinically established agents, and the first candidates of anticancer drug–polymer conjugates are being evaluated in clinical trials.

The advance of well-defined polyvalent and dendritic polymers[15] has paved the way for designing tailor-made systems with self-assembling properties which are also classified as polymer therapeutics. These include: a) polyan-

Table 1: Polymer–protein conjugates with market approval.

Trade name	Protein	Polymer	Indication	Marketed
adagen	adenosine deaminase	5 kDa PEG	severe combined immunodeficiency disease	Enzon
oncaspar	asparaginase	5 kDa PEG	acute lymphatic leukemia	Enzon
pegvisomant	GH antagonist	5 kDa PEG	excessive growth (acromegaly)	Pfizer
PEG-intron	interferon α2b	12 kDa PEG	hepatitis C	Schering-Plough
pegasys	interferon α2a	40 kDa PEG	hepatitis C	Roche
neulasta	granulocyte colony stimulating factor	20 kDa PEG	neutropenia	Amgen
SMANCS/ lipiodol	neocarzinostatin	copolymer of styrene maleic acid	hepatocellular cancer	Yamanouchi Pharmaceutical Company



Rainer Haag obtained his PhD with A. de Meijere at the University of Göttingen in 1995. After postdoctoral work with S. V. Ley, University of Cambridge (UK), and G. M. Whitesides, Harvard University, Cambridge (USA), he completed his habilitation in Macromolecular and Organic Chemistry at the University of Freiburg in 2002. He was Associate Professor at the University of Dortmund and then took the Chair of Organic and Macromolecular Chemistry at the Freie Universität Berlin in 2004. His research interests are dendritic polymers as high-loading supports for synthesis and catalysis, macromolecular nanotransporters for DNA and drugs, as well as protein-resistant surfaces.



Felix Kratz graduated in Chemistry from the University of Heidelberg in 1991. He then carried out postdoctoral research at the Bioinorganic Institute of the University of Florence (Italy) and developed tumor-specific carrier systems with ruthenium(III) complexes. Since 1994 he has been Head of Macromolecular Prodrugs at the Tumor Biology Center in Freiburg, Germany, where he is now in charge of organizing and managing translational research from the laboratory to the clinic. His research areas are drug targeting, drug-delivery systems in oncology, prodrugs, receptor targeting, and bioconjugate chemistry.

 © 2006 Wiley-VCH Verlag GmbH & Co. KGaA, Weinheim

ionic polymers for the inhibition of virus attachment and as heparin analogues; b) polycationic complexes with DNA or RNA (polyplexes); and c) polymer micelles with covalently bound drugs as well as dendritic core–shell architectures for the encapsulation of drugs. In this Review, we present an overview of polymer therapeutics with a focus on concepts and pertinent examples that characterize the salient features of the respective drug-delivery system. Further examples can be found in review articles that have appeared over the past decade on this topic.[5,8,11,16–26] Not included are polymers for galenic applications and slow-release systems based on bulk degradation of the polymer matrix.[27]

2. Macromolecules as Drug-Delivery Systems: Biological Rationale

2.1. Passive Drug Targeting and Specific Tissue Targeting: The EPR Effect

It has long been known that biopolymers play an essential role as free and membrane-bound "therapeutics". Therefore, it is surprising that synthetic polymers were originally only discussed as plasma expanders, for example, pervirlon or poly(vinyl pyrrolidone) during the Second World War.[28]

Passive accumulation of macromolecules and other nanoparticles in solid tumors is a phenomenon which was probably overlooked for several years as a potential biological target for tumor-selective drug delivery. The rationale for using macromolecules as efficient carriers for the delivery of antitumor agents, even if they are not targeted towards an antigen or receptor on the surface of the tumor cell, is based on the pioneering work of Maeda and co-workers[29,30] as well as Jain et al.[31,32] The results of these studies gave detailed insight into the pathophysiology of tumor tissue that is characteristic of angiogenesis, hypervasculature, a defective vascular architecture, and an impaired lymphatic drainage.

Differences in the biochemical and physiological characteristics of healthy and malignant tissue are responsible for the passive accumulation of macromolecules in tumors. This feature has been termed "enhanced permeability and retention" (EPR effect)[30,33] and is depicted schematically in Figure 3.

In general, low-molecular-weight compounds diffuse into normal and tumor tissue through the endothelia cell layer of blood capillaries. Macromolecules, however, cannot pass through the capillary walls of normal tissue. The entry of macromolecules into tumor tissue takes place in the capillaries where blood flow is diminished and nutrients transfer into the tissue. In contrast to the blood capillaries in most normal tissues, the endothelial layer of the capillaries in the tumor tissue is fenestrated and leaky so that macromolecules and other nanoparticles reach the malignant tissue. Tumor tissue generally has a defective lymphatic drainage system with the result that macromolecules are retained and can subsequently accumulate in solid tumors.

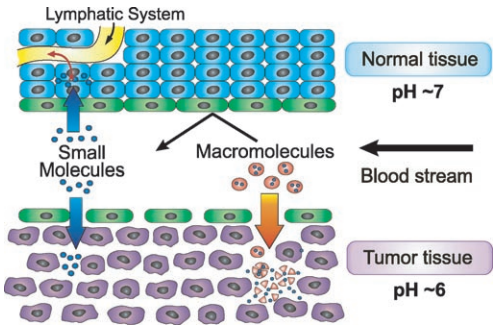


Figure 3. Schematic representation of the anatomical and physiological characteristics of normal and tumor tissue with respect to the vascular permeability and retention of small and large molecules (EPR effect).

The size of the macromolecule is a crucial factor with respect to uptake by the tumor. The EPR effect is observed for macromolecules with molecular weights greater than 20 kDa. Therfore, there is a correlation between the half-life in plasma, the renal clearance, and the accumulation in the tumor of the respective macromolecule. In recent years, most of the research groups involved in the development of drug–polymer conjugates selected macromolecular carriers with molecular weights in the range of 20 to 200 kDa. It is generally assumed that in a healthy organism the renal threshold is in the range of 30–50 kDa to avoid leakage of body proteins into the bladder.[34]

A number of preclinical studies have demonstrated that the physiochemical nature of the biopolymer or synthetic polymer has a strong influence on its pharmacokinetic profile and degree of accumulation in the tumor.[35,36] The biodistribution and uptake by the tumor of the polymer in question is essentially dictated by its molecular weight, charge, conformation, hydrophobicity, and immunogenicity. Preclinical studies have shown that the size of the tumor influences the uptake rate of the polymer in solid tumors: Smaller tumor nodules accumulate larger amounts of the polymer than larger nodules.[37] This observation points to the possibility that polymeric imaging agents could help to detect small tumor nodules.

The influence of the different factors on the EPR-mediated uptake of the polymer in solid tumors is not yet completely understood. As a general rule, a polymer with a molecular weight above the renal threshold (ca. 30 kDa) as well as a neutral charge ensures a long half-life in plasma. This prolonged plasma residence time is an important prerequisite for a significant accumulation of the circulating polymer in the tumor.[35,36] A similar uptake mechanism is also apparent in other leaky tissues, such as inflamed or infected tissue, and can result in an enhanced uptake of macromolecules at the respective sites.[35,36]

In contrast to this simple passive targeting by size, cell-specific targeting using antibodies, oligosaccharides, and peptides has also been addressed by many research groups.[5,38]

2.2. Cellular Uptake of Polymers, Site-Specific Drug Release, and Implications for Drug Design

In general, macromolecules are taken up by the cell through receptor-mediated endocytosis, adsorptive endocytosis, or fluid-phase endocytosis (Figure 4).[39] During endo-

© 2006 Wiley-VCH Verlag GmbH & Co. KGaA, Weinheim

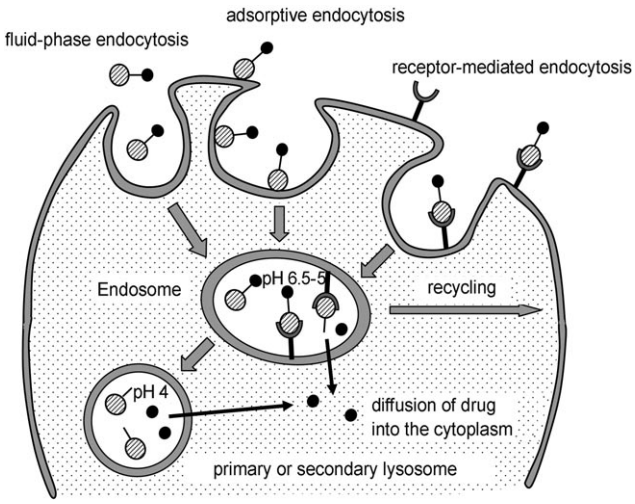


Figure 4. Endocytotic pathway for the cellular uptake of macromolecules and nanocarriers for drug delivery.

cytosis a significant drop in the pH value takes place from the physiological value (7.2–7.4) in the extracellular space to pH 6.5–5.0 in the endosomes and to around pH 4.0 in primary and secondary lysosomes. A great number of lysosomal enzymes become active in the acidic environment of these vesicles, for example, phosphatases, nucleases, proteases, esterases, and lipases.

Drug–polymer conjugates or complexes should be sufficiently stable in the blood stream prior to the drug being liberated at the site of action. In principle, the polymer-bound drug can be released in the body by unspecific hydrolysis by enzymes, by reduction, or in a pH-dependent manner. In an ideal case, cleavage of the drug–polymer conjugate at the tumor site is triggered by a biochemical or physiological property unique for the individual tumor. Although such truly tumor-specific features are rarely encountered, the overexpression of certain enzymes, an acidic and hypoxic environment in solid tumors, as well as the endocytotic pathway of macromolecules offer several options for designing drug–polymer conjugates that are preferentially cleaved within the tumor.

The design of drug–polymer conjugates initially focused on incorporating enzymatically cleavable bonds that allow the prodrug to be cleaved intracellularly after cellular uptake. More recently, a cleavage mechanism involving triggering events that lead to a release cascade have been presented.[40,41] The advantage of this approach is a high local drug concentration with a potential increase in efficacy.[42]

Both the low pH values in endosomes and lysosomes as well as the presence of lysosomal enzymes are therefore intracellular properties which have been exploited for releasing the polymer-bound drug specifically in tumor cells. Furthermore, the microenvironment of tumors has been reported to be slightly acidic in animal models and human patients: Non-invasive techniques have demonstrated that the pH value in tumor tissue is often 0.5–1.0 units lower than in normal tissue (see Figure 3).[43] This difference could contribute to the extracellular release of drugs bound to polymers through acid-sensitive linkers, especially if the drug is trapped by the tumor for longer periods of time.

Finally, drug–polymer conjugates can also be designed to slowly release the polymer-bound drug through hydrolysis under physiological conditions, as exemplified by conjugates of drugs and polyethylene glycol.[44]

2.3. Polymer Conjugates for Protein Stabilization

Coupling polymers to therapeutically relevant proteins imparts several potential advantages: Conjugation can reduce the immunogenicity of the native protein, increase its stability, and prolong its biological half-life, thus resulting in less-frequent administration to the patient. Poly(ethylene glycol) (PEG) has mainly been the polymer of choice for preparing polymer–protein conjugates. In this "PEGylation" technology, linear or branched PEG derivatives are coupled to the surface of the protein.[34,45] The companies Shearwater Polymers and Enzon initiated and refined this technology, which has resulted in the development of clinically as well as commercially successful products such as PEGylated asparaginase, PEGylated adenosine deaminase, PEGylated interferons, and PEGylated granulocyte colony stimulating factor (see Section 3.1).[45–48]

2.4. Multivalent Interactions

In recent years, the development of multivalent drugs which are bridged by polymeric spacers has advanced dramatically (see Section 3.5).[49,50] The great potential of these systems is the high entropic gain in the formation of the multivalent complex (Figure 5). For example, the binding

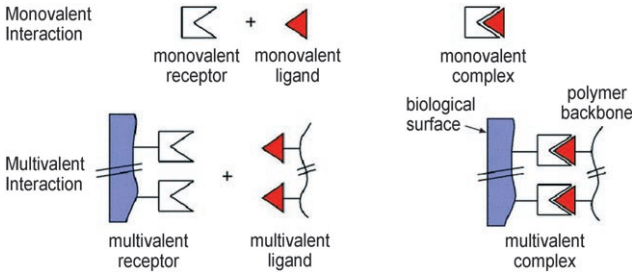


Figure 5. Comparison of monovalent and multivalent interactions.

constants of bivalent interactions can be a factor of 1000 higher than monovalent binding, and for tri- and pentavalent interactions values up to 10^8 have been reported. This possibility allows for completely new ways to develop drugs; however, only a few efforts have been made so far to develop the first candidates for clinical trials.

A challenging approach to the application of multivalent interactions is the mimicry of functional biomacromolecules with therapeutic relevance. Several attempts have been made to mimic specific proteins (e.g., histones) or polysaccharides (e.g., heparin; see Section 3.5). In these cases, mimicry is

 © 2006 Wiley-VCH Verlag GmbH & Co. KGaA, Weinheim

mostly based on the surface charge of the polymer molecules (Figure 6). Applications range from DNA-transfection agents (polycationic systems) to anticoagulating, anti-inflammatory, and anti-HIV drugs (polyanionic systems).

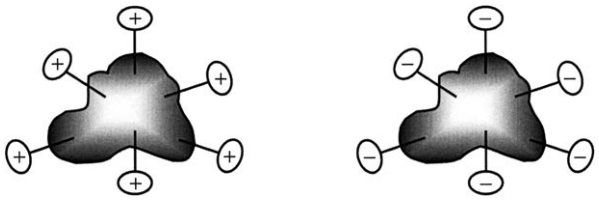


Figure 6. Mimicry of the surface charge of polyionic biomacromolecules and synthetic polymers as an approach for the development for polymer therapeutics.

3. Approaches and Applications: "In Vivo Veritas"

In this section we describe different polymer therapeutics in greater depth, with a focus on their preclinical and clinical potential.

3.1. Polymer Conjugates of Therapeutically Relevant Proteins

Therapeutically relevant proteins such as antibodies, cytokines, growth factors, and enzymes are playing an increasing role in the treatment of viral, malignant, and autoimmune diseases. The development and successful application of therapeutic proteins, however, is often impeded by several difficulties, for example, insufficient stability and shelf-life, costly production, immunogenic and allergic potential, as well as poor bioavailability and sensitivity towards proteases.

An elegant method to overcome most of these difficulties is the attachment of polyethylene glycol chains onto the surface of the protein. PEGylation of the native protein increases its molecular weight and as a result prolongs the half-life in vivo, which in turn allows less frequent administration of the therapeutic protein. In addition, the PEG chains mask the protein, which renders it more resistant to proteases and less immunogenic.

A consequence of the PEGylation of proteins is generally a loss of the protein's biological activity. This loss, however, is outweighed by a substantial increase in the biological half-life of the PEGylated protein.[34]

In the past few years two PEGylation processes have emerged: In the first method one or more linear PEG chains with a molecular weight between 5 and 12 kDa are bound to the surface of the protein (first-generation PEGylated proteins). In the second method a single branched or a multibranched PEG chain is attached to a specific amino acid on the protein's surface (second-generation PEGylated proteins). In most cases activated PEG-carboxylic acids, for example, activated with *N*-hydroxysuccinimide, are bound to the ε-amino groups of lysine residues or the N-terminal amino group, but other chemical modifications with aldehyde, tresylate, or maleimide derivatives of PEG are also used.

The major drawback of first-generation PEGylated proteins was the heterogeneous nature of the pharmaceutical product, since in most cases multiple linear PEGs were attached to the protein. Despite this, several first-generation candidates received regulatory approval. The most prominent examples are adagen (PEGylated adenosine deaminase) for the treatment of severe combined immunodeficiency disease, oncaspar (PEGylated asparaginase) for the treatment of acute leukemia, and PEG-intron (PEGylated interferon α2b) for treating hepatitis C (Table 1).

Second-generation PEGylated proteins, in which a branched or linear PEG chain is attached to a site-specific amino acid on the protein, have the advantage in that they represent defined products with minimal alteration of the three-dimensional conformation of the protein. In 2002, granulocyte colony stimulating factor (G-CSF) PEGylated with a 20-kDa linear PEG chain (neulasta) was the first second-generation PEGylated system to receive market approval (Table 1). Neulasta stimulates the production of white blood cells following bone-marrow depletion in the course of cancer chemotherapy. This treatment is more convenient than with the native protein, human recombinant G-CSF (neupogen); only one injection of neulasta is required every three weeks compared to daily injections of neupogen over two weeks.[51]

Interferon α2a PEGylated with a 40-kDa branched PEG chain (pegasys) is a second-generation PEGylated system that has received market approval, and is a competitor of the first-generation conjugate PEG-intron (Table 1). Both PEG-intron and pegasys have shown significantly better efficacy in the treatment of hepatitis C than the native interferon when combined with the antiviral agent ribavarin.[46,52]

Other examples of PEGylated proteins on the market or in advanced clinical trials are pegvisomant, a PEGylated form of the human growth hormone,[53] and a PEGylated receptor and antibody fragment directed against tumor necrosis factor-α, a major mediator of inflammation (PEG-TNF-RI and PEG-anti-TNF Fab, respectively).[54,55]

Besides PEGylated proteins, one polymer–protein conjugate consisting of the anticancer protein neocarcinostatin and a synthetic copolymer of styrene and a maleic acid anhydride drug (Table 1) has been approved for the treatment of hepatocellular cancer in Japan.[35]

3.2. Drug–Polymer Conjugates with Cleavable Linkers

The development of drug–polymer conjugates is a promising strategy to improve the therapeutic index[1] of toxic drugs, especially in the field of cancer chemotherapy. Several drug–polymer conjugates are being investigated in phase I–III studies at present (Table 2).

Although great efforts are being made to develop novel polymeric carriers, synthetic polymers that have been used in clinically evaluated drug conjugates have been mainly restricted to HPMA, PEG, and poly(glutamic acid) (PG). In addition, albumin, a biopolymer carrier, is being evaluated as a drug-delivery system in anticancer therapy. The cytostatic agents that have been primarily selected for preparing drug–

 © 2006 Wiley-VCH Verlag GmbH & Co. KGaA, Weinheim

Table 2: Drug–polymer conjugates in clinical trials.

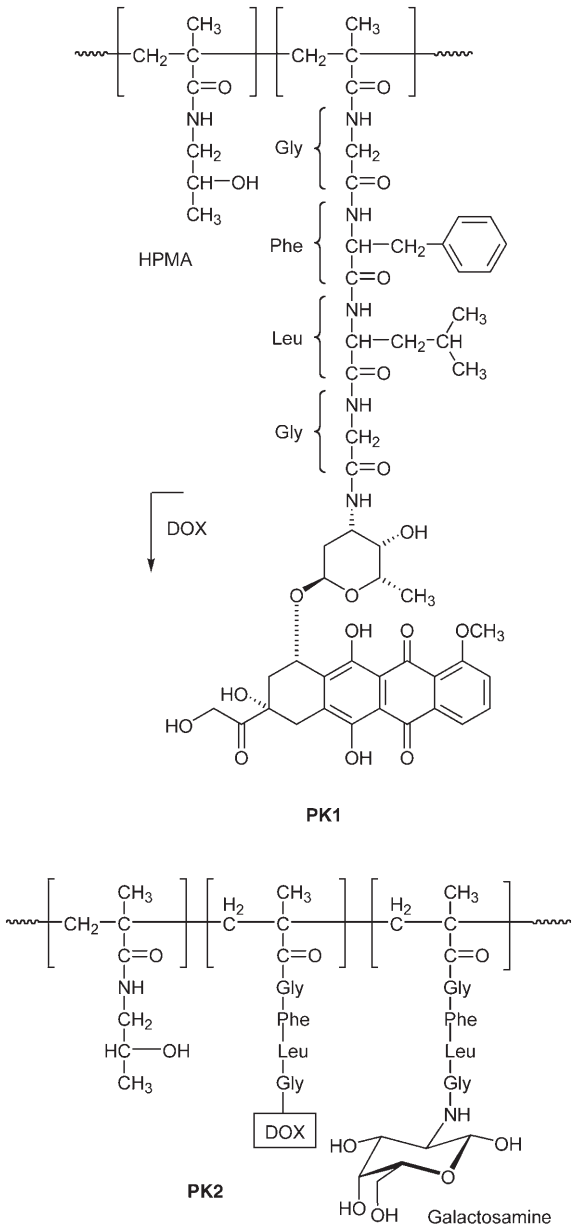
Compound	Spacer	Molecular weight [kDa]	Status of development
PK1, doxorubicin–(HPMA copolymer)	Gly-Phe-Leu-Gly	30	phase II
PK2, galactosaminated doxorubicin–(HPMA-copolymer)	Gly-Phe-Leu-Gly	30	phase I discontinued
PNU-166945, taxol–(HPMA copolymer)	ester	40	phase I completed
MAG-CPT, camptothecin–(HPMA copolymer)	Gly-6-aminohexanoyl-Gly	30	phase I completed
AP5280, diammineplatinum(II)–(HPMA copolymer)	Gly-Phe-Leu-Gly	25	phase I completed
AP5286, diaminocyclohexaneplatinum(II)–(HPMA copolymer)	Gly-Phe-Leu-Gly	25	phase I
prothecan, camptothecin–PEG conjugate	alanine ester	40	phase II
CT-2103, taxol–polyglutamate conjugate	ester	40	phase II/III
CT-2106, camptothecin–polyglutamate conjugate	Gly-ester	50	phase I
MTX-HSA, methotrexate–albumin conjugate	–	67	phase II
DOXO-EMCH, 6-maleinimodcaproyl hydrazone derivative of doxorubicin	acid-sensitive hydrazone	67 (albumin-bound prodrug)	phase I completed

polymer conjugates are doxorubicin, camptothecin, taxol, methotrexate, and platinum complexes.

Several drug–polymer conjugates with HPMA copolymers have been studied clinically. A doxorubicin–(HPMA copolymer) conjugate PK1 was the first drug–polymer conjugate to enter clinical trials.[56] PK1 has a molecular weight of approximately 28 kDa and contains doxorubicin (about 8.5 wt%) linked through its amino sugar to the HPMA copolymer by a tetrapeptide spacer, Gly-Phe-Leu-Gly (Scheme 1). This peptide sequence is cleaved by lysosomal enzymes of tumor cells. Preclinical studies showed that the level of lysosomal enzyme expression in solid tumors, as well as their vascular permeability for macromolecules, correlated with the activity of this conjugate in vivo.[57]

A phase I study revealed that the maximum tolerated dose (MTD) was 320 mg m^{-2} doxorubicin equivalents, which is a fivefold increase relative to the standard dose for doxorubicin.[56] The dose-limiting factors observed in this study were bone-marrow toxicity and mucositis. Other side effects, for example, nausea and diarrhea, were moderate (CTC Grade 1; CTC = common toxicity criteria). A noteworthy finding of this study was that no acute cardiotoxicity was observed even at these high doses. Two partial remissions and two minor responses were seen in four patients with lung, breast, and colorectal cancer. The recommended dose for phase II studies was 280 mg m^{-2} every three weeks. Phase II trials in breast, non-small-cell lung and colon cancer were initiated at the end of 1999; an interim report indicated positive responses in a few cases.[58]

PK2 is a related compound to PK1, but incorporates an additional targeting ligand, namely, a galactosamine group that was designed to be taken up by the asialoglycoprotein receptor of liver tumor cells (Scheme 1). In a phase I study, 31 patients with primary or metastatic liver cancer were evaluated.[59] The MTD of PK2 was 160 mg m^{-2} doxorubicin equivalents which is approximately half the MTD value of PK1, although the molecular weight and the loading ratio are very similar in both conjugates. Dose-limiting toxicity was associated with severe fatigue, neutropenia, and mucositis; a dose of 120 mg m^{-2} doxorubicin equivalents was recommended for phase II studies. Two partial remissions and one minor response were achieved in this study.

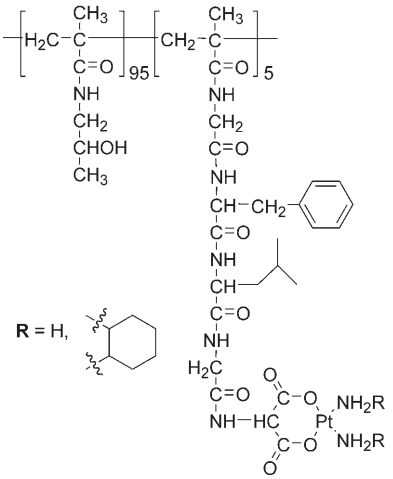


Scheme 1. Chemical structure of the first clinically tested polymeric antitumor therapeutics: PK1 (top) and PK2 (bottom).

 © 2006 Wiley-VCH Verlag GmbH & Co. KGaA, Weinheim

Two other HPMA conjugates with either taxol or camptothecin, respectively, entered phase I trials (Table 2). PNU-166945 is a water-soluble conjugate in which taxol at its 2-OH position is bound through a Gly-Phe-Leu-Gly linker to the polymer backbone. The camptothecin–(HPMA copolymer) conjugate consists of camptothecin linked at its 20-OH group to the HPMA copolymer through a Gly-6-aminohexanoyl-Gly spacer. Although preclinical results in tumor-bearing mice have been promising, both conjugates have had limited success in early clinical trails because of their toxicity profile.[60,61]

Two drug–HPMA conjugates that have only recently entered phase I studies are AP5280 and AP5286, in which a diamine- or a diaminocyclohexaneplatinum(II) moiety is bound to a dicarboxylate ligand that is coupled to the polymer through the tetrapeptide spacer Gly-Phe-Leu-Gly. This cathepsin B sensitive linker is also present in PK1, PK2, and PNU-166945 (Scheme 2).[62,63] Interestingly, during the

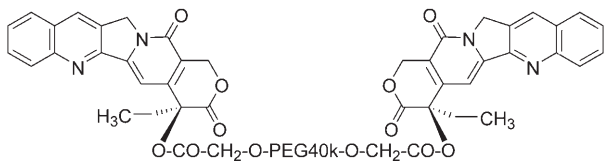


Scheme 2. HPMA–drug conjugates AP5280 and AP5286 with a diamine- or a diaminocyclohexaneplatinum(II) group.

synthesis the platinum(II) group initially forms an O,O chelate which rearranges to the more stable N,O chelate. Preclinical assessment showed a high antitumor efficacy and a significantly increased MTD value for AP5280 compared to the clinical standards (cis- and carboplatin). In a phase I study the dose-limiting toxicity for AP5280 was vomiting (grade 3) at 4500 mg Pt m^{-2} (platinum equivalents); the dose recommendation for a phase II study was 3300 mg(Pt) m^{-2}. Five patients had a stabilization of their disease.[64] Detailed reviews on the clinical studies of drug–polymer conjugates with HPMA copolymer have recently been published by Duncan and Rihova et al.[9,11]

Another approach to doxorubicin–polylactide conjugates was recently reported by Sengupta et al.[65] These conjugates have been embedded into a biodegradable polylactide nanoparticle (ca. 150 nm) to achieve a better tumor selectivity through the EPR effect.

Prothecan, a camptothecin conjugate, is the first drug conjugate with polyethylene glycol that has been clinically assessed (Scheme 3). Conjugating the 20-OH position of

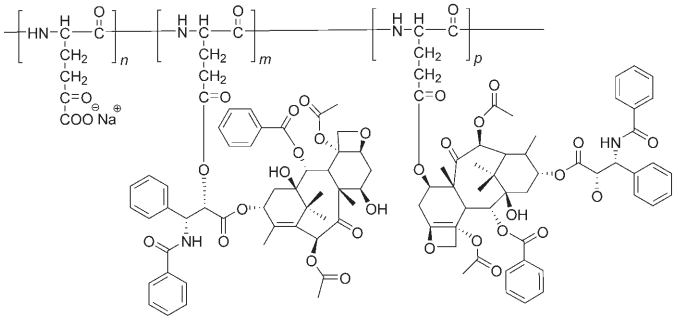


Scheme 3. Prothecan, a camptothecin derivative with 40 kDa PEG.

camptothecin with PEG through a glycine spacer[66–68] proved to have several advantages: a) the EPR effect results in a drug-targeting effect, b) esterifying the 20-hydroxy group of CPT stabilizes the drug in its active lactone form (closed E ring) which otherwise tends to hydrolyze under physiological conditions and lead to the inactive hydroxycarboxylic acid form, c) incorporation of a glycine spacer ensured a controlled release of the drug; and d) use of hydrophilic PEG leads to a highly water-soluble formulation of camptothecin.

Preclinical results with prothecan showed it had better efficacy in animal models of human cancers than free camptothecin.[66–68] Prothecan is currently being assessed in phase II studies for the treatment of gastric and gastro-esophageal tumors after a phase I study showed moderate nonhematologic toxicities at its MTD of 200 mg m^{-2} camptothecin equivalents.[69]

PG-TXL (CT-2103), a poly(L-glutamic acid) conjugate of taxol (Scheme 4), is probably the most successful drug–polymer conjugate to date and is currently undergoing



Scheme 4. PG-TXL (CT-2103), a poly(L-glutamic acid) conjugate of taxol (paclitaxel).

phase III trials in combination with standard chemotherapy against ovarian cancer and non-small-cell lung cancer.[70] PG-TXL has a higher loading ratio (ca. 37 wt% taxol) than other drug–polymer conjugates, and the taxol is linked through its 2′-OH group to the poly(glutamic) acid backbone. Phase I and II studies of various cancers showed promising response rates, even for patients who were resistant to taxane therapy.[71,72] The recommended dose of PG-TXL ranged from 175 to 235 mg m^{-2} (taxol equivalents) which is approximately twice as high as for free taxol. The dose-limiting toxicities of the conjugate are neurotoxicity and neutropenia. A noteworthy feature of PG-TXL is the biodegradability of the polyglutamic acid backbone and the liberation of taxol and taxol glutamic acid derivatives in vitro and in vivo, which, in part, appear to be mediated by cathepsin B.[73] A phase I

 © 2006 Wiley-VCH Verlag GmbH & Co. KGaA, Weinheim

study with an analogously constructed PG conjugate with camptothecin has recently been completed successfully.[74]

Besides synthetic polymers, albumin is also being investigated as a drug carrier in clinical trials. A methotrexate–albumin conjugate (MTX–HSA) was synthesized by directly coupling methotrexate to human serum albumin (HSA). This conjugate showed significant accumulation in rat tumors and high antitumor activity in selected nude mice models.[75,76] Stomatitis proved to be dose-limiting above 50 mg m^{-2} MTX–HSA (MTX equivalents) in a phase I study.[77] Two patients with renal cell carcinoma and one patient with mesothelioma responded to MTX–HSA therapy (one partial remission, two minor responses). Renal cell cancer is a malignancy with low response rates to conventional chemotherapy. Phase II studies are ongoing.

New approaches have concentrated on forming a drug–albumin conjugate in vivo by binding prodrugs selectively to circulating albumin after intravenous administration.[78–81] This prodrug concept is based on two features: a) rapid and selective binding of a maleimide prodrug to the cysteine 34 position of endogenous albumin after intravenous administration, and b) release of the albumin-bound drug at the target site as a result of the incorporation of an acid-sensitive or an enzymatically cleavable bond between the drug and the carrier.

A first clinical candidate is the (6-maleimidocaproyl)hydrazone derivative of doxorubicin (DOXO-EMCH; Figure 7) which incorporates an acid-sensitive carboxylic hydrazone bond as a predetermined breaking point. DOXO-EMCH entered a phase I study in 2003 after demonstrating superior efficacy and an improved toxicity profile relative to free doxorubicin, the clinical standard.[79]

As an example, the therapeutic effects of doxorubicin and DOXO-EMCH against renal cell carcinoma (RENCA) are shown in Figure 8. Mice treated with doxorubicin at its MTD value (4×6 mg kg^{-1}) showed distinct kidney tumors (body weight loss of $-10\,\%$), while the group treated with DOXO-EMCH at 4×12 mg kg^{-1} doxorubicin equivalents showed no body weight loss and complete remission was achieved in nearly all the animals.

In a phase I study with DOXO-EMCH, 37 patients with advanced cancer were treated with an intravenous infusion of DOXO-EMCH once every 3 weeks at a dose of 20–340 mg m^{-2} doxorubicin equivalents. Treatment with DOXO-EMCH was well tolerated up to 200 mg m^{-2}, without manifestation of drug-related side effects. Myleosuppression (grade 1–2), mucositis (grade 1–2), alopecia (grade 1–2), nausea and vomiting (grade 1), mouth dryness (grade 1), and fatigue (grade 1) have been noted at dose levels of 260, and myleosuppression (grade 2–3) as well as mucositis (grade 2–3) were dose-limiting at 340 mg m^{-2}. Of 29/37 evaluable patients, 13 had progressive disease, 13 had disease stabilization, a breast cancer and a liposarcoma patient had partial remission, and a patient with small-cell lung cancer had a complete remission. The recommended dose for phase II studies is 260 mg m^{-2}.

Although the clinical data for drug–polymer conjugates is limited to a few hundred patients, some general trends are apparent. The increase in the maximum tolerated dose (MTD) of the drug–polymer conjugates compared to the parent drug noted in preclinical studies is also manifested in clinical trials. Furthermore, no particular toxicity can be attributed to the polymer, and dose-limiting toxicities are comparable to the free drug. The significance of the molecular weight and of the cleavable linker of the drug–polymer conjugate remains unclear. Although the majority of non-biodegradable polymers have molecular weights close to the renal threshold (30–50 kDa, see Section 2.1), which allows enhanced permeation and retention in solid tumors, as well as a certain degree of renal clearance, a few recent examples of conjugates with albumin, polyglutamic acid, and PEG have molecular weights of 40–80 kDa. Whether the differences in the pharmacokinetic profile as a result of the different molecular weights influence the toxicity and tumor response needs to be evaluated in a larger population of patients.

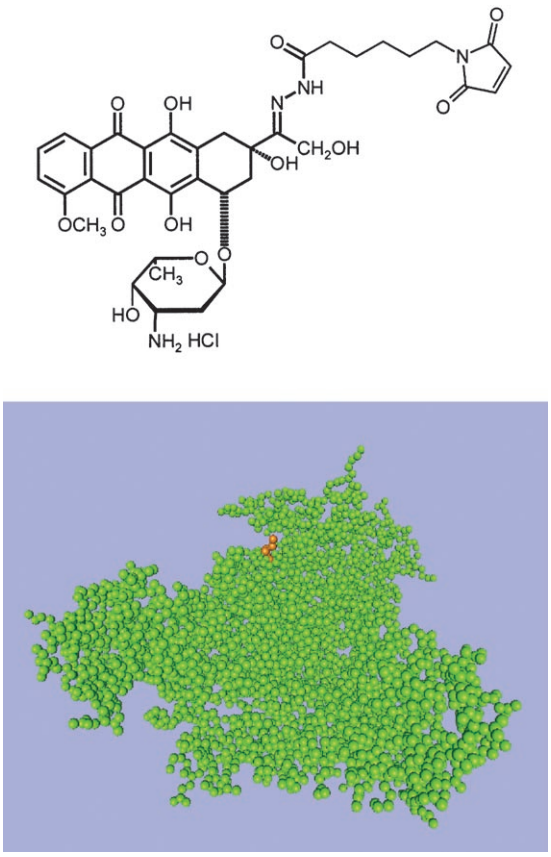


Figure 7. Structure of the prodrug DOXO-EMCH, which is undergoing clinical phase I trials (top), and the structure of human serum albumin (bottom); the prodrug binding position Cys 34 is highlighted in orange.

The effectiveness of the predetermined breaking point incorporated in the drug–polymer conjugate also remains a matter of debate. The majority of drug–HPMA conjugates have made use of the tetrapeptide Gly-Phe-Leu-Gly, which is cleaved by lysosomal enzymes such as cathepsin B. However, preclinical data indicate that antitumor efficacy of such designed conjugates correlates with the expression of cathepsin B in the tumor,[57] a fact that has not been adequately addressed in clinical trials. Detailed knowledge of the

 © 2006 Wiley-VCH Verlag GmbH & Co. KGaA, Weinheim

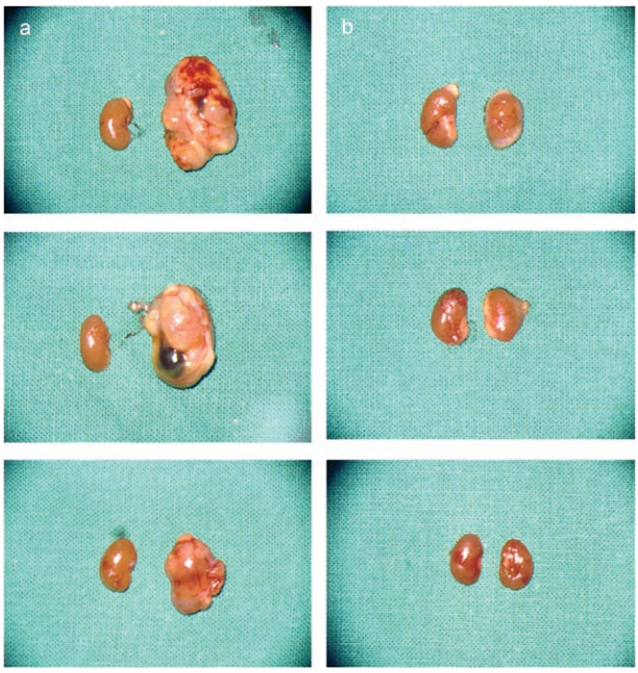


Figure 8. Representative photographic images of the healthy kidneys (left) as well as treated tumor-cell kidneys (right). The three mice from group **A** were treated with 4×12 mg kg^{-1} doxorubicin (body weight change: −10%) and the three mice from group **B** with 4×12 mg kg^{-1} doxorubicin equivalents of DOXO-EMCH (body weight change: +1%) for 24 days.

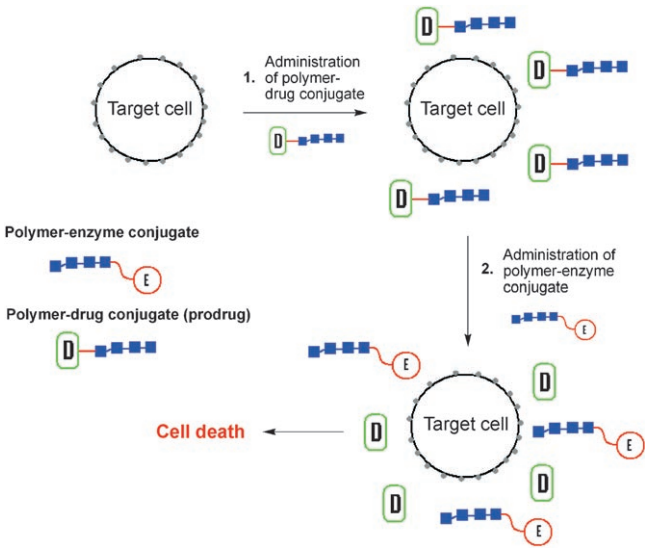


Figure 9. The PDEPT concept: After administration of the polymer–drug conjugate and uptake in the tissue by EPR, the polymer–enzyme conjugate is added to release the drug and induce cell death.

expression of tumor-related proteases in individual tumor entities would certainly be helpful for the future development of cleavable drug–polymer conjugates. Whether drug–polymer conjugates that are cleaved by unspecific hydrolysis or at acidic pH values are more universally applicable needs to be addressed in clinical studies. Preliminary preclinical studies with doxorubicin–HPMA conjugates have indicated that an acid-sensitive linker is more effective than a cathepsin B sensitive one.[82]

3.3. A Combined Approach: The PDEPT Concept

Polymer-directed enzyme–produg therapy (PDEPT) is a novel two-step antitumor approach that combines a polymeric prodrug and a polymer–enzyme conjugate to generate a cytotoxic drug at the tumor site.[83] PDEPT involves initial administration of the polymeric drug to promote tumor targeting before the activating polymer–enzyme conjugate is administrated (Figure 9). PDEPT has certain advantages compared to antibody-directed enzyme–produg therapy (ADEPT): the relatively short residence time of the polymeric prodrug in the plasma allows subsequent administration of the polymer–enzyme conjugate without fear of activation of the prodrug in the blood stream, and also the polymer–enzyme conjugates could have reduced immunogenicity.

Two PDEPT approaches have been investigated with doxorubicin: In the first case, the polymeric prodrug PK1 (FCE 28068; see Scheme 7 in Section 3.6.1), which is currently under phase II clinical evaluation, was selected as a model prodrug in combination with an (HPMA copolymer)–(cathepsin B) conjugate. In the polymer-bound form, the (HPMA copolymer)–(cathepsin B) conjugate retained approximately 20–25% of the cathepsin B activity in vitro. After intravenous administration of the conjugate to tumor-bearing B16F10 mice there was a 4.2-fold increase in its accumulation in tumors relative to the free enzyme. When PK1 and the PDEPT combination were used to treat established B16F10 melanoma tumors, the antitumor activity (% *T*/*C*, the survival time of treated versus control animals) for the PDEPT combination was 168% compared to 152% for PK1 alone, and 144% for free doxorubicin.[84]

Another more successful PDEPT combination consisting of (HPMA-copolymer)–(methacryloyl-gly-gly-cephalosporin)–doxorubicin (HPMA-*co*-MA-GG-C-Dox) as the macromolecular prodrug and an HPMA copolymer conjugate containing the nonmammalian enzyme β-lactamase (HPMA-*co*-MA-GG-β-L) as the activating component has been reported.[85] HPMA-*co*-MA-GG-C-Dox had a molecular weight of about 31600 Da and a doxorubicin–cephalosporin content of 5.85 wt%. Whereas free β-lactamase has a molecular weight of 45 kDa, the HPMA-*co*-MA-GG-β-L conjugate had a molecular weight in the range of 75–150 kDa. The HPMA-*co*-MA-GG-β-L conjugate retained 70% and 80% of its activity against the cephalosporin C and HPMA-*co*-MA-GG-C-Dox substrates, respectively. Intraveneous administration of HPMA-*co*-MA-GG-C-Dox to mice bearing subcutaneously implanted B16F10 melanoma, followed after five hours by HPMA-*co*-MA-GG-β-L induced the release of free doxorubicin in the tumor. Whereas the PDEPT combination caused a significant decrease in the size of the tumor ($T/C = 132\%$), neither free doxorubicin nor HPMA-*co*-MA-GG-C-Dox alone displayed activity. Furthermore the PDEPT combination showed no toxicity at the doses used.[85]

 © 2006 Wiley-VCH Verlag GmbH & Co. KGaA, Weinheim

3.4. Polymeric Angiogenesis Factors

Another therapeutic approach, instead of direct tumor targeting with polymer-bound cytostatic drugs, is the targeting of angiogenesis with an HPMA–polymer conjugate of the angiogenesis inhibitor TNP-470.[86,87] This approach showed very promising results in a mouse model, and no drug-related toxicities were observed.

3.5. Multivalent Therapeutics

A fundamentally different approach to polymer therapeutics is based on the multiple interactions of ligands conjugated with a polymer which interact simultaneously with multiple receptor sites in protein complexes or multiple receptors on the cell surface. This concept is a close mimicry of biological interactions such as cellular recognition and signal transduction where multivalent processes play an important role. Although many interesting approaches have been reported, only a few clinical developments have so far been pursued.

3.5.1. Multivalent Drug Concepts (Toxins and Bacteria)

A number of multivalent inhibitors have been designed that are based on low-molecular-weight drugs and target dimeric or multimeric proteins that contain multiple identical receptor sites.[49,50] For example, a pentavalent starlike carbohydrate ligand has been reported that fitted precisely into the binding pocket of the five subunits of the Shiga-like bacteria toxin, a close analogue of the cholera toxin (Figure 10).[88] An increase in the binding affinity by a factor of 10^7 was observed for this pentavalent interaction relative to the monovalent ligand. This example clearly demonstrates that dendritic and starlike molecules are perfect scaffolds for presenting ligands for multivalent interactions.

Another example is the binding of vancomycin derivatives or oligomers to the D-Ala-D-Ala motive of the bacteria cell wall. Whitesides and co-workers have reported on divalent and trivalent vancomycin derivatives which showed extremely high binding affinities. The trivalent model complex of vancomycin-D-Ala-D-Ala, with a binding constant of 4×10^{-17} M, has a higher affinity than the avidin–biotin complex.[89–91] This concept of multivalent interactions with vancomycin has been taken up in the pharmaceutical industry for in vivo and clinical studies. For example, telavancin, a highly bactericidal injectable antibiotic based on a vancomycin derivative with multiple modes of action, was reported by Theravance (South San Francisco).[92] Part of their research program is dedicated to finding new antibiotics for serious infections arising from *Staphylococcus aureus* (including multidrug-resistant strains) and other Gram-positive pathogens. Telavancin is currently in phase III clinical trials.

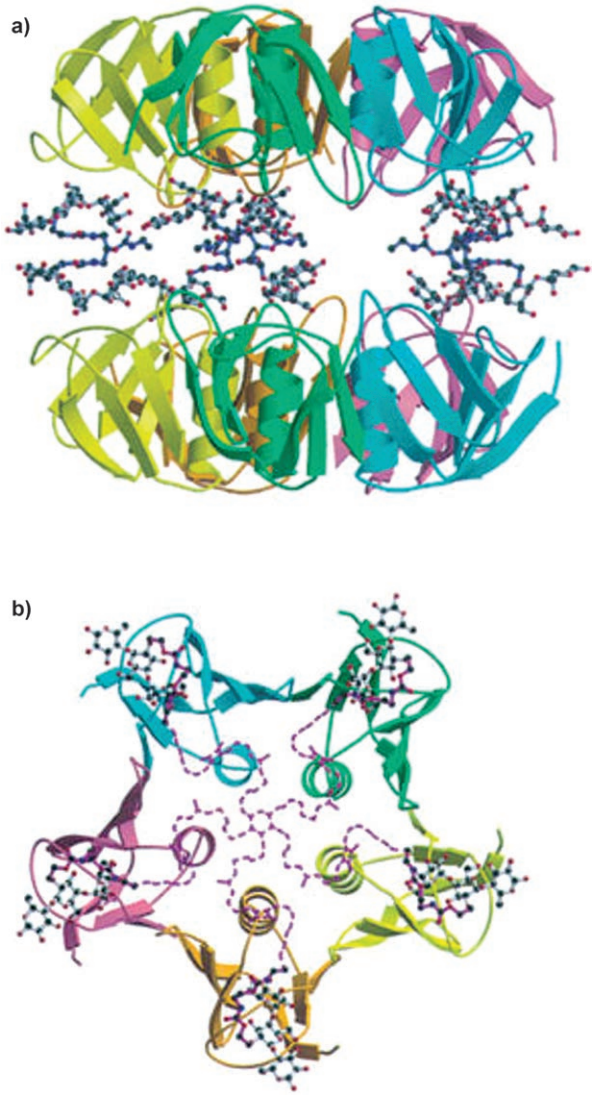


Figure 10. Pentavalent binding of the multivalent polysaccharide inhibitor to the Shiga-like toxin dimer: a) side view, b) top view (adapted from ref. [88]).

3.5.2. Multivalent Interactions at Surfaces—Inhibition of Virus Attachment

The inhibition of virus attachment to cell surfaces is a fundamental problem for the prevention of viral infections, such as influenza and HIV. As depicted in Figure 11, traditional monovalent drugs cannot prevent the multiple adhesion of the virus to the cell surface. Therefore, the development of multivalent ligands (Figure 5) that bind to membrane proteins of viruses is an important goal.

Several polymer architectures, including linear, starlike, and dendritic structures (Figure 2), have been considered as scaffolds for multivalent drugs.[49,50,93–95] Besides linear glycopolymers, various dendrimer structures have been investigated as multivalent ligands for sugar-binding proteins (for example, lectins), with multiple carbohydrate moieties attached at the exterior to form a so-called "sugar-coating". For example, L-lysine dendrimers with 2 to 16 sialic acid units

 © 2006 Wiley-VCH Verlag GmbH & Co. KGaA, Weinheim

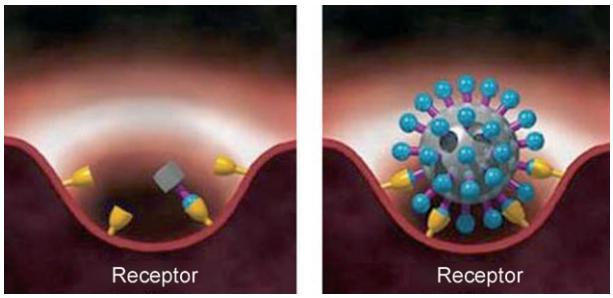


Figure 11. Monovalent binding of a drug (left) versus polyvalent binding of a virus (right) on a cell surface. (Printed with kind permission from Starpharma.)

show enhanced binding affinities in the *Limax flavus* lectin precipitation assay and the hemaglutination assay of erythrocytes.[96] In these systems, four to six sialic acid residues appeared to be an optimal number of functional groups for antiviral activity against the influenza A virus. An approximately 200-fold increase in the binding affinity to the trivalent hemaglutinin as compared to the monovalent ligand was observed. The small size of dendrimers (3–5 nm) relative to the spacing of receptor sites on the virus surface is a major limitation of this approach; hence they can only bind to 1-2 trivalent hemaglutinin receptors (Figure 12). In comparison, a high-molecular weight (10^6 Da) linear acrylamide polymer has shown in vitro an up to 10^8-fold increase in binding affinity, and hence is much more effective in blocking the attack of the influenza virus at the cell surface.[97,98] However, the molecular weight of the polymer is too high to be cleared from the body by the kidneys, and rapid biodegradation is unlikely. In addition to its extremely high binding constant, the polymer can also sterically shield the virus particle when applied in combination with other monovalent ligands.[99]

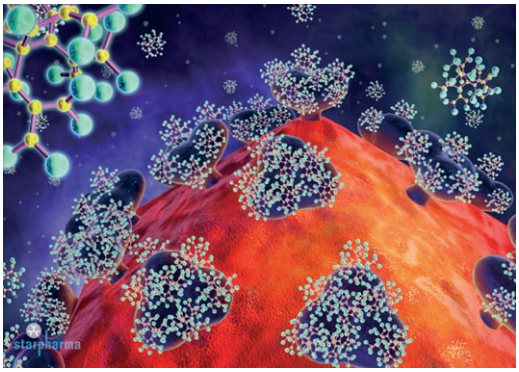


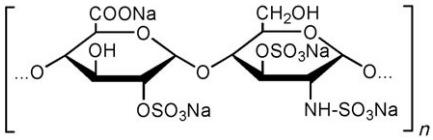
Figure 12. Size relationship between a virus particle with its multivalent cell surface receptors and dendritic drug molecules. (Printed with kind permission from Starpharma.)

Starpharma (Melbourne) is also concentrating on the development of polyvalent drugs. One example is the microbicide VivaGel, a topical vaginal gel that can potentially prevent or reduce transmission of HIV. VivaGel is a dendritic polyanion based on a polylysine core and is currently being evaluated in clinical phase II studies. Many of the approaches used by Starpharmas are based on polyvalent dendrimers which enhance the binding affinity to multivalent receptors or receptors on cell surfaces.[100]

Another approach towards HIV prevention based on polyvalent interactions was reported by Shaunak et al.[101] Dextrin 2-sulfate efficiently blocks HIV infection by binding to cell surfaces. The efficiency of this multivalent interaction has been demonstrated in phase II clinical trials.

3.5.3. *Polyanionic Polymers: Heparin Analogues*

Heparin, a glycosaminoglycan (Scheme 5), has been the drug of choice in the prevention and treatment of thromboembolic disorders for nearly 70 years. There is great interest in finding alternatives to both unfractionated heparin (UFH) and low-molecular-weight heparins (LMWH) because heparin has several disadvantages: First, it has to be isolated from mammalian organs, which implies a potential risk of contamination with pathogens such as viruses or prions, second, the increased use of heparin, especially of LMWH, means there is a growing shortage of the raw material, and third, heparin is a polydisperse mixture of molecules with different chain lengths and chemical structures.[102] Numerous parameters, such as the animal species used for providing heparin, the method of isolation, and the purification step of the product, influence its respective composition and results in wide chemical and subsequent pharmacological variations between different heparin preparations.



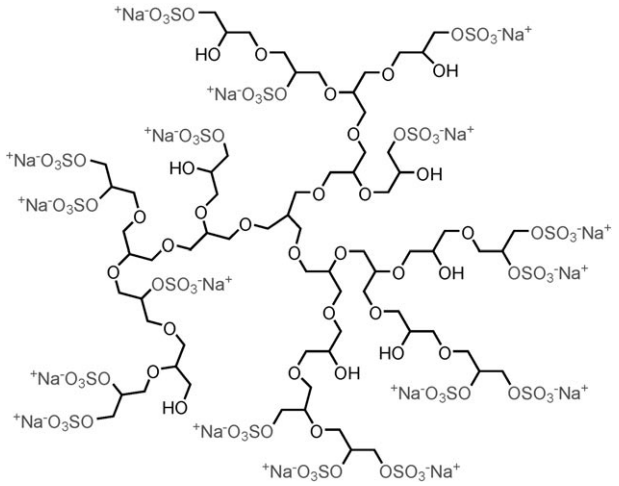
Scheme 5. Structure of a heparin subunit.

In addition to their antithrombic activity, the characteristic feature of heparin and other natural sulfated polysaccharides are complement inhibition,[103] anti-inflammatory,[104,105] antiangiogenic,[106] antimetastatic,[107] antiatherosclerotic,[108] antiproliferative,[109] antiadhesive,[110] and antiviral effects.[111] These additional modes of action can contribute to the overall therapeutic benefit of heparin in some cases.[107]

Consequently, heparin analogues with a similar or even improved pharmacological profile, but lacking the disadvantages of this animal product, are of interest. Besides partially synthetic sulfated linear polysaccharides,[112,113] fully synthetic sulfated linear polymers,[114] which are produced without a starting carbohydrate, may represent promising heparin mimetics.[115] Recently, a new type of polysulfated heparin analogue based on branched polysaccharides was described that possesses a much higher anticoagulant activity than its linear counterparts.[116] However, the accessibility of branched

© 2006 Wiley-VCH Verlag GmbH & Co. KGaA, Weinheim

polysaccharides is problematic because of limited natural sources. Thus, a simple and efficient approach to highly branched polysulfated heparin analogues based on dendritic polyglycerols has been developed (Scheme 6).[117] These



Scheme 6. Dendritic polyglycerol sulfate as an anti-inflammatory heparin analogue.

polyglycerol sulfates prolong the time of activated partial thromboplastin as well as thrombin and inhibit both the classical and alternative complement activation more effectively than heparin itself. In contrast to sulfated polysaccharides, their activities are not directly dependent on the molecular weight, which might be a result of the globular 3D structure of the dendritic polyglycerol sulfates. Since coagulation, complement activation, and inflammation are often present in the pathophysiology of numerous diseases, polyglycerol sulfates with both anticoagulant and anticomplementary activities represent promising candidates for the development of future drugs.

Recently, immunomodulatory and antiangiogenic properties of glucoseamine-modified polyamidoamine (PAMAM) dendrimers have been described. The use of dendrimeric glucosamine and dendrimeric glucosamine 6-sulfate together in a validated and clinically relevant rabbit model of scar-tissue formation after glaucoma filtration surgery resulted in the long-term success of the surgery increasing from 30% to 80%.[118]

3.5.4. Polycationic Polymers as DNA/RNA Transfection Agents

The search for nonviral alternatives remains a challenge because of problems associated with viral gene transfection, such as immune response and limited selectivity,.[119] In the past decade several approaches were pursued in which cationic amphiphiles, polymers, or block copolymers and other pH-responsive polymers were used.[120–125] The colloidal surface and chemical properties of DNA and RNA complexes with polycations are responsible for controlling the extent and rate of delivery of genes to cells. However, additional hurdles on the cellular level have to be overcome on the surface of the cells (Figure 13): Complexes have to enter the cells through the cell membranes, escape degradation in endosomal/lysosomal compartment, traffic through the cytoplasm, and enter the nucleus. The physicochemical characteristics of poly-

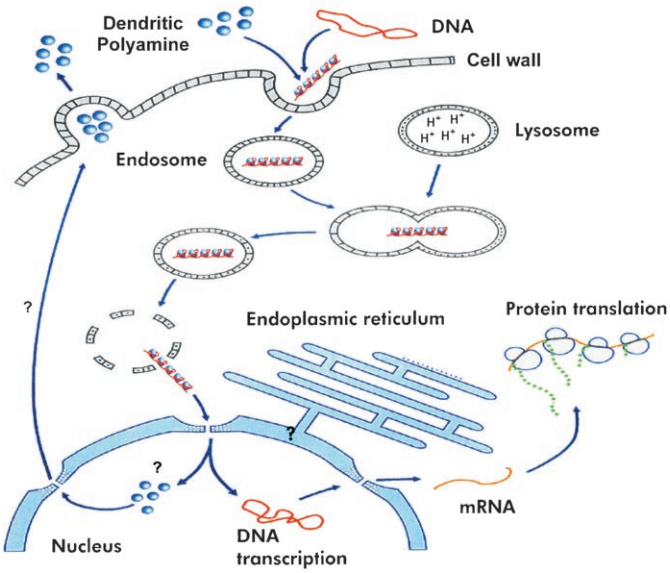


Figure 13. Intracellular uptake of therapeutic DNA or RNA with polycationic polymers, that is, dendritic polyamines.

plexes, such as size, charge, hydrophobicity, and buffering capacity, play a major role in the efficient transport and biological activity of the gene-based drugs.[126]

The "proton-sponge hypothesis" postulates enhanced transgene delivery by cationic polymer–DNA complexes (polyplexes) containing proton-buffering polyamines through enhanced endosomal accumulation of chloride, which leads to osmotic swelling and lysis of the endosome (Figure 13).[127] For therapeutic applications, however, an early endosomal escape mechanism, rather than lysosomal fusion, would be preferable to avoid the release of lysosomal enzymes into the cytosol.[128]

The most frequently used cationic polymers for in vitro gene delivery are poly(ethylene imine) (PEI), poly(L-lysine), and chitosans. Another approach is the use of perfect polyamine-dendrimers[120,129,130] to mimic the globular shape of the natural protein complex. However, the synthetic workload to obtain dendritic structures in the size-range of the natural histone complex (ca. 8 nm) [131] is tremendous (12–18 steps).[132] Also, the observation that a partially destroyed (hydrolyzed) dendritic backbone showed even higher transfection efficiencies[129,133] underlines the significance of readily available alternatives.

A simple approach to dendritic polyamines with different molecular weights and adjustable flexibility (degrees of branching) has been described recently.[134] Both parameters influence transfection efficiency and cytotoxicity. By using a two-step functionalization of hyperbranched PEI, it was possible to generate partially or fully branched pseudodendrimers (poly(propylene imine) (PPI) and poly(amidoamine)

 © 2006 Wiley-VCH Verlag GmbH & Co. KGaA, Weinheim

(PAMAM) dendrimer analogues). The highest DNA transfection efficiencies have been observed for molecular weights in the range $M_n = 5000–10000\ g\,mol^{-1}$ for the nonfunctionalized PEI cores, which is comparable in size to the natural histones (8 nm). A maximum transfection efficiency in the β-gal assay for various cell lines was observed when the degree of branching of the PPI analogue was 58 % and the PEI core had a molecular weight of of $M_n = 10000\ g\,mol^{-1}$.

PEGylated polyethylene imines[135] were recently used for the delivery of siRNA to tumor-bearing mice,[136] thus demonstrating the potential of such polycationic carriers for therapeutic application in vivo. However, the toxicity of these systems have to be further reduced.

3.6. *Supramolecular Drug–Polymer Complexes*

One of the major problems in drug development is the poor solubility of many existing and new drugs. Very often the therapeutic effectiveness of these drugs is diminished by their inability to gain access to the site of action at an appropriate dose. Therefore, these drugs are either not clinically used, delivered in large volumes of aqueous or ethanolic solutions, delivered in conjunction with surfactants, or chemically derivatized to soluble prodrugs. Unfortunately, all of these modifications can result in reduced efficacy or adverse effects.

Many approaches for delivering hydrophobic compounds using polymeric carriers, such as block copolymers and dendritic polymers, have been explored.[4,13]

3.6.1. *Block Copolymer Micelles*

Polymeric micelles (Figure 14) are generally more stable than micelles of small surfactant molecules and can retain the loaded drug for a longer period of time.[137,138] The block-copolymer micelles form spontaneously by self-assembly in water when the concentration of the amphiphilic block copolymer is above the critical micellar concentration (CMC).[139] The driving force can be the hydrophobic interactions of the inner block, for example, a nonpolar poly(caprolactone) block (PCL), or ionic interactions, for example, a poly(aspartate) block (PAsp), complexed to a negatively charged polymer such as DNA that forms a polyion micelle.[140] The outer block often consists of a polar poly(ethylene oxide) (PEO) block which forms the shell of the nanocarrier and protects its core. It has been demonstrated that PEO prevents the adsorption of proteins[141,142] and hence forms a biocompatible polymeric nanocarrier shell.

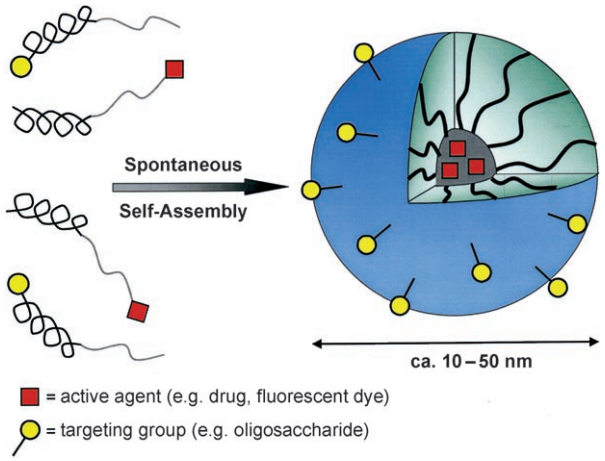


Figure 14. Formation and architecture of block-copolymer micelles which spontaneously form by self-assembly in water. The characteristic features are a pronounced core–shell architecture which can be controlled by the individual polymer blocks. Typical examples of block copolymers are PEO-*b*-PPO, PEO-*b*-PCl, and PEO-*b*-PAsp.

The size of these block-copolymer micelles is determined by thermodynamic parameters, but partial control over the size is possible by variation of the block length of the polymer.[143] Typically, these block-copolymer micelles are 20–50 nm in diameter with a relatively narrow distribution and are therefore similar in size to viruses, lipoproteins, and other naturally occurring transport systems.[137] A major obstacle for these nanocarrier systems is their nonspecific uptake by the reticuloendothelial systems (RES). The size and the surface properties of the nanocarriers based on block copolymers require careful design to achieve long circulation times in the blood and site-specific drug delivery.[144]

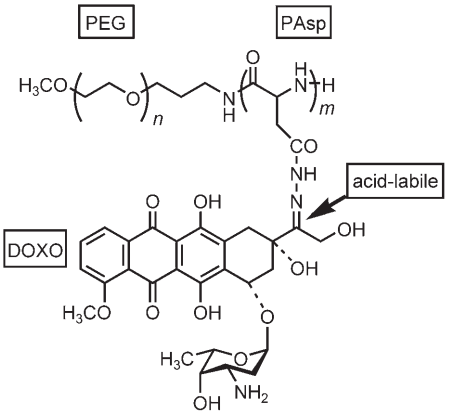
The polarity and functionality of each block allow control over the spontaneously formed core–shell architecture. While terminal functionalities on the outer block (the shell) control biocompatibility and may incorporate potential targeting properties, the inner block of such nanocarriers can be used to complex or covalently couple active drug molecules (Figure 14). This core–shell concept is frequently used to dissolve nonpolar drugs. Examples of block copolymers that have poor solubility in water are the pluronics PEO-*b*-PPO or PEO-*b*-PPO-*b*-PEO.[26]

Supramolecular constructs have also been generated by using block copolymers as shells for dendritic porphyrins.[145] These "blown up" micelles (ca. 100 nm) may have a much higher targeting specificity for tumor tissue as a result of an enhanced EPR effect.

Kataoka and co-workers have recently reported a pH-sensitive supramolecular nanocarrier for doxorubicin based on biocompatible block-copolymer micelles.[146] In contrast to drug–polymer conjugates, in which antitumor agents are covalently attached to a single macromolecule chain, doxorubicin was coupled through an acid-labile hydrazone linker to a PEO-*b*-PAsp copolymer (Scheme 7). After spontaneous self-assembly of the drug-loaded supramolecular nanocarrier (Figure 14), kinetic analysis clearly demonstrated the effective cleavage of the hydrazone bonds at $pH \leq 5$, with concomitant release of doxorubicin. Release of doxorubicin was negligible under physiological conditions in cell culture medium ($pH \approx 7$).

The doxorubicin nanocarrier demonstrated in vitro cytotoxicity against a human small-cell lung cancer cell line (SBC-3) in a time-dependent manner, thus suggesting cellular uptake by endocytosis. The first candidates of antitumor drugs based on polymer micelles have entered clinical trials in Japan.[147]

© 2006 Wiley-VCH Verlag GmbH & Co. KGaA, Weinheim



Scheme 7. A doxorubicin block-copolymer conjugate which self-assembles to form block-copolymer micelles in water. The acid-labile hydrazone bond is cleaved at pH < 6 and doxorubicin is released.

3.6.2. *Nanocarriers Based on Dendritic Polymers*

Although physical aggregates such as liposomes and micelles are frequently used as drug-delivery systems,[5] they can be unstable under shear force and other environmental effects, such as high dilution,[143] temperature, and pressure required, for example, for sterilization. An alternative approach is the covalent modification of dendritic macromolecules with an appropriate shell that results in stable micelle-type structures suitable for noncovalent encapsulation of guest molecules (Figure 15).[148,149,162] The size of these dendritic nanocarriers can be defined precisely between 5 and 20 nm. The encapsulation of guest molecules is driven by noncovalent interactions (ionic, H bonding, and van der Waals interactions) and can be simultaneously tailored for various drugs, while a drug–polymer conjugate has to be synthesized individually.

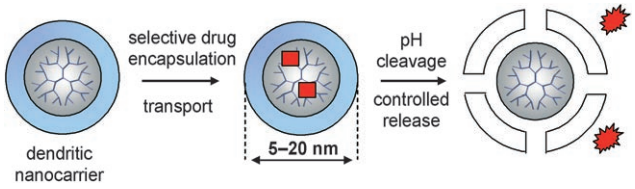


Figure 15. Unimolecular dendritic nanocarriers for encapsulation of biologically active compounds, for example, drugs and oligonucleotides. The drug load can be released selectively in acidic media (such as in tumor tissue) when the acid-labile linkers connecting the shell to the core are cleaved.

Dendritic polymers with their regular and well-defined unimolecular architecture, which can be further chemically modified at either the core (to increase hydrophobicity) or the shell (to increase hydrophilicity), is currently attracting interest as so-called dendritic nanocarriers for applications in drug solubilization and delivery.[15] In previous studies the poorly water-soluble anticancer drug taxol was solubilized in water using polyglycerol dendrimers[150] of the third to the fifth generations.[151] PEGylation of dendritic PEI, PPI, and PAMAM architectures led to water-soluble nanocontainers which were able to solubilize small organic molecules, including anticancer drugs.[152–156]

The encapsulation and the transport of guest molecules in these dendritic architectures have been studied by several research groups.[13,148] However, relatively little is known about the release of the encapsulated guest molecules by pH-triggered cleavage of the shell in the physiological range (Figure 15). In many cases the pH-dependent release from dendritic core–shell architectures has only been achieved under drastic conditions[157] or by protonation of poly(propylene amine) dendrimers[158] and their derivatives.[159]

A simple and general concept for the generation of core–shell-type architectures from readily accessible hyperbranched polymers was recently reported.[160] Several pH-sensitive nanocarriers have been prepared by attaching pH-sensitive shells through acetal or imine bonds to commercially available dendritic core structures (polyglycerol and polyethylene imine; Figure 16). In some cases the pH-responsive nanocarriers showed a very high transport capacity which is an important criterion for efficient drug delivery. Various guest molecules, such as polar dyes, oligonucleotides, and anticancer drugs have been encapsulated inside these dendritic core–shell architectures.

Furthermore, the dendritic polyamine core structure with an imine-linked shell (Figure 16) shows the release profile that is needed for liberating the encapsulated drug in tumor tissue: fast release at pH 5–6 and slow release at pH 7.4.[156] These supramolecular drug-delivery systems are currently being evaluated by us for the transport of cytostatic compounds.

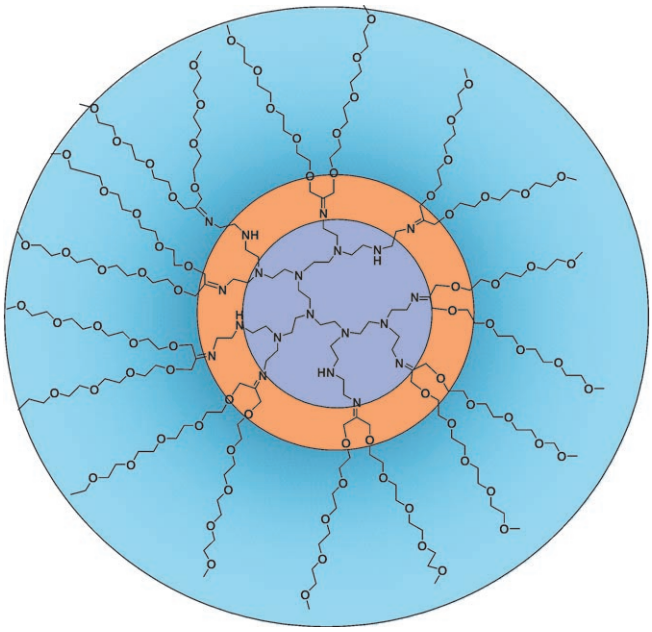


Figure 16. Dendritic core–shell architectures based on commercially available poly(ethylene imine) (PEI) with an acid-labile linker (orange) and PEG shells (blue). Stable supramolecular complexes are formed with various polar guest molecules (dyes, drugs, oligonucleotides). Imine cleavage readily occurs at pH 6 to release the encapsulated guest molecules. The depicted structure shows only an idealized fragment of the much bigger dendritic polyamine core.

© 2006 Wiley-VCH Verlag GmbH & Co. KGaA, Weinheim

4. Summary and Conclusions

The development of polymer therapeutics has emerged as an exciting field of research for improving the therapeutic potential of low-molecular-weight drugs and proteins. PEGylation of therapeutically relevant proteins is an established technology, and it is likely that new PEGylated proteins will attain market approval in the next few years, considering that several hundreds of protein-based therapeutics are under preclinical or clinical development.

The rationale for the development of anticancer drug–polymer conjugates relies on the EPR effect, and various macromolecular prodrugs have shown superior efficacy in preclinical models relative to their low-molecular-weight parent compounds. Several candidates have advanced into clinical studies and have, in most cases, shown a favorable toxicity profile. Comparative studies with established clinical protocols as well as research into the EPR effect in humans and the role of tumor-associated proteases are necessary to select appropriate tumor entities in order to validate the concept of drug–polymer conjugates clinically.

Other concepts, such as multivalent interactions, including the mimicry of functional biomacromolecules by synthetic analogues, have great potential, although the in vivo efficacy data is limited to date.

Finally, bio-nanotechnology has added a new dimension to the development of polymer therapeutics. If nanocarriers based on supramolecular assemblies can be intelligently designed to exploit physiological or biochemical features of infectious or malignant diseases, it should be possible to carry large payloads of the respective drug to the pathogenic site.

In the future more biodegradable polymers with high molecular weights and high precision ($M_n > 30000\ g\,mol^{-1}$, polydispersity < 1.5) as well as new modular approaches to "intelligent" polymeric nanotransporters will be needed. Toxicity and pharmacokinetic issues should be addressed at an early stage when selecting promising new polymer therapeutics, since in vivo studies will primarily decide the fate of a new polymeric drug.

Helmut Ringsdorf's statement on the future perspectives of macromolecular chemistry might serve as a stimulus for the scientists active in the field as well as those of the future:[161]

"It is certainly only a matter of time before pharmaceuticals are required that not only affect cells and tissue specifically, but must also exhibit specific behavior in the cytoplasm of the cell."

We thank the Bundesministerium für Bildung und Forschung (BMBF Nanonachwuchswettbewerb), the Deutsche Forschungsgemeinschaft, the Deutsche Krebshilfe, the Wilhelm Sander-Stiftung, and Fonds der Chemischen Industrie for financial support, and Dr. Pamela Winchester as well as Michal Radowski for their great help in the preparation of this manuscript. Helmut Ringsdorf and Ruth Duncan are gratefully acknowledged for their many helpful and fruitful discussions during the preparation of this manuscript.

Received: June 17, 2005
Published online: January 30, 2006

[1] The therapeutic index of a drug is defined as the ratio of the toxic dose to the therapeutic dose.
[2] The term "polymer therapeutics" was coined by Helmut Ringsdorf and Ruth Duncan. Other research groups use the more general term "nanomedicine".
[3] L. Gros, H. Ringsdorf, H. Schupp, *Angew. Chem.* **1981**, *93*, 311 – 331; *Angew. Chem. Int. Ed. Engl.* **1981**, *20*, 305 – 325.
[4] R. Duncan, *Nat. Rev. Drug Discovery* **2003**, *2*, 347 – 360.
[5] R. Duncan in *Encyclopedia of Molecular Cell Biology and Molecular Medicine, Vol. 14* (Ed.: R. A. Meyers), Wiley-VCH, Weinheim, **2005**, pp. 163 – 204.
[6] G. Kohler, C. Milstein, *Nature* **1975**, *256*, 495 – 497.
[7] H. Ringsdorf, *J. Polym. Sci. Polym. Symp.* **1975**, *51*, 135 – 153.
[8] A. Godwin, K. Bolina, M. Clochard, E. Dinand, S. Rankin, S. Simic, S. Brocchini, *J. Pharm. Pharmacol.* **2001**, *53*, 1175 – 1184.
[9] B. Rihova, K. Kubackova, *Curr. Pharm. Biotechnol.* **2003**, *4*, 311 – 322.
[10] J. Kopecek, P. Kopeckova, T. Minko, Z.-R. Lu, *Eur. J. Pharm. Biopharm.* **2000**, *50*, 61 – 81.
[11] R. Duncan in *Polymeric Drug Delivery Systems* (Ed.: G. S. Kwon), Marcel Dekker, New York, **2005**, pp. 1 – 92.
[12] M. Yokoyama, *Supramol. Des. Biol. Appl.* **2002**, 245 – 267.
[13] R. Haag, *Angew. Chem.* **2004**, *116*, 280 – 284; *Angew. Chem. Int. Ed.* **2004**, *43*, 278 – 282.
[14] J. K. Vasir, M. K. Reddy, V. D. Labhasetwar, *Curr. Nanosci.* **2005**, *1*, 47 – 64.
[15] R. Duncan, L. Izzo, *Adv. Drug Delivery Rev.* **2005**, *57*, 2215 – 2237.
[16] M. Thanou, R. Duncan, *Curr. Opin. Invest. Drugs* **2003**, *4*, 701 – 709.
[17] K. Ulbrich, V. Subr, *Adv. Drug Delivery Rev.* **2004**, *56*, 1023 – 1050.
[18] L. Brannon-Peppas, J. O. Blanchette, *Adv. Drug Delivery Rev.* **2004**, *56*, 1649 – 1659.
[19] A. El-Aneed, *J. Controlled Release* **2004**, *94*, 1 – 14.
[20] T. Sawa, S. K. Sahoo, H. Maeda, *PBM Ser.* **2003**, *1*, 233 – 261.
[21] Y. Luo, G. D. Prestwich, *Curr. Cancer Drug Targets* **2002**, *2*, 209 – 226.
[22] P. S. Huang, A. Oliff, *Curr. Opin. Genet. Dev.* **2001**, *11*, 104 – 110.
[23] G. M. Dubowchik, M. A. Walker, *Pharmacol. Ther.* **1999**, *83*, 67 – 123.
[24] F. Kratz, A. Warnecke, P. C. A. Rodrigues, K. Riebeseel in *Polymeric Biomaterials*, 2nd ed. (Ed.: S. Dumitriu), Marcel Dekker, New York, **2001**, pp. 851 – 894.
[25] F. Kratz, U. Beyer, M. T. Schütte, *Crit. Rev. Ther. Drug Carrier Syst.* **1999**, *16*, 245 – 288.
[26] A. V. Kabanov, T. Okano, *Adv. Exp. Med. Biol.* **2003**, *519*, 1 – 27.
[27] K. E. Uhrich, S. M. Cannizzaro, R. S. Langer, K. M. Shakesheff, *Chem. Rev.* **1999**, *99*, 3181 – 3198.
[28] A. Gresser, *Dtsch. Med. Wochenschr.* **1963**, *88*, 2217.
[29] Y. Matsumura, H. Maeda, *Cancer Res.* **1986**, *46*, 6387 – 6392.
[30] H. Maeda, J. Wu, T. Sawa, Y. Matsumura, K. Hori, *J. Controlled Release* **2000**, *65*, 271 – 284.
[31] R. K. Jain, *Cancer Res.* **1987**, *47*, 3039 – 3051.
[32] R. K. Jain, *Cancer Metastasis Rev.* **1987**, *6*, 559 – 593.
[33] H. Maeda, Y. Matsumura, *Crit. Rev. Ther. Drug Carrier Syst.* **1989**, *6*, 193 – 210.
[34] P. Caliceti, F. M. Veronese, *Drug Deliv. Rev.* **2003**, *55*, 1261 – 1277.
[35] K. Greish, J. Fang, T. Inutsuka, A. Nagamitsu, H. Maeda, *Clin. Pharmacokinet.* **2003**, *42*, 1089 – 1105.
[36] H. Maeda, T. Sawa, T. Konno, *J. Controlled Release* **2001**, *74*, 47 – 61.
[37] R. Satchi-Fainaro, *J. Drug Targeting* **2002**, *10*, 529 – 533.
[38] R. Langer, *Nature* **1998**, *392*, 5 – 10.

 © 2006 Wiley-VCH Verlag GmbH & Co. KGaA, Weinheim

[39] S. Mukherjee, R. N. Ghosh, F. R. Maxfield, *Physiol. Rev.* **1997**, *77*, 759 – 803.
[40] R. J. Amir, N. Pessah, M. Shamis, D. Shabat, *Angew. Chem.* **2003**, *115*, 4632 – 4637; *Angew. Chem. Int. Ed.* **2003**, *42*, 4494 – 4499.
[41] K. Haba, M. Popkov, M. Shamis, R. A. Lerner, C. F. Barbas III, D. Shabat, *Angew. Chem.* **2005**, *117*, 726 – 730; *Angew. Chem. Int. Ed.* **2005**, *44*, 716 – 720.
[42] M. Shamis, H. N. Lode, D. Shabat, *Chem. Commun.* **2004**, *21*.
[43] I. F. Tannock, D. Rotin, *Cancer Res.* **1989**, *49*, 4373 – 4384.
[44] R. B. Greenwald, C. D. Conover, Y. H. Choe, *Crit. Rev. Ther. Drug Carrier Syst.* **2000**, *17*, 101 – 161.
[45] J. M. Harris, R. B. Chess, *Nature Rev. Drug Discovery* **2003**, *2*, 214 – 221.
[46] S. C. Pedder, *Semin. Liver Dis.* **2003**, *23*, 19 – 22.
[47] T. K. Choueiri, T. E. Hutson, R. M. Bukowski, *Expert Rev. Anticancer Ther.* **2003**, *3*, 823 – 829.
[48] G. Molineux, *Anticancer Drugs* **2003**, *14*, 259 – 264.
[49] M. Mammen, S.-K. Choi, G. M. Whitesides, *Angew. Chem.* **1998**, *110*, 2908 – 2935; *Angew. Chem. Int. Ed.* **1998**, *37*, 2754 – 2794.
[50] S.-K. Choi, *Synthetic Multivalent Molecules*, Wiley-Interscience, Hoboken, USA, **2004**.
[51] J. Crawford, *Semin. Oncol.* **2003**, *30*, 24 – 30.
[52] W. Vogel, *Expert Rev. Anti-Infect. Ther.* **2003**, *1*, 423 – 431.
[53] V. Goffin, P. Touraine, *Curr. Opin. Invest. Drugs* **2004**, *5*, 463 – 468.
[54] R. Fernandez-Botran, *Expert Opin. Invest. Drugs* **2000**, *9*, 497 – 514.
[55] E. H. Choy, B. Hazleman, M. Smith, K. Moss, L. Lisi, D. G. Scott, J. Patel, M. Sopwith, D. A. Isenberg, *Rheumatology* **2002**, *41*, 1133 – 1137.
[56] P. A. Vasey, S. B. Kaye, R. Morrison, C. Twelves, P. Wilson, R. Duncan, A. H. Thomson, L. S. Murray, T. E. Hilditch, T. Murray, S. Burtles, D. Fraier, E. Frigerio, J. Cassidy, *Clin. Cancer Res.* **1999**, *5*, 83 – 94.
[57] P. M. Loadman, M. C. Bibby, J. A. Double, W. M. Al-Shakhaa, R. Duncan, *Clin. Cancer Res.* **1999**, *5*, 3682 – 3688.
[58] V. Bilim, *Curr. Opin. Mol. Ther.* **2003**, *5*, 326 – 330.
[59] L. W. Seymour, D. R. Ferry, D. Anderson, S. Hesslewood, P. J. Julyan, R. Poyner, J. Doran, A. M. Young, S. Burtles, D. J. Kerr, *J. Clin. Oncol.* **2002**, *20*, 1668 – 1676.
[60] J. M. Meerum Terwogt, W. W. ten Bokkel Huinink, J. H. Schellens, M. Schot, I. A. Mandjes, M. G. Zurlo, M. Rocchetti, H. Rosing, F. J. Koopman, J. H. Beijnen, *Anticancer Drugs* **2001**, *12*, 315 – 323.
[61] N. E. Schoemaker, C. van Kesteren, H. Rosing, S. Jansen, M. Swart, J. Lieverst, D. Fraier, M. Breda, C. Pellizzoni, R. Spinelli, M. Grazia Porro, J. H. Beijnen, J. H. Schellens, W. W. ten Bokkel Huinink, *Br. J. Cancer* **2002**, *87*, 608 – 614.
[62] E. Gianasi, M. Wasil, E. G. Evagorou, A. Keddle, G. Wilson, R. Duncan, *Eur. J. Cancer* **1999**, *35*, 994 – 1002.
[63] E. Gianasi, R. G. Buckley, J. Latigo, M. Wasil, R. Duncan, *J. Drug Targeting* **2002**, *10*, 549 – 556.
[64] J. M. Rademaker-Lakhai, D. van den Bongard, D. Pluim, J. H. Beijnen, J. H. Schellens, *Clin. Cancer Res.* **2004**, *10*, 3717 – 3727.
[65] S. Sengupta, D. Eavarone, I. Capila, G. Zhao, N. Watson, T. Kiziltepe, R. Sasisekharan, *Nature* **2005**, *436*, 568 – 572.
[66] R. B. Greenwald, A. Pendri, C. D. Conover, C. Lee, Y. H. Choe, C. Gilbert, A. Martinez, Y. Xia, D. Wu, M. Hsue, *Bioorg. Med. Chem.* **1998**, *6*, 551 – 562.
[67] D. Fraier, E. Frigerio, G. Brianceschi, M. Casati, A. Benecchi, C. James, *J. Pharm. Biomed. Anal.* **2000**, *19*, 505 – 514.
[68] J. W. Singer, R. Bhatt, J. Tulinsky, K. R. Buhler, E. Heasley, P. Klein, P. de Vries, *J. Controlled Release* **2001**, *74*, 243 – 247.
[69] E. K. Rowinsky, J. Rizzo, L. Ochoa, C. H. Takimoto, B. Forouzesh, G. Schwartz, L. A. Hammond, A. Patnaik, J. Kwiatek, A. Goetz, L. Denis, J. McGuire, A. W. Tolcher, *J. Clin. Oncol.* **2003**, *21*, 148 – 157.
[70] For further information, see: http.//www.cticseattle.com.
[71] P. Sabbatini, C. Aghajanian, D. Dizon, S. Anderson, J. Dupont, J. V. Brown, W. A. Peters, A. Jacobs, A. Mehdi, S. Rivkin, A. J. Eisenfeld, D. Spriggs, *J. Clin. Oncol.* **2004**, *22*, 4523 – 4531.
[72] J. W. Singer, B. Baker, P. De Vries, A. Kumar, S. Shaffer, E. Vawter, M. Bolton, P. Garzone, *Adv. Exp. Med. Biol.* **2003**, *519*, 81 – 99.
[73] E. Auzenne, N. J. Donato, C. Li, E. Leroux, R. E. Price, D. Farquhar, J. Klostergaard, *Clin. Cancer Res.* **2002**, *8*, 573 – 581.
[74] S. Sayid, J. Dupont, M. McNamara, J. H. Doroshow, P. S. D. Spriggs, E. Eastham, S. Stromatt, C. H. Takimoto, *Clin. Cancer Res.* **2003**, *9*, 16.
[75] A. Wunder, G. Stehle, H. Sinn, H. H. Schrenk, D. Hoff-Biederbeck, F. Bader, E. A. Friedrich, P. Peschke, W. Maier-Borst, D. L. Heene, *Int. J. Oncol.* **1997**, *11*, 497 – 507.
[76] A. M. Burger, G. Hartung, G. Stehle, H. Sinn, H. H. Fiebig, *Int. J. Cancer* **2001**, *92*, 718 – 724.
[77] G. Hartung, G. Stehle, H. Sinn, A. Wunder, H. H. Schrenk, H. S. L. Kränzle, H. H. Fiebig, W. Maier-Borst, D. L. Heene, W. Queißer, *Clin. Cancer Res.* **1999**, *5*, 753 – 759.
[78] F. Kratz, R. Mueller-Driver, I. Hofmann, J. Drevs, C. Unger, *J. Med. Chem.* **2000**, *43*, 1253 – 1256.
[79] F. Kratz, A. Warnecke, K. Scheuermann, C. Stockmar, J. Schwab, P. Lazar, P. Drückes, N. Esser, J. Drevs, D. Rognan, C. Bissantz, C. Hinderling, G. Folkers, I. Fichtner, C. Unger, *J. Med. Chem.* **2002**, *45*, 5523 – 5533.
[80] A. M. Mansour, J. Drevs, N. Esser, F. M. Hamada, O. A. Badary, C. Unger, I. Fichtner, F. Kratz, *Cancer Res.* **2003**, *63*, 4062 – 4066.
[81] A. Warnecke, F. Kratz, *Bioconjugate Chem.* **2003**, *14*, 377 – 387.
[82] B. Rihova, T. Etrych, M. Pechar, M. Jelinkova, M. Stastny, O. Hovorka, M. Kovar, K. Ulbrich, *J. Controlled Release* **2001**, *74*, 225 – 232.
[83] R. Duncan, S. Gac-Breton, R. Keane, R. Musila, Y. N. Sat, R. Satchi, F. Searle, *J. Controlled Release* **2001**, *74*, 135 – 146.
[84] R. Satchi, T. A. Connors, R. Duncan, *Br. J. Cancer* **2001**, *85*, 1070 – 1076.
[85] R. Satchi-Fainaro, H. Hailu, J. W. Davies, C. Summerford, R. Duncan, *Bioconjugate Chem.* **2003**, *14*, 797 – 804.
[86] R. Satchi-Fainaro, M. Puder, J. W. Davies, H. T. Tran, D. A. Sampson, A. K. Greene, G. Corfas, J. Folkman, *Nat. Med.* **2004**, *10*, 255 – 261.
[87] R. Satchi-Fainaro, M. Puder, J. W. Davies, H. T. Tran, D. A. Sampson, A. K. Greene, G. Corfas, J. Folkman, *Cancer Cell* **2005**, *7*, 251 – 261.
[88] P. I. Kitov, J. M. Sadowska, G. Mulvey, G. D. Armstrong, H. Ling, N. S. Pannu, R. J. Read, D. Bundle, *Nature* **2000**, *403*, 669 – 672.
[89] J. H. Rao, L. Yan, J. Lahiri, G. M. Whitesides, R. M. Weis, H. S. Warren, *Chem. Biol.* **1999**, *6*, 353 – 359.
[90] J. H. Rao, J. Lahiri, L. Isaacs, R. M. Weis, G. M. Whitesides, *Science* **1998**, *280*, 708 – 711.
[91] J. H. Rao, J. Lahiri, R. M. Weis, G. M. Whitesides, *J. Am. Chem. Soc.* **2000**, *122*, 2698 – 2710.
[92] A. King, I. Philips, K. Kaniga, *J. Antimicrob. Chemother.* **2004**, *53*, 797 – 803.
[93] R. Roy, *Curr. Opin. Struct. Biol.* **1996**, *6*, 692 – 702.
[94] N. Röckendorf, T. Lindhorst, *Top. Curr. Chem.* **2001**, *217*, 98 – 135.
[95] R. Roy, *Glcycotechnol.* **2003**, *15*, 291 – 310.
[96] D. Zanini, R. Roy, *J. Am. Chem. Soc.* **1997**, *119*, 2088 – 2095.
[97] M. Mammen, G. Dahmann, G. M. Whitesides, *J. Med. Chem.* **1995**, *38*, 4179 – 4190.
[98] S. K. Choi, M. Mammen, G. M. Whitesides, *J. Am. Chem. Soc.* **1997**, *119*, 4103 – 4111.

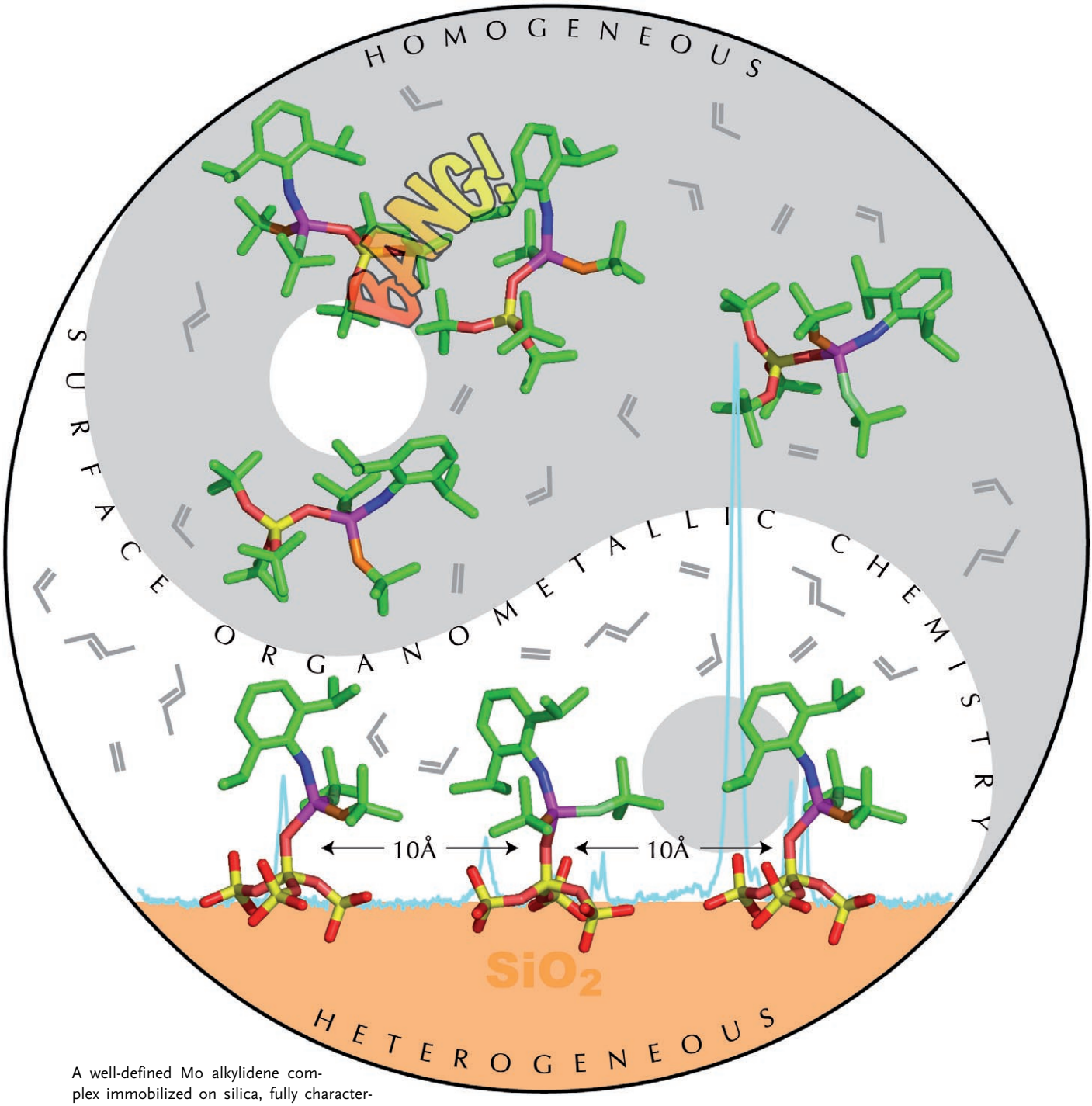
 © 2006 Wiley-VCH Verlag GmbH & Co. KGaA, Weinheim

[99] S. K. Choi, M. Mammen, G. M. Whitesides, *Chem. Biol.* **1996**, *3*, 97 – 104.
[100] For further information, see: http://www.starpharma.com.
[101] S. Shaunak, N. J. Gooderham, R. J. Edwards, N. Payvandi, C. M. Javan, N. Baggett, J. MacDermot, J. N. Weber, D. S. Davies, *Br. J. Pharmacol.* **1994**, *113*, 151 – 158.
[102] J. Hirsh, T. E. Warkentin, S. G. Shaughnessy, S. S. Anand, J. L. Halperin, R. Raschke, C. Granger, E. M. Ohman, J. E. Dalen, *Chest* **2001**, *119*, 64S – 94S.
[103] M. Petitou, P. Ducchaussoy, J.-M. Herbert, G. Duc, M. El Hajji, J.-F. Brannellec, F. Donat, J. Necciari, R. Cariou, J. Bouthier, E. Garrigou, *Semin. Thromb. Hemostasis* **2002**, *28*, 393 – 402.
[104] R. Hopfner, *Curr. Opin. Invest. Drugs* **2002**, *3*, 246 – 251.
[105] J. M. Weiler, R. E. Edens, R. J. Linhardt, D. P. Kapelanski, *J. Immunol.* **1992**, *148*, 3210 – 3215.
[106] J. L. Winkelhake, *Glycoconjugate J.* **1991**, *8*, 381 – 386.
[107] K.-E. Arfors, K. Ley, *J. Lab. Clin. Med.* **1993**, *121*, 201 – 202.
[108] R. J. Linhardt, T. Toida in *Carbohydrates in Drug Design* (Eds.: Z. J. Witczak, K. A. Nieforth), Marcel Dekker, New York, **1997**, pp. 277 – 341.
[109] L. R. Zacharski, D. L. Ornstein, *Thromb. Haemostasis* **1998**, *80*, 10 – 23.
[110] H. Engelberg, *Semin. Thromb. Hemostasis* **1991**, *17*, 5 – 8.
[111] H. G. Garg, B. T. Thompson, C. A. Hales, *Am. J. Physiol.* **2000**, *279*, L779 – L789.
[112] E. DeClercq in *Carbohydrates and Carbohydrate Polymers* (Ed.: M. Yalpani), ATL, Shrewsbury, **1993**, pp. 87 – 100.
[113] M. Petitou, C. A. A. van Boeckel, *Angew. Chem.* **2004**, *116*, 3180 – 3196; *Angew. Chem. Int. Ed.* **2004**, *43*, 3118 – 3133.
[114] L. C. Hsu, *Perfusion* **2001**, *16*, 417 – 428.
[115] G. Franz, D. Pauper, S. Alban, *Proc. Phytochem. Soc. Eur.* **2000**, *44*, 47 – 58.
[116] S. Alban, G. Franz, *Biomacromolecules* **2001**, *2*, 354 – 361.
[117] H. Türk, R. Haag, S. Alban, *Bioconjugate Chem.* **2004**, *15*, 162 – 167.
[118] S. Shaunak, S. Thomas, E. Gianasi, A. Godwin, E. Jones, I. Teo, K. Mireskandari, P. Luthert, R. Duncan, S. Patterson, P. Khaw, S. Brocchini, *Nat. Biotechnol.* **2004**, *22*, 977 – 984.
[119] J. A. Wolff, *Nat. Biotechnol.* **2002**, *20*, 768 – 769.
[120] J. Haensler, F. C. Szoka, *Bioconjugate Chem.* **1993**, *4*, 372 – 379.
[121] O. Boussif, F. Lezoulach, M. A. Zanta, M. D. Mergny, D. Schermann, B. Demeneix, J.-P. Behr, *Proc. Natl. Acad. Sci. USA* **1995**, *92*, 7297 – 7301; J.-P. Behr, *Chimia* **1997**, *51*, 34 – 36.
[122] J. F. Kukowska-Latello, A. U. Bielinska, J. Johnson, R. Spindler, D. A. Tomalia, J. R. Bake, *Proc. Natl. Acad. Sci. USA* **1996**, *93*, 4897 – 4902.
[123] S. Richardson, H. V. Kolbe, R. Duncan, *Int. J. Pharm.* **1999**, *178*, 231 – 243.
[124] D. Joester, M. Losson, R. Pugin, W. Heinzelmann, H. P. Merkle, F. Diederich, *Angew. Chem.* **2003**, *115*, 1524 – 1528; *Angew. Chem. Int. Ed.* **2003**, *42*, 1486 – 1490.
[125] N. Murthy, J. Campbell, N. Fausto, A. S. Hoffman, P. S. Stayton, *Bioconjugate Chem.* **2003**, *14*, 412 – 419.
[126] D. Fischer, *Biomater. Delivery Targeting Proteins Nucleic Acids* **2005**, 295 – 321.
[127] N. D. Sonawane, J. F. C. Szoka, A. S. Verkman, *J. Biol. Chem.* **2003**, *278*, 44826 – 44831.
[128] J.-P. Behr, *Chimia* **1997**, *51*, 27 – 30.
[129] M. X. Tang, C. T. Redemann, F. C. Szoka, *Bioconjugate Chem.* **1996**, *7*, 703 – 714.
[130] A. U. Bielinska, C. Chen, J. Johnson, J. R. Baker, Jr., *Bioconjugate Chem.* **1999**, *10*, 843 – 850.
[131] K. Luger, A. W. Made, R. K. Richmond, D. F. Sargent, T. J. Richmond, *Nature* **1997**, *389*, 251 – 260.
[132] D. A. Tomalia, A. M. Naylor, W. A. Goddard III, *Angew. Chem.* **1990**, *102*, 119 – 156; *Angew. Chem. Int. Ed. Engl.* **1990**, *29*, 138 – 175.
[133] J. Dennig, E. Duncan, *Rev. Mol. Biotechnol.* **2002**, *90*, 339 – 347.
[134] M. Krämer, J.-F. Stumbé, G. Grimm, U. Krüger, B. Kaufmann, M. Weber, R. Haag, *ChemBioChem* **2004**, *5*, 1081 – 1087.
[135] C. Brus, H. Petersen, A. Aigner, F. Czubayko, T. Kissel, *Bioconjugate Chem.* **2004**, *15*, 677 – 684.
[136] R. M. Schiffelers, A. Ansari, J. Xu, Q. Zhou, Q. Tang, G. Storm, G. Molema, P. Y. Lu, P. V. Scaria, M. C. Woodle, *Nucleic Acids Res.* **2004**, *32*, e149.
[137] K. Kataoka, A. Harada, Y. Nagaski, *Adv. Drug Delivery Rev.* **2001**, *47*, 113 – 131.
[138] G. Hoerpel, PhD Thesis, Mainz, **1983**.
[139] G. S. Kwon, M. Naito, K. Kataoka, M. Yokoyama, Y. Sakurai, T. Okano, *Colloids Surf. B* **1994**, *2*, 429 – 434.
[140] Y. Kakizawa, K. Kataoka, *Adv. Drug Delivery Rev.* **2002**, *54*, 203 – 222.
[141] L. Deng, M. Mrksich, G. M. Whitesides, *J. Am. Chem. Soc.* **1996**, *118*, 5136 – 5137.
[142] I. Szleifer, *Curr. Opin. Solid State Mater. Sci.* **1997**, *2*, 337 – 344.
[143] M.-C. Jones, M. Ranger, J.-C. Leroux, *Bioconjugate Chem.* **2003**, *14*, 774 – 781.
[144] K. Kataoka, G. S. Kwon, M. Yokoyama, T. Okano, Y. Sakurai, *J. Controlled Release* **1993**, *24*, 119 – 132.
[145] W.-D. Jang, N. Nishiyama, G.-D. Zhang, A. Harada, D.-L. Jiang, S. Kawauchi, Y. Morimoto, M. Kikuchi, H. Koyama, T. Aida, K. Kataoka, *Angew. Chem.* **2005**, *117*, 423 – 427; *Angew. Chem. Int. Ed.* **2005**, *44*, 419 – 422.
[146] Y. Bae, S. Fukushima, A. Harada, K. Kataoka, *Angew. Chem.* **2003**, *115*, 4788 – 4791; *Angew. Chem. Int. Ed.* **2003**, *42*, 4640 – 4643.
[147] T. Nakanishi, S. Fukushima, K. Okamoto, M. Suzuki, Y. Matsumura, M. Yokoyama, T. Okano, Y. Sakurai, K. Kataoka, *J. Controlled Release* **2001**, *74*, 295 – 302.
[148] M. W. P. L. Baars, E. W. Meijer, *Top. Curr. Chem.* **2000**, *210*, 131 – 182.
[149] L. W. Seymour, Y. Miyamoto, H. Maeda, M. Brereton, J. Strohalm, K. Ulbrich, R. Duncan, *Eur. J. Cancer* **1995**, *31*, 766 – 770.
[150] R. Haag, A. Sunder, J.-F. Stumbé, *J. Am. Chem. Soc.* **2000**, *122*, 2954 – 2955.
[151] T. Ooya, K. P. J. Lee, *Bioconjugate Chem.* **2004**, *15*, 1221 – 1229.
[152] M. W. P. L. Baars, R. Kleppinger, M. H. J. Koch, S.-L. Yeu, E. W. Meijer, *Angew. Chem.* **2000**, *112*, 1341 – 1344; *Angew. Chem. Int. Ed.* **2000**, *39*, 1285 – 1288.
[153] C. Kojima, K. Kono, K. Maruyama, T. Takagishi, *Bioconjugate Chem.* **2000**, *11*, 910 – 917.
[154] C. Kojima, Y. Haba, T. Fukui, K. Kono, T. Takagishi, *Macromolecules* **2003**, *36*, 2183 – 2186.
[155] M. A. Oar, J. M. Serin, W. R. Dichtel, J. M. J. Fréchet, T. Y. Ohulchanskyy, P. N. Prasad, *Chem. Mater.* **2005**, *17*, 2267 – 2275.
[156] S. Xu, M. Krämer, R. Haag, *J. Drug Targeting* **2006**, in press.
[157] J. F. G. A. Jansen, E. W. Meijer, *J. Am. Chem. Soc.* **1995**, *117*, 4417 – 4418.
[158] G. Pistolis, A. Malliaris, D. Tsiourvas, C. M. Paleos, *Chem. Eur. J.* **1999**, *5*, 1440 – 1444.
[159] Z. Sideratou, D. Tsiourvas, C. M. Paleos, *Langmuir* **2000**, *16*, 1766 – 1769.
[160] M. Krämer, J.-F. Stumbé, H. Türk, S. Krause, A. Komp, L. Delineau, S. Prokhorova, H. Kautz, R. Haag, *Angew. Chem.* **2002**, *114*, 4426 – 4431; *Angew. Chem. Int. Ed.* **2002**, *41*, 4252 – 4256.
[161] H. Ringsdorf, *Angew. Chem.* **2004**, *116*, 1082 – 1095; *Angew. Chem. Int. Ed.* **2004**, *43*, 1064 – 1076.
[162] Note added in proof: A recent special issue deals with biomedical applications of dendrimers (*Adv. Drug Delivery Rev.* **2005**, *57*, 2101–2286).

 © 2006 Wiley-VCH Verlag GmbH & Co. KGaA, Weinheim

Communications

DOI: 10.1002/anie.200503205



A well-defined Mo alkylidene complex immobilized on silica, fully characterized by solid-state NMR spectroscopy, leads to better performances in olefin metathesis than the corresponding nonsupported siloxy-containing catalysts, probably because of the isolation of the active sites on a supported system, which prevents decomposition through dimerization. For more details, see the Communication by C. Copéret and coworkers on the following pages.

WILEY InterScience DISCOVER SOMETHING GREAT
© 2006 Wiley-VCH Verlag GmbH & Co. KGaA, Weinheim

Alkene Metathesis

DOI: 10.1002/anie.200503205

Surface versus Molecular Siloxy Ligands in Well-Defined Olefin Metathesis Catalysts: [{(RO)$_3$SiO}Mo(=NAr)(=CH*t*Bu)(CH$_2$*t*Bu)]**

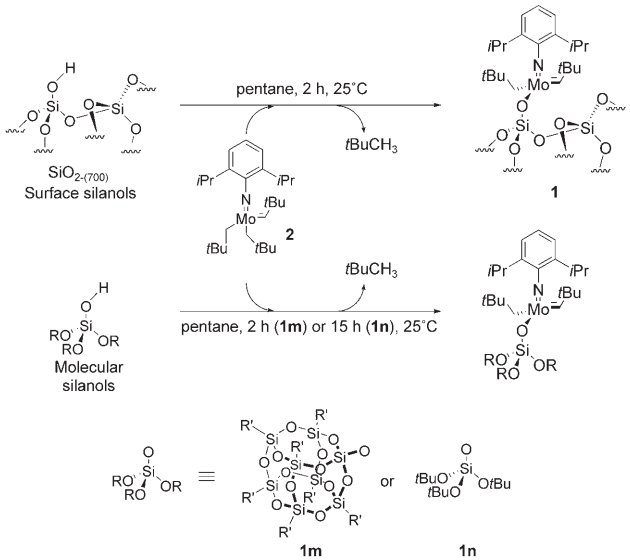
Frédéric Blanc, Christophe Copéret, Jean Thivolle-Cazat, Jean-Marie Basset,* Anne Lesage, Lyndon Emsley,* Amritanshu Sinha, and Richard R. Schrock**

Dedicated to Professor Ei-ichi Negishi on the occasion of his 70th birthday

We report herein the synthesis and characterization of [(≡SiO)Mo(=NAr)(=CH*t*Bu)(CH$_2$*t*Bu)] (**1**), a well-defined heterogeneous catalyst for olefin metathesis, and its molecular equivalents **1m** and **1n**.

We recently reported the preparation and characterization of highly active heterogeneous olefin metathesis catalysts [(≡SiO)Re(≡C*t*Bu)(=CH*t*Bu)(CH$_2$*t*Bu)].[1–3] This system has shown better activity than the best Re-based homogeneous and heterogeneous catalysts and comparable initial activities to Mo- and W-based homogeneous olefin metathesis catalysts. In homogeneous catalysis, well-defined Mo complexes such as [(R$_{F6}$O)$_2$Mo(=NAr)(=CH*t*Bu)][4–7] (R$_{F6}$ = (CF$_3$)$_2$(CH$_3$)C) are much better catalysts than their Re equivalents [(R$_{F6}$O)$_2$Re(≡C*t*Bu)(=CH*t*Bu)].[8,9] However, preparing a supported equivalent to [(R$_{F6}$O)$_2$Mo(=NAr)(=CH*t*Bu)] has remained a challenge.[10–15] In surface organometallic chemistry,[16] the formation of a Mo alkylidene complex requires the use of well-defined Mo alkyl alkylidene molecular precursors, which have become available only recently as [Mo(=NAr)(=CH*t*Bu)(CH$_2$*t*Bu)$_2$] (**2**; Ar = 2,6-diisopropylphenyl).[17–19] Since the surface of silica partially dehydroxylated at 700 °C (SiO$_{2\text{-}(700)}$) can be compared to a bulky monodentate ligand,[16] we investigated the reaction of **2** with SiO$_{2\text{-}(700)}$ in order to generate a well-defined supported olefin metathesis catalyst.

When immersed in a solution of **2** in pentane, a SiO$_{2\text{-}(700)}$ disk immediately turned yellow. After 2 h, the disk was washed three times with pentane, dried under vacuum for 1 h at 25 °C, and analyzed by IR spectroscopy. The IR peaks associated with the surface silanol groups at 3747 cm^{-1} had disappeared while new IR bands associated with ν(C–H) and δ(C–H) of hydrocarbyl ligands appeared in the regions of 3000–2700 and 1500–1350 cm^{-1}, respectively (see Supporting Information). Furthermore, the IR bands at 3065 and 3027 cm^{-1} are attributed to ν(=C–H) of the arylimido group. During these steps the surface silanol groups reacted, as their corresponding IR bands at 3747 cm^{-1} did not reappear. Preparation of larger quantities of this solid was performed by using calibrated silica (40–60 mesh) partially dehydroxylated at 700 °C. When a mixture of SiO$_{2\text{-}(700)}$ (0.26 mmol g^{-1} SiOH) and **2** in pentane was stirred for 2 h at 25 °C, surface organometallic complex **1** was formed together with 1 equivalent of 2,2-dimethylpropane (Scheme 1). The yellow solid thus obtained contains 1.7–2.1 wt % of Mo, which corresponds to 0.17–0.21 mmol of Mo per gram of solids, in agreement with consumption of most of the surface silanol groups (70–80 %). Moreover, the materials contain on average 23 ± 3 C and 1.0 ± 0.3 N per grafted Mo (as obtained from elemental analysis), consistent with the proposed structure **1**, for which 22 C/Mo and 1 N/Mo are expected. Furthermore, the ^{1}H magic-angle spinning (MAS) solid-state NMR spectrum of **1** (Figure 1 a) displays distinct signals at δ = 11.7 (=C*H*t Bu, 1 H), 6.8 (C$_{sp^2}$–H, 3 H), 3.5 (C*H*Me$_2$, 2 H), and



Scheme 1. Formation of surface complex **1** and its homogeneous analogues **1m** and **1n** (R′ = *c*-C$_5$H$_9$).

[*] F. Blanc, Dr. C. Copéret, Dr. J. Thivolle-Cazat, Dr. J.-M. Basset
Laboratoire de Chimie Organométallique de Surface
UMR 9986 CNRS—ESCPE Lyon
43 bd du 11 Novembre 1918, 69616 Villeurbanne Cedex (France)
Fax: (+33) 4-7243-1795
E-mail: coperet@cpe.fr
basset@cpe.fr
Dr. A. Lesage, Prof. Dr. L. Emsley
Laboratoire de Chimie, UMR 5532 CNRS—ENS Lyon
Laboratoire de Recherche Conventionné du CEA (23V/DSM 0432)
Ecole Normale Supérieure de Lyon
46 Allée d'Italie, 69364 Lyon Cedex 07 (France)
Fax: (+33) 4-7272-8483
E-mail: Lyndon.Emsley@ens-lyon.fr
A. Sinha, Prof. Dr. R. R. Schrock
Department of Chemistry
Massachussetts Institute of Technology
Cambridge, MA 02139 (USA)
Fax: (+1) 617-2537670
E-mail: rrs@mit.edu

[**] F.B. is grateful to the French Ministry of Education, Research, and Technology (MENRT) for a predoctoral fellowship. We thank B. Fenet for recording solution-state ^{29}Si{^{1}H} NMR spectra. We are also indebted to the CNRS, ESCPE Lyon, and the National Science Foundation (R.R.S.) for financial support.

Supporting information for this article is available on the WWW under http://www.angewandte.org or from the author.

 © 2006 Wiley-VCH Verlag GmbH & Co. KGaA, Weinheim

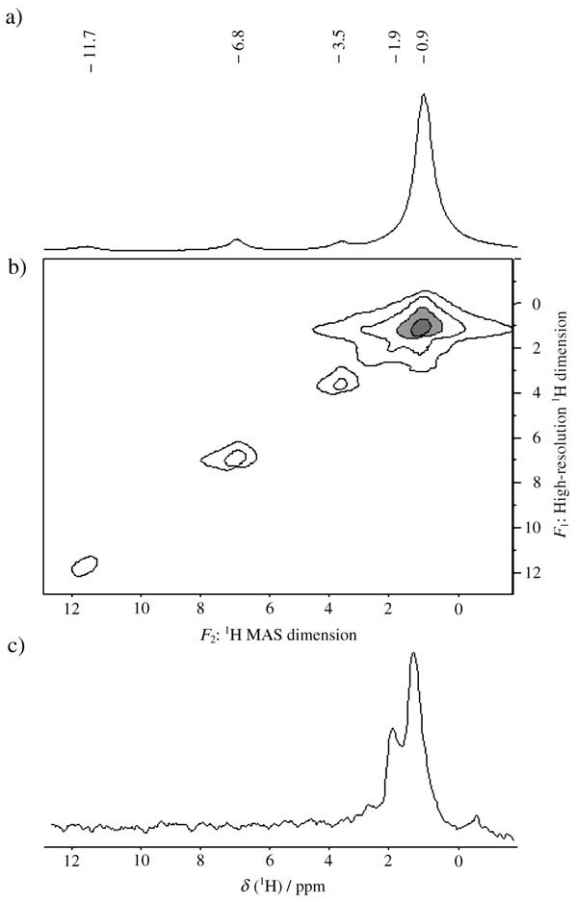


Figure 1. Solid-state NMR spectra of **1**. a) ^{1}H NMR spectrum acquired at a MAS frequency of $\nu_R = 12.5$ kHz with eight scans and a recycle delay of 2 s. The ^{1}H rf field was 83 kHz. b) 2D ^{1}H–^{1}H NMR spectrum recorded at a MAS frequency of $\nu_R = 10.0$ kHz with the DUMBO-1 homonuclear dipolar decoupling sequence[20] in t_1. c) Trace parallel to F_1 extracted along F_2 at $\delta_H = 1.9$ ppm.

0.9 ppm (CH_3, 30 H). The signal of the methylene protons in the position α to Mo is only observed as a shoulder centered around $\delta = 1.9$ ppm. The presence of relatively sharp signals for a solid-state NMR spectrum ($\Delta\nu_{1/2} = 390$ Hz) shows that ^{1}H–^{1}H dipolar coupling is weak, the ligands undergo rapid restricted motion, and the species are dispersed. A 2D ^{1}H–^{1}H homonuclear correlation NMR spectrum recorded with the DUMBO-1 homonuclear dipolar decoupling sequence[20] in t_1 resulted in a slight improvement in the line width of the ^{1}H NMR spectrum ($\Delta\nu_{1/2} =$ 260 Hz; Figure 1 b), in contrast to the much larger effect that is observed for bulk materials. This results, however, in a better resolution of the signal at $\delta = 1.9$ ppm (Figure 1 c).

The ^{13}C cross-polarization (CP) MAS spectrum contains 11 resolved peaks (see Figure 2 a and Supporting Information), which can be tentatively assigned as follows: $\delta = 22$ ($CH(CH_3)_2$), 29 ($=CHC(CH_3)_3$), 31 ($CH_2C(CH_3)_3$), 36 (CH_2CMe_3), 46 ($=CHCMe_3$), 56 (CH_2tBu), 122 (C_{para}), 126 (C_{meta}), 145 (C_{ortho}), 153 (C_{ipso}), and 279 ppm ($=CHtBu$); the signal of the alkylidene carbon atom at $\delta =$ 279 ppm is barely observable. [(≡SiO)Mo(=NAr)(=*CH*t*Bu)-(*CH_2*t*Bu)] (**1***), 33 % ^{13}C-labeled on the carbon atom α to Mo, unambiguously displays signals for both the methine (Mo=*CH*t*Bu) and methylene carbon atoms (Mo−*CH_2*t*Bu) at $\delta = 279$ and 56 ppm, respectively (Figure 2 a). Furthermore, using the 2D ^{1}H–^{13}C dipolar HETCOR NMR method[21,22] (see Figure 2 b and Supporting Information) with different contact times (1 and 5 ms) allowed resolution and assignment of all signals of the ^{13}C spectrum (see Supporting Information).[22,23] The carbene (=*CH*t*Bu) and methylene (*CH_2*t*Bu) signals gave correlations (δ_H [ppm] in F_1; δ_C [ppm] in F_2) at (11.7; 279) and (1.9; 56), respectively. A cross-peak is observed between the proton at $\delta = 3.5$ ppm (C*H*Me_2) and the carbon atom at $\delta = 29$ ppm, showing that *C*HMe_2 (not observed before) also appears at this chemical shift.

The corresponding molecular complexes **1m** and **1n**, with a molecular monosiloxy equivalent, were prepared by using $(RO)_3SiOH$ in place of a siloxy group of the silica surface (Scheme 1).[24–26] The reaction of **2** with 1 equivalent of [(*c*-$C_5H_9)_7Si_7O_{12}SiOH$] in C_6D_6 or pentane for 2 h at 25 °C quantitatively gave [(*c*-$C_5H_9)_7Si_7O_{12}SiO$)Mo(=NAr)(=CH*t*Bu)(CH_2*t*Bu)] (**1m**) and *t*BuCH_3. The closeness of the NMR data of **1m** to those of **1** fully supports the assignments (see Supporting Information). Complex **1m** shows resonances at $\delta = 12.05$ and 281.2 ppm ($^1J_{CH} = 110$ Hz) for the alkylidene ligand in the ^{1}H and ^{13}C NMR spectra, respectively, which is

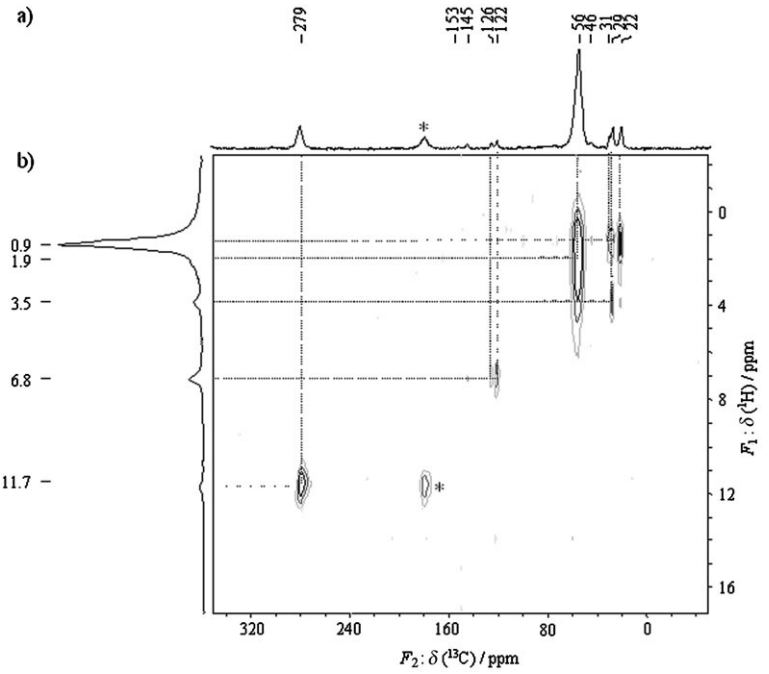
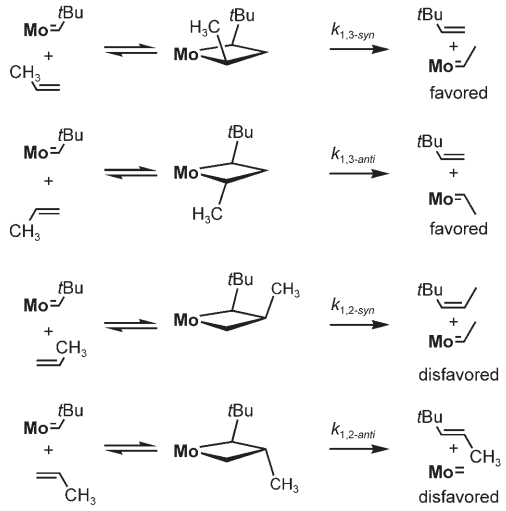


Figure 2. Solid-state NMR spectra acquired at a MAS frequency of $\nu_R = 12.5$ kHz. a) ^{13}C CP MAS NMR spectrum of **1*** recorded with TPPM-15[31] ^{1}H decoupling at $\nu_1^H = 83$ kHz with 56 000 scans. The recycle delay was set to 1 s, and the contact time for the CP step was 1 ms. An exponential line broadening of 80 Hz was applied before Fourier transformation. b) 2D ^{1}H–^{13}C dipolar HETCOR solid-state NMR spectrum of **1*** with a contact time of 1 ms (short-range HETCOR). A total of 32 t_1 were collected with 4096 scans each. Left: Projection along F_2. Asterisks denote spinning side bands.

 © 2006 Wiley-VCH Verlag GmbH & Co. KGaA, Weinheim

consistent with a *syn*-alkylidene complex.[17] A similar reaction carried out over 15 h between **2** and [(tBuO)$_3$SiOH] yielded [{(tBuO)$_3$SiO}Mo(=NAr)(=CHtBu)(CH$_2$$t$Bu)] (**1n**), which displayed similar NMR data and whose X-ray crystal structure (not shown) showed it to be the expected *syn* isomer.

When **1** is contacted with 1350 equivalents of propene at 25 °C (batch reactor), equilibrium is reached within 20 min (around 30% conversion, *E*/*Z*-butene ratio = 2.6) with a turnover frequency (TOF) of 1.0 mol (mol$_{Mo}$)$^{-1}$ s^{-1}, which is four times faster than with [(≡SiO)Re(≡CtBu)(=CHtBu)-(CH$_2$$t$Bu)] (TOF = 0.25 mol (mol$_{Re}$)$^{-1}$ s^{-1}).[1,2] Moreover, roughly 0.7 equivalents of a 2.7:1 mixture of 3,3-dimethylbutene and 4,4-dimethyl-2-pentene is formed, as previously observed for [(≡SiO)Re(≡CtBu)(=CHtBu)(CH$_2$$t$Bu)],[1,2] and shows that initiation is almost quantitative, in agreement with a well-defined system. Moreover, the ratio of cross-metathesis products is in full agreement with the following model: the favored pathway involves reaction intermediates that minimize the interaction between the alkyl substituents (Scheme 2).[27]



Scheme 2. Application of the metallacyclobutane model propene metathesis to explain the favored $k_{1,3}$ pathway.

Moreover, the self-metathesis of 0.5 M solutions of 1-octene and ethyl oleate in toluene in the presence of 1% of **1** gives the equilibrated mixture in 10 and 60 min, respectively (Table 1). The respective initial TOFs are 0.06 and 0.04 mol (mol$_{Mo}$)$^{-1}$ s^{-1}, which is very close to those obtained for [(≡SiO)Re(≡CtBu)(=CHtBu)(CH$_2$$t$Bu)].[28] The initial rates with the corresponding molecular complex **1m** are similar, but the reaction times needed to reach the same conversion (thermodynamic equilibrium) are much longer, which shows that, in this case, decomposition is faster. On the other hand, the quasi-inactivity of molecular complex **2** illustrates the activating effect of the siloxyl group.[3,29]

In conclusion, we have shown that the molecular and surface complexes **1** and **1m** are electronically very similar in terms of both their comparable NMR data and initial TOFs in olefin metathesis. Nonetheless, the supported catalyst has a longer lifetime under catalytic conditions, which shows that the effect of active-site isolation prevents some deactivation pathways such as dimerization of reactive intermediates.[30] Moreover, the formation of about 0.7 equivalents of cross-metathesis product shows that most of the surface complex generates the active species, in agreement with a well-defined heterogeneous catalyst.

Table 1: Olefin metathesis activity at room temperature for **1**, **1m**, and **2**.[a]

Olefin	**1**		**1m**		**2**	
	TOF [s^{-1}][b]	t [h][c]	TOF [s^{-1}][b]	t [h][c]	TOF [s^{-1}][b]	t [h][c]
1-Octene	0.06	1/6	0.06	1	0.02	48[d]
Ethyl oleate	0.04	1	0.03	24	0.005	–[e]

[a] Experimental conditions: 1% Mo, 25 °C, 0.5 M solution of olefin in toluene under Ar atmosphere. All reactions were monitored by gas chromatography. [b] Initial TOF measured after 5 min of reaction and expressed in moles of substrate per mole of Mo per second. [c] Time to reach equilibrium (around 50% conversion). [d] 40% conversion. [e] Deactivation after 2% conversion.

Experimental Section

See Supporting Information for full experimental procedures, the IR and ^{13}C CP MAS NMR spectra of **1**, and the ^{13}C CP MAS NMR spectra, 2D ^{1}H–^{13}C dipolar HETCOR spectra with 1- and 5-ms contact times, and a full assignment of **1***.

Received: September 8, 2005
Published online: January 16, 2006

Keywords: carbene ligands · heterogeneous catalysis · metathesis · molybdenum

[1] M. Chabanas, A. Baudouin, C. Copéret, J.-M. Basset, *J. Am. Chem. Soc.* **2001**, *123*, 2062.
[2] C. Copéret, *New J. Chem.* **2004**, *28*, 1.
[3] X. Solans-Monfort, E. Clot, C. Copéret, O. Eisenstein, *J. Am. Chem. Soc.* **2005**, *127*, 14015.
[4] R. R. Schrock, *Acc. Chem. Res.* **1986**, *19*, 342.
[5] J. S. Murdzek, R. R. Schrock, *Organometallics* **1987**, *6*, 1373.
[6] R. R. Schrock, *Chem. Rev.* **2002**, *102*, 145.
[7] F. J. Feher, T. L. Tajima, *J. Am. Chem. Soc.* **1994**, *116*, 2145.
[8] R. Toreki, R. R. Schrock, *J. Am. Chem. Soc.* **1990**, *112*, 2448.
[9] R. Toreki, G. A. Vaughan, R. R. Schrock, W. M. Davis, *J. Am. Chem. Soc.* **1993**, *115*, 127.
[10] W. A. Herrmann, A. W. Stumpt, T. Priermeier, S. Bogdanović, V. Dufaud, J.-M. Basset, *Angew. Chem.* **1996**, *108*, 2978; *Angew. Chem. Int. Ed. Engl.* **1996**, *36*, 2803.
[11] F. Blanc, M. Chabanas, C. Copéret, B. Fenet, E. Herdtweck, *J. Organometal. Chem.* **2005**, *690*, 5014.
[12] K. C. Hultzsch, J. A. Jernelius, A. H. Hoveyda, R. R. Schrock, *Angew. Chem.* **2002**, *114*, 609; *Angew. Chem. Int. Ed.* **2002**, *41*, 589.
[13] R. M. Kroell, N. Schuler, S. Lubbad, M. R. Buchmeiser, *Chem. Commun.* **2003**, 2742.
[14] S. J. Dolman, K. C. Hultzsch, F. Pezet, X. Teng, A. H. Hoveyda, R. R. Schrock, *J. Am. Chem. Soc.* **2004**, *126*, 10945.
[15] M. Mayr, D. Wang, R. Kroell, N. Schuler, S. Pruehs, A. Fuerstner, M. R. Buchmeiser, *Adv. Synth. Catal.* **2005**, *347*, 484.

 © 2006 Wiley-VCH Verlag GmbH & Co. KGaA, Weinheim

[16] C. Copéret, M. Chabanas, R. Petroff Saint-Arroman, J.-M. Basset, *Angew. Chem.* **2003**, *115*, 164; *Angew. Chem. Int. Ed.* **2003**, *42*, 156.
[17] A. Sinha, R. R. Schrock, *Organometallics* **2004**, *23*, 1643.
[18] D. Ehrenfeld, J. Kress, B. D. Moore, J. A. Osborn, G. Schoettel, *J. Chem. Soc. Chem. Commun.* **1987**, 129.
[19] G. Schoettel, J. Kress, J. A. Osborn, *J. Chem. Soc. Chem. Commun.* **1989**, 1062.
[20] A. Lesage, D. Sakellariou, S. Hediger, B. Elena, P. Charmont, S. Steuernagel, L. Emsley, *J. Magn. Reson.* **2003**, *163*, 105.
[21] S. Hediger, A. Lesage, L. Emsley, *Macromolecules* **2002**, *35*, 5078.
[22] M. Chabanas, A. Baudouin, C. Copéret, J.-M. Basset, W. Lukens, A. Lesage, S. Hediger, L. Emsley, *J. Am. Chem. Soc.* **2003**, *125*, 492.
[23] R. Petroff Saint-Arroman, M. Chabanas, A. Baudouin, C. Copéret, J.-M. Basset, A. Lesage, L. Emsley, *J. Am. Chem. Soc.* **2001**, *123*, 3820.
[24] F. J. Feher, T. A. Budzichowski, *Polyhedron* **1995**, *14*, 3239.
[25] H. C. L. Abbenhuis, *Chem. Eur. J.* **2000**, *6*, 25.
[26] R. Duchateau, *Chem. Rev.* **2002**, *102*, 3525.
[27] J. L. Bilhou, J. M. Basset, R. Mutin, W. F. Graydon, *J. Am. Chem. Soc.* **1977**, *99*, 4083.
[28] M. Chabanas, C. Copéret, J.-M. Basset, *Chem. Eur. J.* **2003**, *9*, 971.
[29] D. G. H. Ballard, *Adv. Catal.* **1973**, *23*, 263.
[30] L. P. H. Lopez, R. R. Schrock, *J. Am. Chem. Soc.* **2004**, *126*, 9526.
[31] S. Hediger, B. H. Meier, N. D. Kurur, G. Bodenhausen, R. R. Ernst, *Chem. Phys. Lett.* **1994**, *223*, 283.

 © 2006 Wiley-VCH Verlag GmbH & Co. KGaA, Weinheim

Magnetic Nanowires

DOI: 10.1002/anie.200503486

Magnetic-Dipolar-Interaction-Induced Self-Assembly Affords Wires of Hollow Nanocrystals of Cobalt Selenide**

*Jinhao Gao, Bei Zhang, Xixiang Zhang, and Bing Xu**

Self-assembly, an attractive and practical methodology, allows the formation of a wide range of nanostructures for promising applications—for example, nanoparticle arrays for new optical band-gap materials[1] or high-density magnetic recording media,[2] self-assembled monolayers (SAM) for nanometer-thick films on a variety of substrates,[3] and nanofibers of self-organized small molecules or oligopeptides for drug delivery and tissue engineering.[4] Hydrogen bonding and/or van der Waals interactions are usually the driving forces that result in self-assembly at the nanoscale.[5] Despite extensive investigation, it is still difficult to control and predict the nanostructures resulting from these two types of forces. Although several recent reports have shown that magnetic dipolar interactions induce rather predictable nanoassemblies,[6,7] methods for maintaining these assemblies when the magnetic force decreases or vanishes have been less thoroughly investigated. Therefore, we decided to use the magnetic dipoles inherently associated with magnetic nanoparticles[8] to form 1D assemblies of hollow nanocrystals of semiconductors.[9]

We chose to make wires of hollow nanocrystals of $CoSe_2$ to demonstrate the concept, because 1) the isolation of a nanonecklace of cobalt nanocrystals on a substrate from a dispersion after removal of the solvent[7] indicated that magnetic dipolar interactions are sufficient to maintain 1D assemblies of nanocrystals in solution; 2) the recently reported formation of hollow CoSe nanocrystals from cobalt nanocrystals through the Kirkendall effect[10] suggested that a similar process could be used to generate hollow $CoSe_2$ nanocrystals from 1D assemblies of cobalt nanocrystals; 3) hollow nanostructures have received considerable attention because they exhibit properties that differ from their solid counterparts;[11] and 4) nanowires of hollow nanocrystals of $CoSe_2$ are unknown. Herein, we show that when their sizes reach approximately 20 nm cobalt nanocrystals self-assemble into wires in solution at temperatures as high as 455 K. Through the nanoscale Kirkendall effect,[10,12] wires of hollow $CoSe_2$ nanocrystals form without loss of the preassembled nanostructure induced by the magnetic dipolar interactions of the cobalt nanocrystals. In control experiments, when the size of the cobalt nanocrystals is 6 nm, or when 20-nm cobalt nanocrystals are in an alternating magnetic field, no wires of hollow $CoSe_2$ nanocrystals form. These observations confirm that the magnetic interaction plays a key role in the formation of the nanowires of hollow $CoSe_2$ crystals. Several types of ferromagnetic metallic nanocrystals (iron, cobalt, nickel, FePt, or CoPt) can be prepared readily, and their self-assembly depends on the magnetic dipolar interactions of particles of a certain size. Therefore, the method shown herein should be a general route to 1D assemblies of hollow nanocrystals.

The synthesis of wires of hollow $CoSe_2$ nanocrystals is easy and straightforward. Cobalt nanocrystals of approximately 20 nm in diameter were prepared according to a modified literature procedure[13] and then dispersed in a solvent (for example, 1,2-dichlorobenzene) by using trioctylphosphine oxide (TOPO) as a surfactant. The injection of a dichlorobenzene solution of selenium into the dispersion of cobalt nanocrystals under reflux at 455 K resulted in a black dispersion of $CoSe_2$ nanocrystals after approximately 30 min. Transmission electron microscope (TEM) images reveal that the $CoSe_2$ nanocrystals form wires of intercon-

[*] J. Gao, Prof. B. Xu
Department of Chemistry
The Hong Kong University of Science & Technology
Clear Water Bay, Hong Kong (China)
Fax: (+852) 2358-1594
E-mail: chbingxu@ust.hk
B. Zhang, Prof. X. Zhang
Department of Physics
The Hong Kong University of Science & Technology
Clear Water Bay, Hong Kong (China)

[**] This work was partially supported by RGC (Hong Kong) and EHIA (HKUST).

Supporting information for this article is available on the WWW under http://www.angewandte.org or from the author.

InterScience
© 2006 Wiley-VCH Verlag GmbH & Co. KGaA, Weinheim

nected hollow spheres (Figure 1a). High-resolution TEM images (inset, Figure 1a) and analysis of the electron diffraction pattern of the sample suggest that these hollow spheres are crystalline. Scanning electron microscope (SEM)

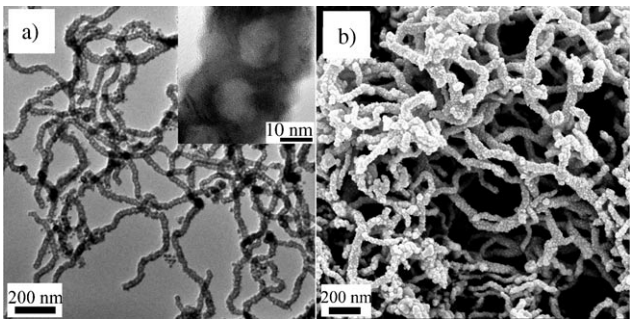


Figure 1. a) TEM image (inset: HR-TEM image), and b) SEM image of the wires of hollow $CoSe_2$ nanocrystals.

images indicate that the wires of hollow $CoSe_2$ nanocrystals are the major nanostructure formed (Figure 1b). This observation suggests that the wires form in high yield, which may allow large-scale production. The X-ray diffraction (XRD) pattern of the $CoSe_2$ nanocrystals (Figure 2) matches that of

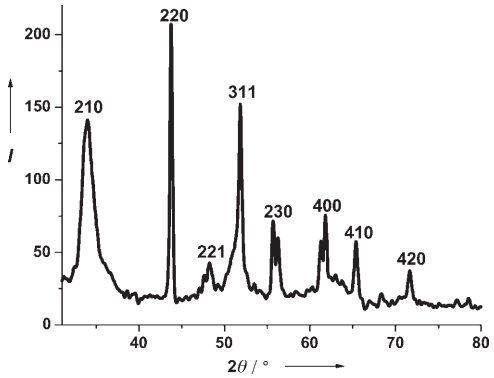
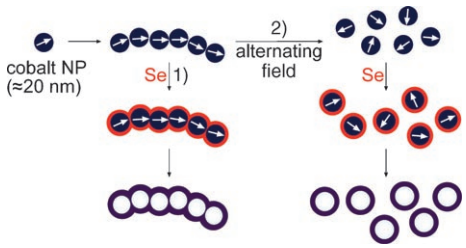


Figure 2. XRD pattern of the wires of hollow $CoSe_2$ nanocrystals.

the primitive cubic phase of $CoSe_2$ (Powder Diffraction File #090234). The X-ray photoelectron spectrum (XPS) of the $CoSe_2$ nanocrystals shows peaks at 778.7 and 54.4 eV, corresponding to the binding energies of the cobalt $2p_{3/2}$ and selenium $3d_{5/2}$ states.[14] In addition, X-ray fluorescence (XRF) analysis indicates that the ratio of Co:Se in the sample is approximately 1:1.80, which suggests that other cobalt selenide phases (for example, CoSe and Co_3Se_4) may be present in small amounts.[15]

Additional TEM analysis of the dispersion of cobalt nanocrystals prior to the addition of selenium showed that the cobalt nanocrystals assemble into wires (see Supporting Information), which are similar to the assemblies of hollow $CoSe_2$ nanocrystals. We also observed a small amount of necklace structures in both the samples of cobalt nanocrystals and hollow $CoSe_2$ nanocrystals (see Supporting Information). Furthermore, the sizes and alignment of the holes of the hollow $CoSe_2$ nanocrystals match with the sizes and alignment of the cobalt nanocrystals in the 1D assembly. These results lead to the proposed mechanism for the formation of wires of hollow $CoSe_2$ nanocrystals (Scheme 1). Each cobalt nano-



Scheme 1. Formation of hollow $CoSe_2$ nanocrystals from cobalt nanoparticles (NP) in the 1) absence and 2) presence of an alternating magnetic field.

crystal behaves as a single magnetic dipole, and the cobalt nanocrystals form chains or necklaces in solution because of strong magnetic dipolar interactions. After being added into the dispersion, selenium reacts with cobalt, and a thin layer of selenium or $CoSe_2$ grows around the wires of cobalt nanocrystals, without disintegration of the wires. Further reaction between selenium and cobalt through the nanoscale Kirkendall process maintains the preassembled nanostructures and affords a 1D assembly of hollow $CoSe_2$ nanocrystals. According to this mechanism, disruption (process 2) in Scheme 1) or reduction of the magnetic dipolar interactions before the addition of selenium should prevent the formation of the wires of hollow $CoSe_2$ nanocrystals. To illustrate this point, we conducted the two following control experiments.

First, we chose cobalt nanocrystals with a smaller size (6 nm) as starting materials, because they have weaker magnetic dipolar interactions than cobalt nanocrystals with diameters of 20 nm. Under the conditions described above, the reaction between 6-nm cobalt nanocrystals and selenium only affords monodispersed hollow nanocrystals (Figure 3a). No 1D assemblies of nanocrystals are observed, probably because the magnetic dipolar interactions between these small cobalt nanocrystals are too weak to form chain or necklace nanostructures at 455 K. Second, we synthesized hollow $CoSe_2$ nanocrystals in an alternating magnetic field,

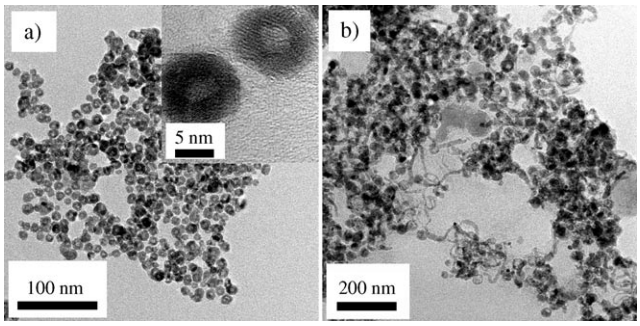


Figure 3. a) TEM image (inset: HR-TEM image) of the monodispersed hollow $CoSe_2$ nanospheres synthesized from 6-nm cobalt nanocrystals; b) TEM image of the hollow $CoSe_2$ nanostructures synthesized in an alternating magnetic field.

 © 2006 Wiley-VCH Verlag GmbH & Co. KGaA, Weinheim

$B(t) = B_0 \sin(\omega t)$, where $B_0 = 35$ G and $\omega = 2\pi f$ with $f = 50$ Hz, generated by a Helmholtz coil. In this field, the reaction of 20-nm cobalt nanocrystals with selenium gives only a small number of individual hollow nanocrystals of $CoSe_2$, in addition to a small number of selenium nanowires (Figure 3b).[16] This result is consistent with process 2) proposed in Scheme 1. Because of the head-to-tail arrangement of the magnetic dipoles of the nanoparticles, it is difficult to "switch" all of the dipoles at the same time. The breaking of the chain is due to the vibrational magnetic torque applied, which disrupts the dipolar interactions between the particles. Once the chain is broken, the alternating magnetic torque causes the particles to rotate and prevents them from reconnecting. This mechanism agrees with our observations. These two experiments confirm that magnetic dipolar interactions play a key role in the formation of 1D assemblies of hollow $CoSe_2$ nanocrystals. The use of magnetic dipolar interactions, which can be easily modified through the application of an alternating magnetic field, in the formation of nanostructures provides a useful alternative to the use of electronic dipolar interactions (as applied in the assembly of nanowires of CdSe[5] and PbTe[17]).

To establish the generality of this procedure, we replaced selenium by sulfur or tellurium in the reaction with 20-nm cobalt nanocrystals. As shown in Figure 4, we obtained wires

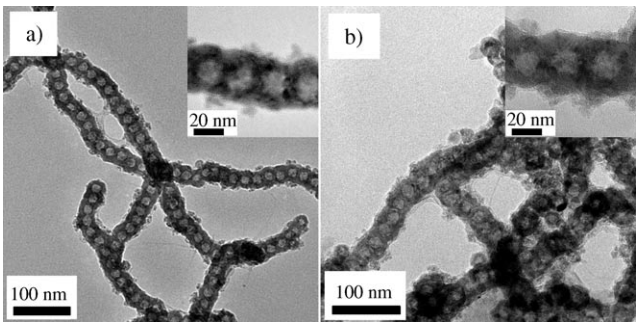


Figure 4. TEM images (insets: HR-TEM images) of the wires of hollow nanocrystals of a) Co_3S_4 and b) CoTe.

of hollow Co_3S_4 and CoTe nanocrystals, which are similar in morphology to the hollow $CoSe_2$ nanocrystals. The XPS of the Co_3S_4 wires shows peaks at 778.9 and 162.2 eV, corresponding to the binding energies of the cobalt $2p_{3/2}$ and sulfur 2p states. XRF analysis indicates that the ratio of Co:S in the sample is 1:1.32, nearly 3:4, which agrees with the ratios of the corresponding precursors. For the CoTe sample, XRF analysis indicates that the ratio of Co:Te is approximately 1:1 (see Supporting Information).

Magnetization measurements indicate that the wires of hollow $CoSe_2$ nanocrystals are ferromagnetic. As shown in Figure 5, the field-dependent magnetization ($M(H)$) of the wires of hollow $CoSe_2$ nanocrystals at 50 K displays hysteresis typical of a ferromagnet. The coercivity (H_c) of the wires of hollow $CoSe_2$ nanocrystals is approximately 600 Oe, roughly half that of the 20-nm cobalt nanocrystals (approximately 1100 Oe; see Supporting Information). Standard zero-field cooling (ZFC) and field cooling (FC) temperature-dependent magnetization ($M(T)$) measurements indicate bulk ferromagnetism. Similar $M(T)$ curves were observed for 20-nm cobalt nanocrystals (see Supporting Information). The magnetic behavior of the wires of hollow $CoSe_2$ nanocrystals suggests that these nanocrystals may actually form a polycrystalline wire with holes. The small peak at 14 K in the ZFC curve (Figure 5, inset) could be due to the unblocking of superparamagnetic $CoSe_2$ nanocrystals, which is evidenced by the FC data from 5 to 30 K. To exclude the possibility that the ferromagnetism solely originates from residual cobalt nanocrystals, we measured the magnetization of the wires of hollow $CoSe_2$ nanocrystals in a 1000-Oe field from 5 to 674 K (Figure 6). We used a SQUID magnetometer to collect the

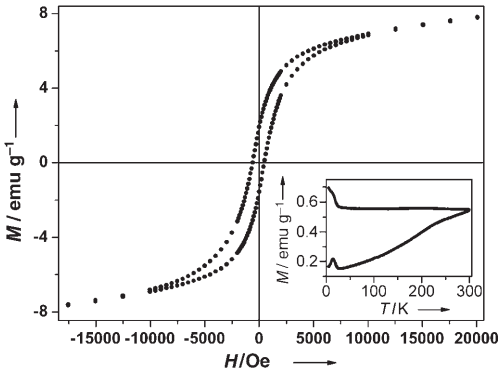


Figure 5. The hysteresis loop for the wires of hollow $CoSe_2$ nanocrystals at 50 K (inset: temperature-dependence of the ZFC (lower) and FC (upper) magnetization of the wires of hollow $CoSe_2$ nanocrystals in a magnetic field of 100 Oe).

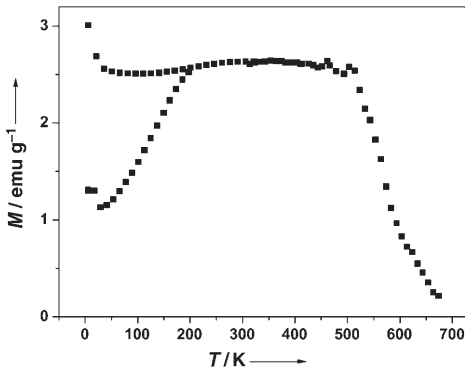


Figure 6. Temperature-dependence of the ZFC (lower) and FC (upper) magnetization of the wires of hollow $CoSe_2$ nanocrystals in a magnetic field of 1000 Oe.

data from 5 to 300 K and a vibrating sample magnetometer to collect the data from 300 to 674 K. The Curie temperature was determined by the position of the maximum of $|dM/dT|$ to be 570 K, which is roughly 1000 K lower than the Curie temperature of cobalt. This result suggests that the ferromagnetism of the wires may arise from $CoSe_2$, although the detailed mechanism has yet to be established.

In summary, we have demonstrated that the nanoscale Kirkendall effect can be applied to a magnetically preassembled nanostructure to form 1D assemblies of hollow nanocrystals of cobalt chalcogenides at elevated temperatures.

 © 2006 Wiley-VCH Verlag GmbH & Co. KGaA, Weinheim

This procedure provides an alternative route to nanowires with a unique morphology (interconnected hollow nanocrystals) that is difficult to achieve using other means. This "magnetic-guiding" strategy is also compatible with other methodologies for creating nanostructures.[9,18] In addition, the magnetic nanostructures produced may have potential applications in the fabrication of nanodevice components. We are currently investigating this possibility.

Received: October 3, 2005
Revised: November 21, 2005
Published online: January 18, 2006

Keywords: chalcogenides · cobalt · magnetic properties · nanostructures · self-assembly

[1] a) S. H. Park, D. Qin, Y. Xia, *Adv. Mater.* **1998**, *10*, 1028; b) B. Gates, Y. Xia, *Appl. Phys. Lett.* **2001**, *78*, 3178.
[2] a) S. Sun, C. B. Murray, D. Weller, L. Folks, A. Moser, *Science* **2000**, *287*, 1989; b) V. F. Puntes, P. Gorostiza, D. M. Aruguete, N. G. Bastus, A. P. Alivisatos, *Nat. Mater.* **2004**, *3*, 263; c) T. Hyeon, *Chem. Commun.* **2003**, 927.
[3] J. C. Love, L. A. Estroff, J. K. Kriebel, R. G. Nuzzo, G. M. Whitesides, *Chem. Rev.* **2005**, *105*, 1103.
[4] a) T. C. Holmes, S. de Lacalle, X. Su, G. S. Liu, A. Rich, S. G. Zhang, *Proc. Natl. Acad. Sci. USA* **2000**, *97*, 6728; b) G. A. Silva, C. Czeisler, K. L. Niece, E. Beniash, D. A. Harrington, J. A. Kessler, S. I. Stupp, *Science* **2004**, *303*, 1352; c) B. G. Xing, C. W. Yu, K. H. Chow, P. L. Ho, D. G. Fu, B. Xu, *J. Am. Chem. Soc.* **2002**, *124*, 14846; d) Z. M. Yang, H. W. Gu, Y. Zhang, L. Wang, B. Xu, *Chem. Commun.* **2004**, 208.
[5] a) Z. Y. Tang, N. A. Kotov, M. Giersig, *Science* **2002**, *297*, 237; b) Z. Y. Tang, N. A. Kotov, *Adv. Mater.* **2005**, *17*, 951.
[6] a) J. C. Love, A. R. Urbach, M. G. Prentiss, G. M. Whitesides, *J. Am. Chem. Soc.* **2003**, *125*, 12696; b) A. R. Urbach, J. C. Love, M. G. Prentiss, G. M. Whitesides, *J. Am. Chem. Soc.* **2003**, *125*, 12704.
[7] a) S. L. Tripp, S. V. Pusztay, A. E. Ribbe, A. Wei, *J. Am. Chem. Soc.* **2002**, *124*, 7914; b) S. L. Tripp, R. E. Dunin-Borkowski, A. Wei, *Angew. Chem.* **2003**, *115*, 5749; *Angew. Chem. Int. Ed.* **2003**, *42*, 5591.
[8] a) T. Hyeon, S. S. Lee, J. Park, Y. Chung, H. Bin Na, *J. Am. Chem. Soc.* **2001**, *123*, 12798; b) J. Park, K. J. An, Y. S. Hwang, J. G. Park, H. J. Noh, J. Y. Kim, J. H. Park, N. M. Hwang, T. Hyeon, *Nat. Mater.* **2004**, *3*, 891; c) J. Park, E. Lee, N. M. Hwang, M. S. Kang, S. C. Kim, Y. Hwang, J. G. Park, H. J. Noh, J. Y. Kini, J. H. Park, T. Hyeon, *Angew. Chem.* **2005**, *117*, 2932; *Angew. Chem. Int. Ed.* **2005**, *44*, 2872.
[9] Y. D. Yin, A. P. Alivisatos, *Nature* **2005**, *437*, 664.
[10] Y. D. Yin, R. M. Rioux, C. K. Erdonmez, S. Hughes, G. A. Somorjai, A. P. Alivisatos, *Science* **2004**, *304*, 711.
[11] a) J. Chen, F. Saeki, B. J. Wiley, H. Cang, M. J. Cobb, Z. Y. Li, L. Au, H. Zhang, M. B. Kimmey, X. D. Li, Y. Xia, *Nano Lett.* **2005**, *5*, 473; b) Y. Sun, Y. Xia, *J. Am. Chem. Soc.* **2004**, *126*, 3892; c) L. Rapoport, N. Fleischer, R. Tenne, *Adv. Mater.* **2003**, *15*, 651; d) L. Rapoport, Y. Bilik, Y. Feldman, M. Homyonfer, S. R. Cohen, R. Tenne, *Nature* **1997**, *387*, 791; e) N. A. Dhas, K. S. Suslick, *J. Am. Chem. Soc.* **2005**, *127*, 2368; f) D. Goll, A. E. Berkowitz, H. N. Bertram, *Phys. Rev. B* **2004**, *70*; g) R. Tenne, *Prog. Inorg. Chem.* **2001**, *50*, 269; h) Y. G. Sun, B. Mayers, Y. N. Xia, *Adv. Mater.* **2003**, *15*, 641; i) X. M. Sun, Y. D. Li, *Angew. Chem.* **2004**, *116*, 3915; *Angew. Chem. Int. Ed.* **2004**, *43*, 3827; j) X. Wang, Y. D. Li, *Angew. Chem.* **2003**, *115*, 3621; *Angew. Chem. Int. Ed.* **2003**, *42*, 3497.
[12] K. N. Tu, U. Gosele, *Appl. Phys. Lett.* **2005**, *86*, 09311.
[13] V. F. Puntes, K. M. Krishnan, A. P. Alivisatos, *Science* **2001**, *291*, 2115.
[14] H. van der Heide, R. Hemmel, C. F. van Bruggen, C. Haas, *J. Solid State Chem.* **1980**, *33*, 17.
[15] C. E. M. Campos, J. C. de Lima, T. A. Grandi, K. D. Machado, V. Drago, P. S. Pizani, *Solid State Commun.* **2004**, *131*, 265.
[16] B. Gates, Y. Yin, Y. Xia, *J. Am. Chem. Soc.* **2000**, *122*, 12582.
[17] K.-S. Cho, D. V. Talapin, W. Gaschler, C. B. Murray, *J. Am. Chem. Soc.* **2005**, *127*, 7140.
[18] a) H. W. Gu, R. K. Zheng, X. X. Zhang, B. Xu, *J. Am. Chem. Soc.* **2004**, *126*, 5664; b) H. W. Gu, Z. M. Yang, J. H. Gao, C. K. Chang, B. Xu, *J. Am. Chem. Soc.* **2005**, *127*, 34.

 © 2006 Wiley-VCH Verlag GmbH & Co. KGaA, Weinheim

Combinatorial Chemistry

DOI: 10.1002/anie.200503663

Screening of a Supramolecular Catalyst Library in the Search for Selective Catalysts for the Asymmetric Hydrogenation of a Difficult Enamide Substrate**

*Xiao-Bin Jiang, Laurent Lefort, P. Elsbeth Goudriaan, André H. M. de Vries, Piet W. N. M. van Leeuwen, Johannes G. de Vries, and Joost N. H. Reek**

Transition-metal-catalyzed asymmetric hydrogenation is one of the classic success stories in transition-metal catalysis because it has resulted in several scientific breakthroughs[1] as well as the development of commercial processes.[2] Many highly enantioselective catalysts for the asymmetric hydrogenation of various classes of prochiral substrates have been reported.[3] However, there are still many challenging substrates that cannot be converted with satisfactory enantioselectivities or yields, which has led to the ongoing intensive research efforts in this area. Although computational techniques are becoming increasingly important, one cannot design an enantioselective chiral catalyst in silico, and therefore, catalyst development for asymmetric reactions relies to a

[*] Dr. X.-B. Jiang, P. E. Goudriaan, Prof. Dr. P. W. N. M. van Leeuwen, Dr. J. N. H. Reek
Homogeneous Catalysis
van't Hoff Institute for Molecular Sciences
University of Amsterdam
Nieuwe Achtergracht 166, 1018 WV Amsterdam (The Netherlands)
Fax: (+31) 20-525-6422
E-mail: reek@science.uva.nl

Dr. L. Lefort, Dr. A. H. M. de Vries, Prof. Dr. J. G. de Vries
DSM research, DSM Pharma Chemicals
Advanced Synthesis, Catalysis & Development
P. O. Box 18, 6160 MD Geleen (The Netherlands)

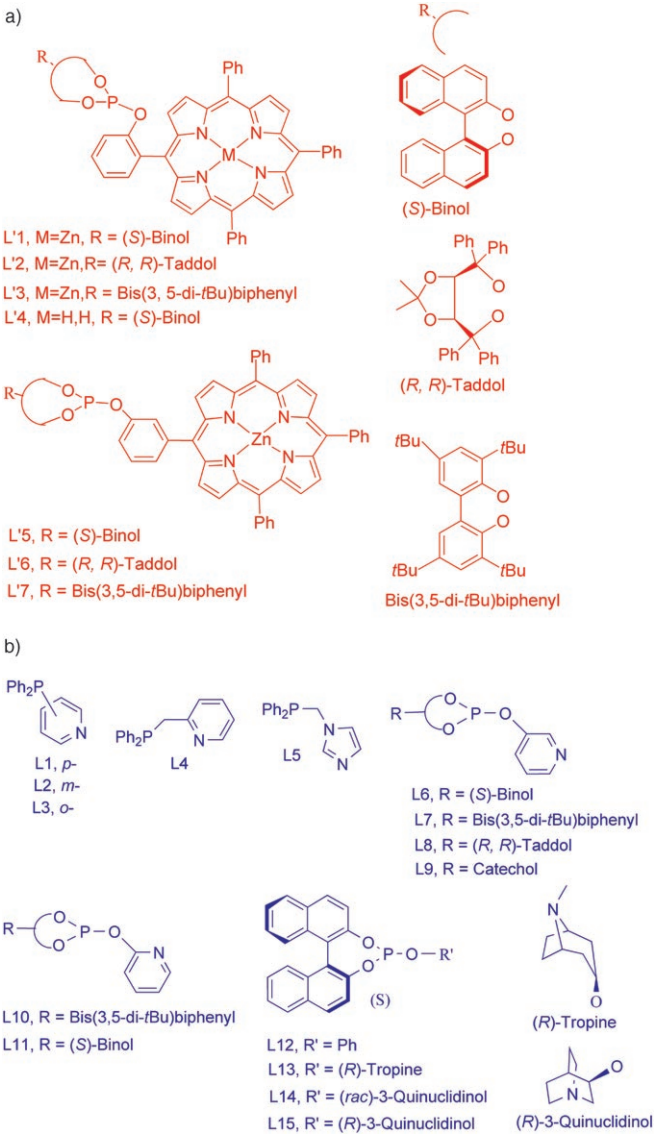
[**] This work was financially supported by NWO.

Supporting information for this article is available on the WWW under http://www.angewandte.org or from the author.

© 2006 Wiley-VCH Verlag GmbH & Co. KGaA, Weinheim

great extent upon a trial-and-error approach and sophisticated guesses. Consequently, combinatorial approaches and high-throughput experimentation have become increasingly important.[4] Several elegant screening techniques for combinatorial catalysis have been developed, but there is only limited technology available to prepare large catalyst libraries with sufficient diversity. Interesting breakthroughs include the revival of the use of monodentate ligands,[5] simultaneously reported by the research groups of Reetz,[6] Feringa and de Vries,[7] and Pringle,[8] and more recently, the successful use of mixtures of monodentate ligands.[9,10] Lefort et al. accomplished the robotic synthesis of 96 monodentate phosphoramidites (instant ligand libraries) and robotic screening in asymmetric hydrogenation in just two days, which demonstrates the value of simple ligand structures.[11] Although some interesting modular bidentate ligands have been reported,[12] a similar breakthrough and revival in the field of bidentate-ligated transition-metal catalysts[13] would be of great impetus for asymmetric catalysis. Consequently, we,[14] and others,[15] have recently introduced a new class of bidentate ligands resulting from the self-assembly of two monodentate ligands (Figure 1). We have used the zinc(II)porphyrin–pyridyl interaction as an assembly motif to generate bidentate phosphorus-based ligands. We have also shown that only 14 building blocks were required to generate a library of 48 bidentate phosphorus ligands,[14b] which have been used successfully in hydroformylation[14a,c] and asymmetric allylic alkylation reactions.[14b,c] Herein we report the extension of the supraphos library and its application in the asymmetric rhodium-catalyzed hydrogenation of a trisubstituted cyclic enamide, which yielded unprecedented selectivities.

The supraphos ligand consists of two components (displayed in red and blue in Figure 1) brought together by the selective and reversible coordination of the nitrogen donor atom of ligand L to the zinc atom of L′, and both phosphorus ligands can then simultaneously coordinate to the rhodium metal (green). For the current study we have used 7 porphyrin–phosphites, including newly prepared zinc(II)porphyrins functionalized with taddol phosphite (L′2 and L′6), and 14 phosphorus ligands containing pyridyl (and other N-donor) groups (Scheme 1). The building blocks were obtained



Scheme 1. a) Structures of porphyrin-functionalized phosphites. b) Structures of N-containing phosphorus ligands.

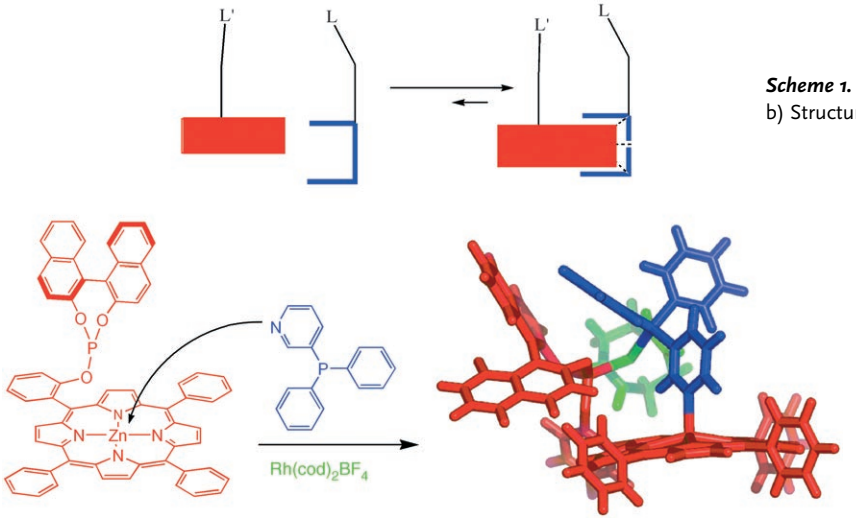
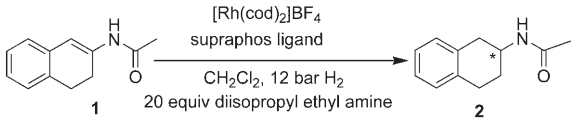


Figure 1. The formation of a bidentate ligand and its transition-metal complex by self-assembly.

by simple synthetic routes (see the Supporting Information), and the supraphos ligand library was constructed with these building blocks according to Figure 1. This library was used in the rhodium-catalyzed hydrogenation of one of the most challenging benchmark substrates in asymmetric hydrogenation, *N*-(3,4-dihydro-2-naphthalenyl)-acetamide (**1**; Scheme 2), by using high-throughput methods to perform 96 reactions in parallel (0.04 mmol scale).[11,16] There are only a few ruthenium-based catalysts known to produce product **2** with high enantioselectivities (up to 90%) from this commercially interesting sub-

 © 2006 Wiley-VCH Verlag GmbH & Co. KGaA, Weinheim



Scheme 2. Rh-catalyzed hydrogenation of *N*-(3,4-dihydro-2-naphthalenyl)acetamide (**1**).

strate.[17] Rhodium catalysts generally result in low to moderate *ee* values (< 72 %) for the product.[18]

The results of the screening experiments displayed in Table 1 show that the supraphos-based catalysts induced conversions from 0 to 100 % and *ee* values between −12 and 94 %. The best results, in terms of conversion and *ee* values, are highlighted in red, and it is clear that there is no correlation between the *ee* value and the conversion. The catalyst based upon supraphos ligand L′1/L2 provides the highest *ee* value (94 %) reported to date and full conversion. Results from five other members of the library indicate that greater than 90 % conversion was obtained, but the highest *ee* value was only 56 %, which represents a significant decrease from 94 %.

In general, both phosphine-phosphite ligands and bisphosphites can provide catalysts that lead to high conversions and *ee* values up to 56 %. Supraphos ligands based on binol-based porphyrin phosphites (L′1, L′5) induced, with a few exceptions, much higher conversions and selectivities than the taddol-based porphyrin phosphites (L′2, L′6). A small variation in ligand structure results in a large change in catalyst performance, as is often observed in asymmetric catalysis. For example, the structural differences between *o*-, *m*-, and *p*-pyridyl-substituted phosphines (L1, L2, and L3) seems small, but in combination with L′1 they result in the formation of rhodium catalysts with substantially different conversions and *ee* values of the product. The same is true when a simple CH_2 group bridges the pyridyl group and phosphorus (L4) or when a methylimidazol group is used instead of pyridyl (L5).

As the performance of L′1/L2 was exceptional we studied this supraphos ligand in more detail. ^{31}P NMR spectroscopy of a 1:1:1 mixture of [Rh(cod)$_2$]BF_4, L′1, and L2 in CD_2Cl_2 showed exclusive formation of the expected [Rh(L′1)(cod)(L2)]BF_4 complex (cod = cycloocta-1,5-diene; see the Supporting Information). The performance of supraphos ligand L′1/L2 as well as some important control experiments were studied on a larger scale (1 mmol of the substrate), and the conversion was monitored by H_2 uptake (Table 2). As expected, the results from the screening experiments were reproduced on this scale (Table 2, entry 1). Similar *ee* values were obtained, and the product was completely characterized after isolation by column chromatography and crystallization.

Several experiments indicate that the bidentate character of the supraphos ligand system is important. In contrast to the catalyst based on supraphos ligand L′1/L2, those based on L′4/L2 (an identical structure but without the zinc metal crucial for bidentate ligand assembly) and L′1/PPh_3, generated the product with only 10 % and 24 % *ee*, and at low conversions (Table 2, entries 2 and 3). The catalysts based on monodentate ligands such as [Rh(L12)$_2$] (Table 2, entry 5) and [Rh(L′1)$_2$] (20 % *ee*) also provided low selectivities and high conversions.

We studied the performance of the catalyst based on supraphos ligand L′1/L2 under various conditions. The reaction carried out with 1 mol % catalyst resulted in formation of the product with a high *ee* value (Table 2, entry 6). The metal-to-ligand ratio as well as the ratio of L′1/L2 is of importance for optimal catalyst performance. At high ligand loading, the *ee* value is high, but the activity is much lower (Rh/L′1/L2 = 1:1.5:1.5; Table 2, entry 7). Interestingly, the presence of only a small excess of L′1 does not affect the results (Rh/L′1/L2 = 1:2:1; Table 2, entry 9), thus indicating that under these conditions catalysis is dominated by the supraphos bidentate ligand. [Rh(L′1)$_2$] is more active and less

Table 1: Conversions (%) of **1** and *ee* values of **2** induced by the rhodium catalysts based on various supraphos ligands as obtained from screening experiments.[a–c]

	L1	L2	L4	L5	L6	L7	L8	L9	L10	L11	L13	L14
L′1	44	100	62	5	80	40	36	20	31	97	86	65
L′2	5	10	2	1	8	4	7	0	9	11	21	14
L′5	38	88	29	28	67	18	19	8	9	100	84	96
L′6	48	54	70	15	59	14	83	8	9	73	93	90

Conversion

	L1	L2	L4	L5	L6	L7	L8	L9	L10	L11	L13	L14
L′1	27	94	47	20	13	54	49	17	11	-2	56	13
L′2	5	7	8	5	16	-3	6	0	3	-12	16	10
L′5	24	46	18	14	21	52	31	11	21	30	34	28
L′6	-1	26	-4	0	5	-7	-12	6	5	4	-9	-5

ee value

100-90 90-80 80-70 70-60 60-50 50-40 40-30 30-20 20-10 10-0

[a] Reaction condition: [Rh(cod)$_2$]BF_4, Rh/L′*n*/L*n* = 1/1.5/1.2, 5 mol % rhodium, CH_2Cl_2, 12 bar H_2, 40 °C, 0.04 mmol of substrate **1**, 20 equiv diisopropyl ethyl amine, 14 h. [b] Conversion and *ee* were determined by chiral GC (Chiralsil-DEXCB). Negative *ee* values indicate that the opposite enantiomer was the major product. [c] Supraphos ligands based on achiral porphyrin-phosphite L′3, L′7 (in combination with chiral building blocks L6, L8, L11, L13, L15) gave *ee* values below 18 %, supraphos ligand L′1/L15 gave only slightly higher *ee* values (17 % *ee*, full conversion) than L′1/L14; for details see the Supporting Information.

 © 2006 Wiley-VCH Verlag GmbH & Co. KGaA, Weinheim

Table 2: Different combinations and ratios of L′*n*/L*n* as catalysts.[a]

Entry	Ligand system	Rh/L′*n*/L*n*	Time [h][b]	Conv. [%][c]	*ee* [%][c]
1	L′1/L2	1/1.5/1.2	4	100	94 (+)
2	L′1/PPh_3	1/1.5/1.2	4	56	24 (+)
3	L′4/L2	1/1.5/1.2	14	19	10 (+)
4	L′1/L3	1/1.5/1.2	4	20	17 (+)
5	L12	1/0/2.1	4	85	1 (−)
6[d]	L′1/L2	1/1.5/1.2	14	86	93 (+)
7	L′1/L2	1/1.5/1.5	14	100	92 (+)
8	L′1/L2	1/1.5/1	14	100	92 (+)
9	L′1/L2	1/2/1	14	100	93 (+)
10	L′1/L2	1/1.2/1	14	100	64 (+)
11	L′1/L2	1/0.5/0.5	14	100	9 (+)
12	binaphos[e]	–	14	100	60 (+)

[a] Reaction conditions: 1 mmol of substrate **1**, 5 mol% $[Rh(cod)_2]BF_4$, CH_2Cl_2, 12 bar H_2, 25 °C, 20 equiv diisopropyl ethyl amine. [b] The time required for the reaction to go to completion based on H_2 uptake and GC analysis. [c] Conversion and *ee* were determined by chiral GC (Chiralsil-DEXCB). The optical signs in brackets are referenced to literature data.[17a] [d] 1 mol% catalyst. [e] 1.1 equiv with respect to Rh.

selective than the Rh/L′1/L2 system so it cannot be a dominant species during this experiment. Using low ligand/rhodium ratios results in faster reactions and lower selectivities, which indicates that other active rhodium species are formed under these conditions (Table 2, entries 10 and 11).

In view of the superior results of supraphos ligand L′1/L2, we considered it likely that the phosphine-phosphite combination plays a crucial role. Therefore we studied binaphos,[19] a covalent bidentate phosphine–phosphite ligand that has been applied successfully to many asymmetric transformations,[20] but in this case the enantioselectivity was moderate (60%, Table 2, entry 12). Chemical modification of binaphos might also lead to better selectivities, but this is a much more tedious process than modification of the supraphos ligand. To date, there is no covalent bidentate ligand that equals the best result obtained with a supraphos-based catalyst, which suggests that the supraphos ligand displays new ligand properties. The large aromatic surface of the porphyrin may play an important role because it creates a pocket to accommodate the substrate. In addition, the supraphos strategy facilitates the formation of ligand combinations that may not form, at least in significant quantities, by only using mixtures of monodentate ligands.[9,10]

In summary, we have demonstrated that the supraphos concept provides easy access to large bidentate ligand libraries and that these ligands can successfully be applied in rhodium-catalyzed asymmetric hydrogenation. High-throughput screening of the current library revealed a catalyst that hydrogenates the trisubstituted cyclic enamide **1** with the highest enantioselectivity known to date. This unambiguously shows that a supramolecular approach to create bidentate ligands is a very powerful tool which leads to new catalysts with properties that surpass those currently available. From the library of 64 supraphos ligands investigated, only one provides a catalyst that induced high *ee* values, which stresses the point that large ligand libraries are required for challenging asymmetric conversions, such as the hydrogenation of the trisubstituted cyclic enamide **1**. One of the advantages typical of supramolecular ligands is the easy access to these large libraries, and we are currently preparing various libraries to widen the scope of asymmetric reactions.

Received: October 16, 2005
Published online: January 13, 2006

Keywords: asymmetric catalysis · combinatorial chemistry · high-throughput screening · self-assembly · supramolecular chemistry

[1] a) W. S. Knowles, *Angew. Chem.* **2002**, *114*, 2096–2107; *Angew. Chem. Int. Ed.* **2002**, *41*, 1998–2007; b) R. Noyori, *Angew. Chem.* **2002**, *114*, 2108–2123; *Angew. Chem. Int. Ed.* **2002**, *41*, 2008–2022; c) W. A. Nugent, T. V. Rajanbabu, M. J. Burk, *Science* **1993**, *259*, 479–483.

[2] a) A. S. C. Chan, S. A. Laneman, R. E. Miller, J. H. Wagenknecht, J. P. Coleman, *Chem. Ind.* **1994**, *53*, 49–68; b) R. Selke in *Asymmetric Catalysis on Industrial Scale* (Eds.: H.-U. Blaser, E. Schmidt), Wiley-VCH, Weinheim, **2004**, pp. 39–53; c) D. J. Ager, S. A. Laneman in *Asymmetric Catalysis on Industrial Scale* (Eds.: H.-U. Blaser, E. Schmidt), Wiley-VCH, Weinheim, **2004**, pp. 259–268; d) T. Iida, T. Mase, *Curr. Opin. Drug Discovery Dev.* **2002**, *5*, 834–851; e) J. G. de Vries in *Encyclopedia of Catalysis I, Vol. 3* (Ed.: T. Horvath), Wiley, New York, **2003**, pp. 295–347; f) *Handbook of Chiral Chemicals*, 2nd ed. (Ed.: D. Ager), CRC, New York, **2005**.

[3] a) *Handbook of Homogeneous Hydrogenation* (Eds.: J. G. de Vries, C. J. Elsevier), Wiley-VCH, Weinheim, **2006**; b) P. A. Chaloner, M. A. Esteruelas, F. Joó, L. A. Oro, *Homogeneous Hydrogenation*, Kluwer, Dordrecht, **1994**; c) J. M. Brown in *Comprehensive Asymmetric Catalysis, Vol. 1* (Eds.: E. N. Jacobsen, A. Pfaltz, H. Yamamoto), Springer, Berlin, **1999**, chap. 5.1, pp. 121–183; d) H.-U. Blaser, F. Spindler in *Comprehensive Asymmetric Catalysis, Vol. 1* (Eds.: E. N. Jacobsen, A. Pfaltz, H. Yamamoto), Springer, Berlin, **1999**, chap. 6.2, pp. 247–267; e) T. Ohkuma, R. Noyori in *Comprehensive Asymmetric Catalysis, Vol. 1* (Eds.: E. N. Jacobsen, A. Pfaltz, H. Yamamoto), Springer, Berlin, **1999**, chap. 6.1, pp. 199–246.

[4] a) A. Hagemeyer, B. Jandeleit, Y. Liu, D. M. Poojary, H. W. Turner, A. F. Volpe, Jr., W. H. Weinberg, *Appl. Catal. A* **2001**, *221*, 23–43; b) M. T. Reetz, *Angew. Chem.* **2001**, *113*, 292–320; *Angew. Chem. Int. Ed.* **2001**, *40*, 284–310; c) S. Dahmen, S. Bräse, *Synthesis* **2001**, 1431–1449; d) A. Hoveyda in *Handbook of Combinatorial Chemistry, Vol. 2* (Eds.: K. C. Nicolaou, R. Hanko, W. Hartwig), Wiley-VCH, Weinheim, **2002**, pp. 991–1016; e) V. Murphy, H. W. Turner, T. Weskamp in *Applied Homogeneous Catalysis with Organometallic Compounds, Vol. 2* (Eds.: B. Cornils, W. A. Herrmann), 2nd ed., Wiley-VCH, Weinheim, **2002**, pp. 740–747; f) C. Gennari, U. Piarulli, *Chem. Rev.* **2003**, *103*, 3071–3100; g) J. G. de Vries, A. H. M. de Vries, *Eur. J. Org. Chem.* **2003**, *5*, 799–811; h) K. Ding, H. Du, Y. Yuan, J. Long, *Chem. Eur. J.* **2004**, *10*, 2872–2884; i) M. T. Reetz in *Comprehensive Coordination Chemistry II, Vol. 9* (Eds.: J. A. McCleverty, T. J. Meyer), Elsevier, Oxford, **2004**, pp. 509–548.

[5] For recent reviews on monodentate ligands, see: a) T. Jerphagnon, J.-L. Renaud, C. Bruneau, *Tetrahedron: Asymmetry* **2004**, *15*, 2101–2111, and references therein; b) J. G. de Vries in *Handbook of Chiral Chemicals*, 2nd ed. (Eds.: D. Ager, S. Laneman), CRC, New York, **2005**.

[6] M. T. Reetz, G. Mehler, *Angew. Chem.* **2000**, *112*, 4047–4049; *Angew. Chem. Int. Ed.* **2000**, *39*, 3889–3890.

[7] M. van den Berg, A. J. Minnaard, E. P. Schudde, J. van Esch, A. H. M. de Vries, J. G. de Vries, B. L. Feringa, *J. Am. Chem. Soc.* **2000**, *122*, 11539–11540.

 © 2006 Wiley-VCH Verlag GmbH & Co. KGaA, Weinheim

[8] C. Claver, E. Fernandez, A. Gillon, K. Heslop, D. J. Hyett, A. Martorell, A. G. Orpen, P. G. Pringle, *Chem. Commun.* **2000**, 961 – 962.
[9] a) M. T. Reetz, X. Li, *Angew. Chem.* **2005**, *117*, 3019 – 3021; *Angew. Chem. Int. Ed.* **2005**, *44*, 2959 – 2962; b) M. T. Reetz, X. Li, *Tetrahedron* **2004**, *60*, 9709 – 9714; c) M. T. Reetz, G. Mehler, A. Meiswinkel, *Tetrahedron: Asymmetry* **2004**, *15*, 2165 – 2167; d) M. T. Reetz, T. Sell, A. Meiswinkel, G. Mehler, *Angew. Chem.* **2003**, *115*, 814 – 817; *Angew. Chem. Int. Ed.* **2003**, *42*, 790 – 793.
[10] a) C. Monti, C. Gennari, U. Piarulli, J. G. de Vries, A. H. M. de Vries, L. Lefort, *Chem. Eur. J.* **2005**, *11*, 6701 – 6717; b) A. H. M. de Vries, L. Lefort, J. A. F. Boogers, J. G. de Vries, D. J. Ager, *Chim. Oggi* **2005**, *23*, 18 – 22 (Supplement on Chiral Technologies); c) R. Hoen, J. A. F. Boogers, H. Bernsmann, A. J. Minnaard, A. Meetsma, T. D. Tiemersma-Wegman, A. H. M. de Vries, J. G. de Vries, B. L. Feringa, *Angew. Chem.* **2005**, *117*, 4281 – 4284; *Angew. Chem. Int. Ed.* **2005**, *44*, 4209 – 4212; d) D. Peña, A. J. Minnaard, J. A. F. Boogers, A. H. M. de Vries, J. G. de Vries, B. L. Feringa, *Org. Biomol. Chem.* **2003**, *1*, 1087 – 1089.
[11] L. Lefort, J. A. F. Boogers, A. H. M. de Vries, J. G. de Vries, *Org. Lett.* **2004**, *6*, 1733 – 1735.
[12] a) J. F. Jensen, I. Sotofte, H. O. Sorensen, M. Johannsen, *J. Org. Chem.* **2003**, *68*, 1258 – 1265; b) F. Blume, S. Zemolka, T. Fey, R. Kranich, H.-G. Schmalz, *Adv. Synth. Catal.* **2002**, *344*, 868 – 883; c) A. Bastero, C. Claver, A. Ruiz, S. Castillón, E. Daura, C. Bo, E. Zangrando, *Chem. Eur. J.* **2004**, *10*, 3747 – 3760; d) R. Kranich, K. Eis, O. Geis, S. Muhle, J. W. Bats, H.-G. Schmalz, *Chem. Eur. J.* **2000**, *6*, 2874 – 2894; e) R. Imbos, A. J. Minnaard, B. L. Feringa, *J. Am. Chem. Soc.* **2002**, *124*, 184 – 185.
[13] For a recent review on bidentate ligands in asymmetric hydrogenation, see: W. Tang, X. Zhang, *Chem. Rev.* **2003**, *103*, 3029 – 3069, and references therein.
[14] a) V. F. Slagt, P. W. N. M. van Leeuwen, J. N. H. Reek, *Chem. Commun.* **2003**, *19*, 2474 – 2475; b) V. F. Slagt, M. Röder, P. C. J. Kamer, P. W. N. M. van Leeuwen, J. N. H. Reek, *J. Am. Chem. Soc.* **2004**, *126*, 4056 – 4057; c) V. F. Slagt, P. W. N. M. van Leeuwen, J. N. H. Reek, *Angew. Chem.* **2003**, *115*, 5771 – 5781; *Angew. Chem. Int. Ed.* **2003**, *42*, 5619 – 5623; d) M. J. Wilkinson, P. W. N. M. van Leeuwen, J. N. H. Reek, *Org. Biomol. Chem.* **2005**, *3*, 2371 – 2383; e) J. N. H. Reek, M. Röder, P. E. Goudriaan, P. C. J. Kamer, P. W. N. M. van Leeuwen, V. F. Slagt, *J. Organomet. Chem.* **2005**, *690*, 4505 – 4516.
[15] a) B. Breit, W. Seiche, *Angew. Chem.* **2005**, *117*, 4401 – 4404; *Angew. Chem. Int. Ed.* **2005**, *44*, 1640 – 1643; b) B. Breit, W. Seiche, *J. Am. Chem. Soc.* **2003**, *125*, 6608 – 6609; c) J. M. Takacs, D. S. Reddy, S. A. Moteki, D. Wu, H. Palencia, *J. Am. Chem. Soc.* **2004**, *126*, 4494 – 4495.
[16] The hydrogenation of a variety of substrates will be reported in a full paper on this topic.
[17] For examples of Ru-catalyzed hydrogenation of **1**, see: a) J. L. Renaud, P. Dupau, A.-E. Hay, M. Guingouain, P. H. Dixneuf, C. Bruneau, *Adv. Synth. Catal.* **2003**, *345*, 230 – 238; b) P. Dupau, P. Le Gendre, C. Bruneau, P. H. Dixneuf, *Synlett* **1999**, *11*, 1832 – 1834; c) P. Dupau, C. Bruneau, P. H. Dixneuf, *Adv. Synth. Catal.* **2001**, *343*, 331 – 334; d) M. Devocelle, A. Mortreux, F. Agbossou, J.-R. Dormoy, *Tetrahedron Lett.* **1999**, *40*, 4551 – 4554; e) D. M. Tschaen, L. Abramson, D. Cai, R. Desmond, U.-H. Dolling, L. Frey, S. Karady, Y.-J. Shi, T. R. Verhoeven, *J. Org. Chem.* **1995**, *60*, 4324 – 4330.
[18] For examples of Rh-catalyzed hydrogenation of **1**, see: a) Z. Zhang, G. Zhu, Q. Jiang, D. Xiao, X. Zhang, *J. Org. Chem.* **1999**, *64*, 1774 – 1775; b) H. Bernsmann, M. van den Berg, R. Hoen, A. J. Minnaard, G. Mehler, M. T. Reetz, J. G. de Vries, B. L. Feringa, *J. Org. Chem.* **2005**, *70*, 943 – 951; c) R. Hoen, M. van den Berg, H. Bernsmann, A. J. Minnaard, J. G. de Vries, B. L. Feringa, *Org. Lett.* **2004**, *6*, 1433 – 1436; d) F. Guillen, M. Rivard, M. Toffano, J. Y. Legros, J. C. Daran, J.-C. Fiaud, *Tetrahedron* **2002**, *58*, 5895 – 5904; e) W. Tang, Y. Chi, X. Zhang, *Org. Lett.* **2002**, *4*, 1695 – 1698.
[19] For binaphos and related ligands in asymmetric hydrogenation, see: Y. Yan, Y. Chi, X. Zhang, *Tetrahedron: Asymmetry* **2004**, *15*, 2173 – 2175, and references therein.
[20] For a recent review on binaphos in asymmetric hydroformylation, see: M. Diéguez, O. Pamies, C. Claver, *Tetrahedron: Asymmetry* **2004**, *15*, 2113 – 2122.

 © 2006 Wiley-VCH Verlag GmbH & Co. KGaA, Weinheim

DNA Recognition

DOI: 10.1002/anie.200503822

Molecular Recognition of a Three-Way DNA Junction by a Metallosupramolecular Helicate**

Aneta Oleksi, Alexandre G. Blanco, Roeland Boer, Isabel Usón, Joan Aymamí, Alison Rodger, Michael J. Hannon, and Miquel Coll**

Although much current drug research focuses on agents that inhibit the action of proteins, nucleic acids are attractive therapeutic targets because of their potential for controlling

[*] Professor M. J. Hannon
School of Chemistry
University of Birmingham
Edgbaston, Birmingham B15 2TT (UK)
Fax: (+44) 121-414-7871
E-mail: m.j.hannon@bham.ac.uk

Dr. A. Oleksi, A. G. Blanco, Dr. R. Boer, Professor M. Coll
Institut de Biologia Molecular de Barcelona-CSIC and
Institut de Recerca Biomèdica
Parc Científic de Barcelona
Josep Samitier 1–5, 08028 Barcelona (Spain)
Fax: (+34) 93-403-4979
E-mail: mcoll@ibmb.csic.es

Prof. I. Usón
Institut de Biologia Molecular de Barcelona-CSIC and
Institució Catalana de Recerca i Estudis Avançats
Jordi Girona 18, 08034 Barcelona (Spain)

Dr. J. Aymamí
Departament d'Enginyeria Química
Universitat Politècnica de Catalunya
Diagonal 647, 08028 Barcelona (Spain)

Professor A. Rodger
Department of Chemistry
University of Warwick
Coventry, CV4 7AL (UK)

[**] This work was supported by an EU Marie Curie Research Training Network (HPRN-CT-2002-00175) and by grants (to M.C.) from the Ministerio de Educación y Ciencia and the Generalitat de Catalunya. M.J.H. is the Royal Society of Chemistry Sir Edward Frankland Fellow 2004-5. A.G.B. is the recipient of a fellowship from the Ministerio de Sanidad y Consumo. We thank Dr. J. Kerckhoffs and J. Peberdy for helicate synthesis.

Supporting information for this article is available on the WWW under http://www.angewandte.org or from the authors.

© 2006 Wiley-VCH Verlag GmbH & Co. KGaA, Weinheim

disease at the source. Indeed, DNA is already the target for widely used anticancer molecules such as intercalators and platinum drugs; consequently the field of DNA recognition has attracted much interest. Existing synthetic agents that bind to DNA do so essentially in one of five distinct modes:[1] They bind covalently (or through coordination bonds) to the DNA bases (as cisplatin), intercalate between the bases, bind in the major groove (often with formation of hydrogen bonds to the bases), bind in the minor groove (as polyamide groove binders), or bind to the sugar–phosphate backbone. In spite of many efforts to redesign their chemical structure and narrow down their binding capacities to specific DNA sequences, DNA-binding drugs (particularly those which have reached the clinic) are, in general, nonspecific drugs with broad cytotoxic effects. The ability to recognize a specific unusual DNA structure—in contrast to strict sequence recognition—is an attractive alternative for gaining specificity. Herein we present a completely new mode of DNA recognition through an atomic resolution X-ray crystal structure of a three-way DNA junction in complex with a synthetic tetracationic supramolecular helicate that fits perfectly into the central-trigonal hydrophobic cavity of the DNA junction. This is not only without precedent as a mode of DNA recognition, but reveals a three-way DNA junction as a well-defined potential structural target for novel, highly specific drugs.

DNA junctions are unique branched structures that consist of several double strands converging at one point. The best-characterized DNA junction is the four-way junction, also known as a Holliday junction, a key intermediate in homologous recombination.[2] Three-dimensional structures of free four-way DNA junctions[3] and different complexes with proteins have been solved.[4] In contrast, three-way junctions, although being the simplest and most abundant nucleic acid branched structures, are not so well characterized. Three-way junctions occur both in RNA and DNA. In RNA they are involved in crucial biological functions such as splicing[5] and translation,[6] and in DNA they are formed transiently during DNA replication (the replication fork).[7] They are also intermediate structures during triplet repeat expansions,[8] anomalies associated with several human genetic diseases such as myotonic dystrophy type 1 and Huntington's disease.[9] Three-way junctions are present in the inverted terminal repeats of certain viral genomes[10] and are intermediates during phage genetic recombination.[11]

Inspired by nature, we have been exploring a new approach for synthetic DNA recognition through the design of agents that possess similar nanoscale molecular surfaces to those of biomolecular DNA-recognition motifs.[12,13] In particular, we have used metallosupramolecular chemistry to generate nanoscale synthetic agents, such as the tetracationic supramolecular helicate (Figure 1 a) $[Fe_2L_3]^{4+}$, which is formed from three bis-pyridylimine organic strands wrapped about two Fe^{2+} ions. We have previously described the binding of this agent to natural polymeric DNAs and the remarkable intramolecular DNA coiling that results.[12] To gain more information we have been attempting to crystallize the agent with oligonucleotides. We report herein the complex with a DNA palindromic hexanucleotide: 5′-d(CGTACG)-3′. To our surprise, we observe molecular recognition not of duplex DNA but rather of a singular DNA structure, a three-way junction (Figure 1 b), which defines a unique triangular-shaped hydrophobic binding site.

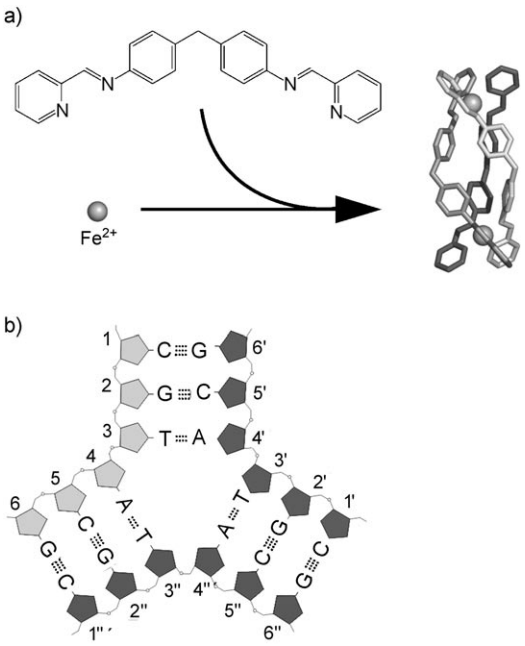


Figure 1. a) The $[Fe_2L_3]^{4+}$ ($L = C_{25}H_{20}N_4$) tetracationic supramolecular helicate with the Fe^{2+} ions represented as spheres; b) The three-way junction of this study showing the DNA sequence used, 5′-d(CGTACG)-3′, and the base-pair arrangement.

The structure of the DNA–supramolecule complex is shown in Figure 2. The DNA has formed a three-way Y-shaped junction and the central hollow space of the junction is occupied by the tetracationic supramolecular compound. The structure of the helicate drug does not suffer any significant conformational change upon binding to DNA (see the Supporting Information). This helicate has remarkable dual characteristics: on one hand it has high positive charge because of the two Fe^{2+} ions axially located at both ends of the drug and, on the other hand, it displays a large hydrophobic surfaces due to the presence of 12 aromatic rings. Both characteristics are driving forces for the noncovalent recognition of the DNA junction by the helicate. First, an electrostatic-dipole interaction occurs between the positively charged supramolecule and the negatively charged DNA phosphates (Figure 3 a). Second, the phenyl rings at the centre of the helicate form extensive π-stacking interactions with the thymine and adenine bases at the junction. Considering a single organic strand, one phenyl ring (B) is stacked on T3, whereas the other phenyl ring (C) is stacked on A4 (Figure 3 b). Because of the threefold symmetry of the drug, which matches the threefold symmetry of the three-way junction, this double stacking interaction is repeated three times. Also, strikingly, the twist between the two phenyl rings B and C of the drug is exactly 60°, which matches the 60° kink in the DNA strand between bases T3 and A4. This therefore allows a perfect stack between consecutive bases and consecutive phenyl rings.

 © 2006 Wiley-VCH Verlag GmbH & Co. KGaA, Weinheim

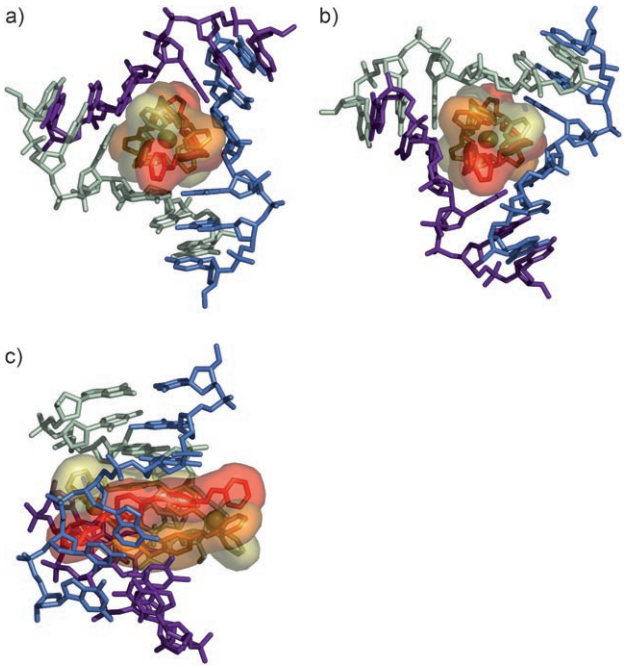


Figure 2. Three-dimensional structure of the $[Fe_2L_3]^{4+}$–DNA complex. The drug is shown with both sticks and surface representations, whereas the Fe^{2+} ions are shown as spheres. a) Major groove side view; b) Minor groove side view; c) Lateral view. One of the Fe^{2+} ions and three terminal phenyl rings stick out from the junction major groove side.

The three pyridine rings (D) at one end of the drug are located at the minor-groove side of the junction and are again twisted 60° with respect to phenyl rings C. This permits them to occupy the DNA minor grooves sandwiched between two opposite DNA-backbone sugar moieties, namely A4 of one strand and C5 of the complementary strand (Figure 3c). This interaction is reminiscent of those observed in minor-groove binders.[14] Similar to the interaction between minor-grove binders and A-tract DNA sequences, the minor groove narrows down, allowing strong van der Waals interactions between the drug and the DNA sugar–phosphate backbone. At the other end of the prismatic supramolecule, the three pyridine rings (A) occupy the major groove sticking away from the DNA and do not interact with it (Figure 2c).

No conventional hydrogen bonds are present between the drug and the DNA because the external surfaces of the drug contain only C–H units. However, short C–H···X interactions are observed between the imino C–H adjacent to rings D and the N3 nitrogen of A4; the (putative) hydrogen atoms are in the appropriate orientation for a C–H···X hydrogen bond (C···N3(A4) = 3.3 Å).

It is noteworthy that, out of several oligonucleotides differing in length (6, 8, 10, and 12 mers) and sequence, we have only obtained complex crystals when the central nucleotides are thymine and adenine (TA). The other crystals diffract to low resolution and thus are not reported further herein, despite that the data are similarly consistent with a three-way junction structure. Although this study is not exhaustive, it suggests that $[Fe_2L_3]^{4+}$ may bind selectively to three-way junctions with a central TA sequence.

A more-detailed analysis of the three-way DNA junction itself is revealing. Its structure corresponds to the open, nonstacked Y-shaped junction.[15–17] It has threefold symmetry which, in this case, corresponds to a crystallographic symmetry favored by the palindromic nature of the oligonucleotide sequence used. The three arms of the junction are therefore identical and there is no coaxial helix-to-helix stacking between them. Instead, the angle between the arms is 110°, with folding in an almost-flat pyramidal arrangement (Figure 2). All the bases are paired in a Watson–Crick manner and the backbone sugar moieties are in the C2′-*endo* conformation. The helical parameters correspond to B-DNA, with an average twist of 35°. The TA bases at the junction point are, at one of their faces, not stacked with other DNA bases, leaving a large triangular hydrophobic tunnel where the drug binds. When going along a single strand, a dramatic kink is apparent at the central T3–A4 segment, where the helical axis suddenly deviates by 60°. This structural feature imposes large deformations of the DNA-backbone geometry, namely an unusual backbone β and glycosidic χ torsion angles (Figure 3). The three-way junction defines two distinct sides or faces, a major groove side (Figure 2a) and a minor groove side (Figure 2b) in which the three respective major or minor grooves converge. At the arms, the minor

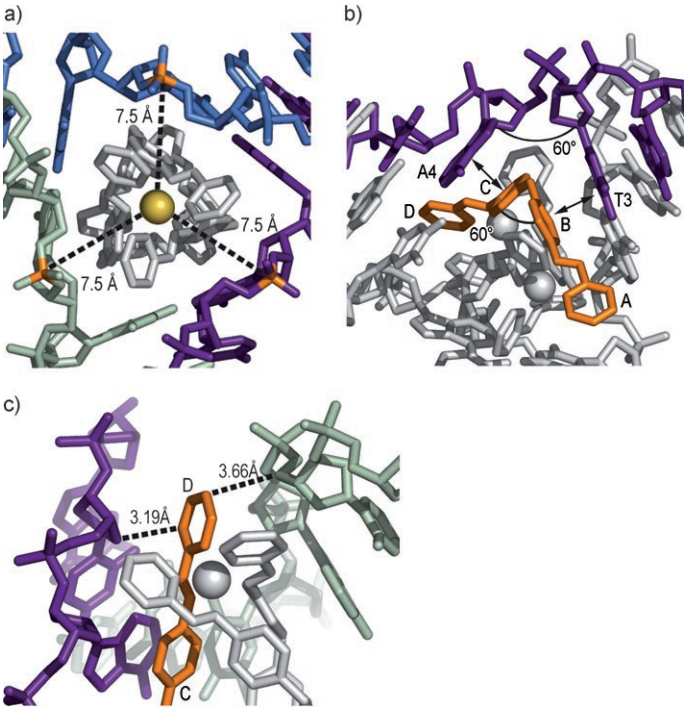


Figure 3. a) View along the junction threefold axis showing the iron–phosphate electrostatic interactions at the minor groove side; b) Stacking interactions (double arrows) between the phenyl rings B and C of the drug and the central T3 and A4 bases of the junction. The DNA strand shows large distortions at the junction point, unstacking of the bases, an unusual backbone β torsion angle (O5′(T3)-C5′(T3)) of 78°, and a glycosidic χ torsion angle of −150° at thymidine T3 ($\beta \approx 180°$ and $\chi \approx -110°$ in regular B-BNA); c) Interaction of the terminal phenyl ring D of the drug at the narrow minor groove of the DNA, reminiscent of minor groove-binding drugs. The Fe^{2+} ions are represented as spheres.

 © 2006 Wiley-VCH Verlag GmbH & Co. KGaA, Weinheim

groove has as narrow a width as the one observed in adenine-track DNA segments,[14] with room only for a single-water spine of hydration. The major groove has a regular B-DNA width.

Excitingly, the only previous example of an X-ray structure of a 3-way junction (of the Cre recombinase protein bound to a three-way junction)[18,19] shows DNA in the same Y conformation as the one we have found (Figure 4). Indeed, the structures are almost superimposable, which indicates that the three-way junction is not significantly perturbed by the drug binding but rather that it is an almost-perfect fit between both structures. Thus the present three-way DNA-junction structure is not an artefact of the crystal packing but rather a structural recognition target for both proteins and drugs.

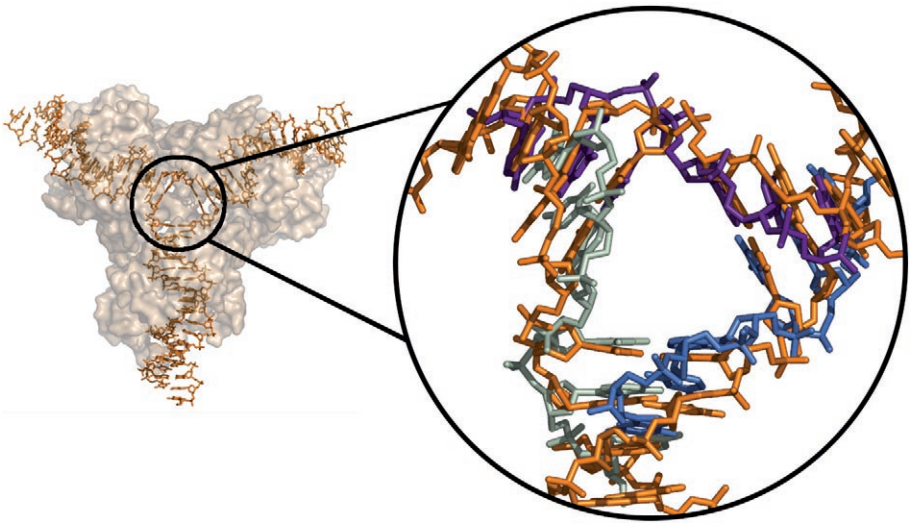


Figure 4. The three-way DNA junction (orange sticks) in the complex structure with Cre recombinase (surface)[18] and (inset) its superimposition with the DNA three-way junction reported herein (colored as in Figure 2). Both junctions have similar unstacked Y forms.

It is pertinent to consider the formation of the junction structure from this palindromic DNA hexanucleotide rather than the more-common double-stranded (ds) B-DNA structure. For a palindromic sequence, full Watson–Crick hydrogen bonding can, in principle, be satisfied within any oligomeric formulation (ds-DNA, three-way junction, four-way junction etc.). Palindromic DNA thus represents a potential dynamic combinatorial library[20] of oligomers, although entropic considerations would normally dictate adoption of a ds-structure. In this instance the triple-helical antiprism selected the member of the library (the three-way junction) to which it binds most effectively, therefore driving the equilibrium exclusively to this structure. Such an effect has implications for the emerging field of DNA nanotechnology.

The key feature in biomolecular DNA-recognition motifs is the size and shape of the molecular surfaces which match to the size and shape of the DNA target and provide a variety of recognition points. The structure herein reveals that our nanoscale supramolecular triple-helical antiprism is similarly matched to the size and shape of the cavity in the three-way DNA junction. It demonstrates that such a three-way DNA-junction structure is an appropriate target for the design of a new family of ligands with a high structural specificity and strong-binding characteristics. Furthermore, this work reveals an unprecedented mode of drug binding to DNA where four kinds of interactions act sinergically: $[Fe_2L_3]^{4+}$ provides both electrostatic interactions, face-to-face π-stacking intercalation-type interactions, C–H···X type H-bond interactions and minor-groove sandwiching interactions. These findings open the way for the development of anti-DNA therapeutic agents with completely novel characteristics and we are actively exploring this further.

Experimental Section

Crystallization and data collection: The synthesis of the helicate $[Fe_2L_3]Cl_4$ ($L = C_{25}H_{20}N_4$) (Figure 1) has been described previously.[12] Crystals were grown at room temperature from sitting drops that contained an aqueous solution of $[Fe_2L_3]Cl_4$ (0.5 μL of 10 mM), d(CGTACG) (1 μL of 3 mM), and reservoir solution (1.5 μL) that contains magnesium acetate (0.08 M), Tris-HCl (2-amino-2-(hydroxymethyl)-1,3-propanediol hydrochloride; 0.05 M; pH 8.5), and PEG 400 (5%). After one week, purple opaque octahedral crystals that measured $0.2 \times 0.2 \times 0.2\ mm^3$ appeared. For freezing, crystals were harvested in reservoir solution that contained glycerol (25%). A multiple wavelength anomalous dispersion (MAD) experiment was performed at the Fe–K-absorption edge at the European synchrotron radiation facility beamline BM16 (Grenoble). Furthermore, a high-resolution data set was collected at beamline ID14-EH2. All data sets were indexed and integrated with XDS[21] and scaled and merged with XSCALE (see the Supporting Information).

Structure determination and refinement: Six Fe atoms were located with SHELXD[22] from anomalous difference data. Initial MAD phases obtained by Harker construction and density modification with SHELXE,[23] allowed us to calculate an experimental 2.6 Å resolution map where one drug–DNA complex was readily interpretable. A second complex was located on a twofold axis, perpendicular to the helicate axis, and therefore disordered in two opposite orientations. The first complex was build by using the X-VIEW graphic software.[24] Once completed, this complex was used to build the second disordered complex in the two alternative conformations. This was done through the superimposition of the metal ions, which had been located clearly. Refinement of the structure followed by using SHELXL97,[25] with restraints for the disordered complex that was linked to the ordered complex and with half occupancy. Bulk solvent correction was applied and atomic isotropic temperature factors refined. TURBO-FRODO graphic software[26] was used for further model building and the introduction of water molecules. The final refinement and model statistics are described in the Supporting Information.

Atomic coordinates: The atomic coordinates have been deposited with the PDB at the European Bioinformatics Institute (EBI) under accession code 2ET0.

Received: October 28, 2005

Keywords: bioinorganic chemistry · biosupramolecular chemistry · DNA recognition · DNA structures · helical structures

 © 2006 Wiley-VCH Verlag GmbH & Co. KGaA, Weinheim

[1] For examples, see: P. B. Dervan, B. S. Edelson, *Curr. Opin. Struct. Biol.* **2003**, *13*, 284 – 299; *Cisplatin, Chemistry and Biochemistry of A Leading Anti-Cancer Drug* (Ed.: B. Lippert), Wiley-VCH, Weinheim, **1999**; J. Reedijk, *Chem. Commun.* **1996**, 801 – 806; Z. J. Guo, P. J. Sadler, *Adv. Inorg. Chem.* **2000**, *49*, 183 – 306; S. Neidle, *Nucleic acid structure and recognition*, Oxford University Press, Oxford, **2002**; S. J. Lippard, J. M. Berg, *Principles of Bioinorganic Chemistry*, University Science Books, Mill Valley, CA, **1994**; J. B. Chaires, *Curr. Opin. Struct. Biol.* **1998**, *8*, 314 – 320.

[2] R. Holliday, *Genet. Res.* **1964**, *5*, 282 – 304.

[3] M. Ortiz-Lombardia, A. Gonzalez, R. Eritja, J. Aymami, F. Azorin, M. Coll, *Nat. Struct. Biol.* **1999**, *6*, 913 – 917; B. F. Eichman, J. M. Vargason, B. H Mooers, P. S. Ho, *Proc. Natl. Acad. Sci. USA* **2000**, *97*, 3971 – 3976.

[4] T. Biswas, H. Aihara, M. Radman-Livaja, D. Filman, A. Landy, T. Ellenberger, *Nature* **2005**, *435*, 1059 – 1066; S. M. Roe, T. Barlow, T. Brown, M. Oram, A. Keeley, I. R. Tsaneva, L. H. Pearl, *Mol. Cell* **1998**, *2*, 361 – 372; D. N. Gopaul, F. Guo, G. D. Van Duyne, *Embo J.* **1998**, *17*, 4175 – 4187; M. Ariyoshi, T. Nishino, H. Iwasaki, H. Shinagawa, K. Morikawa, *Proc. Natl. Acad. Sci. USA* **2000**, *97*, 8257 – 8262; Y. Chen, U. Narendra, L. E. Iype, M. M. Cox, P. A. Rice, *Mol. Cell* **2000**, *6*, 885 – 897.

[5] C. Guthrie, B. Patterson, *Annu. Rev. Genet.* **1988**, *22*, 387 – 419.

[6] A. Nikulin, A. Serganov, E. Ennifar, S. Tishchenko, N. Nevskaya, W. Shepard, C. Portier, M. Garber, B. Ehresmann, C. Ehresmann, S. Nikonov, P. Dumas, *Nat. Struct. Biol.* **2000**, *7*, 273 – 277; B. T. Wimberly, D. E. Brodersen, W. M. Clemons, R. J. Morgan-Warren, A. P. Carter, C. Vonrhein, T. Hartsch, V. Ramakrishnan, *Nature* **2000**, *407*, 327 – 339; N. Ban, P. Nissen, J. Hansen, P. B. Moore, T. A. Steitz, *Science* **2000**, *289*, 905 – 920.

[7] M. R. Singleton, S. Scaife, D. B. Wigley, *Cell* **2001**, *107*, 79 – 89.

[8] C. E. Pearson, M. Tam, Y. H. Wang, S. E. Montgomery, A. C. Dar, J. D. Cleary, K. Nichol, *Nucleic Acids Res.* **2002**, *30*, 4534 – 4547.

[9] R. R. Sinden, *Nature* **2001**, *411*, 757 – 758.

[10] C. J. Leonard, K. I. Berns, *Prog. Nucleic Acid Res. Mol. Biol.* **1994**, *48*, 29 – 52; J. S. Ren, X. G. Qu, J. B. Chaires, J. P. Trempe, S. S. Dignam, J. D. Dignam, *Nucleic Acids Res.* **1999**, *27*, 1985 – 1990.

[11] F. Jensch, B. Kemper, *Embo J.* **1986**, *5*, 181 – 189.

[12] M. J. Hannon, V. Moreno, M. J. Prieto, E. Molderheim, E. Sletten, I. Meistermann, C. J. Isaac, K. J. Sanders, A. Rodger, *Angew. Chem.* **2001**, *113*, 903 – 908; *Angew. Chem. Int. Ed.* **2001**, *40*, 879 – 884; I. Meistermann, V. Moreno, M. J. Prieto, E. Moldrheim, E. Sletten, S. Khalid, P. M. Rodger, J. C. Peberdy, C. J. Isaac, A. Rodger and M. J. Hannon, *Proc. Natl. Acad. Sci. USA* **2002**, *99*, 5069 – 5074; M. J. Hannon, C. L. Painting, A. Jackson, J. Hamblin, W. Errington, *Chem. Commun.* **1997**, 1807 – 1808.

[13] C. Uerpmann, J. Malina, M. Pascu, G. J. Clarkson, V. Moreno, A. Rodger, A. Grandas and M. J. Hannon, *Chem. Eur. J.* **2005**, *11*, 1750 – 1756.

[14] M. Coll, C. A. Frederick, A. H. Wang, A. Rich, *Proc. Natl. Acad. Sci. USA* **1987**, *84*, 8385 – 8389.

[15] D. R. Duckett, D. M. Lilley, *Embo J.* **1990**, *9*, 1659 – 1664.

[16] This three-way junction differs from other three-way junctions derived by NMR (B. N. van Buuren, F. J. Overmars, J. H. Ippel, C. Altona, S. S. Wijmenga, *J. Mol. Biol.* **2000**, *304*, 371 – 383; V. Thiviyanathan, B. A. Luxon, N. B. Leontis, N. Illangasekare, D. G. Donne, D. G. Gorenstein, *J. Biomol. NMR* **1999**, *14*, 209 – 221; B. Wu, F. Girard, B. van Buuren, J. Schleucher, M. Tessari, S. Wijmenga, *Nucleic Acids Res.* **2004**, *32*, 3228 – 3239) in which two arms are stacked coaxially. However, the DNA sequences used in those studies, with unpaired bulged out bases, explains the marked differences compared with our structure.

[17] It is interesting that the three-way junction herein has a completely different geometry from the unliganded four-way junction (reference [3]). That junction was found in the X-stacked form, that is, with the arms coaxially stacked pairwise in two continuous helices rotated 45° and with a very compact structure at the crossing point. In contrast with the three-way junction reported herein, such a four-way junction leaves no room or hollow for ligand binding, except for the DNA grooves. However, the four-way junction is quite flexible and can respond structurally to binding events. Open, nonstacked square-planar four-way junctions are observed in the protein–DNA complex of RuvA and Cre recombinase (reference [4]). Also, several studies indicate that four-way DNA junctions can undergo a transition from a closed, X-stacked conformation to an open, nonstacked planar conformation when lowering the Mg^{2+} or other cation concentrations (D. R. Duckett, A. I. H. Murchie, S. Diekmann, E. Von Kitzing, B. Kemper, D. M. J. Lilley, *Cell* **1988**, *55*, 79 – 89). This is not the case in three-way DNA junctions, where variation in the counterion concentration does not affect the structure, which always remains in the open, nonstacked Y form (reference [15]). The presence of only three double strands drastically restrains the conformation possibilities of the three-way junction when compared with four-way junctions.

[18] K. C. Woods, S. S. Martin, V. C. Chu, E. P. Baldwin, *J. Mol. Biol.* **2001**, *313*, 49 – 69.

[19] Another three-way DNA junction has been reported in complex with the DNA repair protein Ku (J. R. Walker, R. A. Corpina, J. Goldberg, *Nature* **2001**, *412*, 607 – 614). In this case, a DNA junction was used only for the purpose of stabilizing the protein–DNA complex formation and the DNA used was not the natural substrate. Nevertheless, the same nonstacked Y conformation was observed for the junction.

[20] J. M. Lehn, *Chem. Eur. J.* **1999**, *5*, 2455 – 2463.

[21] W. Kabsch, *J. Appl. Crystallogr.* **1993**, *26*, 795 – 800.

[22] G. Sheldrick, H. Hauptmann, C. Weeks, R. Miller, I. Usón in *International Tables for Crystallography F* (Eds.: E. Arnold, M. Rosmann), Kluwer Academic Publishers, Dordrecht, **2001**, pp. 333 – 351.

[23] G. Sheldrick, *Z. Kristallogr.* **2002**, *217*, 644 – 650.

[24] D. E. McRee, *J. Struct. Biol.* **1999**, *125*, 156 – 165.

[25] G. Sheldrick, T. Scheider, *Methods Enzymol.* **1997**, *277*, 319 – 343.

[26] A. Roussel, C. Cambilleau in *Silicon Graphics geometry partners directory* 77–79, Silicon Graphics, Mountain View, CA, **1989**.

 © 2006 Wiley-VCH Verlag GmbH & Co. KGaA, Weinheim

Supramolecular Chemistry

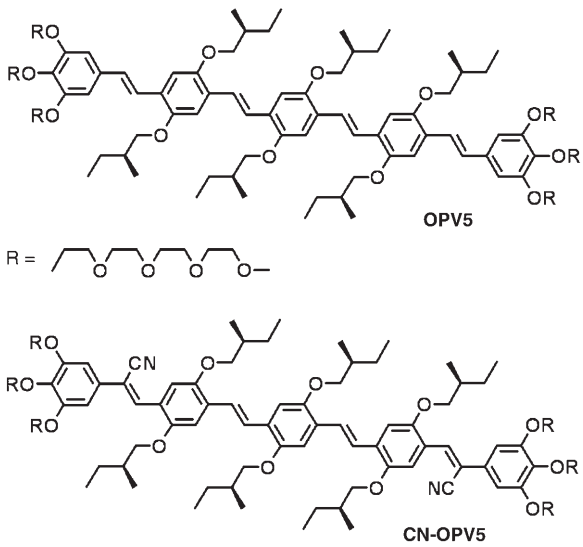
DOI: 10.1002/anie.200502187

Direct Visualization of Efficient Energy Transfer in Single Oligo(*p*-phenylene vinylene) Vesicles**

Freek J. M. Hoeben, Igor O. Shklyarevskiy, Maarten J. Pouderoijen, Hans Engelkamp, Albertus P. H. J. Schenning, Peter C. M. Christianen, Jan C. Maan, and E. W. Meijer**

Addressing the properties and interactions of individual self-assembled architectures is of great importance for the actual implementation of such objects in bio- and nanotechnological applications.[1] Supramolecular electronics depends on the ability to control the ordering of π-conjugated systems into well-defined, functional structures.[2] In natural photosynthetic systems, such a controlled organization yields directional energy and electron transfer in an aqueous environment.[3] Remarkably, only a few reports exist on self-assembled π-conjugated systems in water.[4] Our previous work on energy[5] and electron[6] transfer in self-assembled oligo(*p*-phenylene vinylene) (OPV) assemblies,[7] for example, focused on stacked oligomers in apolar solvents.[8] However, the interactions between self-assembled objects in water has become more appealing and challenging through the opportunities provided by scanning confocal microscopy. Herein we report on the use of fluorescence microscopy to characterize the properties and interactions of OPV assemblies in water by monitoring energy transfer.

OPV5 (Scheme 1) was previously synthesized and shown to form chiral assemblies in water, but no further details with regard to the type of architecture was presented.[4b] By using scanning confocal microscopy we now give direct evidence for the formation of OPV vesicles, an arrangement rarely observed with π-conjugated oligomers.[9] In addition we synthesized the analogous cyano-substituted **CN-OPV5**[10] to study energy transfer in mixed donor/acceptor vesicles in bulk solution as well as in single vesicles, immobilized on a glass surface. Furthermore, the exchange of chromophores between vesicles over time could be monitored.



Scheme 1. Chemical structures of the two oligomers used in this study. **OPV5** is used as an energy donor whereas **CN-OPV5** is used as an energy acceptor.

CN-OPV5 was synthesized according to standard literature procedures, and was obtained as a red waxy solid which was fully characterized.[11] **OPV5** was synthesized and characterized as reported previously.[4b] The optical properties of these two compounds were studied in various solvents by using UV/Vis, fluorescence, and circular dichroism (CD) spectroscopy (Figure 1). In general, **CN-OPV5** displays similar properties to **OPV5**: **CN-OPV5** is molecularly dissolved in chloroform, as indicated by a highly symmetrical π-π* transition at $\lambda_{max} = 482$ nm, intense fluorescence at $\lambda_{em} = 568$ nm, and the absence of any Cotton effect. The effect of cyano substitution in **CN-OPV5** on the HOMO–LUMO separation of the oligomer is clearly observed by comparison of the spectra with those of **OPV5**. The π-π* transition of **CN-OPV5** is shifted 32 nm bathochromically in chloroform, a feature which is desired for making it an energy acceptor for **OPV5**.

The absorption maximum of **CN-OPV5** in water[12] displays a modest hypsochromic shift of 9 nm (to $\lambda_{max} = 473$ nm) relative to that in chloroform, and develops a shoulder extending to $\lambda = 600$ nm. Its fluorescence is strongly quenched and red-shifted to $\lambda_{em} = 638$ nm, and concomitantly, a bisignate Cotton effect is observed, which is positive [+] at high energy and negative [−] at low energy ($g_{max[+]} = +4.9 \times 10^{-4}$ and $g_{max[-]} = -6.8 \times 10^{-4}$).[13] The curve crosses the zero line at $\lambda = 477$ nm, which is close to the wavelength of the absorption maximum. These collective findings indicate that **CN-OPV5** forms chiral, H-type aggregates in an aqueous environment through stacking of the π-conjugated backbones, similar to **OPV5**.[4b] Whereas **OPV5** exhibits quantum yields of $\phi = 0.64$ and $\phi = 0.10$ in THF and water, respectively,

[*] F. J. M. Hoeben, Dr. I. O. Shklyarevskiy, M. J. Pouderoijen, Dr. A. P. H. J. Schenning, Prof. Dr. E. W. Meijer
Laboratory of Macromolecular and Organic Chemistry
Eindhoven University of Technology
P.O. Box 513, 5600 MB Eindhoven (The Netherlands)
Fax: (+31) 40-245-1036
E-mail: a.p.h.j.schenning@tue.nl
e.w.meijer@tue.nl
Dr. I. O. Shklyarevskiy, Dr. H. Engelkamp, Dr. P. C. M. Christianen, Prof. Dr. Ir. J. C. Maan
High Field Magnet Laboratory
Institute for Molecules and Materials
Radboud University Nijmegen
Toernooiveld 7, 6525 ED Nijmegen (The Netherlands)

[**] This work was supported by the Council for Chemical Sciences of the Netherlands Organization for Scientific Research (CW-NWO) and the Royal Dutch Academy for Sciences (KNAW). We thank Dr. Xianwen Lou for matrix-assisted laser desorption ionization time-of-flight (MALDI-TOF) MS measurements.

Supporting information for this article is available on the WWW under http://www.angewandte.org or from the author.

InterScience® DISCOVER SOMETHING GREAT
© 2006 Wiley-VCH Verlag GmbH & Co. KGaA, Weinheim

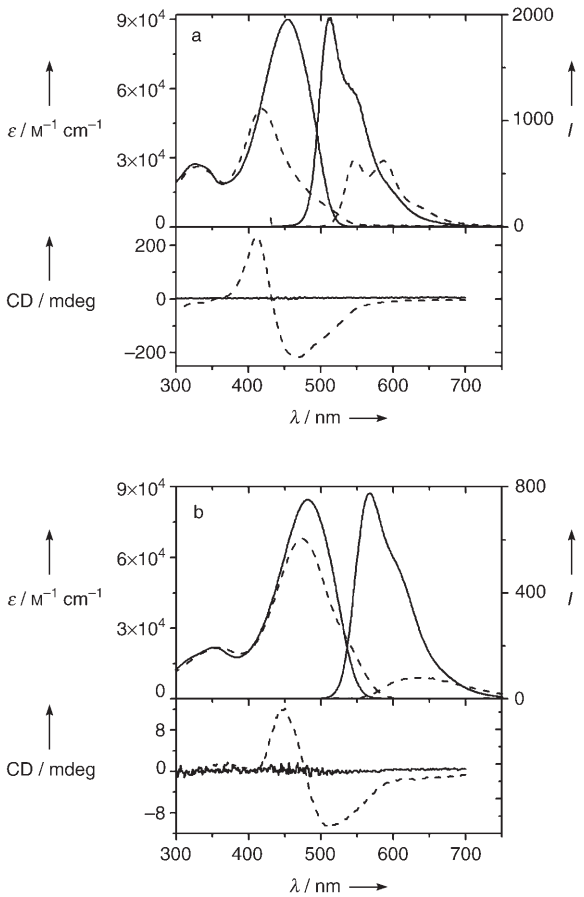


Figure 1. Optical properties of: a) **OPV5** and b) **CN-OPV5** in chloroform (solid line) and water (dashed line) at room temperature as studied by UV/Vis, fluorescence (λ_{exc} = respective λ_{max}), and CD spectroscopy. Concentrations are 1.6×10^{-5} M except for the CD spectroscopic measurements on **CN-OPV5** (7.3×10^{-5} M).

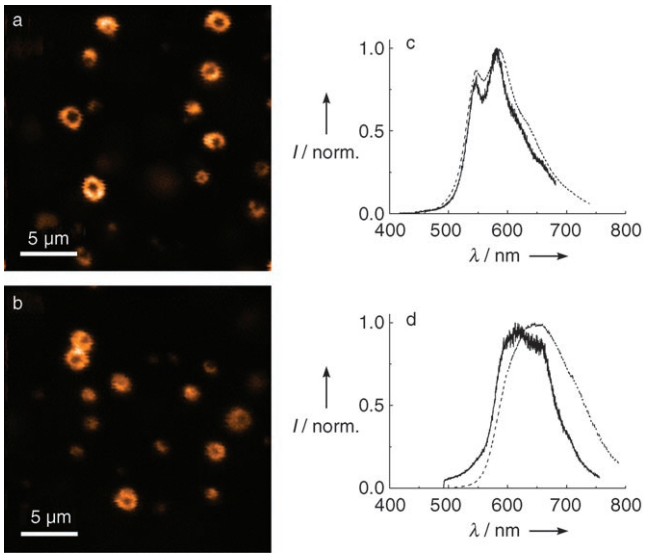


Figure 2. Scanning confocal microscopy images (λ_{exc} = 411 nm) of the vesicles of **OPV5** (a) and **CN-OPV5** (b) and fluorescence of single vesicles (solid lines) of **OPV5** (c) and **CN-OPV5** (d). Solution spectra are shown for comparison (dashed lines).

CN-OPV5 is somewhat less fluorescent, with $\phi = 0.49$ and $\phi = 0.08$ in THF and water, respectively.

To study the stability of the **CN-OPV5** aggregates, temperature-dependent UV/Vis, CD, and fluorescence studies were performed in water.[11] Despite the fact that the Cotton effect gradually disappears, the system is still strongly aggregated at 90 °C. This result is similar to that observed earlier for **OPV5** in water[4b] and was confirmed by dynamic light scattering (DLS) studies.[11] Hence, disorder is introduced at the molecular level, while strong hydrophobic forces hamper vesicle disruption at the microscopic level. The λ_{max} value of **CN-OPV5** recorded at 90 °C displays an additional hypsochromic shift of 35 nm, which suggests that the chromophores in the achiral supramolecular organization at high temperature are more tightly packed.

Dynamic light scattering studies indicated the presence of spheres of several hundreds of nanometers and micrometers in size for **CN-OPV5** and **OPV5**, respectively.[11] Scanning confocal microscopy was used to determine whether these spheres were hollow or solid (Figure 2). For these experiments, the solutions were gelated using 1 mg mL^{-1} gelatine[14] after which they were dropcast onto a glass surface and allowed to dry. It should be noted that the fluorescence spectrum of the parent solution, the undried gel, and the dried gel are similar, thus implying that the confocal images are representative of the solution conditions. Spheres as well as rings of micrometer size could be observed on a glass surface for both **OPV5** and **CN-OPV5**, thus suggesting the presence of vesicles. Slices could be made through the *z*-direction of a single vesicle by adjusting the focal plane of the microscope, which revealed a transition from a solid sphere via a ring back to a solid sphere. The photoluminescence spectra of these separate vesicles (Figure 2, λ_{exc} = 411 nm) were essentially identical to those obtained in solution, thus yielding definitive proof of the formation of OPV vesicles in water. Since supramolecular chirality is expressed in these structures, the vesicles are presumably composed of domains of helical OPV aggregates, as observed before for thiophene vesicles.[9b]

Energy-transfer experiments on **CN-OPV5** and **OPV5** were performed in water (Figure 3), with the aim of generating mixed vesicles and subsequent energy transfer from the **OPV5** donors to the **CN-OPV5** acceptors. Mixtures with various donor/acceptor ratios of were prepared in THF and subsequently injected into water to yield mixed vesicles. These mixtures were first studied in bulk solutions, followed by measurements at the single vesicle level.

Fluorescence data on the mixed samples show a strong decrease of host luminescence at λ_{em} = 546 nm as the acceptor content increases. At 1.6 mol % acceptor, the photoluminescence spectrum is almost completely dominated by **CN-OPV5** as a consequence of efficient energy transfer from **OPV5**. The luminescence of the sensitized acceptor at λ_{em} = 589 and λ_{em} = 634 nm is characteristic of molecularly dissolved species and indicates that **CN-OPV5** exists as isolated chromophores inside the donor vesicles. Increasing the amount of **CN-OPV5** to 31 mol %[11] induces acceptor aggregation, which is expressed in diminished and bathochromically shifted acceptor fluorescence. Time-resolved single-

 © 2006 Wiley-VCH Verlag GmbH & Co. KGaA, Weinheim

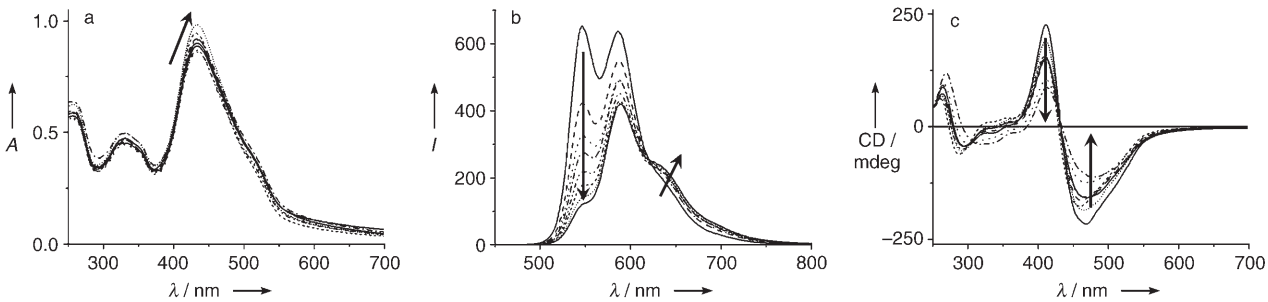


Figure 3. Mixtures containing 0–1.6 mol% **CN-OPV5** in **OPV5** in water as studied by: a) UV/Vis, b) fluorescence ($\lambda_{exc} = 419$ nm), and c) CD spectroscopy ([**OPV5**] $= 1.6 \times 10^{-5}$ M).

photon counting (TCSPC) measurements ($\lambda_{exc} = 400$ nm) were performed on **OPV5** doped with **CN-OPV5** and on both pure oligomers,[11] the latter showing a fluorescence lifetime increase upon cyano substitution of the backbone. Mixed vesicles show a sharp decrease in the lifetime of **OPV5** at $\lambda = 546$ nm, as a consequence of rapid depletion of its first excited state by energy transfer to **CN-OPV5**. The contribution of the longer-lived **CN-OPV5** luminescence at this wavelength becomes more dominant upon increasing the **CN-OPV5** content.

To directly prove the presence of mixed vesicles, a solution of **OPV5** containing 2 mol% **CN-OPV5** was prepared and deposited on a glass surface. The observed size of the vesicles decreased (Figure 4a); this effect was also observed in DLS studies on a similar mixture of the two oligomers.[11] More interestingly, the fluorescence spectra indicated almost complete energy transfer to and subsequent emission from **CN-OPV5** for all vesicles. In agreement with the solution data, the shape of the fluorescence spectrum proved the existence of isolated **CN-OPV5** in the donor **OPV5** vesicles. Furthermore, the sensitized **CN-OPV5** emission was bleached after about 50 s of excitation ($\lambda_{exc} =$ 411 nm) of a single vesicle.[11] As a result, the energy-transfer process was terminated and the fluorescence of the donor oligomer at $\lambda_{exc} = 546$ nm was restored. The luminescence of the donors started to bleach upon prolonged illumination. Interestingly, the bleaching of **CN-OPV5** in a mixed donor/acceptor vesicle occurred much faster than the bleaching of pure **CN-OPV5** vesicles, thus suggesting that **CN-OPV5** is in a state of enhanced excitation, because of light-harvesting from **OPV5**.

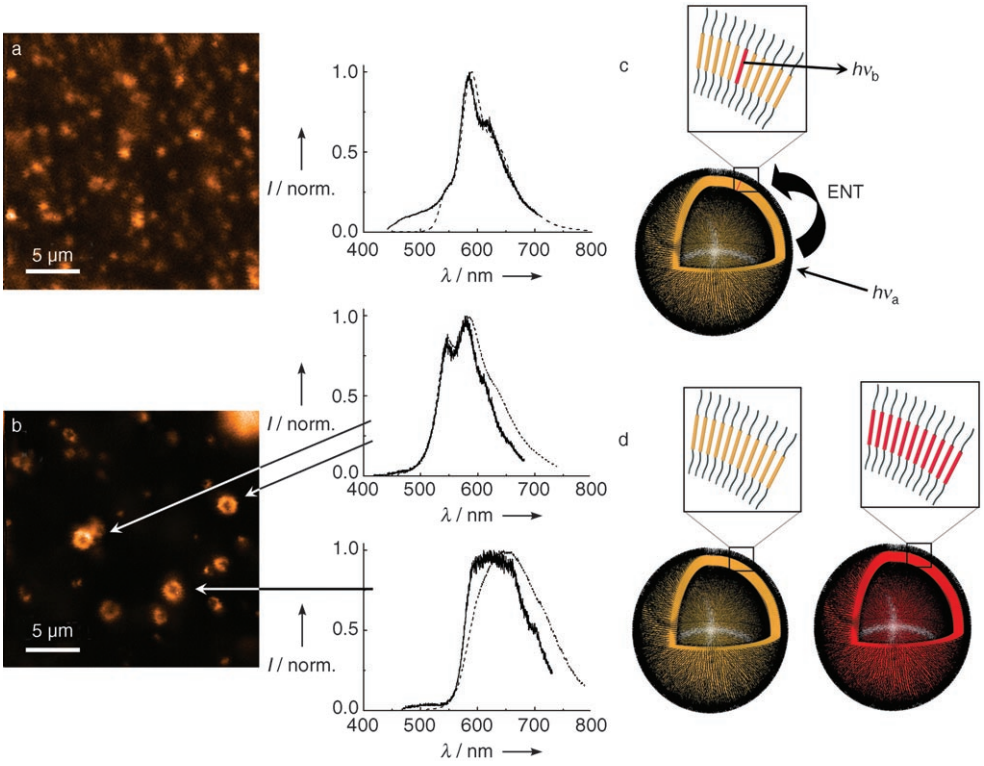


Figure 4. Scanning confocal microscopy images and resulting fluorescence spectra ($\lambda_{exc} = 411$ nm) of mixtures of **OPV5** and **CN-OPV5**: a) with premixing in THF (2 mol% **CN-OPV5**) and b) without premixing in THF (9 mol% **CN-OPV5**). The fluorescence of these single vesicles (solid lines) is compared to the corresponding solution spectra (dashed lines). c), d) Schematic representations of the vesicles formed in (a) and (b), respectively. ENT = energy transfer.

Aqueous solutions of individual vesicles of **OPV5** and **CN-OPV5** were added to study vesicle–vesicle interactions. Since no initial intermixing is possible in this way, the confocal image (Figure 4b) merely shows the presence of either pure **OPV5** or pure **CN-OPV5** vesicles as separate objects, which is concluded on the basis of their fluorescence spectra ($\lambda_{exc} = 411$ nm). The stability of the system containing separate vesicles in solution was examined over time by heating the solution at 35 °C for 48 h (Figure 5). Samples taken over this period were gelated and subsequently studied by confocal microscopy. After 48 h the system showed exclusively mixed vesicles, as characterized by efficient energy transfer from **OPV5** to **CN-OPV5**. Since **OPV5** vesicles could no longer be observed, we attribute this phenomenon to exchange between separate donor and acceptor vesicles. After 2 h, the ongoing exchange process could already be observed

 © 2006 Wiley-VCH Verlag GmbH & Co. KGaA, Weinheim

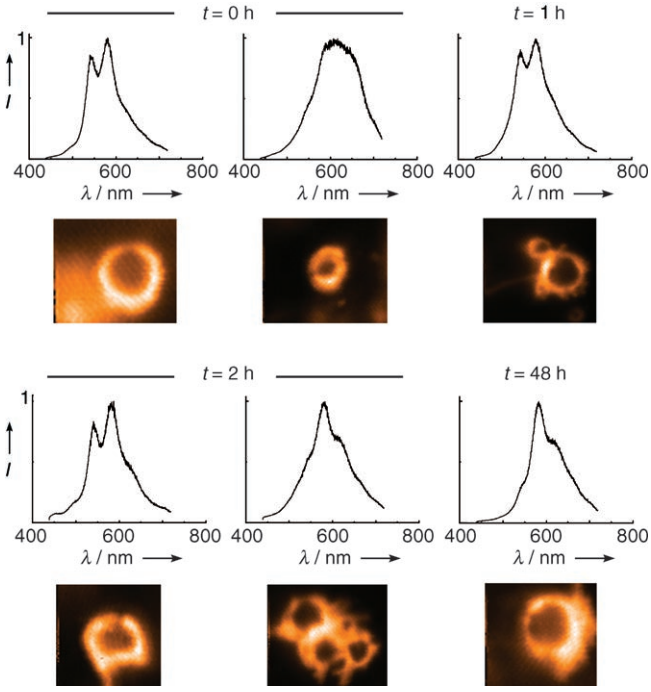


Figure 5. Scanning confocal microscopy images and normalized fluorescence (λ_{exc} = 411 nm) of single vesicles showing the transition from nonmixed to mixed vesicles on prolonged heating of a 2 mol% solution of **CN-OPV5** at 35 °C. At t = 0 h (and t = 1 h), **OPV5** vesicles and some **CN-OPV5** vesicles predominate. At t = 2 h some vesicles show energy transfer. After 48 h all the vesicles are mixed and show almost exclusive **CN-OPV5** luminescence (image sizes are 6×5, 10×9, 10×10, 8×8, 9×9, and 7×6 μm^2 respectively).

for some selected vesicles by scanning confocal microscopy, while the solution spectra[11] still showed an average situation that lacked energy transfer (Figure 5). Energy transfer in those vesicles resulted from the doping of **OPV5** vesicles with small amounts of **CN-OPV5** by the proposed exchange mechanism. These experiments show qualitatively that the OPV vesicles have individual properties which differ from the average solution data.

In conclusion, we have demonstrated the formation of π-conjugated OPV vesicles by using optical studies and scanning confocal microscopy. The synthesis of a cyano-substituted acceptor oligomer enabled us to study energy transfer in doped vesicles in water. Mixed vesicles were visualized on a glass surface by scanning confocal microscopy and thus the energy-transfer process could be studied at the single vesicle level. Moreover, probing the ongoing exchange process between separate donor and acceptor vesicles over time proved that the properties of individual vesicles were different from those of the bulk solution. These data convey the message that the study of single, self-assembled objects and the interaction between such objects yields important and detailed information on their behavior at the molecular level.

Received: June 22, 2005
Revised: December 5, 2005
Published online: January 19, 2006

Keywords: energy transfer · oligomers · scanning probe microscopy · supramolecular chemistry · vesicles

[1] See, for example: I. W. Hamley, *Angew. Chem.* **2003**, *115*, 1730 – 1752; *Angew. Chem. Int. Ed.* **2003**, *42*, 1692 – 1712.
[2] a) A. P. H. J. Schenning, E. W. Meijer, *Nature* **2002**, *419*, 353 – 354; b) F. J. M. Hoeben, P. Jonkheijm, E. W. Meijer, A. P. H. J. Schenning, *Chem. Rev.* **2005**, *105*, 1491 – 1546.
[3] a) W. Kühlbrandt, D. N. Wang, *Nature* **1991**, *350*, 130 – 134; b) W. Kühlbrandt, D. N. Wang, Y. Fujiyoshi, *Nature* **1994**, *367*, 614 – 621; c) Z. Liu, H. Yan, K. Wang. T. Kuang, J. Zhang, L. Gui, X. An, W. Chang, *Nature* **2004**, *428*, 287 – 292; d) G. McDermott, S. M. Prince, A. A. Freer, A. M. Hawthornthwaite-Lawless, M. Z. Papiz, R. J. Cogdell, N. W. Isaacs, *Nature* **1995**, *374*, 517 – 521; e) X. Hu, K. Schulten, *Phys. Today* **1997**, *50*, 28 – 34; f) S. Bahatyrova, R. N. Frese, C. A. Siebert, J. D. Olsen, K. O. van der Werf, R. van Grondelle, R. A. Niederman, P. A. Bullough, C. Otto, C. N. Hunter, *Nature* **2004**, *430*, 1058 – 1062.
[4] For examples with OPVs, see: a) H. Xiong, L. Qin, J. Sun, X. Zhang, J. Shen, *Chem. Lett.* **2000**, *35*, 586 – 587; b) P. Jonkheijm, M. Fransen, A. P. H. J. Schenning, E. W. Meijer, *J. Chem. Soc. Perkin Trans. 2* **2001**, 1280 – 1286; c) B. S. Gaylord, S. Wang, A. J. Heeger, G. C. Bazan, *J. Am. Chem. Soc.* **2001**, *123*, 6417 – 6418; d) B. Liu, B. S. Gaylord, S. Wang, G. C. Bazan, *J. Am. Chem. Soc.* **2003**, *125*, 6705 – 6714; e) J. F. Hulvat, M. Sofos, K. Tajima, S. I. Stupp, *J. Am. Chem. Soc.* **2005**, *127*, 366 – 372.
[5] F. J. M Hoeben, L. M. Herz, C. Daniel, P. Jonkheijm, A. P. H. J. Schenning, C. Silva, S. C. J. Meskers, D. Beljonne, R. T. Phillips, R. H. Friend, E. W. Meijer, *Angew. Chem.* **2004**, *116*, 2010 – 2013; *Angew. Chem. Int. Ed.* **2004**, *43*, 1976 – 1979.
[6] a) A. P. H. J. Schenning, J. van Herrikhuyzen, P. Jonkheijm, Z. Chen, F. Würthner, E. W. Meijer, *J. Am. Chem. Soc.* **2002**, *124*, 10252 – 10253; b) F. Würthner, Z. Chen, F. J. M. Hoeben, P. Osswald, C.-C. You, P. Jonkheijm, J. van Herrikhuyzen, A. P. H. J. Schenning, P. P. A. M. van der Schoot, E. W. Meijer, E. H. A. Beckers, S. C. J. Meskers, R. A. J. Janssen, *J. Am. Chem. Soc.* **2004**, *126*, 10611 – 10618.
[7] a) P. Jonkheijm, F. J. M. Hoeben, R. Kleppinger, J. van Herrikhuyzen, A. P. H. J. Schenning, E. W. Meijer, *J. Am. Chem. Soc.* **2003**, *125*, 15941 – 15949; b) P. Jonkheijm, A. Miura, M. Zdanowska, F. J. M. Hoeben, S. De Feyter, A. P. H. J. Schenning, F. C. De Schryver, E. W. Meijer, *Angew. Chem.* **20034**, *116*, 76 – 80; *Angew. Chem. Int. Ed.* **2004**, *43*, 74 – 78.
[8] a) L. M. Herz, C. Daniel, C. Silva, F. J. M. Hoeben, A. P. H. J. Schenning, E. W. Meijer, R. H. Friend, R. T. Phillips, *Phys. Rev. B* **2003**, *68*, 045203/1 – 045203/7; b) C. Daniel, L. M. Herz, C. Silva, F. J. M. Hoeben, P. Jonkheijm, A. P. H. J. Schenning, E. W. Meijer, *Phys. Rev. B* **2003**, *68*, 235212/1 – 235212/9.
[9] a) L. Jiang, R. C. Hughes, D. Y. Sasaki, *Chem. Commun.* **2004**, 1028 – 1029; b) I. O. Shklyarevskiy, P. Jonkheijm, P. C. M. Christianen, A. P. H. J. Schenning, E. W. Meijer, O. Henze, A. F. M. Kilbinger, W. J. Feast, A. Del Guerzo, J.-P. Desvergne, J. C. Maan, *J. Am. Chem. Soc.* **2005**, *127*, 1112 – 1113.
[10] a) R. W. Lenz, C. E. Handlovits, *J. Org. Chem.* **1960**, *25*, 813 – 817; b) I. D. W. Samuel, G. Rumbles, C. J. Collison, *Phys. Rev. B* **1995**, *52*, 573 – 576; c) R. E. Gill, P. F. van Hutten, A. Meetsma, G. Hadziioannou, *Chem. Mater.* **1996**, *8*, 1341 – 1346; d) P. F. Van Hutten, V. V. Krasnikov, H.-J. Brouwer, G. Hadziioannou, *Chem. Phys.* **1999**, *241*, 139 – 154; e) M. Hohloch, C. Maichle-Mössmer, M. Hanack, *Chem. Mater.* **1998**, *10*, 1327 – 1332; f) D. Oelkrug, A. Tompert, J. Gierschner, H.-J. Egelhaaf, M. Hanack, M. Hohloch, E. Steinhuber, *J. Phys. Chem. B* **1998**, *102*, 1902 – 1907; g) P. Martinez-Ruiz, B. Behnisch, K.-H. Schweikart, M. Hanack, L. Lüer, D. Oelkrug, *Chem. Eur. J.* **2000**, *6*, 1294 – 1301; h) M. Hanack, B. Behnisch, H. Häckl, P. Martinez-Ruiz, K.-H. Schweikart, *Thin Solid Films* **2002**, *417*, 26 – 31; i) H. Detert, D.

 © 2006 Wiley-VCH Verlag GmbH & Co. KGaA, Weinheim

Schollmeyer, E. Sugiono, *Eur. J. Org. Chem.* **2001**, 2927 – 2938; j) C. Löwe, C. Weder, *Adv. Mater.* **2002**, *14*, 1625 – 1629; k) B. R. Crenshaw, C. Weder, *Chem. Mater.* **2003**, *15*, 4517 – 4724.

[11] See the Supporting Information.

[12] In general, OPV aggregates are prepared in water by injecting a concentrated solution of OPV (4×10^{-4} M) in THF into water, followed by removal of the THF at 90 °C.

[13] The less intense CD signal relative to that of **OPV5** is probably a consequence of detrimental steric and electronic effects that accompany close packing between nitrile-substituted OPVs.

[14] Solutions containing OPV vesicles had to be gelated with gelatin prior to the confocal microscopy measurements, since otherwise the vesicles did not stick to the glass surface.

 © 2006 Wiley-VCH Verlag GmbH & Co. KGaA, Weinheim

Directed Evolution

DOI: 10.1002/anie.200502746

Directed Evolution of Enantioselective Enzymes: Iterative Cycles of CASTing for Probing Protein-Sequence Space**

Manfred T. Reetz, Li-Wen Wang, and in part Marco Bocola*

Directed evolution of enantioselective enzymes as catalysts in synthetic organic chemistry has emerged as a fundamentally new and useful approach to asymmetric catalysis.[1] It is based on earlier contributions by molecular biologists, biochemists, and biotechnologists who developed efficient random-gene mutagenesis methods, expression systems, and enzyme assays in the quest to enhance the stability and/or activity of enzymes.[2] By passing through at least two cycles of mutagenesis/screening,[3] Darwinistic character is introduced which forms the general basis of directed evolution. Therein, we first developed high-throughput *ee* assays[4] and applied them in the evolution of active and enantioselective mutants of lipases,[5] monooxygenases,[6] and epoxide hydolases.[7] Other researchers[8] have also contributed to this new area of asymmetric catalysis. Most directed evolution studies either begin with one or more cycles of error-prone polymerase chain reactions (epPCRs)[9] to introduce more or less random mutations that cover the whole gene (and thus enzyme) or a recombinant method such as DNA shuffling[10] is applied.

More recently, the utility of generating focused libraries of mutants that result from amino acid randomization at defined positions in the enzyme, has started to be explored.[2,5c,11] For example, in the case of the directed evolution of enantioselective lipases, we generated a focused library through the simultaneous randomization of four amino acids located adjacent to the binding pocket.[5c] In the quest to enhance enzyme activity, other groups have created focused libraries through the randomization of two, three, four, or more amino acids near the binding site,[11] as in the case of chorismate mutases.[11a]

In another study, systematic saturation mutagenesis at every-single position of the *Bacillus subtilis* lipase, which is composed of 181 amino acids, was considered, thereby generating 181 focused libraries for the purpose of finding enantioselective mutants.[12] This idea was developed independently by scientists at Diversa (USA), who were able to produce highly enantioselective nitrilases by this method.[13] Such saturation mutagenesis can be restricted to selected positions near the active site,[14] thereby lowering the screening effort (although restricting catalyst diversity). Other focused libraries,[2,11] such as those of binary patterning,[11a,b] are also useful tools. Although these strategies lead to improved enzymes, they are not evolutionary in nature unless at least one further round of mutagenesis/screening follows. In many, if not most, practical cases this may be necessary. Efficiency in scanning larger parts of the protein-sequence space with the generation of high-quality libraries is therefore mandatory.[15] It minimizes the undesired formation of inferior (e.g., inactive) enzyme mutants and thus reduces the overall screening effort, which can be substantial in the case of enantioselectivity.[4]

Recently, we introduced a practical method in directed evolution called a combinatorial active site saturation test (CAST). CAST was originally developed with the purpose of expanding the range of substrate acceptance of an enzyme.[16] Based on the 3D structure of the enzyme, two or three amino acids, whose side chains reside next to the binding pocket, are identified and the respective positions are then randomized simultaneously with the creation of relatively small libraries of mutants. Through the use of this method, it was possible to obtain mutant lipases that catalyze the hydrolysis of esters derived from sterically demanding acids that are normally not at all accepted as substrates.[16] CASTing thus means the systematic design and screening of focused libraries around the complete binding pocket. Owing to the fact that two or three amino acids (rather than just one[12–14]) are simultaneously randomized at each site, high catalyst diversity is possible, therefore theoretically allowing the possibility of cooperative effects. The method is a useful alternative to epPCR as the starting point of directed evolution studies. However, it is not, in itself, an evolutionary process because only the initial libraries are considered. In our original paper,[16] we suggested that, for future work, Darwinistic character, which is central to directed evolution,[1,2,10,11,15] can be introduced through the performance of further rounds of mutagenesis/screening. This can be performed by using any

[*] Prof. Dr. M. T. Reetz, L.-W. Wang, Dr. M. Bocola
Max-Planck-Institut für Kohlenforschung
Kaiser-Wilhelm-Platz 1, 45470 Mülheim/Ruhr (Germany)
Fax: (+49) 208-306-2985
E-mail: reetz@mpi-muelheim.mpg.de

[**] Support by the Deutsche Forschungsgemeinschaft (Schwerpunktprogramm 1170 "Directed Evolution to Optimize and Understand Molecular Biocatalysis"; Project RE 359/13-1) and the Fonds der Chemischen Industrie is gratefully acknowledged. L.-W. W. thanks the DAAD for a doctoral stipend. We thank H. Hinrichs for HPLC analyses and J. D. Carballeira, M. Maywald and N. Otte for fruitful discussions.

InterScience
© 2006 Wiley-VCH Verlag GmbH & Co. KGaA, Weinheim

one of the conventional methods, such as epPCR or DNA shuffling after CASTing, which may lead to remote effects.[1,17] As an alternative, we herein propose iterative cycles of CASTing. Consider, for example, an enzyme for which the CAST analysis requires four randomization sites A, B, C, and D. At each site, two or three amino acid positions are randomized simultaneously depending on the CAST analysis. Following the generation and screening of the four respective initial libraries, the gene of each hit is then used as a template for the second round of CASTing. In each case, only two libraries are necessary, for example, the gene of the best mutant arising from A is used as a template for randomization at sites B and C, etc. (Figure 1). In practice, not all branches of this confined protein-sequence space need to be considered, nor is complete over-sampling absolutely mandatory.

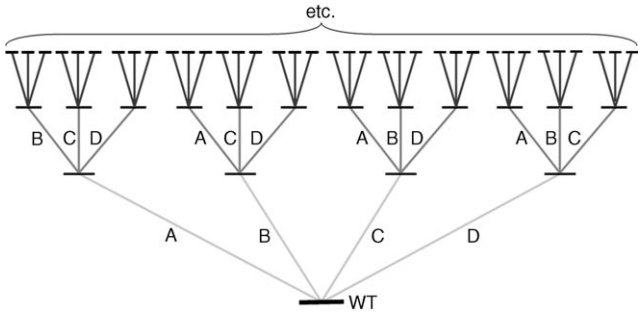
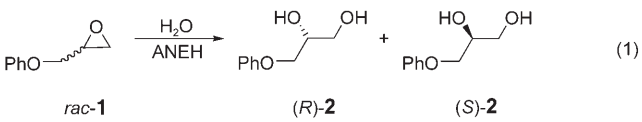


Figure 1. Schematic illustration of iterative CASTing involving (as an example) four randomization sites A, B, C, and D: Confined protein-sequence space for evolutionary enzyme optimization (redundancy in some cases is expected).

The concept of CASTing is illustrated herein with the directed evolution of enantioselective mutants of the epoxide hydrolase from *Aspergillus niger* (ANEH)[18–20] as catalysts in the hydrolytic kinetic resolution of the glycidyl ether **1** with formation of diols (*R*)- and (*S*)-**2**. The wild-type enzyme (WT-ANEH) catalyzes this reaction with a low selectivity factor ($E = 4.6$) in favor of (*S*)-**2** [Eq. (1)]. In previous work, the



rac-**1** (*R*)-**2** (*S*)-**2** (1)

enantioselectivity in this reaction was increased to $E = 10.8$ by screening several libraries produced by epPCR at different mutation rates (the number of total clones amounted to 20000).[7a] The *ee* screening was performed through the application of our previously described MS-based system[21] following a pre-screen[22] to identify the active clones. In the present study, we employed an improved expression system in *E. coli*,[7b] adapted the MS screen, and used an efficient pre-selection system for the elimination of inactive clones.[23]

The X-ray crystal structure[24] of the WT-ANEH reveals, amongst other things, a narrow hydrophobic tunnel as the substrate binding site.[25] The catalytically active triad, the tyrosines 251 and 314 (bind and activate the epoxide through H-bonds), and aspartate 192 (acts as the nucleophile in the rate-determining step) are located in and around the tunnel.[24] Inspection of the 3D structure suggests the creation of six CAST libraries[26] to be produced separately by randomization at sites 193/195/196 (A), 215/217/219 (B), 329/330 (C), 349/350 (D), 317/318 (E), and 244/245/249 (F) (Figure 2).

We have previously pointed out that for 95% coverage of a CAST library resulting from the simultaneous randomization at two (or three) amino acid positions, an excess of about 3000 (or 98000, respectively) clones needs to be screened.[16,27] However, one can settle for a lower degree of over-sampling and still be successful;[28] we have made these and other compromises in the present study. Experimentally, we began by subjecting the WT-ANEH to CASTing with generation of CAST libraries at sites A, B, and C, that is, in three separate experiments, positions 193/195/196, 215/217/219, and 329/330, respectively, were randomized. As shown in Table 1, no enhancement in enantioselectivity was observed in any of the mutants screened in the libraries that originated from the randomization of sites A or C. In contrast, several markedly improved mutants were discovered in the CAST library produced by randomization at positions 215/217/219 (site B). Therefore, the decision was made to continue the evolutionary process on this branch and not to consider, at this point, CAST libraries that potentially originate by randomization at sites D, E, and F, separately. One of the best mutants created by randomizing at site B (215/217/219) by using the WT gene, variant LW081, characterized by the three mutations L215F, A217N, and R219S, leads to an *E* value[29] of 14. This is similar to the structurally related and equally selective mutant LW080 (Table 1). Three other mutants appear to be more active because they showed higher conversions after shorter reaction times,[30] however, they were seen to be less stereoselective.

The mutant gene that corresponds to enzyme LW081 was then used as a template for a second cycle of CASTing, specifically by (arbitrarily) focusing on positions 329/330 (site C). Substantial improvements in enantioselectivity were observed with mutant LW086 ($E = 21$) being the best enzyme (Table 1). Mutant LW086 is characterized by two additional mutational changes of M329P and L330Y. Before continuing the ascent in enantioselectivity, it was of interest to perform CASTing with one of the mutant genes that encodes an enzyme displaying enhanced activity[30] but not improved enantioselectivity. For this purpose, gene LW037 (Table 1) was subjected to randomization at positions 329/330 with the creation of a new library. However, no substantially improved mutants were found (Table 1).

We then refocused our attention on mutant LW086 and used the corresponding gene in another cycle of CASTing. This time, positions 349/350 (site D) were chosen for simultaneous randomization. The best mutant was LW123 with one new mutational change C350V ($E = 24$). At this point, two different decisions for further evolutionary optimization appeared plausible: use of the same gene (LW086) for randomization at the other sites of the enzyme (A, B, C, E,

 © 2006 Wiley-VCH Verlag GmbH & Co. KGaA, Weinheim

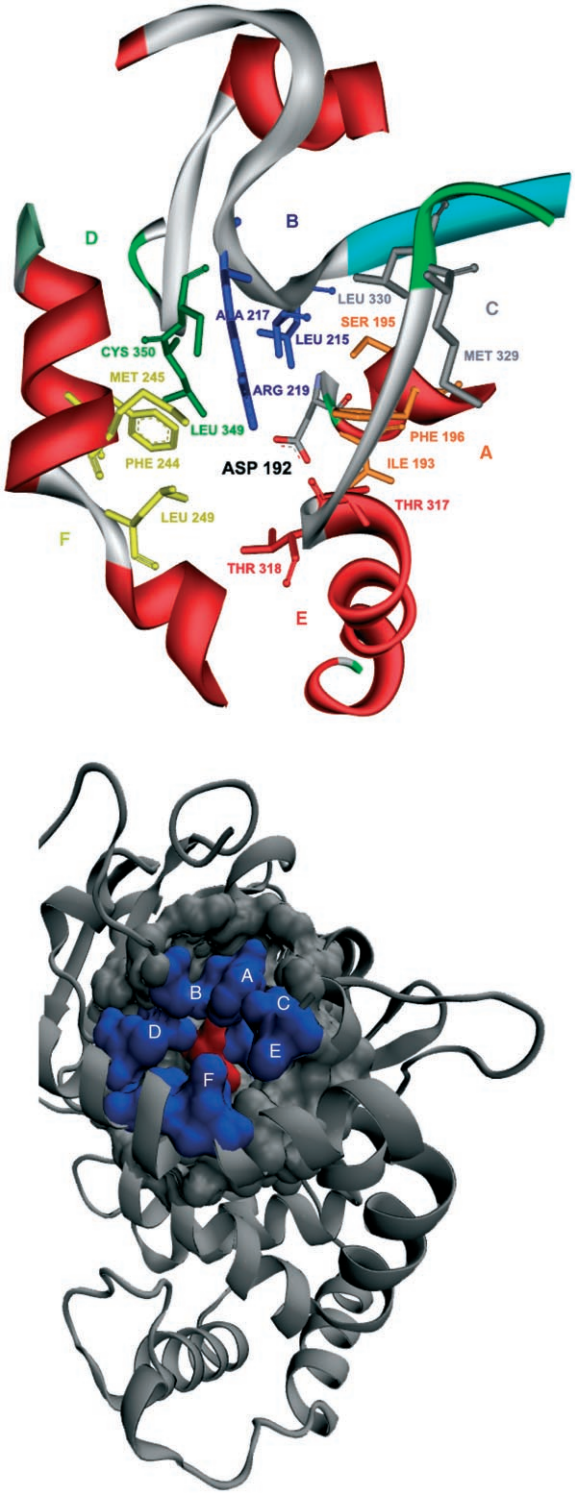


Figure 2. CASTing of the epoxide hydrolase from *Aspergillus niger* (ANEH) based on the X-ray crystal structure of the WT.[24] Top: Defined randomization sites A–E; Bottom: Top view of tunnel-like binding pocket showing sites A–E (blue) and the catalytically active Asp192 (red).

and/or F), or continuation of optimization with LW123. Herein we chose the latter, and created two new CAST libraries by using the LW123 gene as the template and focusing on sites E and F. This led to mutants LW126 ($E = 49$) and LW144 ($E = 35$) as shown in Table 1 and Figure 3.

Upon subjection of the gene LW126 to two separate and independent rounds of CASTing at positions 193/195/196 (site A) and 244/245/249 (site F), no substantial improvements in enantioselectivity were observed. Parallel to these efforts and before examining other positions, such as those defined by B, C, or D, gene LW144 was used as the template for CASTing in a different branch of the protein-sequence space. Randomization at positions 317/318 (site E) resulted in the identification of the, to date, most enantioselective mutant LW202, which shows a selectivity factor of $E = 115 \pm 10$ (Table 1 and Figure 3). This corresponds to a 25-fold increase in enantioselectivity relative to the WT, which therefore shows that iterative CASTing is an efficient way to engineer the ANEH tunnel. Sequencing revealed the presence of two new mutations, T317W and T318V. This means that the best enzyme variant (LW202) is characterized by a total of nine mutational changes (L215F, A217N, R219S, L249Y, T317W, T318V, M329P, L330Y, and C350V). At this stage we refrain from speculating about the origin of enhanced enantioselectivity. Before any sound conclusions can be made, isolation of mutant LW202 in its pure form is necessary, as are kinetic and detailed theoretical studies. Moreover, the question whether all nine mutational changes in the best mutant LW202 are actually necessary for high enantioselectivity needs to be addressed systematically. An initial experiment points to a

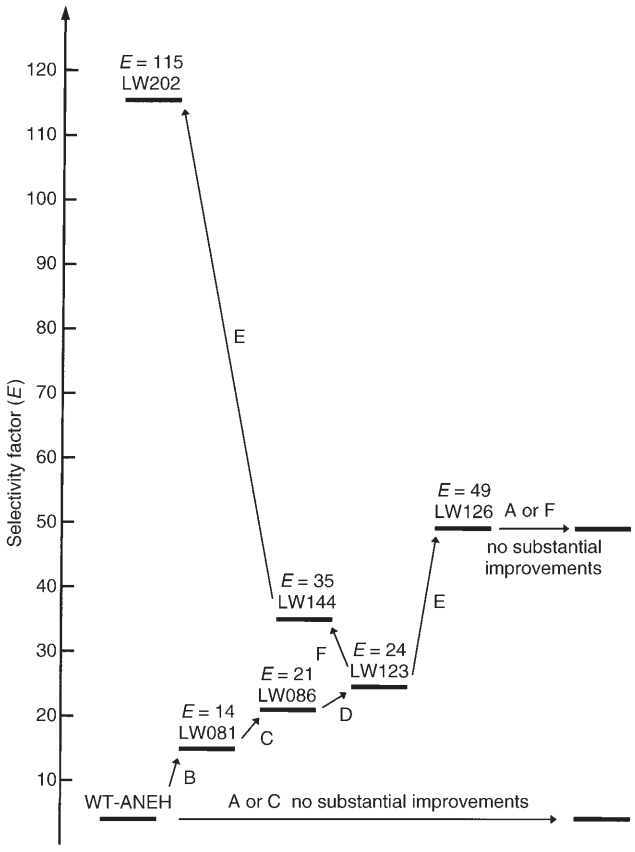


Figure 3. Iterative CASTing in the evolution of enantioselective epoxide hydrolases as catalysts in the hydrolytic kinetic resolution of *rac*-**1**.

 © 2006 Wiley-VCH Verlag GmbH & Co. KGaA, Weinheim

Table 1: Results of CASTing (I) and iterative CASTing (II).[a]

	Randomization sites	Template	Mutant	t_r [min][b]	Conversion [%]	ee_p [%][c]	ee_s [%][d]	Newly introduced mutations			E[e]	No. mutants screened	% active mutants
I	A					No substantial improvements						4000	38
	B	WT-ANEH	LW081	60	34	80	44	L215F	A217N	R219S	14	2200	25
			LW080	60	34	81	45	L215F	A217N	R219T	14		
			LW037	10	42	53	40			R219T	5		
			LW041	10	34	61	32		A217P	R219H	6		
			LW044	10	44	49	39			R219M	4		
	C					No substantial improvements						500	44
II	C	LW081	LW086	60	40	84	60		M329P	L330Y	21	2000	87
			LW102	60	31	86	41		M32K	L330T	19		
		LW037	LW094	60	71	37	97		M329T	L330Q	8		
			LW096	60	78	27	100		M329S	L330P	8		
	D	LW086	LW123	60	50	84	72			C350V	24	2200	6
			LW122	60	27	85	27		L349V	C350V	16		
			LW125	60	32	82	37		L349V		16		
	E	LW123	LW126	60	47	89	86			T318N	49	1600	66
			LW127	60	56	74	99		T317F	T318N	34		
			LW142	30	61	59	100		T317I	T318L	35		
	F		LW144	60	47	87	81			L249Y	35	1300	9
	A	LW126				No substantial improvements						3100	4
	F					No substantial improvements						1600	27
	E	LW144	LW202	60	48	95	94		T317W	T318V	>100	2000	63

[a] CASTing performed as a means to evolve enantioselective epoxide hydrolases as catalysts in the hydrolytic kinetic resolution of *rac*-**1**. [b] t_r = reaction time. [c] ee_p = enantioselectivity of the product. [d] ee_s = enantiopurity of the substrate. [e] E = enantioselectivity of the reaction.

substantial cooperative effect in at least one case. This concerns mutation C350V, introduced in mutant LW086, which raises the E value from 21 to (only) 24 (Figure 3; Table 1). We discovered that upon reintroduction of cysteine at position 350 in the final mutant LW202, enantioselectivity drops sharply from $E = 115$ to $E = 60$. This means that mutation C350V introduced in the early phase of the evolutionary process plays a significant role in the final mutant LW202. The mechanism of this cooperative effect needs to be studied in the future.

The present results were obtained by screening a total of only 20000 clones. This is about the same number of clones previously screened when using epPCR (at different mutation rates) as the method for library formation,[7a] yet the results of the two approaches are dramatically different ($E = 115$ versus $E = 10.8$). In iterative CASTing, the lower numbers of screened mutants are linked with higher numbers of libraries which need to be created. However, the latter is not the bottleneck, because a library of ANEH mutants can be generated in one day. It is likely that if iterative CASTing were to be performed more extensively to cover more of the focused branches of the confined protein-sequence space (Figure 1), even more hits would be discovered. For practical purposes this is not necessary, although we plan to do so for theoretical reasons. We anticipate that iterative CASTing[31] may also be useful when attempting to evolve other enzyme properties such as enhanced activity and/or broadened substrate acceptance.[16,32]

Received: August 4, 2005
Revised: October 28, 2005
Published online: January 13, 2006

Keywords: asymmetric catalysis · directed evolution · enantioselectivity · enzymes · epoxides

[1] For reviews of directed evolution of enantioselective enzymes, see: a) M. T. Reetz, *Proc. Natl. Acad. Sci. USA* **2004**, *101*, 5716–5722; b) M. T. Reetz in *Methods in Enzymology, Vol. 388* (Eds.: D. E. Robertson, J. P. Noel), Elsevier, San Diego, CA, **2004**, pp. 238–256; c) M. T. Reetz, *Tetrahedron* **2002**, *58*, 6595–6602; d) See also N. J. Turner, *Trends Biotechnol.* **2003**, *21*, 474–478.

[2] For reviews of directed evolution, see: a) *Methods in Molecular Biology, Vol. 230* (Eds.: F. H. Arnold, G. Georgiou), Humana, Totowa, NJ, **2003**; b) *Directed Molecular Evolution of Proteins (or How to Improve Enzymes for Biocatalysis)*, (Eds.: S. Brakmann, K. Johnsson), Wiley-VCH, Weinheim, **2002**; c) *Enzyme Functionality—Design, Engineering, and Screening*, (Eds.: A. Svendsen), Marcel Dekker, New York, **2004**; d) *Evolutionary Methods in Biotechnology (Clever Tricks for Directed Evolution)*, (Ed.: S. Brakmann, A. Schwienhorst), Wiley-VCH, Weinheim, **2004**; For a historical account of directed evolution which includes the early contributions of Manfred Eigen, see: e) A. Koltermann, U. Kettling, *Biophys. Chem.* **1997**, *66*, 159–177.

[3] One of the first reports regarding more than one cycle of mutagenesis/selection leading to evolutionary pressure was published in the mid 1980s, although this crucial idea was not generalized until the 1990s: see reference [2] and H. Liao, T. McKenzie, R. Hagemann, *Proc. Natl. Acad. Sci. USA* **1986**, *83*, 576–580.

[4] For reviews of high-throughput *ee* assays, see: a) M. T. Reetz, *Angew. Chem.* **2001**, *113*, 292–320; *Angew. Chem. Int. Ed.* **2001**, *40*, 284–310; b) M. T. Reetz, in *Enzyme Functionality—Design, Engineering, and Screening* (Ed.: A. Svendsen), Marcel Dekker, New York, **2004**, pp. 559–598; c) M. T. Reetz, in *Evolutionary Methods in Biotechnology* (Eds.: S. Brakmann, A. Schwienhorst), Wiley-VCH, Weinheim, **2004**, pp. 113–141; d) M. T.

 © 2006 Wiley-VCH Verlag GmbH & Co. KGaA, Weinheim

Reetz, in *Methods in Molecular Biology, Vol. 230* (Eds.: F. H. Arnold, D. Georgiou), Humana Press, Totowa, NJ, **2003**, pp. 259–282; e) M. T. Reetz, in *Methods in Molecular Biology, Vol. 230* (Eds.: F. H. Arnold, G. Georgiou), Humana Press, Totowa, NJ, **2003**, pp. 283–290; f) D. Wahler, J.-L. Reymond, *Curr. Opin. Biotechnol.* **2001**, *12*, 535–544.

[5] a) M. T. Reetz, A. Zonta, K. Schimossek, K. Liebeton, K.-E. Jaeger, *Angew. Chem.* **1997**, *109*, 2961–2963; *Angew. Chem. Int. Ed. Engl.* **1997**, *36*, 2830–2832; b) K. Liebeton, A. Zonta, K. Schimossek, M. Nardini, D. Lang, B. W. Dijkstra, M. T. Reetz, K.-E. Jaeger, *Chem. Biol.* **2000**, *7*, 709–718; c) M. T. Reetz, S. Wilensek, D. Zha, K.-E. Jaeger, *Angew. Chem.* **2001**, *113*, 3701–3703; *Angew. Chem. Int. Ed.* **2001**, *40*, 3589–3591; d) D. Zha, S. Wilensek, M. Hermes, K.-E. Jaeger, M. T. Reetz, *Chem. Commun.* **2001**, 2664–2665.

[6] a) M. T. Reetz, B. Brunner, T. Schneider, F. Schulz, C. M. Clouthier, M. M. Kayser, *Angew. Chem.* **2004**, *116*, 4167–4170; *Angew. Chem. Int. Ed.* **2004**, *43*, 4075–4078; b) M. T. Reetz, F. Daligault, B. Brunner, H. Hinrichs, A. Deege, *Angew. Chem.* **2004**, *116*, 4170–4173; *Angew. Chem. Int. Ed.* **2004**, *43*, 4078–4081.

[7] a) M. T. Reetz, C. Torre, A. Eipper, R. Lohmer, M. Hermes, B. Brunner, A. Maichele, M. Bocola, M. Arand, A. Cronin, Y. Genzel, A. Archelas, R. Furstoss, *Org. Lett.* **2004**, *6*, 177–180; For an improved expression system of ANEH in *E. coli*, see: b) F. Cedrone, S. Niel, S. Roca, T. Bhatnagar, N. Ait-Abdelkader, C. Torre, H. Krumm, A. Maichele, M. T. Reetz, J. C. Baratti, *Biocatal. Biotransform.* **2003**, *21*, 357–364.

[8] For further examples of enhanced enantioselectivity (evolutionary process was not involved in all cases), see: a) Aminotransferases: G. W. Matcham, A. R. S. Bowen, *Chim. Oggi* **1996**, *14*, 20–24; b) Esterases: U. T. Bornscheuer, J. Altenbuchner, H. H. Meyer, *Biotechnol. Bioeng.* **1998**, *58*, 554–559; c) Hydantoinases: O. May, P. T. Nguyen, F. H. Arnold, *Nat. Biotechnol.* **2000**, *18*, 317–320; d) Phosphotriesterases: M. Chen-Goodspeed, M. A. Sogorb, F. Wu, S.-B. Hong, F. M. Raushel, *Biochemistry* **2001**, *40*, 1325–1331; e) M. Chen-Goodspeed, M. A. Sogorb, F. Wu, F. M. Raushel, *Biochemistry* **2001**, *40*, 1332–1339; f) Monoamine oxidases: M. Alexeeva, A. Enright, M. J. Dawson, M. Mahmoudian, N. J. Turner, *Angew. Chem.* **2002**, *114*, 3309–3312; *Angew. Chem. Int. Ed.* **2002**, *41*, 3177–3180; g) Lipases: Y. Koga, K. Kato, H. Nakano, T. Yamane, *J. Mol. Biol.* **2003**, *331*, 585–592; h) Aldolases: M. Wada, C.-C. Hsu, D. Franke, M. Mitchell, A. Heine, I. Wilson, C.-H. Wong, *Bioorg. Med. Chem.* **2003**, *11*, 2091–2098; i) Epoxide hydrolases: B. van Loo, J. H. L. Spelberg, J. Kingma, T. Sonke, M. G. Wubbolts, D. B. Janssen, *Chem. Biol.* **2004**, *11*, 981–990; j) L. Rui, L. Cao, W. Chen, K. F. Reardon, T. K. Wood, *Appl. Environ. Microbiol* **2005**, *71*, 3995–4003.

[9] a) D. W. Leung, E. Chen, D. V. Goeddel, *Technique* **1989**, *1*, 11–15; b) R. C. Cadwell, G. F. Joyce, *PCR Methods Appl.* **1992**, *2*, 28–33; c) T. Eggert, M. T. Reetz, K.-E. Jaeger, in *Enzyme Functionality—Design, Engineering, and Screening* (Ed.: A. Svendsen), Marcel Dekker, New York, **2004**, pp. 375–390; d) For an illuminating study concerning high-error-rate epPCR, see: D. A. Drummond, B. L. Iverson, G. Georgiou, F. H. Arnold, *J. Mol. Biol.* **2005**, *350*, 806–816.

[10] For a review of DNA shuffling, see: K. A. Powell, S. W. Ramer, S. B. del Cardayré, W. P. C. Stemmer, M. B. Tobin, P. F. Longchamp, G. W. Huisman, *Angew. Chem.* **2001**, *113*, 4068–4080; *Angew. Chem. Int. Ed.* **2001**, *40*, 3948–3959.

[11] For examples of focused libraries, see: references [2,5c,12–15] and a) S. V. Taylor, P. Kast, D. Hilvert, *Angew. Chem.* **2001**, *113*, 3408–3436; *Angew. Chem. Int. Ed.* **2001**, *40*, 3310–3335; b) H. Xiong, B. L. Buckwalter, H. M. Shieh, M. H. Hecht, *Proc. Natl. Acad. Sci. USA* **1995**, *92*, 6349–6353; c) J. U. Bowie, R. T. Sauer, *Proc. Natl. Acad. Sci. USA* **1989**, *86*, 2152–2156; d) Y. Koga, K. Kato, H. Nakano, T. Yamane, *J. Mol. Biol.* **2003**, *331*, 585–592; e) J. A. Wells, M. Vasser, D. B. Powers, *Gene* **1985**, *34*, 315–323; f) J. D. Stevenson, S. J. Benkovic, *J. Chem. Soc. Perkin Trans. 2* **2002**, 1483–1493; g) M. Wilming, A. Iffland, P. Tafelmeyer, C. Arrivoli, C. Saudan, K. Johnsson, *ChemBioChem* **2002**, *3*, 1097–1104; h) A. Juillerat, T. Gronemeyer, A. Keppler, S. Gendreizig, H. Pick, H. Vogel, K. Johnsson, *Chem. Biol.* **2003**, *10*, 313–317; i) L. B. Evnin, J. R. Vásquez, C. S. Craik, *Proc. Natl. Acad. Sci. USA* **1990**, *87*, 6659–6663; j) A. R. Schmitzer, F. Lépine, J. N. Pelletier, *Protein Eng. Des. Sel.* **2004**, *17*, 809–819; k) J. Yang, Y. Koga, H. Nakano, T. Yamane, *Protein Eng.* **2002**, *15*, 147–152; l) M. S. Warren, S. J. Benkovic, *Protein Eng.* **1997**, *10*, 63–68; m) T. Yano, S. Oue, H. Kagamiyana, *Proc. Natl. Acad. Sci. USA* **1998**, *95*, 5511–5515; n) E. M. Gabor, D. B. Janssen, *Protein Eng. Des. Sel.* **2004**, *17*, 571–579; o) D. K. Dube, L. A. Loeb, *Biochemistry* **1989**, *28*, 5703–5707.

[12] S. A. Funke, A. Eipper, M. T. Reetz, N. Otte, W. Thiel, G. van Pouderoyen, B. W. Dijkstra, K.-E. Jaeger, T. Eggert, *Biocatal. Biotransform.* **2003**, *21*, 67–73.

[13] G. DeSantis, K. Wong, B. Farwell, K. Chatman, Z. Zhu, G. Tomlinson, H. Huang, X. Tan, L. Bibbs, P. Chen, K. Kretz, M. J. Burk, *J. Am. Chem. Soc.* **2003**, *125*, 11476–11477.

[14] a) G. P. Horsman, A. M. F. Liu, E. Henke, U. T. Bornscheuer, R. J. Kazlauskas, *Chem. Eur. J.* **2003**, *9*, 1933–1939; b) S. Park, K. L. Morley, G. P. Horsman, M. Holmquist, K. Hult, R. J. Kazlauskas, *Chem. Biol.* **2005**, *12*, 45–54; c) R. Kazlauskas, *Chem. Listy* **2003**, *67*, 329–337.

[15] S. Lutz, W. M. Patrick, *Curr. Opin. Biotechnol.* **2004**, *15*, 291–297.

[16] M. T. Reetz, M. Bocola, J. D. Carballeira, D. Zha, A. Vogel, *Angew. Chem.* **2005**, *117*, 4264–4268; *Angew. Chem. Int. Ed.* **2005**, *44*, 4192–4196.

[17] For examples of remote effects,[14] see: a) M. Bocola, N. Otte, K.-E. Jaeger, M. T. Reetz, W. Thiel, *ChemBioChem* **2004**, *5*, 214–223; b) S. Oue, A. Okamoto, T. Yano, H. Kagamiyama, *J. Biol. Chem.* **1999**, *274*, 2344–2349; c) A. Iffland, P. Tafelmeyer, C. Saudan, J. Johnsson, *Biochemistry* **2000**, *39*, 10790–10798; d) M. Kumar, K. K. Kannan, M. V. Hosur, N. S. Bhavesh, A. Chatterjee, R. Mittal, R. V. Hosur, *Biochem. Biophys. Res. Commun.* **2002**, *294*, 395–401; e) P. K. Agarwal, S. R. Billeter, P. T. R. Rajagopalan, S. J. Benkovic, S. Hammes-Schiffer, *Proc. Natl. Acad. Sci. USA* **2002**, *99*, 2794–2799; f) H. Zhao, F. H. Arnold, *Protein Eng.* **1999**, *12*, 47–53; g) L. K. Jackson, J. Baldwin, R. Akella, E. J. Goldsmith, M. A. Phillips, *Biochemistry* **2004**, *43*, 12990–12999; h) B. Lingen, D. Kolter-Jung, P. Dünkelmann, R. Feldmann, J. Grötzinger, M. Pohl, M. Müller, *ChemBioChem* **2003**, *4*, 721–726; i) S. McQ. Gould, D. S. Tawfik, *Biochemistry* **2005**, *44*, 5444–5452; j) V. G. H. Eijsink, S. Gåseidnes, T. V. Borchert, B. van den Burg, *Biomol. Eng.* **2005**, *22*, 21–30.

[18] a) C. Morisseau, A. Archelas, C. Guitton, D. Faucher, R. Furstoss, J. C. Baratti, *Eur. J. Biochem.* **1999**, *263*, 386–395; b) K. M. Manoj, A. Archelas, J. C. Baratti, R. Furstoss, *Tetrahedron* **2001**, *57*, 695–701; c) M. Arand, H. Hemmer, H. Dürk, J. Baratti, A. Archelas, R. Furstoss, F. Oesch, *Biochem. J.* **1999**, *344*, 273–280.

[19] For reviews of epoxide hydrolases, see: a) K. Faber, R. V. A. Orru in *Enzyme Catalysis in Organic Synthesis* (Eds.: K. Drauz, H. Waldmann), Wiley-VCH, Weinheim, **2002**, pp. 579–608; b) C. Morisseau, B. D. Hammock, *Annu. Rev. Pharmacol. Toxicol.* **2005**, *45*, 311–333; c) A. Archelas, R. Furstoss, *Curr. Opin. Chem. Biol.* **2001**, *5*, 112–119.

[20] For other important work on the directed evolution of enantioselective epoxide hydrolases, see references [8i,j].

[21] a) M. T. Reetz, M. H. Becker, H.-W. Klein, D. Stöckigt, *Angew. Chem.* **1999**, *111*, 1872–1875; *Angew. Chem. Int. Ed.* **1999**, *38*, 1758–1761; W. Schrader, A. Eipper, D. J. Pugh, M. T. Reetz, *Can. J. Chem.* **2002**, *80*, 626–632.

 © 2006 Wiley-VCH Verlag GmbH & Co. KGaA, Weinheim

[22] For information on pre-screens for EH activity, see: a) F. Zocher, M. M. Enzelberger, U. T. Bornscheuer, B. Hauer, R. D. Schmid, *Anal. Chim. Acta* **1999**, *391*, 345 – 351; b) D. Wahler, J.-L. Reymond, *Angew. Chem.* **2002**, *114*, 1277 – 1280; *Angew. Chem. Int. Ed.* **2002**, *41*, 1229 – 1232; c) K. Doderer, R. D. Schmid, *Biotechnol. Lett.* **2004**, *26*, 835 – 839.

[23] Herein, we employed an efficient selection system based on bacterial (*E. coli*) growth. The latter is directly related to the presence of active epoxide hydrolases which catalyze the detoxicating hydrolysis of epoxide substrates such as **1**: M. T. Reetz, L.-W. Wang, *Comb. Chem. High Throughput Screening*, in press.

[24] a) J. Y. Zou, B. M. Hallberg, T. Bergfors, F. Oesch, M. Arand, S. L. Mowbray, T. A. Jones, *Structure* **2000**, *8*, 111 – 122; b) http://www.pdb.ccdc.cam.ac.uk/pdb.

[25] For theoretical analyses of other enzymes with narrow tunnel-like binding pockets, some of which were re-engineered, see: reference [1a]; a) J. Schmitt, S. Brocca, R. D. Schmid, J. Pleiss, *Protein Eng.* **2002**, *15*, 595 – 601; b) H. Henriksson, J. Ståhlberg, R. Isaksson, G. Pettersson, *FEBS Lett.* **1996**, *390*, 339 – 344; c) M. Holmquist, F. Haeffner, T. Norin, K. Hult, *Protein Sci.* **1996**, *5*, 83 – 88.

[26] Based on the X-ray crystal structure of ANEH (see reference [24]), the nonresolved loop from postions 320 to 328 over the binding site was constructed by molecular modeling. The CAST libraries were then defined by using the completed protein model with substrate **1** in the binding pocket.

[27] For the application of mathematical expressions useful in the construction, description, and evaluation of protein libraries, see: a) A. D. Bosley, M. Ostermeier, *Biomol. Eng.* **2005**, *22*, 57 – 61; b) W. M. Patrick, A. E. Firth, J. M. Blackburn, *Protein Eng.* **2003**, *16*, 451 – 457; c) W. M. Patrick, A. E. Firth, *Biomol. Eng.* **2005**, *22*, 105 – 112.

[28] In our previous lipase project (reference [5c]), we created a focused library of mutants through the simultaneous randomization of amino acid positions 160/161/162/163 by using appropriate cassette mutagenesis. For a 95% sequence space coverage, this would require the screening of about three million clones (see references [16,27]). Although only 5000 were actually evaluated, markedly improved mutants were in fact found: The selectivity factor in the kinetic resolution of a chiral ester increased from $E = 1.2$ (WT) to 30 (mutant) (reference [5c]).

[29] All E values were derived through the application of the formula of Sih et al: C.-S. Chen, Y. Fujimoto, G. Girdaukas, C. J. Sih, *J. Am. Chem. Soc.* **1982**, *104*, 7294 – 7299.

[30] The conclusion regarding relative activity is only qualitative and is uncertain because it is based on the assumption of equal expression levels for the various mutants. A sound conclusion can only be made following a kinetic study of the isolated and purified mutants (which we are currently performing).

[31] A different type of evolutionary process can be envisioned through the combination of the mutations of two (or more) enzyme variants identified in the initial CAST libraries.

[32] For a review of practical asymmetric catalysis emphasizing the need to develop systems showing broad substrate scope, see: M. Breuer, K. Ditrich, T. Habicher, B. Hauer, M. Keßeler, R. Stürmer, T. Zelinski, *Angew. Chem.* **2004**, *116*, 806 – 843; *Angew. Chem. Int. Ed.* **2004**, *43*, 788 – 824.

 © 2006 Wiley-VCH Verlag GmbH & Co. KGaA, Weinheim

Homogeneous Catalysis

DOI: 10.1002/anie.200502985

Correlation of Metal Spin State with Catalytic Reactivity: Polymerizations Mediated by α-Diimine–Iron Complexes**

*Michael P. Shaver, Laura E. N. Allan, Henry S. Rzepa, and Vernon C. Gibson**

It has long been recognized that the metal spin state plays a central role in the reactivity of important biomolecules such as the heme-based metalloproteins.[1–5] In nonbiological systems the connection between metal spin state and reactivity, especially in catalysis, has remained largely undeveloped. Herein, we describe a homogeneous catalytic system in which closely related iron complexes with differing metal spin states afford starkly contrasting mechanistic outcomes in catalytic polymerization, to our knowledge the first time such distinct catalytic reaction pathways have been delineated for metal spin state isomers outside a biological manifold.

Four-coordinate α-diimine iron complexes [$^{R}(N,N)FeCl_2$] ($^{R}(N,N)$ = RN=CH−CH=NR) have previously been shown to be active as atom transfer radical polymerization (ATRP) catalysts for the controlled polymerization of styrene.[6,7] In our initial studies, we were surprised to find that ATRP predominates in reactions catalyzed by alkylimine derivatives whereas those catalyzed by arylimine complexes give rise to polymers in which catalytic chain transfer (CCT) is dominant.

Atom transfer radical polymerization is a versatile and increasingly exploited methodology for the synthesis of novel materials by controlled radical polymerization.[8] It involves a dynamic equilibrium between growing and dormant polymer chains using a metal-mediated halogen-exchange process. By ensuring the equilibrium is shifted towards the dormant species, radical concentrations remain low, reducing bimolecular termination and generating polymers with well-defined molecular weights that increase linearly with conversion. If the organoradicals are trapped by the Fe^{II} complex, then an organometallic species is generated which can undergo a β-hydrogen elimination reaction to give short chain, olefin-terminated oligomers, with molecular weights largely independent of conversion. This process is termed catalytic chain transfer.

[*] Dr. M. P. Shaver, L. E. N. Allan, Prof. H. S. Rzepa, Prof. V. C. Gibson
Department of Chemistry
Imperial College of Science, Technology and Medicine
London, SW7 2AZ (UK)
Fax: (+44) 20-7594-5810
E-mail: v.gibson@ic.ac.uk

[**] The Engineering and Physical Sciences Research Council of the United Kingdom and the Natural Sciences and Engineering Research Council of Canada are thanked for funding.

Supporting information for this article is available on the WWW under http://www.angewandte.org or from the author.

© 2006 Wiley-VCH Verlag GmbH & Co. KGaA, Weinheim

The observed polymerization mechanism is determined by the competition between the equilibria shown in Figure 1,[9] which may be viewed as arising from the differing halogenophilicities and carbophilicities of the Fe^{II} species,

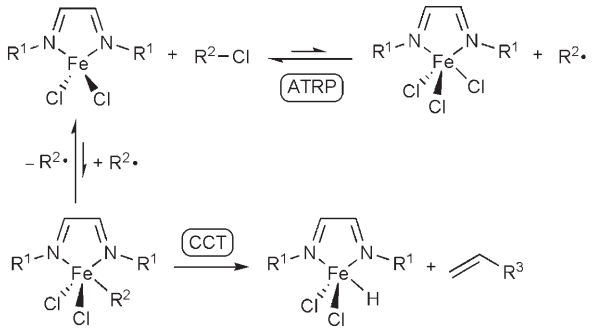


Figure 1. Equilibria involved in ATRP versus CCT polymerization (ATRP = atom transfer radical polymerization, CCT = catalytic chain transfer).

where halogenophilicity and carbophilicity can be defined as the relative predilection for a complex to form metal–halogen and metal–carbon bonds, respectively. In ATRP, an equilibrium is established between Fe^{II} dichloride and Fe^{III} trichloride complexes. The propensity for Fe^{II} complexes to react with a chloroalkane to form the oxidized species and a carbon radical is a function of its halogenophilicity. One mechanism by which catalytic chain transfer may occur involves the formation of a metal–carbon bond, followed by β-hydrogen elimination to generate an alkene-terminated polymer chain. If such a mechanism were operating, it would imply the presence of a second equilibrium in which the dormant Fe^{II} dichloride can trap and stabilize the free radical to form an Fe^{III} alkyl dichloride. The analogous idiom for this equilibrium can be termed carbophilicity.

To investigate the origin of the differing polymerization mechanisms of these iron catalysts, the trivalent derivatives [^{R}(*N*,*N*)$FeCl_3$] (R = cyclohexyl (Cy), **1**; *t*Bu, **2**; 2,6-*i*$Pr_2C_6H_3$ (DIPP), **3**) were prepared by addition of the α-diimines to $FeCl_3$. For **1**, a solution magnetic moment of 5.97 μ_B was obtained, corresponding well with the spin-only value of 5.92 μ_B for a d^5 high-spin iron(III) center (S = 5/2, sextet). The magnetic moment for **3** (3.99 μ_B) corresponds well to a d^5 intermediate-spin iron(III) center (3.87 μ_B, S = 3/2, quartet).[10] While intermediate-spin iron(III) is rare in biological systems,[11,12] numerous iron porphyrinogen and porphyrin complexes exist in quartet spin states.[13–15] This trend persists in other [^{R}(*N*,*N*)$FeCl_3$] complexes; aliphatic α-diimines have high-spin magnetic moments while lower spins are observed in aromatic systems. This difference correlates well with the observed polymerization behaviour; alkylimine iron complexes behave as ATRP catalysts, but arylimine systems promote CCT. Could this change in spin state account for the apparent change in halogenophilicity versus carbophilicity and thus determine the outcome of the polymerization?

All [^{R}(*N*,*N*)$FeCl_2$] complexes react cleanly with R–Cl species under polymerization conditions to give coupled products and the corresponding Fe^{III} species, illustrating the halogenophilic reactivity of each species. To probe the relative carbophilicity of [^{R}(*N*,*N*)$FeCl_2$] complexes, the mono-benzyl Fe^{III} complexes, [^{R}(*N*,*N*)$FeBnCl_2$] (Bn = CH_2Ph), were targeted. Addition of BnMgCl at −78 °C to **1** produced an immediate color change from yellow to deep purple, and [^{Cy}(*N*,*N*)$FeCl_2$] was isolated from the reaction mixture. GC analysis of the reaction products indicated the formation of bibenzyl (Bn_2, $PhCH_2CH_2Ph$) via the coupling of two alkyl radicals formed from the reductive alkylation of **1**. Similarly, alkylation of **2** produced bibenzyl at very low temperatures. The iron–carbon bond is unstable, generating carbon radicals in solution which couple to form the observed product.

The reaction of **3** with BnMgCl at −78 °C produced a markedly different result. GC analysis, after hydrolysis, showed that toluene was the major product, not bibenzyl. Upon warming the solution to −20 °C, a green-black to red color change coincided with the formation of bibenzyl, now the major decomposition product. The radical coupling occurs at a much higher temperature, implying that the alkyl complexes have improved stability. The graph in Figure 2

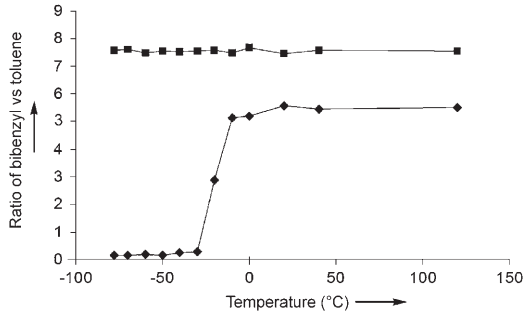


Figure 2. Ratio of integrated GC peaks for the formation of bibenzyl and toluene arising from the decomposition of [^{R}(*N*,*N*)$FeCl_2(CH_2Ph)$] at different temperatures; R = Cy (■), R = DIPP (◆). Higher ratios indicate bibenzyl is the primary decomposition product. Ratios below 1 indicate toluene is the primary decomposition product.

shows the ratio of bibenzyl/toluene formed as a function of temperature. Formation of bibenzyl predominates even at −78 °C when R = Cy (≈7.5 Bn_2/toluene), but toluene outweighs bibenzyl for R = DIPP (≈0.2 Bn_2/toluene) until −20 °C when decomposition occurs (≈5.5 Bn_2/toluene). It is clear that the aryl derivative has improved thermal stability; thus complex **3** is a better alkyl radical trap at low temperatures and therefore may be viewed as being more carbophilic. At polymerization temperatures, where all Fe^{III} species are transient, this increased stability will result in a shift in the relative positions of the equilibria in Figure 1. These experimental observations support the notion that the diisopropylphenyl derivative is more carbophilic and thus a better CCT catalyst than either of the cyclohexyl or *tert*-butyl derivatives. The lower-spin-state complexes will also have a vacant metal d orbital available to facilitate the subsequent β-hydrogen-elimination process.

To learn more about the role of metal spin state, a series of Hartree–Fock-level all-electron [ROHF/6-31G(3d)] calcula-

 © 2006 Wiley-VCH Verlag GmbH & Co. KGaA, Weinheim

tions were performed on model systems for the two competing reactions of [$^{R}(N,N)FeCl_2$]. The chosen basis set effectively reproduces core geometries of first-row transition-metal systems while ensuring reasonable calculation times.[16] Entropic differences required for Equation (2) are estimated by using the model system $CCl_2 + PhCH_2^{\cdot} \rightleftharpoons PhCH_2CCl_2^{\cdot}$. Previous studies[17–19] have shown that the choice of basis set and correlation treatment has a major influence on the relative stabilities of sextet and quartet states in iron systems. Although ROHF calculations overestimate the stability of the sextet state, producing large energy differences between sextet and quartet systems, they more accurately reproduce energy differences between two self-consistent sextet complexes.

Reactions (1) and (2), in which R is either *t*Bu or Ph, were

$$[^{R}(N,N)FeCl_2] + C_6H_5CH_2Cl \rightleftharpoons [^{R}(N,N)FeCl_3] + C_6H_5CH_2^{\cdot} \quad (1)$$

$$[^{R}(N,N)FeCl_2] + C_6H_5CH_2^{\cdot} \rightleftharpoons [^{R}(N,N)FeCl_2(CH_2C_6H_5)] \quad (2)$$

computed with the spin state of the iron complexes specified as either quartet (S = 3/2) or sextet (S = 5/2) for the Fe^{III} species. The relative preference of the two reactions for a particular spin state of iron is a determinant of carbophilicity versus halogenophilicity. For Fe^{III} sextet systems, halogenophilic behavior is favored. For R = *t*Bu and Ph, Reaction (1) is favored over Reaction (2) by 10.6 and 5.5 kcal mol^{-1}, respectively. This trend, however, is reversed for intermediate-spin quartet systems. For R = *t*Bu and Ph, Reaction (2) is now favored by 0.9 and 4.6 kcal mol^{-1}, respectively. The calculations thus predict that systems with S = 3/2 spin states are carbophilic while those with S = 5/2 spin states are halogenophilic. The calculations also show that for R = Ph the carbophilicity is even more pronounced, supporting the experimental evidence for arylimine carbophilicity.

An orbital correlation study between [$^{tBu}(N,N)FeCl_3$] sextet and quartet spin states suggests a rationale for the preference of intermediate spin states for arylimines. The quartet is formally linked to the sextet state by a single electron promotion, and this directly impacts upon the occupied orbital energies and their propensity to include mixing with other atomic orbitals (AOs). In the sextet state, molecular orbital (MO) 84 is singly occupied and predominantly Fe d AO in character with little other mixing. In the quartet state, this MO becomes doubly occupied with a resulting lower energy (61). This introduces metal-based d AOs mixing with ligand AOs of similar energy, creating a delocalized MO in which conjugation with the α-diimine is a prominent feature. This coupling suggests that changes to the electronic characteristics of the ligand substituents would have a strong influence on the nature of the quartet orbital (Figure 3) and hence the quartet/sextet balance.

As the conjugation of this orbital into the ligand backbone includes the 2 and 3 positions of the backbone, these sites will also affect the quartet state and its promotion to a sextet state. Systematic alteration of the backbone substituents should, therefore, control the metal spin state and thus catalyst behavior without significant alteration of the steric environment at the iron center. To tune the catalyst for halogeno- or

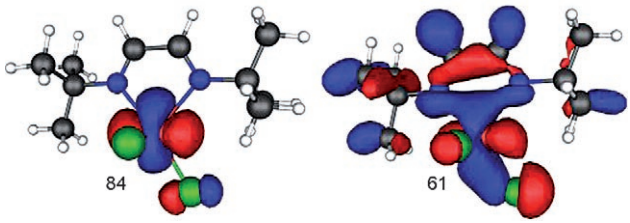


Figure 3. Selected orbital correlation between the singly occupied orbital in the [$^{tBu}(N,N)FeCl_3$] sextet (orbital 84, left) and doubly occupied orbital in the corresponding quartet (orbital 61, right).

carbophilicity, [$^{R}(N,N)FeCl_2$] complexes were targeted containing an electron-withdrawing *para*-fluorophenyl group at the 2 and 3 positions of the ligand backbone. Syntheses of [*t*BuN=C(C_6H_4F)]$_2$ (**4**) and [CyN=C(C_6H_4F)]$_2$ (**5**) were accomplished by condensation of the requisite amine with *para*-fluorobenzil, activated by $TiCl_4$.[20] Reaction of **4** or **5** with $FeCl_2$·1.5 THF[21] generated [$^{tBu,FC_6H_4}(N,N)FeCl_2$] (**6**) and [$^{Cy,FC_6H_4}(N,N)FeCl_2$] (**7**). The atom transfer radical polymerization of styrene initiated using 1-phenylethyl chloride (1-PECl) with [$^{Cy}(N,N)FeCl_2$] and [$^{tBu}(N,N)FeCl_2$] at 120 °C is characterized by low polydispersities and molecular weights that increase linearly with time and conversion.[4] The polymerization of styrene using the aryl-substituted catalysts **6** and **7** monitored under the same conditions generates polymer through a different mechanism. The reactions proceed relatively slowly (e.g. for **6**, $k_{obs.} = 0.02\ h^{-1}$) and the polymer obtained was of low molecular weight (Figure 4).

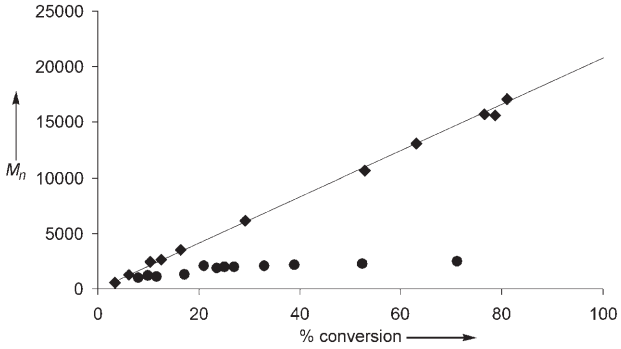


Figure 4. Plot of molecular weight, M_n, versus conversion for polymerization of styrene by [$^{tBu}(N,N)FeCl_2$] (♦) and [$^{tBu,FC_6H_4}(N,N)FeCl_2$] (●).

End-group analysis by multinuclear NMR spectroscopy confirmed that olefin-terminated polymer had formed. The polymerization mechanism has switched, generating low molecular weight polymer presumably by a catalytic chain transfer mechanism. Synthesis of the Fe^{III} complexes [$^{tBu,FC_6H_4}(N,N)FeCl_3$] (**8**) and [$^{Cy,FC_6H_4}(N,N)FeCl_3$] (**9**) established that control over metal spin state has been achieved. The two complexes have solution magnetic moments of 4.01 and 3.85 μ_B, respectively, indicating that both are intermediate-spin S = 3/2 systems. Evans' method NMR spectroscopic measurements over the temperature range 18–120 °C con-

 © 2006 Wiley-VCH Verlag GmbH & Co. KGaA, Weinheim

firmed that the intermediate spin state prevails at the polymerization temperature.

In summary, we have demonstrated a correlation between metal spin state and a simple catalytic chemical reaction, that of polymerization. For Fe^{III} species in a high spin state ($S = 5/2$), living atom transfer radical polymerization predominates, whereas with catalysts in an intermediate spin state ($S = 3/2$), an organometallic pathway leads to catalytic chain transfer. We have further shown that the metal spin state of the iron species can be controlled by judicious choice of α-diimine ligand substituents, highlighting the possibilities for the rational design of catalysts on the basis of metal spin state.

Experimental Section

All solvents were distilled over standard drying agents under nitrogen and were deoxygenated before use. All reactions were performed under an inert atmosphere. Full experimental and calculation details, as well as characterization and polymerization data can be found in the Supporting Information.

Ligand synthesis: To a solution of the appropriate amine (80.0 mmol) in CH_2Cl_2 (30 mL) at 0 °C was added dropwise $TiCl_4$ (1.0 M in CH_2Cl_2, 12.2 mL, 12 mmol). *p*-Fluorobenzene (2.5 g, 10 mmol) in CH_2Cl_2 (10 mL) was added dropwise, and the solution allowed to warm to room temperature and stir overnight. The reaction was quenched with water, filtered, and extracted into CH_2Cl_2. Removal of solvent left a sticky orange solid, which was recrystallized from MeOH (60 mL) to give off-white crystals of **4** (3.06 g, 84 %) and **5** (3.65 g, 88 %), respectively. Other diimine ligands were prepared as described in the literature.[22,23]

[^{R}(*N*,*N*)$FeCl_n$] synthesis: To a mixture of $FeCl_3$ or $FeCl_2$·1.5 THF (6.00 mmol) and ligand (6.00 mmol) was added CH_2Cl_2 (30 mL) and the resulting solution stirred for 24 h. Filtration of the solution, followed by removal of solvent in vacuo gave a greasy solid. Washing with pentane (3 × 15 mL) gave **1** as a yellow solid (67 % yield), **2** as an orange solid (74 %), **6**, **7**, and **8** as purple solids (72, 77, and 60 %, respectively), and **9** as a dark-red solid (70 %). [^{DIPP}(*N*,*N*)$FeCl_3$] (**3**) was prepared by heating a solution of ^{DIPP}(*N*,*N*) and $FeCl_3$ in THF at reflux for 18 h, followed by extraction into diethyl ether, removal of solvent, and washing with pentane to give a green-black solid (78 %).

Alkylation experiments: [^{R}(*N*,*N*)$FeCl_3$] (0.500 mmol) was dissolved in THF (10 mL) and cooled to −78 °C followed by dropwise addition of a solution of RMgCl (0.500 mmol) in THF. An aliquot (1 mL) was removed from the reaction mixture and quenched with distilled H_2O. Subsequent aliquots were removed and quenched over a range of temperatures. Aliquots were filtered through basic alumina and analysed by GC or GC/MS. GC area counts were corrected against organic components present in unreacted RMgCl.

Polymerization experiments: Styrene (5.000 g, 48.00 mmol), 1-phenylethyl chloride (32.0 μL, 0.240 mmol), and catalyst (0.240 mmol) were added to an ampoule equipped with a magnetic stirrer bar. The vessel was then sealed and heated to 120 °C. Conversion was determined by integration of signals for monomer versus polymer backbone in the ^{1}H NMR spectrum of crude aliquots (0.1 mL) removed from the reaction mixture at appropriate intervals. Upon completion of the reaction, the vessel contents were dissolved in THF and added dropwise to acidified methanol to precipitate the poly(styrene), which was washed and dried in vacuo. Samples were analysed by gel permeation chromatography against styrene standards to determine the molecular weight.

Received: August 22, 2005
Revised: October 17, 2005
Published online: January 17, 2006

Keywords: α-diimines · homogeneous catalysis · iron · polymerization · spin state

[1] R. J. P. Williams, *Fed. Proc. Fed. Am. Soc. Exp. Biol.* **1961**, *20*, 5.
[2] J. L. Hoard, M. J. Hoard, T. A. Hamor, W. S. Caughey, *J. Am. Chem. Soc.* **1965**, *87*, 2312.
[3] W. R. Scheidt, C. A. Reed, *Chem. Rev.* **1981**, *81*, 543.
[4] B. Meunier, S. P. de Visser, S. Shaik, *Chem. Rev.* **2004**, *104*, 3947.
[5] M. F. Perutz, A. J. Wilkinson, M. Paoli, G. G. Dodson, *Annu. Rev. Biophys. Biomol. Struct.* **1998**, *27*, 1, and references therein.
[6] V. C. Gibson, R. K. O'Reilly, D. F. Wass, A. J. P. White, D. J. Williams, *Macromolecules* **2003**, *36*, 2591.
[7] V. C. Gibson, R. K. O'Reilly, W. Reed, D. F. Wass, *Chem. Commun.* **2002**, 1850.
[8] K. Matyjaszewski, J. Xia, *Chem. Rev.* **2001**, *101*, 2921.
[9] E. Le Grognec, J. Claverie, R. Poli, *J. Am. Chem. Soc.* **2001**, *123*, 9513.
[10] Alternatively, this may be a mixture of ($S = 5/2$) and low-spin species ($S = 1/2$).
[11] K. Fisher, W. E. Newton, D. J. Lowe, *Biochemistry* **2001**, *40*, 3333.
[12] Y. Zeng, G. A. Caignan, R. A. Bunce, J. C. Rodríguez, A. Wilks, M. Rivera, *J. Am. Chem. Soc.* **2005**, *127*, 9794.
[13] J. Bachmann, D. N. Nocera, *J. Am. Chem. Soc.* **2005**, *127*, 4730.
[14] T. Sakai, Y. Ohgo, T. Ikeue, M. Takahashi, M. Takeda, M. Nakamura, *J. Am. Chem. Soc.* **2003**, *125*, 13028.
[15] T. Sakai, Y. Ohgo, A. Hoshino, T. Ikeue, T. Saitoh, M. Takahashi, M. Nakamura, *Inorg. Chem.* **2004**, *43*, 5034.
[16] K. P. Tellmann, M. J. Humphries, H. S. Rzepa, V. C. Gibson, *Organometallics* **2004**, *23*, 5503.
[17] R. J. Deeth, N. Fey, *J. Comput. Chem.* **2004**, *25*, 1840.
[18] N. J. DeYonker, Y. Yamaguchi, W. D. Allen, C. Pak, H. F. Schaefer, K. A. Peterson, *J. Chem. Phys.* **2004**, *120*, 4726.
[19] M. Swart, A. R. Groenhof, A. W. Ehlers, K. Lammertsma, *J. Phys. Chem. A* **2004**, *108*, 5479.
[20] N. DeKimpe, L. D'Hondt, E. Stanoeva, *Tetrahedron Lett.* **1991**, *32*, 3879.
[21] F. A. Cotton, R. L. Luck, K. A. Son, *Inorg. Chim. Acta* **1991**, *179*, 11.
[22] A. J. Arduengo, R. Krafczyk, R. Schumtzler, *Tetrahedron* **1999**, *55*, 14523.
[23] A. T. T. Hsieh, B. O. West, *J. Organomet. Chem.* **1976**, *112*, 285.

 © 2006 Wiley-VCH Verlag GmbH & Co. KGaA, Weinheim

Helical Structures

DOI: 10.1002/anie.200503136

Two-Dimensional Hierarchical Self-Assembly of One-Handed Helical Polymers on Graphite

Shin-ichiro Sakurai, Kento Okoshi, Jiro Kumaki, and Eiji Yashima**

The control and fabrication of ordered 2D arrays of molecules, in particular chiral (macro)molecules on substrates, is among the great challenges in materials science as these systems have attractive applications in chemical sensing, electro-optical devices, enantioselective adsorbents, and catalysis.[1] The concept of supramolecular self-assembly has been widely applied to the epitaxial alignments of chiral molecules on crystalline graphite and metals to create chiral surfaces, and their enantiomorphic 2D arrangements have been visualized by scanning probe microscopy (SPM).[2] However, it is still difficult to exploit biological and synthetic helical polymers[3] for the creation of 2D chiral surfaces by self-assembly because of their unfavorable strong surface interactions, which can compete with intermolecular interactions and change their inherent helical conformations, except for preorganized DNA with specific sequences[4] and nanopatterned collagen formed by dip-pen nanolithography.[5] Herein we show that cholesteric liquid-crystalline helical polyacetylenes self-assemble into ordered, 2D layered crystals on highly oriented pyrolytic graphite (HOPG). Flat monolayers epitaxially form on the basal plane of the HOPG, on which rodlike helical polyacetylenes further self-assemble into 2D helix-bundles with controlled molecular packing, helical pitch, and handedness upon exposure to organic solvents. The helical conformations in 2D crystals are visualized by atomic force microscopy (AFM) with molecular resolution and the results quantified by X-ray diffraction of the oriented liquid-crystalline polymer films.

Stereoregular (*cis–transoid*) poly(phenylacetylene) bearing L- or D-alanine residues with a long alkyl chain as pendants (namely, poly-**1L** and poly-**1D**, respectively; Figure 1a) were prepared according to a previously reported method.[6] The circular dichroism (CD) spectra of poly-**1L** and poly-**1D** in dilute benzene solution showed characteristic Cotton effects in the polymer backbone region (250–450 nm) that are mirror images of each other (Figure 1b), which indicates that the polymers have a predominantly one-handed

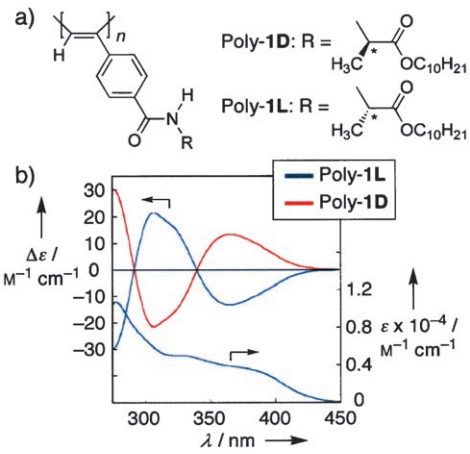


Figure 1. Chiroptical properties of poly-**1** in benzene. a) Structures of poly-**1D** and poly-**1L**. b) CD spectra of poly-**1L** and poly-**1D** in benzene. The absorption spectrum of poly-**1L** in benzene is also shown.

helical conformation with exactly the same helical structure except for the sense of their helicity.[6] Among a variety of helical polyacetylenes prepared so far, the polymers have an exceptionally rigid-rod main-chain character; this has allowed the formation of the first polyacetylene-based cholesteric liquid crystals in concentrated solutions.[6] The interplay between the chirality of the pendant groups, the macromolecular helicity, and the chirality at a macroscopic level is of great interest from fundamental and biological viewpoints. To this end, we have investigated the structures of the helical polymers on HOPG with AFM.

Figure 2a shows a typical AFM image of poly-**1L** spin cast on HOPG from a dilute benzene solution. The poly-**1L** molecules spontaneously self-assembled into a highly ordered monolayer as evidenced by parallel stripes with a periodicity of 4.72 ± 0.21 nm. On this 2D ordered first monolayer, irregular amorphous-like polymers with a height of 0.94 ± 0.3 nm were deposited (second layer as indicated by a red arrow in Figure 2a). The 2D fast Fourier transforms of this first layer showed threefold symmetry, which reflects the crystallographic structure of the HOPG substrate. The average corrugation height of the surface was 0.12 ± 0.02 nm from the profiles of the cross sections included in Figure 2a. The average height of the first monolayer was 0.38 ± 0.04 nm as derived from AFM observations of the isolated poly-**1L** monolayers prepared from a dilute solution in benzene ($0.01\ mg\,mL^{-1}$; see Supporting Information), which was less than the molecular diameter of a helical poly-**1** model (2.1 nm). These results indicate that the poly-**1L** molecules lie flat on the substrate with a planar conformation aligned parallel to the graphite lattice, probably because of the strong and epitaxial adsorption of the long pendant alkyl chains on HOPG; the chain-to-chain spacing of the first layer observed by AFM agreed with that of a model for aligned planar poly-**1** chains (Figure 2d, left). Similar epitaxial alignments on HOPG of long alkyl compounds and some macromolecules with long pendant alkyl chains were reported.[7]

Although the second layer of polymers deposited on the first layer appeared to be amorphous with no specific

[*] Dr. S.-i. Sakurai, Dr. K. Okoshi, Dr. J. Kumaki, Prof. E. Yashima
Yashima Super-Structured Helix Project
Exploratory Research for Advanced Technology (ERATO)
Japan Science and Technology Agency (JST)
101 Creation Core Nagoya, Shimoshidami, Moriyama-ku
Nagoya 463–0003 (Japan)
Fax: (+81) 52-739-2083
E-mail: kumaki@yp-jst.jp
yashima@apchem.nagoya-u.ac.jp

Supporting information for this article is available on the WWW under http://www.angewandte.org or from the author.

© 2006 Wiley-VCH Verlag GmbH & Co. KGaA, Weinheim

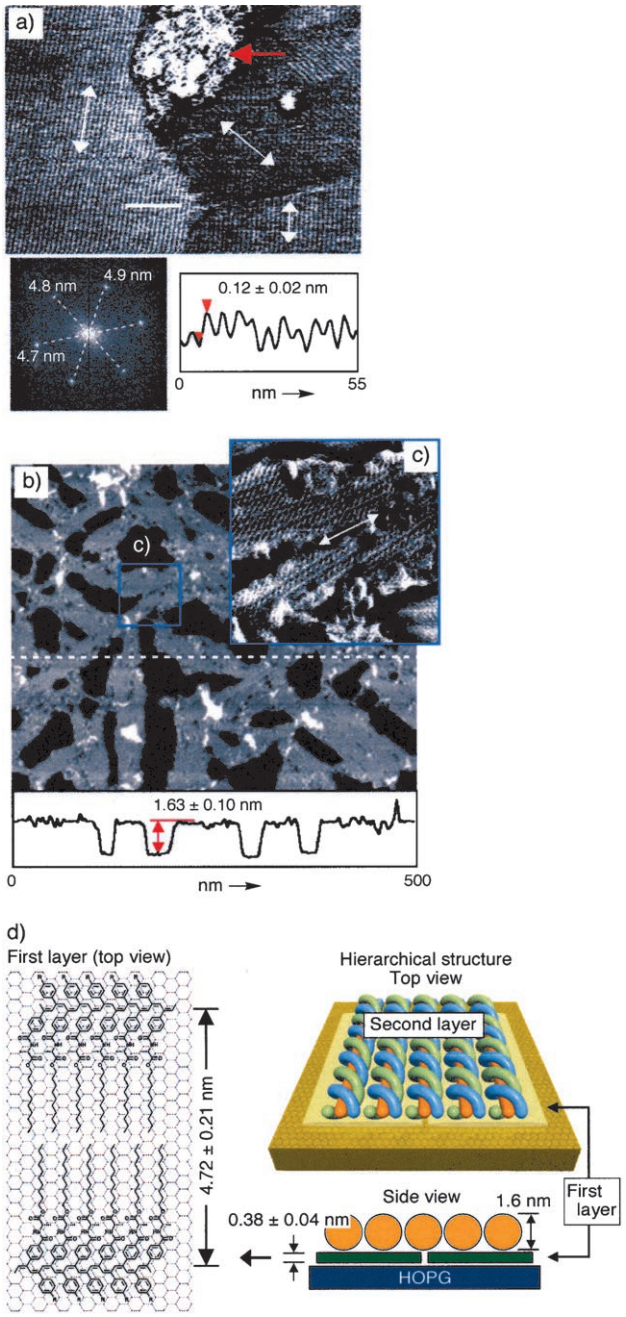


Figure 2. AFM observation of molecular ordering of poly-**1** on HOPG. a) AFM phase image of the epitaxial poly-**1L** crystals prepared by spin casting a dilute solution in benzene (0.05 mg mL^{-1}) on HOPG. The white arrows in the AFM image indicate the direction of the main-chain axes of the polymer; the red arrow indicates the amorphous polymer chains (scale: 250×350 nm). The cross-sectional profile shown by a white line and the typical 2D fast Fourier transform are also shown. b) AFM height image of poly-**1L** prepared by spin casting a solution in benzene (0.1 mg mL^{-1}) on HOPG followed by exposure to benzene vapor for 12 h at ambient temperature (ca. 22 °C; scale: 400×500 nm). The cross-sectional profile denoted by the white dashed line is also shown. c) High-magnification AFM phase image of poly-**1L** corresponding to the area indicated by the blue square in (b). The white arrow in the image indicates the direction of the main-chain axes of the polymer (scale: 70×70 nm). The 2D self-assembled poly-**1L** chains with a left-handed twisted structure can be clearly seen. d) Schematic representation of the hierarchical structure of the self-assembled poly-**1L** on HOPG.

structures, when exposed to benzene vapor for 12 h they further self-assembled into well-defined helix bundles with a constant height of 1.63 ± 0.10 nm (Figure 2b; see Supporting Information for its phase image). The orientation of the polymer strands in the second layer, which was anticipated to be influenced by that of the first layer, was nearly parallel to the polymer backbones underneath (first layer) and had approximately threefold symmetry (see Supporting Information). In the high-resolution AFM image (Figure 2c), the bundle structures are clearly resolved into individual left-handed helical poly-**1L** chains packed parallel to each other. Consequently, the first layer of the poly-**1** lamellae epitaxially deposited on the HOPG basal plane could not only prevent unfavorable direct interactions between helical poly-**1** chains and the HOPG but also serve as a template or soft nanoscopic "rails"[8] for subsequent formation of the upper-layer helix bundle with controlled helicity and lateral packing (Figure 2d, right).

Figure 3a and b show high-resolution AFM phase images of typical 2D arrangements of poly-**1L** and poly-**1D** (second layer) together with their magnified images after exposure to benzene vapor (Figure 3d).[9] These AFM images illustrate possible helical pitch and chain arrangements. As shown in Figure 3d, the 2D molecular ordering of each polymer consists of one-handed helical polymer chains in parallel arrangement; chain–chain spacing (2.13 ± 0.11 nm for poly-**1L** and 2.18 ± 0.10 nm for poly-**1D**) and helical pitch (2.34 ± 0.21 nm for poly-**1L** and 2.47 ± 0.18 nm for poly-**1D**) are similar for poly-**1L** and poly-**1D**.[10] The periodic oblique stripes (blue and green lines in Figure 3d AFM images), which originate from a one-handed helical array of the pendants, were tilted anticlockwise or clockwise at −41 and +42°, respectively, with respect to the axis of the main chain (red arrows in Figure 3a, b, and d). The tilt angles are constant irrespective of the direction of the chains. Some additional AFM images for different areas are shown in the Supporting Information. This remarkable 2D mirror-image relationship suggests that upon exposure to benzene vapor, poly-**1L** and poly-**1D** have enantiomeric left- and right-handed helical structures, respectively, with respect to the pendant arrangements.[11]

The 3D solid-state structure of poly-**1L** was investigated by X-ray analysis. Figure 3c shows a wide-angle X-ray diffraction (WAXD) pattern of a poly-**1L** film prepared from a concentrated cholesteric liquid-crystalline benzene solution and oriented in one direction. The WAXD pattern of the film shows diffuse-but-apparent meridional reflections on the lines of the 5th and 11th layers that are assignable to the turn-layer line and the unit height, respectively, thus giving a helix with 11 units per 5 turns and a translational length per unit of 0.212 nm (for more details, see the Supporting Information). Thus, the helical pitch estimated by AFM is in good agreement with the half pitch of the helical arrangements of the pendants as determined by X-ray analysis (2.33 nm), whereas the chain–chain spacing was slightly larger than that deduced from the WAXD pattern (1.97 nm) because the lateral spacing may be affected by hydrophobic interactions of epitaxially adsorbed pendant alkyl chains of

 © 2006 Wiley-VCH Verlag GmbH & Co. KGaA, Weinheim

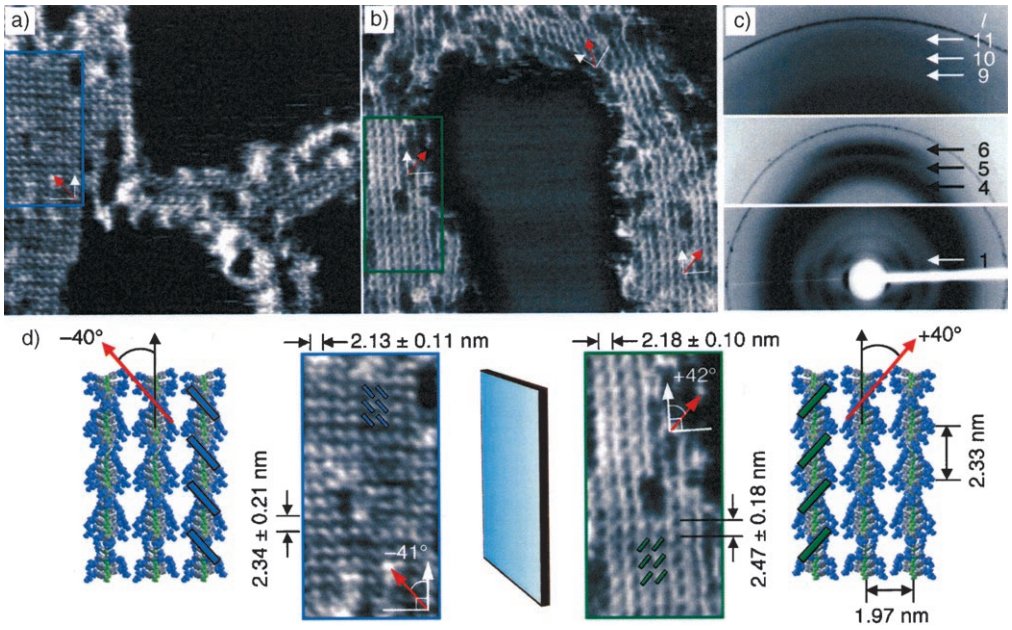


Figure 3. AFM images of self-assembled poly-**1** on HOPG and helical structures of poly-**1** proposed by X-ray analysis. AFM phase images of self-assembled a) poly-**1L** and b) poly-**1D**. The samples were prepared by spin casting solutions in benzene (0.1 mg mL^{-1}) on HOPG, followed by exposure to benzene vapor for 12 h at ambient temperature (ca. 20 °C; scale: 80×90 nm). c) WAXD patterns of an oriented poly-**1L** film prepared from a concentrated cholesteric liquid-crystal benzene solution (ca. 20 wt %). d) Magnified AFM phase images of poly-**1L** (middle left) and poly-**1D** (middle right), which correspond to the area indicated by the squares in (a) and (b), respectively (scale: 20×40 nm). Schematic drawings of the mirror-image relationship of helical poly-**1L** (middle left) and poly-**1D** (middle right; blue and green lines, respectively) 2D crystals with antipodal oblique pendant arrangements are also shown. Possible models (left and right) were constructed on the basis of the results of X-ray structural analysis.

the first layer of the poly-**1** lamellae (for comparison between the AFM and X-ray results, see the Supporting Information).

These AFM observations combined with X-ray structural analysis suggest that the helices of the poly-**1L** and poly-**1D** single chains are enantiomers, and both the enantiomeric left- and right-handed helical poly-**1** polymers provide the enantiomorphic 2D structures on the surface. In spite of extensive studies, determination of the absolute sense of helicity of biological and synthetic polymers still remains a difficult problem. Previous efforts have attempted to observe single macromolecules on surfaces by SPM.[12] Our approach based on the supramolecular self-assembly into a well-defined 2D crystal formation may be superior to previous approaches because the helical conformations are maintained in the 2D lattice, which can be easily recognized at high magnification.

In conclusion, we have demonstrated that upon exposure to solvent vapors rigid-rod helical polymers self-assemble to form ordered 2D crystals with a controlled helical conformation on a solid surface. The structures were visualized by AFM with molecular resolution. This system is conceptually new and provides an approach not only for the construction of chiral materials as chiral selectors and catalysts but also for the rational design of switchable chiral surfaces based on inversion of helicity of macromolecules.[3]

Experimental Section

Polymerization: Poly-**1L** and poly-**1D** were prepared according to a previously reported method by using a rhodium catalyst in THF.[6] The number-average molecular weight ($\bar{M}_n$) and the molecular-weight distribution ($\bar{M}_w/\bar{M}_n$; $\bar{M}_w$ is the weight-average molecular weight) for poly-**1L** was $\bar{M}_n = 2.0\times10^5$ and $\bar{M}_w/\bar{M}_n = 2.3$ and for poly-**1D** $\bar{M}_n = 3.2\times10^5$ and $\bar{M}_w/\bar{M}_n = 2.0$ as determined by size-exclusion chromatography with polystyrene standards and $CHCl_3$ as the eluent. All polymers had a highly *cis–transoidal* structure as deduced from their ^{1}H NMR spectra.[6]

Absorption and CD measurements: The absorption spectra were obtained by using a 0.2-mm quartz cell at 6 °C with a Jasco V570 spectrophotometer and CD spectra were obtained with a Jasco J820 spectropolarimeter. The temperature was controlled with a Jasco CDF-426 L instrument. The polymer concentration was calculated on the basis of the monomer unit and was 1.5 mg mL^{-1}.

AFM measurements: Stock solutions of poly-**1L** and poly-**1D** in dry benzene (0.05 and 0.1 mg mL^{-1}) were prepared. Samples for AFM measurements of poly-**1L** and poly-**1D** were prepared by spin casting 10-μL aliquots of the stock solutions of the polymers. The spin casting was carried out at room temperature at 1800 rpm on freshly cleaved HOPG. After the polymers had been deposited on the HOPG, the HOPG substrates were exposed to benzene vapors, then the substrates were dried under vacuum for 2 h. The organic vapors were prepared by putting benzene (1 mL) into a 2-mL flask that was inside a 50-mL flask, and the HOPG substrates were then placed in the 50-mL flask. The AFM measurements were performed by using a Nanoscope IIIa or Nanoscope IV microscope (Veeco Instruments, Santa Barbara, CA) in air at ambient temperature with standard silicon cantilevers (NCH, NanoWorld, Neuchâtel, Switzerland) and super-sharp cantilevers (SSS-NCH) in the tapping mode. Typical settings of the AFM for the high-magnification observations were as follows: amplitude 1.0–1.5 V; set point 0.9–1.4 V; scan rate 2 Hz. The Nanoscope image processing program was used for the image analysis (see also the Supporting Information).

WAXD analysis: Oriented helical poly-**1L** films for X-ray analyses were prepared by shearing one-directionally lyotropic

 © 2006 Wiley-VCH Verlag GmbH & Co. KGaA, Weinheim

liquid-crystalline solutions of poly-**1L** in benzene cast on a glass plate. After being dried in air, the oriented poly-**1L** films were floated off the glass substrates onto water, carefully collected, then dried. Several oriented poly-**1L** films were prepared and piled up with the orientation direction parallel for X-ray measurement. X-ray measurements were carried out on a Rigaku RINT RAPID-R X-ray diffractometer with a rotating-anode generator with graphite monochromated $Cu_{K\alpha}$ radiation (0.15418 nm) focused through a 0.3-mm pinhole collimator, which was supplied at 50 kV and 100-mA current, equipped with a curved imaging plate of specimen-to-plate distance 127.4 mm. X-ray photographs were taken at ambient temperature (20–25 °C) from the edge-view position with a beam parallel to the film surface (see also the Supporting Information).

Molecular modeling and calculations: Molecular modeling and molecular-mechanics calculations were conducted with the Compass force field as implemented in the MS Modeling program (version 3.1, Accelrys Inc., San Diego, CA) operated by a PC running under Windows XP (see also the Supporting Information).

Received: September 5, 2005
Revised: November 7, 2005
Published online: January 13, 2006

Keywords: chirality · helical structures · scanning probe microscopy · self-assembly

[1] a) S. De Feyter, F. C. De Schryver, *Chem. Soc. Rev.* **2003**, *32*, 139 – 150; b) S. M. Barlow, R. Raval, *Surf. Sci. Rep.* **2003**, *50*, 201 – 341.

[2] a) L. C. Giancarlo, G. W. Flynn, *Acc. Chem. Res.* **2000**, *33*, 491 – 501; b) S. De Feyter, A. Gesquière, M. M. Abdel-Mottaleb, P. C. M. Grim, F. C. De Schryver, C. Meiners, M. Sieffert, S. Valiyaveettil, K. Müllen, *Acc. Chem. Res.* **2000**, *33*, 520 – 531; c) M. Ortega Lorenzo, C. J. Baddeley, C. Muryn, R. Raval, *Nature* **2000**, *404*, 376 – 379; d) A. Kühnle, T. R. Linderoth, B. Hammer, F. Besenbacher, *Nature* **2002**, *415*, 891 – 893.

[3] For reviews on artificial helical polymers, see a) J.-M. Lehn, *Supramolecular Chemistry*, VCH, Weinheim, **1995**; b) M. M. Green, J.-W. Park, T. Sato, A. Teramoto, S. Lifson, R. L. B. Selinger, J. V. Selinger, *Angew. Chem.* **1999**, *111*, 3329 – 3345; *Angew. Chem. Int. Ed.* **1999**, *38*, 3138 – 3154; c) D. J. Hill, M. J. Mio, R. B. Prince, T. S. Hughes, J. S. Moore, *Chem. Rev.* **2001**, *101*, 3893 – 4011; d) T. Nakano, Y. Okamoto, *Chem. Rev.* **2001**, *101*, 4013 – 4038; e) J. J. L. M. Cornelissen, A. E. Rowan, R. J. M. Nolte, N. A. J. M. Sommerdijk, *Chem. Rev.* **2001**, *101*, 4039 – 4070; f) L. Brunsveld, B. J. B. Folmer, E. W. Meijer, R. P. Sijbesma, *Chem. Rev.* **2001**, *101*, 4071 – 4097; g) M. Fujiki, *Macromol. Rapid Commun.* **2001**, *22*, 539 – 563; h) E. Yashima, K. Maeda, T. Nishimura, *Chem. Eur. J.* **2004**, *10*, 42 – 51.

[4] E. Winfree, F. Liu, L. A. Wenzler, N. C. Seeman, *Nature* **1998**, *394*, 539 – 544.

[5] D. L. Wilson, R. Martin, S. Hong, M. Cronin-Golomb, C. A. Mirkin, D. L. Kaplan, *Proc. Natl. Acad. Sci. USA* **2001**, *98*, 13660 – 13664.

[6] K. Okoshi, K. Sakajiri, J. Kumaki, E. Yashima, *Macromolecules* **2005**, *38*, 4061 – 4064.

[7] a) J. P. Rabe, S. Buchholz, *Science* **1991**, *253*, 424 – 427; b) S. A. Prokhorova, S. S. Sheiko, M. Möller, C.-H. Ahn, V. Percec, *Macromol. Rapid Commun.* **1998**, *19*, 359 – 366; c) E. Mena-Osteritz, A. Meyer, B. M. W. Langeveld-Voss, R. A. J. Janssen, E. W. Meijer, P. Bäuerle, *Angew. Chem.* **2000**, *112*, 2791 – 2796; *Angew. Chem. Int. Ed.* **2000**, *39*, 2680 – 2684. For reviews of single macromolecule observations by AFM, see: d) A. D. Schlüter, J. P. Rabe, *Angew. Chem.* **2000**, *112*, 860 – 880; *Angew. Chem. Int. Ed.* **2000**, *39*, 864 – 883; e) S. S. Sheiko, M. Möller, *Chem. Rev.* **2001**, *101*, 4099 – 4123. For recent examples, see: f) S. S. Sheiko, S. A. Prokhorova, K. L. Beers, K. Matyjaszewski, I. I. Potemkin, A. R. Khokhlov, M. Möller, *Macromolecules* **2001**, *34*, 8354 – 8360; g) C. Ecker, N. Severin, L. Shu, A. D. Schlüter, J. P. Rabe, *Macromolecules* **2004**, *37*, 2484 – 2489; h) N. Severin, J. P. Rabe, D. G. Kurth, *J. Am. Chem. Soc.* **2004**, *126*, 3696 – 3697; i) J. Pyun, C. Tang, T. Kowalewski, J. M. J. Fréchet, C. J. Hawker, *Macromolecules* **2005**, *38*, 2674 – 2685.

[8] N. Severin, J. Barner, A. A. Kalachev, J. P. Rabe, *Nano Lett.* **2004**, *4*, 577 – 579.

[9] Both the height (see the Supporting Information) and phase (Figure 3) AFM images showed identical structures. The phase images are presented here for clarity.

[10] The helical pitch was estimated on the basis of the averaged distance between each oblique stripe that appeared in the AFM height images of the polymers (see the Supporting Information).

[11] We note that when poly-**1L** has a left-handed helical array of the pendants, the main-chain has an opposite, right-handed helical structure.

[12] a) T. Kanno, H. Tanaka, T. Nakamura, H. Tabata, T. Kawai, *Jpn. J. Appl. Phys.* **1999**, *38*, L606 – L607; b) K. Furukawa, K. Ebata, M. Fujiki, *Adv. Mater.* **2000**, *12*, 1033 – 1036; c) J. J. L. M. Cornelissen, J. J. J. M. Donners, R. de Gelder, W. S. Graswinckel, G. A. Metselaar, A. E. Rowan, N. A. J. M. Sommerdijk, R. J. M. Nolte, *Science* **2001**, *293*, 676 – 680; d) K. Shinohara, S. Yasuda, G. Kato, M. Fujita, H. Shigekawa, *J. Am. Chem. Soc.* **2001**, *123*, 3619 – 3620; e) B. S. Li, K. K. L. Cheuk, D. Yang, J. W. Y. Lam, L. J. Wan, C. Bai, B. Z. Tang, *Macromolecules* **2003**, *36*, 5447 – 5450; f) S. Sakurai, A. Ohira, Y. Suzuki, R. Fujito, T. Nishimura, M. Kunitake, E. Yashima, *J. Polym. Sci. A* **2004**, *42*, 4621 – 4640.

 © 2006 Wiley-VCH Verlag GmbH & Co. KGaA, Weinheim

Ligation Reactions

DOI: 10.1002/anie.200503991

Chemoselective Amide Ligations by Decarboxylative Condensations of *N*-Alkylhydroxylamines and α-Ketoacids**

Jeffrey W. Bode, Ryan M. Fox, and Kyle D. Baucom*

Chemoselective ligation reactions make possible covalent bond formation between two fragments containing unprotected functional groups. An ideal ligation process proceeds

[*] Prof. Dr. J. W. Bode, R. M. Fox, K. D. Baucom
Department of Chemistry and Biochemistry
University of California
Santa Barbara, CA (USA)
Fax: (+1) 805-893-4120
E-mail: bode@chem.ucsb.edu

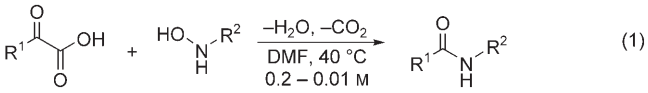
[**] This work was supported by the Donors of the Petroleum Research Fund (administered by the American Chemical Society), the Camille and Henry Dreyfus Foundation (New Faculty Award to J.W.B.), and the University of California. K.D.B. was a 2005 DeWolfe Summer Undergraduate Fellow. We are grateful to Joshua Garretson for preliminary efforts.

Supporting information for this article is available on the WWW under http://www.angewandte.org or from the author.

WILEY InterScience DISCOVER SOMETHING GREAT
© 2006 Wiley-VCH Verlag GmbH & Co. KGaA, Weinheim

under mild, often aqueous, conditions at low molar concentrations, does not require reagents or catalysts, and produces no chemical by-products.[1] The few known reactions that approach these criteria, including oxime formation,[2] thioester-α-bromocarbonyl alkylations,[3] and the copper-promoted alkyne–azide cycloaddition[4] have found diverse and significant applications in drug discovery,[5] functionalized polymer synthesis,[6] and the fabrication of novel nanostructures.[7] Their utility in biomolecule synthesis, however, is limited by the fact that they produce unnatural, and often relatively labile, covalent bonds. The development of chemical ligation reactions that create amide bonds have been a long standing goal.[8] The identification of the native chemical ligation of C-terminal peptide thioesters and N-terminal cysteines has revolutionized the field of synthetic protein chemistry by making possible the coupling of large, unprotected-peptide fragments.[9,10] Despite the utility of this process, the requirement of ligation at relatively rare cysteine residues has encouraged investigations into alternative amide bond-forming reactions.[11,12]

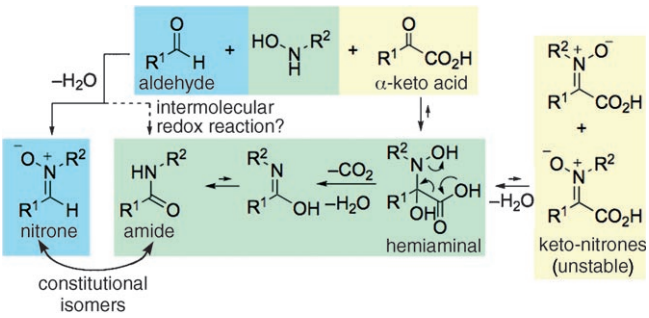
A significant obstacle to the development of new amide ligations is the paucity of reaction types for amide synthesis; nearly all known intermolecular-amide syntheses proceed by addition–elimination reactions of activated carboxylates. Herein we document our discovery of a novel approach to amide synthesis by the decarboxylative condensation of *N*-alkylhydroxylamines and α-keto carboxylic acids [Eq. (1); DMF = *N*,*N*-dimethylformamide]. This process proceeds in polar protic and aprotic solvents, requires no reagents or catalysts, produces only water and carbon dioxide as by-products, and readily tolerates unprotected functional groups. We provide preliminary evaluations of its application to the chemoselective ligation of unprotected-peptide fragments. Investigations into the mechanism and substrate scope of the reaction reveal a rich chemistry that will lead to new solutions for the synthesis of complex molecules and functionalized materials.



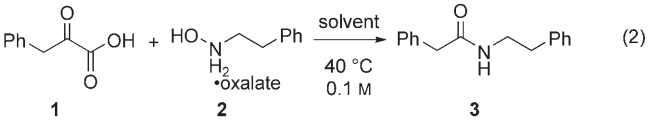
(1)

The discovery of this reaction stemmed from our efforts to develop new approaches to amide and ester synthesis by intramolecular redox reactions of aldehydes.[13] We reasoned that intermolecular redox reactions, for example, between an aldehyde and a hydroxylamine, could also lead to amide formation under appropriate conditions (Scheme 1). These studies, however, were complicated by the propensity of aldehydes and hydroxylamines to rapidly form nitrones. In contrast, ketones rarely condense with *N*-alkylhydroxylamines under mild conditions. Instead, metastable hemiaminals are formed,[14] and we hypothesized that *N*-alkylhydroxylamines would react with α-ketoacids to produce a hemiaminal poised for oxidative decarboxylation to give amide products.[15]

Our hypothesis was tested by mixing two readily available substrates, phenylpyruvic acid (**1**) and *N*-phenethylhydroxylamine (**2**), under a variety of reaction conditions [Eq. (2), Table 1]. Although no amide products were formed in nonpolar solvents, we were pleased to find that simply warming a solution of these two reactants in DMF produced the desired amide product in >70% yield (Table 1, entry 1). A concern in these initial studies was the preparation and handling of the hydroxylamine in its unstable free-base form. Conveniently, we found that salts of the hydroxylamine are equally, and possibly more, efficient in the amidation reaction and as such, we selected the stable, highly crystalline hydroxylamine oxalate salts for further studies (Table 1, entry 2). Likewise, either the protonated ketoacids or their carboxylate salts were suitable reactants (Table 1, entry 3). Amide bond formation occurred in dimethyl sulfoxide (DMSO; Table 1, entry 4), MeOH (Table 1, entry 5), aqueous DMF (Table 1, entry 6), or as suspensions of the reactants in aqueous buffers (Table 1, entries 7–8). Reactions were typically performed at 0.1M by using ketoacid (1.0 equiv) and hydroxylamine oxalate (1.2 equiv) at 40°C, but lower concentrations (0.01M, 0.005M) and other stoichiometric ratios were also viable.



Scheme 1. Reactions of *N*-alkylhydroxylamines with aldehydes and ketones.



(2)

Table 1: Reaction conditions for amide formation from hydroxylamine **1** and α-ketoacid **2**.

Entry	Conditions[a]	*t* [h]	Yield[b] [%]
1	DMF, hydroxylamine free base	15	70
2	DMF	15	79 (88)[c]
3	DMF, ketoacid sodium salt	15	75
4	MeOH	24	72
5	DMSO	15	80
6	DMF/H_2O (5:1)	15	72 (77)[c]
7	acetate buffer (pH 4)	24	(70)[c]
8	6N NH_4Cl, 60°C	15	68 (70)[c]

[a] All reaction performed on a 0.2 mmol scale; [b] Yields following chromatography; [c] HPLC yields of unpurified reaction mixtures given in parentheses.

 © 2006 Wiley-VCH Verlag GmbH & Co. KGaA, Weinheim

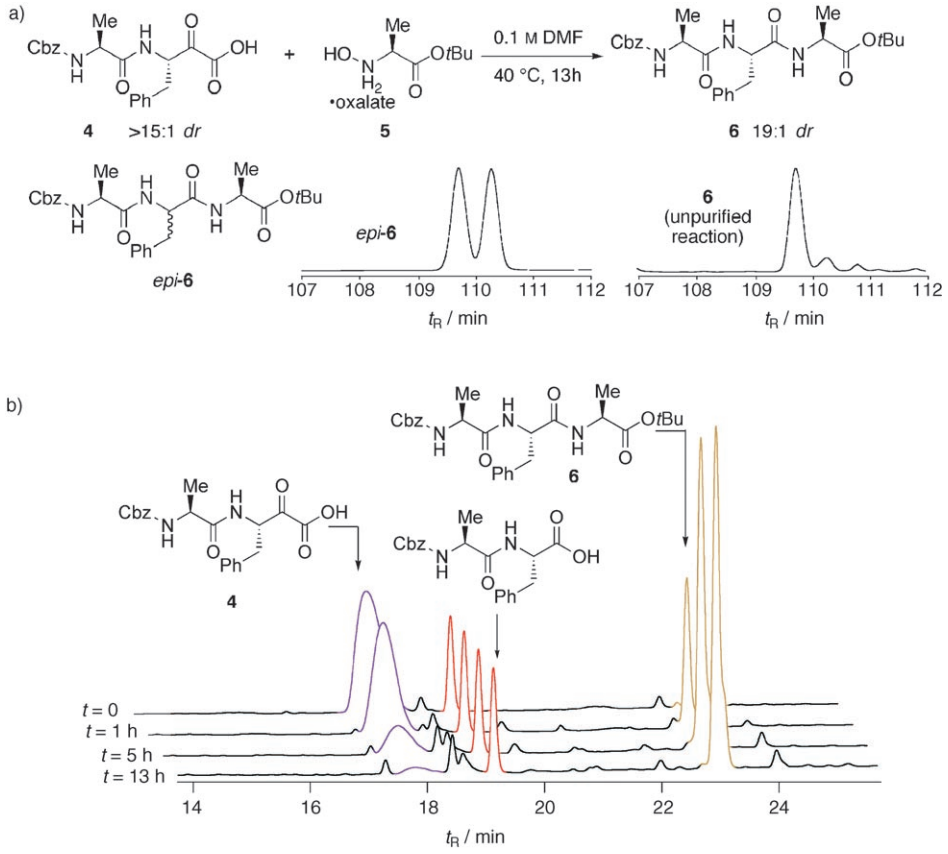
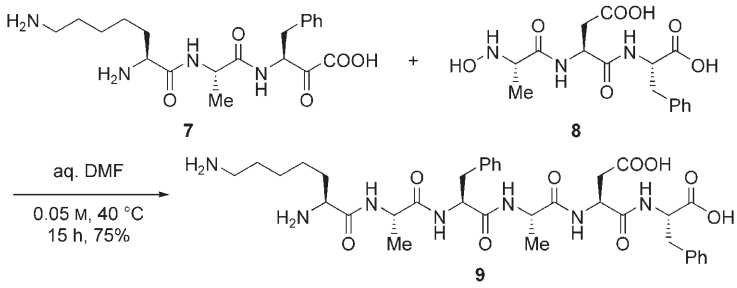


Figure 1. Ketoacid–hydroxylamine ligations of peptide substrates **4** and **5**. a) Demonstration of preservation of stereochemistry during the reaction; b) Monitoring of the reaction by HPLC (samples taken directly from the reaction mixture without purification or workup). A small amount of the carboxylic acid is formed during the synthesis of ketoacid **4**. Cbz = carbobenzyloxycarbonyl.

Ketoacid–hydroxylamine amide ligations occur for a wide range of simple and complex substrates. We have focused our initial investigations on the exploration of the suitability of this process for peptide ligations. Peptide ketoacid **4** was prepared as a >15:1 mixture of diastereomers (with **4** being the major diastereomer) by a variant of Wasserman's ylide method[16,17] and reacted with (*S*)-alanine hydroxylamine oxalate salt **5** (1.2 equiv).[18] The ligation reaction occurred cleanly over the course of 12 h (Figure 1) to give peptide **6** as a 19:1 mixture of diastereomers (peptide **6** is the major form), which demonstrates that epimerization of the ketoacid does not occur during the ligation reaction. Encouraged by these results, we prepared a range of protected- and unprotected-peptide substrates and examined their ligations (Table 2). To further validate the tolerance of this reaction to fully unprotected peptides, ketoacid **7** and hydroxylamine **8** were prepared and shown to undergo efficient ligation in aqueous DMF [Eq. (3)]. Notably, a variety of ligation sites including Phe-Ala, Ala-Phe, Pro-Ala, Val-Gly, and Ala-Ala were feasible.

Several possible reaction pathways can give rise to amide formation, and we have initiated efforts to elucidate the reaction mechanism. Interestingly, although peptide substrates such as **4** and **5** do not appear to condense to form nitrones under the reaction conditions (Figure 1b), less-hindered substrates, including our model reaction [Eq. (2)], rapidly form the isomeric nitrones *cis*-**11** and *trans*-**11** (Figure 2). These nitrone intermediates were detected by reverse-phase HPLC (Figure 2b), liquid chromatography–MS, and in situ ^{1}H and ^{13}C NMR spectroscopy studies of the reaction mixtures. They could be isolated as their methyl esters by being trapped with diazomethane. Although it is clear that these nitrones can form under the reaction



(3)

Table 2: Ketoacid–hydroxylamine peptide ligations of selected protected- and unprotected-peptide substrates.

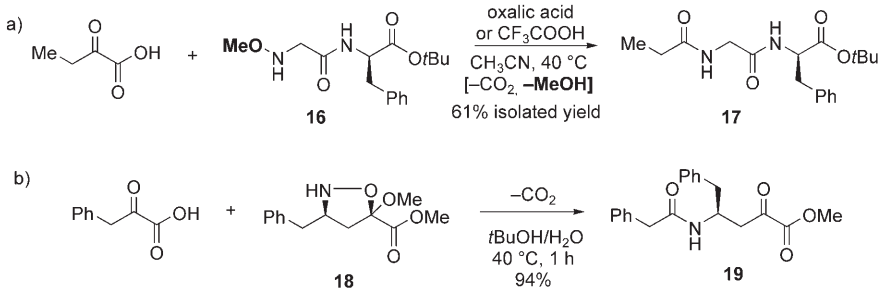
Entry	Ketoacid	Hydroxylamine	Product[a]	Yield[b] [%]
1	FmocAlaPro	AlaO*t*Bu	Fmoc-AlaProAla-O*t*Bu	72
2	FmocAlaVal	GlyOEt	Fmoc-AlaValGly-OEt	58
3	FmocLys(Boc)-Glu(*t*Bu)PheAla	AlaO*t*Bu	Fmoc-Lys(Boc)Glu(*t*Bu)Phe-AlaAla-O*t*Bu[c]	80
4	H_2N-LysAlaPhe	AlaAsp(*t*Bu)PheO*t*Bu	H_2N-LysAlaPhe-AlaAsp(*t*Bu)Phe-O*t*Bu	74
5	FmocAspAlaPhe	AlaAsp(*t*Bu)PheO*t*Bu	Fmoc-AspAlaPhe-AlaAsp(*t*Bu)PheO*t*Bu	74

[a] All reaction performed at 0.02–0.1 M in DMF or DMSO containing ca. 5% H_2O at 40°C for 10–24 h using 1 equiv ketoacid and 1.2–2 equiv hydroxylamine oxalates; [b] Yields of pure products following preparative TLC or RP-HPLC. The reported yields include the preparation of the ketoacids by oxidation of the appropriate cyanoylide followed by coupling with the hydroxylamine; [c] 0.01 M, 48 h.

 © 2006 Wiley-VCH Verlag GmbH & Co. KGaA, Weinheim

conditions, we do not currently believe that they are involved in product formation; all attempts to trap the postulated nitrilium ion **12** by the addition of nucleophiles (MeOH as the reaction solvent, thiophenol, cysteine, glycine) afforded only the usual amide product. Thus, although the rapid formation of nitrone **11** may contribute to the efficiency of the reaction, conversion to the product is likely to proceed through decarboxylation of the tetrahedral intermediate **10**. The question of whether the decarboxylation proceeds through a stepwise or concerted pathway remains to be addressed, although the isolation of small amounts of nitrone **15** suggests that a stepwise reaction is at least a possibility. We note, however, that decarboxylated nitrones are never isolated when peptide-derived ketoacids and hydroxylamines are employed. Although the details remain to be elucidated, the available evidence points to a distinct mechanistic manifold that may have further implications including a role in the prebiotic origin of higher peptides.

This chemoselective amide formation is not limited to *O*-unsubstituted hydroxylamines. For example, *N*-methoxy peptide **16** was coupled with 2-ketobutyric acid in acetonitrile in 61% yield (Scheme 2a).[19] Unexpectedly, and in contrast to the *O*-unsubstituted hydroxylamines, these substrates required added acid and showed increased efficiency in acetronitrile, but were slower in the presence of DMF, DMSO, or water. Cyclic hydroxylamines are exceptional substrates (Scheme 2b); isoxazolidine **18** reacted cleanly with α-ketoacids in either nonpolar (CH_2Cl_2, toluene) or aqueous (0.2 M 1:1 *t*BuOH/H_2O) conditions. The stability of the resultant ketoester product under the reaction conditions is noteworthy.[20]



Scheme 2. Amide-forming ketoacid ligations with *O*-alkyl hydroxylamines.

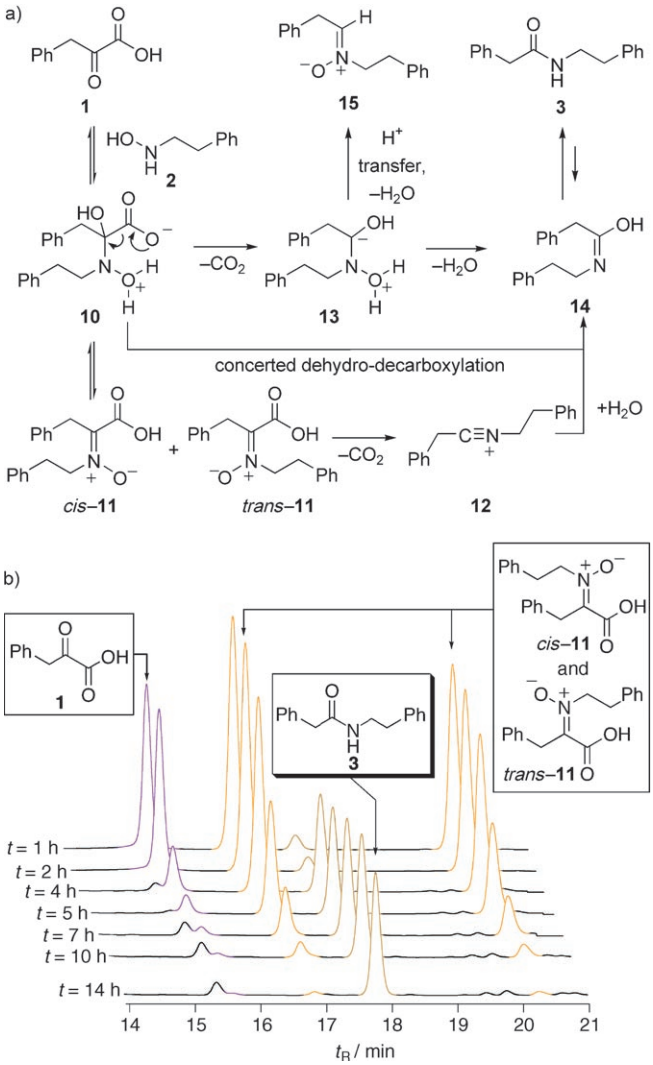


Figure 2. a) Possible reaction pathways for amide formation; b) detection of nitrone intermediates by HPLC.

The coupling of α-ketoacids and hydroxylamines is a powerful, chemoselective amide bond formation that proceeds in the presence of reactive functional groups, requires no reagents or catalysts, and produces only water and CO_2 as by-products. This reaction should be useful for diverse applications that require the coupling of unprotected molecules.

Received: November 9, 2005
Published online: January 17, 2006

Keywords: amides · chemoselectivity · ketoacids · ligation reactions · peptides

[1] J. Rademann, *Angew. Chem.* **2004**, *116*, 4654–4656; *Angew. Chem. Int. Ed.* **2004**, *43*, 4554–4556.
[2] K. Rose, *J. Am. Chem. Soc.* **1994**, ***116***, 30–33.
[3] M. Schnölzer, S. B. H. Kent, *Science* **1992**, *256*, 221–225.
[4] V. V. Rostovtsev, L. G. Green, V. V. Fokin, K. B. Sharpless, *Angew. Chem.* **2002**, *114*, 2708–2711; *Angew. Chem. Int. Ed.* **2002**, *41*, 2596–2599.
[5] W. G. Lewis, L. G. Green, F. Grynszpan, Z. Radic, P. R. Carlier, P. Taylor, M. G. Finn, K. B. Sharpless, *Angew. Chem.* **2002**, *114*, 1095–1099; *Angew. Chem. Int. Ed.* **2002**, *41*, 1053–1057.
[6] C. J. Hawker, K. L Wooley, *Science* **2005**, *309*, 1200–1205.
[7] E. Strable, J. W. Johnson, M. G. Finn, *Nano Lett.* **2004**, *4*, 1385–1389.
[8] L. P. Miranda, P. F. Alewood, *Biopolymers* **2000**, *55*, 3852–3856.
[9] For selected recent examples, see: a) D. Bang, G. I. Makhatadze, V. Tereshko, A. A. Kossiakoff, S. B. Kent, *Angew. Chem.* **2005**, *117*, 3920–3924; *Angew. Chem. Int. Ed.* **2005**, *44*, 2–6; ; b) F. I. Valiyaveetil, M. Sekedat, T. W. Muir, R. MacKinnon, *Angew.*

 © 2006 Wiley-VCH Verlag GmbH & Co. KGaA, Weinheim

Chem. **2004**, *116*, 2558 – 2561; *Angew. Chem. Int. Ed.* **2004**, *43*, 2504 – 2507; .
[10] J. P. Tam, Q. Yu, Z. Miao. *Biopolymers* **1999**, *51*, 311 – 332.
[11] a) B. L. Nilsson, L. L. Kiessling, R. T. Raines, *Org. Lett.* **2001**, *3*, 9 – 12; b) E. Saxon, J. I. Armstrong, C. R. Bertozzi, *Org. Lett.* **2000**, *2*, 2141 – 2143.
[12] a) N. Shangguan, S. Katukojvala, R. Greenberg, L. J. Williams, *J. Am. Chem. Soc.* **2003**, *125*, 7754 – 7755; b) T. Rosen, I. M. Lico, T. W. Chu, *J. Org. Chem.* **1988**, *53*, 1580 – 1582.
[13] a) K. Y.-K. Chow, J. W. Bode, *J. Am. Chem. Soc.* **2004**, *126*, 8126 – 8127; b) S. S. Sohn, J. W. Bode, *Org. Lett.* **2005**, *7*, 3873 – 3876.
[14] T. Ishikawa, K. Nagai, M. Senzaki, A. Tatsukawa, S. Saito, *Tetrahedron* **1998**, *54*, 2433 – 2448.
[15] For other oxidative decarboxylative process of α-ketoacids, see: a) T. R. Beebe, R. Baldridge, M. Beard, D. Cooke, I. DefAys, V. Hensley, D. Hua, J.-C. Lao, D. McMillen, D. Morris, R. Now, E. O'Bryan, C. Spielberger, M. Stolte, J. Waller, *J. Org. Chem.* **1987**, *52*, 3165 – 3166; b) M. D. Corbett, B. R. Corbett, *J. Org. Chem.* **1980**, *45*, 2834 – 2839.
[16] a) H. H. Wasserman, W. B. Ho, *J. Org. Chem.* **1994**, *59*, 4364 – 4366; b) For a solid-supported variant, see: S. Weik, J. Rademann, *Angew. Chem.* **2003**, *115*, 2595 – 2598; *Angew. Chem. Int. Ed.* **2003**, *42*, 2491 – 2494.
[17] Although we have confirmed that epimerization of the peptide ketoacids does not occur during the reaction, the synthesis of enantiopure ketoacids presents some challenges. We have developed a new approach for their preparation that will be reported in due course.
[18] a) For these studies, all peptide hydroxylamines were prepared from the corresponding amines by using the method of Fukuyama, which proceeds with preservation of stereochemistry, see: H. Tokuyama, T. Kuboyama, T. Fukuyama, *Org. Syn.* **2003**, *80*, 207 – 218; b) Peptide hydoxylamines are well-known compounds; for a review, see: H. C. J. Ottenheijm, J. D. M. Herscheid, *Chem. Rev.* **1986**, *86*, 697 – 707.
[19] *O*-Alkyl hydroxylamine amines can be prepared from unprotected *N*-bromoacetyl peptides, see: L. E. Canne, S. J. Bark, S. B. H. Kent, *J. Am. Chem. Soc.* **1996**, *118*, 5891 – 5896.
[20] Further studies on the unique reactivity and synthetic potential of the isoxazolidine substrates will be reported shortly.

 © 2006 Wiley-VCH Verlag GmbH & Co. KGaA, Weinheim

Enzyme Models

DOI: 10.1002/anie.200504027

Primary-Amine-Specific Lactamization of ω-Amino Acids by an Artificial Cyclotransferase Based on [18]Crown-6**

Munetaka Kunishima, Kazuhito Hioki, Takahiro Moriya, Jun Morita, Tomoko Ikuta, and Shohei Tani*

In memory of Kiyoshi Tanaka

Enzyme models are of practical importance for the development of efficient molecular catalysts for organic reactions and of theoretical importance in elucidating mechanisms of enzymatic reactions.[1] In comparison with hydrolase models, an artificial acyltransferase that promotes the reverse reaction of dehydrocondensation is particularly difficult to design.[2] As a representative host compound, [18]crown-6 has received much attention in biomimetic chemistry and, although specific binding of ammonium ions to [18]crown-6 has been extensively investigated,[3–5] application of the complex as an artificial acyltransferase is very limited.[6,7] Among acyltransferase models, cyclotransferase models that catalyze intramolecular dehydrocondensation to lead to the formation of lactams have not been developed. Herein, we report a novel enzyme model of cyclotransferase,[8] which utilizes the specific binding of a primary ammonium ion and [18]crown-6. The artificial enzyme substrate specifically activates the carboxylic acids that possess a primary amino group at the γ-, δ-, or ε-positions, thus leading to the formation of the corresponding lactams.

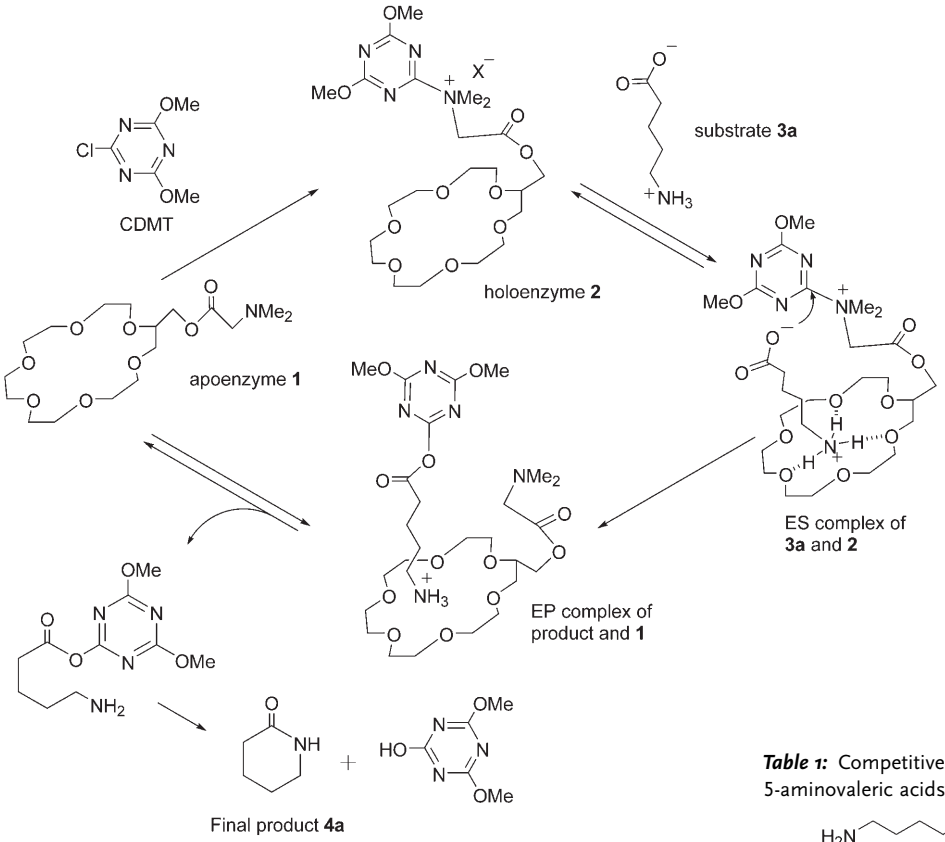
The reaction system is outlined in Scheme 1. Methanol is employed as the solvent as it dissolves the amino acid substrates and stabilizes the complex of the primary ammonium salt and the [18]crown-6.[9–11] A combination system of triazines and tertiary amines which is available in alcohols was attached to the [18]crown-6 and employed for the activation of the substrate carboxyl groups.[12,13] When CDMT was added to a methanolic solution of 5-aminovaleric acid (**3a**) and crown derivative **1**, which can be compared to an apoenzyme,

[*] Prof. Dr. M. Kunishima, Dr. K. Hioki, T. Moriya, J. Morita, T. Ikuta, Prof. Dr. S. Tani
Faculty of Pharmaceutical Sciences
Kobe Gakuin University
Nishi-ku, Kobe 651-2180 (Japan)
Fax: (+81) 78-974-5689
E-mail: kunisima@pharm.kobegakuin.ac.jp
Prof. Dr. M. Kunishima
PRESTO, JST
Nishi-ku, Kobe 651-2180 (Japan)

[**] This work was supported partially by a Grant-in-Aid for Scientific Research (No. 14572025) from the Ministry of Education, Science, Sports, and Culture, Japan.

Supporting information for this article is available on the WWW under http://www.angewandte.org or from the author.

WILEY InterScience DISCOVER SOMETHING GREAT
© 2006 Wiley-VCH Verlag GmbH & Co. KGaA, Weinheim

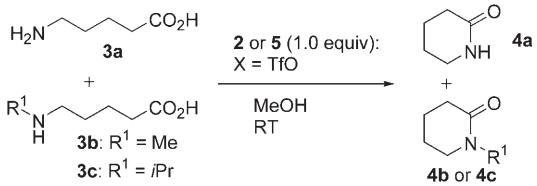


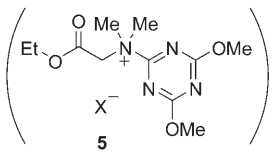
Scheme 1. Substrate-specific lactamization by artificial cyclotransferase. CDMT = 2-chloro-4,6-dimethoxy-1,3,5-triazine, ES = enzyme–substrate, EP = enzyme–product.

a reactive dehydrocondensing reagent **2** (similarly, compared to holoenzyme; X = Cl) was generated by coupling **1** with CDMT through the dimethylamino group. Upon introduction of substrate **3a**, the primary amino group in its ionized form preferentially interacts with **2** to form a so-called ES complex. In the resulting complex, the carboxylate ion of the substrate is brought into proximity with the triazino group and attacks it preferentially, thus giving an EP complex. Intramolecular aminolysis of the resulting acyloxytriazine takes place quickly to give δ-valerolactam with concomitant liberation of **1**, which can be reused in the next catalytic cycle. Since the product **4a** lacks a free amino group, it no longer binds to the crown ring, and thus there is no competitive binding of the product with the catalyst to inhibit the next reaction.

First, to verify that the substrate-specific lactamization takes place through such molecular recognition, we attempted the reaction under stoichiometric conditions using **2** (X = OTf; Tf = trifluoromethanesulfonyl). A competitive reaction between **3a** and *N*-methyl-5-aminovaleric acid (**3b**) was performed. Since the primary amino group of **3a** has a much greater affinity for [18]crown-6 than the secondary amino group of **3b**,[11] **3a** can be expected to react preferentially (Table 1). When a mixture of 1.1 equivalents of both the amino acids was treated with 1.0 equivalents of **2** in methanol at room temperature for 10 min, **4a** was obtained predominantly (**4a**/**4b** = 92:8) in 89% yield (run 1). No significant improvement in either the selectivity or the yield was observed by prolonging the reaction time to 2 h (run 2). The selectivity slightly increased with an excess of **3a** and **3b** (2.0 equiv each; run 3). In the control reaction using **5**, which has the dehydrocondensing group attached to an ethyl group instead of the crown ether, both the selectivity and the yield dropped (54:46, 50% yield; run 4). Prolongation of the reaction time increased the yield to 80%, whereas the selectivity was completely lost (run 5). Similar results were obtained with **3c**, which has an isopropyl group at the nitrogen atom (runs 6 and 7). The reaction rates uniformly decreased when either the methyl or isopropyl group was introduced to the terminal amino group, thus indicating that the mere existence of

Table 1: Competitive lactamization between primary and secondary 5-aminovaleric acids (**3a** vs **3b** or **3c**).





Entry	Substrate[a]	Condensing agent	*t* [min]	Product[b] Yield [%]	Product[b] Ratio (**4a**/**4b** or **4c**)
1	**3a** vs **3b** (1.1:1.1)	**2**	10	89	92:8
2	**3a** vs **3b** (1.1:1.1)	**2**	120	92	90:10
3	**3a** vs **3b** (2.0:2.0)	**2**	10	100	94:6
4	**3a** vs **3b** (1.1:1.1)	**5**[c]	10	50	54:46
5	**3a** vs **3b** (1.1:1.1)	**5**[c]	120	80	51:49
6	**3a** vs **3c** (3.0:3.0)	**2**	20	100	94:6
7	**3a** vs **3c** (3.0:3.0)	**5**[c]	120	88	55:45
8[d]	**3a** vs **3b** (1.1:1.1)	**2**	10	93	94:6

[a] The molar ratios given in parenthesis are based on the amount of **2** or **5** (1.0 equiv). [b] Determined by HPLC. [c] Control. [d] Reaction was carried out in the presence of 2-piperidone (**4a**; 0.85 equiv).

 © 2006 Wiley-VCH Verlag GmbH & Co. KGaA, Weinheim

a substituent at the amino group (rather than size or steric hindrance) was the main factor in decreasing the reaction rate.

To confirm that the observed selectivity is attributable to the supramolecular interaction between the protonated primary amino group of **3a** and the crown ether of **2**, we examined the effect of alkaline-metal ions on the selectivity because the affinity of these cations toward [18]crown-6 correlates with the match of their ionic radii to the diameter of the host.[10,14,15] Competitive reactions under the same conditions as run 2 in Table 1 were conducted in the presence of 2 equivalents of various alkaline-metal triflates. As shown in Table 2, the lithium ion, which has the smallest binding

Table 2: Effect of alkali-metal ions on substrate selectivity.

Entry	CF_3SO_3M (2 equiv)		Product[a]	
		pK_a[b]	Yield [%]	Ratio (**4a**/**4b**)
1	CF_3SO_3Li	< 0.5	96	90:10
2	CF_3SO_3Na	4.38	93	84:16
3	CF_3SO_3K	6.20	69	55:45
4	CF_3SO_3Cs	4.55	84	85:15

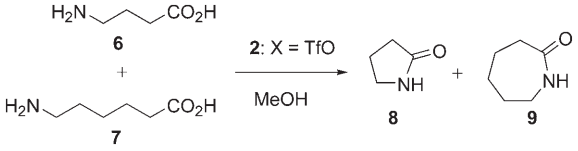
[a] Determined by HPLC. [b] The pK_a values in MeOH/benzene (8:2) are cited from reference [15].

constant ($pK_a = < 0.5$),[15] was found to have almost no effect on selectivity, whereas the potassium ion, well known to have the highest affinity for the crown ring, nearly abolished the selectivity and generated a lower yield (runs 1 and 3). The moderate decrease in the selectivity for **4a** was observed with sodium and cesium salts. The extent to which alkaline-metal ions lowered selectivity correlated very well with their affinity toward [18]crown-6, and we therefore conclude that the observed substrate selectivity for **3a** resulted from the formation of a host–guest complex of the primary ammonium group within the crown ring.

In general, reactions using host compounds suffer from product inhibition because the products retain a high affinity for the host.[1b] In the present case, the primary amino group of **3a**, which is recognized by the crown at the initial stage of the reaction, disappears as it is converted into the amide nitrogen atom of **4a**, which should no longer bind to **2**. In fact, when the competitive reaction was carried out in the presence of **4a**, no decrease in selectivity was observed (Table 1, run 8). Thus, properties intrinsic to this reaction circumvent the problem of product inhibition and, in principle, this benefit applies to all reactions that modify the guest moiety to one with significantly less affinity for the host.[16]

It should be noted that the substrate-specific lactamization proceeds under catalytic conditions. The competitive reaction between **3a** and **3b** was performed using a combination of a catalytic amount of **2** (0.2 equiv) and CDMT (1.0 equiv). To neutralize HCl generated during the reaction, *N*-cyclohexylmorpholine was slowly added by a syringe pump over a period of 5 h. As a result, **4a** and **4b** were obtained in a ratio of 96:4 (yield = 78%). The control reaction using **5** instead of **2** under the same conditions resulted in a low selectivity (**4a**/**4b** = 53:47, 70% yield).

Interestingly, the chain length between the amino group and carboxyl group can be discriminated by **2**. The reactivity of 4-aminobutyric acid (**6**), **3a**, and 6-aminocaproic acid (**7**) toward **2** at room temperature was estimated to be 1:1.5:2.1, respectively, based on their competitive reactions, thus indicating that the kinetically most unfavorable seven-membered ε-caprolactam **9** was formed faster than five- or six-membered lactams (**8** and **4a**). Since the order of observed reactivity of the amino acids does not correlate with their affinity for [18]crown-6,[17] the number of the methylene groups that link the amino group and the carboxyl group could be important. The selectivity of **9**/**8** was improved with decreasing reaction temperature; the ratio of **9** increased up to 85:15 (88% yield) at −40 °C [Eq. (1)].



Conditions	**8**/**9**	Yield [%]
RT, 10 min	32:68	90
0°C, 2 h	28:72	88
-40°C, 48 h	15:85	88

In conclusion, we have succeeded in developing a novel artificial enzyme based on [18]crown-6, which is capable of converting ω-amino acids into their cyclized lactams in a substrate-specific manner. The catalyst can recognize the distance and the degree of substitution of the amino group farthest from the carboxyl group undergoing reaction. Furthermore, although reaction yield and selectivity are sometimes inversely related in organic reactions, both increase in the present system because the reaction rate is enhanced by the formation of the ES complex, which, in turn, is based on molecular recognition. Finally, the present system offers a new concept for circumventing product inhibition.

Experimental Section

General procedure for competitive lactamization using a stoichiometric amount of dehydrocondensing agent (**2** or **5**): A solution of **2** (95.1 mg, 0.142 mmol) in MeOH was added at room temperature to a stirred solution of **3a** (18.3 mg, 0.157 mmol) and **3b** (20.5 mg, 0.157 mmol) in MeOH (the total amount of MeOH = 26 mL). The reaction mixture was stirred at room temperature, and the products were quantified by HPLC at a definite time (1,3-dimethyl-3,4,5,6-tetrahydro-2(1*H*)-pyrimidinone was used as the internal standard).

General procedure for competitive lactamization under the catalytic system of **2** and CDMT: A solution of **2** (19.0 mg, 0.029 mmol) and CDMT (20.0 mg, 0.114 mmol) in MeOH at room temperature was added to a stirred solution of **3a** (18.3 mg, 0.157 mmol) and **3b** (20.5 mg, 0.157 mmol) in MeOH. *N*-cyclohexylmorpholine (0.142 mmol, 0.6 mL of 0.237 M) dissolved in MeOH was added over a period of 5 h by a syringe pump (the total amount of MeOH = 8.5 mL). The reaction mixture was stirred at room temperature, and the products were quantified by HPLC at a definite time.

Received: November 12, 2005
Published online: January 17, 2006

Keywords: condensation · crown compounds · enzyme models · lactams · transferases

 © 2006 Wiley-VCH Verlag GmbH & Co. KGaA, Weinheim

[1] a) R. Breslow, *Acc. Chem. Res.* **1991**, *24*, 317; b) A. J. Kirby, *Angew. Chem.* **1996**, *108*, 770; *Angew. Chem. Int. Ed. Engl.* **1996**, *35*, 707; c) W. B. Motherwell, M. J. Bingham, Y. Six, *Tetrahedron* **2001**, *57*, 4663.

[2] a) D. J. Cram, P. Y.-S. Lam, S. P. Ho, *J. Am. Chem. Soc.* **1986**, *108*, 839; b) D. S. Kemp, N. G. Galakatos, B. Bowen, K. Tan, *J. Org. Chem.* **1986**, *51*, 1829; c) J. S. Nowick, Q. Feng, T. Tjivikua, P. Ballester, J. Rebek, Jr., *J. Am. Chem. Soc.* **1991**, *113*, 8831; d) F. M. Menger, A. V. Eliseev, N. A. Khanjin, M. J. Sherrod, *J. Org. Chem.* **1995**, *60*, 2870; e) I. Huc, R. J. Pieters, J. Rebek, Jr., *J. Am. Chem. Soc.* **1994**, *116*, 10296.

[3] For reviews of [18]crown-6, see: a) J.-M. Lehn, *Angew. Chem.* **1988**, *100*, 91; *Angew. Chem. Int. Ed. Engl.* **1988**, *27*, 89; b) D. J. Cram, *Angew. Chem.* **1988**, *100*, 1041; *Angew. Chem. Int. Ed. Engl.* **1988**, *27*, 1009.

[4] For recent study using [18]crown-6 derivatives, see: a) J. V. Hernández, A. I. Oliva, L. Simón, F. M. Muñiz, M. Grande, J. R. Morán, *Tetrahedron Lett.* **2004**, *45*, 4831; b) N. Solladié, M. E. Walther, M. Gross, T. M. F. Duarte, C. Bourgongne, J.-F. Nierengarten, *Chem. Commun.* **2003**, 2412; c) M. H. Al-Sayah, N. R. Branda, *Org. Lett.* **2002**, *4*, 881; d) K.-S. Jeong, J. W. Park, Y. L. Cho, *Tetrahedron Lett.* **1996**, *37*, 2795; e) C. G. Andrews, C. L. B. Macdonald, *Angew. Chem.* **2005**, *117*, 7619; *Angew. Chem. Int. Ed.* **2005**, *44*, 7453.

[5] For recent study using related compounds of [18]crown-6, see: a) C. P. Mandl, B. König, *J. Org. Chem.* **2005**, *70*, 670; b) N. Demirel, Y. Bulut, *Tetrahedron: Asymmetry* **2003**, *14*, 2633; c) K. Tsubaki, T. Kusumoto, N. Hayashi, M. Nuruzzaman, K. Fuji, *Org. Lett.* **2002**, *4*, 2313.

[6] For the formation of an amide bond, Sasaki et al. developed a very interesting model of peptide synthesis using [18]crown-6; see reference [7].

[7] a) S. Sasaki, M. Shionoya, K. Koga, *J. Am. Chem. Soc.* **1985**, *107*, 3371; b) S. Sasaki, K. Koga, *Chem. Pharm. Bull.* **1989**, *37*, 912.

[8] a) M. Orlowski, A. Meister, *The Enzymes, Vol. 4* (Ed.: P. D. Boyer), Academic Press, New York, **1971**, pp. 123; b) M. Yu, I. Song, W. Wang, R. C. Bateman, Jr., *Arch. Biochem. Biophys.* **1994**, *309*, 300.

[9] The log *K* values for [18]crown-6 with primary ammonium salts are known to be largest in methanol; see references [10] and [11].

[10] R. M. Izatt, K. Pawlak, J. S. Bradshaw, R. L. Bruening, *Chem. Rev.* **1991**, *91*, 1721.

[11] a) R. M. Izatt, N. E. Izatt, B. E. Rossiter, J. J. Christensen, *Science* **1978**, *199*, 994; b) R. M. Izatt, J. D. Lamb, N. E. Izatt, B. E. Rossiter, Jr., J. J. Christensen, B. L. Haymore, *J. Am. Chem. Soc.* **1979**, *101*, 6273; c) V. Rüdiger, H.-J. Schneider, V. P. Solov'ev, V. P. Kazachenko, O. A. Raevsky, *Eur. J. Org. Chem.* **1999**, 1847.

[12] a) M. Kunishima, C. Kawachi, K. Hioki, K. Terao, S. Tani, *Tetrahedron* **2001**, *57*, 1551; b) M. Kunishima, C. Kawachi, J. Morita, K. Terao, F. Iwasaki, S. Tani, *Tetrahedron* **1999**, *55*, 13159.

[13] M. Kunishima, K. Yoshimura, H. Morigaki, R. Kawamata, K. Terao, S. Tani, *J. Am. Chem. Soc.* **2001**, *123*, 10760.

[14] a) V. P. Solov'ev, N. N. Strakhova, O. A. Raevsky, V. Rüdiger, H.-J. Schneider, *J. Org. Chem.* **1996**, *61*, 5221; b) S. Kado, K. Kimura, *J. Am. Chem. Soc.* **2003**, *125*, 4560.

[15] E. Blasius, R. A. Rausch, G. D. Andreetti, J. Rebizant, *Chem. Ber.* **1984**, *117*, 1113.

[16] Systems in which the binding ability of the product to a catalyst is lower than that of a reactant were reported; see: L. G. Mackay, R. S. Wylie, J. K. M Sanders, *J. Am. Chem. Soc.* **1994**, *116*, 3141.

[17] The log*K* values for **6**, **3a**, and **7** with [18]crown-6 determined by NMR titration in [D_4]methanol are 3.24, 3.50, and 3.30, respectively.

 © 2006 Wiley-VCH Verlag GmbH & Co. KGaA, Weinheim

Tin Clusters

DOI: 10.1002/anie.200503738

Organic–Inorganic Sn_{12} and Organic Sn_6 Oxide–Hydroxide Clusters**

Ganesan Prabusankar, Bernard Jousseaume, Thierry Toupance, and Hassan Allouchi*

For many years, it was thought that the hydrolysis of monoorganotin compounds leads only to ill-defined products called organostannonic acids and formulated as $(RSnOOH)_n$. These acids are of industrial importance, as they are used as esterification and transesterification catalysts.[1] Recently, reinvestigation of this reaction showed that it can also give clusters of low molecular weights and variable sizes, which depend on the identity of the organic group linked to the tin atom and on the reaction conditions. A ball-like Sn_{12} cluster bearing two hydroxy groups was formed, together with an undefined oxopolymer, from the hydrolysis of tin halides or alkoxides bearing a simple butyl group as the organic ligand.[2] In this cluster, half of the tin atoms are pentacoordinated and the other half are hexacoordinated. When the very bulky tris(trimethylsilyl)methyl group was used as the ligand in a similar reaction, an adamantane-type Sn_4 cluster containing tetracoordinated tin atoms was isolated. A change in the reaction conditions led to a different result: the use of LiOH instead of Na_2O afforded a small Sn_3 cluster, in which each of the tetracoordinated tin atoms bears a hydroxy group. In this case, the very bulky organic group linked to the tin atom prevented further condensation of the monoorganotin units into distannoxane dimers, which are the building blocks of the Sn_{12} cluster isolated when butyl groups are used as ligands.[3]

Recently, we reported the preparation of trialkynyl tin compounds, which are alternative precursors for organotin oxides and alkoxides.[4] We also demonstrated that the hydrolysis of bis(tripropynylstannyl) derivatives is a facile route to self-assembled hybrid materials with alternating layers of tin oxide and hydrophobic organic chains.[5] The properties of the final materials depend strongly on the identity of the organic groups linked to the tin atoms. To gain deeper insight into the hydrolysis pathway of aryl tin compounds, we investigated monometallic systems such as

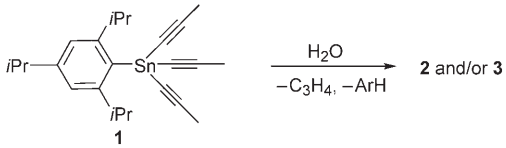
[*] Dr. G. Prabusankar, Dr. B. Jousseaume, Prof. T. Toupance
Laboratoire de Chimie Organique et Organométallique
UMR-CNRS 5802
Université Bordeaux 1
351 cours de la Libération, 33405 Talence (France)
Fax: (+33) 5-4000-6994
E-mail: b.jousseaume@lcoo.u-bordeaux1.fr
Dr. H. Allouchi
Laboratoire de Chimie Physique SPOT, EA 3857
Faculté de Pharmacie
31 Avenue Monge, 37200 Tours (France)

[**] The authors thank the Aquitaine Region, the CNRS (Material Program Grant), and the European Community (FAME Network of Excellence) for partial financial support of this work.

 © 2006 Wiley-VCH Verlag GmbH & Co. KGaA, Weinheim

aryl tripropynyltin compounds. Herein, we describe the first mixed organotin compound in which inorganic tin(IV) atoms coexist with monoorganotin(IV) units. To our knowledge, the isolation and structural characterization of tin oxide fragments embedded between two monoorganotin oxide moieties have not been reported previously. Moreover, slight changes in the reaction conditions produced a new hexameric cage composed of a folded strip of poly(organostannoxane).

Treatment of 2,4,6-iPr$_3$C$_6$H$_2$Sn(CCMe)$_3$ (**1**)[4] with 12 equivalents of water under reflux conditions in THF resulted in the cleavage of the tin–propynyl bonds. Colorless crystals of dodecameric [(2,4,6-iPr$_3$C$_6$H$_2$Sn)$_8$(μ_4-O)$_2$(μ_3-O)$_8$-(μ_2-O)$_4$(μ_2-OH)$_8${Sn(OH)}$_4$] (**2**) were isolated from the pale yellow solution in fairly good yield (Scheme 1). Compound **2**



Scheme 1. Reaction of **1** with water to produce **2** and/or **3**.

is stable under atmospheric conditions, soluble in a large number of common organic solvents, including hydrocarbons such as hexane and pentane, and thermally quite stable (m.p. 202–204 °C). The IR spectrum of **2** revealed the presence of associated hydroxy groups as a broad OH-stretching absorption at 3385 cm^{-1}. The ^{1}H NMR spectrum of **2** revealed that there are two different types of Sn-OH hydrogen atoms, which resonate as singlets at $\delta = 4.93$ ($^2J_{HSn} = 58$ Hz) and 8.83 ppm ($^2J_{HSn} = 17$ Hz). The observation of two singlets indicates that the chemically non-equivalent hydroxy groups in the molecule do not undergo proton exchange (on the NMR timescale). The upfield signal associated with the largest coupling constant is attributed to the hydrogen atoms of bridging hydroxy groups. The solution ^{119}Sn NMR spectrum of **2** consisted of three resonances with an intensity ratio of 1:1:1 at $\delta = -338.0$, -438.2, and -574.1 ppm, which are attributed to the pentacoordinated aryl tin centers, hexacoordinated aryl tin centers, and dearylated hexacoordinated tin centers, respectively. The solid-state CP-MAS ^{119}Sn NMR spectroscopy investigation of **2** was fully consistent with the solution-state study. The spectrum also consisted of three resonances, at $\delta = -343$, -448, and -576 ppm, corresponding to tin atoms in three different environments.

The molecular structure of **2**, which crystallizes as a solvate with 12 molecules of THF, is shown in Figure 1.[6] The oval-shaped cluster consists of 12 tin and 26 oxygen atoms. An adamantane-type inorganic $(SnO_{3/2}OH)_4$ core of tin oxide hydroxide is capped by two identical, perpendicular (2,4,6-iPr$_3$C$_6$H$_2$SnO(OH))$_4$ organostannoxane-type arcs. The four inorganic tin atoms are hexacoordinated and each bear a hydroxy group. The aryl stannoxane arc consists of two hexacoordinated tin units that are linked to two pentacoordinated fragments. There are five different types of oxygen environments in cluster **2**: two tetra-, eight tri-, and four dicoordinated oxygen bridges, eight oxygen atoms in bridging

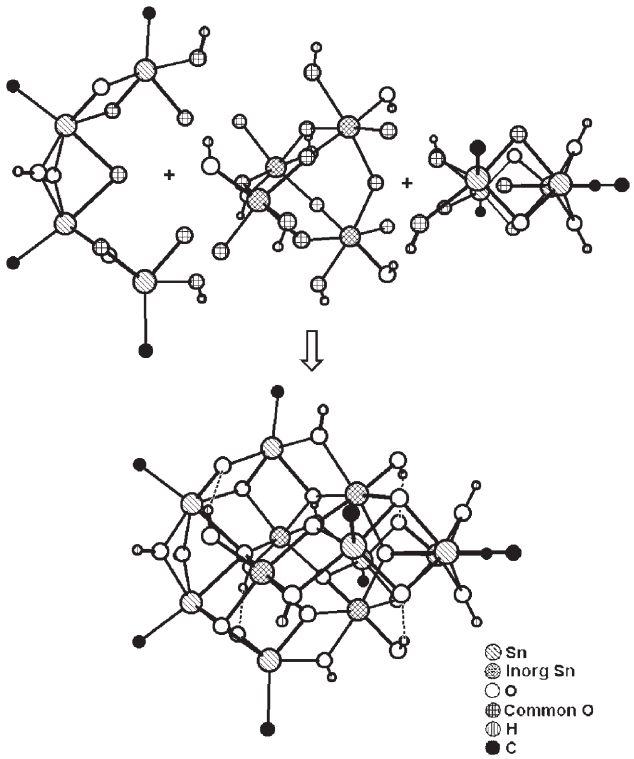


Figure 1. Molecular structure of **2**, showing the tin oxide core. Solvent THF molecules and the noncoordinated atoms of the 2,4,6-iPr$_3$C$_6$H$_2$ ligands are omitted for clarity.

hydroxy groups, and four oxygen atoms in terminal hydroxy groups on the stannonic acid tin atoms. The terminal hydroxy groups participate in intramolecular hydrogen bonding with bridging oxygen atoms.

The formation of the stannonic acid unit in **2** may occur through the partial dearylation of **1** by water during the hydrolysis of the alkynyl groups.[7] The low reactivity of the alkynyl groups in **1** towards hydrolysis (no reaction after 2 months at 20 °C), which is due to the steric hindrance of the bulky 2,4,6-iPr$_3$C$_6$H$_2$ group, led to the use of more severe reaction conditions (65 °C, 9 days), which favored the dearylation. No dearylation was observed for less bulky aryl groups (20 °C, 6 days).[5] Another explanation for the formation of the stannonic acid unit involves the redistribution of the monoaryl tin compound into diaryl tin and dearylated tin compounds.[8] This possibility was ruled out, as the diaryl tin compound was not detected in the reaction mixture. The reaction mixture did, however, contain some 2,4,6-iPr$_3$C$_6$H$_3$ formed through the cleavage of the tin–aryl bond.

Cluster **2** is not the only product that can be isolated from the hydrolysis of **1**. The compound [(2,4,6-iPr$_3$C$_6$H$_2$Sn)$_6$(OH)$_4$(μ_3-O)$_4$(μ_2-O)$_2$(μ_2-OH)$_2$] (**3a**) was isolated in low yield after evaporation of the solvent from the final reaction mixture, extraction of the solid with chloroform, and crystallization (Scheme 1). An analogous compound, **3b**, was obtained in 56 % yield when the hydrolysis of **1** was conducted in *tert*-amyl alcohol (TAA). The IR spectrum of **3a** revealed the presence of hydroxy groups as an absorption band at

 © 2006 Wiley-VCH Verlag GmbH & Co. KGaA, Weinheim

3404 cm^{-1}, but the solution ^1H NMR spectrum was not very informative, owing to the presence of more than 20 signals of varying intensity. The solution ^1H and ^{119}Sn NMR spectra recorded for **3b** were also very complex. The CP-MAS ^{119}Sn NMR spectrum of **3b** showed only two sets of resonances at $\delta = -213$ and -355 ppm.

The molecular structure of **3a** is depicted in Figure 2.[6] The $\{Sn_6O_8\}$ core of cluster **3a** is composed of six puckered

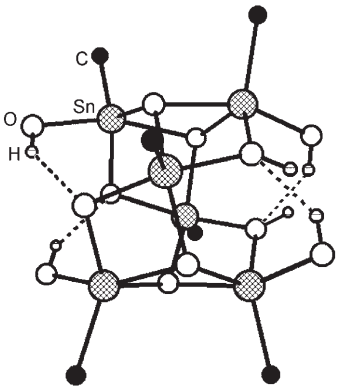
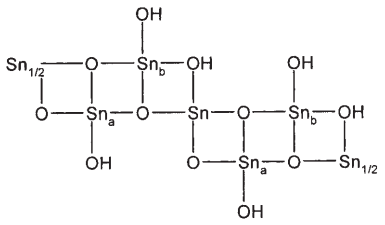


Figure 2. Molecular structure of **3a**. The noncoordinated atoms of the 2,4,6-$iPr_3C_6H_2$ ligands are omitted for clarity.

four-membered $\{Sn_2O_2\}$ rings, in a cagelike arrangement. It can also be described as a double-twist Möbius band of stannoxane units (see Scheme 2). All six tin atoms in **3a** are



Scheme 2. Strip schematic representation of **3**. The 2,4,6-$iPr_3C_6H_2$ ligands have been omitted for clarity.

pentacoordinated. Two tin atoms (Sn_a) are coordinated by three bridging oxygen atoms (two μ_3 and one μ_2), one hydroxy group, and one 2,4,6-$iPr_3C_6H_2$ fragment. Two tin atoms (Sn_b) are surrounded by two μ_3-bridging oxygen atoms, one μ_2-bridging hydroxy group, one terminal hydroxy group, and one 2,4,6-$iPr_3C_6H_2$ fragment. The remaining two tin atoms are bonded to three bridging oxygen atoms (two μ_3 and one μ_2), one μ_2-bridging hydroxy group, and one 2,4,6-$iPr_3C_6H_2$ group. There are four different oxygen environments in **3a**: four tri- and two dicoordinated oxygen bridges, two oxygen atoms in bridging hydroxy groups, and four oxygen atoms in terminal hydroxy groups. The tin oxide inorganic core is completely wrapped by the hydrophobic bulky aryl moiety (2,4,6-$iPr_3C_6H_2$), which leads to the absence of intermolecular hydrogen-bonding interactions in **3a**. However, intramolecular hydrogen bonding occurs between the terminal hydroxy groups and the bridging hydroxy groups. The molecular structure of **3b**, which crystallizes as a solvate with four molecules of TAA, has an identical cage arrangement.[6] The structures of **3a** and **3b** differ mainly in the additional intermolecular hydrogen bonding that occurs between the hydroxy groups of the cage and those of the TAA solvent molecules in **3b** . Unlike **2**, compounds **3a** and **3b** are kinetically labile in solution, as evidenced by the appearance of many signals, which were not assigned, in their ^{119}Sn NMR spectra. However, their decomposition is reversible, as **3a** and **3b** are quantitatively recovered upon crystallization. Thus, the bulky aryl substituent on the tin atom does not allow the formation of the large, soluble NMR-inactive oxopolymers observed for butyltin compounds,[9] but leads to the formation of detectable discrete species.

In summary, the hydrolysis of **1** differs substantially from the hydrolyses of tri(*tert*-amyloxy)phenyltin or tri(propynyl)phenyltin, in which the formation of a ball-like Sn_{12} compound (minor) and an oxopolymer (major) was detected by solution ^{119}Sn NMR spectroscopy.[10] In the present study, either the unprecedented dodecameric oval-shaped cluster **2** or the hexameric cage **3** are formed from the hydrolysis of **1**. The structure of **2** consists of functionalized stannonic acid fragments, derived from **1** through cleavage of the tin–aryl bond, and organotin oxide arcs. The structure of **3** can be described as a circular doubly twisted strip of polystannoxane. In addition, the presence of hydroxy groups on the surfaces of molecules **2** and **3** could allow their further functionalization for use as building blocks in organic–inorganic materials or for solid-acid catalysis. The presence of reactive sites in **2** with different Lewis acidities, corresponding to inorganic tin atoms and organotin moieties, should enhance the catalytic properties of the compound.

Experimental Section

2: A mixture of **1** (2 g, 4.6 mmol) and H_2O (0.98 g, 54.6 mmol) was heated at reflux in THF (30 mL). A large amount of white solid was formed after 24 h, and slowly dissolved within 4 days. The pale yellow reaction mixture became clear after 9 days, and the reaction mixture was then slowly brought to room temperature. Colorless crystals of **2** were obtained at 5 °C (0.32 g, 20 %).[6] M.p. 202–204 °C; ^1H NMR ($CDCl_3$, 300 MHz): $\delta = 0.35$–1.47 (m, 144 H; *i*Pr-CH_3), 1.76–1.81 (m, 48 H; THF-CH_2), 2.61–2.82 (m), 3.06–3.17 (m), 3.49–3.54 (m, 24 H; *i*Pr-C*H*), 3.65–3.68 (m, 48 H; THF-CH_2), 4.93 (s, $^2J_{HSn} = 58$ Hz, 8 H; Sn-O*H*), 6.62–7.06 (m), 7.53 (s, 16 H; aryl-C*H*), 8.83 ppm (s, $^2J_{HSn} = 17$ Hz, 4 H; Sn-O*H*); ^{119}Sn NMR ($CDCl_3$, 74.6 MHz): $\delta = -338.0$ (4 Sn; C-Sn_p), -438.2 (4 Sn; C-Sn_h), -574.1 ppm (4 Sn; HO-Sn_h); CP-MAS ^{119}Sn NMR: $\delta = -343$, -448, -576 ppm; IR (KBr): $\tilde{\nu} = 3385$(w), 2961(vs), 2927(s), 2868(m), 1594(w), 1560(w), 1460(m), 1420(w), 1383(w), 1362(w), 1100(w), 876(w), 717(w), 648(w), 553(m), 496(w), 468 cm^{-1} (m); elemental analysis (%) calcd for $C_{120}H_{196}O_{26}Sn_{12}\cdot 12\,C_4H_8O$ (4344.30): C 46.44, H 6.77, Sn 32.79; found: C 46.10, H 6.22, Sn 31.12.

3a: Compound **3a** was synthesized by the same procedure described for **2**. However, the final reaction mixture was concentrated under vacuum to yield a pale yellow solid, which was extracted with chloroform. Filtration, concentration to approximately 5 mL, and storage at 15 °C afforded colorless crystals of **3a**.[6] ^1H NMR ($CDCl_3$, 300 MHz): $\delta = 0.29$–1.30 (m, 108 H; *i*Pr-CH_3), 2.50–2.60 (m, 18H; *i*Pr-

 © 2006 Wiley-VCH Verlag GmbH & Co. KGaA, Weinheim

C*H*), 6.50–7.08 ppm (m, 12H; aryl-C*H*); IR (KBr): $\tilde{\nu}$ = 3404(w), 3040(w), 2960(vs), 2924(s), 2868(m), 1594(w), 1561(w), 1462(m), 1419(m), 1383(m), 1362(m), 1261(w), 1100(m), 1056(w), 1020(w), 937(w), 876(m), 803(w), 649(w), 554 cm^{-1} (m).

3b: H_2O (0.98 g 54.6 mmol) was added dropwise to a stirred solution of **2** (1 g, 2.3 mmol) in TAA (35 mL) at room temperature. Then the reaction mixture was heated to 60 °C. A large amount of white solid was formed within 3 h. After 9 days, the reaction temperature was raised from 60 to 90 °C. The white precipitate slowly dissolved into the solution, and the reaction mixture became clear. At this stage, the reaction was stopped, and the reaction mixture was slowly brought to 15 °C to afford a large amount of colorless crystals of **3b** (0.53 g, 56 %).[6] M.p. 182–184 °C; ^{1}H NMR ($CDCl_3$, 300 MHz): δ = 0.27–1.38 (m, 152 H; *i*Pr-CH_3, TAA-CH_3, and TAA-CH_2), 1.99 (s, $^2J_{HSn}$ = 40 Hz, 6H; Sn-O*H*), 2.58–2.67 (m, 18H; *i*Pr-C*H*), 6.57–7.08 ppm (m, 12H; aryl-C*H*); ^{119}Sn NMR ($CDCl_3$, 111.92 MHz): δ = −309.5, −321.8, −340.0, −342.6, −350.3, −351.3, −367.0, −375.1, −426.8, −538.7 ppm; CP-MAS ^{119}Sn NMR: δ = −213, −355 ppm; IR (KBr): $\tilde{\nu}$ = 3384(w), 3044(w), 2961(vs), 2928(s), 2870(m), 1595(w), 1561(w), 1463(m), 1412(m), 1384(m), 1363(m), 1101(w), 1070(w), 1057(w), 938(w), 876(m), 743(w), 666(m), 544 cm^{-1} (m); elemental analysis (%) calcd for $C_{90}H_{144}O_{12}Sn_6 \cdot 4\,C_5H_{12}O$ (2483.00): C 53.21, H 7.79, O 10.31, Sn 28.69; found: C 52.09, H 7.73, O 8.29, Sn 28.69.

Received: October 21, 2005
Published online: January 20, 2006

Keywords: arene ligands · hydrolysis · organic–inorganic hybrid composites · stannanes · tin

[1] a) A. G. Davies, *Organotin Chemistry, 2nd ed.*, Wiley-VCH, Weinheim, **2004**; b) B. Jousseaume, C. Laporte, M.-C. Rascle, T. Toupance, *Chem. Commun.* **2003**, 1428; c) C. Camacho-Camacho, M. Biesemans, M. Van Poeck, F. A. G. Mercier, R. Willem, K. Darriet-Jambert, B. Jousseaume, T. Toupance, U. Schneider, U. Gerigk, *Chem. Eur. J.* **2005**, *11*, 2455; d) K. Darriet-Jambert, B. Jousseaume, T. Toupance, U. Schneider, U. Gerigk, EP1598381; *Chem. Abstr.* **2005**, *143*, 460633.

[2] a) H. Puff, H. Reuter, *J. Organomet. Chem.* **1989**, *373*, 173; b) D. Dakternieks, H. Zhu, E. R. Tiekink, R. Coltom, *J. Organomet. Chem.* **1994**, *476*, 33; c) F. Ribot, F. Banse, C. Sanchez, P. Tolédano, J. Maquet, *Inorg. Chem.* **1995**, *34*, 6371.

[3] a) J. Janssen, J. Magull, H. W. Roesky, *Angew. Chem.* **2002**, *114*, 1425; *Angew. Chem. Int. Ed.* **2002**, *41*, 1365; b) K. Wraage, T. Pape, R. Herbst-Irmer, M. Noltemeyer, H.-G. Schmidt, H. W. Roesky, *Eur. J. Inorg. Chem.* **1999**, 869.

[4] a) P. Jaumier, B. Jousseaume, M. Lahcini, F. Ribot, C. Sanchez, *Chem. Commun.* **1998**, 369; b) M. Lahcini, P. Jaumier, B. Jousseaume, *Angew. Chem.* **1999**, *111*, 416; *Angew. Chem. Int. Ed.* **1999**, *38*, 402; c) B. Jousseaume, H. Riague, T. Toupance, M. Lahcini, P. Mountford, B. R. Tyrrell, *Organometallics* **2002**, *21*, 4590.

[5] H. Elhamzaoui, B. Jousseaume, H. Riague, T. Toupance, P. Dieudonné, C. Zakri, M. Maugey, H. Allouchi, *J. Am. Chem. Soc.* **2004**, *126*, 8130.

[6] Crystals of **2**, **3a**, and **3b** were grown from THF (5 °C), chloroform (15 °C), and TAA (15 °C), respectively. In the cases of **2** and **3a**, suitable crystals were covered with mineral oil (Aldrich), mounted onto glass fibers, and transferred directly to the 150-K N_2 stream of a Nonius Kappa CCD diffractometer; in the case of **3b**, a crystal was mounted onto a 1.0-mm glass capillary at room temperature. Structures were solved by direct methods by using SHELXS-97[11] and refined against F^2 by full-matrix least squares by using SHELXL-97.[12] All non-hydrogen atoms were refined anisotropically, with the exception of disordered atoms in the solvent molecules in **2** (THF) and **3b** (TAA). Hydroxy hydrogen atoms were located through difference Fourier synthesis and fixed at these positions during the structure refinements. The largest peaks in the final difference Fourier map were of no chemical significance. **2**: $C_{168}H_{292}O_{38}Sn_{12}$, M_r = 4344.30, monoclinic, space group $P2_1/c$, a = 18.2384(2), b = 26.6625(4), c = 38.7506(5) Å, β = 96.161(1)°, V = 18734.8(4) Å^3, Z = 4, ρ_{calcd} = 1.540 g cm^{-3}, T = 150(2) K, F(000) = 8784, μ($Mo_{K\alpha}$) = 1.637 mm^{-1}, block crystal, 93163 reflections measured, 44564 unique (R_{int} = 0.022), 1874 parameters, R_1 = 0.0414 ($I > 2\sigma(I)$), wR_2 = 0.0964 ($I > 2\sigma(I)$), GOF = 1.062. **3a**: $C_{90}H_{146}O_{12}Sn_6$, M_r = 2132.2, monoclinic, space group $C2/c$, a = 42.6871(13), b = 10.0677(8), c = 30.2690(14) Å, β = 134.642(2)°, V = 9255.6(9) Å^3, Z = 4, ρ_{calcd} = 1.530 g cm^{-3}, T = 150(2) K, F(000) = 4312, μ($Mo_{K\alpha}$) = 1.650 mm^{-1}, plate crystal, 15026 reflections measured, 5789 unique (R_{int} = 0.1194), 488 parameters, R_1 = 0.0828 ($I > 2\sigma(I)$), wR_2 = 0.1702 ($I > 2\sigma(I)$), GOF = 1.052. **3b**: $C_{110}H_{192}O_{16}Sn_6$, M_r = 2483.00, monoclinic, space group $C2/c$, a = 14.9388(2), b = 29.6680(4), c = 28.0134(2) Å, β = 91.772(1)°, V = 12409.7(1) Å^3, Z = 4, ρ_{calcd} = 1.329 g cm^{-3}, T = 296(2) K, F(000) = 5112, μ($Mo_{K\alpha}$) = 1.243 mm^{-1}, plate crystal, 21087 reflections measured, 13136 unique (R_{int} = 0.0242), 525 parameters, R_1 = 0.0548 ($I > 2\sigma(I)$), wR_2 = 0.1457 ($I > 2\sigma(I)$), GOF = 1.013. CCDC-286921 (**2**), CCDC-286922 (**3a**), and CCDC-286923 (**3b**) contain the supplementary crystallographic data for this paper. These data can be obtained free of charge from The Cambridge Crystallographic Data Centre via www.ccdc.cam.ac.uk/data_request/cif.

[7] a) H. W. Roesky, I. Haiduc, N. S. Hosmane, *Chem. Rev.* **2003**, *103*, 2579; b) V. Chandrasekhar, S. Nagendran, V. Baskar, *Coord. Chem. Rev.* **2002**, *235*, 1.

[8] J. D. Kennedy, W. McFarlane, P. J. Smith, R. F. M. White, L. Smith, *J. Chem. Soc. Perkin Trans. 2* **1973**, 1785.

[9] C. Eychenne-Baron, F. Ribot, C. Sanchez, *J. Organomet. Chem.* **1998**, *567*, 137.

[10] a) F. Ribot, personal communication; b) B. Jousseaume, unpublished results.

[11] G. M. Sheldrick, *Acta Crystallogr. Sect. A* **1990**, *46*, 467.

[12] G. M. Sheldrick, SHELXL-97, *Program for Crystal Structure Refinement*, Universität Göttingen, Germany, **1997**.

 © 2006 Wiley-VCH Verlag GmbH & Co. KGaA, Weinheim

Heterogeneous Catalysis

DOI: 10.1002/anie.200503149

Copper-in-Charcoal (Cu/C): Heterogeneous, Copper-Catalyzed Asymmetric Hydrosilylations**

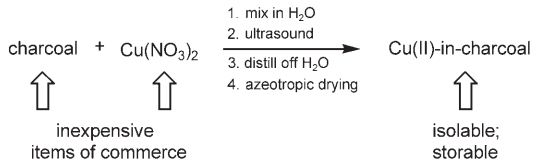
Bruce H. Lipshutz, Bryan A. Frieman, and Anthony E. Tomaso, Jr.*

It has been estimated that 70–80 % of all metal-based catalysis performed in industry is done heterogeneously. The benefits ascribed to this mode of reaction are numerous, including a) simplicity of workup—filtration suffices to remove the catalyst; b) recyclibility—catalysts may retain activity throughout several reaction cycles which leads to high throughput at reduced expense; and c) minimized waste disposal—catalysts that retain impregnated metals reduce environmental concerns.[1] Of the many solid supports that have been used over the past several decades (e.g., SiO_2, Al_2O_3, Kieselgohr, molecular sieves, etc.), inexpensive charcoal is among the most common. Its intricate, albeit ill-defined structure, reveals a large surface area within its matrix, thus allowing for mounting of transition metals in the form of their salts.[2] Usually, this is achieved by evaporation of an aqueous solution in the presence of activated charcoal. Thermal treatment of salt-impregnated charcoal is then used to further reorganize the initial disposition of atoms, on which the extent of heating can have a major impact on metal accessibility through clustering and pore blockage and, hence, catalytic activity.[3]

Copper has been extensively utilized in heterogeneous catalysis following impregnation into charcoal.[4] The species copper-in-charcoal ("Cu/C"), akin to related catalysts "Ni/C",[5] "Co/C",[6] and so forth, exists mainly in its oxidized copper(II) state (CuO), although copper(I) oxide (Cu_2O) is also present within the pores.[7] The nature of each catalyst "Cu/C", however, varies significantly as a function of preparation and handling. Thus, catalysts prepared from $CuCl_2$, $Cu(OAc)_2$, or $Cu(NO_3)_2$ are each likely to be discrete entities,[8] thus displaying highly variable chemical, as well as distinct physical, properties oftentimes manifested by use of sophisticated analytical techniques, such as scanning electron microscopy (SEM) and X-ray diffraction.[9]

The known chemistry of Cu/C can be broadly classified as relating to hydrogenation or dehydrogenation reactions,[10] with few uses reported in the literature applied to synthetic organic chemistry.[11] No precedent exists, to the best of our knowledge, for the use of Cu/C in the field of asymmetric catalysis[12] in which copper is associated with a nonracemic ligand and is capable of inducing chirality in a prochiral substrate. One area in which Cu/C would be of current interest involves its in situ conversion into a heterogeneous form of copper hydride (that is, copper hydride-in-charcoal; "CuH/C") ligated by a nonracemic amine,[13a] phosphine,[13b] or NH carbene ("L*").[13c] Asymmetric hydrosilylations of several functional groups, such as aromatic ketones and imines, α,β-unsaturated ketones and esters, and unsaturated lactones and lactams, can lead to valued nonracemic products upon exposure to [L*CuH] in solution.[14] The first corresponding process under heterogeneous conditions is reported herein.

Although several preparations of Cu/C are known,[15] including the use of $Cu(NO_3)_2$ as a precursor,[16] none derives the benefits of ultrasound as a means of enhancing the level of distribution of Cu^{II} into a solid support under mild conditions. The ultrasound technique, developed originally for the preparation of Ni/C,[17] could be readily applied to the formation of Cu/C (Scheme 1). Our first preparation of Cu/C was similar to that employed for Ni/C, whereby sonication was used followed by distillation of water and in vacuo drying at 100 °C. This method provided a reagent that led to sluggish reactions, apparently because of the detrimental retention of water during formation. Azeotropic drying with toluene afforded a "dry" catalyst which displays far greater reactivity.



Scheme 1. Formation of Cu/C.

Initial attempts to effect asymmetric hydrosilylations of an aryl ketone (e.g., acetophenone) with Cu/C in the presence of excess poly(methylhydrosiloxane) (PMHS) as the source of hydride (obtained from Lancaster)[18] along with catalytic amounts of the Takasago nonracemic 3,5-di-*tert*-butyl-4-methoxydiphenylphosphinyl segphos (DTBM-segphos) ligand (see Table 1)[19] were fruitless; no reduction occurred. The key to catalyst activity was the addition of a sodium salt of an alkyl or aryl alcohol (e.g., *tert*-butanol or phenol, respectively). The use of NaOPh (4 equivalents relative to copper) affords greater rate accelerations relative to NaO*t*Bu, thus leading to complete conversion within one hour at similar concentrations and in comparable enantiomeric excess. Under these conditions, the likely copper(II) species

[*] Prof. B. H. Lipshutz, B. A. Frieman, A. E. Tomaso, Jr.
Department of Chemistry and Biochemistry
University of California
Santa Barbara, CA 93106 (USA)
Fax: (+1) 805-893-8265
E-mail: lipshutz@chem.ucsb.edu

[**] We warmly thank the NSF (CHE 0213522) for financial support, and Dr. Louise Weaver of the Microscopy and Microanalysis Facility at the University of New Brunswick for the surface analyses (http://www.unb.ca/fredericton/science/emunit/). We are also indebted to Dr. Takao Saito and Mr. Hideo Shimizu (Takasago, Co.), Drs. R. Schmid and M. Scalone (Roche, Basel), and Drs. H.-U. Blaser and M. Thommen (Solvias) for supplying the segphos, biphep, and josiphoss ligands, respectively, used in this study. We thank Ms. Danielle Nihan for providing unsaturated lactone **2**.

Supporting information for this article is available on the WWW under http://www.angewandte.org or from the author.

 © 2006 Wiley-VCH Verlag GmbH & Co. KGaA, Weinheim

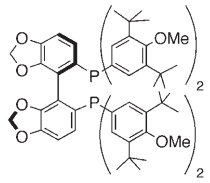
Table 1: Effect of ligand on asymmetric hydrosilylations catalyzed by CuH-in-charcoal.



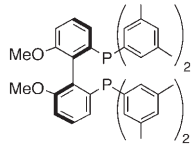
1

Ligand (L*)	Conversion	*ee* [%]
DTBM-segphos	complete in 10 h	88
PPF-P(tBu)$_2$	incomplete after 24 h	12
MeO-biphep	complete in 8 h	80
binap	complete in 18 h	41

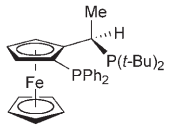
Ar = 3,5-dimethylphenyl.



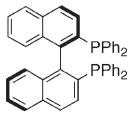
(*R*)-(−)-DTBM-segphos



(*R*)-3,5-xyl-MeO-biphep

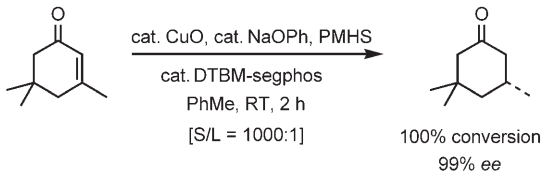


(*R*)-(*S*)-PPF–P(tBu)$_2$



(*R*)-binap

[L*CuO]/C is reduced by the silane presumably via transient species [L*Cu(OR)$_2$] or [L*CuLR] to [L*CuH]/C, after which the intended hydrosilylation takes place smoothly.[7] Indicative that CuO and/or Cu$_2$O may well be the precursor(s) to active CuH under these conditions, the corresponding homogeneous catalyst was prepared using especially inexpensive, black CuO (2.5 mol%). Upon addition of NaOPh, along with PMHS, this new combination leads to an active catalyst that reacts using the homogeneous analogue (Scheme 2).



Scheme 2. Reaction of the homogeneous catalyst system.

Several ligands L* were screened to determine whether this parameter impacts the chemistry of [L*CuH] under these heterogeneous conditions (Table 1). Those studied included nonracemic DTBM-segphos,[19] josiphos,[20] MeO-biphep,[21] and binap,[22] using an iminophosphorane **1** as the substrate. The data pointed to *R*-(−)-DTBM-segphos as the bisphosphine ligand of choice.

Representative examples of functionalities responsive to this new technology at a substrate-to-ligand (S/L) ratio of 1000:1 are illustrated in Table 2, which includes comparison data, where available, for the corresponding reactions carried out previously under homogeneous conditions. Hydrosilylation of acetophenone occurred readily with [(DTBM-segphos)CuH]/C in toluene, even at −50 °C, with 93% *ee* (entry 1). Likewise, heteroaromatic 2-acetylfuran reacts under these mild conditions (entry 2).[14e] The keto ester precursor to the antidepressant prozac (entry 3) is reduced at cold temperatures as well and in high yield with high *ee*. Aryl imines (entries 4 and 5) were found to be the most sluggish of the substrates examined as they required 10 h under ultrasonication conditions and 6% ligand to reach completion. Curiously, the *ee* values observed were noticeably lower than those routinely realized using this catalyst under homogeneous conditions,[14c] even when the sonication-bath temperature was held at 32 °C (or ca. 10 °C below the maximum temperature the bath would normally reach), thus foreshadowing distinctions between [L*CuH] in solution and heterogeneous [L*CuH]/C (see below).

Several 1,4-reductions were also investigated: For example, the reaction with isophorone proceeds in toluene at room temperature within 1 h to afford the desired *R* product in high yield and with >98% *ee* (entry 6). Repeating this experiment at a S/L ratio of 10000:1 afforded identical results (Scheme 3). A cinnamyl enoate (entry 7) was slow to be reduced with Cu/C at ambient temperature using conventional stirring (incomplete after 48 h); with ultrasonication, however, complete conversion took place within 1 h. An unsaturated lactone (entry 8) was reduced without resorting to ultrasonication.

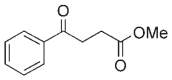
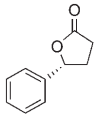
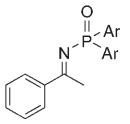
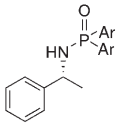
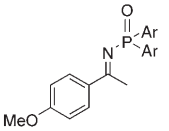
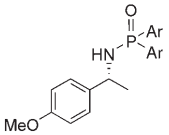
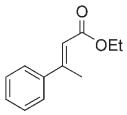
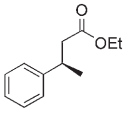
Observations regarding a β,β-disubstituted *Z*-enone **3** (Table 3) were most unexpected, as the Cu/C reagent formed in the presence of a josiphos analogue (namely, [{PPF-P(tBu)$_2$}CuH]/C; PPF-P(tBu)$_2$ = (*R*)-(−)-1-[(*S*)-(diphenylphosphino)ferrocenyl]ethyldi-*tert*-butylphosphine) led to the formation of keto product **4** in only 17% *ee*. Earlier studies on enones in solution with this identical catalyst at low temperatures,[23] and even at 60 °C,[24] had given products such as *ent*-**4** in >90% *ee*. Switching to the segphos system, substantially increased the *ee* value to 64%. Curiously, however, with *tert*-butanol in the reaction mixture, used routinely to enhance reaction rates (by quenching the intermediate copper enolate),[14d,25] the *ee* value was dramatically decreased. Clearly, the solid support can have a significant influence on the selectivity of these hydrosilylations.

The prospects for recycling Cu/C were investigated, notwithstanding its virtually cost-free nature. Collection by filtration from a reaction mixture followed by drying and reuse led to identical results (Scheme 3). Particularly intriguing is the finding that after filtration, direct reuse (no isolation or drying) of the catalyst, and without the addition of more DTBM-segphos or NaOPh, product **5** was afforded in the same yield and with no erosion in reaction rate or enantioselectivity (Scheme 4). Apparently, the phosphine ligand is sequestered and maintained at the copper center.[26]

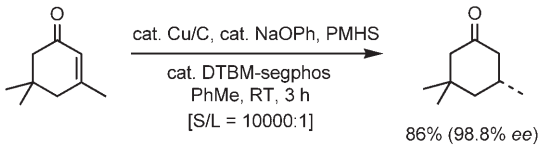
Quantitative inductively coupled plasma atomic emission spectrometry (ICP-AES)[27] was employed to determine the loading of copper within the charcoal, as well as the extent of copper bleed into solution during reactions performed with 0.022 mmol copper at room temperature and under ultrasonication. The loading of Cu/C was found to be 0.344 mmol Cu/g catalyst. Asymmetric conjugate reductions of isophor-

 © 2006 Wiley-VCH Verlag GmbH & Co. KGaA, Weinheim

Table 2: Asymmetric hydrosilylations catalyzed by [{(*R*)-(−)-DTBM-segphos}CuH]-in-charcoal.

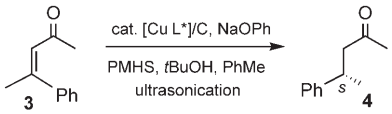
Entry	Substrate	Product	Yield [%][a]	[L*CuH]/C			[L*CuH] (solution)		
				t [h]	*T* [°C]	*ee* [%]	*t* [h]	*T* [°C]	*ee* [%]
1			95	8	−50	93	5	−50	93[14a]
2			91	8	−50	86	12[b]	−50	92[14e]
3			89	8	−45	94	–[c]	–[c]	–[c]
4			92	10	–[d]	88	17	RT	99[14c]
5			90	10	–[d]	84	17	RT	98[14c]
6			70[e]	3	RT	99	8	0	92[14b]
7			99	1	–[d]	99	2[f]	RT	98[14d]
8			83	7	RT	98	3	0	99[14d,24]

[a] Isolated, chromatographically purified materials. [b] Using 0.5 mol% catalyst. [c] Not determined. [d] Using ultrasonication. [e] Product is volatile; some was lost during purification. [f] Using 1 mol% catalyst. Ar = 3,5-dimethylphenyl.



Scheme 3. 1,4-Reduction with isophorone at S/L = 10000:1.

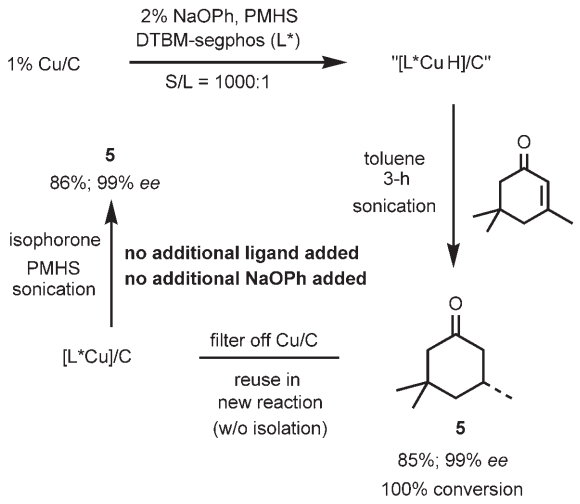
Table 3: Asymmetric hydrosilylations on a representative enone with Cu/C.



Ligand (L*)	*ee* [%]
(*R*)-(−)-DTBM-segphos	64
(*R*)-(−)-DTBM-segphos + *t*BuOH	19
(*R*)-(*S*)-PPF-P(*t*Bu)$_2$	17
(*R*)-(*S*)-PPF-P(*t*Bu)$_2$ + *t*BuOH	3

one (1.00-mmol scale) were performed at room temperature using both conventional stirring and ultrasonication conditions (bath temperature = ≈ 42 °C). ICP-AES analyses showed (as an average of two runs) that 2.5% of the copper used in the reaction had been leached from the support. This value corresponds to 37.0 μg of copper in solution or a substrate/copper ratio of 1667:1. When the control experiment was performed under conventional conditions without substrate, 0.9% of the copper used was found to have leached from the support (13.9 μg). For the reactions performed using sonication, 3.0% of the 2.2 wt.% copper had bled from the support (44.4 μg), which corresponds to a substrate/copper ratio of 1389:1. By comparison, using sonication in the absence of substrate decreased the extent of leaching by half (1.5% of the 2.2 wt.% copper, or 22.2 μg). Reactions

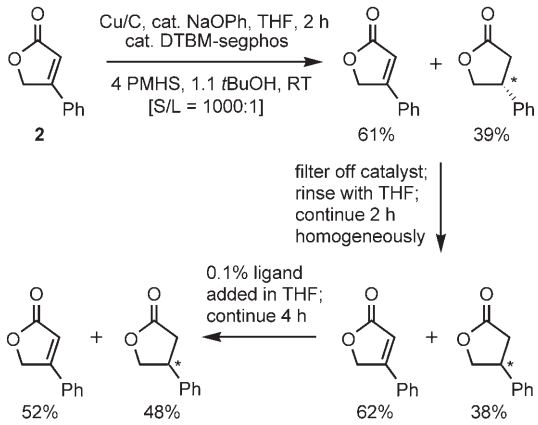
 © 2006 Wiley-VCH Verlag GmbH & Co. KGaA, Weinheim



Scheme 4. Recycling of Cu/C as illustrated by the reduction of isophorone.

conducted at subambient temperatures are likely to afford lower levels of copper in solution.

Additional experiments were carried out to lend further support to the claim that hydrosilylations catalyzed by Cu/C are heterogeneous in nature. Thus, unsaturated lactone **2** was treated with in situ generated catalytic [(DTBM-segphos)-CuH]/C for 2 h at ambient temperature (Scheme 5). An



Scheme 5. Homo- versus heterogeneous catalysis by CuH.

aliquot indicated that the ratio of educt to product was 61:39. The incomplete heterogeneous reaction mixture was filtered free of catalyst and the filtrate, which was shown by TLC to contain no DTBM-segphos, was allowed to stand for an additional 2 h. Analysis showed the ratio was essentially unchanged (62:38). Introduction of additional DTBM-segphos (0.1 mol%) followed by another 4-h reaction period led to some additional product (52:48). These observations support the ICP data that are indicative of a finite amount of copper bleeding into the macroscopic medium, as well as point to the essential role played by the ligand for catalysis to occur in solution. That no additional reaction takes place under homogeneous conditions, notwithstanding the confirmed presence of copper, indicates that reduction occurs within the charcoal matrix where both metal and ligand are present. When considered together with the observed variations in reaction rates and differences in the *ee* values obtained between homogeneous and heterogeneous versions of these hydrosilylations (see Table 2), heterogeneous catalysis is implicated.[28]

Micrographs using transmission electron microscopy (TEM) were recorded from a sample of Cu/C mounted on a grid, which displays 2D images.[29] The brighter grayish portions correspond to charcoal, whereas darker regions correspond to areas with higher copper concentrations. Figure 1a suggests a relatively even distribution of copper

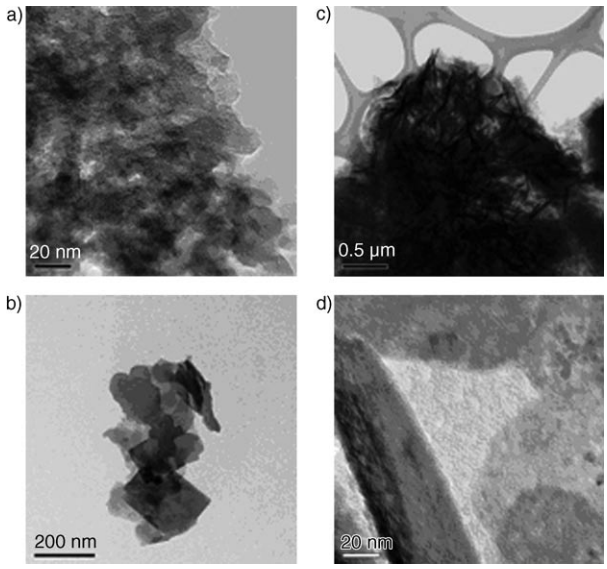


Figure 1. TEM images of Cu^{II}/C: a) bright field image showing dispersion of copper atoms; b) clusters of copper atoms; c) needles of copper atoms in a cluster; d) higher magnification of a copper cluster.

within the charcoal matrix, thought to derive from pretreatment of the catalyst with ultrasound. Figure 1b displays a magnified region of one of these darker regions and shows overlapping copper crystals. Figure 1c shows another perspective of copper conglomerates in the shape of needles on and within the charcoal matrix. Figure 1d illustrates a magnified cross section of a copper conglomerate. Taken together, these initial TEM images indicate a distribution of copper conglomerates on and within the charcoal pores throughout the catalyst. As was the case with Ni/C,[5] in situ reduction from Cu^{II} to reactive $Cu^{I}H$/C by a silane at ambient temperatures is unlikely to alter this array.

In summary, copper(II) has been impregnated within a charcoal matrix using ultrasonication under mild conditions to lead to a heterogeneous reagent, copper-in-charcoal (Cu/C). Once ligated by catalytic amounts of a nonracemic bisphosphine and NaOPh in the presence of a silane, a chiral copper(I) hydride reagent is generated. This species is very effective in asymmetric hydrosilylation reactions of a variety of functional groups, thus affording products in high yields and with excellent *ee* values.[30] ICP and TEM analyses, along with comparison data for the corresponding reactions in

 © 2006 Wiley-VCH Verlag GmbH & Co. KGaA, Weinheim

solution, suggest that the chemistry observed is occurring in a heterogeneous fashion.

Experimental Section

Preparation of Cu^{II}/C: Darco KB (5.00 g, 100 mesh) activated carbon (25% H_2O content) was added to a 100-mL round-bottom flask containing a stirring bar. A solution of $Cu(NO_3)_2 \cdot 3H_2O$ (Acros Organics, Cu content by ICP determination: 127%; 555.7 mg, 2.92 mmol) in deionized H_2O (35 mL) was added to activated carbon, and deionized H_2O (40 mL) was added to wash down the sides of the flask. The flask was purged under argon and stirred vigorously for 1 min. The flask was submerged in an ultrasonic bath under a positive argon flow for 30 min. The flask was attached to an argon-purged distillation setup and placed in a preheated 175–180 °C sand bath with stirring plate. As the distillation ended, the flask temperature rises automatically but should be held below 210 °C for an additional 15 min. Upon cooling to room temperature, toluene (25 mL) was added to wash down the sides of the flask. The flask was again placed into the hot sand bath until the toluene/H_2O azeotrope had distilled. Once the distillation was finished, the azeotropic distillation was repeated. Upon cooling to room temperature, the black solid was washed with toluene (2×30 mL) under argon into a predried (in vacuo) 150-mL coarse-fritted funnel. The toluene (60 mL) used to wash the Cu/C was removed by rotatary evaporation and analyzed for any remaining copper. The fritted funnel was turned upside down under vacuum for 5 h until the Cu/C fell from the frit into the collection flask. The collection flask was then dried in vacuo in a preheated 110–115 °C sand bath for 18 h. Using these specific amounts, the catalyst loading was 0.344 mmol Cu^{II}/g catalyst, or 2.2 wt.% Cu.

Representative asymmetric hydrosilylation: conversion of isophorone into (*R*)-3,3,5-trimethylcyclohexanone (Table 2, entry 6): Cu/C (134.4 mg, 0.05 mmol), NaOPh (24.0 mg, 0.20 mmol), and DTBM-segphos (2.4 mg, 0.002 mmol) were added to a flame-dried, argon-purged 10-mL round-bottom flask. Toluene (2 mL) was added and allowed to stir for 90 min. PMHS (240 μL, 4 mmol H^-) was then added dropwise and allowed to stir for 30 min. Isophorone (300 μL, 2 mmol) was added neat and the reaction was allowed to stir at room temperature until shown to be complete by TLC analysis (3 h; 4:1 hexanes/EtOAc). The reaction mixture was filtered and washed with Et_2O (3×5 mL) to remove the Cu/C. The reaction mixture was quenched with aqueous NaOH (15 mL, 3 M) and allowed to stir at room temperature for 3 h. The residue was purified by flash chromatography (4:1 hexanes/EtOAc) to afford the title product (196.3 mg, 70% yield due to volatility) as a clear oil. Analysis of the residue by GC showed 98.9% *ee* by using a Chiraldex-BDM column with 75 °C isotherm, $R_t = 41.47$ (minor) and 44.94 (major) min. The product matched previously reported spectral data.

Received: September 5, 2005
Published online: January 20, 2006

Keywords: asymmetric catalysis · copper · heterogeneous catalysis · hydrosilylation

[1] H. U. Blaser, A. Baiker, R. Prins, *Heterogeneous Catalysis and Fine Chemicals IV*, Elsevier, Netherlands, **1997**.
[2] J. R. Anderson, *Structure of Metallic Catalysts*, Academic Press, New York, **1975**; E. Bekyarova, D. Mehandjiev, *J. Colloid Interface Sci.* **1996**, *179*, 509; A. B. Stiles, *Catalyst Supports and Supported Catalysts*, Butterworth, Boston, **1987**, chap. 5.
[3] L. M. Gandia, M. Montes, *J. Catal.* **1994**, *145*, 276; M. Domingo-Garcia, I. Fernández-Moráles, F. J. López-Garzón, *Appl. Catal. A* **1994**, *112*, 75.
[4] A. R. Silva, J. L. Figueiredo, C. Freire, B. de Castro, *Catal. Today* **2005**, *102–103*, 154; T. Tsoncheva, S. Vankova, O. Bozhkov, D. Mehandjiev, *J. Mol. Catal. A* **2005**, *225*, 245.
[5] B. H. Lipshutz, S. Tasler, W. Chrisman, B. Spliethoff, B. Tesche, *J. Org. Chem.* **2003**, *68*, 1177.
[6] S. I. Lee, S. U. Son, M. R. Choi, Y. K. Chung, S.-G. Lee, *Tetrahedron Lett.* **2003**, *44*, 4705; S. U. Son, S. I. Lee, Y. K. Chung, *Angew. Chem.* **2000**, *112*, 4318; *Angew. Chem. Int. Ed.* **2000**, *39*, 4158.
[7] T. Tsoncheva, S. Vankova, D. Mehandjiev, *Fuel* **2003**, *82*, 755.
[8] B. H. Lipshutz, B. A. Frieman, *Angew. Chem.* **2005**, *117*, 6503; *Angew. Chem. Int. Ed.* **2005**, *44*, 6345.
[9] A. J. Garrat-Reed, D. C. Bell, *Energy Dispersive X-Ray Analysis in the Electron Microscope BIOS*, Scientific Publishers, Oxfordshire, **2002**; M. Arif Hayat, *Principles and Techniques of Scanning Electron Microscopy*, Van Nostrand Reinhold, New York, **1975**.
[10] I. Kummerow, D. L. Trimm, M. S. Wainwright, *Appl. Catal.* **1986**, *27*, 161.
[11] F. Zaccheria, N. Ravasio, R. Psaro, A. Fusi, *Tetrahedron Lett.* **2005**, *46*, 3695; N. Ravasio, R. Psaro, F. Zaccheria, *Tetrahedron Lett.* **2002**, *43*, 3943; N. , Ravasio, M. Antenori, M. Gargano, P. Mastrorilli, *Tetrahedron Lett.* **1996**, *37*, 3529; N. Ravasio, M. Rossi, *J. Org. Chem.* **1991**, *56*, 4329.
[12] *Comprehensive Asymmetric Catalysis I–III* (Eds.: E. N. Jacobsen, A. Pfaltz, H. Yamamoto), Springer, Berlin, **1999**; *Asymmetric Catalysis in Organic Synthesis* (Ed.: R. Noyori), Wiley, New York, **1994**.
[13] a) C. Bolm, J.-C. Frison, J. Le Paih, C. Moessner, G. Raabe, *J. Organomet. Chem.* **2004**, *689*, 3767; b) A. P. Duncan, J. L. Leighton, *Org. Lett.* **2004**, *6*, 4117; c) W. A. Herrmann, *Angew. Chem.* **2002**, *114*, 1342; *Angew. Chem. Int. Ed.* **2002**, *41*, 1290, and references therein.
[14] a) B. H. Lipshutz, K. Noson, W. Chrisman, A. Lower, *J. Am. Chem. Soc.* **2003**, *125*, 8779; b) B. H. Lipshutz, J. M. Servesko, T. B. Petersen, P. P. Papa, A. Lover, *Org. Lett.* **2004**, *6*, 1273; c) B. H. Lipshutz, H. Shimizu, *Angew. Chem.* **2004**, *114*, 2278; *Angew. Chem. Int. Ed.* **2004**, *43*, 2228; d) B. H. Lipshutz, J. M. Servesko, B. R. Taft, *J. Am. Chem. Soc.* **2004**, *126*, 8352; e) B. H. Lipshutz, A. Lower, K. Noson, *Org. Lett.* **2002**, *4*, 4045.
[15] R. Nickolov, T. Tsoncheva, D. Mehandjiev, *Fuel* **2001**, *81*, 203; B. Park, S. Park, S. Ryu, *J. Colloid Interface Sci.* **1999**, *217*, 142; for the preparation of copper-on-graphite, see: A. Fuerstner, F. Hofer, H. Weidmann, *Carbon* **1991**, *29*, 915; B. H. Lipshutz, M. Koerner, D. A. Parker, *Tetrahedron Lett.* **1987**, *28*, 945.
[16] J. Zhao, Z. Liu, D. Sun, *J. Catal.* **2004**, *227*, 297; H. Tseng, M. Wey, *Carbon* **2004**, *42*, 2269.
[17] B. H. Lipshutz, S. Tasler, *Adv. Synth. Catal.* **2001**, *343*, 327.
[18] While PMHS purchased from Lancaster and used as received works well in this chemistry, the material from Acros was surprisingly ineffective as a source of hydride.
[19] T. Saito, T. Yokozawa, T. Ishizaki, T. Moroi, N. Sayo, T. Miura, H. Kumobayashi, *Adv. Synth. Catal.* **2001**, *343*, 264.
[20] Available from Solvias, Inc.; cf. H.-U. Blaser, W. Brieden, B. Pugin, F. Spindler, M. Studer, A. Togni, *Top. Catal.* **2002**, *19*, 3.
[21] R. Schmid, E. A. Broger, M. Cereghetti, Y. Crameri, J. Foricher, M. Lalonde, R. K. Muller, M. Scalone, G. Schoettel, U. Zutter, *Pure Appl. Chem.* **1996**, *68*, 131; R. Schmid, J. Foricher, M. Ceregetti, P. Schonholzer, *Helv. Chim. Acta* **1991**, *74*, 370.
[22] T. Ohkuma, M. Kitamura, R. Noyori, *Asymmetric Hydrogenation. Catalytic Asymmetric Synthesis* (Ed.: I. Ojima), Wiley-VCH, New York, **2000**, chap. 1, and references therein.
[23] B. H. Lipshutz, J. M. Servesko, *Angew. Chem.* **2003**, *115*, 4937; *Angew. Chem. Int. Ed.* **2003**, *42*, 4789.
[24] B. H. Lipshutz, B. A. Frieman, J. B. Unger, D. M. Nihan, *Can. J. Chem.* **2005**, *83*, 606.

 © 2006 Wiley-VCH Verlag GmbH & Co. KGaA, Weinheim

[25] G. Hughes, M. Kimura, S. L. Buchwald, *J. Am. Chem. Soc.* **2003**, *125*, 11253.
[26] Quantitative determination of the extent of ligand retention has yet to be determined.
[27] A. W. Varnes, *Handbook of Instrumental Techniques for Analytical Chemistry* (Ed.: F. Settle), Prentice Hall, Upper Saddle River, NJ, **1997**, p. 395.
[28] a) Standard workup of organocopper reactions done in solution oftentimes involves aqueous ammonia to sequester copper as its cuprammonium salts,[28b] which at higher concentrations of copper usually display an unmistakable blue coloration in the aqueous phase. Use of this "cuprate quench" (namely, 90% NH_4Cl/10% conc. NH_4OH; pH 10) led to no visible sign of copper in solution; b) B. H. Lipshutz, *Organometallics in Synthesis: A Manual*, 2nd ed. (Ed.: M. Schlosser), Wiley, Chichester, **2002**, chap. 6, and references therein; *Modern Organocopper Chemistry* (Ed.: N. Krause), Wiley-VCH, New York, **2002**; B. H. Lipshutz, S. Sengupta, *Org. React.* **1992**, *41*, 135.
[29] B. Fultz, J. M. Howe, *Transmission Electron Microscopy and Diffractometry of Materials*, Springer, New York, **2002**.
[30] Isolation of the catalyst after treatment with *n*BuLi in THF at room temperature followed by exposure to air over time did not lead to any observable physical change; thus, the catalyst appears to be nonpyrophoric, as is the case with Ni^0/C.

 © 2006 Wiley-VCH Verlag GmbH & Co. KGaA, Weinheim

Tungsten Oxide Films

DOI: 10.1002/anie.200502061

Controlling Wettability and Photochromism in a Dual-Responsive Tungsten Oxide Film**

*Shutao Wang, Xinjian Feng, Jiannian Yao, and Lei Jiang**

Control of the surface wettability of solid substrates has aroused great interest because of their importance in fundamental research and industrial applications.[1–4] Responsive materials have found extensive uses as controllable surfaces because of their intrinsic reaction to environmental stimuli such as light irradiation,[5] electric fields,[6] heating/cooling,[7] and solvent treatment.[8] However, the responsive surface wettability of smooth surfaces is usually very limited. For example, the reported maximum change in contact angle (CA) is only about 11° on flat surfaces coated with azobenzene.[5b] The introduction of surface roughness[9] has recently been used to enhance the responsive wettability of inorganic and organic materials between superhydrophilicity (CA less than 5°) and superhydrophobicity (CA higher than 150°).[10] This responsivity is due to a change of the chemical composition of the surface under an environmental stimulus. For multiresponsive materials, this change of chemical composition may induce multiresponsive properties by combining, for example, wettability conversion between two extreme states with photochromism,[11] which would be a promising starting point for the design of novel, artificial smart surfaces. Herein, we report an intelligent, dual-responsive tungsten oxide film that combines wettability conversion with photochromic behavior.

Tungsten oxide, which is an indirect, broad-gap semiconductor, has been extensively studied because of its unique physical/chemical properties and widespread applications. Tungsten oxide films have been prepared by a variety of methods, such as thermal evaporation, chemical vapor deposition, sputtering, and sol–gel methods.[12–16] Until now, nearly all of its applications are in photo- and electrochromic "smart" windows, erasable optical-storage devices, catalysts, gas sensors, and humidity and temperature sensors. The inorganic oxide film prepared by us shows both reversible wettability conversion between superhydrophobic and superhydrophilic states and photochromism upon alternating between UV irradiation and storage in the dark, and could lead to future uses for tungsten oxide in novel smart devices and help us to understand its chemical and physical properties better.

The rough tungsten oxide films were prepared by an inexpensive and simple electrochemical deposition process.[15] In a typical procedure, aqueous Na_2WO_4 solution was used as the electrolyte for electrodeposition of tungsten oxide films along with oxalic acid to adjust the solution pH in the range 3.1 to 8.6 (this is a suitable pH range for the electrochemical deposition of tungsten oxides; the influence of various experimental conditions on film formation will be discussed elsewhere). An indium tin oxide (ITO) glass was immersed in the electrolyte and electrochemical deposition was conducted at −1.5 eV in single-potential time-based mode with a platinum electrode as the counter electrode and Ag/AgCl as the reference electrode. The morphology of the deposited tungsten oxide film depends on the pH of the precursor solution (see the Supporting Information). Thus, a smooth film composed of nanoparticles is formed at low pH, whereas upon increasing the pH value the oxide films become rough with a remarkable increase of the size of the nanoparticles. When the pH of the precursor solution was about 8.6, a rough, brown film was obtained that exhibits a pebble-beach-like morphology made up of many nanoprotuberances with diameters in the range 40–350 nm (Figure 1). Energy-dispersive X-ray analysis confirmed that this rough film is tungsten oxide (see the Supporting Information).

[*] Dr. S. Wang, Dr. X. Feng, Prof. J. Yao, Prof. L. Jiang
Center of Molecular Sciences
Institute of Chemistry
Chinese Academy of Sciences
Beijing 100080 (P.R. China)
Fax: (+86) 10-8262-7566
E-mail: jianglei@iccas.ac.cn
Dr. S. Wang, Dr. X. Feng
Graduate School of Chinese Academy of Sciences
Beijing 100864 (P.R. China)

[**] The authors thank the National Nature Science Foundation of China (20125102, 90306011, 20421101) and the Innovation Foundation of the Chinese Academy of Sciences for funding this research.

Supporting information for this article is available on the WWW under http://www.angewandte.org or from the author.

 InterScience © 2006 Wiley-VCH Verlag GmbH & Co. KGaA, Weinheim

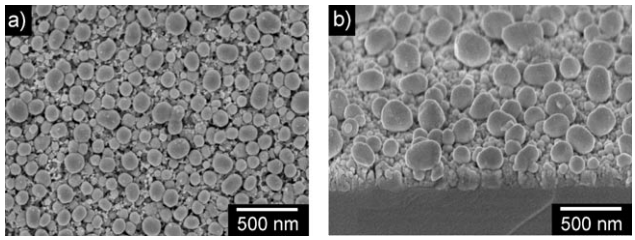


Figure 1. Typical SEM images of tungsten oxide films deposited from the electrolyte at a pH of about 8.6: a) top view; b) side view from 45°. The morphology of the nanostructures resembles a pebble beach.

The surface wettability of the as-prepared rough film was evaluated by water CA measurements. The CA on the film is $151.3 \pm 2.9°$ (the left drop in Figure 2a), thus indicating that

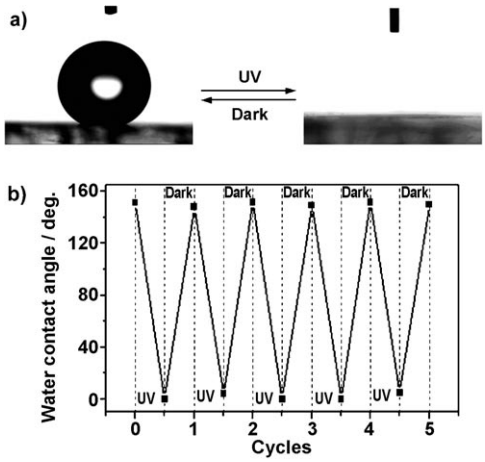


Figure 2. a) Water-drop profiles for the photoresponsive switch between superhydrophobicity and superhydrophilicity of the tungsten oxide film before (left) and after (right) UV irradiation. The water CAs are $151.3 \pm 2.9°$ and less than 5°, respectively. b) Reversible water CA transition on the deposited tungsten oxide film upon alternating UV irradiation and storage in the dark.

the surface is superhydrophobic. We believe that the rough nanostructures play an important role in the surface superhydrophobicity of the film.[2,3] Upon UV irradiation for three hours (a 500-W Hg lamp with a filter centered at 365 ± 10 nm was used as the light source), the water droplet spread out on the film with a CA of less than 5° (the right drop in Figure 2a). UV irradiation therefore induces a change in surface wettability to a superhydrophilic state. Storage of these irradiated films in the dark for 2 weeks caused them to become superhydrophobic again. This cycle was repeated several times, and a good reversibility of surface wettability was observed (Figure 2b).

Surface wettability is determined by the chemical composition of a surface and its nanostructure.[2–9] Our tungsten oxide film shows superhydrophobicity because of the air trapped in the interspaces of the rough surface.[2c] Upon UV irradiation, however, it becomes superhydrophilic. As tungsten oxide is a photosensitive material,[16] when the film is irradiated with UV light the photogenerated electrons will reduce part of the tungsten and the photogenerated holes will react with lattice oxygen to form oxygen vacancies. Water molecules from the air are adsorbed and coordinate kinetically to these oxygen vacancies, which greatly improves the surface hydrophilicity. The X-ray photoelectron spectra of the as-deposited film confirm that a reduction of tungsten to a mixed-valence state occurs (see the Supporting Information). For the as-prepared film, the peaks corresponding to the $W4f_{7/2}$ and $W4f_{5/2}$ orbitals are observed at 35.1 and 37.3 eV, respectively. These values are lower than those for tungsten(VI) trioxide powder (36.0 and 38.2 eV), which indicates that the tungsten in the electrodeposited film may be present as W^{6+}, W^{5+}, and W^{4+}. After UV irradiation, the peaks corresponding to $W4f_{7/2}$ and $W4f_{5/2}$ are observed at energy levels about 0.2 eV lower than those before UV irradiation, thus confirming that the tungsten atoms have been reduced to W^{5+}, W^{4+}, or even to W^{3+}.[15a]

In order to thoroughly understand the role of atmospheric water, the UV-irradiation experiment was also carried out under dry conditions. An evident difference of CA was observed when the sample was irradiated at different humidities (see the Supporting Information). For example, with an irradiation time of 3 hours under the standard conditions (relative humidity of 39–46%), a superhydrophilic state appears, whereas under dry conditions (relative humidity of 9–12%), the CA only changes from 152.3 ± 2.1 to $93.5 \pm 12.4°$. These results indicate that atmospheric water is important for the conversion into a hydrophilic state as water droplets can enter the spaces between the nanoprotuberances by a three-dimensional capillary effect.[17].

Adsorption of hydroxy groups formed in the photochemical surface reaction transforms the surface into an energetically metastable state. When the UV-irradiated film is placed under air in the dark the hydroxy groups are gradually replaced by atmospheric oxygen[18] and the surface evolves back to the initial state. To confirm the function of atmospheric oxygen we performed the following experiment: when the UV-irradiated samples were left under nitrogen in the dark for two weeks the CA only recovered to $30.2 \pm 4.1°$. This slight recovery may be due to oxygen contamination. When these samples were left under air or oxygen instead of nitrogen they returned to the superhydrophobic state. These results provide evidence for the dominant role of atmospheric oxygen in the recovery process[16] leading from superhydrophilicity back to superhydrophobicity. This reversible conversion proceeds only by adsorption and desorption of surface hydroxide ions at the outermost oxide layer.[1b,19] The stability of the surface nanostructures, free from changes in chemical conditions, explains why the reversible wettability switch can be repeated many times.

Since tungsten oxide is an excellent photochromic material, its photochromic behavior was also studied during the wettability conversion. After UV irradiation, the as-prepared film became yellowish green from the initial brown, and when this film was placed in the dark it recovered to brown. As shown in Figure 3, the UV spectra show a change in absorbance, with the greatest absorbance change of 0.34 occurring around 372 nm. In addition, a good reversibility was observed for many cycles of coloration and decoloration. The

 © 2006 Wiley-VCH Verlag GmbH & Co. KGaA, Weinheim

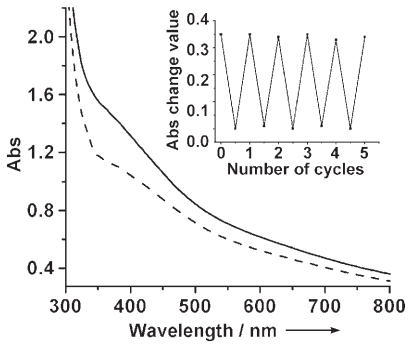


Figure 3. Absorption spectra of an electrodeposited tungsten oxide film before (solid line) and after (dashed line) irradiation with UV light at 365 ± 10 nm. The insert shows the photochromic switching of the absorption change (monitored at 372 nm) during consecutive cycles of UV irradiation and storage in the dark.

photochromic behavior of the as-deposited film is due to the variation of the tungsten valence and the number of oxygen vacancies and water molecules.[16] Importantly, the photochromic behavior and wettability change are linked by the adsorption of atmospheric water by the film.

In conclusion, nanostructured tungsten oxide films with wettability and photochromic dual-responsive properties have been prepared by a facile electrochemical deposition process. A reversible wettability conversion between superhydrophobicity and superhydrophilicity, which is accompanied by photochromism, can be realized for this tungsten oxide material by alternating UV irradiation with storage in the dark. The wettability interconversion and photochromism are coherent in nature and are due to changes in the redox properties of the metal ions and the number of oxygen vacancies and adsorbed water molecules. This study suggests that tungsten oxide materials and other semiconductor oxides with responsive redox properties have a promising future for use in dual- and multifunctional switches in new technological applications such as smart functional windows, microfluidic devices, and bioanalysis.

Experimental Section

The electrodeposition process was performed in a three-electrode system. An aqueous solution of Na_2WO_4 (0.5 M) was used as the electrolyte, and oxalic acid was used to adjust the pH of the solution in the range 3.1 to 8.6. A piece of ITO glass (area 2×3 cm^2) was used as the cathode after it was cleaned with aqueous detergent, acetone, ethanol, and distilled water. The anode was a Pt plate (1.5×1.5 cm^2) and the reference electrode was a CHI110 Ag/AgCl electrode. The cathodic electrodeposition was performed at a constant potential of -1.5 eV for 1–3 min at room temperature. The deposited films were then removed from the solution, washed with distilled water, and blown dry with N_2.

A Hitachi S-4300F scanning electron microscope (SEM) equipped with an energy dispersive X-ray analyzer (Phoenix) was used to determine the morphology and the composition of the porous film. CAs were measured on a dataphysics OCA20 contact-angle system at ambient temperature. The average CA was obtained by measuring more than five different positions of the same sample. X-ray photoelectron spectra were obtained with an ESCALab220i-XL electron spectrometer from VG Scientific using 300-W $Al_{K\alpha}$ radiation. The base pressure was about 3×10^{-9} mbar. UV/Vis spectra were measured with a Hitachi U-4100 spectrophotometer. All measurements were performed at room temperature.

Received: June 15, 2005
Revised: November 28, 2005
Published online: January 13, 2006

Keywords: nanostructures · photochromism · surface chemistry · tungsten · wettability

[1] a) R. Wang, K. Hashimoto, A. Fujishima, M. Chikuni, E. Kojima, A. Kitamura, M. Shimohigoshi, T. Watanabe, *Nature* **1997**, *388*, 431–432; b) R. Wang, N. Sakai, A. Fujishima, T. Watanabe, K. Hashimoto, *J. Phys. Chem. B* **1999**, *103*, 2188–2194.

[2] a) W. Barthlott, C. Neinhuis, *Planta* **1997**, *202*, 1–8; b) P. Aussillous, D. Quéré, *Nature* **2001**, *411*, 924–927; c) L. Feng, S. Li, Y. Li, H. Li, L. Zhang, J. Zhai, Y. Song, B. Liu, L. Jiang, D. Zhu, *Adv. Mater.* **2002**, *14*, 1857–1860; d) R. Blossey, *Nat. Mater.* **2003**, *2*, 301–306.

[3] a) T. Onda, S. Shibuichi, N. Satoh, K. Tsujii, *Langmuir* **1996**, *12*, 2125–2127; b) W. Chen, A. Y. Fadeev, M. C. Heieh, D. Öner, J. Youngblood, T. J. McCarthy, *Langmuir* **1999**, *15*, 3395–3399; c) H. Li, X. Wang, Y. Song, Y. Q. Liu, L. Jiang, D. Zhu, *Angew. Chem.* **2001**, *113*, 1793–1796; *Angew. Chem. Int. Ed.* **2001**, *40*, 1743–1746.

[4] a) H. Y. Erbil, A. L. Demirel, A. Yonca, O. Mert, *Science* **2003**, *299*, 1377–1380; b) I. Woodward, W. C. E. Schofield, V. Roucoules, J. P. S. Badyal, *Langmuir* **2003**, *19*, 3432–3438; c) L. Zhai, F. C. Cebeci, R. E. Cohen, M. F. Rubner, *Nano lett.* **2004**, *4*, 1349–1353; d) X. Zhang, F. Shi, X. Yu, H. Liu, Y. Fu, Z. Wang, L. Jiang, X. Li, *J. Am. Chem. Soc.* **2004**, *126*, 3064–3065; e) J. Han, D. Lee, C. Ryu, K. Cho, *J. Am. Chem. Soc.* **2004**, *126*, 4796–4797.

[5] a) K. Ichimura, S. Oh, M. Nakagawa, *Science* **2000**, *288*, 1624–1626; b) C. Feng, Y. Zhang, J. Jin, Y. Song, L. Xie, G. Qu, L. Jiang, D. Zhu, *Langmuir* **2001**, *17*, 4593–4597; c) T. P. Russell, *Science* **2002**, *297*, 964–967; d) R. Rosario, D. Gust, M. Hayes, F. Jahnke, J. Springer, A. A. Garcia, *Langmuir* **2002**, *18*, 8062–8069.

[6] J. Lahann, S. Mitragotri, T. Tran, H. Kaido, J. Sundaram, I. S. Choi, S. Hoffer, G. A. Somorjai, R. Langer, *Science* **2003**, *299*, 371–374.

[7] D. Crevoisier, P. Fabre, J. Corpart, L. Leibler, *Science* **1999**, *285*, 1246–1249.

[8] S. Minko, M. Müller, M. Motornov, M. Nitschke, *J. Am. Chem. Soc.* **2003**, *125*, 3896–3900.

[9] a) R. N. Wenzel, *Ind. Eng. Chem.* **1936**, *28*, 988–994; b) A. B. D. Cassie, S. Baxter, *Trans. Faraday Soc.* **1944**, *40*, 546–551.

[10] a) T. Sun, G. Wang, L. Feng, B. Liu, Y. Ma, L. Jiang, D. Zhu, *Angew. Chem.* **2004**, *116*, 361–364; *Angew. Chem. Int. Ed.* **2004**, *43*, 357–360; b) Q. Fu, G. V. R. Rao, S. B. Basame, D. J. Keller, K. Artyushkova, J. E. Fulghum, G. P. Lopez, *J. Am. Chem. Soc.* **2004**, *126*, 8904–8905; c) X. Feng, L. Feng, M. Jin, J. Zhai, L. Jiang, D. Zhu, *J. Am. Chem. Soc.* **2004**, *126*, 62–63.

[11] J. N. Yao, K. Hashimoto, A. Fujishima, *Nature* **1992**, *355*, 624–626.

[12] a) M. Sun, N. Xu, J. W. Cao, J. N. Yao, E. G. Wang, *J. Mater. Res.* **2000**, *15*, 927–933; b) I. Turyan, U. O. Krasovec, B. Orel, T. Saraidorov, R. Reisfeld, D. Mandler, *Adv. Mater.* **2000**, *12*, 330–333; c) Y. Koltypin, S. I. Nikitenko, A. Gedanken, *J. Mater. Chem.* **2002**, *12*, 1107–1110.

[13] a) S. K. Deb, *Philos. Mag.* **1973**, *22*, 801; b) T. Oi, K. Miyauchi, K. Uehara, *J. Appl. Phys.* **1982**, *53*, 1832–1833; c) P. K. Shen, J.

 © 2006 Wiley-VCH Verlag GmbH & Co. KGaA, Weinheim

Syed-Bokhari, A. C. C. Tseung, *J. Electrochem. Soc.* **1991**, *138*, 2778 – 2783.
[14] a) A. Nakajima, A. Fujishima, K. Hashimoto, T. Watanabe, *Adv. Mater.* **1999**, *11*, 1365 – 1368; b) N. Xu, M. Sun, J. W. Cao, J. N. Yao, E. G. Wang, *Appl. Surf. Sci.* **2000**, *157*, 81 – 84; c) C. Bigey, G. Maire, *J. Catal.* **2000**, *196*, 224 – 240; d) D. S. Lee, K. H. Nam, D. D. Lee, *Thin Solid Films* **2000**, *375*, 142 – 146.
[15] a) J. N. Yao, P. Chen, A. Fujishima, *J. Electroanal. Chem.* **1996**, *405*, 223 – 226; b) L. Y. Su, H. Wang, Z. H. Lu, *Mater. Chem. Phys.* **1998**, *56*, 266 – 270; c) S.-H. Baeck, K.-S. Choi, T. F. Jaramillo, G. D. Stucky, E. W. McFarland, *Adv. Mater.* **2003**, *15*, 1269 – 1273.
[16] a) C. Bechinger, G. Oefinger, S. Herminghaus, P. Leiderer, *J. Appl. Phys.* **1993**, *74*, 4527 – 4533; b) J. Zhang, D. Benson, C. Tracy, S. K. Deb, A. W. Czanderna, C. Bechinger, *J. Electrochem. Soc.* **1997**, *144*, 2022 – 2026; c) T. He, J. N. Yao, *Res. Chem. Intermed.* **2004**, *30*, 459 – 488.
[17] a) J. Bico, C. Tordeux, D. Quéré, *Europhys. Lett.* **2001**, *55*, 214 – 220; b) J. Bico, U. Thiele, D. Quéré, *Colloids Surf. A* **2002**, *206*, 41 – 46.
[18] M. Miyauchi, A. Nakajima, T. Watanabe, K. Hashimoto, *Chem. Mater.* **2002**, *14*, 2812 – 2816.
[19] a) L. Q. Wang, D. R. Baer, M. H. Engelhard, A. N. Shultz, *Surf. Sci.* **1995**, *344*, 237 – 350; b) R. D. Sun, A. Nakajima, A. Fujishima, T. Watanabe, K. Hashimoto, *J. Phys. Chem. B* **2001**, *105*, 1984 – 1990.

 © 2006 Wiley-VCH Verlag GmbH & Co. KGaA, Weinheim

Drug–Protein Adducts

DOI: 10.1002/anie.200502599

Structural Investigation of Cisplatin–Protein Interactions: Selective Platination of His19 in a Cuprozinc Superoxide Dismutase**

Vito Calderone, Angela Casini, Stefano Mangani, Luigi Messori,* and Pier Luigi Orioli*

Cisplatin (*cis*-$[PtCl_2(NH_3)_2]$) is a leading anticancer drug.[1] Its biological activity is strictly associated with platination of nuclear DNA at guanine sites, the formation of intrastrand cross-links, and the consequent induction of DNA bending.[2] Damage to DNA eventually causes apoptotic cell death through a complex cascade of biochemical processes that are being progressively unraveled.[3] The fact that DNA represents the probable primary target for this metallodrug has prompted a huge number of studies on cisplatin–DNA interactions.[2] In contrast, the interactions of anticancer platinum drugs with proteins have received, until now, far less attention.

Only a very modest fraction of the administered cisplatin reacts with nuclear DNA and produces the critical cytotoxic lesions; the largest amount of cisplatin is reported to bind proteins, both extracellularly and intracellularly.[4] Surprisingly, these latter interactions have been explored only marginally, although they probably constitute the biochemical basis for the relevant systemic toxic effects caused by platinum drugs, and might also play some role in the anticancer mechanism. Thus, it is of great interest, in our opinion, to determine the nature of the platinum-containing molecular fragments that are bound to proteins, their exact location, their strength of binding, and the reversibility of the interactions. A few solution studies on the interactions of cisplatin and analogues with selected proteins have appeared over the years (e.g., ubiquitin,[5] albumin,[6] hemoglobin,[7] transferrin[8]), but we noticed a substantial lack of crystallographic information for protein adducts with platinum drugs. The only kind of structural information available for platinum–protein adducts is that resulting from the use of platinum salts and platinum complexes in the preparation of heavy-atom derivatives of proteins.[9]

These arguments led us to perform new crystallographic investigations of cisplatin derivatives of proteins, to give a detailed structural description of the nature of platinum–protein interactions. Bovine erythrocyte copper–zinc superoxide dismutase (beSOD; EC 1.15.1.1) was selected as the model protein for our study on cisplatin for a number of reasons:[10] the crystal structure of beSOD is available at high resolution;[10] beSOD is a medium-sized protein with several potential binding sites for platinum; it is highly water soluble; it is commercially available; it is known to crystallize easily; and it exhibits great stability under physiological-type conditions.

Crystals of cisplatin-treated beSOD, suitable for X-ray diffraction analysis, were obtained after incubation of the protein with a tenfold molar excess of cisplatin for two weeks. X-ray diffraction data were collected at low temperature and the structure was solved through standard methods to 1.8-Å resolution. To the best of our knowledge, the results presented herein provide the first example of a high-resolution crystal structure for a cisplatin–protein derivative.

The overall structure of cisplatin-treated beSOD (Figure 1) clearly resembles that of the native beSOD used as the starting model for the molecular replacement. The Cα root-mean-square deviation (rmsd) between the two proteins is 0.19 Å and there are no regions where the deviations are significantly high. Also, the physiological copper and zinc atoms are well-defined in the electron-density map of the active site of the enzyme as are the disulfide bridges. The structure seems to be quite rigid as the average *B* factor is 7.3 $Å^2$. In other words, the reaction with cisplatin would cause neither general nor local structural changes of the protein,

[*] Dr. V. Calderone, Prof. S. Mangani
Department of Chemistry
Università degli Studi di Siena
Via Aldo Moro 1, 53100 Siena (Italy)
Fax: (+39) 0577234253
E-mail: mangani@unisi.it
Dr. A. Casini, Prof. L. Messori, Prof. P. L. Orioli
Department of Chemistry
Università degli Studi di Firenze
Via della Lastruccia 3, 50019 Sesto Fiorentino, Firenze (Italy)
Fax: (+39) 055-457-3385
E-mail: luigi.messori@unifi.it

[**] This work was supported by MIUR PRIN 2004, Ente Cassa di Risparmio di Firenze, and COST D20 WG009.

 © 2006 Wiley-VCH Verlag GmbH & Co. KGaA, Weinheim

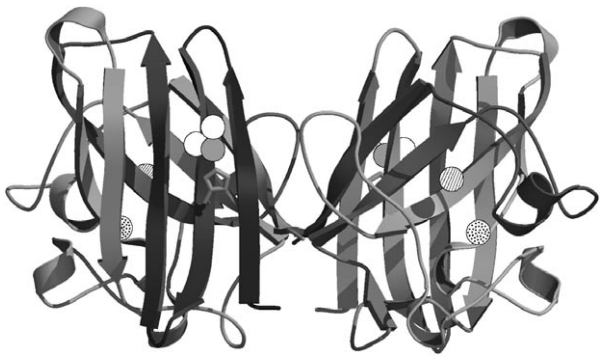


Figure 1. Schematic representation of the asymmetric unit containing the physiological dimer; the side chain of His19 is shown along with Cu (hatched), Zn (dotted), Pt (gray), and Cl (white).

with just monodentate platinum binding occurring on the protein surface.

A detail of the electron-density map around the protein-bound platinum center is shown in Figure 2. The map clearly reveals specific binding of the platinum atom to the NE2

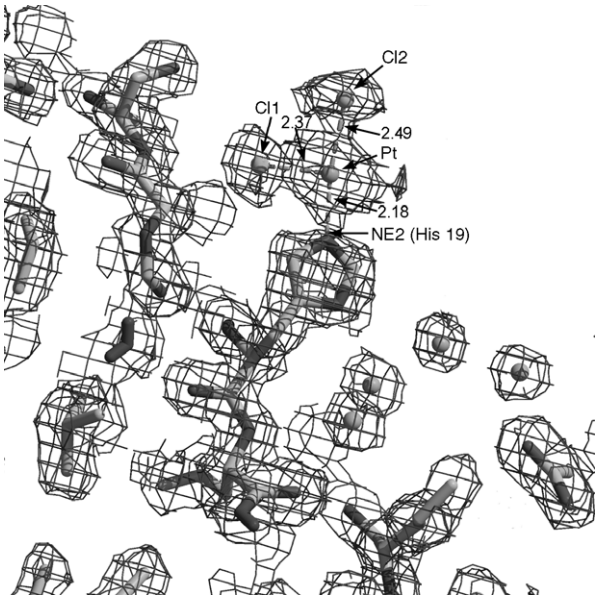


Figure 2. Detail of the $2F_o-F_c$ electron-density map contoured at 1σ showing cisplatin interacting with His19 and the relative bond lengths.

nitrogen atom of His19, in both monomers. The occupancy of the platinum atom is slightly different for the two monomers; the refinement shows values of about 0.7 and 0.6, respectively, which confirm a good binding selectivity. Notably, the electron-density map does not show any presence of additional platinum atoms bound to other residues of either monomer.

Sulfur-containing side chains are known to represent preferred binding sites for platinum compounds; competitive binding of platinum(II) drugs to either nitrogen or sulfur donors is a matter of intense debate.[11] Our structural data on platinated beSOD unambiguously reveal a preference for platinum binding to His compared to Met or Cys residues. This preference may be, at least partially, ascribed to the fact that access to either Met115 or Cys6, the only "free" sulfur-containing groups of beSOD, is somehow sterically hindered. Conversely, Cys55 and Cys144, which are solvent-accessible, are engaged in the formation of an internal disulfide bridge and are thus less prone to react with platinum(II).

Notably, both platinum(II) ions bind the protein in a slightly distorted square-planar arrangement, which is typical for platinum(II) complexes; the coordination environments of the two platinum atoms are very similar but not identical. One of the four ligands is the NE2 nitrogen atom of His19, which anchors the platinum ion to the protein in a monodentate fashion. The adjacent position shows a tiny electron density, which probably results from a very weakly bound water molecule. The remaining coordination positions (one of which is in the *trans* configuration with respect to the histidine nitrogen atom) show a very clear and prominent electron density that was assumed, at first, to arise from the two amino groups of cisplatin.

However, upon careful analysis of the thermal factors of the platinum ligands and of their distances to platinum, it is possible to state quite unambiguously that cisplatin, upon protein binding, releases its two ammonia ligands rather than losing the two chlorine atoms, as might be expected on the grounds of the well-described solution behavior of cisplatin.[1] In fact, if the ligand is refined with the assumption that both adjacent coordination positions (or one of them) are occupied by a nitrogen atom, the *B* factors go down to unrealistic values, whereas, if the two positions are refined assuming the presence of two chlorine atoms, the *B*-factor values obtained are comparable to those of the copper and zinc atoms in the active site of the protein (around 15 Å^2). Also, the interaction distances strongly support this interpretation, as the distances between the platinum atom and these two coordination positions are too large (2.55(12) Å in the case of the *trans* position with respect to the histidine nitrogen atom, and 2.28(12) Å for the other one) compared to the usual Pt–N distances (which should be around 2.1–2.2 Å).[12] A careful inspection of the crystal structure revealed tight contact between a chlorine atom and the main-chain carbonyl group of Thr17 (the distance is 3.23(12) Å).

The proposed release of the ammonia ligands is a quite remarkable and unexpected finding in relation to the classical solution chemistry of cisplatin. However, recent theoretical studies by Deubel and co-workers[13] have established that loss of the ammonia ligands is indeed feasible within the specific protein microenvironment, and may represent a possible mechanism of cisplatin inactivation as both ammonia groups are normally required for its biological activity.[2] These authors showed that the less-polarizable environment, which is likely present when amino acid residues of proteins react with the drug, greatly reduces the *trans* influence and enhances the *trans* effect at the platinum center.[13] Also, the different interactions that can occur between cisplatin and the protein surface might well favor alternative reactivity pathways for the metal center over the time that is needed for crystal formation and growth.

 © 2006 Wiley-VCH Verlag GmbH & Co. KGaA, Weinheim

Overall, the present results are, in our opinion, of significant interest as they represent the first high-resolution crystal structure for a cisplatin–protein adduct. Unambiguous evidence is provided for His19 as the primary anchoring site for cisplatin. Binding is shown to be highly selective: occupation of the His site is relevant (> 60–70 %), while no other binding sites could be detected on the protein surface even at very low occupation percentages. Remarkably, clear evidence for ammonia release from cisplatin is provided. In addition, our study proposes a general X-ray-based strategy for investigating metallodrug–protein interactions, which relies on cocrystallization of adducts of metallodrugs with selected model proteins.

Experimental Section

Crystals of platinated beSOD were obtained by using the hanging-drop method for cocrystallizing the protein (5 mg mL^{-1}) with cisplatin at a platinum/protein molar ratio of 10:1. Cisplatin from Sigma–Aldrich was used (code P4394, lot 124F-0474). The precipitant buffer in the reservoir solution consisted of Tris-HCl (50 mM, pH 7.5), PEG 4000 (18 %), and 2-propanol (20 %). Small crystals appeared within 3 days at 4 °C, and were allowed to grow at room temperature for 2 weeks.

A monochromatic experiment at the Cu_α wavelength was performed on a crystal of beSOD grown in the presence of cisplatin by the rotation method on a PX-Ultra sealed-tube diffractometer (Oxford Diffraction) at 100 K. The crystal diffracted up to 1.7-Å resolution (resolution: 52.0–1.8 Å), with 32303 (3880) unique reflections out of 154261 (8429) reflections, and belonged to space group $P2_12_12_1$ ($a = 47.21$, $b = 50.92$, $c = 146.74$ Å; $\alpha = \beta = \gamma = 90°$) with two molecules (a complete physiological dimer) in the asymmetric unit and a solvent content of about 52 %. The overall completeness was 96.1 (81.4) %, $R_{sym} = 17.5$ (42.6) %, multiplicity: 4.8 (2.2), $I/(\sigma I) = 4.1$ (1.7). The numbers in parentheses refer to the values in the highest resolution shell (1.9–1.8 Å).

The dataset was processed by using the program MOSFLM[14a] and scaled by the program SCALA,[14b] with the TAILS and SECONDARY corrections (the latter restrained with a TIE SURFACE command) to achieve an empirical absorption correction.

The structure of the cisplatin adduct was solved by the molecular replacement technique; the model used was that of a monomer of beSOD (PDB-ID 1SXS) from which all the water molecules and ions were omitted. The correct orientation and translation of the dimer within the crystallographic unit cell were determined with standard Patterson search techniques,[14c,d] as implemented in the program MOLREP.[14e,f] The isotropic refinement was carried out using REFMAC5[14g] for all atoms except Cu, Zn, and Pt, which were refined anisotropically. In between the refinement cycles the model was subjected to manual rebuilding using XtalView.[14h] The same program was used to model the cisplatin adduct into the electron-density map.

Water molecules were added by the standard procedures within the ARP/wARP suite.[14i] The final structure containing 287 water molecules, 2184 protein atoms (two molecules), and 10 ions was refined (resolution range: 37.0–1.8 Å) to a final crystallographic R factor (R_{cryst}) of 0.202 and an R_{free} value of 0.236. The stereochemical quality of the refined models was assessed by using the program Procheck[14j] and is within the standard tolerance, with rmsd values of 0.014 Å for bond lengths and 1.6° for bond angles. The Ramachandran plot is of very good quality, with 88.6 % of residues in the most-favored regions, 11.4 % in the additionally allowed ones, and no residues in generously allowed or in disallowed regions.

The coordinates for the cisplatin–beSOD complex have been deposited in the Protein Data Bank under the accession 2AEO.

Received: July 25, 2005
Revised: November 14, 2005
Published online: January 17, 2006

Keywords: antitumor agents · cisplatin · platinum · superoxide dismutase · X-ray diffraction

[1] B. Lippert, *Cisplatin: Chemistry and Biochemistry of a Leading Anticancer Drug*, Wiley-VCH, Weinheim, **1999**.
[2] a) V. Brabec, *Prog. Nucleic Acid Res. Mol. Biol.* **2002**, *71*, 1–68; b) J. Reedijk, *Proc. Natl. Acad. Sci. USA* **2003**, *100*, 3611–3616.
[3] D. Wang, S. J. Lippard, *Nat. Rev. Drug Discovery* **2005**, *4*, 307–320.
[4] E. R. Jamieson, S. J. Lippard, *Chem. Rev.* **1999**, *99*, 2467–2498.
[5] T. Peleg-Shulman, Y. Najajreh, D. Gibson, *J. Inorg. Biochem.* **2002**, *91*, 306–311.
[6] a) A. I. Ivanov, J. Christodoulou, J. A. Parkinson, K. J. Barnham, A. Tucker, J. Woodrow, P. J. Sadler, *J. Biol. Chem.* **1998**, *273*, 14721–14730; b) P. B. Esposito, R. Najjar, *Coord. Chem. Rev.* **2002**, *232*, 137–149.
[7] R. Mandal, R. Kalke, X. F. Li, *Chem. Res. Toxicol.* **2004**, *17*, 1391–1397.
[8] a) H. Sun, H. Li, P. J. Sadler, *Chem. Rev.* **1999**, *99*, 2817–2842; b) F. Piccioli, S. Sabatini, L. Messori, P. Orioli, C. G. Hartinger, B. K. Keppler, *J. Inorg. Biochem.* **2004**, *98*, 1135–1142; c) C. S. Allardyce, P. J. Dyson, J. Coffey, N. Johnson, *Rapid Commun. Mass Spectrom.* **2002**, *16*, 933–935.
[9] Heavy Atom Databank http://www.bmm.icnet.uk/had/heavyatom.html.
[10] a) C. L. Fisher, R. A. Hallewell, V. A. Roberts, J. A. Tainer, E. D. Getzoff, *Free Radical Res. Commun.* **1991**, *12–13*, 287–296; b) J. A. Tainer, E. D. Getzoff, K. M. Beem, J. S. Richardson, D. C. Richardson, *J. Mol. Biol.* **1982**, *160*, 181–217.
[11] a) S. Manka, F. Becker, O. Hohage, W. S. Sheldrick, *J. Inorg. Biochem.* **2004**, *98*, 1947–1956; b) M. Hahn, M. Kleine, W. S. Sheldrick, *J. Biol. Inorg. Chem.* **2001**, *6*, 556–566; c) J. Reedijk, *Chem. Rev.* **1999**, *99*, 2499–2510.
[12] The Cambridge Structural Database http://www.ccdc.cam.ac.uk/products/csd/.
[13] a) J. K. Lau, D. V. Deubel, *Chem. Eur. J.* **2005**, *11*, 2849–2855; b) D. V. Deubel, *J. Am. Chem. Soc.* **2004**, *126*, 5999–6004; c) D. V. Deubel, *J. Am. Chem. Soc.* **2002**, *124*, 5834–5842.
[14] a) A. G. W. Leslie in *Crystallographic Computing V* (Eds.: D. Moras, A. D. Podjarny, J.-C. Thierry), Oxford University Press, Oxford, **1996**, pp. 50–61; b) P. R. Evans, *"Data Reduction"*, *Proceedings of CCP4 Study Weekend*, Data Collection & Processing, **1993**, 114–122; c) M. G. Rossmann, D. M. Blow, *Acta Crystallogr.* **1962**, *18*, 24–31; d) R. A. Crowther in *The Molecular Replacement Method* (Ed.: M. G. Rossmann), Gordon & Breach, New York, **1972**; e) A. Vagin, A. Teplyakov, *J. Appl. Crystallogr.* **1997**, *30*, 1022–1025; f) A. Vagin, A. Teplyakov, *Acta Crystallogr. Sect. D* **2000**, *56*, 1622–1624; g) G. N. Murshudov, A. Vagin, E. J. Dodson, *Acta Crystallogr. Sect. D* **1997**, *53*, 240–255; h) D. E. McRee, *J. Mol. Graphics* **1992**, *10*, 44–47; i) V. S. Lamzin, K. S. Wilson, *Acta Crystallogr. Sect. D* **1993**, *49*, 129–149; j) R. A. Laskowski, M. W. MacArthur, D. S. Moss, J. M. Thornton, *J. Appl. Crystallogr.* **1993**, *26*, 283–291.

 © 2006 Wiley-VCH Verlag GmbH & Co. KGaA, Weinheim

Phosphane–Diiodine Complexes

DOI: 10.1002/anie.200503007

A Discrete P···I–I···P Assembly: The Large Influence of Weak Interactions on the ^{31}P NMR Spectra of Phosphane–Diiodine Complexes**

Rosario Núñez, Pau Farràs, Francesc Teixidor, Clara Viñas, Reijo Sillanpää, and Raikko Kivekäs*

Thioethers, except derivatives of $[7\text{-R-}7,8\text{-}C_2B_9H_{11}]^-$,[1] are more weakly coordinating ligands than phosphanes.[2] This difference is evidenced by the I–I distances in the spoke-shaped charge-transfer (CT) complexes $R_2S{\cdot}I_2$ and $R_3P{\cdot}I_2$ (Figure 1).[3] The I–I distance is sensitive to the strength of the interaction between the σ* LUMO orbital on I_2 and the HOMO orbital of the donor atom:[4] the stronger the donor, the longer the I–I distance. In these spoke CT complexes, the I–I distance varies from 3.2 ± 0.2 Å in $R_3P{\cdot}I_2$ adducts[5] to 2.80 ± 0.05 Å in $R_2S{\cdot}I_2$ adducts,[6] indicating the weaker donor character of the thioether group. Whereas extended I_2 arrays, spoke adducts of I_2, polyiodides, and other structural configurations involving I_2 molecules are well described,[7] examples of discrete assemblies incorporating an I_2 molecule bridging to two donor atoms are limited. The P···I–I···P assembly is unknown, and only a few examples of the S···I–I···S motif have been reported.[8] As thioethers are weaker donors than phosphanes, we predicted that $R_3P{\cdot}I_2{\cdot}PR_3$ adducts could be generated by using a very weakly coordinating phosphane ligand. By using the carboranyl phosphane (Mecarb)*i*Pr_2P (Mecarb = 1-(2-Me-1,2-$C_2B_{10}H_{10}$)), the complex (Mecarb)*i*$Pr_2P{\cdot}I_2$ containing the shortest I–I distance observed in a spoke adduct was produced.[9] A weaker donor ligand than (Mecarb)*i*Pr_2P can be obtained by replacing the isopropyl fragments by electron-withdrawing phenyl groups, as in (Mecarb)Ph_2P (**1**).[10]

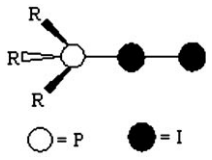


Figure 1. Spoke configuration of $R_3P{\cdot}I_2$ complexes.

Use of ligand **1** allowed the formation of the desired complex **1**·I_2·**1** (**2**), which was isolated as red-brown crystals from a solution of **1** and I_2 (1:1) in CH_2Cl_2 after 2 months at 4 °C. Single-crystal X-ray diffraction confirmed that the structure of **2** consists of one I_2 molecule bridging two molecules of **1** (Figure 2).[11] A nearly linear P···I–I···P arrangement is observed, in which the P···I and I–I distances

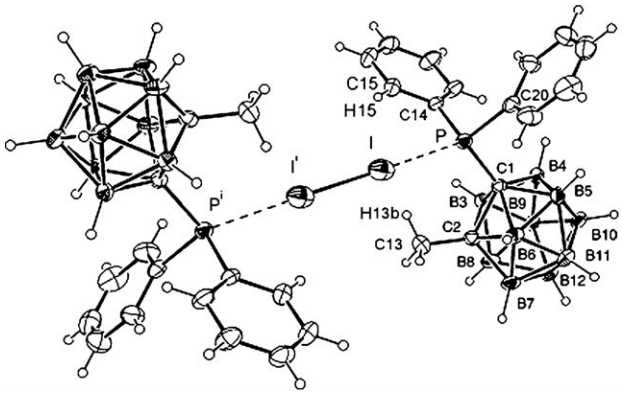


Figure 2. Molecular structure of **2**. The thermal ellipsoids are set at 30% probability. Selected interatomic distances [Å] and angles [°]: I–I^i 2.7753(14) ($i = -x, -y, -z$), P–C1 1.884(6), P–C14 1.831(6), P–C20 1.813(6), C1–C2 1.710(8), I···P 3.3337(18), I···H15 3.15, I···H13b 3.39; P-I-I^i 173.80(4), C1-P-C14 107.6(2), C1-P-C20 101.5(3), C14-P-C20 104.3(3).

are 3.3337(18) and 2.7753(14) Å, respectively. The I–I distance is the shortest found in a phosphane–I_2 adduct, and is only slightly longer than that in solid I_2 at 110 K (2.715(6) Å).[12] The I–I distance in **2** is similar to those in the $R_2S{\cdot}I_2{\cdot}SR_2$ adducts (2.75–2.79 Å).[8] Additionally, two weak I···H(Ph) contacts of 3.15 Å are observed in **2** (Figure 3).

Is the P···I–I···P structural motif observed in the solid state also stable in solution? Monitoring the titration of **1** with I_2 in dry $CDCl_3$ by $^{31}P\{^1H\}$ NMR spectroscopy revealed that increasing the ratio of I_2:**1** leads to a continuous upfield shift of the P-atom signal, from $\delta = 11.5$ (I_2:**1** = 0:1) to −10.2 (1:1) to −12.4 ppm (2:1). The same trend was observed for titrations in 1,2-dichloroethane and CH_2Cl_2. Ratios of I_2:**1** greater than 2:1 do not noticeably alter the chemical shift. These results do not parallel the behavior of other phosphanes, including (Mecarb)*i*Pr_2P,[9] for which an upfield shift of the P-atom resonance is observed when the ratio of I_2:R_3P is increased, up to a ratio of 2:1. Above this ratio, the signal shifts downfield, owing to the formation of $[R_3PI][I_3]$ species.[13] This difference in behavior implies that **1** does not induce the formation of the $[I_3]^-$ ion. To further confirm this point, temperature-dependent ^{31}P NMR spectroscopic studies of solutions of I_2:**1** in CD_2Cl_2 at ratios of 0.25:1, 0.5:1, 1:1, and 1.5:1 were carried out from 1–175 °C. In general, lower temperatures produced an upfield shift of the P-atom signal (see Supporting Information). Likewise, in conductometric titrations of solutions of I_2:**1** in CH_2Cl_2, very low conductance was observed, independent of the I_2:**1** ratio, which is inconsistent with the formation of ionic species. Finally, the I_2:**1** solutions were studied by UV/Vis spectros-

[*] Dr. R. Núñez, P. Farràs, Prof. F. Teixidor, Dr. C. Viñas
Institut de Ciència de Materials de Barcelona (CSIC)
Campus de la U.A.B., 08193 Bellaterra (Spain)
Fax: (+34) 935805729
E-mail: clara@icmab.es
Prof. R. Sillanpää
Department of Chemistry, University of Jyväskylä
FIN-40351 Jyväskylä (Finland)
Dr. R. Kivekäs
Department of Chemistry, PO Box 55
FIN-00014 University of Helsinki (Finland)

[**] This work was supported, in part, by MAT2004-01108 and the Generalitat de Catalunya, 2001/SGR/00337. P. Farràs is enrolled in the UAB PhD program.

Supporting information for this article is available on the WWW under http://www.angewandte.org or from the author.

WILEY InterScience DISCOVER SOMETHING GREAT
© 2006 Wiley-VCH Verlag GmbH & Co. KGaA, Weinheim

copy, which confirmed the absence of $[I_3]^-$ ions.[5a,c] Therefore, in contrast to other phosphanes, **1** is incapable of sufficiently polarizing the I–I bond to allow the splitting required for the formation of $[I_3]^-$ ions, even in the presence of a large excess of I_2. But which species in solution, $\mathbf{1}\cdot I_2$ or $\mathbf{1}\cdot I_2\cdot\mathbf{1}$, best preserves the I–I fragment?

To learn more about the forces that bind phosphane–I_2 adducts, we combined experimental data with density functional theory (DFT) to calculate theoretical NMR spectra for $Ph_3P\cdot I_2$ (in spite of the difficulties encountered in the calculation of accurate NMR spectra for compounds containing P–I interactions using current computational methods[14]). Note that our attempts to reproduce the experimentally observed P···I–I arrangement in $Ph_3P\cdot I_2$ were unsuccessful; therefore, we decided to use geometric parameters from the crystal structure of $Ph_3P\cdot I_2$[5c] as input in our DFT calculations using gauge-including atomic orbitals (GIAO) (see Supporting Information). The calculated chemical shift of the donor P atom depends strongly on the positions of each of the two I atoms along the line defined by the other two atoms in the P···I(1)–I(2) assembly. When the P···I(2) distance is kept constant, moving the I(1) atom towards the P atom increases the shielding of the P nucleus. When the P···I(1) distance is fixed, moving the I(2) atom away from the P atom (and hence increasing the I(1)···I(2) distance) decreases the shielding at the P nucleus. Clearly, a larger number of I atoms in the near proximity of the P donor atom increase its shielding significantly. The results of the calculations are consistent with the upfield shift of the P-atom signal observed when the ratio of I_2:Ph_3P is increased in the titration of Ph_3P with I_2.[13] The removal of I(2) from the Ph_3P···I(1)–I(2) molecule to give the $[Ph_3PI]^+$ ion (along with an $[I_3]^-$ ion) deshields the P nucleus. The $[Ph_3PI]^+$ ion was examined in a separate set of calculations based on geometric parameters from the crystal structure of $[Ph_3PI][I_3]$.[15] The computed chemical shift of the P atom of the naked cation is $\delta = -282$ ppm, far from the experimental value of $\delta = 44$ ppm.[5c] However, if the $[I_3]^-$ ion is incorporated into the calculation the computed chemical shift of the P atom is $\delta = 36$ ppm. Therefore, the chemical shift is very dependent on weak interactions. All of these results suggest that when **1** and I_2 are combined in solution the moiety formed is P···I–I···P, and that the continuous decrease in the chemical shift of the P atoms with either increasing ratios of I_2 or lower temperatures arises from an increase in the number or strength of weak interactions between the P atoms in **1** and I_2 molecules or other I-containing species.

The natural population analysis (NPA) charges on the P atoms in the free ligands Ph_3P and **1**, calculated at the B3LYP/6-311+G(d,p) level of theory, are 0.90 and 0.92, respectively (Figure 3; see Supporting Information). These values suggest that, as expected, the P atoms in PPh_3 are slightly better donors than those in **1**, but do not explain why very dissimilar P···I–I and P···I–I···P motifs are formed (Figure 3). The stabilization of one arrangement over the other may arise from differences in the charges on the phenyl hydrogen atoms in PPh_3 and in **1**. Charges ranging from 0.237 to 0.245 are calculated for those in PPh_3, whereas lower charges of 0.131 to 0.202 are calculated for those in **1** (some of these data are shown in Figure 3). The X-ray crystal structures of $Ph_3P\cdot I_2$[5c] and **2** also demonstrate the importance of the phenyl hydrogen atoms in PPh_3 and **1** for the stabilization of the P···I–I···P arrangement. Intramolecular I···H(Ph) interactions are absent in $Ph_3P\cdot I_2$ but present in **2**. In $Ph_3P\cdot I_2$, I(2) participates in intermolecular interactions with hydrogen atoms in the *para* positions on phenyl groups from two different molecules (Figure 3).

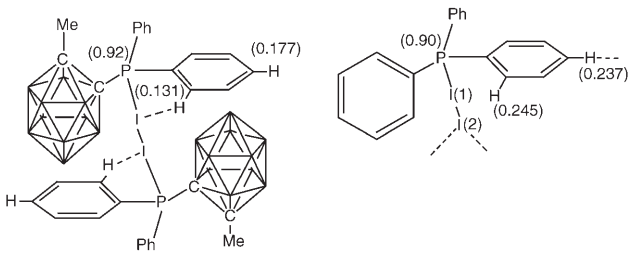


Figure 3. Schematic representation of $\mathbf{1}\cdot I_2\cdot\mathbf{1}$ (**2**) (left) and $Ph_3P\cdot I_2$ (right). Weak I···H contacts shorter than the sum of the van der Waals radii are indicated with dashed lines; those in $Ph_3P\cdot I_2$ are intermolecular contacts. The numbers in parentheses indicate the calculated NPA charges for the P atoms and selected H atoms of the free ligands **1** and PPh_3.

With regard to the influence of the carboranyl group in **1** on the formation of the P···I–I···P motif, it is noted that in addition to having a stronger electron-withdrawing character than a phenyl ring, the carboranyl group also redistributes the charges on the phenyl rings connected to the same P atom. The phenyl hydrogen atoms in **1** with the lowest charges are in the *ortho* positions, and are thus appropriately placed for a weak I···H(Ph) interaction involving a partial electron donation into the σ* orbital on the I_2 molecule in the adduct **2**. This is not the case for the phenyl rings in PPh_3, in which the hydrogen atoms with the lowest charges occupy the *para* positions. Some of these hydrogen atoms do participate in weak intermolecular interactions with I(2) in the crystal structure of the spoke adduct $Ph_3P\cdot I_2$.

The combination of experimental and computational techniques has shed some light on the P–I interactions in $R_3P\cdot I_2$ and $R_3P\cdot I_2\cdot PR_3$ complexes, and on the importance of weak interactions in the interpretation of their ^{31}P NMR spectra, but what can be said about the I–I interactions in these complexes? The I–I distances in $R_3P\cdot I_2\cdot PR_3$ (and $R_2S\cdot I_2\cdot SR_2$) are generally shorter than those in the spoke adducts $R_3P\cdot I_2$. This observation can be explained by considering the orbitals involved in the interaction between the donor P atoms and the I_2 molecule. The combination of the filled lone-pair sp^3 orbitals on each of the two P atoms leads to two filled orbitals, only one of which has the correct symmetry to interact with the σ* orbital on the I_2 molecule. Therefore, the number of electrons transferred from the donor atoms to the I_2 molecule is equal in $R_3P\cdot I_2\cdot PR_3$ and $R_3P\cdot I_2$. However, in $R_3P\cdot I_2$ the electrons in the sp^3 orbital on the donor atom are necessarily more polarizable, and therefore, produce a longer I–I bond. This explanation also accounts also for the similarity of the I–I bond lengths in the spoke $R_2S\cdot I_2$ (2.816(2) Å) and bridging $R_2S\cdot I_2\cdot SR_2$ (2.754(2) Å) adducts with equivalent thioethers in (1,4,7-trithiacyclononane)$_2(I_2)_4$.[3d] An alternative, but equivalent, explanation of

 © 2006 Wiley-VCH Verlag GmbH & Co. KGaA, Weinheim

the bonding in $R_3P{\cdot}I_2{\cdot}PR_3$, based on the butadiene model, is given in the Supporting Information.

This research has substantiated the importance of ligands containing the carboranyl moiety in the formation of phosphane–I_2 adducts with novel structural motifs. Through the use of a carboranyl phosphane ligand, the P···I–I···P assembly was isolated for the first time. X-ray diffraction analysis of **2** demonstrated the presence of this structural motif in the solid state, and a variety of experimental techniques and computational methods suggest that it also exists when **2** is dissolved in halogenated solvents. Furthermore, we have shown that the ^{31}P NMR spectra of phosphane–I_2 adducts are greatly influenced by weak interactions between the adducts and I-containing species. This observation is of great relevance to the calculation of theoretical ^{31}P NMR spectra.

Received: August 23, 2005
Revised: November 22, 2005
Published online: January 20, 2006

Keywords: carboranes · iodine · noncovalent interactions · phosphanes · structure elucidation

[1] "Product Subclass 40: Carboranes and Metallacarboranes": F. Teixidor, C. Viñas in *Science of Synthesis, Vol. 6* (Eds.: D. S. Kaufmann, D. S. Matteson), Georg Thieme, Stuttgart, **2005**, pp. 1235–1275.

[2] W. Levason in *The Chemistry of Organophosphorus Compounds, Vol. 1* (Ed.: F. R. Hartley), Wiley, New York, **1990**, p. 567.

[3] a) P. Deplano, J. R. Ferraro, M. L. Mercuri, E. F. Trogu, *Coord. Chem. Rev.* **1999**, *188*, 71–95; b) M. C. Aragoni, M. Arca, F. A. Devillanova, A. Garau, F. Isaia, V. Lippolis, G. Verani, *Coord. Chem. Rev.* **1999**, *184*, 271–290; c) W.-W. du Mont, F, Ruthe, *Coord. Chem. Rev.* **1999**, *189*, 101–133; d) P. D. Boyle, S. M. Godfrey, *Coord. Chem. Rev.* **2001**, *223*, 265–299; e) S. M. Godfrey, C. A. McAuliffe in *Modern Coordination Chemistry. The Legacy of Joseph Chatt* (Eds.: G. J. Leigh, N. Winterton), The Royal Society of Chemistry, Cambridge, **2002**, pp. 79–89; f) S. Ito, H. Liang, M. Yoshifuji, *Chem. Commun.* **2003**, 398–399.

[4] K. F. Purcell, J. C. Kotz, *Inorganic Chemistry*, Saunders, Philadelphia, PA, **1977**, p. 209.

[5] a) W.-W. du Mont, M. Bätcher, S. Pohl, W. Saak, *Angew. Chem.* **1987**, *99*, 945–947; *Angew. Chem. Int. Ed. Engl.* **1987**, *26*, 912–913; b) F. Ruthe, P. G. Jones, W.-W. du Mont, P. Deplano, M. L. Mercuri, *Z. Anorg. Allg. Chem.* **2000**, *626*, 1105–1111; c) S. M. Godfrey, D. G. Kelly, A. G. Mackie, C. A. McAuliffe, R. G. Pritchard, S. M. Watson, *J. Chem. Soc. Chem. Commun.* **1991**, 1163–1164; d) N. Bricklebank, S. M. Godfrey, H. P. Lane, C. A. McAuliffe, R. G. Pritchard, M. M. Moreno, *J. Chem. Soc. Dalton Trans.* **1995**, 2421–2424.

[6] a) F. H. Herbstein, P. Ashkenazi, M. Kaftory, M. Kapon, G. M. Reisner, D. Ginsburg, *Acta Crystallogr. Sect. B* **1986**, *42*, 575–601; b) A. L. Tipton, M. C. Lonergan, C. L. Stern, D. F. Shriver, *Inorg. Chim. Acta* **1992**, *201*, 23–27; c) A. J. Blake, W.-S. Li, V. Lippolis, M. Schröder, *Acta Crystallogr. Sect. C* **1997**, *53*, 886–888, and references therein.

[7] a) V. Stenzel, J. Jeske, W.-W. du Mont, P. G. Jones, *Inorg. Chem.* **1997**, *36*, 443–448; b) A. J. Blake, F. A. Devillanova, R. O. Gould, W.-S. Li, V. Lippolis, S. Parson, C. Radek, M. Schröder, *Chem. Soc. Rev.* **1998**, *27*, 195–205; c) P. H. Svensson, L. Kloo, *Chem. Rev.* **2003**, *103*, 1649–1684.

[8] a) A. J. Blake, R. O. Gould, C. Radek, M. Schröder, *J. Chem. Soc. Chem. Commun.* **1993**, 1191–1193; b) A. J. Blake, F. Cristiani, F. A. Devillanova, A. Garau, L. M. Gilby, R. O. Gould, F. Isaia, S. Parsons, C. Radek, M. Schröder, *J. Chem. Soc. Dalton Trans.* **1997**, 1337–1346; c) A. J. Blake, F. A. Devillanova, A. Garau, L. M. Gilby, R. O. Gould, F. Isaia, V. Lippolis, S. Parsons, C. Radek, M. Schröder, *J. Chem. Soc. Dalton Trans.* **1998**, 2037–2046.

[9] F. Teixidor, R. Núñez, C. Viñas, R. Sillanpää, R. Kivekäs, *Angew. Chem.* **2000**, *112*, 4460–4462; *Angew. Chem. Int. Ed.* **2000**, *39*, 4290–4292; .

[10] R. Kivekäs, R. Sillanpää, F. Teixidor, C. Viñas, R. Núñez, *Acta Crystallogr. Sect. C* **1994**, *50*, 2027–2030.

[11] CCDC-186442 (**2**) contains the supplementary crystallographic data for this paper. These data can be obtained free of charge from The Cambridge Crystallographic Data Centre via www.ccdc.cam.ac.uk/data_request/cif.

[12] F. Bolhuis, P. B. van Koster, T. Migchelsen, *Acta Crystallogr.* **1967**, *23*, 90–91.

[13] W. I. Cross, S. M. Godfrey, C. A. McAuliffe, R. G. Pritchard, J. M. Sheffield, G. M. Thompson, *J. Chem. Soc. Dalton Trans.* **1999**, 2795–2798, and references therein.

[14] a) S. Patchkovskii, T. Ziegler, *J. Phys. Chem. A* **2002**, *106*, 1088–1099; b) A. Dransfeld, P. V. Schleyer, *Magn. Reson. Chem.* **1998**, *36*, S29-S43; c) C. van Wüllen, *Phys. Chem. Chem. Phys.* **2000**, *2*, 2137–2144.

[15] F. A. Cotton, P. A. Kibala, *J. Am. Chem. Soc.* **1987**, *109*, 3308–3312.

 © 2006 Wiley-VCH Verlag GmbH & Co. KGaA, Weinheim

Phosphoranes

DOI: 10.1002/anie.200503335

Formation of a Dicyanotriorganophosphorane from the Reaction of Triphenylphosphane with Phenylselenocyanate**

Nicholas A. Barnes, Stephen M. Godfrey, Ruth T. A. Halton, Suzanna Law, and Robin G. Pritchard*

Whilst numerous organophosphorus(III) cyanide compounds, such as $R_2PCN/RP(CN)_2$, are known,[1,2] reports of their phosphorus(V) analogues are considerably rarer. The ionic compounds $[R_3PCN]X$ (X = Br, I) are readily formed from

[*] Dr. N. A. Barnes, Dr. S. M. Godfrey, Dr. R. T. A. Halton, S. Law, Dr. R. G. Pritchard
School of Chemistry
The University of Manchester (North Campus)
Manchester, M601QD (UK)
Fax: (+ 44) 161-200-4559
E-mail: stephen.m.godfrey@manchester.ac.uk

[**] We are grateful to the Engineering and Physical Sciences Research Council (EPSRC) for a research studentship to R.T.A.H. and for support of the UMIST FT IR-Raman (Grant No: GR/M30135), NMR (Grant No: GR/L52246), and X-ray (Research Initiative Grant) facilities. The authors thank Dr. A. K. Brisdon for helpful discussions.

WILEY InterScience DISCOVER SOMETHING GREAT
© 2006 Wiley-VCH Verlag GmbH & Co. KGaA, Weinheim

stoichiometric amounts of R_3P and XCN[3,4] and exist in the solid state with either covalent ($[R_3PCN]X$) or ionic ($[R_3PX]CN$) cyanide although the former predominates in solution.[4] Recent work by Verkade and co-workers has shown that Me_3SiCN converts $[(Me_2N)_3PBr]Br$ into $[(Me_2N)_3PCN]Br$, whilst the same reaction with similar azaphosphatrane systems results in the isolation of both cyano (P–CN) and isocyano (P–NC) compounds.[5] In contrast, covalent dicyanotriorganophosphoranes ($R_3P(CN)_2$) are much more elusive with only three examples known ($R_3 = Ph_2Me$, $PhMe_2$, and $(Et_2N)_3$), each obtained from the reaction of $[R_3PCN]I$ with a second equivalent of ICN, although the products were not extensively characterized.[3] Herein, we report the remarkably facile formation of the dicyanotriorganophosphorane $Ph_3P(CN)_2$ by the reaction of triphenylphosphane with phenylselenocyanate.

PhSeCN and Ph_3P were reacted in a 2:1 ratio in dry diethyl ether for 24 h; subsequent solvent reduction and the addition of hexane resulted in the precipitation of a cream solid **1**. The $^{31}P\{^1H\}$ NMR spectrum of **1** ($CDCl_3$) exhibited a resonance at $\delta = -107.3$ ppm, the extremely low frequency of which is consistent with five-coordinate phosphorus, although the signal is considerably shifted from those reported for the trigonal-bipyramidal Ph_3PF_2 ($\delta_P = -58.1$)[6] and Ph_3PCl_2 ($\delta_P = -47.0$).[7] A significantly low-frequency shift in the $^{31}P\{^1H\}$ NMR spectra of P–CN compounds relative to P–Cl analogues is consistent with similar observations for organophosphorus(III) cyanides, for example, Ph_2PCN $\delta_P = -35.7$[2] (relative to Ph_2PCl $\delta_P = 81.9$).[8] The IR spectrum of **1** (nujol) exhibits an absorption at 2150 cm^{-1} (A_2' asymmetric CN mode), whilst the Raman spectrum displays a peak at 2158 cm^{-1} (A_1'' symmetric CN mode). These observations are consistent with group-theory predictions for a $R_3P(CN)_2$ molecule of D_{3h} symmetry. The absence of a band at 2080 cm^{-1} (typical of ionic cyanide)[9] suggests **1** is covalent in the solid state. On the basis of the spectroscopic data, we assigned **1** as the dicyanophosphorane $Ph_3P(CN)_2$. A crop of suitable crystals of **1** were obtained from a solution of diethyl ether, and X-ray crystallographic analysis confirmed the formation of $Ph_3P(CN)_2$ (Figure 1).[10]

To the best of our knowledge, $Ph_3P(CN)_2$ is the first crystallographically characterized dicyanotriorganophosphorane and exhibits trigonal-bipyramidal geometry at the phosphorus center, with axial cyanide groups and equatorial phenyl groups, as predicted by valence-shell electron-pair repulsion (VSEPR) theory. The structure of **1** may be compared with analogous Ph_3PX_2 systems, the solid-state structures of which vary considerably depending upon the nature of X; four-coordinate Ph_3P-X-X "spoke" structures are observed for X = Br or I,[11,12] whereas trigonal-bipyramidal compounds are formed for X = Cl or F,[7,13–14] although the chloride system also yields a dinuclear ionic species in dichloromethane.[15] The trigonal-bipyramidal structure exhibited by **1** is consistent with the high electronegativity of the CN^- ion (3.84 on the Pauling scale),[16] which lies between that of chlorine (3.16) and fluorine (3.98).[17] In $Ph_3P(CN)_2$, the NC-P-CN bond angle is essentially linear (C19-P1-C20: 178.85(16)°) and displays none of the distortions from regular trigonal-bipyramidal geometry observed for Ph_3PCl_2.[7] The P–C bonds to the cyano groups (P1-C19: 1.941(3), P1-C20: 1.929(3) Å) are substantially longer than those to the phenyl rings (P1-C1: 1.801(3), P1-C7: 1.776(4), P1-C13: 1.801(3) Å) and are considerably longer than in ionic $[\{2,4,6\text{-}(MeO)_3C_6H_2\}_3PCN]I$ (P-CN: 1.78(2) Å)[4] and the cyano phosphatrane $[N(CH_2CH_2N\mathit{i}Bu)_3PCN]Br$ (P-CN: 1.854(2) Å);[5] however, these P–CN bonds are closer to the axial P–CN bond length of 1.915(5) Å in the $[P(CN)_3Cl]^-$ ion.[18] The C≡N bond lengths (C19-N1: 1.148(5), C20-N2: 1.147(5) Å) are, however, very similar to the C≡N bond length of 1.148(3) Å in $[N(CH_2CH_2N\mathit{i}Bu)_3PCN]Br$,[5] but rather shorter than that of 1.19(5) Å observed for $[\{2,4,6\text{-}(MeO)_3C_6H_2\}_3PCN]I$.[4]

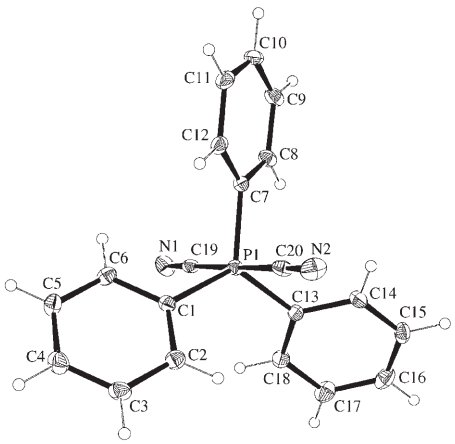


Figure 1. The molecular structure of $Ph_3P(CN)_2$ **1**. Thermal ellipsoids are set at the 30% probability level. Selected bond lengths [Å] and angles [°]: P1-C1 1.801(3), P1-C7 1.776(4), P1-C13 1.801(3), P1-C19 1.941(3), P1-C20 1.929(3), N1-C19 1.148(5), N2-C20 1.147(5); N1-C19-P1 178.7(3), N2-C20-P1 179.0(3), C19-P1-C20 178.85(16), C1-P1-C19 89.90(15), C1-P1-C7 119.16(16).

The formation of $Ph_3P(CN)_2$ in this reaction was unanticipated and is in contrast to the analogous reactions of "PhSeI" (a centrosymmetric dimer $(Ph_2Se_2I_2)_2$ in the solid state)[19] with tertiary phosphanes, which result in cleavage of the weak Se–Se bond and formation of either charge-transfer $R_3PSe(Ph)I$ compounds[20] or ionic $[R_3PSePh]I$ salts,[21] depending on the basicity of the phosphane. Given the significantly different reactivity of PhSeCN and $(Ph_2Se_2I_2)_2$ towards Ph_3P and the intriguing loss of selenium from the former, we sought to further explore the processes involved in the formation of **1** by performing the reaction on an NMR-tube scale with a number of different solvents ($[D_{10}]$diethyl ether, $[D_8]$toluene, and $[D_6]$acetone), thus monitoring the reaction in situ by $^{77}Se\{^1H\}$ and $^{31}P\{^1H\}$ NMR spectroscopy. In all solvents, the only peaks observed in the $^{77}Se\{^1H\}$ NMR spectra were PhSeCN ($\delta_{Se} = 319.2$), Ph_2Se_2 ($\delta_{Se} = 461.9$), and small amounts of Ph_3PSe ($\delta_{Se} = -269.2$). The formation of Ph_2Se_2 may imply the operation of a radical process, which involves homolytic cleavage of the Se–CN bond with subsequent recombination of $PhSe^\bullet$ and $CN^\bullet$ radicals to afford Ph_2Se_2 and $(CN)_2$; the latter species reacting with Ph_3P to produce **1**. However, we have not further explored this supposition.

 © 2006 Wiley-VCH Verlag GmbH & Co. KGaA, Weinheim

The $^{31}P\{^1H\}$ NMR spectrum of the reaction in $[D_6]$acetone recorded immediately after preparation displayed three major resonances at $\delta = -109.0$ (**1**), -4.1 (Ph_3P), and 27.5 ppm. A fourth (minor) resonance, which displayed selenium satellites, $^1J(Se\text{-}P) = 741$ Hz, was observed at $\delta =$ 36.5 ppm and is assigned to Ph_3PSe by comparison with literature values ($\delta_P = 36.1$ ppm, $^1J(Se\text{-}P) = 738$ Hz).[22] The formation of Ph_3PSe suggests that PhSeCN behaves to some degree similarly to KSeCN, which is routinely used to oxidize R_3P to R_3PSe,[23] although the resonance remained a minor product when the sample was monitored over several days. The reaction was monitored over 48 h, with a number of different species being observed (Table 1). The limited stability of **1** in $[D_6]$acetone is highlighted by the rapid disappearance of the resonance at $\delta = -109.0$ ppm, concomitant with the appearance of a peak at $\delta = -25.5$ ppm, which we tentatively assign to the ionized form of **1**, $[Ph_3PCN]CN$, since other $[R_3PCN]^+$ ions have been observed at similar chemical shifts.[4,5] This species is only stable for a few hours in acetone, and after 48 h the only major resonance present in the $^{31}P\{^1H\}$ NMR spectrum is that observed at $\delta = 29.1$ ppm, along with a few minor species. A similar situation was observed when the reaction was followed in $[D_8]$toluene and $[D_{10}]$diethyl ether, although the reaction occurs at a slower rate, with Ph_3P persisting in the mixture over several days. Additionally, **1** is significantly more stable in these solvents, as it survives for several days in both cases. Over longer periods, the $^{31}P\{^1H\}$ NMR spectra in these solvents resemble that observed in $[D_6]$acetone, with the resonance at $\delta = 29.1$ ppm predominating after several weeks.

Whilst the isolation in bulk of the species observed at $\delta =$ 29.1 ppm in the $^{31}P\{^1H\}$ NMR spectrum remains elusive, we were fortuitous in obtaining structural data because of the formation of crystals from the acetone solution upon standing for several days. The structure of the unusual bridged tetracyanodiiminophosphorane **2** was thus elucidated (Figure 2).[24]

The structure of **2** consists of two $\{Ph_3P\}$ units linked by a $-NC(CN)_2C(CN)_2N-$ bridge. The molecule has a centre of symmetry, with the $N-PPh_3$ units adopting an *anti* configuration along the C1–C1_3 bond. The P–N linkage in **2** (P1-N1: 1.577(3) Å) is consistent with a P=N double bond, with the P1-N1-C1 bond angle of 128.3(2)° being somewhat larger than the idealized 120° expected for an sp^2 nitrogen atom. The P=N bond is shorter than those observed for other cyano-substituted imino phosphoranes, for example, 1.615(2) Å for $Ph_3P{=}N\text{-}(cyclo\text{-}C_5(CN)_7)$.[25] The C1–N1 linkage of 1.406(4) Å is typical for a CN single bond, while the terminal CN bond lengths are consistent with C≡N triple bonds. In the extended structure, individual molecules are linked by short intermolecular N···H contacts to phenyl protons (N2···H12: 2.48(4) Å; compared with the sum of the van der Waals radii: 2.75 Å).

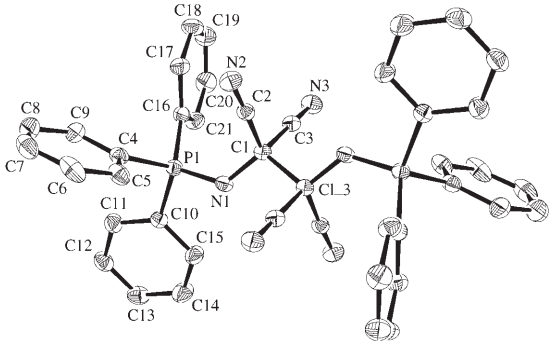


Figure 2. The molecular structure of $Ph_3PNC(CN)_2C(CN)_2NPPh_3 \cdot 2(CH_3)_2CO$ (**2**). Thermal ellipsoids are set at the 30% probability level, and hydrogen atoms and solvent of crystallization are omitted for clarity. Selected bond lengths [Å] and angles [°]: P1-N1 1.577(3), P1-C4 1.809(3), P1-C10 1.800(3), P1-C16 1.797(3), N1-C1 1.406(4), C1-C2 1.502(4), C1-C3 1.505(4), C1-C1_3 1.592(4), C2-N2 1.138(4), C3-N3 1.137(4); C4-P1-N1 113.45(15), P1-N1-C1 128.3(2), N1-C1-C2 116.3(3), N1-C1-C3 113.9(2), N1-C1-C1_3 108.5(2), C1-C2-N2 177.5(3), C1-C3-N3 177.4(3). Symmetry operation used to generate equivalent atoms: $1-x, 1-y, 1-z$.

The origin of **2** remains unclear and provides further evidence for the complexity of this reaction. Whilst **2** has thus far resisted more comprehensive characterization (because of contamination with Ph_2Se_2 and PhSeCN), the $^{31}P\{^1H\}$ NMR spectrum of the crystals confirms that **2** is the species observed at $\delta = 29.1$ ppm and is the most stable phosphorus-containing product obtained from the reaction, thus showing no sensitivity towards air or moisture. The mechanism for the formation of **2** is unclear, but it appears that it forms both in competition with and through the decomposition of **1**. The elimination of $(CN)_2$ from **1**, followed by attack of Ph_3P at the nitrogen atom is likely to result in the initial formation of unsaturated bridged species, such as $Ph_3P{=}N{-}C{\equiv}C{-}N{=}PPh_3$. This unit would be susceptible to successive addition of $(CN)_2$ across the unsaturated carbon–carbon bonds, thus resulting finally in **2**, the stability of which may be enhanced by the presence of cyano groups, which have previously been reported to stabilize iminophosphoranes.[25]

The reaction of PhSeCN with Ph_3P appears to offer a convenient synthetic route to dicyanotriorganophosphoranes, which are otherwise difficult to prepare and have been rarely studied, and $Ph_3P(CN)_2$, described herein, represents the first Group 15 triorganodicyanide compound to be crystallographically characterized. We are continuing to explore the bounds of this fascinating reaction with a view to preparing a range of $R_3P(CN)_2$ compounds, whose reactivity towards metal pow-

Table 1: Relative ratios over time of species present in the $^{31}P\{^1H\}$ NMR spectrum of the reaction of PhSeCN and Ph_3P (2:1) in $[D_6]$acetone.

t [h]	Chemical shift [ppm] of species present in solution							
	36.5 (Ph_3PSe)	29.1 (**2**)	27.5	22.0	15.1	−4.1 (Ph_3P)	−25.5 ((Ph_3PCN)CN)	−109.0 (**1**)
0	1	0	5	0	0	5	0	5
2.5	1	3	0	1	1	0	10	0
6	1	4	0	1	3	0	8	0
48	1	10	0	1	0	0	0	0

 © 2006 Wiley-VCH Verlag GmbH & Co. KGaA, Weinheim

ders may mirror other R_3PX_2 compounds and may yield a new route to novel metal–cyanide complexes.

Experimental Section

All reactions were performed under an inert argon atmosphere using standard Schlenk techniques. Diethyl ether (BDH) was distilled over sodium/benzophenone ketyl and hexane (BDH) was distilled from sodium wire. Triphenylphosphane (Aldrich) and phenylselenocyanate (Acros) were used as supplied without further purification. ^{1}H and ^{13}C{^{1}H} NMR spectra were obtained using a Bruker DPX400 machine operating at 399.9 and 100.6 MHz, respectively. ^{31}P{^{1}H} and ^{77}Se{^{1}H} NMR spectra were obtained using a Bruker DPX200 machine operating at 81.8 and 38.2 MHz, respectively. Peak positions are quoted relative to external trimethylsilane {^{1}H/^{13}C}, 85% H_3PO_4 {^{31}P}, and Me_2Se {^{77}Se} using the high-frequency positive convention throughout. All spectra were recorded at 300 K. IR spectra were recorded on a Nicolet-Nexus combined FT-IR/FT-Raman spectrometer as nujol mulls held between KBr plates. Elemental analyses were performed by the University of Manchester, Chemistry Department, Microanalytical Service.

1: Ph_3P (0.820 g, 3.12 mmol) was dissolved in freshly distilled diethyl ether (30 mL), and PhSeCN (0.797 mL, 6.49 mmol) was added dropwise by syringe. The yellow solution was left to stir overnight, the volume was reduced to 5 mL, and freshly distilled hexane (10 mL) was added, thus resulting in precipitation of a cream solid which was isolated and dried in vacuo (yield = 0.647 g, 65.8%). M.p. 102–104 °C; elemental analysis calcd (%) for $C_{20}H_{15}N_2P$: C 76.4, H 4.8, P 9.9; found: C 75.4, H 4.9, P 9.8; NMR ($CDCl_3$): $\delta_H = 8.12$–8.01 (m, 6H, Ar), 7.74–7.53 ppm (m, 9H, Ar); $\delta_C = 133.9$ (d, $^1J_{PC} = 76.3$ Hz, C_i), 132.3 (d, $^4J_{PC} = 12.6$ Hz, C_p), 132.2 (d, $^2J_{PC} = 18.4$ Hz, C_o), 129.9 ppm (d, $^3J_{PC} = 18.4$ Hz, C_m), (the resonance of the cyanide carbon atom was obscured by aromatic peaks); $\delta_P = -107.3$ ppm (s); IR (Nujol): $\tilde{\nu} = 2150$ cm^{-1}, asymm. ν(CN); Raman: 2158 cm^{-1}, sym. ν(CN).

Crystallography: Diffraction data were recorded on a Nonius κ-CCD four-circle diffractometer using graphite-monochromated $Mo_{K\alpha}$ radiation ($\lambda = 0.71073$ Å) at 150(2) K. Structural data were solved by direct methods, with full-matrix least-squares refinement on F^2 using the SHELX-97 program.[26] Absorption corrections by the multiscan method were applied with the SORTAV program. Non-hydrogen atoms were refined with anisotropic thermal parameters, all hydrogen atoms were located in the data. The figures were generated using ORTEP-3 for Windows.[27] CCDC-282250 (**1**) and -282249 (**2**) contain the supplementary crystallographic data for this paper. These data can be obtained free of charge from The Cambridge Crystallographic Data Centre via www.ccdc.cam.ac.uk/data_request/cif.

Received: September 20, 2005
Published online: January 20, 2006

Keywords: cyanides · phosphoranes · phosphorus · pseudohalogens · selenium

[1] C. E. Jones, K. J. Coskran, *Inorg. Chem.* **1971**, *10*, 1536.
[2] C. A. Wilkie, R. W. Parry, *Inorg. Chem.* **1980**, *19*, 1499.
[3] H. A. Aughsteen, *Indian J. Chem. Sect. A* **1992**, *31*, 951.
[4] S. M. Godfrey, C. A. McAuliffe, R. G. Pritchard, J. M. Sheffield, *J. Chem. Soc. Dalton Trans.* **1998**, 1919.
[5] J. V. Kingston, A. Ellern, J. G. Verkade, *Angew. Chem.* **2005**, *117*, 5040; *Angew. Chem. Int. Ed.* **2005**, *44*, 4960.
[6] F. Ramirez, C. P. Smith, *Tetrahedron Lett.* **1966**, *7*, 3651.
[7] S. M. Godfrey, C. A. McAuliffe, R. G. Pritchard, J. M. Sheffield, *Chem. Commun.* **1998**, 921.
[8] T. J. Hall, J. H. Hargis, *J. Org. Chem.* **1986**, *51*, 4185.
[9] K. Nakamoto, *Infrared and Raman Spectra of Inorganic and Coordination Compounds*, 4th ed., Wiley-Interscience, New York, **1986**.
[10] Crystallographic details for **1** ($C_{20}H_{15}N_2P$): yellow prism, $0.15 \times 0.22 \times 0.22$ mm^3, orthorhombic, $P2_12_12_1$ (no. 19), $a = 11.0951(6)$, $b = 11.9677(7)$, $c = 11.9457(8)$ Å, $\alpha = \beta = \gamma = 90°$, $V = 1586.18(17)$ Å^3, $\rho_{calcd} = 1.316$ g cm^3, $\theta_{max} = 26.99°$, reflections/unique/parameters 4114/2514/209, $F(000)$ 656, $\mu = 0.174$ mm^{-1}, $T_{max} = 0.9742$, $T_{min} = 0.9011$, $R = 0.0526$, $wR2 = 0.1404$, largest diff. peak + hole 0.596, −0.352 Å^{-3}.
[11] N. Bricklebank, S. M. Godfrey, A. G. Mackie, C. A. McAuliffe, R. G. Pritchard, *J. Chem. Soc. Chem. Commun.* **1992**, 355.
[12] S. M. Godfrey, D. G. Kelly, A. G. Mackie, C. A. McAuliffe, R. G. Pritchard, S. M. Watson, *J. Chem. Soc. Chem. Commun.* **1991**, 1163.
[13] E. L. Muetterties, W. Mahler, R. Schmutzler, *Inorg. Chem.* **1963**, *2*, 613.
[14] K. M. Doxsee, E. R. Hanawalt, T. J. R. Wreakly, *Acta. Crystallogr. C* **1992**, *48*, 1288.
[15] S. M. Godfrey, C. A. McAuliffe, R. G. Pritchard, J. M. Sheffield, *Chem. Commun.* **1996**, 2521.
[16] J. E. Huheey, *J. Phys. Chem.* **1966**, *70*, 2086.
[17] L. Pauling, *The Nature of the Chemical Bond*, 3rd ed., Cornell University Press, Ithaca, **1960**.
[18] K. B. Dillon, A. W. G. Platt, A. Schmidpeter, F. Zwaschka, W. S. Sheldrick, *Z. Anorg. Allg. Chem.* **1982**, *488*, 7.
[19] S. Kubiniok, W. W. du Mont, S. Pohl, W. Saak, *Angew. Chem.* **1988**, *100*, 438; *Angew. Chem. Int. Ed. Engl.* **1988**, *27*, 431.
[20] P. D. Boyle, S. M. Godfrey, C. A. McAuliffe, R. G. Pritchard, J. M. Sheffield, *Chem. Commun.* **1999**, 2159.
[21] S. M. Godfrey, R. T. A. Ollerenshaw, R. G. Pritchard, C. L. Richards, *J. Chem. Soc. Dalton Trans.* **2001**, 508.
[22] L. A. Woźniak, W. J. Stec, *Tetrahedron Lett.* **1999**, *40*, 2637.
[23] P. Nicpon, D. W. Meek, *Inorg. Chem.* **1966**, *5*, 1297.
[24] Crystallographic details for **2** ($C_{48}H_{42}N_6P_2O_2$): orange prism, $0.20 \times 0.20 \times 0.20$ mm^3, monoclinic, $P2_1/n$ (no. 14), $a = 9.9274(3)$, $b = 14.9426(5)$, $c = 14.8579(5)$ Å, $\alpha = 90$, $\beta = 92.986(2)$, $\gamma = 90°$, $V = 2201.05(12)$ Å^3, $\rho_{calcd} = 1.202$ g cm^3, $\theta_{max} = 26.00°$, reflections/unique/parameters 15569/4307/325, $F(000)$ 836, $\mu = 0.144$ mm^{-1}, $T_{max} = 0.9718$, $T_{min} = 0.9718$, $R = 0.0722$, $wR2 = 0.2247$, largest diff. peak + hole 0.783, −0.377 Å^{-3}.
[25] P. J. Butterfield, J. C. Tebby, T. J. King, *J. Chem. Soc. Perkin Trans. 1* **1978**, 1237.
[26] G. M. Sheldrick, SHELX-97, University of Göttingen, Gõttingen, Germany, **1998**.
[27] ORTEP 3 for Windows, L. J. Farugia, *J. Appl. Crystallogr.* **1997**, *30*, 565.

 © 2006 Wiley-VCH Verlag GmbH & Co. KGaA, Weinheim

Coupling Reactions

DOI: 10.1002/anie.200503538

Mild Ullmann-Type Biaryl Ether Formation Reaction by Combination of *ortho*-Substituent and Ligand Effects**

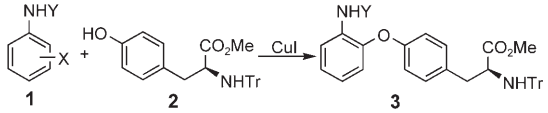
*Qian Cai, Benli Zou, and Dawei Ma**

Many natural cyclopeptides bearing a biaryl ether bridge[1] possess remarkable physiological activities. These include antibiotics (vancomycin,[1,2] ristocetin,[3] and teicoplanin[1,4]), antitumor agents (K-13[5,6e] and bouvardin[6a–c]), neurotensin antagonist RP-66453,[7] and anti-HIV agents (e.g., chloropeptins[8]). For elaboration of these synthetically challenging molecules, several elegant methods that feature biaryl ether formation have been developed. Examples include oxidative phenolic coupling,[1c] *o*-nitro-[1b,2e,f,7] or metal-activated[1c,5a] nucleophilic aromatic substitution, modified Ullmann-type coupling reactions,[1,2a,6] and boronic acid based biaryl ether synthesis.[4,8–10] However, more practical and flexible protocols are still required to improve the synthetic approaches to these biologically important cyclopeptides.

The Ullmann-type coupling reaction of aryl halides and phenols is a reliable method for elaborating biaryl ethers.[10,11] Although this reaction has been employed for the assembly of certain cyclopeptides,[1c,6] the danger of racemization of the amino acid moieties under basic conditions and high reaction temperatures ($\approx 130\,^{\circ}C$) prevents its wide application in this area. In 1997, Nicolaou et al. found that a triazene unit *ortho* to the halogen atom facilitates coupling with phenol moieties so that the reaction proceeds at 80 °C.[2a] Successful application of the method to the total synthesis of vancomycin has been reported.[1a,2b–d] However, good conversion of the substrates requires at least five equivalents of $CuBr{\cdot}SMe_2$. Recently, we and other groups discovered that some special ligands could promote CuI-catalyzed C(aryl)–O bond formation.[10,11] Unfortunately, these new reaction conditions still fall short of that needed for cyclopeptide synthesis because the reaction temperatures are still too high. Recently, we found that the NHCOR groups in 2-haloacetanilides could greatly promote the Ullmann-type biaryl formation reaction, which in combination with the known ligand effect led to this reaction taking place at room temperature. Herein, we wish to disclose these results.

As indicated in Table 1, the reaction of 2-bromotrifluoroacetanilide (**1a**) with L-tyrosine derivative **2** using CuI/*N*,*N*-dimethylglycine in the presence of Cs_2CO_3 at room temperature is completed in 2 h and delivers the coupling product **3a** in 88% yield (entry 1). Low yields were observed with *N*-methyl-L-proline or L-proline as the ligands (entries 2 and 3), and no coupling occurred in the absence of a ligand (entry 4). Relative to aryl bromide **1a**, aryl iodide and chloride were poorer substrates (entries 5 and 6). In addition, a reactivity trend for the *N*-substituent ($Y = COCF_3 > COCH_3 > COPh \gg SO_2Me$) was noted (entries 1 and 7–9). Furthermore, little or no conversion was noticed in the case of 3-bromotrifluoroacetanilide or 4-bromotrifluoroacetanilide as the substrates (entries 10 and 11). These results clearly show the existence of an accelerating effect caused by an *ortho*-amide group and that its combination with ligand effects is essential for this reaction to take place at room temperature.

Table 1: CuI-catalyzed reaction of aryl halides **1** with phenol **2**.[a]



1 2 3

a: Y = $COCF_3$, b: Y = $COCH_3$, c: Y = COPh, d: Y = SO_2Me

Entry	Y	X	Ligand[b]	*t* [h]	Yield [%][c]
1	$COCF_3$	2-Br	A	2	88
2	$COCF_3$	2-Br	B	4	49[d]
3	$COCF_3$	2-Br	C	2	26[d]
4	$COCF_3$	2-Br	–	5	0[d]
5	$COCF_3$	2-I	A	5	43[d]
6	$COCF_3$	2-Cl	A	24	7[d]
7	$COCH_3$	2-Br	A	15	53[d]
8	COPh	2-Br	A	24	14[d]
9	SO_2Me	2-Br	A	24	0[d]
10	$COCF_3$	3-Br	A	2	–[e]
11	$COCF_3$	4-Br	A	2	–[f]

[a] Reaction conditions: CuI (0.15 mmol), ligand (0.5 mmol), **1** (0.5 mmol), **2** (0.75 mmol), Cs_2CO_3 (1.5 mmol), 1,4-dioxane (2 mL), RT. [b] A: *N*,*N*-dimethylglycine, B: *N*-methyl-L-proline, C: L-proline. [c] Yield of the isolated products. [d] Aryl halide was recovered in 40–90% yield. [e] Corresponding cross-coupling product was isolated in less than 3% yield. [f] No conversion was observed. Tr = triphenylmethyl.

With the optimized reaction conditions in hand, we studied the process with a few other aryl bromides and phenols (Table 2). Both *N*-Cbz- and *N*-Boc-L-tyrosine methyl esters were suitable for this reaction and gave **6a** and **6b** in good yields without any racemization, as determined by chiral-column HPLC analysis. Some loss of optical purity was observed when *N*-Boc-(*R*)-4-hydroxyphenylglycine methyl ester was used (see **6c**). Fortunately, this problem could be obviated by changing the *N*-protecting group from Boc to Tr

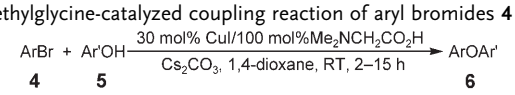
[*] Q. Cai, Prof. Dr. D. Ma
State Key Laboratory of Bioorganic and Natural Products Chemistry
Shanghai Institute of Organic Chemistry
Chinese Academy of Sciences
354 Fenglin Lu, Shanghai 200032 (China)
Fax: (+86) 21-6416-6128
E-mail: madw@mail.sioc.ac.cn
B. Zou
Department of Chemistry
Fudan University
Shanghai 200433 (China)

[**] The authors are grateful to the Chinese Academy of Sciences, National Natural Science Foundation of China (grants 20321202 and 20572119) and the Science and Technology Commission of Shanghai Municipality (grants 02JC14032 and 03XD14001) for their financial support. We also thank Professor T.-L. Ho for helpful discussions.

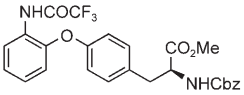
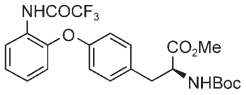
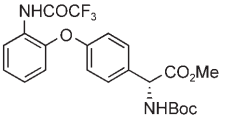
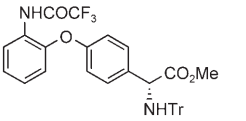
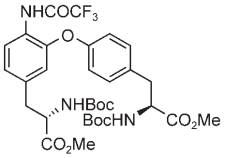
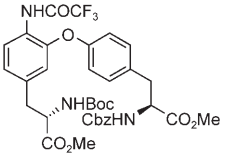
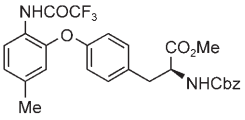
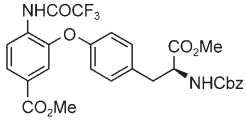
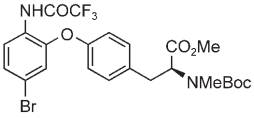
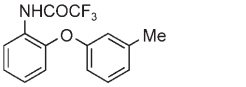
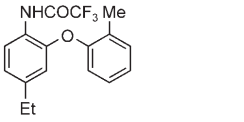
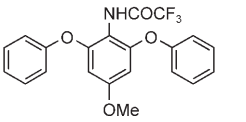
Supporting information for this article is available on the WWW under http://www.angewandte.org or from the author.

InterScience © 2006 Wiley-VCH Verlag GmbH & Co. KGaA, Weinheim

Table 2: CuI/*N*,*N*-dimethylglycine-catalyzed coupling reaction of aryl bromides **4** with phenols **5**.[a]



4 **5** **6**

Product		*t* [h]	Yield [%]	Product		*t* [h]	Yield [%]
	**6a**[b]	5	82		**6b**[b]	5 h	90
	**6c**[c]	8	88		**6d**[b]	8	82
	**6e**	14	85		**6f**	14	80
	**6g**	3	88		**6h**[d]	10	51
	**6i**	4	81		**6j**	4	82
	**6k**	4	76		**6m**[e]	4	70

[a] Reaction conditions: CuI (0.15 mmol), *N*,*N*-dimethylglycine (0.5 mmol), **4** (0.5 mmol), **5** (0.75 mmol), Cs_2CO_3 (1.5 mmol), 1,4-dioxane (2 mL), RT. [b] 99% *ee*, as determined by HPLC. [c] 91% *ee*, as determined by HPLC. [d] 40% aryl bromide was recovered. [e] Phenol (1.5 mmol) was added. Cbz = benzyloxycarbonyl, Boc = *tert*-butoxycarbonyl.

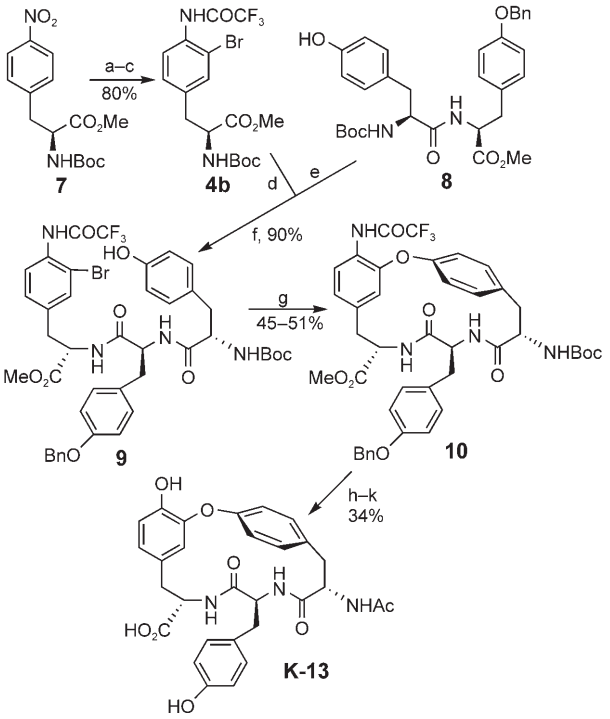
(see **6d**). From a L-phenylalanine-derived bromide **4b** (see Scheme 1 for the preparation), two isodityrosine analogues **6e** and **6f** were produced in good yields. These compounds are promising synthetic intermediates for isodityrosine,[9] K-13,[5] and related natural products. We found that electron-deficient aryl bromides are less reactive (see **6h**). The exclusive formation of **6i** from a coupling of 2,4-dibromotrifluoroacetanilide provided further support of an *ortho*-substituent effect by an NHCOR group. An amino acid residue in the phenol component is not necessary for the reaction, as demonstrated by examples **6j**–**6m**. The formation of **6k** and **6m** also indicated that steric factors might not be critical and a twofold *ortho*-substitution is possible, for example, with 2,6-dibromotrifluoroacetanilides.

Encouraged by the above success, we extended our work to intramolecular macrocyclization, with the total syntheses of antitumor agent K-13 and a cycloisodityrosine derivative. As shown in Scheme 1, **7** was reduced by hydrogenation, brominated with NBS, and treated with $(CF_3CO)_2O$ to afford aryl bromide **4b**. Hydrolysis of **8** with LiOH was followed by coupling with a liberated amine from **4b**. Tripeptide **9**, thus obtained, was subjected to macrocyclization in the presence of CuI (3 equiv) *N*,*N*-dimethylglycine (3 equiv), and Cs_2CO_3 (3 equiv) in dilute dioxane (0.01M), and the desired cyclization product **10** was isolated in 45–51% yields. Next, the macrolactam **10** was converted into K-13 in 34% overall yield through five routine transformations, which included proper changes of the protecting groups, hydrolysis of the ester and trifluoroacetanilide groups, and diazotization of the aniline unit to a phenol moiety.

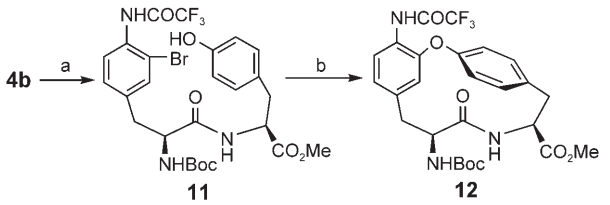
We also carried out a synthesis of **12** (see Scheme 2) from dipeptide **11**, which was obtained by coupling a liberated acid from **4b** with L-tyrosine methyl ester. Although an initial attempt to effect its macrocyclization under our standard conditions failed, when the solvent was changed to MeCN/pyridine (4:1), and the reaction temperature was raised to 45°C, we were pleased to notice that the desired cyclic product **12**, which might serve as an intermediate for synthesizing RP 66453, was isolated in 42% yield.[7] This cyclization is comparable with those reported by two groups who used *o*-nitro-activated nucleophilic aromatic substitution,[7] but in our case two amino acid units could be readily obtained from L-phenylalanine and L-tyrosine. This advantage would allow large-scale preparation.

Since the Hurtley reaction was disclosed in 1929, considerable efforts have been devoted to identifying suitable *ortho*-substituents that can promote Ullmann-type couplings.[2a,12] However, only carboxylate and triazene units have been found to have the desired accelerating effect prior to our present work. Two mesomerism models have been proposed for interpreting the early results,[2a,12c] but a similar model is not suitable for rationalizing the present *ortho*-substituent effect. Consequently, we propose a plausible mechanism as follows (Scheme 3): Oxidative addition of the chelated Cu^I center **A** to ArX produces complex **B**, in which the oxygen of the NHCOR group may coordinate with the Cu center to provide additional stabilization. It is noteworthy that similar Pd^{II} complexes have been determined by Tremont and Rahman in their palladium acetate catalyzed *ortho*-alkylation of acetanilides.[13a] After reaction of **B** with cesium phenoxides to give **C**, reductive elimination occurs to afford the biaryl ethers and regenerate the catalytic species. This model was supported by the difference in reactivity between the trifluoroacetanilides and acetanilides discussed above. The higher reactivity of the aryl bromides might be explained by

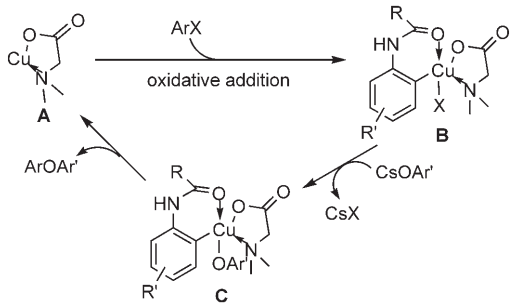
 © 2006 Wiley-VCH Verlag GmbH & Co. KGaA, Weinheim



Scheme 1. Synthesis of K-13. Reagents and conditions: a) $Pd/C/H_2$, MeOH, RT; b) NBS, DMF, RT; c) $(CF_3CO)_2O$, CH_2Cl_2; d) TFA, CH_2Cl_2; e) aq. LiOH, THF, MeOH; f) HATU/DIPEA, DMF; g) Cs_2CO_3, CuI, *N*,*N*-dimethylglycine, 1,4-dioxane, RT; h) TFA then Ac_2O/TEA; i) aq. NaOH, MeOH; j) *t*BuONO/HBF_4, MeCN; k) $Cu(NO_3)_2/Cu_2O$. NBS = *N*-bromosuccinimide, DMF = dimethylformamide, TFA = trifluoroacetic acid, HATU = 2-(7-aza-1*H*-benzotriazole-1-yl)-1,1,3,3-tetramethyluronium hexafluorophosphate, DIPEA = diisopropylethylamine, TEA = triethylamine.



Scheme 2. Synthesis of a cycloisodityrosine derivative. Reagents and conditions: a) 1. aq. LiOH, MeOH, THF; 2. L-tyrosine methyl ester, EDCI, HOBt, DIPEA, CH_2Cl_2, 90% for two steps; b) CuI (3 equiv), $Me_2NCH_2CO_2H$ (4 equiv), Cs_2CO_3 (4 equiv), MeCN/Py (4:1), 0.01 M, 45 °C, 42%. EDCI = 1-(3-dimethylaminopropyl)-3-ethylcarbodiimide hydrochloride.



Scheme 3. Plausible mechanism for mild biaryl formation.

the different contributions of the bromide and iodide anions to the stabilization of **B**. Besides this speculation, more work should be performed to prove this mechanism further or other possible mechanisms should be put forward.

In summary, we have found that the NHCOR group has a strong *ortho*-substituent effect on an Ullmann-type biaryl ether formation reaction. This *ortho*-substituent effect is the third type discovered to date, which should facilitate the development of more mild Ullmann-type coupling reactions.[10] In addition, although the substrates tested so far are limited, our new reaction is rather mild and fast relative to the previous Cu^I-catalyzed coupling reactions of aryl halides with phenols,[11] and therefore should find further applications in organic synthesis.

Received: October 6, 2005
Revised: November 27, 2005
Published online: January 20, 2006

Keywords: biaryl ethers · coupling · ligand effects · *ortho* effect · peptides

[1] For reviews, see: a) K. C. Nicolaou, C. N. C. Boddy, S. Bräse, N. Winssinger, *Angew. Chem.* **1999**, *111*, 2230–2287; *Angew. Chem. Int. Ed.* **1999**, *38*, 2096–2152; b) J. Zhu, *Synlett* **1997**, 133–144; c) A. V. R. Rao, M. K. Gurjar, G. K. L. Reddy, A. S. Rao, *Chem. Rev.* **1995**, *95*, 2135–2167; d) J. Blankenstein, J. Zhu, *Eur. J. Org. Chem.* **2005**, 1949–1964.

[2] a) K. C. Nicolaou, C. N. C. Boddy, S. Natarajan, T.-Y. Yue, H. Li, S. Bräse, J. M. Ramanjulu, *J. Am. Chem. Soc.* **1997**, *119*, 3421–3422; b) K. C. Nicolaou, S. Natarajan, H. Li, N. F. Jain, R. Hughes, M. E. Solomon, J. M. Ramanjulu, C. N. C. Boddy, M. Takayanagi, *Angew. Chem.* **1998**, *110*, 2872–2878; *Angew. Chem. Int. Ed.* **1998**, *37*, 2708–2714; c) K. C. Nicolaou, N. F. Jain, S. Natarajan, R. Hughes, M. E. Solomon, H. Li, J. M. Ramanjulu, M. Takayanagi, A. E. Koumbis, T. Bando, *Angew. Chem.* **1998**, *110*, 2879–2881; *Angew. Chem. Int. Ed.* **1998**, *37*, 2714–2716; d) K. C. Nicolaou, M. Takayanagi, N. F. Jain, S. Natarajan, A. E. Koumbis, T. Bando, J. M. Ramanjulu, *Angew. Chem.* **1998**, *110*, 2881–2883; *Angew. Chem. Int. Ed.* **1998**, *37*, 2717–2719; e) D. A. Evans, M. R. Wood, B. W. Trotter, T. I. Richardson, J. C. Barrow, J. L. Katz, *Angew. Chem.* **1998**, *110*, 2864–2868; *Angew. Chem. Int. Ed.* **1998**, *37*, 2700–2704; f) D. A. Evans, C. J. Dinsmore, P. S. Watson, M. R. Wood, T. I. Richardson, B. W. Trotter, J. L. Katz, *Angew. Chem.* **1998**, *110*, 2868–2872; *Angew. Chem. Int. Ed.* **1998**, *37*, 2704–2708; g) D. L. Boger, S. Miyazaki, S. H. Kim, J. H. Wu, O. Loiseleur, S. L. Castle, *J. Am. Chem. Soc.* **1999**, *121*, 3226–3227.

[3] B. M. Crowley, Y. Mori, C. C. McComas, D. Tang, D. L. Boger, *J. Am. Chem. Soc.* **2004**, *126*, 4310–4317.

[4] a) D. A. Evans, J. L. Katz, G. S. Peterson, T. Hintermann, *J. Am. Chem. Soc.* **2001**, *123*, 12411–12413; b) D. L. Boger, S. H. Kim, S. Miyazaki, H. Strittmatter, J.-H. Wang, Y. Mori, O. Rogel, S. L. Castle, J. J. McAtee, *J. Am. Chem. Soc.* **2000**, *122*, 7416–7417; c) D. L. Boger, S. H. Kim, Y. Mori, J.-H. Wang, O. Rogel, S. L. Castle, J. J. McAtee, *J. Am. Chem. Soc.* **2001**, *123*, 1862–1871.

[5] For selected references, see: a) J. W. Janetka, D. H. Rich, *J. Am. Chem. Soc.* **1997**, *119*, 6488–6495; b) S. Nishiyama, Y. Suzuki, S. Yamamura, *Tetrahedron Lett.* **1989**, *30*, 379–382; c) A. V. R. Rao, T. K. Chakraborty, K. L. Reddy, A. S. Rao, *Tetrahedron Lett.* **1992**, *33*, 4799–4802; d) A. Bigot, M. Bois-Choussy, J. Zhu, *Tetrahedron Lett.* **2000**, *41*, 4573–4577.

 © 2006 Wiley-VCH Verlag GmbH & Co. KGaA, Weinheim

[6] a) D. L. Boger, D. Yohannes, *J. Am. Chem. Soc.* **1991**, *113*, 1427 – 1429; b) D. L. Boger, D. Yohannes, J. Zhou, M. A. Patane, *J. Am. Chem. Soc.* **1993**, *115*, 3420 – 3430; c) D. L. Boger, J. Zhou, *J. Am. Chem. Soc.* **1995**, *117*, 7364 – 7378; for their initial efforts on related studies, see: d) D. L. Boger, D. Yohannes, *Tetrahedron Lett.* **1989**, *30*, 2053 – 2056; e) D. L. Boger, D. Yohannes, *J. Org. Chem.* **1990**, *55*, 6000 – 6017; f) D. L. Boger, D. Yohannes, *J. Org. chem.* **1991**, *56*, 1763 – 1767; g) D. L. Boger, Y. Nomoto, B. R. Teegarden, *J. Org. Chem.* **1993**, *58*, 1425 – 1433.

[7] a) M. Bois-Choussy, P. Cristau, J. Zhu, *Angew. Chem.* **2003**, *115*, 4370 – 4373; *Angew. Chem. Int. Ed.* **2003**, *42*, 4238 – 4241; b) P. J. Krenitsky, D. L. Boger, *Tetrahedron Lett.* **2002**, *43*, 407 – 410.

[8] H. Deng, J.-K. Jung, T. Liu, K. W. Kuntz, M. L. Snapper, A. H. Hoveyda, *J. Am. Chem. Soc.* **2003**, *125*, 9032 – 9034.

[9] M. E. Jung, T. I. Lazarova, *J. Org. Chem.* **1999**, *64*, 2976 – 2977.

[10] For reviews, see: a) S. V. Ley, A. W. Thomas, *Angew. Chem.* **2003**, *115*, 5558 – 5607; *Angew. Chem. Int. Ed.* **2003**, *42*, 5400 – 5449; b) K. Kunz, U. Scholz, D. Ganzer, *Synlett* **2003**, *15*, 2428 – 2439; c) I. P. Beletskaya, A. V. Cheprakov, *Coord. Chem. Rev.* **2004**, *248*, 2337 – 2364.

[11] a) D. Ma, Q. Cai, *Org. Lett.* **2003**, *5*, 3799 – 3802; b) J.-F. Marcoux, S. Doye, S. L. Buchwald, *J. Am. Chem. Soc.* **1997**, *119*, 10539 – 10540; c) E. Buck, Z. J. Song, D. Tschaen, P. G. Dormer, R. P. Volante, P. J. Reider, *Org. Lett.* **2002**, *4*, 1623 – 1626; d) H.-J. Cristau, R. P. Cellier, S. Hamada, J.-F. Spindler, M. Taillefer, *Org. Lett.* **2004**, *6*, 913 – 916.

[12] a) J. Lindley, *Tetrahedron* **1984**, *40*, 1433 – 1456; b) R. Cirigottis, E. Ritchie, W. C. Taylor, *Aust. J. Chem.* **1974**, *27*, 2209 – 2228; c) A. Bruggink, A. Mckillop, *Tetrahedron* **1975**, *31*, 2607 – 2619; d) A. V. Kalinin, J. F. Bower, P. Riebel, V. Snieckus, *J. Org. Chem.* **1999**, *64*, 2986 – 2987.

[13] a) S. J. Tremont, H. U. Rahman, *J. Am. Chem. Soc.* **1984**, *106*, 5759 – 5760; for recent studies using these these complexes as intermediates, see: b) O. Daugulis, V. G. Zaitsev, *Angew. Chem.* **2005**, *117*, 4114 – 4416; *Angew. Chem. Int. Ed.* **2005**, *44*, 4046 – 4048; c) V. G. Zaitsev, O. Daugulis, *J. Am. Chem. Soc.* **2005**, *127*, 4156 – 4157; d) M. D. K. Boele, G. P. F. Strijdonck, A. H. M. Vries, P. C. J. Kamer, J. G. Vries, P. W. N. M. Leeuwen, *J. Am. Chem. Soc.* **2002**, *124*, 1586 – 1587.

 © 2006 Wiley-VCH Verlag GmbH & Co. KGaA, Weinheim

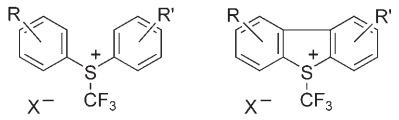
Electrophilic Reagents

DOI: 10.1002/anie.200503776

Straightforward One-Pot Synthesis of Trifluoromethyl Sulfonium Salts**

Emmanuel Magnier, Jean-Claude Blazejewski,* Marc Tordeux, and Claude Wakselman*

The trifluoromethyl group[1] has found widespread use in medicinal,[2] agrochemical,[3] and materials science.[4] Thanks to recent progress in these fields and the skill of organic chemists, methodologies for the direct introduction of the trifluoromethyl group are now available through radical, nucleophilic, or electrophilic approaches.[5] Being the newest, the electrophilic route is the least developed at this time and is scarcely used in the laboratory.[6] However, over the past two decades, electrophilic trifluoromethylation has been made possible by the development of various trifluoromethyl sulfide based reagents. In a pioneering study, Yagupolskii et al. described the preparation of trifluoromethylsulfonium compounds **1** and their reactivity towards some simple nucleophiles (Scheme 1).[7] More recently, Shreeve and co-



Scheme 1. Trifluoromethylating reagents.

workers proposed an alternative route to related reagents with improved electrophilic power.[8] In the meantime, Umemoto and Ishihara succeeded in the preparation of sulfonium salts of type **2**, with a dibenzothiophenium skeleton.[9] The last two research groups clearly demonstrated that the reactivity of both types of reagents **1** or **2** is enhanced by the presence of electron-withdrawing substituents R and R′, such as fluorinated or nitro groups, on the aromatic nucleus.

Although S-(trifluoromethyl) dibenzothiophenium tetrafluoroborate (**2**; $R = R' = H$, $X = BF_4$) is now commercially available, its use and that of related reagents suffers from the

[*] Dr. E. Magnier, Dr. J.-C. Blazejewski, Dr. M. Tordeux, Dr. C. Wakselman
SIRCOB-CNRS, UMR 8086
Université de Versailles
45 Avenue des Etats-Unis, 78035 Versailles Cedex (France)
Fax: (+33) 1-3925-4452
E-mail: magnier@chimie.uvsq.fr
jcblaz@chemie.uvsq.fr

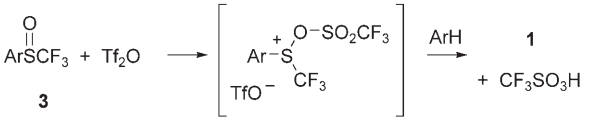
[**] We thank Rhodia for a generous gift of sodium and potassium trifluoromethanesulfinates and Dr. M. E. Popkin for proof-reading the English manuscript.

Supporting information for this article is available on the WWW under http://www.angewandte.org or from the author.

© 2006 Wiley-VCH Verlag GmbH & Co. KGaA, Weinheim

major drawback of their relatively complex synthesis. They are prepared in multistep sequences using either the now-banned ozone-depleting greenhouse gas CF_3Br[10] or expensive silver fluoride,[8] or even lengthier syntheses.[9b] Herein, we propose a multicomponent-reaction process for the preparation of compounds of type **1**.

A close examination of the literature shows that the cornerstone of the previously described syntheses is the formation of an intermediate trifluoromethyl sulfoxide **3**, precursor of the targeted sulfonium compounds **1** or **2** (Scheme 2).



Scheme 2. Mechanism of the formation of the sulfonium compounds.

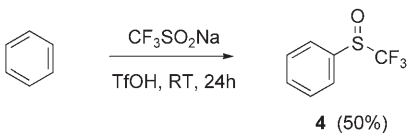
The mechanism proposed by Shreeve and co-workers[8] for the formation of sulfonium **1** involves activation of the sulfoxide function by trifluoromethanesulfonic anhydride ($(CF_3SO_2)_2O$), followed by intermolecular condensation with an arene and concomitant production of trifluoromethanesulfonic acid (CF_3SO_3H; Scheme 2).

In this context, we recently reported an efficient preparation of various aryl trifluoromethyl sulfoxides **3** by treatment of aromatic compounds with a mixture of potassium trifluoromethanesulfinate (CF_3SO_2K), trifluoromethanesulfonic anhydride, and trifluoromethanesulfonic acid.[11] This study could be considered to be the first improvement in the preparation of sulfonium compounds of type **1** as it decreases the number of necessary steps that lead to the synthesis of aryl trifluoromethyl sulfoxides **3**. However, only polymeric material was produced when the methodology was applied to the simplest benzene case.

A reappraisal of this work led us to suspect that the presence of both trifluoromethanesulfonic acid and trifluoromethanesulfonic anhydride at the beginning of the experiment may be deleterious to the outcome of the reaction.

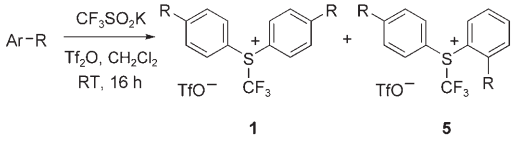
In a first trial, we observed that phenyltrifluoromethyl sulfoxide **4** could be isolated in a satisfactory yield when starting from benzene provided that trifluoromethanesulfonic anhydride was not used (Scheme 3).[12] We assume that this improved procedure can be readily generalized to the synthesis of other aryl trifluoromethyl sulfoxides of type **4**.

However, as shown in Scheme 2, the presence of trifluoromethanesulfonic anhydride is essential for the preparation of sulfonium salts **1**. In a second trial, we thus replaced trifluoromethanesulfonic acid with trifluoromethanesulfonic anhydride. We were very pleased to find that this improvement, with dichloromethane as the solvent, resulted in the straightforward preparation of *S*-(trifluoromethyl)diaryl sulfonium trifluoromethanesulfonates **1** and **5** in a one-pot procedure with low-to-good yields depending on the substrate (Table 1). With an electron-donating substituent on the



Scheme 3. One-step synthesis of phenyltrifluoromethyl sulfoxide **4**.

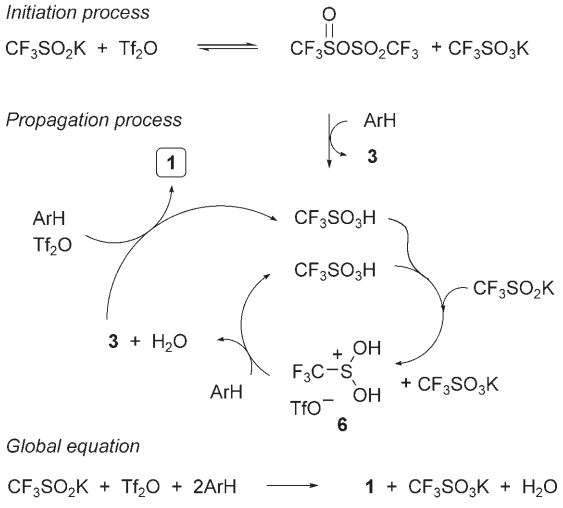
Table 1: One-pot synthesis of trifluoromethyl sulfonium compounds



Entry	R	Compound	Yield of isolated product [%]	**1**/**5**
1	Me	**1a**	73	85:15
2	H	**1b**	60	100:0
3	Cl	**1c**	50	100:0
4	F	**1d**	46	100:0
5	OCF_3	**1e**	15	100:0

aromatic ring (entry 1), the yield of isolated product is good, although associated with incomplete *ortho*/*para* selectivity. Benzene itself gave rise to compound **1b**, already synthesized by Shreeve and co-workers in three steps, in a satisfactory yield (entry 2).[8] Even with less activated substrates (entries 3–5) new trifluoromethyl sulfonium compounds **1c**–**e** could be prepared in fair (**1c**,**d**) to low (**1e**) yield. All compounds have been fully characterized (see the Supporting Information).

The mechanism of this transformation seems rather intriguing, and we propose a possible pathway in Scheme 4. We assume that the process can be divided in two parts, the first being the formation of sulfoxide **3**, the second its transformation into sulfonium **1**. Reaction between potassium trifluoromethanesulfinate and trifluoromethanesulfonic anhydride can produce a mixed sulfonate sulfinate anhydride.[13] This species may be activated enough to react with the aromatic substrate by a Friedel–Crafts-like electrophilic



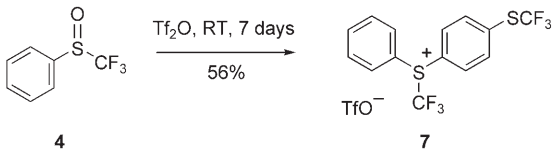
Scheme 4. Proposed mechanism for the formation of the sulfonium compounds **1**.

 © 2006 Wiley-VCH Verlag GmbH & Co. KGaA, Weinheim

substitution. This first reaction is presumably the slower step and may be considered as an initiation process that generates trifluoromethanesulfonic acid and sulfoxide **3**. The acid thus formed may then lead to sulfoxide **3** by the intermediate **6**, as shown in our earlier work.[11] The second part of the mechanism is presumed to be analogous to the one proposed by Shreeve and co-workers (Scheme 2). At this point, the requisite two equivalents of acid necessary for the twofold protonation of potassium trifluoromethanesulfinate (to give **6**) are produced by the propagation reaction. Some experimental observations are in favor of this mechanism. The reaction is inhibited by a base such as 2,6-di-*tert*-butyl-4-methylpyridine. Moreover, in some cases, small quantities of sulfoxide are isolated from the reaction mixture. This last point will be discussed later. The global equation shows that trifluoromethanesulfonic acid does not appear in the reaction equation. The stoichiometry used for the reagents (one equivalent for each) may appear to be in contradiction with this equation. Nevertheless, these conditions gave the best results with respect to the yield of isolated product.[14]

In addition to the aromatic starting material, fine analysis of the crude mixture has revealed the presence of small quantities of aryl trifluoromethyl sulfoxides **3** (as mentioned above), but also reduced aryl trifluoromethyl sulfides, in larger quantities. Part of the aryl trifluoromethyl sulfoxide seems to be reduced in situ, presumably by trifluoromethanesulfonic anhydride. This reagent is better known for its oxidative properties,[13a,15] but some examples of its reducing power have been reported.[13b,16] To the best of our knowledge, no explanation has been proposed yet for this behavior.[17]

This reduction process is peculiarly illustrated by the formation of trifluoromethylthio-substituted sulfonium **7** by treatment of sulfoxide **4** with an excess of neat trifluoromethanesulfonic anhydride (Scheme 5).



4 7

Scheme 5. Preparation of sulfonium **7** in neat Tf_2O.

We suppose that in the first step one equivalent of sulfoxide is reduced to its corresponding sulfide, which can further react with an activated form of the sulfoxide to generate the observed sulfonium **7** (see Scheme 2). We have no experimental evidence for such a mechanism, except the isolation (besides **7**) of nonpolar sulfide derivatives, which result from the reduction of phenyltrifluoromethyl sulfoxide **4** in the reaction medium. Nevertheless, this reaction constitutes a new route to interesting sulfonium derivatives and can be generalized to prepare various aryl trifluoromethyl sulfoxides.

In summary, we have developed a very short and efficient synthesis of aryl trifluoromethyl sulfonium salts, important electrophilic trifluoromethylating reagents. Our strategy allows the preparation of target compounds in a one-pot process for routine laboratory applications. We are currently applying this methodology to more elaborate aromatic compounds, especially biphenyl derivatives, to synthesize new and hopefully more reactive reagents.

Experimental Section

General procedure for the synthesis of sulfonium compounds as exemplified by the preparation of **1b**: Benzene (1.14 mL, 12.8 mmol, 1 equiv) and trifluoromethanesulfonic anhydride (2.14 mL, 12.8 mmol, 1 equiv) were added under argon to a suspension of potassium trifluoromethanesulfinate (2.2 g, 12.8 mmol) in dichloromethane (2 mL, 64 mmol, 5 equiv). The reaction mixture is filtered after 16 h, diluted with CH_2Cl_2 (30 mL), washed with water (3 × 10 mL), dried over $MgSO_4$, and concentrated under reduced pressure. The residue was purified by column chromatography on silica gel using dichloromethane/methanol (90:10) as the eluent to give 1.76 g (70%) of a slightly colored powder. Recrystallization from pentane/ethyl acetate (2:8) afforded 1.5 g (60%) of **1b** as a white solid. M.p. 99.6–100 °C; ^{1}H NMR ($CDCl_3$, 200 MHz): $\delta = 8.27$ (d, $J = 8.8$ Hz, 4H), 7.8 ppm (d, 4H); ^{19}F NMR ($CDCl_3$, 188 MHz): $\delta = -50.7$ (m, 3F, SCF_3), −79.0 ppm (m, 3F, SO_2CF_3); ^{13}C NMR ($CDCl_3$, 75 MHz): $\delta = 145.0$, 134.6, 132.7, 123.0 (q, $J = 328.2$, CF_3), 120.6 (q, $J = 320.0$, CF_3), 114.8 ppm; pos. ESI MS: (m/z): 323 [M^+]; elemental analysis (%) calcd for $C_{14}H_8Cl_2F_6O_3S_2$: C 35.53, H 1.70; found: C 35.51, H 1.69.[18]

Received: October 25, 2005
Published online: January 17, 2006

Keywords: electrophiles · reaction mechanisms · sulfonium salts · trifluoromethyl substituents

[1] a) R. E. Banks, B. E. Smart, J. C. Tatlow in *Organofluorine Chemistry, Principles and Commercial Applications*, Plenum, New York, **1994**; b) B. E. Smart, *J. Fluorine Chem.* **2001**, *109*, 3–11.
[2] a) K. L. Kirk in *Biochemistry of Halogenated Organic Compounds* (Ed.: E. Frieden), Plenum, New York, **1991**; b) F. M. D. Ismail, *J. Fluorine Chem.* **2002**, *118*, 27–33; c) H.-J. Böhm, D. Banner, S. Bendels, M. Kansy, B. Kuhn, K. Müller, U. Obst-Sander, M. Stahl, *ChemBioChem* **2004**, *5*, 637–643.
[3] P. Jeschke, *ChemBioChem* **2004**, *5*, 570–589.
[4] P. Kirsch in *Modern Fluoroorganic Chemistry: Synthesis, Reactivity, Applications*, Wiley-VCH, Weinheim, **2004**.
[5] a) J. T. Welch, S. Eswarakrishnan in *Fluorine in Bioorganic Chemistry*, Wiley, New York, **1991**; b) T. Hiyama in *Organofluorine Compounds, Chemistry and Applications*, Springer, Berlin, **2000**; c) M. A. McClinton, D. A. McClinton, *Tetrahedron* **1992**, *48*, 6555–6666.
[6] T. Umemoto, *Chem. Rev.* **1997**, *97*, 1757–1777.
[7] L. M. Yagupolskii, N. V. Kondratenko, G. N. Timofeeva, *J. Org. Chem. USSR* **1984**, *20*, 103–105.
[8] J. J. Yang, R. L. Kirchmeier, J. M. Shreeve, *J. Org. Chem.* **1998**, *63*, 2656–2660.
[9] a) T. Umemoto, S. Ishihara, *J. Am. Chem. Soc.* **1993**, *115*, 2156–2164; b) T. Umemoto, S. Ishihara, *J. Fluorine Chem.* **1998**, *92*, 181–187.
[10] T. Umemoto, S. Ishihara, *Tetrahedron Lett.* **1990**, *31*, 3579–3582.
[11] C. Wakselman, M. Tordeux, C. Freslon, L. Saint-Jalmes, *Synlett* **2001**, *4*, 550–552.
[12] Sodium or potassium trifluoromethanesulfinate could be interchangeably used without influence on the yield.
[13] a) G. Maas, P. Stang, *J. Org. Chem.* **1981**, *46*, 1606–1610; b) T. Netscher, P. Bohrer, *Tetrahedron Lett.* **1996**, *37*, 8359–8362.

 © 2006 Wiley-VCH Verlag GmbH & Co. KGaA, Weinheim

[14] It should be remembered that water is also formed in this process and may concurrently be protonated by trifluoromethanesulfonic acid and/or hydrolyze trifluoromethanesulfonic anhydride; moreover, although the initiation process is no longer rate determining, it may nevertheless continue to participate in the reaction.
[15] I. L. Baraznenok, V. G. Nenajdenko, E. S. Balenkova, *Tetrahedron* **2000**, *56*, 3077 – 3119.
[16] J. M. Shreeve, J. J. Yang, R. L. Kirchmeier, US Patent 6,215,021, **2001**.
[17] Studies are also ongoing to develop a better understanding of the mechanism of the reduction reaction.
[18] See the Supporting Information for full experimental details, characterization data, and ^{1}H, ^{19}F, and ^{13}C NMR spectra.

 © 2006 Wiley-VCH Verlag GmbH & Co. KGaA, Weinheim

Homogeneous Catalysis

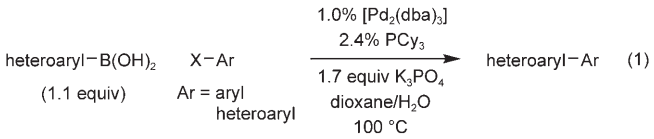
DOI: 10.1002/anie.200503479

A Versatile Method for Suzuki Cross-Coupling Reactions of Nitrogen Heterocycles**

*Noriaki Kudo, Mauro Perseghini, and Gregory C. Fu**

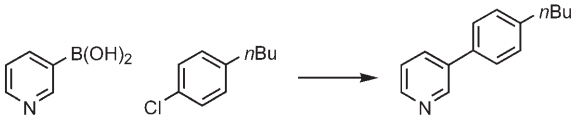
The Suzuki cross-coupling reaction is a powerful method for carbon-carbon bond formation that has been applied in a variety of settings, ranging from natural-products synthesis to materials chemistry, including large-scale production.[1,2] Among the attractive features of the Suzuki reaction are the wide availability, stability to air and moisture, and low toxicity of boronic acids, as well as the facile removal of the boron-containing side products of the coupling process.

In recent years, tremendous progress has been described in the discovery of more active catalysts for the Suzuki reaction. Arguably the most important remaining challenge is the development of a universal method for cross-coupling substrates that include nitrogen heterocycles.[3] The presence of such groups, which are particularly pervasive in medicinal chemistry,[4] can lead to low reactivity in coupling reactions. Herein, we describe an unusually versatile catalyst that achieves Suzuki cross-couplings of an array of nitrogen-containing boronic acids and aryl halides [Eq. (1); dba = dibenzylideneacetone, Cy = cyclohexyl].



Since 1998, we and others have established that trialkylphosphines, including $P(t\mathrm{Bu})_3$ and PCy_3, serve as very effective ligands for a variety of palladium-catalyzed coupling processes.[1,5] In view of the low cost of PCy_3 relative to many of the other ligands that provide highly active cross-coupling catalysts (e.g., $P(t\mathrm{Bu})_3$, aryldialkylphosphines, and carbenes), we decided to examine the possibility of developing a versatile PCy_3-based catalyst for Suzuki reactions of nitrogen heterocycles.

In an earlier study, we employed Pd/PCy_3/KF/THF as a catalyst system for Suzuki cross-couplings of aryl halides.[6,7] Unfortunately, when we applied these conditions to the coupling of 3-pyridineboronic acid with 4-*n*-butylchlorobenzene, we obtained essentially none of the desired biaryl [Eq. (2)]. After considerable exploration of the reaction parameters, we determined that Pd/PCy_3/K_3PO_4/dioxane/H_2O achieves the desired cross-coupling in excellent yield [Eq. (2)].[8,9]



1.5% [$Pd_2(dba)_3$], 4.2% PCy_3, 3.3 equiv KF, THF, 60 °C <2%
1.0% [$Pd_2(dba)_3$], 2.4% PCy_3, 1.7 equiv K_3PO_4, dioxane/H_2O, 100 °C 92%

We were pleased to find that this standard protocol can be applied directly to Suzuki reactions of an array of nitrogen heterocycles. As illustrated in Table 1, a variety of heteroarylboronic acids can even be coupled with challenging aryl halides. Thus, 3-pyridineboronic acid reacts with a range of chlorobenzenes, including *ortho*-substituted and electronically deactivated substrates, in good yield (Table 1, entries 1–4). As might be anticipated, the corresponding aryl bromides and iodides also couple under these conditions (Table 1, entries 5 and 6). In addition, substituted 3-pyridineboronic acids are suitable cross-coupling partners (Table 1, entries 7–9). The method is effective not only for 3-pyridineboronic acids, but also for an array of other heteroarylboronic acids (e.g., 4-pyridine, 5-pyrimidine, and indole; Table 1, entries 10–13).

Although substrates that bear an indole NH group undergo Suzuki cross-coupling smoothly with this procedure (Table 1, entry 13), the catalyst appears to be sensitive to pyrazole NH groups (Table 1, entries 14 and 16). However, simple protection of the nitrogen atom leads to coupling with useful efficiency (Table 1, entries 15 and 17).[10]

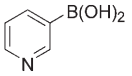
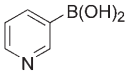
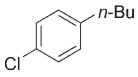
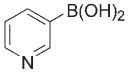
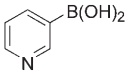
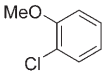
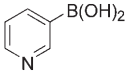
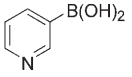
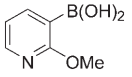
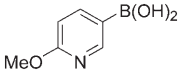
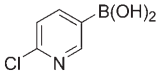
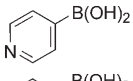
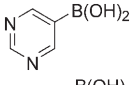
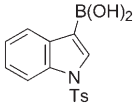
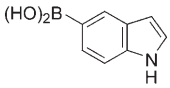
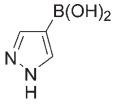
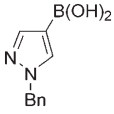
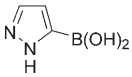
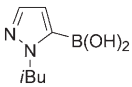
[*] Dr. N. Kudo, Dr. M. Perseghini, Prof. Dr. G. C. Fu
Department of Chemistry
Massachusetts Institute of Technology
Cambridge, MA 02139 (USA)
Fax: (+1) 617-324-3611
E-mail: gcf@mit.edu

[**] We thank Frontier Scientific for boronic acids and Johnson Matthey for $[Pd_2(dba)_3]$. Financial support was provided by the National Institutes of Health (National Institute of General Medical Sciences, R01-GM62871), Merck Research Laboratories, Novartis, Sankyo-Agro Co. Ltd. (N.K.), and Novartis Stiftung (M.P.). Funding for the MIT Department of Chemistry Instrumentation Facility was furnished in part by the National Science Foundation (CHE-9808061 and DBI-9729592).

Supporting information for this article is available on the WWW under http://www.angewandte.org or from the author.

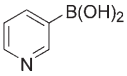
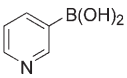
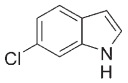
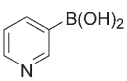
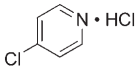
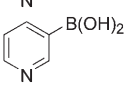
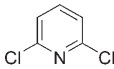
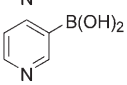
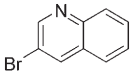
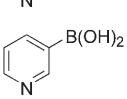
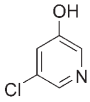
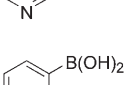
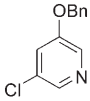
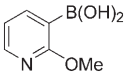
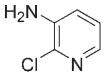
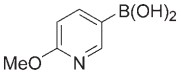
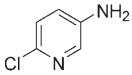
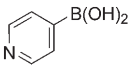
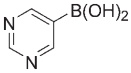
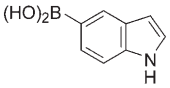
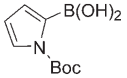
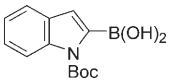
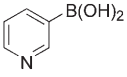
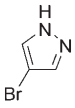
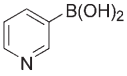
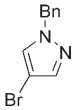
InterScience
© 2006 Wiley-VCH Verlag GmbH & Co. KGaA, Weinheim

Table 1: Suzuki cross-couplings of heteroarylboronic acids with unactivated aryl halides [for the reaction conditions, see Eq. (1)].

Entry	Heteroarylboronic acid	Aryl halide	Yield [%][a]
1			92
2			92
3			95
4			88
5			90
6			91
7			83
8			87
9			85[b]
10			92
11			72
12			85
13			78
14			8
15			64
16			21
17			92

[a] Yield of isolated product (average of two experiments). [b] The product that results from the cross-coupling of the chloride was isolated in 10% yield.

Table 2: Suzuki cross-couplings of heteroarylboronic acids with heteroaryl chlorides and bromides [for the reaction conditions, see Eq. (1)].

Entry	Heteroarylboronic acid	Heteroaryl halide	Yield [%][a]
1			97
2			93
3			98
4			98[b]
5			75
6			87
7			88
8			97
9			95
10			97
11			77
12			89
13			69[c]
14			30[c]
15			< 2
16			73

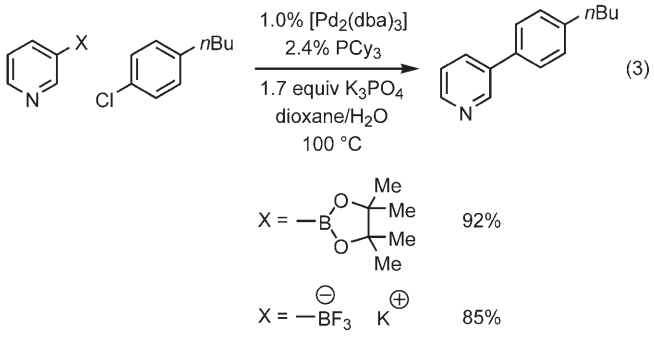
[a] Yield of isolated product (average of two experiments). [b] Double Suzuki cross-coupling (2.2 equiv of the boronic acid, 2.0% $[Pd_2(dba)_3]$, 4.8% PCy_3, and 3.4 equiv of K_3PO_4 were used). [c] The Boc protecting group was removed during the Suzuki reaction.

This catalyst system is also effective for Suzuki cross-couplings in which both of the reaction partners are nitrogen heterocycles, thus providing the desired products in generally good yield (Table 2). Consistent with the example illustrated in entry 13 of Table 1, the method tolerates indole NH groups (Table 2, entries 2 and 12). In addition, pyridines that bear hydroxy (Table 2, entry 6) and NH_2 (Table 2, entries 8 and 9) substituents are suitable substrates. *tert*-Butyloxycarbonyl (Boc) protecting groups at pyrrole and indole nitrogen atoms are cleaved under the cross-coupling conditions

 © 2006 Wiley-VCH Verlag GmbH & Co. KGaA, Weinheim

(entries 13 and 14, respectively).[11] Protection of the pyrazole NH group is necessary for the coupling of a 4-bromopyrazole with 3-pyridineboronic acid (entry 15 vs. 16; see also Table 1, entries 14–17).

In preliminary experiments, we determined that this Pd/PCy_3/K_3PO_4/dioxane/H_2O-based method is effective not only for Suzuki cross-couplings of heteroarylboronic acids, but also for boronate esters and trifluoroborates [Eq. (3)]. Finally, we



(3)

established that the procedure can be conducted on a multigram scale (18 mmol of 4-*n*-butylchlorobenzenechloride + 20 mmol of 3-pyridineboronic acid, yield = 3.4 g (88%) of product).

To the best of our knowledge, this is the most wide-ranging study that has been described for Suzuki reactions of nitrogen-containing cross-coupling partners. Attractive features of this method include its versatility (a single procedure was employed for all of the examples, including boronate esters and trifluoroborates), its compatibility with a variety of unprotected functionalities (e.g., NH_2- and OH-substituted pyridines and unprotected indoles), its convenience (commercially available components), and its efficiency even with inexpensive, unactivated aryl chlorides. We anticipate that this catalyst system will find application in academia and, in particular, in industry.

Experimental Section

General procedure: The heteroarylboronic acid (1.10 mmol), [Pd_2(dba)$_3$] (9.2 mg, 0.010 mmol), and PCy_3 (6.7 mg, 0.024 mmol) were added to a 25-mL Schlenk flask equipped with a stir bar in air. The flask was evacuated and refilled with argon five times. Dioxane (2.67 mL), the (hetero)aryl halide (1.00 mmol; if the halide was a solid, it was added prior to the evacuation/refill cycle), and aqueous K_3PO_4 (1.27 M, 1.33 mL, 1.70 mmol) were added by syringe. The Schlenk flask was sealed and heated in an oil bath at 100 °C for 18 h with vigorous stirring. The mixture was then filtered through a pad of silica gel (washing with EtOAc), the filtrate concentrated under reduced pressure, and the aqueous residue extracted three times with EtOAc. The combined extracts were dried over anhydrous $MgSO_4$, filtered, and concentrated. The residue was then purified by column chromatography on silica gel.

Received: October 1, 2005
Revised: December 12, 2005
Published online: January 19, 2006

Keywords: cross-coupling · heterocycles · homogeneous catalysis · nitrogen · palladium

[1] For leading references, see: a) N. Miyaura in *Metal-Catalyzed Cross-Coupling Reactions* (Eds.: A. de Meijere, F. Diederich), Wiley-VCH, New York, **2004**, chap. 2; b) A. Suzuki in *Handbook of Organopalladium Chemistry for Organic Synthesis* (Ed.: E.-i. Negishi), Wiley Interscience, New York, **2002**, chap. III.2.2.
[2] For an overview, see: A. M. Rouhi, *Chem. Eng. News* **2004**, *82*, 49–58.
[3] For recent reports that include Suzuki reactions of nitrogen heterocycles, see: a) T. E. Barder, S. D. Walker, J. R. Martinelli, S. L. Buchwald, *J. Am. Chem. Soc.* **2005**, *127*, 4685–4696; b) T. E. Barder, S. L. Buchwald, *Org. Lett.* **2004**, *6*, 2649–2652; c) I. Kondolff, H. Doucet, M. Santelli, *Synlett* **2005**, 2057–2061; d) A. E. Thompson, G. Hughes, A. S. Batsanov, M. R. Bryce, P. R. Parry, B. Tarbit, *J. Org. Chem.* **2005**, *70*, 388–390, and references therein.
[4] a) For a discussion of the widespread occurrence of nitrogen heterocycles, particularly pyridines, in pharmaceutically active compounds, see: V. Bonnet, F. Mongin, F. Trecourt, G. Breton, F. Marsais, P. Knochel, G. Queguiner, *Synlett* **2002**, 1008–1010 (footnote 1); b) A. F. Pozharskii, A. T. Soldartenko, A. Katritzky, *Heterocycles in Life and Society*, Wiley, New York, **1997**.
[5] For an overview, see: J. Tsuji, *Palladium Reagents and Catalysts*, Wiley, New York, **2004**.
[6] A. F. Littke, C. Dai, G. C. Fu, *J. Am. Chem. Soc.* **2000**, *122*, 4020–4028; see, also: A. F. Littke, G. C. Fu, *Angew. Chem.* **1998**, *110*, 3586–3587; *Angew. Chem. Int. Ed.* **1998**, *37*, 3387–3388.
[7] For an early report of the use of Pd/PCy_3 for palladium-catalyzed Suzuki reactions, see: W. Shen, *Tetrahedron Lett.* **1997**, *38*, 5575–5578.
[8] For an overview of the use of water as a (co)solvent for Suzuki reactions, see: N. E. Leadbeater, *Chem. Commun.* **2005**, 2881–2902.
[9] For the application of a related system to the cross-coupling of cyclopropylboronic acid with (hetero)aryl bromides, see: D. J. Wallace, C.-y. Chen, *Tetrahedron Lett.* **2002**, *43*, 6987–6990.
[10] For the Suzuki cross-coupling illustrated in entry 15 of Table 1, deboronation is a significant side reaction.
[11] For a previous example, see: C. N. Johnson, G. Stemp, N. Anand, S. C. Stephen, T. Gallagher, *Synlett* **1998**, 1025–1027.

 © 2006 Wiley-VCH Verlag GmbH & Co. KGaA, Weinheim

Enzymes

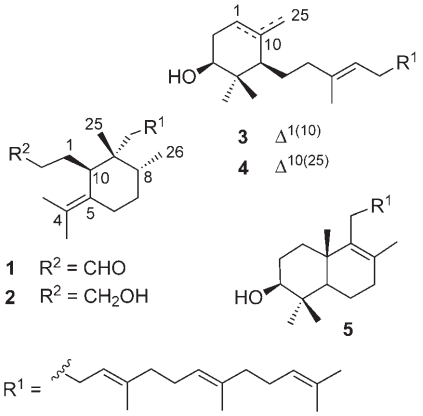
DOI: 10.1002/anie.200503420

An *Arabidopsis* Oxidosqualene Cyclase Catalyzes Iridal Skeleton Formation by Grob Fragmentation**

*Quanbo Xiong, William K. Wilson, and Seiichi P. T. Matsuda**

Oxidosqualene cyclases generate over 100 different triterpene skeletons from a single substrate.[1] This diversity is achieved by variations in three mechanistic motifs: cation–π annulation, cationic migration (including 1,2-shifts and ring expansions), and deprotonation. We encountered a fourth mode while characterizing the *Arabidopsis thaliana* triterpene synthase gene *At5g42600*. The encoded enzyme annulates oxidosqualene to a bicyclic intermediate, which undergoes 1,2-shifts to a C5 cation. Ring A is then cleaved to form the 3,4-*seco* aldehyde **1** by a Grob fragmentation,[2] which has not previously been documented in triterpene biosynthesis. Aldehyde **1** has never been isolated but was hypothesized to be the first carbocyclic precursor[3] in the biosynthesis of iridals. These unusual triterpenoids have been found only in Iridaceae,[3,4] a monocot family that is phylogenetically distant from *Arabidopsis*. Iridals possess diverse biological activities[5] and are the precursors of irones, which give the prized violet scent to orris oil.[3b] Herein, we describe the cloning and heterologous expression of the cyclase gene, the structure elucidation of **1**, the fragmentation mechanism, and phylogenetic implications.

The *At5g42600* gene was amplified by the reverse-transcription polymerase chain reaction (RT-PCR) from *A. thaliana* mRNA and subcloned into the pRS426GAL vector.[6a,b] The resultant plasmid pXQ11.2 was expressed in the yeast hosts SMY8 and RXY6; SMY8 lacks lanosterol synthase,[6c] and RXY6 additionally lacks squalene epoxidase.[6d] Triterpene products were isolated from the non-saponifiable lipids (NSL) of SMY8[pXQ11.2] and identified by GC mass-spectrometric and NMR spectroscopic analysis. We observed only traces of $C_{30}H_{50}O$ triterpene alcohols, namely, **3**,[7a] **4**,[7b] and **5**[7c] (Scheme 1). The predominant product was a novel 3,4-*seco* triterpene alcohol **2** bearing a typical iridal skeleton, and its $C_{30}H_{52}O$ formula suggested a postcyclization reduction. Oxidation of **2** with Dess–Martin periodinane[8] gave the putative precursor **1**, which provided spectral data that enabled us to detect this elusive aldehyde in the NSL of SMY8[pXQ11.2] (Figure 1a). Interestingly, direct hexane extraction of cell homogenates without saponification showed **1** rather than **2** as the major enzymatic product from both in vivo SMY8[pXQ11.2] cultures and an in vitro reaction of RXY6[XQ11.2] with oxidosqualene (Figure 1b,c). These results indicated that **1** was the direct enzymatic product and that **2** arose from further metabolism and/or during saponification.



Scheme 1. MRN1 products: marneral (**1**), marnerol (**2**), camelliol C (**3**), achilleol A (**4**), and tentative structure **5**. Triterpene numbering is used.

The 8α-methyl configuration in **1** and **2** was determined from NOESY spectra and ^{1}H NMR coupling constants.

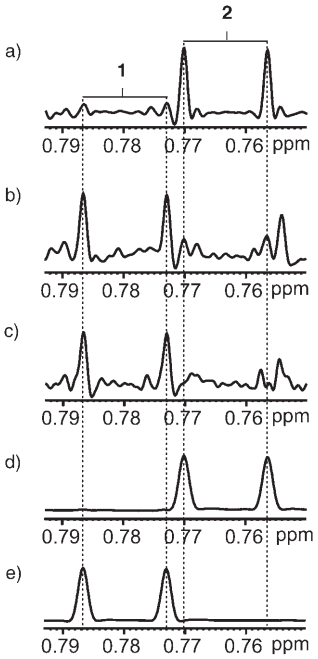


Figure 1. ^{1}H NMR spectra ($CDCl_3$, 500 MHz, 8α-methyl signals) showing the enzymatic formation of **1** versus **2**. a) Hexane extract of the NSL of SMY8[pXQ11.2] cell pellets. b) Hexane extract of SMY8-[pXQ11.2] cell homogenate. c) Hexane extract of RXY6[pXQ11.2] cell homogenates incubated with oxidosqualene. d) Purified sample of **2**. e) Purified sample of **1** from Dess–Martin oxidation. Ratios of **1**/**2** in a), b), and c) were 1:12, 10:3, and 99:1, respectively.

[*] Dr. Q. Xiong, W. K. Wilson, Prof. Dr. S. P. T. Matsuda
Department of Chemistry and
Department of Biochemistry and Cell Biology
Rice University, Houston, TX 77005 (USA)
Fax: (+1) 713-348-5154
E-mail: matsuda@rice.edu

[**] This work was supported by The National Science Foundation (MCB-0209769).

Supporting information for this article is available on the WWW under http://www.angewandte.org or from the author.

© 2006 Wiley-VCH Verlag GmbH & Co. KGaA, Weinheim

Conformational heterogeneity of the cyclohexane ring was taken into account by calculating the Boltzmann distribution from B3PW91/6-311G(2d,p)//B3LYP/6-31G* energies (see the Supporting Information). The results showed the same relative stereochemistry observed in natural 10-deoxy-17-hydroxyiridal,[3a] and thus validated the hypothesis of Marner and Longerich[3] that cyclization of oxidosqualene into iridals proceeds via a B-ring boat intermediate to **1**. In recognition of the pioneering work of Marner on iridals, we named **1** marneral and **2** marnerol. Marneral synthase (MRN1) provides the first definitive example of ring cleavage accompanying oxidosqualene cyclization.

A likely mechanism that leads to **1** is shown in Scheme 2. Oxidosqualene (**6**) is protonated by aspartate 487 and cyclized to the bicyclic carbocation **8**. A series of 1,2-shifts moves H9 to C8, C25 to C9, and H5 to C10 as the positive charge migrates to C5. The last migration forces a conformational reorganization of ring A, which can proceed via twist **9** (inversion of C1) or boat **10** (inversion of C3 and C4) en route to the fully inverted chair **11**. Conformers **10** and **11**, which place the C3–C4 bond in hyperconjugation with the C5 cation, readily form **1** by barrierless[9] Grob fragmentation,[2] with transfer of the 3-hydroxy proton to the hydrogen-bonded aspartate. Conformer **9** may also undergo fragmentation but is hyperconjugatively poised for 4β-methyl migration as well. Other enzymes that generate a C5 cation make Δ5 products by deprotonation at C6 or 3-keto products by 4β-methyl and 3α-hydride shifts. MRN1 avoids these alternatives and accurately selects only the fragmentation pathway. This selectivity appears to be a function of the B-ring conformation and the aspartate mobility.

Sequence alignments for MRN1 revealed distinctive residues that may contribute to its unusual catalytic mechanism (Figure 2). The crystal structure of human lanosterol synthase[14] shows that Cys456 is hydrogen bonded to the protonating aspartate residue (Asp455). Unlike other oxidosqualene cyclases, MRN1 contains glycine in place of cysteine. This modification may facilitate the deprotonation of the axial hydroxy group in **10** and **11** by increasing the mobility and basicity of the aspartate residue in MRN1. MRN1 also differs from other oxidosqualene cyclases by a deletion between positions 730 and 731. Residues in this region are involved in substrate folding to form rings C and D.[1a,c,14] A single-residue deletion in the corresponding region of squalene-hopene cyclase led to incomplete cyclization, with some stereochemical inversion.[15] The deletion in MRN1 may have a similar effect. More detailed understanding of the enzyme mechanism awaits a crystal structure of a marneral synthase.

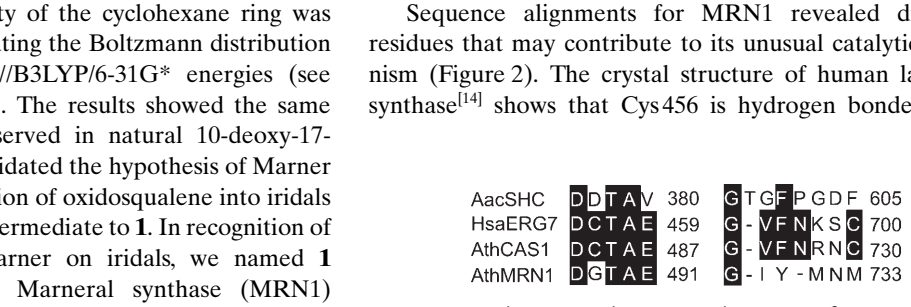
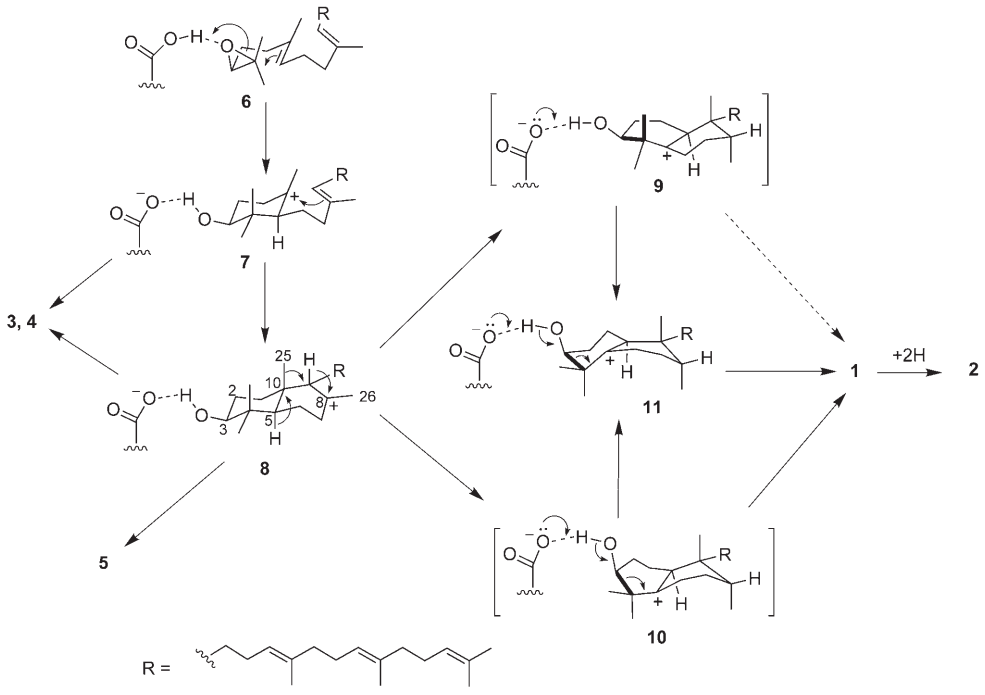


Figure 2. Partial amino acid sequence alignments of MRN1 with squalene-hopene cyclase from *Alicyclobacillus acidocaldarius* (AacSHC),[11] lanosterol synthase from *Homo sapiens* (HsaERG7),[12] and cycloartenol synthase from *A. thaliana* (AthCAS1).[13] More extensive alignments are given in the Supporting Information.



Scheme 2. Suggested mechanistic pathway from oxidosqualene (**6**) to marneral (**1**). Bonds elongated by hyperconjugation with the C5 cation are shown thickened. By-products **3** and **4** could arise from either **8**[10] or **7**.

No monocot marneral synthase has been characterized, but it seems clear that the *Arabidopsis* and *Iris* marneral synthases evolved independently from one another. A phylogenetic tree (see the Supporting Information) shows distant relationships between monocot and eudicot cyclases[16] and indicates that MRN1 arose within the eudicot PEN clade[17] from enzymes that generate the all-chair dammarenyl cation. MRN1 has diverged relatively little from the other PEN genes (70–80% identical) but has developed the ability to cleave ring A and achieved a rare evolutionary transition from a B-ring chair to B-ring boat (**7**) mechanism.[18] This case is a striking example of how enzymes with close phylogenetic affinity can have fundamental differences in mechanism and product structure.

Grob fragmentation is a useful synthetic reaction but its role in natural-products biosynthesis is not widely recognized.[19] Several other 3,4-*seco* triterpenoids with a C4–C5

 © 2006 Wiley-VCH Verlag GmbH & Co. KGaA, Weinheim

tetrasubstituted olefin apparently arise via a B-ring boat intermediate by Grob fragmentation. These include lepidolide[20a] and (24*E*)-3,4-secocucurbita-4,24-diene-3,26-dioic acid[20b] from *Russula lepida*. A similar biosynthetic pathway can be ascribed to camelliol B[7b] and the sesquiterpene coumarins secodriol and secodrial from *Achillea ochroleuca*.[20c] An analogous mechanism via a B-ring chair may pertain to crystallopicrin from *Cortinarius* species,[20d] helianol, isohelianol[20e] and sasanquol from *Camellia sasanqua*,[20f] and graminol A from *Triticum aestivum*.[20g] However, most 3,4-*seco* triterpenoids[21a–d] with a C4–C5 saturated bond arise from a discrete postcyclization step, as do some diterpenoids, such as geayine[21e] and 3,4-secosonderianol.[21f]

In summary, our cloning and characterization of an *Arabidopsis* cyclase uncovered the elusive carbocyclic precursor of iridal triterpenes and provided the first experimental proof of Grob fragmentation in triterpene synthesis. Molecular modeling and sequence comparison suggested how cyclases can modify the reaction kinetics to select either the Grob fragmentation or other termination pathways. The independent development of iridal biosynthesis in monocots and the eudicot PEN clade underscores the complications in using chemotaxonomy to understand phylogenetic relationships and shows that nonsteroidal cyclases can readily evolve to generate diverse triterpene skeletons. Our results exemplify the power of genome mining to reveal novel structures and catalytic activities that conventional analysis of the native organism would not detect.

Experimental Section

cDNA of the *At5g42600* (*PEN5*, 2286 bp) was transcribed from mRNA obtained from 2-day-old *A. thaliana* seedlings. A culture of SMY8[pXQ11.2] (100 mL) was induced with galactose in a synthetic complete medium lacking uracil and grown to saturation with shaking at 30 °C. The cell pellet was saponified with ethanolic KOH at 70 °C for 2 h, followed by extraction with hexane. Analysis of the organic extracts by NMR spectroscopy (500 MHz, $CDCl_3$, 25 °C) and GC-MS (35% phenyl polysiloxane column, 30 m) showed **2** as the only triterpene alcohol. Chromatographic purification (silica gel, CH_2Cl_2/hexane 5:1) of the NSL (48 mg) from a 3-L culture gave, in addition to fractions containing traces of **3**–**5** (< 1% of total enzymatic products), alcohol **2** (1 mg) as a colorless oil: ^{1}H NMR (500 MHz, $CDCl_3$): $\delta =$ 0.764 (d, $J = 6.8$ Hz, 3H), 0.891 (s, 3H), 1.58–1.68 (6 brs, 18H), 1.728 (dqd, $J = 12.8$, 6.8, 4.2 Hz, 1H), 2.560 (dd, $J = 11.6$, 2.6 Hz, 1H), 3.608 (t, $J = 5.6$ Hz, 2H), 5.05–5.11 ppm (m, 3H); ^{13}C NMR (125 MHz, $CDCl_3$): $\delta = 15.6$, 15.9, 16.0, 17.7, 20.2, 20.9, 22.4, 23.4, 24.3, 24.8, 25.7, 26.6, 26.8, 31.0, 31.2, 31.7, 36.2, 39.1, 39.7, 39.8, 44.3, 63.8, 123.4, 124.3, 124.4, 125.7, 131.2, 131.6, 134.2, 134.9 ppm; MS (EI, trimethylsilyl ether) *m*/*z*: 500 [M^+], 69 (base); the carbon skeleton of **2** was elucidated by HSQC, HMBC, and COSYDEC and by comparison with the NMR data for the side chain of thalianol[6d] and camelliol C.[7a] The C8 configuration was deduced as follows: In the NOESY spectrum, H26 correlated with H25 and H11*S*, and H25 correlated with H8 and H10α; the ^{1}H NMR spectrum showed couplings of 12.8 and 4.2 Hz between H8 and the C7 protons; these data are fully compatible with the 8α-methyl chair conformer with the equatorial C8 and C9 methyl groups but are incompatible with any conformer of the 8β-methyl isomer. Conformational analysis and the NOESY spectrum are given in the Supporting Information.

Oxidation of **2** to **1**: Dess–Martin periodinane reagent[8] (100 mg) was added to alcohol **2** (500 μg) in CH_2Cl_2 (2 mL). The reaction mixture was stirred for 24 h at room temperature. After removal of the solvent, the residue was partitioned between hexane/H_2O. The hexane fraction was purified by chromatography on silica gel (CH_2Cl_2/hexane 1:1) to give aldehyde **1** in 80% yield as a colorless oil: ^{1}H NMR (500 MHz, $CDCl_3$): $\delta = 0.780$ (d, 6.8 Hz, 3H), 0.920 (s, 3H), 1.57–1.68 (6 brs, 18H), 1.750 (1H, dqd, $J = 12.5$, 6.8, 4.0 Hz, 1H), 2.556 (dd, $J = 12.0$, 3.8 Hz, 1H), 5.04–5.11 (m, 3H), 9.710 ppm (t, $J =$ 1.8 Hz, 1H); ^{13}C NMR (125 MHz, $CDCl_3$): $\delta = 15.5$, 15.9, 16.0, 17.7, 19.0, 20.2, 20.8, 22.3, 24.2, 24.8, 25.7, 26.7, 26.7, 30.7, 31.6, 36.0, 39.0, 39.7, 39.7, 42.3, 43.9, 124.2, 124.2, 124.8, 125.3, 130.6, 131.2, 134.2, 134.9, 203.2 ppm; MS (EI) *m*/*z*: 426 [M^+], 207, 187, 69 (base).

The samples for the NMR data in Figure 1a,b were obtained from 30-mL cultures of SMY8[pXQ11.2] by a) extraction with hexane of the NSL from the cell pellet or b) by precipitation of homogenized cells with ethanol, partial evaporation of the supernatant, and extraction with hexane. The samples for Figure 1c were obtained by incubation of a cell homogenate from a 30-mL RXY6[pXQ11.2] culture with 2,3-oxidosqualene for 16 h at ambient temperature, followed by the workup used in (b).[22]

Received: September 28, 2005

Keywords: cyclization · fragmentation · iridals · oxidosqualene · terpenoids

[1] a) K. U. Wendt, G. E. Schulz, E. J. Corey, D. R. Liu, *Angew. Chem.* **2000**, *112*, 2930–2952; *Angew. Chem. Int. Ed.* **2000**, *39*, 2812–2833; b) R. Xu, G. C. Fazio, S. P. T. Matsuda, *Phytochemistry* **2004**, *65*, 261–291; c) K. U. Wendt, *Angew. Chem.* **2005**, *117*, 4032–4037; *Angew. Chem. Int. Ed.* **2005**, *44*, 3966–3971.

[2] a) C. A. Grob, P. W. Schiess, *Angew. Chem.* **1967**, *79*, 1–14; *Angew. Chem. Int. Ed. Engl.* **1967**, *6*, 1–15; b) C. A. Grob, *Angew. Chem.* **1969**, *81*, 543–554; *Angew. Chem. Int. Ed. Engl.* **1969**, *8*, 535–546; c) P. Weyerstahl, H. Marschall in *Comprehensive Organic Synthesis, Vol. 6* (Eds.: B. M. Trost, I. Fleming), Pergamon, Oxford, **1991**, pp. 1041–1070; d) T. Constantieux, J. Rodriguez in *Science of Synthesis: Houben–Weyl Methods of Molecular Transformations, Vol. 26* (Ed.: J. Cossy), Georg Thieme, New York, **2005**, pp. 413–462.

[3] a) F.-J. Marner, I. Longerich, *Liebigs Ann. Chem.* **1992**, 269–272; b) F.-J. Marner, *Curr. Org. Chem.* **1997**, *1*, 153–186.

[4] H. Ito, S. Onoue, Y. Miyake, T. Yoshida, *J. Nat. Prod.* **1999**, *62*, 89–93.

[5] a) T. Yoshida, H. Ito, *Curr. Top. Phytochem.* **2000**, *4*, 135–145; b) J.-P. Bonfils, F. Pinguet, S. Culine, Y. Sauvaire, *Planta Med.* **2001**, *67*, 79–81; c) L. Shao, N. E. Lewin, P. S. Lorenzo, Z. Hu, I. J. Enyedy, S. H. Garfield, J. C. Stone, F.-J. Marner, P. M. Blumberg, S. Wang, *J. Med. Chem.* **2001**, *44*, 3872–3880; d) K. Takahashi, S. Suzuki, Y. Hano, T. Nomura, *Biol. Pharm. Bull.* **2002**, *25*, 432–436; e) F. Benoit-Vical, C. Imbert, J. P. Bonfils, Y. Sauvaire, *Phytochemistry* **2003**, *62*, 747–751.

[6] a) H. Liu, J. Krizek, A. Bretscher, *Genetics* **1992**, *132*, 665–673; b) J. B. R. Herrera, B. Bartel, W. K. Wilson, S. P. T. Matsuda, *Phytochemistry* **1998**, *49*, 1905–1911; c) E. J. Corey, S. P. T. Matsuda, C. H. Baker, A. Y. Ting, H. Cheng, *Biochem. Biophys. Res. Commun.* **1996**, *219*, 327–331; d) G. C. Fazio, R. Xu, S. P. T. Matsuda, *J. Am. Chem. Soc.* **2004**, *126*, 5678–5679.

[7] a) T. Akihisa, K. Arai, Y. Kimura, K. Koike, W. C. M. C. Kokke, T. Shibata, T. Nikaido, *J. Nat. Prod.* **1999**, *62*, 265–268; b) A. F. Barrero, E. J. Alvarez-Manzaneda Roldan, R. Alvarez-Manzaneda Roldan, *Tetrahedron Lett.* **1989**, *30*, 3351–3352; c) for the tentative structural evidence suggested by ^{1}H NMR spectroscopic and GC mass-spectrometric analysis, see the Supporting Information.

[8] D. B. Dess, J. C. Martin, *J. Org. Chem.* **1983**, *48*, 4155–4156.

[9] A cross-section of the potential energy surface was obtained by varying the C3–C4 bond lengths in **10** and **11**, as described in the

 © 2006 Wiley-VCH Verlag GmbH & Co. KGaA, Weinheim

Supporting Information; the energy decreased with essentially no barrier as the C3–C4 bond was broken and the 3-hydroxy proton was transferred to aspartate (modeled as acetate stabilized by two hydrogen-bonded water molecules).

[10] Molecular modeling suggested that monocycles **3** and **4** might arise from a bicyclic cation by a mechanism that we now identify as Grob fragmentation; see the Supporting Information for Q. Xiong, X. Zhu, W. K. Wilson, A. Ganesan, S. P. T. Matsuda, *J. Am. Chem. Soc.* **2003**, *125*, 9002 – 9003.

[11] D. Ochs, C. Kaletta, K.-D. Entian, A. Beck-Sickinger, K. Poralla, *J. Bacteriol.* **1992**, *174*, 298 – 302.

[12] a) C. H. Baker, S. P. T. Matsuda, D. R. Liu, E. J. Corey, *Biochem. Biophys. Res. Commun.* **1995**, *213*, 154 – 160; b) C. K. Sung, M. Shibuya, U. Sankawa, Y. Ebizuka, *Biol. Pharm. Bull.* **1995**, *18*, 1459 – 1461.

[13] E. J. Corey, S. P. T. Matsuda, B. Bartel, *Proc. Natl. Acad. Sci. USA* **1993**, *90*, 11628 – 11632.

[14] R. Thoma, T. Schulz-Gasch, B. D'Arcy, J. Benz, J. Aebi, H. Dehmlow, M. Hennig, M. Stihle, A. Ruf, *Nature* **2004**, *432*, 118 – 122.

[15] T. Hoshino, K. Shimizu, T. Sato, *Angew. Chem.* **2004**, *116*, 6868 – 6871; *Angew. Chem. Int. Ed.* **2004**, *43*, 6700 – 6703.

[16] These relationships are also supported by the following reports: a) K. Haralampidis, G. Bryan, X. Qi, K. Papadopoulou, S. Bakht, R. Melton, A. Osbourn, *Proc. Natl. Acad. Sci. USA* **2001**, *98*, 13431 – 134316; b) X. Qi, S. Bakht, M. Leggett, C. Maxwell, R. Melton, A. Osbourn, *Proc. Natl. Acad. Sci. USA* **2004**, *101*, 8233 – 8238.

[17] T. Husselstein-Muller, H. Schaller, P. Benveniste, *Plant Mol. Biol.* **2001**, *45*, 75 – 92.

[18] This mechanistic transition is rare, at least among tetra- and pentacyclic triterpenes: Q. Xiong, F. Rocco, W. K. Wilson, R. Xu, M. Ceruti, S. P. T. Matsuda, *J. Org. Chem.* **2005**, *70*, 5362 – 5375.

[19] The lability of **1** and the weak expression of *MRN1* in *A. thaliana* suggest that **1** and other potential fragmentation products may easily be overlooked in surveys of natural products; for microarray results of MRN1, see: https://www.genevestigator.ethz.ch/ and P. Zimmermann, M. Hirsch-Hoffmann, L. Hennig, W. Gruissem, *Plant Physiol.* **2004**, *136*, 2621 – 2632.

[20] a) J. W. Tan, Z. J. Dong, Z. H. Ding, J. K. Liu, *Z. Naturforsch. C* **2002**, *57*, 963 – 965; b) J. W. Tan, Z. J. Dong, J. K. Liu, *Helv. Chim. Acta* **2000**, *83*, 3191 – 3197; c) H. Greger, O. Hofer, W. Robien, *Phytochemistry* **1983**, *22*, 1997 – 2003; d) W. Steglich in *Biologically Active Molecules* (Ed.: U. P. Schlunegger), Springer, Berlin, **1989**, pp. 1 – 8; e) T. Akihisa, Y. Kimura, K. Koike, T. Shibata, Z. Y. Yoshida, T. Nikaido, T. Tamura, *J. Nat. Prod.* **1998**, *61*, 409 – 412; f) T. Akihisa, K. Yasukawa, Y. Kimura, S. Yamanouchi, T. Tamura, *Phytochemistry* **1998**, *48*, 301 – 305; g) T. Akihisa, K. Koike, Y. Kimura, N. Sashida, T. Matsumoto, M. Ukiya, T. Nikaido, *Lipids* **1999**, *34*, 1151 – 1157.

[21] a) W. J. Baas, *Phytochemistry* **1985**, *24*, 1875 – 1889; b) J. D. Connolly, R. A. Hill, *Nat. Prod. Rep.* **2002**, *19*, 494 – 513; c) J. D. Connolly, R. A. Hill, *Nat. Prod. Rep.* **2003**, *20*, 640 – 659; d) L. M. Liao, P. C. Vieira, E. Rodrigues-Filho, J. B. Fernandes, M. F. G. F. Silva, *Z. Naturforsch. C* **2002**, *57*, 403 – 406; e) G. Palazzino, E. Federici, P. Rasoanaivo, C. Galeffi, F. Delle Monache, *Gazz. Chim. Ital.* **1997**, *127*, 311 – 314; f) A. A. Craveiro, E. R. Silveiro, *Phytochemistry* **1982**, *21*, 2571 – 2574.

[22] The Supporting Information contains additional details on cloning, transformation, expression, saponification, isolation, structure elucidation of **1**–**5**, NMR spectral data, GC-MS data, molecular modeling, sequence alignments, and phylogenetic analysis.

 © 2006 Wiley-VCH Verlag GmbH & Co. KGaA, Weinheim

Rhodium Nanoparticles

DOI: 10.1002/anie.200503174

Synthesis, Stability, and Surface Plasmonic Properties of Rhodium Multipods, and Their Use as Substrates for Surface-Enhanced Raman Scattering**

*Nobuyuki Zettsu, Joseph M. McLellan, Benjamin Wiley, Yadong Yin, Zhi-Yuan Li, and Younan Xia**

Controlling the shape of nanocrystals is critical to modern materials chemistry because the intrinsic properties of most nanomaterials are strongly dependent on their shape.[1] Tripod and tetrapod shapes have recently attracted much attention owing to their potential use as building blocks in the fabrication of complex, multiple-terminal devices through self-assembly.[2] Multipods made of type II–VI semiconductors, such as CdSe,[3] CdS,[4] and CdTe[5], have been known for several years. A key parameter for growing multipods of these solid materials is the energy difference between the zinc blend and wurtzite structures at certain temperatures, as one structure may be preferred during nucleation and the other during growth.[5] As most metals only exist in one crystal structure (often in the face-centered-cubic lattice), it is more challenging to grow branched nanocrystals from metals;[6] it

[*] Dr. N. Zettsu, J. M. McLellan, Prof. Y. Xia
Department of Chemistry
University of Washington
Seattle, WA 98195-1700 (USA)
Fax: (+1) 206-685-8665
E-mail: xia@chem.washington.edu

B. Wiley
Department of Chemical Engineering
University of Washington
Seattle, WA 98195 (USA)

Dr. Y. Yin
The Molecular Foundry
Lawrence Berkeley National Laboratory
Berkeley, CA 94720 (USA)

Prof. Z.-Y. Li
Laboratory of Optical Physics
Institute of Physics
Chinese Academy of Sciences
Beijing 100080 (P.R. China)

[**] This work was supported in part by a grant from the NSF (DMR-0451788) and a fellowship from the David and Lucile Packard Foundation. Y.X. is a Camille Dreyfus Teacher Scholar (2002). N.Z. was partially supported by a research fellowship from the Japan Society for the Promotion of Science (JSPS). B.W. thanks the Center for Nanotechnology at the UW for a fellowship. Z.-Y.L. was supported by the National Key Basic Research Special Foundation of China (Grant No. 2004CB719804). This work used the Nanotech User Facility (NTUF), a member of the National Nanotechnology Infrastructure Network (NNIN) funded by the NSF. We thank the Molecular Foundry at the Lawrence Berkeley National Laboratory for the HRTEM analysis.

Supporting information for this article is available on the WWW under http://www.angewandte.org or from the author.

WILEY InterScience DISCOVER SOMETHING GREAT
© 2006 Wiley-VCH Verlag GmbH & Co. KGaA, Weinheim

will be very difficult at least, if not impossible, to achieve branched growth by means of structural transformation between the nucleation and growth steps. Nevertheless, a number of noble metals including Au,[7] Pt,[8] and Rh[9] have recently been demonstrated to form branched nanocrystals. The use of a capping agent such as cetyltriethylammonium bromide (CTAB) or poly(vinyl pyrrolidone) (PVP) is imperative, however, and this is probably just one of the prerequisites for achieving a branched morphology. The growth mechanism is yet to be completely understood for these systems.

Herein, we report the synthesis of Rh multipods as well as their stability, surface plasmonic properties, and use as substrates for surface-enhanced Raman scattering (SERS). Toshima and co-workers first reported their observation of branched Rh nanocrystals in the late 1970s.[9a] Most recently, Tilley and co-workers reported the polyol synthesis of Rh multipods and proposed a mechanism based on homogenous nucleation and seeded growth to account for the anisotropic growth.[9b] However, neither of these reports described any appealing properties associated with the Rh multipods. We also note that in both cases, the arms of the branched nanostructures were rather short, which could possibly be related to the involvement of water in the reaction media.[10] Here, we demonstrate that Rh multipods can be synthesized in high yields when anhydrous Na_3RhCl_6 (rather than $RhCl_3{\cdot}n\,H_2O$) is used as a precursor of Rh. We also report that the branched morphology can only prevail when oxygen is excluded from the reaction system. Otherwise, oxidative etching and Ostwald ripening would transform the branched nanocrystals into spheres in an effort to minimize the total surface energy.

The branched Rh nanocrystals were synthesized through a polyol process. In a typical procedure, Na_3RhCl_6 and PVP were separately dissolved in ethylene glycol and the two solutions were injected simultaneously into ethylene glycol (preheated to 140 °C) by a syringe pump. The color of the solution rapidly turned from rose pink to dark brown within 1 min, indicating the formation of Rh nanocrystals as $RhCl_6^{3-}$ was reduced by ethylene glycol. The as-obtained Rh nanocrystals were characterized using transmission electron microscopy (TEM). Figure 1 shows TEM images taken from a series of samples that were prepared by increasing the reaction time from 5 min to 48 h. In the initial stage of the reaction (Figure 1a and b), the particles exhibited a well-defined, branched morphology with three (tripod) or four (tetrapod) arms. Among them, tripods were in the majority, comprising approximately 70% of the total particle population. The arms were roughly 11 nm long at $t = 10$ min, but the apparent arm size varied slightly as a result of the difference in their orientation on the TEM grid. High-resolution TEM (HRTEM) studies clearly showed that the same fringe pattern continuously extended throughout each branched nanocrystal, suggesting the formation of a single crystal (Figure 1c). The interplanar distance was measured to be 0.22 nm. This value could be assigned to the spacing between {111} planes, implying that the arms grew in the ⟨111⟩ directions. Powder X-ray diffraction (XRD) patterns (see Supporting Information) of the as-prepared Rh multipods exhibited three peaks

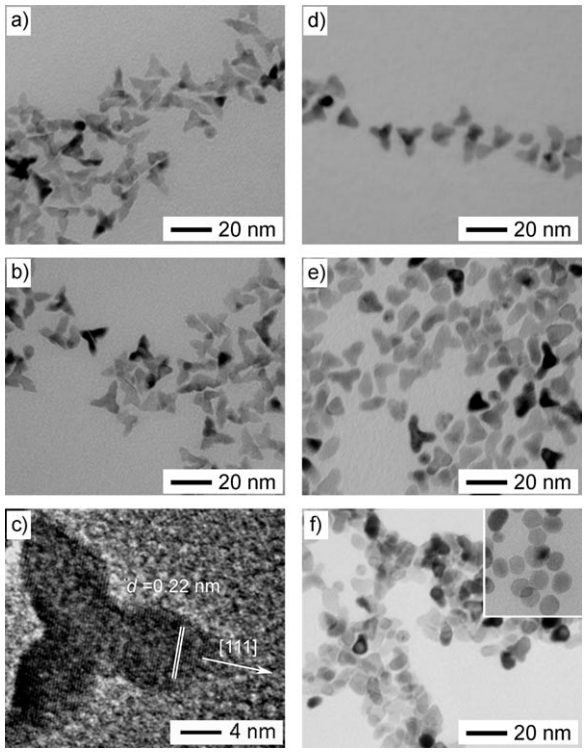


Figure 1. TEM images of Rh nanocrystals synthesized in air at 140 °C for different periods of time: a) 5 min; b) 10 min; c) 10 min (HRTEM image); d) 90 min; e) 6 h; and f) 48 h. The inset in (f) shows a TEM image of the sample at $t = 120$ h.

in the range $35° < 2\theta < 80°$ which correspond to the (111), (200), and (220) diffractions from face-centered-cubic Rh (JCPDS #05-0685).

As the reaction continued (Figure 1d and e), the overall length-to-width aspect ratio of the arm decreased as compared to the sample shown in Figure 1b. The branched Rh nanocrystals slowly evolved into rice-shaped particles at $t =$ 48 h and eventually became spheres at $t = 120$ h. The overall size of the nanocrystal also decreased in this process. The transformation from the branched shape into a spherical one could be interpreted in terms of oxidative etching and Ostwald ripening. Like other face-centered-cubic metals, the surface energy of Rh decreases in the order of (110), (100), and (111).[11] In an effort to minimize the total surface energy, the arm was slowly etched from the tip and the resultant Rh ions were reduced and deposited on the central portion of the nanocrystal to increase the percentage of (111) facets on the surface. Comparison of the intensity ratios of XRD peaks indicates that the transformation of shape resulted in a decrease in the proportion of higher energy (110) facets on the nanocrystals (see Supporting Information). As demonstrated for both Ag and Pd,[12] the oxygen in air plays a key role in the morphological evolution. Continuous bubbling of Ar during the synthesis greatly improved the stability of the branched Rh nanocrystals. Figure 2 shows TEM images of Rh nanocrystals that were obtained under Ar protection at $t = 10$ min and 48 h, respectively. From these images, it is apparent that the branched morphology could be

 © 2006 Wiley-VCH Verlag GmbH & Co. KGaA, Weinheim

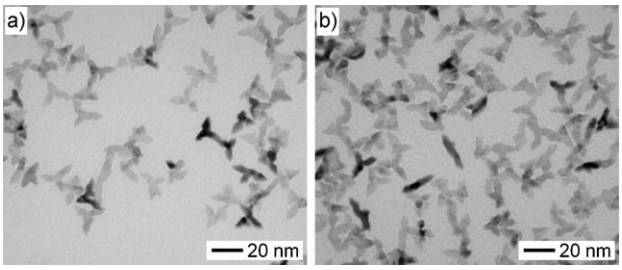


Figure 2. TEM images of Rh nanocrystals synthesized under Ar at 140 °C for a) 10 min and b) 48 h.

preserved for a long period of time when oxidative etching was excluded from the synthesis.

The UV/Vis absorption spectrum of the branched Rh nanocrystals displayed an attractive surface plasmon resonance (SPR) feature (Figure 3 a); a weak and broad peak

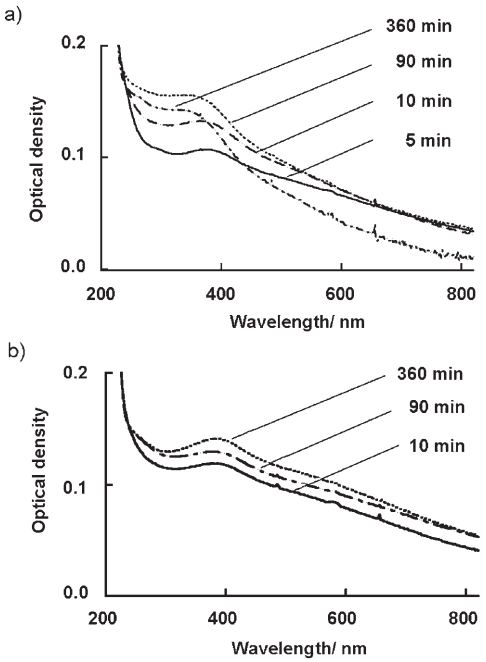


Figure 3. UV/Vis spectra of the Rh nanocrystals as a function of reaction time. The reaction was performed under a) air and b) continuous bubbling of Ar gas. Note that the surface plasmon resonance peak of the Rh multipods was shifted toward shorter wavelengths with increasing reaction time when air was present in the synthesis.

around 380 nm appeared in the initial stage of the reaction. It is well documented that both thin films and spherical nanoparticles of Rh do not exhibit any extinction peaks in the visible region as a result of the very small imaginary part of the dielectric constant.[13] To understand this optical feature, we carried out discrete dipole approximation (DDA) calculations for an individual Rh spherical particle of 10 nm diameter and a tripod nanocrystal featuring an outer triangle of 19 nm, a thickness of 5 nm, and an inner angle of 120° (see Supporting Information).[14] In general, if the geometric parameters are known, DDA calculations can predict the contributions of scattering and absorption to the extinction spectra as well as the peak positions. The calculations indicate that a spherical particle has an SPR peak in the deep UV region while the tripod displays a peak around 380 nm. Although the tripod was assumed to have a planar structure to save computational time, the DDA calculation nearly replicated the observed UV/Vis absorption spectrum of the branched Rh nanocrystals. The experimental spectrum displayed a somewhat broader resonance peak, which is most likely caused by the variation in both shape and size of the Rh nanocrystals in the real sample. In the presence of air, the SPR peak shifted toward shorter wavelengths as the reaction proceeded (Figure 3 a). This shift can be attributed to the transformation from the branched shape into a spherical one. The spectral changes indicate that oxidative etching had already started at about 10 minutes into the reaction. In contrast, the position of the SPR peak remained unchanged over time (see Figure 3 b) when the reaction was carried out under Ar. The peak gradually became more intense with the reaction time. This observation implies that protection by Ar not only promoted anisotropic growth but also helped to preserve the less stable, branched morphology.

We also systematically varied the reaction conditions to find the optimal parameters for generating branched Rh nanocrystals. In general, both the reaction temperature and the concentration of the precursor played important roles in determining the morphology of the product. As compared to the sample prepared at 140 °C, a decrease in the temperature (e.g., to 110 °C, Figure 4 a) led to the formation of branched structures with higher aspect ratios (with arms ca. 2 nm wide by ca. 10–11 nm long). In contrast, relatively isotropic, cubelike nanocrystals were obtained at a higher temperature (180 °C, Figure 4 b). When the reaction conditions were fixed at 140 °C and 10 min, a decrease in the concentration of Na_3RhCl_6 by five times (to 5 mM, Figure 4 c) resulted in embryonic multipods that featured largely faceted rather than

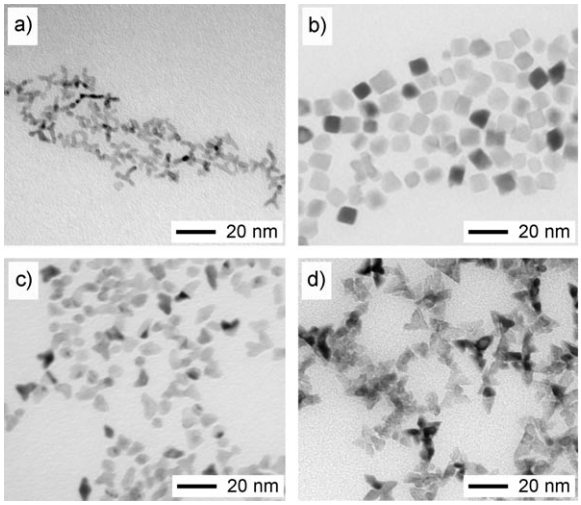


Figure 4. TEM images showing the effects of temperature and the concentration of the precursor on the formation of branched Rh nanocrystals: a) 25 mM Na_3RhCl_6 at 110 °C; b) 25 mM Na_3RhCl_6 at 180 °C; c) 5 mM Na_3RhCl_6 at 140 °C; and d) 50 mM Na_3RhCl_6 at 140 °C. All samples were collected at $t = 10$ min into the reaction.

 © 2006 Wiley-VCH Verlag GmbH & Co. KGaA, Weinheim

spherical nanostructures. When the concentration of Na_3RhCl_6 was doubled (to 50 mM, Figure 4d), the branched morphology was also observed. Interestingly, the majority of these nanostructures were tetrapods rather than tripods.

As the thermodynamically favored particle shape of a face-centered-cubic metal is a truncated octahedron, the branched morphology must be a kinetically controlled product. The finding that anisotropic growth prevailed at relatively lower temperatures is consistent with the results that were recently obtained for Rh multipods synthesized through a different polyol process.[9b] Chen et al. proposed that the shape of a particle of gold (or another face-centered-cubic metal) is mainly determined by the competitive growth along the ⟨111⟩ and ⟨100⟩ directions.[7a] As the reaction temperature was increased, the rates of growth along these two directions were decreased to generate cubic nanocrystals. The shape of Rh nanocrystals was also strongly dependent on the concentration of the precursors. Although branched seeds were formed at all concentrations of Na_3RhCl_6 examined in the present work (5, 25, and 50 mM), TEM studies revealed no additional growth of the crystals and a drastic transformation of their shape with time in the case of 5 mM Na_3RhCl_6. These observations indicate that most of the precursor was consumed in the nucleation stage. In comparison, there was precursor left in the solution after nucleation when higher concentrations (e.g., 25 and 50 mM) of Na_3RhCl_6 were involved. As a result, the arms of each branched seed could continue to grow. As long as the difference in growth rate along the ⟨111⟩ and ⟨100⟩ directions was maintained, the branched nanocrystals could grow into larger dimensions without a change in their morphology.

The interesting plasmonic properties of these multipods may make them attractive for use as SERS substrates. One of the primary enhancement mechanisms in SERS is a result of electromagnetic enhancement arising from the extremely high local fields due to surface plasmon resonance (SPR).[15] Previous explorations of SERS on Group VIIIB metals such as Rh have suffered from fairly weak enhancement.[16] However, these studies have mainly focused on Rh-coated electrodes or Rh particles less than 10 nm in size, none of which exhibited any SPR features in the visible region. Figure 5 compares the SERS activities of thin films cast from three types of Rh nanocrystals: a) multipods synthesized under Ar, b) multipods synthesized in air, and c) nanocubes. The nanocubes of 9 nm in edge length exhibited a SPR peak at 250 nm, while the multipods showed SPR peaks at 360 nm and 380 nm for those synthesized in air and under Ar, respectively. We selected 4-mercaptopyridine (4-MP) as a probe molecule because it has a large scattering cross-section[17] and it has been well studied.[18] Using films that had been modified with 4-MP, it was found that both of the multipod samples gave well-defined, relatively strong SERS signals while the signal from the cubes was quite weak. The multipods prepared under Ar had the highest activity, with an enhancement that was 19 times stronger than that for the nanocubes. These results suggest a trend of stronger SERS signal with a red shift in the SPR peak. It is also possible that the sharp tips of the multipods provided additional enhancement. Recent studies have shown that nanoparticles with

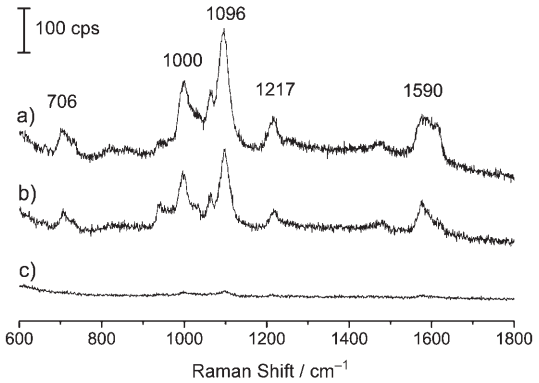


Figure 5. SERS spectra (cps = counts per second) of 4-mercaptopyridine on films of Rh nanocrystals: a) multipods synthesized under Ar (see Figure 2b); b) multipods synthesized in air (see Figure 1a); and c) 9-nm wide cubes (see Figure 4b).

sharp corners or edges are especially active SERS substrates, as the local value of $|E|^2$ at the tips can be more than 500 times that of the applied field.[19] While the SERS results shown here are purely qualitative, the high-quality spectra obtained with the Rh multipods are encouraging and may warrant further exploration.

In summary, we have demonstrated that Rh multipods can be prepared in large quantities by reducing Na_3RhCl_6 with ethylene glycol in the presence of PVP. These highly branched nanocrystals are not stable in air at elevated temperatures; they are slowly converted into spherical particles when the synthesis was allowed to proceed for long periods of time. We believe the formation of multipods is a kinetically controlled process, and thus parameters such as precursor concentration and temperature both play important roles in controlling the morphology of the product. When the synthesis was protected with continuous bubbling of Ar, both the anisotropy in growth and the stability of the product could be enhanced. The optical properties of the tripods were experimentally and theoretically investigated by UV/Vis spectroscopy and DDA calculations, with both methods indicating the presence of an SPR peak around 380 nm for the tripods. These Rh multipods display unprecedented SERS activities, which may find use in applications such as the in situ monitoring of catalytic reactions.[20]

Experimental Section

In a typical synthesis, ethylene glycol (EG; J. T. Baker; 2 mL) was placed in a three-necked flask equipped with a reflux condenser and a magnetic stirrer bar embedded in PYREX glass and heated in air at the designated temperature (e.g., 110, 140, or 180 °C) for 1.5 h. A temperature controller (ACE, 12125–14) equipped with a probe (ChemGlass, 104 TC105) and mantle heater (Electrothermal, HM0050-HS1) was used to maintain the temperature. In separate vials, Na_3RhCl_6 (34.6 mg, 9.0×10^{-2} mmol, Aldrich) and poly(vinyl pyrrolidone) (PVP; $M_r = 55\,000$, Aldrich; 51.3 mg, 4.5×10^{-1} mmol in terms of the repeating unit) were each dissolved in EG (0.8 mL) at room temperature. The molar ratio of Na_3RhCl_6 and the repeating unit of PVP was controlled at 1:5. These two solutions in EG were injected simultaneously into the heated EG using a syringe pump at a rate of 0.2 mL min^{-1}. All of the precursor was reduced to Rh

 © 2006 Wiley-VCH Verlag GmbH & Co. KGaA, Weinheim

multipods, as indicated by UV/Vis spectroscopy. The reaction was continued up to 120 h. A set of samples was taken over the course of each synthesis using a glass pipette. For synthesis performed under Ar, all other experimental parameters were kept the same except for the continuous bubbling of Ar gas. The product was collected by centrifugation and washed with acetone and water several times to remove EG and excess PVP.

The as-obtained samples were characterized by transmission electron microscopy (TEM; JEOL 1200EX II, operated at 80 kV), powder X-ray diffraction (XRD; Philips 1820 diffractometer, $\lambda = 0.154180$ nm), and UV/Vis spectroscopy (Hewlett Packard 8452A diode-array spectrometer). TEM samples were prepared by placing a drop of the aqueous suspension on a carbon-coated copper grid (Ted Pella, Redding, CA), and drying under ambient conditions. The substrate for surface-enhanced Raman scattering (SERS) was prepared by drying a 3-μL aliquot of the final product on a 25-nm thick Al film supported on a Si wafer. The sample was then incubated in an aqueous solution of 4-mercaptopyridine (4 mM) for 1 h, rinsed with deionized water, and dried in air. SERS spectra were obtained with laser excitation (3 mW at the sample) at 785 nm (Renishaw HPNIR785 laser) and a spot size of approcimately 1.6 μm using a Leica DM IRBE optical microscope equipped with a Renishaw inVia Raman spectrometer and a thermoelectrically cooled CCD detector.

Received: September 7, 2005
Published online: January 17, 2006

Keywords: nanostructures · Raman spectroscopy · rhodium · surface plasmon resonance

[1] a) Y. Xia, P. Yang, Y. Sun, Y. Wu, B. Mayers, B. Gates, Y. Yin, F. Kim, H. Yan, *Adv. Mater.* **2003**, *15*, 353 – 389; b) Y. Xia, N. J. Halas, *MRS Bull.* **2005**, *30*, 338 – 348; c) Y. Sun, Y. Xia, *Science* **2002**, *298*, 2176 – 2179; d) E. C. Scher, L. Manna, A. P. Alivisatos, *Philos. Trans. R. Soc. London Ser. A* **2003**, *361*, 241 – 257; e) P. Yang, *MRS Bull.* **2005**, *30*, 85 – 91; f) C. J. Murphy, *Science* **2002**, *298*, 2139 – 2141.

[2] a) D. J. Milliron, S. M. Hughes, Y. Cui, L. Manna, J. Li, L.-W. Wang, A. P. Alivisatos, *Nature* **2004**, *430*, 190 – 195; b) D. L. Wang, C. M. Lieber, *Nat. Mater.* **2003**, *2*, 355 – 356.

[3] a) L. Manna, E. C. Scher, A. P. Alivisatos, *J. Am. Chem. Soc.* **2000**, *122*, 12700 – 12706; b) X. Peng, *Adv. Mater.* **2003**, *15*, 459 – 463; c) Z. A. Peng, X. Peng, *J. Am. Chem. Soc.* **2002**, *124*, 3343 – 3353.

[4] a) Y. W. Jun, S. M. Lee, N. J. Kang, J. Cheon, *J. Am. Chem. Soc.* **2001**, *123*, 5150 – 5151; b) M. Chen, J. Lu, S. Zhang, Y. Xie, Y. Xiong, Y. Qian, X. Liu, *J. Mater. Chem.* **2002**, *12*, 748 – 753.

[5] a) L. Manna, D. J. Milliron, A. Meisel, E. C. Scher, A. P. Alivisatos, *Nat. Mater.* **2003**, *2*, 382 – 385; b) C. Y. Yeh, Z. W. Lu, S. Froyen, A. Zunger, *Phys. Rev. B* **1992**, *46*, 10086 – 10097.

[6] C. Kittel, *Introduction to Solid State Physics*, 7th ed., Wiley, New York, **1996**.

[7] a) S. Chen, Z. L. Wang, J. Ballato, S. H. Foulger, D. Carroll, *J. Am. Chem. Soc.* **2003**, *125*, 16186 – 16187; b) E. Hao, R. C. Bailey, G. C. Schatz, J. T. Hupp, S. Li, *Nano Lett.* **2004**, *4*, 327 – 330.

[8] a) J. Chen, T. Herricks, Y. Xia, *Angew. Chem.* **2005**, *117*, 2645 – 2648; *Angew. Chem. Int. Ed.* **2005**, *44*, 2589 – 2592; b) T. Herricks, J. Chen, Y. Xia, *Nano Lett.* **2004**, *4*, 2367 – 2371; c) X. Teng, H. Yang, *Nano Lett.* **2005**, *5*, 885 – 891.

[9] a) H. Hirai, Y. Nakao, N. Toshima, *J. Macromol. Sci. Chem. A* **1978**, *12*, 1117 – 1141; b) J. D. Hoefelmeyer, K. Niesz, G. A. Somorjai, D. Tilley, *Nano Lett.* **2005**, *5*, 435 – 438.

[10] We were unable to synthesize well-defined Rh multipods when $RhCl_3 \cdot n H_2O$ was used as a precursor. Water seems to enhance oxidative etching and thus greatly modify the shape of a nanocrystal.

[11] Q. Jiang, H. M. Lu, M. Zhao, *J. Phys. Condens. Matter* **2004**, *16*, 521 – 530.

[12] a) B. Wiley, T. Herricks, Y. Sun, Y. Xia, *Nano Lett.* **2004**, *4*, 1733 – 1739; b) Y. Xiong, J. Chen, B. Wiley, Y. Xia, S. Aloni, Y. Yin, *J. Am. Chem. Soc.* **2005**, *127*, 7332 – 7333.

[13] Y. Wang, S. D. Russell, R. L. Shimabukuro, *J. Appl. Phys.* **2005**, *97*, 023708.

[14] a) B. T. Drani, P. J. Flatau, *J. Opt. Soc. Am. A* **1994**, *11*, 1491 – 1499; b) R. Jin, Y. Cao, C. A. Markin, K. L. Kelly, G. Schatz, J.-G. Zheng, *Science* **2001**, *294*, 1901 – 1903; c) Y. Xiong, J. Chen, B. Wiley, Y. Xia, Y. Yin, Z.-Y. Li, *Nano Lett.* **2005**, *5*, 1237 – 1242.

[15] N. Halas, *MRS Bull.* **2005**, *30*, 362 – 367.

[16] Z.-Q. Tian, B. Ren, D.-Yin. Wu, *J. Phys. Chem. B* **2002**, *106*, 9463 – 9482.

[17] W. B. Cai, B. Ren, X. Q. Li, C. X. She, F. M. Liu, X. W. Cai, Z. Q. Tian, *Surf. Sci.* **1998**, *406*, 9 – 22.

[18] Z. Wang, S. Pan, T. D. Krauss, H. Du, L. J. Rothberg, *Proc. Natl. Acad. Sci. USA* **2003**, *100*, 8638 – 8643.

[19] K. L. Kelly, E. Coronado, L. L. Zhao, G. C. Schatz, *J. Phys. Chem. B* **2003**, *107*, 668.

[20] R. Gomez, J. Perez, J. Solla-Gullon, V. Montiel, A. Aldaz, *J. Phys. Chem. B* **2004**, *108*, 9943 – 9949.

 © 2006 Wiley-VCH Verlag GmbH & Co. KGaA, Weinheim

Asymmetric Aldol Reactions

DOI: 10.1002/anie.200503791

Highly Diastereo- and Enantioselective Copper-Catalyzed Domino Reduction/Aldol Reaction of Ketones with Methyl Acrylate**

*Julia Deschamp, Olivier Chuzel, Jérôme Hannedouche, and Olivier Riant**

The development of efficient catalytic asymmetric methodologies for the construction of chiral, nonracemic tertiary alcohols is currently a challenging research area of interest,[1] and a few asymmetric catalytic methods dealing with this demanding task have been described.[2–7] Despite excellent progress in the field of metal-catalyzed enantioselective nucleophilic addition to ketones, only limited success has

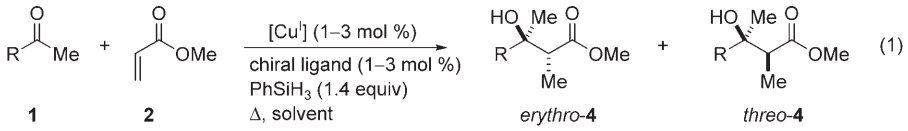
[*] J. Deschamp, O. Chuzel, Dr. J. Hannedouche, Prof. O. Riant
Unité de chimie organique et médicinale
Université catholique de Louvain
Place Louis Pasteur 1, 1348 Louvain-la-Neuve (Belgium)
Fax: (+32) 1047-4168
E-mail: riant@chim.ucl.ac.be

[**] This work was supported by the Université Catholique de Louvain. Dr. B. Pugin (Solvias) and Dr. R. Schmid (Hoffmann–La Roche) are gratefully acknowledged for generous gifts of chiral ligands. Mr. V. Van Tran is also acknowledged for his assistance with the chiral analysis of the new compounds.

Supporting information for this article is available on the WWW under http://www.angewandte.org or from the author.

© 2006 Wiley-VCH Verlag GmbH & Co. KGaA, Weinheim

been achieved in catalytic enantioselective aldol reaction to ketones.[7] The reported systems suffer from either moderate enantioselectivity and/or poor substrate scope and practicality. Moreover, they involve silyl enolate derivatives as nucleophilic partners and thus require an additional and stoichiometric step for their preparation. We are interested in developing an efficient catalytic and enantioselective aldol reaction to simple ketones that overcomes these limitations and does not involve preactivation of the nucleophile in an independent step.[8]

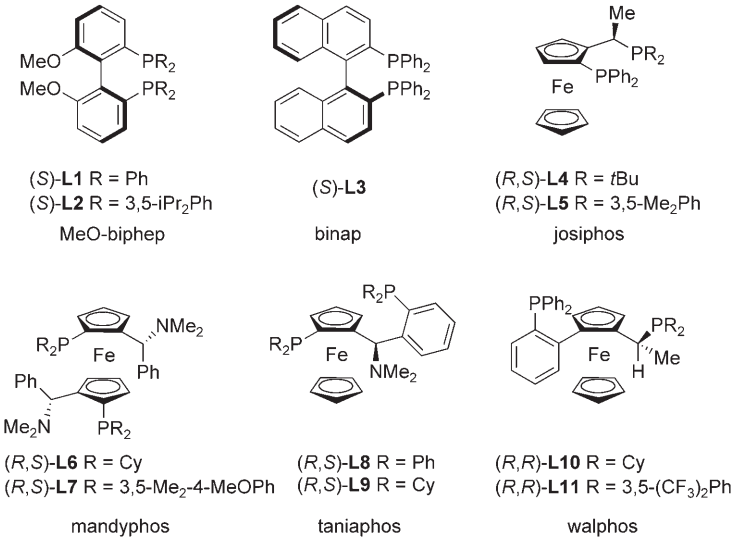


(1)

For this purpose, we turned our intention to the domino conjugate reduction/aldol reaction between α,β-unsaturated carbonyl compounds and ketones with hydrosilane as the reducing agent.[9] This three-component reaction,[10] which allows the preactivation of the nucleophile in situ by generation of a silyl or metal enolate, was successfully employed in the catalytic asymmetric reductive aldol reaction between α,β-unsaturated esters and prochiral aldehydes in the presence of chiral rhodium and iridium complexes.[11,12] Nevertheless, to our knowledge, such a strategy for the development of a catalytic asymmetric aldol process has not been applied to ketones.[13] Herein we disclose our initial studies towards this goal and report the first metal-catalyzed diastereo- and enantioselective intermolecular domino conjugate reduction/aldol reaction between methyl acrylate and simple ketones.[14]

In 1997, pioneer work by Mori et al.[15] suggested that $[CuF(PPh_3)_3]\cdot 2\,EtOH$ was an efficient copper(I) source for the generation of copper hydride species by transmetalation of an hydrogen atom from hydrosilane without any additional silane activator.[16,17] The copper hydride species generated under theses conditions reduced α,β-unsaturated carbonyl compounds stoichiometrically[18] in a 1,4-selective manner.[15,19] Later, various enantioselective copper hydride catalyzed protocols for the 1,4-reduction of a variety of prochiral conjugated compounds were successfully developed by using other copper hydride precursors that were also generated from a stoichiometric amount of silane reagent.[20] These reactions are proposed to proceed by formation of a copper enolate that subsequently undergoes metathesis with a silane to form a silyl enolate. The latter can further participate in an alkylation,[21a] arylation,[21b] or Mukaiyama aldol[21c] reaction to give a one-pot sequential process overall. Trapping the copper enolate by the formation of a C–C bond with an electrophilic ketone partner at a rate faster than the metathesis step could be an opportunity for the development of a copper-catalyzed stereoselective domino reaction between α,β-unsaturated carbonyl compounds and ketones. Shibasaki et al. recently reported a general method for the catalytic aldol reaction between ketene trimethylsilyl acetates and ketones by using catalytic $[CuF(PPh_3)_3]\cdot 2\,EtOH$ in the presence of a stoichiometric amount of $(EtO)_3SiF$ additive.[22] Mechanistic studies showed that the copper enolate intermediate was the reactive nucleophile in this process.[23,24] These observations prompted us to investigate the use of chiral diphosphane-modified copper fluoride as a catalyst for the stereoselective reductive aldol reaction between methyl acrylate and aromatic ketones with hydrosilanes [Eq. (1)].

Our initial experiment was conducted on acetophenone (**1**; $R = C_6H_5$) and methyl acrylate (**2**) with a catalytic amount of $[CuF(PPh_3)_3]\cdot 2\,MeOH$[25] (**3**) and Roche chiral ligand (*S*)-**L1** and a stoichiometric quantity of phenylsilane at 0 °C.[26] In



the presence of **3** and (*S*)-**L1** (1.25 mol %) catalyst, the reaction was almost complete in 2 h (95 % conversion) to afford solely a single product, which was identified as adduct **4**.[27]

Despite high chemoselectivity (99 %), **4** was obtained in a low diastereomeric ratio (d.r. = 41:59) but with an encouraging 51 % *ee* for the major *threo* isomer (Table 1, entry 1).[28] To optimize these results, several parameters were changed. Copper(I) salts were first surveyed to assess the effect of the copper hydride precursor on the reaction. No significant changes in chemo-, diastereo-, and enantioselectivity of the domino reaction between **1** ($R = C_6H_5$) and **2** were observed when using either PPh_3-free CuF–**L1**,[29] CuO*t*Bu–**L1**[30] or CuCl/NaO*t*Bu–**L1** systems under the same conditions.[31] The media effect was then examined by using the easy to handle and air-stable precatalyst **3** and ligand (*S*)-**L1**.

The selectivity of the domino process did not improve by replacing THF with toluene. However, a more polar solvent such as DMF led to poorer conversion and a lower *ee* value of the *threo* isomer. We next investigated the temperature dependence of the reaction. Varying the temperature from 0 to −50 °C raised the *ee* value of *erythro*-**4** from 2 to 25 % (Table 1, entry 1 versus 2), but had hardly any influence on the chemo- and diastereoselectivity of the reaction or on the *ee* value of the *threo* isomer. However, when the reaction was run at −78 °C, chemoselectivity dropped significantly from 99 to 52 % (Table 1, entry 1 versus 3). Diverse chiral ligands were subsequently screened under the optimized conditions (**3**,

 © 2006 Wiley-VCH Verlag GmbH & Co. KGaA, Weinheim

Table 1: Asymmetric copper-catalyzed reductive aldol reaction between methyl acrylate (**2**) and acetophenone (**1**; R = C_6H_5) under various reaction conditions with different chiral ligands **L1**–**L11**.[a]

Entry	Ligand	*t* [h]	Conversion [%][b]	Chemoselectivity [%][b, c]	d.r.[b] *erythro* *threo*	*ee*[b] [%] (*erythro*-**4**)	*ee*[b] [%] (*threo*-**4**)
1 [e,f]	**L1**	2	95	99	41:59	2	51
2 [e]	**L1**	2	80	98	41:59	25	55
3 [e][g]	**L1**	2	77	52	45:55	16	38
4	**L2**	1	99	98	78:22	0	2
5	**L3**	1	98	98	54:46	29	52
6	**L4**	1	99	>99	54:46	−73	−63
7	**L5**	1	98	>99	56:44	40	45
8	**L6**	2	96	98	74:26	16	−1
9	**L7**	2	99	>99	77:23	13	35
10	**L8**	1	99	99	76:24	−85	−94
11	**L9**	1	99	>99	92:8	95[d]	72
12[h]	**L9**	4	92	>99	89:11	87	55
13	**L10**	2	99	99	88:12	−22	37
14	**L11**	2	99	>99	64:36	4	46

[a] Reactions were carried out in solution (0.25 M) in toluene at −50 °C under an oxygen-free argon atmosphere containing **1** (R = C_6H_5) (1.0 equiv), **2** (1.2 equiv), **3** (1 mol %), ligand (1 mol %), $PhSiH_3$ (1.4 equiv) unless otherwise stated. [b] Determined by chiral GC analysis. [c] Chemoselectivity = (**4**/(**4**+phenylethanol) × 100). [d] Absolute configuration: 2*R*,3*S* (see Supporting Information). [e] **1** (0.8 equiv), **2** (1.0 equiv), **3** (1 25 mol %), ligand (1.25 mol %), $PhSiH_3$ (1.2 equiv). [f] At 0 °C. [g] At −78 °C. [h] **3** (0.1 mol %), **L9** (0.1 mol %).

toluene, −50 °C). Among them, diphosphane-based ligands were the most promising ligands in terms of activity and selectivity.[32] Various families of chiral diphosphane ligands **L2**–**L11** were tested, and some results are summarized in Table 1, entries 4–14. To our delight, the reactions were highly chemoselective (> 98 %) and almost complete (95–98 % conversion) in less than 2 h (unoptimized reaction time), regardless of the ligand structure. The *erythro*-**4** isomer was favored in all cases. We first investigated axially chiral biaryl ligands **L2** and **L3**. The substitution of (*S*)-**L1** for (*S*)-**L2** led to a remarkable improvement in the diastereoselectivity (d.r. 41:59→78:22) in favor of the *erythro* isomer (Table 1, entry 2 versus 4). Unfortunately, both isomers were obtained as a racemic mixture. The employ of commonly used (*S*)-**L3** restored some enantioselectivity to the reaction with 29 and 52 % *ee* for the major and minor isomers, respectively, despite a decrease in the diastereoselectivity (Table 1, entry 4 versus 5).

We then assessed chiral ferrocenyl-based diphosphane ligands available from the Solvias kit. Among the different ligand families tested, the josiphos[33a] and taniaphos[33b] ligand families were the most efficient in terms of diastereo- and/or enantioselectivities. For example, the combination of C_1-symmetric (*R*,*S*)-**L4** and precatalyst **3** in the presence of **1**, **2**, and phenylsilane afforded almost quantitatively the adduct **4** with a moderate −73 % *ee* for the *erythro* isomer, despite a low 54:46 d.r. (Table 1, entry 6). The use of **L5**, which bears a more acidic phosphane group on the side chain, did not improve the diastereomeric ratio but led to a significantly lower enantioselectivity (Table 1, entry 7). Improved diastereocontrol of the reaction was observed with mandyphos diphosphane ligands (*R*,*S*)-**L6** and (*R*,*S*)-**L7**, which have a C_2-symmetric backbone (Table 1, entries 8 and 9). Unfortunately, both ligands afforded **4** with low enantioselectivities.

We subsequently tested taniaphos ligand (*R*,*S*)-**L8**, which contains a 1,5-diphosphane unit and hence is capable of forming an eight-membered chelate ring with a metal. Taniaphos ligand (*R*,*S*)-**L8** provided a diastereoselectivity (d.r. 76:24) similar to that obtained with mandyphos ligands (*R*,*S*)-**L6** and (*R*,*S*)-**L7**. However, the enantiodifferentiation was drastically enhanced for both isomers of **4**. Under the optimal conditions, the reaction with (*R*,*S*)-**L8** furnished adduct **4** with −85 *ee* and −94 % *ee* for the *erythro* and *threo* isomers, respectively (Table 1, entry 10). The substitution of phenyl groups attached to phosphorus atoms of **L8** by cyclohexyl substituents further improved the diastereo- and enantioselectivity of the reaction.[34] Indeed, the addition of **1**, **2**, and phenylsilane to **3** (1 mol %) and (*R*,*S*)-**L9** (1 mol %)in toluene gave **4** with 92:8 d.r. in favor of the *erythro* isomer and 95 % *ee* for the major isomer (Table 1, entry 11). The catalyst loading can be decreased to 0.1 mol % without significant variation of chemo- and diastereocontrol (Table 1, entry 12). However, under these conditions, a slight decrease in the enantioselectivity was observed for the preponderant isomer. Notably, for both privileged[35] josiphos and taniaphos ligand families, the opposite absolute configuration of the major compound was observed when the groups on the phosphorus atoms were changed from alkyl to aryl substituents (Table 1, entry 6 versus 7 and entry 10 versus 11). Moreover, a change from josiphos ligands (*R*,*S*)-**L4** and (*R*,*S*)-**L5** to taniaphos ligand (*R*,*S*)-**L9** and (*R*,*S*)-**L8**, respectively, which exhibit the same planar chirality, afforded *erythro*-**4** with the opposite configuration (Table 1, entry 6 versus 11 and entry 7 versus 10).[36] The use of other chiral ligands bearing a 1,5-diphosphane unit such as walphos ligands (*R*,*R*)-**L10** and (*R*,*R*)-**L11** afforded adduct **4** with lower diastereo- and enantioselectivity (Table 1, entries 13 and 14).

Next, we analyzed the scope of the copper-catalyzed asymmetric reductive aldol reaction with respect to the ketone substrate by using taniaphos chiral ligand (*R*,*S*)-**L9** under the optimal conditions. A variety of aromatic and heteroaromatic ketones participate successfully in the reac-

 © 2006 Wiley-VCH Verlag GmbH & Co. KGaA, Weinheim

Table 2: Asymmetric copper-catalyzed reductive aldol reaction between **2** and various aromatic ketones **1** with (*R*,*S*)-**L9** under the optimal conditions.[a]

Entry	R	*t* [h]	Yield [%][h]	Chemoselectivity [%][b][c]	d.r.[b] *erythro*/*threo*	*ee*[b] [%] (*erythro*-**4**)	*ee*[b] [%] (*threo*-**4**)
1	C_6H_5	1	98	>99	92:8	95[d]	72
2	*p*-FC_6H_5	1	88	94	91:9	92	73
3	*p*-$CF_3C_6H_5$	1	87	89	80:20	83	72
4	*p*$MeOC_6H_5$	1	31[f]	97	92:8	90	56
5	*p*-ClC_6H_5	1	95	95	86:14	90	77
6	*m*-ClC_6H_5	1	70	89	88:12	82	n.d.[e]
7[g]	2-thienyl	2	94	>99	96:4	90	15
8	3-thienyl	2	95	>99	95:5	95	65

[a] Reactions were carried out in solution (0.25 M) in toluene at −50 °C under an oxygen-free argon atmosphere containing **1** (1.0 equiv), **2** (1.2 equiv), **3** (1 mol%), (*R*,*S*)-**L9** (1 mol%), $PhSiH_3$ (1.4 equiv) unless otherwise stated. [b] Determined by chiral GC analysis. [c] Chemoselectivity = (**4**/(**4**+phenylethanol) × 100). [d] Absolute configuration: 2*R*,3*S*. [e] Not determined. [f] Conversion determined by GC analysis and not optimized. [g] **3** (3 mol%), (*R*,*S*)-**L9** (3 mol%). [h] Yield of isolated product.

tion (Table 2). For the range of substrates studied, the diastereo- and enantioselectivity of the reaction were moderate to high (*erythro*-**4**: d.r. 80:20–96:4 and 82–95% *ee*). As a general trend, the introduction of a halogen substituent at the *para* or *meta* position of acetophenone slightly decreased the diastereoselectivity of the reaction and the enantioselectivity of the major isomer (Table 2, entry 1 versus entries 2, 5, and 6). The substitution of an electron-withdrawing group at the *para* position of acetophenone by an electron-donating group increased both the diastereomeric ratio and the *ee* of the *erythro* compound (Table 2, entry 3 versus 4). Heteroaromatic ketones such as 2- and 3-thiophene-substituted ketones also took part efficiently in the domino sequence to give the corresponding *erythro*-**4** compound with very high chemo-, diastereo-, and enantioselectivity (Table 2, entries 7 and 8).

In summary, we have developed a new strategy for the catalytic asymmetric aldol reaction of ketones that relies on a domino reduction/aldol reaction sequence between methyl acrylate and aromatic ketones. The process, catalyzed by a diphosphane-modified copper(I) fluoride complex in the presence of phenylsilane, is highly selective (chemo-, diastereo-, and enantioselectivity) for a range of aromatic ketones. This strategy circumvents the need to preactivate the nucleophile prior to the C–C bond-forming step and affords highly functionalized products with two contiguous stereogenic centers, one of which is a chiral tertiary alcohol. Current efforts are focused on exploring the breadth of this domino reaction.

Received: October 26, 2005
Published online: January 20, 2006

Keywords: aldol reaction · copper · enantioselectivity · enolates · hydrosilylation

[1] D. J. Ramon, M. Yus, *Angew. Chem.* **2004**, *116*, 286; *Angew. Chem. Int. Ed.* **2004**, *43*, 284.

[2] For catalytic asymmetric alkylation/phenylation of ketones, see: a) P. I. Dosa, G. C. Fu, *J. Am. Chem. Soc.* **1998**, *120*, 445; b) E. F. DiMauro, M. C. Kozlowski, *J. Am. Chem. Soc.* **2002**, *124*, 12668; c) C. García, L. K. La Rochelle, P. J. Walsh, *J. Am. Chem. Soc.* **2002**, *124*, 10970; d) S.-J. Jeon, P. J. Walsh, *J. Am. Chem. Soc.* **2003**, *125*, 9544; e) C. García, P. J. Walsh, *Org. Lett.* **2003**, *5*, 3641; f) H. Li, C. García, P. J. Walsh, *Proc. Natl. Acad. Sci. USA* **2004**, *101*, 5427; g) J. M. Betancort, C. García, P. J. Walsh, *Synlett* **2004**, 749; h) C. Anaya de Parrodi, P. J. Walsh, *Synlett* **2004**, 2417; i) S.-J. Jeon, H. Li, C. García, L. K. La Rochelle, P. J. Walsh, *J. Org. Chem.* **2005**, *70*, 448; j) D. J. Ramon, M. Yus, *Tetrahedron Lett.* **1998**, *39*, 1239; k) D. J. Ramon, M. Yus, *Tetrahedron* **1998**, *54*, 5651; l) M. Yus, D. J. Ramon, O. Prieto, *Tetrahedron: Asymmetry* **2003**, *14*, 1103; m) K. Funabashi, M. Jachmann, M. Kanai, M. Shibasaki, *Angew. Chem.* **2003**, *115*, 5647; *Angew. Chem. Int. Ed.* **2003**, *42*, 5489; n) M. W. Fennie, E. F. Di Mauro, E. M. O'Brien, V. Annamalai, M. C. Kozlowski, *Tetrahedron* **2005**, *61*, 6249.

[3] For catalytic asymmetric allylation of ketones, see: a) S. Casolari, D. D'Addario, E. Tagliavini, *Org. Lett.* **1999**, *1*, 1061; b) K. M. Waltz, J. Gavenonis, P. J. Walsh, *Angew. Chem.* **2002**, *114*, 3849; *Angew. Chem. Int. Ed.* **2002**, *41*, 3697; c) G. Kim, K. M. Waltz, I. F. Garcia, D. Kwiatkowski, P. J. Walsh, *J. Am. Chem. Soc.* **2004**, *126*, 12580; d) S. Kii, K. Maruoka, *Chirality* **2003**, *15*, 68; e) A. Cunningham, S. Woodward, *Synlett* **2002**, 43; f) A. Cunningham, V. Mokal-Parekh, C. Wilson, S. Woodward, *Org. Biomol. Chem.* **2004**, *2*, 741; g) S. Yamasaki, K. Fujii, R. Wada, M. Kanai, M. Shibasaki, *J. Am. Chem. Soc.* **2002**, *124*, 6536; h) R. Wada, K. Oisaki, M. Kanai, M. Shibasaki, *J. Am. Chem. Soc.* **2004**, *126*, 8910; i) Y. C. Teo, J. D. Goh, T. P. Loh, *Org. Lett.* **2005**, *7*, 2743.

[4] For catalytic asymmetric vinylation, see: a) H. Li, P. J. Walsh, *J. Am. Chem. Soc.* **2004**, *126*, 6538; b) H. M. Li, P. J. Walsh, *J. Am. Chem. Soc.* **2005**, *127*, 8355.

[5] For catalytic asymmetric alkynylation of ketones, see: a) B. Jiang, Z. L. Chen, X. X. Tang, *Org. Lett.* **2002**, *4*, 3451; b) P. G. Cozzi, *Angew. Chem.* **2003**, *115*, 3001; *Angew. Chem. Int. Ed.* **2003**, *42*, 2895; c) P. G. Cozzi, S. Alesi, *Chem. Commun.* **2004**, 2448; d) G. Lu, X. S. Li, X. Jia, W. L. Chan, A. S. C. Chan, *Angew. Chem.* **2003**, *115*, 5211; *Angew. Chem. Int. Ed.* **2003**, *42*, 5057; e) B. Saito, T. Katsuki, *Synlett* **2004**, 1557; f) Y. F. Zhou, R. Wang, Z. Q. Xu, W. J. Yan, L. Liu, Y. F. Kang, Z. J. Han, *Org. Lett.* **2004**, *6*, 4147; g) L. Liu, Y. F. Kang, W. Rui, Y. F. Zhou, C. Chao, N. Ming, M. Z. Gong, *Tetrahedron: Asymmetry* **2004**, *15*, 3757; h) L. Liu, R. Wang, Y. F. Kang, C. Chen, Z. Q. Xu, Y. F. Zhou, M. Ni, H. Q. Cai, M. Z. Gong, *J. Org. Chem.* **2005**, *70*, 1084; i) . F. Kang, L. Liu, R. Wang, Y. F. Zhou, W. J. Yan, *Adv. Synth. Catal.* **2005**, *347*, 243; j) J. C. Mao, B. S. Wan, F. Wu, S. W. Lu, *J. Mol. Catal. A* **2005**, *237*, 126.

[6] For catalytic asymmetric cyanosilylation of ketones, see: a) N. Belokon, B. Green, N. S. Ikonnikov, M. North, T. Parsons, V. I. Tararov, *Tetrahedron* **2001**, *57*, 771; b) S.-K. Tian, L. Deng, *J. Am. Chem. Soc.* **2001**, *123*, 6195; c) S.-K. Tian, R. Hong, L. Deng, *J. Am. Chem. Soc.* **2003**, *125*, 9900; d) H. B. Deng, M. R. Isler,

 © 2006 Wiley-VCH Verlag GmbH & Co. KGaA, Weinheim

M. L. Snapper, A. H. Hoveyda, *Angew. Chem.* **2002**, *114*, 1051; *Angew. Chem. Int. Ed.* **2002**, *41*, 1009; e) Y. Hamashima, M. Kanai, M. Shibasaki, *J. Am. Chem. Soc.* **2000**, *122*, 7412; f) K. Yabu, S. Masumoto, S. Yamasaki, Y. Hamashima, M. Kanai, W. Du, D. P. Curran, M. Shibasaki, *J. Am. Chem. Soc.* **2001**, *123*, 9908; g) F. X. Chen, X. M. Feng, B. Qin, G. L. Zhang, Y. Z. Jiang, *Org. Lett.* **2003**, *5*, 949; h) D. H. Ryu, E. J. Corey, *J. Am. Chem. Soc.* **2005**, *127*, 5384; i) D. E. Fuerst, E. N. Jacobsen, *J. Am. Chem. Soc.* **2005**, *127*, 8964.

[7] a) J. S. Johnson, D. A. Evans, *Acc. Chem. Res.* **2000**, *33*, 325; b) S. E. Denmark, Y. Fan, *J. Am. Chem. Soc.* **2002**, *124*, 4233; c) E. Denmark, Y. Fan, M. D. Eastgate, *J. Org. Chem.* **2005**, *70*, 5235; d) K. Oisaki, D. Zhao, Y. Suto, M. Kanai, M. Shibasaki, *Tetrahedron Lett.* **2005**, *46*, 4325; e) X. Moreau, B. Bazan-Tejeda, J. M. Campagne, *J. Am. Chem. Soc.* **2005**, *127*, 7288.

[8] For a recent review on asymmetric aldol reactions, see: C. Palomo, M. Oiarbide, J. M. Garcia, *Chem. Soc. Rev.* **2004**, *33*, 65.

[9] A. Revis, T. K. Hilty, *Tetrahedron Lett.* **1987**, *28*, 4809.

[10] For a recent review on asymmetric multicomponent reactions, see: D. J. Ramón, M. Yus, *Angew. Chem.* **2005**, *117*, 1628; *Angew. Chem. Int. Ed.* **2005**, *44*, 1602.

[11] a) S. J. Taylor, M. O. Duffey, J. P. Morken, *J. Am. Chem. Soc.* **2000**, *122*, 4528; b) C.-X. Zhao, M. O. Duffey, S. J. Taylor, J. P. Morken, *Org. Lett.* **2001**, *3*, 1829; c) A. E. Russell, N. O. Fuller, S. J. Taylor, P. Aurriset, J. P. Morken, *Org. Lett.* **2004**, *6*, 2309; d) N. O. Fuller, J. P. Morken, *Synlett* **2005**, 1459; e) H. Nishiyama, T. Shiomi, Y. Tsuchiya, I. Matsuda, *J. Am. Chem. Soc.* **2005**, *127*, 6972.

[12] a) S. Isayama, T. Mukaiyama, *Chem. Lett.* **1989**, 2005; b) Matsuda, K. Takahashi, S. Sato, *Tetrahedron Lett.* **1990**, *31*, 5331; c) S.-I. Kiyooka, A. Shimizu, S. Torii, *Tetrahedron Lett.* **1998**, *39*, 5237; d) S. J. Taylor, J. P. Morken, *J. Am. Chem. Soc.* **1999**, *121*, 12202; e) C. X. Zhao, J. Bass, J. P. Morken, *Org. Lett.* **2001**, *3*, 2839; f) I. Shibata, H. Kato, T. Ishida, M. Yasuda, A. Baba, *Angew. Chem.* **2004**, *116*, 729; *Angew. Chem. Int. Ed.* **2004**, *43*, 711; g) M. Freiría, A. J. Whitehead, D. A. Tocher, W. B. Motherwell, *Tetrahedron* **2004**, *60*, 2673.

[13] For the intramolecular reductive aldol reaction of alkenediones with a stoichiometric amount of the Stryker reagent, see: a) P. Chiu, C. P. Szeto, Z. Geng, K. F. Cheng, *Org. Lett.* **2001**, *3*, 1901; b) P. Chiu, B. Chen, K. F. Cheng, *Tetrahedron Lett.* **1998**, *39*, 9229; c) P. Chiu, C. P. Szeto, Z. Geng, K. F. Cheng, *Tetrahedron Lett.* **2001**, *42*, 4091; for intramolecular reductive aldol reaction of alkynediones with stoichiometric or catalytic amounts of the Stryker reagent, see: d) P. Chiu, S. K. Leung, *Chem. Commun.* **2004**, 2308; for an intramolecular reductive Henry reaction with stoichiometric amounts of the Stryker reagent, see: e) W. K. Chung, P. Chiu, *Synlett* **2005**, 55.

[14] During the preparation of this manuscript, a diastereo- and enantioselective copper-catalyzed intramolecular reductive aldol reaction of α,β-unsaturated esters and ketones was reported: H. W. Lam, P. M. Joensuu, *Org. Lett.* **2005**, *7*, 4225.

[15] a) A. Mori, A. Fujita, *Chem. Commun.* **1997**, 2159; b) H. Ito, T. Ishizuka, K. Arimoto, K. Miura, A. Hosomi, *Tetrahedron Lett.* **1997**, *38*, 8887; c) A. Mori, A. Fujita, H. Kajiro, Y. Nishihara, T. Hiyama, *Tetrahedron* **1999**, *55*, 4573.

[16] We have reported the use of copper fluoride–phosphine complexes for the catalytic enantioselective hydrosilylation of aromatic ketones with excellent yields and enantioselectivities: a) S. Sirol, J. Courmarcel, N. Mostefai, O. Riant, *Org. Lett.* **2001**, *3*, 4111; b) J. Courmarcel, N. Mostefai, S. Sirol, S. Choppin, O. Riant, *Isr. J. Chem.* **2002**, *42*, 231; for a review on catalytic asymmetric hydrosilylation to ketones and imines, see: c) O. Riant, N. Mostefai, J. Courmarcel, *Synthesis* **2004**, 2943.

[17] For a special topic on copper-mediated conjugate reductions and reductive aldol reactions with organosilanes as the hydride source, see: P. Chiu, *Synthesis* **2004**, 2943.

[18] A catalytic amount of $[CuF(PPh_3)_3]\cdot 2\,EtOH$ was less efficient.[15c]

[19] For a 1,4-reduction mediated by stoichiometric or catalytic amounts of the Stryker reagent, see: a) W. S. Mahoney, D. M. Brestensky, J. M. Stryker, *J. Am. Chem. Soc.* **1988**, *110*, 291; b) W. S. Mahoney, J. M. Stryker, *J. Am. Chem. Soc.* **1989**, *111*, 8818; c) B. H. Lipshutz, J. Keith, P. Papa, R. Vivian, *Tetrahedron Lett.* **1998**, *39*, 4627.

[20] a) B. H. Lipshutz, J. M. Servesko, *Angew. Chem.* **2003**, *115*, 4937; *Angew. Chem. Int. Ed.* **2003**, *42*, 4789; b) B. H. Lipshutz, J. M. Servesko, T. B. Petersen, P. P. Papa, A. A. Lover, *Org. Lett.* **2004**, *6*, 1273; c) B. H. Lipshutz, J. M. Servesko, B. R. Taft, *J. Am. Chem. Soc.* **2004**, *126*, 8352; d) D. H. Appella, Y. Moritani, R. Shintani, E. M. Ferreira, S. L. Buchwald, *J. Am. Chem. Soc.* **1999**, *121*, 9473; e) Y. Moritani, D. H. Appella, V. Jurkauskas, S. L. Buchwald, *J. Am. Chem. Soc.* **2000**, *122*, 6797; f) G. Hughes, M. Kimura, S. L. Buchwald, *J. Am. Chem. Soc.* **2003**, *125*, 11253; g) . P. Rainka, Y. Aye, S. L. Buchwald, *Proc. Natl. Acad. Sci. USA* **2004**, *101*, 5821; h) C. Czekelius, E. M. Carreira, *Angew. Chem.* **2003**, *115*, 4941; *Angew. Chem. Int. Ed.* **2003**, *42*, 4793; i) C. Czekelius, E. M. Carreira, *Org. Lett.* **2004**, *6*, 4575.

[21] a) B. H. Lipshutz, W. Chrisman, K. Noson, P. Papa, J. A. Sclafani, R. W. Vivian, J. M. Keith, *Tetrahedron* **2000**, *56*, 2779; b) J. Yun, S. L. Buchwald, *Org. Lett.* **2001**, *3*, 1129; c) J. Chae, J. Yun, S. L. Buchwald, *Org. Lett.* **2004**, *6*, 4809.

[22] K. Oisaki, Y. Suto, M. Kanai, M. Shibasaki, *J. Am. Chem. Soc.* **2003**, *125*, 5644; for complementary work, see reference [7d].

[23] The copper enolate intermediate was proposed to be generated by dynamic ligand exchange between silicon and copper;[22] for pioneering work on a CuF–(*S*)-tolbinap-catalyzed enantioselective aldol reaction between silyl dienolate and aldehyde that involved a metalloenolate intermediate, see: a) J. Krüger, E. M. Carreira, *J. Am. Chem. Soc.* **1998**, *120*, 837; b) B. L. Pagenkopf, J. Krüger, A. Stojanovic, E. M. Carreira, *Angew. Chem.* **1998**, *110*, 3312; *Angew. Chem. Int. Ed.* **1998**, *37*, 3124.

[24] For a CuF–tolbinap-catalyzed enantioselective vinylogous Mukaiyama reaction on aliphatic ketones, see reference [7e].

[25] The complex was prepared according to a literature procedure: D. J. Gulliver, W. Levason, M. Webster, *Inorg. Chim. Acta* **1981**, *52*, 153; the amount of methanol molecules contained in the complex was determined by single-crystal X-ray crystallographic analysis of the complex (unpublished results).

[26] $PhSiH_3$ was chosen as hydride source for its tendency not to form stable silyl enol ethers upon transmetalation with copper enolate.[19c]

[27] A minor trace of phenylethanol (< 1 %), the product of reduction of acetophenone, was observed by GC analysis.

[28] Under the same conditions, without any additional ligand, **3** (1.25 mol %) gave only 20 % conversion after a 2-hour reaction.

[29] For the preparation, see: D. Tomita, R. Wada, M. Kanai, M. Shibasaki, *J. Am. Chem. Soc.* **2005**, *127*, 4138.

[30] For the preparation of CuO*t*Bu, see: T. Tsuda, T. Hashimoto, T. Saegusa, *J. Am. Chem. Soc.* **1972**, *94*, 658.

[31] Notably, no effect on the reaction rate was observed when using either preprepared CuO*t*Bu or CuO*t*Bu prepared in situ (from CuCl/NaO*t*Bu); for a report on the salt effect on the rate of the enantioselective 1,4-reduction of β,β-disubstituted nitroalkenes when using both methods of CuO*t*Bu preparation, see reference [20 h].

[32] For example, monodentate Feringa phosphonite, tridentate *t*Bu-pybox, and tetradentate Trost ligand gave very low activity and/or no enantioselectivity.

[33] For original work, see: a) A. Togni, C. Breutel, A. Schnyder, F. Spindler, H. Landert, A. Tijani, *J. Am. Chem. Soc.* **1994**, *116*, 4062; b) T. Ireland, G. Grossheimann, C. Wieser-Jeunesse, P. Knochel, *Angew. Chem.* **1999**, *111*, 1560; *Angew. Chem. Int. Ed.* **1999**, *38*, 3212.

 © 2006 Wiley-VCH Verlag GmbH & Co. KGaA, Weinheim

[34] These observations are in contrast to those usually made in other processes using taniaphos-derived ligands containing either alkyl or aromatic substituents on phosphorus atoms. Generally, a change from electron-rich aromatic groups to cyclohexyl groups has a negative effect on the enantioselectivity of the process. For some examples, see: a) B. L. Feringa, R. Badorrey, D. Peòa, S. R. Harutyunyan, A. J. Minnaard, *Proc. Natl. Acad. Sci. USA* **2004**, *101*, 5834; b) F. Spindler, C. Malan, M. Lotz, M. Kesselgruber, U. Pittelkow, A. Rivas-Nass, O. Briel, H.-U. Blaser, *Tetrahedron: Asymmetry* **2004**, *15*, 2299.

[35] T. P. Yoon, E. N. Jacobsen, *Science* **2003**, *299*, 1691.

[36] A similar observation was previously made in the copper-catalyzed asymmetric conjugate addition of Grignard reagents to cyclic enones.[34a]

 © 2006 Wiley-VCH Verlag GmbH & Co. KGaA, Weinheim

Fullerenes

DOI: 10.1002/anie.200502417

Di- and Tridysprosium Endohedral Metallofullerenes with Cages from C_{94} to C_{100}**

Shangfeng Yang and Lothar Dunsch**

Endohedral fullerenes, the novel form of fullerenes with atoms, ions, or clusters trapped in their inner space,[1–5] exhibit a variety of structural, magnetic, and electronic properties, which are important for potential applications in electronics and medicine.[1–7] To date, the majority of the isolated endohedral fullerenes, including both the conventional metallofullerenes and the clusterfullerenes,[1–5,8–13] is based on mainly Group 3 elements, especially La, Y, and Sc. Among them, dimetallofullerenes appear unique because of the equivalence of the two encaged atoms and the accessibility of a large variety of cage sizes such as C_{80}, C_{82}, and C_{84}. Whereas dimetallofullerenes with cages smaller than C_{80} have been extensively studied,[14–18] few studies on higher dimetallofullerenes with cages larger than C_{84} have been reported.[19,20]

The largest fullerene cage isolated and characterized up to now within the fullerene family, including the empty fullerenes,[1–13,21] is C_{94}. As many fullerene cages are accessible only in the endohedral form such as the non-IPR cages C_{66}[17] and C_{68}[8] and large fullerene cages tend to be preferably stabilized as the endohedral structures,[19,20] the investigation of the larger fullerene cages, preferentially in endohedral form, appears quite important and challenging.

On the other hand, trimetallofullerenes are even more intriguing because of the encapsulation of three metal atoms. To date only $Sc_3@C_{82}$,[1,22] $Er_3@C_{74}$, [20] and $Tb_3@C_{80}$[23] have been obtained in extremely low yields. Higher trimetallofullerenes have not yet been described.

Very recently we isolated a family of dysprosium nitride clusterfullerenes and found that the application of NH_3 (reactive gas atmosphere[5]) benefited simultaneously the production of a large series of di- and trimetallofullerenes (multimetallofullerenes).[12] Herein we report the efficient production and facile isolation of a stable didysprosium fullerene of C_{100} and a tridysprosium fullerene of C_{98} for the first time as well as two isomeric didysprosium fullerenes of C_{94}. The higher multimetallofullerenes were isolated to high purity by single-stage HPLC and identified by LD-TOF mass spectrometry. Their electronic properties and band-gaps were investigated by UV/Vis/NIR spectroscopy. FTIR spectroscopy was used to examine their vibrational patterns and stabilities in solid form as well.

The typical chromatogram of a fullerene extract indicates a large variety of the endohedral fullerenes formed (Figure 1 a). In particular, the mass spectrometric (MS) analysis

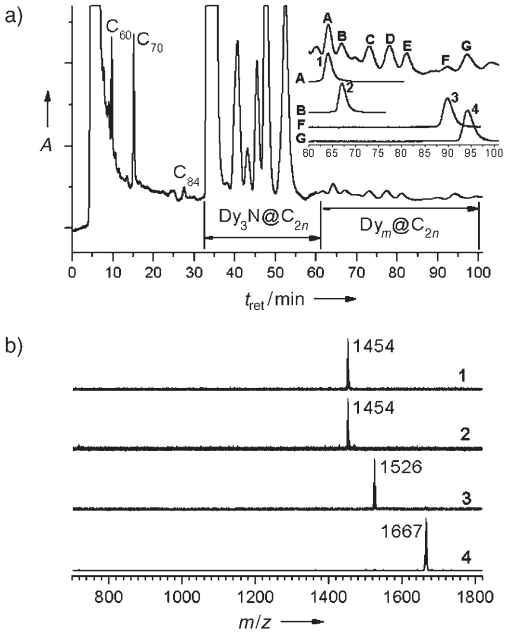


Figure 1. a) Chromatogram of the fullerene extract mixture produced by the reactive gas atmosphere synthesis method (linear combination of two 4.6×250-mm Buckyprep columns; flow rate 1.6 mL min^{-1}; injection volume 100 μL; toluene as eluent; column temperature 40 °C). Inset: Chromatogram of the higher multimetallofullerenes (top trace) and the isolated products **1**–**4**, conditions as for (a). b) Positive-ion LD-TOF mass spectra of **1**–**4**.

provides direct evidence for the formation of a series of multimetallofullerenes $Dy_m@C_{2n}$ with two ($m=2$, $40 \le n \le 57$) and three ($m=3$, $40 \le n \le 50$) cage metal atoms.[12] The detected dimetallofullerene family is much larger than the reported series of Dy- and Er-based dimetallofullerenes isolated by recycling HPLC.[19,20] Among them, the multimetallofullerenes with cages smaller than C_{94} ($n \le 46$, $t_{ret} <$ 61.0 min) overlap with the clusterfullerene main products $Dy_3N@C_{2n}$ ($39 \le n \le 46$, t_{ret}: 32.7 $\approx$61.0 min), while their yields are significantly lower.[12] In contrast, the higher $Dy_m@C_{2n}$ multimetallofullerenes with cages larger than C_{94} ($n \ge 47$) are produced in relatively high yields, comparable to that of the empty C_{84} ($t_{ret}=26.8$ min; see Figure 1 a). Such yields have never been achieved by the conventional arc discharging method without the addition of NH_3, by which the dominant products are always the empty fullerenes such as C_{60}, C_{70}, C_{76}, C_{78}, and C_{84}, as well as mono- and dimetallofullerenes. In this case, the yields of the metallofullerenes are generally lower than that of C_{84}.[1–4,6,19,20] By using C_{84} as the reference, we could then infer that the yields of the higher multimetallo-

[*] Dr. S. Yang, Prof. Dr. L. Dunsch
Group of Electrochemistry and Conducting Polymers
Leibniz-Institute for Solid State and Materials Research Dresden
01171 Dresden (Germany)
Fax: (+49) 351-4659-745
E-mail: s.yang@ifw-dresden.de
l.dunsch@ifw-dresden.de

[**] We cordially thank Dr. M. Krause for valuable discussions and Mrs. H. Zöller, Ms. K. Leger, Mr. F. Ziegs, and Ms. S. Döcke for technical assistance. S.Y. thanks the Alexander von Humboldt (AvH) Foundation for financial support.

Supporting information for this article is available on the WWW under http://www.angewandte.org or from the author.

 © 2006 Wiley-VCH Verlag GmbH & Co. KGaA, Weinheim

fullerenes in the present case are higher than those of all of the monometallofullerenes and those dimetallofullerenes with relatively smaller cages. A plausible interpretation for the enhanced yields of the higher multimetallofullerenes has been proposed previously.[12]

The whole portion of the multimetallofullerenes ($Dy_m@C_{2n}$) was examined with HPLC, and the absence of obvious shoulder peaks in the chromatogram suggests the efficient isolation of each fraction (A–G) under the present isolation conditions as shown in the inset of Figure 1a (top trace). Each fraction collected after the single-step HPLC separation step was subjected to further HPLC analysis (see inset of Figure 1a) and laser desorption time-of-flight (LD-TOF) MS analysis (Figure 1b) so as to identify their chemical forms and ascertain the purity. Among them, fractions A, B, F, G are found to be composed of single components: $Dy_2@C_{94}$ (I) (**1**), $Dy_2@C_{94}$ (II) (**2**), $Dy_2@C_{100}$ (**3**), and $Dy_3@C_{98}$ (**4**; see Table 1 and Supporting Information for further analysis including fractions C–E). As a matter of fact, **3** has the largest fullerene cage isolated to date and **4** is the largest trimetallofullerene ever isolated. In addition to the preferential production of these higher multimetallofullerenes in high yields as discussed above, the facile isolation by single-stage HPLC, even for the two $Dy_2@C_{94}$ isomers (**1** and **2**), highlights another advantage of the present method.

UV/Vis/NIR spectra of the products **1**–**4** in toluene (Figure 2) are generally very rich in features and show clear absorptions in the NIR region (Table 1). Based on the absorption spectral onsets of 1403, 1497, 1590, and 1370 nm for **1**–**4**, the optical band-gaps are calculated to be 0.88, 0.83, 0.78, and 0.91 eV, respectively,[1,5,10–12,19,20] indicating that **1**–**4** are all small band-gap fullerenes. In this sense, for the two isomers of $Dy_2@C_{94}$, the optical band-gap of **2** is slightly smaller than that of **1**, suggesting a relatively lower stability of **2**. Moreover, the distinct difference in the strongest absorptions between **1** and **2** should be highlighted (see Figure 2a and Table 1). The UV/Vis/NIR spectra of **1** and **2** are consistent with the spectra reported in reference [19] (although the detailed comparison of these two isomers was not available there). On the other hand, the C_{100} cage in **3** shows a less structured electronic absorption spectrum. As shown in Figure 2b, **3** shows an even stronger absorption in the NIR region than that in the UV and visible regions. As a result, the strongest absorption of **3** lies at 1056 nm and the visible absorptions at 624 and 690 nm are much weaker. Notably, compound **3** also has the smallest optical band-gap among **1**–**4**, which points to its low stability. The UV/Vis/NIR spectrum of **4** exhibits a strong HOMO–LUMO transition at 664 nm and three weak shoulder peaks at 341, 442, and 578 nm (see inset in Figure 2b).

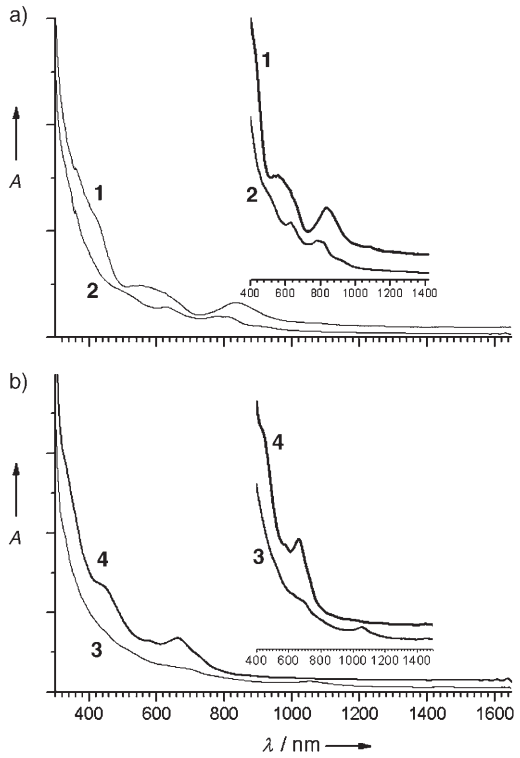


Figure 2. UV/Vis/NIR spectra of the isolated products **1** and **2** (a) as well as **3** and **4** (b) in toluene. The insets show the compressed spectral range (400–1500 nm) with the characteristic absorption bands.

The FTIR spectra of **1**–**4** display bands for the intramolecular modes mostly in the mid-IR region. It is found that **2** and **3** (Figure 3, curves c and d) are unstable in the solid form, as confirmed by the strong, but unresolved absorption bands between 870 and 1260 cm^{-1}. Such broad bands, which are attributed to a graphitization upon decomposition of the dimetallofullerenes,[24] do not occur for compounds **1** and **4** (Figure 3). In fact, the lower stabilities of **2** and **3** revealed by FTIR spectroscopy are consistent with their smaller optical band-gaps.

Since **1** and **4** are reasonably stable in the solid form, their FTIR spectra can be evaluated for the analysis of the structures. The large number of lines in the spectra reflects the expectedly low molecular symmetry of the C_{94} and C_{98}

Table 1: Characteristics of the dysprosium multimetallofullerenes **1**–**4**.

No.	Product	t_{ret}(min)		Purity[a] [%]	Onset [nm]	Band-gap[b] [eV]	UV/Vis/NIR absorptions [nm]	Color[c]
		Buckyprep	Buckyclutcher					
1	$Dy_2@C_{94}$(I)	63.9	26.2	≥99	1403	0.88	421, 551, 839, 1077	green-yellow
2	$Dy_2@C_{94}$(II)	67.1	25.6	≥98	1497	0.83	493, 628, 782, 813, 914	yellow
3	$Dy_2@C_{100}$	90.2	29.0	≥99	1590	0.78	624, 690, 1056	yellow
4	$Dy_3@C_{98}$	94.8	27.9	≥99	1370	0.91	341, 442, 578, 664	yellow-green

[a] Based on the integration results of the chromatograms running on both Buckyprep and Buckyclutcher columns and LD-TOF mass spectra run in positive-ion mode. [b] The band-gap is calculated from the spectral onset (band-gap [eV] ≈ 1240/onset [nm]). [c] Dissolved in toluene.

 © 2006 Wiley-VCH Verlag GmbH & Co. KGaA, Weinheim

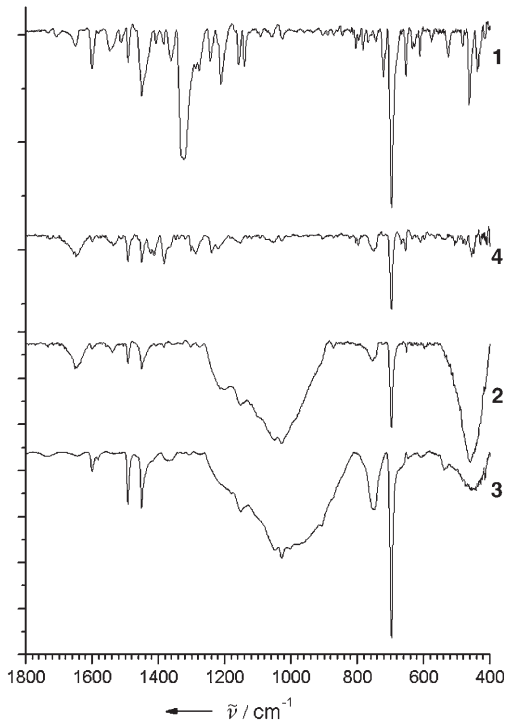


Figure 3. FTIR spectra of compounds **1**–**4**.

cages. Compounds **1** and **4** exhibit similar bands in the radial vibrational part (below 800 cm^{-1}),[10,11,25] and interestingly the most intense low-energy IR line remains constant at around 697 cm^{-1} for **1** and **4**. However, in the tangential vibrational part (above 1100 cm^{-1})[10,11,25], the strongest IR bands for **1** and **4** lie at around 1325 and 1383 cm^{-1}, respectively. Such differences are due to the different cage symmetries and the charge state of the fullerene cage.

When the fullerene cage becomes larger, the number of structural isomers increases dramatically and the molecular symmetry is significantly reduced:[26] as a result the number of IPR structural isomers for the $C_{94,}$ C_{96}, C_{98}, and C_{100} cages are 134, 187, 259, and 450, respectively.[21,26,27] Numerous theoretical calculations have revealed that the stability of the IPR isomer of fullerenes (empty[27,28] and endohedral fullerenes[25]) depends strongly on the cage symmetry. It is therefore reasonable to assume that the experimentally isolated stable isomer correlates preferably to the energetically most stable cage structure.[25,27,28] However, it should be noted that in some cases the stability of the IPR isomer of the endohedral fullerene is somewhat different to that of the empty fullerene with the same cage due to the charge transfer between the encaged species and the fullerene cage.[1,2] So far no theoretical study on endohedral fullerenes with a charged cage higher than C_{84} is available because of the tremendous difficulties associated with the effect of the charge state and the significantly lowered molecular symmetry of higher cages.[29] Nevertheless, previous studies on C_{84} and $Sc_2@C_{84}$ revealed that the isomeric structure of empty C_{84} (23:D_{2d}) was largely preserved by $Sc_2@C_{84}$ despite the charge transfer between the two encaged Sc atoms and the C_{84} cage.[25,28] For even larger cages it thus appears that the effect of the charge state of the cage could be neglected since most of the isomers of these cages have essentially quite low molecular symmetries.[26,27,29] Hence, by neglecting the effect of the charge state of the cage, such a correlation can be made for **1**–**4** on the basis of the corresponding empty fullerene cages.

The lowest-energy structure of C_{100} has been calculated to be 449:D_2.[27d] Furthermore, the five isomers 18:C_2, 426:C_1, 425:C_1, 442:C_2, and 148:C_1 are preferentially populated within a wide temperature interval.[27d] As fullerenes are generated at extremely high temperature in arc discharges, all of these six thermodynamically most stable isomers are expected to be the probable cage candidates of **3** (Figure 4; see Supporting Information for the analysis on **1**, **2**, and **4**).

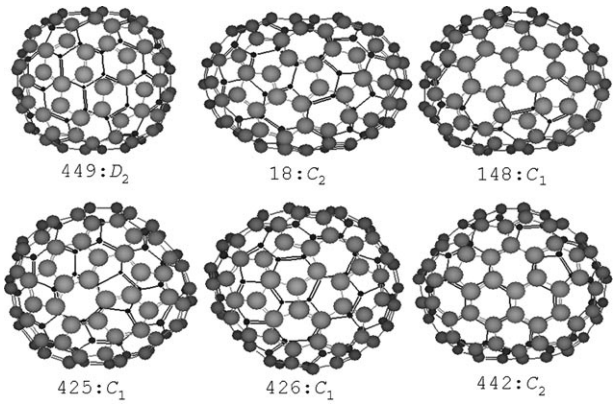


Figure 4. The structures of the six most probable cage isomers of **3** (Dy atoms are omitted for clarity), which are also the thermodynamically most stable IPR isomers of the empty C_{100} fullerene.

In summary, we have successfully produced the stable $Dy_2@C_{100}$ dimetallofullerene **3** (the largest fullerene cage isolated to date), the $Dy_3@C_{98}$ trimetallofullerene **4**, and two $Dy_2@C_{94}$ isomers (**1**, **2**) in high yields. The new higher multimetallofullerenes **1**–**4** were isolated in high purity by single-stage HPLC. The UV/Vis/NIR spectra indicate that **1**–**4** are all small band-gap fullerenes. The large number of lines in the FTIR spectra of **1** and **4** indicates the low symmetries of their cages; in contrast, **2** and **3** are unstable in the solid form. These results open a route to produce new fullerenes with large cages.

Experimental Section

General procedures for the production of fullerenes by a modified Krätschmer-Huffman DC-arc discharging method with the addition of NH_3 (20 mbar) have been described elsewhere.[5,10–12] After DC-arc discharging, the resulting soot was pre-extracted with acetone and further Soxhlet-extracted with CS_2 for 20 h. The fullerenes were separated by single-stage HPLC running in a Hewlett-Packard instrument (series 1050), with toluene used as the eluent. A linear combination of two analytical Buckyprep columns (4.6 × 250 mm; Nacalai Tesque, Japan) was applied to separate the products. A UV detector set to 320 nm was used for fullerene detection. The purity of the isolated products was further checked by HPLC runs performed on a 10 × 250 mm Buckyclutcher column (Regis, USA), followed by LD-TOF MS analysis running in both positive- and negative-ion

 © 2006 Wiley-VCH Verlag GmbH & Co. KGaA, Weinheim

modes (Biflex III, Bruker, Germany). Sample preparation and experimental details for UV/Vis/NIR and FTIR spectroscopic measurements were described previously.[5,10–12]

Received: July 11, 2005
Revised: September 13, 2005
Published online: January 17, 2006

Keywords: dysprosium · endohedral fullerenes · fullerenes · IR spectroscopy · UV/Vis spectroscopy

[1] H. Shinohara, *Rep. Prog. Phys.* **2000**, *63*, 843 – 892.
[2] *Endofullerenes: A New Family of Carbon Clusters* (Eds.: T. Akasaka, S. Nagase), Kluwer, Dordrecht, **2002**.
[3] S. Y. Liu, S. Q. Sun, *J. Organomet. Chem.* **2000**, *599*, 74 – 86.
[4] S. H. Yang, *Trends Chem. Phys.* **2001**, *9*, 31 – 43.
[5] L. Dunsch, M. Krause, J. Noack, P. Georgi, *J. Phys. Chem. Solids* **2004**, *65*, 309 – 315.
[6] S. F. Yang, PhD thesis, Hong Kong University of Science & Technology, **2003**; See also a) S. F. Yang, S. H. Yang, *J. Phys. Chem. B* **2001**, *105*, 9406 – 9412; b) S. F. Yang, L. Z. Fan, S. H. Yang, *J. Phys. Chem. B* **2003**, *107*, 8403 – 8411; c) S. F. Yang, L. Z. Fan, S. H. Yang, *J. Phys. Chem. B* **2004**, *108*, 4394 – 4404; d) S. F. Yang, L. Z. Fan, S. H. Yang, *Chem. Phys. Lett.* **2004**, *388*, 253 – 258.
[7] L. J. Wilson, D. W. Cagle, T. P. Thrash, S. J. Kennel, S. Mirzadeh, J. M. Alford, G. J. Ehrhardt, *Coord. Chem. Rev.* **1999**, *192*, 199 – 207.
[8] S. Stevenson, P. W. Fowler, T. Heine, J. C. Duchamp, G. Rice, T. Glass, K. Harich, E. Hajdu, R. Bible, H. C. Dorn, *Nature* **2000**, *408*, 427 – 428.
[9] a) L. Dunsch, P. Georgi, F. Ziegs, H. Zöller, German Patent DE 10301722A1, **2003**; b) M. Wolf, K.-H. Müller, Y. Skourski, D. Eckert, P. Georgi, M. Krause, L. Dunsch, *Angew. Chem.* **2005**, *117*, 3371 – 3374; *Angew. Chem. Int. Ed.* **2005**, *44*, 3306 – 3309.
[10] a) M. Krause, L. Dunsch, *Angew. Chem.* **2005**, *117*, 1581 – 1584; *Angew. Chem. Int. Ed.* **2005**, *44*, 1557 – 1560; b) M. Krause, J. Wong, L. Dunsch, *Chem. Eur. J.* **2005**, *11*, 706 – 711; c) M. Krause, L. Dunsch, *ChemPhysChem* **2004**, *5*, 1445 – 1449.
[11] S. F. Yang, L. Dunsch, *Chem. Eur. J.* **2005**, *12*, 413 – 419.
[12] S. F. Yang, L. Dunsch, *J. Phys. Chem. B* **2005**, *109*, 12320 – 12328.
[13] C. R. Wang, T. Kai, T. Tomiyama, T. Yoshida, Y. Kobayashi, E. Nishibori, M. Takata, M. Sakata, H. Shinohara, *Angew. Chem.* **2001**, *113*, 411 – 413; *Angew. Chem. Int. Ed.* **2001**, *40*, 397 – 399.
[14] L. Dunsch, A. Bartl, P. Georgi, P. Kuran, *Synth. Met.* **2001**, *121*, 1113 – 1114.
[15] H. Kato, A. Taninaka, T. Sugai, H. Shinohara, *J. Am. Chem. Soc.* **2003**, *125*, 7782 – 7783.
[16] C. R. Wang, P. Georgi, L. Dunsch, T. Kai, T. Tomiyama, H. Shinohara, *Curr. Appl. Phys.* **2002**, *2*, 141 – 143.
[17] C. R. Wang, T. Kai, T. Tomiyama, T. Yoshida, Y. Kobayashi, E. Nishibori, M. Takata, M. Sakata, H. Shinohara, *Nature* **2000**, *408*, 426 – 427.
[18] B. P. Cao, T. Wakahara, T. Tsuchiya, M. Kondo, Y. Maeda, G. M. A. Rahman, T. Akasaka, K. Kobayashi, S. Nagase, K. Yamamoto, *J. Am. Chem. Soc.* **2004**, *126*, 9164 – 9165.
[19] N. Tagmatarchis, H. Shinohara, *Chem. Mater.* **2000**, *12*, 3222 – 3226.
[20] N. Tagmatarchis, E. Aslanis, K. Prassides, H. Shinohara, *Chem. Mater.* **2001**, *13*, 2374 – 2379.
[21] Z. Slanina, X. Zhao, F. Uhlik, S.-L. Lee, *J. Mol. Struct. (Theochem)* **2003**, *630*, 205 – 213.
[22] a) H. Shinohara, H. Sato, M. Ohkohchi, Y. Ando, T. Kodama, T. Shida, T. Kato, *Nature* **1992**, *357*, 52 – 54; b) M. Takata, E. Nishibori, M. Sakata, M. Inakuma, E. Yamamoto, H. Shinohara, *Phys. Rev. Lett.* **1999**, *83*, 2214 – 2217.
[23] Y. F. Lian, Z. J. Shi, X. H. Zhou, Z. N. Gu, *Chem. Mater.* **2004**, *16*, 1704 – 1714.
[24] M. Krause, S. Baes-Fischlmair, R. Pfeifer, W. Plank, T. Pichler, H. Kuzmany, N. Tagmatarchis, K. Prassides, *J. Phys. Chem. B* **2001**, *105*, 11964 – 11969.
[25] a) M. Inakuma, E. Yamamoto, T. Kai, C. R. Wang, T. Tomiyama, H. Shinohara, T. J. S. Dennis, M. Hulman, M. Krause, H. Kuzmany, *J. Phys. Chem. B* **2000**, *104*, 5072 – 5077; b) M. Krause, M. Hulman, H. Kuzmany, T. J. S. Dennis, M. Inakuma, H. Shinohara, *J. Chem. Phys.* **1999**, *111*, 7976 – 7984.
[26] P. W. Fowler, D. E. Manolopoulos, *An Atlas of Fullerenes*, Clarendon, Oxford, **1995**.
[27] a) X. Zhao, Z. Slanina, H. Goto, E. Osawa, *J. Chem. Phys.* **2003**, *118*, 10534 – 10540; b) X. Zhao, Z. Slanina, *J. Mol. Struct. (Theochem)* **2003**, *636*, 195 – 201; c) X. Zhao, Z. Slanina, H. Goto, *J. Phys. Chem. A* **2004**, *108*, 4479 – 4484; d) X. Zhao, H. Goto, Z. Slanina, *Chem. Phys.* **2004**, *306*, 93 – 104.
[28] G. Sun, M. Kertesz, *J. Phys. Chem. A* **2001**, *105*, 5212 – 5220.
[29] Z. Slanina, private communication.

 © 2006 Wiley-VCH Verlag GmbH & Co. KGaA, Weinheim

Metathesis

DOI: 10.1002/anie.200503321

Diastereoselective Ring-Rearrangement Metathesis**

*Verena Böhrsch, Jürgen Neidhöfer, and Siegfried Blechert**

Olefin metathesis is one of the most versatile tools in organic synthesis because of its broad applicability and its compatibility with functional groups.[1] Among the different types of the metathesis reactions that have been developed, ring-rearrangement metathesis (RRM) has proven to be especially powerful. Stereocenters are easily established in a ring and transferred to the side chain. RRM has been applied in the synthesis of fused carbocycles[2] and polycyclic ethers[3] as well as piperidines,[4,5] pyrrolidines,[5] and various natural products.[6]

We were interested in extending this methodology to create new stereocenters by RRM. Some years ago, we presented the first example of diastereoselective ring-closing metathesis.[7] The selectivity was catalyst-dependent. Diastereoselective RCM has been applied in the synthesis of highly functionalized rings,[8] also those containing quaternary

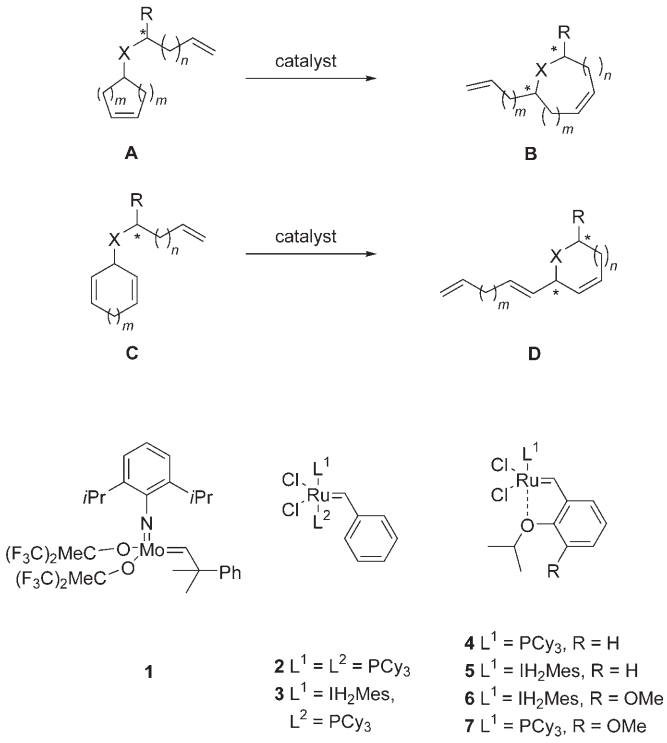
[*] V. Böhrsch, J. Neidhöfer, Prof. Dr. S. Blechert
Institut für Chemie
Technische Universität Berlin
Strasse des 17. Juni 135, 10623 Berlin (Germany)
Fax: (+49) 30-314-23619
E-mail: blechert@chem.tu-berlin.de

[**] V.B. thanks the Graduiertenkolleg 352 for a scholarship.

Supporting information for this article is available on the WWW under http://www.angewandte.org or from the author.

WILEY InterScience DISCOVER SOMETHING GREAT
© 2006 Wiley-VCH Verlag GmbH & Co. KGaA, Weinheim

stereocenters[9] as well as natural products, for example, in the synthesis of (−)-limaspermine[10] and in the formal synthesis of (−)-eburnamorine.[11] Herein we present the concept of diastereoselective ring-rearrangement metathesis. RRM of prochiral rings with stereocenters in the side chain like **A** and **C** should lead to respective carbo- and heterocycles like **B** and **D** containing a new stereocenter (Scheme 1). The challenge



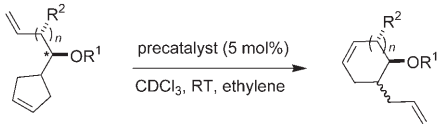
Scheme 1. Concept of the diastereoselective RRM. Mes = 2,4,6-trimethylphenyl, Cy = cyclohexyl.

for such a process is to shift the reaction to the desired product. Mechanistically, the reaction can start either at the terminal or the cyclic double bond and can be thermodynamically or kinetically controlled.

In the first experiments we used 1-cyclopent-3-enyl-but-3-en-1-ol (**8a**) and the *tert*-butyldimethylsilyl (TBDMS)-protected derivative **9a** as substrates under different conditions and with different precatalysts (**1**–**7**). We found that an ethylene atmosphere prevented dimerization and oligomerization and enhanced the catalyst initiation rate.

The monosubstituted cyclopentenes **8a**–**9a** ($n = 0$) underwent rearrangement to give the more substituted five-membered ring (Table 1). As expected, conversions and diastereoselectivities were catalyst dependant. For example, with precatalyst **3** cyclopentene **8a** rearranged to give **8b** in 79% conversion (d.r. (*trans*/*cis*) = 4:1). The use of **4** resulted in only 19% conversion. The protected allylic alcohol **9a** underwent rearrangement with 5 mol% of **4** in 79% conversion with a diastereoselectivity of 4:1, whereas 10 mol% of **1** led to a diastereoselectivity of 3:1 and 70% conversion. Selected results are given in Table 1. The conversions and diastereoselectivities were determined by ^{1}H NMR spectroscopy. In most cases, the pure diastereoisomers were isolable by silica gel chromatography and obtained in good to excellent yields. For details see the Supporting Information.

Table 1: Rearrangement of cyclopentenes.



8a–14a 8b–14b

Cmpd	n	R^1	R^2	Cat.	Conv. [%][d]	*trans*/*cis*[d]
8a	0	H	H	**3**	79	4:1
9a	0	TBDMS	H	**4**	79	4:1
10a	1	H	H	**3**[b]	88	1:4[a]
11a	1	TBDMS	H	**3**	95	2:1
12a	1	MEM	H	**3**	95	2:1
13a	1	H	TMS	**4**	86	1:6
14a	1	H	Ph	**3**	82	3:1[c]

[a] Reaction conducted with 1.5 equiv of $Ti(OiPr)_4$ as an additive. [b] Reaction conducted with 3 mol% catalyst. [c] Reaction performed at 50°C. [d] Determined by ^{1}H NMR spectroscopy.

In case of the allylic alcohol **8a**, the thermodynamic control of the reaction was demonstrated by equilibration experiments. Thus, subjecting pure *trans*-**8b** to the rearrangement conditions resulted again in a mixture of **8a**, *trans*-**8b**, and *cis*-**8b** (3:9:2).

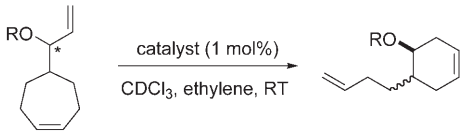
Homologous substrates ($n = 1$) also undergoes RRM giving cyclohexenes. Notably, the free homoallylic alcohol **10a** provided the *cis* product (d.r. = 3:2) as the main product. To increase the steric bulk of the alcohol $Ti(OiPr)_4$ was added to the reaction mixture, which led to an enhancement of selectivity in favor of the *cis* product (d.r. = 4:1) and not, as expected for steric reasons, the *trans* product. Equilibration experiments did not lead to changes in the diastereomeric ratio, which is consistent with kinetic control for this case. To investigate the influence of precoordination of the metal center versus the steric influence, different protecting groups were introduced. We compared the effect of a sterically demanding, noncoordinating TBDMS group and a coordinating (2-methoxyethoxy)methyl (MEM) group. Cyclopentenes **11a** and **12a** gave predominantly the *trans* products with precatalyst **3**, although in moderate selectivity (d.r. = 2:1). The first-generation precatalysts **2, 4**, and **7** gave complete conversion but gave no diastereoselectivity. The second-generation precatalysts **5** and **6** showed the same selectivity as **3**. In all cases the structure of the protecting group did not affect the stereoselectivity.

To probe the reaction further, a second stereocenter was introduced in the side chain. As examples the trimethylsilyl (TMS)- and phenyl-substituted compounds **13a** and **14a**, respectively, were chosen. The stereocenters in the allylic position were found to strongly influence the diastereoselectivity. The rearrangement of **13a** with 5 mol% of **4** gave **13b** in 86% conversion with a ratio of 6:1 in favor of the *cis* isomer. In this example, identical selectivities were achieved with the precatalysts **3** and **4**, but the reactivity of **4** was superior to that of **3**. To our surprise, the phenyl-substituted compound **14a** gave the all-*trans*-configurated product **14b**

 © 2006 Wiley-VCH Verlag GmbH & Co. KGaA, Weinheim

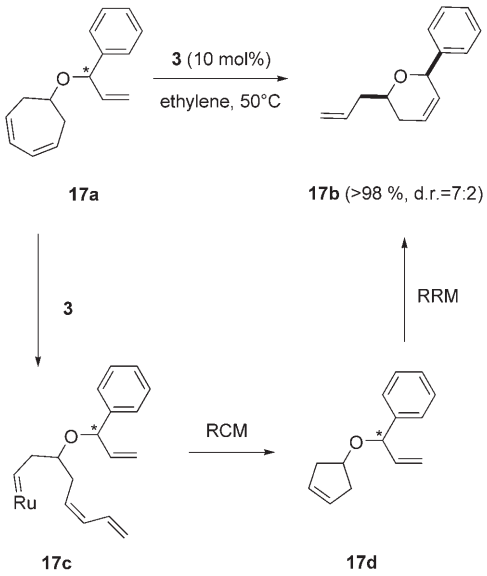
with inversed selectivity (d.r. = 3:1) compared to that with the unsubstituted substrate **10a**. The use of $Ti(OiPr)_4$ did not result in different selectivities.

Following the promising results obtained with cyclopentenes, we investigated prochiral rings of different sizes in order to vary the length of the side chain in the product. The reactions of cycloheptenes **15a** and **16a** did not show significant selectivities with any of the precatalysts (Scheme 2), though the conversion was complete with a precatalyst loading as low as 1 mol% at room temperature. The addition of $Ti(OiPr)_4$ to the free alcohol **15a** did not influence the result.



Scheme 2. RRM of cycloheptenes.

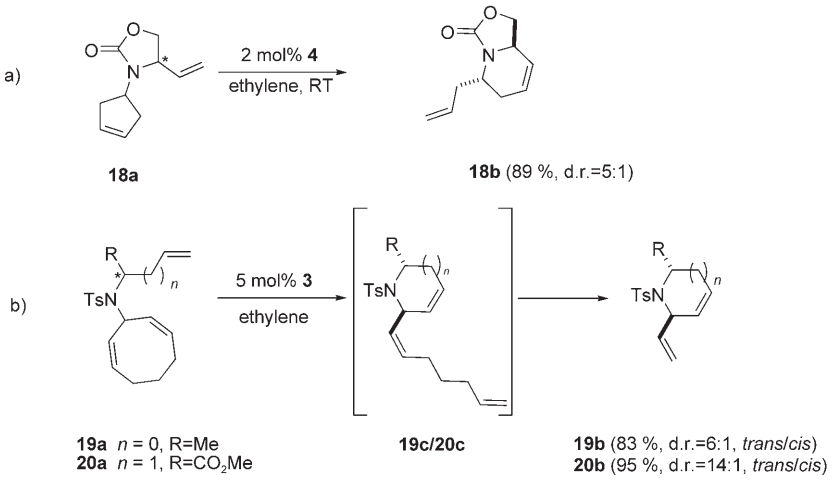
As heterocycles are present in a large number of biologically and synthetically interesting natural products, we were also interested in applying our method to their synthesis. We envisaged that cyclodienes such as **17a** would rearrange to give products with an internal double bond in the side chain. Instead, **17a** was converted into the dihydropyran **17b** with a diastereomeric ratio of 7:2 in favor of the 2,6 *cis* product (Scheme 3). GC–MS determination and NMR control showed the cyclopentene derivative **17d** to be an intermediate, which appeared and disappeared during the course of the reaction. A reasonable explanation for these observations is that the precatalyst attacks the ring double bond giving the carbene complex **17c**, which then reacts by RCM to give **17d** while butadiene is cleaved. The new prochiral substrate now rearranges to give the isolated dihydropyran **17b**.



Scheme 3. Preparation of dihydropyrans by RRM.

We next focused on using a cyclopentene to prepare nitrogen heterocycles. Carbamate **18a** underwent rearrangement most effectively with the Hoveyda I precatalyst **4** (Scheme 4a). We were pleased to observe a good diastereomeric ratio (5:1) and high conversion (89%) with low precatalyst loading (2 mol%). With precatalyst **2** the diastereomeric ratio was almost identical, but a higher loading of **2** was necessary for good conversions (4 mol%). To our surprise, in this example the second-generation precatalysts **3** and **5** provided the product with lower selectivities (2:1).[12] To examine the reversibility of the reaction, the *cis*-configured carbamate **18b** was submitted to the rearrangement conditions (4 mol% **2**). As no reaction took place, we assume kinetic control for this substrate.

Finally we investigated the reactions of 1,4-cyclooctadienes, which cannot undergo ring contraction. Because pyrroles and piperidines are important core structures of natural products, the cyclooctadienes **19a** and **20a** were examined (Scheme 4b). Upon reaction with 5 mol% of **3**, dihydropyrrole **19b** was obtained with a good selectivity of 6:1, although higher temperatures were necessary for good conversions. RRM first leads to the intermediate **19c**, whose side chain bears a 1,6-diene moiety. This chain is severed in the cross-metathesis with ethylene or in the cyclization of the side chain giving cyclopentene, preventing equilibration. With the first-generation precatalysts **2** and **4**, a mixture of **19b** and **19c** was obtained. The major product **19b** was deduced to be the *trans* isomer by comparison of its NMR spectra with that reported for the *cis* compound.[13] The allylglycine-derived cyclooctadiene derivative **20a** was rearranged to give the piperideine derivative **20b** with high conversion and excellent



Scheme 4. RRM leading to pyrroles and piperideines as rearrangement products. Ts = toluene-4-sulfonyl.

 © 2006 Wiley-VCH Verlag GmbH & Co. KGaA, Weinheim

diastereoselectivity (95%, 14:1) at room temperature (Scheme 4b). This example is of particular interest, as piperideines such as **20b** are found in various natural products.[14]

In summary, we have developed the new concept of diastereoselective ring-rearrangement metathesis. Various carbo- and heterocycles were prepared in moderate to excellent stereoselectivities and in good conversions. We observed a strong influence of the substitution pattern of the directing stereocenter on the configuration of the new stereocenter. The diastereoselectivity depended on the pre-catalyst applied. Differently substituted cyclopentenes and cyclohexenes as well as 2,5-substituted dihydropyrans, dihydropyrroles, and dihydropyridines were prepared. The application of the method in total synthesis is in progress and will be reported in due course. Spectroscopic data and experimental procedures are given in the Supporting Information.

Received: September 19, 2005
Published online: January 19, 2006

Keywords: diastereoselectivity · heterocycles · metathesis · rearrangement · synthetic methods

[1] Selected reviews: K. C. Nicolaou, P. G. Bulger, D. Sarlah, *Angew. Chem.* **2005**, *117*, 4564 – 4601; *Angew. Chem. Int. Ed.* **2005**, *44*, 4490; R. H. Grubbs, *Tetrahedron* **2004**, *60*, 7117; S. J. Connon, S. Blechert, *Angew. Chem. Int. Ed.* **2003**, *42*, 1900; *Angew. Chem.* **2003**, *115*, 1944; A. Fürstner, *Angew. Chem.* **2000**, *112*, 3140; *Angew. Chem. Int. Ed.* **2000**, *39*, 3012.
[2] R. Stragies, S. Blechert, *Synlett* **1998**, 169.
[3] S. D. Burke, K. J. Quinn, V. J. Chen, *J. Org. Chem.* **1998**, *63*, 8626; J. P. A. Harrity, M. S. Visser, J. D. Gleason, A. H. Hoveyda, *J. Am. Chem. Soc.* **1997**, *119*, 1488; W. J. Zuercher, M. Hashimoto, R. H. Grubbs, *J. Am. Chem. Soc.* **1996**, *118*, 6634.
[4] J. Neidhöfer, S. Blechert, *Synthesis* **2004**, *18*, 3047; U. Voigtmann, S. Blechert, *Synthesis* **2000**, *6*, 893 – 898.
[5] H. Ovaa, C. Stapper, G. A. van der Marel, H. S. Overkleeft, J. H. van Boom, S. Blechert, *Tetrahedron* **2002**, *58*, 7503.
[6] N. Holub, J. Neidhöfer, S. Blechert, *Org. Lett.* **2005**, *7*, 1227; S. Basra, S. Blechert, *Strategies Tactics Org. Synth.* **2004**, *4*, 315.
[7] C. M. Huwe, J. Velder, S. Blechert, *Angew. Chem.* **1996**, *108*, 2542 – 2544; *Angew. Chem. Int. Ed. Engl.* **1996**, *35*, 2376.
[8] P. A. Evans, J. Cui, G. P. Buffone, *Angew. Chem.* **2003**, *115*, 1776; *Angew. Chem. Int. Ed.* **2003**, *42*, 1734 – 1737.
[9] Y.-i. Fukuda, H. Sasaki, M. Shindo, K. Shishido, *Tetrahedron Lett.* **2002**, *43*, 2047; B. Schmidt, B. Costisella, R. Roggenbuck, M. Westhus, H. Wildemann, P. Eilbracht, *J. Org. Chem.* **2001**, *66*, 7658.
[10] Y.-i. Fukuda, M. Shindo, K. Shishido, *Heterocycles* **2004**, *62*, 787.
[11] Y. Murakami, M. Shindo, K. Shishido, *Synlett* **2005**, *4*, 664.
[12] A similar effect was observed by Wallace in double RCM: D. J. Wallace, *Tetrahedron Lett.* **2005**, *46*, 591 – 594.
[13] K. Fugami, K. Oshima, K. Utimoto, H. Nozaki, *Bull. Chem. Soc. Jpn.* **1987**, *60*, 2509.
[14] F.-X. Felpin, J. Lebreton, *Curr. Org. Synth.* **2004**, *1*, 83.

 © 2006 Wiley-VCH Verlag GmbH & Co. KGaA, Weinheim

Magnetic Properties

DOI: 10.1002/anie.200503140

Two Compounds Containing the Mixed Germanium–Vanadium Polyoxothioanion $[V_{14}Ge_8O_{42}S_8]^{12-}$**

*Dragan Pitzschke, Jing Wang, Rolf-Dieter Hoffmann, Rainer Pöttgen, and Wolfgang Bensch**

The variety of microporous polyhedral framework solids has increased severely in the last years.[1] The largest classes of microporous materials are still aluminosilicates (Al-O-Si) and aluminophosphates (Al-O-P) as well as their isomorphic substituted forms. These compounds have been studied extensively because of their interesting properties and applications in industrial processes as, for instance, catalysts and ion-exchange materials. A promising strategy for the synthesis of new open-framework materials with elements others than Al or Si is to connect larger building units like clusters in vanadates and molybdates or secondary building units (SBUs) in large-pore indium sulfides.[2–7] The interconnection of polyoxometal building blocks like polyoxovanadates by means of covalent bonds could create new porous materials with ultralow framework densities and high porosity. The catalytic or photochemical reactivity of such transition-metal-based materials could be enhanced relative to that of Si- or Al-containing materials. Vanadium is of particular interest because it shows a flexible coordination behavior as well as a great variety of valence states. VO_4 tetrahedra, VO_5 square pyramids, and VO_6 octahedra are often observed as primary building units in polyoxovandate compounds.[8] These building units are able to form larger aggregates and/or clusters by condensation of the polyhedra. The clusters or aggregates may then be joined through metal coordination complexes to create three-dimensional framework structures. During the last years a number of pure and mixed vanadates like vanadiumborates, -arsenates, -germanates, and -phosphates with organic and inorganic counterions have been prepared.[9–14]

In our investigations we attempted to incorporate sulfur and germanium in anionic vanadium clusters in order to enhance the structural diversity of the building units and to generate possible porous compounds. Here we report the synthesis and characterization of the two new mixed Ge/V polyoxothio compounds (dien-H_3)$_4$[$V_{14}Ge_8O_{42}S_8$]·5H_2O (**1**)

[*] Dipl.-Chem. D. Pitzschke, J. Wang, Prof. Dr. W. Bensch
Institut für Anorganische Chemie
Universität Kiel
Olshausenstrasse 40, 24098 Kiel (Germany)
Fax: (+49) 431-880-1520
E-mail: wbensch@ac.uni-kiel.de
Dr. R.-D. Hoffmann, Prof. Dr. R. Pöttgen
Institut für Anorganische und Analytische Chemie
Westfälische Wilhelms-Universität Münster (Germany)

[**] This work was supported by the State of Schleswig-Holstein.

 © 2006 Wiley-VCH Verlag GmbH & Co. KGaA, Weinheim

and (aep-H_3)$_4$[$V_{14}Ge_8O_{42}S_8$] (**2**). The two compounds were prepared hydrothermally using diethylenetriamine (dien) and 1-(2-aminoethyl)piperazine (aep) as bases. The structures consist of isolated $[V_{14}Ge_8O_{42}S_8]^{12-}$ anions with protonated amines as counterions. The $[V_{14}Ge_8O_{42}S_8]^{12-}$ units represent the first known germanium vanadium polyoxothioanion compounds and are composed of 12 slightly distorted VO_5 square pyramids and 8 GeO_3S tetrahedra (Figure 1, top).

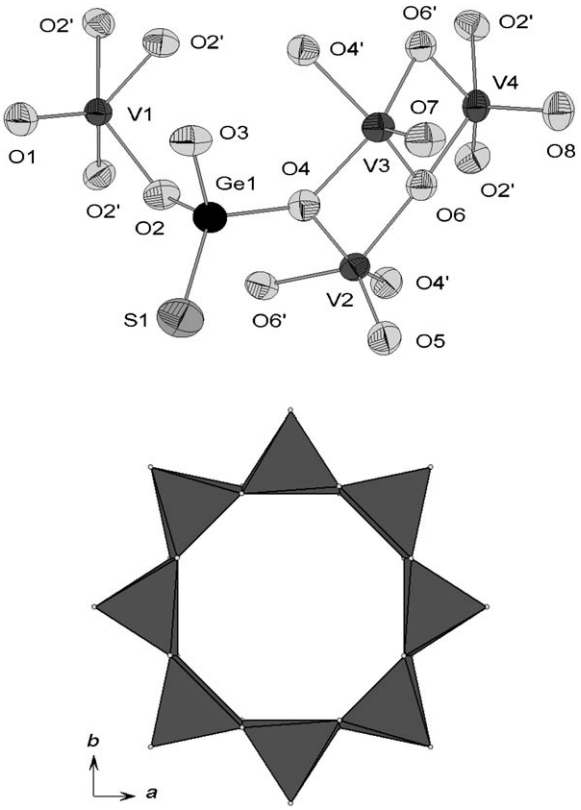


Figure 1. Top: Asymmetric unit of **2** with labeling and displacement ellipsoids drawn at the 50% probability level (atoms with superscripts are generated by symmetry operations). Bottom: Ring built by interconnection of the eight VO_5 square pyramids located in the middle of the cluster in compound **2**.

The VO_5 pyramids in **1** and **2** have typical geometric parameters with basal and apical bond lengths of 1.919(5)–1.998(5) Å and 1.592(11)–1.630(8) Å, respectively. The O-V-O angles vary between 76.5(3) and 149.9(3)°. The bond valence sums for all V atoms in **1** and **2** were determined according to the method of Brown and Altermatt.[15] The average value of 4.10 justify the assignment of V^{4+}. The GeO_3S tetrahedra are moderately distorted with Ge–O bond lengths between 1.778(6) and 1.809(4) Å and Ge–S bond lengths from 2.096(3) to 2.122(3) Å. The angles vary between 103.4(2) and 105.1(3)° for O-Ge-O angles and are between 110.5(2) and 117.2(2)° for O-Ge-S. The bond lengths and angles in **1** and **2** are comparable with those found in other vanadates and in thiogermanates.[2,3,16] Within the cluster eight VO_5 square pyramids are condensed to form a ring (Figure 1, bottom). Each VO_5 unit in the ring is connected with two other square pyramids sharing common edges. On each side of the ring three VO_5 pyramids and four GeO_3S tetrahedra are connected through common edges and corners forming the anionic cluster (Figure 2). The cluster diameter is

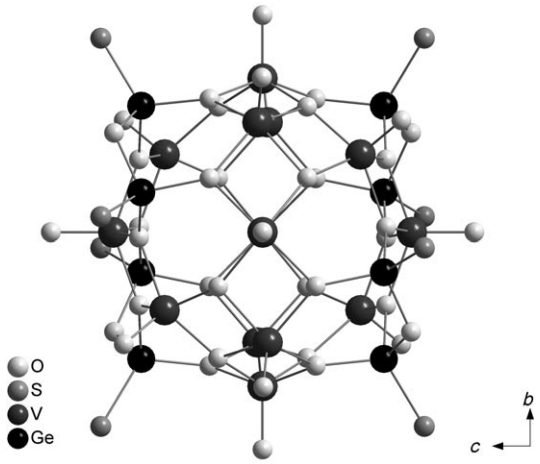


Figure 2. $[V_{14}Ge_8O_{42}S_8]^{12-}$ unit of the title compounds.

7.450 Å for **1** and 7.316 Å for **2**, measured from coordinate to coordinate. The organic cations are located between the clusters. The $[V_{14}Ge_8O_{42}S_8]^{12-}$ clusters in **1** are stacked along the *c* axis in an AB sequence, reminiscent of hexagonal closed packing. The anions in every A layer of **1** are rotated by 90° with respect to the clusters in the B layers. In compound **2** the anions are also arranged in an AB sequence, but the orientation of the clusters is identical in the two layers.

The thermal stability of **1** and **2** was investigated by simultaneous difference thermoanalysis (DTA) and thermogravimetry analysis (TGA) in air at temperatures between 25 and 725 °C. Compound **1** decomposes in two steps with a total mass loss of $\Delta m_{exp} = 27.9\,\%$, which is in good agreement with that calculated for the removal of the organic cations ($\Delta m_{theo} = 16.1\,\%$), S ($\Delta m_{theo} = 9.7\,\%$), and H_2O ($\Delta m_{theo} = 3.3\,\%$). The first thermal event (30–180 °C) is accompanied by $\Delta m_{exp} = 3.3\,\%$. The second thermal process ($\Delta m_{exp} = 24.6\,\%$) covering $T = 180$–660° shows three exothermic events (at $T_P = 302$, 525, and 589 °C; T_P = peak temperature). In the brown residue only small amounts of organic components and S were found (C 0.484 %, H 0.042 %, N 0.173 %, S 0.359 %, $CHNS_{sum} = 1.058\,\%$). In further experiments the heating process was stopped at 180 °C. CHNS analysis revealed no loss of organic components. DTA-TGA-MS measurements showed the loss of H_2O (m/z 18) in this temperature range. The loss of water is reversible, and when the dehydrated product is stored in a wet atmosphere, water is incorporated again. The weight loss during the first step corresponds to five H_2O molecules per formula unit. Compound **2** is decomposed in two steps with an overall weight loss of $\Delta m_{exp} = 29.9\,\%$, which agrees well with the expulsion of the organic cation ($\Delta m_{theo} = 19.4\,\%$) and S ($\Delta m_{theo} = 9.4\,\%$). The first step ranges from 30 to 430 °C ($\Delta m_{exp} = 15.2\,\%$) and the second step from 430 to 725 °C ($\Delta m_{exp} = 14.7\,\%$). Three

 © 2006 Wiley-VCH Verlag GmbH & Co. KGaA, Weinheim

exothermic events ($T_P = 305$, 443 and 583 °C) are seen in the DTA curve. The CHNS analysis revealed a contamination of less than 0.1 % in the brown residue (C 0.069 %, H 0.0 %, N 0.0 %, S 0.0 %, $CHNS_{sum} = 0.069$ %). In further experiments the heating process was stopped at 430 °C. The powder pattern of the product is X-ray amorphous. In the X-ray powder patterns of the final decomposition products of **1** and **2** crystalline V_2O_5 and GeO_2 could be identified.

The cluster $[V_{14}Ge_8O_{42}S_8]^{12-}$ contains 14 V^{4+} ions with d^1 electronic configuration. This arrangements is reminiscent of that observed earlier in a V_{14}-containing vanadate.[2d] The asymmetric unit (Figure 1) contains three oxygen-bridged V^{4+} ions. If one assumes antiferromagnetic interactions through superexchange between V2, V3, and V4, magnetic frustration results and therefore a net magnetic moment may occur regardless of the orientation of the three coupled spins. The temperature dependence of the magnetic susceptibility of solvent-free **2** was measured to determine the magnetic behavior of the cluster. Figure 3 shows the temperature

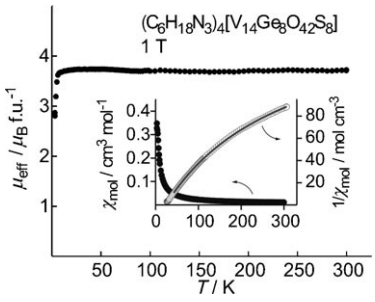


Figure 3. Temperature dependence of the effective magnetic moment, μ_{eff}, of **2** at 1 T. The solid line in the insert was obtained from equation $\mu_{eff}^2 = 8\,(\chi - TIP)\,T\mu_B$.

dependence of the effective magnetic moment, calculated using Equation (1) and corrected for diamagnetism (1313.6×10^{-6} cm^3 mol^{-1}).

$$\mu_{eff}^2 = 8\,(\chi - TIP)\,T\,\mu_B \qquad (1)$$

The inset of Figure 3 depicts χ_{mol} and χ_{mol}^{-1} emphasizing the deviation from a simple Curie law. The solid line corresponds to the calculated value employing the above formula. Nevertheless, the temperature dependence of the magnetic moment is described well by the modified Curie law down to low temperatures. The occurrence of a temperature-independent paramagnetism (TIP) can be understood considering the $^2D_{3/2}$ ground state of the V^{4+} ions, it was 5562×10^{-6} cm^3 mol^{-1}. The magnetic moment stays constant from very low temperatures (20 K) up to room temperature and it amounts to 3.71 μ_B. This value is much smaller than that expected for 14 independent V^{4+} ions, which would yield 6.48 μ_B with $g = 2$ and $S = 1/2$ ($1.732 \times \sqrt{14} = 6.48$). Thus, to a large extent antiferromagnetic coupling must be assumed. To further elucidate the magnetic behavior, isothermal field dependence was examined (Figure 4). While at 300 K paramagnetic saturation determines the magnetization, at 3 K magnetization increases

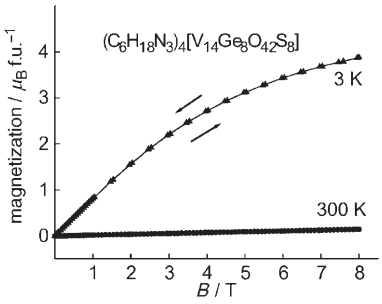


Figure 4. Field dependence of the molar magnetization of **2** measured at 300 K and 3 K after zero-field cooling of the sample.

linearly up to ca. 1.5 T. At that point the magnetization levels off and saturation is not reached yet at 8 T with $\mu_{SM} = 3.88\,\mu_B$. The maximum saturation moment would be $14\,g\,S = 14\,\mu_B$ for 14 independent V^{4+} ions. Gradually the spins undergo field-induced flipping, but considering the arrangement of the 14 V^{4+} ions in the cluster which would clearly not give a trivial spin system, the maximum moment cannot be reached. Spontaneous magnetization was not observed, and this was further supported by FC measurements at 0.01 T (see the Experimental Section). Additional alternating-current magnetization measurements, which distort the spin system to a lesser extent than direct-current magnetization, did not reveal any energy losses in the imaginary part of the magnetic susceptibility nor any frequency dependence suggesting predominant antiferromagnetic spin interactions for **2**.

The promising results presented here can be regarded as a starting point for further systematic exploration of the Ge-V-S-O system. It is highly likely that systematic variation of the synthesis conditions might yield new and fascinating materials with new structural architectures and interesting physical properties.

Experimental Section

Compounds **1** and **2** were synthesized under hydrothermal conditions using germanium (146 mg, 2 mmol), NH_4VO_3 (468 mg, 4 mmol), and sulfur (128 mg, 4 mmol). For **1**, diethylenetriamine (50 % in H_2O; 4 mL, 18 mmol) was applied and **2** was synthesized in 1-(2-aminoethyl)piperazine (75 % in H_2O; 4 mL, 23 mmol). The mixtures were heated to 160 °C (**1**) and 170 °C (**2**), respectively, for seven days in Teflon-lined steel autoclaves (ca. 30 mL). The homogeneous products consisting of black octahedral crystals were filtered off, washed with distilled water, and dried in air. The yield based on Ge is about 60 %. Typical dimensions of the crystals are $0.1 \times 0.1 \times 0.1$ mm^3. The compounds are stable in air and not soluble in water or conventional organic solvents.

X-ray structure analysis and crystallographic data for **1**: $C_{16}H_{74}N_{12}Ge_8O_{47}S_8V_{14}$, $M_r = 2737.25$, tetragonal, space group $P\bar{4}2c$, $a = 14.2358(8)$, $c = 23.142(2)$ Å, $V = 4689.9(5)$ Å^3; $Z = 2$; $\rho_{calcd} = 1.875$ g cm^{-3}, $F(000) = 2572$, $T = 293$ K, $\lambda(Mo_{K\alpha}) = 0.71073$ Å, Flack parameter $x = 0.01(2)$. Single-crystal X-ray work was performed using an Imaging Plate Diffraction System (IPDS-1). 10977 reflections collected, 4500 independent ($R_{int} = 0.0478$). 216 parameters, the final residues were $R1$ ($I \geq 2\sigma(I)$) = 0.0528, wR2 ($I \geq 2\sigma(I)$) = 0.1419, GoF = 1.000. H_2O molecules are heavily disordered and could not be located. Residual electron density: 1.412/−0.578 e Å^{-3}. X-ray

 © 2006 Wiley-VCH Verlag GmbH & Co. KGaA, Weinheim

structure analysis and crystallographic data for **2**: $C_{24}H_{72}N_{12}Ge_8O_{42}S_8V_{14}$, $M_r = 2751.32$, tetragonal, space group $I\bar{4}2m$, $a = 14.536(2)$, $c = 22.688(4)$ Å, $V = 4793.5(10)$ Å^3; $Z = 2$; $\rho_{calcd} = 1.901$ g cm^{-3}, $F(000) = 2668$, $T = 293$ K, $\lambda(Mo_{K\alpha}) = 0.71073$ Å, Flack parameter $x = 0.00(5)$. Single crystal X-ray work was performed using a STOE AED-II four-circle diffractometer. 4747 reflections collected, 2151 independent ($R_{int} = 0.0232$). 161 parameters, the final residues were $R1$ ($I \geq 2\sigma(I)$) = 0.0468, $wR2$ ($I \geq 2\sigma(I)$) = 0.1385, GoF = 1.122. Residual electron density: 2.894/−0.667 e Å^{-3}. Face-indexed absorption correction; structure solution with SHELXS-97;[17] structure refinement against F^2 using SHELXL-97.[17]

CCDC-273447 (**1**) and -273446 (**2**) contain the supplementary crystallographic data for this paper. These data can be obtained free of charge from The Cambridge Crystallographic Data Centre via www.ccdc.cam.ac.uk/data_request/cif.

DTA-TGA measurements were performed simultaneously in Al_2O_3 crucibles under a dynamic air atmosphere (flow rate: 75 mL min^{-1}) using different heating rates with the STA-429CD thermobalance from Netzsch. DTA-TGA-MS measurements were performed simultaneously in Al_2O_3 crucibles under a dynamic helium or nitrogen atmosphere (flow rate: 75 mL min^{-1}, purity: 5.0) using different heating rates with the STA-409CD thermobalance with Skimmer coupling from Netzsch, which is equipped with a quadrupole mass spectrometer QMA 400 from Balzers. X-ray powder diffraction experiments were conducted on a STOE STADI P transmission powder diffractometer with a position-sensitive detector and $Cu_{K\alpha1}$ radiation ($\lambda = 1.540598$ Å).

Magnetic susceptibilities of polycrystalline agglomerates of **2** were measured with a Physical Property Measurement System (PPMS, Quantum Design, Inc.) between 3 K and 300 K. Direct-current measurements were performed in zero-field-cooled (ZFC, 1 T) and field-cooled (FC, 0.01 T) mode. Isothermal magnetization was measured after ZFC with magnetic flux densities up to 8 T. Alternating-current measurements were used to analyze a possible frequency dependence of the real and imaginary part of the magnetic susceptibility with amplitudes of 3 and 10 Oe in the frequency range from 11 Hz up to 9999 Hz.

Received: September 5, 2005
Published online: January 20, 2006

Keywords: magnetic properties · polyoxothio anions · solvothermal synthesis · structure elucidation · thermal stability

[1] a) A. K. Cheetham, G. Férey, T. Loiseau, *Angew. Chem.* **1999**, *111*, 3466 – 3492; *Angew. Chem. Int. Ed.* **1999**, *38*, 3268 – 3292.
[2] a) A. Müller, E. Krickemeyer, M. Penk, H.-J. Walberg, H. Bögge, *Angew. Chem.* **1987**, *99*, 1060 – 1061; *Angew. Chem. Int. Ed. Engl.* **1987**, *26*, 1045 – 1046; b) A. Müller, M. Penk, R. Rohlfing, E. Krickemeyer, J. Döring, *Angew. Chem.* **1990**, *102*, 927 – 929; *Angew. Chem. Int. Ed. Engl.* **1990**, *29*, 927 – 929; c) A. Müller, E. Krickemeyer, M. Penk, R. Rohlfing, A. Armatage, H. Bögge, *Angew. Chem.* **1991**, *103*, 1720 – 1722; *Angew. Chem. Int. Ed. Engl.* **1991**, *30*, 1674 – 1676; d) A.-L. Barra, D. Gatteschi, L. Pardi, A. Müller, J. Döring, *J. Am. Chem. Soc.* **1992**, *114*, 8509 – 8514.
[3] a) T. Drezen, O. Joubert, M. Ganne, L. Brohan, *J. Solid State Chem.* **1998**, *136*, 298 – 304; b) T. Drezen, M. Ganne, *J. Solid State Chem.* **1999**, *147*, 552 – 560.
[4] a) A. Müller, E. Beckmann, H. Bögge, M. Schmidtmann, A. Dress, *Angew. Chem.* **2002**, *114*, 1210 – 1215; *Angew. Chem. Int. Ed.* **2002**, *41*, 1162 – 1167; b) A. Müller, E. Krickemeyer, H. Bögge, M. Schmidtmann, F. Peters, *Angew. Chem.* **1998**, *110*, 3567 – 3571; *Angew. Chem. Int. Ed.* **1998**, *37*, 1220 – 1223; c) A. Müller, P. Kögerler, C. Kuhlmann, *Chem. Commun.* **1999**, 1347 – 1358.
[5] a) C. L. Cahill, J. B. Parise, *J. Chem. Soc. Dalton Trans.* **2000**, 1475 – 1482; b) C. L. Cahill, B. Gugliotta, J. B. Parise, *Chem. Commun.* **1998**, 1715 – 1716.
[6] a) H. Li, J. Kim, T. L. Groy, M. O'Keeffe, O. M. Yaghi, *J. Am. Chem. Soc.* **2001**, *123*, 4867 – 4868; b) H. Li, A. Laine, M. O'Keeffe, O. M. Yaghi, *Science* **1999**, *283*, 1145 – 1147.
[7] a) C. Wang, Y. Li, X. Bu, N. Zheng, O. Zivkovic, C.-S. Yang, P. Feng, *J. Am. Chem. Soc.* **2001**, *123*, 11506 – 11507; b) N. Zheng, X. Bu, B. Wang, P. Feng, *Science* **2002**, *298*, 2366 – 2369.
[8] M. T. Pope, *Heteropoly and Isopoly Oxometalates*, Springer, Berlin, **1983**.
[9] a) D. Riou, G. Férey, *J. Solid State Chem.* **1995**, *120*, 137 – 145; b) D. Riou, G. Férey, *Inorg. Chem.* **1995**, *34*, 6520 – 6523; c) Y. Zhang, R. C. Haushalter, A. Clearfield, *Inorg. Chem.* **1996**, *35*, 4950 – 4956.
[10] a) I. D. Williams, M. Wu, H. H.-Y. Sung, X. X. Zhang, J. Yu, *Chem. Commun.* **1998**, 2463 – 2464; b) Y. Zhao, G. Zhu, W. Liu, Y. Zou, W. Pang, *Chem. Commun.* **1999**, 2219 – 2220.
[11] a) R. C. Haushalter, Z. Wang, L. M. Meyer, S. S. Dhingra, M. E. Thompson, J. Zubieta, *Chem. Mater.* **1994**, *6*, 1463 – 1464; b) A.-H. Liu, S.-L. Wang, *Inorg. Chem.* **1998**, *37*, 3415 – 3418.
[12] a) Y.-M. Chen, E.-B. Wang, B.-Z. Lin, S.-T. Wang, *J. Chem. Soc. Dalton Trans.* **2003**, 519 – 520; b) T. Whitfield, X. Wang, A. J. Jacobson, *Inorg. Chem.* **2003**, *42*, 3728 – 3733.
[13] a) V. Soghomonian, R. C. Haushalter, J. Zubieta, C. J. O'Connor, *Inorg. Chem.* **1996**, *35*, 2826 – 2830; b) V. Soghomonian, R. C. Haushalter, Q. Chen, J. Zubieta, *Inorg. Chem.* **1994**, *33*, 1700 – 1704.
[14] R. C. Finn, R. C. Haushalter, J. Zubieta, *Prog. Inorg. Chem.* **2003**, *51*, 421 – 601.
[15] a) I. D. Brown, D. Altermatt, *Acta Crystallogr. Sect. B* **1985**, *41*, 244 – 247; b) I. D. Brown, K. K. Wu, *Acta Crystallogr. Sect. B* **1976**, *32*, 1957 – 1959.
[16] a) B. Krebs, S. Pohl, *Z. Naturforsch. B* **1971**, *26*, 853 – 854; b) B. Krebs, *Angew. Chem.* **1983**, *95*, 113 – 134; *Angew. Chem. Int. Ed. Engl.* **1983**, *22*, 113 – 134; c) S. Pohl, B. Krebs, *Z. Anorg. Allg. Chem.* **1976**, *424*, 265 – 272.
[17] a) G. M. Sheldrick, SHELXS-97, Program for Crystal Structure Determination, University of Göttingen (Germany), **1997**; b) G. M. Sheldrick, SHELXL-97, Program for the Refinement of Crystal Structures, University of Göttingen (Germany), **1997**.

 © 2006 Wiley-VCH Verlag GmbH & Co. KGaA, Weinheim

Kinetic Resolution

DOI: 10.1002/anie.200503291

Self-Assembled Nanoreactors as Highly Active Catalysts in the Hydrolytic Kinetic Resolution (HKR) of Epoxides in Water

*Benjamin M. Rossbach, Kerstin Leopold, and Ralf Weberskirch**

The synthesis of optically active organic compounds is a central research topic in chemistry because of their widespread use in the pharmaceutical industry as well as in the production of fine chemicals.[1] Catalytic enantioselective organic reactions can be achieved by metal catalysis,[2] by biocatalysis,[3] and more recently also by organocatalysis.[4] Despite the increased industrial demand for enantiomerically pure compounds, to date only a few catalytic asymmetric processes have found commercial application.[5] One rare exception is the hydrolytic kinetic resolution (HKR) of terminal epoxides, which allows the production of enantiopure epoxides and diols from the racemic stating materials.[6] These chiral compounds play a key role as intermediates in the production of pharmaceuticals and agricultural chemicals.[7]

Studies of HKR of epoxides catalyzed by Co^{III}(salen) complexes (H_2salen = *N*,*N*′-bis(salicylidene)ethylenediamine) support a cooperative mechanism involving two catalyst metal centers that leads to the dual activation of the epoxide as an electrophile and water as a nucleophile.[6] This synergistic activation seems to be a common feature of Lewis acid catalysis in general and asymmetric catalysis in particular. Two discrete cobalt centers bring the nucleophilic and electrophilic reaction partners into proximity and with the correct relative geometry for the selective conversion of only one enantiomer, thus reducing the energetic barrier in a similar way to enzyme catalysis.[8a] The asymmetric ring-opening reaction of epoxides by azide nucleophiles catalyzed by related Cr^{VI}(salen) complexes follows a similar mechanism.[9] Also, Shibasaka and co-workers reported already in 1995 on the use of heterobimetallic binol complexes that enable asymmetric Michael additions by a dual activation of the reagents (binol = 1,1′-bi-2-naphthol).[8b,c]

Catalyst immobilization and environmentally benign solvents are important issues in the development of sustainable industrial processes. The use of water as a reaction medium has attracted increasing attention because it is economical and has no associated health and safety risks.[10] In the past couple of years several groups have reported the application of polymer-supported catalysts in water without the use of any organic cosolvent.[11] Water plays a particular role in the Co^{III}(salen)-catalyzed HKR in acting as reagent in the epoxide opening as well as a ligand for the Co(salen) complex.[12] As a consequence the amount of water in the reaction mixture is a very sensitive factor. In general, 0.55–0.70 equivalents of water with respect to the racemic epoxides is employed to achieve high enantioselectivity, and residual water must be removed carefully before workup so as not to diminish the enantiomeric excess and yield of the chiral products. As the enantioselective kinetic resolution of the terminal epoxides is also exothermic, the addition of water must be continuous and at constant temperature.[6,13] Therefore, carrying out HKR in water seems to be possible only if the amount of water in the immediate environment of catalyst and the racemic epoxides can be strictly controlled.

Jacobsen and co-workers utilized dendrimers as a support material for Co^{III}(salen) complexes and showed the beneficial effects of high local concentrations of catalyst on the activity without loss of enantioselectivity.[14] Inspired by this work, we aimed to prepare a core–shell-type nanoreactor in which the hydrophobic core provides a favorable environment for the Co^{III}(salen) complex and the racemic epoxide, while the hydrophilic shell guarantees water-solubility of the nanoreactor. Several approaches can be used to prepare such amphiphilic structures, for example, with either core–shell-like dendrimers[15] or by simple amphiphilic block copolymers that self-assemble in water to form micellar aggregates with a hydrophobic core and a water-soluble shell.[16] Although dendrimers can enhance reaction rates and have therefore been regarded as "unimolecular micelles",[14,17] elaborate preparation of the functionalized dendrimers through multistep synthesis is required. For that reason we decided to prepare amphiphilic block copolymers with pendant Co^{III}-(salen) moieties covalently attached to the hydrophobic block. These functionalized block copolymers should form micellar aggregates in water, thereby creating a nanoenvironment with high local concentration of the Co^{III}(salen) complex in the hydrophobic core along with a hydrophilic shell ensuring the water-solubility of the whole aggregate. The approach was based on several considerations: Firstly, it was anticipated that the hydrophobic core would exclude any excess water from the catalyst and epoxides. Secondly, the high local concentration of catalyst should be beneficial for catalytic activity. Thirdly, covalent attachment of the catalyst to the polymer should also allow separation and recycling of the catalyst.

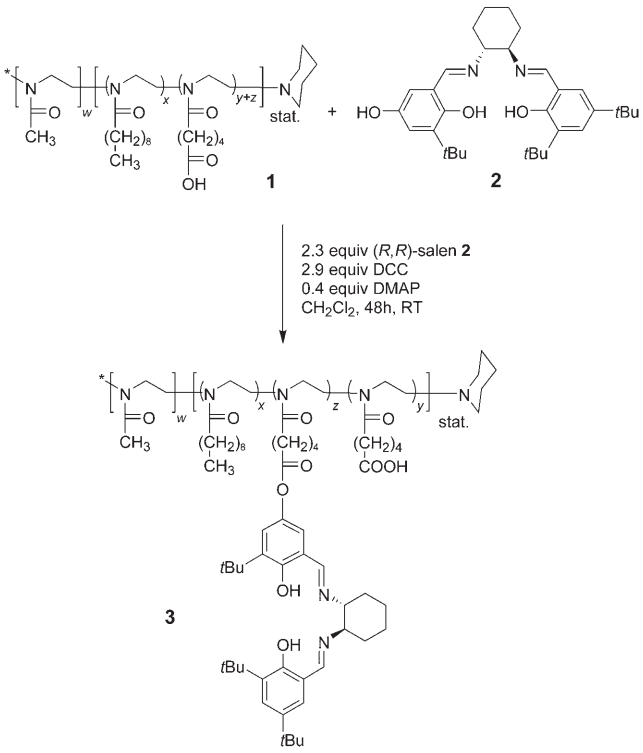
As the presence of functional moieties could disturb the polymerization of the 2-alkyl-2-oxaline-based monomers, the salen moiety was introduced in a polymer-analogous coupling reaction. In the first step, the amphiphilic block copolymer **1**

[*] Dipl.-Chem. B. M. Rossbach, Dr. R. Weberskirch
Department Chemie
Lehrstuhl für Makromolekulare Stoffe
Technische Universität München
Lichtenbergstrasse 4, 85747 Garching (Germany)
Fax: (+49) 89-289-13562
E-mail: ralf.weberskirch@ch.tum.de
Dr. K. Leopold
Department Chemie
Lehrbereich Anorganische Chemie
Arbeitskreis Analytische Chemie
Technische Universität München
Lichtenbergstrasse 4, 85747 Garching (Germany)

Supporting information for this article is available on the WWW under http://www.angewandte.org or from the author.

 © 2006 Wiley-VCH Verlag GmbH & Co. KGaA, Weinheim

with pendant carboxylic acid groups was prepared according to a literature procedure.[18] Its structure and composition was confirmed by ^{1}H NMR spectroscopy, and size-exclusion chromatography (SEC) revealed a molar mass of 6153 g mol^{-1} and a polydispersity of 1.12. The chiral salen ligand **2**, featuring a hydroxy group for covalent attachment to the polymer, was prepared in a three-step synthesis,[13a,19] and its structure and purity were confirmed by ^{1}H NMR and ^{13}C NMR spectroscopy as well as by elemental analysis. The precursor polymer **1** was treated with two equivalents of salen ligand **2** in the presence of *N*,*N*′-dicyclohexylcarbodiimide (DCC) as an activation reagent (Scheme 1).



Scheme 1. Synthesis of the amphiphilic (*R*,*R*)-macrosalen ligand **3** ($w = 41$, $x = 4.5$, $y = 2.8$, $z = 2.3$). DCC = *N*,*N*′-dicyclohexylcarbodiimide; DMAP = 4-dimethylaminopyridine; stat. = statistical.

An excess of the carboxylic acid groups in the polymer (2.1 equiv relative to the salen ligand) guaranteed quantitative binding. The immobilized salen ligand **3** was analyzed by ^{1}H and ^{13}C NMR spectroscopy as well as by SEC. The ^{1}H NMR spectrum of macrosalen ligand **3** is depicted in Figure 1. The signals labeled 9 and 6,6′ can be clearly assigned to the polymer backbone and the methyl or methylene group neighboring the amide in the side chain, respectively. Also, the salen ligand can be identified by the signals at $\delta = 1.25$ and 1.35 ppm corresponding to the *tert*-butyl groups and the signals between $\delta = 6.66$ and 7.32 ppm that belong to the aromatic salen protons. The broad signal at $\delta = 13.84$ ppm can be assigned to the internal hydroxy groups of the salen ligand. Quantitative NMR analysis revealed that approximately 2.3 ligand moieties were bound on average to each polymer chain. SEC measurements indicate an increase in molar mass

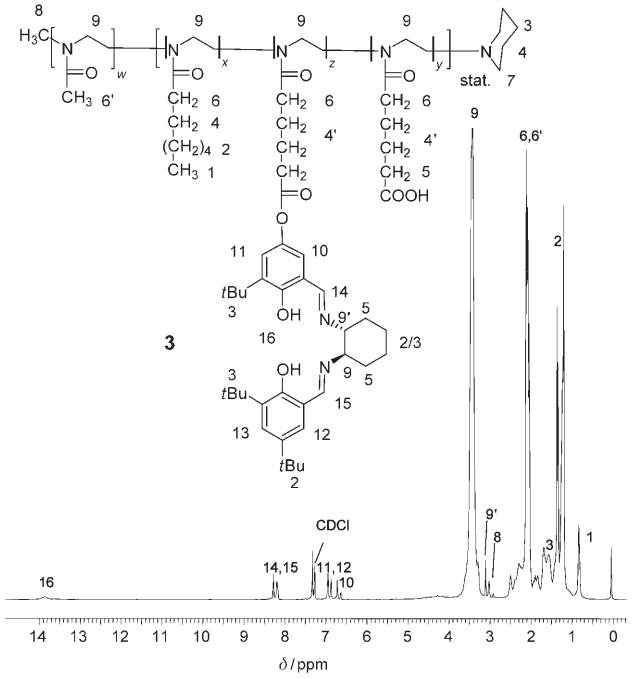
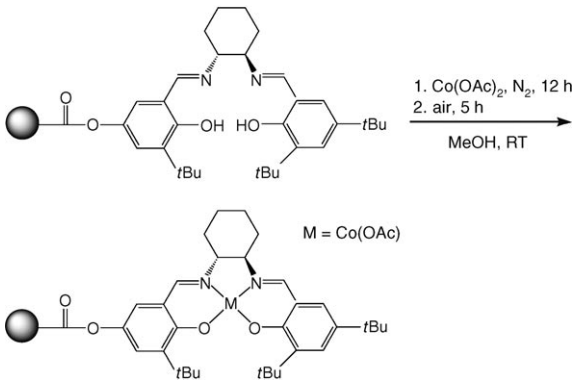


Figure 1. ^{1}H NMR spectrum of **3** ($CDCl_3$, 500.1 MHz, $T = 297.0$ K).

to 7667 g mol^{-1} for the polymer-bound salen ligand **3** with a narrow polydispersity of 1.07.

The polymer–Co^{III}(salen) complex **4** was prepared by reaction of a solution of **3** in methanol with two equivalents of $Co(OAc)_2 \cdot 4H_2O$ under inert gas (Scheme 2). The typically



Scheme 2. Metalation followed by oxidation of (*R*,*R*)-**3** to give the polymeric Co^{III}(salen) complex **4**.

red Co^{II} complex immediately turned dark brown upon exposure to air. The metal content was determined by graphite-furnace atomic-absorption spectrometry (GFAAS) to be 0.0179 g Co per gram of polymer, which corresponds to one Co atom per polymer chain.

The aggregation behavior of **4** in water was studied by dynamic light scattering (DLS) and TEM analysis. The hydrodynamic radii of the particles measured at three different concentrations ($c_p = 1.0$, 2.0, and 4.0 mg mL^{-1}) were in the range of 10 to 12 nm. TEM analysis (Figure 2) revealed

 © 2006 Wiley-VCH Verlag GmbH & Co. KGaA, Weinheim

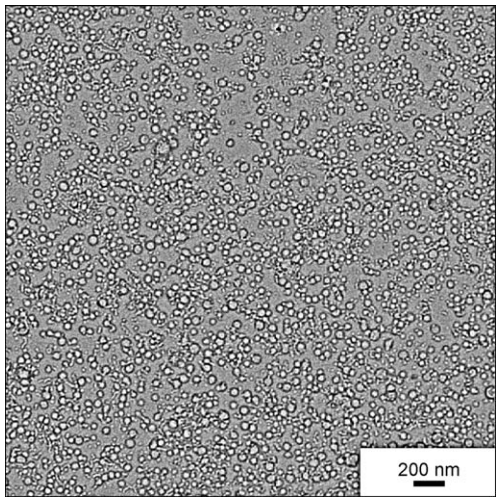


Figure 2. TEM micrograph of micellar aggregates of **4** ($c_p = 2$ mg mL^{-1}, 0.31 mmol).

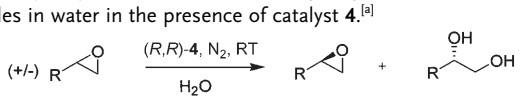
spherical aggregates with an average radius of 14.3 nm, which is in good agreement with the DLS data.

The activity and selectivity of the self-assembled aggregates were investigated with four different aromatic epoxides, chosen because they are known to require higher amounts of catalyst and longer reaction times than aliphatic epoxides for HKR. For these experiments, **4** was dissolved in degassed water in concentrations suitable for the formation of micellar aggregates (1.2–2.6 mg mL^{-1}; 0.18–0.39 mmol L^{-1}). The racemic epoxide was then added, and the reaction mixture was stirred at room temperature. When the reaction was complete, as indicated by chiral gas chromatography (GC), the aqueous phase was extracted twice with ethyl acetate to separate the enantio-enriched epoxide and diol from the reduced catalyst, which remains completely in the aqueous phase. The aromatic diols precipitated upon addition of hexane to the organic extracts and were separated from the epoxides by filtration.

Following this procedure we first investigated the catalytic efficacy of **4** in HKR of ether-containing terminal epoxides (Table 1, entries 1–4). As an example, the reaction in water of 2-phenoxymethyloxirane with **4** at room temperature gave of an enantiomeric excess of 99.1 % *ee* of (*S*)-phenoxymethyloxirane after 4.5 h when a catalyst loading of 0.02 mol % was used, and 96.6 % *ee* after a shorter reaction time of 1 h and with a catalyst loading of 0.08 mol % (Table 1, see entries 1 and 2). The enantiomeric excess of the diol fraction was determined to be at least 88.9 % *ee* in the latter (entry 1) and 95.9 % *ee* in the former experiment (entry 2). Most remarkable, however, is that the micellar catalytic approach allows the use of low amounts of catalyst (0.02–0.08 mol %) and shorter reaction times (1–4.5 h) than the homogeneous approach ($c_{cat} = 0.5$ mol %, $t = 16$–18 h) to achieve the same enantioselectivity (> 99 % *ee*).[20]

Similar results were obtained with racemic 2-benzyloxymethyloxirane under the same reaction conditions ($c_{cat} =$ 0.10 mol %, $t = 1$ h, $T =$ room temperature): (*S*)-2-benzyloxymethyloxirane was obtained with 95.6 % ee and the diol derivative with 87.4 % *ee* (Table 1, entry 3). Greater than

Table 1: Hydrolytic kinetic resolution (HKR) of aromatic terminal epoxides in water in the presence of catalyst **4**.[a]



No.	R	$c_{cat.}$[b] [mol %]	c_p [mmol L^{-1}]	t[c] [h]	ee_{epox}[d] [%]	ee_{diol}[e] [%]	Conv.[f] [%]
1	CH_2OPh	0.08	0.177	1	96.6	88.9	52.2
2	CH_2OPh	0.02	0.168	4.5	99.1	95.9	51.1
3	CH_2OBn	0.10	0.220	1	95.6	87.4	52.3
4	CH_2OBn	0.02	0.178	4	> 99.9	86.9	53.5
5	Ph	0.09	0.331	6	91.3	91.3	50.0
6	Ph	0.06	0.229	24	98.1	91.5	51.8
7	*p*-ClC_6H_4	0.10	0.265	6	> 99.9	95.1	51.2
8	*p*-ClC_6H_4	0.06	0.393	7.5	97.8	95.1	50.9

[a] A detailed description of the catalysis is given in the Supporting Information. Bn = benzyl. [b] Ratio of Co to racemic epoxide. [c] The reaction was terminated by extraction of the diol and epoxides fraction. [d] Enantiomeric excess of the epoxides was determined by chiral GC or chiral HPLC immediately after the aliquot was removed. [e] Diols were treated with 2,2-dimethoxypropane and a catalytic amount of *p*-TsOH and the enantiomeric excess was determined by chiral GC. *p*-TsOH = *p*-toluenesulfonic acid. [f] Estimated on the basis of the *ee* value of the recovered epoxide and diol products (see the Supporting Information).

99.9 % *ee* for the epoxide was achieved by reducing the cobalt loading to 0.02 mol % (Table 1, entry 4). The increased reaction time evidently led to a slight consumption of the less reactive enantiomer, which explains the relatively high overall yield and the low enantiomeric excess for the diol product (86.9 % *ee*).

The effects of the nanoreactor in improving catalytic activity become even clearer with the less-reactive HKR substrates 2-phenyloxirane and 2-(4-chlorophenyl)oxirane. 2-Phenyloxirane could be isolated in up to 98 % *ee* after 24 h with only 0.06–0.09 mol % catalyst (Table 1, entries 5 and 6), whereas similar *ee* values could be obtained from the homogeneous reaction only after 48 h and with 0.8 mol % catalyst.[20] The results in Table 1 demonstrate the advantages of the nanoreactor approach. The high local concentration of catalyst leads to enhanced activity similar to that obtained by Jacobsen and co-workers with dendrimer and oligomeric salen systems. More important, however, is the fact that the hydrophobic core limits the penetration of water into the nanoreactors and thus prevents the early hydrolysis of the racemic and chiral epoxides.

For the complete characterization of (*R*,*R*)-**4**, we investigated its recycling and reuse in four consecutive cycles with the substrate 2-phenyloxirane. The catalyst was recovered from the aqueous phase and regenerated by treatment with diluted acetic acid and exposure to air. The results of the recycling experiments are summarized in Table 2. Although the reaction time had to be increased, *ee* values greater than 99.9 % could still be obtained in the fourth run. We assume that the increased reaction times are due to partial oxidation of Co^{III} to give an unreactive Co^{IV} species and that acetic acid was sometimes difficult to remove completely (even by lyophilization) after the regeneration of the catalyst. The leaching of cobalt from **4** after isolation of the substrate by repeated extraction of the aqueous phase with ethyl acetate

 © 2006 Wiley-VCH Verlag GmbH & Co. KGaA, Weinheim

Table 2: Catalyst recycling of **4** in the HKR of 2-phenyloxirane in water.

Cycle	$c_{cat.}$[a] [mol%]	t [h]	$ee_{max,epox}$[b] [%]	$ee_{max,diol}$[c] [%]	Conv.[d] [%]
1	0.06	24	98.1	91.5	51.8
2	0.29	20	97.6	72.6	57.9
3	0.30	44	>99.9	80.9	54.7
4	0.12	96	>99.9	87.5	53.3

[a] Ratio of Co to racemic epoxide. [b] The *ee* values of the *S* epoxide were determined by chiral GC or HPLC analysis after workup. [c] The *ee* values were determined by chiral GC after reaction of the diols with 2,2-dimethoxypropane and a catalytic amount of *p*-TsOH. [d] Estimated on the basis of the *ee* value of the recovered epoxide and diol products (see the Supporting Information).

and hexane was analyzed by GFAAS. The metal content of the product fraction was below the analytical detection limit (7.4 ppb), which suggests that the immobilization of the Co^{III}(salen) catalyst to the polymer is stable, even after extended reaction times.

In summary, we have demonstrated the first HKR of various racemic aromatic epoxides in pure water using a Co^{III}(salen) complex supported on an amphiphilic, water-soluble block copolymer. The aggregation of the polymer and the formation of micellar aggregates are key steps in the preparation of functional nanoreactors. The high local concentration of catalyst in the hydrophobic core and the limited amount of water that can penetrate into the micellar core during catalysis are crucial to achieving high activity while maintaining excellent enantioselectivity comparable to that obtained under homogeneous reaction conditions in organic media. Finally, the polymeric catalyst could be separated and reused in four consecutive cycles, without loss of enantioselectivity. Studies are continuing on the optimization of the catalyst regeneration.

Received: September 16, 2005
Published online: January 20, 2006

Keywords: epoxides · immobilization · kinetic resolution · polymers · self-assembly

[1] For recent reviews, see: a) J. M. Janey, *Angew. Chem.* **2005**, *117*, 4364; *Angew. Chem. Int. Ed.* **2005**, *44*, 4292; b) A. M. Carroll, T. P. O'Sullivan, P. J. Guiry, *Adv. Synth. Catal.* **2005**, *347*, 609; c) H. Yamamoto, K. Futatsugi, *Angew. Chem.* **2005**, *117*, 1958; *Angew. Chem. Int. Ed.* **2005**, *44*, 1924; d) Y. Uozumi, *Top. Curr. Chem.* **2004**, *242*, 77; e) V. Cesar, S. Bellemin-Laponnaz, L. H. Gade, *Chem. Soc. Rev.* **2004**, *33*, 619; f) J. A. Ma, D. Cahard, *Angew. Chem.* **2004**, *116*, 4666; *Angew. Chem. Int. Ed.* **2004**, *43*, 4566; g) M. Dieguez, O. P. Pamies, C. Claver, *Chem. Rev.* **2004**, *104*, 3189; h) P. J. Guiry, C. P. Saunders, *Adv. Synth. Catal.* **2004**, *346*, 497; i) P. McMorn, G. J. Hutchings, *Chem. Soc. Rev.* **2004**, *33*, 108; j) O. Pamies, J. E. Bäckvall, *Chem. Rev.* **2003**, *103*, 3247.

[2] For examples, see: a) T. Uchida, R. Irie, T. Katsuki, *J. Synth. Org. Chem. Jpn.* **2005**, *63*, 478; b) J. J. Van Veldhuizen, J. E. Campbell, R. E. Giudici, A. H. Hoveyda, *J. Am. Chem. Soc.* **2005**, *127*, 6877; c) K. C. Hultzsch, *Adv. Synth. Catal.* **2005**, *347*, 367.

[3] For examples, see: a) A. I. Kallenberg, F. van Rantwijk, R. A. Sheldon, *Adv. Synth. Catal.* **2005**, *347*, 905; b) J. Sukumaran, U. Hanefeld, *Chem. Soc. Rev.* **2005**, *34*, 530; c) T. Ishige, K. Honda, S. Shimizu, *Curr. Opin. Chem. Biol.* **2005**, *9*, 174; d) N. End, K. U. Schoning, *Top. Curr. Chem.* **2004**, *242*, 273; e) M. T. Reetz, K. E. Jaeger, *Top. Curr. Chem.* **1999**, *200*, 31.

[4] a) P. I. Dalko, L. Moisan, *Angew. Chem.* **2004**, *116*, 5248; *Angew. Chem. Int. Ed.* **2004**, *43*, 5138; b) P. I. Dalko, L. Moisan, *Angew. Chem.* **2001**, *113*, 3840; *Angew. Chem. Int. Ed.* **2001**, *40*, 3726; c) E. R. Jarvo, S. J. Miller, *Tetrahedron* **2002**, *58*, 2481; d) P. R. Schreiner, *Chem. Soc. Rev.* **2003**, *32*, 289.

[5] H. U. Blaser, E. Schmidt in *Asymmetric Catalysis on Industrial Scale*, Wiley-VCH, Weinheim, **2004**.

[6] M. Tokunaga, J. F. Larrow, F. Kakiuchi, E. N. Jacobsen, *Science* **1997**, *277*, 936.

[7] a) H. C. Kolb, M. S. VanNieuwenhze, K. B. Sharpless, *Chem. Rev.* **1994**, *94*, 2483; b) B. M. Chourdary, N. S. Chowdari, S. Madhi, M. L. Kantam, *J. Org. Chem.* **2003**, *68*, 1736.

[8] a) J.-A. Ma, D. Cahard, *Angew. Chem.* **2004**, *116*, 4666; *Angew. Chem. Int. Ed.* **2004**, *43*, 4566; b) H. Sasai, Y. Satow, K. N. Houk, M. Shibasaka, *J. Am. Chem. Soc.* **1995**, *117*, 6194; c) M. Shibasaka, H. Sasai, T. Arai, *Angew. Chem.* **1997**, *109*, 1290; *Angew. Chem. Int. Ed. Engl.* **1997**, *36*, 1236.

[9] K. B. Hansen, J. L. Leighton, E. N. Jacobsen, *J. Am. Chem. Soc.* **1996**, *118*, 10924.

[10] P. Tundo, P. Anastas, D. StC. Black, J. Breen, T. Collins, S. Memoli, J. Miyamoto, M. Polyakoff, W. Tunes, *Pure Appl. Chem.* **2000**, *72*, 1207.

[11] See, for example: a) Y. Uozumi, M. Nakazono, *Adv. Synth. Catal.* **2002**, *344*, 274; b) Y. Uozumi, T. Watanabe, *J. Org. Chem.* **1999**, *64*, 6921; c) Y. Uozumi, H. Danjo, T. Hayashi, *Tetrahedron Lett.* **1998**, *39*, 8303; d) Y. M. A. Yamada, K. Takeda, H. Takahashi, S. Ikegami, *Org. Lett.* **2002**, *4*, 3371; e) D. Schönfelder, K. Fischer, M. Schmidt, O. Nuyken, R. Weberskirch, *Macromolecules* **2005**, *38*, 254; f) M. T. Zarka, M. Bortenschlager, K. Wurst, O. Nuyken, R. Weberskirch, *Organometallics* **2004**, *23*, 4817; g) T. Kotre, O. Nuyken, R. Weberskirch, *Macromol. Chem. Phys.* **2004**, *205*, 1187; h) M. T. Zarka, O. Nuyken, R. Weberskirch, *Macromol. Rapid Commun.* **2004**, *25*, 858; i) T. Malmström, C. Andersson, *Chem. Commun.* **1996**, 1135; j) D. E. Bergbreiter, B. L. Case, Y. S. Liu, J. W. Caraway, *Macromolecules* **1998**, *31*, 6053; k) D. E. Bergbreiter, L. Zhang, V. M. Martagnanam, *J. Am. Chem. Soc.* **1993**, *115*, 9295; l) D. E. Bergbreiter, P. L. Osburn, A. Wilson, E. M. Sink, *J. Am. Chem. Soc.* **2000**, *122*, 9058.

[12] L. P. C. Nielsen, C. P. Stevenson, D. G. Blackmond, E. N. Jacobsen, *J. Am. Chem. Soc.* **2004**, *126*, 1360.

[13] a) D. A. Annis, E. N. Jacobsen, *J. Am. Chem. Soc.* **1999**, *121*, 4147; b) S. D. Choi, G. J. Kim, *Catal. Lett.* **2004**, *92*, 35; c) L. L. Welbs, R. C. Scarrow, A. S. Borovik, *Chem. Commun.* **2004**, *22*, 2544.

[14] R. Breinbauer, E. N. Jacobsen, *Angew. Chem.* **2000**, *112*, 3750; *Angew. Chem. Int. Ed.* **2000**, *39*, 3604.

[15] a) S. W. Krska, D. Seyferth, *J. Am. Chem. Soc.* **1998**, *120*, 3604; b) A. P. H. J. Schenning, C. Elissen-Roman, J. W. Weener, M. W. P. L. Baars, S. J. van der Gaast, E. W. Meijer, *J. Am. Chem. Soc.* **1998**, *120*, 8199.

[16] a) B. Chu, *Langmuir* **1995**, *11*, 414; b) P. Alexandridis, T. A. Hatton, *Colloids Surf. A* **1995**, *96*, 1; c) G. Riess, *Prog. Polym. Sci.* **2003**, *28*, 1107.

[17] a) C. J. Hawker, K. L. Wooley, J. M. J. Frechet, *J. Chem. Soc. Perkin Trans. 1* **1993**, 1287; b) G. R. Newkome, C. N. Moorefield, J. M. Keith, G. R. Baker, G. H. Escamilla, *Angew. Chem.* **1994**, *106*, 701; *Angew. Chem. Int. Ed. Engl.* **1994**, *33*, 666.

[18] M. T. Zarka, O. Nuyken, R. Weberskirch, *Chem. Eur. J.* **2003**, *9*, 3228.

[19] J. M. Ready, E. N. Jacobsen, *J. Am. Chem. Soc.* **2001**, *123*, 2687.

[20] S. E. Schaus, B. D. Brandes, J. F. Larrow, M. Tokunaga, K. B. Hansen, A. E. Gould, M. E. Furrow, E. N. Jacobsen, *J. Am. Chem. Soc.* **2002**, *124*, 1307.

 © 2006 Wiley-VCH Verlag GmbH & Co. KGaA, Weinheim

Crystal Engineering

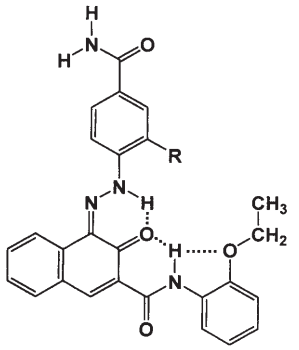
DOI: 10.1002/anie.200502468

Crystal Structures of Pigment Red 170 and Derivatives, as Determined by X-ray Powder Diffraction**

Martin U. Schmidt, Detlef W. M. Hofmann, Christian Buchsbaum, and Hans Joachim Metz*

Pigment Red 170 (**1a**) is currently one of the most important organic pigments for paints and coatings with an estimated market share of roughly 50 million euros annually. The γ phase is used for automotive coatings, but the coatings start to fade after five to ten years. For a better understanding of the pigment's properties we determined the crystal structures of the α and γ phases from X-ray powder diagrams, even in the cases when indexing was not possible. The structures served as the starting point for structure variations by crystal-engineering methods which finally led to γ polymorphs of new chemical identity with improved durability under weathering conditions.

Pigments, which are by definition insoluble in application media e.g. paints, resins, plastics or inks, develop their coloristic properties through dispersion. The crystal structures are not altered during this process and therefore play an important role in determining properties of the final products such as hue and photostability.[1] Surprisingly the crystal structures of the Pigment Red 170 polymorphs were hitherto not known. The reason lies in the very low solubility of the pigment in all solvents, impeding the growth of single crystals suitable for X-ray analyses. We therefore determined the crystal structures from powder diffraction data.



1a: R = H (Pigment Red 170)
1b: R = CH_3
1c: R = F
1d: R = Cl
1e: R = Br
1f: R = NO_2

Most methods[2] for the determination of crystal structures from X-ray powder diagrams require the diagram to be indexed, that is, all lattice parameters and the possible space groups must be known. There are two alternative approaches: 1) search for an isotypical compound with known structure, or 2) predict the crystal structures by global minimization of the lattice energy, followed by simulation of powder diagrams and comparison with the experimental diffractogram.[3] To solve the structure of α-**1a** we had to combine the two approaches.

Pigment **1a** is synthesized industrially by diazotation of *p*-aminobenzamide and subsequent coupling with 3-hydroxy-2-naphththoic acid (2-ethoxy)anilide. In the solid state these azo pigments assume the hydrazo form (see formula).[4]

The primary product of the syntheses is a nanocrystalline precipitate of the α polymorph (α-**1a**), which cannot be recrystallized. The crystal quality is low, with a domain size of about 10 nm.[5] The X-ray powder diagram contains at best only about 10 relatively broad reflections (Figure 1a, black line). All attempts for indexing the diagram failed.

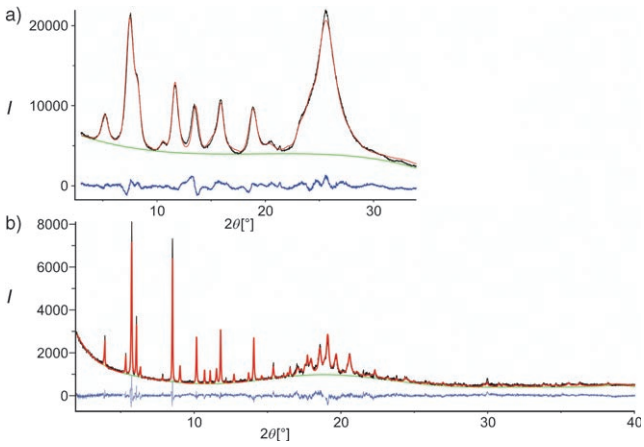


Figure 1. Rietveld refinement of a) α-**1a** (λ = 1.540598 Å), b) α-**1b** (λ = 1.149914 Å). Experimental powder diagrams shown in black, simulated diagrams in red, background curves in green, difference curves in blue.

[*] Prof. Dr. M. U. Schmidt, Dr. D. W. M. Hofmann, Dipl.-Chem. C. Buchsbaum
Institut für Anorganische und Analytische Chemie
Johann Wolfgang Goethe-Universität
Marie-Curie-Strasse 11, 60439 Frankfurt am Main (Germany)
Fax: (+49) 69-798-29235
E-mail: m.schmidt@chemie.uni-frankfurt.de

Dr. H. J. Metz
Clariant GmbH
Div. Pigments & Additives, G834
65926 Frankfurt am Main (Germany)

[**] The authors thank Dr. Felix Grimm and Jörg Wolka (Clariant GmbH, Frankfurt) for the syntheses of starting materials, Frank Becker, Dennis Thamm, and Dr. Andreas Wacker (Clariant GmbH, Frankfurt) for the syntheses of the pigments, Prof. Dr. Erich F. Paulus, Dipl.-Ing. Ursula Conrad (both formerly at Hoechst AG, Frankfurt), Dr. Martin Ermrich (Röntgenlabor Dr. Ermrich, Reinheim), and Edith Alig (Univ. of Frankfurt) for X-ray powder diagrams, Prof. Peter W. Stephens (NSLS Brookhaven) for synchrotron measurements, PD Dr. Robert E. Dinnebier (MPI for Solid-State Research, Stuttgart), Dr. Stephan Rühl (Univ. of Göttingen) and Jan Schnorr (Univ. of Frankfurt) for the support on the Rietveld refinements with GSAS, and Dr. Hans Klee and his group (Clariant GmbH) for electron microscopy. Financial support from the Deutsche Forschungsgemeinschaft (Forschergruppe 412) is gratefully acknowledged.

Supporting information for this article is available on the WWW under http://www.angewandte.org or from the author.

© 2006 Wiley-VCH Verlag GmbH & Co. KGaA, Weinheim

In the course of our investigations to improve the properties of the γ-**1a** phase (see below) we synthesized the previously unknown methyl derivative **1b**. Comparison of the powder diagrams of α-**1a** and α-**1b** revealed that the structures are isotypic (see Figure 1 and the Supporting Information). Compounds **1a** and **1b** were shown to form a continuous series of mixed crystals. Although α-**1b** exhibits a powder diagram of considerably higher quality (Figure 1b, black line) than that of α-**1a**, a complete indexing of **1b** was still not possible, because 30 out of 33 observed peaks correspond to the *hk*0 reflections; thus the lattice parameters a^*, b^* and γ^*, could be determined, but the information on the remaining three parameters (c^*, α^*, β^*), as well as on the crystal system and the space group remained obscure.

The structure of α-**1b** was solved by a crystal-structure prediction[6] using FlexCryst.[7,8] The molecular geometry was derived from crystal data of other azo pigments[9,10] and held constant during the structure-prediction step. Calculations were performed with fixed values for a, b, and γ in the 11 most frequent space groups. Simulation of powder diagrams and automated comparison with the experimental diagram pointed to a structure having $P2_12_12_1$ symmetry. Subsequently the crystal structure was optimized with CRYSCA[11] including the optimization of the molecular conformation. The similarity between calculated and experimental powder diagram increased even further, although there was no fit to the experimental data in this step. Finally we recorded a high-resolution powder diffraction pattern with synchrotron radiation and refined the structure by the Rietveld method with the program GSAS[12] (Figure 1b).[13,14] The structure changed only very slightly, underlining the accuracy of the CRYSCA calculations.

The crystal structure of α-**1b** was then used as a starting point for the Rietveld refinement of α-**1a** (Figure 1a).[15] In α-**1a** (and α-**1b**) the molecules are almost planar. They are arranged in a herringbone pattern (Figure 2). Each molecule

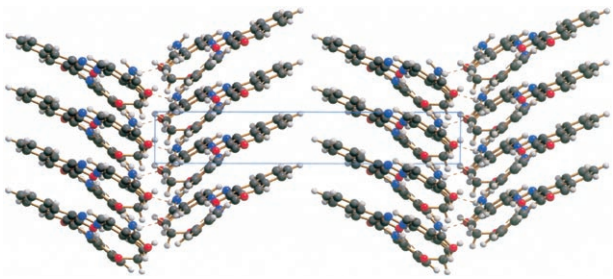


Figure 2. Section of the crystal structure of the α phase of Pigment Red 170 (α-**1a**) (SCHAKAL plot[28]). View direction [100], *b* axis horizontal, *c* axis vertical. C atoms are shown in black, O in red, N in blue, H in white.

is connected through four hydrogen bonds (C=O···H–N) to its neighbors. The $CONH_2$ groups form a helix perpendicular to the molecular planes, thus creating a three-dimensional network.

The corresponding derivatives with fluoro-, chloro-, bromo-, and nitro substituents were synthesized as well (**1c**–**f**).[16] Their α polymorphs are isotypical to α-**1a** and α-**1b**. The Rietveld refinements of α-**1c**–**f** proved the remarkable similarity between the crystal structures of all α phases (see the Supporting Information).[17]

For α-**1a**–**f**, the size of the substituents R was calculated from Hofmann's volume increments for atoms in molecular crystals.[18] This leads to the conclusion that medium-sized substituents produce a preference for the α polymorph. In the case of the smallest substituent, hydrogen ($V = 5.1$ Å^3), the α polymorph becomes less stable than the β and γ phases; the α structure no longer corresponds to the optimal packing of the molecules of **1a**; this is also reflected by the lower density of the α phase (1.395(1) g cm^{-3}) relative to that of the γ phase (1.4020(2) g cm^{-3}), and by the difference in lattice energies (α: −198.17, γ: −200.47 kJ mol^{-1}).[19] For larger substituents like CH_3 ($V = 29.1$ Å^3) the α phase becomes significantly more stable; for chlorine (25.8 Å^3) and bromine (32.7 Å^3) the α phase is the only phase known. The nitro substituent, which requires even more space (34.6 Å^3, coplanar with the adjacent phenyl ring), destabilizes the α structure and leads to two new polymorphs (δ and ε).[16]

The γ phase of Pigment Red 170 (γ-**1a**) is produced industrially by thermal treatment of the α polymorph in water at 130 °C under pressure.[20] γ-**1a** is a brilliant red pigment and has been used for many years in car coatings. In the past 30 years empirical search programs have focused on new red pigments with improved light- and weatherfastness, and hundreds of derivatives have been synthesized. In terms of the relevant application properties, however, all of them are inferior to γ-**1a**.

Pigments with desirable properties are generally characterized by very dense packings (e.g., 1.74 g cm^{-1} for the triphenedioxazine $C_{22}H_{12}Cl_2N_6O_4$[3] and 2.03 g cm^{-1} for the anthanthrone pigment $C_{22}H_8Br_2O_2$[6c]). Dense packings impede photochemical reactions that require a change in molecular geometry; in the case of photodissociation the fragments remain trapped at their locations and have a good chance for recombination. Structures with unfavorable lattice energies correspond to pigments with enhanced solubilities in the application medium, increasing the chances for photochemical or radical degradation of the dissolved molecules.

When the ethoxy moiety in **1a** is replaced by a methoxy or propoxy group, products with increased solubilities and lower durabilites are obtained. A similar effect is observed when the position of the ethoxy group is changed. The key reasons for these observations were unclear hitherto because no crystal structures were known.

The crystal structure of γ-**1a** could be solved from a standard powder diagram recorded in the lab. The diagram could be indexed by TREOR.[21,22] The structure was solved by crystal-structure prediction using the program CRYSCA. CRYSCA performs global lattice energy mimimizations for flexible molecules;[6,11,23,24] with this approach we could recently solve the structure of the violet pigment $C_{22}H_{12}Cl_2N_6O_4$ from a non-indexed powder diagram containing only 12 peaks.[3] For γ-**1a**, several thousand crystal structures with given lattice parameters were generated with the symmetries $P2_1/c$, $P2_1/n$, and $P2_1/a$ ($Z = 4$). The lattice energy was optimized simultaneously with the molecular geometry. For all energetically favorable structures, the

 © 2006 Wiley-VCH Verlag GmbH & Co. KGaA, Weinheim

simulated powder diagrams were compared with the experimental difractogram, revealing that the calculated structure with the lowest energy had a powder diagram very similar to the experimental one. Finally a Rietveld refinement, based on a carefully recorded data set, was carried out.[25]

The structure of γ-**1a** features almost planar molecules, arranged in weakly undulating layers (Figure 3). Within these layers, each molecule is connected with its neighbors by four hydrogen bonds (Figure 4). Between the layers there are only van der Waals interactions.

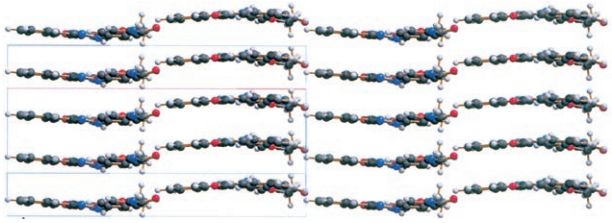


Figure 3. Crystal structure of the γ phase of Pigment Red 170 (γ-**1a**). View direction [103], *b* axis horizontal, *a* and *c* axes vertical. C atoms are shown in black, O in red, N in blue, H in white.

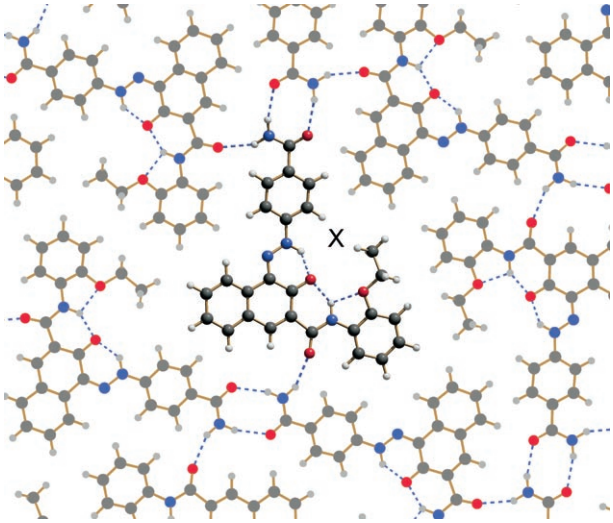


Figure 4. Crystal structure of the γ phase of Pigment Red 170 (γ-**1a**). View direction [30$\bar{1}$]. Only one layer is shown. C atoms are shown in black, O in red, N in blue, H in white. At the position marked with an X, there a small empty space that may be filled by an additional substituent.

Based on these crystal structures we are now able to draw some conclusions on structure–property relationships: The ethoxy groups seem to be a good choice to fill the space between the molecules in one layer, resulting in a quite dense packing. Replacement of the ethoxy substituent by a methoxy group would leave space vacant, while a propoxy group in the standard all-*trans* conformation would generate steric interactions with neighboring molecules. Similarly other structural variations, for example, additional substituents on the naphthalene moiety or the phenyl rings, would also lead in most cases to a less efficient packing resulting in higher solubilities and poorer application properties.

Despite the generally efficient packing of γ-**1a**, a small void still remains between the ethoxy group and the phenyl moiety (marked with an "X" in Figure 4). In a crystal-engineering approach, filling this void with an additional substituent was predicted to improve the pigment properties of γ-**1a**. Previous synthetic studies omitted this substitution pattern because the percursors are more difficult to synthesize. However, a close examination of the structures led to the conclusion that no ideal substituent exists: all potential choices are too large for the void. We therefore chose to fill only a given fraction of the voids by producing mixed crystals (solid solutions) of γ-**1a** and γ-**1b–f**.

Such solid solutions are readily formed, if the syntheses are conducted with a mixture of the corresponding diazonium salts. Experimental evidence proved our hypothesis: while the new pigments have coloristic properties very similar to those of γ-**1a**, some of them exhibit considerably improved light- and weatherfastness; in other words, the corresponding automotive coatings show less fading.[26,27] This remarkable improvement in performance was thought to be impossible for this chemical class of colorants.

This work shows that it may be possible to determine crystal structures from X-ray powder diagrams even if the powder data are of low quality and indexing fails. The only prerequisite is a sufficiently accurate molecular geometry. Structural details, such as bond lengths and bond angles, are difficult to deduce from powder data, but in many cases information about the molecular arrangement in the crystal can lead to new insights in structure–property relationships. Crystal engineering based on this information can lead to new materials with improved properties. We are convinced this approach will be used more and more in organic solid-state science as well as in application-oriented research.

Experimental Section

1b: 4-Amino-3-methyl-benzamide (15.0 g, 0.1 mol) was stirred into 5 N hydrochloric acid (60 mL). The mixture was diluted with water and diazotized at 10 °C with 5 N sodium nitrate (20 mL). Subsequently glacial acetic acid (7 mL) and 2 N sodium acetate (50 mL) were added. Meanwhile 3-hydroxy-2-naphthoic acid (2-ethoxy)anilide ("Naphtol AS-PH", technical grade, 30 g, 0.1 mol) was dissolved in water (450 mL) and 5 N NaOH (42 mL) at elevated temperature. This solution was added slowly over 1 h to the stirred solution of the diazonium salt, which was cooled at 10 to 15 °C. The α-**1b** precipitated as a fine red powder, which was isolated by filtration and washed with water. Yield: 350 g press cake. To improve crystallite size and crystal quality, the water-containing press cake of **1b** was suspended in 800 mL of *N*-methylpyrrolidone (NMP) and heated to 105 °C for 1 h. The pigment powder was isolated by filtration, washed with NMP and then with water, and dried in vacuo at 50–60 °C, giving 44.5 g (95 %) of α-**1b**. When the final treatment was conducted with chlorobenzene at 120 °C under pressure, γ-**1b** formed.

The α phases of **1c–f** were synthesized analogously from the appropriately substituted 4-aminobenzamide derivatives. The final treatment was done with glacial acetic acid at 114 °C for **1c** (R = F), with water under pressure at 160 °C for **1d** (R = Cl), and with water at 140 °C for **1e** (R = Br). The α phase of **1f** (R = NO_2) formed when the press cake was heated in dimethylformamide at 106 °C for 35 min; when the press cake was stirred in water at 98 °C for 2 h, δ-**1f** resulted with small admixtures of the α phase; heating in water at 140 °C for

 © 2006 Wiley-VCH Verlag GmbH & Co. KGaA, Weinheim

1 h resulted in the formation of the ε phase with small amounts of the α and δ phases.

Solid solutions of **1a** and **1d** (9:1 and 4:1) in the γ phase: The corresponding amounts of 4-aminobenzamide and 4-amino-3-chlorobenzamide were combined, diazotized, and coupled with 3-hydroxy-2-naphthoic acid (2-ethoxy)anilide, as described for **1b**. For the final treatment the press cake was suspended in water and heated under pressure to 140 °C for 1 h, then filtered and dried. The solid solutions formed with a yield of 95 %.

4-Amino-3-chlorobenzamide: 4-Amino-3-chlorobenzonitrile (5 g, 0.032 mol) was dissolved in acetone (25 mL). This solution was cooled while 30 % H_2O_2 solution (16 mL), tetrabutylammonium hydrogen sulphate (2.4 g), and 20 % NaOH (15 mL) were added. The mixture was stirred at 30–40 °C for 90 min, and an alkaline pH was maintained. The mixture was neutralized with sulfuric acid, and extracted with chloroform (25 mL). When a saturated NaCl solution (50 mL) was added to the organic phase, the product precipitated. Yield: 3.5 g (63 %). Purity (HPLC-MS): 98.7 % ($M^+ = 170$). ^{1}H NMR (400 MHz, [D$_6$]DMSO, 25 °C, TMS): $\delta = 7.76$ (d, $^5J = 2$ Hz, 1 H; H2), 7.66 (s, 1 H; CONH), 7.58 (dd, $^4J = 9$ Hz, $^5J = 2$ Hz, 1 H; H6), 7.00 (s, 1 H; CONH), 6.76 (d, $^4J = 9$ Hz, 1 H; H5), 5.86 ppm (s, 2 H; NH_2). IR: $\tilde{\nu} = 3439$ (m), 3328 (m), 3144 (m), 1703 (w), 1665 (m), 1618 (s), 1508 (w), 1430 (s), 1387 (s), 1309 (m), 1169 (m), 1117 cm^{-1} (m).

X-ray powder diagrams: All measurements were performed in transmission geometry on a STOE-STADI-P diffractometer equipped with a curved Ge(111) primary monochromator and a linear-position-sensitive detector. $Cu_{K\alpha 1}$ radiation ($\lambda = 1.540598$ Å) was used. The diffractogram of α-**1a** was additionally recorded with synchrotron radiation (NSLS Brookhaven, beamline X3B1, $\lambda = 1.149914$ Å).

Rietveld refinements: All refinements were carried out with the program GSAS, using restraints for bond lengths, bond angles, and planar groups.

Received: July 14, 2005
Revised: October 25, 2005
Published online: January 20, 2006

Keywords: crystal engineering · dyes/pigments · Rietveld refinement · X-ray powder diffraction

[1] W. Herbst, K. Hunger, *Industrial Organic Pigments*, 3rd ed., Wiley-VCH, Weinheim, **2004**.

[2] For structure solution by direct methods see e.g.: a) G. Cascarano, L. Favia, C. Giacovazzo, *J. Appl. Crystallogr.* **1992**, *25*, 310–317; b) A. Altomare, M. C. Burla, M. Camalli, B. Carrozzini, G. L. Cascarano, C. Giacovazzo, A. Guagliardi, A. C. G. Moliterni, G. Polidori, R. Rizzi, *J. Appl. Crystallogr.* **1999**, *32*, 339–340; c) F. C. Chan, J. Anwar, R. Cernik, P. Barnes, R. M. Wilson, *J. Appl. Crystallogr.* **1999**, *32*, 436–441; For Patterson methods: d) K. Wagner, J. Hirschler, E. Egert, *Z. Kristallogr.* **2001**, *216*, 565–572; e) W. Lasocha, J. Czapkiewicz, P. Milart, H. Schenk, *Z. Kristallogr.* **2001**, *216*, 291–294; For real-space methods see e.g.: f) K. D. M. Harris, M. Tremayne, *Chem. Mater.* **1996**, *8*, 2554–2570 (Review); g) K. D. M. Harris, M. Tremayne, B. M. Kariuki, *Angew. Chem.* **2001**, *113*, 1674–1700; *Angew. Chem. Int. Ed.* **2001**, *40*, 1626–1651 (Review); h) V. B. Zlokazov, V. V. Chernyshev, *J. Appl. Crystallogr.* **1992**, *25*, 447–451; i) V. V. Chernyshev, H. Schenk, *Z. Kristallogr.* **1998**, *213*, 1–3; j) W. I. F. David, K. Shankland, N. Shankland, *Chem. Commun.* **1998**, 931–932; k) Y. G. Andreev, P. G. Bruce, *J. Chem. Soc. Dalton Trans.* **1998**, 4071–4080; l) G. E. Engel, S. Wilke, O. König, K. D. M. Harris, F. J. J. Leusen, *J. Appl. Crystallogr.* **1999**, *32*, 1169–1179; m) A. A. Coelho, *J. Appl. Crystallogr.* **2000**, *33*, 899–908; n) S. Pagola, P. W. Stephens, *Mater. Sci. Forum* **2000**, *321–324*, 40–45; o) S. G. Zhukov, V. V. Chernyshev, E. V. Babaev, E. J. Sonneveld, H. Schenk, *Z. Kristallogr.* **2001**, *216*, 5–9; p) A. Le Bail, *Mater. Sci. Forum* **2001**, *378–381*, 65–70; q) V. Favre-Nicolin, R. Cerny, *J. Appl. Crystallogr.* **2002**, *35*, 734–743; r) J. C. Johnston, W. I. F. David, A. J. Markvardsen, K. Shankland, *Acta Crystallogr. Sect. A* **2002**, *58*, 441–447.

[3] M. U. Schmidt, M. Ermrich, R. E. Dinnebier, *Acta Crystallogr. Sect. B* **2005**, *61*, 37–45.

[4] E. F. Paulus, *Z. Kristallogr.* **1982**, *160*, 235–243.

[5] Estimated from the peak widths in the powder diagram by applying the formula of Scherrer (P. Scherrer, *Nachr. K. Ges. Wiss. Göttingen* **1918**, 98–100), cf.: R. Allmann, *Röntgenpulverdiffraktometrie*, Verlag Sven von Loga, Cologne, **1994**, p. 194. The total particle sizes are approximately 100 nm, as shown by transmission electron microscopy.

[6] a) J. P. M. Lommerse, W. D. S. Motherwell, H. L. Ammon, J. D. Dunitz, A. Gavezzotti, D. W. M. Hofmann, F. J. J. Leusen, W. T. M. Mooij, S. L. Price, B. Schweizer, M. U. Schmidt, B. P. van Eijck, P. Verwer, D. E. Williams, *Acta Crystallogr. Sect. B* **2000**, *56*, 697–714; b) W. D. S. Motherwell, H. L. Ammon, J. D. Dunitz, A. Dzyabchenko, P. Erk, A. Gavezzotti, D. W. M. Hofmann, F. J. J. Leusen, J. P. M. Lommerse, W. T. M. Mooij, S. L. Price, H. Scheraga, B. Schweizer, M. U. Schmidt, B. P. van Eijck, P. Verwer, D. E. Williams, *Acta Crystallogr. Sect. B* **2002**, *58*, 647–661; c) G. M. Day, W. D. S. Motherwell, H. L. Ammon, S. X. M. Boerrigter, R. G. Della Valle, E. Venuti, A. Dzyabchenko, J. D. Dunitz, B. Schweizer, B. P. van Eijck, P. Erk, J. C. Facelli, V. E. Bazterra, M. B. Ferraro, D. W. M. Hofmann, F. J. J. Leusen, C. Liang, C. C. Pantelides, P. G. Karamertzanis, S. L. Price, T. C. Lewis, H. Nowell, A. Torrisi, H. A. Scheraga, Y. A. Arnautova, M. U. Schmidt, P. Verwer, *Acta Crystallogr. Sect. B* **2005**, *61*, 511–527.

[7] D. W. M. Hofmann, J. Apostolakis, *J. Mol. Struct.* **2003**, *647*, 17–39.

[8] D. W. M. Hofmann, L. N. Kuleshova, M. Yu. Antipin, *Cryst. Growth Des.* **2004**, *4*, 1395–1402.

[9] Cambridge Structural Database, Cambridge Crystallographic Data Centre, 12 Union Road, Cambridge, UK.

[10] D. Kobelt, E. F. Paulus, W. Kunstmann, *Z. Kristallogr.* **1974**, *139*, 15–32.

[11] M. U. Schmidt, H. Kalkhof, *CRYSCA. Program for Crystal Structure Calculations for Flexible Molecules*, Frankfurt am Main, **1999**.

[12] A. C. Larson, R. B. von Dreele, General Structure Analysis System (GSAS), Los Alamos National Laboratory Report LAUR **1994**, pp. 86–748.

[13] α-**1b**: Red powder, $C_{27}H_{24}N_4O_4$, $M_r = 468.50$, orthorhombic, $P2_12_12_1$, $Z = 4$, $a = 24.6208(9)$ Å, $b = 22.8877(9)$ Å, $c = 3.9388(2)$ Å, $\alpha = \beta = \gamma = 90°$, $V = 2219.6(2)$ Å^3, $\rho_{calcd} = 1.4020(2)$ g cm^{-3}, $R_{wp} = 6.65\,\%$, $R_p = 5.19\,\%$, red. $\chi^2 = 4.459$.

[14] CCDC-270077 (α-**1a**), 270078 (α-**1b**), 270079 (α-**1e**), 270080 (α-**1f**), 270081 (α-**1c**), 270082 (α-**1d**), and 276530 (γ-**1a**) contain the supplementary crystallographic data for this paper. These data can be obtained free of charge from the Cambridge Crystallographic Data Centre via www.ccdc.cam.ac.uk/data_request/cif.

[15] α-**1a**: Red powder, $C_{26}H_{22}N_4O_4$, $M_r = 454.48$, orthorhombic, $P2_12_12_1$, $Z = 4$, $a = 23.960(9)$ Å, $b = 23.234(9)$ Å, $c = 3.887(1)$ Å, $\alpha = \beta = \gamma = 90°$, $V = 2164(1)$ Å^3, $\rho_{calcd} = 1.395(1)$ g cm^{-3}, $R_{wp} = 4.95\,\%$, $R_p = 3.70\,\%$, red. $\chi^2 = 23.16$. Restraints for planar groups were applied for each of the the two phenyl rings, and for the naphthalene moiety, but not for the relative movement of these fragments or for the conformation of the ethoxy group. Nevertheless a chemically sensible, almost planar molecular conformation was obtained. A previous careful and cautious fit of the strongly anisotropic peak shapes turned out to be crucial.

[16] a) M. U. Schmidt, A. Wacker, H. J. Metz (Clariant GmbH), German Patent DE 10224279A1, **2003**; b) M. U. Schmidt, A.

 © 2006 Wiley-VCH Verlag GmbH & Co. KGaA, Weinheim

Wacker, H. J. Metz (Clariant GmbH), International Patent WO 2003099936A1, **2003** [*Chem. Abstr. 140*, 6180].

[17] α-**1c**–**1f**: Red powders, orthorhombic, $P2_12_12_1$, $Z=4$. α-**1c**: $C_{26}H_{21}N_4O_4F$, $M_r=472.47$, $a=24.429(9)$ Å, $b=23.014(9)$ Å, $c=3.816(3)$ Å, $V=2145(2)$ Å^3, $\rho_{calcd}=1.463(2)$ g cm^{-3}, $R_{wp}=8.28\,\%$, $R_p=6.60\,\%$, red. $\chi^2=13.39$; α-**1d**: $C_{26}H_{21}N_4O_4Cl$, $M_r=488.92$, $a=25.370(6)$ Å, $b=23.573(5)$ Å, $c=3.958(3)$ Å, $V=2367(2)$ Å^3, $\rho_{calcd}=1.372(2)$ g cm^{-3}, $R_{wp}=5.51\,\%$, $R_p=4.17\,\%$, red. $\chi^2=3.581$; α-**1e**: $C_{26}H_{21}N_4O_4Br$, $M_r=533.37$, $a=24.58(7)$ Å, $b=22.74(7)$ Å, $c=3.914(12)$ Å, $V=2188(20)$ Å^3, $\rho_{calcd}=1.62(1)$ g cm^{-3}, $R_{wp}=9.97\,\%$, $R_p=6.45\,\%$, red. $\chi^2=6.080$; α-**1f**: $C_{26}H_{21}N_5O_6$, $M_r=499.47$, $a=24.270(3)$ Å, $b=23.713(2)$ Å, $c=3.9164(4)$ Å, $V=2253.9(3)$ Å^3, $\rho_{calcd}=1.4719(2)$ g cm^{-3}, $R_{wp}=5.63\,\%$, $R_p=4.50\,\%$, red. $\chi^2=6.258$. Rietveld plots of α-**1c**–**1f** as well as figures of the crystal structures of α-**1a**–**1f** are included in the Supporting Information.

[18] D. W. M. Hofmann, *Acta Crystallogr. Sect. B* **2002**, *58*, 489 – 493; these atomic volumes were derived from a fit to more than 200 000 molecular crystal structures.

[19] Dreiding force field (S. L. Mayo, B. D. Olafson, W. A. Goddard III, *J. Phys. Chem.* **1990**, *94*, 8897 – 8909); atomic charges calculated according to J. Gasteiger, M. Marsili, *Tetrahedron* **1980**, *36*, 3219 – 3228.

[20] J. Ribka (Hoechst AG), German Patent DE 2043482, **1970** [*Chem. Abstr. 77*, 36379].

[21] P.-E. Werner, *Z. Kristallogr.* **1964**, *120*, 375 – 389.

[22] $a=10.855$ Å, $b=24.097$ Å, $c=8.354$ Å, $\beta=100.225°$, $V=2150.6$ Å^3, $Z=4$, space group ambiguous.

[23] M. U. Schmidt, *Kristallstrukturberechnungen metallorganischer Molekülverbindungen*, Shaker Verlag, Aachen, **1995**.

[24] M. U. Schmidt, U. Englert, *J. Chem. Soc. Dalton Trans.* **1996**, 2077 – 2082.

[25] γ-**1a**: Red powder, $C_{26}H_{22}N_4O_4$, $M_r=454.48$. Sample measured in capillary, $2\theta=3°$ to 80°; 85 distinguishable peaks or peak groups, 1458 Bragg positions, max. intensity 730 000 counts. Monoclinic, space group $P2_1/n$ (No. 14), $a=10.8222(3)$ Å, $b=24.1690(15)$ Å, $c=8.3623(5)$ Å, $\beta=100.576(3)°$, $V=2150.1(2)$ Å^3, $\rho_{calcd}=1.4040(2)$ g cm^{-3}, $R_{wp}=7.7\,\%$, $R_p=5.4\,\%$, red. $\chi^2=8.00$. (Rietveld plot included in the Supporting Information.)

[26] For example, a coating containing a solid solution (γ phase) of 90 % **1a** and 10 % **1d** shows only a slight color change (color difference $\Delta E=2.2$) during a 2000-hour weatherfastness test in a rapid-weathering apparatus (Xenotest Beta X1200). In contrast, the simultaneously tested coating containing the pure γ-**1a** showed a remarkably stronger color change ($\Delta E=3.3$). A solid solution with 5 % **1d** resulted in color changes of medium extent ($\Delta E=2.6$). Lightfastness tests gave corresponding results. Physical mixtures of γ-**1a** und α-**1d** exhibit considerably poorer light- and weatherfastness.

[27] M. U. Schmidt, A. Wacker, H. J. Metz (Clariant GmbH), International Patent WO 2005019346A1, **2005** [*Chem. Abstr. 142*, 263085].

[28] E. Keller, SCHAKAL99. Kristallographisches Institut der Universität, Freiburg, **1999**.

 © 2006 Wiley-VCH Verlag GmbH & Co. KGaA, Weinheim

DOI: 10.1002/anie.200503292

Tailored Mesostructuring and Biofunctionalization of Gold for Increased Electroactivity**

*Rafael Szamocki, Stephane Reculusa, Serge Ravaine, Phil N. Bartlett, Alexander Kuhn, and Rolf Hempelmann**

Redox reactions play an important role in biochemistry and are often catalyzed by dehydrogenases and oxidoreductases.[1] This is not only the case for physiological reactions under biological conditions and for biotechnology but also for the detection of biochemical species by transduction into an electrical signal in a biosensor[1] or into electrical current in a biofuel cell.[2–5]

While in the case of "inorganic" electrochemistry the electrocatalysts employed (e.g. Pt nanoparticles for fuel cells) are electron conductors and act themselves as electrodes, the catalysts in biochemistry, redox-active enzymes, are non-conductive. Thus for the transfer of electrons from the substrate through the active center of the enzyme to the electrode it is generally necessary to have a cofactor and a mediator.[1]

To achieve a sufficiently high rate of electrochemical conversion, the electrode surface area must be increased artificially by using rough or porous materials. In doing so it is important to control and to fine-tune the interior surface area. An ideal way to control the pore size and the spatial

[*] R. Szamocki, Prof. R. Hempelmann
Physikalische Chemie
Universität des Saarlandes
66123 Saarbrücken (Germany)
Fax: (+49) 681-302-4759
E-mail: r.hempelmann@mx.uni-saarland.de

R. Szamocki, Prof. A. Kuhn
Laboratoire d'Analyse Chimique par Reconnaissance Moléculaire
ENSCPB, Université Bordeaux 1
33607 Pessac (France)

Dr. S. Reculusa, Prof. S. Ravaine
Centre de Recherche Paul Pascal, CNRS
33600 Pessac (France)

Prof. P. N. Bartlett
School of Chemistry
University of Southampton
Southampton (UK) SO171BJ (UK)

[**] Financial support by the DFG (SFB277), the DAAD, and the CNRS through the "Programme Matériaux" (A.K. and S.R.) is gratefully acknowledged. The authors are indebted to the French Ministry of Research for a Cotutelle grant and the French–British Alliance programme for supporting this collaboration. We also thank Prof. Frank Mücklich and Alexandra Velichko from the Materials Science Department of Saarland University for ion-beam cuts and SEM micrographs.

Supporting information for this article (Experimental) is available on the WWW under http://www.angewandte.org or from the author.

 © 2006 Wiley-VCH Verlag GmbH & Co. KGaA, Weinheim InterScience

arrangement of the pores is to use colloidal crystals built from monodisperse SiO_2[6] or polymer particles[7–9] as endo templates for subsequent electrodeposition. This technique has often been used with templates synthesized by methods including controlled evaporation, sedimentation, and convective self-assembly, or by formation of an ordered hydrogel.[9–17] However with these methods it is quite difficult to generate surfaces with an exactly predefined number of pore layers, especially for thick films, and to control the opening of the final pore layer.

In the present work we use the Langmuir–Blodgett (LB) technique to prepare colloidal crystals of up to 50 layers as templates for the synthesis of metallic macroporous materials. This technique offers the advantage of perfectly controlling the ordering of the colloids in the *z* direction and, unlike other methods, no cracks are formed in the template structure, which ensures a homogeneous electrodeposition of the metal through the structure. As a consequence, as a result of the higher order, the thickness of the macroporous material can be well controlled, guided by regular current oscillations during the electrodeposition. The inner surface of the macroporous electrodes increases linearly with the number of the pore layers, and the whole inner surface can be coated with an electrochemical chain which represents a bioelectrocatalytic system.

We used gold-coated glass plates, which we modified with cysteamine in order to obtain a more hydrophilic surface, as substrates for the macroporous electrodes. The colloidal crystals were built layer by layer using the LB technique (Figure 1 a).[18–22] To define the geometric area for the electrodeposition step, the electrodes together with the template were coated with a thin varnish-film leaving a square window with a characteristic size of 6 mm. The template-covered electrodes were then carefully immersed in the gold electrolyte solution. After 10 min during which the plating solution infiltrated the template, electrodeposition was started using a deposition potential of −0.66 V vs. Ag/AgCl as recommended by the manufacturer of the plating bath.

During the electrodeposition of gold through the template we observed temporal oscillations in the reduction current (Figure 2), which allowed us to control the thickness of macroporous gold with a precision of approximately 10 nm. These oscillations can be explained by the periodic variation of the active electrode surface area during the growth of gold in the template. At the beginning of the deposition each SiO_2 bead of the first deposited layer is in contact with the electrode surface at only one point, and therefore both the electrode surface and the deposition current are maximal. As the gold grows into the template, the active electrode surface area decreases continuously and goes through a minimum when the metal thickness reaches the middle of the first layer of beads because the particles are touching each other at this level. The current then increases as the film grows beyond this point, and the active electrode area increases. Oscillations of this kind have been observed by others in the case of Ni deposition through opal-like structures but were much less pronounced, most likely because of the lower degree of order in the template.[23] In the present case the oscillations are extremely high in amplitude and give us an easy and reliable way to control the number of penetrated sphere layers and thus the thickness of the final deposit. After the electrodeposition step the templates are removed by etching with 5% HF for 3 min leading to a highly ordered porous structure (Figure 1 b).

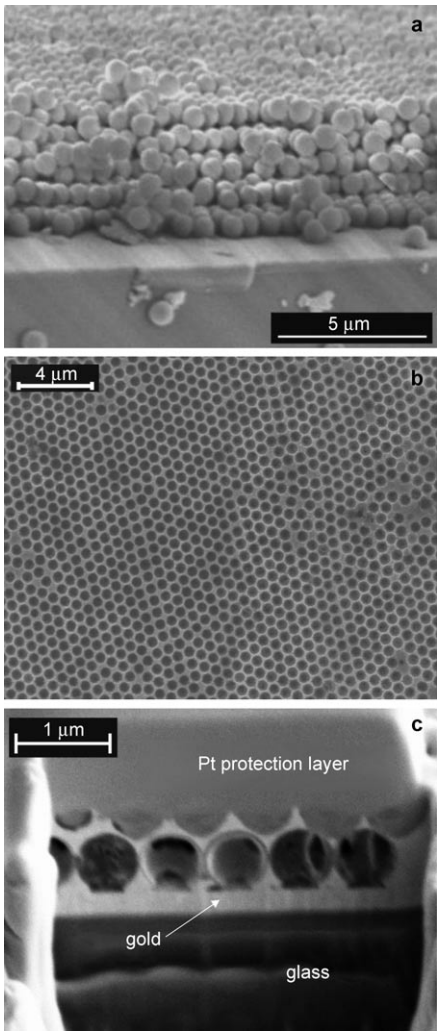


Figure 1. a) Image obtained by scanning electron microscopy (SEM) of the section of a colloidal crystal made up of five layers of 680-nm silica particles using the Langmuir–Blodgett technique. b) Top view of macroporous gold, $^1/_2$ layer of hollow spheres, $d = 680$ nm. c) Cross section of macroporous gold, $1^1/_2$ layers of hollow spheres, $d = 680$ nm. The sample was covered with a Pt protection layer before it was cut with an ion beam.

In Figure 1 c the side view of a layer of a macroporous gold electrode is shown where the deposition has been stopped at the second minimum of the deposition current resulting in a thickness of $1^1/_2$ layers of hollow spheres. The porous gold is highly organized and the pore diameter correlates exactly with the diameter of the precursor beads. Dark points, representing the interconnection between the pores, can also be observed (Figure 1 c).

When the diameter of the template colloids is varied, the period of the oscillations also changes and, as expected, the period decreases (Figure 2 a–c). During a quite large number of oscillations (up to seven) the amplitude decreases, that is,

 © 2006 Wiley-VCH Verlag GmbH & Co. KGaA, Weinheim

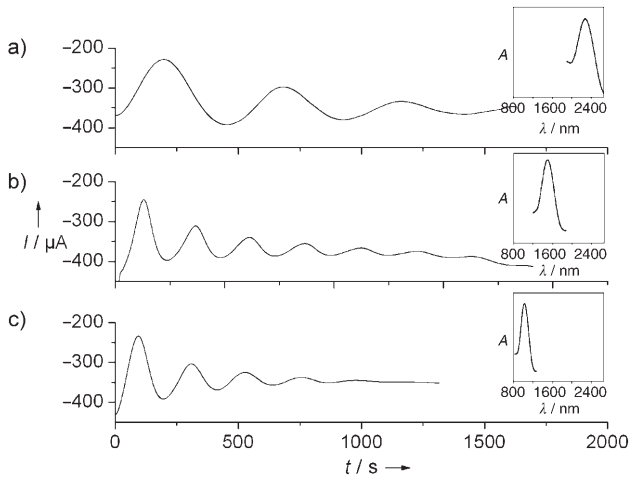


Figure 2. a) Current–time plots recorded during the electrodeposition of macroporous gold. a) $3^1/_2$ layers of hollow spheres, $d = 1100$ nm; inset: Bragg diffraction peak of a crystal made of five layers of 1100-nm silica particles. b) $7^1/_2$ layers of hollow spheres, $d = 680$ nm; inset: Bragg diffraction peak of a crystal made of five layers of 680-nm silica particles. c) $5^1/_2$ layers of hollow spheres, $d = 460$ nm; inset: Bragg diffraction peak of a crystal made of five layers of 460-nm silica particles.

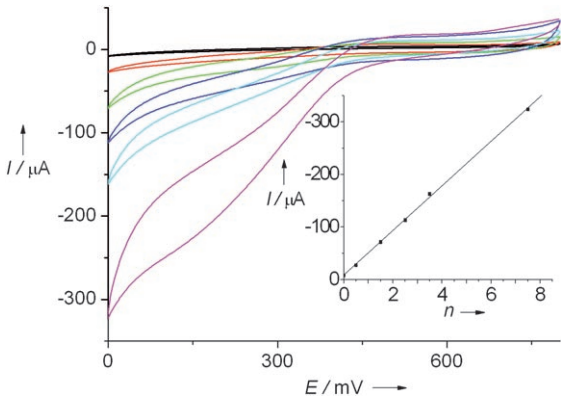


Figure 3. Comparison of the H_2O_2 (10 mM in 0.5 M H_2SO_4) reduction current on macroporous gold electrodes with different numbers of pore layers: smooth electrode (black), $^1/_2$ layer (red), $1^1/_2$ layers (green), $2^1/_2$ layers (blue), $3^1/_2$ layers (green blue), $7^1/_2$ layers (violet); $\nu = 10$ mV s^{-1}. Inset: Reduction current at 0 V as function of the number of porous layers n.

the gold deposition becomes less uniform in the z direction, and therefore the local current variations cancel each other.

The electrochemical characterization of the macroporous gold was performed by cyclic voltammetry. With this technique the ratio between active and geometric surface area, which is an important property of the macroporous electrodes, can be determined. To measure the active area, we recorded the cyclic voltammogram in 0.5 M H_2SO_4 (not shown) and calculated the charge transferred by integrating the reduction peak of gold oxide since this charge is proportional to the active surface area. We observed a linear relation between the surface area and the number of layers of hollow spheres. For a layer thickness of $7^1/_2$ hollow spheres with a pore diameter of 680 nm, we measured an active surface area that is about 30 times greater than that for a flat electrode, in accordance with geometrical calculations. This result indicates that almost all of the pores are interconnected by channels and consequently contribute to the active surface area.

This increase of active surface area results in a higher turnover for electrochemical reactions at the electrode surface, and a higher faradaic current can be observed. For the reduction of H_2O_2 to water (Figure 3), a prototypical, slow electrochemical reaction, the reduction current shows a linear increase: the turnover for an electrode with $7^1/_2$ layers of spheres is, just like the inner surface area, about 30 times greater than for a flat electrode. In contrast, for fast redox couples like $[Ru(NH_3)_6]^{3+}/[Ru(NH_3)_6]^{2+}$, we did not observe any significant increase in redox activity with the number of pore layers. A possible explanation of this behavior is that because of the high reaction rate the molecules react completely at the outermost pore half-layer before they are able to diffuse into the pores, thus only a small part of the whole active area is used for the reaction.

Since the NADH/NAD^+ system is a cofactor of many enzymes, the electrochemical conversion of this biomolecule, which also shows slow reaction kinetics at electrodes, is of great interest both for biosensors and preparative electroenzymatics.[24] For that reason we coated the surface of the gold electrodes with a monolayer of the redox mediator (4-carboxy-2,5,7-trinitro-9-fluorenylidene)malononitrile (TNF), which is an efficient catalyst for the electrooxidation of NADH.[25] In recent work we could show that macroporous electrodes obtained by evaporation of colloidal latex bead solutions could also be modified with this mediator, but precise control of the electrode thickness was impossible for more than three pore layers.[26,27] In their recent report on macroporous gold films modified with hemoglobin, Xia et al monitored the thickness of the porous material by the charge flow during electrodeposition.[28] In our experience, however, this does not give perfect control over the number of pore layers. With the Langmuir–Blodgett approach in our study, we could generate samples with more than ten pore layers still with a very high accuracy.

First the electrodes were cleaned by cyclic voltammetry and then dipped into a 5 mM TNF solution in Tris buffer overnight. To activate the mediator, a potential of −500 mV was applied, and thus two of the three nitro groups were reduced to hydroxylamine groups.[29] In a further immobilization step, a monolayer of NADH or NAD^+ was bound to the monolayer of TNF. For this purpose the mediator-modified electrodes were dipped into a solution of 0.2 M $CaCl_2$ and 3.2 mM NADH in Tris buffer and left overnight. Both the carboxyl group of the TNF and the phosphate groups of the NADH can form a complex with Ca^{2+}, which therefore acts as an electrostatic bridge.[30–32] The NADH adsorbed at the surface can be detected in the first cycle by cyclic voltammetry (Figure 4a). As expected, the oxidation current increases linearly with the number of pore layers. The LB technique allows us to generate well-ordered porous deposits with a thickness of more than ten half-pore layers, and even for fifteen half-pore layers no current saturation could be observed.

 © 2006 Wiley-VCH Verlag GmbH & Co. KGaA, Weinheim

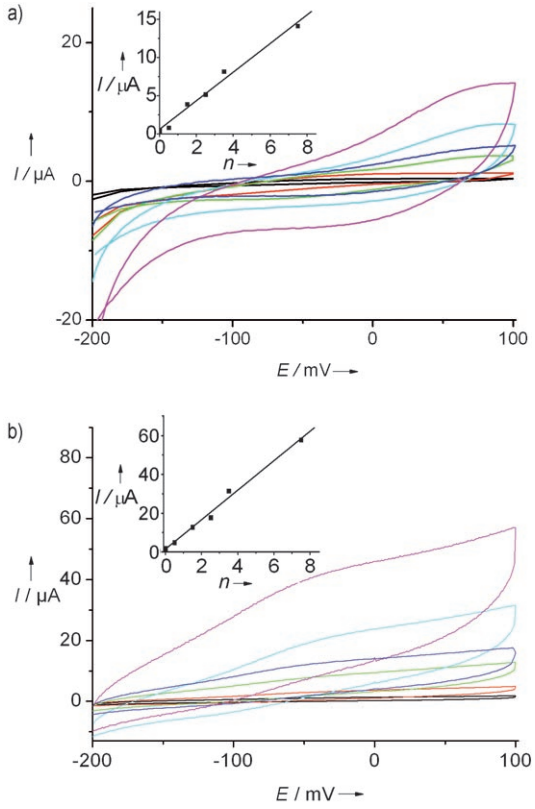


Figure 4. a) First CV cycles recorded for mediator/Ca^{2+}/NADH-modified macroporous gold ($d = 680$ nm) with different numbers of pore layers in Tris buffer; smooth electrode (black), $^1/_2$ layer (red), $1^1/_2$ layers (green), $2^1/_2$ layers (blue), $3^1/_2$ layers (green blue), $7^1/_2$ layers (violet); $\nu = 10$ mV s^{-1}. Inset: Oxidation current at 100 mV as a function of the number of porous layers. b) Cyclovoltammograms recorded with mediator/Ca^{2+}/NAD^+-modified macroporous gold electrodes (d = 680 nm) with different numbers of pore layers in Tris buffer in the presence of GDH (3 u mL^{-1}) and 10 mM glucose: smooth electrode (black), $^1/_2$ layer (red), $1^1/_2$ layers (green), $2^1/_2$ layers (blue), $3^1/_2$ layers (green blue), $7^1/_2$ layers (violet); $\nu = 10$ mV s^{-1}. Inset: Oxidation current at 100 mV as a function of the number of porous layers.

To achieve electroenzymatic turnover on macroporous electrodes, the target enzyme must be able to diffuse into the porous system such that the entire inner surface becomes active. We verified this by using glucose dehydrogenase (GDH) and glucose as the substrate. For this purpose we cycled mediator-modified electrodes in a buffer solution containing GDH or GDH and glucose, respectively, together with NAD^+ and $CaCl_2$ (Figure 4b). If the solution contained no glucose the NAD^+ was not reduced to NADH by the enzyme so that no electrochemical oxidation was observed. When glucose was added, it was oxidized enzymatically by NAD^+, which reacted to give NADH, which in turn was detected by a current increase as in the previous experiments. We found that for an electrode with $7^1/_2$ layers of hollow spheres the oxidation current increased by a factor of 25 compared to that of a flat electrode. Thus we conclude that for a pore diameter of 680 nm the interconnections are wide enough to allow the enzyme to diffuse into all the pores (Figure 5).

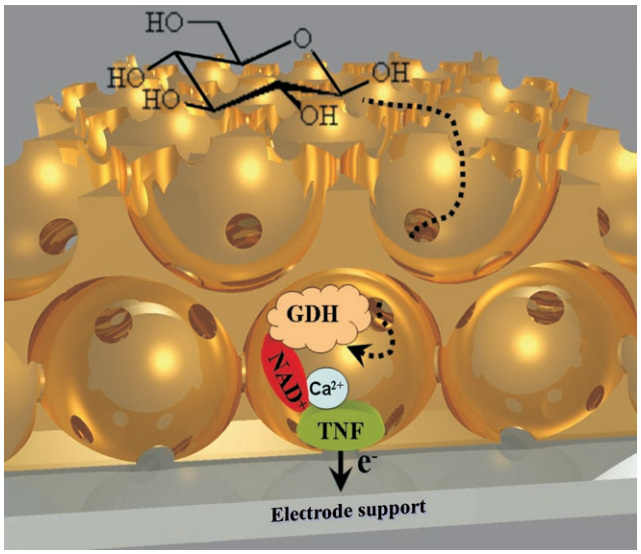


Figure 5. Representation of an electrode with $1^1/_2$ layers of hollow spheres modified with a mediator monolayer (TNF), Ca^{2+}, and NAD^+, and its reaction in a solution containing the enzyme GDH and the substrate glucose.

Another possibility to increase the active area for a given thickness of the porous electrode is to generate smaller pores by using smaller beads as templates during the synthesis of the

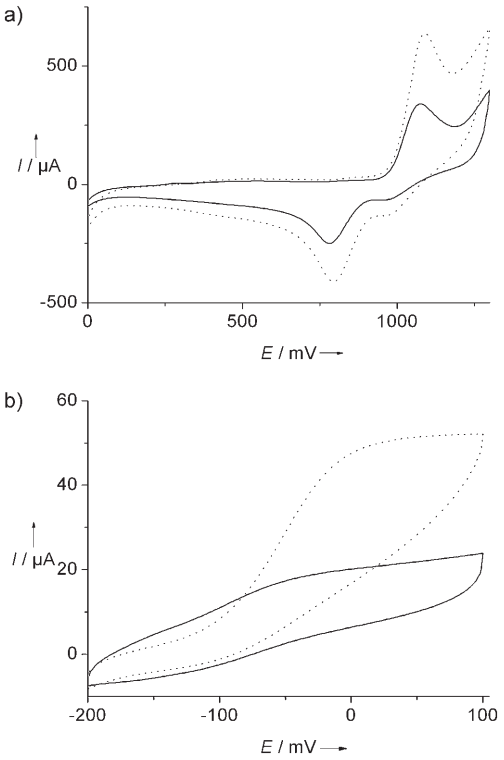


Figure 6. Comparision of macroporous gold electrodes of the same thickness (2.2 μm) but with different pore sizes; solid line: $d = 1100$ nm, $2^1/_2$ layers; dotted line: $d = 460$ nm, $5^1/_2$ layers. a) Potential cycles in pure 0.5 M H_2SO_4; $\nu = 100$ mV s^{-1}. b) Modified with mediator in 3.2 mM NADH and 0.1 M $CaCl_2$ in 0.1 M Tris buffer; $\nu = 10$ mV s^{-1}.

 © 2006 Wiley-VCH Verlag GmbH & Co. KGaA, Weinheim

macroporous gold. An electrode with, for example, $2^1/_2$ layers of hollow spheres and a pore diameter of 1100 nm has the same thickness (2.2 μm) as one with $5^1/_2$ layers and a pore diameter of 460 nm, but the electrode with 460-nm pores has a greater inner surface area. The electrochemical activity was determined by cyclic voltammetry and shows exactly the expected increase relative to the gold oxide striping peak (Figure 6 a). Analogous behavior was observed for the catalytic NADH oxidation described above (Figure 6 b).

By a combination of the Langmuir–Blodgett technique using colloidal particles and electrochemistry we have synthesized highly ordered macroporous gold with very precise control over the pore size, the spatial arrangement of the pores, and the number of pore layers. For electrochemical reactions exhibiting slow reaction rates the redox current is proportional to the number of hollow-sphere layers. The whole inner surface can be completely modified with a monolayer of the mediator TNF, Ca^{2+}, and the cofactor NAD^+. The current for the electroenzymatic oxidation of glucose with GDH on these modified electrodes can be easily increased by more than one order of magnitude compared to that on a nonporous electrode. This gain in signal is very interesting especially for the use of microelectrodes as biosensors or for biofuel cells.

Received: September 16, 2005
Revised: November 29, 2005
Published online: January 20, 2006

Keywords: bioelectrochemistry · electrocatalysis · porous materials · self-assembly · template synthesis

[1] A. J. Bard, M. Stratmann, *Encyclopedia of Electrochemistry, Vol. 9*, Wiley-VCH, **2002**.
[2] A. Heller, *Phys. Chem. Chem. Phys.* **2004**, *6*, 209 – 216.
[3] S. C. Barton, J. Gallaway, P. Atanassov, *Chem. Rev.* **2004**, *104*, 4867 – 4886.
[4] I. Willner, E. Katz, *Angew. Chem.* **2000**, *112*, 1230 – 1269; *Angew. Chem. Int. Ed.* **2000**, *39*, 1180 – 1218.
[5] "Biofuel Cells: Functional Design and Operation": E. Katz, A. N. Shipway, I. Willner in *Handbook of Fuel Cell Technology* (Eds.: W. Vielstich, H. Gasteiger, A. Lamm), Wiley, New York, **2002**.
[6] E. G. Wijnhoven, S. J. M. Zevenhuisen, M. A. Hendriks, D. Vanmaekelbergh, J. J. Kelly, W. L. Vos, *Adv. Mater.* **2000**, *12*, 888 – 890.
[7] O. D. Velev, P. M. Tessier, A. M. Lenhoff, E. W. Kaler, *Nature* **1999**, *401*, 548.
[8] P. N. Bartlett, P. R. Birkin, M. A. Ghanem, *Chem. Commun.* **2000**, 1671 – 1672.
[9] P. Jiang, J. F. Bertone, K. S. Hwang, V. L. Colvin, *Chem. Mater.* **1999**, *11*, 2132 – 2140.
[10] T. S. Eagleton, P. C. Searson, *Chem. Mater.* **2004**, *16*, 5027 – 5032.
[11] P. M. Tessier, O. D. Velev, A. T. Kalambur, A. M. Lenhoff, J. F. Rabolt, E. W. Kaler, *Adv. Mater.* **2001**, *13*, 396 – 400.
[12] Z. Gu, A. Fujishima, O. Sato, *Chem. Mater.* **2002**, *14*, 760 – 765.
[13] C. Lellig, W. Härtl, J. Wagner, R. Hempelmann, *Angew. Chem.* **2002**, *114*, 108 – 110; *Angew. Chem. Int. Ed.* **2002**, *41*, 102 – 104.
[14] D. J. Norris, E. G. Arlinghaus, L. Meng, R. Heiny, L. E. Scriven, *Adv. Mater.* **2004**, *16*, 1393 – 1399.
[15] P. Jiang, *Angew. Chem.* **2004**, *116*, 5743 – 5746; *Angew. Chem. Int. Ed.* **2004**, *43*, 5625 – 5628.
[16] F. Yan, W. A. Goedel, *Adv. Mater.* **2004**, *16*, 911 – 915.
[17] M. E. Abdelsalam, P. N. Bartlett, J. J. Baumberg, S. Coyle, *Adv. Mater.* **2004**, *16*, 90 – 93.
[18] M. Szekeres, O. Kamalin, R. A. Schoonheydt, K. Wostyn, K. Clays, A. Persoons, I. Dekany, *J. Mater. Chem.* **2002**, *12*, 3268 – 3274.
[19] M. Szekeres, O. Kamalin, P. G. Grobet, R. A. Schoonheydt, K. Wostyn, K. Clays, A. Persoons, I. Dékány, *Colloids Surf. A* **2003**, *227*, 77 – 83.
[20] S. Reculusa, S. Ravaine, *Chem. Mater.* **2003**, *15*, 598 – 605.
[21] S. Reculusa, P. Massé, S. Ravaine, *J. Colloid Interface Sci.* **2004**, *279*, 471 – 478.
[22] S. Reculusa, S. Ravaine, *Appl. Surf. Sci.* **2005**, *246*, 409 – 414.
[23] T. Sumida, Y. Wada, T. Kitamura, S. Yanagida, *Langmuir* **2002**, *18*, 3886 – 3894.
[24] E. Steckhan, *Top. Curr. Chem.* **1994**, *170*, 83 – 111.
[25] N. Mano, A. Thienpont, A. Kuhn, *Electrochem. Commun.* **2001**, *3*, 585 – 588.
[26] S. Ben-Ali, D. A. Cook, S. A. G. Evans, A. Thienpont, P. N. Bartlett, A. Kuhn, *Electrochem. Commun.* **2003**, *5*, 747 – 751.
[27] S. Ben-Ali, D. A. Cook, P. N. Bartlett, A. Kuhn, *J. Electroanal. Chem.* **2005**, *579*, 181 – 187.
[28] C. Wang, C. Yang, Y. Song, W. Gao, X. Xia, *Adv. Funct. Mater.* **2005**, *15*, 1267 – 1275.
[29] N. Mano, A. Kuhn, *J. Electroanal. Chem.* **1999**, *477*, 79 – 88.
[30] E. Katz, T. Lötzbeyer, D. D. Schlereth, W. Schuhmann, H.-L. Schmidt, *J. Electroanal. Chem.* **1994**, *373*, 189 – 200.
[31] N. Mano, P. Peyrou, A. Kuhn, *Electroanalysis* **2001**, *12*, 770 – 774.
[32] N. Mano, A. Kuhn, S. Menu, E. J. Dufourc, *Phys. Chem. Chem. Phys.* **2003**, *5*, 2082 – 2088.

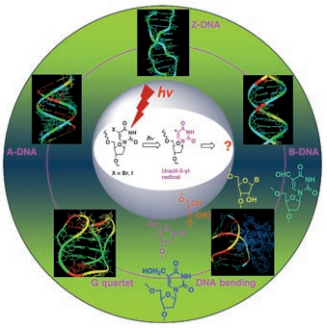
 © 2006 Wiley-VCH Verlag GmbH & Co. KGaA, Weinheim

Cover Picture

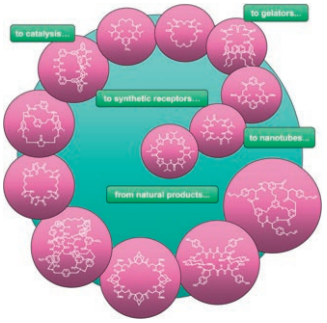


Dieter Enders,* Oliver Niemeier, and Tim Balensiefer

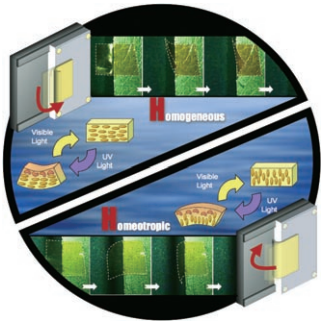
Enantioselective intramolecular crossed-benzoin reactions can be effected by using chiral N-heterocyclic carbene catalysts. The tetracyclic chiral carbene catalyst shown in the cover picture enables the reaction to proceed with formation of only one enantiomer of the α-hydroxy-substituted tetralones. D. Enders and co-workers disclose the development of the quaternary stereocenters in the organocatalytic reaction in their Communication on page 1463 ff.



DNA Structures
The local conformation in DNA governs the abstraction of hydrogen through uracil-5-yl radicals. How this principle is used to analyze DNA structures is shown by H. Sugiyama and Y. Xu in their Minireview on page 1354 ff.



Macrocycles
In their Review on page 1364 ff., S. E. Gibson and C. Lecci take a closer look at amino acid derived macrocycles. How advanced is their synthesis? What are the applications of these compounds?



Liquid Crystals
The photoresponsive behavior of liquid-crystalline elastomer films with different types of mesogen alignment is discussed by T. Ikeda and co-workers in their Communication on page 1378 ff.

DOI: 10.1002/anie.200600208

Chemistry—An Asian Journal: Lift-Off in Hawaii

Several events organized around the Pacifichem 2005 marked the beginning of *Chemistry—An Asian Journal*, the new sister journal of *Angewandte Chemie* and *Chemistry—A European Journal*. In the afternoon of December 16, an official meeting took place between representatives of the four co-publishing chemical societies, Wiley-VCH, and the supporting society, the Gesellschaft Deutscher Chemiker (German Chemical Society, GDCh), to discuss organizational matters. The four societies,



- the Chinese Chemical Society (CCS),
- the Chemical Research Society of India (CRSI),
- the Chemical Society of Japan (CSJ), and
- the Korean Chemical Society (KCS)

together form the Asian Chemical Editorial Society (ACES). The most important result of the meeting was certainly the decision to invite the Chemical Society Located in Taipei and the Singapore National Institute of Chemistry to join the circle of publishing societies.

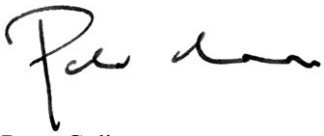
The ACES meeting was followed directly by a reception hosted by *Angewandte Chemie* and its sister journals as well as Wiley-VCH. The response was overwhelming: Over 400 Editorial and Advisory Board members, authors, and referees joined in the celebration to mark the launch of *Chemistry—An Asian Journal*. Besides many prominent chemists, including the guests of honor George A. Olah and Koji Nakanishi as well as the Presidents of the GDCh (Henning Hopf), the Chemical Society of Japan (Shinji Murai), and the Korean Chemical Society (Kook Joe Shin), the launch was attended by many younger authors from around the world; the photo gallery on the opposite page gives a good impression of the event. The packed room and the Hawaiian sunset provided an excellent platform for an exchange of ideas across all subject areas.

The guests were greeted by Eva-E. Wille (responsible for the worldwide chemistry program of John Wiley and Sons). On behalf of ACES, Shinji Murai then addressed the participants, and my speech followed (both are summarized on page 1332). Subsequently, Koji Nakanishi, who is also Editor-in-Chief of *The Chemical Record*, underscored the importance of *Chemistry—An Asian Journal* for all Asian chemists, and wished the journal much success. The tremendous response to the invitation is a good omen!

The next day saw a meeting for the members of the Editorial Board and the International Advisory Board of *Chemistry—An Asian Journal* which was also attended by Neville Compton, Editor of *Chemistry—A European Journal*, to show the "sister relationship" and close ties we wish to foster between the two journals.

Naturally, the Editorial Board is made up of top-notch Asian chemists. The International Advisory Board, however, is truly international (see right column) and is a striking list of high-caliber chemists, which includes seven Nobel Laureates who have pledged their support for *Chemistry—An Asian Journal!*

The Chairman of the Editorial Board, Ryoji Noyori, was unfortunately unable to attend the conference, but his strong support for *Chemistry—An Asian Journal* is always felt. On his behalf, I wish to invite the readers of *Angewandte Chemie* to submit their next high-quality Full Paper of broad interest to *Chemistry—An Asian Journal*.



Peter Gölitz

Editorial Board

Chairman: Ryoji **Noyori**, Riken, Nagoya
Members: Kankan **Bhattacharyya**, Kolkata; Makoto **Fujita**, Tokyo; Krishna N. **Ganesh**, Pune; Minoru **Isobe**, Nagoya; Kwang S. **Kim**, Pohang; Shu **Kobayashi**, Tokyo; Myongsoo **Lee**, Yonsei University, Seoul; Can **Li**, Dalian; Zongfan **Liu**, Beijing; Tien-Yau **Luh**, Taipei; Eiichi **Nakamura**, Tokyo; Mitsuo **Sawamoto**, Kyoto; Kazuyuki **Tatsumi**, Nagoya; Yoshio **Umezawa**, Tokyo; Henry **Wong**, Hong Kong; Dongyuan **Zhao**, Shanghai; Daoben **Zhu**, Beijing

International Advisory Board

Varinder **Aggarwal**, Bristol; Takuzo **Aida**, Tokyo; Ayyappanpillai **Ajayaghosh**, Kerala; Chunli **Bai**, Beijing; Martin **Banwell**, Canberra; Ad **Bax**, Bethesda, MD; Guy **Bertrand**, Riverside, CA; Srinivasan **Chandrasekaran**, Bangalore; Chi-Ming **Che**, Hong Kong; Jin-Ho **Choy**, Seoul; Gautam R. **Desiraju**, Hyderabad; François **Diederich**, Zürich; Norman **Dovichi**, Seattle, WA; Ben **Feringa**, Groningen; Alan **Fersht**, Cambridge; Akira **Fujishima**, Kanagawa; Tohru **Fukuyama**, Tokyo; Ernest **Giralt**, Barcelona; Robert H. **Grubbs**, Pasadena, CA; Charles **Han**, Beijing; Tamejiro **Hiyama**, Kyoto; Roald **Hoffmann**, Ithaca, NY; Andy **Hor**, Singapore; Jianguo **Hou**, Hefei; Vadim T. **Ivanov**, Moscow; Yasuhiro **Iwasawa**, Tokyo; Eric **Jacobsen**, Cambridge, MA; Kimoon **Kim**, Pohang; Susumu **Kitagawa**, Kyoto; Paul **Knochel**, Munich; Peter **Kündig**, Geneva; Eun **Lee**, Seoul; Yuan-Tseh **Lee**, Taipei; Jean-Marie **Lehn**, Strasbourg; Guoqiang **Lin**, Shanghai; David **MacMillan**, Pasadena, CA; Keiji **Maruoka**, Kyoto; Goverdhan **Mehta**, Bangalore; Keiji **Morokuma**, Atlanta, GA; Klaus **Müllen**, Mainz; Teruaki **Mukaiyama**, Tokyo; Shinji **Murai**, Osaka; Koji **Nakanishi**, New York; K. C. **Nicolaou**, La Jolla, CA; Jun **Okuda**, Aachen; Hiroyuki **Osada**, Saitama; Chintamani N. R. **Rao**, Bangalore; Richard R. **Schrock**, Cambridge, MA; Ferdi **Schüth**, Mülheim; K. Barry **Sharpless**, La Jolla, CA; Masakatsu **Shibasaki**, Tokyo; Kook Joe **Shin**, Seoul; Seiji **Shinkai**, Fukuoka; Yukio **Sugiura**, Kyoto; Junghun **Suh**, Seoul; Kohei **Tamao**, Saitama; Reshef **Tenne**, Rehovot; Barry M. **Trost**, Stanford, CA; Chen-Ho **Tung**, Beijing; Huilin **Wan**, Xiamen; Erkang **Wang**, Changchun; George **Whitesides**, Cambridge, MA; Chi-Huey **Wong**, La Jolla, CA; Hisashi **Yamamoto**, Chicago, IL; Do **Yoon**, Seoul; Xiao-Zeng **You**, Nanjing; Ahmed **Zewail**, Pasadena, CA

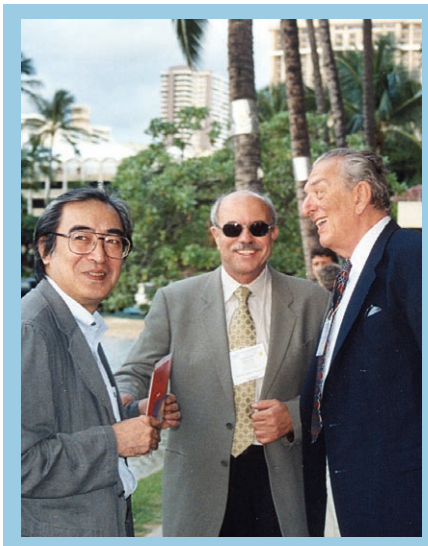
Editorial Office

Editor: Peter **Gölitz**; Deputy Editor: José **Oliveira**; Assistant Editor: Clara **Tan**; Editorial Assistant: Renata **Doczi**

 © 2006 Wiley-VCH Verlag GmbH & Co. KGaA, Weinheim

Aloha

Chemistry—An Asian Journal



M. Shibasaki (left), K. C. Nicolaou, G. A. Olah



K. Nakanishi



S. Murai



P. Pyykkö (left), M. Schädel



Can Li (left), N. Tatsumi, K. Tatsumi



M. Isobe (left), K. J. Shin



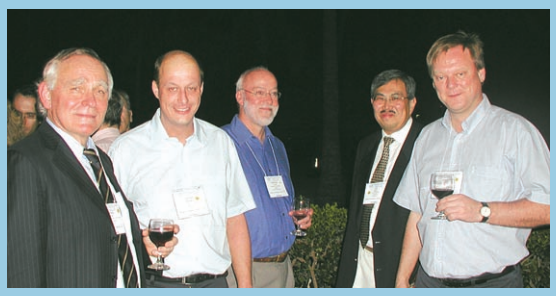
G. Bodwell (left), H. M. L. Davies, J. S. Clark, J. Selegue, B. Feringa



E.-E. Wille (left), P. Gölitz, M. Banwell



K. N. Ganesh (left), R. T. Raines



H. Hopf (left), P. Roesky, K. Cavell, J. Okuda, E. Hahn



R. R. Schmidt (left), A. de Meijere



L. Oro (left), E.-E. Wille, K. Nozaki



O. Kappe (right), C. Wentrup, G. Maier, B. Maier



J. L. Sessler (left), P. Gölitz, A. B. Holmes, S. G. Withers



P. Dixneuf (left), U. Siehl, Y. Do

© 2006 Wiley-VCH Verlag GmbH & Co. KGaA, Weinheim

Editorial



Shinji Murai (right) and Peter Gölitz toast the success of *Chemistry—An Asian Journal* after having presented their speeches (see text on this page).

Dear Friends,
We are celebrating the start of a new journal. It is still a newborn baby. Imagine your family: If you have only one child, there can be no intersibling relationship. If you have two children, a relationship is formed between them. However, if you have three children, many more relationships can flourish: A and B; B and C; C and A; A and (B+C); B and (C+A); C and (A+B); A and B and C.
This is why we need a new focal point. To date, the strong journals have been published in Europe and in the USA. We need Asia as a new hub for the publication of a leading journal to keep the journal relationships healthy and to promote further cooperation in chemical science and technology.
On behalf of the Chemical Society of Japan, which boasts 40 000 members distributed almost evenly between industry and academia, I assure you that we will make the best efforts for the success of the new journal.
Thank you.
Shinji Murai

Ladies and Gentlemen,
dear guests of honor,
"Some people believe football is a matter of life and death. I am very disappointed with that attitude. I can assure you it is much, much more important than that."
As scientists you will easily agree that you can replace the word football in this quote from Bill Shankly, a famous English football team manager, with "science" or in our case with "chemistry". I have worked as an editor for more than 25 years and it is therefore no wonder that my game would be "publishing".
Football, or soccer, as the Americans call it, and scientific publishing must have something in common and at least this is true for 2006. In June/July of next year the world will get excited about the Football World Cup which this time will be taking place in Germany. At exactly the same time the chemical world will get excited about the first issue of *Chemistry—An Asian Journal*. As of today manuscripts can be submitted: Full Papers and Focus Reviews.
On an occasion like this, one likes to say "a dream has come true" or some other similar poetic phrases. From Professor Seiji Shinkai I had heard another dream metaphor earlier this year; he said: "Two people in the same bed have different dreams". In the past in Europe and Asia every individual country—being in the United States one likes to say "every little country"—dreamed of the premier league for its own journal: they were in the same bed—Europe or Asia—but had different dreams. A decade ago many European chemical societies and foremost Jean-Marie Lehn, Nobel Laureate of 1987, got behind *Chemistry—A European Journal*, which celebrated its phenomenal success earlier this year at a special symposium to mark its 10th anniversary. The Editor-in-chief Dr. Neville Compton is with us today and he should be congratulated on the achievements. A testimony of its popularity is the fact that in 2006 *Chemistry—A European Journal* increases its frequency of publication from 24 to 36 issues.
Akin to the situation in Europe in the early 1990s was the situation for Asian chemical societies. Not anymore! Thanks to the farsightedness of the presidents and secretaries of major Asian chemical societies we celebrate today the launch of *Chemistry—An Asian Journal*. Let me mention a few of the farsighted people who were instrumental in quickly reaching an agreement between the societies and Wiley-VCH.
Foremost I must mention Professor Ryoji Noyori, Nobel Laureate of 2001 and President of RIKEN. His response to our initial thoughts was most encouraging and his acceptance of the role "Chairman of the Editorial Board" will be a guarantee for success. The discussions with the Chemical Society of Japan were led by Dr. Teruto Ohta, the Executive Director of the society, Professor Shinji Murai, the current President, and Professor Eiichi Nakamura from The University of Tokyo. From China we got immediate support from Professor Chunli Bai, the current President of the Chinese Chemical Society and Executive Vice President of the Chinese Academy of Science, and Professor Jiannian Yao, Secretary General of the Chinese Chemical Society; the current President of the Chemical Research Society of India, Professor Animesh Chakravorty, but also the former President Professor C. N. R. Rao were instrumental, as was Professor Kook Joe Shin, the current President of the Korean Chemical Society.
Since the idea was to start *Chemistry—An Asian Journal* in exactly the same way as *Chemistry—A European Journal* the support of the German Chemical Society (GDCh) was also needed, and its current President Professor Henning Hopf as well as Professor Wolfram Koch, the Executive Director of the GDCh were both immediately excited once they heard about the project. The GDCh is the owner society of *Angewandte Chemie*, and *Chemistry—An Asian Journal* will be distributed to all institutional subscribers of *Angewandte* guaranteeing the highest possible visibility for the new journal from the start. "Good things come in threes" is a saying, and certainly *Angewandte Chemie* with its two sister publications *Chemistry—A European Journal* and *Chemistry—An Asian Journal* will prove that this holds true.
This picture also applies to another journal the first issue of which will be published in January: *ChemBioChem* and *ChemPhysChem* will be complemented by *ChemMedChem*! *ChemMedChem* is co-published by the Italian, the German and many other European chemical societies and covers all aspects of the drug discovery process. It's bound to be the premier medicinal chemistry journal in Europe and to succeed in the world.
ChemMedChem and even more *Chemistry—An Asian Journal* could not have been started without support from within the publishers, Wiley-VCH. I had the permanent encouragement of Dr. Eva Wille and the great help of Dr. Carina Kniep on both projects.
It has been an exciting year. But I would not have ventured into these new projects if I were not sure of having **your** support. As an Editor you work for authors and readers. Listening to **your** lectures, reading **your** papers, hearing **your** advice—that's what makes me tick! I thank you all for making my professional life so enjoyable and I look forward to many fruitful interactions with you in the future and to celebrating the success of *Chemistry—An Asian Journal* at the next Pacifichem in five years.
Cheers!
Peter Goelitz

© 2006 Wiley-VCH Verlag GmbH & Co. KGaA, Weinheim

Commments on *CHEMISTRY—AN ASIAN JOURNAL*



Ryoji Noyori
Chairman of the Editorial Board of Chemistry—An Asian Journal
Nobel Laureate

Chemistry—An Asian Journal offers a highly visible arena for top papers from researchers around the world and especially Asia. With their unique cultural backgrounds, Asian researchers will significantly expand the horizons of chemical science. Complementing the existing top European and American journals, *Chemistry—An Asian Journal* will spur a "quantum leap" in Asian chemistry.



Chunli Bai
President of the Chinese Chemical Society

The inauguration of *Chemistry—An Asian Journal* is a milestone marking the new beginning of the alliance of Asian chemists. The journal will bring about great advances in Asian chemistry, and the Chinese Chemical Society will do its utmost to promote its success.



Animesh Chakravorty
President of the Chemical Research Society of India

At an accelerating pace, the present century will witness many great findings in chemical science originating from the East. The launch of *Chemistry—An Asian Journal*, driven by the four major Asian chemical societies, is thus truly symbolic of this outlook. *Chemistry—An Asian Journal* is destined to be a top chemistry journal that will publish much of the best from the East and the world over.



Shinji Murai
President of the Chemical Society of Japan

The Asian societies have joined forces to establish a world-class chemistry journal. United, we can push forward the boundaries of chemical science and technology.



Kook Joe Shin
President of the Korean Chemical Society Kook Joe Shin

Inaugurating a first-class Asian journal in chemistry for which chemical societies from China, India, Japan, and Korea collaborate is a truly historic event. Its success will be guaranteed with the prestigious editorial leadership of Professor Ryoji Noyori and with the support from *Angewandte Chemie* which is the carrier journal during the initial stage.



Henning Hopf
President of the GDCh

Chemists all over the world have witnessed the stunning development of Asian chemistry during the last decades. This requires a world-class chemical journal that has its roots in Asia. The German Chemical Society is proud to support *Chemistry—An Asian Journal*, the new sister publication of *Angewandte Chemie* and *Chemistry—A European Journal*.



Jean-Marie Lehn
Founding Chairman of the Editorial Board of Chemistry—A European Journal
Nobel Laureate

The great activity displayed by chemists of Asian countries requires a high-visibility journal. Like *Chemistry—A European Journal* has done at the European level, through the united action of European chemical societies, *Chemistry—An Asian Journal* will offer to chemists in Asian countries a forum for the disclosure of top-level chemical research.

© 2006 Wiley-VCH Verlag GmbH & Co. KGaA, Weinheim

Contents

VIP *The following Communications have been judged by at least two referees to be "very important papers" and will be published online at www.angewandte.org soon:*

H. Zhang, H. Xia, G. He, T. B. Wen, L. Gong, G. Jia**
Synthesis and Characterization of Stable Ruthenabenzenes

*X. Mo, Y. An, C.-S. Yun, S. M. Yu**
Nanoparticle-Assisted Visualization of Binding Interactions between Collagen Mimetic Peptide and Collagen Fibers

*M. B. Harney, Y. Zhang, L. R. Sita**
Discrete, Multiblock Isotactic–Atactic Stereoblock Polypropene Microstructures of Differing Block Architectures by Programmable Stereomodulated Living Ziegler–Natta Polymerization

*Y. Weizmann, Z. Cheglakov, V. Pavlov, I. Willner**
Autonomous Fueled Mechanical Replication of Nucleic Acid Templates for the Amplified Optical Detection of DNA

B. Botta, F. Caporuscio, D. Subissati, A. Tafi, M. Botta, A. Filippi, M. Speranza**
Flattened-Cone 2,8,14,20-Tetrakis(L-valinamido)[4]resorcinarene: Enantioselective Allosteric Receptors in the Gas Phase

*B. Wang, C. Chi, W. Shan, Y. Zhang, N. Ren, W. Yang, Y. Tang**
Chiral MCM-41 Mesostructured Silica Nanofibers

News

Bioorganic Chemistry: K. Sandhoff, H. Kessler, F. Diederich, and K. C. Nicolaou awarded ____ **1346**

Books

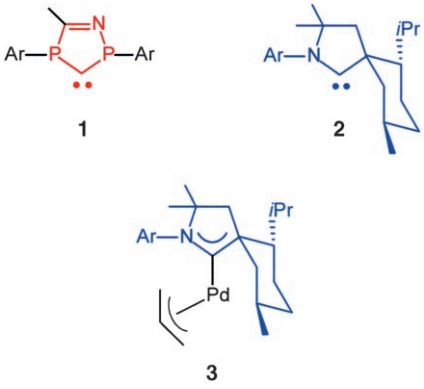
Handbook of Reagents for Organic Synthesis — Peter Wipf — *reviewed by J. Rademann* ____ **1347**

Highlights

Carbenes

F. E. Hahn* ____ **1348 – 1352**

Heterocyclic Carbenes



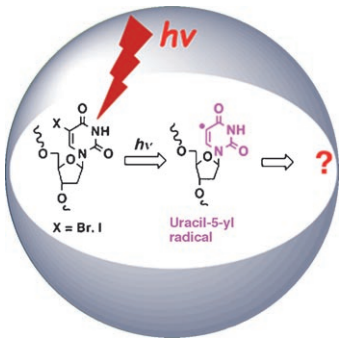
New carbenes open up new vistas. The P-heterocyclic carbene **1** was obtained after planarization of the P atoms in the heterocycle with sterically demanding substituents. The cyclohexyl substituent in the cyclic alkylaminocarbene **2** can be locked by proper substitution in the most sterically demanding conformation such that a low-coordinate metal center, as in complex **3**, is stabilized.

Minireviews

DNA Structures

Y. Xu, H. Sugiyama* ____ **1354 – 1362**

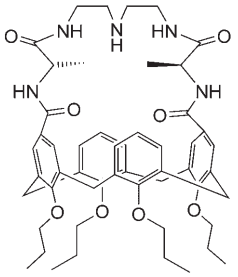
Photochemical Approach to Probing Different DNA Structures



Shedding light on DNA structures: Investigation of local DNA conformational changes associated with biological events is essential for understanding the function of DNA. A modern approach to this is the use of 5-halouracil as a probe molecule. Upon irradiation with UV light, a uracil-5-yl radical is formed and initiates a follow-up reaction in the DNA that depends on the local conformation of the DNA (see picture).

WILEY InterScience DISCOVER SOMETHING GREAT
© 2006 Wiley-VCH Verlag GmbH & Co. KGaA, Weinheim

Reviews



1

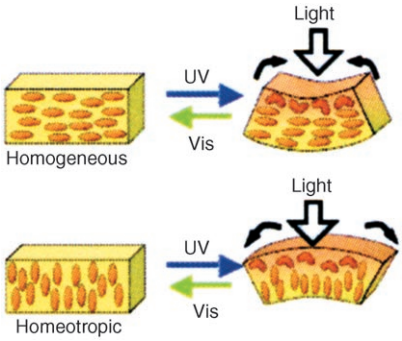
A vancomycin mimic: Synthetic macrocycle **1** shows promising antibiotic activity towards Gram-positive bacterial strands owing to its ability to bind the (*R*)-alanyl-(*R*)-alanine terminus of peptoglycans. But how useful are other amino acid derived macrocycles?

Macrocycles

S. E. Gibson,* C. Lecci ____ **1364 – 1377**

Amino Acid Derived Macrocycles—An Area Driven by Synthesis or Application?

Communications

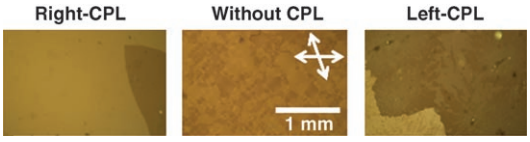


Light moves: Azobenzene liquid-crystalline elastomer (LCE) films with completely different types of mesogen alignment have been prepared by in situ photopolymerization. Upon irradiation with UV light, an LCE film with homogeneous (parallel) alignment bends toward the light source, whereas an LCE film with homeotropic (normal) alignment bends away from it.

Liquid Crystals

M. Kondo, Y. Yu, T. Ikeda* _ **1378 – 1382**

How Does the Initial Alignment of Mesogens Affect the Photoinduced Bending Behavior of Liquid-Crystalline Elastomers?

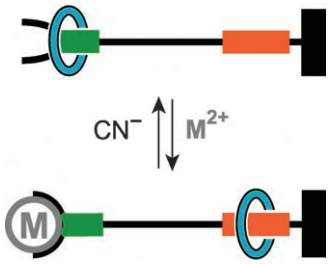


Imperative irradiation: A large enantiomeric excess in a liquid-crystal phase can be induced by circularly polarized light (CPL) as an external stimulus, and an imbalance in the two chiral domains becomes remarkable in the B_X phase (see pictures), which is similar to the B_4 phase made up by classical bent-core mesogens.

Liquid Crystals

S.-W. Choi, T. Izumi, Y. Hoshino, Y. Takanishi, K. Ishikawa, J. Watanabe, H. Takezoe* ____ **1382 – 1385**

Circular-Polarization-Induced Enantiomeric Excess in Liquid Crystals of an Achiral, Bent-Shaped Mesogen



When push comes to shove: A switchable [2]rotaxane has been developed in which the binding of a metal ion (e.g. Cd^{2+}, see scheme) to a bis(picolyl)amine fragment that acts as one of the stoppers induces a shift of the macrocyclic component along the thread from one binding site (green) to another weaker binding site (orange).

Rotaxanes

D. S. Marlin, D. González Cabrera, D. A. Leigh,* A. M. Z. Slawin ____ **1385 – 1390**

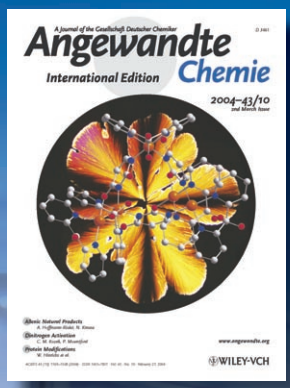
An Allosterically Regulated Molecular Shuttle

For the USA and Canada:
ANGEWANDTE CHEMIE International Edition (ISSN 1433-7851) is published weekly by Wiley-VCH PO Box 191161, D 69451 Weinheim, Germany. Air freight and mailing in the USA by Publications Expediting Inc. 200 Meacham Ave., Elmont, NY 11003. Periodicals postage paid at Jamaica NY 11431. US POSTMASTER: send address changes to *Angewandte Chemie*, Wiley-VCH, 111 River Street, Hoboken, NJ 07030. Annual subscription price for institutions: US$ 5685/5168 (valid for print and electronic / print or electronic delivery); for individuals who are personal members of a national chemical society prices are available on request. Postage and handling charges included. All prices are subject to local VAT/sales tax.

© 2006 Wiley-VCH Verlag GmbH & Co. KGaA, Weinheim

The best in chemistry –

for more than a hundred years



A Journal of the Gesellschaft Deutscher Chemiker

Angewandte
International Edition **Chemie**

www.angewandte.org

1888: ***The beginning of a success story***

Constant Innovations

1962: *First issue of the International Edition*
1976: *Graphical abstracts*
1979: *Cover pictures*
1988: *Centenary of Angewandte*
1989: *Routine use of color*
1991: *New section: Highlights*
1992: *Computerized editorial tracking system*
1995: *Internet service for readers*
1998: *Regular press service; full-text online*
2000: *New section: Essays; EarlyView: Communications available online ahead of the printed version*
2001: *New section: Minireviews*
2002: *Online submission of manuscripts*
2003: *Weekly publication; new section: News; new layout*
2004: *Backfiles (1962-1997); ManuscriptXpress: Online system for authors and referees*



Angewandte's advisors...

Seiji Shinkai
Kyushu University, Fukuoka

» ***Angewandte Chemie*** *is my favorite journal and I am honored to serve on its International Advisory Board. The research essence of an article can be understood rapidly because text and illustrations are finely harmonized. Furthermore, the high quality contents, which have a strong impact, are published very quickly.* «

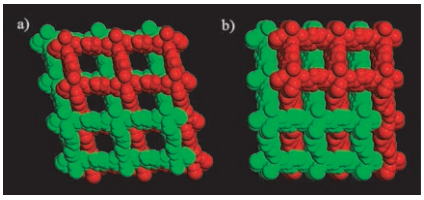
Angewandte Chemie International Edition *is a journal of the German Chemical Society (GDCh)*

GDCh

WILEY InterScience® DISCOVER SOMETHING GREAT

WILEY-VCH

1190104_gu



Filling the pores: A zinc-based metal–organic framework (MOF) can be transformed reversibly from an open (a) to a dense (b) configuration. The microporous solid is the first example of a MOF that is highly selective in the gas-chromatographic separation of alkanes.

Microporous Materials

B. Chen,* C. Liang, J. Yang, D. S. Contreras, Y. L. Clancy, E. B. Lobkovsky, O. M. Yaghi, S. Dai* _____ **1390 – 1393**

A Microporous Metal–Organic Framework for Gas-Chromatographic Separation of Alkanes



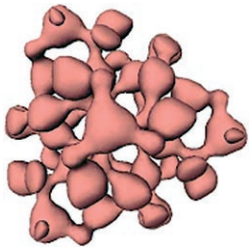
C-substituted zwitterionic 6π + 6π benzoquinonemonoimines are obtained by a C–C bond formation reaction. A selective, formal insertion of tetracyanoethylene (TCNE) or 7,7′,8,8′-tetracyanoquinodimethane (TCNQ) into a C–H bond of a quinonoid ring provides a new, general synthetic method in quinonoid chemistry.

C–C Coupling

P. Braunstein,* O. Siri,* J.-p. Taquet, Q.-Z. Yang _____ **1393 – 1397**

Regioselective Carbon–Carbon Bond Formation Reactions between TCNE or TCNQ and a Quinonoid Ring

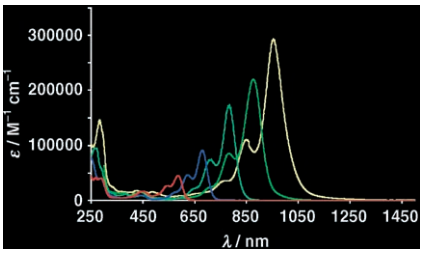
Swapping structures and cations: In an acid-induced 3D-to-3D transformation at room temperature, $K_6Cd_4Sn_3Se_{13}$ is converted into $K_{14-x}H_xCd_{15}Sn_{12}Se_{46}$. The $[Cd_{15}Sn_{12}Se_{46}]^{14-}$ framework, which contains a tunnel network of accessible cages of labyrinthine complexity (see picture), is highly robust, acid resistant, and has excellent ion-exchange properties.



Chalcogenides

N. Ding, M. G. Kanatzidis* **1397 – 1401**

Acid-Induced Conversions in Open-Framework Semiconductors: From $[Cd_4Sn_3Se_{13}]^{6-}$ to $[Cd_{15}Sn_{12}Se_{46}]^{14-}$, a Remarkable Disassembly/Reassembly Process



In the red: The synthesis and optical properties of homologous ladder-type near-infrared-absorbing chromophores, namely, two pentarylenebis(dicarboximide)s (green traces; see picture) as well as a hexarylenebis(dicarboximide) (yellow trace) have been studied. A strong bathochromic shift of the absorption maximum is noted with an increasing degree of annulation as is evident from the other traces.

NIR Dyes

N. G. Pschirer, C. Kohl, F. Nolde, J. Qu, K. Müllen* _____ **1401 – 1404**

Pentarylene- and Hexarylenebis(dicarboximide)s: Near-Infrared-Absorbing Polyaromatic Dyes

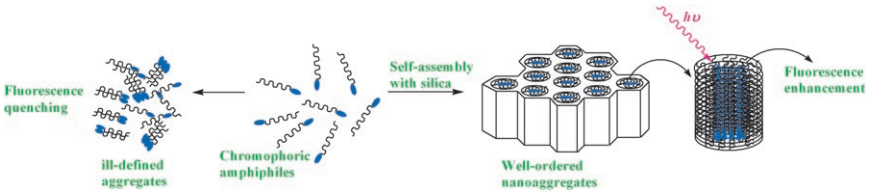
© 2006 Wiley-VCH Verlag GmbH & Co. KGaA, Weinheim

Contents

Hybrid Nanocomposites

C. J. Bhongale, C.-S. Hsu* — **1404 – 1408**

Emission Enhancement by Formation of Aggregates in Hybrid Chromophoric Surfactant Amphiphile/Silica Nanocomposites



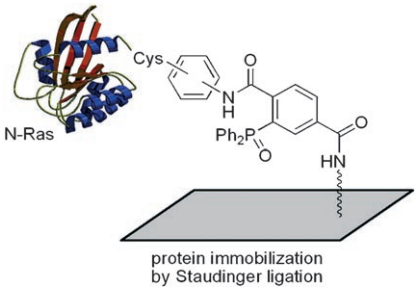
In best order: Nanoaggregates of chromophores formed in a controlled fashion in self-assembled functional hybrid nanocomposites enhance fluorescence (see scheme). These hybrids minimize the problem of solid-state quenching and are thus applicable in the fabrication of electroluminescence devices.

Protein Microarrays

A. Watzke, M. Köhn, M. Gutierrez-Rodriguez, R. Wacker, H. Schröder, R. Breinbauer, J. Kuhlmann, K. Alexandrov, C. M. Niemeyer, R. S. Goody,* H. Waldmann* — **1408 – 1412**

Site-Selective Protein Immobilization by Staudinger Ligation

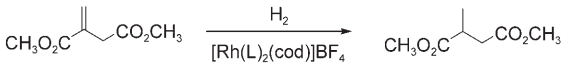
A sticky situation: A site-specific immobilization of proteins onto a glass surface may allow the creation of protein microarrays. This approach relies on the Staudinger ligation between azide-modified proteins and a phosphane-functionalized glass surface.



Asymmetric Catalysis

M. T. Reetz,* Y. Fu, A. Meiswinkel — **1412 – 1415**

Nonlinear Effects in Rh-Catalyzed Asymmetric Olefin Hydrogenation Using Mixtures of Chiral Monodentate P Ligands

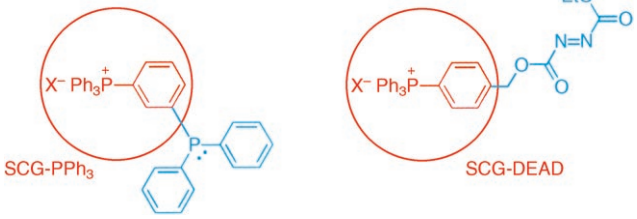


Well mixed: A 1:1 mixture of two different binaphthol-derived monophosphonite ligands (L) is employed in the Rh-catalyzed hydrogenation of prochiral olefins (see scheme; cod = cyclooctadiene). Variation of the enantiopurity of the ligands results in unusual nonlinear effects; furthermore, > 92 % *ee* can be achieved even if one component is racemic.

Supported Catalysts

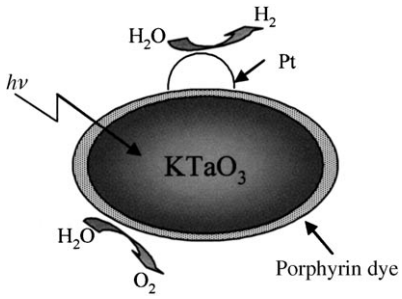
J.-C. Poupon, A. A. Boezio, A. B. Charette* — **1415 – 1420**

Tetraarylphosphonium Salts as Solubility-Control Groups: Phosphonium-Supported Triphenylphosphine and Azodicarboxylate Reagents



Predictable solubilities! Reagents supported on a tetraarylphosphonium group have solubilities that can be predicted. The reagents and their by-products can be readily removed, recovered, and recycled after reaction by a precipitation/filtration sequence initiated by the addition of a low-polarity solvent, such as diethyl ether. Furthermore, the supported reagents are robust and exhibit reactivities similar to their parent compounds.

© 2006 Wiley-VCH Verlag GmbH & Co. KGaA, Weinheim



Back to the elements: The activity of Pt/$K_{0.95}Ta_{0.92}Zr_{0.08}O_3$ for the photocatalytic splitting of water into H_2 and O_2 is greatly improved by dye sensitization (see picture). Among the organic dyes examined, the highest photocatalytic activity is obtained with cyanocobalamin (vitamin B_{12}) as a sensitizer.

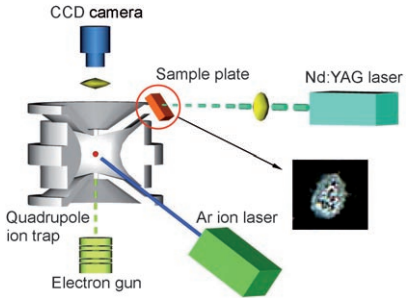
Photocatalysis

H. Hagiwara, N. Ono, T. Inoue, H. Matsumoto, T. Ishihara* **1420 – 1422**

Dye-Sensitizer Effects on a Pt/KTa(Zr)O_3 Catalyst for the Photocatalytic Splitting of Water

---

Single charged bioparticles such as viruses, bacteria, and mammalian whole cells have been successfully desorbed by laser-induced acoustic waves and analyzed with a quadrupole ion-trap mass spectrometer (see picture). This approach offers a high sensitivity of detection and good accuracy of the mass measurement. The capability to measure the mass of an entire cell has broad potential in biomedical applications.

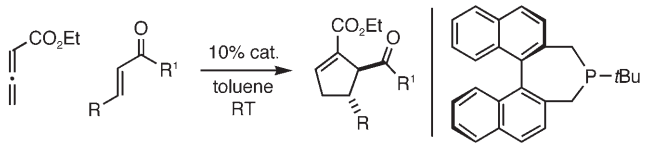


Mass Spectrometry

W.-P. Peng, Y.-C. Yang, M.-W. Kang, Y.-K. Tzeng, Z. Nie, H.-C. Chang,* W. Chang, C.-H. Chen **1423 – 1426**

Laser-Induced Acoustic Desorption Mass Spectrometry of Single Bioparticles

---



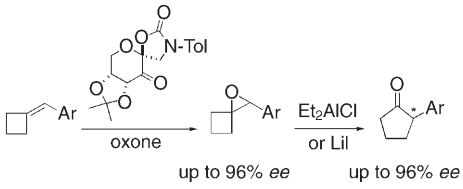
A phosphepine catalyst mediates enantioselective [3+2] cycloadditions of allenes with a variety of β-substituted α,β-unsaturated enones to produce highly functionalized cyclopentenes that contain two contiguous stereocenters (see scheme). Surprisingly, opposite regioisomers are produced as compared to reactions with β-unsubstituted enones.

Asymmetric Synthesis

J. E. Wilson, G. C. Fu* **1426 – 1429**

Synthesis of Functionalized Cyclopentenes through Catalytic Asymmetric [3+2] Cycloadditions of Allenes with Enones

---



Optically active epoxides are prepared by the highly enantioselective epoxidation of benzylidenecyclobutanes using a glucose-derived ketone as the catalyst and oxone as the oxidant. A subsequent Lewis acid catalyzed rearrangement of the resulting epoxides with Et_2AlCl or LiI provides α-aryl substituted cyclopentanones in high enantiomeric excess (see scheme; Tol = tolyl).

Synthetic Methods

Y.-M. Shen, B. Wang, Y. Shi* **1429 – 1432**

Enantioselective Synthesis of 2-Aryl Cyclopentanones by Asymmetric Epoxidation and Epoxide Rearrangement

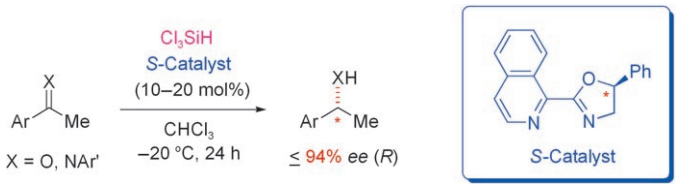
© 2006 Wiley-VCH Verlag GmbH & Co. KGaA, Weinheim

Contents

Asymmetric Reduction

A. V. Malkov,* A. J. P. S. Liddon, P. Ramírez-López, L. Bendová, D. Haigh, P. Kočovský* _____ **1432 – 1435**

Remote Chiral Induction in the Organocatalytic Hydrosilylation of Aromatic Ketones and Ketimines

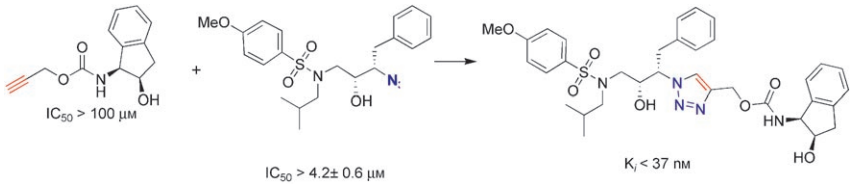


Lewis basic, metal-free pyridyloxazolines catalyze the reduction of prochiral aromatic ketones and ketimines with Cl_3SiH in good enantioselectivity (up to 94% *ee*). Arene–arene interactions between the substrate and the catalyst are likely to play a role in the enantiodifferentiation process.

Drug Design

M. Whiting, J. Muldoon, Y.-C. Lin, S. M. Silverman, W. Lindstrom, A. J. Olson, H. C. Kolb, M. G. Finn, K. B. Sharpless, J. H. Elder,* V. V. Fokin* _____ **1435 – 1439**

Inhibitors of HIV-1 Protease by Using In Situ Click Chemistry

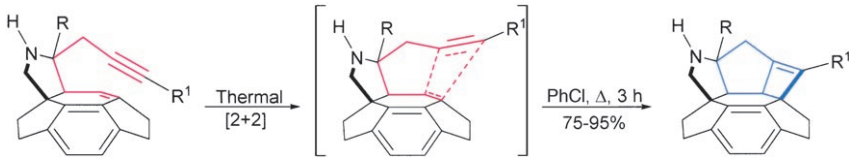


Twice poor equals potent: HIV-1 Protease assembles its own potent inhibitor through formation of the triazole linkage from azide- and alkyne-containing fragments that are themselves poor binders.

Fullerenes

N. Martín,* M. Altable, S. Filippone, A. Martín-Domenech, M. Güell, M. Solà _____ **1439 – 1442**

Thermal [2+2] Intramolecular Cycloadditions of Fuller-1,6-enynes



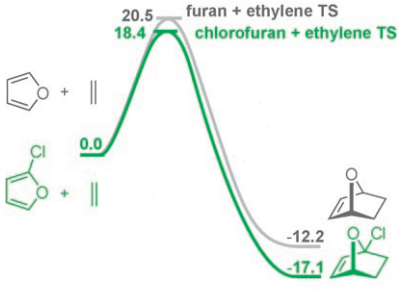
More fused rings for fullerenes: Fuller-1,6-enynes are a peculiar class of 1,6-enynes that involve a highly strained double-bond component as well as a curved molecular surface. They undergo an unprecedented thermal [2+2] cycloaddition to afford products with three neighboring fused rings on one six-membered ring of the C_{60} core as shown in the scheme.

Computer Chemistry

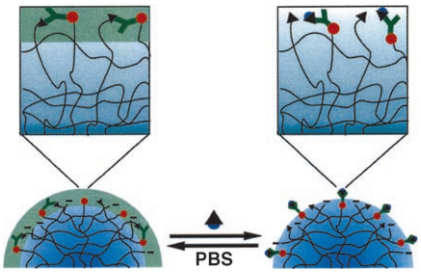
S. N. Pieniazek, K. N. Houk* _____ **1442 – 1445**

The Origin of the Halogen Effect on Reactivity and Reversibility of Diels–Alder Cycloadditions Involving Furan

Origin and generality of the halogen effect in Diels–Alder reactions were explored with high-accuracy CBS–QB3 computations. Halogen substitution increases cycloaddition exergonicities and decreases activation barriers. This effect is attributed to the energetic preference for electronegative halogen substituents to be attached to a more highly alkylated, and therefore more electropositive, carbon framework.



© 2006 Wiley-VCH Verlag GmbH & Co. KGaA, Weinheim

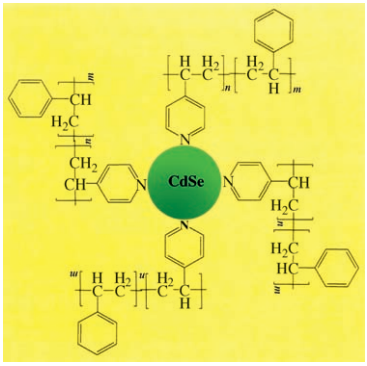


Soft lenses: Reversible antibody–antigen cross-links at the surface of a hydrogel microlens allow focal tuning of the microlens in response to soluble antigens (see picture; PBS = phosphate-buffered saline) to form the basis of a label-free biosensor/bioassay technique, whose sensitivity can be tuned by controlling the number of cross-links required to effect a specific swelling response.

Microlenses

J. Kim, N. Singh, L. A. Lyon* **1446 – 1449**

Label-Free Biosensing with Hydrogel Microlenses

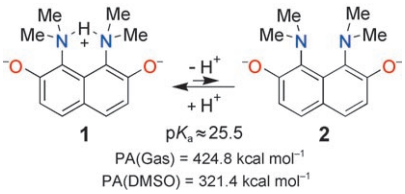


Selective incorporation of CdSe quantum dots (QDs) in the poly(4-vinylpyridine) nanodomains of a poly(styrene-*b*-4-vinylpyridine) diblock copolymer thin film (see structure) results in much higher conductivity and faster electron tunneling than in a random distribution of the same QDs in poly(4-vinylpyridine) homopolymer.

Quantum Dots

C.-P. Li, K.-H. Wei,* J. Y. Huang **1449 – 1453**

Enhanced Collective Electron Transport by CdSe Quantum Dots Confined in the Poly(4-vinylpyridine) Nanodomains of a Poly(styrene-*b*-4-vinylpyridine) Diblock Copolymer Thin Film



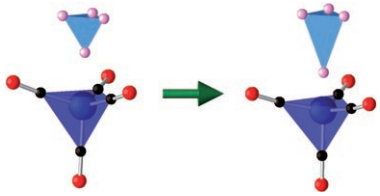
The strongest nitrogen base is 1,8-bis(dimethylamino)naphthalene-2,7-diolate according to experimental data and DFT calculations. Its proton affinity (PA) is comparable to those of simple ions such as OH^-, NH_2^-, and H^-. The diaminonaphthalene diolate **2** is protonated at the neutral amino groups with extremely high gas-phase and solution proton affinity to form highly stable H-bonded conjugate acid **1**. DMSO = dimethyl sulfoxide.

Proton Sponges

V. A. Ozeryanskii,* A. A. Milov, V. I. Minkin, A. F. Pozharskii **1453 – 1456**

1,8-Bis(dimethylamino)naphthalene-2,7-diolate: A Simple Arylamine Nitrogen Base with Hydride-Ion-Comparable Proton Affinity

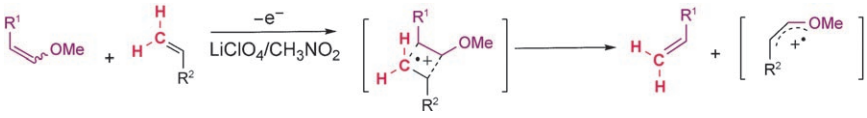
Changes in polyhedral shapes around Co and N atoms in a polyhedral-interconversion reaction coupled to a proton-transfer process are followed in a theoretical study through a generalized polyhedral-interconversion coordinate within the framework of the Avnir continuous shape measures.



Coordination Modes

D. Casanova, P. Alemany, S. Alvarez* **1457 – 1460**

Polyhedral Interconversion Coupled with Proton Transfer between an Ammonium Cation and the $[Co(CO)_4]^-$ Ion



Electrolytically generated four-membered-ring radical-cation intermediates are involved in the anodic olefin cross-metathesis of enol ethers and olefins in a lithium perchlorate/nitromethane electrolyte solution (see scheme). The reaction mechanism was investigated through deuterium-labeling studies.

Electrochemistry

T. Miura, S. Kim, Y. Kitano, M. Tada, K. Chiba* **1461 – 1463**

Electrochemical Enol Ether/Olefin Cross-Metathesis in a Lithium Perchlorate/Nitromethane Electrolyte Solution

© 2006 Wiley-VCH Verlag GmbH & Co. KGaA, Weinheim

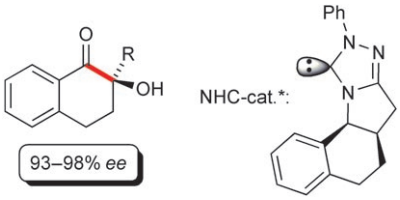
Contents

Homogeneous Catalysis

D. Enders,* O. Niemeier, T. Balensiefer ——— **1463 – 1467**

Asymmetric Intramolecular Crossed-Benzoin Reactions by N-Heterocyclic Carbene Catalysis

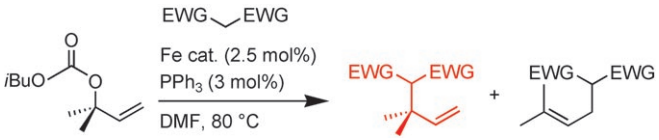
Getting cross: Excellent asymmetric inductions and very good yields are achieved in the generation of a quaternary stereocenter in α-hydroxy-substituted tetralones by using chiral N-heterocyclic carbene catalysts in an enantioselective intramolecular crossed-benzoin reaction. The synthesis of the corresponding α-hydroxyindanones with good *ee* values is also possible by this route.



Allylic Alkylation

B. Plietker* ——— **1469 – 1473**

A Highly Regioselective Salt-Free Iron-Catalyzed Allylic Alkylation

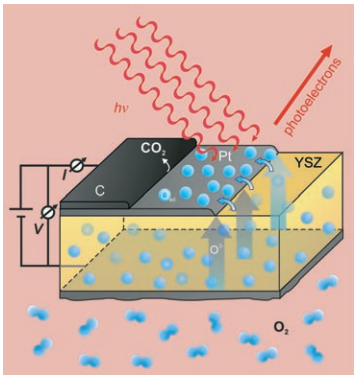


Ironing out the kinks: A highly regioselective allylic alkylation can be performed in the presence of catalytic amounts of an iron(−II) complex and triphenylphosphane (see scheme; EWG = electron-withdrawing group). Allyl carbonates and pronucleophiles are coupled in high yields with a high regioselectivity comparable only with that obtained with Rh catalysts. The reaction is broadly applicable and does not require external base.

Surface Reactions

B. Luerßen, E. Mutoro, H. Fischer, S. Günther, R. Imbihl, J. Janek* ——— **1473 – 1476**

In Situ Imaging of Electrochemically Induced Oxygen Spillover on Pt/YSZ Catalysts



Over the top: Electrochemically induced oxygen spillover on a Pt film has been investigated by photoelectron emission microscopy. Oxygen ions migrate through the YSZ substrate to the triple-phase boundary, where they are converted into adsorbed oxygen atoms that can oxidize the carbon layer on the Pt surface (see scheme; YSZ = yttria-stabilized zirconia).

Aluminum Clusters

R. Burgert, H. Schnöckel,* M. Olzmann, K. H. Bowen, Jr. ——— **1476 – 1479**

The Chlorination of the $[Al_{13}]^-$ Cluster and the Stepwise Formation of Its Intermediate Products, $[Al_{11}]^-$, $[Al_9]^-$, and $[Al_7]^-$: A Model Reaction for the Oxidation of Metals?

Watch your step! The individual steps during the chlorination of $[Al_{13}]^-$ clusters via $[Al_{11}]^-$, $[Al_9]^-$, and $[Al_7]^-$ intermediates (see picture) can be "visualized" by means of Fourier transform ion cyclotron resonance (FT-ICR) mass spectrometry. The reaction can be interpreted as a model reaction for the chlorination of bulk aluminum.



The issues for February 2006 appeared online on the following dates
Issue 5: January 17 · Issue 6: January 23 · Issue 7: January 30 · Issue 8: February 6

© 2006 Wiley-VCH Verlag GmbH & Co. KGaA, Weinheim

Sources

Product and Company Directory

You can start the entry for your company in "Sources" in any issue of *Angewandte Chemie*.

If you would like more information, please do not hesitate to contact us.

Wiley-VCH Verlag – Advertising Department
Tel.: 0 62 01 - 60 65 65
Fax: 0 62 01 - 60 65 50
E-Mail: MSchulz@wiley-vch.de

Service

Keywords ____ *1480*

Authors ____ *1481*

Sources ____ *A11*

Preview ____ *1483*



For more information on ChemMedChem see www.chemmedchem.org

© 2006 Wiley-VCH Verlag GmbH & Co. KGaA, Weinheim



Awarded...

Burckhardt Helferich Prizes to K. Sandhoff, H. Kessler, F. Diederich, and K. C. Nicolaou

In December 2005, the Institute of Organic Chemistry at the University of Leipzig (Germany) handed out the first Burckhardt Helferich Prize for Bioorganic Chemistry. Helferich (1887–1982)[1] was a professor at the Universities of Leipzig and Bonn, and was President of the Gesellschaft Deutscher Chemiker (German Chemical Society) during 1956–1957.



K. Sandhoff

Konrad Sandhoff (University of Bonn) was recognized for his pioneering work on the function, biosynthesis, and degradation of glycosphingolipids. A hereditary neurodegenerative disease has been named after him. Sandhoff completed his PhD in 1965 with H. Jatzkewitz at the University of Munich and then joined the Max Planck Institute for Psychiatry. He completed his habilitation in 1972, and after visiting professorships at the Johns Hopkins University (Baltimore, MD) and the Weizmann Institute in Rehovot (Israel) he joined the University of Bonn in 1979. He was a member of the editorial board for *Angewandte Chemie* during 1994–2003. Together with T. Kolter in 1999 he discussed metabolic pathways of sphingolipids and the pathobiochemistry of neurodegenerative diseases in a review in *Angewandte Chemie*. More recently they reported in *ChemBioChem* on a model system for the identification of lipid-modified glutamate residues in proteins.[2]

Horst Kessler (Technical University of Munich, TUM) received the prize for his outstanding work on the structure elucidation and dynamics of biologically important macromolecules, using NMR techniques that he partly developed. His work has made possible the development of new drugs. Kessler obtained his PhD in 1966 working with E. Müller at the University of Tübingen and completed his habilitation there in 1969. In 1971 he joined the University of Frankfurt (Main) as professor, and since 1989 he has been working at the TUM. He has also had short stays as visiting professor in Wisconsin and Haifa (Technion). Kessler has served on the editorial board of *Angewandte Chemie* since 1995 and was its President from 2000–2003. He recently reported in *ChemBioChem* on the biocompatibility of titanium implant materials that have been coated with cyclic RGD peptides and discussed the folding and aggregation of domains in p53 from diffusion NMR spectroscopy studies.[3]

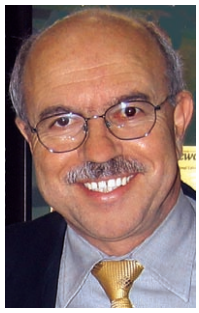


H. Kessler

François Diederich (ETH Zürich) was recognized for his important work in biologically and medicinally oriented organic chemistry, in particular on molecular modeling and recognition, which has enabled the development of enzyme and receptor blockers. His work also deals with novel materials, fullerene chemistry, and supramolecular nanostructures. Diederich completed his PhD in 1979 at the University of Heidelberg with H. Staab. He carried out postdoctoral research at the University of California in Los Angeles (UCLA) and at the Max Planck Institute for Medicinal Research in Heidelberg. After completing his habiliation in 1985 he returned to UCLA, and in 1992 he joined the ETH. Diederich has served on the editorial board of *Angewandte Chemie* since 1995 and is its President since 2004. Another focus of his research is antimalarial therapy, which he discussed recently in *Angewandte Chemie*.[4]



F. Diederich



K. C. Nicolaou

K. C. Nicolaou (Scripps Research Institute, La Jolla, CA) will receive the Burkhardt Helferich Prize 2006. The audience at his lecture (May 23, 2006) can look forward to hearing about many aspects of organic synthesis, especially the total synthesis of natural products. In 2005 he reported many total syntheses in *Angewandte Chemie* and discussed metathesis reactions[5a] and palladium catalysis cross-couplings[5b] in total synthesis. Nicolaou has been a member of the international advisory board of *Angewandte Chemie* for many years. Cypriot-born Nicolaou studied chemistry in London and obtained his PhD in 1972 under the guidance of F. Sondheimer and P. J. Garratt. He carried out postdoctoral research with T. J. Katz (Columbia University, New York) and E. J. Corey (Harvard University, Cambridge, MA). In 1976 he joined the University of Pennsylvania as professor, and in 1989 he accepted joint appointments, which he still holds today, at the University of California in San Diego and the Scripps Research Institute.

[1] H. Bredereck, *Angew. Chem.* **1957**, *69*, 405.
[2] a) T. Kolter, K. Sandhoff, *Angew. Chem.* **1999**, *111*, 1632; *Angew. Chem. Int. Ed.* **1999**, *38*, 1532; b) P. Sawatzki, I. Damm, B. Pierstorff, H. Hupfer, K. Sandhoff, T. Kolter, *ChemBioChem* **2005**, *6*, 178.
[3] a) J. Auernheimer, D. Zukowski, C. Dahmen, M. Kantlehner, A. Enderle, S. L. Goodman, H. Kessler, *ChemBioChem* **2005**, *6*, 2034; b) A. Dehner, H. Kessler, *ChemBioChem* **2005**, *6*, 1550.
[4] C. M. Crane, J. Kaiser, N. L. Ramsden, S. Lauw, F. Rohdich, W. Eisenreich, W. N. Hunter, A. Bacher, F. Diederich, *Angew. Chem.* **2006**, *118*, 1082; *Angew. Chem. Int. Ed.* **2006**, *45*, 1069.
[5] a) K. C. Nicolaou, P. G. Bulger, D. Sarlah, *Angew. Chem.* **2005**, *117*, 4564; *Angew. Chem. Int. Ed.* **2005**, *44*, 4490; b) K. C. Nicolaou, P. G. Bulger, D. Sarlah, *Angew. Chem.* **2005**, *117*, 4516; *Angew. Chem. Int. Ed.* **2005**, *44*, 4442.

DOI: 10.1002/anie.200600226

InterScience
© 2006 Wiley-VCH Verlag GmbH & Co. KGaA, Weinheim

Carbenes

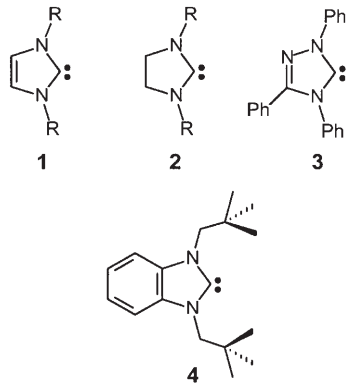
DOI: 10.1002/anie.200503858

Heterocyclic Carbenes**

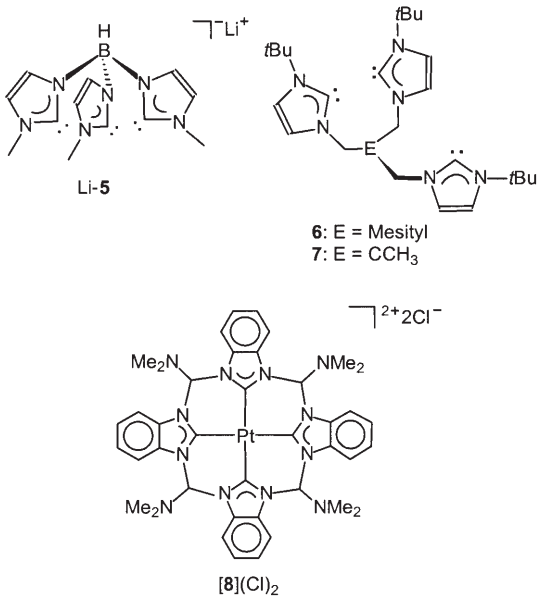
*F. Ekkehardt Hahn**

Keywords:
carbene homologues · carbene ligands · iridium · palladium · rhodium

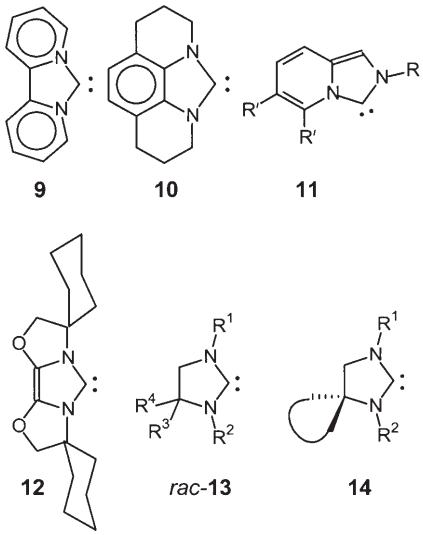
About 30 years elapsed between the proposal of stable N-heterocyclic carbenes (NHCs)[1] and the preparation of the first member of this class of compounds by Arduengo et al. The isolation of the stable imidazolin-2-ylidene **1**[2] and the saturated imidazolidin-2-ylidene derivative **2**[3] sparked renewed interest in the chemistry of N-heterocyclic carbenes and their metal complexes. Initially, the triazole derivative **3**[4] and the benzannulated carbene **4**[5] were prepared, both containing a diamine-stabilized carbene center as part of a five-membered ring.



Diazolium salts have been reported, which after in situ deprotonation react to give metal complexes with bidentate carbene ligands containing donor groups of types **1**[6] and **4**.[5,7] However, the free carbene ligands have been isolated only rarely.[6b,7b] The tripodal tricarbene **5** and its homoleptic metal complexes $[M(\mathbf{5})_2]^+$ ($M = Fe^{III}$, Cr^{III}) have been described.[8] The free tripodal tricarbenes **6**[9] and **7**[10] have been isolated, characterized by X-ray diffraction, and subsequently employed for the preparation of various metal complexes.[11] In addition, a tetracarbene ligand as in the complex cation $[\mathbf{8}]^{2+}$ is known. Such ligands can be obtained by template-controlled cyclization of 2-functionalized phenyl[12] or ethyl isocyanides[13] and subsequent introduction of alkyl bridges between the transiently formed NH,NH-stabilized carbene ligands.[14]



The carbenes with a substituted five-membered N-heterocyclic ring—**9**,[15] **10**,[16] **11**,[17] and **12**[18]—have been described as well as the unsymmetrically substituted compound *rac*-**13**[19] and the spirocyclic derivative **14**.[20] NHC **12** exhibits remarkable flexible steric bulk, which is caused by conformation changes of the cyclohexyl rings.



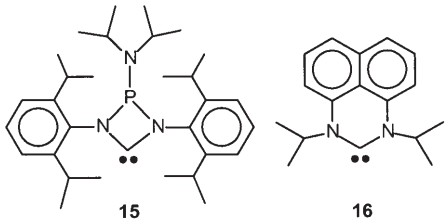
Cyclic diaminocarbenes derived from four-, six-, and seven-membered N-heterocyclic rings and their metal complexes are also known. Carbene **15** was obtained from the corresponding cyclic iminium salt by deprotonation with KHMDS (KHMDS = potassium 1,1,1,3,3,3-hexamethyldisilazane).[21]

Carbenes **16**,[22] **17a**,[23] and **17b**[24] derived from six-membered heterocycles were prepared by deprotonation of cyclic azolium salts with $LiN[Si(CH_3)_3]_2$, LiO*t*Bu, or KHMDS. The N-heterocy-

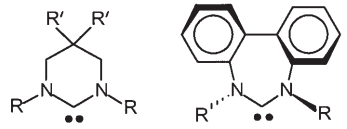
[*] Prof. Dr. F. E. Hahn
Institut für Anorganische und Analytische Chemie
Westfälische Wilhelms-Universität Münster
Wilhelm Klemm-Strasse 8
48149 Münster (Germany)
Fax: (+49) 251-833-3108
E-mail: fehahn@uni-muenster.de

[**] This work was supported by the Deutsche Forschungsgemeinschaft (SFB 424) and the International Graduate College "Template-Directed Chemical Synthesis" (GRK 673).

InterScience
© 2006 Wiley-VCH Verlag GmbH & Co. KGaA, Weinheim



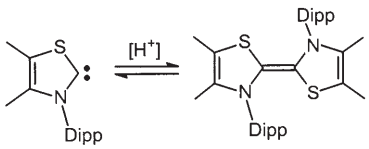
15 16



17a: R = *i*Pr, R′ = H
17b: R= Mesityl, R′ = Me **18**: R = Adamantyl

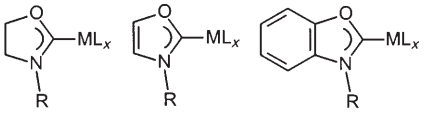
clic carbenes derived from four- to six-membered rings have a nearly planar heterocyclic framework. This is not the case for the seven-membered N-heterocyclic carbene ligand **18**. Condensation of 2,2′-diaminobiphenyl with two equivalents of 2-adamantone followed by reduction of the resulting imine and cyclization with triethyl orthoformate gave a cyclic, nonplanar C_2-symmetric amidinium salt. Deprotonation of this salt with KO*t*Bu in the presence of $[PdCl(allyl)_2]$ gave the palladium complex with the nonplanar, C_2-symmetric carbene **18**.[25]

Attempts to replace the nitrogen atoms in NHCs with other heteroatoms were carried out shortly after the first reports on stable NHCs appeared. Arduengo et al. described as early as 1997 the stable thiazol-2-ylidene **19**, which exists in a proton-catalyzed chemical equilibrium with its dimer **20**.[26] The mechanism for the dimerization of N-heterocyclic carbenes has recently been discussed in detail.[27] Free ylidenes derived from the oxazoline, oxazole, or



Dipp = 1-(2,6-Diisopropylphenyl)

19 **20**

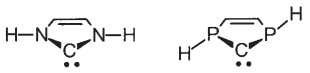


R = H, Alkyl, Aryl

21 **22** **23**

benzoxazole frameworks are not stable. However, carbene complexes of types **21**,[28] **22**,[29] and **23**[30] can be generated from complexes with 2-functionalized alkyl or phenyl isocyanides in template syntheses.

The unusual stablity of free N-heterocyclic carbenes has been attributed the ability of the nitrogen atoms in the heterocycle to act as π donors, thereby decreasing the electron deficiency at the adjacent carbene center. It is therefore surprising that until recently the heavier elements of Group 15 like phosphorus have not been employed for the stabilization of cyclic carbene centers[31] although ab initio calculations show[32] that the π-donor capabilities of third-row elements are as great, or greater than, those of their second-row counterparts. However, these calculations also show that the nitrogen atoms of a hypothetical N-heterocyclic carbene **24** are in a perfectly planar environment,[33] whereas the phosphorus centers in a hypothetical P-heterocyclic carbene (PHC) **25** are, as



24 **25**

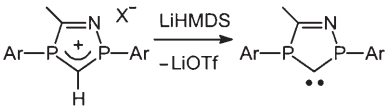
expected, strongly pyramidalized,[34] thereby preventing efficient stabilization of the carbene center. Bertrand and co-workers have solved this problem elegantly and reported recently on the synthesis of the first stable PHC **29**,[35] wherein pyramidalization of the phosphorus atoms[36] is prevented and the carbene center is stabilized by use of sterically demanding P substituents.

NHCs are often obtained by deprotonation of azolium salts. The corresponding phosphorus derivatives are unknown. In addition, preparative methods for the synthesis of substituted imidazoles or imidazolium salts cannot be used for the construction of phosphorus heterocycles. Therefore Bertrand and co-workers developed a new method for the synthesis of the salts **28a** and **28b**. It involves the dehalogenation of phosphaalkene **26** with AgOTf or $GaCl_3$ and subsequent reaction of the transiently formed diphosphaallyl cation **27** in a formal [3+2] cycloaddition with acetonitrile as the dipolarophile. The cations in **28a**/**28b** were deprotonated with LiHMDS to give the free, stable (m.p. 123–127 °C) PHC **29**.



26 **27**

Ar = 2,4,6-Tri-*tert*-butylphenyl



28a: X = OTf
28b: X = $GaCl_4$ **29**

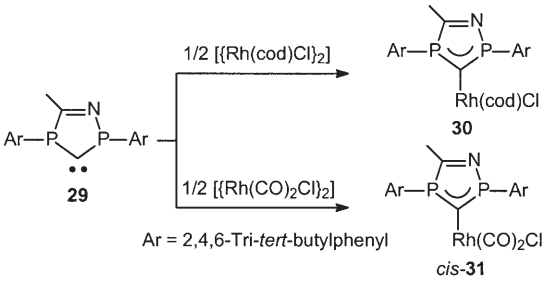
The molecular structures of **28b** and **29** demonstrate that the use of the sterically demanding 2,4,6-tri-*tert*-butylphenyl substituents has the desired effect. The phosphorus atoms in these compounds have a nearly planar bonding geometry (sum of angles at the phosphorus atoms: 354° and 348° for **28b**, 353° and 348° for **29**). The small deviation from planarity together with the *trans* arrangement of the aryl substituents leads to chiral compounds in the solid state. In solution both ^1H and ^{13}C NMR spectroscopy allows, even at low temperature (−100 °C), the detection of only one resonance for the diastereotopic groups indicating a rapid interconversion of the enantiomers and a low inversion barrier at the phosphorus atoms. The strong π donation of the phosphorus lone pairs was demonstrated by the short $P–C_{carbene}$ distances, which are significantly shorter than P–C single bonds. A significant reduction des P-C-P angle of 106.2(5)° in **28b** to 98.2(3)° in **29** was observed upon deprotonation of the salt **28b**. Similar behavior was observed previously for NHCs and their NHC(H^+) precursors. The ^{13}C NMR signal for the carbene carbon atom in PHC **29** ($\delta = 184$ ppm) is strongly deshielded compared to that of **28a** ($\delta = 119$ ppm) and is observed at a slightly higher field than the analogous signals of NHCs.

Ab initio calculations showed that a reduction of the steric bulk of the P substituents (substitution of 2,4,6-tri-*tert*-butylphenyl for hydrogen) in car-

© 2006 Wiley-VCH Verlag GmbH & Co. KGaA, Weinheim

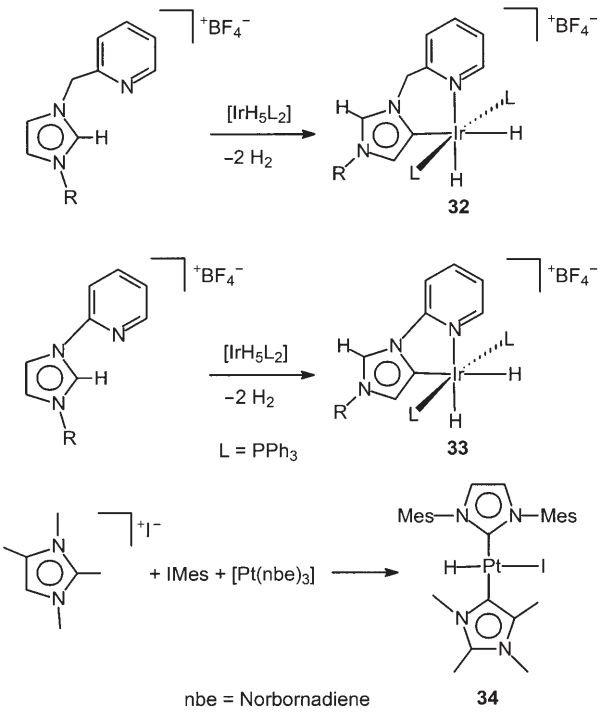
benes of type **29** leads to a pyramidalization of the phosphorus atoms (sum of angles 328° and 342°) and to a reduction of the singlet–triplet energy gap, which in turn destabilizes the P-heterocyclic carbene. These data confirm the validity of Bertrand's synthetic concept for PHCs.

NHCs and PHCs possess similar properties as ligands. PHC **29** reacts with $[\{Rh(cod)Cl\}_2]$ (cod = cyclooctadiene) under formation of the air-stable complex **30**. No pyramidalization at the



phosphorus atoms was observed upon complex formation, and the sum of angles at these atoms remains in the complex essentially the same as in the free ligand. This is indicative of only weak π back-bonding from the metal to the carbene center. This hypothesis was also corroborated by the relatively long $Rh-C_{carbene}$ distance (2.064(8) Å), which is at the upper limit of the range for $Rh-C_{NHC}$ bond lengths. IR spectroscopic investigations (CO-stretching frequencies) on *cis*-**31** reveal σ-donor properties for PHC **29** that compare well with those of related NHCs including the particularly basic acyclic diaminocarbene ligand.[37] Based on their properties it can be assumed that PHCs will serve as interesting and potentially useful additions to the family of heterocyclic carbene ligands.

The last years have seen an increasing number of reports describing the observation that imidazolium salts are not always metalated at the C2 ring atom. Recently, Crabtree et al. discussed the factors that lead to the surprising formation of complexes **32** and **33** which contain an abnormal, C,N-stabilized carbene center (C4–Ir bond).[38] In a planned synthesis Cavell et al.[39] prepared the carbene complex **34** with an abnormal carbene ligand

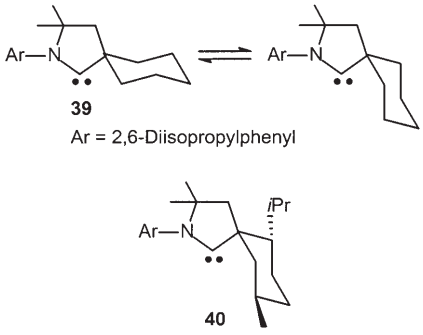


(C4–Pt bond) by oxidative addition of a C2-alkylated imidazolium salt to a Pt^0 center.

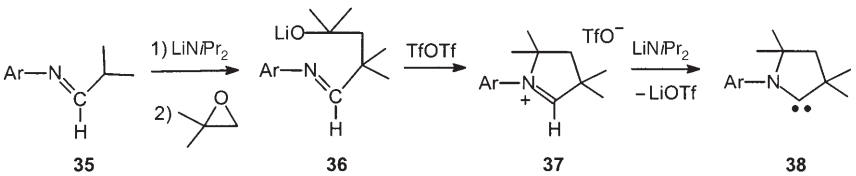
Uncomplexed abnormal carbene ligands have not been isolated yet. However, Bertrand et al. succeeded recently with the preparation of the first stable cyclic alkylaminocarbenes (CAACs).[40] The same group had previously described the first acyclic arylamino- and alkylaminocarbene ligands.[41]

CAAC **38** was prepared from the imine **35**. Deprotonation of **35** with lithium diisopropylamide and ring-opening attack of the generated azaallyl anion on 1,2-epoxy-2-methylpropane gave **36**. The cyclic aldiminium salt **37** was obtained by reaction of **36** with the anhydride of trifluoromethansulfonic acid. Deprotonation of **37** with lithium diisopropylamide gave CAAC **38** as a colorless solid, which is also stable in solution over weeks at room temperature. CAAC **39** contains a spiro carbon adjacent to the carbene center. It was obtained starting from an imine similar to **35**, which was prepared from 2,6-diisopropylaniline and cyclohexylcarbaldehyde.

Ligand **39** exhibits, similarly to carbenes of type **12**, a flexible steric bulk based on conformational changes of the cyclohexyl ring. In contrast to **12**, this "flexible wing" is located directly adjacent to the carbene center in **39**, so that its influence on the steric demand of the carbene ligand in metal complexes is even more pronounced. The most remarkable ligand in this series is CAAC **40**.[40] By ingenious substitution of the cyclohexyl ring the conformation of the "flexible wing" is locked in the most sterically demanding conformation with respect to a metal center coordinated by **40**. The steric demand of CAACs like **39** or **40** is quite

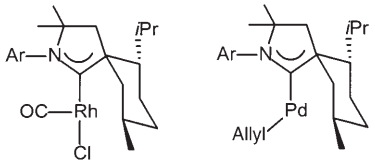


different from that of phosphines or normal NHCs. In addition, CAACs function as excellent donor ligands with a σ-donor power higher than that of electron-rich phosphines or even NHC ligands.



 © 2006 Wiley-VCH Verlag GmbH & Co. KGaA, Weinheim

The rigid CAAC **40** allows the preparation of unusual, low-coordinate transition-metal complexes like **41** and **42**.[42] The conformationally locked cyclohexyl ring protects the Rh^I center in **41** (Ar = 2,6-$iPr_2C_6H_3$) like a wall and thus stabilizes the 14-valence-electron Rh^I complex. Complex **42** is the first stable cationic [Pd(allyl)(NHC)] complex with 14 valence electrons. The stabilization of the low-coordinate complexes **41** and **42** was most likely supported by agostic interactions between the hydrogen atoms of the cyclohexyl ring and the metal centers.



41 **42**

Published online: January 31, 2006

[1] a) H.-W. Wanzlick, E. Schikora, *Angew. Chem.* **1960**, *72*, 494; b) H.-W. Wanzlick, H.-J. Kleiner, *Angew. Chem.* **1961**, *73*, 493; c) H.-W. Wanzlick, *Angew. Chem.* **1962**, *74*, 129–134; *Angew. Chem. Int. Ed. Engl.* **1972**, *11*, 75–80; d) H.-J. Schönherr, H.-W. Wanzlick, *Justus Liebigs Ann. Chem.* **1970**, *731*, 176–179.

[2] A. J. Arduengo III, R. L. Harlow, M. Kline, *J. Am. Chem. Soc.* **1991**, *113*, 361–363.

[3] a) A. J. Arduengo III, J. R. Goerlich, W. J. Marshall, *J. Am. Chem. Soc.* **1995**, *117*, 11027–11028; b) M. K. Denk, A. Thadani, K. Hatano, A. J. Lough, *Angew. Chem.* **1997**, *109*, 2719–2721; *Angew. Chem. Int. Ed. Engl.* **1997**, *36*, 2607–2609.

[4] a) D. Enders, K. Breuer, G. Raabe, J. Runsink, J. H. Teles, J.-P. Melder, K. Ebel, S. Brode, *Angew. Chem.* **1995**, *107*, 1119–1122; *Angew. Chem. Int. Ed. Engl.* **1995**, *34*, 1021–1023; b) D. Enders, T. Balensiefer, *Acc. Chem. Res.* **2004**, *37*, 534–541.

[5] a) F. E. Hahn, L. Wittenbecher, R. Boese, D. Bläser, *Chem. Eur. J.* **1999**, *5*, 1931–1935; b) F. E. Hahn, L. Wittenbecher, D. Le Van, R. Fröhlich, *Angew. Chem.* **2000**, *112*, 551–554; *Angew. Chem. Int. Ed.* **2000**, *39*, 541–544.

[6] a) W. A. Herrmann, J. Schwarz, M. G. Gardiner, M. Spiegler, *J. Organomet. Chem.* **1999**, *575*, 80–86; b) R. E. Douthwaite, D. Haüssinger, M. L. H. Green, P. J. Silcock, P. T. Gomes, A. M. Martins, A. A. Danopoulos, *Organometallics* **1999**, *18*, 4584–4590; c) M. V. Baker, B. W. Skelton, A. H. White, C. C. Williams, *J. Chem. Soc. Dalton Trans.* **2001**, 111–120; d) R. E. Douthwaite, M. L. H. Green, P. J. Silcock, P. T. Gomes, *Organometallics* **2001**, *20*, 2611–2615; e) J. E. Mata, A. R. Chianese, J. R. Miecznikowski, M. Poyatos, E. Peris, J. W. Faller, R. H. Crabtree, *Organometallics* **2004**, *23*, 1253–1263.

[7] a) F. E. Hahn, M. Foth, *J. Organomet. Chem.* **1999**, *585*, 241–245; b) F. E. Hahn, T. von Fehren, L. Wittenbecher, R. Fröhlich, *Z. Naturforsch. B* **2004**, *59*, 541–543.

[8] a) U. Kernbach, M. Ramm, P. Luger, W. P. Fehlhammer, *Angew. Chem.* **1996**, *108*, 333–335; *Angew. Chem. Int. Ed. Engl.* **1996**, *35*, 310–312; b) R. Fränkel, U. Kernbach, M. Bakola-Christianopoulou, U. Plaia, M. Suter, W. Ponikwar, H. Nöth, C. Moinet, W. P. Fehlhammer, *J. Organomet. Chem.* **2001**, *617–618*, 530–545.

[9] a) H. V. Rasika Dias, W. Jin, *Tetrahedron Lett.* **1994**, *35*, 1365–1366; b) H. Nakai, Y. Tang, P. Gantzel, K. Meyer, *Chem. Commun.* **2003**, 24–25.

[10] X. Hu, I. Castro-Rodriguez, K. Meyer, *Organometallics* **2003**, *22*, 3016–3018.

[11] X. Hu, K. Meyer, *J. Organomet. Chem.* **2005**, *690*, 5474–5484.

[12] a) F. E. Hahn, V. Langenhahn, N. Meier, T. Lügger, W. P. Fehlhammer, *Chem. Eur. J.* **2003**, *9*, 704–712; b) F. E. Hahn, C. García Plumed, M. Münder, T. Lügger, *Chem. Eur. J.* **2004**, *10*, 6285–6293.

[13] F. E. Hahn, V. Langenhahn, T. Pape, *Chem. Commun.* **2005**, 5390–5392.

[14] F. E. Hahn, V. Langenhahn, T. Lügger, T. Pape, D. Le Van, *Angew. Chem.* **2005**, *117*, 3825–3829; *Angew. Chem. Int. Ed.* **2005**, *44*, 3759–3763.

[15] R. Weiss, S. Reichel, M. Handke, F. Hampel, *Angew. Chem.* **1998**, *110*, 352–354; *Angew. Chem. Int. Ed.* **1998**, *37*, 344–347.

[16] C. Metallinos, F. B. Barrett, J. L. Chaytor, M. E. A. Heska, *Org. Lett.* **2004**, *6*, 3641–3644.

[17] M. Alcarazo, S. J. Roseblade, A. R. Cowley, R. Fernández, J. M. Brown, J. M. Lassaletta, *J. Am. Chem. Soc.* **2005**, *127*, 3290–3291.

[18] a) G. Altenhoff, R. Goddard, C. W. Lehmann, F. Glorius, *Angew. Chem.* **2003**, *115*, 3818–3821; *Angew. Chem. Int. Ed.* **2003**, *42*, 3690–3693; b) G. Altenhoff, R. Goddard, C. W. Lehmann, F. Glorius, *J. Am. Chem. Soc.* **2004**, *126*, 15195–15201.

[19] F. E. Hahn, M. Paas, D. Le Van, T. Lügger, *Angew. Chem.* **2003**, *115*, 5402–5405; *Angew. Chem. Int. Ed.* **2003**, *42*, 5243–5246.

[20] F. E. Hahn, M. Paas, D. Le Van, R. Fröhlich, *Chem. Eur. J.* **2005**, *11*, 5080–5085.

[21] E. Despagnet-Ayoub, R. H. Grubbs, *J. Am. Chem. Soc.* **2004**, *126*, 10198–10199.

[22] P. Bazinet, G. P. A. Yap, D. S. Richeson, *J. Am. Chem. Soc.* **2003**, *125*, 13314–13315.

[23] M. Mayr, K. Wurst, K.-H. Ongania, M. R. Buchmeiser, *Chem. Eur. J.* **2004**, *10*, 1256–1266.

[24] J. Yun, E. R. Marinez, R. H. Grubbs, *Organometallics* **2004**, *23*, 4172–4173.

[25] C. C. Scarborough, M. J. W. Grady, I. A. Guzei, B. A. Gandhi, E. E. Bunel, S. S. Stahl, *Angew. Chem.* **2005**, *117*, 5403–5406; *Angew. Chem. Int. Ed.* **2005**, *44*, 5269–5272.

[26] A. J. Arduengo III, J. R. Goerlich, W. J. Mashall, *Liebigs Ann.* **1997**, 365–374.

[27] R. W. Alder, M. E. Blake, L. Chaker, J. N. Harvey, F. Paolini, J. Schütz, *Angew. Chem.* **2004**, *116*, 6020–6036; *Angew. Chem. Int. Ed.* **2004**, *43*, 5896–5911.

[28] a) W. P. Fehlhammer, K. Bartel, U. Plaia, A. Völkl, A. T. Liu, *Chem. Ber.* **1985**, *118*, 2235–2254; b) U. Plaia, H. Stolzenberg, W. P. Fehlhammer, *J. Am. Chem. Soc.* **1985**, *107*, 2171–2172.

[29] J. Ruiz, G. García, M. E. G. Mosquera, B. F. Perandones, M. P. Gonzalo, M. Vivanco, *J. Am. Chem. Soc.* **2005**, *127*, 8584–8585.

[30] a) M. Tamm, F. E. Hahn, *Coord. Chem. Rev.* **1999**, *182*, 175–209; b) M. Basato, R. A. Michelin, M. Mozzon, P. Sgarbossa, A. Tassan, *J. Organomet. Chem.* **2005**, *690*, 5414–5420.

[31] In marked contrast with the cyclic series, phosphorus has been used to prepare several acyclic stable carbenes, including the first one ever reported. a) A. Igau, H. Grützmacher, A Baceiredo, G. Bertrand, *J. Am. Chem. Soc.* **1988**, *110*, 6463–6466; b) A. Igau, A. Baceiredo, G. Trinquier, G. Bertrand, *Angew. Chem.* **1989**, *101*, 617–618; *Angew. Chem. Int. Ed. Engl.* **1989**, *28*, 621–622; c) C. Buron, H. Gornitzka, V. Romanenko, G. Bertrand, *Science* **2000**, *288*, 834–836.

[32] J. Kapp, C. Schade, A. M. El-Nahas, P. von R. Schleyer, *Angew. Chem.* **1996**, *108*, 2373–2376; *Angew. Chem. Int. Ed. Engl.* **1996**, *35*, 2236–2238.

[33] a) D. A. Dixon, A. J. Arduengo III, *J. Phys. Chem.* **1991**, *95*, 4180–4182; b) C. Boehme, G. Frenking, *J. Am. Chem. Soc.* **1996**, *118*, 2039–2046.

[34] a) A. Fekete, L. Nyulászi, *J. Organomet. Chem.* **2002**, *643–644*, 278–284; b) W. W. Schoeller, D. Eisner, *Inorg. Chem.* **2004**, *43*, 2585–2589.

 © 2006 Wiley-VCH Verlag GmbH & Co. KGaA, Weinheim

[35] D. Martin, A. Baceiredo, H. Gornitzka, W. W. Schoeller, G. Bertrand, *Angew. Chem.* **2005**, *117*, 1728–1731; *Angew. Chem. Int. Ed.* **2005**, *44*, 1700–1703.
[36] L. Nyulászi, *Tetrahedron* **2000**, *56*, 79–84.
[37] a) R. W. Alder, P. R. Allen, M. Murray, A. G. Orpen, *Angew. Chem.* **1996**, *108*, 1211–1213; *Angew. Chem. Int. Ed. Engl.* **1996**, *35*, 1121–1123; b) K. Denk, P. Sirsch, W. A. Herrmann, *J. Organomet. Chem.* **2002**, *649*, 219–224.
[38] S. Gründermann, A. Kovacevic, M. Albrecht, J. W. Faller, R. H. Crabtree, *J. Am. Chem. Soc.* **2002**, *124*, 10473–10481.
[39] D. Bacciu, K. J. Cavell, I. A. Fallis, L. Ooi, *Angew. Chem.* **2005**, *117*, 5416–5418; *Angew. Chem. Int. Ed.* **2005**, *44*, 5282–5284.
[40] V. Lavallo, Y. Canac, C. Präsang, B. Donnadieu, G. Bertrand, *Angew. Chem.* **2005**, *117*, 5851–5855; *Angew. Chem. Int. Ed.* **2005**, *44*, 5705–5709.
[41] a) S. Solé, H. Gornitzka, W. W. Schoeller, D. Bourissou, G. Bertrand, *Science* **2001**, *292*, 1901–1903; b) X. Cattoën, H. Gornitzka, D. Bourissou, G. Bertrand, *J. Am. Chem. Soc.* **2004**, *126*, 1342–1343; c) V. Lavallo, J. Mafhouz, Y. Canac, B. Donnadieu, W. W. Schoeller, G. Bertrand, *J. Am. Chem. Soc.* **2004**, *126*, 8670–8671.
[42] V. Lavallo, Y. Canac, A. DeHope, B. Donnadieu, G. Bertrand, *Angew. Chem.* **2005**, *117*, 7402–7405; *Angew. Chem. Int. Ed.* **2005**, *44*, 7236–7239.



 © 2006 Wiley-VCH Verlag GmbH & Co. KGaA, Weinheim

DOI: 10.1002/anie.200501962

DNA Structures

Photochemical Approach to Probing Different DNA Structures

*Yan Xu and Hiroshi Sugiyama**

Keywords:
DNA structures · DNA · hydrogen abstraction · photochemistry · uracil

The various conformations of DNA—the A, B, and Z forms, the protein-induced DNA kink, and the G-quartet form—are thought to play important biological roles in processes such as DNA replication, gene expression and regulation, and the repair of DNA damage. The investigation of local DNA conformational changes associated with biological events is therefore essential for understanding the function of DNA. In this Minireview, we discuss the use of photochemical dehalogenation of 5-halouracil-containing DNA to probe the structure of DNA. Hydrogen abstraction by the resultant uracil-5-yl radicals is atom-specific and highly dependent on the structure of the DNA, suggesting that this photochemical approach could be applied as a probe of DNA conformations in living cells.

1. Introduction

Polymorphic DNA exists in a variety of distinct conformations.[1] Duplex DNA can adopt a variety of sequence-dependent secondary structures that range from the canonical right-handed B form through to the left-handed Z form.[2,3] Triplex and tetraplex structures of DNA are also known to exist.[3–5] Figure 1 shows the characteristic deviation of DNA structures: the A, B, and Z forms, the protein-induced DNA kink, and the G-quartet form. These conformations are thought to play important biological roles in processes such as DNA replication, gene expression and regulation, and the repair of DNA damage.[6,7] For example, human telomeric DNA, which forms G-quartet (quadruplex) structures, serves to protect the cell from recombination and degradation.[7,8] Disruption of telomere maintenance leads to eventual cell death, which can be exploited for therapeutic intervention in cancer treatment.[8–14] Recently, Rich and co-workers shed more light on the biological relevance of Z-DNA in a report that double-stranded RNA adenosine deaminase (ADAR1), the tumor-associated protein DLM-1, and the E3L protein of vaccinia virus bind specifically to Z-form DNA.[6] Furthermore, Liu et al. presented evidence that Z-DNA-forming sequences are required for chromatin-dependent activation of the CSF1 (colony-stimulating factor 1) promoter.[15] Besides the structure itself of DNA, its binding of a transcription factor such as a TATA

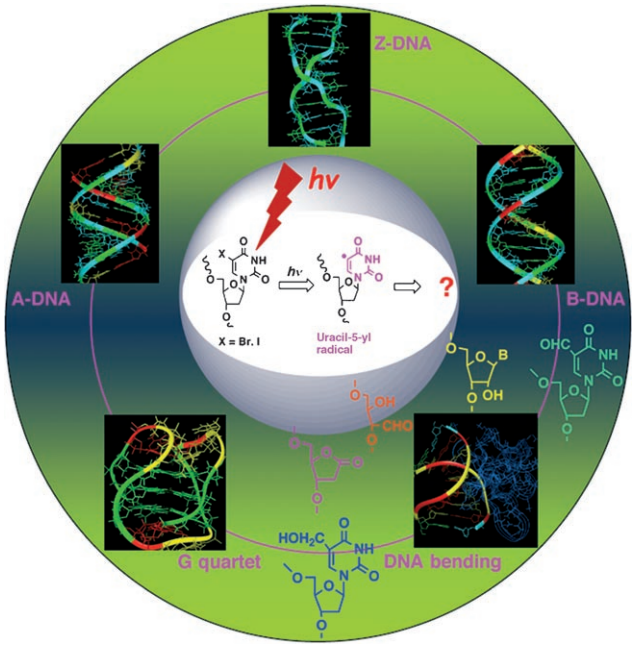


Figure 1. Structure-dependent atom-specific hydrogen abstraction from various important DNA local structures by the uracilyl radical generated from 5-halouracil upon irradiation with UV light.

[*] Dr. Y. Xu, Prof. H. Sugiyama
Department of Chemistry, Graduate School of Science
Kyoto University, Kitashirakawa-Oiwakecho
Sakyo, Kyoto, 606-8502 (Japan)
and
SORST (Japan) Science and Technology Corporation
Fax: (+81) 757-533-670
E-mail: hs@kuchem.kyoto-u.ac.jp

InterScience

© 2006 Wiley-VCH Verlag GmbH & Co. KGaA, Weinheim

box-binding protein induces significant bending of the DNA which is believed to be essential for the initiation of transcription.[16–22] For these reasons, investigation of local DNA conformational changes associated with biological events is essential for understanding the function of DNA.

Methods such as X-ray crystal structure analysis[23] and NMR spectroscopy[24,25] provide structural information with atomic resolution about DNA with defined sequences. Other spectroscopic methods such as circular dichroism and Raman spectroscopy can also be used to study DNA structures. These methods deal with model systems of DNA, such as synthetic oligonucleotides or homopolymers; however, they report the average conformation of the entire sample and cannot be used to pinpoint local conformational differences. Moreover, these approaches cannot be applied directly to probe local DNA structures inside living cells. Although various chemical probes and antibodies have been developed, these methods usually require the isolation of DNA from the nucleus.

Light can be made to permeate into a cell by selecting a suitable wavelength and by focusing on a certain locus within the cell. Because conformational changes in DNA are likely to occur in a short period within the living cell, a method that uses the DNA photoreaction and is capable of fixing the DNA conformation in vivo would be very useful. The products of the photochemical reaction should reflect the DNA local structure and provide information at sequence resolution on the conformational change of the DNA during the irradiation. In this Minireview, we describe the photoreactivities of 5-halouracil in the five characteristic local DNA structures: the A, B, and Z forms, the protein-induced DNA kinks, and the G-quartet form (Figure 1). Hydrogen abstraction from DNA by the uracil-5-yl radical generated upon UV irradiation of the 5-halouracil residue is atom-specific and highly dependent on the structure of the DNA. This photochemical method, which reflects DNA structure, could be applied as a unique probe of DNA conformations in living cells.

2. Competitive 1′- and 2′α-Hydrogen Abstraction by the Uracilyl Radical in B-Form DNA

Thymine (T) in DNA can be replaced with 5-halouracil (^{Br}U or ^{I}U), and the resultant 5-halouracil-substituted DNA remains functional in vivo. Replacement of thymine in DNA by 5-halouracil enhances the photosensitivity of the cell with respect to DNA–protein cross-linking, breakage of DNA strands, and the creation of alkali-labile sites through the formation of uracilyl radicals upon irradiation.[26–29] Therefore, we reasoned that the photoreactivity of 5-halouracil could be used to probe the local conformation of DNA. We started our project to elucidate the structure of DNA lesions by careful analysis of the products of photoirradiated 5-halouracil-containing hexanucleotides. Photoirradiation of the self-complementary B-form duplex d(GCA^{Br}UGC)$_2$ and d(GCA^{I}UGC)$_2$ resulted in the release of adenine together with the formation of deoxyribonolactone **1** as a C1′ oxidation product and erythrose-containing hexameric product **2** as a C2′ oxidation product (Scheme 1).[27–29] By using a stereospecifically C2′-deuterated oligonucleotide of the deoxyribose moiety, we demonstrated that the formation of the C2′ oxidation product **2** occurs by a rate-limiting abstraction of the 2′α-hydrogen atom of the deoxyribose moiety by the uracilyl radical.[29] The results clearly indicate that the uracilyl radical competitively abstracts the 1′- and 2′α-hydrogen atoms of the deoxyribose residue of adenine on the 5′ side.

In contrast to the behavior of d(GCA^{Br}UGC)$_2$ upon photoirradiation whereby C1′ and C2′ oxidation products were efficiently formed, hexanucleotides that lack the A^{Br}U sequence, such as 5′-d(GCG^{Br}UCG)-3′/5′-d(CGACGC)-3′, showed very poor photoreactivity. On the basis of these results, we initially proposed the mechanism that sequence-specific electron transfer occurs from the adjacent adenine moiety on the 5′ side to ^{Br}U, to form the ^{Br}U anion radical in the duplex structure. Formation of a uracilyl anion radical eliminates the Br anion to generate a uracilyl radical that abstracts the C1′-hydrogen atom of adenosine, and subsequent oxidation of the C1′ radical by the cation radical of adenine produces ribonolactone through a C1′ cation. This type of selectivity was confirmed by others.[30] However, as guanine is a better electron-donating base the reactivity was called a "contrathermodynamic reaction".[30] Recently, ^{Br}U was used as a probe of excess electron transfer.[31] We investigated the electron transfer along DNA by using uniformly 5-halouracil-substituted DNA.[32] By PCR, we prepared 450-base-pair DNA fragments in which all thymine residues were substituted with ^{Br}U or ^{I}U. The DNA fragments were irradiated with monochromatic UV light ($\lambda = 302$ nm) and then analyzed on sequencing gels. Surprisingly, specific cleavage at 5′-(G/C)AA^{X}U^{X}U-3′ and 5′-(G/C)A^{X}U^{X}U-3′ sequences in both ^{Br}U- and ^{I}U-containing DNA fragments

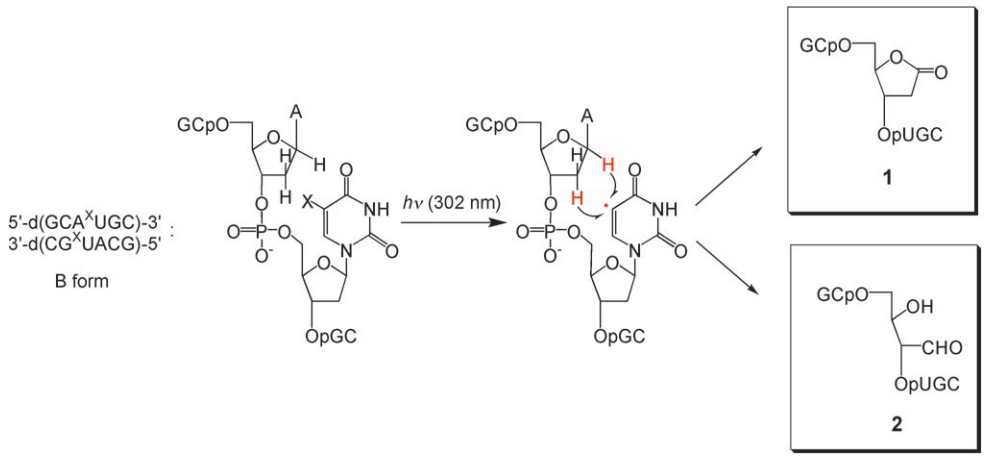


Hiroshi Sugiyama, born in 1956, received his PhD in 1984 with Teruo Matuura at Kyoto University. After postdoctoral studies at the University of Virginia with Sidney M. Hecht, he returned to Kyoto University in 1986 as assistant professor and became associate professor in 1993. In 1996, he joined the Institute of Biomaterials and Bioengineering at Tokyo Medical and Dental University. Since 2003 he is a professor of chemical biology at Kyoto University. His honors include the Nippon IBM award and the Chemical Society of Japan Award for Creative Work.



Yan Xu studied chemistry at Liaoning University of Petroleum and Chemical Technology (China). In 2004, he completed his PhD under the guidance of Prof. Hiroshi Sugiyama at Tokyo Medical and Dental University, where he studied non-natural nucleic acids and small molecules to stabilize Z-form DNA and photochemical methods of probing G-quartet structures. Currently, he is a Japan Science and Technology Fellow in the group of Prof. Sugiyama at Kyoto University, studying the structure and function of DNA by a chemical approach.

© 2006 Wiley-VCH Verlag GmbH & Co. KGaA, Weinheim



Scheme 1. Competitive hydrogen abstraction from C1′ and C2′ positions in B-form DNA. X = Br, I; G = guanine, C = cytosine, A = adenine, U = uracil.

was observed only after heat treatment. Analysis of the oligonucleotide products by HPLC indicated that the major products were ribonolactone-containing octamers. When oligonucleotides were irradiated in $H_2{}^{18}O$, incorporation of ^{18}O atoms into ribonolactone residues from $H_2{}^{18}O$ was observed, indicating that H_2O is the source of the carbonyl oxygen center of the ribonolactone. From these observations, we proposed a possible mechanism for the efficient photoreactions at 5′-GAA^{X}U^{X}U-3′ sequences (see Figure 2). The initial electron transfer would occur from guanine to the electron-deficient ^{X}U^{X}U step through stacked AA and A moieties.[33] Release of the halide ion from the ^{X}U^{X}U anion radical generates uracilyl radicals to abstract the hydrogen atom at C1′ from the adjacent adenine moiety of the ^{X}U^{X}U step. One-electron oxidation of the C1′ radical of deoxyadenine (dA) by the cation radical of guanine gives rise to a C1′ cation and regeneration of guanine. The intervening adenine bases between guanine and the ^{X}U^{X}U step are considered to act as a bridge between the electron donor and acceptor for charge separation after electron transfer from guanine to the ^{X}U^{X}U step, thus preventing rapid electron back transfer. Previously observed A^{Br}U sequence specificity can be explained by the same role of adenine.

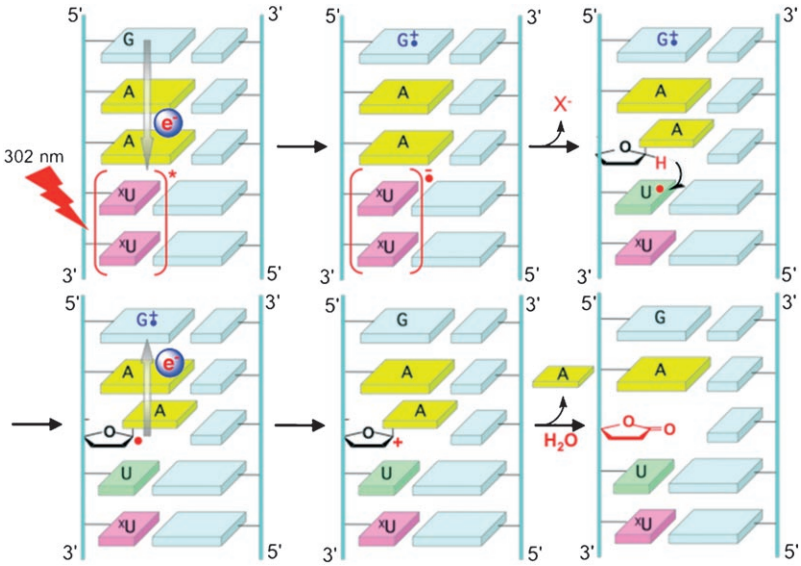


Figure 2. Proposed mechanism for the efficient photochemical reaction at 5′-(G/C)AA^{X}U^{X}U-3′ sequences.

3. Selective 1′-Hydrogen Abstraction in A-Form DNA

Analysis of the photolysates of the DNA–RNA hybrid 5′-d(CGA^{I}UGC)-3′/5′-r(GCAUCG)-3′, which adopts the A-type structure, indicated that the selective 1′ oxidation product **1** was obtained as a major product with release of free adenine (Figure 3a).[34] Similar results were obtained for ^{Br}U-containing DNA–RNA hybrids and for DNA oligomers.[28,29,34] ^{1}H NMR NOE experiments with 5′-d(CGAUGC)-3′/5′-r(GCAUCG)-3′ and 5′-d(CGAUGC)-3′/5′-d(GCATCG)-3′ suggest that there is no correlation between the distances and the selectivity of hydrogen abstraction. To examine the origin of the selectivity of hydrogen abstraction, a putative transition state for the process in a DNA duplex and a DNA–RNA hybrid was constructed and the conformational energy required to achieve their transition states was evaluated.[34] New sets of parameters for the transition state of hydrogen abstraction for the AMBER force field were prepared by ab initio molecular orbital calculations of the abstraction of hydrogen from ethanol by vinyl radicals. In the DNA–RNA hybrid, the minimized energy of the C1′ transition state was the lowest, which explains the observed selective C1′-hydrogen abstraction. The calculated structure of the AU step, which contains the putative transition state of C1′-hydrogen abstraction in the DNA–RNA hybrid, is shown in Figure 3b. Contrary to the A form, for which the C1′ radical is more stabilized than that resulting from C2′-hydrogen abstraction, the activation energy levels of the C1′ and C2′ radicals of the B form are roughly equivalent,[29] which would explain the competitive C1′- and C2′-

© 2006 Wiley-VCH Verlag GmbH & Co. KGaA, Weinheim

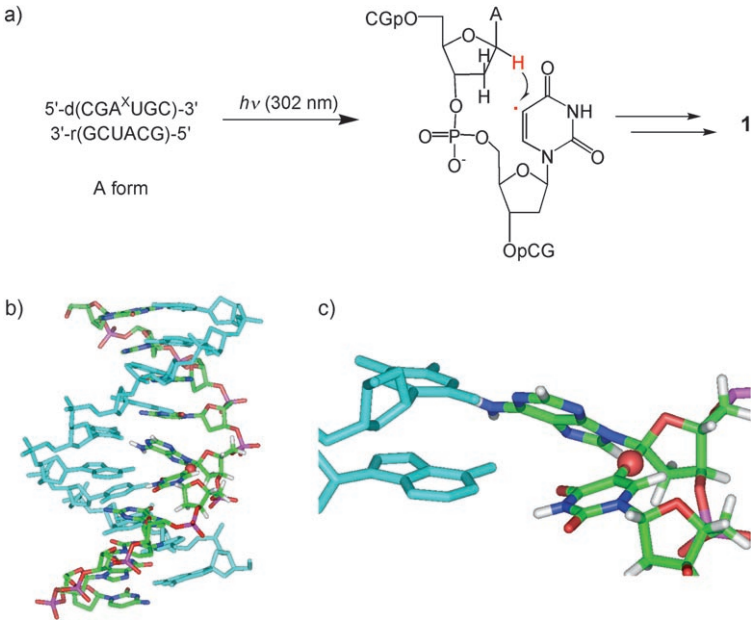


Figure 3. a) Photochemical products of hexanucleotides in A-type DNA–RNA hybrids upon irradiation with UV light. Selective 1′-hydrogen abstraction occurred in the A-like structure. X = Br, I. b) Structure of the AU step for a minimized octamer, showing the putative transition state for C1′-hydrogen abstraction in the DNA–RNA hybrid, and c) a close-up view of one AU step.

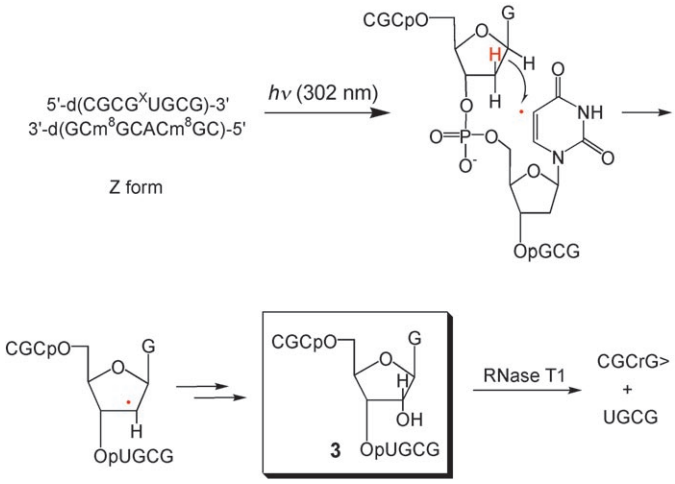
hydrogen abstraction observed. Although a more precise description of hydrogen abstraction would require the dynamic aspects of the nucleic acids to be accounted for, the results provide a qualitative explanation of conformation-dependent hydrogen abstraction by the uracil-5-yl radical in a DNA duplex and DNA–RNA hybrid.

In a model system using monomers, the reaction of the 2′-deoxyuridin-1′-yl radical with molecular oxygen gave the peroxyl intermediate, which ultimately led to the formation of 2′-deoxyribonolactone via the C1′ cation.[35–37] The source of oxygen of the ribonolactone in A-form DNA has not been elucidated, although the peroxyl intermediate is possibly involved in the formation of 2′-deoxyribonolactone.

4. Stereospecific 2′α-Hydroxylation in Z-Form DNA

The Z form of DNA is one of the characteristic local structures of DNA revealed by X-ray crystallography and has been extensively investigated in relation to transcription,[38,39] the methylation of cytosine,[40] and the extent of DNA supercoiling.[41–43] However, the biological relevance of Z-DNA is not well understood, presumably because of its short lifetime under torsional stress caused by unwinding of DNA during transcription. To investigate hydrogen abstraction by the uracilyl radical in Z-DNA, we need to overcome the experimental difficulty in obtaining stable Z-form oligonucleotides under physiological salt conditions. For example, the duplex deoxyoctadecamer, $d(Gm^5C)_4A^{Br}U(Gm^5C)_4$, which has an $A^{Br}U$ sequence in the middle, retains the typical B form even in solution in 4 M NaCl. To obtain stable Z-form DNA, various modified guanine units were synthesized and introduced into duplex oligonucleotides to evaluate their capacity to stabilize Z-form DNA. It was found that incorporation of 8-methyl-2′-deoxyguanosine (m^8G)[44] and 8-methylguanosine (m^8rG)[45] into DNA dramatically stabilized the Z form. The development of the Z-stabilizing monomeric unit, the so-called Z stabilizer, has allowed us to understand the photochemical reaction of ^{I}U in Z-DNA. We found that the iodouracil-containing Z form, 5′-d(CGCG^{I}UGCG)-3′/5′-d(Cm^{8}GCACm^{8}GCG)-3′, undergoes 2′α-hydroxylation of the duplex under UV irradiation (λ = 302 nm), as shown in Scheme 2.[46] Stereospecific 2′β-hydrogen abstraction to give 2′α-hydroxylation, as in **3**, was demonstrated by using a stereospecifically deuterated octanucleotide in Z-form DNA. Importantly, because the 2′α-hydroxylation site in DNA can be easily hydrolyzed by ribonuclease T1, this photochemical and enzymatic hydrolysis is useful for detecting Z-form regions in DNA (Scheme 2).

Rich and co-workers recently reported that several proteins bind specifically to Z-form DNA, including the ubiquitous enzyme double-stranded RNA adenosine deaminase (ADAR1).[47,48] The possible biological roles of Z-DNA have come to attract much current interest. We examined the photochemical reaction of Z-DNA induced by the binding of Zα, that is, the NH_2 terminus of ADAR1 which is responsible for high-affinity binding to Z-DNA.[49] Stereospecific 2′α-hydroxylation occurred efficiently at the 5′ side of ^{I}U in the Z form induced by Zα. The X-ray crystal structure of the Zα–$d(CGCGCG)_2$ complex suggests that the deoxyribose C2′β hydrogen atom of the guanine at the 5′ side is located very close to the uracilyl



Scheme 2. Irradiation of d(CGCG^{X}UGCG)/d(Cm^{8}GCACm^{8}GCG) with UV light in the presence of Zα (2 equiv/DNA), indicating that specific 2′β-hydrogen abstraction gives rise to 2′α-hydroxylation, followed by enzymatic digestion of the hydroxylated product with ribonuclease T_1. X = Br, I.

 © 2006 Wiley-VCH Verlag GmbH & Co. KGaA, Weinheim

radical, whereas C1′- and C2′α-hydrogen atoms are located very far from the C5 position of uracil, as depicted in Figure 4.[49] The calculated structure of the $G^{Br}U$ step, which contains the putative transition state of the C2′β-hydrogen abstraction in Z-DNA, is shown in Figure 4c. These results suggest that Zα packs tightly in Z-DNA, with the C3′-*endo*-sugar puckering the guanine of the duplex, and promotes specific C2′β-hydrogen abstraction by the uracilyl radical to exclude 1′ and 2′ oxidation.

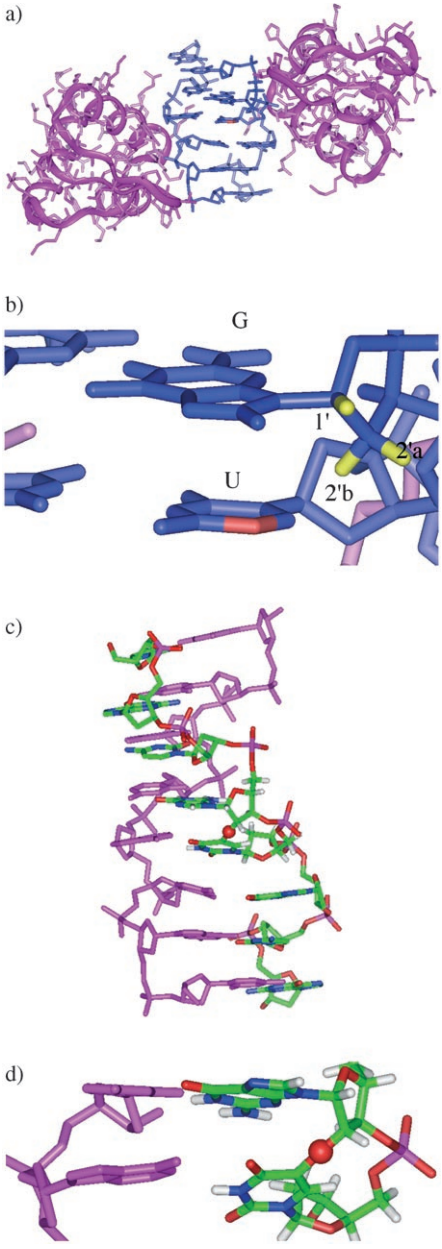
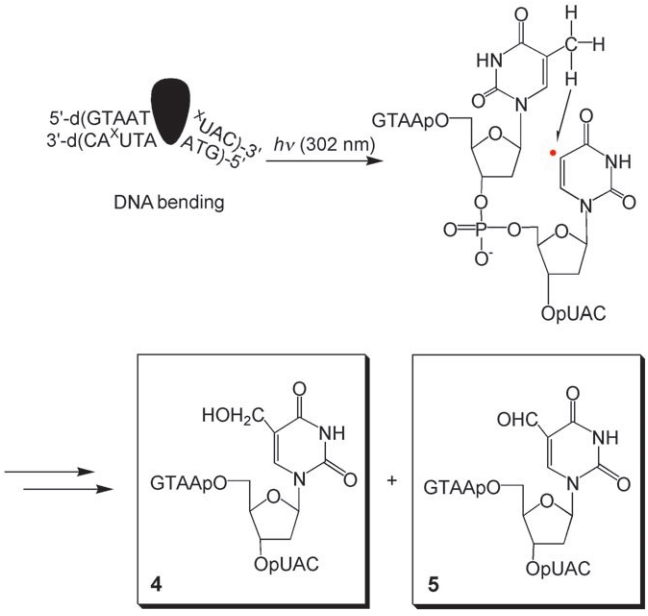


Figure 4. a) Crystal structure of the Zα–d(CGCGCG)$_2$ complex and b) a close-up view of one 5′-GC-3′ region. The carbon atom at the 5-position of uracil is shown in red, and abstracted hydrogen atoms of guanine are shown in yellow. c) Structure of the $G^{Br}U$ step for a minimized Z-DNA structure showing the putative transition state of C2′β-hydrogen abstraction and d) a close-up view of one $G^{Br}U$ step.

5. Intrastrand Hydrogen Abstraction from the 5-Methyl Group of Thymine in Protein-Induced DNA Kinks

Over the past decade, resolution of the crystal structures of many DNA–protein complexes has increased our understanding of DNA–protein interactions. In some instances, the binding of a protein induces significant conformational changes in DNA which are thought to play important biological roles.[17–22] For example, the TATA box-binding protein induces DNA bending, which is essential for the initiation of transcription. To detect the DNA kink induced by the protein, the photoreaction of 5-halouracil-containing DNA in the presence of Sso7d protein was examined. Sso7d is a small chromosomal protein from the hyperthermophilic archaeabacterium *Sulfolobus solfataricus* that displays stability towards heat, acids, and other chemicals. The crystal structure of the complex of Sso7d and d(GTAATTAC)$_2$ was solved at high resolution.[50] The protein binds in the minor groove, causing a sharp bending (60°) at the TpT step; this kink results from the intercalation of the hydrophobic side chains of Val26 and Met29. Consistent with previous observations of B-form DNA, photoirradiation of d(GTAAT^{I}UAC)$_2$ produced 1′ and 2′ oxidation products in the absence of Sso7d. In the presence of Sso7d, the formation of two new products, **4** and **5**, was observed as shown in Scheme 3.[51] These results clearly indicate that the protein-induced DNA kink causes an intrastrand hydrogen abstraction from the 5-methyl group of thymine in the same strand. Inspection of the crystal structure indicates that the 5-methyl group in thymine is in close proximity to the uracilyl radical, whereas the T5-1′- and T5-2′-hydrogen atoms are located far from the adjacent uracilyl radical, as shown in Figure 5. We conclude that the unusual intrastrand hydrogen abstraction from T5-Me by the



Scheme 3. Irradiation of d(GTAAT^{I}UAC)$_2$–Sso7d with UV light. The formation of new products was observed, indicating an intrastrand hydrogen abstraction from the 5-methyl group of thymine.

© 2006 Wiley-VCH Verlag GmbH & Co. KGaA, Weinheim

radical occurred efficiently at the observed bending site in the crystal structure.[51] This specific intrastrand methyl hydrogen abstraction provides a powerful tool to detect directly DNA kinks in solution.

HPLC analysis of the photoirradiated d(GTAAT^{I}UAC)$_2$–Sso7d complex also indicated that the protein Sso7d was efficiently oxidized to Sso7dOH. Upon treatment with lysyl endopeptidase, oxidation of Sso7dOH occurred mainly at the fragment from residues 29 to 40 (78%). Post-source-decay mass spectrometry (PSD-MS/MS) was performed to elucidate the site of the oxidized amino acid residue in fragment 29–40 (Figure 6). Fragment b2 was found in oxidized fragment 29–40 but not in the unmodified fragment, whereas fragment y11 was constant in both cases. These results indicate that specific oxidation occurred at Met29 during irradiation of the d(GTAAT^{I}UAC)$_2$–Sso7d complex. Inspection of the X-ray crystal structure suggests that residue Met29 is in close proximity to the uracilyl radical, which is intercalated with the major groove at the bending site. These results suggest that the interaction of DNA–Sso7d in solution is substantially similar to its crystal structure.

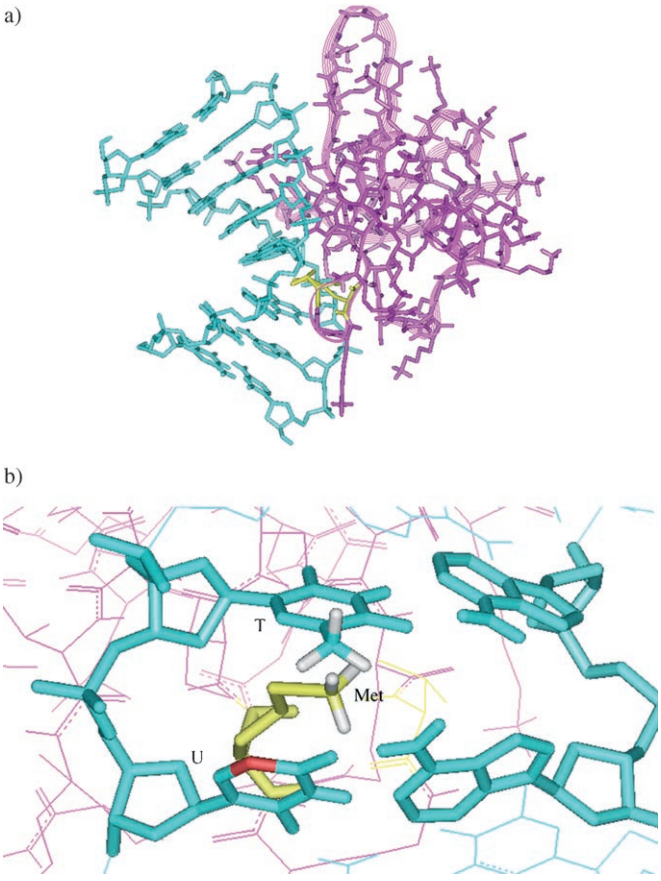


Figure 5. a) Crystal structure of the photoirradiated Sso7d–d(GTAAT^{I}UAC)$_2$ complex and b) a close-up view of the reacting region. In (a) the intercalated Met29 and Val26 moieties are shown in yellow; in (b) residues U6 and T5 of d(GTAATUAC)$_2$ are colored blue, the carbon atom at the 5-position of U6 is red, and the putative abstracted hydrogen atoms of thymine are white.

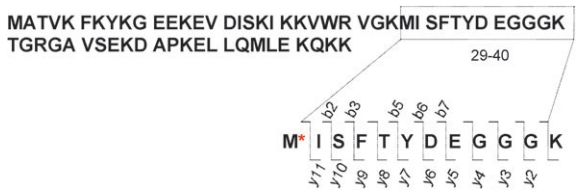


Figure 6. Sequence of the fragment 29–40 of Sso7d. The oxidized fragment 29–40 produced fragment b2, whereas fragment y11 remained constant in both the oxidized and unmodified fragments 29–40.

6. Highly Efficient Photochemical Formation of 2′-Deoxyribonolactone in the Antiparallel G Quartet

DNA tetraplexes, otherwise known as DNA quadruplexes or G quartets, are four-stranded DNA structures formed by guanine-rich sequences.[52–54] Although G quartets have so far been studied in vitro only, they are attracting increasing attention because of their postulated involvement in a variety of biological processes. The DNA of human telomeres consists of repeat units of the nucleotide sequence TTAGGG, ending in a single-stranded segment that overhangs at the end of the double-stranded DNA helix. The single-stranded repeat units can form four-stranded G-quartet structures.[55–57] NMR spectroscopic analysis demonstrated that a 22-mer of 5′-d[AGGG(TTAGGG)$_3$]-3′ in the solution state in the presence of Na^+ ions adopts an antiparallel G-quartet structure in which the opposing GGG columns are antiparallel, with one diagonal and two lateral TTA loops (Figure 7).[58] In contrast, the same 22-mer adopts a completely different G-quartet architecture in a crystal grown in the presence of K^+ ions, in which four core GGG units are parallel, with the three linking external loops positioned on the exterior of the G-quartet core.[59]

To explore the structure-dependent abstraction of hydrogen atoms in antiparallel and parallel G quartets, one of the six thymine residues in 22-mer human telomeric DNA 5′-d(AGGGT^{1}T^{2}AGGGT^{3}T^{4}AGGGT^{5}T^{6}AGGG)-3′ was substituted with ^{I}U to generate six types of oligodeoxynucleotide (ODNs 1–6).[60] Upon irradiation with UV light, more than 60% of antiparallel ODN 4, in which T^4 in the middle of the

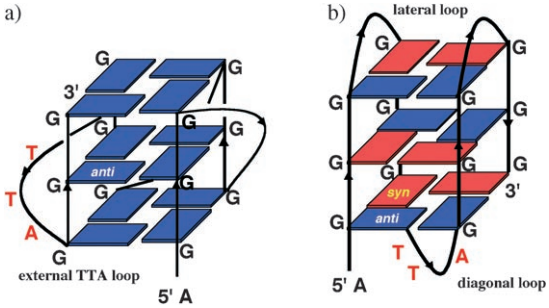


Figure 7. Schematic representations of the folded structures of d[AG$_3$(T$_2$AG$_3$)$_3$]: a) the K^+-stabilized crystal structure, with TTA external loops abutting the sides of the G quartet and parallel GGG columns; b) the Na^+-stabilized solution-state structure, with one diagonal and two lateral TTA units.

© 2006 Wiley-VCH Verlag GmbH & Co. KGaA, Weinheim

diagonal loop was substituted with ^{I}U, was consumed. In marked contrast to the photoreactivity of the antiparallel ODN 4, the parallel ODNs 1–6 were not consumed (< 2%) under the same irradiation conditions. Analysis of the products indicated that 2′-deoxyribonolactone was efficiently produced with release of thymine from photoirradiated ODN 4 in the antiparallel structure (Figure 8).

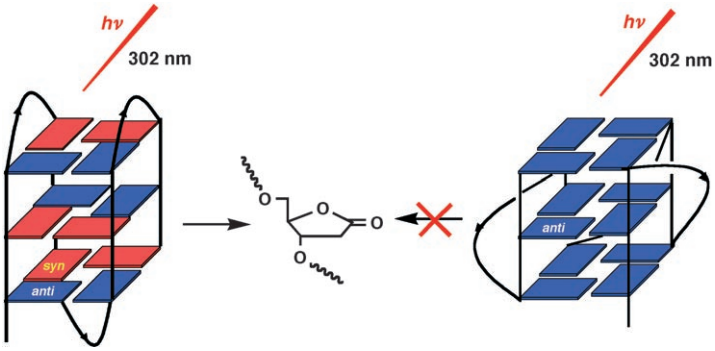


Figure 8. ^{I}U in the diagonal loop of an antiparallel G quartet undergoes an extremely facile photochemical reaction to produce a 2′-deoxyribonolactone residue. A similar reaction does *not* occur in parallel G quartets.

The high photochemical reactivity of ODN 4 in the antiparallel G quartet and its poor photoreactivity in the parallel G quartet can be explained by comparing the loop regions of the two structures (Figure 9).[58,59] In the parallel G quartet, the adenine in the TTA external loop intercalates between the two thymines to prevent hydrogen abstraction. In contrast, there is no such intercalation of the adenine base in the diagonal loop structure of the antiparallel G quartet, thereby allowing 1′-hydrogen abstraction by the uracilyl radical in the loop. Furthermore, the structure determined by NMR experiments suggests that the uracilyl radical is positioned closer to the 1′-hydrogen atom of the adjacent T_3 than the other hydrogen atoms in the diagonal loop.

Several other guanine-rich sequences have also been proposed to function biologically through the formation of a G quartet. For instance, G quartets have been associated with site-specific genetic recombination in immunoglobulin switch regions (IgG), the insulin gene linked polymorphic region, the retinoblastoma susceptibility gene (Rb), and the *c*-myc oncogene.[61–64] Numerous potential G-quartet-forming sequences have been identified in many important genes.[65] The sequence motif required for intrastrand G quartets can be written as $G_nN_{m1}G_nN_{m2}G_nN_{m3}G_n$, where n is the number of guanine tetrads; $m1$, $m2$, and $m3$ are the loop lengths; and the diagonal loop (N_{m2}) of antiparallel structures is common in the sequence motif (Figure 10a). To test the efficacy of the photochemical method, we examined the photoreactions of the ^{I}U-substituted IgG switch regions and the 5′ termini of the Rb gene.[60] Photoirradiation was performed at $\lambda = 302$ nm for 5′-d(AGGGGAGCTGGGG^{I}UAGGTGGGA)-3′ (IgG) and 5′-d(CGGGGGGTT^{I}UTGGGCGGC)-3′ (Rb). HPLC analysis of the photolysates indicated that the photoproducts (≈90% yield) were 2′-deoxyribonolactone-containing oligomers, which were obtained as the major products with

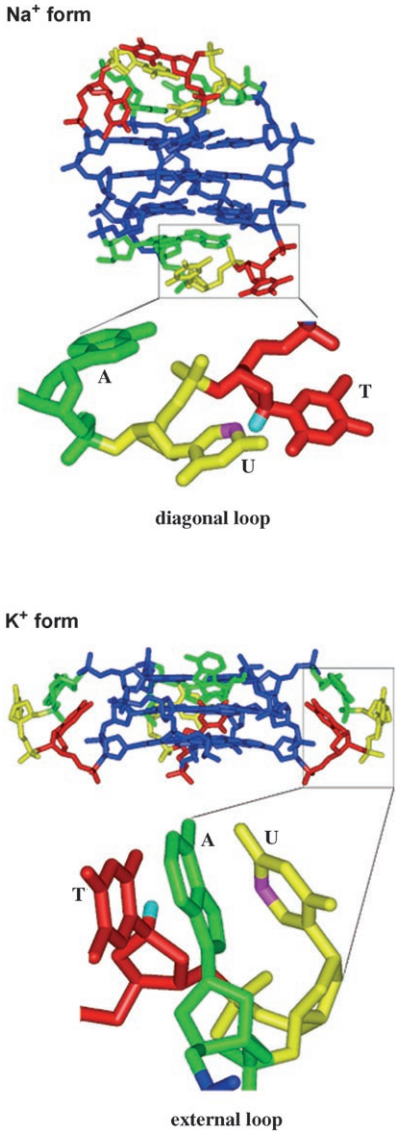


Figure 9. Structure of photoirradiated oligonucleotide d(AGGGTTAGGGT^{I}UAGGGTTAGGG) (ODN 4) based on NMR experiments (Na^+ form) and X-ray crystallography (K^+ form) and close-up views of the loop regions. Guanine moieties are colored blue; carbon atom C5 of uracil is pink; abstracted hydrogen atoms of thymine are cyan; thymine red, uracil yellow, and adenine green.

release of free guanine or thymine. This highly efficient production of 2′-deoxyribonolactone strongly suggests the formation of an antiparallel G quartet with a diagonal loop for these guanine-rich sequences. Figure 10b and c show the proposed G-quartet structure based on our photochemical studies, showing two stacked guanine tetrads and a diagonal four-base loop for both IgG and Rb.

7. Summary and Outlook

Our results indicate that the hydrogen abstraction of DNA by the uracil-5-yl radical generated from 5-halouracil under irradiation is atom-specific and highly dependent on

© 2006 Wiley-VCH Verlag GmbH & Co. KGaA, Weinheim

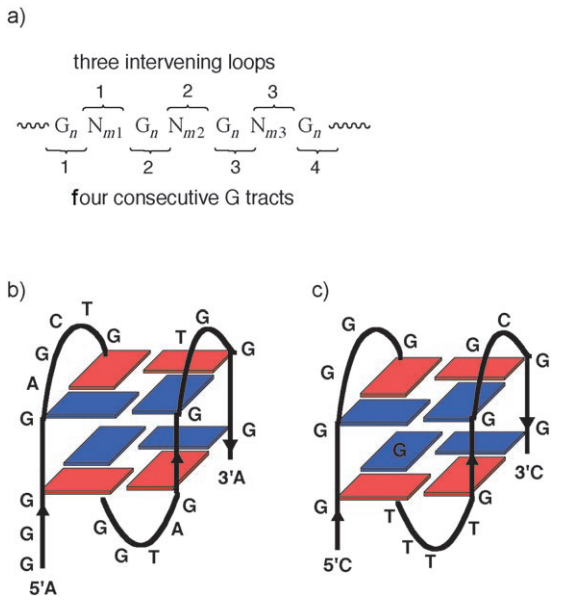
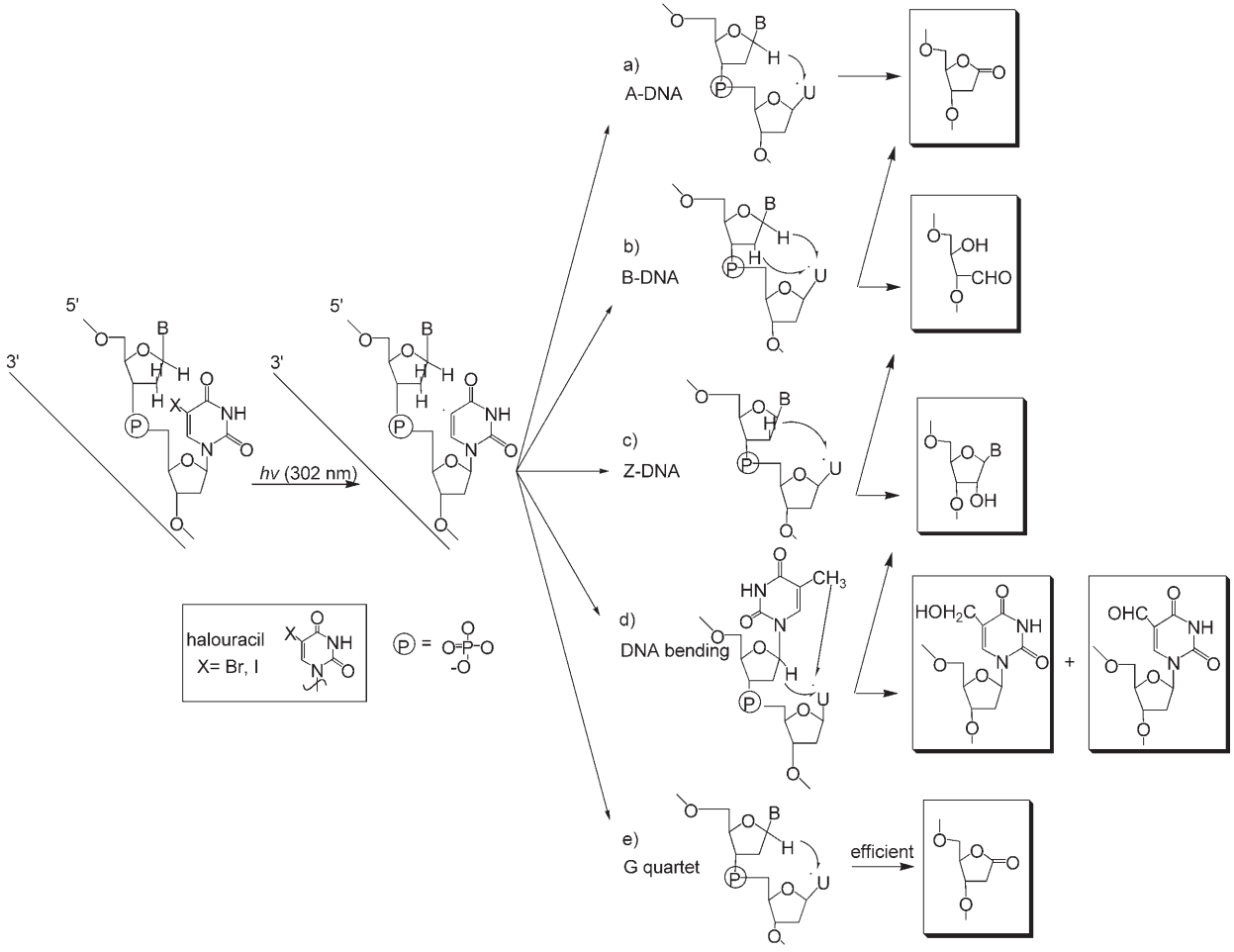


Figure 10. The generic G-quartet-forming sequence, G_n, from four guanine-rich tracts undergoes hydrogen bonding to form tetrads, which then stack to form the G-quartet stem. a) 1, 2, and 3 form the three loops. b,c) Schematic representation showing the K^+-induced G-quartet forms of IgG (b) and Rb (c).

the conformation of the DNA (Scheme 4). Competitive 1′- and 2′α-hydrogen abstractions were observed in B-DNA, whereas selective 1′-hydrogen abstraction occurred in the A-like structure of DNA–RNA hybrids. In Z-form DNA, stereospecific 2′β-hydrogen abstraction gave rise to 2′α-hydroxylation. In protein-induced DNA kinks, photoirradiation caused intrastrand hydrogen abstraction from the 5-methyl group of thymine at the 5′ side. The photoreactivity of iodouracil-containing telomeric DNA depends on the orientation of the G quartet: the 2′-deoxyribonolactone residue is effectively produced only in the diagonal loop of the antiparallel G quartet. These studies have demonstrated the detailed relationship between the DNA local structure and the photochemical product, and show the potential of this photochemical method in detecting DNA structure. Irradiation with UV light leads to the formation of two major types of photoadducts: cyclobutane dimers and the (6–4) photoproduct in DNA.[66] Ligation-mediated polymerase chain reaction (LMPCR) is a useful technique to detect these products in vivo.[67] As 5-halouracil-substituted DNA is functional in living cell systems such as *E. coli*, use of the photochemical reactions of 5-halouracil-containing DNA



Scheme 4. Photochemical products formed by hydrogen abstraction in the five different structures of 5-halouracil-containing DNA upon irradiation with UV light.

 © 2006 Wiley-VCH Verlag GmbH & Co. KGaA, Weinheim

would provide a powerful tool to probe local DNA conformations in vivo.

Received: June 7, 2005
Published online: January 16, 2006

[1] N. R. Cozzarelli, J. C. Wang, *DNA Topology and Its Biological Effects*, Cold Spring Harbor Laboratory Press, New York, **1990**.
[2] "DNA Conformation and Protein Binding": A. Travers, *Annu. Rev. Biochem.* **1989**, *58*, 427 – 452.
[3] A. H.-J. Wang, G. J. Quigley, F. J. Kolpak, J. L. Crawford, J. H. van Boom, G. A. van der Marel, A. Rich, *Nature* **1979**, *282*, 680 – 686.
[4] R. R. Sinden, *DNA Structure and Function*, Academic Press, New York, **1994**.
[5] S. Neidle, *DNA Structure and Recognition*, IRL, Oxford, **1994**.
[6] A. Rich, S. Zhang, *Nat. Rev. Genet.* **2003**, *4*, 566 – 572.
[7] J. A. Hackett, D. M. Feldser, C. W. Greider, *Cell* **2001**, *106*, 275 – 286.
[8] M. Lei, E. R. Podell, P. Baumann, T. R. Cech, *Nature* **2003**, *426*, 198 – 203.
[9] H. Han, D. R. Langley, A. Rangan, L. H. Hurley, *J. Am. Chem. Soc.* **2001**, *123*, 8902 – 8913.
[10] W. Tuntiwechapikul, T. L. Jeong, M. Salazar, *J. Am. Chem. Soc.* **2001**, *123*, 5606 – 5607.
[11] J. L. Mergny, L. Lacroix, M. P. Teulade-Fichou, C. Hounsou, L. Guittat, M. Hoarau, P. B. Arimondo, J. P. Vigneron, J.-M. Lehn, J. F. Riou, T. Garestier, C. Helene, *Proc. Natl. Acad. Sci. USA* **2001**, *98*, 3062 – 3067.
[12] J.-L. Mergny, J.-F. Riou, P. Mailliet, M. P. Teulade-Fichou, E. Gilson, *Nucleic Acids Res.* **2002**, *30*, 839 – 865.
[13] H. Arthanari, P. H. Bolton, *Chem. Biol.* **2001**, *8*, 222 – 230.
[14] J. W. Shay, Y. Zou, E. Hiyama, W. E. Wright, *Hum. Mol. Genet.* **2001**, *10*, 677 – 685.
[15] R. Liu, H. Liu, X. Chen, M. Kirby, P. O. Brown, K. Zhao, *Cell* **2001**, *106*, 309 – 318.
[16] E. H. Blackburn, *Nature* **1991**, *350*, 569 – 573.
[17] J. L. Kim, D. B. Nikolov, S. K. Burley, *Nature* **1993**, *365*, 520 – 527.
[18] D. B. Nikolov, H. Chen, E. D. Halay, A. Hoffmann, R. G. Roeder, S. K. Burley, *Proc. Natl. Acad. Sci. USA* **1996**, *93*, 4862 – 4867.
[19] Y. Kim, J. H. Geiger, S. Hahn, P. B. Sigler, *Nature* **1993**, *365*, 512 – 520.
[20] M. H. Werner, G. M. Clore, C. L. Fisher, R. J. Fisher, L. Trinh, J. Shiloach, A. M. Gronenborn, *Cell* **1995**, *83*, 761 – 771.
[21] M. A. Schumacher, K. Y. Choi, H. Zalkin, R. G. Brennan, *Science* **1994**, *266*, 763 – 770.
[22] M. H. Werner, J. R. Huth, A. M. Gronenborn, G. M. Clore, *Cell* **1995**, *81*, 705 – 714.
[23] S. B. Zimmerman, B. H. Pheiffer, *J. Mol. Biol.* **1979**, *135*, 1023 – 1027.
[24] D. G. Reid, S. A. Salisbury, S. Bellard, Z. Schakked, D. H. Williams, *Biochemistry* **1983**, *22*, 2019 – 2025.
[25] G. M. Clore, A. M. Gronenborn, *FEBS Lett.* **1985**, *179*, 187 – 198.
[26] M. C. Willis, B. J. Hicke, O. C. Uhlenbeck, T. R. Cech, T. H. Koch, *Science* **1993**, *262*, 1255 – 1257.
[27] H. Sugiyama, Y. Tsutsumi, I. Saito, *J. Am. Chem. Soc.* **1990**, *112*, 6720 – 6721.
[28] H. Sugiyama, Y. Tsutsumi, K. Fujimoto, I. Saito, *J. Am. Chem. Soc.* **1993**, *115*, 4443 – 4447.
[29] H. Sugiyama, K. Fujimoto, I. Saito, E. Kawashima, T. Sekine, Y. Ishido, *Tetrahedron Lett.* **1996**, *37*, 1805 – 1808.
[30] T. Chen, G. P. Cook, A. T. Koppisch, M. M. Greenberg, *J. Am. Chem. Soc.* **2000**, *122*, 3861 – 3866.
[31] T. Ito, S. E. Rokita, *J. Am. Chem. Soc.* **2004**, *126*, 11480 – 11481.
[32] T. Watanabe, T. Bando, Y. Xu, R. Tashiro, H. Sugiyama, *J. Am. Chem. Soc.* **2005**, *127*, 44 – 45.
[33] C. Behrens, T. Carell, *Chem. Commun.* **2003**, 1632 – 1633.
[34] H. Sugiyama, K. Fujimoto, I. Saito, *Tetrahedron Lett.* **1997**, *38*, 8057 – 8060.
[35] C. J. Manuel, M. Newcomb, C. Ferreri, C. Chatgilialoglu, *J. Am. Chem. Soc.* **1999**, *121*, 2927 – 2928.
[36] C. Chatgilialoglu, T. Gimisis, *Chem. Commun.* **1998**, 1249 – 1250.
[37] T. Christopher, B. K. Goodman, M. M. Greenberg, *Chem. Biol.* **1998**, *5*, 263.
[38] S. Wolfl, C. Martines, A. Rich, J. A. Majzoub, *Proc. Natl. Acad. Sci. USA* **1996**, *93*, 3664 – 3668.
[39] A. Herbert, A. Rich, *J. Biol. Chem.* **1996**, *271*, 11595 – 11598.
[40] W. Zacharias, T. R. O'Connor, J. E. Larson, *Biochemistry* **1988**, *27*, 2970 – 2978.
[41] S. D. Sheridan, C. J. Benham, G. W. Hatfield, *J. Biol. Chem.* **1999**, *274*, 8169 – 8174.
[42] G. P. Schroth, P.-J. Chou, P. S. Ho, *J. Biol. Chem.* **1992**, *267*, 11846 – 11855.
[43] A. J. Jaworski, N. P. Higgins, R. D. Wells, W. J. Zacharias, *Biol. Chem.* **1991**, *266*, 2576 – 2581.
[44] H. Sugiyama, K. Kawai, A. Matsunaga, K. Fujimoto, I. Saito, H. Robinson, A. H.-J. Wang, *Nucleic Acids Res.* **1996**, *24*, 1272 – 1278.
[45] Y. Xu, R. Ikeda, H. Sugiyama, *J. Am. Chem. Soc.* **2003**, *125*, 13519 – 13524.
[46] K. Kawai, I. Saito, H. Sugiyama, *J. Am. Chem. Soc.* **1999**, *121*, 1391 – 1932.
[47] T. Schwartz, M. A. Rould, K. Lowenhaupt, A. Herbert, A. Rich, *Science* **1999**, *284*, 1841 – 1845.
[48] T. Schwartz, J. Behlke, K. Lowenhaupt, U. Heinemann, A. Rich, *Nat. Struct. Biol.* **2001**, *8*, 761 – 765.
[49] T. Oyoshi, K. Kawai, H. Sugiyama, *J. Am. Chem. Soc.* **2003**, *125*, 1526 – 1531.
[50] Y.-G. Gao, S.-Y. Su, H. Robinson, S. Padmanabhan, L. Lim, B. S. McCrary, S. P. Edmondson, J. W. Shriver, A. H.-J. Wang, *Nat. Struct. Biol.* **1998**, *5*, 782 – 786.
[51] T. Oyoshi, A. H.-J. Wang, H. Sugiyama, *J. Am. Chem. Soc.* **2002**, *124*, 2086 – 2087.
[52] W. I. Sundguist, A. Klug, *Nature* **1989**, *342*, 825 – 829.
[53] D. Sen, W. Gilbert, *Nature* **1990**, *344*, 410 – 414.
[54] F. W. Smith, J. Feigon, *Nature* **1992**, *356*, 164 – 168.
[55] Y. Wang, D. J. Patel, *Biochemistry* **1992**, *31*, 8112 – 8119.
[56] M. P. Horvath, S. C. Schultz, *J. Mol. Biol.* **2001**, *310*, 367 – 377.
[57] C. Schaffitzel, I. Berger, J. Postberg, J. Hanes, H. J. Lipps, A. Plückthun, *Proc. Natl. Acad. Sci. USA* **2001**, *98*, 8572 – 8577.
[58] Y. Wang, D. J. Patel, *Structure* **1993**, *1*, 263 – 282.
[59] G. N. Parkinson, M. P. Lee, S. Neidle, *Nature* **2002**, *417*, 876 – 880.
[60] Y. Xu, H. Sugiyama, *J. Am. Chem. Soc.* **2004**, *126*, 6274 – 6279.
[61] P. Catasti, X. M. Chen, R. K. Moyzis, E. M. Bradbury, G. Gupta, *J. Mol. Biol.* **1996**, *264*, 534 – 545.
[62] A. I. Murchie, D. M. Lilly, *Nucleic Acids Res.* **1992**, *20*, 49 – 53.
[63] T. Simonsson, P. Pecinka, M. Kubista, *Nucleic Acids Res.* **1998**, *26*, 1167 – 1172.
[64] A. Siddiqui-Jain, C. L. Grand, D. J. Bearss, L. H. Hurley, *Proc. Natl. Acad. Sci. USA* **2002**, *99*, 11593 – 11598.
[65] M. N. Weitzmann, K. J. Woodford, K. Usdin, *J. Biol. Chem.* **1996**, *271*, 20958 – 20964.
[66] T. Matsunaga, K. Hieda, O. Nikaido, *Photochem. Photobiol.* **1991**, *54*, 403 – 410.
[67] F. Thoma, *EMBO J.* **1999**, *18*, 6585 – 6598.

 © 2006 Wiley-VCH Verlag GmbH & Co. KGaA, Weinheim

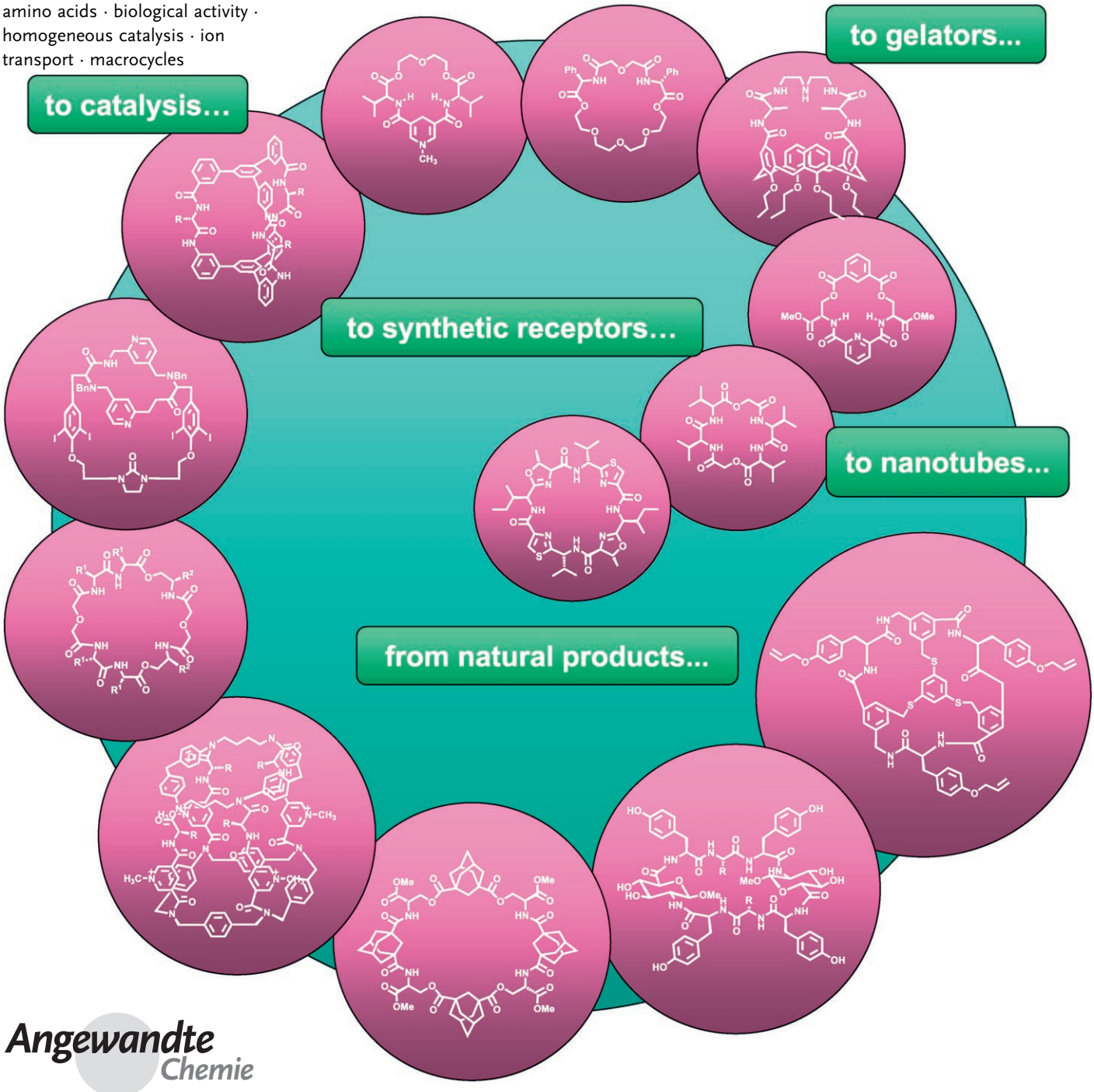
DOI: 10.1002/anie.200503428

Macrocycles

Amino Acid Derived Macrocycles—An Area Driven by Synthesis or Application?

Susan E. Gibson and Cristina Lecci*

Keywords:
amino acids · biological activity · homogeneous catalysis · ion transport · macrocycles



© 2006 Wiley-VCH Verlag GmbH & Co. KGaA, Weinheim

The synthesis, structure, and physical properties of macrocycles have fascinated chemists for many years. Their inherent properties make them useful in areas as diverse as ion transport across membranes, development of new antibiotics, and catalysis. In this Review, the authors examine the chemistry of macrocycles containing non-peptidic amino acid derived molecules; the analysis is discussed in terms of function, rather than structure or synthesis. It is revealed that the diverse and imaginative structures created by synthetic chemists are not being fully exploited in application-driven endeavors.

From the Contents

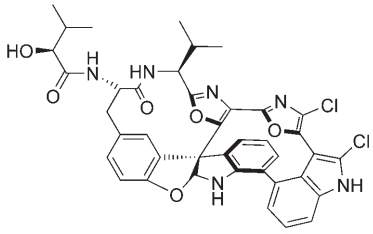
1. Introduction 1365
2. Transport across Membranes 1366
3. Amino Acid Derived Macrocycles in Catalysis 1369
4. Gelators 1371
5. Organic Nanotubes 1371
6. Recognition of Biologically Important Molecules 1372
7. Summary and Outlook 1374

1. Introduction

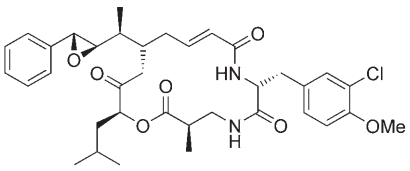
Macrocycles form a major class of molecules that encompasses a wide range of structures and functional groups.[1] They also perform a wide range of functions in areas as diverse as, for example, ion transport, gelation, and catalysis. Chemists have been fascinated for many years by the inherent physical properties of macrocycles and by the synthetic challenge that these structures represent.[2] Contemporary chemistry, however, is increasingly directed towards the creation of molecules that are tailored to perform a well-defined function. We thus thought it would be interesting to carry out an analysis of macrocyclic chemistry that would determine how much progress has been made towards using currently available synthetic expertise to create macrocycles that perform a well-defined function. Given the volume of research conducted on macrocycles, however, we decided to focus on one area that would act as a representative of the whole subject. We thus chose to confine our search and analysis to non-peptidic macrocycles derived from amino acids, as we hypothesized that these may act as a bridge between many of nature's macrocycles and man's attempts to mimic and improve on the function of these molecules.

Before discussing how synthetic non-peptidic macrocycles derived from amino acids are being used in a range of applications (Sections 2–6), it is instructive to look at the functions performed by naturally occurring macrocycles of this type.

Diazonamide A[3] (**1**), isolated from the marine ascidian *Diazona angulata*, is a potent inhibitor of tubulin assembly in human carcinoma cells; even though its overall mode of action is unclear, several hypotheses about the nature of its interaction with tubulin have been formulated.[4] For example, it has been proposed that diazonamide A binds to tubulin at a site remote from that where the *Vinca* alkaloids bind; it has also been proposed that it binds weakly to unpolymerized tubulin but strongly to microtubule ends.[4] Cryptophycin-1 (**2**), the major cryptophycin extracted from cyanobacterium *Nostoc* sp. GSV224, is also a potent inhibitor of tubulin polymerization and is believed to have therapeutic advantages over paclitaxel (taxol).[5] Examination of the effects of incubating cryptophycin-1 with tubulin in vitro led to the hypothesis that **2** does not form a covalent bond to the protein, despite the presence of a very reactive epoxide ring.[5c]



diazonamide A (**1**)

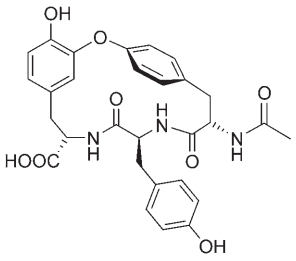


cryptophycin-1 (**2**)

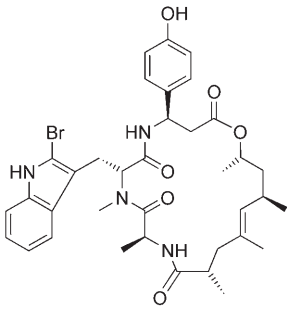
Some naturally occurring amino acid containing macrocycles derive their biological activity from the proposed or proven formation of complexes with metal cations. The biaryl ether K-13 (**3**), isolated from the culture broth of *Micromonospora halophytica* subsp. *exilisia* K-13, is an inhibitor of the angiotensin I-converting enzyme, a member of the family of zinc metalloproteinases.[6] Its mechanism of inhibition is believed to rely on its coordination to the Zn^{II} ion in the active site of angiotensin I. The Li^{I} complex of jaspamide (**4**; jasplakinolide), isolated from the marine sponge *Jaspis johnstoni*, has been the subject of extensive recent investigations as a model for cation–π interactions, which are acknowledged to be important in protein–DNA complexes[7] and

[*] Prof. S. E. Gibson, C. Lecci
Department of Chemistry
Imperial College London
South Kensington Campus, London SW7 2AY (UK)
Fax: (+44) 207-594-5804
E-mail: s.gibson@imperial.ac.uk

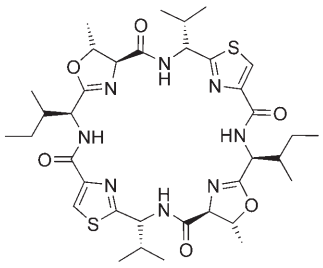
© 2006 Wiley-VCH Verlag GmbH & Co. KGaA, Weinheim



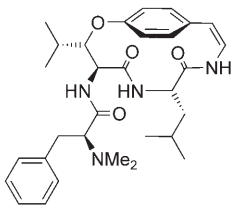
K-13 (**3**)



jaspamide (jasplakinolide, **4**)



ascidiacyclamide (**5**)



frangufoline (sanjoinine A, **6**)

which may explain the anticancer activity of jaspamide and how it stabilizes actin polymerization. Ascidiacyclamide (**5**), isolated from ascidian *Lissoclinum patella* found on the Great Barrier Reef,[8] features a hydrophobic pocket capable of accommodating two copper ions, a metal whose concentration is 10^5-fold higher in the ascidian organisms than in the surrounding sea water and which is able to capture CO_2 and CO_3^{2-}. This macrocycle, characterized by the presence of oxazoline/thiazole heterocycles alternating with amino acid residues, may therefore be involved in the uptake and transport of CO_2/CO_3^{2-} in ascidians, which are known to concentrate CO_3^{2-} in their spicules.[9] Frangufoline (**6**; sanjoinine A) is an alkaloid isolated from *Rhamnus frangula* leaves and from the seeds of *Zizyphus vulgaris*.[10] It is reported to exhibit ionophore activity[11] and to be an effective inhibitor of calmodulin-induced activation of Ca^{II} ATPase.[12]

2. Transport across Membranes

2.1. Introduction

Increasing attention has been devoted in recent years to the development of synthetic systems that mimic the ionophore activity of membrane proteins. Valinomycin, a cyclopeptide obtained from *Streptomyces* fermentation, is a much studied natural ion carrier that derives its antibiotic properties from its specific binding to potassium ions. Normal cells contain a high concentration of potassium ions and a low concentration of sodium ions, and thus the specific binding and transport of potassium from the inside to the outside of the cell operated by valinomycin causes the death of the cell. Unfortunately valinomycin, along with other naturally occurring ionophore peptides, shows no selective toxicity for bacterial cells over mammalian cells and is therefore useless as a therapeutic agent.[13] Synthetic low-molecular-weight compounds that could be tailored to exhibit well-defined ion-transport properties across model membranes would therefore represent a useful alternative to natural ion channels.

Two main methods have emerged over the years for modeling in vitro the conditions for transport of small molecules across natural biological membranes. The simplest, introduced by Cram and co-workers in the late 1970s but still considered a benchmark in this area, uses a chloroform/water interface as a model for a liquid membrane.[14] The transport experiments are usually conducted in a U-tube to assess, for example, the differential transport of a racemic mixture of enantiomeric salts by a single enantiomer of the host, or in a W-tube when both enantiomers of the host are employed in the differential, simultaneous transport of both enantiomers of the guest.[14b] In the U-tube experiment, a solution of the host in chloroform is stirred at the bottom of the tube; a solution of the guest and $LiPF_6$ (picrate salts of lithium, potassium, ammonium, rubidium, and cesium have also been used)[14a] in water floats on the $CHCl_3$ pool in one of the arms, and water floats on the $CHCl_3$ in the remaining arm. The rates of transport of the hexafluorophosphate salt of each guest from one arm of the tube to the other are measured by monitoring the increase in absorbance (with time) in the UV spectrum of the solution in the receiving arm. When a racemic mixture of enantiomers is used as the guest, the enantiomeric



Sue E. Gibson did her first degree in Cambridge and her DPhil in Oxford with S. G. Davies. She was awarded a Royal Society European Fellowship to study at the ETH, Zürich, with A. Eschenmoser. She returned to the UK to a lectureship in organic chemistry at the Univ. of Warwick (1985) and was appointed to a lectureship at Imperial College, London (1990). She took up the Daniell Chair of Chemistry at King's College London (1999), returning to Imperial College London and a Chair of Chemistry (2003). Her research interests lie in the the application of transition metals in organic synthesis.

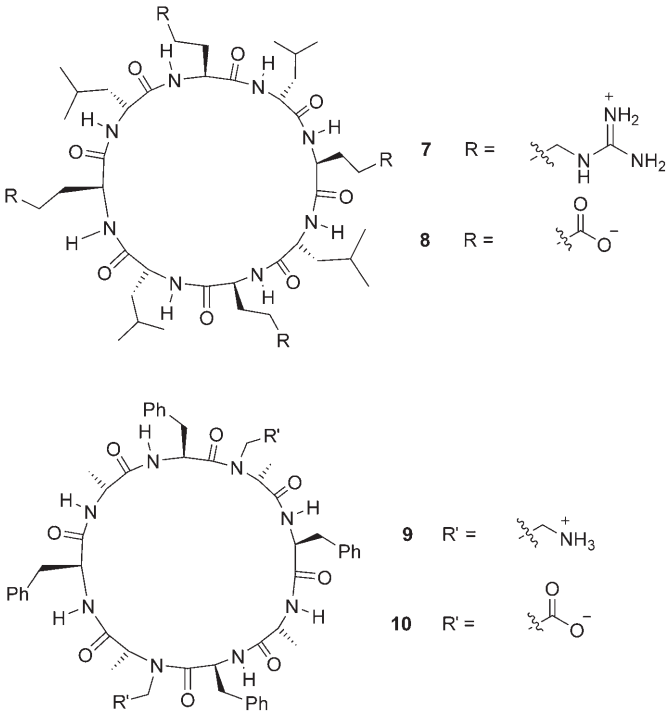


Cristina Lecci graduated from the University of Pisa (Italy) in April 2002 under the supervision of Anna Iuliano. Her research project involved the synthesis and evaluation of new biselector chiral stationary phases for the separation of racemic mixtures of biologically important substrates by HPLC. During her PhD studies (2002–2005) with Sue Gibson she worked on the synthesis and applications of tricarbonylchromium(0) complexes of small and medium-sized paracyclophanes. She also carried out work on amino acid derived chiral macrocycles.

© 2006 Wiley-VCH Verlag GmbH & Co. KGaA, Weinheim

excess of the guest transported to the receiving arm may be determined polarimetrically.[14b]

A more advanced model, which more closely resembles naturally occurring lipid bilayers is based on a study published in the mid-1970s.[15] In this report the changes in the spectral properties (e.g. fluorescence) of several cyanine dyes upon association with red blood cells and the natural ionophore valinomycin were examined, and various hypotheses were put forward to explain how the dye "senses" the change in the membrane potential induced by valinomycin. Given the poor reproducibility of some spectroscopic experiments performed on blood cells, the authors turned their attention to a model synthetic membrane, which was obtained by sonicating a mixture of phosphatidylcholine, cholesterol, and KCl–Tris (Tris = tris(hydroxymethyl)aminomethane) to obtain a vesicle suspension. A cyanine dye was added to this suspension and the fluorescence emission of the resulting system was recorded. Upon addition of valinomycin, the fluorescence of the dye decreased sharply. The authors postulated that this was the result of membrane polarization induced by valinomycin-mediated transport of potassium ions out of the vesicles; this leads to an increased concentration of the dye on the inner membrane surface with subsequent formation of dye multimers, which are known to quench fluorescence. A variant of this type of model membrane was developed to perform studies on planar lipid bilayers,[16] but the procedure already described,[15] along with the use of valinomycin and a fluorescent dye as a standard reference, has remained basically unchanged to date.



2.2. Transport of Small Molecules across a Lipid Membrane

Although this Review is focused on non-peptidic amino acid derived macrocycles, this section begins with a report on the modification of ion-transport channels by synthetic cyclopeptides in order to place the subsequent work with non-peptidic molecules in perspective. Synthetic cyclopeptides **7**–**10**[17] were used to modify the pore of staphylococcal α-hemolysin (αHL), a 239-residue exotoxin that forms a mushroom-shaped heptameric pore (100-Å-long channel) in lipid bilayers.[18]

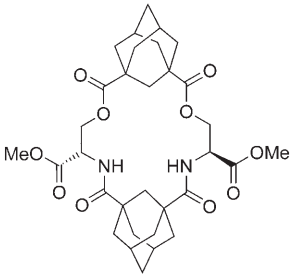
Cyclopeptides **7**–**10** do not form channels by themselves but rather are designed to alter the conductance and ion selectivity of the αHL pore. In fact while lodged in the channel lumen (the authors propose that the peptides are held at a single binding site within the protein), the two positively charged peptides **7** and **9** increase the natural anion selectivity of αHL,[19] while the negatively charged peptide **8** converts αHL into a weakly cation-selective pore. Peptide **10** gave different results depending on the intensity of the reversal potential applied. This study also demonstrated that the positively charged peptides **7** and **9** bind to various polyanions that block the channel[20] and reduce the channel current (small polyanions such as 1,2,3,4,5,6-benzenehexacarboxylate (mellitic acid), L-*myo*-inositol 1,4,5-triphosphate hexapotassium salt, and D-*myo*-inositol 1,4,5-triphosphate hexasodium salt were used as blockers). This result reinforces the idea that the use of noncovalent adapters is a versatile way of programming the properties of αHL and perhaps other channel pores.

The ion-transporting properties of non-peptidic serine-based macrocycles incorporating an adamantane moiety have been the focus of extensive research over the last decade.[21] Using the fluorescent dye method described previously, and valinomycin as a standard reference,[15] it was found that although macrocycle **11** did not transport any ions,[22] the larger macrocycles **12**–**16** were all effective in translocating Na^{I}, Mg^{II}, and Ca^{II} ions across model membranes (small unilamellar vesiscles).[21c] Macrocycle **14**, featuring two exocyclic (*S*)-leucine residues, showed maximum efficiency and was demonstrated to be almost as efficient as valinomycin in quenching the fluorescence of the dye. Interestingly, studies conducted on similar macrocycles featuring only one adamantane unit were found to be completely devoid of any ion-transport capability, in spite of containing strong metal-complexing moieties in their cyclic framework.

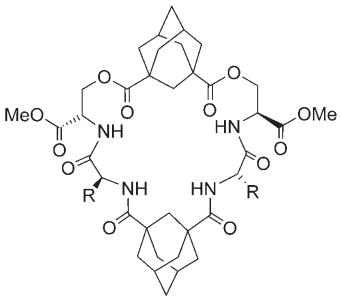
In a more recent development from the same group,[21d] serine-based 20-membered macrocycles **17a**–**c** and cysteine-based 15-membered macrocycles **18a**–**c** were synthesized and it was shown that **17c** and **18c** are capable of transporting Na^{I} across a lipid bilayer. None of the prepared macrocycles in this case transport Ca^{II} and Mg^{II} ions, which highlights how a judicious choice of complexing moieties on the ring can effectively tune the performance of synthetic systems.

Calixarene-like macrocycles **19**–**25** form ion channels in bilayer membranes by the creation of tail-to-tail dimers and the alignment of their hydrophobic alkyl chains (R^2).[23] How the nature of an amino acid residue (R^1), the length of the alkyl chain (R^2), and the size of the macrocycle (*n*) affected the activity of the ion channel was assessed. The synthetic macrocycles **19**–**25** show similar conductance, charge selec-

© 2006 Wiley-VCH Verlag GmbH & Co. KGaA, Weinheim

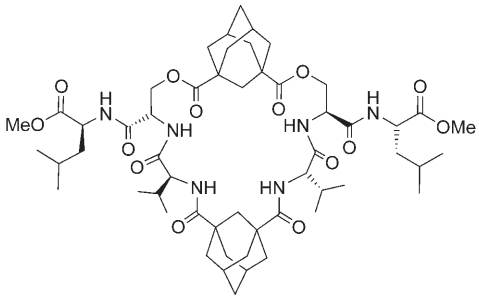


11

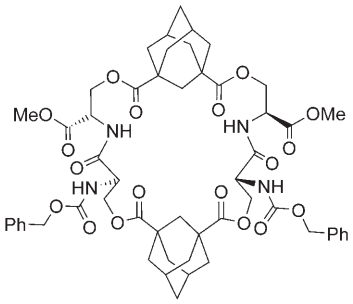


12 R =

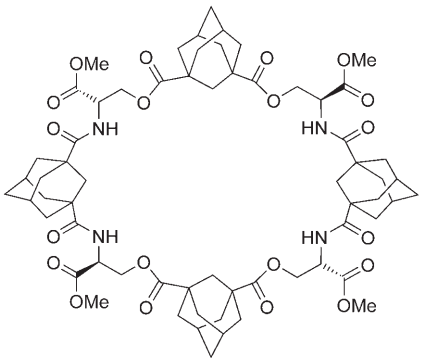
13 R =



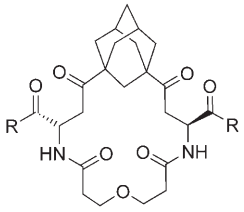
14



15



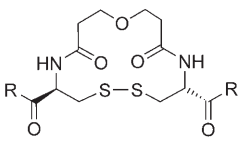
16



17a R = OMe

17b R = LeuOMe

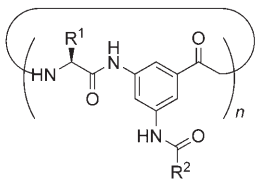
17c R =



18a R = OMe

18b R = LeuOMe

18c R =



19 $R^1 = CH_3$, $R^2 = n\text{-}C_9H_{19}$, $n = 3$
20 $R^1 = CH_3$, $R^2 = n\text{-}C_9H_{19}$, $n = 4$
21 $R^1 = CH_3$, $R^2 = n\text{-}C_{15}H_{31}$, $n = 4$
22 $R^1 = CH_3$, $R^2 = n\text{-}C_{15}H_{31}$, $n = 5$
23 $R^1 = CH_2COO^-$, $R^2 = n\text{-}C_{15}H_{31}$, $n = 4$
24 $R^1 = (CH_2)_4NH_3^+$, $R^2 = n\text{-}C_{17}H_{35}$, $n = 4$
25 $R^1 = CH_2OH$, $R^2 = n\text{-}C_{17}H_{35}$, $n = 4$

tivity (K^I over Cl^-), and cation selectivity (K^I over Na^I) in spite of their quite different structures. The authors ascribe this quite surprising result to the fact that the rate-determining step for ion permeation through all these channels is migration through the hydrophobic alkyl chain region. The current of an ion permeating across a channel is an integration of the whole energy profile the ion experiences during the permeation.[24] Therefore, it was reasoned that the alkyl chain region, which is much longer than the amino acid containing region, contributes significantly to the current, and ultimately to the conductance, of the channel. Altering the length of the alkyl chain, though, did not produce any effect on the conductance; this apparently unexpected behavior was rationalized by assuming that the degree of ordered interaction between the alkyl chains increases with increasing chain length. This produces a more-ordered pore, which facilitates ion permeation.

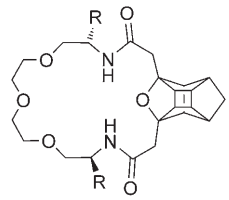
2.3. Transport of Small Molecules across a Chloroform/Water Membrane

The undeniable practicality of the U-tube liquid membrane over the lipid-membrane experiment for assessing the transport properties of synthetic macrocycles has certainly contributed to its popularity as an initial screen for transport properties. Several amino acid derived macrocycles of various sizes and nature have been used as hosts to extract metal ions

 © 2006 Wiley-VCH Verlag GmbH & Co. KGaA, Weinheim

or charged organic species from an aqueous to a chloroform layer.

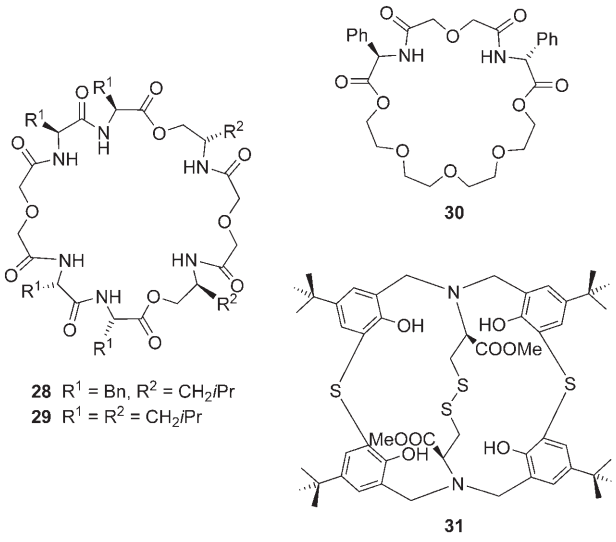
It has been reported both for chiral guests[25] and for metal ion guests[26] that the presence of a cage in the macrocyclic backbone enhances the lipophilicity and hence the transport ability of the resulting system. In light of this, macrocycles derived from (*S*)-α-phenylglycine (**26**) and (*S*)-valine (**27**) and



26 R = Ph
27 R = *i*Pr

incorporating a pentacycloundecane backbone were studied[27] by using the U-tube transport experiment and measuring the optical rotation in the receiving arm of the tube.[14b] (±)-Methyl-α-phenylglycinate hydrochloride was used as the guest in the transport experiment, and macrocycles **26** and **27** showed a moderate enantioselectivity for the (*R*)-enantiomer (29 and 68% *ee*, respectively). Analogous macrocycles containing a pyridine ring in place of the pentacycloundecane moiety displayed poor transport ability, probably as a result of their low lipophilicity.

Studies on the differential transport of amino ester hydrochlorides and various amines through a liquid membrane showed that macrocycles **28** and **29** (Scheme 1), which contain predominantly aromatic or exclusively alkyl side chains, display increased affinity for organic molecules with matching substituents.[28] The smaller macrocycle **30** showed selective transport properties towards K^I and Na^I across a liquid membrane, and a degree of preference for M^I over M^{II} cations was established.[29] Chiral (dithiatetrahomodiaza)calix[4]arene (**31**), in which four methylene bridges (-CH_2-) were replaced by two epithio (-S-) groups and two dihomoaza bridges (-CH_2-$NRCH_2$-), proved capable of extracting Zn^{II} (61% extraction) and Cu^{II} (83% extraction) from water to chloroform.[30] Given that the parent calixarene did not extract any metal ions, this result suggested that the epithio groups and the dihomoaza bridges contained in **31** may play an important role in determining the host–guest properties of the synthetic macrocycle.



28 R^1 = Bn, R^2 = CH_2*i*Pr
29 R^1 = R^2 = CH_2*i*Pr

30

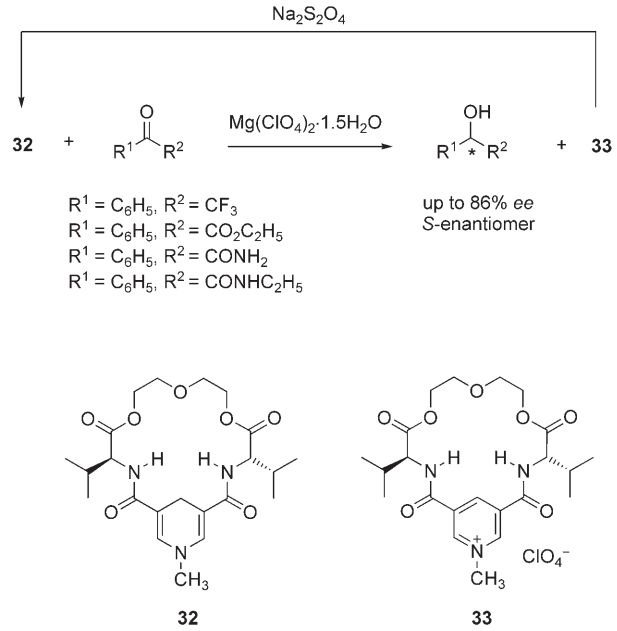
31

Scheme 1. Macrocycles **28** and **29** transport organic molecules with matching substituents.[28] Macrocycles **30**[29] and **31**[30] transport metal ions selectively.

3. Amino Acid Derived Macrocycles in Catalysis

Synthetic macrocyclic ligands derived from amino acids offer an attractive way of holding chiral groups in close proximity to each other to create a situation that resembles the chiral environment surrounding the metal in many metalloenzyme-catalyzed reactions.[31] In designing potential ligands for catalytically active transition metals, the ligand should: a) be able to sustain a range of metal oxidation states, b) feature readily available and modifiable chiral residues close to the metal, capable of influencing the stereoselective approach of a substrate, and c) be sufficiently stable to allow multiple turnovers under a range of catalytic reaction conditions.

The first example of the synthesis and application of amino acid containing macrocycles to an asymmetric transformation dates back to 1979:[32] (*S*)-Valine was used as the starting material for the synthesis of a 1,4-dihydropyridine-containing system **32** (Scheme 2), which encapsulates Mg^{II} and catalyzes the asymmetric reduction of ketones to alcohols at room temperature. Upon hydride transfer from the



R^1 = C_6H_5, R^2 = CF_3
R^1 = C_6H_5, R^2 = $CO_2C_2H_5$
R^1 = C_6H_5, R^2 = $CONH_2$
R^1 = C_6H_5, R^2 = $CONHC_2H_5$

up to 86% *ee*
S-enantiomer

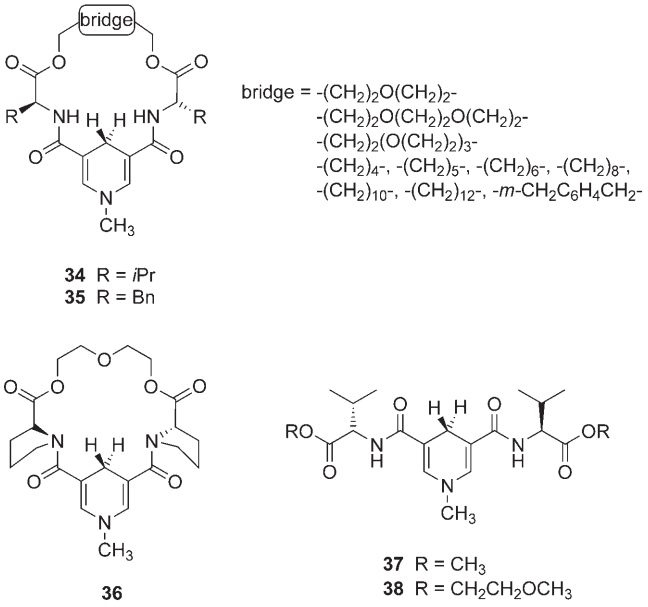
32 **33**

Scheme 2. Compounds **32** and **33** and the proposed catalytic cycle for the reduction of ketones to alcohols.[32]

© 2006 Wiley-VCH Verlag GmbH & Co. KGaA, Weinheim

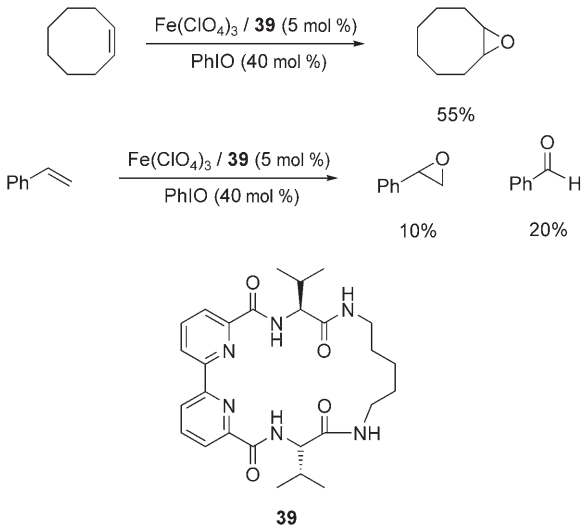
dihydropyridine ring to the carbonyl moiety, **32** is oxidized to the corresponding pyridinium salt **33**, which is reduced back to **32** with $Na_2S_2O_4$ without loss of enantiopurity (measured polarimetrically). The reduction proceeds with asymmetric induction of up to 86% *ee*, and this result represented at the time one of the highest asymmetric inductions ever achieved with a 1,4-dihydropyridine.

On the basis of shielding effects in ^{1}H NMR spectroscopic studies, the consistent formation of the *S* enantiomer of the alcohol product was attributed to a transition state in which the Mg^{II} coordination site was close to the diethylene glycol bridge. This initial hypothesis was reformulated, however, in light of further studies.[33] In a second report the consequences of changing the configuration and the structure of the amino acid along with the length of the bridge embedded in the macrocycle were assessed. "Open" analogues **37** and **38** of the synthetic macrocycles **34–36** were also prepared in order to evaluate the effect of the cyclic structure on the enantiomeric excess of the alcohol product.



Good to excellent enantioselectivities (up to 90% *ee*) of the alcohol were obtained with compounds **34** and **35**, which feature a wide range of bridges. Consistent formation of the *S* enantiomer indicated that the length and the nature of the bridge were not crucial in determining the stereochemical course of the reaction. This led to the conclusion that the magnesium ion does not bind to the bridge in the complex formed prior to hydride transfer. Remarkably, proline-derived macrocycle **36** was the only system that failed to transfer chirality, affording the racemic alcohol in 50% yield. Finally, "open" derivatives **37** and **38** gave very low enantioselectivity (10 and 18% *ee*, respectively) of alcohol product, which confirmed that the presence of a bridge is a minimum requirement for good transfer of chirality. These reports[32,33] represent important milestones towards the development of quite simple systems that resemble the structure and the selectivity of the naturally occurring redox systems NAD^+/NADH and $NADP^+$/NADPH.

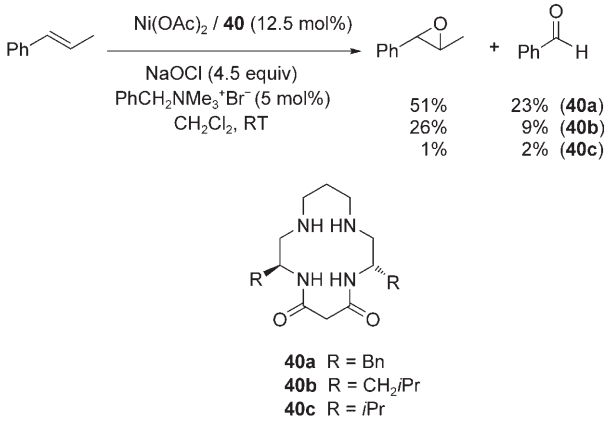
An iron(III) complex of chiral macrocycle **39** (Scheme 3) was shown to catalyze the conversion of alkenes into the



Scheme 3. Macrocycle **39** and its application to the epoxidation of alkenes (yields based on iodosylbenzene).[34]

corresponding epoxides in the presence of iodosylbenzene as terminal oxidant.[34] Cyclooctene gave exclusively epoxidized product in a reasonable yield (relative to iodosylbenzene amount employed), whereas styrene produced its epoxide and benzaldehyde. Analysis of the styrene epoxide with a chiral shift reagent[35] revealed an essentially racemic product, which suggested minimal chiral interactions had occurred between the alkene and the metal-bound oxidizing reagent.

Dioxycyclam macrocycles **40a,b** (Scheme 4) form catalytically active complexes with Ni^{II} for the conversion of *trans*-2-methylstyrene into the corresponding epoxide with sodium hypochlorite as terminal oxidant.[36] The phenylalanine-derived macrocycle **40a** afforded complete conversion of the substrate into the corresponding epoxide and benzalde-



Scheme 4. Dioxycyclam macrocycles **40a,b** and their application to the epoxidation of *trans*-2-methylstyrene.[36]

 © 2006 Wiley-VCH Verlag GmbH & Co. KGaA, Weinheim

hyde (acetaldehyde, which is also presumed to be formed during the reaction, could not be detected under the GC conditions chosen for the analysis).[36] The leucine-derived complex **40b** showed only moderate activity, whereas the valine analogue **40c** gave very low conversions. Spectroscopic investigation of the epoxide product obtained with **40a** revealed its racemic nature, which was ascribed to the low steric demands of the benzyl side chain. Previous studies had proven that simple nickel salts such as $Ni(OAc)_2$ are inactive as oxidation catalysts with NaOCl alone and that no epoxidation occurred in the absence of a Ni^{II}–cyclam complex;[37] hence the presence of the dioxocyclam ligand was considered essential for the reactivity.

4. Gelators

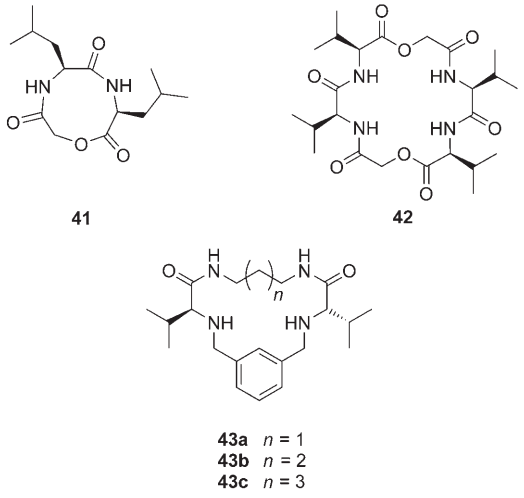
In the last decade a large number of low-molecular-weight compounds capable of reversibly forming gels in both organic liquids and water were reported.[38,39] These compounds can self-assemble into fibers of considerable length (several micrometers) that crosslink and entrap solvent molecules, thus forming a soft, solidlike material. Given their interesting physical and chemical properties, organic gelators have been studied for use in drug-delivery processes,[40] responsive materials,[41] and catalysis.[42]

Amino acid derived building blocks have been widely used for the construction of low-molecular-weight compounds that form gels in organic solvents.[43] The first example of amino acid containing systems capable of gelating both polar (acetonitrile, water) and nonpolar (diethyl ether, dichloromethane) solvents was reported in 1993 (**41** and **42**, Scheme 5).[44] More-recent studies show that in some cases the chirality of the system is expressed at a supramolecular level by the formation of helical architectures.[45] In fact, scanning electron microscopy of the gel formed by macrocycle **43a** ($n=1$) revealed the presence of isolated right-handed twisted ribbons several micrometers long.[45a] The self-assembly of chiral cyclophanes **43a–c** and of their analogues containing different amino acid side chains proved to be very sensitive to small structural changes (the nature of the amino acid residue or of the aromatic moiety, the length of the aliphatic spacer).[45b] These factors have an important influence on the conformational preference of these types of molecules as well as on their supramolecular self-assembly.

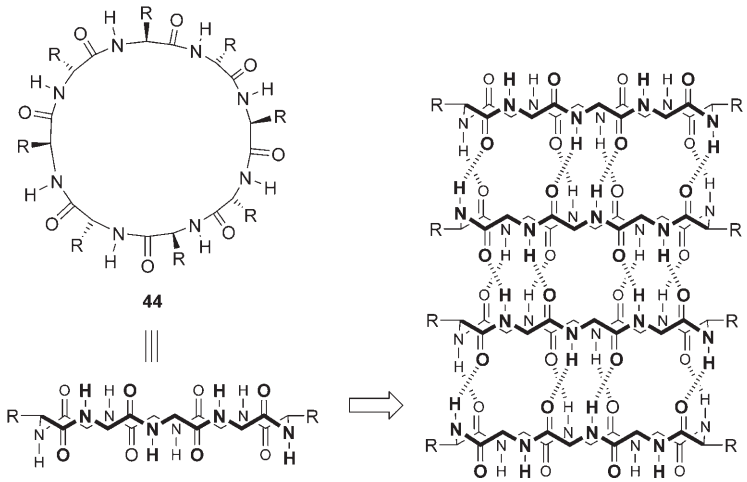
The relationship between the absolute configuration of the chiral macrocycle used to form the gel and the handedness of the resulting helix was also studied.[45c] The two enantiomers of compound **43a** contain helixlike aggregates of opposite handedness in their benzene gels. Results obtained with nonenantiopure mixtures, though, suggest that under these conditions compound **43a** could self-assemble into enantiopure crystalline conglomerates disrupted by racemic aggregates or could be made up by layers of opposite enantiomers stacked above each other to form a *meso* aggregate. In either case, the presence of the other enantiomer results in smaller aggregates and prevents gelation.

5. Organic Nanotubes

Synthetic nanotubes have been the subject of extensive investigations over the last few years given their potential utility in chemical, biological, and materials science.[46] The hypothesis that cyclic peptides with an even number of alternating *R* and *S* amino acids should stack through backbone–backbone hydrogen bonding to form hollow cylinders was first formulated in 1974.[47] Almost two decades later this concept was put into practice with the synthesis of octapeptide *cyclo*[-{(*S*)-Gln-(*R*)-Ala-(*S*)-Glu-(*S*)-Ala}$_2$-] **44** (Scheme 6), which provided the first example of a self-assembling nanotube formed by ring stacking of cyclic *R*,*S* peptides.[48] More recently, the high efficacy of this class of materials against lethal methicillin-resistant *Staphilococcus aureus* infections in mice was reported, revealing that *R*,*S* α-peptides are attractive alternatives to naturally derived antibiotics.[49]



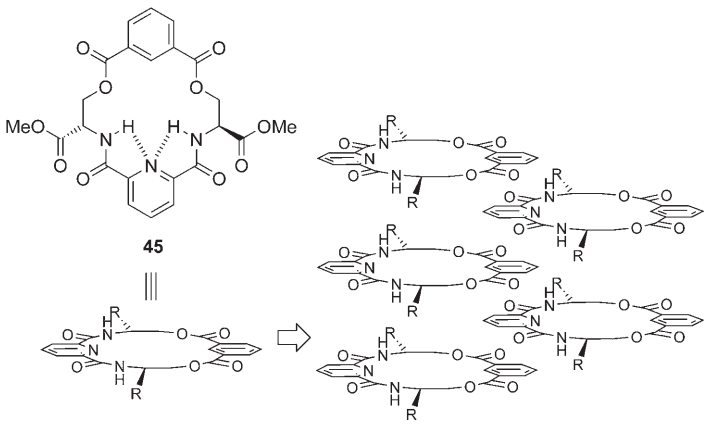
Scheme 5. Cyclic compounds **41** and **42** gelate polar and nonpolar solvents,[44] and **43a** forms supramolecular right-handed twisted ribbons.[45a]



Scheme 6. The first example of a self-assembling nanotube based on cyclic α-peptide **44**.[48] (Some of the R groups have been removed for clarity.)

© 2006 Wiley-VCH Verlag GmbH & Co. KGaA, Weinheim

Non-peptidic synthetic macrocycles also form tubelike structures by stacking above one another through hydrogen bonds or π–π interactions between aromatic rings.[46c,50] For example, serine-based cyclophane **45** (Scheme 7) self-assembles into a supramolecular structure containing two tubes.[51] A crucial requirement for π–π stacking between the aromatic and pyridyl bridging units is the presence of the pyridyl unit next to the amide moiety; this locks the amide NH groups into NH···N hydrogen bonding, thereby creating an almost flat ring conformation, a prerequisite for vertical stacking.



Scheme 7. The 18-membered serinophane **45**, which contains pyridyl and phenyl rings as bridges, and schematic representation of the multiple π–π stacks in the self-assembly.[51]

6. Recognition of Biologically Important Molecules

6.1. Introduction

Many biological processes vital to life involve interactions between the active sites of receptor proteins and relatively small molecules such as carbohydrates, amino acids, peptides, glycoconjugates, and hormones. Specific molecular recognition phenomena also play an important role in the highly selective chemical reactions that occur in living systems. Much attention has thus been devoted in recent years to the study of synthetic models that could provide a understanding of these processes.[52]

NMR spectroscopy and HPLC are important techniques for studying the binding of synthetic receptors to substrates of biological interest.[53,54] In both cases the molecular-recognition process is translated into a physical phenomenon (shift of NMR peaks or separated peaks in the chromatogram), which expresses and quantifies the free energy of formation of the supramolecular aggregates.

6.2. Recognition of Amino Acid and Peptide Derivatives

Amino acid residues in a receptor molecule and/or a substrate molecule play a significant role in artificial systems as they can be arranged to form multipoint binding sites, thus mimicking many naturally occurring receptors and enzymes. The tertiary structure and function of complex biological molecules such as enzymes rely strongly on noncovalent, specific inter- and intramolecular interactions that involve amino acid residues, and the binding between a substrate and a receptor is significantly enhanced when the receptor structure is inherently complementary to that of the substrate. The development of synthetic systems derived from amino acids and capable of binding amino acid or peptide derivatives is therefore a powerful tool for understanding the phenomena that govern molecular recognition in biological environments.[55]

The C_3-symmetric receptor **46**[56] (Figure 1) features a concave, rigid binding site and an array of hydrogen-bond donors and acceptors located around the macrocycle periphery. It was anchored to silica to obtain a chiral stationary phase (CSP), which showed exceptional affinity for the *S* enantiomer of *N*-Boc-amino acid methylamides (Boc = *tert*-butoxycarbonyl).[57]

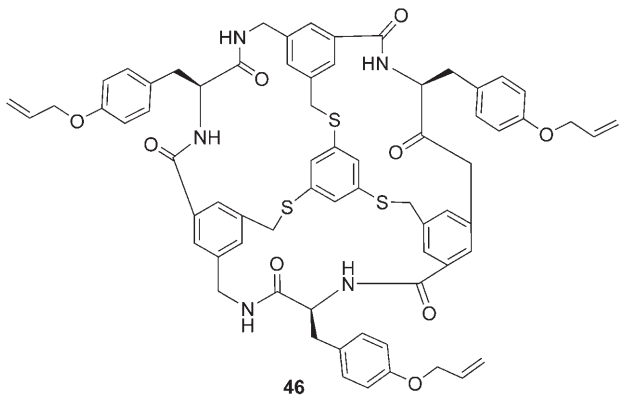
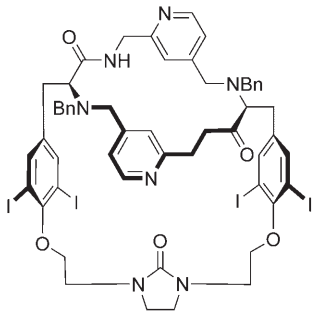


Figure 1. A CSP derived from macrocycle **46** readily separates the enantiomers of some simple amino acid derivatives.[56,57]

An enantioselectivity factor α_{RS} (defined as the ratio between the partition coefficients for the formation of the two diastereomeric adsorbates)[54] of **46** was obtained for the enantiomers of threonine, corresponding to a difference in binding affinities $\Delta(\Delta G_{ass}) = -2.2$ kcal mol^{-1}. Notably, even a small $\Delta(\Delta G_{ass})$ value is enough to allow a good separation on HPLC. For example, when $\Delta(\Delta G_{ass}) = 50.0$ cal mol^{-1}, $\alpha = 1.09$, which corresponds to well-resolved peaks on the chromatogram.[54]

NMR titration has been used to explore the binding properties of another tyrosine-derived macrocycle. Compound **47** (Figure 2), which is a superior version to a previously reported receptor,[58] exhibited enantioselectivity for the *S* enantiomer of acetylalanineamides (Ac-(*S*)-Ala-NHBn (Bn = Benzyl): $\Delta G_{ass} = -2.36$ kcal mol^{-1}; Ac-(*R*)-Ala-NHBn: $\Delta G_{ass} = -1.36$ kcal mol^{-1}; hence $\Delta(\Delta G_{ass}) = -1.0$ kcal mol^{-1}) and alanine dipeptides ($-0.8 < \Delta(\Delta G_{ass}) < -1.3$ kcal mol^{-1}).[59] A series of experiments performed with structurally different alanine derivatives (obtained by varying the nature of the protecting groups at the C and N termini) showed that the binding properties of the receptor are a direct conse-

 © 2006 Wiley-VCH Verlag GmbH & Co. KGaA, Weinheim

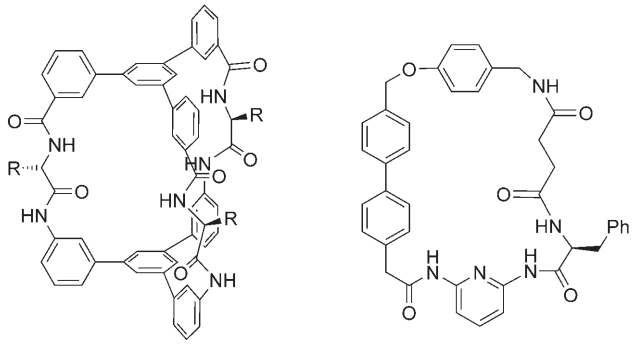


47

Figure 2. Macrocycle **47** selectively binds the *S* enantiomer of acetylalanineamides.[59]

quence of a good match between the substituents on the host and the guest and therefore of their capability to give rise to stable interactions.

Cagelike selectors **48**–**49** (Scheme 8) showed good enantioselectivity ($-0.6 < \Delta(\Delta G_{ass}) < -1.1$ kcal mol^{-1}) for the *S* enantiomer of N-protected amino acids in solution, but



48 R = CH_2*i*Pr
49 R = Bn

50

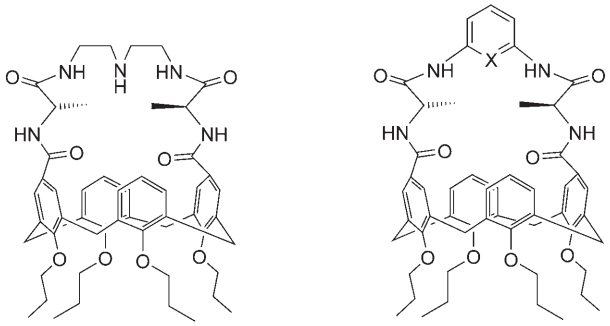
Scheme 8. Cagelike macrocycles **48** and **49**[60] and a macrocycle with minimal chirality **50**[61] are selective towards N-protected amino acids and dipeptides, respectively.

they were unable to resolve the same class of compounds when anchored to silica.[60] The (*S*)-phenylalanine-derived macrocycle **50**, carefully designed to feature a diamidopyridine unit (which serves as a carboxylic acid binding site) and to contain a rigid biaryl fragment (to hold open the binding cavity), binds selectively to the carboxylic acid terminus of *N*-Cbz-β-alanyl-(*S*)-amino acids.[61] Although the observed binding ($-0.1 < \Delta(\Delta G_{ass}) < -1.0$ kcal mol^{-1}) is not comparable with the high enantioselectivities observed for some other peptide-binding systems ($-2\Delta(\Delta G_{ass}) < -3$ kcal mol^{-1}),[62] it is surprisingly good given the minimal chirality incorporated in the macrocycle.

6.3. Recognition of Carboxylic Anions

Carboxylate anions are involved in several processes of biological interest. A much-studied example is carboxypeptidase A, an enzyme that coordinates to the C-terminal carboxylate group of polypeptides by the formation of an arginine–aspartate salt bridge, and then catalyzes the hydrolysis of the C-terminal residue.[63] Carboxylate anions also play a special role in the biological activity of the vancomycin family of glycopeptide antibiotics.[64] Vancomycin, produced by the microorganism *Amycolatopsis orientalis*, is widely prescribed for infections arising from *Staphylococcus aureus*; it is known to bind to bacterial-cell-wall mucopeptide precursors (intermediates in the process of bacterial cell-wall biosynthesis)[65] by forming three hydrogen bonds with the carboxylate anion of the C-terminal (*R*)-alanine. The enantioselective recognition and separation of chiral carboxylates[66,67] is also an important goal because several pharmaceutical compounds bear this functional group.

Chiral C_2-symmetric macrocycles **51**–**52** are examples of synthetic receptors for carboxylates derived partially from natural amino acids (Scheme 9).[68] The potential of this type



51

52a X = CH
52b X = N

Scheme 9. Macrocycle **51** behaves as a vancomycin mimic,[69] and macrocycles **52a**,**b** selectively bind carboxylate anions.[68]

of compound is demonstrated by the fact that **51** behaves as a vancomycin mimic, showing promising antibiotic activity against Gram-positive bacterial strands owing to its ability to bind the (*R*)-alanyl-(*R*)-alanine terminus of peptoglycans.[69]

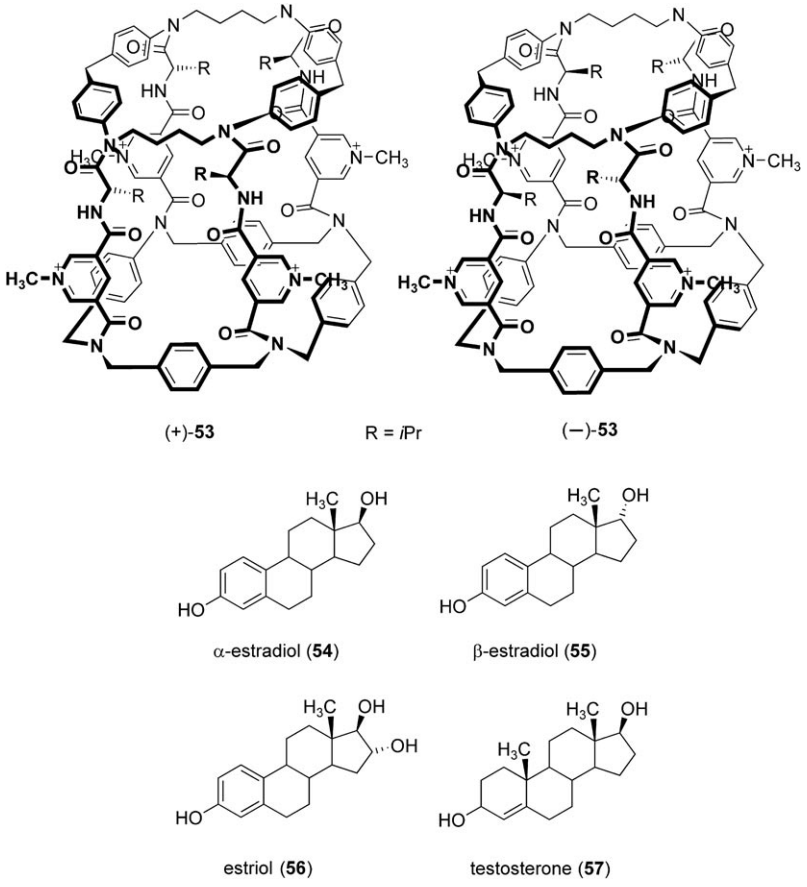
A preliminary screening of the binding properties of macrocycles **52a**–**b** was performed by mass spectrometry, which has become a powerful tool for the characterization of noncovalent adducts since the development of mild ionization techniques such as FAB, MALDI, and ESI.[70] In fact, if supramolecular entities can be successfully charged and transferred into the gas phase without destruction, then mass spectrometry has clear advantages over other methods such as vapor-phase osmometry, size-exclusion chromatography (SEC), gel-permeation chromatography, GPC), or light scattering, all of which give only estimates of molecular weights. Macrocycles **52a**–**b** showed good selectivity for organic carboxylates over inorganic anions such as Cl^- and NO_3^- in the gas phase. Subsequent NMR spectroscopic

 © 2006 Wiley-VCH Verlag GmbH & Co. KGaA, Weinheim

investigations confirmed that **52b** has a higher affinity for carboxylate anions, with particularly strong binding to benzoate. Disappointingly, **52a–b** showed only very modest enantioselectivity for the *R* enantiomer of *N*-acetyl amino acid carboxylates.

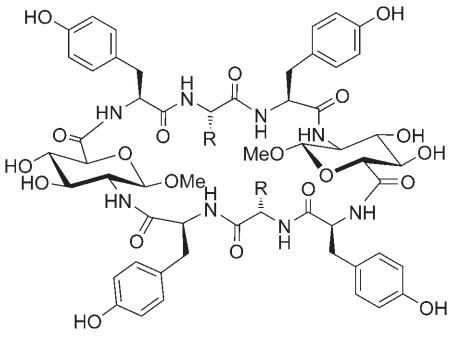
6.4. Recognition of Steroids and Purine Derivatives

Steroid recognition by protein receptors has several essential and diverse roles in eukaryotic cells.[71] Steroid-binding proteins (SBPs) exhibit a wide range of affinities ($K_{ass} \approx 10^5$–$10^{10}\,M^{-1}$) depending on their involvement in steroid transport, metabolism, or gene regulation.[72] The development of water-soluble synthetic steroid receptors featuring rigid cavities, known to be present also in steroid-binding proteins, may help to elucidate the mechanism of recognition of naturally occurring SBPs. Water-soluble cage-type enantiomeric macrocycles (−)-**53** and (+)-**53** have been used for the selective uptake of steroid hormones containing an aromatic moiety (α-estradiol (**54**), β-estradiol (**55**), and estriol (**56**); Scheme 10), but do not bind a fully aliphatic guest (testosterone (**57**)).[73,74] NMR spectroscopic studies revealed that the binding constant for complexation of (−)-**53** with α-estradiol is greater than the corresponding constant for β-estradiol ($\Delta(\Delta G_{ass}) = 0.34\,kcal\,mol^{-1}$), and the situation is reversed for the binding of (+)-**53** to these two epimers.



Scheme 10. Enantiomeric macrocycles (+)-**53** and (−)-**53** show diastereoselective binding for steroids.[73]

Studies of the selective complexation of purines and pyrimidines by synthetic host compounds may lead to a better understanding of noncovalent interactions involving nucleic acids, which contain purines and pyrimidines as structural building blocks. Very recently the binding properties of synthetic macrocycles **58–60** towards purine derivatives were reported (Figure 3).[75] Although the binding proved to be weak ($K_{ass} \approx 10\,M^{-1}$), these macrocycles exhibit an interesting framework derived from amino acids and sugars whose potential has yet to be fully exploited.



58 R = tyrosine side chain
59 R = CH_2CH_2COOH
60 R = $CH_2CH_2CH_2NHC(NH)NH_2$

Figure 3. Macrocycles **58–60** bind weakly to purine derivatives.[75]

7. Summary and Outlook

Our initial analysis of the literature covering non-peptidic amino acid derived macrocycles revealed that approximately 60% of the published papers dealt with synthesis alone, and remarkably few were truly driven by development of the function of the macrocycle. Against this background it is interesting to analyze the studies of ion transport across membranes. In this area remarkable advances are currently being made by using relatively readily available cyclopeptides. Studies that challenge synthetic non-peptidic macrocycles with sophisticated membrane models for ion transport, however, are scarce, but some of those, such as that based on the adamantyl-containing systems **11–16**, have produced very encouraging results in terms of activity and ion selectivity.

Macrocycles offer an attractive way of holding chiral groups in close proximity to each other to create a situation that resembles the chiral environment in a metalloenzyme. Despite some very elegant and encouraging work on mimicking naturally occurring $NAD(P)^+/NAD(P)H$ redox systems aimed at producing asymmetric catalysts for the reduction of carbonyl compounds, the use of this class of macrocycle in catalysis is remarkably underdeveloped to date.

Hydrogen-bonding interactions facilitate the formation of extended structures, and hence it is not surprising that amino acid derived macrocycles have been shown to act as gelators and to form tubular

 © 2006 Wiley-VCH Verlag GmbH & Co. KGaA, Weinheim

structures. Given the recent observation that cyclopeptides that form tubes are active against methicillin-resistant *Staphilococcus aureus* infections in mice, it is perhaps surprising that more structurally diverse macrocycles available by synthetic methods have not been tested for cylinder formation and antibiotic activity.

Several structurally diverse types of synthetic amino acid derived macrocycles have been designed to promote selective binding of biologically important organic molecules. In particular, the ability of a calixarene/amino acid/polyamine macrocycle to act as a mimic of the antibiotic vancomycin by binding the (*R*)-alanyl-(*R*)-alanine terminus of peptoglycans points to the exciting potential therapeutic uses of macrocycles only accessible by organic synthesis.

In summary, potential applications of non-peptidic amino acid derived macrocycles are exciting and varied, but this potential has only just started to be addressed. By discussing the applications investigated to date, it is intended that this Review should inspire more application-driven research in the future.

The authors thank the EPSRC for a studentship (to C.L.).

Received: September 28, 2005
Published online: January 30, 2006

[1] For recent reviews on macrocyclic chemistry, see: a) F. Arico, T. Chang, S. J. Cantrill, S. I. Khan, J. F. Stoddart, *Chem. Eur. J.* **2005**, *11*, 4655 – 4666; b) K. Bowman-James, *Acc. Chem. Res.* **2005**, *38*, 671 – 678; c) C. A. Schalley, T. Wielandt, J. Bruggemann, F. Vogtle, *Top. Curr. Chem.* **2004**, *248*, 141 – 200; d) L. A. Wessjohann, E. Ruijter, *Top. Curr. Chem.* **2005**, *243*, 137 – 184; e) B. Botta, M. Cassani, I. D'Acquarica, D. Misiti, D. Subissati, G. Delle Monache, *Curr. Org. Chem.* **2005**, *9*, 337 – 355.

[2] For recent reviews on the synthetic challenges represented by macrocycles, see: a) J. Blankenstein, J. P. Zhu, *Eur. J. Org. Chem.* **2005**, 1949 – 1964; b) L. V. R. Bonaga, H. C. Zhang, A. F. Moretto, H. Ye, D. A. Gauthier, J. Li, G. C. Leo, B. E. Maryanoff, *J. Am. Chem. Soc.* **2005**, *127*, 3473 – 3485; c) I. P. Beletskaya, A. G. Bessmertnykh, A. D. Averin, F. Denat, R. Guilard, *Eur. J. Org. Chem.* **2005**, 281 – 305; d) C. A. Schalley, W. Reckien, S. Peyerimhoff, B. Baytekin, F. Vogtle, *Chem. Eur. J.* **2004**, *10*, 4777 – 4789; e) A. G. M. Barrett, A. J. Hennessy, R. Le Vezouet, P. A. Procopiou, P. W. Seale, S. Stefaniak, R. J. Upton, A. J. P. White, D. J. Williams, *J. Org. Chem.* **2004**, *69*, 1028 – 1037.

[3] a) For a Review, see: K. C. Nicolaou, S. A. Snyder, *Angew. Chem.* **2005**, *117*, 1036 – 1069; *Angew. Chem. Int. Ed.* **2005**, *44*, 1012 – 1044; b) for a total synthesis, see: K. C. Nicolaou, D. Y.-K. Chen, X. Huang, T. Ling, M. Bella, S. A. Snyder, *J. Am. Chem. Soc.* **2004**, *126*, 12888 – 12896.

[4] Z. Cruz-Monserrate, H. C. Vervoort, R. Bai, D. J. Newman, S. B. Howell, G. Los, J. T. Mullaney, M. D. Williams, G. R. Pettit, W. Fenical, E. Hamel, *Mol. Pharmacol.* **2003**, *63*, 1273 – 1280.

[5] a) For a report on the clinical efficacy of synthetic analogues of cryptophycin-1, see: J. Liang, R. E. Moore, E. D. Moher, J. E. Munroe, R. S. Al-awar, D. A. Hay, D. L. Varie, T. Y. Zhang, J. A. Aikins, M. J. Martinelli, C. Shih, J. E. Ray, L. L. Gibson, V. Vasudevan, L. Polin, K. White, J. Kushner, C. Simpson, S. Pugh, T. H. Corbett, *Invest. New Drugs* **2005**, *23*, 213 – 224; b) N. R. Watts, N. Cheng, W. West, A. C. Steven, D. L. Sackett, *Biochemistry* **2002**, *41*, 12662 – 12669; c) D. Panda, R. H. Himes, R. E. Moore, L. Wilson, M. A. Jordan, *Biochemistry* **1997**, *36*, 12948 – 12953; d) for a total synthesis, see: L.-H. Li, M. A. Tius, *Org. Lett.* **2002**, *4*, 1637 – 1640.

[6] a) For a synthesis of K-13 analogues, see: P. Cristau, J. P. Vors, J. Zhu, *Org. Lett.* **2003**, *5*, 5575 – 5578; b) for a synthesis of K-13, see: D. L. Boger, D. Yohannes, *J. Org. Chem.* **1989**, *54*, 2498 – 2502; c) for fermentation, isolation, and biological properties, see: H. Kase, M. Kaneko, K. Yamada, *J. Antibiot.* **1987**, *40*, 450 – 454.

[7] a) J. N. Tabudravu, L. A. Morris, B. F. Milne, M. Jaspars, *Org. Biomol. Chem.* **2005**, *3*, 745 – 749; b) R. Wintjens, J. Liévin, M. Rooman, E. Buisine, *J. Mol. Biol.* **2000**, *302*, 395 – 410; c) D. P. Cioca, K. Kitano, *Cell. Mol. Life Sci.* **2002**, *59*, 1377 – 1387; d) M. R. Bubb, I. Spector, B. B. Beyer, K. M. Fosen, *J. Biol. Chem.* **2000**, *275*, 5163 – 5170; e) for a total synthesis of jaspamide, see: H. Yoshiro, Y. Katsuyuki, M. Takefumi, *Heterocycles* **1994**, *39*, 603 – 612.

[8] For a review on synthetic studies of biologically active marine cyclopeptides, see: P. Wipf, *Chem. Rev.* **1995**, *95*, 2115 – 2134.

[9] a) For a review on oxazole and thiazole alkaloids, see: Z. Jin, Z. Li, R. Huang, *Nat. Prod. Rep.* **2002**, *19*, 454 – 476; b) for a conformational study on cyclic octapeptides of marine origin, see: G. Abbenante, D. P. Fairlie, L. R. Gahan, G. R. Hanson, G. K. Pierens, A. L. van den Brenk, *J. Am. Chem. Soc.* **1996**, *118*, 10384 – 10388; c) for a synthesis of some analogues of ascidiacyclamide **5**, see: A. J. Blake, J. S. Hannam, K. A. Jolliffe, G. Pattenden, *Synlett* **2000**, 1515 – 1518, and references therein.

[10] a) For a recent report on the synthesis and biological properties of cyclopeptide alkaloids see: M. M. Joullié, D. J. Richard, *Chem. Commun.* **2004**, 2011 – 2015; b) for a total synthesis of sanjoinine A, see: D. Xiao, S. P. East, M. M. Joullié, *Tetrahedron Lett.* **1998**, *39*, 9631 – 9632.

[11] M. K. Park, J. H. Park, J. H. Cho, J. K. Park, Y. N. Han, B. H. Han, *Arch. Pharmacal Res.* **1991**, *14*, 103 – 104.

[12] K. H. Hwang, Y. N. Han, B. H. Han, *Arch. Pharmacal Res.* **2001**, *24*, 202 – 206.

[13] a) F. M. Harold, J. R. Baarda, *J. Bacteriol.* **1967**, *149*, 53 – 60; b) M. C. Blok, J. De Gier, L. L. Van Deenen, *Biochim. Biophys. Acta* **1974**, *367*, 202 – 209; c) L. Kovac, E. Bohmerova, P. Butko, *Biochim. Biophys. Acta* **1982**, *721*, 341 – 348; d) K. Altendorf, W. Epstein, A. Lohmann, *J. Bacteriol.* **1986**, *168*, 334 – 337; e) M. Jackson, H. H. Mantsch, *Biopolymers* **1991**, *31*, 1205 – 1212.

[14] a) S. S. Moore, T. L. Tarnowski, M. Newcomb, D. J. Cram, *J. Am. Chem. Soc.* **1977**, *99*, 6398 – 6405; b) M. Newcomb, J. L. Toner, R. C. Helgeson, D. J. Cram, *J. Am. Chem. Soc.* **1979**, *101*, 4941 – 4947.

[15] P. J. Sims, A. S. Waggoner, C. H. Wang, J. F. Hoffman, *Biochemistry* **1974**, *13*, 3315 – 3330.

[16] A. J. Minn, P. Vélez, S. L. Schendel, H. Liang, S. W. Muchmore, S. W. Fesik, M. Fill, C. B. Thompson, *Nature* **1997**, *385*, 353 – 357.

[17] J. Sanchez-Quesada, M. R. Ghadiri, H. Bayley, O. Braha, *J. Am. Chem. Soc.* **2000**, *122*, 11757 – 11766.

[18] L. Song, M. R. Hobaugh, C. Shustak, S. Cheley, H. Bayley, J. E. Gouaux, *Science* **1996**, *274*, 1859 – 1866.

[19] a) G. Menestrina, *J. Membr. Biol.* **1986**, *90*, 177 – 190; b) L.-Q. Gu, M. Dalla Serra, J. B. Vincent, G. Vigh, S. Cheley, O. Braha, H. Bayley, *Proc. Natl. Acad. Sci. USA* **2000**, *97*, 3959 – 3964.

[20] a) L.-Q. Gu, O. Braha, S. Conlan, S. Cheley, H. Bayley, *Nature* **1999**, *398*, 686 – 690; b) H. Bayley, O. Braha, L.-Q. Gu, *Adv. Mater.* **2000**, *12*, 139 – 142.

[21] a) D. Ranganathan, V. Haridas, K. P. Madhusudanan, R. Roy, R. Nagaraj, G. B. John, M. B. Sukhaswami, *Angew. Chem.* **1996**, *108*, 1193 – 1195; *Angew. Chem. Int. Ed. Engl.* **1996**, *35*, 1105 – 1107; b) I. L. Karle, D. Ranganathan, V. Haridas, *J. Am. Chem. Soc.* **1996**, *118*, 10916 – 10917; c) D. Ranganathan, V. Haridas, K. P. Madhusudanan, R. Roy, R. Nagaraj, G. B. John, *J. Am. Chem. Soc.* **1997**, *119*, 11578 – 11584; d) D. Ranganathan, M. P.

 © 2006 Wiley-VCH Verlag GmbH & Co. KGaA, Weinheim

Samant, R. Nagaraj, E. Bikshapathy, *Tetrahedron Lett.* **2002**, *43*, 5145 – 5147.
[22] Given the small size of this macrocycle, the formation of a complex with metal ions is prevented due to the fact that its carbonyl groups are oriented outward: R. W. Roeske, S. J. Kennedy in *Chemistry and Biochemistry of Amino Acids, Peptides and Proteins, Vol. 7* (Ed.: B. Weinstein), Marcel Dekker, New York, **1983**, pp. 205 – 256.
[23] H. Ishida, Z. Qi, M. Sokabe, K. Donowaki, Y. Inoue, *J. Org. Chem.* **2001**, *66*, 2978 – 2989.
[24] D. G. Levitt, *Annu. Rev. Biophys. Biophys. Chem.* **1986**, *15*, 29 – 57.
[25] A. P. Marchand, H.-S. Chong, B. Ganguly, *Tetrahedron: Asymmetry* **1999**, *10*, 4695 – 4700.
[26] a) A. P. Marchand, K. A. Kumar, A. S. McKim, K. Mlinarić-Majerski, G. Kragol, *Tetrahedron* **1997**, *53*, 3467 – 3474; b) A. P. Marchand, S. Alihodžič, A. S. McKim, K. A. Kumar, K. Mlinarić-Majerski, T. Šumanovac, S. G. Bott, *Tetrahedron Lett.* **1998**, *39*, 1861 – 1864.
[27] T. Govender, H. K. Hariprakasha, H. G. Kruger, A. P. Marchand, *Tetrahedron: Asymmetry* **2003**, *14*, 1553 – 1557.
[28] a) H. Kataoka, T. Katagi, *Tetrahedron* **1987**, *43*, 4519 – 4530; b) H. Kataoka, T. Katagi, *Chem. Pharm. Bull.* **1988**, *36*, 3199 – 3201.
[29] M. Žinić, V. Škarić, *J. Org. Chem.* **1988**, *53*, 2582 – 2588.
[30] K. Ito, A. Suzuki, N. Ito, H. Teraura, Y. Ohba, *J. Heterocycl. Chem.* **2003**, *40*, 405 – 409, and references therein.
[31] a) J. H. Hartley, T. D. James, C. J. Ward, *J. Chem. Soc. Perkin Trans. 1* **2000**, 3155 – 3184; b) X. X. Zhang, J. S. Bradshaw, R. M. Izatt, *Chem. Rev.* **1997**, *97*, 3313 – 3361.
[32] J. G. de Vries, R. M. Kellogg, *J. Am. Chem. Soc.* **1979**, *101*, 2759 – 2761, and references therein.
[33] P. Jouin, C. B. Troostwijk, R. M. Kellogg, *J. Am. Chem. Soc.* **1981**, *103*, 2091 – 2093.
[34] R. B. Hopkins, A. D. Hamilton, *J. Chem. Soc. Chem. Commun.* **1987**, 171 – 173.
[35] J. T. Groves, R. S. Myers, *J. Am. Chem. Soc.* **1983**, *105*, 5791 – 5796.
[36] T. R. Wagler, Y. Fang, C. J. Burrows, *J. Org. Chem.* **1989**, *54*, 1584 – 1589.
[37] a) J. D. Koola, J. K. Kochi, *Inorg. Chem.* **1987**, *26*, 908 – 916; b) H. Yoon, C. J. Burrows, *J. Am. Chem. Soc.* **1988**, *110*, 4087 – 4089.
[38] N. M. Sangeetha, U. Maitra, *Chem. Soc. Rev.* **2005**, *34*, 821 – 836.
[39] For an example, see: a) P. Terech, R. G. Weiss, *Chem. Rev.* **1997**, *97*, 3133 – 3159; b) D. J. Abdallah, R. G. Weiss, *Adv. Mater.* **2000**, *12*, 1237 – 1247; c) J. van Esch, B. L. Feringa, *Angew. Chem.* **2000**, *112*, 2351 – 2354; *Angew. Chem. Int. Ed.* **2000**, *39*, 2263 – 2266; d) O. Gronwald, E. Snip, S. Shinkai, *Curr. Opin. Colloid Interface Sci.* **2002**, *7*, 148 – 156; e) G. Wang, A. D. Hamilton, *Chem. Eur. J.* **2002**, *8*, 1954 – 1961; f) J. J. van Gorp, J. A. J. M. Vekemans, E. W. Meijer, *J. Am. Chem. Soc.* **2002**, *124*, 14759 – 14769; g) M. George, R. G. Weiss, *Langmuir* **2002**, *18*, 7124 – 7135; h) M. George, R. G. Weiss, *Langmuir* **2003**, *19*, 1017 – 1025; i) C. Wang, A. Robertson, R. G. Weiss, *Langmuir* **2003**, *19*, 1036 – 1046; j) C. Wang, R. G. Weiss, *Chem. Commun.* **2003**, 310 – 311; k) G. Bühler, M. C. Feiters, R. J. M. Nolte, *Angew. Chem.* **2003**, *115*, 2599 – 2602; *Angew. Chem. Int. Ed.* **2003**, *42*, 2494 – 2497; l) Y. Watanabe, T. Miyasou, M. Hayashi, *Org. Lett.* **2004**, *6*, 1547 – 1550; m) V. Caplar, M. Zinic, J.-L. Pozzo, F. Fages, G. Mieden-Gundert, F. Vögtle, *Eur. J. Org. Chem.* **2004**, 4048 – 4059.
[40] For a recent short account, see: J. C. Tiller, *Angew. Chem.* **2003**, *115*, 3180 – 3183; *Angew. Chem. Int. Ed.* **2003**, *42*, 3072 – 3075.
[41] For an example, see: I. Sato, K. Kadowaki, H. Urabe, J. H. Jung, Y. Ono, S. Shinkai, K. Soai, *Tetrahedron Lett.* **2003**, *44*, 721 – 724.
[42] For a review, see: N. W. Fadnavis, A. Deshpande, *Curr. Org. Chem.* **2002**, *6*, 393 – 410.
[43] For an example, see: a) K. Hanabusa, K. Hiratsuka, M. Kimura, H. Shirai, *Chem. Mater.* **1999**, *11*, 649 – 655; b) R. Jayakumar, M. Murugesan, C. Asokan, M. A. Scibioh, *Langmuir* **2000**, *16*, 1489 – 1496; c) G. Mieden-Gundert, L. Klein, M. Fischer, F. Vögtle, K. Heuzé, J.-L. Pozzo, M. Vallier, F. Fages, *Angew. Chem.* **2001**, *113*, 3266 – 3267; *Angew. Chem. Int. Ed.* **2001**, *40*, 3164 – 3166; d) X. Luo, B. Liu, Y. Liang, *Chem. Commun.* **2001**, 1556 – 1557; e) J. Makarević, M. Jokić, B. Perić, V. Tomišić, B. Kojić-Prodić, M. Žinić, *Chem. Eur. J.* **2001**, *7*, 3328 – 3341; f) A. Carré, P. Le Grel, M. Baudy-Floch, *Tetrahedron Lett.* **2001**, *42*, 1887 – 1889; g) N. Yamada, T. Imai, E. Koyama, *Langmuir* **2001**, *17*, 961 – 963; h) J. Makarević, M. Jokić, L. Frkanec, D. Katalenić, M. Žinić, *Chem. Commun.* **2002**, 2238 – 2239; i) L. Frkanec, M. Jokić, J. Makarević, K. Wolsperger, M. Žinić, *J. Am. Chem. Soc.* **2002**, *124*, 9716 – 9717; j) I. Ihara, T. Sakurai, T. Yamada, T. Hashimoto, M. Takafuji, T. Sagawa, H. Hachisako, *Langmuir* **2002**, *18*, 7120 – 7123; k) S. K. Maji, D. Haldar, A. Banerjee, A. Banerjee, *Tetrahedron* **2002**, *58*, 8695 – 8702; l) S. Malik, S. K. Maji, A. Banerjee, A. K. Nandi, *J. Chem. Soc. Perkin Trans. 2* **2002**, 1177 – 1186; m) S. A. Ahmed, X. Sallenave, F. Fages, G. Mieden-Gundert, W. M. Müller, U. Müller, F. Vögtle, J.-L. Pozzo, *Langmuir* **2002**, *18*, 7096 – 7101; n) S. Kiyonaka, S. Shinkai, I. Hamachi, *Chem. Eur. J.* **2003**, *9*, 976 – 998.
[44] E. J. de Vries, R. M. Kellogg, *J. Chem. Soc. Chem. Commun.* **1993**, 238 – 240.
[45] a) J. Becerril, M. I. Burguete, B. Escuder, S. V. Luis, J. F. Miravet, M. Querol, *Chem. Commun.* **2002**, 738 – 739; b) J. Becerril, M. I. Burguete, B. Escuder, F. Galindo, R. Gavara, J. F. Miravet, S. V. Luis, G. Peris, *Chem. Eur. J.* **2004**, *10*, 3879 – 3890; c) J. Becerril, B. Escuder, J. F. Miravet, R. Gavara, S. V. Luis, *Eur. J. Org. Chem.* **2005**, 481 – 485.
[46] For recent reviews on organic nanotubes, see: a) M. A. Balbo Block, C. Kaiser, A. Khan, S. Hecht, *Top. Curr. Chem.* **2005**, *245*, 89 – 150; b) D. T. Bong, T. D. Clark, J. R. Granja, M. R. Ghadiri, *Angew. Chem.* **2001**, *113*, 1016 – 1041; *Angew. Chem. Int. Ed.* **2001**, *40*, 988 – 1011; c) D. Ranganathan, *Acc. Chem. Res.* **2001**, *34*, 919 – 930; d) J. D. Hartgerink, T. D. Clark, M. R. Ghadiri, *Chem. Eur. J.* **1998**, *4*, 1367 – 1372.
[47] P. De Santis, S. Morosetti, R. Rizzo, *Macromolecules* **1974**, *7*, 52 – 58.
[48] M. R. Ghadiri, J. R. Granja, R. A. Milligan, D. E. McRee, N. Khazanovich, *Nature* **1993**, *366*, 324 – 327.
[49] S. Fernandez-Lopez, H.-S. Kim, E. C. Choi, M. Delgado, J. R. Granja, A. Khasanov, K. Kraehenbuehl, G. Long, D. A. Weinberger, K. M. Wilcoxen, M. R. Ghadiri, *Nature* **2001**, *412*, 452 – 455.
[50] See: also W. Guo, X.-L. Mi, J. Wang, J.-Q. He, J.-P. Cheng, *Chem. J. Chin. Univ.* **2005**, *26*, 1086 – 1089.
[51] D. Ranganathan, A. Thomas, V. Haridas, S. Kurur, K. P. Madhusudanan, R. Roy, A. C. Kunwar, A. V. S. Sarma, M. Vairamani, K. D. Sarma, *J. Org. Chem.* **1999**, *64*, 3620 – 3629.
[52] For a review on synthetic receptors, see: J. H. Hartley, T. D. James, C. J. Ward, *J. Chem. Soc. Perkin Trans. 1* **2000**, 3155 – 3184.
[53] a) C. S. Wilcox, J. C. Adrian Jr., T. H. Webb, F. J. Zawacki, *J. Am. Chem. Soc.* **1992**, *114*, 10189 – 10197; b) I. Horman, B. Dreux, *Helv. Chim. Acta* **1984**, *67*, 754 – 764; c) C. J. Cresswell, A. L. Allred, *J. Phys. Chem.* **1962**, *66*, 1469 – 1470.
[54] W. H. Pirkle, T. C. Pochapsky, *Chem. Rev.* **1989**, *89*, 347 – 362.
[55] For examples of amino acid derived macrocycles as receptors for amino acids and peptide derivatives, see: a) J. Gong, B. C. Gibb, *Chem. Commun.* **2005**, 3319 – 3321; b) F. Galindo, J. Becerril, M. I. Burguete, S. V. Luis, L. Vigara, *Tetrahedron Lett.* **2004**, *45*, 1659 – 1662; c) X. Chen, D.-M. Du, W.-T. Hua, *Tetrahedron: Asymmetry* **2003**, *14*, 999 – 1007; d) T. Bhattacharyya, A. Sundin,

 © 2006 Wiley-VCH Verlag GmbH & Co. KGaA, Weinheim

U. J. Nilsson, *Tetrahedron* **2003**, *59*, 7921 – 7928; e) H. Zhao, W. Hua, *J. Org. Chem.* **2000**, *65*, 2933 – 2938; f) J. A. Gavin, M. E. Garcia, A. J. Benesi, T. E. Mallouk, *J. Org. Chem.* **1998**, *63*, 7663 – 7669; g) G. J. Pernia, J. D. Kilburn, J. W. Essex, R. J. Mortishire-Smith, M. Rowley, *J. Am. Chem. Soc.* **1996**, *118*, 10220 – 10227; h) M. F. Cristofaro, A. R. Chamberlin, *J. Am. Chem. Soc.* **1994**, *116*, 5089 – 5098; i) C. P. Waymark, J. D. Kilburn, I. Gillies, *Tetrahedron Lett.* **1995**, *36*, 3051 – 3054; j) G. J. Pernía, J. D. Kilburn, M. Rowley, *J. Chem. Soc. Chem. Commun.* **1995**, 305 – 306; k) R. Liu, P. E. J. Sanderson, W. C. Still, *J. Org. Chem.* **1990**, *55*, 5184 – 5186.

[56] For analogous receptors exhibiting enantioselectivity in solution, see: a) J.-I. Hong, S. K. Namgoong, A. Barnardi, W. C. Still, *J. Am. Chem. Soc.* **1991**, *113*, 5111 – 5112; b) R. Liu, W. C. Still, *Tetrahedron Lett.* **1993**, *34*, 2573 – 2576; c) S. D. Erickson, J. A. Simon, W. C. Still, *J. Org. Chem.* **1993**, *58*, 1305 – 1308; d) M. R. Carrasco, W. C. Still, *Chem. Biol.* **1995**, *2*, 205 – 212; e) A. Borchardt, W. C. Still, *J. Am. Chem. Soc.* **1994**, *116*, 7467 – 7468.

[57] F. Gasparrini, D. Misiti, C. Villani, *J. Org. Chem.* **1995**, *60*, 4314 – 4315.

[58] P. E. J. Sanderson, J. D. Kilburn, W. C. Still, *J. Am. Chem. Soc.* **1989**, *111*, 8314 – 8315.

[59] R. Liu, P. E. J. Sanderson, W. C. Still, *J. Org. Chem.* **1990**, *55*, 5184 – 5186.

[60] R. J. Pieters, J. Cuntze, M. Bonnet, F. Diederich, *J. Chem. Soc. Perkin Trans. 2* **1997**, 1891 – 1900.

[61] J. Dowden, P. D. Edwards, S. S. Flack, J. D. Kilburn, *Chem. Eur. J.* **1999**, *5*, 79 – 89.

[62] W. C. Still, *Acc. Chem. Res.* **1996**, *29*, 155 – 163.

[63] D. W. Christianson, *Acc. Chem. Res.* **1989**, *22*, 62 – 69.

[64] D. H. Williams, B. Bardsley, *Angew. Chem.* **1999**, *111*, 1264 – 1286; *Angew. Chem. Int. Ed.* **1999**, *38*, 1173 – 1193.

[65] H. R. Perkins, *Biochem. J.* **1969**, *111*, 195 – 205.

[66] For a review on synthetic receptors for carboxylic acids and carboxylates, see: R. J. Fitzmaurice, G. M. Kyne, D. Douheret, J. D. Kilburn, *J. Chem. Soc. Perkin Trans. 1* **2002**, 841 – 864.

[67] For examples of amino acid-containing synthetic macrocycles used as receptors for carboxylate anions and carboxylic acids, see: a) T. K. Chakraborty, S. Tapadar, T. V. Raju, J. Annapurna, H. Singh, *Synlett* **2004**, 2484 – 2488; b) X. Yang, X. Wu, M. Fang, Q. Yuan, E. Fu, *Tetrahedron: Asymmetry* **2004**, *15*, 2491 – 2497; c) Q. Yuan, E. Fu, X. Wu, M. Fang, P. Xue, C. Wu, J. Chen, *Tetrahedron Lett.* **2002**, *43*, 3935 – 3937; d) A. Tanaka, S. Fujiyoshi, K. Motomura, O. Hayashida, Y. Hisaeda, Y. Murakami, *Tetrahedron* **1998**, *54*, 5187 – 5206; e) O. Hayashida, A. Tanaka, S. Fujiyoshi, Y. Hisaeda, Y. Murakami, *Tetrahedron Lett.* **1997**, *38*, 1219 – 1222.

[68] F. Sansone, L. Baldini, A. Casnati, M. Lazzarotto, F. Ugozzoli, R. Ungaro, *Proc. Natl. Acad. Sci. USA* **2002**, *99*, 4842 – 4847.

[69] a) A. Casnati, M. Fabbi, N. Pelizzi, A. Pochini, F. Sansone, R. Ungaro, E. Di Modugno, G. Tarzia, *Bioorg. Med. Chem. Lett.* **1996**, *6*, 2699 – 2704; b) L. Frish, F. Sansone, A. Casnati, R. Ungaro, Y. Cohen, *J. Org. Chem.* **2000**, *65*, 5026 – 5030.

[70] For excellent reviews, see: a) C. A. Schalley, *Mass Spectrom. Rev.* **2001**, *20*, 253 – 309; b) C. A. Schalley, *Int. J. Mass Spectrom.* **2000**, *194*, 11 – 39.

[71] a) R. M. Evans, *Science* **1988**, *240*, 889 – 895; b) F. J. Zeelen in *Medicinal Chemistry of Steroids*, Elsevier, Amsterdam, **1990**, pp. 15 – 42.

[72] F. Schroeder, P. Butko, G. Nemecz, T. J. Scallen, *J. Biol. Chem.* **1990**, *265*, 151 – 157.

[73] Y. Murakami, O. Hayashida, T. Ito, Y. Hisaeda, *Chem. Lett.* **1992**, 497 – 500.

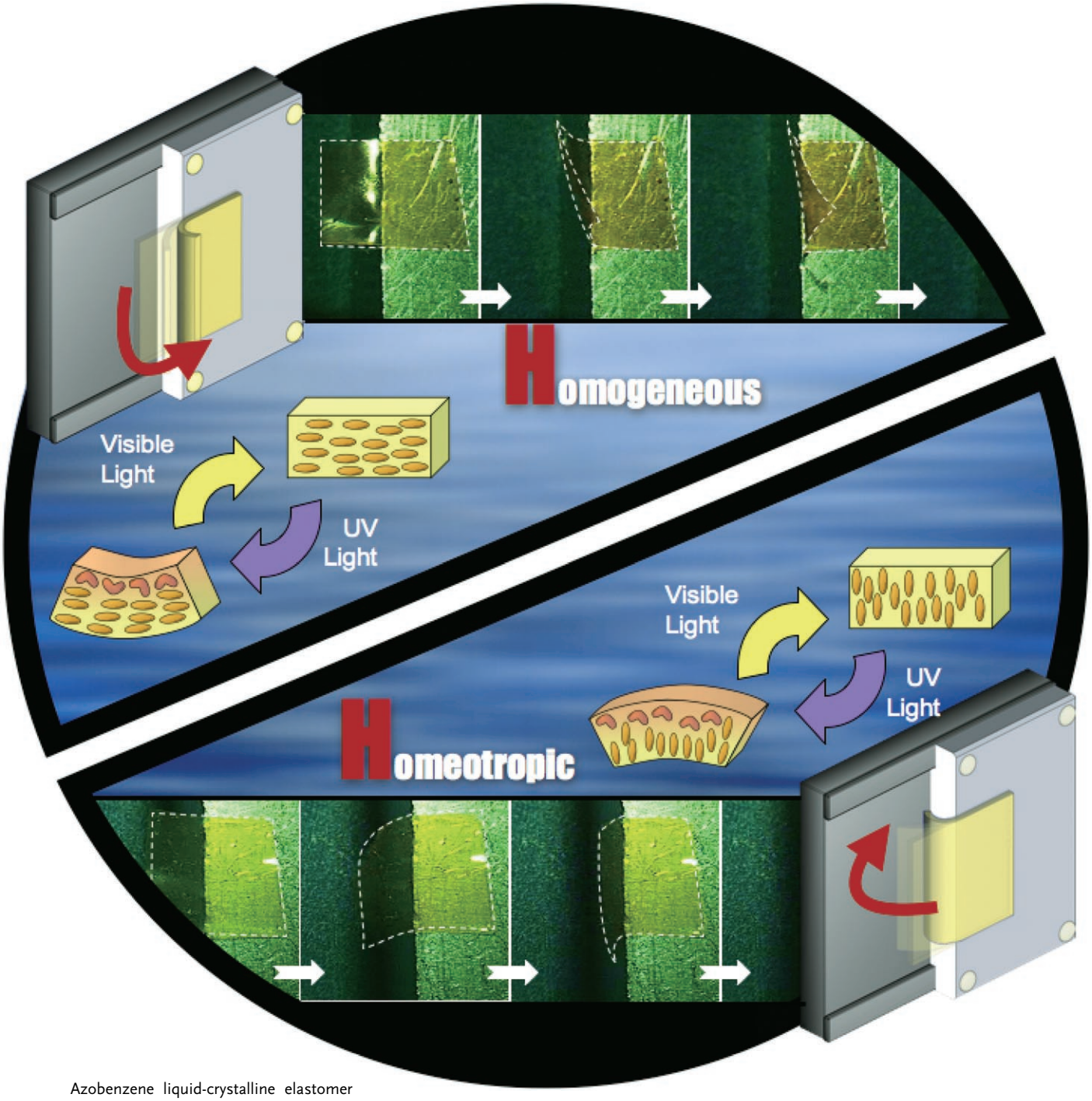
[74] For further applications of the same type of macrocycles, see: O. Hayashida, K. Ono, Y. Hisaeda, Y. Murakami, *Tetrahedron* **1995**, *51*, 8423 – 8436.

[75] a) J. F. Billing, U. J. Nilsson, *Tetrahedron* **2005**, *61*, 863 – 874; for the synthesis of related systems, see: b) J. F. Billing, U. J. Nilsson, *Tetrahedron Lett.* **2005**, *46*, 991 – 993; c) J. F. Billing, U. J. Nilsson, *J. Org. Chem.* **2005**, *70*, 4847 – 4850.

© 2006 Wiley-VCH Verlag GmbH & Co. KGaA, Weinheim

Communications

DOI: 10.1002/anie.200503684



Azobenzene liquid-crystalline elastomer films with two types of mesogen alignment, parallel (homogeneous) and normal (homeotropic) to the film surface, have been prepared by photopolymerization. T. Ikeda and co-workers discuss how the alignment of the mesogens dictates the bending behavior of the films on irradiation with UV/Vis light in their Communication on the following pages.

WILEY InterScience DISCOVER SOMETHING GREAT
© 2006 Wiley-VCH Verlag GmbH & Co. KGaA, Weinheim

Liquid Crystals

DOI: 10.1002/anie.200503684

How Does the Initial Alignment of Mesogens Affect the Photoinduced Bending Behavior of Liquid-Crystalline Elastomers?

*Mizuho Kondo, Yanlei Yu, and Tomiki Ikeda**

The development of actuators that show bending movement is of increasing interest. The bending movement is usually induced by an asymmetric contraction or expansion in the materials.[1–4] This type of actuator has more advantages than the actuators that show only two-dimensional movements, such as expansion and contraction, from the viewpoint of precise three-dimensional actuation and long lifetime owing to small deformation for the bending action. Because of these unique properties, the bending actuators are expected to be used for cantilevers, micropumps, and many other micromechanical applications.

Various materials have been reported as the bending actuators, such as piezoelectric transducers,[5] shape-memory alloys,[6] and polymers.[2] In comparison with other materials, the polymer actuators are much softer, lighter, and highly processible, which makes them easily made into various shapes; consequently, studies have been performed on the actuation of polymer materials and many applications have been proposed.[7] In addition, the bending of most polymer actuators, such as conducting polymers is driven by electrical energy; thus, these materials require wires to acquire electrical power.[3] On the other hand, elastomeric polymers, including gels and shape-memory polymers, can undergo mechanical actuation in response to various physical stimuli, such as pH,[8] solvent composition,[9] heat,[10–12] and light.[13,14]

Light can be controlled remotely and rapidly as an external stimulus, so it is of great importance in developing simple, efficient, and compact elastomeric polymer actuators that can be driven by light. It is known that liquid-crystalline elastomers (LCEs) exhibit a spontaneous contraction along the director axis when heated above their nematic (N)–isotropic (I) phase-transition temperatures.[15–17] On the other hand, when azobenzene chromophores are incorporated into LCEs, they can undergo the contraction isothermally because of the change in alignment order by light.[18–20] Furthermore, as the extinction coefficient of the azobenzene moieties at approximately 360 nm is large (about $2.0 \times 10^4\ L\,mol^{-1}\,cm^{-1}$) and more than 99% of the incident photons are absorbed by the surface with a thickness of less than 1 μm, LCE films with a high concentration of azobenzene moieties can generate an alignment change only in the film surface upon exposure to actinic UV light. As a result, an uneven distribution of the anisotropic deformation is formed along the film normal and the bending action can be realized in the film. Previously, we found that monodomain and polydomain LCE films showed different bending behavior: the bending of the former took place just along the alignment direction of the mesogens,[21] while in the latter the bending in any direction could be evoked.[22] These results indicate that the initial alignment of photoactive mesogens strongly affects the bending behavior of the LCE films. In this study, therefore, we explored the effect of the initial alignment of the azobenzene mesogens on the bending behavior of the LCE films. For this purpose, we prepared LCE films with two extreme alignment modes, parallel (homogeneous) and normal (homeotropic) to the film surface, and investigated their photoresponsive behavior in detail.

The structures of the monofunctional LC monomer 6-4-(4-hexyloxyphenylazo)phenoxyhexyl acrylate (A6AB6) and difunctional monomer 4,4′-bis[6-(acryloyloxy)hexyloxy]azobenzene (DA6AB) used in this study are shown in Figure 1a.

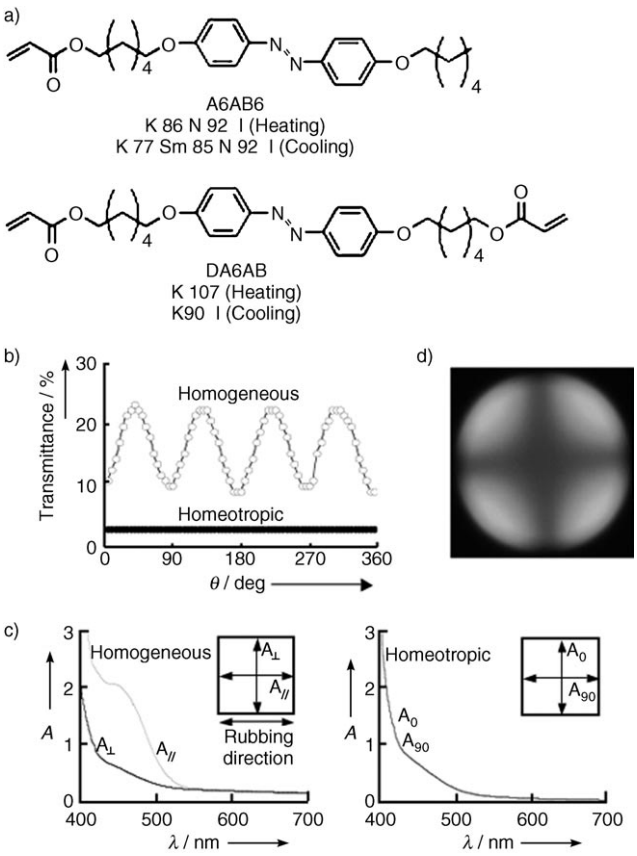


Figure 1. Structures of the LC monomer and cross-linker used in this study (a), and optical properties of the homogeneous and homeotropic films analyzed by POM (b), polarized UV/Vis absorption spectroscopy (c), and conoscopic observation by POM (d). Thickness of the films: 10 μm.

[*] M. Kondo, Prof. Dr. T. Ikeda
Chemical Resources Laboratory
Tokyo Institute of Technology, R1–11
4259 Nagatsuta, Midori-ku, Yokohama 226-8503 (Japan)
Fax: (+81) 45-924-5275
E-mail: tikeda@res.titech.ac.jp
Prof. Dr. Y. Yu
Department of Materials Science
Fudan University, 220 Handan Road
Shanghai 200433 (China)

Supporting information for this article is available on the WWW under http://www.angewandte.org or from the author.

© 2006 Wiley-VCH Verlag GmbH & Co. KGaA, Weinheim

The mesomorphic properties of the monomers were studied by polarized-light optical microscopy (POM) and differential scanning calorimetry (DSC; see the Experimental Section). The typical schlieren texture of an N phase was observed at 86 °C for A6AB6, and isotropization occurred at 92 °C upon heating. When cooled from the I phase, the N phase appeared at 92 °C and a monotropic smectic (Sm) phase at 85 °C. Crystallization started at 77 °C. However, DA6AB did not show any mesomorphism.

It was found by DSC studies that the glass-transition temperature (T_g) of the LCE films appeared at approximately 60 °C, and the DSC curve also exhibited a broad endothermic peak at approximately 147 °C, which was assigned to the LC–I phase transition. The optical anisotropy in the LCE films was evaluated at room temperature by measuring the transmittance of the probe light through crossed polarizers with a sample film between them as a function of the rotation angle (Figure 1b). For the homogeneous films, the rotation angle indicates the direction of the polarizer with respect to the rubbing direction of the alignment layers. The regular maximum and minimum values with 90° separations show that the azobenzene mesogens in the homogeneous films are preferentially aligned along the rubbing direction of the alignment layers. On the other hand, the transmittance was quite low ($<3\%$) in the homeotropic films and showed no angular dependence.

We also investigated the alignment behavior of the azobenzene mesogens by polarized absorption spectroscopy (Figure 1c). In the homogeneous films, $A_{\parallel}$ and $A_{\perp}$ are the absorbance measured with light polarized parallel and perpendicular to the rubbing direction of the alignment layers, respectively. In the homeotropic films, the polarization directions of the measurement beam for A_0 and A_{90} were perpendicular to each other. It is clear that the homogeneous films show high dichroism along the alignment direction, whereas the homeotropic films exhibit low absorption and no dichroism. In addition, the conoscopic observation of the homeotropic films by POM showed a dark cross image (Figure 1d). The cross point represents the optic axis of the LC phase; therefore, it is clear that the azobenzene mesogens are aligned normal to the film surface in the homeotropic films.

We observed the photoinduced-bending behavior of the LCE films under the experimental setup shown in Figure 2a. A part of a free-standing LCE film was pasted onto an aluminum block, heated by a hot stage, and irradiated with unpolarized UV light. We set the film vertically to eliminate the influence of gravity. When the homogeneous film was exposed to UV light at 366 nm, the film bent toward the irradiation direction of the actinic light along the alignment direction (see Figure 2b and the Supporting Information). On the other hand, when the homeotropic film was exposed to the actinic light, it bent away from the actinic light source (see Figure 2c and the Supporting Information). We observed completely different bending behavior in the LCE films with different alignment of azobenzene mesogens. Additionally, both the homogeneous and homeotropic films reverted to the initial flat states when irradiated with visible light at >540 nm.

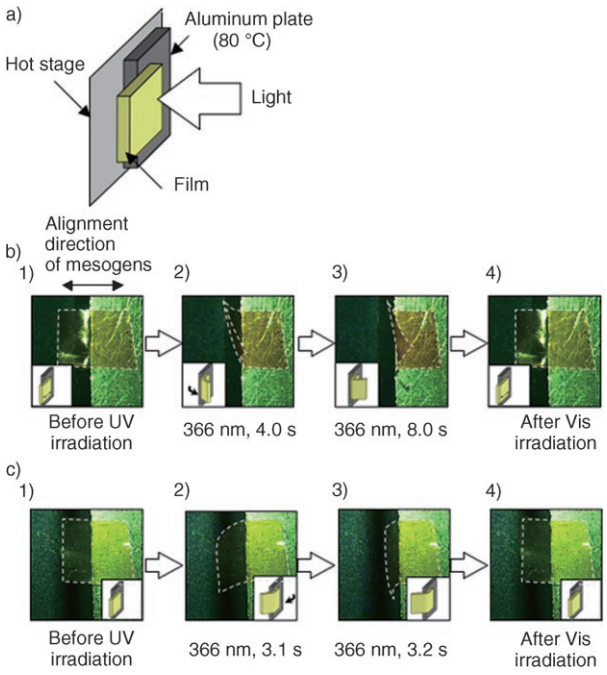


Figure 2. Schematic illustration of the experimental setup (a) and photographs of the homogeneous film (b) and the homeotropic film (c) that exhibits photoinduced bending and unbending behavior. The white dash lines show the edges of the films and the inset of each photograph is a schematic illustration of the film state. The intensity of 366 nm light was 50 mW cm^{-2}. Size of the films: 4 mm × 4 mm × 20 μm. Vis = visible.

To observe the bending behavior of the homeotropic film in a more free-standing state, we set the film on a copper stick fixed to a copper plate, with which the temperature of the film was controlled (Figure 3a). When the film was irradiated with

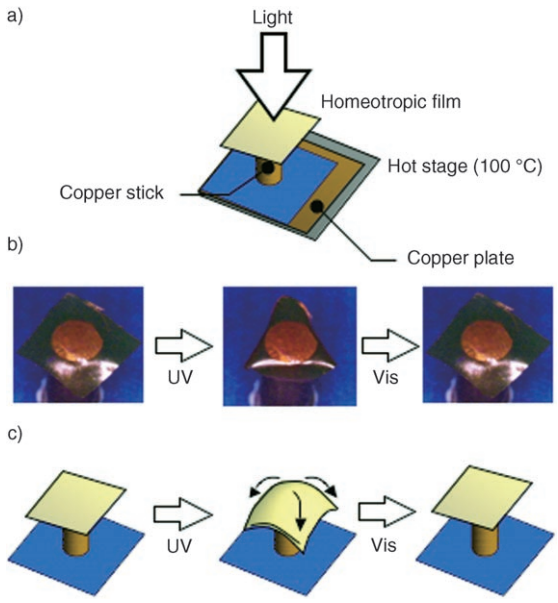


Figure 3. Schematic illustration of the experimental setup (a), photographs of the bending behavior of the homeotropic film (b), and schematic illustration of the film state (c). The intensity of 366 nm light was 35 mW cm^{-2}. Size of the film: 5 mm × 5 mm × 20 μm.

 © 2006 Wiley-VCH Verlag GmbH & Co. KGaA, Weinheim

366 nm light, all sides of the film bent away from the actinic light source simultaneously until they wrapped around the top of the copper stick (Figure 3b). This behavior indicates that the bending of the homeotropic film occurs isotropically without a preferential direction (Figure 3c), in a completely opposite way from the homogeneous film whose bending takes place anisotropically only along the alignment direction of mesogens.

A plausible mechanism of the bending behavior of the homogeneous and homeotropic films is illustrated in Figure 4a. It has been known that the irradiation of UV light gives rise to *trans–cis* isomerization and alignment change of the azobenzene mesogens in LCEs. In the homogeneous films, as the azobenzene mesogens are aligned parallel to the rubbing direction, an anisotropic contraction is generated along this direction upon UV-light irradiation (Figure 4a(1)). On the other hand, the alignment direction of the azobenzene mesogens in the homeotropic films is perpendicular to the film surface; thus, exposure to UV light induces an isotropic expansion (Figure 4a(2)). In addition, because of the high concentration of the azobenzene moieties in both LCE films and the high extinction coefficient of the azobenzene moieties at the irradiation wavelength, the actinic UV light hardly permeates through either film. As a result, an uneven distribution of anisotropic deformation is generated along the film normal in both films: contraction of the surface layer in the homogenous film while expansion of the surface layer occurs in the homeotropic film. This change in the mode of deformation leads to the bending behavior in a completely opposite direction.

The influence of temperature and light intensity on the bending behavior was examined by measuring the time taken by both films to bend by 90°. It was observed that the bending was accelerated by increasing the temperature and the light intensity.

To confirm the mechanism of bending in these two films, we measured the mechanical force generated from photoirradiation by thermomechanical analysis. As shown in Figure 4b(1), a film was first fixed by clamping both ends of the film and heated to 75 °C, which is higher than the T_g value of the film. An external force was loaded onto the film to keep the length of the film unchanged. The stretching direction was parallel to the alignment direction for the homogeneous film. Upon irradiation of UV light, the load of the homogeneous film increased from approximately 120 to 140 kPa after photoirradiation for 10 minutes (Figure 4b(2)). On the contrary, the load of the homeotropic film decreased from approximately 120 to 110 kPa after photoirradiation for 10 minutes (Figure 4b(3)). These results clearly indicate that the surface region in the homeotropic film expands, while that in the homogeneous film contracts along the alignment direction. In addition, it was found that the time taken for the homeotropic film to reach the maximum force was faster than that of the homogeneous film, presumably because the absorbance of the homeotropic film is lower than that of the homogeneous film. Thus, the light penetrates the film more deeply in the homeotropic film than the homogeneous film and the change in alignment of mesogens is induced in a thicker layer in the former than in the latter, which would lead to the observed difference in the photomechanical effect in the two films.

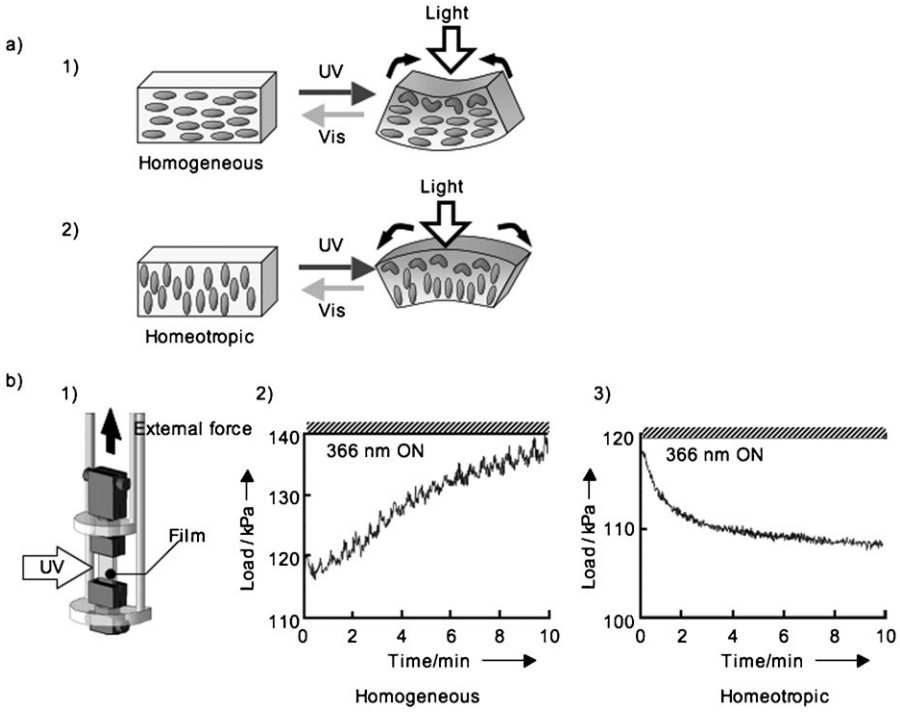


Figure 4. Schematic illustration of the bending mechanism in the homogeneous and the homeotropic films (a) and force generated by photoirradiation (b). Schematic illustration of the experimental setup (1), the force generated upon exposure to UV light at 366 nm (4.8 mW cm^{-2}) in the homogeneous film (2), and the homeotropic film (3). Size of the films: 4.5 mm × 5 mm × 20 μm.

In conclusion, the initial alignment of photoactive mesogens significantly affects the bending behavior of the LCE films: the homogeneous films bent toward the irradiation direction of the actinic UV light, while the homeotropic films bent away from the light source. The change in the photoinduced bending behavior is assumed to arise from the different mode of deformation of the surface layer of the two films. The surface of the homogeneous films contracts and the load on the films increases, while the surface of the homeotropic films expands and the load on the films decreases upon exposure to UV light.

 © 2006 Wiley-VCH Verlag GmbH & Co. KGaA, Weinheim

Experimental Section

LC monomer A6AB6 and cross-linker DA6AB were prepared according to a previously reported method.[23] The LCE films were prepared by in situ photopolymerization of a mixture of A6AB6 and DA6AB (90:10 (mol/mol)) containing 1 mol% of photoinitiator (Ciba Specialty, Irgacure 784). First, the melt of the mixture was injected into a glass cell, which had been treated for homogeneous or homeotropic alignment. The homogeneous cell was coated with polyimide alignment layers that had been rubbed to align LC mesogens, while the homeotropic cell was treated with *n*-octadecyltrimethoxysilane. After the sample was cooled down slowly ($0.5\,^{\circ}C\,min^{-1}$) to a polymerization temperature at 88 °C (in the N phase), photoirradiation was performed at >540 nm (547 nm, $3\,mW\,cm^{-2}$) with a 500-W high-pressure mercury lamp through glass filters (Toshiba, Y-52 + IRA-25) for 2 h. The LCE films were taken off from the cells after polymerization.

The thermodynamic properties of the monomers and the LCE films were determined by DSC (Seiko I&E, SSC-5200 and DSC220C) at heating and cooling rates of $2\,^{\circ}C\,min^{-1}$ for the monomers and $10\,^{\circ}C\,min^{-1}$ for the films. At least three scans were performed to check the reproducibility. The films were washed with $CHCl_3$ to completely remove the starting monomers and dried under reduced pressure. The mesomorphic properties and the phase-transition behavior were examined with a polarizing optical microscope (POM; Olympus, BH-2) equipped with a Mettler hot stage (models FP-90 and FP-82). The polarized UV spectra of the films were measured at room temperature with a UV/Vis absorption spectrometer (Jasco, V-550). Thermomechanical analysis was performed in a stretch mode under an external tension at a constant temperature, using a thermomechanical analyzer (TMA; Simadzu, TMA-60).

Received: October 18, 2005
Published online: January 20, 2006

Keywords: alignment · azobenzene derivatives · elastomers · liquid crystals · surface chemistry

[1] M. V. Gandhi, B. S. Thompson, *Smart Materials and Structures*, Chapman and Hall, London, **1992**.
[2] Y. Osada, D. E. E. Derossi, *Polymer Sensors and Actuators*, Springer, Heidelberg, **2000**.
[3] E. Smela, *Adv. Mater.* **2003**, *15*, 481 – 494.
[4] R. Pelrine, R. D. Kornbluh, Q. Pei, J. Joseph, *Science* **2000**, *287*, 836 – 839.
[5] G. H. Haertling, *Proc. SPIE-Int. Soc. Opt. Eng.* **1997**, *3040*, 81 – 92.
[6] A. D. Johnson, V. Martnov, V. Gupta, *Proc. SPIE-Int. Soc. Opt. Eng.* **2001**, *4557*, 341 – 351.
[7] R. D. Kornbluh, R. Pelrine, Q. Pei, R. Heydt, S. Stanford, S. Oh, J. Eckerle, *Proc. SPIE-Int. Soc. Opt. Eng.* **2002**, *4698*, 254 – 270.
[8] M. Torres-Lungo, N. A. Pappas, *Macromolecules* **1997**, *30*, 6646 – 6651.
[9] Z. Hu, X. Zhang, Y. Li, *Science* **1995**, *269*, 525 – 527.
[10] H. Wermter, H. Finkelmann, *Liquid Crystalline Elastomers as Artificial Muscles*, http://www.e-polymers.org Report No. 013, **2001**.
[11] D. L. Thomsen III, P. Keller, J. Naciri, R. Pink, H. Jeon, D. Shenoy, B. R. Ratna, *Macromolecules* **2001**, *34*, 5868 – 5875.
[12] J. Naciri, A. Srinvasan, H. Jeon, N. Nikolov, P. Keller, B. R. Ratna, *Macromolecules* **2003**, *36*, 8499 – 8505.
[13] A. Lendlein, J. Jiang, O. Jüngerand, R. Langer, *Nature* **2005**, *434*, 879 – 882.
[14] S. V. Ahir, E. M. Terentjev, *Nat. Mater.* **2005**, *4*, 491 – 495.
[15] M. Warner, E. M. Terentjev, *Liquid Crystal Elastomers*, Oxford University Press, Oxford, UK, **2003**.
[16] P.-G. de Gennes, M. Hebert, R. Kant, *Macromol. Symp.* **1997**, *113*, 39 – 49.
[17] P. Xie, R. Zhang, *J. Mater. Chem.* **2005**, *15*, 2529 – 2550.
[18] H. Finkelmann, E. Nishikawa, G. G. Pereira, M. Warner, *Phys. Rev. Lett.* **2001**, *87*, 015501.
[19] M. Camacho-Lopez, H. Finkelmann, P. Palffy-Muhoray, M. Shelley, *Nat. Mater.* **2003**, *2*, 307 – 310.
[20] M.-H. Li, P. Keller, B. Li, X. Wang, M. Brunet, *Adv. Mater.* **2003**, *15*, 569 – 572.
[21] T. Ikeda, M. Nakano, Y. Yu, O. Tsutsumi, A. Kanazawa, *Adv. Mater.* **2003**, *15*, 201 – 205.
[22] Y. Yu, M. Nakano, T. Ikeda, *Nature* **2003**, *425*, 145.
[23] D. Caretti, A. S. Angeloni, C. Carlini, M. Laus, E. Chiellini, G. Galli, A. Altomare, R. Solaro, *Liq. Cryst.* **1989**, *4*, 513 – 527.

 © 2006 Wiley-VCH Verlag GmbH & Co. KGaA, Weinheim

Liquid Crystals

DOI: 10.1002/anie.200503767

Circular-Polarization-Induced Enantiomeric Excess in Liquid Crystals of an Achiral, Bent-Shaped Mesogen

*Suk-Won Choi, Tatsuya Izumi, Yusuke Hoshino, Yoichi Takanishi, Ken Ishikawa, Junji Watanabe, and Hideo Takezoe**

Achiral, bent-shaped mesogens have opened up a new era in liquid-crystal science with respect to polarity and chirality.[1,2] Bent-shaped mesogens are known to segregate into two self-assembling, chiral domains in which the molecules are believed to have chiral conformations.[3] In this sense the system is regarded as a racemate, despite being composed of achiral molecules.[4] Hence, the numbers of the two enantiomers are equivalent and the enantiomeric excess is zero in an unperturbed state. However, the system is not necessarily racemic because an imbalance of chirality can be produced by an external chiral stimulus. At least two methods have been elucidated for this: 1) a small amount of chiral dopant is effective in inducing almost 100% *ee*,[5] and 2) a chiral surface has been successfully used to induce a finite *ee*.[6] Herein we demonstrate another method that does not involve chiral molecular species. Novel, achiral, bent-shaped dimers with photochromic moieties on both side wings form large, chiral domains enantioselectively when the samples are cooled from the conventional anticlinic SmC_A phase to a low-temperature B_X phase similar to B_4 while being irradiated with circularly

[*] S.-W. Choi, T. Izumi, Y. Hoshino, Dr. Y. Takanishi, Prof. Dr. K. Ishikawa, Prof. Dr. J. Watanabe, Prof. Dr. H. Takezoe
Department of Organic and Polymeric Materials
Tokyo Institute of Technology
O-okayama, Meguro-ku, Tokyo 152-8552 (Japan)
Fax: (+81) 3-5734-2876
E-mail: htakezoe@o.cc.titech.ac.jp

WILEY InterScience DISCOVER SOMETHING GREAT
© 2006 Wiley-VCH Verlag GmbH & Co. KGaA, Weinheim

polarized light (CPL). The enantioselectivity can be controlled by the handedness of the CPL.

Many chemical and physical systems can occur in two forms that are mirror images of each other. This phenomenon, known as chirality, is found in biological molecular systems because of enantioselective interactions.[7] Thus, the control of chirality is important in science as well as technology,[8–10] and several reactions can proceed enantioselectively if chiral dopants are involved[11] or if an external, chiral bias is present.[7,12,13] One such external bias is irradiation with CPL, and deracemization has been reported in several systems upon CPL irradiation.[14–18] However, the induced *ee* was rather low (a few percent). We demonstrate herein that irradiation with CPL can induce a large imbalance in two chiral domains, leading to large *ee* values in an achiral, bent-shaped mesogenic dimer with azo linkages at both side wings.

We used the bent-core dimer α,ω-bis(4-alkoxyazobenzene-4′-carbonyloxy)alkene (12OAz5AzO12; Figure 1), in

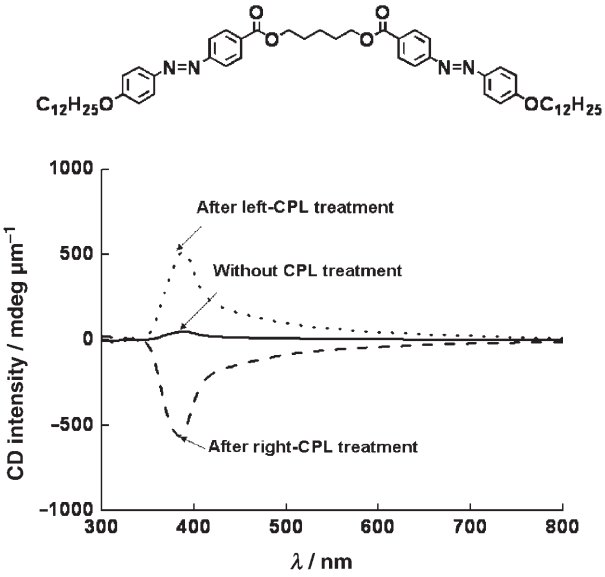


Figure 1. The chemical structure of 12OAz5AzO12 and three typical CD spectra of the B_X phase of achiral, bent-shaped 12OAz5AzO12. The spot size for the CD measurements covers the whole area irradiated by the CPL (10 mm).

which two azobenzene moieties with alkoxy tails are linked by a polymethylene spacer (12 and 5 are the number of carbon atoms in the alkoxy tails and the central spacer, respectively). The detailed synthesis and properties of the homologous molecules have been described elsewhere.[19] This compound shows the following phase sequence: isotropic (108 °C)–SmC_A (94 °C)–B_X. The assignment of the higher-temperature phase to the smectic C_A (SmC_A) phase[20] was made by texture observations: spherelike textures coalesce into the well-known, fan-shaped texture upon cooling from the isotropic phase. A clear birefringence with Schlieren textures having singularities of $s = 1$ and 1/2 was also observed.[21] The actual structure is not the conventional SmC_A,[20] but is an interdigitated layer with a periodicity of half a molecular length.[22] The low-temperature B_X phase is a solidlike phase that is considerably different from a crystal in several aspects, like the B_4 phase of classical bent-core (banana-shaped) molecules.[23] The most notable feature is that spontaneous chiral segregation occurs in the B_X phase, in which no layer chirality[2] exists because of the nontilted phases. A chiral conformation[3–5] is the origin of this type of chiral domain. In the SmC_A phase, a spontaneous segregation into two chiral domains was not observed.

The *ee* values were determined by circular dichroism (CD) measurements and direct polarizing microscope observations using 2-μm-thick cells. CD measurements were carried out first to confirm that macroscopic chirality occurs in the B_X phase. Figure 1 shows three typical CD spectra observed for the B_X phase after three different treatments. Without CPL irradiation, only a negligible CD signal ($\Delta\varepsilon \leq 50\ \mathrm{mdeg\,\mu m^{-1}}$) was observed. However, remarkably strong CD signals were observed at about 380 nm after right-CPL or left-CPL irradiation through a 10-mm-diameter aperture for 1 h. These CD signals are due to an induced circular dichroism (CD) and indicate the nucleation of macroscopic chiral domains. A positive intensity is induced by left-CPL, whereas a negative signal is induced by right-CPL. The CD spectra were recorded 10 times after heating the cell to form the isotropic liquid. Without the CPL stimuli, a CD with negligible positive or negative signals was observed, whereas the B_X phase exhibited large CD intensities ($\Delta\varepsilon \geq 300\ \mathrm{mdeg\,\mu m^{-1}}$) with a negative (positive) sign after right-CPL (left-CPL) irradiation every time. Thus, an intrinsically macroscopic achiral system can be converted into a macroscopic, chiral system by a CPL stimulus.

Next, we directly observed the textures under a polarizing microscope. The existence of chiral domains in the B_X phase was confirmed by a conventional method whereby the two domains become apparent as bright and dark regions when one of the polarizers is rotated clockwise by a small angle ($\theta = 5°$) with respect to the crossed position. The brightness of the two domains interchanges when the polarizer is rotated counterclockwise. The textures of the cells are shown in Figure 2. In the B_X phase without the CPL stimulus the observed texture exhibits grainy domains segregated into (+) or (−) chiral domains of equal probabilities (Figure 2a), whereas the imbalance between these chiral domains becomes notable upon CPL irradiation (Figures 2b and 2c). Although the texture still includes two opposite chiral domains, an imbalanced domain with a size larger than a few millimeters can be prepared by CPL irradiation. Large, distinct (−) chiral domains with a large, negative CD peak are produced by right-CPL irradiation (Figure 2b), whereas large, distinct (+) chiral domains with a large, positive CD peak are nucleated by left-CPL irradiation (Figure 2c).

We also calculated the value of the induced enantioselectivity in the B_X phase of the 12OAz5AzO12 cell after CPL irradiation. This was done by two methods, namely direct texture observation and CD. Optical microphotographs of B_X were taken of a region including both (+) and (−) chiral domains after irradiation (Figure 3a). The ratio of the (+) and (−) chirality domains was analyzed by using a computer software package (Adobe Photoshop Elements 2.0). Image processing allowed the overall domain to be assigned clearly

 © 2006 Wiley-VCH Verlag GmbH & Co. KGaA, Weinheim

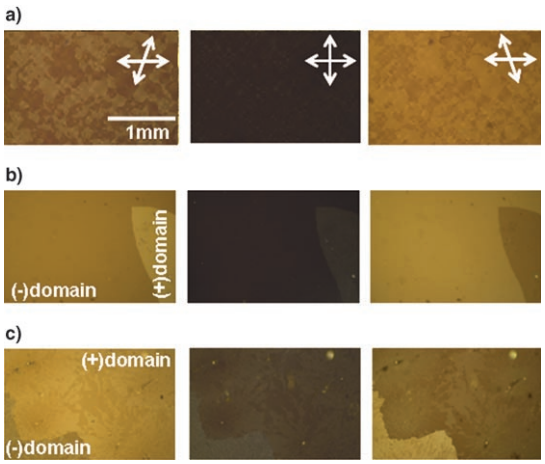


Figure 2. Optical microphotographs of the B_X phase of the achiral 12OAz5AzO12 cell under decrossed and crossed polarizers: a) without CPL treatment, b) after right-CPL treatment, and c) after left-CPL treatment. The arrows indicate the directions of the polarizers.

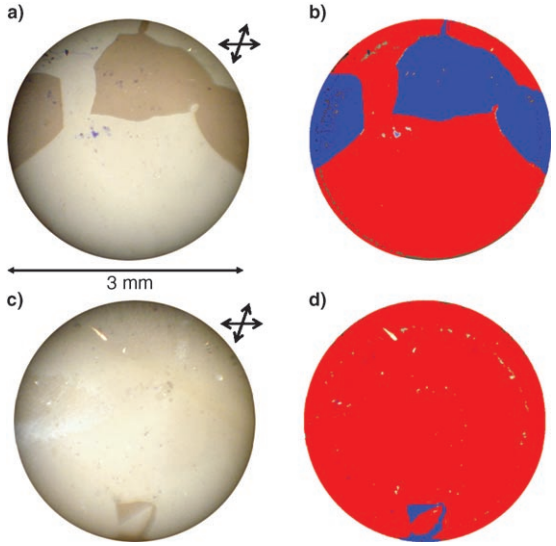


Figure 3. a) An overall view taken with an optical microscope showing the texture of B_X obtained by left-CPL stimuli (30 $mW cm^{-2}$ for 60 minutes) of an area with a diameter of 3 mm where the value of the observed CD intensity is about +1000 mdeg μm^{-1}. b) Image processing allows the overall domain to be divided into two colors (red and blue) indicating the (+) and (−) chiral domains, respectively. c) An almost purely chiral domain 3 mm in diameter and d) its processed image. The arrows indicate the directions of the polarizers.

to two colors—red and blue—corresponding to the (+) and (−) chiral domains, respectively (Figure 3b). A ratio of 70:30 (i.e., 40% *ee*) can be easily obtained by counting the number of red and blue pixels. If we choose appropriate chiral domains, such as those shown in Figures 3c and 3d, we find domains with almost 100% *ee*. The CD intensity of these homochiral domains exceeds the detection limit of our CD instrument (>2000 mdeg). Thus, we can conclude that a remarkably large *ee* values can be induced by CPL. Optimization of the irradiation and cell conditions should produce a homochiral domain in the whole of the irradiated area of this system.

This is the first report of a large *ee* value being attained and visualized and where macroscopic chirality is controllable in achiral, bent-shaped molecular systems by irradiation with CPL. However, a basic question arises: How can CPL stimuli, particularly exposure of a higher-temperature, liquid-crystalline SmC_A phase, give rise to enantioselectivity in a B_X phase with two chiral domains and induce a large *ee* value in achiral, bent-shaped 12OAz5AzO12 molecules? CPL is a chiral electromagnetic radiation that is theoretically able to induce enantioselective conversion.[13] Three types of asymmetric photoreactions are known to be effected by CPL irradiation: 1) preferential photodestruction, in which one of the enantiomers of a racemate is preferentially destroyed and the remaining enantiomer is therefore enriched,[14] 2) photoresolution, namely a deracemization of photochemically interconvertible enantiomers,[15,16] and 3) asymmetric photosynthesis, namely an enantioselective photochemical formation of an optically active compound from a prochiral starting material.[17,18] However, the *ee* values in these cases are very low (a few percent at most),[13] except for the photodestructive reaction.[14]

Bent-shaped molecules like the one used here can be regarded as racemic mixtures rather than as an achiral system because of their spontaneous segregation into chiral domains. Therefore, our asymmetric photoreaction by CPL irradiation can be seen as a kind of photoresolution. Furthermore, this chirality is not inherent in phases formed from bent-shaped molecules and can be switched easily to the opposite by changing the external chiral stimulus; chiral *S* and *R* conformers cannot be interchanged. In this sense, the present enantioselectivity is unique.

The higher-temperature, liquid-crystalline SmC_A phase is a fluid phase in which two axially twisted conformers interchange such that the system is either achiral or racemic. Photochromic azobenzenes have been utilized extensively in supramolecular chemistry, catalysis, and materials science because of their efficient, reversible *trans–cis* photoisomerization, which leads to large changes in molecular geometry.[24] It is well known that rod-like, azo-containing molecules tend to reorient under linearly polarized light irradiation to the direction perpendicular to the polarization.[25] The same scenario may apply here: preferential conversion into a particular chiral conformation could occur under CPL irradiation because of a finite CD (absorption difference) between two chiral conformations. This preference triggers and accelerates the conversion and is fixed when the system is brought into the B_X phase, where spontaneous chiral resolution takes place, meaning that a large imbalance of optical purity and high *ee* are induced by CPL irradiation. This CPL-induced enantioselectivity is observed only in systems containing azobenzene bonds, thus photochromic *trans–cis* isomerization is most important for this phenomenon. It is also notable that the enantioselectivity induced in the B_X phase can be maintained for several months at least at room temperature.

In conclusion, we have succeeded in obtaining a large imbalance in the two chiral domains and inducing large *ee* values in a B_X phase that is similar to the B_4 phase in classical bent-core (banana-shaped) molecules using circularly polar-

 © 2006 Wiley-VCH Verlag GmbH & Co. KGaA, Weinheim

ized light. This technique opens up the possibility of enantioselectively converting an achiral molecular system into a chiral system for practical use in functional materials. Our future goals include enantioselective syntheses in a chiral domain to provide a new method of photopolymerization in the B_X phase with high *ee* values that may lead to chiral films for chiral segregation.

Experimental Section

Sandwich cells were fabricated from fused-quartz slides without alignment treatments such as coating with an alignment layer or rubbing. The dimensions and thickness of the cell were about $1.2 \times 1.2\ cm^2$ and 2 μm, respectively. Irradiation was performed with light from a Mercury lamp after passing it through a Fresnel rhomb and an aperture with a diameter of 10 mm to produce circular polarization. Irradiation was performed at the absorption wavelength of *trans*-12OAz5AzO12 (365 nm; intensity $30\ mW\,cm^{-2}$). The temperature was adjusted within ±2 °C by a temperature control unit (Chino, DB1150). Better enantioselectivity control was achieved by irradiation of a heated cell (103 °C) in the SmC_A phase with right- or left-CPL for 1 h. Then, while maintaining the irradiation, the cell was allowed to cool to 80 °C, which is below the SmC_A–B_X phase-transition temperature, at more than $10\ K\,min^{-1}$.

The imbalance between the two chiral domains was evaluated by means of circular dichroism (CD) spectroscopic analysis (JASCO J-720WI) and direct observation of the texture under a polarizing microscope (Nikon, OPTIPHOT-POL). All evaluations were carried out at room temperature and atmospheric pressure.

Received: October 24, 2005
Published online: January 27, 2006

Keywords: azo compounds · chirality · chromophores · enantioselectivity · liquid crystals

[1] T. Niori, T. Sekine, J. Watanabe, T. Furukawa, H. Takezoe, *J. Mater. Chem.* **1996**, *6*, 1231 – 1233.
[2] D. R. Link, G. Natale, R. Shao, J. E. Maclennan, N. A. Clark, E. Korblova, D. M. Walba, *Science* **1997**, *278*, 1924 – 1927.
[3] H. Niwano, M. Nakata, J. Thisayukta, D. R. Link, H. Takezoe, J. Watanabe, *J. Phys. Chem. B* **2004**, *108*, 14889 – 14896.
[4] D. J. Earl, M. A. Osipov, H. Takezoe, Y. Takanishi, M. R. Wilson, *Phys. Rev. E* **2005**, *71*, 021706-1-11.
[5] J. Thisayukata, Y. Nakayama, S. Kawauchi, H. Takezoe, J. Watanabe, *J. Am. Chem. Soc.* **2000**, *122*, 7441 – 7448.
[6] K. Shiromo, D. A. Sahade, T. Oda, T. Nihira, Y. Takanishi, K. Ishikawa, H. Takezoe, *Angew. Chem.* **2005**, *117*, 1984 – 1987; *Angew. Chem. Int. Ed.* **2005**, *44*, 1948 – 1951.
[7] G. L. J. A. Rikken, E. Raupach, *Nature* **2000**, *405*, 932 – 935.
[8] C. Viedma, *Phys. Rev. Lett.* **2005**, *94*, 065504-1-4.
[9] J. J. D. de Jong, L. N. Lucas, R. M. Kellogg, J. H. van Esch, B. L. Feringa, *Science* **2004**, *304*, 278 – 281.
[10] J. M. Ribo, J. Crusats, F. Sagues, J. Claret, R. Rubires, *Science* **2001**, *292*, 2063 – 2066.
[11] G. Solladie, R. G. Zimmermann, *Angew. Chem.* **1984**, *96*, 335 – 349; *Angew. Chem. Int. Ed. Engl.* **1984**, *23*, 348 – 362.
[12] L. D. Barron, *Science* **1994**, *266*, 1491 – 1492.
[13] B. L. Feringa, R. A. van Delden, *Angew. Chem.* **1999**, *111*, 3624 – 3645; *Angew. Chem. Int. Ed.* **1999**, *38*, 3419 – 3438.
[14] T. Kawasaki, M. Sato, S. Ishiguro, T. Saito, Y. Morishita, I. Sato, H. Nishino, Y. Inoue, K. Soai, *J. Am. Chem. Soc.* **2005**, *127*, 3274 – 3275.
[15] K. S. Burnham, G. B. Schuster, *J. Am. Chem. Soc.* **1999**, *121*, 10245 – 10246.
[16] N. P. M. Huck, W. F. Jager, B. de Lange, B. L. Feringa, *Science* **1996**, *273*, 1686 – 1688.
[17] T. Fujiwara, N. Nanba, K. Hamada, F. Toda, K. Tanaka, *J. Org. Chem.* **1990**, *55*, 4532 – 4537.
[18] A. Moradpour, J. F. Nicoud, G. Balavoine, H. Kagan, G. Tsoucaris, *J. Am. Chem. Soc.* **1971**, *93*, 2353 – 2354.
[19] T. Niori, S. Adachi, J. Watanabe, *Liq. Cryst.* **1995**, *19*, 139 – 148.
[20] A. D. L. Chandani, E. Gorecka, Y. Ouchi, H. Takezoe, A. Fukuda, *Jpn. J. Appl. Phys., Part 1* **1989**, *28*, L1265 – L1268.
[21] Y. Takanishi, H. Takezoe, A. Fukuda, J. Watanabe, *Phys. Rev. B* **1992**, *45*, 7684 – 7689.
[22] S. W. Choi, M. Zennyoji, Y. Takanishi, H. Takezoe, T. Niori, J. Watanabe, *Mol. Cryst. Liq. Cryst.* **1999**, *328*, 185 – 192.
[23] J. Thisayukta, H. Takezoe, J. Watanabe, *Jpn. J. Appl. Phys., Part 1* **2001**, *40*, 3277 – 3287.
[24] H. Asanuma, T. Takarada, T. Yoshida, D. Tamaru, X. Liang, M. Komiyama, *Angew. Chem.* **2001**, *113*, 2743 – 2745; *Angew. Chem. Int. Ed.* **2001**, *40*, 2671 – 2673.
[25] W. M. Gibbons, P. J. Shannon, S. T. Sun, B. J. Swetlin, *Nature* **1991**, *351*, 49 – 50.

 © 2006 Wiley-VCH Verlag GmbH & Co. KGaA, Weinheim

Rotaxanes

DOI: 10.1002/anie.200502624

An Allosterically Regulated Molecular Shuttle**

Dana S. Marlin, Diego González Cabrera, David A. Leigh, and Alexandra M. Z. Slawin*

One of Nature's most effective ways of influencing function from afar is through allosteric control.[1] This occurs—most typically in proteins—when activity at a substrate-binding site is modulated by the complexation of an effector molecule or

[*] Dr. D. S. Marlin, D. González Cabrera, Prof. D. A. Leigh
School of Chemistry
University of Edinburgh
The King's Buildings
West Mains Road
Edinburgh EH9 3JJ (UK)
Fax: (+44) 131-667-9085
E-mail: David.Leigh@ed.ac.uk
Prof. A. M. Z. Slawin
School of Chemistry
University of St. Andrews
Purdie Building
St. Andrews
Fife KY16 9ST (UK)

[**] This work was supported by the European Union Future and Emerging Technology Program Hy3M and the EPSRC. D.S.M. is a Marie Curie Fellow; D.A.L. is an EPSRC Senior Research Fellow and holds a Royal Society–Wolfson Research Merit Award.

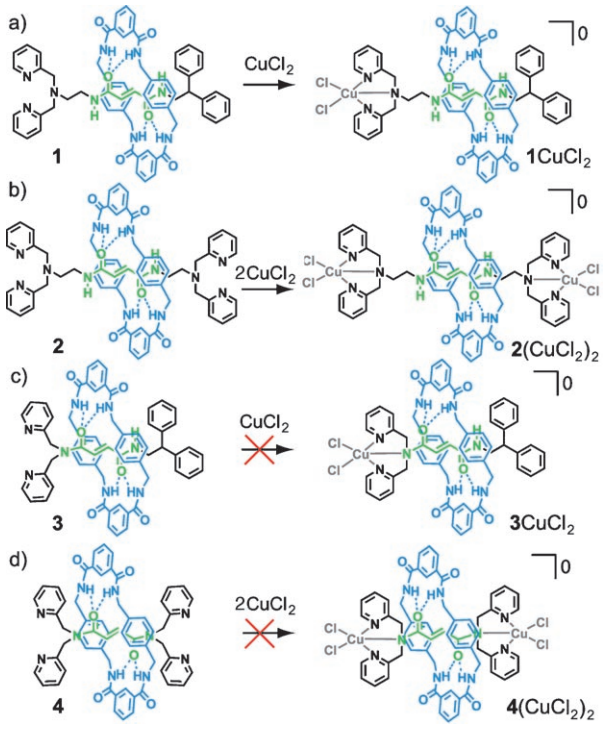
Supporting information for this article is available on the WWW under http://www.angewandte.org or from the author.

© 2006 Wiley-VCH Verlag GmbH & Co. KGaA, Weinheim

ion at a second site. The binding sites are frequently several nanometers apart, and communication between them is achieved through a variety of mechanisms, the details of which are not well understood but often involve multiple substrate-binding sites and cooperative complexation events that are accompanied by large amplitude movements of polypeptide chains and other molecular subunits.[2] However, to achieve any kind of distant control in response to binding in synthetic systems is far from trivial. Most of the artificial allosteric receptors developed to date feature one or more substrate-interaction sites directly conformationally coupled to an effector-binding site.[3] Herein, we report on a mechanically linked substrate/host ensemble (a [2]rotaxane), which contains two spatially and chemically distinct "substrate" hydrogen-bonding sites, only one of which is influenced by the coordination of a metal ion (the "effector") to an adjacent tridentate ligand fragment. The result is a stimuli-responsive molecular shuttle[4] that undergoes a large amplitude internal motion (change in the position and binding strength of the macrocycle), allosterically regulated through a small, but highly significant, conformational change brought about by complexation of a transition metal at the effector site.

The molecular shuttle allosteric control mechanism has its origins in anomalous behavior observed for some simple hydrogen-bonded rotaxanes that bear metal-chelating stoppers containing a bis(2-picolyl)amine (BPA)[5] moiety (Scheme 1). Rotaxanes **1** and **2**, in which the BPA unit is connected to the hydrogen-bonding groups of the thread by an ethylene spacer, react readily with various transition-metal salts including $CuCl_2$, which yields complexes **1**$CuCl_2$ and **2**$(CuCl_2)_2$, respectively (Scheme 1a and b). The X-ray crystal structures of **1**$CuCl_2$ and **2**$(CuCl_2)_2$ (Figure 1a and b) show the typical four intercomponent hydrogen bonds between the benzylamide groups of the macrocycle and the amide groups of the thread,[6] together with the predicted coordination of the BPA ligands to each metal ion in a tridentate fashion. However, to our surprise, rotaxanes **3** and **4**, in which the ethylene spacer is absent and the BPA unit is attached directly to the hydrogen-bonding station of the thread, were found *not* to react[7] with $CuCl_2$ or similar transition-metal salts even under forcing conditions (Scheme 1c and d). This behavior is in marked contrast to that of their parent threads, which react like rotaxanes **1** and **2** to give the expected coordination complexes, indicating that the reduced electron density on the nitrogen atom caused by the adjacent carbonyl group is not the reason for the lack of reaction of **3** and **4**.[5]

The X-ray crystal structures of **3** and **4** (Figure 1c–f) reveal the reason for their lack of reactivity. Although the macrocycles in **3** and **4** form hydrogen bonds to the thread through the four intercomponent hydrogen bonds (shown in the stick representation, Figure 1c and d) analogous to rotaxanes **1** and **2**, the pyridine arms of the BPA groups are forced close-to-parallel with the isophthalamide groups of the macrocycle (concomitantly forming favorable π–π-stacking interactions) to accommodate the ring on the hydrogen-bonding site. To chelate to a metal ion by using all three nitrogen atoms of the BPA group, the pyridine arms must twist orthogonally, causing them to enter space that is already occupied by the benzylamide macrocycle. However, the



Scheme 1. Rotaxanes **1**–**4** and their attempted complexation reactions with one (a, c) or two (b, d) equivalents of $CuCl_2$ in DMF at room temperature. Complexes **1**$CuCl_2$ and **2**$(CuCl_2)_2$ are formed in near-quantitative yield and were purified by recrystallization from CH_3CN/DMF;[8] **3**$CuCl_2$ and **4**$(CuCl_2)_2$ could not be detected even upon heating at 80 °C for 12 h.[7] The free threads of **1**–**4** each react readily with $CuCl_2$ in DMF at room temperature to form coordination complexes that are analogous to **1**$CuCl_2$ and **2**$(CuCl_2)_2$.

macrocycle physically has nowhere else to move to in either **3** or **4** (see the space-filling representations, Figure 1e and f) and so the conformational change required for the BPA group to chelate to a transition metal cannot take place in these short congested rotaxane structures.

The prospect of a situation where, despite binding at different sites, metal- and macrocycle-binding modes compete for the same 3D space led us to consider whether translocation of the macrocycle to a second hydrogen-bonding site on a thread could be induced by a metal-binding interaction. As a model we designed rotaxane **5** (Scheme 2), which contains three carbonyl hydrogen-bond acceptors on the thread in what can be viewed as an elongated hydrogen-bonding station (for clarity in interpreting the ^{1}H NMR spectra (Figure 2), one half of this unit is colored in green and the other in orange). With this extended station the macrocycle in **5** has space to occupy (and hydrogen-bonding partners) when a metal binds to, and rearranges the conformation of, the BPA-containing stopper. The solid-state structure of **5** (Scheme 2b) reveals that the macrocycle is bound to the central carbonyl group (O41) of the thread through hydrogen bonds between the carboxamide hydrogen donors (N20H and N29H) and the amide carbonyl group adjacent to the diphenylacetyl stopper (O44). However, the carbonyl group (O38) adjacent to the BPA station is also in the plane of the other two carbonyl groups (O41 and O44) on the thread, and in solution one

 © 2006 Wiley-VCH Verlag GmbH & Co. KGaA, Weinheim

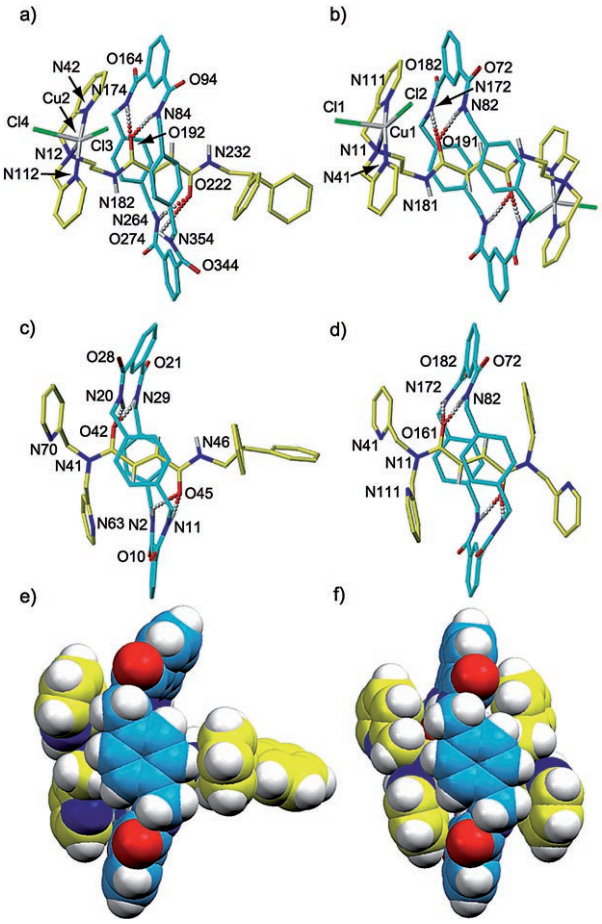
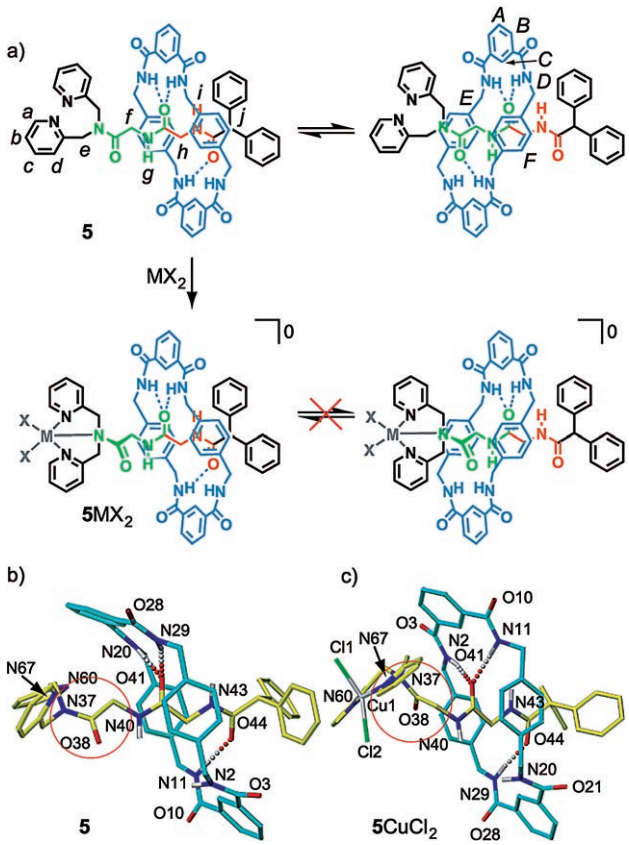


Figure 1. X-ray crystal structures[8] of a) **1**$CuCl_2$, b) **2**$(CuCl_2)_2$, c) **3**, and d) **4** in stick representation, and e) **3** and f) **4** in space-filling van der Waals radius form. C (thread) yellow, C (macrocycle) turquoise, O red, N dark blue, Cu gray, Cl green, H white. In the stick representations, all hydrogen atoms except for the amide and olefin protons have been omitted for clarity. Selected bond lengths [Å]: **1**$CuCl_2$: N12–Cu2 2.075, N42–Cu2 1.987, N112–Cu2 1.987, Cl3–Cu2 2.235, Cl4–Cu2 2.563, N264H–O222 2.236, N354H–O222 2.353, N174H–O192 2.260, N84H–O192 2.290; **2**$(CuCl_2)_2$: N11–Cu1 2.076, N41–Cu1 2.001, N111–Cu1 2.027, Cu1–Cl1 2.497, Cu1–Cl1 2.232, N172H–O191 2.140, N82H–O191 2.260; **3**: N20H–O42 2.239, N29H–O42 2.136, N2H–O45 2.687, N11H–O45 1.957; **4**: N172H–O161 1.985, N82H–O161 2.212.



Scheme 2. Synthesis of [2]rotaxane **5** with an extended hydrogen-bonding site and its subsequent complexation to generate **5**MX_2 ($MX_2 = CuCl_2$ or $Cd(NO_3)_2$): a) the solution positional equilibrium of the macrocycle in **5** (atom-lettering scheme corresponds to ^{1}H NMR assignments in Figure 2). The complexes **5**MX_2 were prepared by addition of a solution of the appropriate metal salt in acetonitrile to a solution of **5** in acetonitrile at room temperature and purified by crystallization. b, c) X-ray crystal structures[8] of **5** and **5**$CuCl_2$, respectively. C (thread) yellow, C (macrocycle) turquoise, O red, N dark blue, Cu gray, Cl green, H white; all hydrogen atoms except for the amide protons have been omitted for clarity. Selected bond lengths [Å]: **5**: N20H–O41 2.026, N29H–O41 2.192, N11H–O44 1.888; **5**$CuCl_2$: N37–Cu1 2.432, N60–Cu1 1.976, N67–Cu1 1.987, Cl1–Cu1 2.256, Cl2–Cu1 2.227, N2H–O41 2.190, N11H–O41 2.153, N29H–O44 1.885. The red circles highlight the enforced change in conformation of the BPA ligand and adjacent peptide unit upon coordination to a metal ion.

would expect an equilibrium to exist between the hydrogen bonding of N11H and O44 and a similar interaction between O38 and N2H (Scheme 2a). Indeed, the ^{1}H NMR spectrum of rotaxane **5** in CD_3CN (Figure 2b) reveals that this is the case, with the chemical shifts of both internal methylene groups H_f and H_h (green and orange, respectively) shifted upfield ($\Delta\delta H_f = 0.7$ ppm; $\Delta\delta H_h = 1.0$ ppm) relative to those of the free thread (Figure 2a), as a result of shielding from the macrocycle.

Addition of $CuCl_2$ to **5** results in formation of complex **5**$CuCl_2$, the X-ray crystal structure of which is shown in Scheme 2c. The most striking characteristics of this solid-state structure are the chelation of all three BPA nitrogen atoms (including the carboxamide nitrogen, N71) to the Cu^{II} ion, together with the out-of-plane tilting of carbonyl oxygen O38 relative to the plane in which the other two carbonyl oxygen atoms (O41 and O43) of the thread lie. As cadmium is a diamagnetic metal with similar binding properties to Cu^{II}, treatment of **5** with $Cd(NO_3)_2$ allowed us to study the solution behavior of metal chelation to **5** using ^{1}H NMR spectroscopy (compare Figure 2c with Figure 2b and d). As expected, the binding of a metal ion to the BPA stopper alters the equilibrium of hydrogen bonding between the three carbonyl hydrogen-bond acceptors in **5**, causing a shift of the signal for H_h (orange) further upfield and a slight downfield shift of the resonance for H_f (green) in **5**$Cd(NO_3)_2$ relative to those in the free rotaxane. Comparison of the ^{1}H NMR spectra of **5**$Cd(NO_3)_2$ with the $Cd(NO_3)_2$–thread complex revealed a similar trend, that is, a large upfield shift of the signal for H_h and a much smaller shift for that of H_f. The changes indicate that the

 © 2006 Wiley-VCH Verlag GmbH & Co. KGaA, Weinheim

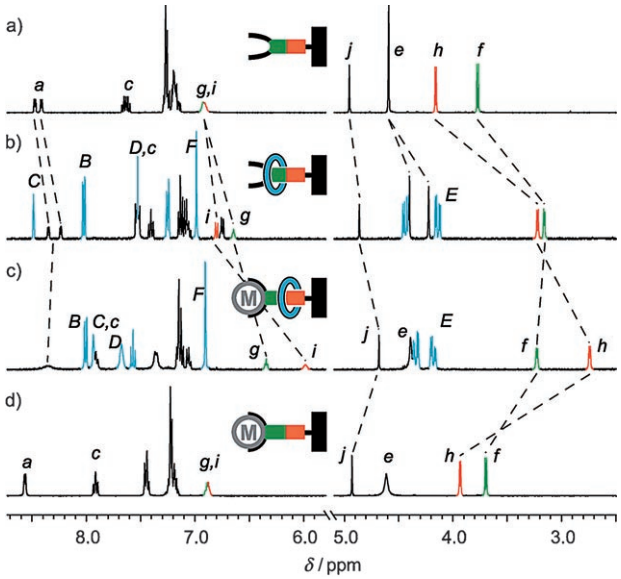
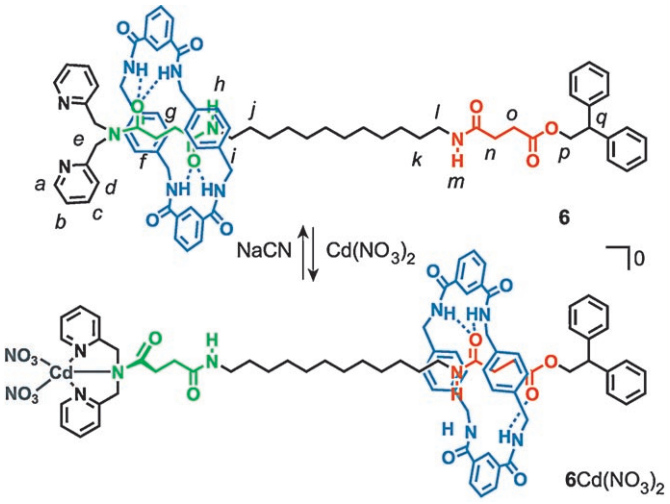


Figure 2. Partial ^{1}H NMR spectra (400 MHz, CD_3CN, 298 K) of a) the thread of rotaxane **5**, b) **5**, c) **5**$Cd(NO_3)_2$, and d) the complex of the thread of rotaxane **5** with $Cd(NO_3)_2$. Resonances are colored and labeled as shown in Scheme 2.



Scheme 3. An allosterically regulated molecular shuttle. Rotaxane **6** consists of a BPA metal-chelating site (the "effector" binding site), two hydrogen-bonding stations of different intrinsic affinities (substrate-binding sites), and a benzylamide macrocycle substrate. Metal complexation of **6** occurs quantitatively at room temperature with $Cd(NO_3)_2$ in CD_3CN. The reverse transformation is accomplished by treatment with excess NaCN (5 equiv).

macrocycle no longer shuttles back and forth along the thread in **5**$Cd(NO_3)_2$ but is restricted mainly to a position over the H_h methylene group between carbonyl oxygen atoms O41 and O43.

Encouraged by the results from this model system we prepared a two-station [2]rotaxane, **6**, with hydrogen-bonding sites of substantially differing affinities[9] for the macrocycle separated by a C_{12} alkyl chain. The station of known[9] higher binding affinity (succinamide, shown in green) is directly attached to the metal-binding BPA unit, while the station of inherent lower affinity[9] (succinic amide ester, shown in orange) is attached to a nonchelating diphenylacetyl stopper (Scheme 3). In **6**, the macrocycle occupies the position over the green station more than 95% of the time at 273 K in CD_3CN, as revealed by the large ($\Delta\delta = 1.5$ ppm) upfield shift of the signals for protons H_f and H_g (compare Figure 3b and a). In comparison, the signals for protons H_n and H_o (orange station) appear at similar chemical shifts in rotaxane **6** (Figure 3a) and the parent thread (Figure 3a).

The addition of one equivalent of $Cd(NO_3)_2$ to **6** in CD_3CN results in a dramatic change in the ^{1}H NMR spectrum (Figure 3c). The major differences in the spectra of **6** and **6**$Cd(NO_3)_2$ are the large ($\Delta\delta = 1.1$ ppm) downfield shift of the signals for protons H_f and H_g (green station) and the upfield shift ($\Delta\delta = 0.7$ ppm) of the peaks for H_n and H_o (orange station) in the metal-coordinated rotaxane. In addition, protons H_l, H_p, and H_q at the periphery of the orange station are also shielded by the macrocycle ($\Delta\delta \approx 0.3$ ppm). Collectively these data indicate that the macrocycle has moved from residing predominantly over the green station to being positioned mainly over the orange station. The difference in the chemical shifts of **6**$Cd(NO_3)_2$ relative to those of the parent thread bound to $Cd(NO_3)_2$ (Figure 3d) confirms the change in position of the macrocycle. The coordination

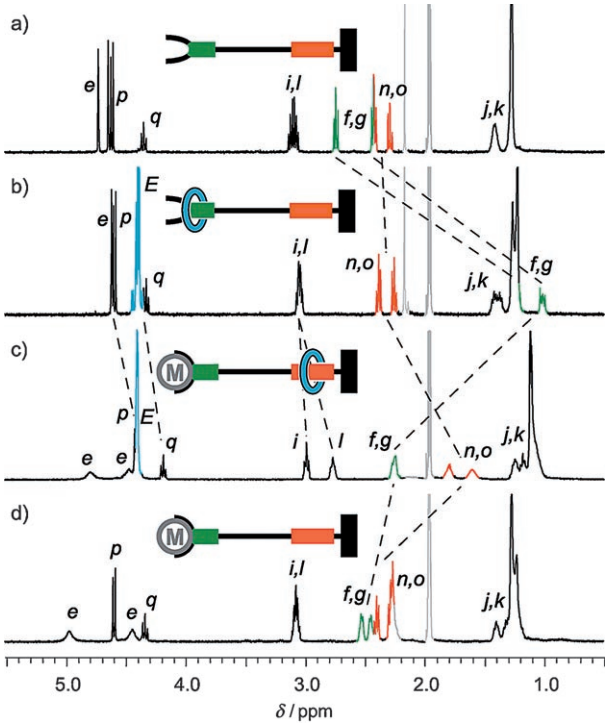


Figure 3. Partial ^{1}H NMR spectra (400 MHz, CD_3CN, 273 K) of a) the parent thread of **6**, b) **6**, c) **6**$Cd(NO_3)_2$, and d) the complex of the parent thread of **6** with $Cd(NO_3)_2$. Resonances are colored and labeled as shown in Scheme 3. Peaks shown in light gray arise from residual non-deuterated solvent and water.

reaction, and change in position of the macrocycle, is reversed by treatment with NaCN (Scheme 3).

The stimuli-induced shuttling between **6** and **6**$Cd(NO_3)_2$ (Scheme 3) corresponds to a negative heterotropic allosteric

 © 2006 Wiley-VCH Verlag GmbH & Co. KGaA, Weinheim

binding event[10]—inhibition of hydrogen bonding of the macrocycle at the succinamide unit through the conformational change induced by metal chelation at the BPA site—that leads to translocation of the macrocycle to the inherently weaker hydrogen-bonding succinic amide ester site, which lies 1.5 nm away. Similarly large movements in rotaxanes have been used to bring about changes in conductivity,[4d,11] circular dichroism,[12] fluorescence,[13] porosity,[14] and surface energy,[15] and to carry out mechanical work,[15,16] largely as a result of chemical (redox, acid-base, and photochemical) reactions on the covalent structure of the rotaxane. An allosteric shuttling mechanism offers the possibility of using metal-binding events as the energy source or operating stimulus for functional synthetic molecular machines.

Received: July 26, 2005
Revised: October 1, 2005
Published online: January 30, 2006

Keywords: allosterism · hydrogen bonds · molecular devices · rotaxanes · transition metals

[1] For recent reviews on allostery in biological systems, see: a) J.-P. Changeux, S. J. Edelstein, *Neuron* **1998**, *21*, 959–980; b) R. R. Breaker, *Nature* **2004**, *432*, 838–845; c) J.-P. Changeux, S. J. Edelstein, *Science* **2005**, *308*, 1424–1428.

[2] a) A. Mattevi, M. Rizzi, M. Bolognesi, *Curr. Opin. Struct. Biol.* **1996**, *6*, 762–769; b) J. Goldberg, A. C. Nairn, J. Kuriyan, *Cell* **1996**, *84*, 875–887; c) B. Kobe, B. E. Kemp, *Nature* **1999**, *402*, 373–376; d) G. Licini, P. Scrimin, *Angew. Chem.* **2003**, *115*, 4720–4723; *Angew. Chem. Int. Ed.* **2003**, *42*, 4572–4575; e) W. A. Lim, *Curr. Opin. Struct. Biol.* **2002**, *12*, 61–68; f) J. A. Hardy, J. A. Wells, *Curr. Opin. Struct. Biol.* **2004**, *14*, 706–715.

[3] For reviews on synthetic allosteric receptor systems, see: a) T. Nabeshima, *Coord. Chem. Rev.* **1996**, 151–169; b) S. Shinkai, M. Ikeda, A. Sugasaki, M. Takeuchi, *Acc. Chem. Res.* **2001**, *34*, 494–503; c) M. Takeuchi, M. Ikeda, A. Sugasaki, S. Shinkai, *Acc. Chem. Res.* **2001**, *34*, 865–873; d) L. Kovbasyuk, R. Krämer, *Chem. Rev.* **2004**, *104*, 3161–3187; e) S. Shinkai, M. Takeuchi, *Bull. Chem. Soc. Jpn.* **2005**, *78*, 40–51.

[4] a) *Molecular Catenanes, Rotaxanes, and Knots*: *A Journey Through the World of Molecular Topology* (Eds.: J.-P. Sauvage, C. Dietrich-Buchecker), Wiley-VCH, Weinheim, **1999**; b) V. Balzani, A. Credi, F. M. Raymo, J. F. Stoddart, *Angew. Chem.* **2000**, *112*, 3484–3530; *Angew. Chem. Int. Ed.* **2000**, *39*, 3348–3391; c) V. Balzani, M. Venturi, A. Credi, *Molecular Devices and Machines—A Journey into the Nanoworld*, Wiley-VCH, Weinheim, **2003**; d) A. H. Flood, R. J. A. Ramirez, W.-Q. Deng, R. P. Muller, W. A. Goddard, J. F. Stoddart, *Aust. J. Chem.* **2004**, *57*, 301–322; e) "Synthetic Molecular Machines": E. R. Kay, D. A. Leigh in *Functional Artificial Receptors* (Eds.: T. Schrader, A. D. Hamilton), Wiley-VCH, Weinheim, **2005**, pp. 333–406.

[5] For examples of Cu^{II} and Cd^{II} bound to BPA tertiary amide ligands, including several with a central carboxamide nitrogen and discussions of the thermodynamics and kinetics of these coordination modes, see: a) C. Cox, D. Ferraris, N. N. Murthy, T. Lectka, *J. Am. Chem. Soc.* **1996**, *118*, 5332–5333; b) N. Niklas, F. Hampel, G. Liehr, A. Zahl, R. Alsfasser, *Chem. Eur. J.* **2001**, *7*, 5135–5142; c) N. Niklas, F. W. Heinemann, F. Hampel, R. Alsfasser, *Angew. Chem.* **2002**, *114*, 3535–3537; *Angew. Chem. Int. Ed.* **2002**, *41*, 3386–3388; d) N. Niklas, F. W. Heinemann, F. Hampel, T. Clark, R. Alsfasser, *Inorg. Chem.* **2004**, *43*, 4663–4673; e) S. Novokmet, F. W. Heinemann, A. Zahl, R. Alsfasser, *Inorg. Chem.* **2005**, *44*, 4796–4805; f) D. S. Marlin, D. González Cabrera, D. A. Leigh, A. M. Z. Slawin, *Angew. Chem.* **2006**, *118*, 83–89; *Angew. Chem. Int. Ed.* **2006**, *45*, 77–83.

[6] F. G. Gatti, D. A. Leigh, S. A. Nepogodiev, A. M. Z. Slawin, S. J. Teat, J. K. Y. Wong, *J. Am. Chem. Soc.* **2001**, *123*, 5983–5989.

[7] There was no indication of reaction by color change, mass spectrometry, or thin-layer chromatography.

[8] Crystals of **1**$CuCl_2$ and **2**$(CuCl_2)_2$ of suitable quality for X-ray diffraction studies were obtained by carefully layering a solution of the appropriate complex in *N*,*N*-dimethylformamide (DMF) with CH_3CN (approximately 1:10 v/v). Single crystals of **3**, **4**, **5**, and **5**$CuCl_2$ were grown from slow evaporation of saturated solutions in CH_3CN, $CHCl_3$, CH_2Cl_2, and CH_2Cl_2/DMF (5:1 v/v), respectively. Data for **1**$CuCl_2$, **2**$(CuCl_2)_2$, **3**, **4**, and **5**$CuCl_2$ were collected on a Bruker SMART CCD diffractometer, whereas data for **5** were collected on a Rigaku Saturn (MM007 high flux RA/$Mo_{K\alpha}$ radiation, confocal optic). Data were collected at 150 K for **1**$CuCl_2$, **2**$(CuCl_2)_2$, and and **4**, at 125 K for **3** and **5**$CuCl_2$, and at 93 K for **5**. All data collections employed narrow frames (0.3–1.0°) to obtain at least a full hemisphere of data. Intensities were corrected for Lorentz polarization and absorption effects (multiple equivalent reflections). Structures were solved by direct methods, non-hydrogen atoms were refined anisotropically with CH protons being refined in riding geometries (SHELXTL) against F^2. In most cases, amide protons were refined isotropically subject to a distant constraint. Data for **1**$CuCl_2$·3.75 DMF: $C_{73.75}H_{83.75}N_{12.25}O_{9.25}Cl_2Cu$, $M_r = 1424.22$, crystal size $2.07 \times 0.37 \times 0.35\ mm^3$, monoclinic, $P21/c$, $a = 15.5009(8)$, $b = 43.623(2)$, $c = 23.9057(11)$ Å, $Z = 8$, $\rho_{calcd} = 1.231\ Mg\,m^{-3}$; $\mu = 0.415\ mm^{-1}$, 92715 reflections collected, 27020 unique ($R_{int} = 0.0521$) giving $R = 0.0702$ for 18444 observed data [$F_o > 4\sigma(F_o)$], $S = 0.994$ for 1481 parameters; residual electron density extremes were 0.549 and $-0.566\ eÅ^{-3}$. Data for **2**$(CuCl_2)_2$: $C_{70}H_{78}Cl_4Cu_2N_{14}O_8$, $M_r = 1512.34$, crystal size $0.19 \times 0.18 \times 0.08\ mm^3$, monoclinic, $P21/c$, $a = 12.7343(5)$, $b = 19.0061(8)$, $c = 15.7470(7)$ Å, $Z = 2$, $\rho_{calcd} = 1.438\ Mg\,m^{-3}$; $\mu = 0.828\ mm^{-1}$, 20841 reflections collected, 7515 unique ($R_{int} = 0.0450$) giving $R = 0.0791$ for 5367 observed data [$Fo > 4\sigma(F_o)$], $S = 1.112$ for 444 parameters; residual electron density extremes were 0.663 and $-0.851\ eÅ^{-3}$. Data for **3**: $C_{62}H_{56}N_8O_6$, $M_r = 1009.15$, crystal size $0.21 \times 0.1 \times 0.1\ mm^3$, monoclinic, $C2/c$, $a = 31.107(10)$, $b = 18.677(6)$, $c = 21.001(7)$ Å, $Z = 8$, $\rho_{calcd} = 1.318\ Mg\,m^{-3}$; $\mu = 0.086\ mm^{-1}$, 31645 reflections collected, 9198 unique ($R_{int} = 0.5301$) giving $R = 0.1611$ for 2791 observed data [$F_o > 4\sigma(F_o)$], $S = 0.994$ for 707 parameters; residual electron density extremes were 0.383 and $-0.380\ eÅ^{-3}$. Data for **4**·$(CHCl_3)_3$: $C_{64}H_{58}Cl_{12}N_{10}O_6$, $M_r = 1488.66$, crystal size $0.59 \times 0.46 \times 0.41\ mm^3$, triclinic, $P\bar{1}$, $a = 11.8069(7)$, $b = 12.2006(7)$ Å, $Z = 4$, $\rho_{calcd} = 1.485\ Mg\,m^{-3}$; $\mu = 0.559\ mm^{-1}$, 16004 reflections collected, 7684 unique ($R_{int} = 0.04$) giving $R = 0.0526$ for 6362 observed data [$F_o > 4\sigma(F_o)$], $S = 0.9917$ for 415 parameters; residual electron density extremes were 0.44 and $-0.36\ eÅ^{-3}$. Data for **5**: $C_{62}H_{59}N_9O_8$, $M_r = 1058.18$, crystal size $0.1 \times 0.03 \times 0.03\ mm^3$, triclinic, $P\bar{1}$, $a = 10.9491(5)$, $b = 14.8382(2)$, $c = 18.5719(8)$ Å, $Z = 2$, $\rho_{calcd} = 1.311\ Mg\,m^{-3}$; $\mu = 0.716\ mm^{-1}$, 32650 reflections collected, 7414 unique ($R_{int} = 0.0782$) giving $R = 0.0806$ for 5270 observed data [$F_o > 4\sigma(F_o)$], $S = 1.051$ for 746 parameters; residual electron density extremes were 0.288 and $-0.313\ eÅ^{-3}$. Data for **5**$CuCl_2$·3 DMF·2 H_2O: $C_{68.75}H_{75.75}Cl_2CuN_{11.25}O_{10.75}$, $M_r = 1366.1$, crystal size $0.16 \times 0.1 \times 0.1\ mm^3$, monoclinic, $P2(1)/n$, $a = 25.279(6)$, $b = 10.970(3)$, $c = 25.649(6)$ Å, $Z = 4$, $\rho_{calcd} = 1.288\ Mg\,m^{-3}$; $\mu = 0.451\ mm^{-1}$, 44451 reflections collected, 12876 unique ($R_{int} = 0.4536$) giving $R = 0.1614$ for 4795 observed data [$F_o > 4\sigma(F_o)$], $S = 1.038$ for 856 parameters; residual electron density extremes were 1.180 and $-0.718\ eÅ^{-3}$. The protons on solvate molecules were not allowed for in the refinement. CCDC 281563–281568 (**1**$CuCl_2$, **2**$(CuCl_2)_2$,

 © 2006 Wiley-VCH Verlag GmbH & Co. KGaA, Weinheim

3, **4**, **5**, and **5**$CuCl_2$, respectively) contain the supplementary crystallographic data for this paper. These data can be obtained free of charge from The Cambridge Crystallographic Data Centre via www.ccdc.cam.ac.uk/data_request/cif.

[9] A. Altieri, G. Bottari, F. Dehez, D. A. Leigh, J. K. Y. Wong, F. Zerbetto, *Angew. Chem.* **2003**, *115*, 2398 – 2402; *Angew. Chem. Int. Ed.* **2003**, *42*, 2296 – 2300.

[10] For other examples of negative heterotropic allostery in artificial systems, see: a) M. H. Al-Sayah, N. R. Branda, *Angew. Chem.* **2000**, *112*, 975 – 977; *Angew. Chem. Int. Ed.* **2000**, *39*, 945 – 947; b) M. H. Al-Sayah, N. R. Branda, *Chem. Commun.* **2002**, 178 – 179; c) P. Thordarson, E. J. A. Bijsterveld, J. A. A. W. Elemans, P. Kasak, R. J. M. Nolte, A. E. Rowan, *J. Am. Chem. Soc.* **2003**, *125*, 1186 – 1187; d) M. H. Al-Sayah, R. McDonald, N. R. Branda, *Eur. J. Org. Chem.* **2004**, 173 – 182.

[11] A. H. Flood, J. F. Stoddart, D. W. Steuerman, J. R. Heath, *Science* **2004**, *306*, 2055 – 2056.

[12] G. Bottari, D. A. Leigh, E. M. Pérez, *J. Am. Chem. Soc.* **2003**, *125*, 13360 – 13361.

[13] a) Q.-C. Wang, D.-H. Qu, J. Ren, K. Chen, H. Tian, *Angew. Chem.* **2004**, *116*, 2715 – 2719; *Angew. Chem. Int. Ed.* **2004**, *43*, 2661 – 2665; b) D.-H. Qu, Q.-C. Wang, J. Ren, H. Tian, *Org. Lett.* **2004**, *6*, 2085 – 2088; c) E. M. Pérez, D. T. F. Dryden, D. A. Leigh, G. Teobaldi, F. Zerbetto, *J. Am. Chem. Soc.* **2004**, *126*, 12210 – 12211; d) D. A. Leigh, M. Á. F. Morales, E. M. Pérez, J. K. Y. Wong, C. G. Saiz, A. M. Z. Slawin, A. J. Carmichael, D. M. Haddleton, A. M. Brouwer, W. J. Buma, G. W. H. Wurpel, S. León, F. Zerbetto, *Angew. Chem.* **2005**, *117*, 3122 – 3127; *Angew. Chem. Int. Ed.* **2005**, *44*, 3062 – 3067.

[14] T. D. Nguyen, H.-R. Tseng, P. C. Celestre, A. H. Flood, Y. Liu, J. F. Stoddart, J. I. Zink, *Proc. Natl. Acad. Sci. USA* **2005**,*102*, 10029 – 10034.

[15] J. Berná, D. A. Leigh, M. Lubomska, S. M. Mendoza, E. M. Pérez, P. Rudolf, G. Teobaldi, F. Zerbetto, *Nat. Mater.* **2005**, *4*, 704 – 710.

[16] Y. Liu, A. H. Flood, P. A. Bonvallet, S. A. Vignon, B. H. Northrop, H.-R. Tseng, J. O. Jeppesen, T. J. Huang, B. Brough, M. Baller, S. Magonov, S. D. Solares, W. A. Goddard, C.-M. Ho, J. F. Stoddart, *J. Am. Chem. Soc.* **2005**, *127*, 9745 – 9759.

 © 2006 Wiley-VCH Verlag GmbH & Co. KGaA, Weinheim

Microporous Materials

DOI: 10.1002/anie.200502844

A Microporous Metal–Organic Framework for Gas-Chromatographic Separation of Alkanes**

Banglin Chen, Chengdu Liang, Jun Yang, Damacio S. Contreras, Yvette L. Clancy, Emil B. Lobkovsky, Omar M. Yaghi, and Sheng Dai**

Microporous metal–organic frameworks (MOFs),[1] which are new types of zeolite analogues, have been paid extensive attention because of their potential applications in gas storage,[2] separation,[3] and catalysis.[4] The modular construction of MOFs allows their pore size and shape to be systematically tuned by the judicious choice of metal-containing secondary building units (SBUs) and/or bridging linkers, and by making use of framework interpenetration or interweaving.[5] Their selective adsorption and high thermal stability make these microporous materials potentially useful for alkane separation. However, this application has not yet been developed. In the petroleum industry, the separation of alkane isomers is a very important process, and some narrow-pore zeolites have been used to sieve linear from branched alkanes, to boost octane ratings in gasoline.[6] To match the alkane molecule sizes, the microporous compound Zn-

[*] Prof. Dr. B. Chen, D. S. Contreras, Y. L. Clancy
Department of Chemistry
University of Texas-Pan American
Edinburg, TX 78541-2999 (USA)
Fax: (+1) 956-384-5006
E-mail: banglin@utpa.edu

Dr. C. Liang, Dr. S. Dai
Chemical Sciences Divisions
Oak Ridge National Laboratory
Oak Ridge, TN 37831 (USA)
Fax: (+1) 865-576-5235
E-mail: dais@ornl.gov

J. Yang, Prof. Dr. O. M. Yaghi
Materials Design and Discovery Group
Department of Chemistry, University of Michigan
Ann Arbor, MI 48109-1055 (USA)

Dr. E. B. Lobkovsky
Department of Chemistry and Chemical Biology
Baker Laboratory, Cornell University
Ithaca, NY 14853-1301 (USA)

[**] This work was supported by the University of Texas-Pan American through a Faculty Research Council award to B.C., by the Welch Foundation grant (BG-0017) to the Department of Chemistry at UTPA, by an appointment to the Higher Education Research Experiences (HERE) at the Oak Ridge National Laboratory (ORNL) for faculty (B.C.), which is sponsored by the US Department of Energy and administered by the Oak Ridge Institute for Science and Education, and by the Office of Basic Energy Sciences, US Department of Energy, under contract No. DE-AC05-00OR22725 with UT-Battelle, LLC (S.D.). We thank Dr. Jing-Feng Huang for his help with the GC separation of alkanes.

Supporting information for this article is available on the WWW under http://www.angewandte.org or from the author.

WILEY InterScience DISCOVER SOMETHING GREAT
© 2006 Wiley-VCH Verlag GmbH & Co. KGaA, Weinheim

(BDC)(4,4′-Bipy)$_{0.5}$ (MOF-508; BDC = 1,4-benzenedicarboxylic acid, 4,4′-Bipy = 4,4′-bipyridine) was designed to have a primitive cubic framework with pores that can be tuned by double interpenetration to have 1D channels of approximately 4.0 × 4.0 Å in cross section. Herein, we report the first example of a microporous MOF that is highly selective in the GC separation of alkanes.

A guest-filled phase, MOF-508a, was synthesized by the solvothermal reaction of H_2BDC, 4,4′-Bipy, and $Zn(NO_3)_2 \cdot 6H_2O$ in DMF/ethanol at 90 °C for 24 h, and isolated as colorless block-shaped crystals. The formula of the compound was determined to be Zn(BDC)(4,4′-Bipy)$_{0.5}$·(DMF)(H_2O)$_{0.5}$ by elemental microanalysis and single-crystal X-ray diffraction studies,[7] and the phase purity of the bulk material was independently confirmed by both powder X-ray diffraction (PXRD) and thermal gravimetric analysis (TGA). TGA data indicate that MOF-508a releases its guest molecules over the temperature range 25–145 °C to form the guest-free phase Zn(BDC)(4,4′-Bipy)$_{0.5}$ (MOF-508b), which is thermally stable to 360 °C. Interestingly, the PXRD pattern of the guest-free phase MOF-508b is significantly different from that of the as-synthesized MOF-508a (see Supporting Information), indicating the formation of a new phase whose structure was also characterized by single-crystal X-ray crystallography.[7]

As expected, the framework of MOF-508a is composed of paddle-wheel dinuclear zinc carboxylate units {$Zn_2(COO)_4$}, which are bridged by the BDC ligands to form a distorted 2D square grid. The 2D square grids are pillared by 4,4′-Bipy molecules, whose nitrogen atoms occupy the axial sites of the {$Zn_2(COO)_4$} paddle wheels, to form a 3D framework with a topology that can be described as an elongated primitive cubic lattice (see Supporting Information). Two of the 3D frameworks interpenetrate in MOF-508a, reducing the pore size. A 1D channel occurs in the direction of the rectangular diagonal of the paddle-wheel clusters (Figure 1a). This channel has a cross section of approximately 4.0 × 4.0 Å. The X-ray crystal structure of the guest-free phase MOF-508b reveals that the framework retains the overall connectivity, but the {$Zn_2(COO)_4$} paddle-wheel clusters are significantly distorted, and the 4,4′-Bipy linkers are bent. These changes compress the framework considerably: the volume per formula unit decreases from 410.7 (MOF-508a) to 342.3 Å^3 (MOF-508b), a 16.7% reduction. Thus, a dense doubly interpenetrating 3D framework is formed (Figure 1b).

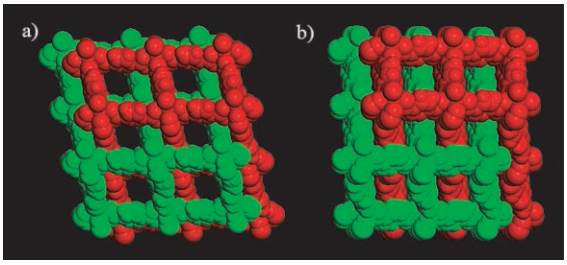


Figure 1. Space-filling representations of the structures of a) the open phase Zn(BDC)(4,4′-Bipy)$_{0.5}$·(DMF)(H_2O)$_{0.5}$ (MOF-508a), which contains 1D channels of 4.0 × 4.0 Å, and b) the dense phase Zn(BDC)(4,4′-Bipy)$_{0.5}$ (MOF-508b), viewed along the rectangular diagonal of the paddle-wheel clusters. The two interpenetrating frameworks are shown in red and green. The disordered guest molecules in MOF-508a are omitted for clarity.

Soaking the guest-free phase MOF-508b in DMF/ethanol for one day regenerated the guest-filled phase MOF-508a. The PXRD pattern of the product is exactly the same as that of the as-synthesized MOF-508a (see Supporting Information). Therefore, the host framework expands back to its former volume upon guest inclusion. This reversible cycle can be repeated many times without loss of crystallinity. Note that, although some dynamic microporous MOFs are known, MOFs exhibiting reversible open–dense framework transformations in the crystalline state are still very rare.[8] Clearly, this reversible open–dense framework transformation is responsible for the dynamic features and hysteresis of the compound's gas sorption isotherms for N_2 and H_2 at 77 K, and for CO_2 at 195 K (Figure 2). Similar sorption behavior was also observed for the copper analogue of MOF-508a, Cu(BDC)(4,4′-Bipy)$_{0.5}$.[9] The overall Langmuir surface area (A_s), calculated using the Langmuir equation from the N_2 sorption isotherm of the compound, is 946 m^2 g^{-1}.[10] The material can take up 90 cm^3 g^{-1} or 0.8 wt.% H_2 at standard temperature and pressure (STP).

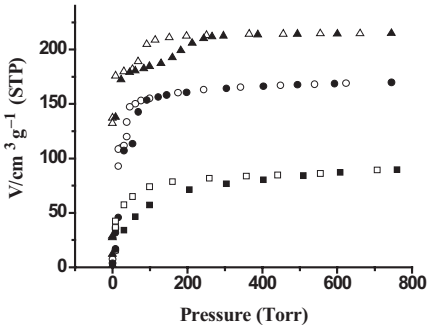


Figure 2. N_2 (△), CO_2 (○), and H_2 (□) sorption isotherms for MOF-508b (N_2 and H_2 at 77 K; CO_2 at 195 K). Adsorption: filled symbols; desorption: open symbols.

The 4.0 × 4.0 Å cross section of the 1D channels in the guest-filled phase MOF-508a is slightly larger than a methane molecule (3.8 × 3.8 Å). Thus, we initially examined the possibility of using MOF-508 phases for the chromatographic separation of natural gas. A chromatographic column of 120 cm was packed with single crystals of MOF-508b with sizes of 25–100 μm (3 g). The GC separation of natural gas was carried out at an inlet pressure of 60 psi with helium as the carrier gas over the temperature range 40–150 °C. Preliminary results indicated that the MOF-508 column can efficiently separate natural gas mixtures (see Supporting Information).

The GC separation was examined in detail for linear and branched isomers of pentane and hexane, because of their availability and industrial relevance in petroleum refining. The MOF-508 column can clearly separate *n*-pentane from *n*-hexane with retention times of 6.39 min and 12.06 min, respectively (Figure 3a). Branched 2-methylbutane (retention time of 5.31 min) elutes from the column before its linear isomer *n*-pentane (Figure 3b). Similarly, 2-methylpentane

 © 2006 Wiley-VCH Verlag GmbH & Co. KGaA, Weinheim

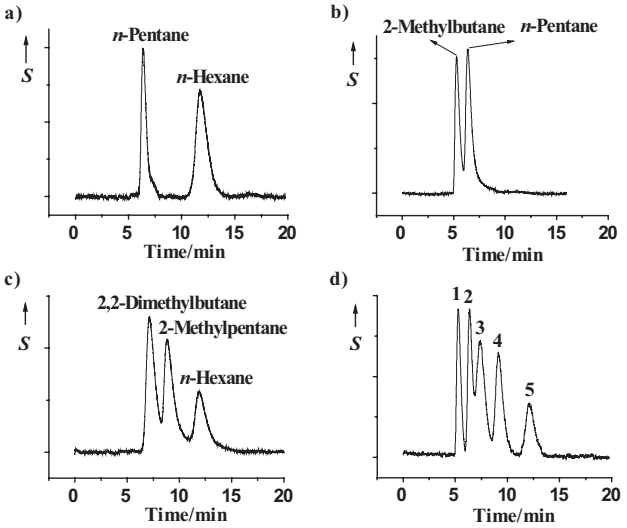


Figure 3. Chromatograms of alkane mixtures separated on a MOF-508 column: a) separation of *n*-pentane and *n*-hexane, b) separation of 2-methylbutane and *n*-pentane, c) separation of 2,2-dimethylbutane, 2-methylpentane, and *n*-hexane, and d) separation of an alkane mixture containing 2-methylbutane (**1**), *n*-pentane (**2**), 2,2-dimethylbutane (**3**), 2-methylpentane (**4**), and *n*-hexane (**5**). S = thermal conductivity detector response.

(retention time of 9.16 min) runs through the column faster than its linear isomer *n*-hexane, while 2,2-dimethylbutane, the isomer of hexane with the shortest linear chain, elutes even faster at a time of 7.40 min (Figure 3c). Thus, mixtures of 2-methylbutane, *n*-pentane, 2,2-dimethylbutane, 2-methylpentane, and *n*-hexane can be easily separated with this new type of microporous MOF column (Figure 3d). The potential applications of this microporous MOF column in the efficient GC separation of natural gas and alkane mixtures are remarkable and foreseeable: the column could be used to identify the impurities in natural gas, and to monitor the amounts of mono- and multibranched alkanes formed in cracking reactions.

The selective GC separation of alkanes on the MOF-508 column is the result of their different van der Waals interactions with the microporous MOF-508 walls, which arise from the subtle matching of the size and shape of the alkanes with the MOF-508 micropores.[11] The 4.0×4.0 Å channels of in the open phases of MOF-508 are accessible to the linear chains, but not to the branched parts of the alkanes. Thus, the retention of alkanes on the column mainly depends on the length of the linear part of the alkane, which contributes to its van der Waals interactions with the microporous MOF walls. The 2-methylbutane molecule, with its shorter linear chain of two carbon atoms, has a weaker van der Waals interaction and elutes faster than its linear isomer *n*-pentane. The same trend is observed for 2,2-dimethylbutane, 2-methylpentane, and *n*-hexane. This behavior is analogous to the pore and pore-mouth adsorption effect observed in mordenite and ZSM-22, which have small 1D channels.[12]

In conclusion, we present a rare example of a MOF exhibiting a reversible open–dense framework transformation in the crystalline state. This transformation is attributed to the rigid and flexible nature of the 4,4′-Bipy linkers and the variable distortion of the paddle-wheel clusters. Most importantly, for the first time, we demonstrated the application of a microporous MOF in the GC separation of alkanes based on their different van der Waals interactions arising from subtle size- and shape-selective matching. The unique features of MOF-508 are its 1D pores of 4.0×4.0 Å, which selectively accommodate linear alkanes and discriminate branched alkanes. Thus, its good GC separation capability is a result of its differential interactions with the alkane isomers. Compared with inorganic zeolite analogues, the specific interactions between the analytes and the organic moieties of MOFs might further enhance their separation capabilities. Further studies on related microporous MOFs and their applications in highly selective separation are in progress.

Experimental Section

MOF-508a: A mixture of $Zn(NO_3)_2 \cdot 6H_2O$ (1.407 g, 4.73 mmol), H_2BDC (0.786 g, 4.73 mmol), and 4,4′-Bipy (0.369 g, 2.36 mmol) was suspended in DMF/ethanol (1:1, 400 mL), and heated in a teflon vessel (500 mL) at 90 °C for 24 h. The colorless block-shaped crystals formed were collected, washed with DMF and hexane, and dried in air (1.82 g, 95 %). Elemental analysis (%) calcd for $Zn(BDC)(4,4'\text{-}Bipy)_{0.5} \cdot (DMF)(H_2O)_{0.5}$ ($C_{16}H_{16}N_2O_{5.5}Zn$): C 47.37, H 3.98, N 6.90, Zn 16.12; found: C 47.60, H 3.97, N 6.40, Zn 16.80; TGA data, calcd weight loss (%) for $1\,DMF + 0.5\,H_2O$: 15.1; found: 15.1. MOF-508b: A sample of MOF-508a was heated at 120 °C under vacuum for 24 h to produce MOF-508b. TGA indicated that there was no further weight loss.

GC separation of natural gas: GC measurements were performed with a Buck Scientific 910 GC system. The instrument control and data acquisition were carried out by the software Peakwin, which runs on a laptop with the Windows XP operating system. A thermal conductivity detector was used for data collection. Helium was used as the carrier gas and was driven at the inlet pressure of 60 psi. Fresh columns of MOF-508b were conditioned at 160 °C overnight before injection. The GC measurements were conducted with a temperature program consisting of two steps: 40 °C for the first 4 min, and 150 °C for the remainder of the measurement. For a typical run, 1 mL of natural gas was manually injected through the injection port. Each run ended after 20 min.

GC separation of linear and branched pentane and hexane isomers: The GC measurement was conducted with a temperature program consisting of three steps: 120 °C for 2 min, ramp from 120–160 °C over 2 min, and 160 °C for the remainder of the measurement. For a typical run, 1 (two components) to 2 μL (five components) of the alkane mixture was manually injected through the injection port. Each run ended after 20 min.

Received: August 10, 2005
Revised: November 15, 2005
Published online: January 20, 2006

Keywords: alkanes · gas chromatography · metal–organic frameworks · microporous materials · sorption

[1] a) O. M. Yaghi, M. O'Keeffe, N. W. Ockwig, H. K. Chae, M. Eddaoudi, J. Kim, *Nature* **2003**, *423*, 705; b) C. Janiak, *Dalton Trans.* **2003**, 2781; c) S. Kitagawa, R. Kitaura, S. Noro, *Angew. Chem.* **2004**, *116*, 2388; *Angew. Chem. Int. Ed.* **2004**, *43*, 2334; d) C. N. R. Rao, S. Natarajan, R. Vaidhyanathan, *Angew. Chem.*

 © 2006 Wiley-VCH Verlag GmbH & Co. KGaA, Weinheim

2004, *116*, 1490; *Angew. Chem. Int. Ed.* **2004**, *43*, 1466; e) D. Bradshaw, J. B. Claridge, E. J. Cussen, T. J. Prior, M. J. Rosseinsky, *Acc. Chem. Res.* **2005**, *38*, 273; f) G. Férey, C. Mellot-Draznieks, C. Serre, F. Millange, *Acc. Chem. Res.* **2005**, *38*, 217.

[2] a) J. L. C. Rowsell, A. R. Millward, K. S. Park, O. M. Yaghi, *J. Am. Chem. Soc.* **2004**, *126*, 5666; b) D. N. Dybstev, H. Chun, K. Kim, *Angew. Chem.* **2004**, *116*, 5143; *Angew. Chem. Int. Ed.* **2004**, *43*, 5033; c) L. Pan, M. B. Sander, X. Huang, J. Li, M. Smith, E. Bittner, B. Bockrath, J. K. Johnson, *J. Am. Chem. Soc.* **2004**, *126*, 1308; d) X. Zhao, B. Xiao, A. J. Fletcher, K. M. Thomas, D. Bradshaw, M. J. Rosseinsky, *Science* **2004**, *306*, 1012; e) B. Chen, N. W. Ockwig, A. R. Millward, D. S. Contreras, O. M. Yaghi, *Angew. Chem.* **2005**, *117*, 4823; *Angew. Chem. Int. Ed.* **2005**, *44*, 4745; f) J. L. C. Rowsell, O. M. Yaghi, *Angew. Chem.* **2005**, 117, 4748; *Angew. Chem. Int. Ed.* **2005**, *44*, 4670.

[3] a) O. M. Yaghi, C. E. Davis, G. Li, H. Li, *J. Am. Chem. Soc.* **1997**, *119*, 2861; b) H. J. Choi, T. S. Lee, M. P. Suh, *Angew. Chem.* **1999**, *111*, 1490; *Angew. Chem. Int. Ed.* **1999**, *38*, 1405; c) R. Kitaura, K. Fujimoto, S. Noro, M. Kondo, S. Kitagawa, *Angew. Chem.* **2002**, *114*, 141; *Angew. Chem. Int. Ed.* **2002**, *41*, 133; d) T. K. Maji, K. Uemura, H.-C. Chang, R. Matsuda, S. Kitagawa, *Angew. Chem.* **2004**, *116*, 3331; *Angew. Chem. Int. Ed.* **2004**, *43*, 3269; e) E. Y. Lee, M. P. Suh, *Angew. Chem.* **2004**, *116*, 2858; *Angew. Chem. Int. Ed.* **2004**, *43*, 2798.

[4] a) M. Fujita, Y. J. Kwon, S. Washizu, K. Ogura, *J. Am. Chem. Soc.* **1994**, *116*, 1151; b) J. S. Seo, D. Whang, H. Lee, S. I. Jun, J. Oh, Y. J. Jeon, K. Kim, *Nature* **2000**, *404*, 982; c) L. Pan, H. Liu, X. Lei, X. Huang, D. H. Olson, N. J. Turro, J. Li, *Angew. Chem.* **2003**, *115*, 560; *Angew. Chem. Int. Ed.* **2003**, *42*, 542; d) A. Hu, H. L. Ngo, W. Lin, *J. Am. Chem. Soc.* **2003**, *125*, 11490; e) A. Hu, H. L. Ngo, W. Lin, *Angew. Chem.* **2003**, *115*, 6182; *Angew. Chem. Int. Ed.* **2003**, *42*, 6000.

[5] a) B. Chen, M. Eddaoudi, T. M. Reineke, J. W. Kampf, M. O'Keeffe, O. M. Yaghi, *J. Am. Chem. Soc.* **2000**, *122*, 11559; b) B. Chen, M. Eddaoudi, S. T. Hyde, M. O'Keeffe, O. M. Yaghi, *Science* **2001**, *291*, 1021; c) M. Eddaoudi, D. B. Moler, H. Li, B. Chen, T. M. Reineke, M. O'Keeffe, O. M. Yaghi, *Acc. Chem. Res.* **2001**, *34*, 319; d) M. Eddaoudi, J. Kim, N. Rosi, D. Vodak, J. Wachter, M. O'Keeffe, O. M. Yaghi, *Science* **2002**, *295*, 469.

[6] S. Kulprathipanja, R. W. Neuzil, US Patent 4 445 444, **1984**, UOP; [*Chem. Abs. 101*, 75824].

[7] Single-crystal X-ray diffraction data were collected on a Bruker X8 APEX II diffractometer at 173 K. The data sets were corrected for absorption with the SADABS program (G. M. Sheldrick, SADABS). The structures were solved by direct methods and refined by full-matrix least-squares methods with the SHELXTL-97 program package. For MOF-508a, the electron density contribution of the diffuse scattering of the disordered guest molecules (DMF and H_2O) was handled using the SQUEEZE procedure in the PLATON software suite. Crystal data for MOF-508a ($C_{13}H_8NO_4Zn$; the contribution of the disordered guest molecules is not included in the derived data): triclinic, $P\bar{1}$, $a = 10.880(3)$, $b = 10.918(3)$, $c = 14.122(4)$ Å, $\alpha = 89.335(16)$, $\beta = 89.171(17)$, $\gamma = 78.380(16)°$, $V = 1643.0(8)$ Å^3, $Z = 4$, $\rho_{calcd} = 1.243$ g cm^{-3}, $\mu(Mo_{K\alpha}) = 1.501$ mm^{-1}; $2\theta_{max} = 49.42°$, total number of reflections 5144 ($R_{int} = 0.0729$), 417 parameters, $R_1 = 0.0655$ (3426 reflections with $I > 2\sigma(I)$), w$R_2 = 0.1826$ (all data), GOF = 0.933. Crystal data for MOF-508b ($C_{13}H_8NO_4Zn$): triclinic, $P\bar{1}$, $a = 7.7911(18)$, $b = 9.2984(18)$, $c = 10.6284(19)$ Å, $\alpha = 65.320(7)$, $\beta = 86.199(7)$, $\gamma = 78.145(7)°$, $V = 684.6(2)$ Å^3, $Z = 2$, $\rho_{calcd} = 1.492$ g cm^{-3}, $\mu(Mo_{K\alpha}) = 1.801$ mm^{-1}; $2\theta_{max} = 51.28°$, total number of reflections 2507 ($R_{int} = 0.0301$), 207 parameters, $R_1 = 0.0325$ (2225 reflections with $I > 2\sigma(I)$), w$R_2 = 0.0930$ (all data), GOF = 1.037. CCDC-265850 (MOF-508a) and CCDC-265851 (MOF-508b) contain the supplementary crystallographic data for this paper. These data can be obtained free of charge from The Cambridge Crystallographic Data Centre via www.ccdc.cam.ac.uk/data_request/cif. The structure of MOF-508a was also published by other groups while this paper was being written and revised (H. Chun, D. N. Dybstev, H. Kim, K. Kim, *Chem. Eur. J.* **2005**, *11*, 3521; B. Ma, K. L. Mulfort, J. T. Hupp, *Inorg. Chem.* **2005**, *44*, 4912).

[8] D. V. Soldatov, J. A. Ripmeester, S. I. Shergina, I. E. Sokolov, A. S. Zanina, S. A. Gromilov, Yu. A. Dyadin, *J. Am. Chem. Soc.* **1999**, *121*, 4179.

[9] a) K. Seki, *Phys. Chem. Chem. Phys.* **2002**, *4*, 1968; b) R. Kitaura, K. Seki, G. Akiyama, S. Kitagawa, *Angew. Chem.* **2003**, *115*, 444; *Angew. Chem. Int. Ed.* **2003**, *42*, 428.

[10] F. Rouquerol, J. Rouqerol, K. Sing, *Absorption by Porous Solids*, Academic Press, London, UK, **1999**.

[11] N. Y. Chen, W. E. Garwood, F. G. Dwyer, *Shape-Selective Catalysis in Industrial Applications*, Marcel Dekker, New York, **1989**.

[12] J. F. M. Denayer, R. A. Ocakoglu, I. C. Arik, C. E. A. Kirschhock, J. A. Martens, G. V. Baron, *Angew. Chem.* **2005**, *117*, 404; *Angew. Chem. Int. Ed.* **2005**, *44*, 400; R. A. Ocakoglu, J. F. M. Denayer, G. B. Marin, J. A. Martens, G. V. Baron, *J. Phys. Chem. B* **2003**, *107*, 398.

 © 2006 Wiley-VCH Verlag GmbH & Co. KGaA, Weinheim

C–C Coupling

DOI: 10.1002/anie.200502574

Regioselective Carbon–Carbon Bond Formation Reactions between TCNE or TCNQ and a Quinonoid Ring**

Pierre Braunstein, Olivier Siri,* Jean-philippe Taquet, and Qing-Zheng Yang*

Dedicated to Prof. Arthur J. Carty

Tetracyanoethylene (TCNE) and 7,7′,8,8′-tetracyanoquinodimethane (TCNQ) are strong organic, one-electron acceptors, and as such are much used as precursors to electron-transfer salts and superconducting or magnetic materials.[1] The coordination chemistry of TCNE and TCNQ has been much

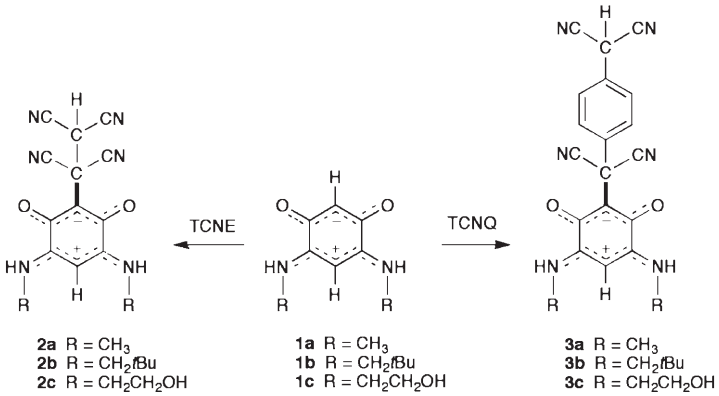
[*] Dr. P. Braunstein, Dr. O. Siri, J.-p. Taquet, Dr. Q.-Z. Yang
Laboratoire de Chimie de Coordination
Institut de Chimie, UMR 7177 CNRS
Université Louis Pasteur
4 Rue Blaise Pascal, 67070 Strasbourg Cedex (France)
Fax: (+33) 390-241-322
E-mail: braunst@chimie.u-strasbg.fr
siri@luminy.univ-mrs.fr

[**] This work was supported by the Centre National de la Recherche Scientifique, the Ministère de la Recherche et des Nouvelles Technologies, and Clariant. We thank Prof. R. Welter and Dr. A. DeCian (ULP, Strasbourg) for the determination of the crystal structures, Dr. G. Royal (UJF, Grenoble) for preliminary electrochemical studies on compound **1b**, and the referees for constructive comments. TCNE = tetracyanoethylene, TCNQ = 7,7′,8,8′-tetracyanoquinodimethane.

© 2006 Wiley-VCH Verlag GmbH & Co. KGaA, Weinheim
WILEY InterScience DISCOVER SOMETHING GREAT

investigated,[2] and their reactions with organometallic compounds include: 1) insertion into M–H,[3a,b] M–C,[3c–f] or M–OR bonds;[3g] 2) [2+2], [4+2], or [3+2] additions on the ligand;[4] 3) α,β-additions to an acetylide group;[5] 4) cycloadditions;[6] and 5) insertions into an aromatic C–H bond.[7] Although numerous reactions of TCNE and TCNQ with organic compounds have been reported,[8] only insertion reactions into a C–C bond of a spiroanellated bicyclopropyl system[9] or a C–H bond of 4-hydroxycoumarins,[10] cyclic enol ethers,[11] phenols,[12] or a mesoionic thiazolium system[13] have been observed.

Quinonoid compounds also form an important class of molecules owing to their remarkable chemical and physical properties.[14] Recently, unusual quinonoid zwitterions (molecules of type **1** in Scheme 1) have been reported,[15,16b] the



Scheme 1. Reactions of zwitterions **1** with TCNE or TCNQ.

unprecedented electronic features of which immediately attracted considerable theoretical interest.[16] These molecules display interesting chemical and structural features, including when they act as ligands,[16b,17] and have relevant applications in color chemistry.[18] Whereas the reactivity at their oxygen and/or nitrogen centers has been demonstrated, a C-substitution reaction that preserves the zwitterionic form represented a challenge that could only be taken up by C–H insertion chemistry, so far unknown in quinonoid chemistry. Probably because quinones and TCNX (TCN = tetracyano; X = E or Q) are both well-known electron acceptors, to the best of our knowledge, no work has been reported so far on their reactivity with each other.

Notwithstanding the fact that quinonoids **1** are rather unusual as they have substituents that make them poorer electron acceptors than quinones, we describe herein the hitherto unknown reactions of TCNE and TCNQ with zwitterionic quinone monoimine derivatives, which afforded new C-substituted zwitterions.

When TCNE and the purple 6π + 6π zwitterions **1a–c**[15,16b,17c] were reacted together at room temperature in a 1:1 ratio, an orange precipitate (**2a,b**) or solution (**2c**) formed (see the Experimental section and Scheme 1).

The ^{1}H NMR data of **2a–c** are similar to those for **1a–c**, except for the C(sp^2)–H resonances of the latter, which are replaced with new, downfield shifted singlets (for example, δ(C-H) = 5.19 and 5.49 ppm for **1b**[15] and δ(C-H) = 5.39 and 6.00 ppm for **2b**). The ^{13}C{^{1}H} spectra (DEPT 135 experiment) revealed the presence of a new sp^3 carbon atom bearing only one proton (δ(C-H) = 31.25, 30.61, and 31.26 ppm for **2a**, **2b**, and **2c**, respectively) and showed that the O=C–*C*–H carbon atom in **1** has become a quaternary center in **2**. The formation of 1:1 addition products was further supported by mass-spectrometric, IR spectroscopic, and elemental-analysis data.

An X-ray analysis of **2a** established that regioselective C–C bond formation had occurred between TCNE and the zwitterion CH carbon atom adjacent to the C=O bonds (Figure 1a).[20] The length of the newly formed C1–C9 bond

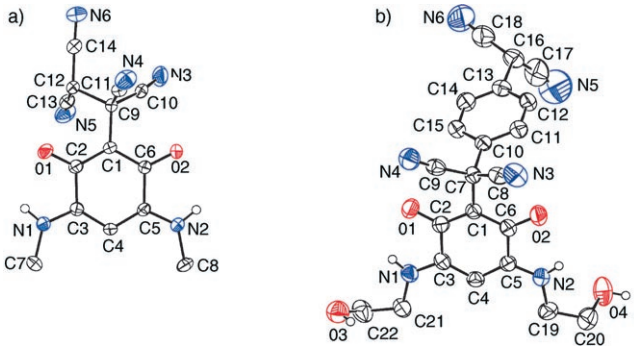


Figure 1. a) ORTEP view of the crystal structure of **2a** in **2a**·0.5 acetone. The H atom at C12 is not shown. Selected bond lengths [Å] and bond angles [°]: O1–C2 1.241(2), O2–C6 1.243(2), C1–C2 1.410(3), C1–C6 1.408(3), N1–C3 1.309(3), C5–N2 1.314(2), C4–C3 1.394(3), C4–C5 1.383(3), C2–C3 1.520(3), C5–C6 1.516(3), C1–C9 1.521(3), C12–C9 1.578(3), C12–C13 1.465(4), C10–N3 1.139(3); O1-C2-C1 125.9(2), O1-C2-C3 117.1(2), C2-C1-C9 120.6(2), C10-C9-C1 112.4(2), N3-C10-C9 169.2(2), C1-C9-C12 112.4(2), C11-C9-C10 108.1(2), N1-C3-C2 112.8(2), N1-C3-C4 125.1(2). b) ORTEP view of the crystal structure of **3c** in **3c**·0.5 Et_2O. The H atom at C16 is not shown. Selected bond lengths [Å] and bond angles [°]: C2–O1 1.246(4), O2–C6 1.238(4), C2–C1 1.400(4), C6–C1 1.408(4), N1–C3 1.311(4), N2–C5 1.310(4), C4–C3 1.384(4), C4–C5 1.381(4), C2–C3 1.521(5), C5–C6 1.533(5), C7–C1 1.530(4), C7–C8 1.500(5), C7–C10 1.549(4), C10–C11 1.378(4), C12–C11 1.393(5), C13–C16 1.535(5), C8–N3 1.133(4); O1-C2-C1 125.6(3), O1-C2-C3 116.6(3), C2-C1-C7 119.4(3), C8-C7-C1 110.8(3), N3-C8-C7 174.6(4), C1-C7-C10 112.5(2), C9-C7-C8 103.5(3), N1-C3-C2 113.2(3), N1-C3-C4 125.1(3).

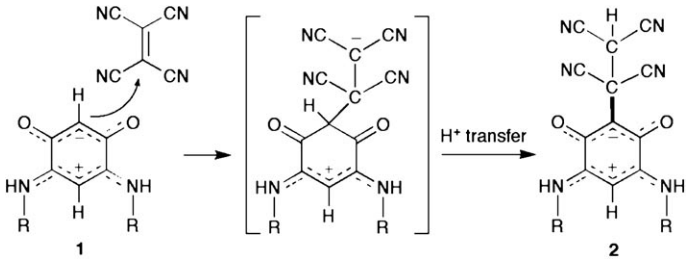
(1.521(3) Å) corresponds to a C–C single bond. Examination of the bond lengths within the O1-C2-C1-C6-O2 and N1-C3-C4-C5-N2 moieties shows an equalization of the C–C and C–O bond lengths and the C–C and C–N bond lengths, respectively, which is consistent with the zwitterionic structure;[15,16b] that is, delocalization of the two 6π electrons subunits that remain connected by two single bonds: C2–C3 and C5–C6 (1.520(3) and 1.516(3) Å, respectively).

These results prompted us to investigate the reaction with TCNQ. Orange-pink solids **3a–c** were similarly obtained from **1a–c**, respectively (Scheme 1), and fully characterized (see the Experimental Section). Owing to the weaker electron-withdrawing ability of the $HC(CN)_2$-C_6H_4-$C(CN)_2$ moiety, the ^{1}H NMR chemical shifts are shifted upfield with respect to those of **2**. The presence of well-defined resonances for AA′BB′ spin systems at approximately δ = 7.60 and 7.90 ppm,

 © 2006 Wiley-VCH Verlag GmbH & Co. KGaA, Weinheim

with ^3J(H,H) and ^4J(H,H) coupling constants of 8.7 and 2.1 Hz, respectively, is consistent with the presence of aromatic protons in a *para*-disubstituted ring. An X-ray diffraction study of **3c**[20] also established the regioselective, formal insertion of TCNQ into the C–H bond of **1c** adjacent to the C=O bonds, which preserves the zwitterionic character of its core, as observed for TCNE (Figure 1b). Furthermore, the conversion of the quinonoid ring of TCNQ into an aromatic ring is confirmed by the C7–C10 and C13–C16 bond lengths of 1.535(4) and 1.535(5) Å, respectively, which correspond to a C–C single bond. The $CH(CN)_2$ and $C(CN)_2$ groups adopt a staggered conformation, similar to their orientation in **2a**.

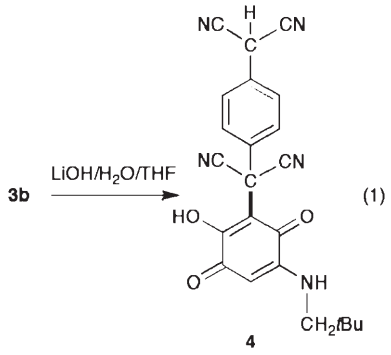
The cyclic voltammogram of **1b** reveals a reversible reduction process centered at −1.38 V and an irreversible oxidation wave at +0.96 V versus a Ag/Ag^+ electrode (that is, −1.09 and +1.25 V versus a saturated calomel electrode (SCE), respectively), which results from a one-electron oxidation process. When we compared these data with the first reduction potential of TCNE or TCNQ, in the range +0.10 to +0.25 V versus SCE,[21] it appears that the latter are much better one-electron acceptors than zwitterion **1b**. No reaction was observed between **1b** and dimethylacetylenedicarboxylate, maleic anhydride, or CO_2 in THF at room temperature or under reflux, thus it would appear that these reagents are not electrophilic enough. We have no spectroscopic indication that the formation of the C-substituted zwitterions **2** or **3** takes place by initial formation of charge-transfer complexes, as suggested in other cases.[3b,7c] Rather, we believe that C–C bond formation results from a Michael-type addition reaction, that is, the nucleophilic sp^2 C1 atom of the quinonemonoimine **1** attacks the double bond of TCNE or TCNQ (Scheme 2).



Scheme 2. Proposed mechanism for the formation of **2**.

Because the zwitterionic quinonoid compounds **1** can be considered as coupled polymethines composed from a cationic trimethine cyanine moiety and an anionic trimethine oxonol moiety that are chemically connected but electronically independent,[15,17c,22a–c] they should be able to react, as known from the chemistry of polymethines,[22d,e] with certain electrophiles. This behavior has now been demonstrated with TCNE and TCNQ, and the chemoselectivity of the reaction which occurs only on the electron-richer trimethine oxonol part of the molecule is fully consistent with the allopolarization principle.[23] This C–C bond formation reaction is thermally irreversible, as verified with **3b**.

In addition, **2** and **3** may be used to prepare C-substituted benzoquinones of type **4** in high yield [Eq. (1)].[17a] Related hydroxyquinones are known as efficient bioinhibitors.[19]



In conclusion, we have reported the first regioselective, formal insertion reactions of TCNE and TCNQ into a C–H bond of a quinonoid ring. This reaction between sp^2-hybridized carbon centers, which results in the formation of a new $C(sp^2)$–$C(sp^3)$ bond, provides general synthetic access to functional, C-substituted $6\pi+6\pi$ quinonoid zwitterions. The potential of these new multifunctional ligands, bearing two (N,O) chelation sites and four cyano groups, is particularly high in coordination chemistry, homogeneous catalysis (cooperative effects), and biochemistry.

Experimental Section

NMR spectra were obtained by using a Bruker AC-300 instrument. MALDI-TOF mass spectra were recorded on a Biflex III Bruker mass spectrometer and ESI mass spectra on a Bruker micrOTOF instrument. Elemental analyses were performed by the "Service de Microanalyse, Université Louis Pasteur (Strasbourg, France)". All reactions were carried out under purified N_2, using Schlenk techniques, and the solvents were freshly distilled under nitrogen prior to use. Compounds **1a–c** were prepared following literature procedures.[15,16b,17a,c,d]

2a: A solution of TCNE (154 mg, 1.20 mmol) in THF (5 mL) was added to a solution of **1a** (200 mg, 1.20 mmol) in ethanol (30 mL). After the solution was stirred at room temperature for 3 h, the orange precipitate was filtered off, washed with ethanol, and dried in air (166 mg, 47% yield). Compound **2a** is highly soluble in acetone, poorly soluble in CH_2Cl_2, and almost insoluble in MeOH and EtOH. ^{1}H NMR (300 MHz, [D$_6$]acetone): $\delta = 3.31$ (d, ^3J(H,H) = 5.4 Hz, 6H, CH_3), 5.84 (s, 1H, $C(sp^3)$-H), 6.49 (s, 1H, N=C=C-H), 9.03 ppm (br s, 2H, N-H); ^{13}C{^{1}H} NMR (75 MHz, [D$_6$]acetone): $\delta = 29.80$ (CH_3-N), 31.25 ($C(sp^3)$-H), 37.80 (HC-*C*(CN)), 83.06 (N=C=*C*-H), 93.77 (O=C=*C*), 110.18 and 112.00 (C≡N), 155.45 (C=N), 170.00 ppm (C=O); IR (KBr): $\tilde{\nu} = \nu_{C\equiv N}$ 2246 (w), 2255 cm^{-1} (w); UV/Vis (CH_2Cl_2): $\lambda_{max} = 331$ nm (log $\varepsilon = 4.42$), 345 nm (log $\varepsilon = 4.43$), 475 nm (br, log $\varepsilon = 2.96$); HRMS (ESI): 317.08 ([*M*+Na]$^+$); found: 317.08; elemental analysis (%) calcd for $C_{14}H_{10}N_6O_2$: C 57.14, H 3.43, N 28.56; found: C 57.01, H 3.68, N 28.78.

2b: Solid TCNE (115 mg, 0.90 mmol) was added to a solution of **1b** (250 mg, 0.90 mmol) in THF (25 mL). After the solution was stirred at room temperature for 2 h, the solvent was evaporated to 5 mL and hexane was added. The orange precipitate was filtered off and **2b** was recrystallized from a dichloromethane/pentane mixture and dried in air (350 mg, 96% yield). Compound **2b** is highly soluble in chlorinated solvents, acetone, or THF. ^{1}H NMR (300 MHz,

 © 2006 Wiley-VCH Verlag GmbH & Co. KGaA, Weinheim

$CDCl_3$): $\delta = 1.08$ (s, 18H, CH_3), 3.20 (d, $^3J(H,H) = 6.6$ Hz, 4H, CH_2), 5.39 (s, 1H, C(sp^3)-H), 6.00 (s, 1H, N=C=C-H), 8.28 (brt, 2H, N-H); $^{13}C\{^1H\}$ NMR (75 MHz, $CDCl_3$): $\delta = 27.42$ (CMe_3), 30.61 (C(sp^3)-H), 32.63 (CMe_3), 37.63 (HC-C(CN)), 55.21 (CH_2-N), 82.72 (N=C=C-H), 94.25 (O=C=C), 111.05 and 108.86 (C≡N), 154.83 (C=N), 169.35 (C=O); IR (KBr): $\tilde{\nu} = \nu_{C\equiv N}$ 2243 (w), 2256 cm^{-1} (w); UV/Vis (CH_2Cl_2): $\lambda_{max} = 336$ nm (log $\varepsilon = 4.36$), 350 nm (log $\varepsilon = 4.35$), 478 nm (br, log $\varepsilon = 3.09$); HRMS (ESI): 429.20 ($[M+Na]^+$); found: 429.21; elemental analysis (%) calcd for $C_{22}H_{26}N_6O_2 \cdot 1/6\,CH_2Cl_2$: C 63.29, H 6.31, N 19.98; found: C 63.26, H 6.40, N 20.30.

2c: Solid TCNE (170 mg, 1.33 mmol, 1 equiv) was added to a suspension of **1c** (300 mg, 1.33 mmol) in acetonitrile (50 mL), and the solution was stirred overnight at room temperature. After filtration to remove the small amount of unreacted **1c**, the filtrate was concentrated and diethyl ether was added to precipitate the product. After filtration, washing with diethyl ether, and drying in air, **2c** was obtained as an orange powder (362 mg, 77% yield). Compound **2c** is highly soluble in acetone and poorly soluble in CH_2Cl_2. ^1H NMR (300 MHz, [D_6]acetone): $\delta = 3.78$ (m, 4H, NHCH_2), 3.95 (q, ^3J-(H,H) = 5.5 Hz, 4H, CH_2OH), 4.36 (t, $^3J(H,H) = 5.5$ Hz, 2H, OH), 6.09 (s, 1H, C(sp^3)-H), 6.49 (s, 1H, N=C=CH), 8.84 ppm (brs, 2H, NH); $^{13}C\{^1H\}$ NMR (75 MHz, [D_6]acetone): $\delta = 31.26$ (C(sp^3)-H), 37.86 (HC-C($CN)_2$), 45.90 and 46.03 (CH_2NH), 59.23 and 59.35 (CH_2OH), 84.05 (N=C=C), 93.69 (O=C=C), 110.18 (C≡N), 111.98 (C≡N), 155.06 (N=C), 169.98 ppm (O=C); IR (KBr): $\tilde{\nu} = \nu_{C\equiv N}$ 2113 (w), 2216 cm^{-1} (w); MALDI-TOF: m/z 353.1 $[M-1]^-$; elemental analysis (%) calcd for $C_{16}H_{14}N_6O_4$: C 54.24, H 3.98, N 23.72; found: C 54.24, H 4.17, N 23.86.

3a: Prepared by a similar method to that of **2a**, from **1a** (100 mg, 0.60 mmol) and TCNQ (123 mg, 0.60 mmol, 1 equiv), instead of TCNE. Yield of isolated product = 48% (107 mg). Compound **3a** is soluble in dimethyl sulfoxide (DMSO) and almost insoluble in most common organic solvents. ^1H NMR (300 MHz, [D_6]DMSO): $\delta = 3.10$ (d, $^3J(HH) = 5.4$ Hz, 6H, CH_3), 5.48 (s, 1H, C(sp^3)-H), 5.60 (s, 1H, N=C=C-H), 7.64 (dt, AA′ part of an AA′BB′ spin system, 2H, $^3J(HH) = 8.7$ Hz, $^4J(HH) = 2.1$ Hz, aromatic C-H), 7.82 (dt, BB′ part of an AA′BB′ spin system, 2H, $^3J(H,H) = 8.7$ Hz, $^4J(H,H) = 2.1$ Hz, aromatic C-H), 8.38 ppm (brs, 2H, N-H); $^{13}C\{^1H\}$ NMR (100 MHz, [D_6]DMSO): $\delta = 30.50$ (CH_3-N), 38.97 (C(sp^3)-H), 82.91 (N=C-C-H), 100.65 (O=C=C), 116.26 (C≡N), 127.49 (aromatic C-H), 155.80 (C=N), 169.35 ppm (C=O); we could not observe all ^{13}C NMR resonances owing to the poor solubility of **3a** in DMSO; IR (KBr): $\tilde{\nu} = \nu_{C\equiv N}$ 2250 cm^{-1} (vw); UV/Vis (CH_2Cl_2): $\lambda_{max} = 333$ nm (log $\varepsilon =$ 4.42), 347 nm (log $\varepsilon = 4.45$), 478 nm (br, log $\varepsilon = 2.99$); HRMS (ESI): 393.11 ($[M+Na]^+$); found: 393.15; elemental analysis (%) calcd for $C_{20}H_{14}N_6O_2$: C 64.86, H 3.81, N 22.69; found: C 64.23, H 4.19, N 22.39.

3b: Prepared by a similar method to that of **2a**, from **1b** (100 mg, 0.36 mmol) with TCNQ (73 mg, 0.36 mmol, 1 equiv), instead of TCNE. Yield of isolated product = 98% (170 mg). Compound **3b** is highly soluble in chlorinated solvents, acetone, and THF. It remains unchanged after refluxing in a solution of THF overnight. ^1H NMR (300 MHz, $CDCl_3$): $\delta = 1.06$ (s, 18H, CH_3), 3.14 (d, $^3J(H,H) = 6.3$ Hz, 4H, CH_2), 5.16 (brs, 1H, C(sp^3)-H), 5.28 (s, 1H, N=C=C-H), 7.54 (dt, AA′ part of an AA′BB′ spin system, 2H, $^3J(H,H) = 8.7$ Hz, $^4J(H,H) =$ 2.1 Hz, C-H aromatic), 7.93 (dt, BB′ part of an AA′BB′ spin system, 2H, $^3J(H,H) = 8.7$ Hz, $^4J(H,H) = 2.1$ Hz, C-H aromatic), 8.30 ppm (brt, 2H, N-H); $^{13}C\{^1H\}$ NMR (100 MHz, $CDCl_3$): $\delta = 27.47$ (CMe_3), 27.81 (C_{sp3}-H), 32.54 (CMe_3), 32.76 (aryl-C(CN)), 55.16 (CH_2-N), 81.74 (N=C-C-H), 101.35 (O=C=C), 111.48 and 114.78 (C≡N), 126.84 and 138.07 (aromatic C), 127.98 and 128.06 (aromatic C-H), 155.62 (C=N), 168.02 ppm (C=O); IR (KBr): $\tilde{\nu} = \nu_{C\equiv N}$ 2243 cm^{-1} (vw); UV/Vis (CH_2Cl_2): $\lambda_{max} = 338$ nm (log $\varepsilon = 4.31$), 351 nm (log $\varepsilon = 4.33$), 478 nm (br, log $\varepsilon = 3.04$); HRMS (ESI): 505.23 ($[M+Na]^+$); found: 505.27; elemental analysis (%) calcd for $C_{26}H_{30}N_6O_2 \cdot 1/2\,C_4H_8O$: C 69.48, H 6.61, N 16.20; found: C 69.45, H 6.64, N 16.38.

3c: Prepared by a similar method to that of **2c**, from **1c** (100 mg, 0.44 mmol) with of TCNQ (90 mg, 0.44 mmol, 1 equiv), instead of TCNE. Yield of isolated product = 91% (173 mg). Compound **3c** is highly soluble in acetone and poorly soluble in CH_2Cl_2. ^1H NMR (300 MHz, [D_6]acetone): $\delta = 3.71$ (q, $^3J(H,H) = 5.6$ Hz, 4H, NHCH_2), 3.91 (q, $^3J = 5.3$ Hz, 4H, CH_2OH), 4.34 (t, $^3J(H,H) = 5.6$ Hz, 2H, OH), 5.92 (s, 1H, C_{sp3}-H), 6.13 (s, 1H, N=C=CH), 7.75 and 7.91 (AA′BB′ spin system, 4H, aromatic C-H), 8.70 ppm (brs, NH); IR (KBr): $\tilde{\nu} = \nu_{C\equiv N}$ 2121 (w), 2174 (w); 2250 cm^{-1} (w); MALDI-TOF: m/z 429.2 $[M-1]^-$; elemental analysis (%) calcd for $C_{22}H_{18}N_6O_4 \cdot 1/2$ $(CH_3CH_2)_2O$: C 61.66, H 4.96, N 17.98; found: C 61.04, H 4.94, N 18.08.

4: Compound **3b** (200 mg, 0.414 mmol) was dissolved in a solution of LiOH in THF/H_2O (100 mL, pH > 10) and then stirred overnight at room temperature. Protonation of the alcoholate, followed by extraction with CH_2Cl_2 and evaporation of the solvent afforded **4** as a purple powder (158 mg, 92% yield). ^1H NMR (300 MHz, [D_6]acetone): $\delta = 1.05$ (s, 9H, CH_3), 3.35 (brd, 2H, CH_2), 5.93 (s, 1H, C(sp^3)-H), 6.18 (s, 1H, NC=CH), 7.84 and 7.97 ppm (AA′BB′ spin system, 4H, aromatic C-H); the OH and NH protons could not be observed; IR (KBr): $\tilde{\nu} = \nu_{C\equiv N}$ 2121 (w), 2253 cm^{-1} (w); MALDI-TOF: m/z 412.1 $[M-1]^-$; elemental analysis (%) calcd for $C_{23}H_{19}N_5O_3$: C 66.82, H 4.63, N 16.94; found: C 66.25, H 5.18, N 16.52.

Received: July 22, 2005
Revised: November 6, 2005
Published online: January 20, 2006

Keywords: C–C coupling · chemoselectivity · insertion · quinones · zwitterions

[1] For recent review articles, see: a) N. Martin, J. L. Segura, C. Seoane, *J. Mater. Chem.* **1997**, *7*, 1661; b) J. S. Miller, A. J. Epstein, *Coord. Chem. Rev.* **2000**, *206–207*, 651; c) J.-P. Farges, A. Brau, *Handbook of Advanced Electronic and Photonic Materials and Devices*, *Vol. 3* **2001**, p. 329; d) D. Jérome, H. J. Schulz, *Adv. Phys.* **2002**, *51*, 293; e) E. B. Yagubskii, *NATO Sci. Ser. II* **2004**, *139*, 45; f) P. Batail, *Chem. Rev.* **2004**, *104*, 4887; g) D. Jérome, *Chem. Rev.* **2004**, *104*, 5565.

[2] W. Kaim, M. Moscherosch, *Coord. Chem. Rev.* **1994**, *129*, 157.

[3] a) J. S. Ricci, J. A. Ibers, *J. Am. Chem. Soc.* **1971**, *93*, 2391; b) J. R. Klingler, K. Mochida, J. K. Kochi, *J. Am. Chem. Soc.* **1979**, *101*, 6626; c) S. R. Su, A. Wojcicki, *Inorg. Chem.* **1975**, *14*, 89; d) O. A. Reutov, V. I. Rosenberg, G. V. Gavrilova, V. A. Nikanorov, *J. Organomet. Chem.* **1979**, *177*, 101; e) S. Fukuzumi, K. Mochida, J. K. Kochi, *J. Am. Chem. Soc.* **1979**, *101*, 5961; f) M. H. Chisholm, L. A. Rankel, *Inorg. Chem.* **1977**, *16*, 2177; g) E. Hevia, J. Pérez, L. Riera, V. Riera, I. del Rio, S. Garcia-Granda, D. Miguel, *Chem. Eur. J.* **2002**, *8*, 4510.

[4] a) A. Davison, J. P. Solar, *J. Organomet. Chem.* **1979**, *166*, C13; b) P. Hong, K. Sonogashira, N. Hagihara, *J. Organomet. Chem.* **1981**, *219*, 363; c) M. I. Bruce, T. W. Hambley, M. R. Snow, A. G. Swincer, *Organometallics* **1985**, *4*, 494; d) G.-H. Lee, S.-M. Peng, G.-M. Yang, S.-F. Lush, R.-S. Liu, *Organometallics* **1989**, *8*, 1106.

[5] a) M. I. Bruce, T. W. Hambley, M. R. Snow, A. G. Swincer, *Organometallics* **1985**, *4*, 501; b) Y. Yamamoto, R. Satoh, T. Tanase, *J. Chem. Soc. Dalton Trans.* **1995**, 307; c) M. I. Bruce, M. E. Smith, N. N. Zaitseva, B. W. Skelton, A. H. White, *J. Organomet. Chem.* **2003**, *670*, 170; d) M. I. Bruce, P. J. Low, F. Hartl, P. A. Humphrey, F. de Montigny, M. Jevric, C. Lapinte, G. J. Perkins, R. L. Roberts, B. W. Skelton, A. H. White, *Organometallics* **2005**, *24*, 5241.

[6] a) D. R. Lantero, M. E. Welker, *J. Organomet. Chem.* **2002**, *656*, 217; b) D. E. Kadlecek, D. Hong, P. J. Carroll, L. G. Sneddon, *Inorg. Chem.* **2004**, *43*, 1933.

[7] a) K. Onitsuka, H. Urayama, K. Sonogashira, F. Ozawa, *Chem. Lett.* **1995**, 1019; b) Y. Yamamoto, X.-H. Han, K.-i. Sugawara, S. Nishimura, *Angew. Chem.* **1999**, *111*, 1318; *Angew. Chem. Int.*

 © 2006 Wiley-VCH Verlag GmbH & Co. KGaA, Weinheim

Ed. **1999**, *38*, 1242; c) Y. Yamamoto, X.-H. Han, S. Nishimura, K.-i. Sugawara, N. Nezu, T. Tanase, *Organometallics* **2001**, *20*, 266; d) Y. Yamamoto, H. Settu, K. Nishiyama, K. Kuge, K. Tatsumi, *Eur. J. Inorg. Chem.* **2002**, 2447.

[8] a) E. Ciganek, W. J. Lin, O. W. Webster in *The Chemistry of the Cyano Group* (Ed.: Z. Rappoport), Wiley-Interscience, New York, **1970**, p. 446; b) Z. Rappoport, D. Ladkani, *J. Chem. Soc. Perkin Trans. 1* **1974**, 2595; c) R. Huisgen, *Acc. Chem. Res.* **1977**, *10*, 117; d) R. Huisgen, *Acc. Chem. Res.* **1977**, *10*, 199; e) J.-M. Fang, C.-C. Yang, Y.-W. Wang, *J. Org. Chem.* **1989**, *54*, 477; f) Y.-W. Wang, J.-M. Fang, Y.-K. Wang, M.-H. Wang, T.-Y. Ko, Y.-J. Cherng, *J. Chem. Soc. Perkin Trans. 1* **1992**, 1209; g) S. Nishida, N. Asanuma, M. Murakami, T. Tsuji, T. Imai, *J. Org. Chem.* **1992**, *57*, 4658.

[9] B. König, D. Kaufmann, R. Näder, A. de Meijere, *J. Chem. Soc. Chem. Commun.* **1983**, 771.

[10] a) H. Junek, *Monatsh. Chem.* **1965**, *96*, 1421; b) H. Junek, H. Aigner, *Monatsh. Chem.* **1971**, *102*, 622.

[11] A. Kondo, S. Iwatsuki, *J. Org. Chem.* **1982**, *47*, 1965.

[12] B. P. Bespalov, E. V. Getmanova, V. V. Titov, *Tetrahedron Lett.* **1976**, 1867.

[13] K. T. Potts, J. Baum, E. Houghton, D. N. Roy, U. P. Singh, *J. Org. Chem.* **1974**, *39*, 3619.

[14] S. Pataï, Z. Rappoport, *The Chemistry of the Quinonoid Compounds*, *Vols 1, 2*, Wiley, New York, **1988**.

[15] O. Siri, P. Braunstein, *Chem. Commun.* **2002**, 208.

[16] a) A. Sawicka, P. Skurski, J. Simons, *Chem. Phys. Lett.* **2002**, *362*, 527; b) P. Braunstein, O. Siri, J.-p. Taquet, M.-M. Rohmer, M. Bénard, R. Welter, *J. Am. Chem. Soc.* **2003**, *125*, 12246; c) D. Delaere, P. C. Nam, M. T. Nguyen, *Chem. Phys. Lett.* **2003**, *382*, 349; d) H. T. Le, P. C. Nam, V. L. Dao, T. Veszprémi, M. T. Nguyen, *Mol. Phys.* **2003**, *101*, 2437; e) C. P. Constantinides, P. A. Koutentis, J. Schatz, *J. Am. Chem. Soc.* **2004**, *126*, 16232; f) Y. Haas, S. Zilberg, *J. Am. Chem. Soc.* **2004**, *126*, 8991; g) T. Höltzl, T. Veszprémi, M.T. Nguyen, *J. Phys. Org. Chem.*, **2005**, *18*, 1123.

[17] a) P. Braunstein, O. Siri, J.-p. Taquet, Q.-Z. Yang, *Chem. Eur. J.* **2004**, *10*, 3817; b) J.-p. Taquet, O. Siri, P. Braunstein, R. Welter, *Inorg. Chem.* **2004**, *43*, 6944; c) Q.-Z. Yang, O. Siri, P. Braunstein, *Chem. Commun.* **2005**, 2660; d) Q.-Z. Yang, O. Siri, P. Braunstein, *Chem. Eur. J.*, **2005**, *11*, 7237.

[18] a) J. F. Corbett, *Hair Colorants: Chemistry and Toxicology*, Micelle Press, Weymouth, **1998**; b) P. Braunstein, O. Siri, PCT Int. Appl. WO 2002072533A1; c) P. Braunstein, O. Siri, J. P. Taquet, FR2002–09144.

[19] a) B. S. Joshi, V. N. Kamat, *Indian J. Chem.* **1975**, *13*, 795; b) N. Subbarayudu, Y. D. Satyanarayana, E. Venkata-Rao, D. Venkata-Rao, *Indian J. Pharm. Sci.* **1978**, *40*, 173; c) N. R. Bachur, S. L. Gordon, M. V. Gee, *Cancer Res.* **1978**, *38*, 1745; d) N. U. Frigaard, S. Tokita, K. Matsuura, *Biochim. Biophys. Acta* **1999**, *1413*, 108; e) J. J. Inbaraj, R. Gandhidasan, R. Murugesan, *Free Radical Biol. Med.* **1999**, *26*, 1072; f) M. Aguilar-Martìnez, J. A. Bautista-Martìnez, N. Macìas-Ruvalcaba, I. Gonzàles, E. Tovar, T. Marin del Alizal, O. Collera, G. Cuevas, *J. Org. Chem.* **2001**, *66*, 8349; g) P. Stahl, L. Kissau, R. Matzischek, A. Giannis, H. Waldmann, *Angew. Chem.* **2002**, *114*, 1222; *Angew. Chem. Int. Ed.* **2002**, *41*, 1174; h) T. Ling, E. Poupon, E. J. Rueden, S. H. Kim, E. A. Theodorakis, *J. Am. Chem. Soc.* **2002**, *124*, 12261; i) G. Meazza, B. E. Scheffler, M. R. Tellez, A. M. Rimando, J. G. Romagni, S. O. Duke, D. Nanayakkara, I. A. Khan, E. A. Abourashed, F. E. Dayan, *Phytochemistry* **2002**, *60*, 281.

[20] Red crystals of **2a**·0.5 suitable for X-ray diffraction studies were obtained by slow diffusion of heptane into an solution of **2a** in acetone. Data for **2a**·0.5 acetone: triclinic space group, $P\bar{1}$, a = 9.7610(2), b = 11.9030(3), c = 15.8030(4) Å, α = 68.040(14), β = 80.380(12), γ = 73.100(11)°, 173(2) K, Z = 2; refinement of 10326 reflections and 465 parameters, yielded $R1$ = 0.0859 and $wR2$ = 0.1757 for all data (5599 reflections with $I > 2\sigma(I)$). Single crystals of **3c**·0.5 Et_2O suitable for X-ray diffraction studies were obtained from a mixture of acetone/Et_2O; data for **3c**·0.5 Et_2O: triclinic space group, $P\bar{1}$, with a = 11.617(5), b = 14.726(5), c = 14.990(5) Å, α = 80.25(5), β = 74.05(5), γ = 67.78(5)°, 173(2) K, Z = 2; refinement of 13224 reflections and 630 parameters yielded $R1$ = 0.0902 and $wR2$ = 0.2336 for all data (7537 reflections with $I > 2\sigma(I)$). CCDC-279100 and -279101 contain the supplementary crystallographic data for this paper. These data can be obtained free of charge from The Cambridge Crystallographic Data Center via www.ccdc.cam.ac.uk/data_request/cif.

[21] a) B. Olbrich-Deussner, W. Kaim, R. Gross-Lannert, *Inorg. Chem.* **1989**, *28*, 3113; b) R. C. Wheland, J. L. Gibson, *J. Am. Chem. Soc.* **1976**, *98*, 3916.

[22] a) S. Dähne, D. Leupold, *Angew. Chem.* **1966**, *78*, 1029; *Angew. Chem. Int. Ed. Engl.* **1966**, *5*, 984; b) J. Fabian, *J. Prakt. Chem.* **1978**, *320*, 361; c) J. Fabian, *Int. J. Quantum Chem.* **1977**, *11*, 259; d) N. Tyutyulkov, J. Fabian, A. Mehlhorn, F. Dietz, A. Tader, *Polymethine Dyes; Structure and Properties*, St. Kliment Ohrdski University Press, Sofia, **1991**; e) J. Kucera, Z. Arnold, *Collect. Czech. Chem. Commun.* **1967**, *32*, 1704.

[23] a) R. Gompper, H.-U. Wagner, *Angew. Chem.* **1976**, *88*, 389; b) R. Gompper, H.-H. Vogt, H.-U. Wagner, *Z. Naturforsch. B* **1981**, *36*, 1644.

 © 2006 Wiley-VCH Verlag GmbH & Co. KGaA, Weinheim

Chalcogenides

DOI: 10.1002/anie.200502787

Acid-Induced Conversions in Open-Framework Semiconductors: From $[Cd_4Sn_3Se_{13}]^{6-}$ to $[Cd_{15}Sn_{12}Se_{46}]^{14-}$, a Remarkable Disassembly/Reassembly Process**

*Nan Ding and Mercouri G. Kanatzidis**

The assembly of chalcogenides with 3D open frameworks is of considerable scientific interest because, like the zeolites, they have large free spaces.[1–3] Yet due to their greater chemical, compositional, and structural diversity, the chalcogenides present a wider variety and broader scope of properties. These materials can be relevant in molecular recognition,[2a] ion conduction,[3c] environmental remediation,[4] and photocatalysis.[5] The chalcogen elements can impart novel photonic or electronic properties that are not found in zeolites.[3]

[*] N. Ding, Prof. M. G. Kanatzidis
Department of Chemistry
Michigan State University
East Lansing MI 48842-1793 (USA)
Fax: (+1) 517-355-1793
E-mail: kanatzid@cem.msu.edu

[**] Financial support from the National Science Foundation (DMR-0443785 and CHE-0211029 Chemistry Research Group) is gratefully acknowledged.

Supporting information for this article is available on the WWW under http://www.angewandte.org or from the author.

© 2006 Wiley-VCH Verlag GmbH & Co. KGaA, Weinheim
InterScience

However, the ability of zeolites (for example, H-Y, H-ZSM-5[6]) to act as solid-acid catalysts is not shared by open-framework chalcogenides, because the chalcogenides are more vulnerable to attack by acid. The 3D open framework of $K_6Cd_4Sn_3Se_{13}$ contains intersecting tunnels that enable fast ion exchange with alkali-metal cations.[7] The observation of efficient ion exchange in $K_6Cd_4Sn_3Se_{13}$ led to our idea of making proton-exchanged $H_6Cd_4Sn_3Se_{13}$, which would contain alkali-metal-free tunnels, through the direct reaction of $K_6Cd_4Sn_3Se_{13}$ with acid. Our attempt to make $H_6Cd_4Sn_3Se_{13}$ led to the generation of the new 3D anionic framework $[Cd_{15}Sn_{12}Se_{46}]^{14-}$, which shows surprising resistance to acids, as well as excellent ion-exchange properties. Although the number of open-framework chalcogenides has been steadily increasing, reactivity studies on these materials have not been emphasized to date. Herein, we give one of the first reports on the reactivity of these compounds.

After stirring $K_6Cd_4Sn_3Se_{13}$ in a concentrated aqueous solution of HI (pH 1.1–1.8) for 1 h, the original cube-shaped crystals (Figure 1a) disappeared and new crystals with a tetrahedral morphology (Figure 1b) were formed. Single-crystal X-ray diffraction analysis revealed that the new compound has the formula $K_{14-x}H_xCd_{15}Sn_{12}Se_{46}$ ($x \approx 7$) and a unit cell that is unrelated to that of $K_6Cd_4Sn_3Se_{13}$.[8] Furthermore, the new structure is comprised of $[Sn_2Se_7]^{6-}$ ions, rather than the $[SnSe_4]^{4-}$ ions found in $K_6Cd_4Sn_3Se_{13}$.

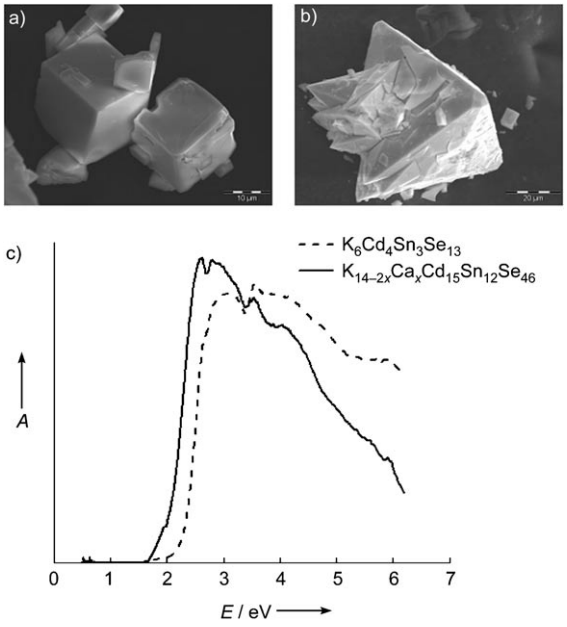


Figure 1. a) Scanning electron microscope (SEM) image of the original crystals of $K_6Cd_4Sn_3Se_{13}$. b) SEM image of the new crystals of $K_{14-x}H_xCd_{15}Sn_{12}Se_{46}$. c) Electronic spectra of $K_6Cd_4Sn_3Se_{13}$ (dashed line) and $K_{14-2x}Ca_xCd_{15}Sn_{12}Se_{46}$ (solid line).

Interestingly, the isostructural compounds $K_{14-2x}M_xCd_{15}Sn_{12}Se_{46}$ (M = Ca, Mg; $x \approx 1.5$, 4) were formed under the hydrothermal conditions used to synthesize the original compound $K_6Cd_4Sn_3Se_{13}$,[7] by simply adding Ca^{2+} or Mg^{2+} ions. The hydrothermal synthesis of $K_{14-2x}M_xCd_{15}Sn_{12}Se_{46}$, in a yield of approximately 70%, is complete within 18–24 h, whereas the formation of $K_6Cd_4Sn_3Se_{13}$ usually requires 3–4 days.[9,10] To obtain an analogue with only K^+ ions, it was necessary to carry out the hydrothermal reaction of the starting materials K_2Se, Cd, Sn, and Se at a higher temperature.[11,12] The greater dissociation rate of water at higher temperatures and pressures generates more H^+ ions, which may help in the formation of the $[Sn_2Se_7]^{6-}$ ions. The compound $K_{14-2x}Ca_xCd_{15}Sn_{12}Se_{46}$ is a wide-gap semiconductor with an energy gap of approximately 2.00 eV, which is narrower than that of $K_6Cd_4Sn_3Se_{13}$ (2.33 eV), Figure 1c.

Although the mechanism behind the transformation of $K_6Cd_4Sn_3Se_{13}$ to $K_{14-x}H_xCd_{15}Sn_{12}Se_{46}$ is not clear, the reaction is not topotactic, but involves a dissolution/reassembly process. We describe the process on the basis of the building blocks of the two anionic frameworks $[Cd_4Sn_3Se_{13}]^{6-}$ and $[Cd_{15}Sn_{12}Se_{46}]^{14-}$ in Equation (1). In this reaction, either a protogenic acid or a Lewis acid such as an M^{2+} ion, can be used to condense two of the original $[SnSe_4]^{4-}$ units into a single $[Sn_2Se_7]^{6-}$ dimeric unit, with the expulsion of Se^{2-} ions. In addition, some Cd^{2+} ions are expelled during the formation of the final structure. Considering that selenides are generally vulnerable to acid attack, one of the most amazing properties of the $[Cd_{15}Sn_{12}Se_{46}]^{14-}$ framework is its high resistance to acid (up to pH 1.1). This feature may be due to the compact 3D arrangement of the building fragments.

$$4\,[Cd_4(SnSe_4)_3(Se)]^{6-} \xrightarrow{\text{acid}} [Cd_{15}(Sn_2Se_7)_6(Se)_4]^{14-} + Cd^{2+} + 6\,Se^{2-} \quad (1)$$

The new compounds crystallize in the noncentrosymmetric space group $I\bar{4}3d$. Figure 2a shows a [100] projection of the $[Cd_{15}Sn_{12}Se_{46}]^{14-}$ framework in the structure of $K_{14-2x}Ca_xCd_{15}Sn_{12}Se_{46}$. Surprisingly, the unique framework is based on dimeric $[Sn_2Se_7]^{6-}$ units linked by Cd^{2+} ions. The formula of the framework can be more expressly written as $[Cd_{15}(Sn_2Se_7)_6(\mu_3\text{-}Se)_4]^{14-}$.

The high structural complexity makes it difficult to define a suitable building block in this extended framework. One possibility is the complex fragment with the formula $[Cd_{15}(Sn_2Se_7)_6(\mu_3\text{-}Se)_4]^{14-}$ shown in Figure 2b. At its center there is a μ_3-Se atom (Se5) with a triangular planar geometry. To simplify the description, one third of the building block ($[Cd_5(Sn_2Se_7)_2(\mu_3\text{-}Se)_{4/3}]^{14/3-}$) is singled out and shown in Figure 2c. The inset of Figure 2c shows the spatial disposition of the metal atoms in this fragment—two vertex-sharing trigonal bipyramids whose trigonal axes are perpendicular to each other. The five Cd atoms (one Cd1 atom and four Cd2 atoms) in this fragment define the center and four vertices of a tetrahedron, which can be used to represent the whole $[Cd_5(Sn_2Se_7)_2(\mu_3\text{-}Se)_{4/3}]^{14/3-}$ unit. As shown in Figure 2d, one way of viewing the $[Cd_{15}(Sn_2Se_7)_6(\mu_3\text{-}Se)_4]^{14-}$ building block is simply as three such tetrahedra linked through a μ_3-Se5 atom.

Two of these large $[Cd_{15}(Sn_2Se_7)_6(\mu_3\text{-}Se)_4]^{14-}$ building blocks connect to form a distorted trigonal prism, shown in polyhedral representations viewed perpendicular and parallel to the trigonal axis of the cage in Figures 3a and 3b, respectively. The height of the cage is approximately 6.3 Å (excluding the van der Waals radii of the Se atoms), and in

 © 2006 Wiley-VCH Verlag GmbH & Co. KGaA, Weinheim

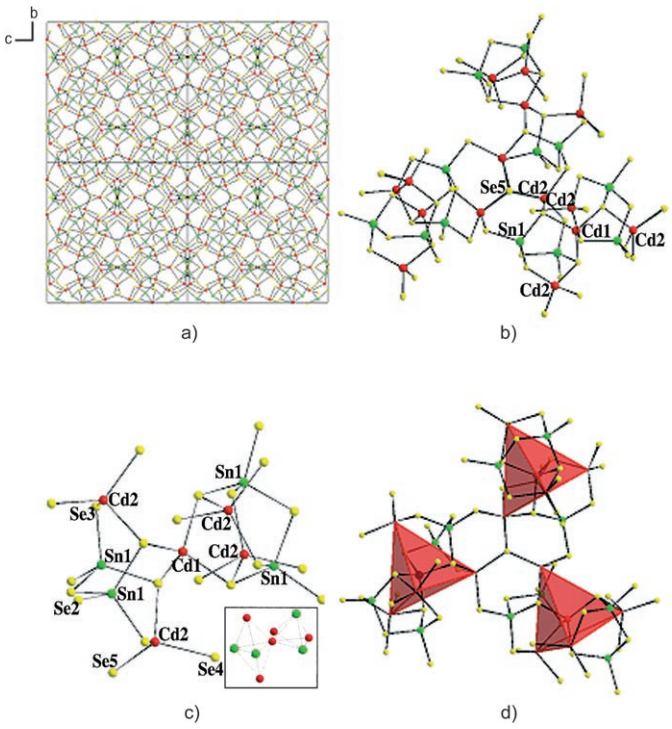


Figure 2. a) A [100] projection of the extended $[Cd_{15}Sn_{12}Se_{46}]^{14-}$ framework, in the structure of $K_{14-2x}Ca_xCd_{15}Sn_{12}Se_{46}$. b) The $[Cd_{15}(Sn_2Se_7)_6(\mu_3\text{-}Se)_4]^{14-}$ building block, which is composed of three of the cluster units shown in (c) linked through a μ_3-Se5 atom. c) A $[Cd_5(Sn_2Se_7)_2(\mu_3\text{-}Se)_{4/3}]^{14/3-}$ cluster unit. The inset shows the spatial disposition of the metal atoms. d) A polyhedral representation of the $[Cd_{15}(Sn_2Se_7)_6(\mu_3\text{-}Se)_4]^{14-}$ building block. The red tetrahedra are defined by the five Cd atoms in the cluster unit shown in (c). Cd red, Sn green, Se yellow. Selected bond lengths [Å]: Sn1–Se1 2.530(3), Sn1–Se2 2.547(3), Sn1–Se3 2.500(3), Sn1–Se4 2.492(3), Cd1–Se1 2.632(2), Cd2–Se1 2.688(3), Cd2–Se3 2.625(3), Cd2–Se4 2.652(3), Cd2–Se5 2.6150(17).

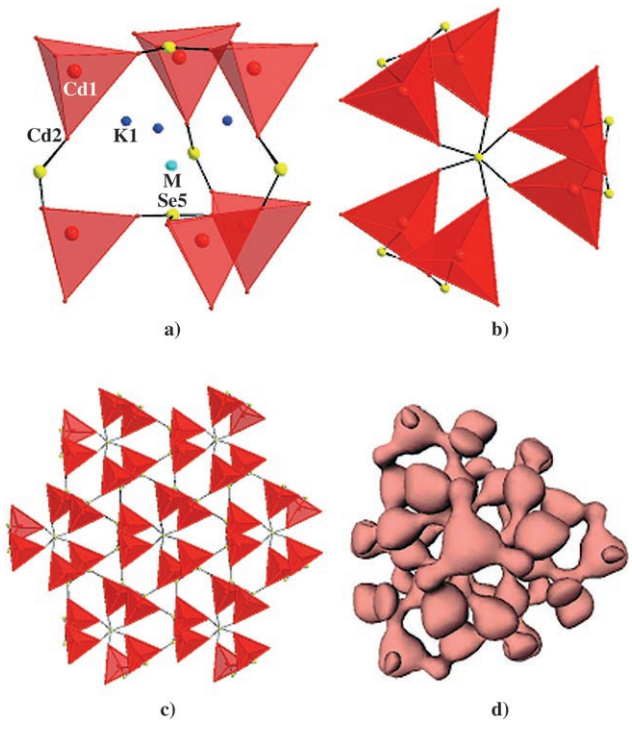


Figure 3. a) Polyhedral representation of a single cage, and the K^+ and M^{2+} ions (M = Ca, Mg) contained within it, in the structure of $K_{14-2x}M_xCd_{15}Sn_{12}Se_{46}$. b) The same cage viewed down its threefold axis. c) Polyhedral representation of the $[Cd_{15}Sn_{12}Se_{46}]^{14-}$ framework viewed down the [111] direction. The red polyhedra are defined by the five Cd atoms in Figure 2c, and the yellow balls are μ_3-Se5 atoms. d) Depiction of the void space in $[Cd_{15}Sn_{12}Se_{46}]^{14-}$ along the [111] direction. See text for details.

$K_{14}Cd_{15}Sn_{12}Se_{46}$ disordered K^+ ions occupy approximately half of its space.

In $K_{14-2x}M_xCd_{15}Sn_{12}Se_{46}$, M^{2+} ions replace the K^+ ions in the site near the center of the cage (Figure 3a).[13] A view down the [111] direction of the $[Cd_{15}Sn_{12}Se_{46}]^{14-}$ framework, in which only the cages whose axial directions are parallel to [111] are visible, is shown in Figure 3c. The same pattern is obtained in views down the $[11\bar{1}]$, $[\bar{1}11]$, and $[\bar{1}1\bar{1}]$ directions. Therefore, there are cages of four different orientations in the framework, and they are connected by sharing the $[Cd_5(Sn_2Se_7)_2(\mu_3\text{-}Se)_{4/3}]^{14/3-}$ units. Since the cages are capped by the tetrahedral building blocks, no open channels are readily seen in the unit cell.

The relative size, shape, and interconnection of the open channels in the $[Cd_{15}Sn_{12}Se_{46}]^{14-}$ framework is revealed by plotting the isosurface lying between the framework atoms and the voids,[14] as depicted in Figure 3d along the [111] direction. There are two types of cavities: a) the small spherical voids, which correspond to the small spaces inside the Cd_3Sn_2 trigonal bipyramids shown in Figure 2c and have a diameter of only approximately 2.5 Å, and b) the larger trigonal cavities, which lie inside the distorted trigonal prisms shown in Figure 3a and have a diameter of approximately 6 Å. These two types of cavities are connected by narrow channels whose width is approximately 2 Å to form a 3D labyrinthine network of cages.

The presence of interconnected cages in the structure enables large ion mobilities and fast ion exchange. Ion-exchange reactions with the ions Cs^+, Rb^+, Na^+, Li^+, and H^+ were performed on $K_{14}Cd_{15}Sn_{12}Se_{46}$ at room temperature (Table 1).[15,16] The mobility of the K^+ ions is surprisingly high, despite the relatively small diameter of the tunnels. As also observed for $K_6Cd_4Sn_3Se_{13}$,[7] Rb^+ ions can replace almost all the K^+ ions in $K_{14}Cd_{15}Sn_{12}Se_{46}$ to form $Rb_{14}Cd_{15}Sn_{12}Se_{46}$. The strongly hydrated Li^+ ion is a larger entity and gives a lower exchange yield than the Cs^+, Rb^+, and Na^+ ions. In the case of

Table 1: Energy dispersive spectroscopy (EDS) analysis of the ion-exchange products.

Exchanged cation	EDS analysis	Exchange yield[a] [%]
Cs^+	$K_{1.44}Cs_{8.64}Cd_{15.12}Sn_{12}Se_{43.08}$	86
Rb^+	$K_{0.84}Rb_{13.92}Cd_{14.76}Sn_{12}Se_{42.36}$	94
Na^+	$K_{1.56}Na_{11.40}Cd_{14.04}Sn_{12}Se_{48.0}$	88
Li^+	$K_{8.88}Cd_{13.32}Sn_{12}Se_{46.08}$	37
H^+	$K_{4.68}Cd_{12.48}Sn_{12}Se_{43.08}$	67

[a] In the cases of Li^+ and H^+ ion exchange, the yield is calculated based on the theoretical formula $K_{14}Cd_{15}Sn_{12}Se_{46}$; all other yields are calculated based on the amount of cations detected.

© 2006 Wiley-VCH Verlag GmbH & Co. KGaA, Weinheim

H^+ ion exchange, approximately 2/3 of the K^+ ions were exchanged when a concentrated acid solution (pH 1.7) was used. When the pH was 2.3, almost no exchange of K^+ ions was observed.

In a remarkable acid-induced 3D-to-3D transformation at room temperature, $K_6Cd_4Sn_3Se_{13}$ was converted into $K_{14-x}H_xCd_{15}Sn_{12}Se_{46}$, which adopts a new structure type. The $[Cd_{15}Sn_{12}Se_{46}]^{14-}$ framework, which contains a tunnel network of accessible cages of labyrinthine complexity, is highly robust and acid resistant. The new structure type may serve as a suitable model for understanding the structures of amorphous mesostructured chalcogenides,[17,18] for example, the mesostructured "Pt-$SnSe_4$," which also shows marked resistance to acids and excellent ion-exchange properties.[19]

Received: August 5, 2005
Revised: November 22, 2005
Published online: January 20, 2006

Keywords: chalcogenides · hydrothermal synthesis · ion-exchange · open-framework structures · semiconductors

[1] a) S. Dhingra, M. G. Kanatzidis, *Science* **1992**, *258*, 1769; b) T. J. McCarthy, T. A. Tanzer, M. G. Kanatzidis, *J. Am. Chem. Soc.* **1995**, *117*, 1294; c) J. A. Hanko, M. G. Kanatzidis, *Angew. Chem.* **1998**, *110*, 354; *Angew. Chem. Int. Ed.* **1998**, *37*, 342; d) A. Enos Axtell III, Y. Park, K. Chondroudis, M. G. Kanatzidis, *J. Am. Chem. Soc.* **1998**, *120*, 124; e) M. J. Manos, R. G. Iyer, E. Quarez, J. H. Liao, M. G. Kanatzidis, *Angew. Chem.* **2005**, *117*, 3552; *Angew. Chem. Int. Ed.* **2005**, *44*, 3618.

[2] a) H. Li, A. Laine, M. O'Keeffe, O. M. Yaghi, *Science* **1999**, *283*, 1145; b) H. Li, J. Kim, T. L. Groy, M. O'Keefe, O. M. Yaghi, *J. Am. Chem. Soc.* **2001**, *123*, 4867; c) H. Li, J. Kim, M. O'Keefe, O. M. Yaghi, *Angew. Chem.* **2003**, *115*, 1817; *Angew. Chem. Int. Ed.* **2003**, *42*, 1819.

[3] a) N. Zheng, X. Bu, P. Feng, *Angew. Chem.* **2004**, *116*, 4857; *Angew. Chem. Int. Ed.* **2004**, *43*, 4753; b) N. Zheng, X. Bu, P. Feng, *Nature* **2003**, *426*, 428; c) X. Bu, N. Zheng, Y. Li, P. Feng, *J. Am. Chem. Soc.* **2003**, *125*, 6024; d) N. Zheng, X. Bu, B. Wang, P. Feng, *Science* **2002**, *298*, 2366; e) C. Wang, X. Bu, N. Zheng, P. Feng, *J. Am. Chem. Soc.* **2002**, *124*, 10268.

[4] C. L. Cahill, J. B. Parise, *J. Chem. Soc. Dalton Trans.* **2000**, 1475.

[5] a) N. Zheng, X. Bu, P. Feng, *J. Am. Chem. Soc.* **2005**, *127*, 5286; b) N. Zheng, X. Bu, P. Feng, *Chem. Commun.* **2005**, 2805.

[6] T. Okuhara, *Chem. Rev.* **2002**, *102*, 3641.

[7] N. Ding, D.-Y. Chung, M. G. Kanatzidis, *Chem. Commun.* **2004**, 1170.

[8] $K_{14-x}H_xCd_{15}Sn_{12}Se_{46}$ ($x \approx 7$) crystal data: A tetrahedron-shaped crystal with dimensions $0.065 \times 0.059 \times 0.053$ mm^3 was chosen for the single-crystal X-ray diffraction experiment. An empirical absorption correction was applied to the data using SADABS. The structure was solved by direct methods and refined using SHELX-97. $K_{7.92}H_{6.08}Cd_{15}Sn_{12}Se_{46}$, $M_r = 7058.38$, cubic, space group $I\bar{4}3d$ (No. 220), $a = 23.0897(5)$ Å, $V = 12309.9(5)$ Å^3, $Z = 4$, $\rho_{calcd} = 3.790$ mg m^{-3}, $\mu = 18.763$ mm^{-1}; index range $-27 \le h \le 27$, $-27 \le k \le 27$, $-27 \le l \le 27$; total reflections 42734, independent reflections 1815, parameters 65, $R1 = 0.0840$, $wR2 = 0.2085$, GOF = 0.950. The crystals diffracted X-rays poorly. The K^+ ions are disordered over several sites in the cavity. Energy dispersive spectroscopy (EDS) analysis of the single crystal: $K_{4.8}Cd_{12.0}Sn_{12}Se_{45.6}$. The structure was not deposited with the ICSD because of the poor diffraction quality of the crystals and the availability of the much better refined structures of the isostructural compounds $K_{14-2x}M_xCd_{15}Sn_{12}Se_{46}$.

[9] Synthesis of $K_{14-2x}M_xCd_{15}Sn_{12}Se_{46}$ (M = Ca, Mg; $x \approx 1.5, 4$): K_2Se (0.093 g, 0.6 mmol), Cd (0.143 g, 1.3 mmol), Sn (0.120 g, 1.0 mmol), and Se (0.260 g, 3.3 mmol) were combined in an evacuated and flame-sealed fused-silica tube, and melted at 900 °C. The product was loaded into a 9-mm pyrex tube along with $CaCl_2$ (0.066 g, 0.6 mmol) or $MgCl_2 \cdot 6H_2O$ (0.145 g, 0,7 mmol), and deionized water (0.2 mL). The tube was then evacuated to 3×10^{-3} Torr and flame sealed. The tube was kept at 115 °C for 18–24 h. The products, dark orange tetrahedral or polyhedral crystals, were collected by filtration, and washed with water, ethanol, and diethyl ether. Yield: 70%. The main impurity is $K_2CdSnSe_4$ (ca. 30%). The crystals are stable in air for months. The powder X-ray diffraction patterns of $K_{14-2x}M_xCd_{15}Sn_{12}Se_{46}$ are identical to that of $K_{14-x}H_xCd_{15}Sn_{12}Se_{46}$, demonstrating that the compounds are isostructural.

[10] $K_{14-2x}Ca_xCd_{15}Sn_{12}Se_{46}$ ($x \approx 1.5$) crystal data: A polyhedron-shaped crystal with dimensions $0.085 \times 0.102 \times 0.093$ mm^3 was chosen for the single-crystal X-ray diffraction experiment. An empirical absorption correction was applied to the data using SADABS. The structure was solved with direct methods and refined using SHELX-97. $K_{6.6}Ca_{0.8}Cd_{15}Sn_{12}Se_{46}$, $M_r = 7031.99$, cubic, $I\bar{4}3d$ (No. 220), $a = 23.2807(4)$ Å, $V = 12617.9(4)$ Å^3, $Z = 4$, $\rho_{calcd} = 3.807$ mg m^{-3}, $\mu = 18.500$ mm^{-1}; index range $-27 \le h \le 27$, $-27 \le k \le 27$, $-27 \le l \le 15$; total reflections 30752, independent reflections 1855, parameters 66, $R1 = 0.0516$, $wR2 = 0.1337$, GOF = 1.140. The K^+ and Ca^{2+} ions are disordered over several sites in the cavity. EDS analysis of the single crystal: $K_{10.4}Ca_{1.3}Cd_{14.9}Sn_{12}Se_{43.7}$. Further details of the crystal structure investigation may be obtained from the Fachinformationszentrum Karlsruhe, 76344 Eggenstein-Leopoldshafen, Germany (fax: (+49) 7247-808-666; e-mail: crysdata@fiz-karlsruhe.de) on quoting the deposition number CSD-415497.

[11] Synthesis of $K_{14}Cd_{15}Sn_{12}Se_{46}$: K_2Se (0.186 g, 1.2 mmol), Cd (0.286 g, 2.6 mmol), Sn (0.240 g, 2.0 mmol), and Se (0.520 g, 6.6 mmol) were combined in an evacuated and flame-sealed fused-silica tube, and melted at 900 °C. The product was loaded into a 13-mm pyrex tube along with deionized water (0.3 mL). The tube was then evacuated to 3×10^{-3} Torr and flame sealed. The tube was kept at 180 °C for 6 days. Dark orange polyhedral crystals were isolated in 61% yield. The impurities are $K_2CdSnSe_4$ (ca. 29%), CdSe (ca. 10%), and a small amount of Se.

[12] $K_{14}Cd_{15}Sn_{12}Se_{46}$ crystal data: A polyhedron-shaped crystal with dimensions $0.115 \times 0.096 \times 0.098$ mm^3 was chosen for the single-crystal X-ray diffraction experiment. An empirical absorption correction was applied to the data using SADABS. The structure was solved with direct methods and refined using SHELX-97. $K_{14}Cd_{15}Sn_{12}Se_{46}$, $M_r = 7989.84$, cubic, $I\bar{4}3d$ (No. 220), $a = 23.090(3)$ Å, $V = 12311(3)$ Å^3, $Z = 4$, $\rho_{calcd} = 3.933$ mg m^{-3}, $\mu = 19.001$ mm^{-1}; index range $-27 \le h \le 27$, $-27 \le k \le 27$, $-27 \le l \le 27$; total reflections 73484, independent reflections 1815, parameters 67, $R1 = 0.0768$, $wR2 = 0.1874$, GOF = 1.210. The K^+ ions are disordered over several sites in the cavity. EDS analysis of the single crystal: $K_{12.4}Cd_{14.5}Sn_{12}Se_{44.0}$. Further details of the crystal structure investigation may be obtained from the Fachinformationszentrum Karlsruhe, 76344 Eggenstein-Leopoldshafen, Germany (fax: (+49) 7247-808-666; e-mail: crysdata@fiz-karlsruhe.de) on quoting the deposition number CSD-415498.

[13] See Supporting Information for further discussion of the cationic site occupancy.

[14] T. F. Nagy, S. D. Mahanti, J. L. Dye, *Zeolites* **1997**, *19*, 57. See Supporting Information for further explanation of the calculation of the free space.

 © 2006 Wiley-VCH Verlag GmbH & Co. KGaA, Weinheim

[15] A typical ion-exchange reaction with H^+ ions: $K_{14}Cd_{15}Sn_{12}Se_{46}$ (20 mg) was mixed with an aqueous solution of HI (pH 1.7, 15 mL). The mixture was left at room temperature for 5.5 h without stirring. The product was collected by filtration, and washed with water, ethanol, and diethyl ether. The crystallinity of the sample was confirmed by X-ray powder diffraction before and after the ion exchange. The extent of the ion exchange was assessed with EDS analysis.

[16] A typical ion-exchange reaction with A^+ ions (A = Li, Na, Rb, Cs): $K_{14}Cd_{15}Sn_{12}Se_{46}$ (40 mg) was mixed with and aqueous solution of A^+ ions (LiI, NaI, RbCl, or $CsCH_3COO$; ca. 20 equiv, 10 mL) at room temperature and stirred for 5 h. The products were collected by filtration, and washed with water, ethanol, and diethyl ether. The crystallinity of the samples was confirmed by X-ray powder diffraction before and after the ion exchange. The extent of the ion exchange was assessed with EDS analysis.

[17] P. N. Trikalitis, K. K. Rangan, M. G. Kanatzidis, *J. Am. Chem. Soc.* **2002**, *124*, 2604.

[18] P. N. Trikalitis, K. K. Rangan, T. Bakas, M. G. Kanatzidis, *Nature* **2001**, *410*, 671.

[19] P. N. Trikalitis, N. Ding, C. Malliakas, S. J. L. Billinge, M. G. Kanatzidis, *J. Am. Chem. Soc.* **2004**, *126*, 15326.

 © 2006 Wiley-VCH Verlag GmbH & Co. KGaA, Weinheim

NIR Dyes

DOI: 10.1002/anie.200502998

Pentarylene- and Hexarylenebis(dicarboximide)s: Near-Infrared-Absorbing Polyaromatic Dyes**

*Neil G. Pschirer, Christopher Kohl, Fabian Nolde, Jianqiang Qu, and Klaus Müllen**

Although a large variety of dyes are commercially available today, there is an ongoing need for new chromophoric systems[1–3] and low-band-gap materials.[4] For example, near-infrared (NIR) emission has received increased attention for applications in bioassays and medicine[5] while NIR absorption is demanded for laser-welding of plastics or efficient blocking of heat rays. Most of the commercially available NIR materials are not suitable for such purposes owing to their insufficient stability.[6] Over the last decade we have developed several NIR-absorbing polyaromatic dyes.[7–9] By extending the π system of perylenebis(dicarboximide)s along the molecular long axis, we have obtained the higher homologues terrylenebis(dicarboximide) (**2**) and quaterrylenebis(dicarboximide) (**3**; Figure 1). In comparison to the absorption maximum of perylenebis(dicarboximide) (**1**), those of **2** and **3** are shifted bathochromically. Quaterrylenebis(dicarboximide) (**3**) is a deeply colored dye with a strong absorption in the NIR region.[9] Both chromophores exhibit high thermal, chemical, and photochemical stabilities together with high extinction coefficients.[8–11] Recently we introduced an alternative and surprisingly facile approach toward NIR absorbers by the coupling and fusion of a perylenedicarboximide with a 1,5-diaminoanthraquinone to afford bis(perylenedicarboximide)-*a*,*d*-1,5-diaminoanthraquinone (**4**), a NIR absorber with a remarkably strong absorption around 1100 nm and extraordinary thermal and photochemical inertness.[7]

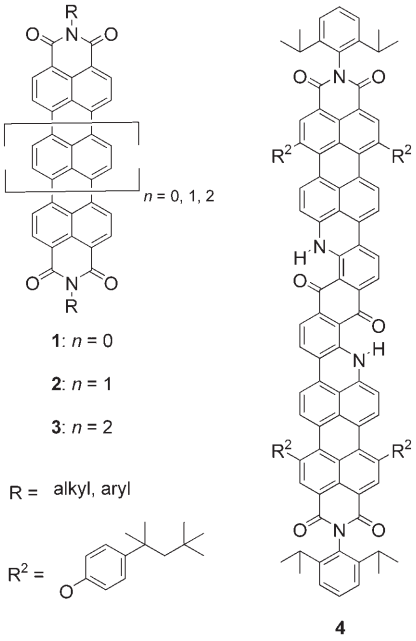


Figure 1. Chemical structures of rylenebis(dicarboximide)s and bis(rylenedicarboximide)-*a*,*d*-1,5-diaminoanthraquinone.

If we take into consideration the outstanding role of quaterrylenebis(dicarboximide) (**3**), then the extension of the framework of rylenebis(dicarboximide)s appears a logical next step to induce a narrowing of the HOMO–LUMO gap, thereby causing a further bathochromic shift in the absorption spectrum.[12] Herein, we describe the synthesis and attractive optical properties of homologous ladder-type chromophores, namely the pentarylenebis(dicarboximide)s **6** and **7** as well as the hexarylenebis(dicarboximide) **8**.

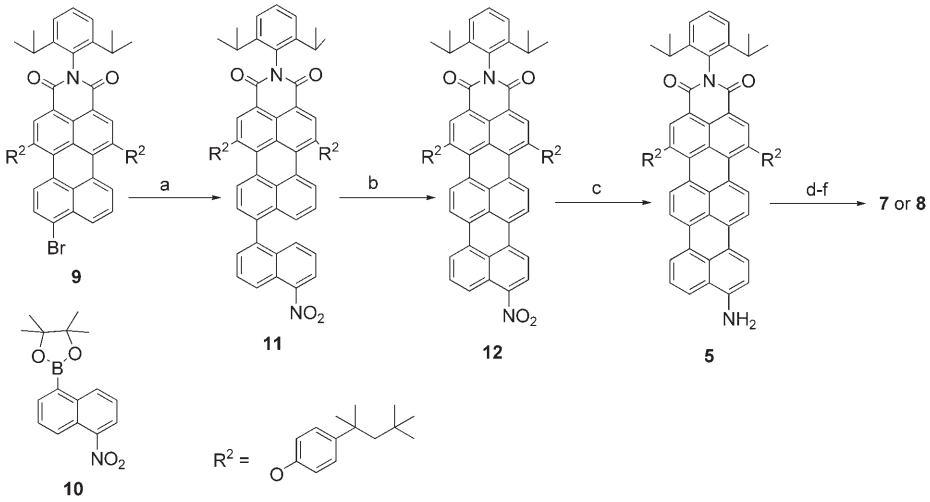
We selected two different construction concepts for the penta- and hexarylenebis(dicarboximide)s **6**, **7**, and **8**: 1) The "nitronaphthalene method" in which one nitronaphthalene unit is attached to a perylenedicarboximide, the bisaryl product is fused, and the nitro group is replaced by a halide to provide a halogen-substituted terrylenedicarboximide as a precursor for the penta- or hexarylenebis(dicarboximide)s **7** and **8** (Scheme 1); or 2) the "bisbromorylene method" in

[*] Dr. N. G. Pschirer, Dr. C. Kohl, F. Nolde, Dr. J. Qu, Prof. Dr. K. Müllen
Max Planck Institute for Polymer Research
Ackermannweg 10, 55128 Mainz (Germany)
Fax: (+49) 6131-379-350
E-mail: muellen@mpip-mainz.mpg.de

[**] We gratefully acknowledge BASF AG and the Deutsche Forschungsgemeinschaft (Sonderforschungsbereich 625) for financial support, as well as Dr. R. Sens and Dr. C. Lennartz (BASF AG) for their calculations.

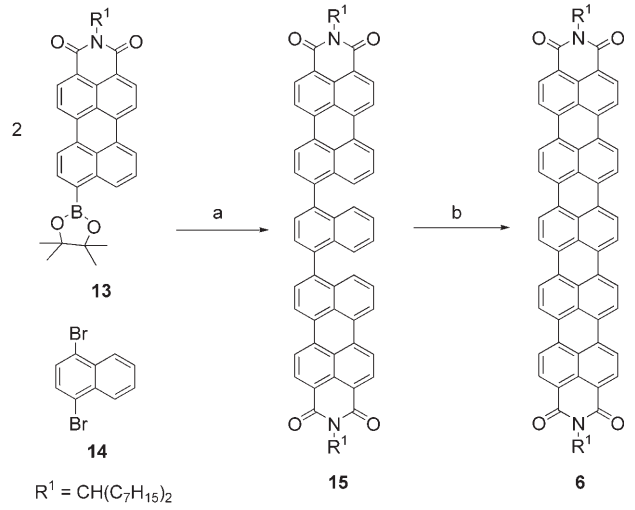
Supporting information for this article is available on the WWW under http://www.angewandte.org or from the author.

 © 2006 Wiley-VCH Verlag GmbH & Co. KGaA, Weinheim



Scheme 1. Reagents and conditions: a) $[Pd(PPh_3)_4]$, K_2CO_3 (aq), ethanol/toluene, 80 °C, 16 h, 100%; b) DBN, NaO*t*Bu, diglyme, 70 °C, 2 h 35%; c) Pd/C, H_2, ethanol/$CHCl_3$, room temperature, 15 h, 78%; d) $NaNO_2$, HCl, THF, Et_2O, MeCN, −10 °C, NaI; e) for **8**: $B(OR)_2$, $[Pd(PPh_3)_4]$, KOAc, toluene; for **7**: **9**, K_2CO_3 (aq), $[Pd(PPh_3)_4]$, ethanol/toluene; f) K_2CO_3, ethanolamine, 135 °C. DBN = 1,5-diazabicyclo-[4.3.0]non-5-ene.

which two perylenedicarboximides are coupled to a bisbromonaphthalene or -perylene and fused in a one-step (**6**) or two-step (**7** and **8**) sequence to form the corresponding penta- or hexarylenediimide (Schemes 2 and 3).



Scheme 2. Reagents and conditions: a) $[Pd(PPh_3)_4]$, K_2CO_3 (aq), ethanol/toluene, 80 °C, 72%; b) $AlCl_3$, chlorobenzene, 75 °C, 20 min, 24%.

The nitronaphthalene method requires the boronic ester of 1-bromo-5-nitronaphthalene (**10**) which was prepared according to the procedure of Miyaura et al.[13] with bis(pinacolato)diboron and $[PdCl_2(dppf)]$ (dppf = 1,1′-bis(diphenylphosphino)ferrocene). The boronic ester was coupled to the diphenoxy-substituted 9-bromoperylenedicarboximide (**9**) under standard Suzuki conditions to form the terrylene precursor **11** in quantitative yield (Scheme 1). In the subsequent step, **11** was cyclized with sodium *tert*-butoxide/1,5-diazabicyclo[4.3.0]non-5-ene as base in diglyme to give 11-nitroterrylenedicarboximide (**12**) in 35% yield, after isolation and purification by column chromatography.

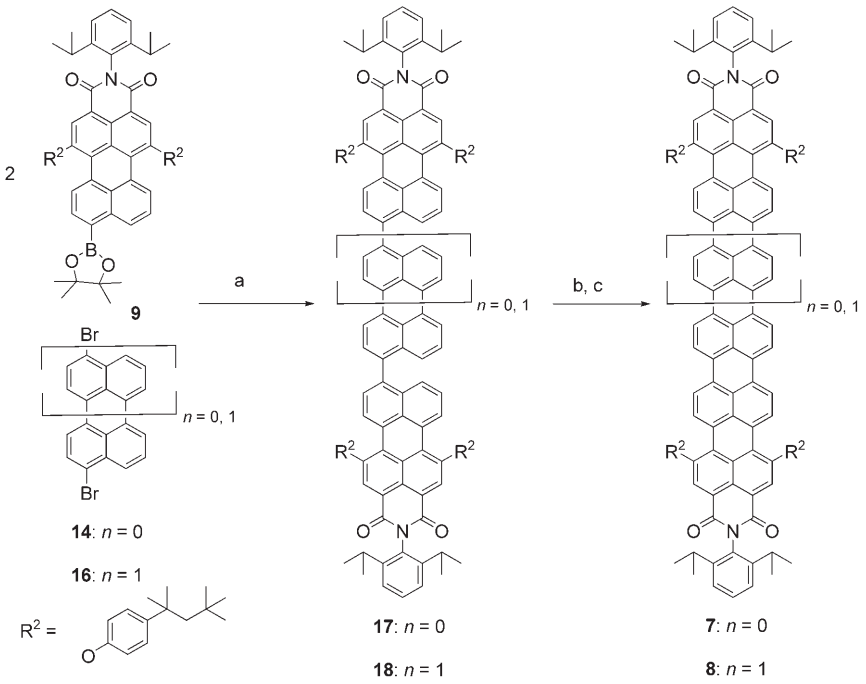
11-Nitroterrylenedicarboximide (**12**) is readily soluble in all common organic solvents (120 mg mL^{-1} CH_2Cl_2) at room temperature and serves as a starting material for the preparation of **7** and **8**. Reduction of **12** with Pd/C and hydrogen gave 11-aminoterrylene (**5**) in 78% yield. Attempts to produce a halogenated terrylene by the Sandmeyer reaction delivered the non-halogenated terrylene as the major product and only small quantities of the desired compound. The amount obtained, however, was sufficient for the homocoupling of the iodinated terrylenemonoimide or the Suzuki coupling of the monoimide with perylenemonoimide **9** to form the bis(terrylenemonoimide) or perylenemonoimide-terrylenemonoimide bichromophores, respectively, which were then directly cyclized (without isolation) through an oxidative cyclodehydrogenation to yield **8** or **7** in high purity and yield (last step) after purification.

To obtain these higher rylenediimides in an improved overall yield, a second approach was investigated. Extension of the framework by introducing a naphthalene or perylene unit between two perylenemonoimides (the bisbromorylene method) involves the palladium-catalyzed coupling reaction of perylenemonoimides with a bisbromo-functionalized naphthalene or perylene followed by a final bond closure to a double-stranded rylene structure. To avoid the use of toxic stannyl compounds as intermediates in the Stille coupling reaction, the boronic esters of 9-bromoperylenedicarboximide (**13**) and **9** were subjected to Suzuki coupling with 1,4-bisbromonaphthalene (**14**) to give the bisperylenylnapthalene derivatives **15** and **17** in good yields (**15** 72%, **17** 75%). The boronic ester of **9** was coupled with 1,9(10)-bisbromoperylene (**16**) to provide **18** in 79% yield (Scheme 3).

The final cyclization steps were carried out through an oxidative cyclodehydrogenation. Several dehydrogenation methods to form rylene structures from polynaphthalene and/or polyperylene units are described in the literature. Clar et al. applied successfully an aluminum chloride/sodium chloride melt to "cake" polynaphthalene derivatives together.[14,15] We developed milder conditions for the cyclization to oligorylenes under the influence of $AlCl_3/CuCl_2$ and $FeCl_3$.[16]

While both 2,6-diisopropylphenyl and 1-heptyloctyl substituents at the imide structure improve the synthesis of pentarylenediimide by enhancing the solubility, the alkyl substitution has the advantage that no dealkylation has to be feared during the Lewis acid assisted cyclization step. To obtain the fully annulated ladder-type structure **6**, the bisperylenyl(naphthalene) derivative **15** was allowed to react with aluminum chloride in chlorobenzene to afford **6**, which was obtained as a black–green precipitate in 24% yield. The pentarylenediimide **6** is only slightly soluble in organic

 © 2006 Wiley-VCH Verlag GmbH & Co. KGaA, Weinheim



Scheme 3. Reagents and conditions: a) $[Pd(PPh_3)_4]$, K_2CO_3 (aq), ethanol/toluene, 80 °C; b) $FeCl_3$/nitromethane, CH_2Cl_2, room temperature, 24 h; c) K_2CO_3, ethanolamine, 135 °C, 4 h.

solvents ($< 0.5\ mg\,mL^{-1}\ CH_2Cl_2$) at room temperature and is better regarded as a pigment than a dye.

It was then of particular interest to see if we could synthesize , through the bisbromorylene method the more-soluble tetraphenoxy-substituted derivatives **7** and **8**, which were already obtained by the nitronapthalene method. The cyclization of **17** and **18** to the tetraphenoxy-pentarylene **7** and -hexarylene **8** was achieved under milder conditions in a two-step process to avoid the undesirable dealkylation of phenoxy and imide substituents by strong Lewis acids. The first cyclization of **17** and **18** was obtained with $FeCl_3$/nitromethane in CH_2Cl_2 at room temperature. After hydrolysis and washing, the target compounds were formed by a mild base-promoted cyclization with K_2CO_3/ethanolamine. This method provides the NIR absorbers **7** and **8** in an overall yield of over 25 %.

As a result of the substitution with four *tert*-octylphenoxy groups in the bay positions, penta- and hexarylene derivative **7** and **8** are soluble in all common organic solvents ($> 1\ mg\,mL^{-1}\ CH_2Cl_2$). The synthesized penta- and hexarylenediimides were characterized by mass spectrometry and IR and UV/Vis/NIR spectroscopy, while the measurement of ^1H NMR spectra was only successful in the case of **7**. The absorption spectra of penta- and hexarylene derivatives **7** and **8** demonstrate a strong bathochromic shift of the absorption maximum with an increasing degree of annulation (Figure 2). The absorption maximum of **7** is found at 877 nm whereas that for **8** lies at 953 nm. By examining the entire rylenediimide series (perylenediimide **1** to hexarylenediimide **8**), it is apparent that the energy of the absorption maximum is shifted to lower energies upon increasing the length of the π system, as is to be expected from a simple particle-in-a-box picture. When the maximum absorption energy was plotted against the inverse squared length of the π system, where the length L is taken as the N–N distance of the force-field geometries of rylenes **1**, **2**, **3**, **7**, and **8**, an ideal particle-in-the-box behavior ($E \approx 1/L^2$) was indeed observed (see Figure 3).

In the case of the pentarylene derivatives **6** and **7**, the absorption maximum is additionally influenced by the number of phenoxy substituents in the bay region of the chromophore. The maximum absorption of the unsubstituted pentarylene **6** lies at 831 nm, whereas that for the tetrasubstituted pentarylene **7** lies at 877 nm. This is a consequence of the destabilization of the HOMO by antibonding contributions of the phenoxy groups. The bathochromic shift of the first electronic transition upon phenoxy substitution in the bay position of **6** is best reproduced by ZINDO/s calculations, which give values of 745 nm for **6** and 777 nm for **7**. These calculations show a bathochromic shift of approximately 100 nm compared to the observed values, a typical effect of gas-phase calculations. In each case, the absorption bands exhibit a similar vibrational structure, which is typical for rylenediimides.

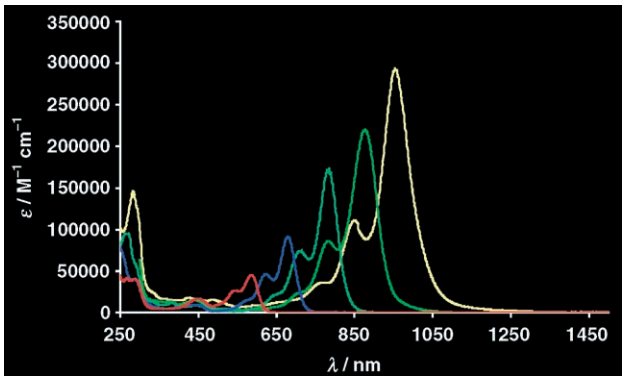


Figure 2. Absorption spectra of the entire tetraphenoxy-substituted rylenediimide series in $CHCl_3$: perylenebis(dicarboximide) (red), terrylenebis(dicarboximide) (blue), quaterrylenebis(dicarboximide) (turquoise), pentarylenebis(dicarboximide) **7** (green), and hexarylenebis(dicarboximide) **8** (yellow).

As a result of the extension of the aromatic π system along the molecular long axis, not only does a bathochromic shift become apparent but the absorption coefficients increase also: $\varepsilon = 235\ M^{-1}cm^{-1}$ for the pentarylenediimide **7**, $\varepsilon = 293\ M^{-1}cm^{-1}$ for the hexarylenediimide **8**. Such absorption coefficients are phenomenal and, to our knowledge, are the highest reported among all the known organic dyes in this region of the NIR spectrum. Theoretic elucidation of the electronic transition properties of penta- and hexarylene as

 © 2006 Wiley-VCH Verlag GmbH & Co. KGaA, Weinheim

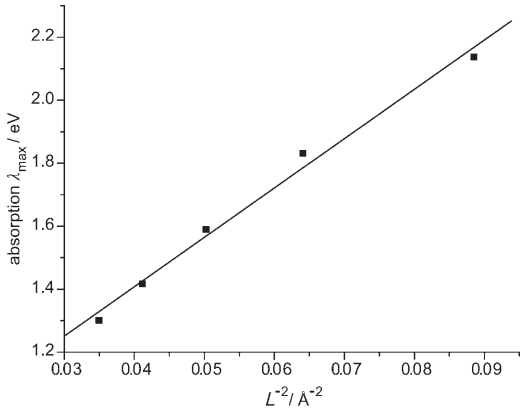


Figure 3. Correlation between the maximum absorption energy and the inverse squared length of the π system (see text). A particle-in-the-box behavior is observed ($E \approx 1/L^2$). Plotted points represent the tetraphenoxy-substituted rylene dyes (left to right) **8**, **7**, **3**, **2**, and **1**.

extended π-conjugated derivatives of perylenediimide substantiate these excellent spectral properties. Compounds **6**, **7**, and **8** display an impressive stability and their solutions remained unchanged over weeks in sunlight. The photostability of **8** was compared with its lower homologue, the quaterrylenediimide **2**, whose excellent photochemical stability was reported previously.[10] Exposure of solutions of **8** and **2** in THF (10^{-6} M^{-1}) in quartz cuvettes to UV light ($\lambda =$ 365 nm) for 9 h led to no significant changes in their absorption intensities. From a practical point of view, it is important to mention the almost colorless solutions of the penta- and hexarylenediimide derivatives **6**, **7**, and **8**. A negligible absorption in the visible region together with their extraordinary high extinction coefficients in the NIR, which is only comparable to a few squarylium dyes,[17] predestine them for many technological applications, such as security printing.

In conclusion, two synthetic approaches give access to an extended homologous series of NIR-absorbing rylenebis(dicarboximide)s. The absorption spectra of pentarylenediimide **6** and **7** as well as hexarylenediimide **8** are characterized by an extremely intense absorption between 830 and 960 nm. In addition to these remarkable photophysical properties, the penta- and hexarylene derivatives still display good chemical and thermal stability, as already observed for their smaller homologues, the perylene-, terrylene-, and quaterrylenediimides.

Received: August 23, 2005
Published online: January 20, 2006

Keywords: aromaticity · dyes/pigments · fused-ring systems · perylenes · UV/Vis spectroscopy

[1] M. Linke-Schätzel, A. D. Bhise, H. Gliemann, T. Koch, T. Schimmel, T. S. Balaban, *Thin Solid Films* **2004**, *451*, 16 – 21.
[2] F. Würthner, S. Ahmed, C. Thalacker, T. Debaerdemaeker, *Chem. Eur. J.* **2002**, *8*, 4742 – 4750.
[3] P. Coppo, M. Duati, V. N. Kozhevnikov, J. W. Hofstraat, L. De Cola, *Angew. Chem.* **2005**, *117*, 1840 – 1844; *Angew. Chem. Int. Ed.* **2005**, *44*, 1806 – 1810.
[4] L. Groenendaal, F. Jonas, D. Freitag, H. Pielartzik, J. R. Reynolds, *Adv. Mater.* **2000**, *12*, 481 – 494.
[5] V. Mantareva, D. Petrova, L. Avramov, I. Angelov, E. Borisova, M. Peeva, D. Wöhrle, *J. Porphyrins Phthalocyanines* **2005**, *9*, 47 – 53.
[6] P. Gregory, *High-Technology Applications of Organic Colorants*, Plenum, New York, **1991**.
[7] C. Kohl, S. Becker, K. Müllen, *Chem. Commun.* **2002**, *23*, 2778 – 2779.
[8] F. Holtrup, G. Müller, H. Quante, S. de Feyter, F. C. De Schryver, K. Müllen, *Chem. Eur. J.* **1997**, *3*, 219 – 225.
[9] H. Quante, K. Müllen, *Angew. Chem.* **1995**, *107*, 1487 – 1489; *Angew. Chem. Int. Ed. Engl.* **1995**, *34*, 1323 – 1325.
[10] Y. Nagao, H. Iwawaki, K. Kozawa, *Heterocycles* **2002**, *56*, 331 – 340.
[11] Y. Geerts, H. Quante, H. Platz, R. Mahrt, M. Hopmeier, A. Böhm, K. Müllen, *J. Mater. Chem.* **1998**, *8*, 2357 – 2369.
[12] M. Adachi, Y. Nagao, *Chem. Mater.* **1999**, *11*, 2107 – 2114.
[13] T. Ishiyama, M. Murata, N. Miyaura, *J. Org. Chem.* **1995**, *60*, 7508 – 7510.
[14] E. Clar, *Chem. Ber.* **1948**, *81*, 52 – 63.
[15] E. Clar, W. Kelly, R. M. Laird, *Monatsh. Chem.* **1956**, *87*, 391.
[16] K.-H. Koch, K. Müllen, *Chem. Ber.* **1991**, *124*, 2091 – 2100.
[17] J. Fabian, R. Zahradnik, *Angew. Chem.* **1989**, *101*, 693 – 710; *Angew. Chem. Int. Ed. Engl.* **1989**, *28*, 677 – 694; J. Fabian, M. Nakazumi, T. J. Matsuoka, *Chem. Rev.* **1992**, *92*, 1197 – 1226.

 © 2006 Wiley-VCH Verlag GmbH & Co. KGaA, Weinheim

Hybrid Nanocomposites

DOI: 10.1002/anie.200503067

Emission Enhancement by Formation of Aggregates in Hybrid Chromophoric Surfactant Amphiphile/Silica Nanocomposites**

*Chetan Jagdish Bhongale and Chain-Shu Hsu**

Following to the recent development of the organic-templated growth of materials, new types of photonic hybrid composite materials have emerged whose structure and function are organized hierarchically. Ordered, periodic mesoscopic materials allow the construction of composites with many types of guest, such as organic molecules or polymers. These host–guest materials combine the high stability of the inorganic host system, a new structure-forming mechanism due to the confinement of guests in well-defined

[*] C. J. Bhongale, Prof. C.-S. Hsu
Department of Applied Chemistry
National Chiao-Tung University
Hsinchu, Taiwan (R.O.C.)
Fax: (+886) 3513-1523
E-mail: cshsu@mail.nctu.edu.tw

[**] We thank the National Science Council of the Republic of China (NSC94-2129M009-009) for financial support.

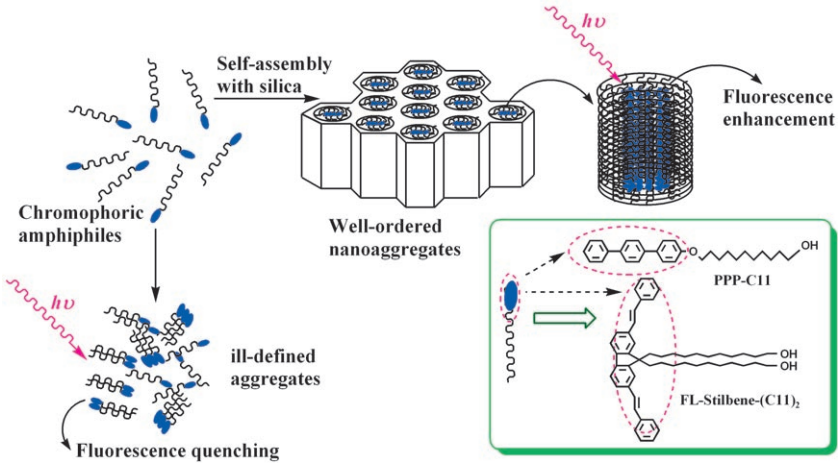
Supporting information for this article is available on the WWW under http://www.angewandte.org or from the author.

WILEY InterScience DISCOVER SOMETHING GREAT
© 2006 Wiley-VCH Verlag GmbH & Co. KGaA, Weinheim

pore channels, and a modular composition. The inorganic framework serves to protect, stabilize, and orient the organic moiety inside it. Preparation methods, properties, and possible applications of chromophores in porous silica, molecular sieves, and minerals have been summarized in a recent review article.[1] Inclusion of dye molecules such as Coumarin 40, Rhodamine BE50, or Oxazine 1 inside the nanopores has been demonstrated by Schulz-Ekloff's and Wöhrle's group,[2–4] and in several other papers on this topic the concentration of dye molecules within the mesopores has been optimized by either inclusion of the dye molecules within preformed mesopores or during sol–gel synthesis. These materials showed an increase in photoluminescence intensity at only moderate dye concentrations.[5–7] An MEH-PPV/silica nanocomposite[8] that was produced for control of energy transfer and prepared by infiltration of MEH-PPV into a preformed, oriented, hexagonal silica mesophase was found to be heterogeneous, exhibiting two distinct conjugated polymer environments, that is, polymers inside and outside the hexagonally arranged pore channels of the silica particles.

Self-assembly is the spontaneous organization of materials (or micelles) through noncovalent interactions without external intervention[9] into periodic hexagonal, cubic, or lamellar mesophases. It typically employs nonsymmetric molecules that are programmed to organize into well-defined supramolecular assemblies.[9] Amphiphilic surfactant molecules or polymers bearing hydrophilic and hydrophobic parts are the most common examples. Despite the excellent control of pore size, early mesoporous materials, following the pioneering work at Mobil on surfactant-templated materials,[10] were isolated in the form of powders, which precludes their use in thin-film applications like membranes, catalysts, etc. Stable, supported, mesoporous silica films were first prepared by the groups of Ozin[11] and Brinker[9,12] by evaporation-induced self-assembly (EISA). These films can be processed into porous or composite mesostructures with potential utility for a variety of applications such as membranes,[13] sensors,[14] waveguides,[15] lasers,[4,15,16] low-dielectric-constant (low-k) insulators,[17,18] and other still-evolving fields of activities. More recently, Okabe et al.[19] have demonstrated the immobilization and tuning of one-dimensional, columnar, charge-transfer (CT) assemblies in mesoporous silica films consisting of a hexagonal array of nanoscopic channels. The fabrication and characterization of multiply doped nanostructured silicate sol–gel thin films has also been reported.[20,21]

We have exploited the EISA approach to make mesostructured, functional, hybrid nanocomposite films for potential use in electroluminescence devices, where fluorescence quenching in the solid state is the most challenging problem. EISA can organize hydrophilic, inorganic and hydrophobic, organic precursors into ordered nanostructures.[22] It is well known that organic nanoparticles have special properties that lie between the properties of molecules and those of bulk materials,[23] and aggregation-induced emission (AIE) enhancement has been observed for a diverse range of conjugated organic nanoparticles.[24–26] However, these studies were focused mostly on the photophysical properties of nanoparticle suspensions rather than using nanoparticles systematically in thin-film formation. We have designed and synthesized the amphiphilic surfactant organic compounds PPP-C11 and FL-stilbene-$(C11)_2$, which have special conjugated chromophoric groups at the ends of their hydrophobic tails (see Scheme 1 for the chemical structures and the Supporting Information for synthetic procedures and characterization data). Our basic idea was to form the core or clusters of the chromophoric groups as nanopackets by self-assembly, which could enhance the photoluminescence (PL) of the nanocomposite films prepared, a seemingly ideal solution for the solid-state quenching of fluorescence. Indeed, we observed a higher photoluminescence intensity and quantum efficiency depending on the orientation and packing of the chromophoric groups at the tail end. The chromophore amphiphiles act as photoactive molecules as well as structure-directing agents. The organic–inorganic functional hybrid nanocomposites were characterized by SEM, TEM, XRD, and steady-state-absorbance and photoluminescence measurements.



Scheme 1. Formation of the chromophore-bearing amphiphile/silica self-assembled hybrid nanocomposite and the chemical structures of the chromophore amphiphiles used.

The SEM image in Figure 1a shows the formation of nanosheets of the PPP-C11 nanocomposite that are somewhat

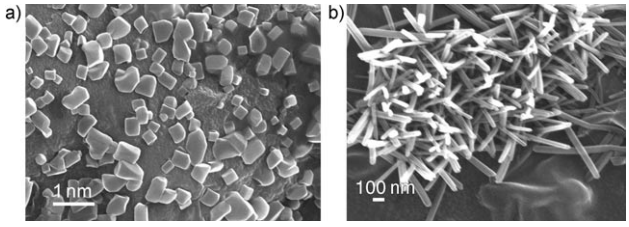


Figure 1. SEM images of the chromophoric amphiphile/silica self-assembled nanocomposites formed from a) PPP-C11 and b) FL-Stilbene-$(C11)_2$.

 © 2006 Wiley-VCH Verlag GmbH & Co. KGaA, Weinheim

rectangular in shape and a few nanometers thick. The FL-stilbene-$(C11)_2$ nanocomposite formed as uniform nanorods with diameters of about 75 nm and lengths below 1 μm (Figure 1b). X-ray diffraction (XRD) analysis of the nanocomposite thin films showed peaks characteristic of a periodic, mesoscopic silicate structure with single peaks around $2\theta = 1.53$ and 1.57°, thus indicating periodic, short-range structural order with a *d*-spacing for the (100) diffraction peak of 57.9 and 56.2 Å for the nanocomposite films of PPP-C11 and FL-stilbene-$(C11)_2$, respectively (Figure 2). The presence of higher-order Bragg peaks

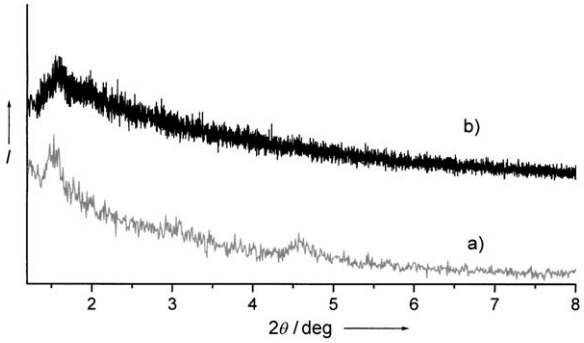


Figure 2. XRD profiles of mesostructured chromophoric amphiphile/silica self-assembled nanocomposites formed from a) PPP-C11 and b) FL-Stilbene-$(C11)_2$.

around $2\theta = 3$ and 4.5° in Figure 2a indicates that the PPP-C11 nanocomposite also displays a high degree of long-range structural order. TEM images of the nanocomposites revealed that the composite with FL-stilbene-$(C11)_2$ has a uniform mesostructure, but with no apparent long-range ordering[27] (Figure 3b), whereas the nanocomposite produced with PPP-

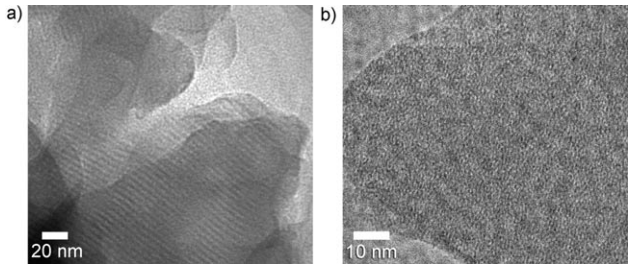


Figure 3. TEM images of chromophoric amphiphile/silica self-assembled nanocomposites formed from a) PPP-C11 and b) FL-Stilbene-$(C11)_2$.

C11 displays a highly uniform periodic mesostructure (Figure 3a). This difference is due to the size and orientation of the chromophore groups attached at the tail ends and the length and size of the surfactant in the nanocomposites as both these factors affect the topology of amphiphile surfactants and consequently the packing of the chromophores within the channels—the bulkier the group is the greater the steric hindrance, hence the loose packing of the chromophores. Similar results were obtained for the composites prepared by surfactant/silica self-assembly with CTAB and Brij-58 as surfactant templates.[27] We propose that increasing the surfactant tail area, and consequently that of the chromophore, might reduce the value of the surfactant packing parameter (g)[28] and thus affect the mesostructure formation. An apparent decrease in the *d*-spacing with respect to the XRD results may be due to the shrinkage of the samples in the TEM chamber.[29] Although a future detailed structural study is needed, the present results show that these precursors have the ability to form mesophases by self-assembly.

The UV/Vis absorption and PL spectra for the PPP-C11 nanocomposite are shown in Figure 4a and b, respectively. PPP-C11 is an amphiphile with a terphenyl chromophore as the hydrophobic part and a single alkyl chain with a hydroxy head-group as the hydrophilic part. The absorption band of PPP-C11 in solution in THF is observed at 292 nm, but when a thin film of PPP-C11 is formed its absorption undergoes a blue shift of about 17 nm. The nanocomposite thin film also shows a maximum peak around $\lambda_{max} \approx 275$ nm. The PL spectrum of PPP-C11 in THF shows a single band with a maximum peak at 365 nm. In the solid state it undergoes a large decrease, with a maximum peak at 390 nm and two weak shoulders at longer wavelength. This is a red shift of 25 nm relative to the solution spectrum. However, in the nanocomposite we observe a strong emission enhancement in the UV-blue region, with a maximum peak at 390 nm and two pronounced shoulders at 406 and 435 nm with an evident vibrational structure. This fluorescence change, with about a fourteen-fold increase in the intensity, is quite unusual considering that the fluorescence efficiency of organic chromophores generally decreases in the solid state, although they show high fluorescence efficiency in solution. This quite general decrease is attributed mainly to intermolecular vibronic interactions, which induce a nonradiative deactivation process—fluorescence quenching—by excitonic coupling, excimer formation, and excitation energy migration to the impurity traps.[30] The emission enhancement observed in the nanocomposite films is due to the well-ordered arrangement of the chromophore groups on the nanoscale. The external quantum efficiency (Φ), as measured by an integrating sphere method, for the PPP-C11 chromophore film is 10%, and this increases to 56% in the PPP-C11 nanocomposite film.

The other chromophore amphiphile studied, FL-stilbene-$(C11)_2$, has a bulky chromophore group that contains fluorene and stilbene moieties and two long alkyl chains as the hydrophobic tail, with hydroxy head-groups as the hydrophilic part. A solution of FL-stilbene-$(C11)_2$ in THF shows an absorption at 372 nm with two shoulders at 355 and 390 nm (Figure 4c). This band is red-shifted for the chromophore and nanocomposite films by 5 nm ($\lambda_{max} = 377$ nm) and the shoulder peaks are also shifted to higher wavelengths by about five and ten nanometers, respectively. FL-stilbene-$(C11)_2$ in THF solution shows bright blue fluorescence with two clearly resolved vibronic features at 410 and 428 nm in the PL spectrum (Figure 4d). In the pure chromophore amphiphile film the PL intensity is quenched and red-shifted, although it still shows the well-resolved vibronic features at 418 and 440 nm and a broad shoulder at longer wavelength.

 © 2006 Wiley-VCH Verlag GmbH & Co. KGaA, Weinheim

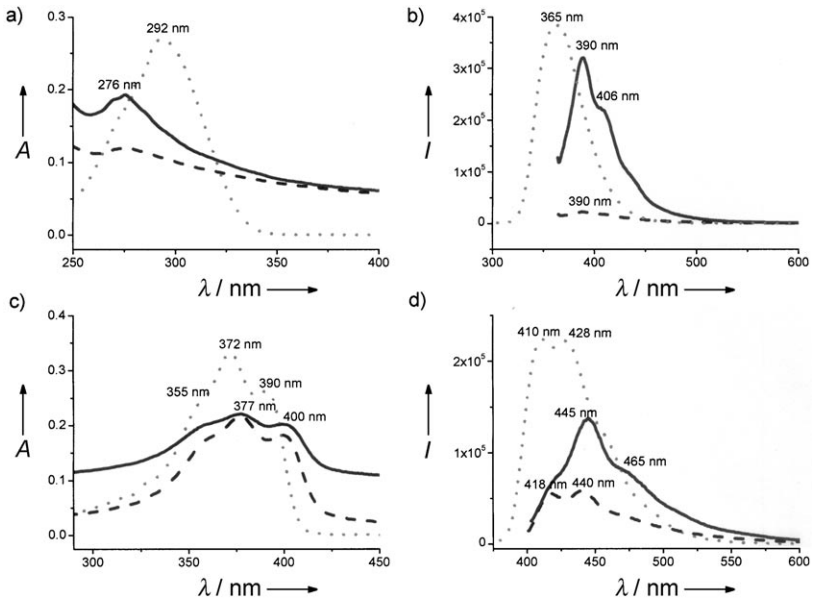


Figure 4. UV/Vis spectra for a THF solution (dotted lines) and chromophore (dashed lines) and nanocomposite films (solid lines) of PPP-C11 (a) and FL-Stilbene-$(C11)_2$ (c). Photoluminescence spectra for a THF solution (dotted lines) and chromophore (dashed lines) and nanocomposite films (solid lines) of PPP-C11 (b) and FL-Stilbene-$(C11)_2$ (d). (The PL intensities of solutions were normalized for comparison.)

However, when the nanocomposite film of FL-stilbene-$(C11)_2$ is formed by EISA, its emission intensity is enhanced more than twofold compared to the chromophore amphiphile film alone, with λ_{max} at 445 nm and shoulders at around 428 and 465 nm. The external quantum efficiency (Φ) for the FL-stilbene-$(C11)_2$ chromophore film is 24%, and this increases to 31% in the FL-stilbene-$(C11)_2$ nanocomposite film. This increase in absorbance in the nanocomposite indicates an increase in the effective conjugation length of the chromophores and, consequently, enhancement in the fluorescence is observed. The "controlled" aggregation of the chromophore groups within the hydrophobic core of the nanocomposite minimizes the formation of larger crystals and thus enhances the fluorescence. The nanopackets in the hybrid composites could provide a controlled concentration of active dots or chromophores, which are better defined systems, and could prevent coalescence into larger, ill-defined aggregates. A similar enhancement has been observed for C540A residing in the organic, hydrophobic regions of a nanocomposite.[20] Although Forster quenching[31,32] is observed in most cases for fluorescent molecules in molecular sieves, the fluorescence enhancement induced in this case is attributed to the well-ordered nanopackets of "controlled" chromophore aggregates formed in the self-assembled nanocomposites, as is evident from the above results. The intensity increase may be due to an increased quantum efficiency of the chromophore nanoaggregates within silica. Such a fluorescence enhancement has also been observed for the well-packed chains and aggregates in conjugated polymers[33] and for fullerene aggregates in organic–inorganic nanocomposites.[5] The mode of interaction amongst the chromophore amphiphile molecules in functional hybrid nanocomposites is a topic of great research interest and will be discussed in future publications.

In summary, we have demonstrated the preparation of chromophore amphiphile/silica self-assembled nanocomposite films of PPP-C11 and FL-stilbene-$(C11)_2$ with enhanced emission, and have thus tried to solve the problem of solid-state quenching of organic chromophores. These nanocomposites show a nanosheet or nanorod morphology. The ability to tailor the orientation of the chromophore surfactant amphiphiles within the mesoscopic structures by solvent-evaporation induced self-assembly in thin films, and the subsequent formation of well-ordered chromophore nanopackets, dramatically affects the photophysical properties of these materials. Moreover, this chromophore amphiphile/silica self-assembly approach to overcome the problem of solid-state quenching in the development of organic light emitting devices with high efficiencies should be broadly applicable and will enable new physical studies and new devices with these nanocomposite materials. Furthermore, this method obviates the chromophore leaching problem that is common in inclusion chemistry. The design of further surfactant amphiphiles with other chromophores at the tail-ends will allow the variation and improvement of the architecture on a molecular and nanometer scale. The demonstration of "controlled" chromophore aggregation and emission enhancement in self-assembled functional hybrid nanocomposites may stimulate new molecular engineering endeavors in the design of luminescent organic compounds with highly emissive aggregation states.

Received: August 29, 2005
Revised: November 18, 2005
Published online: January 30, 2006

Keywords: aggregation · fluorescence · nanostructures · organic–inorganic hybrid composites · self-assembly

[1] G. Schulz-Ekloff, D. Wöhrle, B. van Duffel, R. A. Schoonheydt, *Microporous Mesoporous Mater.* **2002**, *51*, 91.
[2] M. Ganschow, C. Hellriegel, E. Kneuper, M. Wark, C. Thiel, G. Schulz-Ekloff, C. Bräuchle, D. Wöhrle, *Adv. Funct. Mater.* **2004**, *14*, 269.
[3] M. Ganschow, M. Wark, D. Wöhrle, G. Schulz-Ekloff, *Angew. Chem.* **2000**, *112*, 167; *Angew. Chem. Int. Ed.* **2000**, *39*, 160.
[4] M. Ganschow, I. Braun, G. Schulz-Ekloff, D. Wöhrle, *Host–Guest Systems Based on Nanoporous Crystals*, Wiley-VCH, Weinheim, **2003**.
[5] P. Innocenzi, G. Brusatin, *Chem. Mater.* **2001**, *13*, 3126.
[6] A. Costela, I. Garcia-Moreno, C. Gomez, O. Garcia, R. Sastre, *Appl. Phys. B* **2002**, *75*, 827.
[7] C. Peng, H. Zhang, J. Yu, Q. Meng, L. Fu, H. Li, L. Sun, X. Guo, *J. Phys. Chem. B* **2005**, *109*, 15278.

 © 2006 Wiley-VCH Verlag GmbH & Co. KGaA, Weinheim

[8] T.-Q. Nguyen, J. Wu, V. Doan, B. J. Schwartz, S. H. Tolbert, *Science* **2000**, *288*, 651.
[9] C. J. Brinker, Y. Lu, A. Sellinger, H. Fan, *Adv. Mater.* **1999**, *11*, 579.
[10] C. T. Kresge, M. E. Leonowicz, W. J. Roth, J. C. Vartuli, J. S. Beck, *Nature* **1992**, *359*, 710.
[11] H. Yang, N. Coombs, I. Sokolov, G. A. Ozin, *Nature* **1996**, *381*, 589.
[12] Y. Lu, H. Fan, A. Stump, T. L. Ward, T. Rieker, C. J. Brinker, *Nature* **1999**, *398*, 223.
[13] C. Tsai, S. Tam, Y. Lu, C. J. Brinker, *J. Membr. Sci.* **2000**, *169*, 255.
[14] K. Domansky, J. Liu, L.-Q. Wang, M. H. Engelhard, S. Baskaran, *J. Mater. Res.* **2001**, *16*, 2810.
[15] P. D. Yang, G. Wirnsberger, H. C. Huang, S. R. Cordero, M. D. McGehee, B. Scott, T. Deng, G. M. Whitesides, B. F. Chmelka, S. K. Buratto, G. D. Stucky, *Science* **2000**, *287*, 465.
[16] I. Braun, G. Ihlein, F. Laeri, J. Nockel, G. Schulz-Ekloff, F. Schüth, U. Vietze, O. Weiss, D. Wöhrle, *Appl. Phys. B* **2000**, *70*, 335.
[17] R. D. Miller, *Science* **1999**, *286*, 421.
[18] H.-Y. Fan, H. R. Bentley, K. R. Kathan, P. Clem, Y.-F. Lu, C. J. Brinker, *J. Non-Cryst. Solids* **2001**, *285*, 79.
[19] A. Okabe, T. Fukushima, K. Ariga, T. Aida, *Angew. Chem.* **2002**, *114*, 3564; *Angew. Chem. Int. Ed.* **2002**, *41*, 3414.
[20] P. N. Minoofar, R. Hernandez, S. Chia, B. Dunn, J. I. Zink, A.-C. Franville, *J. Am. Chem. Soc.* **2002**, *124*, 14388.
[21] P. N. Minoofar, B. Dunn, J. I. Zink, *J. Am. Chem. Soc.* **2005**, *127*, 2656.
[22] A. Sellinger, P. M. Weiss, A. Nguyen, Y. Lu, R. A. Assink, W. Gong, C. J. Brinker, *Nature* **1998**, *394*, 256.
[23] D. Horn, J. Rieger, *Angew. Chem.* **2001**, *113*, 4460; *Angew. Chem. Int. Ed.* **2001**, *40*, 4330.
[24] B.-K. An, S.-K. Kwon, S.-D. Jung, S.-Y. Park, *J. Am. Chem. Soc.* **2001**, *123*, 14410.
[25] C. J. Bhongale, C.-W. Chang, C. S. Lee, E. W. G. Diau, C. S. Hsu, *J. Phys. Chem. B* **2005**, *109*, 13472 – 13482.
[26] J. Luo, Z. Xie, J. W. Y. Lam, L. Cheng, H. Chen, C. Qiu, H. S. Kwok, X. Zhan, Y. Liu, D. Zhu, B. Z. Tang, *Chem. Commun.* **2001**, 1740.
[27] G. V. Rama Rao, G. P. Lopez, J. Bravo, H. Pham, A. K. Datye, H. Xu, T. L. Ward, *Adv. Mater.* **2002**, *14*, 1301.
[28] Y. Lu, Y. Yang, A. Sellinger, M. Lu, J. Huang, H. Fan, G. Lopez, A. R. Burns, D. Y. Sasaki, J. Shelnutt, C. J. Brinker, *Nature* **2001**, *410*, 913.
[29] B. McCaughey, C. Costello, D. Wang, J. E. Hampsey, Z. Yang, C. Li, C. J. Brinker, Y. Lu, *Adv. Mater.* **2003**, *15*, 1266.
[30] J. B. Birks, *Photophysics of Aromatic Molecules*, Wiley, London, **1970**.
[31] M. Cotlet, T. Vosch, S. Habuchi, T. Weil, K. Müllen, J. Hofkens, F. De Schryver, *J. Am. Chem. Soc.* **2005**, *127*, 9760.
[32] I. Gopich, A. Szabo, *J. Phys. Chem. B* **2005**, *109*, 6845.
[33] K.-Y. Peng, S.-A. Chen, W.-S. Fann, S.-H. Chen, A.-C. Su, *J. Phys. Chem. B* **2005**, *109*, 9368.

 © 2006 Wiley-VCH Verlag GmbH & Co. KGaA, Weinheim

Protein Microarrays

DOI: 10.1002/anie.200502057

Site-Selective Protein Immobilization by Staudinger Ligation**

Anja Watzke, Maja Köhn, Marta Gutierrez-Rodriguez, Ron Wacker, Hendrik Schröder, Rolf Breinbauer, Jürgen Kuhlmann, Kirill Alexandrov, Christof M. Niemeyer, Roger S. Goody, and Herbert Waldmann**

The site- and chemoselective immobilization of proteins through regions of the macromolecules that are not involved in interactions with other molecules is preferable or even required for the application of protein arrays in proteomics research.[1–4] Recently, expressed protein ligation was employed for this purpose,[5] and Raines and co-workers[6] and Bertozzi and co-workers[7] demonstrated the use of the Staudinger ligation[8,9] for protein immobilization by means of a two-step process in which a peptide is first immobilized followed by noncovalent binding of a protein to the peptide sequence.

Herein, we report the successful site-selective covalent immobilization of proteins by reaction of the azide-modified C terminus of a protein generated by expressed protein

[*] Dr. K. Alexandrov, Prof. R. S. Goody
Department of Physical Biochemistry
Max-Planck-Institut für molekulare Physiologie
Otto-Hahn-Strasse 11, 44227 Dortmund (Germany)
Fax: (+49) 231-133-2399
E-mail: roger.goody@mpi-dortmund.mpg.de

Dr. A. Watzke, Dr. M. Köhn, Dr. M. Gutierrez-Rodriguez, Prof. R. Breinbauer, Prof. H. Waldmann
Department of Chemical Biology
Max-Planck-Institut für molekulare Physiologie
Otto-Hahn-Strasse 11, 44227 Dortmund (Germany)
and
Chemische Biologie, Fachbereich Chemie
Universität Dortmund
44227 Dortmund (Germany)
Fax: (+49) 231-133-2499
E-mail: herbert.waldmann@mpi-dortmund.mpg.de

Dr. J. Kuhlmann
Department of Structural Biology
Max-Planck-Institut für molekulare Physiologie
Otto-Hahn-Strasse 11, 44227 Dortmund (Germany)

Prof. C. M. Niemeyer
Biologisch-Chemische Mikrostrukturtechnik, Fachbereich Chemie
Universität Dortmund
44227 Dortmund (Germany)

Dr. R. Wacker, Dr. H. Schröder
Chimera Biotec GmbH
Emil-Figge-Strasse 76a, 44227 Dortmund (Germany)

[**] This research was supported by the Volkswagen Stiftung, the Max Planck Gesellschaft, and the Fonds der Chemischen Industrie.

Supporting information for this article is available on the WWW under http://www.angewandte.org or from the author.

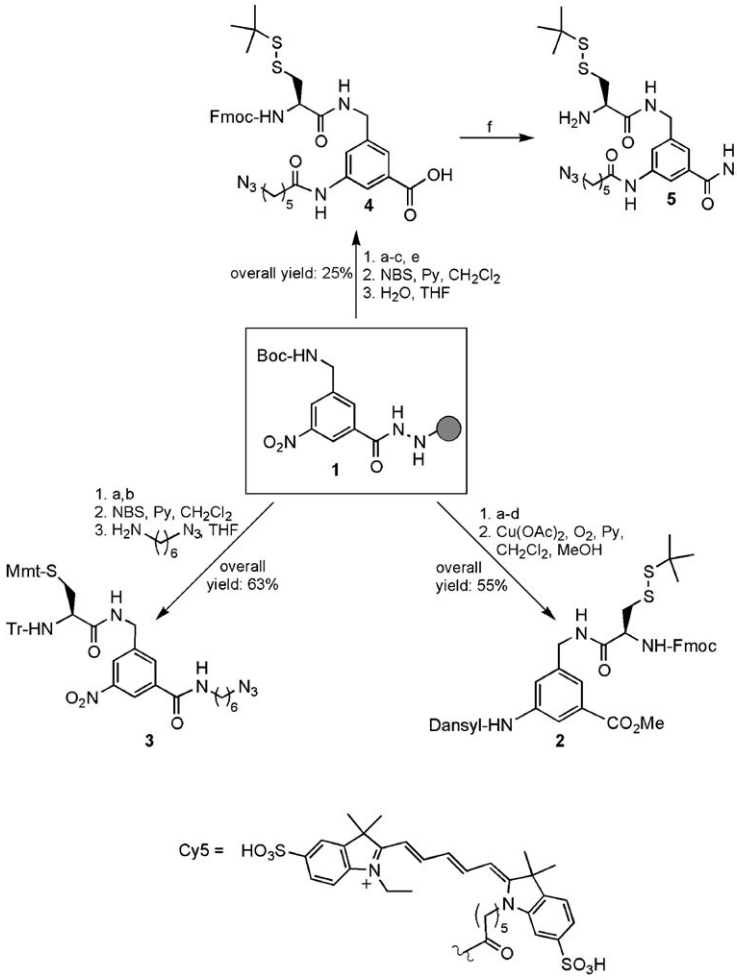
WILEY InterScience DISCOVER SOMETHING GREAT
© 2006 Wiley-VCH Verlag GmbH & Co. KGaA, Weinheim

ligation (EPL) in vitro[10] with a phosphane-functionalized glass surface.

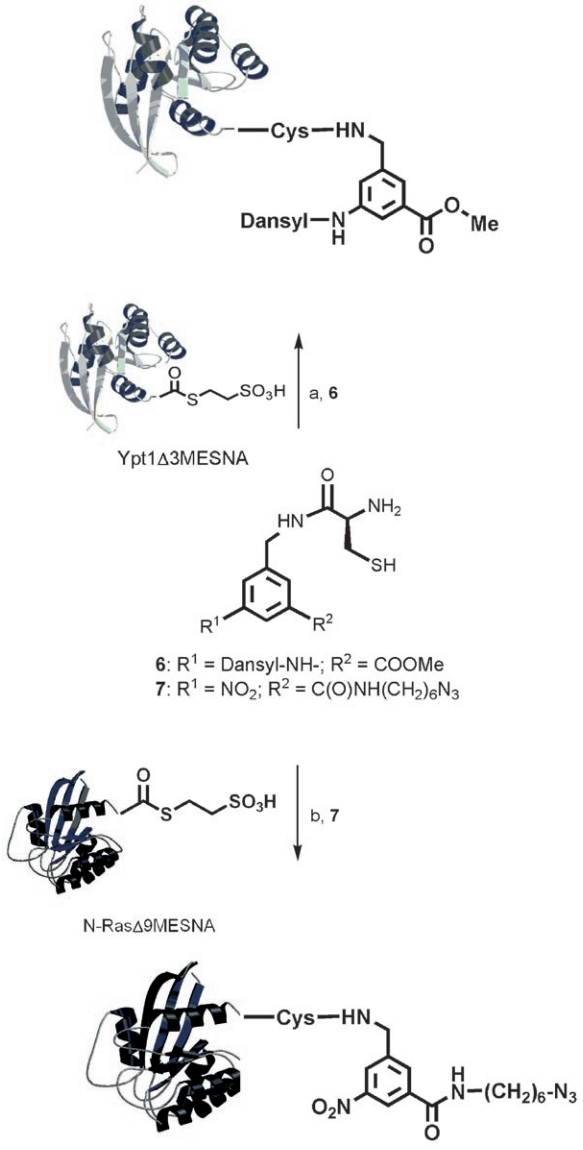
To devise a flexible method we developed a general building block that 1) can be coupled to a protein of interest by EPL, 2) carries an azide group for immobilization to a surface, and 3) embodies a third site that can be equipped with a further functional tag, label, or reporter group, for example, a fluorophore.

To this end, immobilized benzene derivative **1** (Scheme 1) equipped with a triply orthogonal set of functional groups was synthesized. Selective cleavage of the Boc group allowed attachment of a side-chain-protected cysteine derivative for coupling to a thioester group of a protein by EPL (see **2**, **3**, and **4**; Scheme 1). Selective "on-resin" reduction of the nitro group with $SnCl_2$ yielded an amine that can, for instance, be used to introduce a fluorescent label (see **2**; Scheme 1) or an azide-containing amide group (see **4**; Scheme 1). Oxidative activation of the hydrazide linker[11] followed by attack of an appropriate nucleophile on the intermediate acyldiazene gives an ester **2**, the free carboxylic acid **4**, or an amide **3**.

To demonstrate that these building blocks can be coupled successfully to proteins by EPL, the Fmoc group was removed from compound **2**, and the resulting cysteine amide **6** was ligated with the mercaptoethanesulfonic acid (MESNA) thioester of Ypt1Δ3 (Scheme 2), the yeast homologue of the human Rab7 protein that was generated by means of intein technology as described previously.[12] Analysis of the ligation reaction by SDS-PAGE (see the Supporting Information) clearly revealed that the coupling had proceeded successfully. The desired protein was obtained quantitatively.



Scheme 1. Synthesis of fluorescently labeled and azide-functionalized building blocks. a) TFA/CH_2Cl_2 (50%), 30 min; b) Fmoc-Cys(*St*Bu)-OH or Tr-Cys(SMmt)-OH (4 equiv), HOBt (4 equiv), DIC, $(iPr)_2NEt$; c) $SnCl_2{\cdot}2H_2O$, DMF, 2 h, room temperature; d) DansylCl (2 equiv), DMAP (0.5 equiv), pyridine (2 equiv), DMF; e) N_3-$(CH_2)_5$-CO_2H (3 equiv), HOBt, DIC, $(iPr)_2NEt$, CH_2Cl_2, 12 h, room temperature; f) Cy5-Et-NH_2 (4 equiv), HOBt (4 equiv), HBTU, $(iPr)_2NEt$, 12 h, room temperature, 45%. Dansyl = 5-(dimethylamino)naphthalene-1-sulfonyl; DIC = 1,3-diisopropylcarbodiimide; DMF = *N*,*N*-dimethylformamide; Fmoc = 9-fluorenylmethyloxycarbonyl; HBTU = *O*-(benzotriazol-1-yl)-*N*,*N*,*N*′,*N*′-tetramethyluronium hexafluorophosphate; HOBt = 1-hydroxy-1*H*-benzotriazole; Mmt = (4-methoxyphenyl)-(diphenyl)methyl; TFA = trifluoroacetic acid; Tr = trityl = triphenylmethyl.

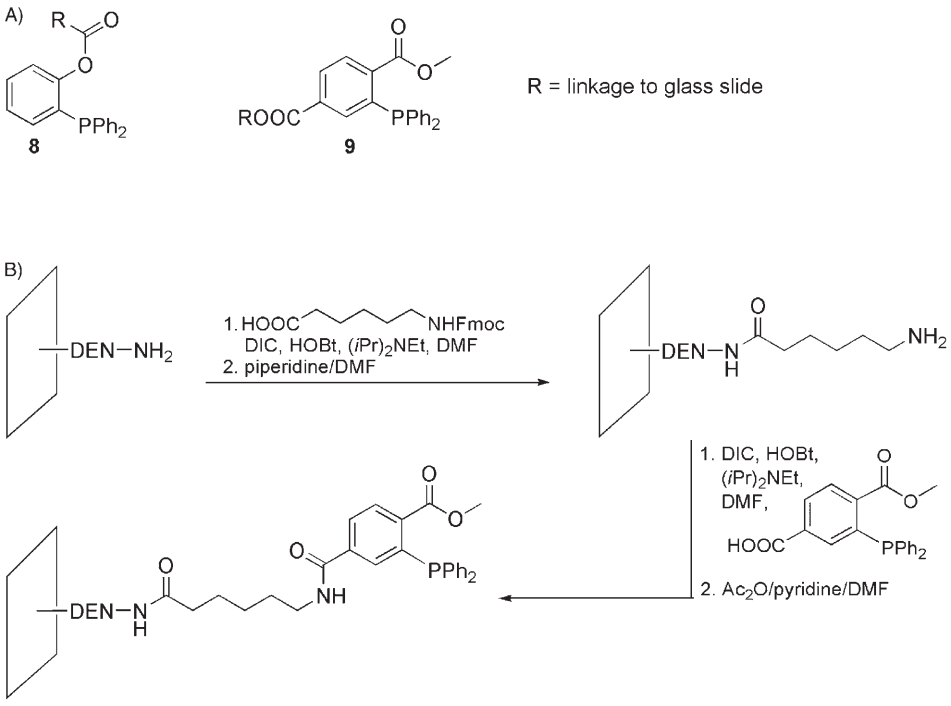


Scheme 2. Ligation of building blocks **6** and **7** to Ypt1 thioester and N-Ras thioester. a) Na_2HPO_4/NaH_2PO_4 (50 mM), pH 7.5, $MgCl_2$ (0.1 mM), GDP (2 μM), MESNA (150 mM), 12 h, room temperature. GDP = guanosine-5′-diphosphate; YptΔ3 = Ypt truncated by three amino acids; MESNA = 2-mercaptoethanesulfonic acid.

 © 2006 Wiley-VCH Verlag GmbH & Co. KGaA, Weinheim

Encouraged by this finding we aimed at the synthesis of an azide-tagged Ras protein[13] suitable for immobilization on a surface. The hypervariable C-terminal region of the signal-transducing Ras oncoproteins is believed primarily to mediate protein–membrane interactions and to be less important for Ras-effector interactions than other regions of the protein.[13] Therefore, immobilization of Ras through the C terminus is desirable.

Accordingly, we planned to ligate Ras to an azide-carrying building block (Scheme 1) and to immobilize it to a phosphane-functionalized surface by means of the Staudinger ligation technique. To this end, compound **3** was deprotected, and the resulting cysteine derivative **7** was treated with the MESNA thioester of a C-terminally truncated N-RasΔ9 protein (Scheme 2).[14]



Scheme 3. Preparation of phosphane-modified glass slides. A) Phosphanes used for Staudinger ligation; B) functionalization of the glass slides. DEN = fourth-generation polyamidoamine dendrimer.

After incubation with a fivefold excess of **7** for 12 h, the semisynthetic protein was obtained pure in 95% yield (see the Supporting Information for details). Notably, the ligation reaction with azide-carrying building block **7** is efficient in the presence of excess thiol, that is, the azide incorporated into **7** is not reduced to the amine under these conditions.

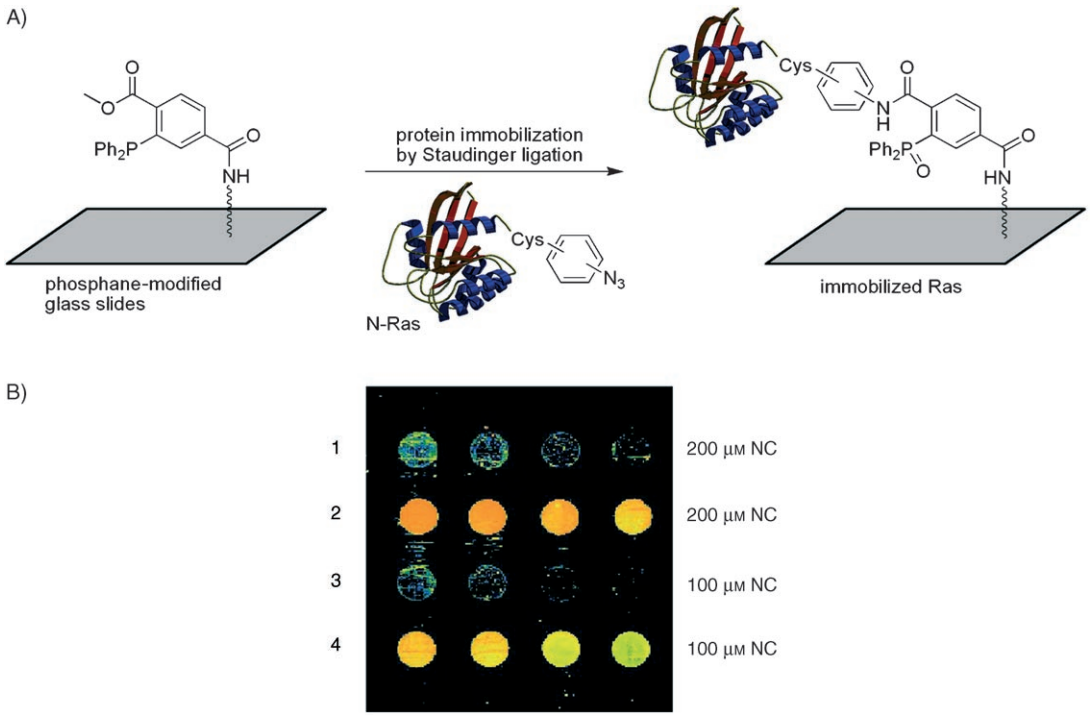
For the immobilization of the azide-functionalized Ras protein, glass slides initially modified with an intermediate layer of generation 4 PAMAM dendrimers were chosen as carriers to allow maximum surface coverage.[9,15] For covalent attachment of the protein by means of Staudinger ligation the surfaces of the slides were decorated with an appropriately functionalized phosphane. Initially it was planned to functionalize the surface with phosphane **8** (Scheme 3). However, Liskamp and co-workers found that 2-diphenylphosphanylphenol ester **8** (Scheme 3A) not only reacts with an azide to give an amide but also undergoes side reactions with the amine groups of lysine side chains,[16] and hence phosphane **9** introduced by Bertozzi and Saxon[8a] was chosen for the immobilization of proteins. This phosphane has been used for in vivo studies in which the Staudinger ligation was applied.[8c] Phosphane groups on surfaces are generally prone to oxidation, but the phosphane used in this case was developed by Bertozzi and co-workers to limit air oxidation.[8d]

For the preparation of the phosphane-functionalized surface an aminocaproic acid linker was introduced to generate distance between the functional groups and the surface, followed by coupling of the phosphane through amide formation (Scheme 3B).

For the immobilization experiments, the azide-modified N-Ras protein (positive control; PC) as well as the unmodified Ras protein as a negative control (NC) (Scheme 4) were dissolved in different buffers at various concentrations and spotted onto the phosphane-modified substrates by using a piezo-driven spotting robot (see the Supporting Information). The slides were washed with buffer at different time intervals and incubated with BSA-containing (BSA = bovine serum albumin) blocking solution to prevent nonspecific binding of protein reagents. The slides were then treated with Cy5-labeled Ras antibody (50 nM, 1 h at room temperature).[17] The fluorescence signals were recorded and quantified after removal of excess reagent. A representative result for the immobilization of azide-modified Ras protein is shown in Scheme 4B. The immobilization of azide-modified N-Ras protein (PC) gave clear fluorescent signals depending on the concentration of N-Ras in the spotting solution. The minimum concentration for acceptable levels of immobilization was found to be approximately 50 μM. An immobilization time of 4 h was sufficient for obtaining clear and reproducible signals. Several buffers are compatible with the immobilization reaction (see the Supporting Information). The immobilization was carried out at pH 7.4–7.6 owing to the pH-dependant stability of the Ras protein. We note, however, that the Staudinger ligation proceeds well over a relatively wide pH range (5–8.5).[18]

These results demonstrate that the immobilization of the azide-modified Ras protein onto the phosphane-modified glass slides was successful. Although the data provide no formal proof of the orientation of the protein on the surface,

 © 2006 Wiley-VCH Verlag GmbH & Co. KGaA, Weinheim



Scheme 4. A) Immobilization of the azide-functionalized N-Ras protein on phosphane-functionalized glass slides. B) Binding of Cy5-labeled Ras antibody to immobilized azide-functionalized N-Ras protein (2 and 4) as positive control (PC) and unmodified N-Ras protein (1 and 3) as negative control (NC).

circumstantial evidence suggests that the immobilization occurred regioselectively at the C terminus.

In conclusion, we have developed a new strategy for the site-specific immobilization of proteins onto a glass surface that may be used for the creation of protein microarrays. This approach relies on the Staudinger ligation between azide-modified proteins and a phosphane-functionalized glass surface and employs a central triply orthogonally functionalized building block together with expressed protein ligation for the synthesis of the azide-modified proteins.

The method requires manipulation of expressed proteins before immobilization. Although this extra step may limit the generality of the method, it should still be applicable to the immobilization of numerous proteins.

Received: June 15, 2005
Revised: December 7, 2005
Published online: January 27, 2006

Keywords: bioorganic chemistry · protein microarrays · protein modification · solid-phase synthesis · Staudinger ligation

[1] a) H. Zhu, M. Snyder, *Curr. Opin. Chem. Biol.* **2001**, *5*, 40–45; b) H. Zhu, M. Snyder, *Curr. Opin. Chem. Biol.* **2003**, *7*, 55–63; c) E. Phizicky, P. I. Bastiaens, H. Zhu, M. Snyder, S. Fields, *Nature* **2003**, *422*, 208–215.

[2] a) M. F. Templin, D. Stoll, J. M. Schwenk, O. Pötz, S. Kramer, T. O. Joos, *Proteomics* **2003**, *3*, 2155–2166; b) B. Schweitzer, P. Prediki, M. Snyder, *Proteomics* **2003**, *3*, 2190–2199.

[3] G. MacBeath, S. L. Schreiber, *Science* **2000**, *289*, 1760–1763.

[4] K.-Y. Tomizaki, K. Usui, H. Mihara, *ChemBioChem* **2005**, *6*, 1–18.

[5] J. A. Camarero, Y. Kwon, M. A. Coleman, *J. Am. Chem. Soc.* **2004**, *126*, 14730–14731.

[6] M. B. Soellner, K. A. Dickson, B. L. Nilsson, R. T. Raines, *J. Am. Chem. Soc.* **2003**, *125*, 11790–11791.

[7] a) H. C. Hang, C. Yu, D. L. Kato, C. R. Bertozzi, *Proc. Natl. Acad. Sci. USA* **2003**, *100*, 14846–14851; b) H. C. Hang, C. Yu, M. R. Pratt, C. R. Bertozzi, *J. Am. Chem. Soc.* **2004**, *126*, 6–7.

[8] a) E. Saxon, C. R. Bertozzi, *Science* **2000**, *287*, 2007–2010; b) S. Luchansky, H. C. Hang, E. Saxon, J. R. Grunwell, C. Yu, D. H. Dube, C. R. Bertozzi, *Methods Enzymol.* **2003**, *362*, 249–272; c) J. A. Prescher, D. H. Dube, A. R. Bertozzi, *Nature* **2004**, *430*, 873–877; d) K. Kiich, E. Saxon, D. A. Tirrell, C. R. Bertozzi, *Proc. Natl. Acad. Sci. USA* **2002**, *99*, 19–24.

[9] a) M. Köhn, R. Wacker, C. Peters, H. Schroeder, R. Breinbauer, C. M. Niemeyer, H. Waldmann, *Angew. Chem.* **2003**, *115*, 6010–6014; *Angew. Chem. Int. Ed.* **2003**, *42*, 5830–5834; b) M. Köhn, R. Breinbauer, *Angew. Chem.* **2004**, *116*, 3168–3178; *Angew. Chem. Int. Ed.* **2004**, *43*, 3106–3116.

[10] a) R. M. Hofmann, T. W. Muir, *Curr. Opin. Biotechnol.* **2002**, *13*, 297–303; b) U. K. Blaschke, J. Silberstein, T. W. Muir, *Methods Enzymol.* **2000**, *328*, 478–496; c) T. J. Tolbert, C. H. Wong, *J. Am. Chem. Soc.* **2000**, *122*, 5421–5428; d) J. P. Tam, J. X. Xu, K. D. Eom, *Biopolymers* **2001**, *60*, 194–205; e) G. G. Kochendoerfer, S. B. H. Kent, *Curr. Opin. Chem. Biol.* **1999**, *3*, 665–671; f) P. E. Dawson, T. W. Muir, I. Clark-Lewis, S. B. H. Kent, *Science* **1994**, *266*, 776–779.

[11] a) F. Stieber, U. Grether, H. Waldmann, *Angew. Chem.* **1999**, *111*, 1142–1145; *Angew. Chem. Int. Ed.* **1999**, *111*, 1073–1077; b) L. Brunsveld, A. Watzke, T. Durek, K. Alexandrov, R. S. Goody, H. Waldmann, *Chem. Eur. J.* **2005**, *11*, 2756–2772.

[12] A. Rak, O. Pylypenko, T. Durek, A. Watzke, S. Kushnir, L. Brunsveld, H. Waldmann, R. S. Goody, K. Alexandrov, *Science* **2003**, *302*, 646–650.

 © 2006 Wiley-VCH Verlag GmbH & Co. KGaA, Weinheim

[13] Review: A. Wittinghofer, H. Waldmann, *Angew. Chem.* **2000**, *112*, 4360 – 4383; *Angew. Chem. Int. Ed.* **2000**, *39*, 4192 – 4212.
[14] For the preparation of the N-Ras thioester, see: D. Gottlieb, C. Grunwald, C. Nowak, J. Kuhlmann, H. Waldmann, *Chem. Commun.* **2006**, 260 – 262.
[15] R. Benters, C. M. Niemeyer, D. Wöhrle, *ChemBioChem* **2001**, *2*, 686 – 694.
[16] R. Merkx, D. T. S. Rijkers, J. Kemmink, R. M. J. Liskamp, *Tetrahedron Lett.* **2003**, *44*, 4515 – 4518.
[17] The Ras antibody was obtained from Santa Cruz Biotechnology (product number sc-35). This antibody recognizes an amino acid sequence on a correctly folded active site helix of Ras (I. S. Sigal, J. B. Gibbs, J. S. D'Alonzo, E. M. Scolnick, *Proc. Natl. Acad. Sci. USA* **1986**, *83*, 4725 – 4729; M. E. Furth, L. J. Davis, B. Fleurdelys, E. M. Scolnick, *J. Virol.* **1982**, *43*, 294 – 304); if it is exposed to denatured Ras only weak binding is observed (C. Becker, MPI Dortmund, personal communication).
[18] E. Saxon, S. J. Luchansky, H. C. Hang, C. Yu, S. C. Lee, C. R. Bertozzi, *J. Am. Chem. Soc.* **2002**, *124*, 14893 – 14902.

 © 2006 Wiley-VCH Verlag GmbH & Co. KGaA, Weinheim

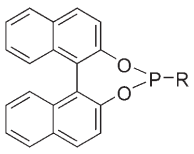
Asymmetric Catalysis

DOI: 10.1002/anie.200503604

Nonlinear Effects in Rh-Catalyzed Asymmetric Olefin Hydrogenation Using Mixtures of Chiral Monodentate P Ligands**

Manfred T. Reetz, Yu Fu, and Andreas Meiswinkel*

Several years ago three groups reported that certain binaphthol (BINOL)-derived monodentate phosphorus compounds are excellent chiral ligands in Rh-catalyzed olefin hydrogenation, namely, phosphites **1**,[1] phosphonites **1** (R = alkyl, aryl)[2] and phosphoramidites **1**.[3] This came as a surprise



1a R = CH_3
b R = $C(CH_3)_3$

because it had been accepted for decades that chelating bidentate diphosphines are necessary for high enantioselectivity.[4] A recent mechanistic study by our group focused on the phosphites and showed that two monodentate P ligands are bonded to rhodium in the transition state of hydrogenation, which is in accord with NMR data, kinetic investigations, and observations of conventional positive nonlinear effects (NLEs).[5] Such detailed mechanistic investigations have not yet been completed for the catalyst systems involving the analogous phosphonites[2] or phosphoramidites,[3a] but preliminary results point to a similar mechanism.[3b,6]

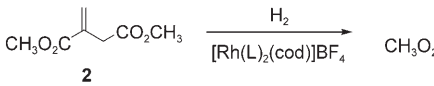
In 2002, we proposed a new tool in combinatorial asymmetric transition-metal-catalyzed reactions:[7] The use of mixtures of two different chiral monodentate ligands L^a and L^b that led to the presence of three different catalysts in a given reaction mixture, two homo-combinations ML^aL^a and ML^bL^b and one hetero-combination ML^aL^b. If the hetero-combination is more reactive and more enantioselective than either of the homo-combinations, enhanced enantioselectivity will result. We demonstrated this effect in Rh-catalyzed olefin hydrogenation.[7] Thus, the method allows for high catalyst diversity with the possibility of discovering superior catalysts, but without the need to synthesize new ligands. Following our initial report, Feringa and co-workers reported related results using the analogous monodentate phosphoramidites **1**.[8]

Herein, we address for the first time the question of possible NLEs when using such mixtures. The situation is considerably more complex than in the case of classical systems that display conventional NLEs,[9] which means that the usual mathematical treatment does not apply. When varying the enantiomeric purity of L^a from 100 to 0% *ee* (racemate) while keeping the partner ligand pure, for example, L^b_S, six different catalytic reactions need to be considered [Eq. (1)]:



$ML^a_SL^a_S \xrightarrow{k_1}$
$ML^a_RL^a_R \xrightarrow{k'_1}$
$ML^a_RL^a_S \xrightarrow{k_2}$
$\Big|$
$ML^b_SL^b_S \xrightarrow{k_3}$
$ML^a_RL^b_S \xrightarrow{k_4}$
$ML^a_SL^b_S \xrightarrow{k_5}$ (1)

The stereochemical outcome of a given hydrogenation reaction depends upon the inherent enantioselectivity of each of these processes, but also on the relative amounts of catalysts present in the mixture and the six rate constants, which can be expected to be different (except for $k_1 = k'_1$). Because we are unable to separate the homo- from the hetero-complexes and to use the latter without ligand exchange, only k_1 (or k'_1) and k_3 can be measured directly in separate experiments. In the other cases, the rate of product formation results from the combined action of the relevant rate processes. As a model reaction, we chose the Rh-catalyzed hydrogenation of itaconic acid dimethyl ester (**2**), with compounds **1a** and **1b** serving as the two P ligands [Eq. (2)]. In all cases, $[Rh(cod)_2]BF_4$ (cod = cyclooctadiene) was treated with two equivalents of **1** to form $[Rh(L)_2(cod)]$ (L = ligand) complexes as the precatalysts.



CH_3O_2C, CO_2CH_3 $\xrightarrow[[Rh(L)_2(cod)]BF_4]{H_2}$ CH_3O_2C, CO_2CH_3 (2)

2 **3**

[*] Prof. Dr. M. T. Reetz, Dr. Y. Fu, Dr. A. Meiswinkel
Max-Planck-Institut für Kohlenforschung
Kaiser-Wilhelm-Platz 1
45470 Mülheim/Ruhr (Germany)
Fax: (+49) 208-306-2985
E-mail: reetz@mpi-muelheim.mpg.de

[**] We thank the Fonds der Chemischen Industrie for generous support and Nils Theyssen for advice in measuring the hydrogenation rates.

InterScience
© 2006 Wiley-VCH Verlag GmbH & Co. KGaA, Weinheim

When utilizing the enantiopure homo-combinations [Rh]/(*S*)-**1a** and [Rh]/(*S*)-**1b** in separate experiments, product **3** was shown to have the *S* configuration with 90 and 57% *ee*, respectively.[7b] Upon using a 1:1 mixture of (*S*)-**1a** and (*S*)-**1b**, the *ee* value increased to 96% (*S*).[7b] In the present study, we first varied the enantiopurity of (*S*)-**1a** stepwise from 100 to 0% *ee*, while maintaining 100% *ee* of (*S*)-**1b**. The result of these experiments show that the *ee* value of **3** decreases only slightly from 96 to 92% *ee* (S enantiomer) as the racemic state is approached (Figure 1, black line). Thus, one of the components can be a racemate, and the result from a practical point of view is still acceptable.

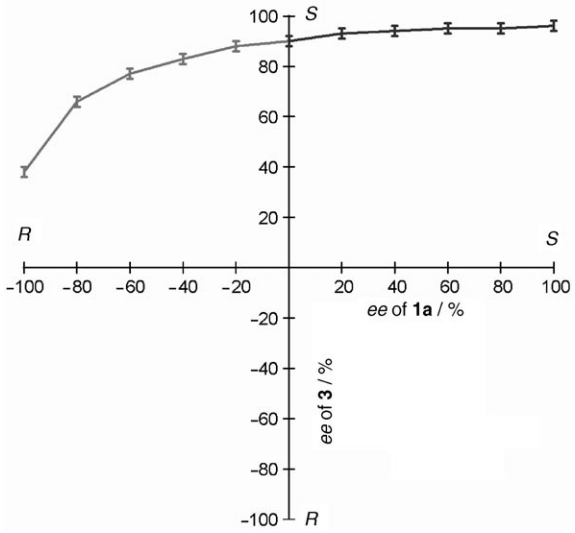


Figure 1. NLE in the Rh-catalyzed hydrogenation of **2** using enantiopure (*S*)-**1b** and **1a** of varying enantiopurity.

It was also of interest to scan the other region of stereochemical space by once again maintaining 100% *S* purity of **1b**, but working in a regime in which the *R* configuration of **1a** dominates, namely, using (*R*)-**1a** at different levels of enantiopurity. The experimental result is also shown in Figure 1 (gray curve). In the extreme case of enantiomerically pure (*R*)-**1a** and (*S*)-**1b** in a mixture, the configuration of **3** remains as *S*, but the *ee* value decreases to 39%. This behavior indicates that the influence of the *tert*-butyl component **1b** dominates the stereochemical outcome.

We then performed the analogous series of experiments in which the enantiopurity of (*S*)-**1a** was maintained at 100% and the *ee* value of **1b** was varied (Figure 2). The results point to a similar behavior when varying the enantiopurity of (*S*)-**1b** from 100 to 0% *ee* (Figure 2, black line). When working in the regime in which more (*R*)- than (*S*)-**1b** is present (gray curve), the quantitative results are somewhat different from those in Figure 1. Nevertheless, the influence of the *tert*-butyl component **1b** dominates again. In this case, the effect finally leads to inversion of configuration, with (*R*)-**3** being formed preferentially with 43% *ee*. This value does not quite correspond to the expected 39% *ee* observed previously in the case of (*R*)-**1a**/(*S*)-**1b**, but may be within experimental error (±2%).

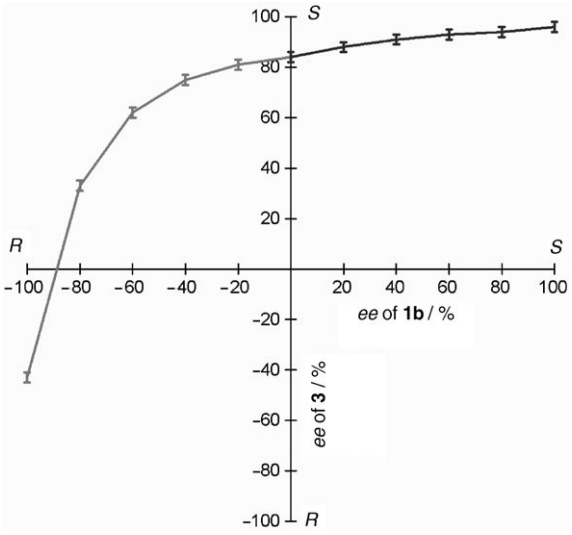


Figure 2. NLE in the Rh-catalyzed hydrogenation of **2** using enantiopure (*S*)-**1a** and **1b** of varying enantiopurity.

To gain some mechanistic insight, we first performed NMR experiments. Upon treating $[Rh(cod)_2]BF_4$ with a 1:1 mixture of (*S*)-**1a** and (*S*)-**1b**, three species were identified by NMR spectroscopy: [Rh{(*S*)-**1a**}$_2$(cod)], [Rh{(*S*)-**1b**}$_2$(cod)], and [Rh{(*S*)-**1a**}{(*S*)-**1b**}(cod)] catalysts in a ratio of 1:1:3, which is not the statistical but rather the thermodynamic value.[6,7b] Of course, once the precatalysts convert into the active species, the ratio may change (which we could not measure). When performing the experiment with a 1:1 mixture of pure (*S*)-**1a** and *rac*-**1b**, a complex NMR spectrum results which displays the same peaks as before in addition to new signals that correspond to diastereomeric complexes. Extensive work is required before a final NMR analysis can be presented.

Kinetic studies of asymmetric catalytic processes are extremely useful in a mechanistic sense and therefore in designing improved catalyst systems.[10] In the present case, the relative rates of hydrogenation of **2** were first measured using the conventional homo-combinations [Rh]/(*S*)-**1a** and [Rh]/(*S*)-**1b**. As shown in Figure 3, the bulky *tert*-butyl ligand (*S*)-**1b** leads to the lowest catalyst activity followed by (*S*)-**1a**. The synthetically useful combination that arises from a mixture of (*S*)-**1a** and (*S*)-**1b** results in the highest rate (Figure 3, red curve), which of course is the result of three reactions. As required by the mixture concept,[7] the two homo-combinations are not only less enantioselective, they are also less active, which is another way of stating that the hetero-combination displays enhanced enantioselectivity and an increased rate. The pure mixed Rh complex of (*S*)-**1a**/(*S*)-**1b**, if it were possible to prepare as the sole species in the reaction, would be even more enantioselective and reactive than the mixture of the three species (the total amount of Rh being constant).

In previous synthetic work regarding the use of mixtures,[6,7] a trend was observed (with exceptions): Hetero-combinations show enhanced enantioselectivity whenever one component is "small" and the other is "large", as in the

 © 2006 Wiley-VCH Verlag GmbH & Co. KGaA, Weinheim

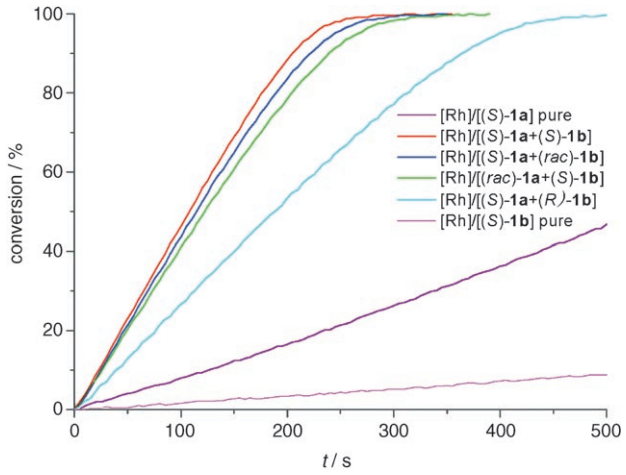


Figure 3. Relative rates of hydrogenation of **2** (Rh/**2** = 1:5000, Rh/**1** = 1:2, **1a**/**1b** = 1:1, 1.3 bar H_2, room temperature, CH_2Cl_2 as the solvent).

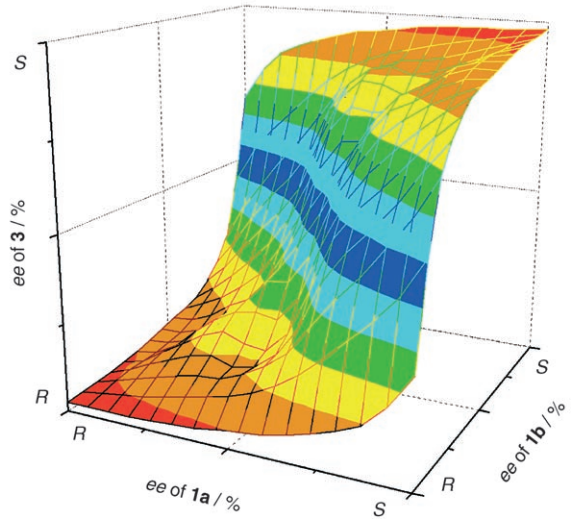
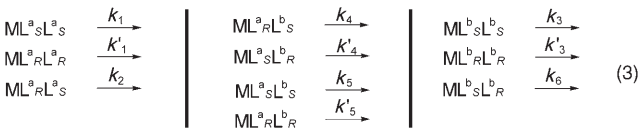


Figure 4. NLE in the Rh-catalyzed hydrogenation of **2** using mixtures of **1a** and **1b**, each with varying degrees of enantiopurity.

present case.[7] Rate enhancement because of this structural feature is observed even when the absolute configurations of the two components are opposite (mismatched), as in the case of (*S*)-**1a**/(*R*)-**1b** (Figure 3, blue curve). Of course, this effect is less pronounced relative to the use of the matched case (*S*)-**1a**/(*S*)-**1b**. The fact that the systems using the racemate of one of the components are more reactive than (*S*)-**1a**/(*R*)-**1b** is now easily understood.

Although the rates of the six individual processes that occur in a system comprising *rac*-**1a**/(*S*)-**1b** (or (*S*)-**1a**/*rac*-**1b**) cannot be measured separately, the results of the kinetic study are in line with the following conclusion: The combination (*S*)-**1a**/(*S*)-**1b** constitutes the most reactive system, all others such as diastereomeric (*S*)-**1a**/(*R*)-**1b** are less able to compete effectively. If the amount of the diastereomeric ligand combination (*S*)-**1a**/(*R*)-**1b** increases in the mixture by using **1b** enriched with the *R* enantiomer, the reaction catalyzed by the respective Rh complex begins to compete and in the extreme case dominates, thus resulting in markedly lower or even opposite enantioselectivity.

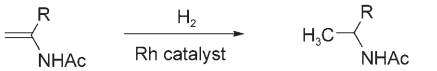
The present results are not only of mechanistic value; they also point to a practical feature, namely, the fact that complete enantiopurity of the ligands is not essential. Indeed, one of the components can even be racemic, with the process still leading to > 92 % *ee*. Although of only partial practical value, we were interested from a theoretical viewpoint to see how the system performs when varying the enantiopurity of both components simultaneously. This means that a total of ten reactions needs to be considered [Eq. (3)].



(3)

The graphic representation of the data of such a systematic search requires a three-dimensional format (Figure 4). It can be seen that the *ee* values vary from 96 % *ee* (*S*) to 96 % *ee* (*R*) in the extremes and that an enantioselectivity of > 90 % *ee* can be achieved even when both components have enantiopurities of only 80 % *ee* and even less (Figure 4, red areas).

The basic phenomenon described above for itaconic acid diester (**2**) was also observed in the case of two other substrates **4a** and **4b** [Eq. (4)], although only a small portion of the data points were collected in these cases (Table 1). For example, in the case of substrate **4b**, racemic **1a** can be used with enantiopure **1b** and the *ee* value is still a respectable 93 % (Table 1, entry 6).



(4)

4a R = Ph
b R = CO_2CH_3

5a R = Ph
b R = CO_2CH_3

Table 1: Asymmetric hydrogenation of olefins **4a**, **b** using ligands **1a**, **b**.

Entry	Ligand	*ee* of **5a** [%][a] (configuration)	*ee* of **5b** [%][b] (configuration)
1	(*S*)-**1a**	76 (*R*)	92 (*R*)
2	(*S*)-**1b**	13 (*R*)	93 (*R*)
3	(*S*)-**1a**/(*S*)-**1b**	95 (*R*)	98 (*R*)
4	(*S*)-**1a**/(*R*)-**1b**	49 (*R*)	82 (*S*)
5	(*S*)-**1a**/*rac*-**1b**	83 (*R*)	62 (*R*)
6	*rac*-**1a**/(*S*)-**1b**	70 (*R*)	93 (*R*)

[a] Conditions: Rh/**4a** = 1:100, Rh/**1** = 1:2, **1a**/**1b** = 1:1, 1.3 bar H_2, room temperature, CH_2Cl_2 as the solvent. [b] Conditions: Rh/**4b** = 1:200, Rh/**1** = 1:2, **1a**/**1b** = 1:1, 1.3 bar H_2, room temperature, CH_2Cl_2 as the solvent.

In summary, we have addressed for the first time the question of nonlinear effects in Rh-catalyzed olefin hydrogenation using a mixture of two different chiral monodentate

 © 2006 Wiley-VCH Verlag GmbH & Co. KGaA, Weinheim

P ligands. Apart from the theoretical interest, the results are of practical significance because the ligands do not need to be 100% enantiopure. Indeed, in some cases one of the ligand components can be racemic[11] while still leading to >92% *ee*. It remains to be seen if the molecular basis of the observed kinetic and stereochemical behavior can be uncovered by theoretical studies.

Received: October 12, 2005
Published online: January 20, 2006

Keywords: asymmetric catalysis · hydrogenation · kinetics · nonlinear effects · rhodium

[1] a) M. T. Reetz, G. Mehler, *Angew. Chem.* **2000**, *112*, 4047 – 4049; *Angew. Chem. Int. Ed.* **2000**, *39*, 3889 – 3890; review: b) M. T. Reetz, *Chim. Oggi* **2003**, *21*, 5 – 8; see also: c) I. V. Komarov, A. Börner, *Angew. Chem.* **2001**, *113*, 1237 – 1240; *Angew. Chem. Int. Ed.* **2001**, *40*, 1197 – 1200; d) T. Jerphagnon, J.-L. Renaud, P. Demonchaux, A. Ferreira, C. Bruneau, *Adv. Synth. Catal.* **2004**, *346*, 33 – 36; e) J. Ansell, M. Wills, *Chem. Soc. Rev.* **2002**, *31*, 259 – 268; review of monodentate P ligands in general: f) F. Lagasse, H. B. Kagan, *Chem. Pharm. Bull.* **2000**, *48*, 315 – 324.

[2] a) M. T. Reetz, T. Sell, *Tetrahedron Lett.* **2000**, *41*, 6333 – 6336; b) C. Claver, E. Fernandez, A. Gillon, K. Heslop, D. J. Hyett, A. Martorell, A. G. Orpen, P. G. Pringle, *Chem. Commun.* **2000**, 961 – 962.

[3] a) M. van den Berg, A. J. Minnaard, E. P. Schudde, J. van Esch, A. H. M. de Vries, J. G. de Vries, B. L. Feringa, *J. Am. Chem. Soc.* **2000**, *122*, 11539 – 11540; b) M. van den Berg, A. J. Minnaard, R. M. Haak, M. Leeman, E. P. Schudde, A. Meetsma, B. L. Feringa, A. H. M. de Vries, C. E. P. Maljaars, C. E. Willans, D. Hyett, J. A. F. Boogers, H. J. W. Henderickx, J. G. de Vries, *Adv. Synth. Catal.* **2003**, *345*, 308 – 323; c) H. Bernsmann, M. van den Berg, R. Hoen, A. J. Minnaard, G. Mehler, M. T. Reetz, J. G. de Vries, B. L. Feringa, *J. Org. Chem.* **2005**, *70*, 943 – 951.

[4] a) W. S. Knowles, *Angew. Chem.* **2002**, *114*, 2096 – 2107; *Angew. Chem. Int. Ed.* **2002**, *41*, 1998 – 2007; b) R. Noyori, *Angew. Chem.* **2002**, *114*, 2108 – 2123; *Angew. Chem. Int. Ed.* **2002**, *41*, 2008 – 2022.

[5] M. T. Reetz, A. Meiswinkel, G. Mehler, K. Angermund, M. Graf, W. Thiel, R. Mynott, D. G. Blackmond, *J. Am. Chem. Soc.* **2005**, *127*, 10305 – 10313.

[6] T. Sell, Dissertation Ruhr-Universität Bochum, **2002**.

[7] a) M. T. Reetz, A. Meiswinkel, T. Sell, G. Mehler, patent application DE-A 102476330, **2002**; b) M. T. Reetz, T. Sell, A. Meiswinkel, G. Mehler, *Angew. Chem.* **2003**, *115*, 814 – 817; *Angew. Chem. Int. Ed.* **2003**, *42*, 790 – 793; c) M. T. Reetz, G. Mehler, *Tetrahedron Lett.* **2003**, *44*, 4593 – 4596; d) M. T. Reetz, X. Li, *Tetrahedron* **2004**, *60*, 9709 – 9714; e) M. T. Reetz, G. Mehler, A. Meiswinkel, T. Sell, *Tetrahedron: Asymmetry* **2004**, *15*, 2165 – 2167.

[8] a) D. Peña, A. J. Minnaard, J. A. F. Boogers, A. H. M. de Vries, J. G. de Vries, B. L. Feringa, *Org. Biomol. Chem.* **2003**, *1*, 1087 – 1089; b) A. Duursma, R. Hoen, J. Schuppan, R. Hulst, A. J. Minnaard, B. L. Feringa, *Org. Lett.* **2003**, *5*, 3111 – 3113.

[9] Reviews: a) C. Girard, H. B. Kagan, *Angew. Chem.* **1998**, *110*, 3088 – 3127; *Angew. Chem. Int. Ed.* **1998**, *37*, 2922 – 2959; b) H. B. Kagan, *Synlett* **2001**, 888 – 899; c) D. G. Blackmond, *Acc. Chem. Res.* **2000**, *33*, 402 – 411; d) M. Avalos, R. Babiano, P. Cintas, J. L. Jiménez, J. C. Palacios, *Tetrahedron: Asymmetry* **1997**, *8*, 2997 – 3017.

[10] D. G. Blackmond, *Angew. Chem.* **2005**, *117*, 4374 – 4393; *Angew. Chem. Int. Ed.* **2005**, *44*, 4302 – 4320.

[11] a) This observation bears some resemblance to our previous work involving a diphosphite composed of a chiral-backbone diol and configurationally fluxional atropisomeric diphenol-derived P heterocycles that lead to three diastereomeric ligand/metal complexes with different kinetic profiles (D. G. Blackmond, T. Rosner, T. Neugebauer, M. T. Reetz, *Angew. Chem.* **1999**, *111*, 2333 – 2335; *Angew. Chem. Int. Ed.* **1999**, *38*, 2196 – 2199; M. T. Reetz, T. Neugebauer, *Angew. Chem.* **1999**, *111*, 134 – 137; *Angew. Chem. Int. Ed.* **1999**, *38*, 179 – 181). Diphenol itself is achiral, but atropisomerism is created in the synthesis of the P heterocycle. This basic phenomenon was reported indepently by Noyori, Mikami, and co-workers in a study in which they describe a Ru complex composed of a chiral diamine and an achiral diphenyl-derived diphosphine; upon complexation, the latter turns into a configurationally fluxional atropisomeric system that leads to two diastereomeric complexes with different reaction rates and enantioselectivity (K. Mikami, T. Korenaga, M. Terada, T. Ohkuma, T. Pham, R. Noyori, *Angew. Chem.* **1999**, *111*, 517 – 519; *Angew. Chem. Int. Ed.* **1999**, *38*, 495 – 497). Since these papers appeared, many further examples have been reported, including the extension by Balsells and Walsh who showed that the enantioselectivity of the addition of Et_2Zn to aldehydes catalyzed by a chiral titanium alkoxide can be increased by the addition of "achiral" *meso*-1,2-diamine, which is really a pair of fluxional enantiomers (J. B. Balsells, P. J. Walsh, *J. Am. Chem. Soc.* **2000**, *122*, 1802 – 1803); see also: b) K. Mikami, M. Yamanaka, *Chem. Rev.* **2003**, *103*, 3369 – 3400; c) J. W. Faller, A. R. Lavoie, J. Parr, *Chem. Rev.* **2003**, *103*, 3345 – 3367; d) P. J. Walsh, A. E. Lurain, J. Balsells, *Chem. Rev.* **2003**, *103*, 3297 – 3344.

 © 2006 Wiley-VCH Verlag GmbH & Co. KGaA, Weinheim

Supported Catalysts

DOI: 10.1002/anie.200503599

Tetraarylphosphonium Salts as Solubility-Control Groups: Phosphonium-Supported Triphenylphosphine and Azodicarboxylate Reagents**

*Jean-Christophe Poupon, Alessandro A. Boezio, and André B. Charette**

Tremendous effort has been invested over the last few decades to develop novel supports to facilitate organic synthesis. These supports have been used not only to carry out multistep syntheses,[1] but also to bind catalysts, reagents,

[*] J.-C. Poupon, A. A. Boezio, Prof. A. B. Charette
Département de Chimie
Université de Montréal, P.O. Box 6128
Station Downtown, Montréal, Québec H3C 3J7 (Canada)
Fax: (+1) 514-343-5900
E-mail: andre.charette@umontreal.ca

[**] This work was supported by Valorisation-Recherche Québec (VRQ), Valorisation-Recherche s.e.c. (Univalor), and the Université de Montréal. A.A.B. is grateful to the NSERC (PGF B) and FCAR (B2) for postgraduate fellowships.

Supporting information for this article is available on the WWW under http://www.angewandte.org or from the author.

© 2006 Wiley-VCH Verlag GmbH & Co. KGaA, Weinheim

and scavengers to facilitate either the purification process of a product or the recovery of a potentially expensive or toxic catalyst or reagent.[2]

A landmark achievement by Merrifield[3] used functionalized cross-linked, insoluble polymers as a solid support.[4] This solid-phase technology revolutionized peptide and polynucleotide synthesis and was soon used to develop solid-supported reagents and catalysts.[5] As an attempt to restore classical homogeneous organic-chemistry conditions, the replacement of insoluble resins by a soluble polymer support became a popular modification.[6] The non-cross-linked support is typically soluble in some solvents and insoluble in others. Among the soluble polymers, polyethylene glycols (PEGs)[7] and non-cross-linked polystyrene (NCLP)[8] have been by far the most widely used for the recovery and recycling of reagents or catalysts. A recent approach using solid supports derived from ring-opening metathesis polymerization (ROMP) has been reported.[9] Silica-bound scavengers or reagents have also been extensively used recently.[10] The rigid and nonswelling backbone of the silica eliminates the issue of solvent compatibility. Complementary approaches have involved linking a catalyst or reagent on a dendrimeric structure[11] or encapsulating it (homogenous or heterogeneous) in some porous species framework.[12]

Another area of interest is the ionic liquids that consist of pyridinium, imidazolium, ammonium, or phosphonium salts.[13] The structural variations of the salts allow modulation of their melting points. The most popular ionic liquid is $[BMIM]^+[X]^-$ (BMIM = 1-*n*-butyl-3-methylimidazolium, X = OTf, BF_4, PF_6, SbF_6; Tf = triflate). As ionic liquids are highly polar and non-coordinating solvents, they readily dissolve transition-metal complexes without changing their properties. An additional versatile alternative is to use the fluorous phase.[14] Reagents and catalysts can be labeled with a certain number of fluorine atoms to increase their solubilities in the fluorous phase. Perfluoro protecting groups have been developed, thus allowing a substrate to be temporarily tagged for its purification on a fluorous reverse-phase column or to be soluble in the fluorous phase. Finally, reagents that carry basic or acidic moieties (free or masked),[15] polyaromatic tags,[16] or stilbene tags (precipiton)[17] have also been used. The main advantage of those approaches is the use of low-molecular-weight molecules, which are easy to purify and characterize.

Our interest in phosphorus chemistry led us to contemplate the possibility of using tetraarylphosphonium and related phosphonium salts as potential solubility-control groups for reagents and catalysts. Obviously, our goal was to develop small stable entities that are soluble in well-defined solvents but that precipitate completely when a minimum amount of an orthogonal solvent is added. The alkyltriarylphosphonium compounds are readily used as ylide precursors for the Wittig reaction. A general characteristic of these reagents is their insolubility in diethyl ether.[18] As diethyl ether is a good solvent for most organic compounds, we first considered quantifying the solubility of some arylphosphonium salts with various counterions (X = Br, ClO_4, PF_6) in a system of CH_2Cl_2/Et_2O. Several arylphosphonium salts were dissolved in CH_2Cl_2, and the amount of Et_2O required to achieve a quantitative precipitation was evaluated by ^{31}P NMR spectroscopic analysis with triphenylphosphine as the internal standard (Figure 1). Two general trends were

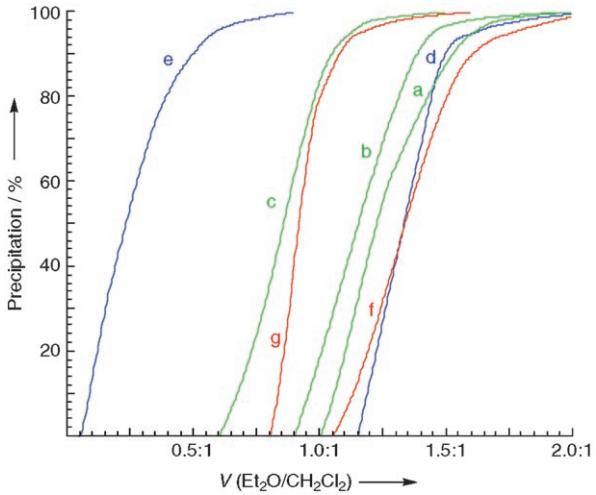


Figure 1. Relative solubility of arylphosphonium salts in Et_2O/CH_2Cl_2. Ph_3PMe; a) Ph_4PX, X = Br; b) Ph_4PX, X = ClO_4; c) Ph_4PX, X = PF_6; d) Ph_4PX, X = Br; e) Ph_4PX, X = ClO_4, X = PF_6 (insoluble); f) **3**; g) **5**.

observed: the amount of diethyl ether required to obtain a quantitative precipitation of the arylphosphonium salts is counterion dependent ($Br > ClO_4 > PF_6$), and the amount of diethyl ether required is generally less for tetraarylphosphonium salts than for triarylalkylphosphonium salts for the same counterion.

Another unique property of tetraarylphosphonium salts is that they have little propensity to trap organic compounds upon precipitation under these conditions. This behavior is an important property that supports for reagents and catalysts should ideally possess. For example, when diethyl ether was added to a solution containing Ph_4PBr and sudan red 7B (Figure 2 A), quantitative precipitation of an easily filtered

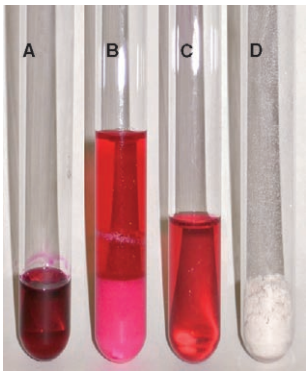
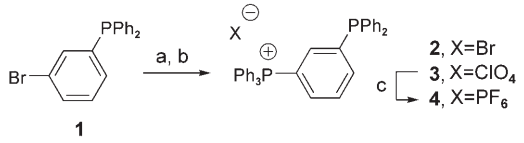


Figure 2. Precipitation/filtration/dissolution sequence of a solution of Ph_4PBr and sudan red 7B. A) Ph_4PBr (250 mg), sudan red 7B (5 mg), and CH_2Cl_2 (1 mL); B) addition of Et_2O (3 mL); C) filtrate; D) filtered phosphonium salt (247 mg) after washing with Et_2O (25 mL) and drying.

 © 2006 Wiley-VCH Verlag GmbH & Co. KGaA, Weinheim

solid occurred (Figure 2B). Filtration produced a clear red solution of the dye exempt of phosphonium (Figure 2C) and a clean, white solid (Figure 2D).

In light of these promising properties, we evaluated the ability of this group to control the solubility properties of a supported reagent. To insure improved chemical stability, a tetraarylphosphonium group was selected as the solubility-control group. Furthermore, we assumed that the shielding of the phosphorus center by the four aryl moieties should lead to more reproducible solvent interactions and interionic distances that are largely responsible for the solubility properties.[19] Two recent reviews dealing with the advances in the separation-friendly reagents for the Mitsunobu reaction[20] confirmed the great interest of the chemical community in settling the problems of the elimination of phosphine oxide and hydrazine by-products. We felt that the elaboration of a phosphonium-supported triphenylphosphine moiety would constitute an excellent model to evaluate the efficiency of the tetraarylphosphonium species as a potentially useful solubility-control group. The desired compound **2** was synthesized using the Horner reaction,[21] which involved a nickel-mediated coupling of bromophosphine **1** and triphenylphosphine (Scheme 1). A subsequent anion-exchange reaction led either to the perchlorate or hexafluorophosphate salts **3** and **4**.



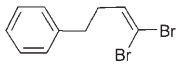
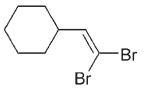
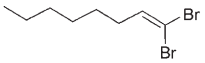
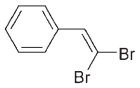
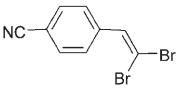
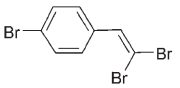
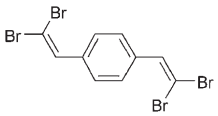
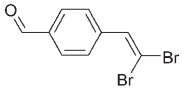
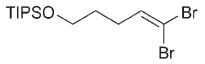
Scheme 1. Reagents and conditions: a) $NiBr_2$, PPh_3, PhCN, reflux, 4 h (78%); b) $LiClO_4$, MeCN, CH_2Cl_2, 15 min (95%); c) $LiPF_6$, MeCN, CH_2Cl_2, H_2O, 1 h (95%).

Gratifyingly, the solubility of both the phosphine **3** and the related phosphine oxide **5** closely followed that of the parent tetraphenylphosphonium salt, thus indicating the predominant influence of the solubility-control group (Figure 1, curves f and g). Both compounds were precipitated quantitatively when a two-volume excess of diethyl ether or less was added.

Although the perchlorate ion is known to be both a powerful oxidant (perchloric acid[22]) and a solid-rocket propellant (ammonium perchlorate[23]), its nonlability in the present compounds makes it slow to react.[24] However, as little chemistry is known regarding tetraarylphosphonium perchlorate, a thermogravimetric experiment was performed to ensure its dynamic thermal stability. The comparison between phosphonium perchlorate and bromide showed comparable behavior: decomposition occurred at a comparable rate and very high temperature (360°C for the perchlorate and 380°C for the bromide).[25] Nevertheless, care must be taken during their use because of the lack of general data about phosphonium percholorate. Alternatively, the hexafluorophosphate salt **4** could be used as well.

With phosphine **3** in hand, its reactivity, recovery, and recyclability were initially tested in the Corey–Fuchs olefination[26,27] as substantial amounts of triphenylphosphine oxide are produced in this reaction. Phosphine **3** was mixed with CBr_4 and zinc dust, and the reaction mixture was heated under reflux prior to the addition of aldehyde. Under these conditions, the ylide was cleanly formed and high yields of the 1,1-dibromoalkenes were obtained (Table 1). The yields

Table 1: Synthesis of 1,1-dibromoalkenes using the Corey–Fuchs reaction with phosphine **3**.

Entry			Yield [%][a]
1		**6**	94[b]
2		**7**	90[b]
3		**8**	90[b]
4		**9**	96[b]
5		**10**	96[b]
6		**11**	98[c]
7		**12**	95[d]
8		**13**	85[b]
9		**14**	96[b]

[a] After flash chromatography. [b] Phosphine **3** (2.5 equiv), CBr_4 (2.5 equiv), Zn dust (2.5 equiv), CH_2Cl_2 (0.2 M), reflux (0.5 h); then addition of aldehyde, RT, 3 h. [c] Three equivalents of all reagents, RT, 6 h. [d] Six equivalents of all reagents, RT, 6 h.

obtained with phosphine **3** are usually comparable with those obtained with triphenylphosphine. When the reaction was complete, the zinc salts were filtered and the addition of Et_2O to the filtrate to allow complete precipitation of the phosphine oxide **5** by-product, followed by filtration, led to an organic layer free of phosphine/phosphine oxide. Concentration under reduced pressure afforded a quantitative recovery of a very clean crude product for which the NMR spectroscopic analysis did not show any traces of phosphonium salts (Figure 3).

It is also possible to recycle phosphine **3** in high yield as the only product of the reduction of the resulting phosphine oxide **5** with trichlorosilane and dimethylaniline [Eq. (1)].[28]

Our next study was the Mitsunobu reaction involving relatively hindered secondary alcohols using *p*-nitrobenzoic acid[29] as the nucleophile. Although the optimal solvent for this reaction is THF or toluene, the use of phosphine **3** forced us to opt for a 2:1 mixture of toluene and dichloromethane.

 © 2006 Wiley-VCH Verlag GmbH & Co. KGaA, Weinheim

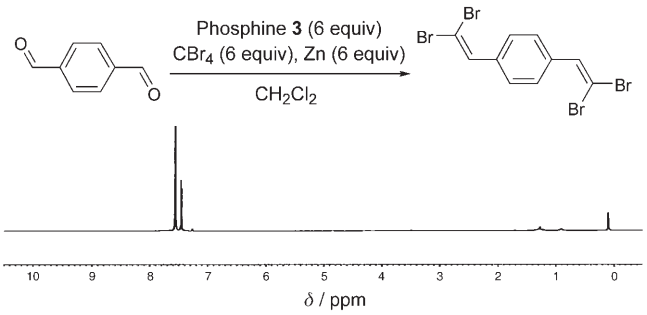
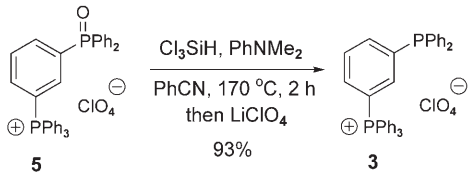


Figure 3. Crude NMR spectrum for the Corey–Fuchs reaction (Table 1, entry 7; quantitative mass recovery).



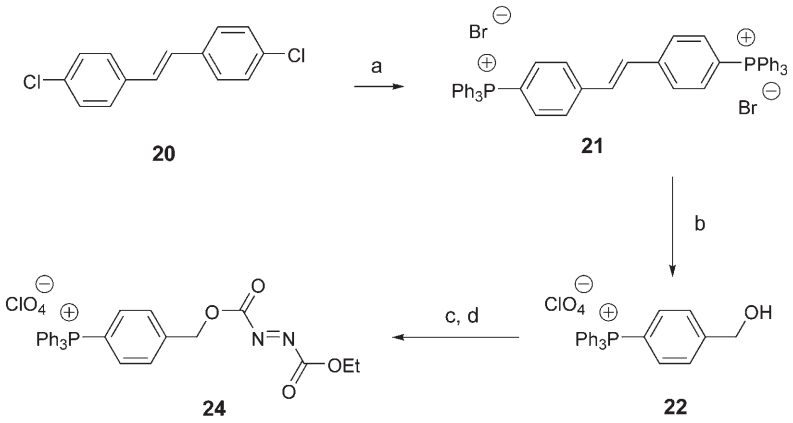
(1)

The results are shown in Table 1, and they indicate that the reactivity of phosphine **3** is quite similar to that of triphenylphosphine.[30] Interestingly, in this solvent system, the phosphine oxide **12** was precipitated, thus allowing a visual indication of the reaction progress. When the reaction was complete, 5 volumes of Et_2O (relative to CH_2Cl_2) were added to complete the precipitation of the phosphonium-derived by-products. Filtration and concentration of the crude mixture led to a phosphorus-free product, as determined by ^{31}P NMR spectroscopic analysis. Conversely, the NMR spectroscopic analysis of the phosphonium salt showed only traces of the reaction products (less than 2%). The Mitsunobu reaction of several alcohols led to esters **15**–**18** in yields comparable to those obtained with triphenylphosphine or other supported phosphines (Table 1, entries 1–4) and with complete inversion of configuration (determined by HPLC for **17**).

The next step was to develop a diethyl azodicarboxylate (DEAD) reagent supported on the phosphonium solubility-control group and examine whether it can be used in conjunction with phosphine **3**. The direct Horner reaction of triphenylphosphine with 4-chlorobenzaldehyde did not give a clean phosphonium salt. Alternatively, a double Horner reaction of 4,4′-dichlorostilbene[31] led to the clean formation of the bis(phosphonium) salt **21**. After an anion-exchange reaction and reductive ozonolysis, benzyl alcohol **22** was obtained in an 77% overall yield from **20**. The elaboration of the DEAD reagent was accomplished by treatment of **22** with triphosgene to generate the chlorocarbonyl pyridinium intermediate followed by the addition of ethyl carbazate to lead to hydrazine dicarboxylate **23**. A final oxidation with *N*-bromosuccinimide (NBS)[32] afforded the DEAD reagent **24** in excellent yield (Scheme 2). The desired product was therefore obtained in five steps and 60% overall yield from 4-chlorobenzaldehyde without the need to purify any of the intermediates by chromatography.

The Mitsunobu reaction of 2-octanol with 4-nitrobenzoic acid, phosphine **3** (1.5 equiv), and DEAD **24** (1.5 equiv) led to the clean formation of the ester (Table 2, entry 3). Addition of diethyl ether followed by filtration allowed quantitative removal of the by-products. To the best of our knowledge, this case is the first time that two supported reagents are used simultaneously with such effectiveness. In a recent report, Hanson and co-workers[33] used five equivalents of both reagents supported on a soluble ROMP polymer to esterify a primary alcohol in 64% yield.

In conclusion, we have developed a highly reactive triphenylphosphine and DEAD reagent supported on a novel solubility-control group. The main advantage of this system is the use of a novel low-molecular-weight support that is soluble in solvents of medium polarities (CH_3CN, dimethyl sulfoxide (DMSO), dimethylformamide (DMF), CH_2Cl_2, $ClCH_2CH_2Cl$, etc.) for the attachment of reagents and insoluble in solvents of low polarities (Et_2O, PhMe, hexane) for clean precipitation. In addition, the reagents display a similar reactivity to their parent nonsupported analogues, there is no need to use extra equivalents because of the availability of all the reactive sites, and the reactions can easily be followed by NMR spectroscopic and mass-spectrometric analysis. Furthermore, they are not hygroscopic (completely insoluble in water) and are easily handled solids that can be quickly and easily be filtered upon precipitation. We are currently introducing additional reagents, catalysts, and substrates on the phosphonium support, and the results will be reported in due course.



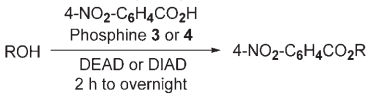
Scheme 2. Synthesis of the DEAD reagent. Reagents and conditions: a) $NiBr_2$, PPh_3, PhCN, reflux, 2 h; b) $LiClO_4$, CH_2Cl_2, MeOH, 15 min, O_3, −78 °C then $NaBH_4$ (77% for two steps); c) triphosgene, pyridine, CH_2Cl_2, −78 °C then $EtOOCNHNH_2$, −78 °C→RT (95%); d) pyridine, NBS, 0 °C, 0.5 h (91%).

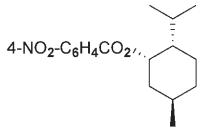
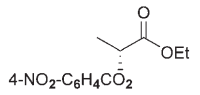
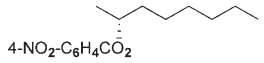
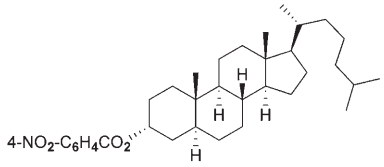
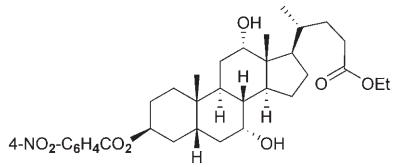
Received: October 11, 2005
Published online: January 20, 2006

Keywords: phosphonium ions · phosphorus · separation · supported catalysts · Wittig reaction

 © 2006 Wiley-VCH Verlag GmbH & Co. KGaA, Weinheim

Table 2: Mitsunobu reactions with phosphine **3**.



Entry	ROH		Yield [%][a]	Yield [%][f]
1		**15**	79[b] 84[c]	65–84
2		**16**	83[b]	71–91
3		**17**	91[b] 84[d]	83
4		**18**	78[b]	70–89
5		**19**	89[e]	–

[a] After flash chromatography. [b] Phosphine **3** and DEAD reagent. [c] Phosphine **4** and DEAD reagent. [d] Phosphine **3** and azodicarboxylate **24** at −10 °C. [e] Phosphine **3** and DIAD reagent. [f] PPh_3 or other supported systems.[18,27,29]

[1] a) P. H. H. Hermkens, H. C. J. Ottenheijm, D. Rees, *Tetrahedron* **1996**, *52*, 4527–4554; b) A. Nefzi, J. M. Ostresh, R. A. Houghten, *Chem. Rev.* **1997**, *97*, 449–472; c) A. R. Brown, P. H. H. Hermkens, H. C. J. Ottenheijm, D. C. Rees, *Synlett* **1998**, 817–827; d) S. Kobayashi, *Chem. Soc. Rev.* **1999**, *28*, 1–15; e) B. A. Lorsbach, M. J. Kurth, *Chem. Rev.* **1999**, *99*, 1549–1581; f) D. A. Horton, G. T. Bourne, M. L. Smythe, *Chem. Rev.* **2003**, *103*, 893–930.

[2] a) A. Kirschning, H. Monenschein, R. Wittenberg, *Angew. Chem.* **2001**, *113*, 670–701; Angew. *Chem. Int. Ed.* **2001**, *40*, 650–679; b) C. C. Tzschucke, C. Markert, W. Bannwarth, S. Roller, A. Hebel, R. Haag, *Angew. Chem.* **2002**, *114*, 4136–4173; *Angew. Chem. Int. Ed.* **2002**, *41*, 3964–4000.

[3] R. B. Merrifield, *J. Am. Chem. Soc.* **1963**, *85*, 2149–2154.

[4] a) I. W. James, *Tetrahedron* **1999**, *55*, 4846–4855–4946; b) F. Guiller, D. Orain, M. Bradley, *Chem. Rev.* **2000**, *100*, 2091–2157.

[5] a) A. Akelah, D. C. Sherrington, *Chem. Rev.* **1981**, *81*, 557–587; b) S. J. Shuttleworth, S. M. Allin, P. K. Sharma, *Synthesis* **1997**, 1217–1239; c) D. H. Drewry, D. M. Coe, S. Poon, *Med. Res. Rev.* **1999**, *19*, 97–148; d) R. J. Booth, J. C. Hodges, *Acc. Chem. Res.* **1999**, *32*, 18–26; e) S. V. Ley, I. R. Baxendale, R. N. Bream, P. S. Jackson, A. G. Leach, D. A. Longbottom, M. Nesi, J. S. Scott, R. I. Storer, S. Taylor, *J. Chem. Soc. Perkin Trans. 1* **2000**, 3815–4195; f) G. Bhalay, A. Dunstan, A. Glen, *Synlett* **2000**, 1846–1859; g) N. E. Leadbeater, M. Marco, *Chem. Rev.* **2002**, *102*, 3217–3274; h) C. A. McNamara, M. J. Dixon, M. Bradley, *Chem. Rev.* **2002**, *102*, 3275–3300; i) M. Benaglia, A. Puglisi, F. Cozzi, *Chem. Rev.* **2003**, *103*, 3401–3429.

[6] a) P. H. Toy, K. D. Janda, *Acc. Chem. Res.* **2000**, *33*, 546–554; b) T. J. Dickerson, N. N. Reed, K. D. Janda, *Chem. Rev.* **2002**, *102*, 3325–3344; c) D. E. Bergbreiter, *Chem. Rev.* **2002**, *102*, 3345–3384.

[7] Sharpless dihydroxylation catalyst: H. Han, K. D. Janda, *J. Am. Chem. Soc.* **1996**, *118*, 7632–7633; the Grubbs catalyst: Q. Yao, *Angew. Chem.* **2000**, *112*, 4060–4062; *Angew. Chem. Int. Ed.* **2000**, *39*, 3896–3898.

[8] a) E. J. Enholm, M. E. Gallagher, K. M. Moran, J. S. Lombardi, J. P. Schulte II, *Org. Lett.* **1999**, *1*, 689–691; b) J.-M. Ahn, P. Wentworth Jr., K. D. Janda, *Chem. Commun.* **2003**, 480–481; c) A. B. Charette, A. A. Boezio, M. K. Janes, *Org. Lett.* **2000**, *2*, 3777–3779; d) A. B. Charette, A. A. Boezio, M. K. Janes, *J. Org. Chem.* **2001**, *66*, 2178–2180.

[9] a) A. G. M. Barrett, B. T. Hopkins, J. Köbberling, *Chem. Rev.* **2002**, *102*, 3301–3324; b) J. D. Moore, R. J. Byrne, P. Vedantham, D. L. Flynn, P. R. Hanson, *Org. Lett.* **2003**, *5*, 4241–4244; c) A. M. Harned, M. Zhang, P. Vedantham, S. Mukherjee, R. H. Herpel, D. L. Flynn, P. R. Hanson, *Aldrichimica Acta* **2005**, *38*, 3–16.

[10] For reviews: a) C. E. Song, S.-G. Lee, *Chem. Rev.* **2002**, *102*, 3495–3524; b) Z.-L. L. Lu, E. Lindner, H. A. Mayer, *Chem. Rev.* **2002**, *102*, 3543–3578.

[11] a) S. B. Garber, J. S. Kingsbury, B. L. Gray, A. H. Hoveyda, *J. Am. Chem. Soc.* **2000**, *122*, 8168–8179; b) B. M. Ji, Y. Yuan, K. L. Ding, A. B. Meng, *Chem. Eur. J.* **2003**, *9*, 5989–5996; c) Y. Ribourdouille, G. D. Engel, L. H. Gade, *C. R. Chim.* **2003**, *6*, 1087–1096; d) S. M. Lu, H. Alper, *J. Am. Chem. Soc.* **2003**, *125*, 13126–13131.

[12] For a review: I. F. Vankelecom, *Chem. Rev.* **2002**, *102*, 3779–3810.

[13] a) P. Wasserscheid, W. Kleim, *Angew. Chem.* **2000**, *112*, 3926–3945; *Angew. Chem. Int. Ed.* **2000**, *39*, 3772–3789; b) J. Dupont, R. F. Souza, P. A. Suarez, *Chem. Rev.* **2002**, *102*, 3667–3692; c) Q. Yao, Y. Zhang, *Angew. Chem.* **2003**, *115*, 3517–3520; *Angew. Chem. Int. Ed.* **2003**, *42*, 3395–3398; d) N. Audic, H. Clavier, M. Mauduit, J.-C. Guillemin, *J. Am. Chem. Soc.* **2003**, *125*, 9248–9249; e) D. W. Kim, D. Y. Chi, *Angew. Chem.* **2004**, *116*, 489–491; *Angew. Chem. Int. Ed.* **2004**, *43*, 483–485.

[14] a) D. P. Curran, *Angew. Chem.* **1998**, *110*, 1230–1255; *Angew. Chem. Int. Ed.* **1998**, *37*, 1174–1196; b) H. Nakamura, B. Linclau, D. P. Curran, *J. Am. Chem. Soc.* **2001**, *123*, 10119–10120; c) W. Zhang, *Chem. Rev.* **2004**, *104*, 2531–2556.

[15] a) M. Von Itzstein, M. Mocerino, *Synth. Commun.* **1990**, *20*, 2049–2059; b) H. Perrier, M. Labelle, *J. Org. Chem.* **1999**, *64*, 2110–2113; c) J. Yoshida, K. Itami, K. Mitsudo, S. Suga, *Tetrahedron Lett.* **1999**, *40*, 3403–3406; d) M. Karlsson, M. Johansson, C. Andersson, *J. Chem. Soc. Dalton Trans.* **1999**, 4187–4192; e) C. Yoakim, I. Guse, J. A. O'Meara, B. Thavonekham, *Synlett* **2003**, 473–476; f) S. Hanessian, D. Ducharme, R. Massé, M. L. Capmau, *Carbohydr. Res.* **1978**, *63*, 265–269.

[16] J. S. Warmus, M. I. da Silva, *Org. Lett.* **2000**, *2*, 1807–1809.

[17] T. Bosanac, C. S. Wilcox, *Org. Lett.* **2004**, *6*, 2321–2324.

[18] A. Maercker, *Org. React.* **1965**, *14*, 389–490.

[19] a) E. Grunwald, G. Baughman, G. Kohnstan, *J. Am. Chem. Soc.* **1960**, *82*, 5801–5811; b) M. H. Abraham, Y. H. Zhao, *J. Org. Chem.* **2004**, *69*, 4677–4685.

[20] a) R. Dembinski, *Eur. J. Org. Chem.* **2004**, 2763–2772; b) S. Dandapani, D. P. Curran, *Chem. Eur. J.* **2004**, *10*, 3130–3138.

[21] L. Horner, G. Mummenthey, H. Moses, P. Beck, *Chem. Ber.* **1966**, *99*, 2782–2788; see also: H. H. Willard, L. R. Perkins, F. F. Blicke, *J. Am. Chem. Soc.* **1948**, *70*, 737–738.

[22] J. Long, *Chem. Health Saf.* **2002**, *9*, 12–18.

 © 2006 Wiley-VCH Verlag GmbH & Co. KGaA, Weinheim

[23] a) P. W. M. Jacobs, H. M. Whiteheat, *Chem. Rev.* **1969**, *69*, 551 – 590; b) L. Liu, F. Li, L. Tan, L. Ming, Y. Yi, *Propellants Explos. Pyrotech.* **2004**, *29*, 34 – 38.
[24] M. M. Abu-Omar, L. D. McPherson, J. Arias, V. M. Bereau, *Angew. Chem.* **2000**, *112*, 4480 – 4483; *Angew. Chem. Int. Ed.* **2000**, *39*, 4310 – 4313.
[25] The authors are thankful to Marie-Ève Perron for carrying this experiment and to Professor James D. Wuest for providing the access to the instrument.
[26] F. Ramirez, N. B. Desai, N. McKelvie, *J. Am. Chem. Soc.* **1962**, *84*, 1745 – 1747.
[27] E. J. Corey, P. L. Fuchs, *Tetrahedron Lett.* **1972**, *13*, 3769 – 3772.
[28] The compound is blue because of a possible reduction of the ClO_4^- ion; an exchange with ClO_4^- gave a colorless compound.
[29] a) S. F. Martin, J. A. Dodge, *Tetrahedron Lett.* **1991**, *32*, 3017 – 4320; b) J. A. Dodge, J. I. Trujillo, M. J. Presnell, *J. Org. Chem.* **1994**, *59*, 234 – 236; c) T. Tsunoda, Y. Yamamiya, Y. Kawamura, S. Itô, *Tetrahedron Lett.* **1995**, *36*, 2529 – 2530.
[30] It is important to point out that the related perchlorate salt of (4-triphenylphosphonium)diphenylphosphinobenzene is substantially less reactive in the Mitsunobu reaction than phosphine **3**.
[31] Prepared by the McMurry reaction from 4-chlorobenzaldhyde: D. Lenoir, *Synthesis* **1989**, 883 – 897.
[32] M. A. Brimble, C. K. Y. Lee, *Tetrahedron: Asymmetry* **1998**, *9*, 873 – 884.
[33] A. M. Harned, H. Song He, P. H. Toy, D. L. Flynn, P. R. Hanson, *J. Am. Chem. Soc.* **2005**, *127*, 52 – 53.

 © 2006 Wiley-VCH Verlag GmbH & Co. KGaA, Weinheim

Photocatalysis

DOI: 10.1002/anie.200503316

Dye-Sensitizer Effects on a Pt/KTa(Zr)O_3 Catalyst for the Photocatalytic Splitting of Water**

*Hidehisa Hagiwara, Naoko Ono, Takanori Inoue, Hiroshige Matsumoto, and Tatsumi Ishihara**

The development of an active catalyst for the photocatalytic decomposition of pure water into H_2 and O_2 is urgently required from an energy-saving viewpoint. Various semiconductor oxides, mainly TiO_2- and Nb-based mixed oxides, have been investigated for this reaction.[1,2] Recently, however, various Ta-based oxides reported by Kato and Kudo et al. have attracted interest as new photocatalytic materials because of their fairly high activity for the photocatalytic splitting of H_2O.[3–5] In addition, Zou et al. have found that Ni-doped $InTaO_4$ can decompose H_2O upon activation with visible light,[6] as can the mixed $SrTiO_3/WO_3$ compound reported by Sayama et al.[7,8] In a previous study we found that Zr-doped $KTaO_3$ exhibits a high activity, splitting H_2O into almost stoichiometric amounts of H_2 and O_2.[9,10] However, these photocatalysts mainly consist of oxide semiconductors combined with a metal or metal oxide such as Pt or NiO. On the other hand, dye-sensitized solar cells are attracting a great deal of interest because of their simple structure and high efficiency.[11,12] In these cells a free electron is excited in the organic dye and passes through a TiO_2 electrode to the counter electrode. Although the structure of these solar cells is simple, a high energy conversion up to 11% can be achieved, and the electron-transfer step resembles that in photocatalysis. Indeed, the application of dye-sensitized solar cells to the photolysis of water has also been reported,[12] therefore a dye-sensitized TiO_2 electrode should also function as a photocatalyst for the splitting of water into H_2 and O_2.

Photocatalysts sensitized by various organic dyes have been investigated, and it has been reported that hydrogen forms under visible-light irradiation of Pt/TiO_2 in the presence of bipyridyl–ruthenium complex, albeit in a small amount.[13,14] However, the splitting of pure water by a dye-sensitized oxide semiconductor has not yet been achieved. This study reports the sensitizing effects of porphyrinoids on the photocatalytic splitting of H_2O into H_2 and O_2 by Pt/KTa(Zr)O_3 and shows that the addition of porphyrinoids to $KTaO_3$ increases the activity of this compound.

Figure 1 shows a TEM image of $K_{0.95}Ta_{0.92}Zr_{0.08}O_3$ coated with tetraphenylporphyrinatochromium(III). The surface of the particle is covered with an amorphous film of the chromium complex. Therefore, the $KTaO_3$-based oxide is encapsulated with the organic dye and good electronic contact between the oxide semiconductor and organic dye seems to have been achieved. The prepared $KTaO_3$ also appears to have good crystallinity since the lattice image is also observed. The UV/Vis spectrum of the prepared catalyst

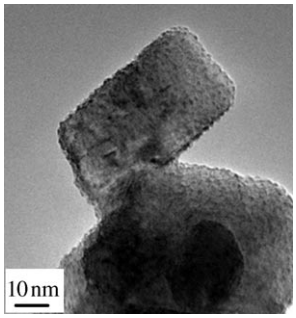


Figure 1. TEM image of Pt-loaded $K_{0.95}Ta_{0.92}Zr_{0.08}O_3$ sensitized by Cr–TPP (rough, thin surface layer).

[*] H. Hagiwara, H. Matsumoto, Dr. T. Ishihara
Department of Applied Chemistry
Faculty of Engineering
Kyushu University
Motooka 744, Nishi-Ku, Fukuoka, 819-0395 (Japan)
Fax: (+81) 92-802-2871
E-mail: ishihara@cstf.kyushu-u.ac.jp
N. Ono, T. Inoue
Department of Applied Chemistry
Faculty of Engineering
Oita University
Dannoharu 700, Oita, 870-1192 (Japan)

[**] The authors are grateful for financial support from the Nissan Science Research Foundation.

InterScience DISCOVER SOMETHING GREAT
© 2006 Wiley-VCH Verlag GmbH & Co. KGaA, Weinheim

is the sum of those of $KTaO_3$ and tetraphenylporphyrinatochromium(III) (Cr–TPP). This also supports the uniform distribution of organic dye on the $KTaO_3$-based oxide.

Table 1 summarizes the photocatalytic activity of the $KTaO_3$ catalyst sensitized by various organic dyes. The observed formation rate of O_2 is almost half that of H_2, and the lowest formation rate of H_2 is 2.1 μmol h^{-1} g^{-1} for Pt/$K_{0.95}Ta_{0.92}Zr_{0.08}O_3$. It can also be seen that almost no H_2 or O_2 was formed with Pt/cyanocobalamin (vitamin B_{12}) or cyanocobalamin/$KTaO_3$. The formation rate of H_2 and O_2 was greatly increased relative to that for Pt/$K_{0.95}Ta_{0.92}Zr_{0.08}O_3$ by addition of various porphyrinoids. The formation rate of H_2 increases as follows: TPPS < TCPP < Co–TPP ≪ Cr–TPP < TMPyP < cyanocobalamin. Although the rate of formation of H_2 is slightly larger than that of O_2, almost stoichiometric amounts of H_2 and O_2 are formed with respect to H_2O splitting with the various dye-sensitized catalysts studied. In particular, the rate of formation of H_2 is almost twice as large as that of O_2 on Cr–TPP-sensitized Pt/$KTaO_3$. The metal cation of the porphyrin complex also has a large influence on the rate of formation of H_2 and O_2, as can be seen by comparing the results for catalysts sensitized with Co–TPP and Cr–TPP. Among the porphyrinoids examined, cyanocobalamin shows the strongest effect on the photocatalytic splitting of water. Although it would be difficult, changing the central cation of cyanocobalamin from Co^{2+} to Cr^{3+} should greatly improve the photocatalytic activity. In any case, the formation rate of H_2 and O_2 with this cyanocobalamin-based catalyst is the highest obtained in this study (575.0 and 280.4 μmol g^{-1} h^{-1}, respectively). Almost no H_2 and O_2 were observed with Pt/cyanocobalamin as the photocatalyst (Table 1), therefore cyanocobalamin is a promoter rather than a photocatalyst. In view of the narrow bandgap of cyanocobalamin, this result is to be expected. A further study examined the dye-sensitizer effects of cyanocobalamin.

Table 1: Photocatalytic splitting of water into H_2 and O_2 by $K_{0.95}Ta_{0.92}Zr_{0.08}O_3$ sensitized by various organic dyes.[a]

Organic dye	Formation rate [μmol g^{-1} h^{-1}]	
	H_2	O_2
Pt/$K_{0.95}Ta_{0.92}Zr_{0.08}O_3$	2.1	0.7
Pt/cyanocobalamin	4.5	trace
Cyanocobalamin/$K_{0.95}Ta_{0.92}Zr_{0.08}O_3$	6.1	0.5
Pt/organic dye/$K_{0.95}Ta_{0.92}Zr_{0.08}O_3$		
Tetraphenylporphine tetrasulfonic acid (TPPS)	376.8	106.0
Tetrakis(4-carboxyphenyl)porphine (TCPP)	404.2	95.6
Zn–TPP dimer[b]	365.2	152.0
Co–phthalocyanine	22.3	9.3
Cr–phthalocyanine	52.0	25.1
Co–tetraphenylporphyrin (Co–TPP)	145.3	44.8
Cr–tetraphenylporphyrin (Cr–TPP)	512.6	257.0
Chlorophyll a	371.5	122.6
Cyanocobalamin	575.0	280.4

[a] Pt was added for all catalysts except for cyanocobalamin/$K_{0.95}Ta_{0.92}Zr_{0.08}O_3$, and the Pt load and the amount of organic dye are 0.2 and 0.8 wt.%, respectively. Photolysis was performed at pH 11. [b] Pentamethylene bis[4-(10,15,20-triphenylporphin-5-yl)benzoate]dizinc(II).

Figure 2 shows the rate of formation of H_2 and O_2 with different amounts of cyanocobalamin added for $K_{0.95}Ta_{0.92}Zr_{0.08}O_3$. It can be seen that the rate of formation of H_2 and O_2 increases upon increasing the amount of cyanocobalamin, with the highest formation rate achieved at 0.6 wt.%. Since the light absorbed by cyanocobalamin cannot reach the central part of the photocatalyst ($KTaO_3$), addition of a large excess of cyanocobalamin only serves to lower the activity of the catalyst. Therefore an optimum cyanocobalamin load was achieved with 0.8 wt.%.

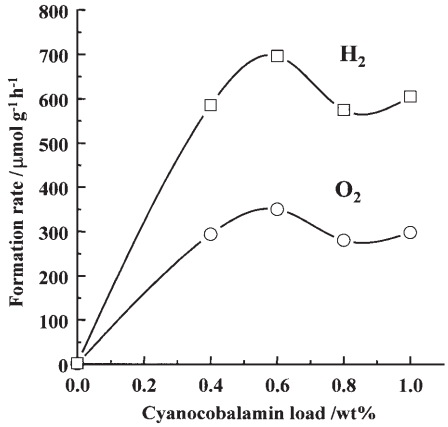


Figure 2. Rate of formation of H_2 and O_2 as a function of amount of added cyanocobalamin for $K_{0.95}Ta_{0.92}Zr_{0.08}O_3$.

Figure 3 shows the amount of H_2 and O_2 formed by Pt/$K_{0.95}Ta_{0.92}Zr_{0.08}O_3$ sensitized by cyanocobalamin after various reaction times. Formation of H_2 and O_2 occurs immediately upon irradiation, and although the rate of formation decreases slightly from the initial rate, it is sustained over the time period examined (9 h). The total amount of H_2 evolved during these 9 hours was 1370 molar times larger than that obtained with cyanocobalamin supported on $KTaO_3$, therefore cyanocobalamin is a promoter rather than

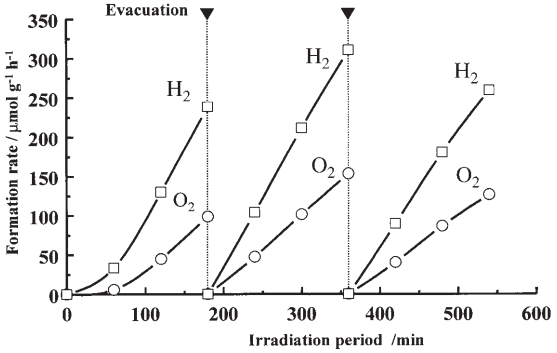


Figure 3. Amount of H_2 and O_2 formed by cyanocobalamin-sensitized Pt/$K_{0.95}Ta_{0.92}Zr_{0.08}O_3$ as a function of reaction time.

 © 2006 Wiley-VCH Verlag GmbH & Co. KGaA, Weinheim

a sacrificial agent. The estimated apparent quantum yield of the catalyst for this experiment is 12.2% with 300-nm light, which is smaller than that reported for La-doped $NaTaO_3$, although it is known that this catalyst exhibits a high quantum yield with UV light.

To identify the effect of the sensitizer, the photovoltaic behavior of $Pt/KTa_{0.92}Zr_{0.08}O_3$ with and without added Cr–TPP was studied as a function of time. Figure 4 shows the decay curve of the photovoltaic potential after irradiation

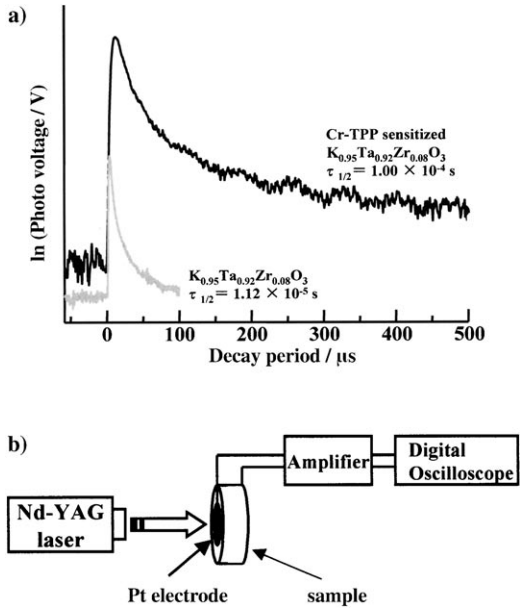


Figure 4. Decay curve of the photovoltaic potential of $KTaO_3$ with and without Cr–TPP sensitization after irradiation for 8–10 ns with a 263-nm laser.

with a 8–10-ns pulse from a 263-nm Nd-YAG laser. When $Pt/KTa_{0.92}Zr_{0.08}O_3$ was irradiated, the photovoltaic potential was observed over 4.0 μs with an estimated half-life of 11.2 μs. It is evident from this figure that the half-life of the photovoltaic potential is increased upon addition of Cr–TPP. This suggests that the lifetime of the photo-excited electron and hole can be increased by coating with Cr–TPP. Therefore the positive effects of porphyrinoids can be explained by the improved efficiency of charge separation. In light of the small bandgap of the organic dye, it is likely that the excited free electron in the $KTaO_3$-based oxide passes to the organic dye, where it is excited again, and then passes to Pt, which is the effective site for H_2 formation, in analogy to photosynthesis. This is because the photovoltaic potential increases upon irradiation with a 263- and 526-nm mixed-laser compared with that of a single 263-nm laser. As previously discussed, TEM observation suggests that the $KTaO_3$ oxide semiconductor is encapsulated by the organic dye, therefore the electron in $KTaO_3$ can easily transfer to the organic dye, resulting in the efficient separation of hole and electron.

This study has demonstrated that the photocatalytic splitting of water by $KTaO_3$ can be greatly improved by addition of an organic dye as sensitizer and that cyanocobalamin is the most effective dye in this respect.

Experimental Section

The $KTaO_3$ catalyst was prepared by calcination of a mixture of Ta_2O_5, K_2CO_3, and $ZrO(NO_3)_2{\cdot}6H_2O$ at 1173 K in air for 10 h. Commercially available organic dye, mainly porphyrin, was used in this study after exchanging the metal center. The various metal porphyrins were prepared by refluxing with the appropriate metal chloride in pyridine. Loading of the dye sensitizer onto the obtained $KTaO_3$ was performed by an impregnation method with pyridine as solvent. Pt was also loaded by an impregnation method with an aqueous solution of $[Pt(NH_3)_4(NO_3)_2]$. The photodecomposition of water was performed in a conventional closed circulating system with a dead volume of about 500 mL. The catalyst (100 mg) was suspended in 30 mL of pure water pre-saturated with Ar. KOH was used to adjust the pH to pH 11. The quartz reaction cell was irradiated by an external light source (500-W Xenon lamp, Ushio). During the photodecomposition the water and catalyst were mixed with a magnetic stirring bar. Argon at a pressure of 10.67 kPa was used as the circulating carrier gas. The H_2 and O_2 formed were measured with a TCD gas chromatograph (Shimadzu GC-8APT) connected to the circulating line with a sampling valve.

Received: September 19, 2005
Published online: January 20, 2006

Keywords: dyes/pigments · heterogeneous catalysis · photolysis · porphyrinoids · sensitizers

[1] S. Moon, H. Mametsuka, E. Suzuki, M. Anpo, *Chem. Lett.* **1998**, 117–118.
[2] T. Takata, A. Tanaka, M. Hara, J. N. Kondo, K. Domen, *Catal. Today* **1998**, *44*, 17–26.
[3] H. Kato, A. Kudo, *Catal. Today* **2003**, *78*, 561–569.
[4] A. Kudo, H. Kato, *Chem. Phys. Lett.* **2000**, *331*, 373–377.
[5] H. Kato, K. Asakura, A. Kudo, *J. Am. Chem. Soc.* **2003**, *125*, 3082–3089.
[6] Z. Zou, J. Ye, K. Sayama, H. Arakawa, *Nature* **2001**, *414*, 625–627.
[7] K. Sayama, K. Mukasa, R. Abe, Y. Abe, H. Arakawa, *Chem. Commun.* **2001**, 2416–2417.
[8] K. Sayama, K. Mukasa, R. Abe, Y. Abe, H. Arakawa, *J. Photochem. Photobiol. A* **2002**, *148*, 71–77.
[9] T. Ishihara, H. Nishiguchi, K. Fukamachi, Y. Takita, *J. Phys. Chem. B* **1999**, *103*, 1–3.
[10] C. Mitsui, H. Nishiguchi, K. Fukamachi, T. Ishihara, Y. Takita, *Chem. Lett.* **1999**, 1327–1328.
[11] T. Renouard, R.-A. Fallahpour, M. K. Nazeeruddin, R. Humphry-Baker, S. I. Gorelsky, A. B. P. Lever, M. Grätzel, *Inorg. Chem.* **2002**, *41*, 367–378.
[12] M. Grätzel, *Chem. Lett.* **2005**, *34*, 8–13.
[13] E. A. Malinka, G. L. Kamalov, S. V. Vodzinskii, V. I. Melnik, Z. I. Zhilina, *J. Photochem. Photobiol. A* **1995**, *90*, 153–158.
[14] R. Abe, K. Sayama, H. Arakawa, *Chem. Phys. Lett.* **2003**, *379*, 230–235.

 © 2006 Wiley-VCH Verlag GmbH & Co. KGaA, Weinheim

Mass Spectrometry

DOI: 10.1002/anie.200503271

Laser-Induced Acoustic Desorption Mass Spectrometry of Single Bioparticles**

Wen-Ping Peng, Yi-Chang Yang, Ming-Wei Kang, Yan-Kai Tzeng, Zongxiu Nie, Huan-Cheng Chang, Wen Chang, and Chung-Hsuan Chen*

The pioneering work on electrospray ionization (ESI) by Fenn and co-workers[1] as well as matrix-assisted laser desorption/ionization (MALDI) mass spectrometry (MS) by Tanaka et al.[2] and Karas and Hillenkamp[3] now allows the soft ionization and mass measurement of large biomolecules. With the simplicity of the mass spectra, MALDI-MS has become a major tool for current proteomic research and in the diagnosis of diseases.[4] We previously demonstrated that MALDI is also a useful technique for laser desorption/ionization of intact bacterial particles such as *Escherichia coli*.[5] However, to produce gas-phase ions of viruses and cells that do not have rigid walls, the method is not so applicable because these bioparticles can disintegrate easily when mixed with the matrix and the disintegration proceeds further during the course of matrix crystallization and subsequent laser desorption/ionization processes. Herein, we report a laser-induced acoustic desorption (LIAD) method that allows facile desorption of intact bioparticles (including viruses, bacteria, and mammalian whole cells) for the determination of absolute mass with a quadrupole ion trap (QIT). While LIAD has been demonstrated previously for desorption of intact organic and biomolecular ions,[6–9] the mass range was limited to less than 20 kDa.

The LIAD method developed here involves laser ablation of a silicon wafer at a site opposite to the surface that contains the biological samples. Acoustic waves generated by the laser ablation desorb the analyte. Interestingly, some bioparticles with mass $m > 1 \times 10^9$ Da are desorbed as "precharged" ions and therefore their analysis by mass spectrometric can be performed without the need of external ionization. Although the efficiency of the desorption/ionization process is low, only a single particle is required for each mass measurement. Compared to ESI, which has been applied successfully to the time-of-flight mass measurement of intact MS2 virus capsids[10] and plant viruses,[11] LIAD is advantageous that pathogenic or potentially dangerous bioparticles can be analyzed more safely in an environment without aerosol production.

The experimental setup comprised a quadrupole ion trap that operated in the audiofrequency region for analyzing charged particles with very high masses (Figure 1).[12,13] The biological sample of interest was first loaded on a bare Si(100) wafer (0.5-mm thickness)[14] devoid of any energy-absorbing organic matrix. A frequency-doubled Nd:YAG laser beam (532 nm) was then applied to the backside of the sample plate to desorb the bioparticles, which entered the ion trap through the gap between the ring and end-cap electrodes. Each end-cap was drilled with separate holes for the collection of scattered laser light and for the entrance of an electron beam. An argon ion laser (488 nm) illuminated the trapped particles

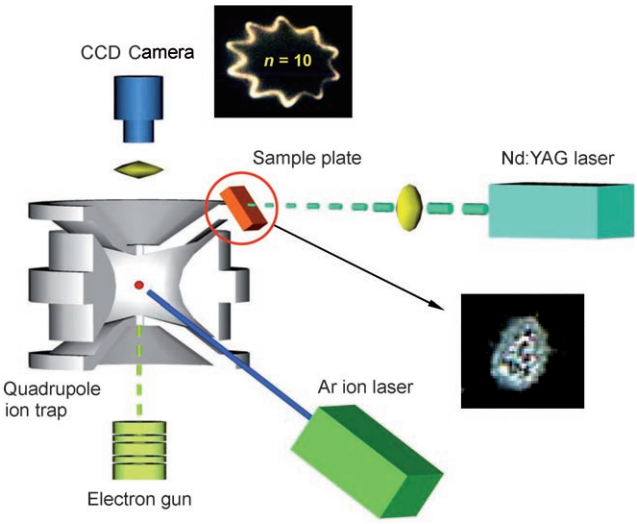


Figure 1. Experimental setup: The charged bioparticles were generated by laser-induced acoustic desorption and introduced to the quadrupole ion trap through the gap between the ring and end-cap electrodes. The typical laser fluence used for desorption was 3 J cm^{-2}, above the ablation threshold of Si.[27] The photo (top) shows a starlike oscillation trajectory of the trapped particle when the radial oscillation frequency is in resonance with the trap-driving frequency (*n* is the number of branches in the star). Observation of the stationary starlike light-scattering pattern ensures confinement of a single bioparticle in the ion trap. The image (right) is an enlarged image of the laser-ablated spot with a size of approximately 1 mm along the long axis on the sample plate (0.5-mm-thick Si wafer).

[*] Dr. W.-P. Peng, Y.-C. Yang, M.-W. Kang, Dr. Z. Nie, Dr. H.-C. Chang
Institute of Atomic and Molecular Sciences
Academia Sinica
Taipei, 106 (Taiwan)
Fax: (+886) 2-2362-0200
E-mail: hcchang@po.iams.sinica.edu.tw
Dr. W.-P. Peng, Dr. H.-C. Chang, Dr. C.-H. Chen
Genomics Research Center
Academia Sinica
Nankang, 115 (Taiwan)
Y.-K. Tzeng, Dr. H.-C. Chang
Department of Chemistry
National Taiwan Normal University
Taipei, 106 (Taiwan)
Dr. Z. Nie
Department of Physics
Wuhan University
Wuhan 430072 (China)
Dr. W. Chang
Institute of Molecular Biology
Academia Sinica
Nankang, 115 (Taiwan)

[**] This work was supported by grants from the Academia Sinica and the National Science Council (grant no. NSC 92-3112-B-001-012-Y) of Taiwan. We thank Y.-Y. Cheng for donating anemic blood samples, C. S. Chung for virus preparations, and Prof. Y. T. Lee for stimulating discussions.

© 2006 Wiley-VCH Verlag GmbH & Co. KGaA, Weinheim

for light-scattering measurement. A 55° forward light-scattering path and an electron-multiplier charge-coupling device (CCD) were adopted to assure high collection and detection efficiencies of the scattered photons. Trapping of the bioparticles from the laser desorption was achieved with 100–2000 Hz ac field (depending on the particle size) and approximately 1 mTorr helium buffer gas.[15] By observing the light-scattering pattern (Figure 1) associated with the trap-driving frequency ($\Omega/2\pi$) and voltage amplitude (V_{ac}), highly precise mass-to-charge ratios (m/z) were obtained for a single trapped particle.[16] The typical accuracy of the m/z measurement was on the order of 10^{-3}, primarily limited by the machining errors and mechanical misalignments of the ion-trap electrodes.[15,17] To determine the mass m, accurate measurement of the charge z was made by creating one-electron differentials[18] in the charge states by electron bombardment of the bioparticle.[19] After a few (typically five to seven) measurements for the same particle carrying different numbers of charges, mass information was deduced with a procedure that iteratively tried all possible mass-to-charge ratios for various charge states and then selected the set of the assigned m/z values that produced the lowest standard deviation.[20] The signs of the charges were finally determined from the changes (either increase or decrease) of the charge states upon secondary electron emission[19] owing to the electron bombardment.

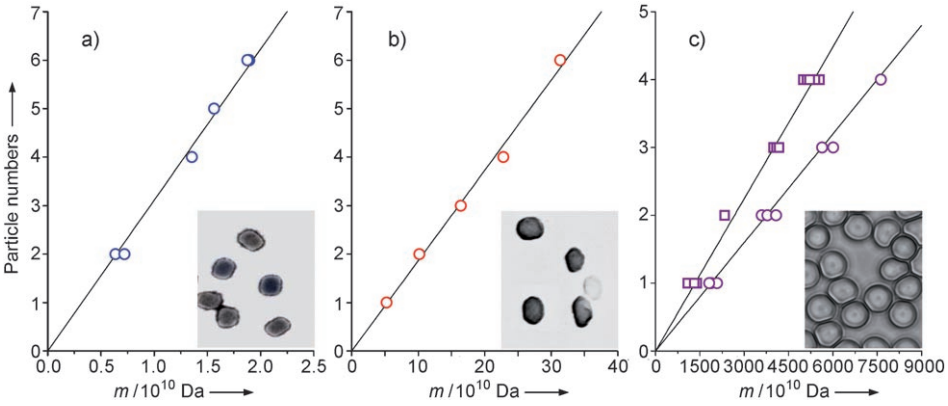


Figure 2. Plots of measured masses versus particle numbers for a) vaccinia viruses, b) *E. coli* K-12 bacteria, and c) human red blood cells. Insets: electron microscopy images of vaccinia viruses (ca. 0.33-μm long and 0.27-μm diameter; a), *E. coli* bacteria (ca. 1-μm long and 0.6-μm diameter; b), and optical microscopy image of normal red blood cells (ca. 1.7-μm thick and 7.3-μm diameter; c). The typical trapping parameters ($\Omega/2\pi$ and V_{ac}, respectively) used in each measurement were: a) 1500 Hz and 300 V, b) 300 Hz and 300 V, and c) 300 Hz and 1000 V. The two data sets shown in (c) are those of normal (○) and anemic (□) red blood cells. Note that the lack of the data point for single viruses in (a) is mainly because the light scattering from these particles is too weak to be detected.

Three different kinds of bioparticles were examined in this study:[21] vaccinia viruses, *E. coli* K-12 bacteria, and human red blood cells (representatives of viruses, bacteria, and mammalian whole cells, respectively). Furthermore, they cover the mass range from 1×10^{9} to 1×10^{14} Da (1.6 fg to 160 pg in weight) or the size range from 200 nm to 10 μm. As reported elsewhere,[20] polystyrene particle size standards (NIST SRM 1690) with a nominal diameter of 1 μm were examined with the same setup to ensure high-accuracy mass measurement. We obtained a mass of $2.38\pm0.03\times10^{11}$ Da,[22] which is in excellent agreement with the value of $2.38\pm0.07\times10^{11}$ Da calculated from the size of 0.895 ± 0.008 μm for SRM 1690[23] and the density of 1.055 ± 0.001 g cm^{-3} [24] for the polystyrene sphere.

The greatest advantage of using LIAD is that the technique can be applied to desorption of viruses and cells without rigid envelopments. As cluster particles are formed during the laser desorption process,[5,8,20] least-squares fitting of measured masses versus particle numbers was used to derive the mass of the monomeric particle (see Figure 2). For vaccinia virus, we determined a mass of $3.26\pm0.15\times10^{9}$ Da, which is equivalent to a dry weight of 5.4 ± 0.2 fg (Figure 2a). This weight is in good agreement with the median weight of 5.26 fg determined by quantitative electron microscopy,[25] suggesting that the desorbed viral particles are intact. Application of the same technique to the mass measurement of *E. coli* K-12 gave a number-average mass of $5.35\pm0.24\times10^{10}$ Da (Figure 2b), which is also consistent with our previous measurement ($5.03\pm0.14\times10^{10}$ Da) for the dehydrated bacterial particle using MALDI as the ion source.[5] Similar successful applications were made for human red blood cells (Figure 2c). Note that because only a single bioparticle and an ion-trap device were used in each measurement, poor mass resolution associated with the position spread and velocity spread in an ensemble measurement with a time-of-flight mass spectrometer is eliminated.

An interesting application of LIAD-QIT-MS is to distinguish normal from abnormal red blood cells. For human red blood cells, an index commonly used to characterize the corpuscles is MCH (mean corpuscular hemoglobin), which is a measure of the average weight of hemoglobin within a cell. The normal result of the MCH index for a healthy adult is 27–31 pg.[26] Shown in Figure 2c are the results of the mass measurements for red blood cells from normal (circles) and anemic (squares) male adults in this work. The former gave a number-average mass of $1.9\pm0.1\times10^{13}$ Da, with a mass variation of about 5%. This measured mass (or 32 ± 2 pg in weight) corresponds to the mean mass of a dehydrated erythrocyte that consists mainly of hemoglobin.[26] Notably, the weight matches closely with the MCH value of a normal red blood cell. In comparison, the mean mass of the anemic red blood cells from a patient with α-thalassemia is substantially lower at $1.3\pm0.1\times10^{13}$ Da (or 22 ± 2 pg in weight). The difference in mass between these two types of dehydrated corpuscles is approximately 30%, beyond the limit of our experimental uncertainty (≈1%) as well as the mass variation of each sample (≈10%). The ability to distinguish these two types of red blood cells substantiates the utility of this method for biomedical applications.

 © 2006 Wiley-VCH Verlag GmbH & Co. KGaA, Weinheim

In this experiment, shock waves are generated by laser ablation due to material ejection from the Si surface (Figure 1 and Figure 3a).[27,28] These waves decay rapidly to acoustic waves that propagate through the 0.5-mm-thick substrate to the other surface and desorb the biological cells. We repeated the measurements for the same kind of bioparticles many times. The distribution of the charge number shows that more than 100 charges (up to 2000 charges for red blood cells) can be attached to each bioparticle without external ionization. Both positively and negatively charged particles are observed with nearly equal probability when an undoped Si wafer is used as the substrate in the measurement (Figure 3a). The result stands as an interesting contrast to the observation that predominantly only positively charged particles are produced by MALDI using sinapinic acid as the matrix (Figure 3b).[5,17]

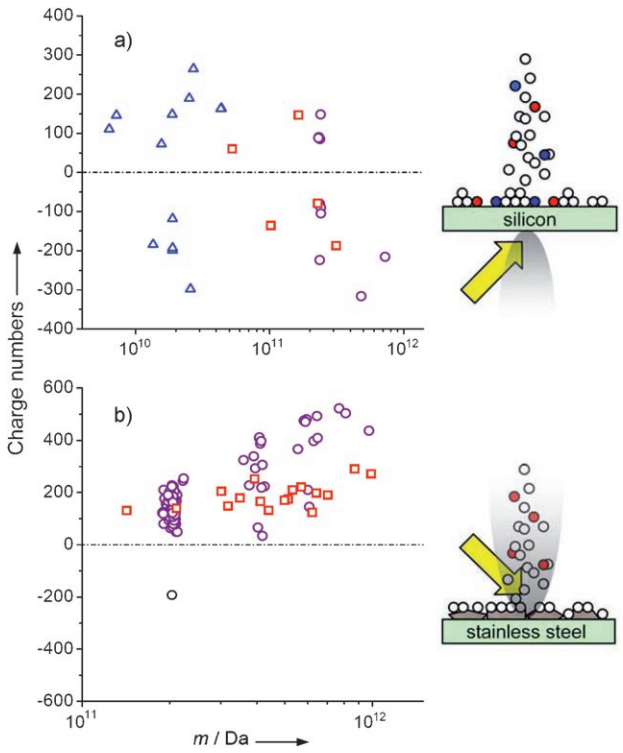


Figure 3. a) Charge-state distribution of particles generated by LIAD using an undoped Si wafer as the substrate. The three samples used were polystyrene size standards (NIST SRM 1690; ○), *E. coli* K-12 bacteria (□), and vaccinia viruses (△). b) Charge-state distribution of aminopolystyrene spheres (○) and *E. coli* K-12 particles (□) generated by MALDI using sinapinic acid as the matrix.[5,17] The corresponding laser desorption processes are illustrated on the right, where neutral, positively charged, and negatively charged particles are denoted by white, red, and blue spheres, respectively.

For LIAD, the process is mostly based on mechanical shaking forces and the desorption/ionization efficiency is usually low. The production of hundreds to thousands of charges with one particle by acoustic desorption, conceivably, is an unlikely process. Also, the ionization during acoustic desorption to produce such a large number of charges on a bioparticle is unlikely to occur. To explain our observations, we consider that a small percentage of bioparticles are present as precharged ions and that they are liberated from the surface by LIAD.[29] These charges originate from either electron-transfer or proton-transfer processes.[30] If the net charge of a sample is neutral, the number of particles with positive charges should be counterbalanced by particles with negative charges and therefore both types of charged bioparticles should be seen. This expectation is indeed in accord with our observation that the number of desorbed particles with negative charges is about equal to the number with positive charges, for three different samples deposited on the undoped Si wafer (Figure 3a). To elucidate this mechanism further, we conducted the same acoustic desorption measurement for a variety of particles (including organic, inorganic, and biological particles) from the surface of an *n*-type Si wafer biased at different dc voltages (up to 500 V). The observed charge-state distribution showed no direct correlation with the voltage applied to the wafer, indicating that acoustic forces dominated the desorption process in all cases.

Mass spectrometry without the need of matrix and external ionization offers major advantages in terms of sensitivity as well as background and fragmentation interference. Micron-sized bioparticles, including cellular organelles (such as chromosomes and mitochondria) and whole cells, are particularly amendable to this type of analysis because they can be easily charged by electron bombardment and detected by light scattering, and their masses can be measured directly and accurately with a quadrupole ion trap on a single-particle basis. The present demonstration of single mammalian cell experiments, in which the normal red blood cells were distinguished from the anemic red blood cells, can lead to possible detection of cancer cells (or even stem cells) with mass spectrometry. If the mass of a cancer cell is distinctly different from that of a normal cell, the spectrometer developed in this work can become a rapid cell sorter in the future.

Received: September 15, 2005
Revised: November 14, 2005
Published online: January 27, 2006

Keywords: analytical methods · mass spectrometry · single-particle studies · viruses

[1] S. F. Wong, C. K. Meng, J. B. Fenn, *J. Phys. Chem.* **1988**, *92*, 546.
[2] K. Tanaka, H. Waki, Y. Ido, S. Akita, Y. Yoshida, T. Yoshida, *Rapid Commun. Mass Spectrom.* **1988**, *2*, 151.
[3] M. Karas, F. Hillenkamp, *Anal. Chem.* **1988**, *60*, 2299.
[4] C. Dass, *Principles and Practices of Biological Mass Spectrometry*, Wiley, New York, **2001**.
[5] W.-P. Peng, Y.-C. Yang, M.-W. Kang, Y. T. Lee, H.-C. Chang, *J. Am. Chem. Soc.* **2004**, *126*, 11766.
[6] M. A. Posthumus, P. G. Kistemaker, H. L. C. Meuzelaar, M. C. T. de Brauw, *Anal. Chem.* **1978**, *50*, 985.
[7] B. Lindner, U. Seydel, *Anal. Chem.* **1985**, *57*, 895.
[8] V. V. Golovlev, S. L. Allman, W. R. Garrett, N. I. Taranenko, C. H. Chen, *Int. J. Mass Spectrom. Ion Processes* **1997**, *169*, 69.
[9] J. Perez, L. E. Ramirez-Arizmendi, C. J. Petzold, L. P. Guler, E. D. Nelson, H. I. Kenttamaa, *Int. J. Mass Spectrom.* **2000**, *198*, 173.

 © 2006 Wiley-VCH Verlag GmbH & Co. KGaA, Weinheim

[10] M. A. Tito, K. Tars, K. Valegard, J. Hajdu, C. V. Robinson, *J. Am. Chem. Soc.* **2000**, *122*, 3550.
[11] S. D. Fuerstenau, W. H. Benner, J. J. Thomas, C. Brugidou, B. Bothner, G. Siuzdak, *Angew. Chem.* **2001**, *113*, 559; *Angew. Chem. Int. Ed.* **2001**, *40*, 541.
[12] R. F. Wuerker, H. Shelton, R. V. Langmuir, *J. Appl. Phys.* **1959**, *30*, 342.
[13] R. E. March, J. F. Todd, *Quadrupole Ion Trap Mass Spectrometry*, Wiley, New York, **2005**.
[14] Thin foils such as that made of tantalum also worked well as the sample substrates. The 0.5-mm Si wafer was chosen in this study for its rigidity and versatility of surface modification.
[15] The efficiency of the overall process (including ionization and ion trapping) is approximately 10^{-6}; that is, a loading of 10^7 bioparticles on the sample plate allows the analysis of the mass of about 10 charged particles.
[16] G. Hars, Z. Tass, *J. Appl. Phys.* **1995**, *77*, 4245.
[17] W.-P. Peng, Y. T. Lee, J. W. Ting, H.-C. Chang, *Rev. Sci. Instrum.* **2005**, *76*, 023108.
[18] M. A. Philip, F. Gelbard, S. Arnold, *J. Colloid Interface Sci.* **1983**, *91*, 507.
[19] S. Schlemmer, J. Illemann, S. Wellert, D. Gerlich, *J. Appl. Phys.* **2001**, *90*, 5410.
[20] W.-P. Peng, Y.-C. Yang, C.-W. Lin, H.-C. Chang, *Anal. Chem.* **2005**, *77*, 7084.
[21] Wild-type vaccinia viruses were prepared as intracellular mature virus stocks in BSC40 cells. They were purified according to published procedures (see: C. S. Chung, J. C. Hsiao, Y. S. Chang, W. Chang, *J. Virol.* **1998**, *72*, 1577) and resuspended in filtered (0.2-μm pore-size filter) deionized water before use. *E. coli* K-12 bacteria were obtained from Sigma and purified by repeated centrifugation in filtered distilled water. Both samples were prepared as suspensions at a concentration of about 1×10^{10} particles mL^{-1}. An aliquot (10 μL) of each solution of sample was deposited on a bare Si wafer and dried in air prior to laser desorption. Peripheral blood samples were taken from a healthy individual and a patient with α-thalassemia (a type of hereditary anemia). Red blood cells were separated by centrifugation and rinsed three times in phosphate-buffered saline at room temperature. A thin layer of red blood cells was smeared on the Si wafer and dried in air. The MCH values of these two blood samples were measured independently with an automated hematology analyzer (Sysmex K-1000) to be 31 and 22 pg, respectively.
[22] As the accuracy of the mass measurement for each particle is better than 1%, the reported variation in mass represents the intrinsic mass distribution of these particles.
[23] Certificate of analysis for NIST Standard Reference Material 1690.
[24] H. Kahler, B. J. Lloyd, Jr., *Science* **1951**, *114*, 34.
[25] G. F. Bahr, W. D. Foster, D. Peters, E. H. Zeitler, *Biophys. J.* **1980**, *29*, 305.
[26] *Mosby's Manual of Diagnostic and Laboratory Tests*, (Eds.: K. D. Pagana, T. J. Pagana), Mosby, St. Louis, **1998**.
[27] W. P. Leung, A. C. Tam, *Appl. Phys. Lett.* **1992**, *60*, 23.
[28] A. A. Kolomenskii, H. A. Schuessler, V. G. Mikhalevich, A. A. Maznev, *J. Appl. Phys.* **1998**, *84*, 2404.
[29] Besides bioparticles, we found that some nano- and microparticles composed of metals, inorganic salts, organic compounds, and polymers were also liberated in charged forms. The masses of sinapinic acid powders, NaCl crystallites, gold nanoparticles, and polystyrene microparticles were all measured with this approach. The result indicates that the setup presently described may become a convenient mass spectrometer for the determination of mass of micro- and nanoparticles without the need of external ionization.
[30] Although the mechanism of the particle-charging process is not exactly known, the surface charge density of these desorbed precharged ions is actually very low. For a red blood cell carrying 1000 charges as an example, the calculated surface charge density is on the order of 10^{-7} $C m^{-2}$, a value which is much lower than that of small molecular ions desorbed/ionized by LIAD (Ref. [8]). Because of this low charge density, electron bombardment of negatively charged particles is possible.

 © 2006 Wiley-VCH Verlag GmbH & Co. KGaA, Weinheim

Asymmetric Synthesis

DOI: 10.1002/anie.200503312

Synthesis of Functionalized Cyclopentenes through Catalytic Asymmetric [3+2] Cycloadditions of Allenes with Enones**

*Jonathan E. Wilson and Gregory C. Fu**

Five-membered carbocycles are a common substructure in a wide array of natural and nonnatural products.[1] Among this family of compounds, cyclopentenes are particularly important targets, in part because derivatization of the olefin often occurs with good diastereoselectivity, thereby providing access to highly functionalized, stereochemically complex cyclopentanes. Although considerable progress has been described in developing methods for the asymmetric synthesis of cyclopentenes, the number of effective *catalytic* enantioselective processes is comparatively small.[2]

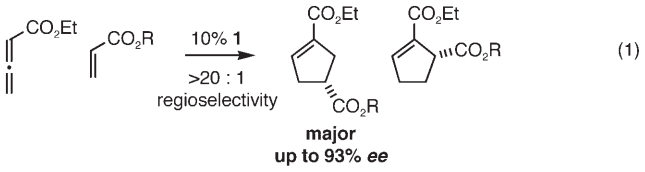
Recently, nucleophilic catalysis by phosphines has emerged as a powerful tool in synthetic organic chemistry.[3] For example, tertiary phosphines catalyze a variety of annulation reactions, including Lu's [3+2] cycloaddition of allenes with olefins to generate cyclopentenes.[4] In 1997, Zhang et al. reported a pioneering study in which he established that a chiral phosphine can furnish good enantioselectivity in this process; with respect to scope, only unsubstituted acrylate esters and diethyl maleate react with the allene to form the target cyclopentenes in high enantiomeric excess (*ee*) [Eq. (1) and (2)].[5]

[*] J. E. Wilson, Prof. Dr. G. C. Fu
Department of Chemistry
Massachusetts Institute of Technology
Cambridge, MA 02139 (USA)
Fax: (+1) 617-324-3611
E-mail: gcf@mit.edu

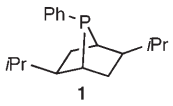
[**] We thank Luke Firmansjah and Dr. Peter Mueller for assistance (X-ray crystallography) and the Jamison group for a sample of (*R*)-nmdpp. Support has been provided by the NIH (National Institute of General Medical Sciences: R01-GM57034; National Cancer Institute: training grant CA009112), Merck Research Laboratories, and Novartis. Funding for the MIT Department of Chemistry Instrumentation Facility has been furnished in part by NSF CHE-9808061 and NSF DBI-9729592.

Supporting information for this article is available on the WWW under http://www.angewandte.org or from the author.

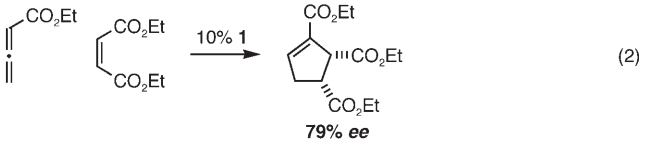
WILEY InterScience DISCOVER SOMETHING GREAT
© 2006 Wiley-VCH Verlag GmbH & Co. KGaA, Weinheim



(1)

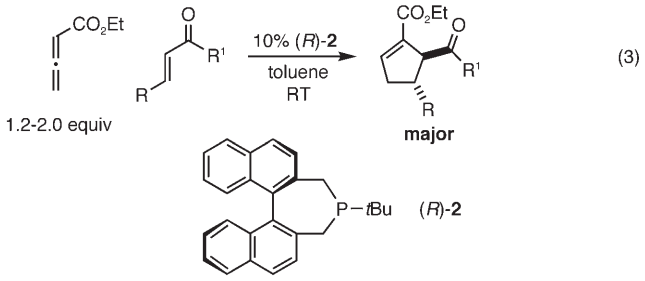


1



(2)

In general, there has been only very limited progress to date in the development of effective phosphine-based methods for asymmetric nucleophilic catalysis.[6] We recently reported that phosphepine **2**, which was originally designed as a ligand for metal-catalyzed processes,[7] catalyzes [4+2] annulations of allenes with imines to generate piperidine derivatives with good enantioselectivity.[6c,8] Since that initial study, we have been exploring the utilization of this phosphepine for a wide array of nucleophile-catalyzed reactions. Herein, we establish that **2** catalyzes enantioselective [3+2] cycloadditions of allenes with a variety of β-substituted α,β-unsaturated enones to produce highly functionalized cyclopentenes that contain two contiguous stereocenters [Eq. (3)].



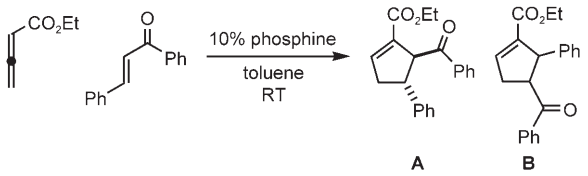
(3)

In a preliminary investigation, we surveyed the use of phosphepine **2** and a variety of commercially available mono- and bisphosphines as catalysts for the asymmetric cycloaddition of ethyl-2,3-butadienoate and chalcone (Table 1). Whereas **2** furnishes the target cyclopentene in good yield, *ee*, and regioselectivity (Table 1, entry 1), the other phosphines are either ineffective as catalysts (Table 1, entries 2–4) or provide relatively poor enantiomeric excess (Table 1, entries 5–7).

Phosphepine **2** catalyzes the asymmetric [3+2] cycloaddition of allenes with a wide array of enones (Table 2).[9] It is worth noting that these are the first such processes that employ β-substituted α,β-unsaturated carbonyl compounds (other than diethyl maleate)[10] and that the opposite regioisomer is produced preferentially as compared with substrates that lack a β substituent [cf. Eq. (1)].[4,5]

The desired cyclopentene is generated in good enantiomeric excess for both electron-rich and electron-poor chalcone derivatives (Table 2, entries 2–6), although cycloadditions of electron-rich substrates proceed somewhat less efficiently and therefore require additional allene (2.0 equivalents, rather than 1.2; Table 2, entries 4 and 6). The method tolerates heterocyclic substituents in either the β position (Table 2, entries 7 and 8) or attached to the carbonyl group (Table 2, entries 9 and 10) of the enone.

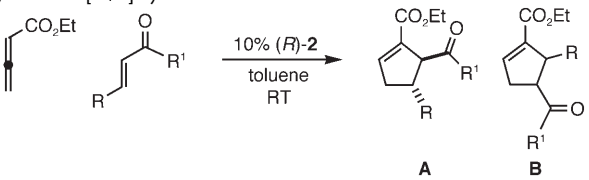
Table 1: Survey of chiral phosphine catalysts for the [3+2] cycloaddition of allenes with enones.[a]



Entry	Phosphine[b]	Yield [%][c]	*ee* [%][d]	**A**:**B**
1	(*R*)-**2**	64	88	13:1
2	(*S*)-binapine	0	–	–
3	(*R*)-binap	2	50	>20:1
4	(*R*)-nmdpp	4	−4	11:1
5	(*R*,*R*)-Me-bpe	61	−4	6:1
6	(*R*,*R*)-ferrotane	64	11	7:1
7	(*R*,*R*)-Et-DuPhos	61	58	7:1

[a] All data are the average of two experiments. [b] binap = 2,2'-Bis(diphenylphosphanyl)-1,1′-binaphthyl, nmdpp = neomenthyldiphenylphosphine. Molecular structures of (*S*)-binapine, (*R*,*R*)-Me-bpe, (*R*,*R*)-ferrotane, and (*R*,*R*)-Et-DuPhos are shown in Ref. [17]. [c] Yield of isolated **A** and **B**. [d] Enantiomeric excess of **A**. A negative value for *ee* signifies that the shown enantiomer of cyclopentene **A** is the minor product, rather than the major.

Table 2: Synthesis of functionalized cyclopentenes through catalytic asymmetric [3+2] cycloadditions.[a]



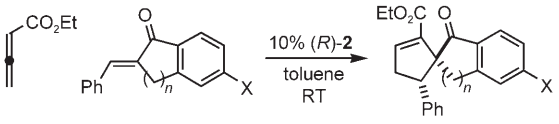
Entry	R	R^1	Yield [%][b]	*ee* [%][c]	**A**:**B**
1	Ph	Ph	64	88	13:1
2	Ph	4-chlorophenyl	76	82	7:1
3	Ph	4-methylphenyl	61	87	20:1
4	Ph	4-methoxyphenyl	54	88	>20:1
5	4-chlorophenyl	Ph	74	87	9:1
6	4-methoxyphenyl	Ph	67	87	10:1
7	2-furyl	Ph	69	88	3:1
8[d]	2-quinolyl	Ph	52	88	20:1
9[d]	4-chlorophenyl	2-(5-methylfuryl)	54	89	>20:1
10	Ph	2-thienyl	74	90	6:1
11	C≡CC_5H_{11}	Ph	65	85	6:1
12	C≡CTES	Ph	70	87	>20:1
13	C_5H_{11}	Ph	39[e]	75	>20:1

[a] All data are the average of two experiments. All cycloadditions employed 1.2 equiv of allene, except for entries 4, 6, 7, and 13, for which 2.0 equiv was used. [b] Yield of isolated **A** and **B**. [c] Enantiomeric excess of **A**. [d] Because of the low solubility of the enone in toluene, CH_2Cl_2 was employed as a co-solvent. [e] The enone can be recovered in 56% yield.

 © 2006 Wiley-VCH Verlag GmbH & Co. KGaA, Weinheim

This process is not limited to β-(hetero)aryl enones. For example, phosphepine **2** catalyzes cycloadditions of enones that bear a β-alkynyl group with good enantiomeric excess (Table 2, entries 11 and 12). Under our standard conditions, if an alkyl substituent occupies the β position, formation of the cyclopentene proceeds sluggishly, but with fairly good selectivity (Table 2, entry 13).

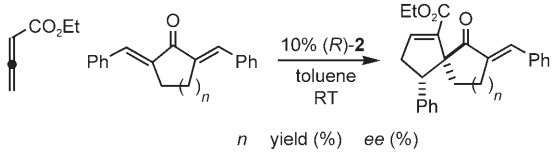
Catalyst **2** can achieve the enantioselective synthesis of spirocyclic compounds through reactions of trisubstituted enones, thereby generating adjacent quaternary[11] and tertiary stereocenters [Eq. (4); a single regioisomer is produced].[12–14] This method is not entirely general—the cycloaddition of an indanone proceeds in excellent yield, however, the reaction of a closely related tetralone is considerably less efficient [but highly enantioselective; Eq. (4)].[15]



(4)

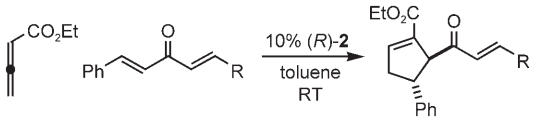
n	X	yield (%)	*ee* (%)
1	Br	97	89
2	H	32	95

Dienones are also suitable substrates, undergoing a single phosphine-catalyzed [3+2] cycloaddition [Eq. (5) and (6); only one regioisomer is observed]). Although for symmetrical dienones there is no issue of site selectivity, this complication does arise for unsymmetrical compounds. Interestingly, phosphepine **2** can achieve enantioselective cycloadditions with complete site selectivity [Eq. (6)].



(5)

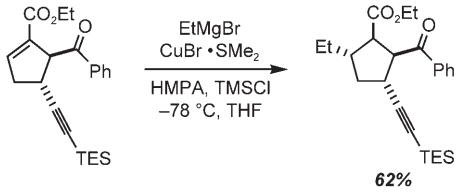
n	yield (%)	*ee* (%)
1	81	89
2	57	93



(6)

R	yield (%)	*ee* (%)
Ph	75	89
2,6-dichlorophenyl	68	73

We had anticipated that the enantiomerically enriched cyclopentenes generated in these asymmetric [3+2] cycloadditions should be attractive substrates for further functionalization. An example of such a process, which produces a diastereomerically pure cyclopentane that bears four contiguous stereocenters, is illustrated in Equation (7).[16]



(7)

In summary, we have described the first nucleophile-catalyzed asymmetric [3+2] cycloadditions of allenes with enones. We have determined that β-substituted enones undergo reaction with a different regiochemical preference compared with previously described cycloadditions of β-unsubstituted α,β-unsaturated carbonyl compounds. We have applied our method to reactions of trisubstituted olefins, thereby generating adjacent quaternary and tertiary stereocenters. Finally, we have established that the product cyclopentenes can be stereoselectively derivatized to provide cyclopentanes that bear four contiguous stereocenters. Ongoing efforts are directed at further expanding the currently limited range of enantioselective processes catalyzed by chiral phosphine nucleophiles.

Received: September 17, 2005
Published online: January 30, 2006

Keywords: asymmetric synthesis · cycloaddition · homogeneous catalysis · phosphanes

[1] For leading references and examples, see: a) R. C. Hartley, S. T. Caldwell, *J. Chem. Soc. Perkin Trans. 1* **2000**, 477–501, and previous reviews in this series; b) Prostaglandins: *Prostaglandins, Leukotrienes and Essential Fatty Acids* (Eds.: D. F. Horrobin, M. S. Manku, P. Sirois, P. Borgeat), Churchill Livingston, Edinburgh, **2002**; c) Carbasugars: G. Rassu, L. Auzzas, L. Pinna, L. Battistini, C. Curti, *Stud. Nat. Prod. Chem.* **2003**, *29*, 449–520; d) Polymers: I. Kuntz, *Encycl. Polym. Sci. Eng.* **1985**, *4*, 537–542.

[2] For recent examples of processes in which the asymmetry is introduced during the ring-forming reaction, see: a) H. M. L. Davies, B. Xiang, N. Kong, D. G. Stafford, *J. Am. Chem. Soc.* **2001**, *123*, 7461–7462; b) S. E. Gibson, A. Stevenazzi, *Angew. Chem.* **2003**, *115*, 1844–1855; *Angew. Chem. Int. Ed.* **2003**, *42*, 1800–1810.

[3] For a review, see: J. L. Methot, W. R. Roush, *Adv. Synth. Catal.* **2004**, *346*, 1035–1050.

[4] a) C. Zhang, X. Lu, *J. Org. Chem.* **1995**, *60*, 2906–2908; b) Z. Xu, X. Lu, *Tetrahedron Lett.* **1999**, *40*, 549–552; c) X. Lu, C. Zhang, Z. Xu, *Acc. Chem. Res.* **2001**, *34*, 535–544; d) Y. Du, X. Lu, Y. Yu, *J. Org. Chem.* **2002**, *67*, 8901–8905; e) Y. Du, X. Lu, *J. Org. Chem.* **2003**, *68*, 6463–6465.

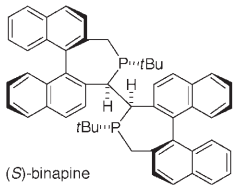
[5] G. Zhu, Z. Chen, Q. Jiang, D. Xiao, P. Cao, X. Zhang, *J. Am. Chem. Soc.* **1997**, *119*, 3836–3837.

[6] a) E. Vedejs, O. Daugulis, S. T. Diver, *J. Org. Chem.* **1996**, *61*, 430–431; E. Vedejs, O. Daugulis, *J. Am. Chem. Soc.* **1999**, *121*, 5813–5814; S. A. Shaw, P. Aleman, E. Vedejs, *J. Am. Chem. Soc.* **2003**, *125*, 13368–13369; b) M. Shi, L.-H. Chen, C.-Q. Li, *J. Am. Chem. Soc.* **2005**, *127*, 3790–3800; c) R. P. Wurz, G. C. Fu, *J. Am. Chem. Soc.* **2005**, *127*, 12234–12235. See also: Z. Chen, G. Zhu, Q. Jiang, D. Xiao, P. Cao, X. Zhang, *J. Org. Chem.* **1998**, *63*, 5631–5635.

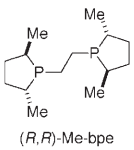
[7] a) S. Gladiali, A. Dore, D. Fabbri, O. De Lucchi, M. Manassero, *Tetrahedron: Asymmetry* **1994**, *5*, 511–514; b) K. Junge, B. Hagemann, S. Enthaler, G. Oehme, M. Michalik, A. Monsees, T. Riermeier, U. Dingerdissen, M. Beller, *Angew. Chem.* **2004**, *116*,

 © 2006 Wiley-VCH Verlag GmbH & Co. KGaA, Weinheim

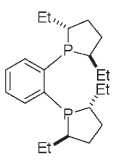
5176 – 5179; *Angew. Chem. Int. Ed.* **2004**, *43*, 5066 – 5069, and references therein.
[8] For the initial report of this annulation method, see: X.-F. Zhu, J. Lan, O. Kwon, *J. Am. Chem. Soc.* **2003**, *125*, 4716 – 4717.
[9] Notes: a) Under these conditions, α,β-unsaturated ketones in which R^1 = alkyl or alkynyl or R = alkenyl (Table 2), α,β-unsaturated esters that bear a β substituent, *p*-benzoquinone, and *N*-phenylmaleimide are not suitable coupling partners. Benzyl and allyl-2,3-butadienoate are less reactive than ethyl-2,3-butadienoate. b) If access to racemic cyclopentenes is desired, PPh_3 or PBu_3 can be employed as the catalyst. c) Use of THF or CH_2Cl_2 as the solvent leads to poorer yield and regioselectivity. d) At lower temperature, the rate of cycloaddition decreases significantly, with only a small gain in *ee*. e) According to ^{31}P NMR spectroscopy, phosphepine **2** is the predominant phosphorus-containing species that is present during the [3+2] cycloaddition process. f) To the best of our knowledge, the stereochemistry of the enone is preserved in the cyclopentene.
[10] For non-asymmetric reactions, only maleates and fumarates have been shown to be suitable substrates. Lu et al. (e.g., ref. [4a]) and Zhang et al. (ref. [5]) were unable to achieve cycloadditions of other β-substituted α,β-unsaturated carbonyl compounds.
[11] For a recent discussion of the challenge of developing catalytic asymmetric methods for the synthesis of quaternary all-carbon centers, see: C. J. Douglas, L. E. Overman, *Proc. Natl. Acad. Sci. USA* **2004**, *101*, 5363 – 5367.
[12] Lu et al. have described phosphine-catalyzed [3+2] cycloadditions that generate spirocycles from enones that lack a β substituent (refs. [4d] and [4e]). They observe predominant formation of a different regioisomer (the two carbonyl groups are in a 1,3 relationship on the cyclopentene ring) from that depicted in Equation (4).
[13] For leading references to an example of a naturally occurring spiroindanone that bears an all-carbon quaternary stereocenter (fredericamycin A), see: Y. Kita, K. Higuchi, Y. Yoshida, K. Iio, S. Kitagaki, K. Ueda, S. Akai, H. Fujioka, *J. Am. Chem. Soc.* **2001**, *123*, 3214 – 3222.
[14] For another recent example of a catalytic asymmetric method for the synthesis of spirocyclic compounds wherein an all-carbon quaternary stereocenter is established in the cyclization process, see: M. Hatano, K. Mikami, *J. Am. Chem. Soc.* **2003**, *125*, 4704 – 4705.
[15] For the tetralone, a considerable quantity of unreacted starting material was observed. Increasing the amount of allene did not improve the yield.
[16] These conditions were developed by Nakamura and Kuwajima: S. Matsuzawa, Y. Horiguchi, E. Nakamura, I. Kuwajima, *Tetrahedron* **1989**, *45*, 349 – 362.
[17] Molecular structures of phosphine catalysts given in Table 1:



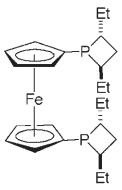
(*S*)-binapine



(*R*,*R*)-Me-bpe



(*R*,*R*)-Et-DuPhos



(*R*,*R*)-ferrotane

 © 2006 Wiley-VCH Verlag GmbH & Co. KGaA, Weinheim

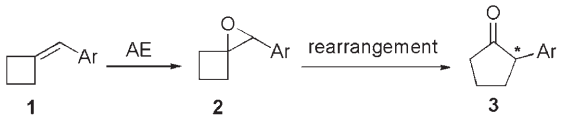
Synthetic Methods

DOI: 10.1002/anie.200501520

Enantioselective Synthesis of 2-Aryl Cyclopentanones by Asymmetric Epoxidation and Epoxide Rearrangement**

*Yu-Mei Shen, Bin Wang, and Yian Shi**

Optically active 2-aryl cycloalkanones are a class of useful molecules for organic synthesis and have received extensive attention. A number of effective approaches have been developed for the synthesis of 2-alkyl-2-aryl disubstituted cycloalkanones,[1–7] including the Pd-catalyzed asymmetric α-arylation of alkyl substituted cycloalkanones,[1] the allylic alkylation of 2-aryl cycloalkanones,[2] and the chelation-controlled Heck arylation of enol ethers.[3] In the preparation of monosubstituted 2-aryl cycloalkanones, high *ee* values have also been obtained for 2-aryl cyclohexanones and cycloheptanones through the asymmetric protonation of the corresponding silyl enol ethers and enolates.[7] Thus far, monosubstituted 2-aryl cyclopentanones are still a challenge to obtain, presumably because of facile racemization under the reaction conditions. Herein, we wish to report our preliminary efforts on the asymmetric epoxidation of benzylidenecyclobutane and subsequent epoxide rearrangement (Scheme 1).[8–12]



Scheme 1. Asymmetric epoxidation of benzylidenecyclobutane (**1**) and subsequent epoxide rearrangement. AE = asymmetric epoxidation.

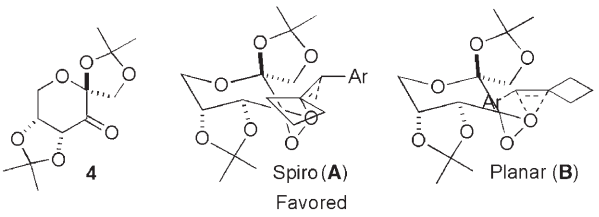
The initial epoxidation of benzylidenecyclobutane with fructose-derived ketone **4**, which has been shown to be effective for a variety of *trans*- and trisubstituted olefins,[13] gave only 42% *ee*. The low *ee* value obtained with **4** could be attributed to the severe competition of the planar transition state **B** with the favored spiro transition state **A** (Scheme 2). Our recent studies with oxazolidinone-containing ketones have shown that there is an attractive interaction between the

[*] Y.-M. Shen, B. Wang, Prof. Dr. Y. Shi
Department of Chemistry
Colorado State University
Fort Collins, CO 80523 (USA)
Fax: (+1) 970-491-1801
E-mail: yian@lamar.colostate.edu

[**] We are grateful for generous financial support from the General Medical Sciences of the National Institutes of Health (GM59705-06).

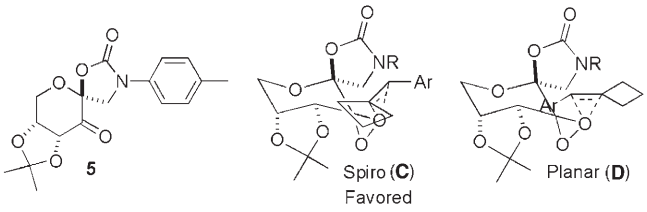
Supporting information for this article is available on the WWW under http://www.angewandte.org or from the author.

© 2006 Wiley-VCH Verlag GmbH & Co. KGaA, Weinheim



Scheme 2. Transition states of ketone **4**.

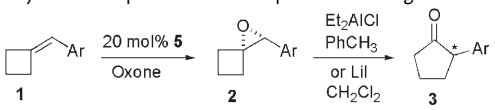
aryl group of the olefin and the oxazolidinone moiety of the ketone catalyst.[14] These studies indicate that the desired spiro transition state **C** could be further favored by such an attraction (Scheme 3), thus resulting in higher enantioselectivity. The *ee* value of the epoxide increased to 90% when the epoxidation was carried out with 20 mol% ketone **5** at −10°C (Table 1, entry 1). High enantioselectivities were also obtained for a variety of other substituted benzylidenecyclobutanes (Table 1).[15]

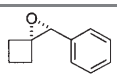
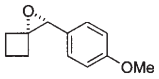
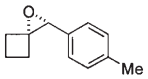
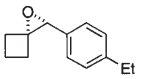
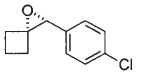
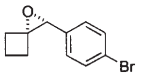
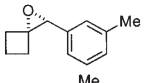
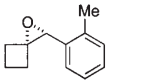
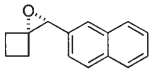


Scheme 3. Transition states of ketone **5**.

With optically active epoxides in hand, the Lewis acid catalyzed epoxide rearrangement was explored. The stereoselectivity of the rearrangement was found to be highly sensitive to the Lewis acid and solvent. After optimization, the rearrangement was effectively achieved with Et_2AlCl in toluene at −78°C. The cyclopentanone product was obtained cleanly after careful work up,[16] and high *ee* values were generally maintained (Table 1). The rearrangement with Et_2AlCl is likely to go through a concerted process with inversion of the configuration (pathway a; Scheme 4). Slightly more enantioselectivity is lost for epoxides with electron-donating groups, such as the 4-MeO moiety (Table 1, entry 2), during the rearrangement. This lowered enantioselectivity could be because of the competition from a stepwise S_N1-type process via a carbocation which is stabilized by electron-donating groups. To probe the reaction mechanism further, the rearrangement was then carried out with LiI.[17] The opposite enantiomer of the rearrangement product was obtained under these conditions (Table 1), and good *ee* values were also obtained in most cases. The rearrangement with LiI is likely to go via intermediate **6** with double inversion (pathway b; Scheme 4). The low *ee* value obtained with the 4-MeO substituted epoxide (Table 1, entry 2) could be because of the competition from pathway a and/or the S_N1-type process. To support the above mechanistic pathways further, the configurations of the 4-Cl substituted epoxide (Table 1, entry 5) and the corresponding rearranged cyclopentanone product with Et_2AlCl were determined by using vibrational circular dichroism (VCD; BioTools).[18] It is shown that the epoxide has an *R* configuration and the rearranged cyclopentanone has an *S* configuration. The configuration of the rearranged cyclopentanone was also determined for entry 1 by comparison with the measured optical-rotation value of the lactone product (obtained from the Baeyer–Villiger

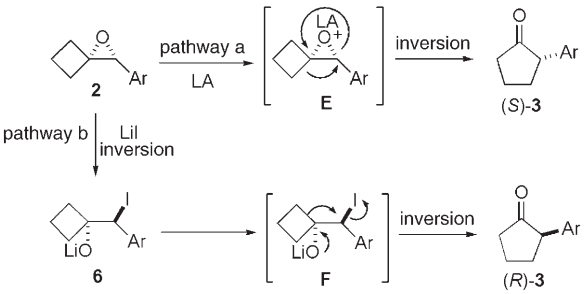
Table 1: Asymmetric epoxidation and epoxide rearrangement.[a–c]



Entry	Epoxide	Yield of (**2**) [%] (*ee*)[d]	Conditions	Yield of **3** [%] (*ee*)[e]
1		93 (90)	Et_2AlCl LiI	90 (90) (*S*) 81 (90) (*R*)
2		95 (91)	Et_2AlCl LiI	98 (82) (*S*) 81 (40) (*R*)
3		84 (93)	Et_2AlCl LiI	82 (88) (*S*) 91 (92) (*R*)
4		67 (94)	Et_2AlCl LiI	99 (91) (*S*) 86 (92) (*R*)
5		78 (96)	Et_2AlCl LiI	89 (94) (*S*) 87 (84) (*R*)
6		80 (96)	Et_2AlCl LiI	94 (93) (*S*) 87 (84) (*R*)
7		80 (95)	Et_2AlCl LiI	82 (92) (*S*) 92 (93) (*R*)
8		77 (86)	Et_2AlCl LiI	83 (84) (*S*) 90 (80) (*R*)
9		88 (95)	Et_2AlCl LiI	94 (96) (*S*) 84 (87) (*R*)

[a] All epoxidations were carried out with the substrate (0.5 mmol), **5** (0.1 mmol), oxone (0.8 mmol), and K_2CO_3 (3.36 mmol) in dimethoxyethane (DME)/dimethoxymethane (DMM) (3:1, v/v; 7.5 mL) and buffer (0.1 M K_2CO_3/AcOH, pH 9.3; 5 mL) at −10 or 0°C for 4–12 h, except for entry 9, in which the reaction was carried out in DME/DMM (1:1, v/v; 9.4 mL) and buffer (3.1 mL) at 0°C for 8 h. The epoxides in entries 4, 5, 6, 8, and 9 were purified by column chromatography on silica gel (buffered with Et_3N). [b] All rearrangements were carried out with epoxide (1.0 equiv) and Et_2AlCl (0.25 or 1.0 equiv) in $PhCH_3$ at −78°C for 0.25–3 h. The ketone products were not purified by column chromatography on silica gel and were clean as judged by NMR spectroscopy. [c] All rearrangements were carried out with LiI (1.0–3.0 equiv) in CH_2Cl_2 at room temperature for 5–30 min, except for entry 2, in which the reaction was carried out at 0°C. [d] The *ee* value (%) of the epoxide was determined by chiral GC (Chiraldex B-DM), except for entry 2, for which the *ee* value was determined by chiral HPLC (Chiralcel AD). The absolute configuration was tentatively assigned based on the spiro reaction mode. The absolute configuration of entry 5 was determined by using the VCD spectra (BioTools). [e] The *ee* value (%) of the cyclopentanone was determined by chiral HPLC (Chiralcel AD). The absolute configuration was tentatively assigned based on the mechanistic consideration. The absolute configuration was determined for entry 1 by comparison of the measured optical-rotation value of the lactone product (obtained from the Baeyer–Villiger oxidation of the ketone with *m*CPBA) with the reported value.[20] The absolute configuration of entry 5 was determined by using the VCD spectra (BioTools).

 © 2006 Wiley-VCH Verlag GmbH & Co. KGaA, Weinheim



Scheme 4. Possible reaction pathways for the epoxide rearrangement. LA = Lewis acid.

oxidation of the ketone with *meta*-chloroperoxybenzoic acid (*m*CPBA)[19]) with the reported value.[20]

In conclusion, we have shown that benzylidenecyclobutanes can undergo epoxidation with the readily available glucose-derived ketone **5** in high enantioselectivity. The resulting epoxides can be rearranged to 2-aryl cyclopentanones with either inversion or retention of configuration using Et_2AlCl or LiI. High *ee* values have been obtained for cyclopentanones in most cases. This two-step process provides a viable entry to optically active 2-aryl cyclopentanones, which until now could not be readily obtained.

Experimental Section

Representative procedure for asymmetric epoxidation (Table 1, entry 5): Buffer (0.1 M K_2CO_3/AcOH in aqueous ethylenediaminetetraacetate (EDTA; 4×10^{-4} M), pH 9.3; 5 mL) was added to a solution of **1** (0.089 g, 0.5 mmol) and **5** (0.033 g, 0.1 mmol) in DME/DMM (3:1 v/v; 7.5 mL). After the mixture was cooled to −10 °C by using a NaCl/ice bath, a 0.20 M solution of oxone (0.492 g, 0.80 mmol) in aqueous EDTA (4×10^{-4} M, 4.0 mL) and a solution of 0.84 M K_2CO_3 (0.464 g, 3.36 mmol) in aqueous EDTA (4×10^{-4} M, 4.0 mL) were added separately yet simultaneously by a syringe pump over a period of 10 h. The reaction mixture was quenched and extracted with hexane, washed with brine, dried over Na_2SO_4, filtered, concentrated, and purified by flash column chromatography (the silica gel was buffered with 1% Et_3N in organic solvent; hexane/EtOAc as the eluent) to give the epoxide as a colorless oil (0.076 g, 78% yield, 96% *ee*).

Representative procedure for the epoxide rearrangement with Et_2AlCl (Table 1, entry 1): A solution of Et_2AlCl (1.0 M in hexane; 50 μL, 0.05 mmol) was added to a solution of the epoxide (90% *ee*; 0.032 g, 0.2 mmol) in dry toluene (2 mL) at −78 °C. The reaction mixture was stirred at −78 °C until completion (about 3 h) and quenched with saturated aqueous $NaHCO_3$ (0.10 mL) at −78 °C. Upon warming up to 0 °C, the reaction mixture was diluted with hexane, washed with brine, dried over Na_2SO_4, filtered, and concentrated to give the ketone product as a colorless oil (0.029 g, 90% yield, 90% *ee*).[21]

Received: May 3, 2005
Published online: January 30, 2006

Keywords: asymmetric synthesis · chirality · cyclopentanones · epoxidation · rearrangement

[1] a) J. Ahman, J. P. Wolfe, M. V. Troutman, M. Palucki, S. L. Buchwald, *J. Am. Chem. Soc.* **1998**, *120*, 1918; b) T. Hamada, A. Chieffi, J. Ahman, S. L. Buchwald, *J. Am. Chem. Soc.* **2002**, *124*, 1261.

[2] B. M. Trost, G. M. Schroeder, J. Kristensen, *Angew. Chem.* **2002**, *114*, 3642; *Angew. Chem. Int. Ed.* **2002**, *41*, 3492.

[3] P. Nilsson, M. Larhed, A. Hallberg, *J. Am. Chem. Soc.* **2003**, *125*, 3430.

[4] For the catalytic asymmetric phase-transfer alkylation of 2-phenyl-1-indanone, see: U.-H. Dolling, P. Davis, E. J. J. Grabowski, *J. Am. Chem. Soc.* **1984**, *106*, 446.

[5] For examples of enzymatic resolution approach, see: a) S. Takano, K. Inomata, T. Sato, M. Takahashi, K. Ogasawara, *J. Chem. Soc. Chem. Commun.* **1990**, 290; b) K. Tanaka, T. Taniguchi, K. Ogasawara, *Tetrahedron Lett.* **2001**, *42*, 1049.

[6] For examples of the rearrangement of aryl substituted 2,3-epoxy acylates and sulfonates, see: a) Y. Kita, A. Furukawa, J. Futamura, K. Higuchi, K. Ueda, H. Fujioka, *Tetrahedron Lett.* **2000**, *41*, 2133; b) Y. Kita, A. Furukawa, J. Futamura, K. Ueda, Y. Sawama, H. Hamamoto, H. Fujioka, *J. Org. Chem.* **2001**, *66*, 8779; c) Y. Kita, J. Futamura, Y. Ohba, Y. Sawama, J. K. Ganesh, H. Fujioka, *J. Org. Chem.* **2003**, *68*, 5917.

[7] For the asymmetric protonation of enol derivatives, see: a) K. Ishihara, M. Kaneeda, H. Yamamoto, *J. Am. Chem. Soc.* **1994**, *116*, 11179; b) K. Ishihara, S. Nakamura, M. Kaneeda, H. Yamamoto, *J. Am. Chem. Soc.* **1996**, *118*, 12854; c) A. Yanagisawa, H. Inanami, H. Yamamoto, *Chem. Commun.* **1998**, 1573; d) S. Nakamura, M. Kaneeda, K. Ishihara, H. Yamamoto, *J. Am. Chem. Soc.* **2000**, *122*, 8120; e) K. Ishihara, D. Nakashima, Y. Hiraiwa, H. Yamamoto, *J. Am. Chem. Soc.* **2003**, *125*, 24.

[8] For reviews on acid-promoted epoxide rearrangements, see: a) G. Magnusson, *Org. Prep. Proced. Int.* **1990**, *22*, 547; b) B. Rickborn in *Comprehensive Organic Synthesis, Vol. 3* (Eds.: B. M. Trost, I. Fleming), Pergamon, Oxford, **1991**, p. 733; c) H. Fujioka, Y. Yoshida, Y. Kita, *Yuki Gosei Kagaku Kyokaishi* **2003**, *61*, 133.

[9] For the rearrangement of oxaspiropentanes and oxaspirohexanes, see: a) B. M. Trost, M. J. Bogdanowicz, *J. Am. Chem. Soc.* **1972**, *94*, 4777; b) B. M. Trost, M. J. Bogdanowicz, *J. Am. Chem. Soc.* **1973**, *95*, 5321; c) B. M. Trost, P. H. Scudder, *J. Am. Chem. Soc.* **1977**, *99*, 7601; d) J. K. Crandall, W. W. Conover, *J. Org. Chem.* **1978**, *43*, 3533.

[10] For the asymmetric epoxidation of cyclopropylideneethanol and subsequent rearrangement, see: a) H. Nemoto, H. Ishibashi, M. Nagamochi, K. Fukumoto, *J. Org. Chem.* **1992**, *57*, 1707; b) H. Nemoto, M. Nagamochi, H. Ishibashi, K. Fukumoto, *J. Org. Chem.* **1994**, *59*, 74; c) H. Nemoto, T. Tanabe, K. Fukumoto, *J. Org. Chem.* **1995**, *60*, 6785; d) H. Nemoto, K. Fukumoto, *Synlett* **1997**, 863.

[11] For asymmetric epoxidations of unfunctionalized cyclopropylidene derivatives and subsequent rearrangement, see: a) M. Yoshida, M. A.-H. Ismail, H. Nemoto, M. Ihara, *Heterocycles* **1999**, *50*, 673; b) H. Nemoto, M. Yoshida, K. Fukumoto, M. Ihara, *Tetrahedron Lett.* **1999**, *40*, 907; c) M. Yoshida, M. A.-H. Ismail, H. Nemoto, M. Ihara, *J. Chem. Soc. Perkin Trans. 1* **2000**, 2629.

[12] For asymmetric dihydroxylations of cyclopropylidene derivatives and subsequent rearrangements, see: a) A. Krief, A. Ronvaux, A. Tuch, *Bull. Soc. Chim. Belg.* **1997**, *106*, 699; b) A. Krief, A. Ronvaux, A. Tuch, *Tetrahedron* **1998**, *54*, 6903; c) H. Nemoto, J. Miyata, H. Hakamata, K. Fukumoto, *Tetrahedron Lett.* **1995**, *36*, 1055; d) H. Nemoto, J. Miyata, H. Hakamata, M. Nagamochi, K. Fukumoto, *Tetrahedron* **1995**, *51*, 5511; e) J. M. Diffendal, J. Filan, P. G. Spoors, *Tetrahedron Lett.* **1999**, *40*, 6137; f) J. Miyata, H. Nemoto, M. Ihara, *J. Org. Chem.* **2000**, *65*, 504.

[13] a) Z.-X. Wang, Y. Tu, M. Frohn, J.-R. Zhang, Y. Shi, *J. Am. Chem. Soc.* **1997**, *119*, 11224; b) Y. Shi, *Acc. Chem. Res.* **2004**, *37*, 488, and references therein.

 © 2006 Wiley-VCH Verlag GmbH & Co. KGaA, Weinheim

[14] a) H. Tian, X. She, L. Shu, H. Yu, Y. Shi, *J. Am. Chem. Soc.* **2000**, *122*, 11551; b) H. Tian, X. She, H. Yu, L. Shu, Y. Shi, *J. Org. Chem.* **2002**, *67*, 2435; c) L. Shu, P. Wang, Y. Gan, Y. Shi, *Org. Lett.* **2003**, *5*, 293; d) L. Shu, Y. Shi, *Tetrahedron Lett.* **2004**, *45*, 8115.

[15] Some epoxides underwent rearrangement on silica gel, thus they were used directly without purification; these epoxides were clean as judged by analysis with NMR spectroscopy and GC analysis (see the Supporting Information).

[16] It was found that α-aryl cyclopentanones readily underwent racemization on silica gel; the ketone products were not purified by column chromatography on silica gel and were clean as judged by NMR spectroscopy.

[17] For examples of LiI- and LiBr-mediated rearrangements of oxaspiropentanes and oxaspirohexanes, see: a) J. R. Salaun, J. M. Conia, *J. Chem. Soc. Chem. Commun.* **1971**, 1579; b) P. Leriverend, M.-L. Leriverend, *C. R. Hebd. Seances Acad. Sci. Ser. C* **1975**, *280*, 791; c) D. H. Aue, M. J. Meshishnek, D. F. Shellhamer, *Tetrahedron Lett.* **1973**, 4799; d) B. M. Trost, L. H. Latimer, *J. Org. Chem.* **1978**, *43*, 1031; e) D. R. Morton, Jr., F. C. Brokaw, *J. Org. Chem.* **1979**, *44*, 2880; f) F. Huet, A. Lechevallier, J.-M. Conia, *Chem. Lett.* **1981**, 1515; g) S. Halazy, A. Krief, *J. Chem. Soc. Chem. Commun.* **1982**, *1200*; h) Y. Tobe, T. Yamashita, K. Kakiuchi, Y. Odaira, *J. Chem. Soc. Chem. Commun.* **1985**, 888; i) T. W. Hart, M.-T. Comte, *Tetrahedron Lett.* **1985**, *26*, 2713; j) M. C. Pirrung, S. A. Thomson, *J. Org. Chem.* **1988**, *53*, 227; k) T. Chevtchouk, J. Ollivier, J. Salaun, *Tetrahedron: Asymmetry* **1997**, *8*, 1011; l) F. Mahuteau-Betzer, L. Ghosez, *Tetrahedron Lett.* **1999**, *40*, 5183; m) A. M. Bernard, C. Floris, A. Frongia, P. P. Piras, *Synlett* **2002**, 796.

[18] T. B. Freedman, X. Cao, R. K. Dukor, L. A. Nafie, *Chirality* **2003**, *15*, 743.

[19] H. Suginome, K. Orito, K. Yorita, M. Ishikawa, N. Shimoyama, T. Sasaki, *J. Org. Chem.* **1995**, *60*, 3052; the Baeyer–Villiger oxidation was carried out based on the procedure reported above with a slight modification: cyclopentanone, solid $NaHCO_3$ (2.0 equiv), and *m*CPBA (2.0 equiv) were mixed and then CH_2Cl_2 was added.

[20] R. Downham, P. J. Edwards, D. A. Entwistle, A. B. Hughes, K. S. Kim, S. V. Ley, *Tetrahedron: Asymmetry* **1995**, *6*, 2403.

[21] Experimental procedures for the asymmetric epoxidation and epoxide rearrangement, the characterization of the epoxides and cyclopentanones, the determination of the *ee* values of the epoxides and cyclopentanones, and the VCD spectra are given in the Supporting Information.

 © 2006 Wiley-VCH Verlag GmbH & Co. KGaA, Weinheim

Asymmetric Reduction

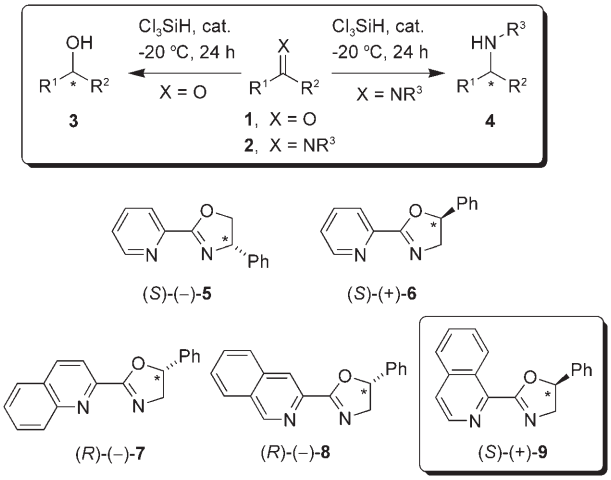
DOI: 10.1002/anie.200503941

Remote Chiral Induction in the Organocatalytic Hydrosilylation of Aromatic Ketones and Ketimines**

Andrei V. Malkov, Angus J. P. Stewart Liddon, Pedro Ramírez-López, Lada Bendová, David Haigh, and Pavel Kočovský**

Dedicated to Professor Henri Kagan on the occasion of his 75th birthday

Asymmetric hydrogenation, hydroboration, and hydrosilylation are the most frequently used catalytic methods for the reduction of prochiral ketones **1** and imines **2** (Scheme 1).[1]



Scheme 1. Catalytic reduction of ketones and ketimines; for R^1–R^3, see Tables 1 and 2.

[*] Dr. A. V. Malkov, A. J. P. S. Liddon, Dr. P. Ramírez-López, L. Bendová, Prof. Dr. P. Kočovský
Department of Chemistry, WestChem
Joseph Black Building
University of Glasgow, Glasgow G12 8QQ (UK)
Fax: (+44) 141-33-488
E-mail: amalkov@chem.gla.ac.uk
p.kocovsky@chem.gla.ac.uk
Dr. D. Haigh
Department of Medicinal Chemistry
Metabolic and Viral Centre of Excellence for Drug Discovery
GlaxoSmithKline Pharmaceuticals
Medicines Research Centre
Stevenage, Hertfordshire, SG1 2NY, (UK)

[**] We thank the GSK and EPSRC for an industrial CASE awards to A.J.P.S.L., the Ministry of Education and Science of Spain for a postdoctoral fellowship to P.R.-L., the Socrates Exchange program, and Dr. Alfred Bader and the University of Glasgow for an additional support.

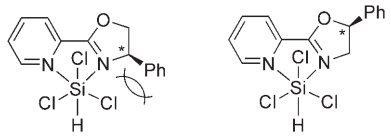
Supporting information for this article is available on the WWW under http://www.angewandte.org or from the author.

WILEY InterScience DISCOVER SOMETHING GREAT
© 2006 Wiley-VCH Verlag GmbH & Co. KGaA, Weinheim

Although asymmetric hydrogenation remains favored by industry in general, it is not free of problems, namely, those associated with metal leaching, high pressure, and the cost of the catalyst and its regeneration. Stoichiometric borane reduction, catalyzed by chiral oxazaborolidine, avoids most of these problems and offers high levels of enantioselection,[1] but its cost is prohibitive for large-scale industrial application. The recently developed reduction of imines, which uses the Hantsch dihydropyridine as a stoichiometric reducing agent and a chiral Brønsted acid as an organocatalyst,[2] is also tainted by the cost implications. Transition-metal-catalyzed hydrosilylation[1,3,4] on the other hand relies on much cheaper silanes as reducing agents but shares the problem of metal leaching with hydrogenation. Furthermore, the current methods usually perform well with either ketones or imines, but rarely with both classes.[4] The alternative metal-free methods[2,5] are rare and considerably less effective;[6] nevertheless, a promising development has recently been reported,[7] which relies on Cl_3SiH, an inexpensive and easy-to-handle reducing agent.[8] Herein, we report an organocatalytic hydrosilylation applicable to both ketones and ketimines.

As part of our program focusing on the activation of organosilicon reagents by Lewis bases,[9] we examined 2-pyridyloxazolines of type **5**, derived from (*S*)-phenylglycinol, as potential organocatalysts in the hydrosilylation of aromatic ketones with Cl_3SiH (Scheme 1, **1**→**3**). Initial attempts to reduce acetophenone (**1a**) in the presence of **5** (20 mol%, $CHCl_3$, −20°C, 24 h) resulted in a rather low conversion into alcohol **3a** (Table 1, entry 1). By contrast, the isomeric oxazoline **6**, obtained from (*S*)-mandelic acid, proved much more reactive and furnished **3a** in 78% *ee* (entry 2).[10] Reduction of a series of aromatic ketones **1b–e**, catalyzed by **6**, proceeded in a similar fashion, with 70–80% *ee* (entries 3–6). On the other hand, reduction of the non-aromatic ketone **1f** resulted in the formation of a racemic product (entry 7). Other solvents, such as toluene, diethyl ether, and THF, proved inferior.

The lower reactivity of **5** relative to **6** can be conjectured to originate from an increase in the steric radius of the extra-coordinate silicon moiety by coordination to the ligand. Thus, the coordination of Cl_3SiH to **5** is impaired by the adjacent phenyl group (Scheme 2, **A**), whereas this adverse effect is absent in chelate **B**, derived from **6**.[11]



Scheme 2. Coordination of Cl_3SiH to (2-pyridyl)oxazolines.

To improve the efficacy of the catalyst and to shed more light on the mechanism, related oxazolines were prepared with the quinoline **7** or isoquinoline **8** and **9** fragments in place of the pyridine moiety (Scheme 1). No reduction was observed with **7** ($CHCl_3$, −20°C; Table 1, entry 8), presumably because of the steric constraints imposed by the quinoline moiety, thus mirroring the behavior of **5**. The 3-isoquinoline catalyst **8** was approximately as efficient as the parent (pyridyl)oxazoline **6** (entry 9; compare with entry 2). A real improvement over a range of substrates (**1a–e, g, h**) was attained with the 1-isoquinolyl catalyst **9** (entries 10–16), which allowed the catalyst loading to be lowered to 10 mol% and provided by far the best enantioselectivities in the metal-free hydrosilylation of ketones to date (≤94% *ee*).

Importantly, catalyst **9** was also found to exhibit high efficiency in the reduction of *N*-aryl imines **2a–f** (Table 2). Therefore, it can be regarded as the first organocatalyst that

Table 1: Reduction of ketones (**1**→**3**) with trichlorosilane catalyzed by **5–9**.[a]

Entry	Catalyst (mol%)	Ketone	R^1, R^2	Yield [%]	*ee* [%][b,c]
1	(*S*)-**5** (20)	**1a**	Ph, Me	29[d]	66[g]
2	(*S*)-**6** (20)	**1a**	Ph, Me	85[d]	78
3	(*S*)-**6** (20)	**1b**	2-MeO-C_6H_4, Me	100[d]	77
4	(*S*)-**6** (20)	**1c**	2-F-C_6H_4, Me	30[d]	70
5	(*S*)-**6** (20)	**1d**	4-Me-C_6H_4, Me	100[d]	80
6	(*S*)-**6** (20)	**1e**	Ph, Et	91[d]	80
7	(*S*)-**6** (20)	**1f**	*c*-C_6H_{11}, Me	67[d,e]	0
8	(*R*)-**7** (20)	**1a**	Ph, Me	0	–
9	(*R*)-**8** (20)	**1a**	Ph, Me	41[e,f]	73[g]
10	(*S*)-**9** (10)	**1a**	Ph, Me	85[f]	84
11	(*S*)-**9** (10)	**1b**	2-MeO-C_6H_4, Me	50[f]	87
12	(*S*)-**9** (10)	**1c**	2-F-C_6H_4, Me	35[f]	70
13	(*S*)-**9** (10)	**1d**	4-Me-C_6H_4, Me	90[f]	85
14	(*S*)-**9** (10)	**1e**	Ph, Et	55[f]	86
15	(*S*)-**9** (10)	**1g**	2-naphth, Me	93[f]	94
16	(*S*)-**9** (10)	**1h**	6-Me-2-naphth, Me	93[f]	92

[a] The reactions were carried out on a 0.4-mmol scale with Cl_3SiH (2.1 equiv) in $CHCl_3$ in the presence of the catalyst at −20°C for 24 h. [b] Determined by chiral GC or HPLC. [c] All products **3** were *R* configured (unless stated otherwise), as revealed by comparison of their optical rotation with the literature data. [d] Conversion determined by GC of the reaction mixture after a standard work up. [e] The reaction was carried out in CH_2Cl_2. [f] Yield of the isolated product (shown to be pure by ^1H NMR spectroscopic analysis). [g] The product was *S* configured. naphth = napthyl.

Table 2: Reduction of ketimines (**2–4**) with trichlorosilane catalyzed by **9**.[a]

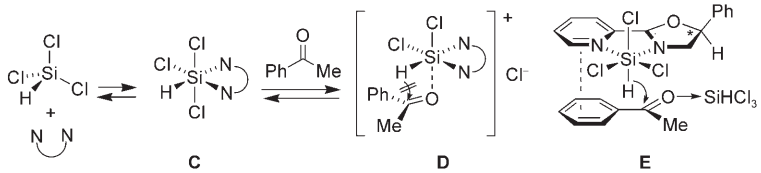
Entry	Imine	R^1, R^2, R^3	Yield [%][b]	*ee* [%][c,d]
1	**2a**	Ph, Me, Ph	65	87
2	**2b**	Ph, Me, PMP[e]	60	85
3	**2c**	2-naphth, Me, Ph	67	87 (98[f])
4	**2d**	2-naphth, Me, PMP[e]	67	86
5	**2e**	4-MeO-C_6H_4, Me, PMP[e]	51	87
6	**2f**	4-CF_3-C_6H_4, Me, PMP[e]	65	87

[a] The reactions were carried out on a 0.4-mmol scale with $HSiCl_3$ (2.0 equiv) in $CHCl_3$ in the presence of catalyst **9** (20 mol%) at −20°C for 24 h. [b] Yield of the isolated product (product shown to be pure by ^1H NMR spectroscopic analysis). [c] Amines **4** were *R* configured, as revealed by comparison of their optical rotation and their HPLC retention times with the literature data. [d] Enantiomeric excess was determined by HPLC. [e] PMP = *p*-methoxyphenyl. [f] After a single recrystallization from methanol.

 © 2006 Wiley-VCH Verlag GmbH & Co. KGaA, Weinheim

allows reduction of both ketones and ketimines with a practically useful enantioselectivity.

To rationalize the high selectivity of catalysts **6**, **8**, and **9**, the following issues have to be taken into account: 1) Table 1 reveals that the order of reactivity of the ketones displays a good correlation with their Brønsted basicity[12] (pK_{HB}): 2-MeO-C_6H_4COMe (1.34) > PhCOMe (1.11) > 2-F-C_6H_4COMe (0.90). If we accept that this trend can be extrapolated to Lewis basicity, the results would suggest that the carbonyl oxygen atom is coordinated to the weakly Lewis acidic Cl_3SiH in the transition state.[13] 2) Trichlorosilane does not reduce carbonyl or heterocarbonyl compounds unless activated by Lewis bases through the formation of extra-coordinate silicon species, such as **C**, in the case of bidentate activators (Scheme 3).[7] Coordination of the carbonyl group



Scheme 3. Mechanism of hydrosilylation.

(**D**) might be presumed (upon replacement of a chloride atom at the silicon center) but can be regarded as unproductive, since the corresponding four-membered transition state (TS) for the reduction is unlikely.[13,14] 3) A linear relationship between the enantiopurity of catalyst **6** and the product was observed for the reduction of acetophenone (**1a**→**3a**), thus suggesting that only one molecule of the catalyst is actively involved in the enantiodifferentiating event. 4) The role of the substituent on the oxazoline rings in **6**, **8**, and **9** can be attributed to the shielding of one of the faces of the catalyst by the Ph group.[15]

Accordingly, the following mechanistic picture can be drawn: the *N*,*N*-chelation of Cl_3SiH by the catalyst creates an activated hydrosilylating species, while another molecule of Cl_3SiH is likely to activate the ketone by coordination to the oxygen atom in the *E* fashion.[16] The ketone–Cl_3SiH complex will then approach the catalyst–Cl_3SiH complex from the less-hindered side (as dictated by the remote chiral center in the catalyst). Transition state **E**, which accommodates all these effects, is consistent with the experimentally observed *si*-facial selectivity of the reaction and with the features discussed herein. It can also be hypothesized that **E** will be stabilized by arene–arene interactions between the heteroaromatic systems of the catalyst and the substrate.[17]

The potential role of the latter π–π interactions in shaping the TS[17] was assessed by a computational analysis of the pyridine–acetophenone model complex (Figure 1).[18] The successive scans, according to the steering angle (θ), the distance between the planes (r_1), and the parallel displacement of the two molecules (r), were carried out (each scan starting at the geometry of interaction energy minimum of the previous scan). The lowest interaction energy found by the potential-energy surface scans was at $-6.3\ kcal\,mol^{-1}$. The

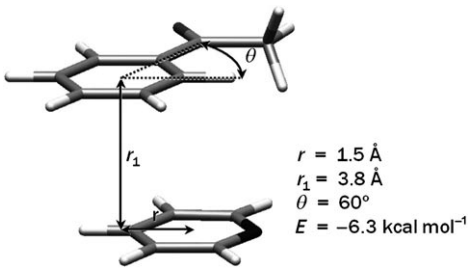


Figure 1. Arene–arene interactions of acetophenone (**1a**) with pyridine as the model TS **E**.

magnitude of this interaction lends credence to the proposed involvement of π stacking in the transition state **E**.

A similar mechanism can be envisaged for the reduction of imines. However, the coordination of Cl_3SiH to the nitrogen atom is unlikely, as this would create a very crowded environment. Hence, the R^3 group of imine **2** can be assumed to fill the space that the $SiHCl_3$ group fills in **E**. Experimental data support this hypothesis: Note that the electron-rich ketones react faster than their electron-poor counterparts (Table 1, entries 3 versus 4 and 11 versus 12), which is consistent with the carbonyl basicity (see below) and, therefore, its propensity to coordinate the Lewis acidic Cl_3SiH. By contrast, imines exhibit the opposite trend (Table 2, entries 5 versus 6).

In conclusion, we have developed a new, practical, metal-free protocol for the enantioselective reduction of aromatic ketones (≤94% *ee*) and ketimines (≤87% *ee*). The reaction is characterized by an unusual, long-ranging chiral induction. The enantiodifferentiation is presumed to be aided by aromatic interactions between the catalyst and the substrate.

Experimental Section

General procedure for the asymmetric reduction of ketones **1** and ketimines **2** with trichlorosilane: Trichlorosilane (86 μL, 0.84 mmol, 2.1 equiv) was slowly added dropwise to a solution of the catalyst (11.0 mg, 0.04 mmol or 21.9 mg, 0.08 mmol) and the corresponding ketone or imine (0.40 mmol, 1.0 equiv) in $CHCl_3$ (2 mL) at −20 °C. The reaction mixture was stirred at −20 °C for 24 h, after which time saturated aqueous $NaHCO_3$ (1 mL) was added to quench the reaction. The mixture was extracted with CH_2Cl_2 (3 × 10 mL) and the combined organic extracts were dried over $MgSO_4$. Concentration in vacuo followed by flash chromatography on silica gel (2 × 15 cm) with petroleum ether/ethyl acetate (20:1) or CH_2Cl_2 as the eluent afforded alcohols **3a**–**3h** or amines **4a**–**4f**.

Received: November 7, 2005
Published online: January 20, 2006

Keywords: arene–arene interactions · asymmetric catalysis · N ligands · organocatalysis · reduction

[1] E. N. Jacobsen, A. Pfaltz, H. Yamamoto, *Comprehensive Asymmetric Catalysis, Vol. I–III*, Springer, Heidelberg, **1999**.
[2] a) S. Singh, U. K. Batra, *Indian J. Chem.* **1989**, *27*, 1; b) M. Rueping, E. Sugiono, C. Azap, T. Theissmann, M. Bolte, *Org. Lett.* **2005**, *7*, 3781; c) S. Hoffmann, A. M. Seayad, B. List,

 © 2006 Wiley-VCH Verlag GmbH & Co. KGaA, Weinheim

Angew. Chem. **2005**, *117*, 7590; *Angew. Chem. Int. Ed.* **2005**, *44*, 7424.

[3] O. Riant, N. Mostefai, J. Courmarcel, *Synthesis* **2004**, 2943.

[4] A highly efficient Cu-catalyzed hydrosilylation of ketones and ketimines has been developed: a) B. H. Lipshutz, K. Noson, W. Chrisman, A. Lower, *J. Am. Chem. Soc.* **2003**, *125*, 8779; b) B. H. Lipshutz, H. Shimizu, *Angew. Chem.* **2004**, *116*, 2278; *Angew. Chem. Int. Ed.* **2004**, *43*, 2228.

[5] a) P. I. Dalko, L. Moisan, *Angew. Chem.* **2001**, *113*, 3840; *Angew. Chem. Int. Ed.* **2001**, *40*, 3726; b) P. I. Dalko, L. Moisan, *Angew. Chem.* **2004**, *116*, 5248; *Angew. Chem. Int. Ed.* **2004**, *43*, 5138; c) E. R. Jarvo, S. J. Miller, *Tetrahedron* **2002**, *58*, 2481; d) A. Berkessel, H. Gröger, *Asymmetric Organocatalysis*, Wiley-VCH, Weinheim, **2005**.

[6] a) R. Schiffers, H. B. Kagan, *Synlett* **1997**, 1175; b) H. Nishikori, R. Yoshihara, A. Hosomi, *Synlett* **2003**, 561; c) F. J. LaRonde, M. A. Brook, *Tetrahedron Lett.* **1999**, *40*, 3507; d) F. J. LaRonde, M. A. Brook, *Inorg. Chim. Acta* **1999**, *296*, 208; e) M. D. Drew, N. J. Lawrence, W. Watson, S. A. Bowles, *Tetrahedron Lett.* **1997**, *38*, 5857.

[7] a) R. A. Benkeser, D. Snyder, *J. Organomet. Chem.* **1982**, *225*, 107; b) S. Kobayashi, M. Yasuda, I. Hachiya, *Chem. Lett.* **1996**, 407; c) M. A. Brook, *Silicon in Organic, Organometallic and Polymeric Chemistry*, Wiley, New York, **2000**, pp. 133 – 136; d) F. Iwasaki, O. Onomura, K. Mishima, T. Maki, Y. Matsumura, *Tetrahedron Lett.* **1999**, *40*, 7507; e) F. Iwasaki, O. Onomura, K. Mishima, T. Kanematsu, T. Maki, Y. Matsumura, *Tetrahedron Lett.* **2001**, *42*, 2525.

[8] A very efficient organocatalytic protocol for the hydrosilylation of ketimines (with $\leq 92\%$ *ee*) has been developed by us recently: a) A. V. Malkov, A. Mariani, K. MacDougall, P. Kočovský, *Org. Lett.* **2004**, *6*, 2253; b) A. V. Malkov, S. Stončius, K. N. MacDougall, A. Mariani, G. D. McGeoch, P. Kočovský, *Tetrahedron* **2006**, *62*, 264.

[9] a) A. V. Malkov, M. Orsini, D. Pernazza, K. W. Muir, V. Langer, P. Meghani, P. Kočovský, *Org. Lett.* **2002**, *4*, 1047; b) A. V. Malkov, M. Bell, M. Orsini, D. Pernazza, A. Massa, P. Herrmann, P. Meghani, P. Kočovský, *J. Org. Chem.* **2003**, *68*, 9659; c) A. V. Malkov, M. Bell, M. Vassieu, V. Bugatti, P. Kočovský, *J. Mol. Catal. A* **2003**, *196*, 179; d) A. V. Malkov, L. Dufková, L. Farrugia, P. Kočovský, *Angew. Chem.* **2003**, *115*, 3802; *Angew. Chem. Int. Ed.* **2003**, *42*, 3674; e) A. V. Malkov, M. Bell, F. Castelluzzo, P. Kočovský, *Org. Lett.* **2005**, *7*, 3219.

[10] Hydrosilylation of **1a**, catalyzed by Rh complexes of **5** and **6**, produced alcohol **2a** in 69% *ee* and 9% *ee*, respectively: H. Brunner, U. Obermann, *Chem. Ber.* **1989**, *122*, 499.

[11] Similar effects have been observed by us for substituted bipyridines, in which the increased bulk prevented coordination of $[Mo(CO)_6]$ and other metal complexes: A. V. Malkov, I. R. Baxendale, J. Fawcett, D. R. Russel, V. Langer, D. J. Mansfield, M. Valko, P. Kočovský, *Organometallics* **2001**, *20*, 673.

[12] F. Besseau, M. Luçon, C. Laurence, M. Berthelot, *J. Chem. Soc. Perkin Trans. 2* **1998**, 101.

[13] T. Kudo, T. Higashide, S. Ikedate, and H. Yamataka, *J. Org. Chem.* **2005**, *70*, 5157.

[14] Transfer hydrogenation and oxazaborolidine-catalyzed reduction of ketones with borane have been shown to proceed through a six-membered transition state: a) M. Yamakawa, H. Ito, R. Noyori, *J. Am. Chem. Soc.* **2000**, *122*, 1466; b) S. Itsuno in *Comprehensive Asymmetric Catalysis, Vol. 1*, Springer, Heidelberg, **1999**, pp. 290 – 315.

[15] Replacing the Ph in **6** with *t*Bu led to virtually identical results, which rules out arene–arene interactions of the substrate with the Ph in **6**.

[16] For a review on the carbonyl coordination (*E* vs *Z*; η^1 vs η^2), see: S. Shambayati, W. E. Crowe, S. L. Schreiber, *Angew. Chem.* **1990**, *102*, 273; *Angew. Chem. Int. Ed. Engl.* **1990**, *29*, 256.

[17] Arene–arene interactions have been suggested by us to account for the stereochemical outcome of allyl silane addition to aromatic aldehydes;[9d,e] Hayashi and co-workers arrived at a similar conclusion: a) T. Shimada, A. Kina, T. Hayashi, *J. Org. Chem.* **2003**, *68*, 6329; Birman et al. recently invoked arene – arene interactions to rationalize the kinetic resolution in the acylation of racemic alcohols: b) V. B. Birman, H. Jiang, *Org. Lett.* **2005**, *7*, 3445.

[18] The geometries of monomers were determined by the cc-pVTZ/RI-MP2 gradient optimization in the Turbomole v.5.6 package (R. Ahlrichs, M. Bär, M. Häser, H. Horn, C. Kölmel, *Chem. Phys. Lett.* **1989**, *162*, 165); the optimized geometries of monomers were kept frozen throughout the scans. Interaction energies were computed with aug-cc-pVDZ basis set at RI-MP2 level in Turbomole v.5.6 and are BSSE-corrected. Only the face-to-face geometry was examined, thus keeping the planes of the monomers parallel throughout the scans.

 © 2006 Wiley-VCH Verlag GmbH & Co. KGaA, Weinheim

Drug Design

DOI: 10.1002/anie.200502161

Inhibitors of HIV-1 Protease by Using In Situ Click Chemistry**

Matthew Whiting, John Muldoon, Ying-Chuan Lin, Steven M. Silverman, William Lindstrom, Arthur J. Olson, Hartmuth C. Kolb, M. G. Finn, K. Barry Sharpless, John H. Elder, and Valery V. Fokin**

The global AIDS epidemic has claimed the lives of more than 20 million people since 1981. Another 10 million are now living with HIV and most of these are likely to develop AIDS over the course of the next decade. In spite of the various treatment protocols available, including the mainstream

[*] Dr. Y.-C. Lin, Dr. W. Lindstrom, Prof. A. J. Olson, Prof. J. H. Elder
Department of Molecular Biology
The Scripps Research Institute
10550 North Torrey Pines Road, La Jolla, CA 92037 (USA)
Fax: (+1) 858-784-2750
E-mail: jelder@scripps.edu

Dr. M. Whiting, Dr. J. Muldoon, S. M. Silverman, Prof. H. C. Kolb, Prof. M. G. Finn, Prof. K. B. Sharpless, Prof. V. V. Fokin
Department of Chemistry and
The Skaggs Institute for Chemical Biology
The Scripps Research Institute
10550 North Torrey Pines Road, BCC-315, La Jolla, CA 92037 (USA)
Fax: (+1) 858-784-7562
E-mail: fokin@scripps.edu

[**] We thank the National Institute of General Medical Sciences, the National Institutes of Health (GM048870), the Skaggs Institute for Chemical Biology, and the W. M. Keck Foundation (K.B.S.) for financial support.

Supporting information for this article is available on the WWW under http://www.angewandte.org or from the author.

© 2006 Wiley-VCH Verlag GmbH & Co. KGaA, Weinheim

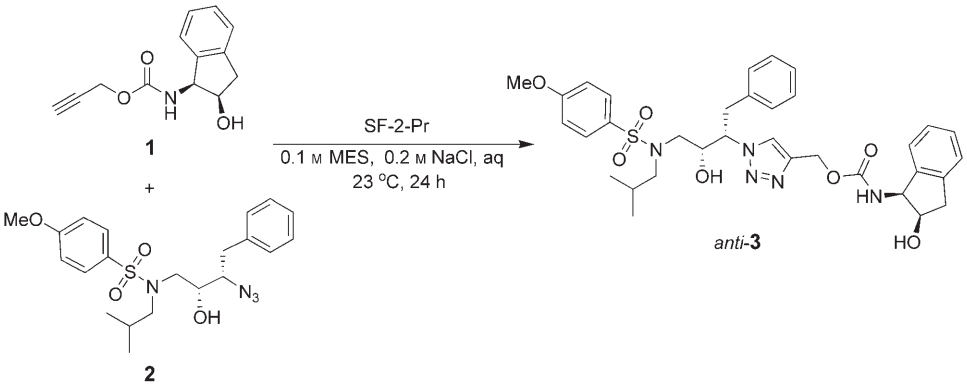
highly active antiretroviral therapy (HAART),[1] the number of people infected with HIV continues to rise. The most recent UNAIDS (United Nations Programme on HIV/AIDS)/world health organization estimates show that, in 2004 alone, 4.9 million people were newly infected with HIV.[2]

HIV-1 protease (HIV-1-Pr)[3] has been recognized as an important target for inhibition of viral replication. Although seven inhibitors have been approved by the food and drug association since 1995 and a number more are currently undergoing clinical evaluation, their success has been undermined by rapid mutation of the virus.[4] The alarming rate at which strains of HIV-1 that are resistant to the currently available drugs and their combinations emerge underscores the urgent need for new, broad-spectrum protease inhibitors that are effective against the new mutants as well as the wild-type virus.

Herein we describe the early results of our investigation into the application of a multidisciplinary, chemistry-driven approach for the rapid discovery of bioactive molecules, termed in situ click chemistry, for the elucidation of novel HIV-1-Pr inhibitors. The goal of in situ click chemistry is to accelerate the identification of novel pharmaceutical candidates through involvement of a biological target in the selection and covalent assembly of its own inhibitors. Although the concept has been previously demonstrated by several researchers,[5] the in situ click-chemistry approach[6] is unique in that it relies on the completely bio-orthogonal 1,3-dipolar cycloaddition of organic azides and alkynes.[7] This highly exergonic reaction produces five-membered nitrogen heterocycles, 1,2,3-triazoles, which are exceedingly stable to acidic and basic hydrolysis as well as severe reductive/oxidative conditions. At the same time, the triazoles produced are capable of active participation in hydrogen bonding as well as dipole–dipole and π-stacking interactions.

Even though both azides and alkynes are energetic species, their reactivity profiles are quite narrow, at least under physiological conditions. Furthermore, despite the large thermodynamic driving force for cycloaddition, the high kinetic barrier effectively hides the reactants until they are brought into close proximity by a biological template or activated towards each other by alternative means (e.g., catalysis). These features allow the target to sample numerous combinations of building blocks, but synthesize only the best binders. The efficacy of in situ click chemistry has already been demonstrated by the discovery of novel, highly potent inhibitors of acetylcholinesterase and carbonic anhydrase.[6] Previous studies have, however, always utilized building blocks with a high affinity for the target ($K_i < 37$ nM).[6c,d] In the HIV-1-Pr case, we do not have such a luxury and as such, we were pleased to find that the enzyme selectively formed an inhibitor from components that exhibited only weak binding to the target.

To probe the protease-templated reaction, alkyne **1** (500 μM, $IC_{50} > 100$ μM) and azide **2** (100 μM, $IC_{50} = 4.2 \pm 0.6$ μM) were incubated in the presence of the HIV-1,-Pr SF-2-WTQ7K-Pr,[8] (henceforth simply denoted SF-2-Pr; 15 μM) in 2-morpholinomethanesulfonic acid (MES; 0.1M)/NaCl (0.2M) buffer solution at 23 °C for 24 h (Scheme 1). Controls



Scheme 1. SF-2-Pr templated in situ click-chemistry formation of protease inhibitor *anti*-**3**.

were performed both in the absence of the enzyme, to confirm the background rate of the cycloaddition, and in the presence of bovine serum albumin (BSA), to determine any non-specific peptidic catalysis. Analysis of the crude reaction mixtures was carried out by HPLC and mass spectrometry in single-ion mode (LCMS-SIM), which was previously demonstrated to be a sensitive, medium-throughput method for the detection of a desired product.[6b] Comparison of the enzyme and background reactions showed that the triazole *anti*-**3**, which has previously been shown to be an inhibitor of the wild-type HIV-1-Pr ($IC_{50} = 6$ nM, $K_i = 1.7$ nM) and also of several mutant strains,[9] was indeed formed in an increased rate in the presence of the enzyme. In contrast to other systems,[6b,c] the background reaction was observable under our chosen conditions and produced a detectable amount of the regioisomeric triazoles *anti*- and *syn*-**3** in a 2:1 ratio, favoring the 1,4-disubstituted product *anti*-**3**. Surprisingly, the presence of BSA gave an increase in the observed rate of product formation, which led to a small increase in the final product concentration without affecting the regioisomeric ratio. However, a marked acceleration in the rate of formation of only one of the regioisomers was observed in the presence of the enzyme with an approximately tenfold increase in the overall product formation. The triazole product was formed with a much enhanced regioisomeric ratio of 18:1 in favor of the same 1,4-isomer, *anti*-**3** (Figure 1). In a further control experiment, a known HIV-1-Pr active-site ligand, TL3[10] (15 μM), was added to both the background and enzyme reactions prior to incubation with the azide and alkyne fragments. The added inhibitor showed no effect on the background reaction[11] but completely suppressed the increase in product formation in the presence of the enzyme,

 © 2006 Wiley-VCH Verlag GmbH & Co. KGaA, Weinheim

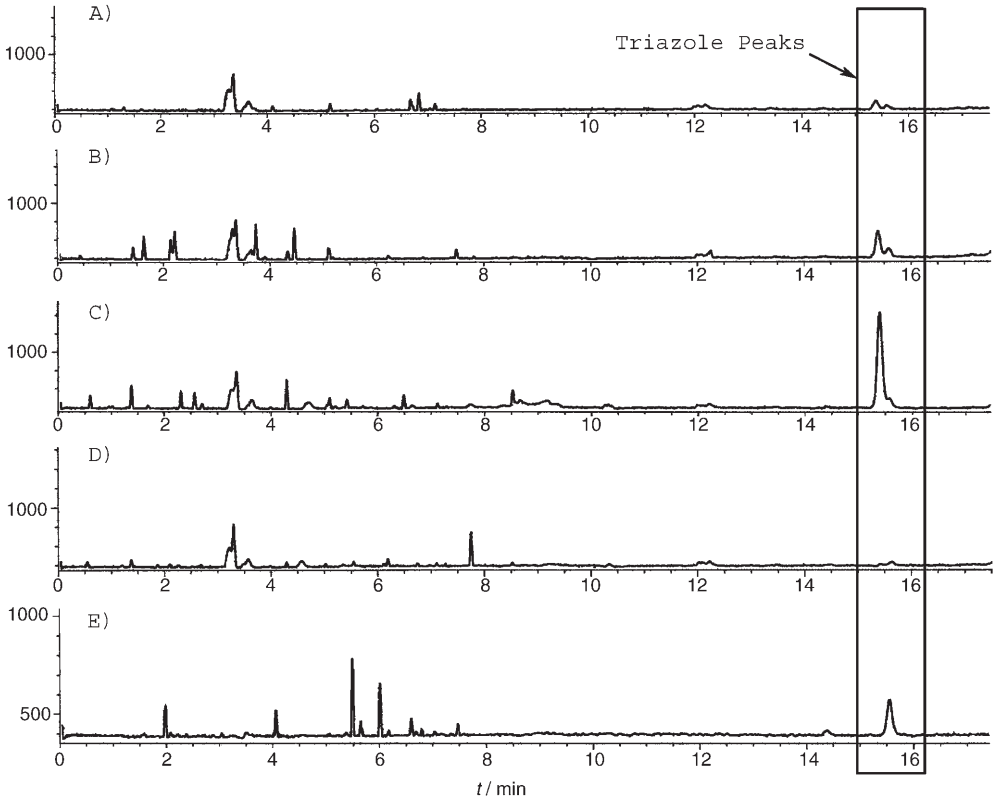
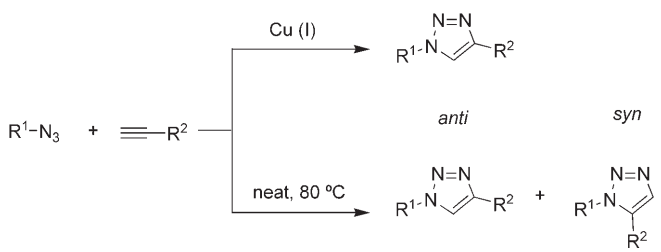


Figure 1. In situ formation of **3** determined by LCMS-SIM. A) Background reaction, alkyne **1** (500 μM) and azide **2** (100 μM) were incubated in MES (0.1 M) and NaCl aqueous buffer (0.2 M) for 24 h. B) Compounds **1** and **2** incubated in the presence of BSA (0.5 mg mL^{-1}, 7.5 μM). C) Compounds **1** and **2** were incubated in the presence of SF-2-Pr (15 μM). D) Compounds **1** and **2** incubated in the presence of SF-2-Pr (15 μM) and protease inhibitor TL3 (15 μM). E) Authentic sample of *anti*-**3**.

We next investigated whether the enzyme could select a pair of fragments that form a potent binder from a number of building blocks that are concurrently present in a single reaction mixture. In the context of a drug-discovery program, this would be a major advantage, enabling more-rapid screening and reducing the amount of enzyme required for each individual analysis. In the present system, azide **2** was known to be the tightest-binding fragment; we therefore hoped to show that it could recruit a complimentary fragment from an array of alkynes. Alkynes **4**–**7** (Figure 2) were chosen as test substrates owing to their similar molecular weight and degree of functionality when compared with **1**. It was also determined that, as expected, none of the individual fragments gave strong protease inhibition (IC_{50} of Alkynes **4**–**7** > 100 μM).

thereby demonstrating that the active site does indeed act as a template for the cycloaddition reaction. The reaction, performed in situ, was also carried out in the presence of the more clinically relevant HIV-1-Pr, NL4-3-WTQ7K-Pr,[12] which gave essentially identical results.

To determine the regiochemistry of the triazole formed by the enzyme, a mixture of both regioisomers, *syn*- and *anti*-**3**, was obtained by thermal cycloaddition, and the regioisomerically pure 1,4-disubstituted triazole product, *anti*-**3**, was prepared by a copper(I)-catalyzed reaction of the corresponding azide and alkyne blocks[13] (Scheme 2). Co-injection of the crude, enzyme-promoted reaction with both a mixture of the triazoles and the pure 1,4-regioisomer revealed that the enzyme had preferentially formed the expected 1,4-triazole, *anti*-**3**.[11]



Scheme 2. Preparation of regioisomeric triazoles by copper(I)-catalyzed and thermal cycloaddition reactions.

Thus, instead of screening binary mixtures of azide and alkyne fragments, azide **2** (100 μM) was incubated with the five alkynes **1** and **4**–**7** (200 μM each) in the presence of both SF-2-Pr (15 μM) and BSA (to monitor the background reaction). After incubation for 24 h at 23 °C, the crude reaction mixtures were directly analyzed by LCMS-SIM (monitoring for MH^+ and MNa^+ of all potential products[14]). Comparison of the total ion count and the extracted-ion traces of each possible product from the enzyme and background reaction showed an increased amount of only one triazole product (**3**) in the presence of the enzyme (Figure 3).[15]

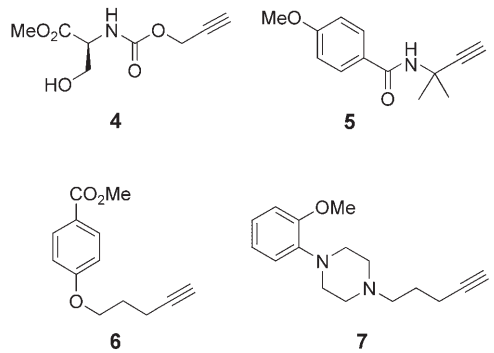


Figure 2. Alkynes **4**–**7**.

© 2006 Wiley-VCH Verlag GmbH & Co. KGaA, Weinheim

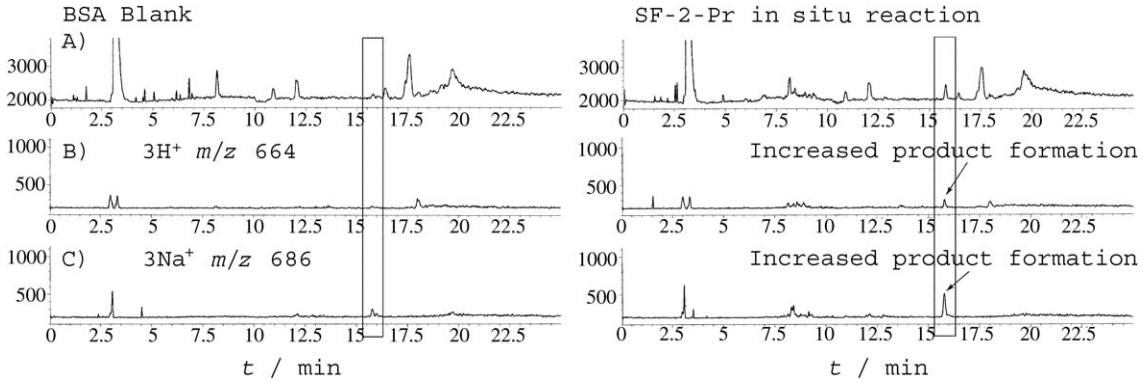


Figure 3. LCMS-SIM and extracted-ion traces for the in situ mixture experiment as described above. The combined traces (A) are shown as well as the extracted-ion traces for both **3**H^+ (B) and **3**Na^+ (C). The left-hand traces show the BSA background reaction and the right-hand traces show the corresponding in situ reaction with SF-2-Pr. Extracted-ion traces for all alternative-product masses showed no increased product formation.[11]

In summary, this work has demonstrated that the in situ click-chemistry approach can be successfully applied to the formation of HIV-1-Pr inhibitors. The protease itself acts as a template for the reaction and greatly increases the rate of formation of the 1,4-triazole product, *anti*-**3**. This rate acceleration is readily detected by simple comparison with the LCMS-SIM traces for the in situ reaction and a background reaction by using BSA in place of the enzyme. In this study, the use of building blocks with much lower affinities for the biological target than in previous examples should greatly facilitate the transfer of this technology to new systems in which the structures of high affinity binders are not known. Further studies are currently underway that apply this methodology to the discovery of entirely novel protease inhibitors by using even lower affinity fragments as well as efforts to directly employ drug resistant, mutant proteases in the in situ discovery process.

Received: June 21, 2005
Revised: October 28, 2005
Published online: January 20, 2006

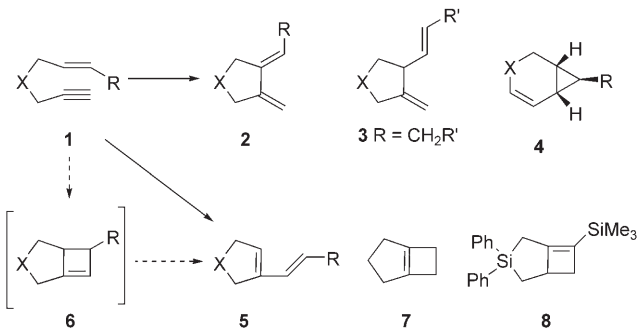
Keywords: click chemistry · drug design · HIV-1 protease · inhibitors · triazoles

[1] J. A. Bartlett, R. Demasi, J. Quinn, C. Moxham, F. Rousseau, *AIDS* **2001**, *15*, 1369 – 1377.
[2] UNAIDS 2005 report, http://www.unaids.org.
[3] N. E. Kohl, E. A. Emini, W. A. Schleif, L. J. Davis, J. C. Davis, J. C. Heimbach, R. A. F. Dixon, E. M. Scolnick, I. S. Sigal, *Proc. Natl. Acad. Sci. USA* **1988**, *85*, 4686 – 4690.
[4] J. H. Condra, W. A. Schleif, O. M. Blahy, L. J. Gabryelski, D. J. Graham, J. C. Quintero, A. Rhodes, H. L. Robbins, E. Roth, M. Shivaprakash, *Nature* **1995**, *374*, 569 – 571.
[5] a) D. Rideout, *Science* **1986**, *233*, 561 – 563; b) D. Rideout, T. Calogeropoulou, J. Jaworski, M. McCarthy, *Biopolymers* **1990**, *29*, 247 – 262; c) O. Ramstrom, J.-M. Lehn, *Nat. Rev. Drug Discovery* **2002**, *1*, 26 – 36, and references therein; d) S. Otto, *Curr. Opin. Drug Discovery Dev.* **2003**, *6*, 509 – 520; e) D. A. Erlanson, S. K. Hansen, *Curr. Opin. Chem. Biol.* **2004**, *8*, 399 – 406, and references therein; f) R. Nguyen, I. Huc, *Angew. Chem.* **2001**, *113*, 1824 – 1826; *Angew. Chem. Int. Ed.* **2001**, *40*, 1774 – 1776; g) K. C. Nicolaou, R. Hughes, S. Y. Cho, N. Winssinger, H. Labischinski, R. Endermann, *Chem. Eur. J.* **2001**, *7*, 3824 – 3843; h) S. E. Greasley, T. H. Marsilje, H. Cai, S. Baker, S. J. Benkovic, D. L. Boger, I. A. Wilson, *Biochemistry* **2001**, *40*, 13538 – 13547, and references therein; i) A. T. Poulin-Kerstien, P. B. Dervan, *J. Am. Chem. Soc.* **2003**, *125*, 15811 – 15821.
[6] a) W. G. Lewis, L. G. Green, F. Grynszpan, Z. Radic, P. R. Carlier, P. Taylor, M. G. Finn, K. B. Sharpless, *Angew. Chem.* **2002**, *114*, 1095 – 1099; *Angew. Chem. Int. Ed.* **2002**, *41*, 1053 – 1057; b) R. Manetsch, A. Krasinski, Z. Radic, J. Raushel, P. Taylor, K. B. Sharpless, H. C. Kolb, *J. Am. Chem. Soc.* **2004**, *126*, 12809 – 12818; c) V. P. Mocharla, B. Colasson, L. Lee, S. Roeper, K. B. Sharpless, C-H. Wong, H. C. Kolb, *Angew. Chem.* **2004**, *116*,118 – 122; *Angew. Chem. Int. Ed.* **2005**, *44*, 116 – 120; d) A. Krasinski, Z. Radic, R. Manetsch, J. Raushel, P. Taylor, K. B. Sharpless, H. C. Kolb, *J. Am. Chem. Soc.* **2005**, *127*, 6686 – 6692.
[7] R. Huisgen in *1,3-Dipolar Cycloaddition Chemistry, Vol. 1* (Ed.: A. Padwa), Wiley, New York, **1984**, pp. 1 – 176.
[8] R. Sanchez-Pescador, M. D. Power, P. J. Barr, K. S. Steimer, M. M. Stempien, S. L. Brown-Shimer, W. W. Gee, A. Renard, A. Randolph, J. A. Levy, D. Dina, P. A. Luciw, *Science* **1985**, *227*, 484 – 492.
[9] a) A. Brik, J. Muldoon, Y-C. Lin, J. H. Elder, D. S. Goodsell, A. J. Olson, V. V. Fokin, K. B. Sharpless, C-H. Wong, *ChemBioChem* **2003**, *4*, 1246 – 1248; b) A. Brik, J. Alexandratos, Y.-C. Lin, J. H. Elder, A. J. Olsen, A. Wlodawer, D. S. Goodsell, C.-H. Wong, *ChemBioChem* **2005**, *6*, 1167 – 1169.
[10] a) C. C. Mak, V.-D. Le, Y.-C. Lin, J. H. Elder, C.-H. Wong, *Bioorg. Med. Chem. Lett.* **2001**, *11*, 219 – 222; b) T. Lee, G. S. Laco, B. E. Torbett, H. S. Fox, D. L. Lerner, J. H. Elder, C.-H. Wong, *Proc. Natl. Acad. Sci. USA* **1998**, *95*, 939 – 944.
[11] See the Supporting Information for full spectral details.
[12] A. Adachi, H. E. Gendelman, S. Koenig, T. Folks, R. Wiley, A. Rabson, M. A. Martin, *J. Virol.* **1986**, 284 – 291.
[13] a) V. V. Rostovtsev, L. G. Green, V. V. Fokin, K. B. Sharpless, *Angew. Chem.* **2002**, *114*, 2708 – 2711; *Angew. Chem. Int. Ed.* **2002**, *41*, 2596 – 2599; b) C. W. Tornøe, C. Christensen, M. Meldal, *J. Org. Chem.* **2002**, *67*, 3057 – 3064.
[14] There is a possibility that potential products could be mass-spectrometry silent and thus would be left undetected if they had significantly different ionization energies. In the present study this was demonstrated not to be the case as the common azide fragment **2** gave a relatively large ESI-MS signal compared with alkyne **1** (see the Supporting Information for a more detailed explanation).
[15] One advantage of the in situ click-chemistry approach over the traditional drug-discovery techniques is that the need to independently synthesize each individual compound for screening is eliminated. Increased rate of formation of a triazole

 © 2006 Wiley-VCH Verlag GmbH & Co. KGaA, Weinheim

product(s) indicates possible hits that can then be further investigated individually (again, very quickly thanks to the "guaranteed" nature of the cycloaddition reaction). To ascertain that no binders were overlooked in this particular case, we also carried out thermal cycloaddition reactions of each individual azide/alkyne combination and determined the product retention times by LCMS. This confirmed our initial determination that only one triazole was formed with an increased rate in the presence of the biological target, thereby illustrating that the enzyme was able to sample an array of potential inhibitor fragments and select only one productive combination, the one leading to the inhibitor **3**.

© 2006 Wiley-VCH Verlag GmbH & Co. KGaA, Weinheim



Scheme 1. Possible dienes prepared from 1,6-enynes.

Fullerenes

DOI: 10.1002/anie.200502404

Thermal [2+2] Intramolecular Cycloadditions of Fuller-1,6-enynes**

Nazario Martín, Margarita Altable, Salvatore Filippone, Angel Martín-Domenech, Mireia Güell, and Miquel Solà*

The transition-metal-catalyzed cyclization of enynes (mostly 1,6-enynes) **1** has been extensively studied as it provides a powerful method for the construction of carbo- and heterocyclic systems (**2**–**5**) in a simple manner (Scheme 1).[1] Cycloisomerization of enynes to form novel diene structures is currently a major challenge both synthetically and mechanistically. Among the different cyclic products obtained, metathesis-type product **5** is a useful building block whose formation involves an interesting mechanism in which the carbon–carbon double bond of the enyne is completely cleaved.[2] In this chemical transformation, cyclobutene species **6** were suggested as precursors of dienes **5**.[3] Cyclobutenes **6** have been considered to be highly strained species as they are the equivalent of a *trans*-cycloheptene, a species not known to exist at ambient temperature.[4] However, the cyclobutene isomer **7** is an olefin that is stable at 118 °C.[5] Furthermore, cyclobutene **8** has recently been isolated as a stable and well-characterized silane derivative.[6]

Recently, we reported that 1,6-enynes in which fullerene C_{60} was used as the alkene component (fuller-1,6-enynes) undergo a highly efficient and regioselective [2+2+1] intramolecular Pauson–Khand reaction with $[Co(CO)_8]$ to form a new type of fullerene derivative with an unprecedented three or five fused pentagonal rings on the fullerene surface.[7] Herein, we report that the thermal treatment of fuller-1,6-enynes leads very efficiently and in a totally regioselective manner to the formation of stable cyclobutene adducts without the need of any catalyst. To the best of our knowledge, this is the first example of a thermal [2+2] cyclization that involves a fullerene double bond as the alkene unit of the reactive 1,6-enyne to form novel organofullerenes endowed with the rather unusual cyclobutene moiety **6**. These findings confirm that species of type **6** are stable at room temperature and can be easily obtained from the appropriate strained 1,6-enynes by thermal treatment. The reaction, which has proven to be generally applicable, takes place through a concerted [2+2] mechanism according to ONIOM (UB3LYP/6-31G*:AM1) theoretical calculations.

Although [2+2] cycloadditions of fullerenes are not common, several examples in which mostly photochemical methods were employed are known. Hoke et al. first reported that benzene reacted with C_{60} to give a series of [2+2] cycloadducts, from which the monoadduct was isolated and characterized.[8] Since then, other photochemical [2+2] cycloadditions of fullerenes have been reported.[9]

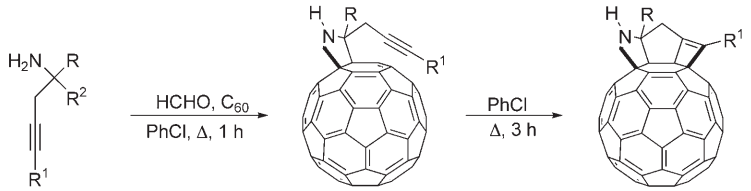
The synthesis of the starting fuller-1,6-enynes **10a–e** was carried out by 1,3-dipolar cycloaddition reaction of the azomethine ylides, which were generated in situ from propargyl-containing glycine derivatives[10] **9a–e** and formaldehyde, to [60]fullerene in refluxing chlorobenzene for 1 h following Prato's procedure.[11] The novel fulleropyrrolidines **10a–c** and previously reported compounds **10d–e**[7a–b] were obtained as stable brown solids in moderate yields (30–49 %; 55–65 % based on recovered C_{60}; Scheme 2). Fuller-1,6-enynes **10a–e** are suitable precursors for further chemical transformations: They undergo thermal intramolecular cyclization upon heating in refluxing chlorobenzene for 3 h,

[*] Prof. Dr. N. Martín, M. Altable, Dr. S. Filippone, Dr. A. Martín-Domenech
Departamento de Química Orgánica I
Facultad de Ciencias Químicas
Universidad Complutense de Madrid
Ciudad Universitaria s/n, 28040 Madrid (Spain)
Fax: (+34) 91-394-4103
E-mail: nazmar@quim.ucm.es
M. Güell, Prof. Dr. M. Solà
Institut de Química Computacional y Dpto de Química
Universidad de Girona
17071 Girona, Catalonia (Spain)

[**] These investigations were financially supported by the MEC of Spain (Projects BQU2002-00855 and BQU2002-0412-C02-02). S.F. thanks the CAM for a postdoctoral contract. M.A. and M.G. thank the MEC for research grants.

Supporting information for this article is available on the WWW under http://www.angewandte.org or from the author.

 © 2006 Wiley-VCH Verlag GmbH & Co. KGaA, Weinheim



9a: R=CO_2Et; R^1=R^2=H
9b: R=CO_2Et; R^1=TMS; R^2=H
9c: R=Me; R^1=H; R^2=CO_2H
9d: R=propargyl; R^1=H; R^2=CO_2H
9e: R=R^1=R^2=H

Scheme 2. [2+2] cycloaddition reaction of fuller-1,6-enynes **10a–e**. TMS = trimethylsilyl.

leading to the novel fullerocyclobutenes **11** in excellent yields (75–95%).

Note that substitution on the pyrrolidine ring in compounds **10** plays an important role on the outcome of the reaction. Thus, *gem*-disubstituted fuller-1,6-enynes **10a–d** afforded the respective cyclobutenes **11a–d** as stable solids in very high yields. In contrast, cyclobutene **11e** (R = R^1 = H) was obtained in low yield (15%) and found to be unstable. These findings clearly indicate that the reactivity of fuller-1,6-enynes is controlled by the rigid geometry between the reactive ene and yne groups, which in turn depends on the substitution pattern at atom C2 of the pyrrolidine ring.[12] Fuller-1,6-enyne **10d** is suitably functionalized with two propargyl groups that are able to undergo a twofold thermal cyclization reaction. However, only compound **11d**, resulting from a single thermal cyclization, was obtained, probably as a result of the high strain of the expected bis(cyclobutene).

The structures of the novel compounds **10** and **11** were unambiguously established by UV/Vis, FTIR, and ^{1}H and ^{13}C NMR spectroscopic techniques, as well as by mass spectrometry. As diagnostic signals in the ^{1}H NMR spectra, the alkynyl proton of fuller-1,6-enynes **10** appears at around $\delta = 2.3$ ppm whereas the olefinic protons of cyclobutenes **11** appear around $\delta = 7.0$ ppm. In the ^{13}C NMR spectra of compounds **11**, the bridgehead olefinic carbon atom appears at $\delta \approx 150$–161 ppm. However, compound **11b** presents a deshielded signal at $\delta \approx 169.4$ ppm owing to the presence of the TMS group on the adjacent olefinic carbon, in agreement with previous reports for compound **8**.[6]

The heteronuclear multiple-bond connectivity (HMBC) NMR spectrum of representative compound **11d** is shown in Figure 1, and it clearly shows that the protons of the three methylene groups present in the molecule are coupled to the quaternary carbon atoms of the pyrrolidine ring (C^a: δ = 76.8 ppm; C^b: $\delta = 84.1$ ppm). Moreover, the methylene group of the cyclopentane ring ($\delta = 3.34$, 3.58 ppm) and the olefinic proton ($\delta = 7.56$ ppm) are coupled ($^2J_{CH}$) to the bridgehead olefinic carbon (C^c) at $\delta = 161.0$ ppm, thus supporting the structural assignment (see Supporting Information). The structures of all new compounds were further confirmed by HMQC and HMBC experiments, through comparison with UV/Vis spectra, which exhibit the typical signatures for the *cis*-1-bis-adducts,[13] and by mass spectroscopy.

To further support the structural assignments, we carried out a cyclic voltammetry study of compounds **10a–c** and **11a–c** in *o*-dichlorobenzene/MeCN (4:1) as solvent and with tetra-*n*-butylammonium perchlorate as the supporting electrolyte at room temperature (see Supporting Information). Precursor fulleropyrrolidines **10a–c** showed four reversible reduction waves, whereas only three reversible reduction waves were observed for compounds **11a–c** under the same experimental conditions. A remarkable negative shift in the redox potentials (34–65 mV) relative to the values for pristine C_{60} ($E^{1/2}_{red} = -0.800$, -1.209, -1.673, -2.127 V) was observed for **10a–c** which is attributed to the saturation of one double bond in the fullerene, thus raising the energy of the LUMO. *Cis*-1-biscycloadducts **11a–c** resulting from the [2+2] cycloaddition exhibit half-wave reduction potentials that are shifted to more-negative values (80–130 mV) relative to those for the parent C_{60}, and a significant shift (46–67 mV) compared with their respective precursors. These findings are in full agreement with the results of previous electrochemical studies of related fullerene derivatives containing one or two saturated double bonds and confirm the cathodic shift of biscycloadducts relative to related monocycloadducts.[14]

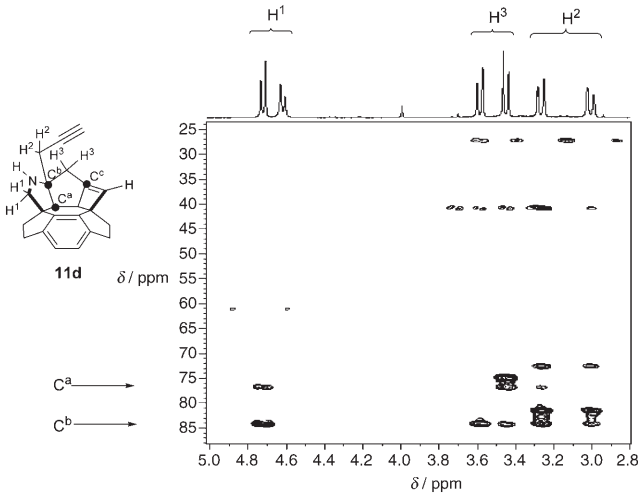


Figure 1. Part of the ^{1}H–^{13}C multiple-bond shift-correlation spectrum of compound **11d**.

Together, these data support the unambiguous structure of the novel C_{60}-based cyclobutene derivatives and thus remove the possibility of other structures stemming from thermal rearrangements.

The intramolecular thermal reaction of compounds **10** leads regioselectively to the formation of the respective *cis*-1 regioisomers, which are also obtained as a mixture of enantiomers provided that the thermal cyclization yields, besides the stereogenic center on the pyrrolidine ring, two new stereogenic carbon atoms on the fullerene surface with well-defined stereochemistry. To the best of our knowledge, this is the first example of three fused rings on the same hexagonal ring of the fullerene surface containing a cyclo-

 © 2006 Wiley-VCH Verlag GmbH & Co. KGaA, Weinheim

butene moiety. Furthermore, these results confirm that cyclobutene structures **6** are stable and that their thermal formation is possible from strained 1,6-enynes.

To determine the reaction mechanism, a theoretical analysis of three different possible reaction paths was carried out.[15] First, we studied the mechanism proposed by Gilbert and co-workers that involves a [2+1] cycloaddition to give a cyclopropylcarbene intermediate, which in a subsequent step evolves through a 1,2-carbon shift to the final product.[16] We were able to locate the two possible cyclopropylcarbene intermediates. However, the energy barriers involved in the paths from reactants to products through these cyclopropylcarbene intermediates were found to be larger than 50 kcal mol^{-1} and, for this reason, this mechanism was rejected. Second, we analyzed another mechanism that involves a diradical intermediate that already comprises one of the two C–C bonds to be formed. This radical mechanism was also considered by Bachrach and Gilbert for the reaction between cyclopentyne and ethene.[16b] A systematic search for the two possible diradical intermediates always reverted to the final product. Finally, we investigated the possibility of a concerted pathway. In this case, we located the transition state (TS) depicted in Figure 2 which has an energy barrier of 27.5 kcal mol^{-1}. The structure of this TS points to a concerted but very asynchronous addition, as suggested in previous work on similar chemical processes.[17,18] The energy barrier and the structure of this TS bear some resemblance to those found for the addition of ethylene to ketene and isocyanate[17] and also for the addition of ethylene to ethyne. In this latter case, the energy barrier computed at the UB3LYP/6-31G* level is about 7 kcal mol^{-1} higher than that of the corresponding **10a**→**11a** reaction, as expected from the fact that the double bond in C_{60} is more activated toward cycloaddition reactions than that of ethylene.[19] The TS has some diradical character with the carbon atom of the CH terminus of the 1,6-enyne structure containing a localized α electron, while the unpaired β electron is delocalized mainly around the darkened pyracylene unit of C_{60} in Figure 2. This transition state also has a molecular structure that denotes productlike (late) character. The process is found to be exothermic by 14.9 kcal mol^{-1}.

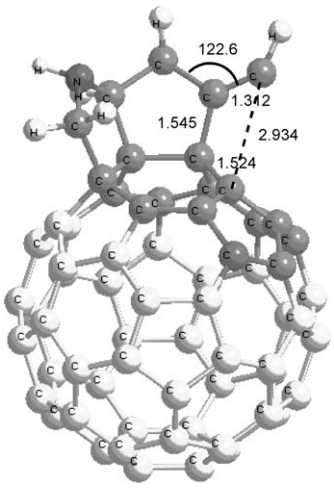


Figure 2. Optimized transition-state structure (ONIOM(UB3LYP/6-31G*:UAM1)) with the most relevant bond lengths [Å] and angles [°]. Darkened atoms constitute the model system treated at high level in the ONIOM approach.

In summary, we have discovered novel reactivity of suitable functionalized fuller-1,6-enynes **10**, which efficiently undergo regioselective *cis*-1 thermal intramolecular [2+2] cyclization to afford a new type of fullerene derivative that contains elusive fused cyclobutenes, thus confirming the stability and synthetic availability of important intermediates of type **6**. Theoretical calculations reveal that the cyclization proceeds through an unusual concerted reaction mechanism which is favored by the strain of the enyne moiety. These results shed some light on the controversial stability of fused cyclobutenes and show that they can be thermally generated from strained 1,6-enynes, thus paving the way to an interesting scenario for further chemical transformations.

Received: July 11, 2005
Revised: November 18, 2005
Published online: January 20, 2006

Keywords: cycloaddition · enynes · fullerenes · fused-ring systems · regioselectivity

[1] Reviews: a) G. C. Lloyd-Jones, *Org. Biomol. Chem.* **2003**, *1*, 215–236; b) C. Aubert, O. Buisine, M. Malacria, *Chem. Rev.* **2002**, *102*, 813–834; c) S. T. Diver, A. Giessert, *Chem. Rev.* **2004**, *104*, 1317–1382; d) A. M. Echavarren, C. Nevado, *Chem. Soc. Rev.* **2004**, *33*, 431–436.

[2] Reviews: a) M. Mori, *Top. Organomet. Chem.* **1998**, *1*, 133–154; b) C. S. Poulsen, R. Madsen, *Synthesis* **2003**, 1–18.

[3] a) R. J. Madhushaw, Ch.-Y. Lo, Ch.-W. Hwang, M.-D. Su, H.-C. Shen, S. Pal, I. R. Shaikh, R.-S. Liu, *J. Am. Chem. Soc.* **2004**, *126*, 15560–15565; b) N. Chatani, H. Inoue, T. Kotsuma, S. Murai, *J. Am. Chem. Soc.* **2002**, *124*, 10294–10295; c) C. Nieto-Oberhuber, S. López, A. M. Echavarren, *J. Am. Chem. Soc.* **2005**, *127*, 6178–6179.

[4] a) B. M. Trost, M. Yanai, K. Hoogsteen, *J. Am. Chem. Soc.* **1993**, *115*, 5294–5295; b) E. J. Corey, F. A. Carey, R. A. E. Winter, *J. Am. Chem. Soc.* **1965**, *87*, 934–935; c) For a review, see: J. F. Liebman, A. Greenberg, *Chem. Rev.* **1976**, *76*, 311–365.

[5] W. F. Maier, P. v. R. Schleyer, *J. Am. Chem. Soc.* **1981**, *103*, 1891–1900.

[6] G. Oba, G. Moreira, G. Manuel, M. Koenig, *J. Organomet. Chem.* **2002**, *643–644*, 324–330.

[7] a) N. Martín, M. Altable, S. Filippone, A. Martín-Domenech, *Chem. Commun.* **2004**, 1338–1339; b) N. Martín, M. Altable, S. Filippone, A. Martín-Domenech, A. Poater, M. Solà, *Chem. Eur. J.* **2005**, *11*, 2716–2729; c) G. Schick, T. Jarrosson, Y. Rubin, *Angew. Chem.* **1999**, *111*, 2508–2512; *Angew. Chem. Int. Ed.* **1999**, *38*, 2360–2363; d) W. Qian, S.-C. Chuang, R. B. Amador, T. Jarrosson, M. Sander, S. Pieniazek, S. I. Khan, Y. Rubin, *J. Am. Chem. Soc.* **2003**, *125*, 2066–2067.

[8] S. H. Hoke, J. Molstad, D. Dilettato, M. J. Jay, D. Carlson, B. Kahr, R. G. Cooks, *J. Org. Chem.* **1992**, *57*, 5069–5071.

[9] a) S. R. Wilson, N. Kaprinidis, Y. Wu, D. I. Schuster, *J. Am. Chem. Soc.* **1993**, *115*, 8495–8496; b) G. Vassilikogiannakis, M. Orfanopoulos, *J. Am. Chem. Soc.* **1997**, *119*, 7394–7395; c) B. Bildstein, M. Schweiger, H. Angleitner, H. Kopacka, K. Wurst, K.-H. Ongania, M. Fontani, P. Zanello, *Organometallics* **1999**, *18*, 4286–4295; d) T.-Y. Hsiao, S. K. Chidambareswaran, Ch.-H. Cheng, *J. Org. Chem.* **1998**, *63*, 6119–6122.

 © 2006 Wiley-VCH Verlag GmbH & Co. KGaA, Weinheim

[10] A. López, R. Pleixats, *Tetrahedron: Asymmetry* **1998**, *9*, 1967 – 1977.
[11] a) M. Prato, M. Maggini, *Acc. Chem. Res.* **1998**, *31*, 519 – 526; b) N. Tagmatarchis, M. Prato, *Synlett* **2003**, 768 – 779.
[12] This geometrical effect has also been observed in the Pauson–Khand reaction of related fullerenynes (see reference [7]).
[13] a) K. Kordatos, S. Bosi, T. Da Ros, A. Zambon, V. Lucchini, M. Prato, *J. Org. Chem.* **2001**, *66*, 2802 – 2808; b) Y. Nakamura, N. Takano, T. Nishimura, E. Yashima, M. Sato, T. Kudo, J. Nishimura, *Org. Lett.* **2001**, *3*, 1193 – 1196.
[14] a) L. Echegoyen, L. E. Echegoyen, *Acc. Chem. Res.* **1998**, *31*, 593 – 601; b) N. Martín, L. Sánchez, B. Illescas, I. Pérez, *Chem. Rev.* **1998**, *98*, 2527 – 2547; c) M. Carano, T. Da Ros, M. Fanti, K. Kordatos, M. Paolucci, M. Prato, S. Bofia, F. Zerbetto, *J. Am. Chem. Soc.* **2003**, *125*, 7139 – 7144.
[15] Calculations were performed with a two-layered ONIOM-(B3LYP/6-31G*:AM1) approach using the Gaussian 03 program (Gaussian 03 (Revision B.02), M. J. Frisch, G. W. Trucks, H. B. Schlegel, G. E. Scuseria, M. A. Robb, J. R. Cheeseman, J. A. Montgomery, Jr., T. Vreven, K. N. Kudin, J. C. Burant, J. M. Millam, S. S. Iyengar, J. Tomasi, V. Barone, B. Mennucci, M. Cossi, G. Scalmani, N. Rega, G. A. Petersson, H. Nakatsuji, M. Hada, M. Ehara, K. Toyota, R. Fukuda, J. Hasegawa, M. Ishida, T. Nakajima, Y. Honda, O. Kitao, H. Nakai, M. Klene, X. Li, J. E. Knox, H. P. Hratchian, J. B. Cross, C. Adamo, J. Jaramillo, R. Gomperts, R. E. Stratmann, O. Yazyev, A. J. Austin, R. Cammi, C. Pomelli, J. W. Ochterski, P. Y. Ayala, K. Morokuma, G. A. Voth, P. Salvador, J. J. Dannenberg, V. G. Zakrzewski, S. Dapprich, A. D. Daniels, M. C. Strain, O. Farkas, D. K. Malick, A. D. Rabuck, K. Raghavachari, J. B. Foresman, J. V. Ortiz, Q. Cui, A. G. Baboul, S. Clifford, J. Cioslowski, B. B. Stefanov, G. Liu, A. Liashenko, P. Piskorz, I. Komaromi, R. L. Martin, D. J. Fox, T. Keith, M. A. Al-Laham, C. Y. Peng, A. Nanayakkara, M. Challacombe, P. M. W. Gill, B. Johnson, W. Chen, M. W. Wong, C. Gonzalez, J. A. Pople, Gaussian, Inc., Pittsburgh, PA, **2003**). For open-shell species the geometry optimizations were performed within the unrestricted methodology, while the closed-shell singlet molecules were optimized using the restricted formalism. Single-point ONIOM(UB3LYP/6-31G*:UAM1) energies were computed for all species using the unrestricted method to obtain the reported energy barriers and reaction energies. To ensure that the TS connects reactants and products, full optimizations were performed by slightly shifting the geometry of the TS in either sense.
[16] a) D. W. Laird, J. C. Gilbert, *J. Am. Chem. Soc.* **2001**, *123*, 6704 – 6705; b) S. M. Bachrach, J. C. Gilbert, *J. Org. Chem.* **2004**, *69*, 6357 – 6364.
[17] a) F. P. Cossío, G. Roa, B. Lecea, J. M. Ugalde, *J. Am. Chem. Soc.* **1995**, *117*, 12306 – 12313; b) S. Yamabe, K. Kuwata, T. Minao, *Theor. Chem. Acc.* **1999**, 102, 139 – 146; c) D. Freitag, M. Drees, S. Goutal, T. Strassner, P. Metz, *Tetrahedron* **2005**, *61*, 5616 – 5621.
[18] H. Cao, S. G. Van Ornum, J. Deschamps, J. Flippen-Anderson, F. Laib, J. M. Cook, *J. Am. Chem. Soc.* **2005**, *127*, 933 – 943.
[19] M. Solà, J. Mestres, J. Martí, M. Duran, *Chem. Phys. Lett.* **1994**, *231*, 325 – 330.

 © 2006 Wiley-VCH Verlag GmbH & Co. KGaA, Weinheim

Computer Chemistry

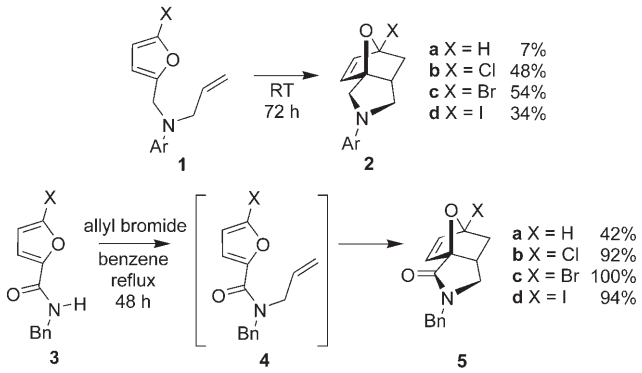
DOI: 10.1002/anie.200502677

The Origin of the Halogen Effect on Reactivity and Reversibility of Diels–Alder Cycloadditions Involving Furan**

*Susan N. Pieniazek and Kendall N. Houk**

Diels–Alder reactions involving furan as a diene are valuable processes, yielding versatile oxanorbornenes that have been used in the syntheses of numerous complex molecular architectures[1] such as prostaglandins[2] and terpenoids.[3] Furan substitution greatly affects the viability of these reactions. Halogen substituents have been found to increase rates and yields. In addition, halogen atoms can be easily removed[4] or used as handles in carbon–carbon bond-forming reactions.[5] Klepo and Jakopcic found that chlorine, bromine, or iodine substituents on furan increase cycloaddition yields and cycloadduct stability (see yields for conversion of **1** to **2**).[6] More recently, Padwa and co-workers found that conversions of furanylamides **3b–d** to **5b–d** proceed at higher rates and increased yields than the unsubstituted system **3a** to **5a** (Scheme 1).[7]

The possibility that simple halogen substitution might convert previously failed furan cycloadditions into successes



Scheme 1. Intramolecular reactions. Bn = benzyl.

[*] S. N. Pieniazek, Prof. Dr. K. N. Houk
Department of Chemistry and Biochemistry
University of California
Los Angeles, CA 90095-1569 (USA)
Fax (+1) 310-206-1843
E-mail: houk@chem.ucla.edu

[**] We are grateful to the National Science Foundation and the Partnerships for Advanced Computational Infrastructure (PACI) for financial support of this research. The computations were performed on the National Science Foundation Terascale Computing System at the Pittsburgh Supercomputing Center (PSC) and on the UCLA Academic Technology Services (ATS) Hoffman Beowulf cluster. We are grateful to Albert Padwa and Michael E. Jung for discussions.

Supporting information for this article is available on the WWW under http://www.angewandte.org or from the author.

WILEY InterScience DISCOVER SOMETHING GREAT
© 2006 Wiley-VCH Verlag GmbH & Co. KGaA, Weinheim

caused us to explore the origin and generality of this halogen effect. A number of apparently reasonable cycloadditions have been found to be unsuccessful, usually due to substrate inertness[8] or the tendency for products to undergo retro-cycloadditions.[9–11] A celebrated example is the unattainable direct synthesis of cantharidin (**6**).[12] Figure 1 illustrates

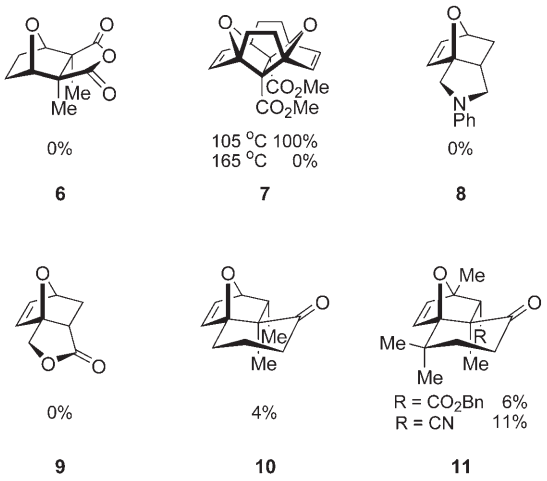


Figure 1. Furan-Diels–Alder adducts formed in low or negligible yields (**6**–**11**).

products of failed cycloadditions (**8** and **9**) as well as low-yielding cycloadditions (**10** and **11**).[11,13] Cram's polycycle (**7**) exemplifies the sensitivity of these reactions to retrocycloadditions at increased temperatures.[14] This reversibility has been used to advantage for self-healing polymers prepared by Wudl et al.[15]

The halogen effect and the possibility that it might facilitate these unsuccessful cycloadditions were explored with high-accuracy CBS–QB3[16] computations.[17] The much faster B3LYP/6-31G(d) calculations of energetics are accurate for many hydrocarbon pericyclic reactions,[18] but we have found systematic errors for hetero systems[19] and had to resort to the more CPU-intensive calculations. The nature of stationary points was confirmed by frequency analysis.

Diels–Alder cycloadditions of furan and 2-chlorofuran with ethylene are predicted to have activation enthalpies of 20.5 and 18.4 kcal mol^{-1}, respectively (Figure 2). The corresponding reaction enthalpies are −12.2 and −17.1 kcal mol^{-1}. The larger stabilization of the product by the chlorine substituent, as compared to reactants and transition state, produces a change in activation enthalpy (2.1 kcal mol^{-1}) that is about one-half the change in reaction energy (4.9 kcal mol^{-1}). This increase in exothermicity upon substitution is accompanied by a smaller decrease in activation barriers, indicating that the stabilizing effect of halogens increases with bond formation between diene and dienophile.

The kinetic and thermodynamic facilitation of furan cycloadditions are general with halogen substitution on the diene (Table 1). Halogen substitution increases reaction exothermicities by 4–9 kcal mol^{-1}, and decreases activation barriers by 2–3 kcal mol^{-1}. Reactions involving 2-fluorofuran are predicted to have the greatest increases in exothermicity,

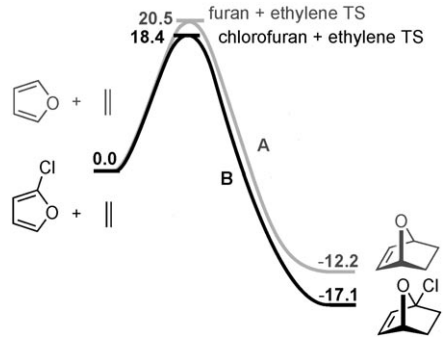
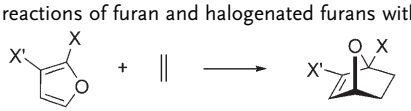


Figure 2. The Diels–Alder reaction of 2-chlorofuran and ethylene (curve B) has a lower activation enthalpy and is more exothermic than the reaction of furan (curve A). Enthalpies are given in [kcal mol^{-1}].

Table 1: CBS–QB3-calculated activation and reaction enthalpies [kcal mol^{-1}] for the reactions of furan and halogenated furans with ethylene.

a X = H
b X = Br
c X = Cl
d X = F



(1)–(2)

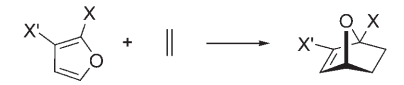
Reaction		$\Delta H^{\neq}$		ΔH_r
1a		20.5		−12.2
1b		18.3		−17.3
1c		18.4		−17.1
1d		17.1		−20.9
2b		18.0		−16.0
2c		18.1		−16.0
2d		18.6		−16.2

while bromine and chlorine should affect exothermicities to the same extent. This trend is also found for the cycloaddition energy barriers. Halogenation has a greater effect on the exothermicities at the 2- rather than at the 3-position of furan. Since $-T\Delta S$ is approximately $+12$ kcal mol^{-1} at 25 °C for each of these reactions, the halogen causes a reversible reaction ($\Delta G \approx 0$) to become significantly exergonic.

Several other representative substituents were investigated for comparison (Table 2). Methyl substitution lowers activation enthalpies by less than 1 kcal mol^{-1} and increases exothermicities by less than 2 kcal mol^{-1}. These energy

Table 2: Calculated activation and reaction enthalpies [kcal mol^{-1}] for the reactions of methyl-, trifluoromethyl-, and methoxyfuran with ethylene.

a X = H
b X = CH_3
c X = CF_3
d X = OCH_3



(3)–(4)

Reaction		$\Delta H^{\neq}$		ΔH_r
1a		20.5		−12.2
3b		19.9		−13.2
3c		18.1		−16.9
3d		18.8		−17.9
4b		19.5		−14.0
4c		19.4		−14.1
4d		18.3		−18.3

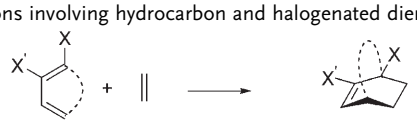
© 2006 Wiley-VCH Verlag GmbH & Co. KGaA, Weinheim

changes are significantly smaller than those caused by halogen substitution and reflect the general energetic preference for branching hydrocarbons. The trifluoromethyl group, which is comparable in electronegativity to chlorine and bromine, lowers activation enthalpies by 1–2 kcal mol^{-1} and increases exothermicities by 2–5 kcal mol^{-1}. As observed for halogens, the greatest changes in energetics occur in reactions involving 2-substituted furans. The methoxy group is a commonly used substituent in furan cycloadditions,[1b] and is predicted to lower activation enthalpies by 2 kcal mol^{-1} and increase exothermicities by 6 kcal mol^{-1}.

To determine if the halogen effect is unique for furans, hydrocarbon diene cycloadditions were explored (Table 3).

Table 3: Activation and reaction enthalpies [kcal mol^{-1}] for the Diels–Alder reactions involving hydrocarbon and halogenated dienes.

a X = H
b X = Br
c X = Cl
d X = F



(5)–(8)

Reaction		$\Delta H^{\neq}$		ΔH_r
5a		21.5		−40.3
5b		19.8		−44.2
5c		20.0		−42.5
5d		20.6		−43.3
6a		16.1		−26.4
6b		14.6		−29.9
6c		14.9		−29.4
6d		14.6		−31.3
7b		20.0		−42.6
7c		20.5		−42.4
7d		22.0		−41.6
8b		14.5		−28.3
8c		14.8		−28.0
8d		16.1		−26.8

The same kinetic and thermodynamic effects found for furan are also observed in the hydrocarbon dienes. Activation barriers are decreased by 0–2 kcal mol^{-1} and reaction exothermicities are increased by 0–4 kcal mol^{-1}. Halogen substitution has a smaller effect on hydrocarbon dienes than on furan. Reaction enthalpies are significantly larger for reactions involving unsubstituted hydrocarbon dienes than for furan ($\Delta\Delta H = 14$–28 kcal mol^{-1}). As a result, halogen substitution greatly impacts furan cycloaddition energetics, in contrast with their hydrocarbon counterparts.

Isodesmic Equations (9)–(11) were examined to determine the effect of halogenation on diene, transition state, and product, separately. The increased exothermicities in the reactions involving halogenated furans (Table 1) correspond with a larger stabilization of the adducts (3.6–14.0 kcal mol^{-1}) over the reactants (−0.2–5.3 kcal mol^{-1}; Table 4). The stabilizations are approximately in the order of electronegativities, although chlorine and fluorine are sometimes reversed. This stabilization is parallel for bromine and chlorine substituents along the reaction coordinate, resulting in identical overall effects on reaction enthalpies (Table 1).

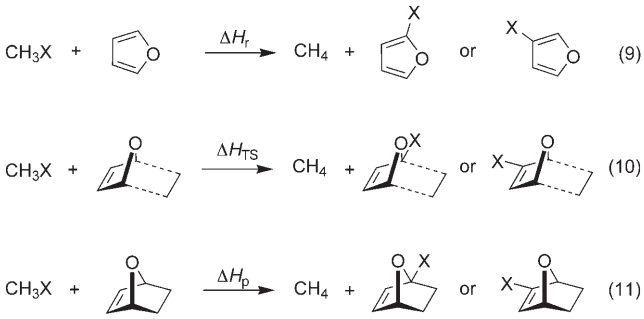
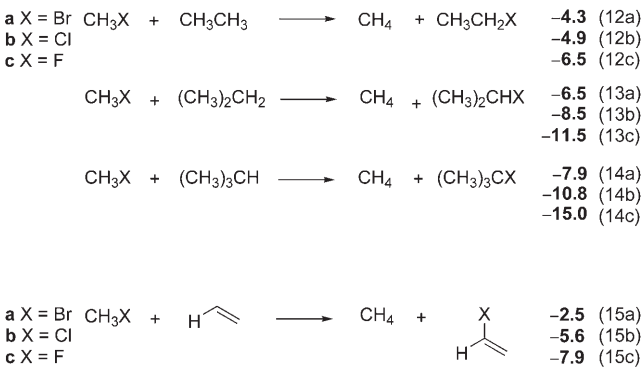


Table 4: Decomposition of reactant, transition state, and product stabilization [kcal mol^{-1}] using isodesmic Equations (9)–(11).

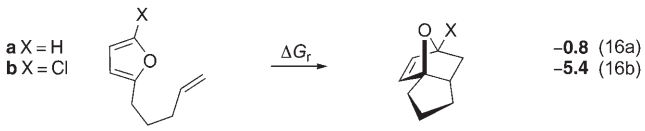
	Diene	ΔH_r	ΔH_{TS}	Product	ΔH_p
X = H		0.0	0.0		0.0
X = Br		0.2	−1.9		−4.8
X = Cl		−3.5	−5.7		−8.5
X = F		−5.3	−8.8		−14.0
X = H		0.0	0.0		0.0
X = Br		0.2	−2.3		−3.6
X = Cl		−2.9	−5.4		−6.7
X = F		−1.9	−3.7		−5.9

Comparison of isodesmic Equations (12a)–(12c) with (15a)–(15c) suggests a small effect due to change of hybridization from sp^2 to sp^3. Stabilization of these systems by electronegative substituents has been ascribed to a combination of n→π* resonance in unsaturated systems, hyperconjugation, and orbital electronegativity effects.[20] The larger effect is the energetic preference for electronegative halogens to be attached to a more highly alkylated, and therefore more electropositive, carbon framework as provided in the Diels–Alder product. The series of isodesmic reactions in Equations (12)–(14) illustrates the generality of this preference. Exothermicity increases substantially with each additional methyl group on the carbon bearing the electronegative substituent (tertiary > secondary > primary), a general effect widely observed.[21] These observations have been explained by Schleyer using an analogy with carbocations.[20] Electropositive groups stabilize both carbocations and carbon centers carrying electronegative substituents by means of hyperconjugative and σ-inductive effects.



 © 2006 Wiley-VCH Verlag GmbH & Co. KGaA, Weinheim

The results show that halogenation of dienes is beneficial in Diels–Alder reactions, both increasing the rates and yields of these reactions. Intramolecular Diels–Alder reactions involving furan have a tendency for retrocycloaddition,[10] but halogenation makes the reaction more exergonic. For example, an unsubstituted analog of systems **1** and **3** [Eq. (16a)] is predicted to have $\Delta G_r = -0.8$ kcal mol^{-1}, essentially zero within expected error. Halogen substitution would cause this reaction [Eq. (16b)] to become more clearly exergonic ($\Delta G_r = -5.4$ kcal mol^{-1}). The large effects of halogen substitution in experimental cases **1b–d** and **3b–d**, are in good agreement with calculations.



Alkyl substitution has a small and similar effect on both activation and reaction energies, while electronegative groups are much more influential. The trifluoromethyl group exhibits comparable effects to halogens at the 2-position of furan. Alkoxy groups and halogens are not only beneficial to the energetics of these reactions, but provide functionalities for further transformations. A detailed analysis of other substituent effects involving attachment of two electronegative atoms to one carbon atom (e.g. anomeric effect), and the study of synthetically useful intramolecular Diels–Alder reactions involving halogenated furans are in progress.

Received: July 29, 2005
Revised: October 8, 2005
Published online: January 20, 2006

Keywords: computer chemistry · cycloaddition · halogenation · oxygen heterocycles · retro reactions

[1] a) P. Vogel, J. Cossy, J. Plumet, O. Arjona, *Tetrahedron* **1999**, *55*, 13521 – 13642; b) C. O. Kappe, S. S. Murphree, A. Padwa, *Tetrahedron* **1997**, *53*, 14179 – 14233; c) B. H. Lipshutz, *Chem. Rev.* **1986**, *86*, 795 – 819; d) L. L. Klein, *J. Am. Chem. Soc.* **1985**, *107*, 2573 – 2574; e) L. L. Klein, M. S. Shanklin, *J. Org. Chem.* **1988**, *53*, 5202 – 5209; f) P. R. Ashton et al., *J. Am. Chem. Soc.* **1992**, *114*, 6330 – 6353; g) M. Löffler, A.-D. Schlüter, K. Gessler, W. Saenger, J.-M. Toussaint, J.-L. Brédas, *Angew. Chem.* **1994**, *106*, 2281 – 2284; *Angew. Chem. Int. Ed. Engl.* **1994**, *33*, 2209 – 2212; h) C. Valdés, U. P. Spitz, S. W. Kubik, J. Rebek, Jr., *Angew. Chem.* **1995**, *107*, 2031 – 2033; *Angew. Chem. Int. Ed. Engl.* **1995**, *34*, 1885 – 1887.

[2] P. W. Sprague, J. E. Heikes, J. Z. Gougoutas, M. F. Malley, D. N. Harris, R. Greenberg, *J. Med. Chem.* **1985**, *28*, 1580 – 1590.

[3] a) Y. Shuyuan, G. Beese, B. A. Keay, *J. Chem. Soc. Perkin Trans. 1* **1992**, 2729 – 2731; b) A. T. Sneden, *Synlett* **1993**, 313 – 322.

[4] M. E. Jung, J. P. Hudspeth, *J. Am. Chem. Soc.* **1978**, *100*, 4309 – 4311.

[5] K. L. Milkiewicz, I. B. Neagu, D. J. Parks, T. Lu, *Tetrahedron Lett.* **2003**, *44*, 7341 – 7343.

[6] Z. Klepo, K. Jakopcic, *J. Heterocycl. Chem.* **1987**, *24*, 1787 – 1791.

[7] K. R. Crawford, S. K. Bur, C. S. Straub, A. Padwa, *Org. Lett.* **2003**, *5*, 3337 – 3340.

[8] E. Wenkert, P. D. R. Moeller, S. R. Piettre, *J. Am. Chem. Soc.* **1988**, *110*, 7188 – 7194.

[9] H. Kwart, K. King, *Chem. Rev.* **1968**, *68*, 415 – 447.

[10] a) H. W. Gschwend, M. J. Hillman, B. Kisis, *J. Org. Chem.* **1976**, *41*, 104 – 110; b) L. L. Klein, *J. Org. Chem.* **1985**, *50*, 1770 – 1773; c) D. D. Sternbach, D. M. Rossana, *Tetrahedron Lett.* **1985**, *26*, 591 – 594; d) S. Cauwbergs, P. J. De Clercq, B. Tinant, J. P. Declercq, *Tetrahedron Lett.* **1988**, *29*, 2493 – 2496; e) B. J. McNelis, D. D. Sternbach, A. T. MacPhail, *Tetrahedron* **1994**, *50*, 6767 – 6782; f) T. Hudlicky, G. Butora, S. P. Fearnley, A. G. Gum, P. J. Persichini III, M. R. Stabile, J. S. Merola, *J. Chem. Soc. Perkin Trans. 1* **1995**, 2393 – 2398; g) T. Heiner, S. I. Kozhushkov, M. Noltemeyer, T. Haumann, R. Boese, A. de Meijere, *Tetrahedron* **1996**, *52*, 12185 – 12196; h) D. Prajapati, D. D. Laskar, J. S. Sandhu, *Tetrahedron Lett.* **2000**, *41*, 8639 – 8643.

[11] M. E. Jung, S.-J. Min, *J. Am. Chem. Soc.* **2005**, *127*, 10834 – 10835.

[12] a) G. Stork, E. E. van Tamelen, L. J. Friedman, A. W. Burgstahler, *J. Am. Chem. Soc.* **1951**, *73*, 4501 – 4501; b) G. Stork, E. E. van Tamelen, L. J. Friedman, A. W. Burgstahler, *J. Am. Chem. Soc.* **1953**, *75*, 384 – 392; c) W. G. Dauben, C. R. Kessel, K. H. Takemura, *J. Am. Chem. Soc.* **1980**, *102*, 6893 – 6894; d) P. A. Grieco, J. J. Nunes, M. D. Gaul, *J. Am. Chem. Soc.* **1990**, *112*, 4595 – 4596.

[13] a) D. Bilovic, Z. Stojanac, V. Hahn, *Tetrahedron Lett.* **1964**, *5*, 2071 – 2074; b) K. A. Parker, M. R. Adamchuk, *Tetrahedron Lett.* **1978**, *19*, 1689 – 1692; c) C. Rogers, B. A. Keay, *Can. J. Chem.* **1992**, *70*, 2929 – 2947.

[14] D. G. Cram, C. S. Montgomery, G. R. Knox, *J. Am. Chem. Soc.* **1966**, *88*, 515 – 525.

[15] X. Chen, M. A. Dam, K. Ono, A. Mal, H. Shen, S. R. Mutt, K. Sheran, F. Wudl, *Science* **2002**, *295*, 1698 – 1702.

[16] a) M. R. Nyden, G. A. Petersson, *J. Chem. Phys.* **1981**, *75*, 1843 – 1862; b) G. A Petersson, M. A. Al-Laham, *J. Chem. Phys.* **1991**, *94*, 6081 – 6090; c) G. A. Petersson, T. Tensfeldt, J. A. Montgomery, *J. Chem. Phys.* **1991**, *94*, 6091 – 6101; d) J. A. Montgomery, J. W. Ochterski, G. A. Petersson, *J. Chem. Phys.* **1994**, *101*, 5900 – 5909.

[17] Gaussian 03 (Revision C.02): M. J. Frisch et al., see Supporting Information.

[18] a) V. A. Guner, K. S. Khuong, K. N. Houk, A. Chuma, P. Pulay, *J. Phys. Chem. A* **2004**, *108*, 2959 – 2965; b) V. Guner, K. S. Khuong, A. G. Leach, P. S. Lee, M. D. Bartberger, K. N. Houk, *J. Phys. Chem. A* **2003**, *107*, 11445 – 11459.

[19] S. N. Pieniazek, K. N. Houk, unpublished results.

[20] P. von R. Schleyer, *Pure Appl. Chem.* **1987**, *59*, 1647 – 1660.

[21] a) J. D. Dill, P. von R. Schleyer, J. A. Pople, *J. Am. Chem. Soc.* **1976**, *98*, 1663 – 1668; b) T. Clark, G. W. Spitznagel, R. Klose, P. von R. Schleyer, *J. Am. Chem. Soc.* **1984**, *106*, 4412 – 4419; c) Y.-R. Luo, S. W. Benson, *J. Phys. Chem.* **1988**, *92*, 5255 – 5257; d) A. E. Dorigo, K. N. Houk, T. Cohen, *J. Am. Chem. Soc.* **1989**, *111*, 8976 – 8978; e) K. B. Wiberg, *J. Org. Chem.* **1991**, *56*, 544 – 550; f) J. N. Harvey, H. G. Viehe, *J. Prakt. Chem.* **1995**, *337*, 253 – 256.

 © 2006 Wiley-VCH Verlag GmbH & Co. KGaA, Weinheim

Microlenses

DOI: 10.1002/anie.200503102

Label-Free Biosensing with Hydrogel Microlenses**

*Jongseong Kim, Neetu Singh, and L. Andrew Lyon**

Bioresponsive soft materials, which undergo structural and/or morphological changes in response to a biological stimulus, have been investigated for numerous applications in drug-delivery, tissue-regeneration, bioassay/biosensor, and biomimetic systems.[1–11] Simple stimuli-sensitive hydrogels are of interest in a number of fields as they allow the use of external stimuli such as temperature, pH, and photon flux to induce physicochemical changes in the material.[12–21] More complex hydrogels that are bioresponsive have been engineered by varying the polymer composition, polymeric structure, and the display of specific functional groups.[1,2,5,7–9,22,23] While these materials have been successfully employed for various biological applications such as controlled drug-delivery systems and in tissue engineering,[1–4] they are still of enormous interest for developing more-sophisticated materials that display more complex responsivities. One potential application of such bioresponsive hydrogels is in biosensing, in which a physicochemical change of a hydrogel is monitored and related to a protein, oligonucleotide, or ligand-binding event.[5,6,11]

Our group recently developed hydrogel microlenses in which specific protein-binding events[11] were monitored as changes in the focal length of the microlens by brightfield optical microscopy. We observed that the focal length of the microlens could be tuned by multivalent protein binding, where the protein–ligand association formed a cross-linker in the hydrogel network. Herein, we take advantage of that fundamental observation by coupling an antigen/antibody pair directly to the microlens, thereby providing a reversibly switchable cross-link on the microlens. This forms the basis of a new biosensing construct that is reversible and simultaneously acts as the biosensor scaffolding/immobilization architecture, transducer, and amplifier, while providing broad tunability of the concentration of the analyte to which the microlens is sensitive. Furthermore, this construct is exceedingly resistant to false signals due to nonspecific binding, as the microlens bioresponsivity is dependent on the reversible displacement of protein-to-ligand interactions.

To achieve these goals, we prepared hydrogel microparticles (>1 micron in diameter) composed of poly(*N*-isopropylacrylamide-co-acrylic acid) (pNIPAm-co-AAc) through aqueous free-radical precipitation polymerization. We previously demonstrated that similar particles can be used to create self-assembled arrays of hydrogel microlenses on solid supports.[11,20,24,25] To render the microgels reactive to antibodies, a portion of the AAc groups were used to couple an antigen (biotin, as H_2N-biotin) and aminobenzophenone (ABP) using EDC and DCC, respectively.[26] Functionalization with ABP allows for photochemical tethering of anti-biotin after it is associated to the microlens through native antibody–antigen association. The biotin/ABP-functionalized microgels were then coulombically assembled onto a 3-aminopropyltrimethoxysilane (APTMS)-functionalized glass substrate to form supported microlenses. Bioresponsive microlenses were then prepared by exposure to a buffered solution of polyclonal anti-biotin, which binds to the microlenses through antibody–antigen interactions. Photochemical ligation of the surface-tethered ABP to the antigen-bound antibody was accomplished by using UV irradiation. Thus, the surface of the microlens is decorated with multiple antibody–antigen-based cross-links, which can then be disrupted by the introduction of free antigen to the surrounding medium. As the antibody is covalently tethered to the surface of the microlens, washing with antigen-free media results in reassembly of the tethered antibody/antigen pairs, thereby providing for a reversible biosensing microlens. This approach is outlined in Scheme 1.

The behavior of the microlenses following incubation with different concentrations of polyclonal anti-biotin is shown in Figure 1a,b. Under these conditions, microlenses not only showed a dependence on the concentration of antibody in the differential interference contrast (DIC) images, with the formation of a dark circle at the particle periphery, but also showed changes in the image projection through the microlenses. The details of image projection through microlenses by optical microscopy have been described previously (see Supporting Information also for a schematic of the microscope setup).[11,20,24,25] Above a critical concentration of the antibody the lens is in the "on" configuration, while below that concentration the lens is "off". These optical effects are a result of the change in the local refractive index (n) of the hydrogel microlenses caused by the formation of biotin–anti-biotin cross-links at the surface of the microlens. The critical concentration of anti-biotin represents the point at which the number of cross-linking points is sufficient to cause the microgel periphery to deswell. Below that concentration, the elastic restoring force of the network exceeds the free energy change associated with multivalent antibody binding. In this fashion, the intrinsic binding affinity of the antibody/antigen pair is modulated by the negative entropy associated with gel restriction.

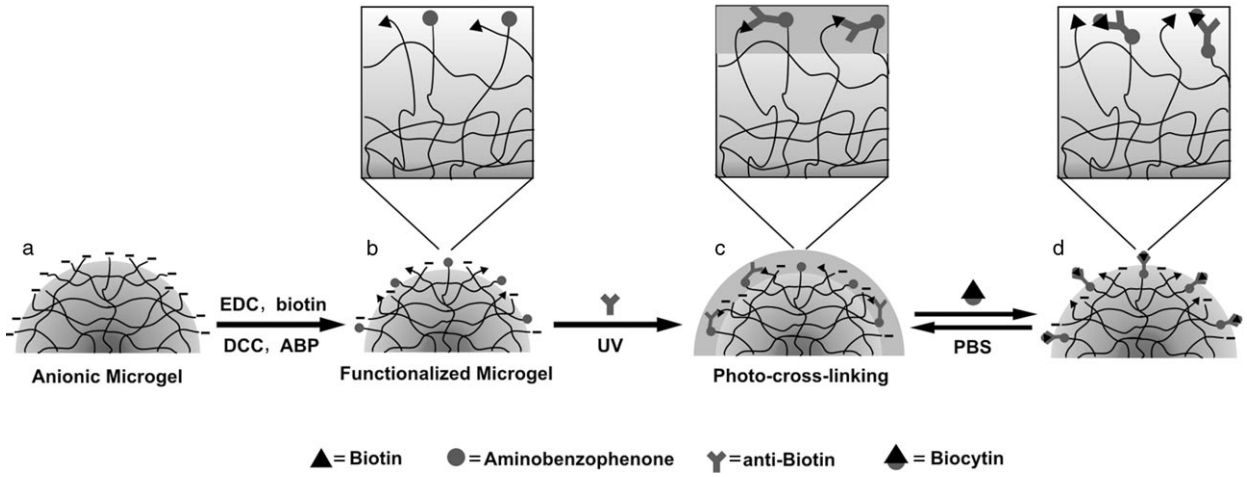
To illustrate the effect of deswelling of the surface of the microlens on the overall optical properties, a series of 2D optical ray-tracing simulations (Raytrace v.2.18) were performed in a medium with $n = 1.33$ (refractive index of water).

[*] J. Kim, N. Singh, Prof. L. A. Lyon
School of Chemistry and Biochemistry
Petit Institute for Bioengineering and Bioscience
Georgia Institute of Technology
Atlanta, GA 30332-0400 (USA)
Fax: (+1) 404-894-7452
E-mail: lyon@chemistry.gatech.edu

[**] L.A.L. acknowledges support from a Sloan Fellowship and a Camille Dreyfus Teacher–Scholar Award.

Supporting information for this article is available on the WWW under http://www.angewandte.org or from the author.

InterScience
© 2006 Wiley-VCH Verlag GmbH & Co. KGaA, Weinheim



Scheme 1. General strategy for label-free biosensing using bioresponsive hydrogel microlenses: a) pNIPAm-co-AAc hydrogel microparticles are assembled as microlenses on a glass substrate; b) conjugation of biotin and ABP to the microlenses; c) assembly of antibodies followed by photochemical ligation; d) reversible displacement of the antibody–antigen cross-link with antigen. EDC = 1-ethyl-3-(3-dimethylaminopropyl)carbodiimide; DCC = dicyclohexyl carbodiimide; PBS = phosphate-buffered saline.

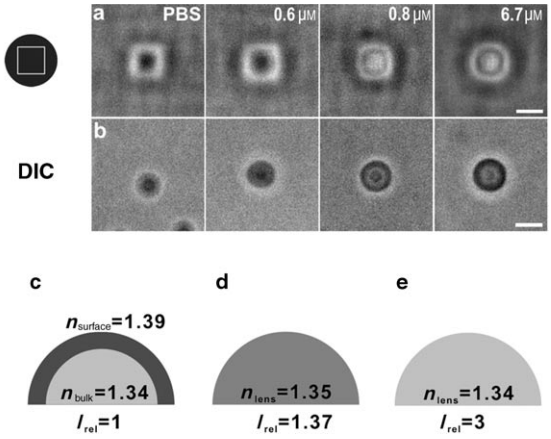


Figure 1. Influence of the concentration of polyclonal anti-biotin on lensing and the optical model of the lens structure. a) Projection of a square pattern (shown on left) through a biotin/APB-modified hydrogel microlens upon UV irradiation during incubation with anti-biotin at the concentrations indicated. b) DIC microscopy images taken under the same conditions as in (a). Scale bars: 2 μm. c–e) Results of ray-tracing simulations of the relative focusing powers of the microlens: c) a meniscus + plano-convex compound lens arising from the formation of antibody–antigen cross-links at the microgel periphery; d) a simple plano-convex lens arising from uniform distribution of the two refractive indices in (c); e) a uniform plano-convex lens in the absence of antibody–antigen cross-links. The relevant refractive indices (n) and the relative focal lengths (l_{rel}) are indicated. Note that the refractive index of the medium is considered to be $n = 1.33$.

In the "on" state of the lens (Figure 1c), the microlens is modeled as a "meniscus + plano-convex" compound lens with a slightly higher refractive index at the periphery ($n_{surface} = 1.39$ vs $n_{bulk} = 1.34$) as a result of a surface-localized binding of biotin to anti-biotin. The simulations show that the compound lens structure produces a significantly shorter relative focal length ($l_{rel} = 1.00$) as compared to the unmodified hydrogel microlens, which is modeled as a "uniform plano-convex" lens ($n = 1.34$; $l_{rel} = 3.00$; Figure 1e). In the compound lens, we have somewhat arbitrarily assumed that antibody–antigen binding, and hence the increase in refractive index, is limited to the outer 25% of the lens volume (≈ 170 nm deep into the particle). It is clear that the dimensions of the dark circle at the particle periphery are at or below the diffraction limit for visible-light imaging (≈ 250 nm), so this is a reasonable initial estimate. We have also illustrated previously that avidin can diffuse fairly deep into microgels with a similar cross-linking density.[27] In Figure 1d, we also compare the surface-localized binding case to a plano-convex lens in which the increase in the refractive index due to antibody–antigen binding is uniformly distributed over the entire optic ($n = 1.35$; $l_{rel} = 1.37$). In light of the results from the simulation, it is clear that by limiting the hydrogel responsivity to the particle periphery a higher sensitivity to binding events can potentially be obtained as a result of a concomitant localization of the changes in the refractive index. Furthermore, we expect that these structures should display fast response times owing to the short mass-transport distance required to elicit an optical response.

The bioresponsivity of the lens is highly reversible as shown in Figure 2. In this example, the biotin/ABP-functionalized hydrogel microlenses were incubated with a solution of polyclonal anti-biotin (6.7 μM; equivalent to 670 pmol) and then irradiated with UV light to covalently tether the antigen-associated antibodies to the microlens. The changes in the microlens-projected image were then monitored during exposure to 10 mM PBS (panels a, c, and e) and 1 mM solution of biocytin (panels b, d, and f), which is a water-soluble analogue of biotin. The microlens was initially observed to be in the "on" state in PBS solution which we characterize as the formation of a double-square image in image-projection mode and the dark circle at the particle periphery in the DIC image. Then, when the microlenses were exposed to a solution of free biocytin, they were observed to switch to the "off" state, as characterized by a single square image (projection mode) and the disappearance of the black circle (DIC mode). This change in focal length of the microlens arises from the

 © 2006 Wiley-VCH Verlag GmbH & Co. KGaA, Weinheim

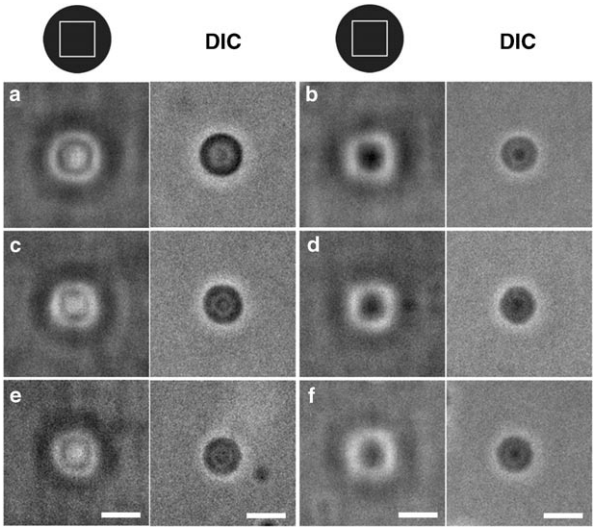


Figure 2. Reversibility of the bioresponsive microlenses. In each panel, the left image is the projection of the square pattern and the right image is the DIC image of the microlens. a) Initial "on" state; b) the lens turned "off" with 1 mM biocytin; c, e) the lens reverts to the "on" state upon washing with PBS; d, f) the same conditions as (b), which turns the lens "off". Scale bars: 2 μm.

disruption of the bound antibody–antigen pairs by competitive displacement with free antigens from solution. When the microlens is returned to an antigen-free buffer, the tethered antibody–antigen pairs reassemble as the free antigens dissociate from the microlens. This response can then be cycled by repeated exposures to either antigen-containing or antigen-free buffer. These results indicate that 1) the microlens response is thermodynamically reversible, that is, the initially photochemically coupled state is a relatively low-energy state, and 2) the antibodies are indeed coupled to the microlens, as reversibility would not be expected if the first displacement interaction led to dissolution of the antibody from the surface of the microlens. Note that this displacement-based mode of action yields microlenses that are insensitive to nonspecific binding as well as specific binding to non-paratope regions of the tethered antibody (see Supporting Information).

In designing any sensor system, selectivity, sensitivity, and dynamic range are key factors to consider. In light of the results discussed above, we have shown that we can prepare bioresponsive hydrogel microlenses that display high specificity in a label-free format as a result of the use of a displacement/competitive binding scheme. However, the response is essentially a binary (on/off) one that does not allow for quantitative analysis over a wide range of analyte concentrations. Therefore, it should be possible to tune the sensitivity of the microlenses by changing the number of antibody–antigen cross-links present on the microlens, and hence the number that must be displaced to induce a response. This can be trivially accomplished by changing the concentration of polyclonal anti-biotin used in the photochemical cross-linking step to set an initial "on" state of the lens (see Figure 3). As expected, the minimum concentration of biocytin required to switch the microlens state is dependent on the concentration of antibody used in the photochemical cross-linking step. This behavior can be understood by considering the thermodynamics of the system. In the tethered antibody–antigen system, the thermodynamics of hydrogel swelling are intimately coupled with those of the biological affinity pair. That is, the effective affinity of an individual binding pair must be reduced in the case where the gel is deswollen relative to its equilibrium state. Essentially this is a state in which the total free energies of antibody–antigen binding overcome the reduction of network entropy required for deswelling. Thus, there should be a critical number of cross-linking points that result in observable hydrogel deswelling. If the hydrogel microlenses are prepared with excess binding pairs above that critical point, then the individual hydrogel microlenses will reswell only after a suitably large number of displacement events have occurred. However, if the number of cross-linking points is just slightly above this critical point, only a few displacement events will result in gel swelling. Also, note that row (d) shows a lens incubated with 0.6 μM anti-biotin, which is insufficient to turn the lens "on", even in PBS that is lacking added biocytin.

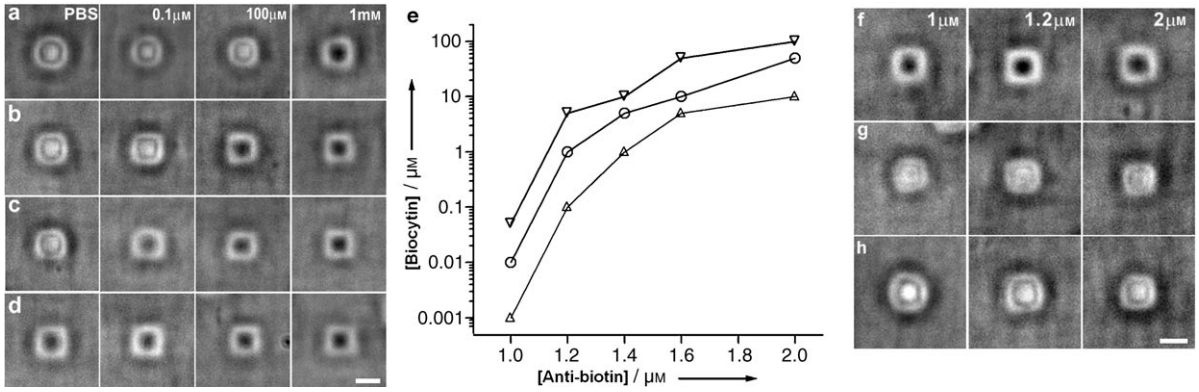


Figure 3. Tuning the microlens sensitivity: Row a) projection of the square pattern through a microlens incubated with 6.7 μM anti-biotin before photochemical cross-linking. The biocytin concentrations are indicated at the top of each column. b–d) Incubation with 2 μM anti-biotin (row b), 1 μM anti-biotin (row c), and 0.6 μM anti-biotin (row d). e) Graph of the microlens focusing "state" as a function of the concentration of the solution of biocytin and the initial concentration of anti-biotin. △: fully "on" state (as shown in row f), ○: transition point (row g), ▽: fully "off" state (row h). Note that 150 μL of each biocytin solution was used for this experiment (10 nM is equivalent to 1.5 pmol). Scale bars: 2 μm.

 © 2006 Wiley-VCH Verlag GmbH & Co. KGaA, Weinheim

These results suggest that the digital nature of an individual microlens response can be overcome by creating microlens arrays in which the individual array elements exhibit differing analyte sensitivities.

To observe microlens switching in more detail, we exposed the hydrogel microlenses to a narrower range of biocytin concentrations (Figure 3e and f). These experiments reveal that hydrogel microlenses show at least three distinct image projection modes, which we refer to here as "off", "intermediate", and "on", in response to different concentrations of anti-biotin (Figure 3f–h). Figure 3e shows the occurrence of each state upon changing the biocytin concentration as a function of the initial concentration of anti-biotin. From these data it is clear that the bioresponsive microlenses do display a transition range of finite width and are hence not purely binary response elements, thereby coupling the ultimate sensitivity of the element with our ability to observe subtle changes in microlens focal length. Most importantly, Figure 3e shows a modulation of microlens sensitivity over approximately four orders of magnitude, clearly illustrating the potential for using gel-swelling thermodynamics to modulate the sensitivity of a bioaffinity-based sensor element.

In conclusion, we have demonstrated a new approach to label-free biosensing by combining antibody–antigen cross-linked hydrogel microlenses with a simple brightfield optical microscopy technique. The utility of the construct for the detection of small molecules, its resistance to interferences from nonspecific adsorption, the ability to tune the sensitivity, the requirement of only a small volume of the sample, and the inexpensive, rapid, and simple fabrication method make this a potentially powerful and general biosensing construct. Furthermore, these fundamental advantages make this material attractive for the future development of bioresponsive materials in applications far beyond bioanalysis.

Received: August 31, 2005
Published online: January 27, 2006

Keywords: antibodies · antigens · biosensors · gels · polymers

[1] B. Jeong, Y. H. Bae, D. S. Lee, S. W. Kim, *Nature* **1997**, *388*, 860.
[2] P. F. Kiser, G. Wilson, D. Needham, *Nature* **1998**, *394*, 459.
[3] R. Langer, *Nature* **1998**, *392*, 5.
[4] M. P. Lutolf, J. L. Lauer-Fields, H. G. Schmoekel, A. T. Metters, F. E. Weber, G. B. Fields, J. A. Hubbell, *Proc. Natl. Acad. Sci. USA* **2003**, *100*, 5413.
[5] T. Miyata, N. Asami, T. Uragami, *Nature* **1999**, *399*, 766.
[6] J. H. Holtz, S. A. Asher, *Nature* **1997**, *389*, 829.
[7] C. Wang, R. J. Stewart, J. Kopecek, *Nature* **1999**, *397*, 417.
[8] A. Aggeli, M. Bell, N. Boden, J. N. Keen, P. F. Knowles, T. C. McLeish, M. Pitkeathly, S. E. Radford, *Nature* **1997**, *386*, 259.
[9] K. N. Plunkett, K. L. Berkowski, J. S. Moore, *Biomacromolecules* **2005**, *6*, 632.
[10] D. G. Anderson, J. A. Nurdick, R. Langer, *Science* **2004**, *305*, 1923.
[11] J. Kim, S. Nayak, L. A. Lyon, *J. Am. Chem. Soc.* **2005**, *127*, 9588.
[12] K. Dusek, K. Patterson, *J. Polym. Sci. Polym. Phys. Ed.* **1968**, *6*, 1209.
[13] T. Tanaka, D. J. Fillmore, *J. Chem. Phys.* **1979**, *70*, 1214.
[14] B. R. Saunders, B. Vincent, *Adv. Colloid Interface Sci.* **1999**, *80*, 1.
[15] R. Pelton, *Adv. Colloid Interface Sci.* **2000**, *85*, 1.
[16] M. Arotcarena, B. Heise, S. Ishaya, A. Laschewsky, *J. Am. Chem. Soc.* **2002**, *124*, 3787.
[17] V. T. Pinkrah, A. E. Beezer, B. Z. Chowdhry, L. H. Gracia, J. C. Mitchell, M. J. Snowden, *Langmuir* **2004**, *20*, 8531.
[18] M. Bradley, B. Vincent, *Langmuir* **2005**, *21*, 8630.
[19] Y. Luo, M. S. Shoichet, *Nat. Mater.* **2004**, *3*, 249.
[20] J. Kim, M. J. Serpe, L. A. Lyon, *J. Am. Chem. Soc.* **2004**, *126*, 9512.
[21] I. Berndt, J. S. Pedersen, W. Richtering, *J. Am. Chem. Soc.* **2005**, *127*, 9372.
[22] K. Dusek, M. Duskova-Smrckova, M. Ilavsky, R. Stewart, J. Kopecek, *Biomacromolecules* **2003**, *4*, 1818.
[23] S. Nayak, H. Lee, J. Chmielewski, L. A. Lyon, *J. Am. Chem. Soc.* **2004**, *126*, 10258.
[24] M. J. Serpe, J. Kim, L. A. Lyon, *Adv. Mater.* **2004**, *16*, 184.
[25] J. Kim, M. J. Serpe, L. A. Lyon, *Angew. Chem. Int. Ed.* **2005**, *44*, 1333; *Angew. Chem.* **2005**, *117*, 1357.
[26] G. T. Hermanson, *Bioconjugate Techniques*, Academic Press, San Diego, **1996**.
[27] S. Nayak, L. A. Lyon, *Angew. Chem. Int. Ed.* **2004**, *43*, 6706; *Angew. Chem.* **2004**, *116*, 6874.

 © 2006 Wiley-VCH Verlag GmbH & Co. KGaA, Weinheim

Quantum Dots

DOI: 10.1002/anie.200503152

Enhanced Collective Electron Transport by CdSe Quantum Dots Confined in the Poly(4-vinylpyridine) Nanodomains of a Poly(styrene-*b*-4-vinylpyridine) Diblock Copolymer Thin Film**

Chung-Ping Li, Kung-Hwa Wei, and Jung Y. Huang*

Semiconductor nanoparticle (NP) quantum dots (QDs) that have sizes close to their Bohr exciton radius (typically between 1 and 10 nm) display size-dependent band gaps and hence tunable optical properties.[1] As a result, they exhibit a wide range of electrical and optical properties and can be used for various applications, such as light-emitting diodes, solar cells, lasers, and transistors. In these applications, composite materials consisting of nanoparticles and organic materials are often adopted. Thus, an understanding of the collective

[*] C.-P. Li, Prof. K.-H. Wei
Department of Materials Science and Engineering
National Chiao Tung University
1001 Ta Hsueh Road, Hsinch 30050 (Taiwan ROC)
Fax: (+886) 35-724-727
E-mail: khwei@cc.nctu.edu.tw
Prof. J. Y. Huang
Department of Electro-Optical Engineering
National Chiao Tung University
1001 Ta Hsueh Road, Hsinch 30050 (Taiwan ROC)

[**] The authors acknowledge the National Science Council in Taiwan for funding (NSC 94-2120M-009-001).

Supporting information for this article is available on the WWW under http://www.angewandte.org or from the author.

© 2006 Wiley-VCH Verlag GmbH & Co. KGaA, Weinheim

electron transport of QDs dispersed in organic materials is of both scientific and technological importance. A number of reports have described three- and two-dimensional electron transport in ordered arrays of Au NPs in SiO_2 superlattices,[2] ZnO QD assemblies,[3] and organically capped CdSe QDs.[4] Electron transport also has been examined in granular films of Au NPs linked by alkanethiol molecules[5] or poly(4-vinylpyridine)[6] and Au/spacer/CdSe QD[7] assemblies. Orbital-selective electron transport through a single CdSe QD has been measured by scanning tunneling microscopy.[8]

Thin films of diblock copolymers are versatile templates for the preparation of long-range-ordered arrays of nanostructures, because their periodic thickness can be tuned between 10 and 100 nm.[9] For example, the selective sequestration of presynthesized CdS,[10a] CdSe,[11] and TiO_2[10b] nanoparticles into one block of a diblock copolymer is performed through strong interactions between one block of the copolymer and the surface ligands of the nanoparticles. Encapsulation of Au nanoparticles in a block copolymer has also been reported.[12] In the present study, we prepared self-assembled thin films that consisted of CdSe QDs sequestered in the poly(4-vinylpyridine) nanodomains of poly(styrene-*b*-4-vinylpyridine) (S4VP) diblock copolymer, following a previously reported approach.[10] By conductive atomic force microscopy (C-AFM) and measurements on devices, we found that the electron-tunneling rate constant of CdSe QDs confined in poly(4-vinylpyridine) nanodomains is much larger than that in a random distribution. To our knowledge, this is the first report on the nanodomain-confinement effect on the collective electron-transport behavior of quantum dots. This has large implications for application in hybrid photovoltaic cells and light-emitting diodes, because collective electron transport by CdSe QDs and hole transport by organic materials, respectively, are critical for producing highly efficient hybrid photovoltaic cells[1] and light-emitting diodes.[13]

Figure 1 shows the process for preparing a monolayered (CdSe/P4VP)-*b*-PS thin film. First, the trioctylphosphine oxide (TOPO) ligands on the CdSe QDs were exchanged by hydrophilic pyridine ligands. Then, pyridine-modified CdSe QDs and PS-*b*-P4VP block copolymer were dissolved and mixed in pyridine, whereby the CdSe QDs are distributed selectively in the P4VP phase due to dipole–dipole interactions. After drying, (CdSe/P4VP)-*b*-PS in bulk form was obtained. Subsequently, toluene, which is a good solvent for PS but a poor one for P4VP, was used to form a solution containing micelles with CdSe/P4VP cores and PS shells. The micellar solutions were then spin-coated at 5000 rpm for 60 s on carbon-coated silicon wafers to form thin films for transmission electron microscopy study and device measurements, respectively. Figure 2a shows a transmission electron microscopy (TEM) image of a thin film of 48% (CdSe/P4VP)-*b*-PS recorded without staining. The dark regions

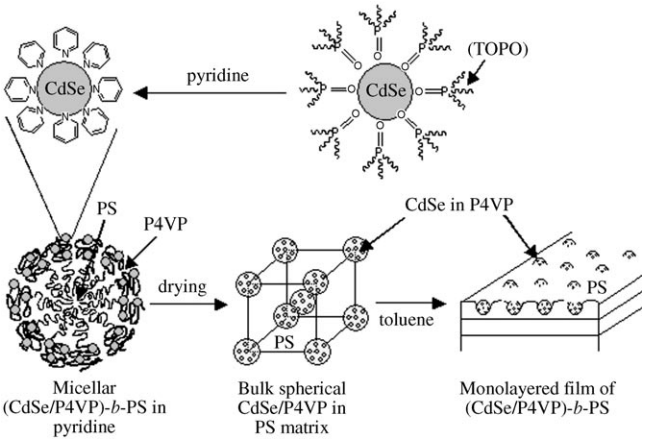


Figure 1. Preparation of a monolayered (CdSe/P4VP)-*b*-PS thin film by incorporation of selectively dispersed pre-synthesized CdSe QDs in P4VP domains.

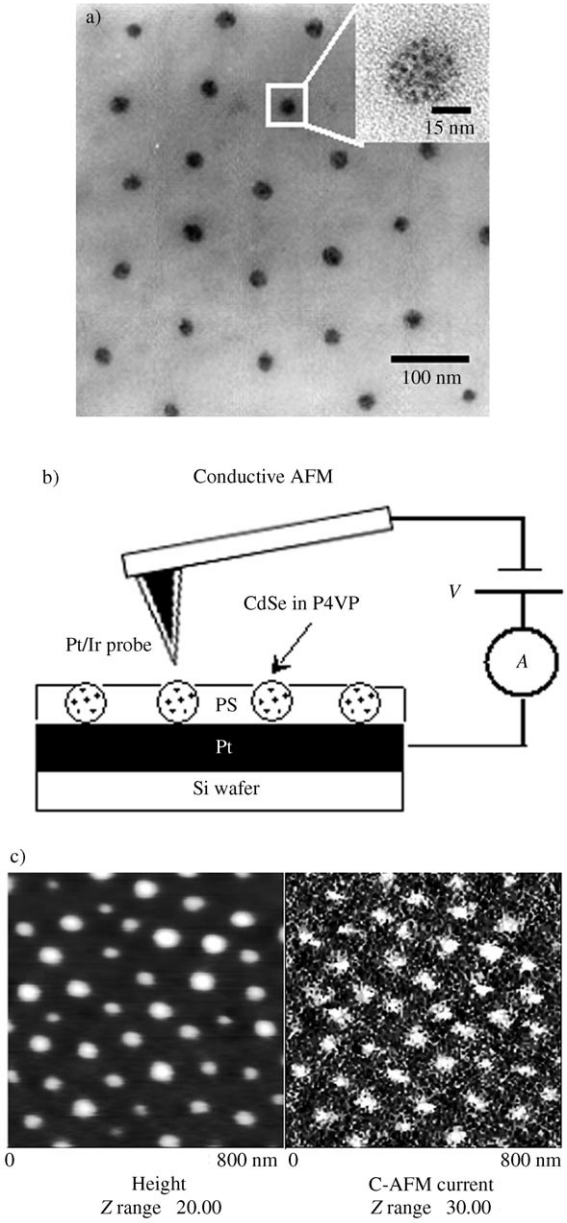


Figure 2. a) TEM image of a thin film of 48% (CdSe/P4VP)-*b*-PS obtained without staining. b) Schematic representation of the C-AFM imaging mode. c) C-AFM topographic (left) and current (right) images of a thin film of 48% (CdSe/P4VP)-*b*-PS.

 © 2006 Wiley-VCH Verlag GmbH & Co. KGaA, Weinheim

show the CdSe/P4VP composite phase representing the higher electron density of cadmium. The PS-*b*-P4VP nanospheres are thus revealed clearly. The diameter of the CdSe/P4VP spheres is about 35 nm, and the interdomain distance about 100 nm. The inset of Figure 2a reveals that CdSe QDs are dispersed homogeneously in a P4VP nanodomain. Figure 2b shows a schematic representation of the C-AFM method we used to analyze the CdSe/P4VP spheres embedded in polystyrene. The current image was measured at a sample bias of $V_B = 8$ V. Figure 2c shows the topographic and current images of a section of the thin film of 48% (CdSe/P4VP)-*b*-PS. In the height image, the light regions with a size of about 35 nm represent the CdSe/P4VP domains, and the dark area the polystyrene matrix. Because the thickness of the film is smaller than the size of the CdSe/P4VP domains (23 vs 30 nm), this image indicates that microphase-separated (CdSe/P4VP)-*b*-PS exists as a monolayered thin film. In the current image, the currents of the P4VP/CdSe phases (light regions) were about 30–40 pA, whereas that of the PS phase (dark regions) was at the level of the noise (ca. 0.5 pA).

Figure 3a displays the current–voltage (*I*–*V*) curves of a single CdSe/P4VP nanodomain, as measured by C-AFM. The turn-on voltage of the CdSe/P4VP nanodomains decreases with increasing number of incorporated CdSe QDs. This phenomenon occurs because the electron mobility from the probe to the nanodomains increases with increasing density of CdSe QDs. The linear regions of the *I*–*V* curves represent Ohmic behavior[17] and indicate constant conductivities σ that can be calculated from the slope of the curves.[14] The nonlinear regions are due to electron tunneling from the probe tip to the conduction band of CdSe QDs, which must overcome the barrier height ϕ_e of the P4VP between the tip and CdSe (inset of Figure 3a).[14,19] A tunneling process in which electron injection occurs under a forward bias can be properly modeled by using the Fowler–Nordheim (FN) equation to determine the electron barrier height ϕ_e.[14] The ϕ_e values for the 10, 15, 26, 33, and 48% CdSe QDs in the P4VP block were 2.4, 2.2, 2.0, 1.8, and 1.5 eV, respectively.[14] The ϕ_e value decreases monotonically with increasing amount of CdSe QDs in the P4VP block because the distance between the tip and CdSe QDs decreases at higher densities of CdSe QDs. Figure 3b shows the conductivity of a single CdSe/P4VP nanodomain as a function of the volume fraction of incorporated CdSe in P4VP. The conductivity of the CdSe/P4VP nanodomain displays only a slight change at low CdSe loadings, exhibits a sharp increase at a critical loading, and becomes saturated at high loading. Hence, the conductivity of polymers incorporating CdSe QDs is best described by a percolation theory (the solid curve in Figure 3b represents the best fit to the experimental data).[14] The conductivity σ of a single CdSe/P4VP nanodomain is on the order of 10^{-5} to $10^{-7}\ \Omega^{-1}\,cm^{-1}$ (Table 1). The conductivity increases with increasing amount of CdSe because the distance between CdSe QDs decreases at higher densities of CdSe QDs. We also obtained the averaged current–voltage (I_{av}–*V*) curve of a single CdSe/P4VP nanodomain in PS matrix in a sandwich device.[14] The conductivity of the device also increases with increasing amount of CdSe and is on the same order of magnitude (10^{-7} to $10^{-5}\ \Omega^{-1}\,cm^{-1}$) as that measured by C-AFM (Table 1).

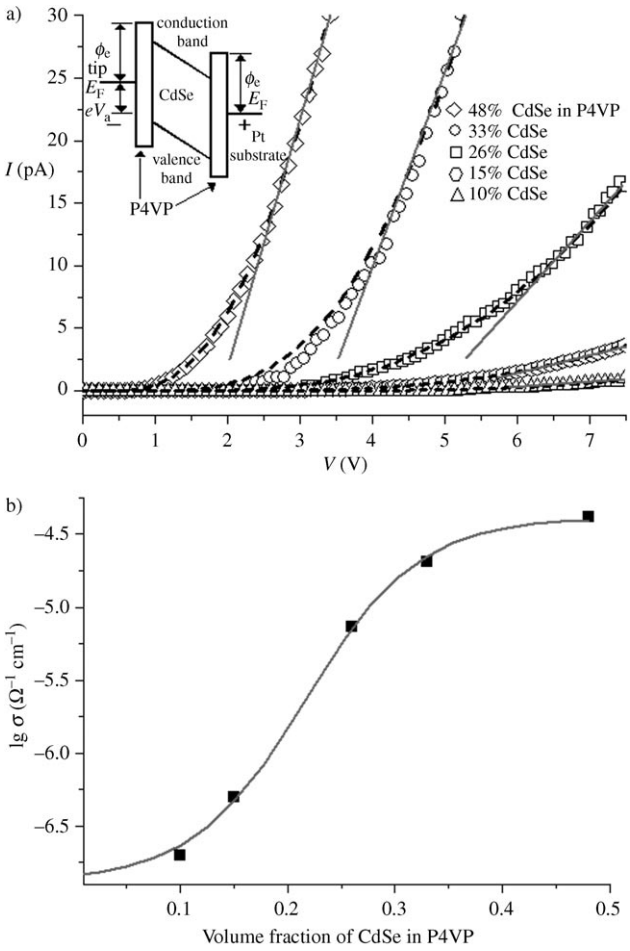


Figure 3. a) *I*–*V* curves of a single CdSe/P4VP nanodomain in (CdSe/P4VP)-*b*-PS thin films, as measured by C-AFM. The dotted lines are best fits of the FN equation. Inset: The energy bands of the C-AFM tip, CdSe/P4VP monolayer, and substrate. E_F is the electron Fermi energy inside Pt, and ϕ_e is the barrier height between Pt and CdSe/P4VP. eV_a is the applied potential energy difference between the tip and the substrate. b) Plot of conductivity versus amount of CdSe in P4VP.

Table 1: Conductivity σ and electron-tunneling rate constant k_{ET} for nanodomain-confined and randomly distributed CdSe in P4VP, as measured by C-AFM and in a device.

CdSe in P4VP [vol%]	$10^6\sigma$ [$\Omega^{-1}\,cm^{-1}$]				$10^{-3}\,k_{ET}$ [s^{-1}]			
	(CdSe/P4VP)-*b*-PS (nanodomain-confined)		CdSe/P4VP (randomly distributed)		(CdSe/P4VP)-*b*-PS (nanodomain-confined)		CdSe/P4VP (randomly distributed)	
	C-AFM	device	C-AFM	device	C-AFM	device	C-AFM	device
10	0.2	0.13	0.03	0.01	1.4	0.9	0.2	0.09
15	0.6	0.46	0.08	0.05	4.2	3.2	0.5	0.4
26	7.4	5.2	0.82	0.6	39	27	4.3	3.1
33	20	14	2.2	1.6	87	60	9.6	6.9
48	41	28	4.8	2.9	179	127	21.3	13.2

© 2006 Wiley-VCH Verlag GmbH & Co. KGaA, Weinheim

Figure 4a shows a plot of $-\ln\sigma$ versus the edge-to-edge interparticle distance δ_e, as measured by C-AFM and in a device. The conductivity in terms of δ_e and temperature T is described[5,15] by Equation (1) where σ is the conductivity of

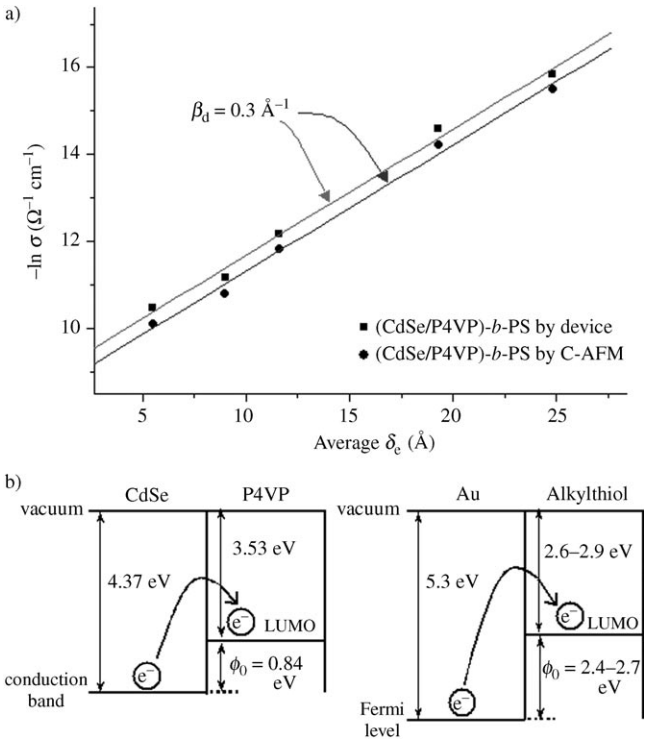


Figure 4. a) Plot of $-\ln\sigma_{(CdSe/P4VP)\text{-}b\text{-}PS}$ versus δ_e, as measured by C-AFM and in a device. b) Schematic diagram of the barrier height for electron tunneling from the conduction band of CdSe to the LUMO of P4VP[18] and from the Fermi level of Au to the LUMO of an alkanethiol.[15,16]

the resulting composite, β_d the electron-tunneling coefficient, δ_e the edge-to-edge interparticle distance,[14] E_A the activation barrier energy, R the gas constant, and T the temperature.

$$\sigma(\delta_e,T) = \sigma_0 \exp[-\beta_d \delta_e]\exp\left[\frac{-E_A}{RT}\right] \quad (1)$$

The linear slope of the plot of $-\ln\sigma$ versus δ_e indicates an electron-hopping mechanism, and the value of the slope (i.e., β_d) is 0.3 Å^{-1}. In our system, the value of β_d differs from that found in other cases. For instance, the value of β_d is 0.2–0.6 Å^{-1} for electron tunneling through π-bonded molecules, and about 0.6–1.0 Å^{-1} for saturated molecules.[16] The electron-tunneling coefficient β_d can be described[16] by Equation (2) where m^* is the electron effective mass, ϕ_0 the electron-tunneling barrier height between the dots, and $\hbar$ the reduced Planck constant.

$$\beta_d = 2\sqrt{\frac{2m^*\phi_0}{\hbar^2}} \quad (2)$$

Electron tunneling from one dot to the next must overcome the tunneling barrier height ϕ_0 of the spacer between the two dots. We found that the value of β_d in the CdSe–P4VP–CdSe system (0.3 Å^{-1}) is small when compared to that in the Au–alkanethiol–Au system (0.8–1.2 Å^{-1}), because the tunneling barrier height between the conduction band of CdSe and the LUMO of P4VP is smaller than that between the Fermi level of Au and the LUMO of an alkanethiol (Figure 4b).[5,6] The smaller β_d value for (CdSe/P4VP)-*b*-PS than for Au–alkanethiol indicates that the edge-to-edge interparticle distance has less effect on the conductivity for (CdSe/P4VP)-*b*-PS than for the Au–alkanethiol–Au system. The effective electron mass $m^* = 0.14m$ was calculated by Equation (2), where m is the free electron mass.

To compare the effect that nanodomain confinement has on the CdSe QDs with respect to their randomly distributed state, we prepared four samples that had the same density of P4VP: the first two contained 48 vol% CdSe with respect to the P4VP blocks in a PS-*b*-P4VP diblock copolymer, and the second two contained 48 vol% CdSe in a P4VP homopolymer. The electron-tunneling rate constant k_{ET} can be estimated from the conductivity by assuming a cubic-lattice model described by an equation.[5,14] Table 1 indicates that both k_{ET} and σ for the nanodomain-confined case are about seven times larger than those for the randomly distributed case. This can be explained by the fact that the collective electron transport of CdSe QDs in the nanodomain-confined case is restricted by the P4VP sphere, while the collective electron transport for the randomly distributed CdSe QDs follows a free-pathway behavior. The k_{ET} value increases with increasing amount of CdSe.

In conclusion, we have demonstrated that the electron-tunneling rate constant of CdSe QDs confined in a poly(4-vinylpyridine) nanodomain is much larger than that in a random distribution, and it increases with increasing amount of CdSe. The electron-tunneling coefficient of the CdSe–P4VP–CdSe system is 0.3 A^{-1}. The electron barrier height from the tip of the probe to the nanodomain decreases monotonically and the conductivity of the CdSe/P4VP nanodomain increases in accordance with a percolation model with increasing amount of CdSe.

Received: September 6, 2005
Revised: November 24, 2005
Published online: January 30, 2006

Keywords: block copolymers · electron transport · monolayers · quantum dots · semiconductors

[1] W. Huynh, J. J. Dittmer, A. P. Alivisatos, *Science* **2002**, *295*, 2425–2427.
[2] H. Fan, K. Yang, D. M. Boye, T. Sigmon, K. J. Malloy, H. Xu, G. P. Lopez, C. J. Brinker, *Science* **2004**, *304*, 567–571.
[3] a) A. L. Roest, J. J. Kelly, D. Vanmaekelbergh, *Phys. Rev. Lett.* **2002**, *89*, 036801; b) A. L. Roest, J. J. Kelly, D. Vanmaekelbergh, *Appl. Phys. Lett.* **2003**, *83*, 5530–5532.
[4] D. Yu, C. Wang, P. Guyot-Sionnest, *Science* **2003**, *300*, 1277–1280.
[5] W. P. Wuelfing, S. J. Green, J. J. Pietron, D. E. Cliffel, R. W. Murry, *J. Am. Chem. Soc.* **2000**, *122*, 11465–11472.
[6] R. J. Forster, L. Keane, *J. Electroanal. Chem.* **2003**, *554–555*, 345–354.

 © 2006 Wiley-VCH Verlag GmbH & Co. KGaA, Weinheim

[7] E. P. A. M. Bakkers, A. W. Marsman, L. W. Jenneskens, D. Vanmaekelbergh, *Angew. Chem.* **2000**, *112*, 2385 – 2388; *Angew. Chem. Int. Ed.* **2000**, *39*, 2297 – 2299.
[8] E. P. A. M. Bakkers, Z. Hens, A. Zunger, A. Franceschetti, L. P. Kouwenhoven, L. Gurevich, D. Vanmaekelbergh, *Nano Lett.* **2001**, *1*, 551 – 556.
[9] J. P. Spatz, S. Mossmer, C. Hartmann, M. Möller, T. Herzog, M. Krieger, H. G. Boyen, P. Ziemann, B. Kabius, *Langmuir* **2000**, *16*, 407 – 415.
[10] a) S. W. Yeh, K. H. Wei, Y. S. Sun, U. S. Jeng, K. S. Liang, *Macromolecules* **2003**, *36*, 7903 – 7907; b) C. C. Weng, K. H. Wei, *Chem. Mater.* **2003**, *15*, 2936 – 2941; c) S. W. Yeh, T. L. Wu, K. H. Wei, *Nanotechnology* **2005**, *16*, 683 – 687; d) C. C. Weng, C. P. Chen, C. H. Ting, K. H. Wei, *Chem. Mater.* **2005**, *17*, 3328 – 3330.
[11] Y. Lin, A. Böker, J. He, K. Sill, H. Xiang, C. Abetz, X. Li, J. Wang, T. Emrick, S. Long, Q. Wang, A. Balazs, T. P. Russell, *Nature* **2005**, *434*, 55 – 59.
[12] Y. Kang, T. A. Taton, *Angew. Chem.* **2005**, *117*, 413 – 416; *Angew. Chem. Int. Ed.* **2005**, *44*, 409 – 412.
[13] N. Tesster, V. Medvedev, M. Kazes, S. Kan, U. Banin, *Science* **2002**, *295*, 1506.
[14] See the Supporting Information.
[15] F. P. Zamborini, L. E. Smart, M. C. Leopold, R. W. Murry, *Anal. Chim. Acta* **2003**, *496*, 3 – 16.
[16] a) A. Salomon, D. Cahen, S. Lindsay, J. Tomfohr, V. B. Engelkes, C. D. Frisbie, *Adv. Mater.* **2003**, *15*, 1881 – 1890; b) X. D. Cui, X. Zarate, J. Tomfohr, O. F. Sankey, A. Primak, A. L. Moore, T. A. Moore, D. Gust, G. Harris, S. M. Lindsay, *Nanotechnology* **2002**, *13*, 5 – 14.
[17] N. Boden, R. J. Bushby, J. Clements, B. Movaghar, *J. Appl. Phys.* **1998**, *83*, 3207 – 3216.
[18] We measured the HOMO and LUMO levels of P4VP by cyclic voltammetry (CV).
[19] D. Xu, G. D. Watt, J. N. Harb, R. C. Davis, *Nano Lett.* **2005**, *5*, 571 – 577.

 © 2006 Wiley-VCH Verlag GmbH & Co. KGaA, Weinheim

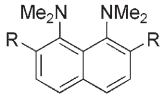
Proton Sponges

DOI: 10.1002/anie.200503472

1,8-Bis(dimethylamino)naphthalene-2,7-diolate: A Simple Arylamine Nitrogen Base with Hydride-Ion-Comparable Proton Affinity**

Valery A. Ozeryanskii, Aleksey A. Milov, Vladimir I. Minkin, and Alexander F. Pozharskii*

Since the discovery by Alder et al.[1] of the anomalously high basicity ($pK_a = 12.1$, H_2O, 25 °C) of 1,8-bis(dimethylamino)-naphthalene (**1**), widely known as a "proton sponge", much



1 R = H; **2** R = OMe; **3** R = NMe_2; **4** R = OH; **5** R = O^-

effort has been made to design even stronger bases of similar type.[2] The synthesis of 2,7-dimethoxy-1,8-bis(dimethylamino)naphthalene (**2**) with $pK_a = 16.1$ has become the currently unsurpassed success in this direction.[3] The high basicity of **2**[4] was attributed to the +M effect of the two MeO groups, which in conjunction with their "buttressing effect" destabilizes the base and leads to a large gain in free energy on protonation. This explanation allows one to expect that further increases in pK_a may be achieved by substitution of methoxy groups in **2** by more strongly electron-donating dimethylamino groups in **3**. However, due to steric hindrance, the electron-donating ability of the NMe_2 groups at C-2 and C-7 is diminished, and the basicity of **3** ($pK_a = 15.8$)[5] does not exceed that of **2**. We therefore assumed that more promising and more basic candidates are **4** and **5** with less sterically demanding OH and O^- substituents in the *ortho* positions.

[*] Dr. V. A. Ozeryanskii, Prof. A. F. Pozharskii
Department of Organic Chemistry
Rostov State University
7, Zorge str., 344090 Rostov-on-Don (Russia)
Fax: (+7) 863-2975-146
E-mail: vv_ozer2@rsu.ru
Dr. A. A. Milov, Prof. V. I. Minkin
Southern Research Centre
Russian Academy of Sciences
41, Chekhov ave., 344006 Rostov-on-Don (Russia)
and
Institute of Physical and Organic Chemistry
Rostov State University
194/2, Stachki ave., 344090 Rostov-on-Don (Russia)

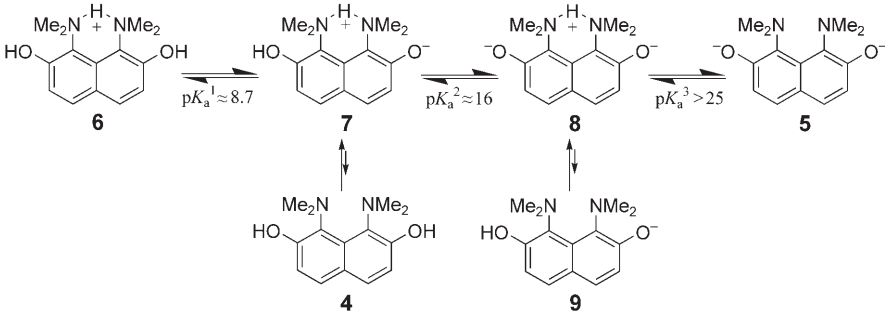
[**] This work was in part supported by the Russian Foundation for Basic Research (grants RFBR No's 05-03-32110, 04-03-32538 and N. Sh. 945.2003.03). We thank Dr. A. G. Starikov, Rostov-on-Don, for computational assistance.

Supporting information for this article is available on the WWW under http://www.angewandte.org or from the author.

© 2006 Wiley-VCH Verlag GmbH & Co. KGaA, Weinheim

This assumption has been fully confirmed, and herein we report a novel 1,8-bis(dimethylamino)naphthalene derivative with the highest basicity among all currently studied aminoarene systems.

Heating a solution of **2** in 46% aqueous HBr gave the protonated form **6** of naphthalenediol **4** as hydrobromide monohydrate in nearly quantitative yield. In the ^{1}H NMR spectrum (Table 1, entries 3–5), the



Scheme 1. Protonation equilibria and possible tautomeric forms between **6** and diolate **5**.

Table 1: Selected ^{1}H NMR spectroscopic data for **2** and the bromide of **6** and deprotonation of hydrobromide **6**.

Entry	Starting material	Solvents and conditions	Species in solution	NMe_2	δ_H [ppm] H-3, H-6	N–H···N[a]
1	**2**	[D$_6$]DMSO	**2**	2.82 (s)	7.16	–
2	**2**·HBr	[D$_6$]DMSO	**2**+H$^+$	3.18 (d)	7.53	19.38
3	**6**	[D$_6$]DMSO	**6**	3.19 (d)	7.14	19.30
4	**6**	D$_2$O/[D$_6$]DMSO (1:3)	**6**	3.12 (d)	7.07	19.33
5	**6**	CD$_3$OD	**6**	3.31 (d)	7.11	19.65
6	**6**	CD$_3$OD + KOH (1 equiv)	**7**	3.27 (br s)	6.78	18.70
7	**6**	CD$_3$OD + KOH (3 equiv)	**8**	3.26 (s)	6.58	19.66
8	**6**	D$_2$O/[D$_6$]DMSO (1:3) + KOH (6 equiv)	**8**	3.03 (s)	6.23	19.26
9	**6**	D$_2$O/[D$_6$]DMSO (1:3) + KOH (18 equiv)	**8**	3.04 (s)	6.22	19.25
10	**6**	D$_2$O/[D$_6$]DMSO (1:3) + KOH (18 equiv), 100 °C	**8**	3.08 (s)	6.21	–[b]
11	**6**	[D$_6$]DMSO + LiH (10 equiv)[c]	**8**	3.12	6.17	19.12

[a] Chemical shift of the chelated proton. [b] Complete H/D exchange. [c] See also text.

N-H-N chelated proton resonates at very low field ($\delta = 19.30$ and 19.65 ppm in [D$_6$]DMSO and CD$_3$OD, respectively), as is typical for conjugate acids of 2,7-disubstituted proton sponges (e.g., entry 2 in Table 1).[2a,4] In contrast to the hydroxy protons ($\delta \approx 11.0$ ppm), which readily undergo rapid H/D exchange in CD$_3$OD- or D$_2$O-containing solutions, H/D exchange of the NH proton is complete only after several weeks at room temperature. Gradual addition of solid KOH to a solution of **6** in CD$_3$OD or D$_2$O/DMSO leads to consecutive formation of ions **7** (Table 1, entry 6) and **8** (Table 1, entries 7–10) in which the NH proton remains intact (Scheme 1). This process is accompanied by strong shielding of H-3 and H-6, the signals of which are shifted upfield to $\delta \approx 6.2$ ppm (cf. Table 1, entry 2). At the same time, the downfield shift (by more than 3 ppm) observed for the NMe_2 groups leaves no doubt to their involvement in N-H(D)-N bonding (Table 1, entries 9 and 10; cf. entry 1). Surprisingly, all attempts to deprotonate the diolate anion **8** further were unsuccessful. Thus, even after prolonged heating of **6** in KOH/D$_2$O/[D$_6$]DMSO (Table 1, entry 10) or with a large excess of LiH in [D$_6$]DMSO (Table 1, entry 11), the ^{1}H NMR spectra contained the well-defined low-field signal of the chelated proton.

Estimation of pK_a values for **6**–**8** seemed especially intriguing. We could measure directly only the first ionization constant for the phenolic hydroxy group in **6**. The pK_a^1 value determined potentiometrically in H$_2$O/EtOH (1:1) at 20 °C was 8.93 ± 0.04, which corresponds to approximately 8.6–8.7 for aqueous solution (cf. pK_a for β-naphthol: 9.63 in H$_2$O;[6] 9.94 ± 0.04 in H$_2$O/EtOH 1:1 (this work)). To estimate pK_a^2, the transprotonation NMR procedure was employed.[7] For example, the room-temperature ^{1}H NMR spectrum of a 3:1 mixture of **2** and **6** in [D$_6$]DMSO showed that only one equivalent of **2** was protonated to give a 2/1/1 mixture of **2**, **2**+H$^+$, and **7**. Hence, pK_a^2 definitely exceeds 11 (on the DMSO scale) or approaches 16 (in H$_2$O). The pK_a^3 value was evaluated by correlating known pK_a values for proton sponge **1** and some of its 2,7-disubstituted derivatives in DMSO with the sum of Hammett constants σ_p^+[8,9] of the *ortho* susbstituents (see Ref. [4]). The resulting linear relationship ($r^2 = 0.9970$) is shown in Figure 1. Extrapolation to $(O^-)_2$ gives a pK_a^3 value for dianion **5** of 21.0 in DMSO or about 25.5 on the water scale. It can be

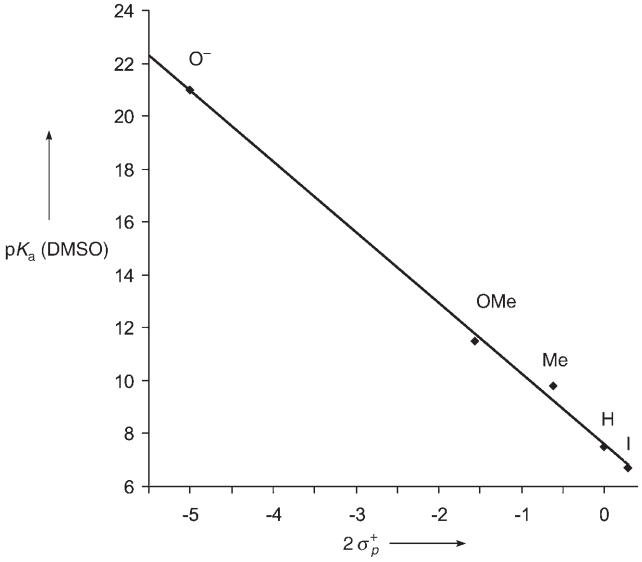
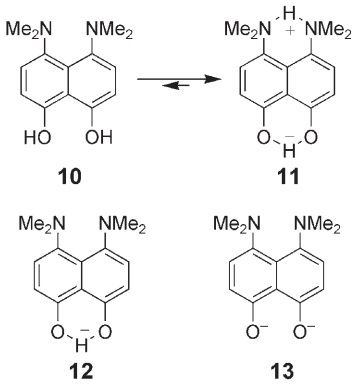


Figure 1. Correlation of basicities of 2,7-disubstituted proton sponges with the sum of the σ_p^+ constants of *ortho*-substituents.

 © 2006 Wiley-VCH Verlag GmbH & Co. KGaA, Weinheim

assumed that the true basicity of **5** is even higher, since abstraction of the NH proton occurs neither on heating **5** with LiH/DMSO at 130–140 °C for 1–2 h nor under ultrasonic irradiation of the mixture (140 W) for 20–25 min.

The existence of naphthols **4** and **9** exclusively in tautomeric forms **7** and **8** is similar to the behavior of 4,5-dihydroxy-1,8-bis(dimethylamino)naphthalene (**10**), for which the zwitterionic structure **11** was found to be the only molecular form existing in solution and in the solid state.[10] No estimation of pK_a for **11** was reported.



To provide a theoretical basis for the above observations and to check whether dianion **5** is the most basic and simple system in which neutral amino groups are protonated, quantum-chemical calculations on molecules and ions **1**, **2**, **4**–**9**, and related compounds **10**–**13** were carried out. Selected results of the calculations are listed in Table 2 and shown in Figure 2. Further details are collected in the Experimental Section and in the Supporting Information.

Calculations with various basis sets yielded essentially identical results; hence, we concluded that the 6-31G** basis is quite sufficient for evaluating proton affinities (PA values) of such systems. Moreover, the results of single-point calculations are sufficient for correctly accounting for the influence of a solvent on PA values. The difference between

Table 2: B3LYP/6-31G** and B3LYP/6-311++G** gas-phase [PA(Gas)] and solution [PA(DMSO)[a]] proton affinities [kcal mol^{-1}] for structures **1**, **2**, **4**, **5**, **9**, **10**, **12**, and **13** and simple anions H^-, OH^-, and NH_2^-.

	R	B3LYP/6-31G**		B3LYP/6-311++G**	
		PA(Gas)	PA(DMSO)	PA(Gas)	PA(DMSO)
1	H	259.6[b]	293.5 (293.3)	253.4	287.3
2	2,7-$(OMe)_2$	274.7	303.9	268.2	298.2
4	2,7-$(OH)_2$	272.6	304.4 (304.2)	265.3	297.5
5	2,7-$(O^-)_2$	440.4	334.6 (334.8)	424.8	321.4
9	2-OH, 7-O^-	359.8	322.0 (322.7)	349.0	312.0
10	4,5-$(OH)_2$	263.5	296.8 (297.0)	256.6	290.5
12	4-OH, 5-O^-	340.5	310.1 (311.0)	331.5	301.5
13	4,5-$(O^-)_2$	419.8	312.7	406.1	301.7
OH^-	–	435.1	348.5 (348.4)	396.0	313.3 (313.3)
NH_2^-	–	445.2	369.9 (369.7)	412.5	340.0 (339.9)
H^-	–	449.7	–	405.0	–

[a] Single-point IEFPCM calculations; results of calculations with full geometry optimization in the presence of solvent in parentheses. [b] 245.9 (experimentally), see ref. [11].

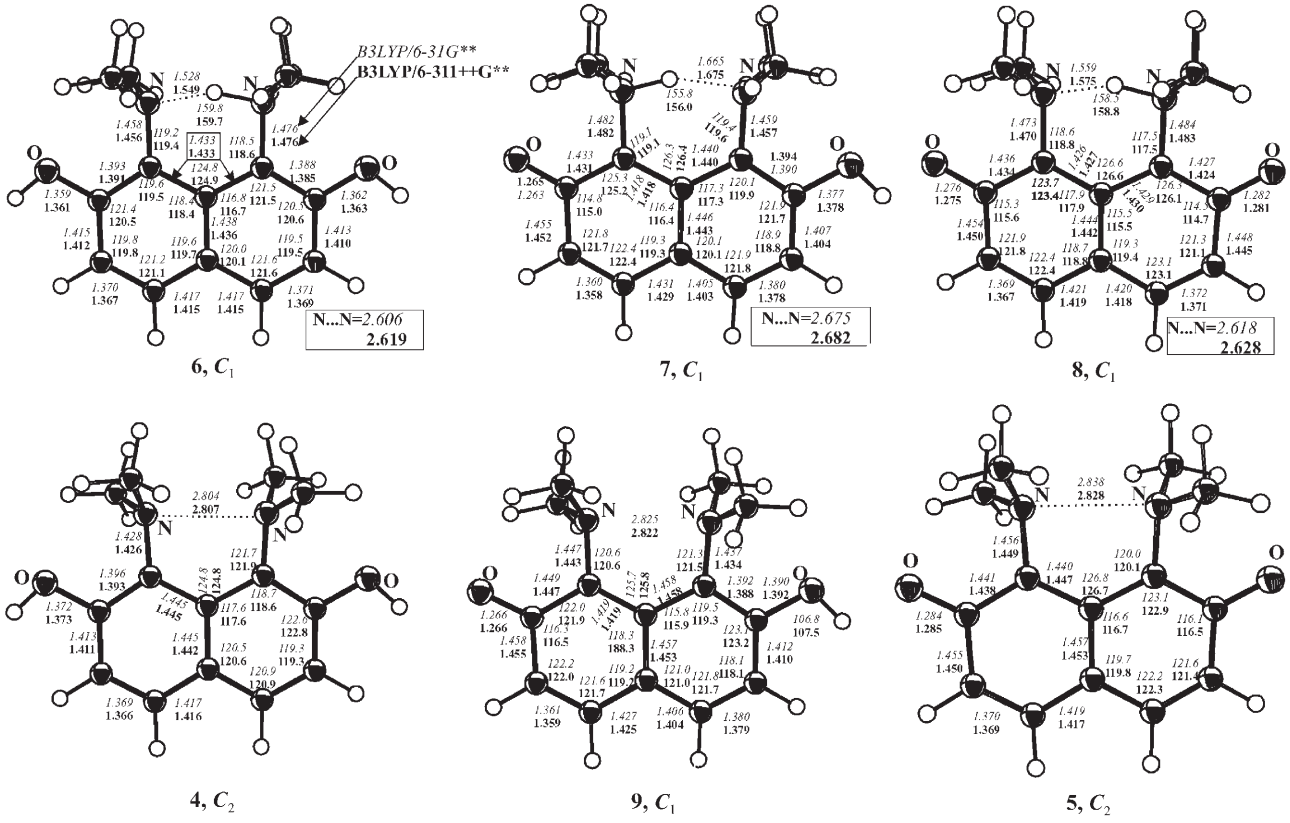


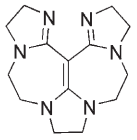
Figure 2. Optimized geometries of **4**–**9** calculated by B3LYP/6-311++G** and B3LYP/6-31G** methods. Bond lengths and angles are indicated in angstroms and degrees, respectively.

 © 2006 Wiley-VCH Verlag GmbH & Co. KGaA, Weinheim

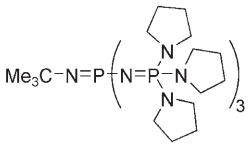
the results of the single-point and geometry-optimized calculations is less than 1 kcal mol^{-1}.

The calculations confirmed the observed experimental data and are in agreement with Scheme 1. For example, deprotonation of cation **6** results in zwitterion **7**, which, depending on the basis set used, is stabilized by 8.7–9.7 kcal mol^{-1} (in DMSO) relative to neutral structure **4**. Further deprotonation occurs with participation of the OH group to give anion **8**, which is 11.9–12.8 kcal mol^{-1} (in DMSO) more stable than its isomer **9**.

Structure **8** as the conjugate acid of dianion **5** is stabilized by an unsymmetrical, charge-assisted, intramolecular hydrogen bond (see Figure 2), and the gas-phase barrier to N–H···N proton transfer is calculated to be 0.91 kcal mol^{-1} (cf. 1.36 kcal mol^{-1} for the **2**+H$^+$ cation[12]). Compound **5** is indeed the most basic, both in solution and, predictably, in the gas phase. Remarkably, the PA value of **5** is as high as those of the simplest ions such as OH^-, NH_2^-, or even H^- (see Table 2). This value substantially exceeds the PAs calculated for amidines such as **14** (269.5), phosphazenes such as **15**



14



15

(301.0 kcal mol^{-1}),[13] the phosphatranes of Verkade and coworkers, and 1,8-bis(tetramethylguanidino)naphthalene,[14] as well as other computationally designed nitrogen superbases.[15]

Experimental Section

6: A solution of **2** (0.137 g, 0.5 mmol) in aqueous HBr (46% 5 mL) was heated to reflux under a nitrogen atmosphere for 2 h. The reaction mixture was then evaporated to dryness to leave 0.16 g (100%) of **6**-Br hydrate as gray lustrous needles (m.p. 285°C, decomp., from MeCN/EtOH 3:1). Elemental analysis (%) calcd for $C_{14}H_{19}BrN_2O_2{\cdot}H_2O$: C 48.74, H 6.14, Br 23.16; found: C 45.15, H 5.66, Br 22.33. IR (nujol): $\tilde{\nu}$ = 3370, 3130, 2680 (OH); 1620, 1500 (ring); 460 cm^{-1} (br). ^{13}C NMR (75 MHz, [D$_6$]DMSO, TMS): δ = 42.1 ($^2J_{C-N\cdots H}$ = 2.7 Hz; NMe), 116.5 (^1J = 163.1 Hz; C-3, C-6), 122.9 (C-9), 123.1 (C-10), 123.7 (C-1, C-8), 130.1 (^1J = 162.2 Hz; C-4, C-5), 153.1 ppm ($^2J_{COH}$ = 9.9 Hz; C-2, C-7).

DFT[16] calculations were carried out by the restricted Hartree–Fock method with the Gaussian 98 program suite[17] with the 6-31G** and 6-311++G** basis sets. Becke's three-parameter hybrid functional with the Lee–Yang–Parr correlation functional (B3LYP)[18] was used in the DFT calculations. All the structures corresponded to the stationary points on the respective potential energy surfaces (PES). Analytic harmonic frequencies at the same level of theory were used to characterize the nature of the stationary point corresponding to the gas-phase structure under study. The influence of solvent was taken into account by carrying out single-point and full-geometry optimization calculations with the PCM solvation method and the integral equation formalism model (IEFPCM).[19]

Received: September 30, 2005
Published online: January 20, 2006

Keywords: amines · basicity · density functional calculations · hydrogen bonds · organic bases

[1] R. W. Alder, P. S. Bowman, W. R. S. Steele, D. R. Winterman, *Chem. Commun.* **1968**, 723–724.
[2] Reviews: a) A. F. Pozharskii, *Russ. Chem. Rev.* **1998**, *67*, 1–24; b) A. L. Llamas-Saiz, C. Foces-Foces, J. Elguero, *J. Mol. Struct.* **1994**, *328*, 297–323; c) H. A. Staab, T. Saupe, *Angew. Chem.* **1988**, *100*, 895–1040; *Angew. Chem. Int. Ed. Engl.* **1988**, *27*, 865–879.
[3] F. Hibbert, K. P. P. Hunte, *J. Chem. Soc. Perkin Trans. 2* **1983**, 1895–1899.
[4] A. F. Pozharskii, O. V. Ryabtsova, V. A. Ozeryanskii, A. V. Degtyarev, O. N. Kazheva, G. G. Alexandrov, O. A. Dyachenko, *J. Org. Chem.* **2003**, *68*, 10109–10122.
[5] A. Kirsch, C. Krieger, H. A. Staab, F. A. Neugebauer, *Tetrahedron Lett.* **1994**, *35*, 8365–8368.
[6] A. Bryson, R. W. Mattews, *Aust. J. Chem.* **1963**, *16*, 401–410.
[7] F. Hibbert, G. R. Simpson, *J. Chem. Soc. Perkin Trans. 2* **1987**, 243–246.
[8] The following Hammett σ_p^+ constants were taken: H: 0, I: +0.135, Me: −0.311, MeO: −0.778 (H. C. Brown, Y. Okamoto, *J. Am. Chem. Soc.* **1958**, *80*, 4979–4987), O$^-$: −2.5 (I. N. Juchnovski, I. G. Binev, *Tetrahedron* **1977**, *33*, 2993–2995).
[9] The correlation with common Hammett σ_p constants is less accurate (r^2 = 0.9383).
[10] H. A. Staab, C. Krieger, G. Hieber, R. Oberdorf, *Angew. Chem.* **1997**, *109*, 1884–1886; *Angew. Chem. Int. Ed. Engl.* **1997**, *36*, 1884–1886.
[11] Y. K. Lau, P. P. S. Saluja, P. Kebarle, R. W. Alder, *J. Am. Chem. Soc.* **1978**, *100*, 7328–7333.
[12] V. A. Ozeryanskii, A. F. Pozharskii, A. J. Bieńko, W. Sawka-Dobrowolska, L. Sobczyk, *J. Phys. Chem. A* **2005**, *109*, 1637–1642.
[13] B. Kovačević, Z. B. Maksić, R. Vianello, *J. Chem. Soc. Perkin Trans. 2* **2001**, 886–891.
[14] a) J. Tang, J. Dopke, J. G. Verkade, *J. Am. Chem. Soc.* **1993**, *115*, 5015–5020; b) B. Kovačević, D. Barić, Z. B. Maksić, *New J. Chem.* **2004**, *28*, 284–288; c) V. Raab, J. Kipke, R. M. Gschwind, J. Sundermeyer, *Chem. Eur. J.* **2002**, *8*, 1682–1693; d) B. Kovačević, Z. B. Maksić, *Chem. Eur. J.* **2002**, *8*, 1694–1702.
[15] a) B. Kovačević, Z. B. Maksić, R. Vianello, M. Primorac, *New J. Chem.* **2002**, *26*, 1329–1334; b) G. Bucher, *Angew. Chem.* **2003**, *115*, 4172–4175; *Angew. Chem. Int. Ed.* **2003**, *42*, 4039–4042; c) Z. Gattin, B. Kovačević, Z. B. Maksić, *Eur. J. Org. Chem.* **2005**, 3206–3213.
[16] J. B. Foresman, E. Frisch, *Exploring Chemistry with Electronic Structure Methods*, 2nd ed., Gaussian, Inc., Pittsburg, **1996**.
[17] Gaussian 98 (Revision A.5), M. J. Frisch, G. W. Trucks, H. B. Schlegel, G. E. Scuseria, M. A. Robb, J. R. Cheeseman, V. G. Zakrzewski, J. A. Montgomery, R. E. Stratmann, J. C. Burant, S. Dapprich, J. M. Millam, A. D. Daniels, K. N. Kudin, M. C. Strain, O. Farkas, J. Tomasi, V. Barone, M. Cossi, R. Cammi, B. Mennucci, C. Pomelli, C. Adamo, S. Clifford, J. Ochterski, G. A. Petersson, P. Y. Ayala, Q. Cui, K. Morokuma, D. K. Malick, A. D. Rabuck, K. Raghavachari, J. B. Foresman, J. Cioslowski, J. V. Ortiz, B. B. Stefanov, G. Liu, A. Liashenko, P. Piskorz, I. Komaromi, R. Gomperts, R. L. Martin, D. J. Fox, T. Keith, M. A. Al-Laham, C. Y. Peng, A. Nanayakkara, C. Gonzalez, M. Challacombe, P. M. W. Gill, B. G. Johnson, W. Chen, M. W. Wong, J. L. Andres, M. Head-Gordon, E. S. Replogle, J. A. Pople, Gaussian, Inc., Pittsburgh, PA, **1998**.
[18] a) A. D. Becke, *Phys. Rev. B* **1988**, *38*, 3098; b) C. Lee, W. Yang, R. G. Parr, *Phys. Rev. B* **1988**, *37*, 785; c) P. J. Stevens, F. J. Devlin, C. F. Chabalowski, M. J. Frisch, *J. Phys. Chem.* **1994**, *98*, 11623–11627.
[19] J. Tomasi, B. Mennucci, E. Cancès, *J. Mol. Struct. (Theochem)* **1999**, *464*, 211–226.

 © 2006 Wiley-VCH Verlag GmbH & Co. KGaA, Weinheim

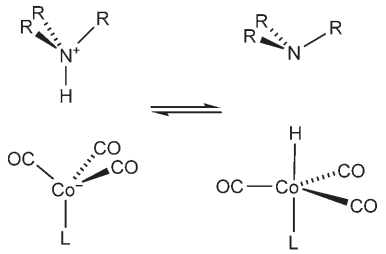
Coordination Modes

DOI: 10.1002/anie.200503597

Polyhedral Interconversion Coupled with Proton Transfer between an Ammonium Cation and the $[Co(CO)_4]^-$ Ion**

*David Casanova, Pere Alemany, and Santiago Alvarez**

Proton transfer between ammonium cations and $[CoL(CO)_3]^-$ ions (L = CO, PR_3) has been illustrated by Brammer et al.[1] through a series of crystal structures according to the structure-correlation principle, which states that "if a correlation can be found between two or more independent parameters describing the structure of a given fragment in a variety of environments, then the correlation function maps a minimum energy path in the corresponding parameter space".[2] The two ends of the proton transfer reaction correspond to an ionic pair formed by an ammonium cation and the $[CoL(CO)_3]^-$ ion (**1a**) and independent amine



1a **1b**

and hydrido carbonyl complexes **1b**. The structures analyzed by Brammer et al. correspond to compounds with N–H···Co hydrogen bonds, a behavior consistent with the acidity of the hydrido carbonyl complex in water.[3] According to the structure-correlation principle, the variety of H···Co distances found (between 2.63 Å for a N–H···Co hydrogen-bonded species and 1.43 Å for the hydrido complex) should correspond to snapshots along the proton-transfer reaction coordinate. Since the coordination spheres of both the N and Co atoms are significantly affected by the progress of the proton-transfer reaction, these systems provide an excellent opportunity to test the applicability of the polyhedral-shape measures as reaction coordinates and to correlate the potential-energy surface with the structural evolution. Therefore, the aim of this communication is to show how DFT calculations provide an energy profile for such a reaction that accounts for the fine details of the distribution of structures along the path and how the proton transfer is coupled to changes in the coordination polyhedra of the N and Co atoms. An outcome of this study is that the energy and the stereochemical changes that accompany the proton transfer can be described as a function of a single parameter, the generalized polyhedral-interconversion coordinate[4] for the transformation of a $[CoL(CO)_3]^-$ (L = ligand) tetrahedron into a vacant trigonal bipyramid.

To represent the general case of an ammonium cation, we took the NH_4^+ ion as the simplest example, whereas the family of the $[CoL(CO)_3]^-$ ions was represented in our calculations by the $[Co(CO)_4]^-$ ion. To explore the potential-energy surface, we calculated a linear-transit reaction coordinate for the $NH_4{\cdot}[CoL(CO)_3]$ aggregate keeping the Co···H distance fixed and optimizing the rest of the geometry.[5] The two minima and one maximum obtained were fully optimized and could be characterized as stationary points on the potential-energy surface through frequency analysis (geometries and frequencies for the three stationary points are provided in the Supporting Information). The two minima correspond to the two alternative hydrogen-bonding situations: a) N–H···Co, referred to herein as the ion pair, to avoid confusion with the second minimum, and b) N···H–Co, which we term the hydrogen-bonded complex. The maximum corresponds to a transition state with a delocalized hydrogen bond of the type N···H···Co. The isolated fragments $[Co(CO)_4]^-$, NH_4^+, NH_3, and $[HCo(CO)_4]$ were also optimized. The optimized structures are shown in Figure 1, those of the cobalt complexes are in good agreement with the experimentally determined structures for $[HCo(CO)_4]$[6] and a variety of salts of the $[Co(CO)_4]^-$ ion, as found in a structural database search.[7]

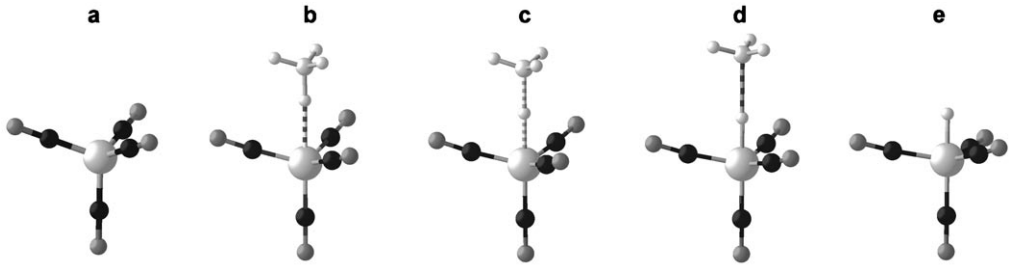
The changes in the coordination spheres of the N and Co atoms can be monitored by using continuous-shape measures (CShM).[8,9] In short, a shape measure is a dimensionless continuous function that calibrates the degree of distortion of a set of atoms from a predetermined shape (typically a polyhedron), thus yielding zero for those structures that exactly match the reference shape and increasingly higher values as the distortions are more pronounced. As a rule of thumb, small but chemically significant distortions give shape measures of the order of 0.1 units, whereas values of 1 unit or more indicate important-to-severe distortions. In Figure 2, we represent the evolution of different shape measures as a function of the Co···H distance: 1) that of the NH_3 group relative to a vacant tetrahedron and those of the $\{Co(CO)_4\}$ fragment relative to 2) the tetrahedron and 3) the vacant trigonal bipyramid (a trigonal bipyramid with one axial ligand missing, termed vTBP herein). The stereochemistry around the Co atom, which is perfectly tetrahedral at the early stages of the reaction (Co···H ≈ 2.4 Å), is gradually distorted as the

[*] D. Casanova, Prof. S. Alvarez
Departament de Química Inorgànica and
Centre de Recerca en Química Teòrica
Universitat de Barcelona
Martí i Franquès 1–11, 08028 Barcelona (Spain)
Fax: (+34) 93-4907725
E-mail: santiago.alvarez@qi.ub.es
Dr. P. Alemany
Departament de Química Física and
Centre de Recerca en Química Teòrica
Universitat de Barcelona (Spain)

[**] Work supported by the Dirección General de Investigación (MCyT), projects CTQ2005-08123-C02-01/BQU, and –02/BQU.

Supporting information for this article is available on the WWW under http://www.angewandte.org or from the author.

 © 2006 Wiley-VCH Verlag GmbH & Co. KGaA, Weinheim



	a	b	c	d	e
$\varphi(T_d$–vTBP)	0 %	22 %	34 %	42 %	54 %
Co···H (Å)	-	2.09	1.70	1.52	1.49
N···H (Å)	-	1.12	1.49	2.09	-

Figure 1. Structures along the path for proton transfer between the NH_4^+ and $[Co(CO)_4]^-$ moieties: a) Isolated $[Co(CO)_4]^-$ ion, b) ion pair with an N–H···Co bond, c) transition state, d) hydrogen-bonded species with N···H–Co bond, and e) isolated $[HCo(CO)_4]$. The generalized coordinates along the interconversion path from the tetrahedron to the vTBP, $\varphi(T_d$–vTBP), are given alongside each optimized structure.

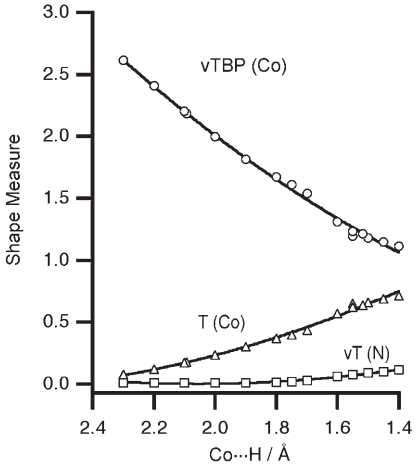


Figure 2. Evolution of the polyhedral measures of the N and Co coordination spheres along the proton-transfer reaction, vacant tetrahedron (vT) for NH_3 (squares), tetrahedron (T; triangles), and vacant trigonal bipyramid (vTBP; circles) for the $\{Co(CO)_4\}$ fragment.

ammonium cation approaches, and such a loss of tetrahedricity is seen to correlate with a tendency to adopt a vTBP geometry. However, the final product of the proton transfer, $[HCo(CO)_4]$, is still far from being a perfect trigonal bipyramid, according to the nonzero value of the CShM of its $\{Co(CO)_4\}$ fragment relative to the vTBP, in good agreement with its experimental structure (calculated and experimental C_{ax}-Co-C_{eq} bond angles of 105 and 99°, respectively). The stereochemistry around the N atom, in contrast, varies very little at the early stages of the reaction, remaining nearly tetrahedral even at Co···H: 2.1 Å, the equilibrium geometry for the N–H···Co bonded ion pair. At Co···H distances of 1.8 Å or shorter, though, that shape measure increases gradually, thus reflecting the loss of the proton and the adjustment of the remaining H–N–H bond angles to the pyramidal geometry of ammonia. The rather small changes in shape measures of the NH_3 fragment relative to those experienced by the $\{Co(CO)_4\}$ unit reflects their different degree of geometrical change: while bond angles vary from 109.5° in NH_4^+ to 115.5° in NH_3, the C_{ax}-Co-C_{eq} bond angles change from 109.5° in $[Co(CO)_4]^-$ to 99.1° in $[CoH(CO)_4]$.

Not only are the shape measures correlated to the Co···H distance along the reaction path, but it is also seen that all the points in our linear transit pathway have shape measures for the $\{Co(CO)_4\}$ fragment that correspond to the minimal-distortion interconversion path between the tetrahedron and the vTBP according to the very small values of the path-deviation function.[10] For that reason, we can describe the proton-transfer reaction by means of the generalized reaction coordinate[4] that corresponds to the conversion of a $\{Co(CO)_4\}$ tetrahedron into a vTBP (Figure 3). Using such a coordinate, the independent reactants are represented by 0 % of the polyhedral path, as the isolated $[Co(CO)_4]^-$ ion is perfectly tetrahedral. One hundred percent of the reaction coordinate would correspond to a vTBP shape for the $\{Co(CO)_4\}$ fragment. However, the products of the reaction, represented by the position of $[HCo(CO)_4]$ along the reaction coordinate, appear at 54 % of the polyhedral-interconversion

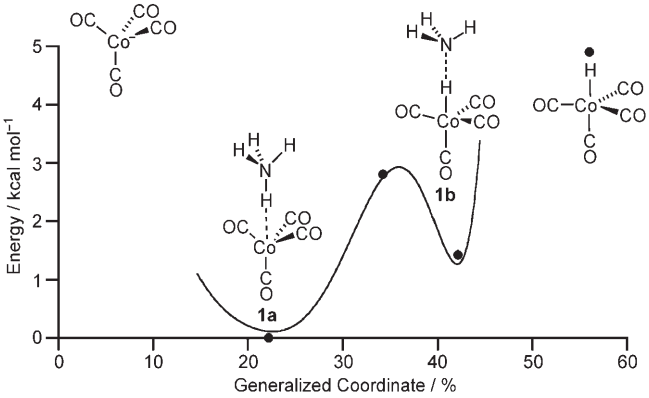


Figure 3. Calculated energy (gas phase) for the $NH_4{\cdot}[Co(CO)_4]$ composite along the proton-transfer path, as a function of the generalized coordinate for the polyhedral rearrangement of the $\{Co(CO)_4\}$ fragment from a tetrahedral to vTBP shape. The continuous line represents the points along the linear transit pathway, the circles correspond to stationary points.

 © 2006 Wiley-VCH Verlag GmbH & Co. KGaA, Weinheim

path, as the hydrido carbonyl complex does not reach the trigonal bipyramidal shape (Figure 1e). In-between, we can see that the ion pair with N–H···Co bonding appears at 22%, the transition state at 35%, and the N···H-Co hydrogen-bonded complex at 42% of the polyhedral transformation around the Co atom. It is worth noting that the isolated $[HCo(CO)_4]$ complex is closer (54% of the path) to the vTBP than when hydrogen bonded (42%).

If we look now at the relative energies of the stationary points along the reaction path in the gas phase (relative energies at the B3LYP and CCSD(T) levels are given in the Supporting Information), we notice that the ion pair **1a** is much more stable than the independent ions (93 kcal mol^{-1}), the hydrogen-bonded species **1b** is nearly isoenergetic with **1a**, and the barrier for the proton transfer is about 2 kcal mol^{-1}. The dissociation of the hydrogen-bonded species into the two neutral molecules is calculated to cost some 3 kcal mol^{-1}. The fact that the ionicity of the species involved changes along the proton-transfer process made us worry about the effect of solvents of different polarities on the energy profile. Single-point calculations at the geometries optimized for the gas phase were carried out at the B3LYP level with the polarizable continuum model (PCM) approach, using dielectric constants that correspond to water, CH_2Cl_2, and CH_3Cl (energy profiles provided in the Supporting Information). As expected, the ionic forms are increasingly stabilized as the polarity of the solvent increases to the point that the independent ions become more stable than the ion pair **1a** for the case of water (by 2.5 kcal mol^{-1}). As a result, both the hydrogen-bonded species **1b** and the independent neutral molecules become unstable relative to the ion pair in the three solvents tested by more than 10 kcal mol^{-1}. Notice that the PCM model does not take into account possible bonding interactions between solvent molecules and the species that participate in the reaction, such as hydrogen bonding or weak coordination. Therefore, the energy profile given herein should not be taken as a quantitative representation of the corresponding proton-transfer reaction in solution.

Once we have a simple and clear description of the stereochemistry and the energetics of this proton-transfer process, we can go back to the structural correlation based on experimental distances and angles proposed by Brammer et al.[11] To that end, our theoretical results and some related experimental data plotted on shape maps are shown side by side in Figure 4.[9] There, the lower continuous line represents the minimal-distortion interconversion path between the tetrahedron and the vTBP; its two extremes correspond to these two ideal figures. All calculated points, both the optimized geometries (Figure 4, left) and the structures of the linear-transit reaction coordinate, are seen to follow the minimal distortion path.

The experimental structural data for the ternary ammonium salts of the $[Co(CO)_4]^-$ ion (Figure 4, right) are found in the shape map between the position predicted by calculations for the isolated anion and that of the ion pair, thus reflecting the shallowness of the potential well around the latter and the presence of steric hindrance in some cases that keeps the Co and N atoms at a relatively long distance (e.g., Co···H: 2.73 Å

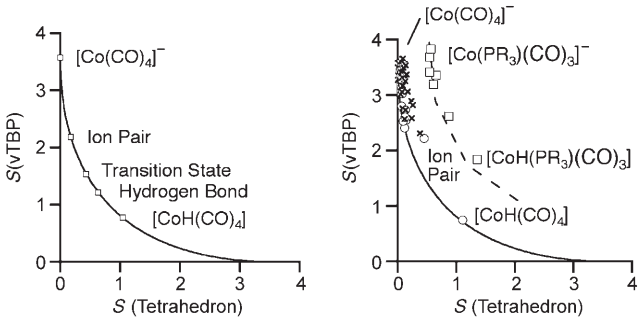
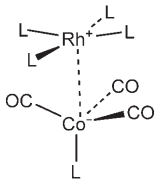


Figure 4. Calculated (left) and experimental (right) data on shape maps for tetracoordinate fragments in the tetrahedron–vTBP space, thus showing the minimal-distortion interconversion path (continuous line), and a distortion path with the axial ligand at a longer distance ($d'/d = 1.27$) than the rest (dashed line in the right-hand-side plot). The theoretical data plotted are those of the optimized structures (left, squares). The experimental X-ray structural data shown (right) are those of the ternary ammonium salts of the $[Co(CO)_4]^-$ ion (circles), other salts of the same anion (crosses), $[HCo(CO)_4]$ and the phosphine substituted analogues, $[Co(PR_3)(CO)_3]^-$ and $[HCo(PR_3)(CO)_3]$ (squares).

for the quinuclidinium salt[11]). The fact that all structurally characterized ammonium salts of the cobalt carbonylate present the ion-pair structure **1a**, while no hydrido carbonyl complex seems to exist in the presence of an amine, is consistent with our finding that the hydrido carbonyl complex is stable in the presence of an amine only in the gas phase. The experimental gas-phase structure of $[HCo(CO)_4]$ also occupies the position predicted along the minimal polyhedral distortion path. The absence of experimental structures in the region that corresponds to the transition state completes a rather accurate cross-section of the potential-energy surface.

If we include the structures of salts of the same carbonylate anion with other cations in the shape map, we find them aligned along the expected reaction path as well. As the countercations in those cases are not proton donors, it is surprising at first sight to find such significant deviations of the $[Co(CO)_4]^-$ ion from the tetrahedron. Let us focus on the most extreme case to illustrate the usefulness of the shape map, that of a structure practically at the same position in which we find the ion pair with the shortest hydrogen bond: this structure corresponds to a carbonylate of the square planar $[Rh(CNR)_4]^+$ ion.[12] Since hydrogen bonding must be precluded in this case, the shape measures suggest that some sort of interaction between the two ions may drive the distortion of the tetrahedral carbonylate toward a trigonal bipyramid, as confirmed by a relatively short Co···Rh distance of 3.38 Å and a significant distortion of the Rh coordination sphere from square planar toward a square pyramid **2**. In other words, the rhodium center of the cationic complex is a Lewis acid that plays the role of the proton in the ammonium salts. Precedents of d^8 square-planar metals that act as Lewis acids are known,[13] and the existence of bonding that is as weak as the Co···Rh interaction found herein and the corresponding pyramidali-



2

 © 2006 Wiley-VCH Verlag GmbH & Co. KGaA, Weinheim

zation of the metal coordination sphere have been explained with molecular-orbital arguments.

To show how the use of shape maps can provide further insight into the details of reaction pathways through structural correlations, we have separately analyzed the families of $[Co(PR_3)(CO)_3]^-$ and $[Co(PR_3)_4]^-$ ions. The former were included by Brammer et al. in the structural correlation of the cobalt carbonylate discussed above. The position of the mixed ligand complexes in the shape map (Figure 4, right, squares) shows that they follow a pathway parallel to the minimal distortion path as a result of the differences between Co–C and Co–P bond lengths with a product of the proton-transfer reaction, $[CoH(PR_3)(CO)_3]$, thus also presenting a geometry that is about halfway in the direction of the trigonal bipyramid. These similarities confirm the validity of the proposal of a common structural correlation for the two families of molecules at the qualitative level. Full substitution of carbonyls by phosphines in the $[Co(PR_3)_4]^-$ ions (not shown in Figure 4 for simplicity; see the Supporting Information) should bring us back to the minimal-distortion path, as all the bonds of the analyzed $\{CoP_4\}$ polyhedral fragment are practically identical. Even if no such anions have been structurally characterized, there is one hydrido derivative $[CoH(PR_3)_4]$[14] that appears right along the minimal distortion pathway. Analogous hydrido complexes with tripod tetradentate ligands present geometries much closer to the trigonal bipyramid,[15] as the tripod ligand enforces P_{axial}-Co-$P_{equatorial}$ bond angles much closer to 90°. The fact that the homoleptic phosphine complexes go back to the same path of the homoleptic carbonyl ones confirms that the changes in the reaction path upon substitution in the heteroleptic complexes are because of an asymmetric substitution pattern.

In summary, the present study of the proton transfer reaction between an ammonium cation and a cobalt carbonylate shows that the evolution of the polyhedral shape measure of the $\{Co(CO)_4\}$ fragment along the reaction path can be used as a reaction coordinate. Changes in bond distances and angles and the potential energy of the system can be adequately described by this reaction coordinate. The geometries of experimental structures of families of compounds with the general formulae $[Co(CO)_4]^-$, $[Co(PR_3)(CO)_3]^-$, $[CoH(CO)_4]$, $[CoH(PR_3)(CO)_3]$, and $[CoH(PR_3)_4]$ offer snapshots of the low-energy regions of the potential-energy surface for the proton-transfer reaction in the gas phase. Furthermore, there is a good correspondence between the optimized structures of the species that participate in this reaction and those found experimentally, thus providing an excellent illustration of the structure-correlation principle. Paradoxally, the proton-transfer reaction seems to be disfavored in solution and only the ion pair or the dissociated ions are expected to exist depending on the polarity of the solvent used.[16]

Received: October 11, 2005
Published online: January 20, 2006

Keywords: cobalt · continuous shape measures · coordination modes · proton transfer · reaction coordinates

[1] L. Brammer, J. C. Mareque Rivas, C. D. Spilling, *J. Organomet. Chem.* **2000**, *609*, 36.
[2] H.-B. Bürgi in *Perspectives in Coordination Chemistry* (Eds.: A. F. Williams, C. Floriani, A. E. Meerbach), Verlag Helvetica Chimica Acta, Basel, **1992**; H.-B. Bürgi, *Acta Crystallogr. Sect. A* **1998**, *54*, 873; P. Murray-Rust, H.-B. Bürgi, J. D. Dunitz, *J. Am. Chem. Soc.* **1975**, *97*, 921; H.-B. Bürgi, J. D. Dunitz, *Structure Correlations*, VCH, Weinheim, **1994**.
[3] W. Hieber, E. Lindner, *Chem. Ber.* **1961**, *94*, 1417.
[4] J. Cirera, S. Alvarez, *Chem. Eur. J.*, in press.
[5] DFT calculations at the B3LYP level were performed using the Ahlrichs triple-ζ all-electron basis set with two p-polarization functions at the Co atom. Interaction energies were corrected for the basis-set superposition error by means of the counterpoise method. All calculations were performed with the Gaussian package (Gaussian 03 Revision B.4), M. J. Frisch et al., Gaussian, Inc., Pittsburgh, PA, **2003**). Single-point calculations on the B3LYP-optimized geometries at the CCSD(T) level were also carried out (see the Supporting Information).
[6] E. A. McNeill, F. R. Scholer, *J. Am. Chem. Soc.* **1977**, *99*, 6243.
[7] Structural searches were carried out in the Cambridge Structural Database (F. H. Allen, O. Kennard, *Chem. Des. Autom. News* **1993**, *8*, 31), version 5.26.
[8] H. Zabrodsky, S. Peleg, D. Avnir, *J. Am. Chem. Soc.* **1992**, *114*, 7843; D. Avnir, O. Katzenelson, S. Keinan, M. Pinsky, Y. Pinto, Y. Salomon, H. Zabrodsky Hel-Or in *Concepts in Chemistry: A Contemporary Challenge* (Ed.: D. H. Rouvray), Research Studies Press Ltd., Taunton, **1996**. All continuous shape measures and path-deviation functions reported herein were calculated with the *SHAPE* program (version 1.1): M. Llunell, D. Casanova, J. Cirera, J. M. Bofill, P. Alemany, S. Alvarez, M. Pinsky, D. Avnir, Barcelona, **2003**.
[9] S. Alvarez, P. Alemany, D. Casanova, J. Cirera, M. Llunell, D. Avnir, *Coord. Chem. Rev.* **2005**, *249*, 1693.
[10] D. Casanova, J. Cirera, M. Llunell, P. Alemany, D. Avnir, S. Alvarez, *J. Am. Chem. Soc.* **2005**, *127*, 1755.
[11] L. Brammer, J. C. Mareque Rivas, D. Zhao, *Inorg. Chem.* **1998**, *37*, 5512.
[12] I. Ojima, N. Clos, R. J. Donovan, P. Ingallina, *Organometallics* **1991**, *10*, 3211.
[13] G. Aullón, S. Alvarez, *Inorg. Chem.* **1996**, *35*, 3137.
[14] J. D. Crane, N. Young, *Acta Crystallogr. Sect. E* **2004**, *60*, m487.
[15] C. A. Ghilardi, S. Midollini, L. Sacconi, *Inorg. Chem.* **1975**, *14*, 1790; C. Bianchini, D. Masi, C. Mealli, A. Meli, M. Sabat, *Gazz. Chim. Ital.* **1986**, *116*, 201; A. Orlandini, L. Sacconi, *Cryst. Struct. Commun.* **1975**, *4*, 157; A. Orlandini, L. Sacconi, *Inorg. Chim. Acta* **1976**, *19*, 61.
[16] See the Supporting Information for optimized atomic coordinates and calculated vibrational spectra for $[Co(CO)_4]^-$, $[CoH(CO)_4]$, ion pair, and N···H–Co hydrogen-bonded species; calculated B3LYP and CCSD(T) energies of the stationary points of the B3LYP potential energy surface; shape measures and CSD reference codes for the experimental structures of $[Co(CO)_4]^-$, $[CoH(CO)_4]$, $[Co(PR_3)(CO)_3]^-$, $[CoH(PR_3)(CO)_3]$, and $[CoH(PR_3)_4]$ complexes; plot of the B3LYP energy profile in different solvents and at the CCSD(T) level in the gas phase.

 © 2006 Wiley-VCH Verlag GmbH & Co. KGaA, Weinheim

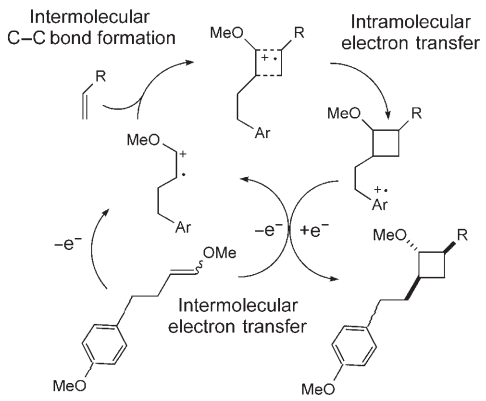
Electrochemistry

DOI: 10.1002/anie.200503656

Electrochemical Enol Ether/Olefin Cross-Metathesis in a Lithium Perchlorate/Nitromethane Electrolyte Solution**

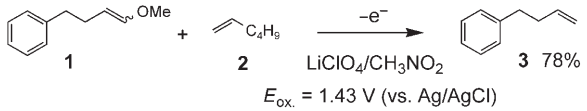
*Teppei Miura, Shokaku Kim, Yoshikazu Kitano, Masahiro Tada, and Kazuhiro Chiba**

Transition-metal-catalyzed olefin cross-metathesis plays an important role in the construction of various carbogenic skeletons by allowing the exchange of substituents between different olefins via an activated key intermediate consisting of a four-membered ring coordinated to a transition metal.[1] Alternatively, electrochemical reactions have proven to be a viable method in triggering reactions between different olefins by reversing the polarity of alkenes[2] and initiating radical anion-[3] (or cation-[4]) based reactions.[5] Electrochemically activated olefin cyclodimerization, for example, can effectively lead to the intermolecular formation of four-membered rings.[6] Moreover, we reported an electrocatalytic intermolecular formal [2+2] cross-coupling of electron-rich olefins (Scheme 1).[7] The anodic oxidation of enol ethers[8] that bear a methoxyphenyl group can be used to trigger an intermolecular formal [2+2] cycloaddition with varied alkenes. In this case, the intermolecular olefin coupling was assisted by a unique lithium perchlorate/nitromethane electrolyte solution[9] and the methoxyphenyl group of the substrates served as an intramolecular electron donor[10] to form the cyclobutane ring. Herein, we describe novel electrochemical olefin cross-metatheses between anodically activated enol ethers and aliphatic alkenes.



Scheme 1. Anodic intermolecular formal [2+2] cross-coupling of olefins.

Initially, the electrolytic intermolecular reaction between 4-methoxybut-3-enylbenzene (**1**) and hex-1-ene (**2**) was investigated. The anodic oxidation of enol ether **1** involved a carbon felt anode, a constant potential of 1.43 V (vs. Ag/AgCl), a carbon felt counter electrode, and a lithium perchlorate/nitromethane electrolyte solution (1.0 M) in an undivided cell under argon. Remarkably, the anodic activation of enol ether **1** in the presence of **2** resulted in the formation of but-3-enylbenzene (**3**) in 78% yield (Scheme 2).



Scheme 2. Electrochemical olefin cross-metathesis of 4-methoxybut-3-enylbenzene (**1**) and hex-1-ene (**2**) in lithium perchlorate/nitromethane electrolyte solution.

In our experiments, the reaction was deemed complete after the passage of approximately 1.0 F mole^{-1} of electricity. Under different electrolytic conditions, the desired product was obtained in trace or in unacceptable yields (Table 1). In the absence of electrolysis, a mixture of **1** and **2** in lithium perchlorate/nitromethane electrolyte solution at ambient temperature did not react, even after more than 10 h.

Table 1: Electrolytic cross-metathesis of 4-methoxybut-3-enylbenzene (**1**) and hex-1-ene (**2**) under different conditions.

Electrolyte	Solvent	Electricity [F mole^{-1}]	Yield (**3**)[a] [%]
$LiClO_4$	CH_3NO_2	1.0	78
$LiClO_4$	CH_3NO_2	0.5	40[b]
$LiClO_4$	CH_3NO_2	0.3	30[c]
$LiClO_4$	CH_3NO_2	0	n.d.[d]
Me_4NClO_4	CH_3NO_2	1.0	4
Bu_4NClO_4	CH_3NO_2	1.0	n.d.
Me_4NClO_4	CH_3CN	1.0	n.d.
$LiClO_4$	CH_3CN	1.0	3

[a] Yields were determined by gas chromatography (n.d. = not detected). [b] 38% of **1** was recovered. [c] 55% of **1** was recovered. [d] More than 99% of **1** was recovered.

Furthermore, the reaction was responsive to a stepwise application of the electricity. Because the amount of the product for each stage remained essentially unchanged during the intervals of electrolysis, an external switch of the electrolysis allows the regulation of the reaction process.

The electrochemical enol ether/olefin cross-metathesis can also be extended to the combination of simple alkyl enol ethers and alkenes. For example, anodic oxidation of 1-methoxy-tridec-1-ene (**4**) in the presence of **2** afforded the desired tridec-1-ene (**5**) in 76% yield (Scheme 3).

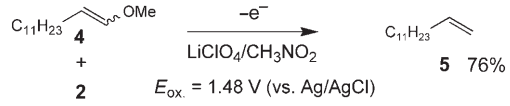
To gain insight into the reaction mechanism, the anodic activation of enol ether **1** was carried out with deuterium-

[*] T. Miura, Dr. S. Kim, Prof. Y. Kitano, Prof. M. Tada, Prof. K. Chiba
Laboratory of Bioorganic Chemistry
Tokyo University of Agriculture and Technology
3-5-8 Saiwai-cho, Fuchu, Tokyo 183-8509 (Japan)
Fax: (+81) 42-360-7167
E-mail: chiba@cc.tuat.ac.jp

[**] This work was partially supported by a Grant-in-Aid for Scientific Research from the Ministry of Education, Culture, Sports, Science, and Technology and the Japan Society for the Promotion of Science.

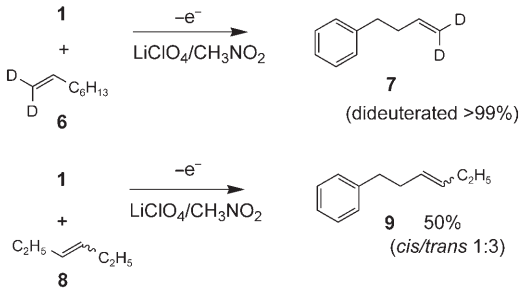
Supporting information for this article is available on the WWW under http://www.angewandte.org or from the author.

 © 2006 Wiley-VCH Verlag GmbH & Co. KGaA, Weinheim



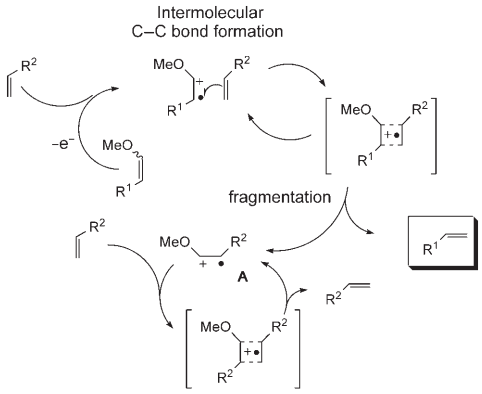
Scheme 3. Electrochemical olefin cross-metathesis between alkyl enol ether **4** and hex-1-ene (**2**).

labeled olefin **6** (Scheme 4). The formation of almost completely dideuterated product **7**[11] helped to verify our proposed cross-metathesis pathway. Moreover, under the same reaction conditions, an internal olefin, hex-3-ene (**8**), resulted in the carbon-chain-elongated product **9**.



Scheme 4. Electrochemical olefin cross-metathesis of enol ether **1** with deuterated olefin **6** or internal olefin **8**.

Notably, these electrochemical enol ether/olefin cross-metathesis reactions also give rise to a trace amount of the alternate fragment as the enol ether—for example, **4** was detected in the electrochemical reaction mixture of **1** and **5** along with main product **3**. Accordingly, a radical-cation-assisted fragmentation must have taken place to complete the formation of the metathesis products. The radical cation (fragment **A**) generated in situ from the enol ether could regenerate the radical cation of the starting enol ether by intermolecular electron transfer. On the other hand, the presence of a methoxyphenyl group should complete the formation of the corresponding four-membered ring. Except for specific enol ethers with neighboring oxidizable moieties that exhibit oxidation potentials of reasonable relative values, most enol ethers, however, should form the cross-metathesis products without completion of the intramolecular electron-transfer-assisted cyclobutane formation. In a cyclic voltammetry study, the anodic oxidation peak of **1** appeared at 1.43 V (vs. Ag/AgCl) with no cathodic peak.[12] The oxidation current of enol ether **1** was observed in the region 0.8–1.55 V (vs. Ag/AgCl). Anodic oxidation of the mixture of **1** and **2** in lithium perchlorate/nitromethane at around the lowest potential of the region (0.8–1.0 V vs. Ag/AgCl) also gave the desired product **3**. On the other hand, aliphatic alkene **2** in lithium perchlorate/nitromethane gave no clear oxidation peak in the region 0–1.6 V (vs. Ag/AgCl). The results suggest that cross-metathesis is initiated by anodic oxidation of the enol ether, followed by the formation of the key intermediate—a four-membered radical-cation ring—from the activated enol ether and alkene (Scheme 5).



Scheme 5. Proposed reaction mechanism of electrochemical olefin cross-metathesis.

In conclusion, anodic-oxidation triggers olefin cross-metathesis reactions between enol ethers and alkenes in a lithium perchlorate/nitromethane electrolyte solution. Intermolecular reactions allow the exchange of carbon fragments between even simple alkyl enol ethers and alkenes. Because the oxidation potentials of enol ethers are relatively low, the reaction may involve inter- and intramolecular enol ether/olefin cross-metathesis, thus avoiding overoxidation of substrates. In this reaction system, the synergistic effects of the electrochemical activation of the enol ether and the stabilization of the radical-cation intermediates in a suitable electrolyte solution should effectively help to form the active key intermediate. Efforts to expand the scope of this electrochemical methodology for the synthesis of various alkenes and to extend the work to intramolecular reactions are currently underway.

Received: October 15, 2005
Published online: January 27, 2006

Keywords: alkenes · electrochemistry · enol ethers · metathesis · oxidation

[1] For a Review of alkene cross-metathesis, see: S. J. Connon, S. Blechert, *Angew. Chem.* **2003**, *115*, 1944–1968; *Angew. Chem. Int. Ed.* **2003**, *42*, 1900–1923.
[2] a) K. D. Moeller, *Tetrahedron* **2000**, *56*, 9527–9554; b) J. B. Sperry, C. R. Whitehead, I. Ghiviriga, R. M. Walczak, D. L. Wright, *J. Org. Chem.* **2004**, *69*, 3726–3734; c) J. Mihelcic, K. D. Moeller, *J. Am. Chem. Soc.* **2004**, *126*, 9106–9111.
[3] For a review of electrolytic reductive coupling, see: M. F. Nielsen, J. H. P. Utley in *Organic Electrochemistry, 4th ed.* (Eds.: H. Lund, O. Hammerich), Marcel Dekker, New York, NY, **2001**, pp. 795–882.
[4] For a review of electrolytic oxidative coupling, see: H. J. Schaefer in *Organic Electrochemistry, 4th ed.* (Eds.: H. Lund, O. Hammerich), Marcel Dekker, New York, NY, **2001**, pp. 883–967.
[5] a) R. D. Little, K. D. Moeller, *Electrochem. Soc. Interface* **2002**, *11*, 36–42; b) R. D. Little, M. K. Schwaebe in *Electrochemistry VI: Electroorganic Synthesis: Bond Formation at Anode and Cathode, Topics in Current Chemistry 185* (Ed.: E. Steckhan) Springer, Berlin, **1997**, pp. 1–48; c) J. D. Anderson, M. M. Baizer, J. P. J. Petrovich, *Org. Chem.* **1966**, *31*, 3890–3897.

 © 2006 Wiley-VCH Verlag GmbH & Co. KGaA, Weinheim

[6] a) A. Ledwith, *Acc. Chem. Res.* **1972**, *5*, 133–139; b) J. Delaunay, G. Mabon, A. Orliac, J. Simonet, *Tetrahedron Lett.* **1990**, *31*, 667–668; c) J. Delaunary, A. Orliac, J. Simonet, *Tetrahedron Lett.* **1995**, *36*, 2083–2084; d) O. Fourets, P. Cauliez, J. Simonet, *Tetrahedron Lett.* **1998**, *39*, 565–566; e) R. G. Janssen, M. Motevalli, J. H. P. Utley, *Chem. Commun.* **1998**, 539–540.

[7] K. Chiba, T. Miura, S. Kim, Y. Kitano, M. Tada, *J. Am. Chem. Soc.* **2001**, *123*, 11314–11315.

[8] For related chemical oxidations to form enol ether radical cations, see: a) B. B. Snider, T. Kwon, *J. Org. Chem.* **1990**, *55*, 4786–4788; b) B. B. Snider, T. Kwon, *J. Org. Chem.* **1992**, *57*, 2399–2410; c) T. Fujii, T. Hirao, Y. Ohshiro, *Tetrahedron Lett.* **1992**, *33*, 5823–5826; d) A. Heidbreder, J. Mattay, *Tetrahedron Lett.* **1992**, *33*, 1973–1976; e) K. Ryter, T. Livinghouse, *J. Am. Chem. Soc.* **1998**, *120*, 2658–2659; f) M. Schmittel, A. Burghart, H. Werner, M. Laubender, R. Söllner, *J. Org. Chem.* **1999**, *64*, 3077–3085.

[9] a) K. Chiba, M. Tada, *J. Chem. Soc. Chem. Commun.* **1994**, 2485–2486; b) M. Ayerbe, F. P. Cossio, F. Kim, H. U. Euskal, D. San Sebastian, *Tetrahedron Lett.* **1995**, *36*, 4447–4450; c) C. Chapuis, A. Kucharska, P. Rzepecki, J. Jurczak, *Helv. Chim. Acta* **1998**, *81*, 2314–2325; d) R. Kumareswaran, P. S. Vankar, M. V. R. Reddy, S. V. Pitre, R. Roy, Y. D. Vankar, *Tetrahedron* **1999**, *55*, 1099–1110; e) S. Sankararaman, R. Sudha, *J. Org. Chem.* **1999**, *64*, 2155–2157.

[10] a) S. Duan, K. D. Moeller, *J. Am. Chem. Soc.* **2002**, *124*, 9368–9369; b) B. Marciniak, G. L. Hug, J. Rozwadowski, K. Bobrowski, *J. Am. Chem. Soc.* **1995**, *117*, 127–134.

[11] P. C. H. Eichinger, J. H. Bowie, R. N. Hayes, *J. Org. Chem.* **1987**, *52*, 5224–5228.

[12] Cyclic voltammograms and experimental details are provided in the Supporting Information.

 © 2006 Wiley-VCH Verlag GmbH & Co. KGaA, Weinheim

Homogeneous Catalysis

DOI: 10.1002/anie.200503885

Asymmetric Intramolecular Crossed-Benzoin Reactions by N-Heterocyclic Carbene Catalysis**

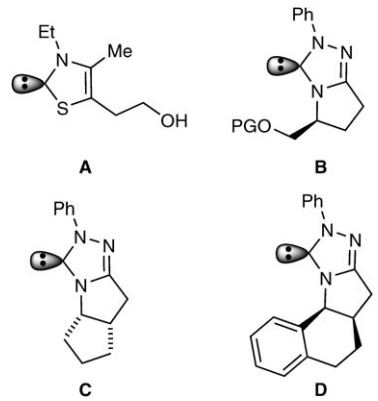
Dieter Enders, Oliver Niemeier, and Tim Balensiefer*

The discovery of stable carbenes in the last decade of the 20th century[1] has brought about extensive research on the chemistry of N-heterocyclic carbenes. With respect to the biochemistry of the coenzyme thiamine (vitamin B_1, a natural thiazolium salt), where the catalytically active species has been proposed to be a carbene, investigations on N-heterocyclic carbenes focussed on the catalysis of organic reactions[2] side by side with their use as ligands for organometallic chemistry.[3]

The powerful catalytic capacities of N-heterocyclic carbenes have been demonstrated by new organocatalytic transformations, for example, conjugate nucleophilic acylations,[4] transesterifications,[5] and polymerizations.[6] Great efforts have been made to conduct carbene-catalyzed reactions in an enantioselective way, and the 21st century has already witnessed remarkable achievements, such as, the efficient enantioselective benzoin condensation,[7] the asymmetric intramolecular Stetter reaction,[8] and the stereoselective intermolecular aldehyde-imine cross-coupling.[9]

The crossed-benzoin reaction also belongs to the family of nucleophilic acylation reactions. Chemoselectivity and stereocontrol were first reached with the thiamine-dependent enzyme benzoylformate decarboxylase that linked various, mostly aromatic, aldehydes to acetaldehyde to form the corresponding 2-hydroxy ketones.[10] Synthetic thiazolium salts developed by Stetter and co-workers, and similar to thiamine itself,[11] have been used successfully by Suzuki and co-workers for the first intramolecular crossed-aldehyde-ketone benzoin reactions in the course of an elegant natural product synthesis.[12] Stereocontrol was exerted by preexisting stereocenters in these specific substrates—the catalysts being achiral.

As it was highly desirable to develop a general protocol for the intramolecular benzoin reaction, we started investigations on simple aldehyde-ketones as substrates for the carbene-catalyzed intramolecular crossed-benzoin condensation. We were able to show that various five- and six-membered cyclic acyloins could be obtained in moderate to good yields by employing a commercially available thiazolium salt as precatalyst and 1,8-diazabicyclo[5.4.0]undec-7-ene (DBU) or triethylamine as the base to generate the carbene (**A**, Scheme 1).[13] Synchronously to our report, Suzuki and co-workers published similar results emphasizing that the competing intramolecular aldol reaction could be suppressed when a substoichiometric amount of base was employed relative to the precatalyst.[14]



Scheme 1. Carbenes derived from thiazolium and triazolium salts. PG = protecting group.

[*] Prof. Dr. D. Enders, Dipl.-Chem. O. Niemeier, Dipl.-Chem. T. Balensiefer
Institute of Organic Chemistry
RWTH Aachen University
Landoltweg 1, 52074 Aachen (Germany)
Fax: (+49) 241-8092127
E-mail: enders@rwth-aachen.de

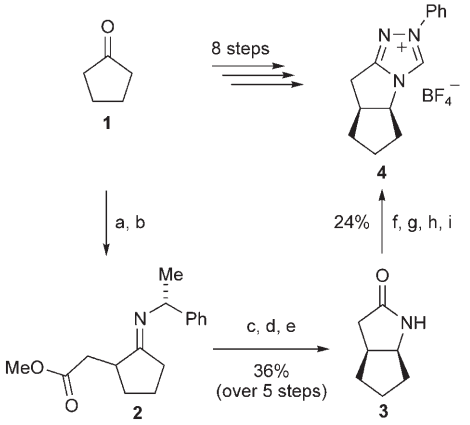
[**] This work was supported by the Deutsche Forschungsgemeinschaft (Schwerpunktprogramm Organokatalyse) and the Fonds der Chemischen Industrie. We thank Degussa AG, BASF AG, Bayer AG, and Wacker Chemie for the donation of chemicals.

© 2006 Wiley-VCH Verlag GmbH & Co. KGaA, Weinheim

With the crossed intramolecular aldehyde-ketone benzoin condensation thus established as a synthetic method, we continued our research to further optimize the reaction and to devise an enantioselective variant. We report herein the synthesis of various novel enantiopure polycyclic triazolium salts and their application as efficient chiral N-heterocyclic carbene catalysts of type **B**–**D** (Scheme 1) for the first enantioselective intramolecular crossed-benzoin reaction creating a quaternary stereocenter.[15]

Unfortunately the bicyclic triazolium salt that had successfully been used in our research group for the enantioselective intermolecular benzoin condensation[7] did not show any catalytic activity in the intramolecular reaction. We thus searched for alternative, easily accessible enantiopure polycyclic γ-lactams as precursors for the synthesis of novel triazolium salts. The rigid polycyclic structure of the catalysts should allow for high asymmetric inductions in catalysis.

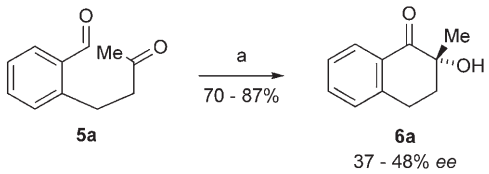
A first target was found in the *cis*-bicyclic lactam **3** which was obtained in a diastereo- and enantioselective manner in five steps starting from cyclopentanone (**1**) in 36% yield following a modified procedure developed by Omar and Frahm (Scheme 2).[16] After α-alkylation of **1** with methyl



Scheme 2. Preparation of the tricyclic triazolium salt **4**. a) LDA, $BrCH_2CO_2Me$, THF, DMPU, −78 °C to RT, 18 h; b) (*R*)-phenethylamine, cyclohexane, 4-Å molecular sieves, room temperature, 72 h; c) Raney Ni/H_2 (20 bar), EtOH, room temperature, 16 h; d) 3 N NaOH, MeOH, room temperature, 1 h; e) Li, liq. NH_3, THF/*t*BuOH (9:1), −78 °C, 20 min; f) Me_3OBF_4, CH_2Cl_2, room temperature, 24 h; g) $PhNHNH_2$, THF, 80 °C, 3 h; h) HBF_4/Et_2O, CH_2Cl_2, room temperature, 30 min; i) $HC(OMe)_3$, MeOH, 80 °C, 12 h. LDA = lithium diisopropylamide, DMPU = 1,3-dimethylhexahydro-2-pyrimidone.

bromoacetate and subsequent condensation with (*R*)-phenethylamine, the resulting imine **2** was diastereoselectively hydrogenated, cyclized, and deprotected to give lactam **3**. The *cis*-tricyclic triazolium salt **4** was then obtained as a solid in 24% yield by a modified three-step procedure reported by Knight and Leeper.[17]

The asymmetric intramolecular benzoin condensation with model substrate **5a** and the chiral triazolium salt **4** as precatalyst gave rise to the desired acyloin **6a** in good yields by utilizing toluene as solvent and DBU or KO*t*Bu as the base (Scheme 3). Unfortunately only moderate enantiomeric excess (37–48%) could be achieved, even at 5 °C (Table 1).



5a **6a**
37 - 48% *ee*

Scheme 3. First investigations with model substrate **5a**. a) **4**, base, toluene (0.1 M).

Table 1: Asymmetric intramolecular crossed-benzoin reaction with **4**.

4 [mol%]	Base (mol%)	*t* [h]	*T*	Yield [%]	*ee* [%][a] (config.)[b]
10	DBU (10)	3	RT	76	38 (*R*)
10	KO*t*Bu (10)	3	RT	87	37 (*R*)
20	DBU (20)	24	5 °C	70	48 (*R*)

[a] Determined by HPLC with a chiral stationary phase (Daicel Chiralpak AD). [b] Based on the measured optical rotation value in comparison with the literature data.[18]

Two different concepts were chosen to increase the steric demand of the carbene catalysts and thus increase the asymmetric induction. A triazolium salt synthesis starting from L-pyroglutamic acid (**7**), which is among the cheapest chiral sources available, might generate an extremely flexible catalyst system. Furthermore, the promising results with precatalyst **4** showed that modifications of this structure could also be fruitful.

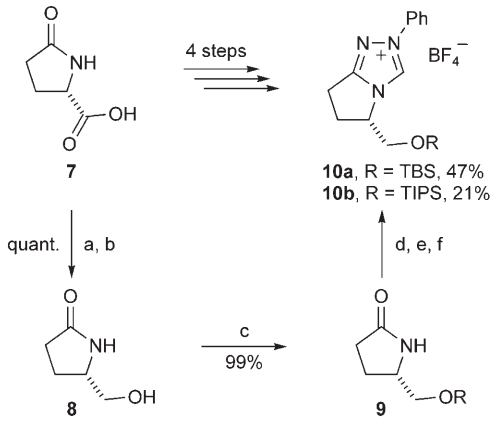
The *tert*-butyldimethylsilyl (TBS) and triisopropylsilyl (TIPS) protected lactams **9** could be synthesized in almost quantitative yields from L-pyroglutamic acid (**7**) by reduction to the hydroxymethyl-substituted lactam **8** and subsequent reaction with the silyl chlorides.[19] The bulkiness at the stereogenic center might be modified by a simple exchange of the protecting group. Conversion into the triazolium salts could be achieved by following an optimized one-pot procedure recently reported by Rovis and co-workers.[20] The lactams **9** were methylated with Meerwein's reagent to form the corresponding amidates. These were treated in situ with phenylhydrazine to yield the hydrazonium salts, which were directly cyclized with trimethyl orthoformate in methanol to give the triazolium salts **10** in moderate yields as crystalline solids (Scheme 4).

For the structural optimization of the tricyclic triazolium salt **4** the *cis*-tricyclic lactam **13** was chosen as the precursor for the synthesis of the tetracyclic triazolium salt **14**. The diastereo- and enantiopure γ-lactam **13** was synthesized following a procedure reported by Ennis et al. (Scheme 5).[21]

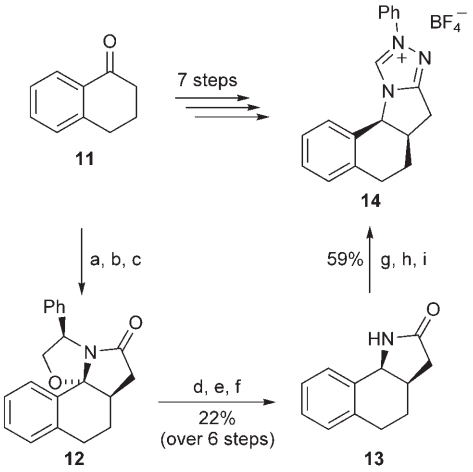
α-Tetralone (**11**) was α-alkylated with ethyl bromoacetate and subsequently hydrolyzed to the corresponding carboxylic acid. Condensation with (*R*)-phenylglycinol yielded the lactam **12** as a single stereoisomer. Stereoselective reduction, dehydration of the alcohol, and acid-catalyzed enamine hydrolysis provided the *cis*-tricyclic lactam **13**. The one-pot procedure that had previously been successful in the synthesis of **10** also gave access to the chiral tetracyclic triazolium salt **14**, which was obtained as a solid in 59% yield.

With these novel chiral carbene precursors in hand, several aldehyde ketones **5a**–**e** could be transformed into

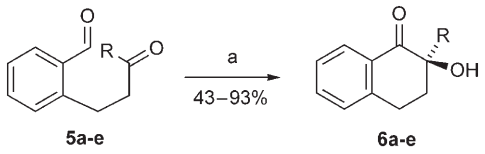
 © 2006 Wiley-VCH Verlag GmbH & Co. KGaA, Weinheim



Scheme 4. Preparation of triazolium salts **10** derived from pyroglutamic acid. a) $SOCl_2$, MeOH, −15 °C, 2 h; b) $NaBH_4$, EtOH, 0 °C, 12 h; c) RCl, imidazole, DMF, room temperature, 20 h; d) Me_3OBF_4, CH_2Cl_2, room temperature, 3 h; e) $PhNHNH_2$, CH_2Cl_2, room temperature, 3 h; f) $HC(OMe)_3$, MeOH, 80 °C, 12 h.



Scheme 5. Preparation of the tetracyclic triazolium salt **14**. a) LDA, $BrCH_2CO_2Et$, THF, DMPU, −78 °C to RT, 18 h; b) $LiOH{\cdot}H_2O$, THF/H_2O (2:1), room temperature, 20 h; c) (*R*)-phenylglycinol, toluene, 4-Å molecular sieves, reflux, 20 h; d) Et_3SiH, $TiCl_4$, CH_2Cl_2, −78 °C to RT, 3 h; e) $LiOH{\cdot}H_2O$, DMSO, 140 °C, 72 h; f) 1 N HCl, THF, reflux, 8 h; g) Me_3OBF_4, CH_2Cl_2, room temperature, 3 h; h) $PhNHNH_2$, CH_2Cl_2, room temperature, 3 h; i) $HC(OMe)_3$, MeOH, 80 °C, 12 h.



Scheme 6. Asymmetric intramolecular crossed-benzoin reaction with substrates **5a–e**. a) Precatalyst **10** or **14**, solvent (0.1 M), base, 1 day.

the corresponding six-membered acyloins **6a–e** (Scheme 6, Table 2).

The use of 10 mol% of the TBS-substituted catalyst **10a** and stoichiometric amounts of DBU in toluene at room temperature enabled the methyl-substituted acyloin **6a** to be obtained in high yield (92%) but with only moderate enantioselectivity (61%). Application of the TIPS-substituted catalyst **10b** under the same conditions resulted in an increased enantiomeric excess of 77%, which could be further improved to 84% with almost unchanged yields by performing the reaction at 5 °C.

The reactions with the tetracyclic catalyst **14** were conducted in THF for better solubility. Furthermore, DBU was found to cause side reactions which could be suppressed when KO*t*Bu was used in substoichiometric amounts (9 mol%). Product **6a** could be obtained in high yield (93%) with an excellent enantiomeric excess of 94%. Attempts to increase the *ee* value further by performing the reaction at 5 °C gave only very low conversion even after five days, presumably because of the low activity of the catalyst at this temperature.

The increased steric demand at the ketone function of the substrates **5** resulted in the reaction rate being much lower and reaction times of two days were necessary. Furthermore, higher catalyst loadings were required to achieve good conversions. We were pleased to see that the steric bulk of the ketone function had a significant influence on the enantiomeric excess, and almost complete inductions could be achieved. α-Hydroxy-α-ethyl tetralone (**6b**) was obtained with 95% *ee* and in still excellent yields. An excellent enantiomeric excess of 98% was obtained with the *n*-butyl- and *iso*-butyl-substituted substrates **5c**,**d**. The α-butyl-α-hydroxytetralone (**6c**) could be synthesized in excellent yields with only 10 mol% of the catalyst **14**. A significant decrease in the chemical yield, albeit with the enantiomeric excess remaining very good (93%), was observed when the benzyl-substituted aldehyde ketone **5e** was used.

In general, the TIPS-substituted triazolium salt **10b** derived from pyroglutamic acid delivered lower enantiomeric excess values than the tetracyclic carbene precursor **14**. However, the ease of its preparation and the low price of L-pyroglutamic acid also make it an attractive catalyst. Reaction times are less than catalyses performed with **14**, and the reaction can be performed at 5 °C for better enantioselectivity.

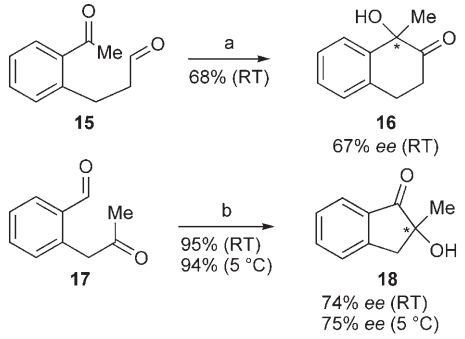
Table 2: Asymmetric intramolecular crossed-benzoin reaction with **5**.

5	R	Catalyst (mol%)	Base (mol%)	*T*	Yield [%]	*ee* [%][a] (config.)[b]
a	Me	**10a** (10)[c]	DBU (10)	RT	92	61 (*S*)
a	Me	**10b** (10)[d]	DBU (10)	RT	89	77 (*S*)
a	Me	**10b** (10)[d]	DBU (10)	5 °C	90	84 (*S*)
a	Me	**14** (10)[c]	KO*t*Bu (9)	RT	93	94 (*S*)
b	Et	**14** (20)[c]	KO*t*Bu (19)	RT	90[e]	95 (*S*)
c	*n*Bu	**10b** (10)[d]	DBU (10)	RT	88	79 (*S*)
c	*n*Bu	**14** (10)[c]	KO*t*Bu (9)	RT	85[e]	98 (*S*)
d	*i*Bu	**14** (20)[c]	KO*t*Bu (19)	RT	91[e]	98 (*S*)
e	Bn	**10b** (10)[d]	DBU (10)	RT	90	63 (*R*)
e	Bn	**14** (20)[c]	KO*t*Bu (19)	RT	43[e]	93 (*R*)

[a] Determined by GC (Lipodex E) or HPLC (Daicel Chiralpak AD) with a chiral stationary phase. [b] Based on the measured optical rotation value in comparison with the literature data,[18] adaptation of computational calculations,[22] and assuming a uniform reaction mechanism. [c] Reaction in THF (0.1 M). [d] Reaction in toluene (0.1 M). [e] Reaction time 2 days.

© 2006 Wiley-VCH Verlag GmbH & Co. KGaA, Weinheim

Investigations to widen the scope of the asymmetric intramolecular benzoin reaction by utilizing aldehyde-ketone **15**, where the aldehyde and the ketone function are interchanged relative to **5**, show a promising 67% *ee* for the resulting acyloin **16** as well as high yields (68%). First experiments with substrate **17** to synthesize the five-membered cyclic acyloin **18** resulted in an excellent yield and a good enantiomeric excess (74%). When the reaction was carried out at 5°C, the enantiomeric excess could be slightly increased to 75% (Scheme 7).



Scheme 7. Further substrate scope for the asymmetric intramolecular crossed-benzoin reaction. a) **14** (20 mol%), KO*t*Bu (19 mol%), THF (0.1 M), room temperature, 4 days; b) **14** (10 mol%), KHMDS (10 mol%, 0.5 M in toluene), THF (0.1 M), 2 days. KHMDS = potassium hexamethyldisilazide.

The absolute configuration of the produced quarternary stereocenter of the acyloin **6a** was determined to be *S* by comparison of the measured optical rotation value with the corresponding literature data.[18] This stereochemical outcome might be explained by the transition state shown in Figure 1, which is an adaptation of the transition state

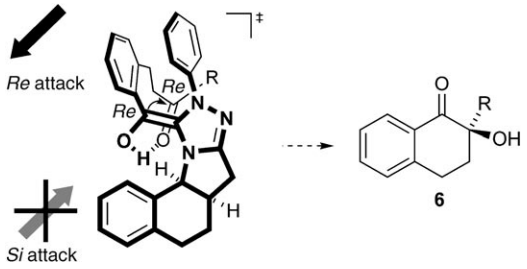


Figure 1. Proposed transition state.

proposed by Dudding and Houk on the basis of computational calculations.[22] The *Si* face of the Breslow intermediate,[23] which is formed as its *E* isomer in the hypothetical catalytic cycle, would be sterically shielded by the tetrahydronaphthalene residue of the tetracyclic catalyst. The *Re* face of the intermediate would attack the ketone function at its *Re* face (R ≠ Bn). Furthermore, a favorable pre-arrangement for the formation of the C–C bond might be caused by the activation of the ketone function by an intramolecular H bridge. Thus, the *S* configuration of the new stereocenter would be preferred, which in fact is observed.

In conclusion we have developed the first enantioselective intramolecular crossed-benzoin reaction catalyzed by novel chiral N-heterocyclic carbenes. The tetracyclic triazolium salt **14** catalyzes the cyclization with generation of a quaternary stereocenter in high yields and excellent enantiomeric excess. An interchange of the functional groups of the title α-hydroxy-substituted tetralones is possible as well as the synthesis of the corresponding α-hydroxyindanone derivatives with still good enantiomeric excess values.

Experimental Section

Typical procedure for the asymmetric intramolecular crossed-benzoin reaction, as exemplified for the formation of **6d**: Precatalyst **14** (20.6 mg, 0.055 mmol, 20 mol%) was suspended with anhydrous THF (1.7 mL) in a Schlenk tube under argon at room temperature. A solution of freshly sublimed KO*t*Bu (5.9 mg, 0.052 mmol, 19 mol%) in anhydrous THF (0.6 mL) was added slowly, and the solution was stirred for 5 min. Aldehyde-ketone **5d** (60 mg, 0.275 mmol) was dissolved in anhydrous THF (0.5 mL) and added to the carbene solution. The reaction mixture was stirred for 48 h, diluted with CH_2Cl_2, quenched with water, extracted two times with CH_2Cl_2, and dried over $MgSO_4$. The solvent was evaporated and the crude product was purified by flash chromatography on silica gel (dichloromethane/*n*-pentane 2:1) to yield **6d** (54 mg, 91%) as a colorless liquid. *ee* = 98% (determined by HPLC on a chiral stationary phase (Daicel Chiralpak AD)). $[\alpha]_D^{23} = -30.0$ ($c = 1.5$ in $CHCl_3$); ^{1}H NMR (300 MHz, $CDCl_3$, TMS): $\delta = 0.85$ (d, 3H, $J = 6.6$ Hz, CH_3CH), 0.96 (d, 3H, $J = 6.9$ Hz, CH_3CH), 1.50 (dd, 1H, $J = 5.5$, 14.3 Hz, C*H*HCH), 1.68 (dd, 1H, $J = 4.7$, 14.6 Hz, CH*H*CH), 1.84–1.97 (m, 1H, CH), 2.15 (ddd, 1H, $J = 6.0$, 13.5, 13.5 Hz, CC*H*H), 2.36 (ddd, 1H, $J = 2.2$, 5.0, 13.5 Hz, CCH*H*), 2.93–3.17 (m, 2H, CH_2), 3.92 (s, 1H, OH), 7.24–8.00 ppm (m, 4H, ArH); ^{13}C NMR (75 MHz, $CDCl_3$): $\delta = 23.5$, 23.7, 24.7, 26.5, 34.7, 43.8, 75.9, 126.7, 127.8, 128.8, 130.4, 133.7, 143.1, 202.5 ppm.

The analytical and spectroscopic data of all new compounds were correct.

Received: November 3, 2005
Published online: January 3, 2006

Keywords: asymmetric synthesis · benzoin reaction · heterocycles · homogeneous catalysis · N-heterocyclic carbenes

[1] a) A. J. Arduengo III, R. L. Harlow, M. Kline, *J. Am. Chem. Soc.* **1991**, *113*, 361–363; b) review: A. J. Arduengo III, R. Krafczyk, *Chem. Unserer Zeit* **1998**, *32*, 6–14; c) D. Enders, K. Breuer, G. Raabe, J. Runsink, J. H. Teles, J.-P. Melder, K. Ebel, S. Brode, *Angew. Chem.* **1995**, *107*, 1119–1122; *Angew. Chem. Int. Ed. Engl.* **1995**, *34*, 2021–2024.
[2] Review: D. Enders, T. Balensiefer, *Acc. Chem. Res.* **2004**, *37*, 534–541.
[3] Review: W. A. Herrmann, *Angew. Chem.* **2002**, *114*, 1342–1363; *Angew. Chem. Int. Ed.* **2002**, *41*, 1290–1311.
[4] a) C. Burstein, F. Glorius, *Angew. Chem.* **2004**, *116*, 6331–6334; *Angew. Chem. Int. Ed.* **2004**, *43*, 6205–6208; b) S. S. Sohn, E. L. Rosen, J. W. Bode, *J. Am. Chem. Soc.* **2004**, *126*, 14370–14371; c) M. He, J. W. Bode, *Org. Lett.* **2005**, *7*, 3131–3134.
[5] R. Singh, R. M. Kissling, M.-A. Letellier, S. P. Nolan, *J. Org. Chem.* **2004**, *69*, 209–212.
[6] O. Coulembier, A. P. Dove, R. C. Pratt, A. C. Sentman, D. A. Culkin, L. Mespouille, P. Dubois, R. M. Waymouth, J. L. Hedrick, *Angew. Chem.* **2005**, *117*, 5044–5048; *Angew. Chem. Int. Ed.* **2005**, *44*, 4964–4968.

 © 2006 Wiley-VCH Verlag GmbH & Co. KGaA, Weinheim

[7] D. Enders, U. Kallfass, *Angew. Chem.* **2002**, *114*, 1822 – 1824; *Angew. Chem. Int. Ed.* **2002**, *41*, 1743 – 1745.
[8] a) M. S. Kerr, J. Read de Alaniz, T. Rovis, *J. Am. Chem. Soc.* **2002**, *124*, 10298 – 10299; b) Short review: M. Christmann, *Angew. Chem.* **2005**, *117*, 2688 – 2690; *Angew. Chem. Int. Ed.* **2005**, *44*, 2632 – 2634.
[9] S. M. Mennen, J. D. Gipson, Y. R. Kim, S. J. Miller, *J. Am. Chem. Soc.* **2005**, *127*, 1654 – 1655.
[10] H. Iding, T. Dünnwald, L. Greiner, A. Liese, M. Müller, P. Siegert, J. Grötzinger, A. S. Demir, M. Pohl, *Chem. Eur. J.* **2000**, *6*, 1483 – 1495.
[11] H. Stetter, *Angew. Chem.* **1976**, *88*, 695 – 704; *Angew. Chem. Int. Ed. Engl.* **1976**, *15*, 639 – 648.
[12] Y. Hachisu, J. W. Bode, K. Suzuki, *J. Am. Chem. Soc.* **2003**, *125*, 8432 – 8433.
[13] D. Enders, O. Niemeier, *Synlett* **2004**, 2111 – 2114.
[14] Y. Hachisu, J. W. Bode, K. Suzuki, *Adv. Synth. Catal.* **2004**, *346*, 1097 – 1100.
[15] Reviews: a) K. Fuji, *Chem. Rev.* **1993**, *93*, 2037 – 2066; b) E. J. Corey, A. Guzman-Perez, *Angew. Chem.* **1998**, *110*, 402 – 415; *Angew. Chem. Int. Ed.* **1998**, *37*, 388 – 401; c) J. Christoffers, A. Mann, *Angew. Chem.* **2001**, *113*, 4725 – 4732; *Angew. Chem. Int. Ed.* **2001**, *40*, 4591 – 4597; d) I. Denissova, L. Barriault, *Tetrahedron* **2003**, *59*, 10105 – 10146.
[16] a) F. Omar, A. W. Frahm, *Arch. Pharm.* **1989**, *322*, 461 – 471; b) F. Omar, A. W. Frahm, *Arch. Pharm.* **1990**, *323*, 923 – 928.
[17] R. L. Knight, F. J. Leeper, *J. Chem. Soc. Perkin Trans. 1* **1998**, 1891 – 1893.
[18] F. A. Davis, M. C. Weismiller, *J. Org. Chem.* **1990**, *55*, 3715 – 3717.
[19] C. M. Acevedo, E. F. Kogut, M. A. Lipton, *Tetrahedron* **2001**, *57*, 6353 – 6359.
[20] M. S. Kerr, J. Read de Alaniz, T. Rovis, *J. Org. Chem.* **2005**, *70*, 5725 – 5728.
[21] a) M. D. Ennis, R. L. Hoffman, N. B. Ghazal, D. W. Old, P. A. Mooney, *J. Org. Chem.* **1996**, *61*, 5813 – 5817; b) J. A. Nieman, M. D. Ennis, *Org. Lett.* **2000**, *2*, 1395 – 1397.
[22] T. Dudding, K. N. Houk, *Proc. Natl. Acad. Sci. USA* **2004**, *101*, 5770 – 5775.
[23] R. Breslow, *J. Am. Chem. Soc.* **1958**, *80*, 3719 – 3726.

 © 2006 Wiley-VCH Verlag GmbH & Co. KGaA, Weinheim

Allylic Alkylation

DOI: 10.1002/anie.200503274

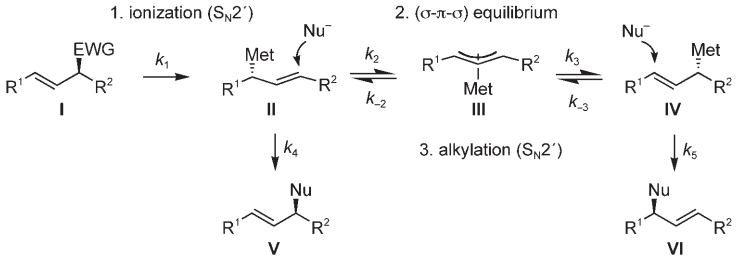
A Highly Regioselective Salt-Free Iron-Catalyzed Allylic Alkylation**

*Bernd Plietker**

Transition-metal-catalyzed reactions belong to the most important tools in synthetic organic chemistry. Over the past 30 years the productive collaboration between organic and inorganic chemists has led to a dynamic evolution in this field and, as a consequence, to the development of a variety of new transformations.[1] Apart from the invention of new reactions, the use of only small amounts of a catalyst is advantageous with regard to environmental aspects. Although the amount of catalyst employed is usually very low the high price of these compounds often prevents their application on a large scale. Hence, the search for new catalysts based on inexpensive nontoxic metals such as iron has gained increasing attention in the past years.[2]

Allylic alkylation is among the most successful catalytic C–C bond formations in organic chemistry.[3] A variety of transition metals can be used for the selective reaction between a C nucleophile and allylic activated substrates. Detailed investigations, especially in the field of palladium catalysis, have made allylic alkylation a versatile synthetic tool in preparative organic chemistry.[4] Although palladium is the predominant metal in this field, various procedures involving ruthenium,[5] iridium,[6] nickel,[7] tungsten,[8] copper,[9] or molybdenum catalysts[10] have been published. In most cases, intermediate π-allyl metal complexes are formed that allow asymmetric allylic alkylation through addition of chiral ligands. However, the reaction of unsymmetrically substituted substrates often leads to the formation of regioisomers.[11,12]

To date, a catalytic regioselective allylic alkylation in which the new C–C bond is formed at the carbon atom that bears the leaving group in the starting material was only observed in the presence of rhodium catalysts by the groups of Evans[13] and Martin.[14] To favor such a reaction, a fast alkylation of **II** ($k_1,k_4 \gg k_2,k_3$; Scheme 1) might prevent the formation of the undesired π-allyl metal intermediate **III**, thus leading to the observed regioselective C–C bond formation in the product **V** (σ-allyl metal mechanism).[13a]



Scheme 1. Allylic alkylation through σ-allyl ($k_1,k_4 \gg k_2,k_3$) or π-allyl metal mechanism ($k_2,k_3 \gg k_4,k_5$). EWG = electron-withdrawing group.

Roustan et al.[15] and Xu and Zhou[16] reported a regioselective, allylic alkylation in the presence of the formal Fe^{-II} complex $[Bu_4N][Fe(CO)_3(NO)]$. Although from an economical and ecological point of view this catalyst represents an interesting alternative to the commonly used transition-metal complexes, this catalytic process was not studied further owing to the high catalyst loading (25 mol%) and the need for a toxic CO atmosphere.[17,18]

Within the course of the synthesis of a natural product, we sought a regioselective allylic alkylation method in which the new C–C bond is formed at the carbon atom that bears the nucleofuge in the starting material. Although almost ignored, C–C bond formation in the presence of a Fe^{-II} complex appeared remarkable to us with regard to both practicability and stability of the catalyst.[14,15] Herein we summarize the results of our investigations based on the pioneering work of Roustan and Xu that have led to the development of an efficient, regioselective, salt-free, iron-catalyzed allylic alkylation.[19] The scope of the reaction for different pronucleophiles and allyl carbonates is discussed below.[20]

The primary goal of our initial investigations in this field was the replacement of the toxic CO atmosphere. The low conversion in the absence of CO indicated a deactivation of the catalyst within the first catalytic cycle (Table 1, entry 1). Based on the assumption that the CO atmosphere should suppress deactivating ligand-exchange processes at the metal center, various ligands were tested in order to replace the CO atmosphere (Table 1). A probable coordination at the metal center could maintain the catalyst activity, thus taking over the function of the CO atmosphere. Surprisingly, triphenylphosphane, a monodentate basic ligand, showed optimum results (Table 1, entry 3).[21] Furthermore, the separate deprotonation of the pronucleophile proved to be unnecessary, thus allowing a salt-free reaction procedure.

Subsequent investigations on the influence of the carbonate structure indicated an isobutyl carbonate to be beneficial for the reaction. The change in the carbonate structure improved the yield significantly from 41% to 68%. A subsequent optimization of the solvent indicated that strongly coordinating solvents such as *N*,*N*-dimethylformamide increase the reactivity of the catalyst (Table 2, entry 8).[22] The moderate regioselectivity in the presence of acetonitrile is surprising and suggests an alternative π-allyl metal mechanism (Table 2, entry 7). Investigations on the mechanism are

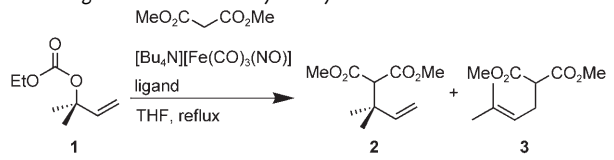
[*] Priv.-Doz. Dr. B. Plietker
Organische Chemie II, FB Chemie
Universität Dortmund
Otto-Hahn-Strasse 6, 44221 Dortmund (Germany)
Fax: (+49) 231-755-3884
E-mail: bernd.plietker@uni-dortmund.de

[**] Financial support by the Fonds der Chemischen Industrie, the Deutsche Forschungsgemeinschaft, the Otto-Röhm-Gedächtnisstiftung, and the Fonds zur Förderung des wissenschaftlichen Nachwuchses im Fachbereich Chemie der Universität Dortmund is gratefully acknowledged.

Supporting information for this article is available on the WWW under http://www.angewandte.org or from the author.

© 2006 Wiley-VCH Verlag GmbH & Co. KGaA, Weinheim

Table 1: Ligand effect in the allylic alkylation of **1**.[a]



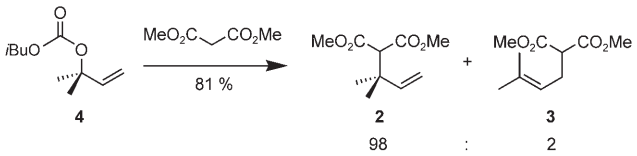
Entry	Ligand	**2**/**3**[b]	Conversion [%][c]
1	–	n.d.[d]	8
2	pyridine	n.d.	6
3	PPh_3	96:4	41
4	PBu_3	92:8	26
5	$P(OEt)_3$	n.d.	12
6	dppe[e]	n.d.	8
7	dppp[e]	n.d.	11
8	dppf[e]	n.d.	13

[a] All reactions were performed on a 1-mmol scale under argon in the presence of the Fe catalyst (10 mol%), ligand (10 mol%), and pronucleophile (2 equiv) in absolute THF (5 mL) and stopped after 12 h. [b] Determined by GC. [c] Determined by GC relative to undecane as internal standard. [d] Not determined. [e] dppe = Ethane-1,2-diylbis-(diphenylphosphane), dppp = propane-1,3-diylbis(diphenylphosphane), dppf = 1,1′-bis(diphenylphosphanyl)ferrocene.

Table 2: Solvent effect in the allylic alkylation.[a]

Entry	Solvent	**2**/**3**[b]	Conversion [%][c]
1	THF	96:4	68
2	DME[d]	92:8	43
3	acetone	n.d.	12
4	CH_2Cl_2	n.d.	–
5	toluene	97:3	39
6	DMSO	96:4	46
7	CH_3CN	58:42	60
8	DMF[d]	98:2	95
9	NMP[d]	97:3	82

[a] All reaction were carried out in the presence of the Fe catalyst (10 mol%) and PPh_3 under otherwise identical conditions as described in Table 1. [b] Determined by GC. [c] Determined by GC relative to undecane as internal standard.



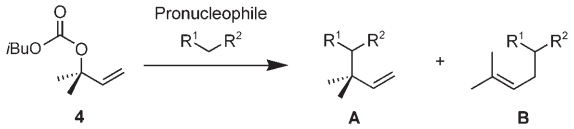
Scheme 2. Iron-catalyzed allylic alkylation. Reagents and conditions: substrate (1 mmol), pronucleophile (2 mmol), $[Bu_4N][Fe(CO)_3(NO)]$ (2.5 mol%), PPh_3 (3 mol%), DMF (1 mL), 80°C, 24 h.

currently being carried out in our laboratories. An increase in the substrate concentration from 0.2 to 1 mol L^{-1} allowed a further decrease in the catalyst loading to as little as 2.5 mol% while maintaining the regioselectivity. The optimized conditions are shown in Scheme 2.

The iron-catalyzed allylic alkylation is applicable to a variety of different C nucleophiles (Table 3). Nitrile-containing pronucleophiles proved to be most reactive. The presence of only one CN group decreases the reaction time significantly (Table 3, entries 3–6). The formation of two adjacent quaternary carbon centers in the presence of the iron catalyst proceeds in good yields (Table 3, entry 6). However, this C–C bond formation is not as regioselective as the formation of only one quaternary center. Apparently, the steric repulsion between the substituents at the allyl fragment and the nucleophile leads to a lower selectivity. However, the branched product is still the major product.

The iron-catalyzed allylic alkylation is applicable to a variety of differently substituted allyl carbonates (Table 4). In

Table 3: Iron-catalyzed allylic alkylation of different pronucleophiles.[a]

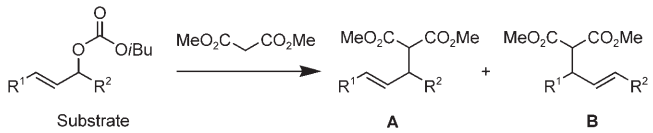


Entry	Pronucleophile		Product **A**		*t* [h]	**A**/**B**[b]	Yield [%][c]
1	MeO_2C CO_2Me	**5**	MeO_2C CO_2Me	**2**	24	98:2	81
2	O CO_2Me	**6**	O CO_2Me	**7**	24	96:4	71
3	NC CN	**8**	NC CN	**9**	12	92:8	74
4	NC CO_2Me	**10**	NC CO_2Me	**11**	12	94:6	79
5	PhO_2S CN	**12**	PhO_2S CN	**13**	12	94:6	92
6	O CN	**14**	O CN	**15**	12	87:13	81

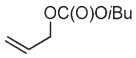
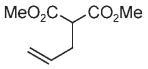
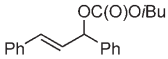
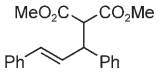
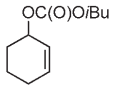
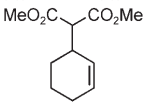
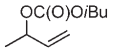
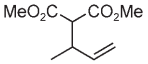
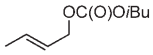
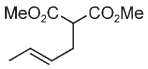
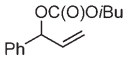
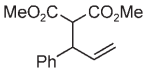
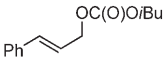
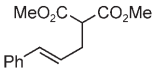
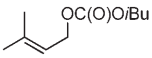
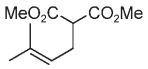
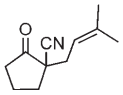
[a] All reactions were carried out on a 1-mmol scale in the presence of the Fe catalyst (2.5 mol%), PPh_3 (3 mol%), and the pronucleophile (2 equiv) in absolute DMF (1 mL) at 80°C. [b] Determined by GC. [c] Yield of both regioisomers after isolation.

 © 2006 Wiley-VCH Verlag GmbH & Co. KGaA, Weinheim

Table 4: Iron-catalyzed allylic alkylation of various carbonates.[a]



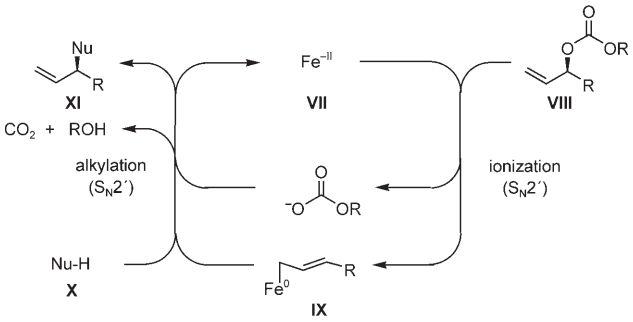
Substrate A B

Entry	Substrate		Product **A**		*t* [h]	**A**:**B**[b]	Yield [%][c]
1		**16**		**17**	12	93:7	84
2		**18**		**19**	48	–	53
3		**20**		**21**	48	–	69
4		**22**		**23**	24	98:2	78
5		**24**		**25**	36	96:4	76
6		**26**		**27**	24	98:2	78
7		**28**		**29**	48	92:8	56
8		**30**		**3**	48	93:7	61
9		**30**		**31**	24	84:16	65

[a] All reactions were performed as indicated in Table 3. [b] Determined by GC. [c] Combined yield of both regioisomers after isolation.

every case the substitution takes place at the carbon atom that bears the original leaving group. The introduction of further olefin substituents has a significant influence on the course of the reaction. More substituents lead to longer reaction times.[23] However, we were pleased to find that the regioselectivity is not influenced (Table 4). Whereas aliphatic substituents solely prolong the reaction times, a phenyl substituent at C3 of the allyl fragment leads to a significantly lower yield (Table 4, entries 2 and 7). The regioselectivity of the reaction is defined exclusively by the substitution pattern of the allyl carbonate (Table 4, entries 4/5 and 6/7). In contrast, the nature of the pronucleophile does not influence the regioselectivity (Table 3, entry 1 and Table 4, entry 8; Table 3, entry 6 and Table 4, entry 9).

From the observed high regioselectivity in the alkylation it can be concluded that, in contrast to most common transition-metal-catalyzed allylic alkylations, no η^3-allyl intermediate is formed in this reaction. A selective double S_N2' addition both of the metal **VII** (Scheme 3) in the first and of the nucleophile **X** in the second step allows the observed high regioselectivity. An oxidative addition through an S_N2 mechanism appears to be unlikely as both reaction time and conversion rate in the alkylation of primary allyl carbonates clearly depends on the substitution pattern at C3 of the allyl fragment (Table 4, entries 1, 5, and 9).[23] A preliminary mechanistic proposal is shown in Scheme 3.

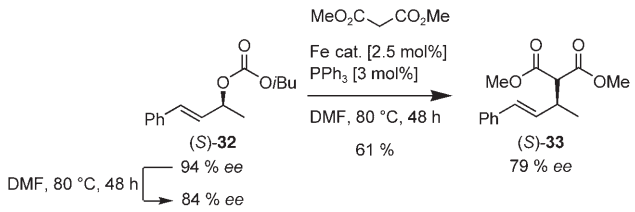


Scheme 3. Postulated catalytic cycle for the iron-catalyzed allylic alkylation.[24]

The proposed mechanism has stereochemical consequences. If indeed only a σ-allyl metal species such as **IX** is formed in situ, the allylic alkylation of enantiomerically enriched carbonates should lead to the formation of enantiomerically and regioisomerically enriched substitution products with retention of the configuration. To test this hypothesis (*S*)-allyl carbonate **33** was subjected to the alkylation conditions. The

 © 2006 Wiley-VCH Verlag GmbH & Co. KGaA, Weinheim

enantiomeric ratios of the starting material and of the product were analyzed by means of chiral HPLC (Scheme 4). The enantiomeric excess decreased to a certain extent; however, the *S*-configured malonic ester derivative **34** was formed as



Scheme 4. Iron-catalyzed allylic alkylation of enantiopure carbonate (*S*)-**33**.

the main product. The lower *ee* values are probably the result of epimerization of the starting material under the reaction conditions. This hypothesis was proven by a control experiment in which (*S*)-**33** was subjected to the reaction conditions in the absence of the iron catalyst. After 48 h a decrease in the enantiopurity to 83 % *ee* was observed. Hence, at the current state of research such an epimerization event might be responsible for the observed loss in enantioselectivity. However, this test reaction serves as a first indication that a σ-allyl metal mechanism takes place in the iron-catalyzed allylic alkylation.

In summary, we have described an efficient, salt-free, regioselective iron-catalyzed allylic alkylation of allyl carbonates. The addition of triphenylphosphane led to a significant increase in reactivity of the $[Fe(CO)_5]$-derived stable iron(−II) complex $[Bu_4N][Fe(CO)_3(NO)]$. In the presence of the catalyst (2.5 mol %) and PPh_3 (3 mol %) a variety of different allyl carbonates and pronucleophiles were coupled in good to excellent yields. The use of a carbonate as leaving group avoids a separate deprotonation of the pronucleophile by external bases. Apart from the possible salt-free reaction course, a fact that is especially attractive for applications on a preparative scale, the high regioselectivity of the alkylation is remarkable. The new C–C bond is formed selectively at the carbon atom in the allyl fragment that bears the leaving group in the starting material. Comparable high regioselectivities were previously only observed in the presence of rhodium catalysts. Further investigations on the mechanism, stereo- and regioselectivity aspects, and scope and limitations are currently underway in our laboratories.

Experimental Section

2: A 10-mL Schlenk tube was charged with the iron catalyst (10.6 mg, 0.025 mmol, 2.5 mol %) and PPh_3 (7.3 mg, 0.03 mmol, 3 mol %), which were then dissolved under argon in dry DMF (1 mL) and heated to 80 °C for 30 min. The mixture was cooled to room temperature, and the allyl carbonate **4** (186 mg, 1 mmol) and dimethyl malonate (232 mg, 2 mmol) were then added. The reaction mixture was heated in the sealed Schlenk tube for 24 h at 80 °C. The mixture was cooled to room temperature, and dichloromethane (20 mL) was then added. The organic layer was extracted with water (2 × 10 mL) and dried over a mixture of Na_2SO_4 and charcoal (1:1; ≈5 g). After filtration and evaporation of the solvent a pale yellow liquid was obtained which was purified by flash column chromatography (isohexane/diethyl ether, 5:1). Yield: 162 mg (0.81 mmol, 81 %).

Received: September 15, 2005
Revised: October 26, 2005
Published online: January 27, 2006

Keywords: alkylation · carboxylic acids · iron · nucleophiles · regioselectivity

[1] a) *Transition Metals for Organic Synthesis, Vol. 1 and 2* (Eds.: M. Beller, C. Bolm), Wiley-VCH, Weinheim, **1998**; b) *Comprehensive Asymmetric Catalysis I–III* (Eds.: E. N. Jacobsen, A. Pfaltz, H. Yamamoto), Springer, Berlin, **1999**.
[2] For a review on iron-catalyzed cross-coupling, see: A. Fürstner, R. Martin, *Chem. Lett.* **2005**, *34*, 624.
[3] B. M. Trost, M. L. Crawley, *Chem. Rev.* **2003**, *103*, 2921.
[4] J. Tsuji in *Palladium Reagents and Catalysts* (Ed.: J. Tsuji), Wiley, New York, **1995**, p. 290.
[5] a) Y. Morisaki, T. Kondo, T.-A. Misudo, *Organometallics* **1999**, *18*, 4742; b) B. M. Trost, P. Fraisse, Z. Ball *Angew. Chem.* **2002**, *114*, 1101; *Angew. Chem. Int. Ed.* **2002**, *41*, 1059.
[6] a) R. Takeuchi, N. Shiga, *Org. Lett.* **1999**, *1*, 265; b) B. Bartels, G. Helmchen, *Chem. Commun.* **1999**, 741.
[7] a) K.-G. Chung, Y. Miyake, S. Uemura, *J. Chem. Soc. Perkin Trans. 1* **2000**, 15; b) M. T. Didiuk, J. P. Morken, A. H. Hoveyda, *J. Am. Chem. Soc.* **1995**, *117*, 7273.
[8] a) G. C. Lloyd-Jones, A. Pfaltz, *Angew. Chem.* **1995**, *107*, 534; *Angew. Chem. Int. Ed. Engl.* **1995**, *34*, 462; b) B. M. Trost, M. -Hung, *J. Am. Chem. Soc.* **1987**, *109*, 2176; c) B. M. Trost, M.-H. Hung, *J. Am. Chem. Soc.* **1983**, *105*, 7757.
[9] E. S. M. Persson, M. van Kaveren, D. M. Grove, J.-E. Bäckvall, G. van Koten, *Chem. Eur. J.* **1995**, *1*, 351.
[10] B. M. Trost, K. Dogra, I. Hachiya, T. Emura, D. L. Hughes, S. W. Krska, R. A. Reamer, M. Palucki, N. Yasuda, P. J. Reider, *Angew. Chem.* **2002**, *114*, 2009; *Angew. Chem. Int. Ed.* **2002**, *41*, 1929.
[11] The use of ligands sometimes leads to a shift in the regioisomer ratio towards the branched products; for example, see: J. W. Fuller, J. C. Wilt, J. Parr, *Org. Lett.* **2004**, *6*, 1301.
[12] The character of the metal influences the regiochemical course of allylic alkylations. Ruthenium, molybdenum, rhodium, tungsten, and iridium catalysts often lead to the formation of the branched product, regardless of the substitution pattern of the starting material.
[13] a) P. A. Evans, J. D. Nelson, *J. Am. Chem. Soc.* **1998**, *120*, 5581; b) P. A. Evans, J. D. Nelson, *Tetrahedron Lett.* **1998**, *39*, 1725.
[14] B. L. Ashfeld, K. A. Miller, S. F. Martin, *Org. Lett.* **2004**, *6*, 1321.
[15] J. L. Roustan, J. Y. Merour, F. Houlihan, *Tetrahedron Lett.* **1979**, 3721.
[16] a) Y. Xu, B. Zhou, *J. Org. Chem.* **1987**, *52*, 974; b) B. Zhou, Y. Xu, *J. Org. Chem.* **1988**, *53*, 4421.
[17] For reviews on the chemistry of tricarbonyl iron complexes, see: a) M. Periasamy, C. Rameshkumar, U. Radhahrishnan, A. Devasagayaraj, *Curr. Sci.* **2002**, *71*, 1307; b) H.-J. Knölker, *Chem. Rev.* **2000**, *100*, 2941.
[18] For a comprehensive study on iron-mediated allylic alkylations, see: D. Enders, B. Jandeleit, S. von Berg, G. Raabe, J. Runsink, *Organometallics* **2001**, *20*, 4312.
[19] For an interesting Fe-catalyzed allylic alkylation of allyl halides, see: R. Martin, A. Fürstner, *Angew. Chem.* **2004**, *116*, 4045; *Angew. Chem. Int. Ed.* **2004**, *43*, 3955.
[20] B. Plietker, patent pending (102005040752.8)
[21] A ligand exchange in the presence of $P(OPh)_3$ was previously reported: K. Itoh, S. Nakanishi, Y. Otsuji, *Bull. Chem. Soc. Jpn.* **1991**, *64*, 2965.

 © 2006 Wiley-VCH Verlag GmbH & Co. KGaA, Weinheim

[22] The positive effect of *N*,*N*-dimethylformamide on the ligand exchange has been described.[21]
[23] A similar effect was observed by Evans and Nelson in rhodium-catalyzed allylic alkylations.[13a]
[24] The presented mechanism, including the molecular structures, represents a model. Detailed spectroscopic investigations on the structure of the active catalyst as well as on reactive intermediates are currently underway in our laboratories.

 © 2006 Wiley-VCH Verlag GmbH & Co. KGaA, Weinheim

Surface Reactions

DOI: 10.1002/anie.200503708

In Situ Imaging of Electrochemically Induced Oxygen Spillover on Pt/YSZ Catalysts**

*Bjoern Luerßen, Eva Mutoro, Holger Fischer, Sebastian Günther, Ronald Imbihl, and Jürgen Janek**

Following the pioneering work of Vayenas and co-workers, the feasibility of electrochemical promotion of heterogeneously catalyzed reactions has been demonstrated in the past two decades with porous metal catalysts interfaced to solid electrolytes.[1–3] The catalytic activity of electrically polarized porous metal electrodes on solid electrolytes has been investigated in over 100 reaction systems, and up to 200-fold increases in rate have been reported. Mechanistically, the promotion effect has been attributed to a charged mobile species that is (partially) discharged at the triple-phase boundary (tpb) (solid electrolyte/metal/gas) and then diffuses over the metal surface, thereby modifying its catalytic activity.[3–6] The crucial role of the electrochemically generated spillover species and its chemical identity have been proven in recent years by surface analytical techniques for only two systems: the oxygen-ion-conducting Pt/YSZ system (YSZ = yttria-stabilized zirconia, $ZrO_2 + Y_2O_3$)[4,6–9] and the alkali-ion-conducting Pt/β″-Al_2O_3 system.[10,11] We report herein the imaging of the spillover process itself. We observe the diffusional spreading of oxygen upon electrochemical pumping on a dense platinum film interfaced with YSZ. The experiments provide a better basis for a detailed mechanistic understanding of the electrochemical promotion of surface reactions.

The typical cell arrangement of an electrochemical promotion experiment is shown in Figure 1a, and the generation of spillover oxygen at the tpb is illustrated. Oxygen ions are transported through the YSZ solid electrolyte during the anodic (positive) polarization of the metal catalyst (working electrode), and the following reaction [Eq. (1)] takes place at the tpb:

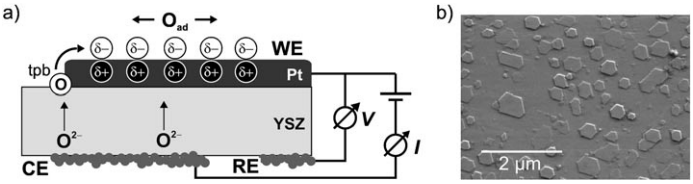


Figure 1. a) Formation of an outer electrochemical double layer during electrical polarization of the cell Pt|YSZ|Pt. A standard three-electrode setup was used. WE = working electrode, CE = counter electrode, RE = reference electrode. b) SEM image of a Pt(111) film deposited on YSZ(111) by pulsed laser deposition (PLD) after annealing.

$$O^{2-}{}_{YSZ} - 2e^- \rightarrow O_{tpb} \rightarrow O_{ad} \quad (1)$$

The atomic oxygen generated at the tpb (O_{tpb}) spills over the electrode surface forming a layer of chemisorbed oxygen (O_{ad}). It was demonstrated with planar YSZ/Pt model catalysts studied in an ultrahigh-vacuum (UHV) chamber that the electrochemically generated spillover oxygen is identical to oxygen adsorbed from the gas phase.[8,12] However, instead of the expected diffusion from the tpb, a seemingly uniform increase in the oxygen concentration across the metal surface was observed. This uniform increase in oxygen coverage could be attributed to a high density of pores (grain boundaries) in the metal film, which act as fast-diffusion paths to transport oxygen from the Pt/YSZ interface to the outer metal surface.

To obtain a planar model catalyst, a pore-free, 200- to 250-nm thick Pt film was deposited by pulsed laser deposition on the (111) plane of YSZ. Subsequent annealing produced a dense Pt film with (111) surface orientation as shown in Figure 1b. Two spatially resolving methods were applied to image the spillover process in situ. With photoelectron emission microscopy (PEEM), the photoelectrons ejected during illumination by a D_2 discharge lamp (5.5 eV–6.2 eV) are used to image the local work function (WF) with a spatial resolution of approximately 1 μm and a temporal resolution of 20 ms (on the order of video frames). Information about the chemical identity of the imaged species was obtained with scanning photoelectron microscopy (SPEM) at the synchro-

[*] Dr. B. Luerßen, Dipl.-Chem. E. Mutoro, Dipl.-Chem. H. Fischer, Prof. Dr. J. Janek
Institute for Physical Chemistry
Justus Liebig University Giessen
Heinrich-Buff-Ring 58, 35392 Giessen (Germany)
Fax: (+49) 641-99-34509
E-mail: juergen.janek@phys.chemie.uni-giessen.de
Dr. S. Günther
Department of Chemistry
Ludwig Maximilian University Munich
Butenandtstrasse 11, 81377 Munich (Germany)
Prof. Dr. R. Imbihl
Institute for Physical Chemistry and Electrochemistry
University Hannover
Callinstrasse 3–3A, 30167 Hannover (Germany)

[**] We thank L. Gregoratti, A. Barinov, and M. Kiskinova (Sincrotrone ELETTRA, Trieste, Italy) for their invaluable support. We gratefully acknowledge the support of C. Korte for establishing the PLD technique and of L. Majdandzic in sample preparation. Financial support by the DFG (German Science Foundation) and the FCI (Fund of the German Chemical Industry) and the state of Hessia is also acknowledged.

 © 2006 Wiley-VCH Verlag GmbH & Co. KGaA, Weinheim

tron light source ELETTRA (Trieste, Italy). In SPEM, intense synchrotron radiation in the X-ray range (ca. 600 eV) is focused by means of a zone plate into a narrow spot (diameter 0.15 μm). An image of the elemental distribution is obtained by scanning the sample with the energy analyzer tuned to the energy of the specific core level.[13] The experimental setup for our experiments (Figure 1a) is located in a UHV chamber with base pressure p of approximately 10^{-9} mbar. The electrochemical pumping voltage is controlled by a potentiostat (Jaissle IMP83). Owing to O_2 desorption, the pressure rises reproducibly during electrochemical pumping from 10^{-9} up to approximately 10^{-7} mbar, and a current of a few μA flows through the electrochemical cell.

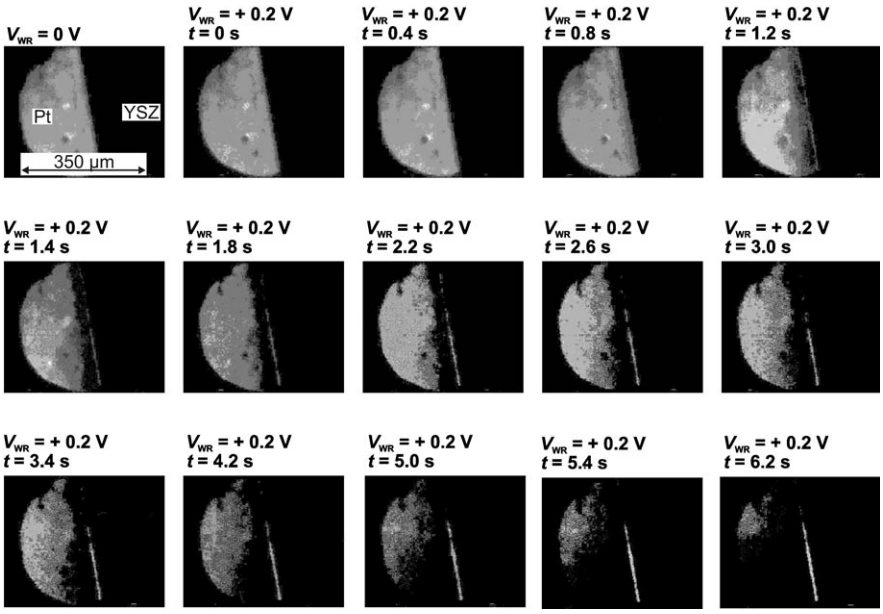


Figure 2. Sequence of PEEM images taken during anodic polarization of a dense Pt electrode. An anodic polarization potential of $V_{WR} = +0.2$ V was applied at $T = 670$ K (base pressure $p = 1 \times 10^{-9}$ mbar).

Figure 2 displays a series of PEEM images recorded during anodic polarization of the working electrode ($V_{WR} = 0.20$ V). Oxygen adsorbed on platinum is observed as a dark area, because the surface dipole caused by the negatively charged oxygen atoms increases the local work function.[7]

Shortly after the pumping voltage is applied, a dark area forms at the tpb and spreads out onto the platinum electrode until the whole metal electrode is uniformly dark. The front velocity of approximately 25 μm s^{-1} remains roughly constant throughout this process. SPEM analysis proves that the spillover species is chemisorbed oxygen with an O 1s binding energy of 530.6 eV.[8,12] After the voltage has been switched off, the chemisorbed oxygen desorbs slowly into the gas phase. This diffusion experiment was repeated several times, but bubbles of oxygen gas (formed during electrochemical polarization) were observed on the dense platinum electrode after some time, which proves that the electrode surface is gas tight.

In a second type of experiment, we used a surface reaction to prove that the electrochemically generated spillover species is in fact reactive oxygen. We created a thin layer of carbon on a Pt electrode by thermal decomposition of ethylene. As shown schematically in Figure 3a, small holes (with diameter of 2 μm) in the Pt electrode create tpb sites from which oxygen atoms can spill over onto adjacent Pt sites during electrochemical pumping. In essence, the holes represent small sources of atomic oxygen. These spillover oxygen atoms react with the carbonaceous film to produce CO and CO_2, which immediately desorb and leave behind a clean metal surface. As grain boundaries in platinum can act as fast-diffusion paths for oxygen, such reaction fronts can be observed only on Pt films with sufficiently large grains.

As shown by the series of C 1s and Pt 4f SPEM images in Figure 3b, the hole in the carbon film grows as the reacting spillover oxygen consumes carbon. The rate of carbon consumption is controlled by the spillover rate of oxygen if the desorption of the electrochemically generated oxygen into the gas phase and possible kinetic control by the oxidation of

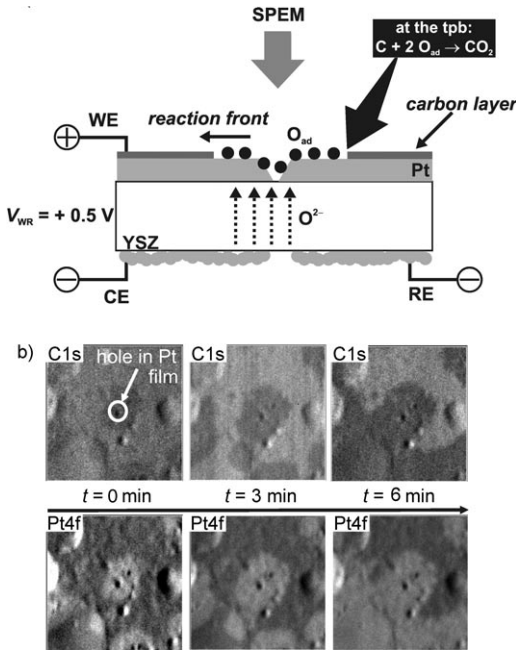


Figure 3. a) Electrochemically controlled surface reaction experiment: The working electrode is initially covered with a layer of carbon, produced by exposure of the electrode to ethylene ($p(C_2H_4) = 5 \times 10^{-8}$ mbar, $T = 673$ K) followed by thermal annealing. Upon anodic polarization ($V_{WR} = +0.5$ V), oxygen spreads from a small hole in the electrode and reacts with the carbon layer to form a propagating reaction front. b) Time sequence of SPEM images taken during anodic polarization ($V_{WR} = +0.5$ V). The upper and lower rows show the Pt 4f and C 1s maps, respectively.

 © 2006 Wiley-VCH Verlag GmbH & Co. KGaA, Weinheim

carbon at the reaction front are neglected. Setting the pumping voltage to zero immediately stops the reaction front, and the carbon concentration and distribution on the Pt surface remain constant. As the experiment is performed in a UHV chamber and as molecular oxygen is known to react very slowly with graphite layers, we exclude transport of oxygen through the gas phase. Diffusion through the Pt layer can also be neglected because other experiments on identical platinum layers prove the negligible solubility of oxygen in platinum. Therefore, the moving surface reaction front is a direct proof for the mobility and reactivity of electrochemically generated oxygen spillover.

The application of a pumping voltage raises the electrochemical potential of the ionic oxygen species at the tpb. If this species is in thermodynamic equilibrium with the chemisorbed neutral oxygen species on the metal surface, then the chemical potential of the chemisorbed oxygen will also increase. A potential of only 0.2 V corresponds to an increase in the oxygen activity $a(O_2)$ by a factor of 10^6 (at $T=$ 670 K) according to the Nernst equation. Depending on the reference oxygen activity, very high oxygen activities at the tpb can be reached; this high activity constitutes the thermodynamic basis for electrochemically induced oxygen spillover and the NEMCA (non-Faradaic electrochemical modification of catalytic activity) effect.[14] In our case ($p_{ref}(O_2) = 1 \times 10^{-9}$ mbar), we obtain a surface activity for oxygen of $a(O_2) = 1 \times 10^{-3}$.

To extract the diffusion coefficient of the spillover species, we performed a quantitative analysis of the diffusion profile (Figure 2) by relating the local gray values $G(x,t)$ of the PEEM images to the local spillover concentration $\theta(x,t)$. We assumed that $G(x,t)$ is proportional to the photocurrent I and that the work function Φ of the Pt electrode scales linearly with the surface coverage $\theta(x,t)$ of oxygen. The relationship between I and Φ is given by the Fowler equation ($I \propto \Phi^2$). Additionally, we assumed that the maximum coverage corresponds to $\theta = 0.25$ ML (assumption: 1 ML adsorbed oxygen on Pt(111) corresponds to 1.5×10^{15} atoms cm^{-2}). The resulting $\theta(t)$ curves at a given position x were analyzed with the appropriate solution of Fick's second law of diffusion.[15] This solution includes a constant diffusion coefficient D and a constant flow rate of oxygen at the tpb. The decrease of θ by desorption and the dependence of D on the coverage θ are neglected at this stage. Thus, the solution of Fick's second law we use here can only be regarded as an approximation. Nevertheless, the experimental data are in excellent agreement with the fitted diffusion equation, as shown by Figure 4.

We extract a diffusion coefficient of $D_O = (9.2 \pm 1.8) \times 10^{-4}$ cm^2 s^{-1} at 670 K. This value is distinctly larger than reported values for the diffusion coefficient of chemisorbed oxygen on Pt(111).[16] One reason may be that the Pt film we used shows microscopically small defects, the density of which increase close to the tpb. Further systematic measurements of diffusion profiles on microscopically well-defined electrodes should resolve this problem.

In summary, we were able by both work-function microscopy (PEEM) and μ-XPS (SPEM) to image in situ the spillover process that occurs as electrochemically pumped oxygen ions are discharged at the tpb. The spillover species is identified as chemisorbed oxygen, which spreads out by diffusion over the Pt surface. This spillover oxygen also reacts with a carbonaceous surface layer to form CO and CO_2. Firstly, these experiments clearly prove the concept of electrochemically generated surface species. We expect that further systematic and quantitative PEEM and SPEM experiments on chemically and geometrically well-defined electrodes will help in understanding the mechanism of electrochemical promotion in more detail. Secondly, this example of the electrochemical cleaning of a carbon-covered Pt surface by spillover oxygen documents vividly the potential of electrochemically controlled surface reactions.

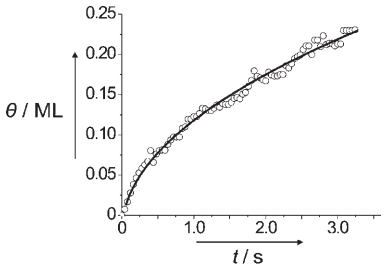


Figure 4. $\theta(t)$ diagram for a position 50 μm from the tpb; dots: measurement, line: calculation.

Received: October 19, 2005
Published online: January 20, 2006

Keywords: electrochemistry · electrode kinetics · heterogeneous catalysis · surface chemistry · zirconia

[1] C. G. Vayenas, S. Bebelis, S. Ladas, *Nature* **1990**, *343*, 625–627.
[2] C. G. Vayenas, S. Bebelis, C. Pliangos, S. Brosda, D. Tsiplakides, T. S. Stein, *Electrochemical Activation of Catalysis: Promotion, Electrochemical Promotion, and Metal–Support Interactions*, Plenum, New York, **2002**.
[3] *Catalysis and Electrocatalysis at Nanoparticle Surfaces* (Eds.: A. Wieckowski, E. R. Savinova, C. G. Vayenas), Marcel Dekker, New York, **2003**.
[4] S. Ladas, S. Kennou, S. Bebelis, C. G. Vayenas, *J. Phys. Chem.* **1993**, *97*, 8845–8848.
[5] I. Metcalfe, *J. Catal.* **2001**, *199*, 247; I. Metcalfe, *J. Catal.* **2001**, *199*, 259–272.
[6] I. Riess, C. G. Vayenas, *Solid State Ionics* **2003**, *159*, 313–329.
[7] J. Poppe, A. Schaak, J. Janek, R. Imbihl, *Ber. Bunsen-Ges.* **1998**, *102*, 1019–1022; Erratum: J. Poppe, A. Schaak, J. Janek, R. Imbihl, *Ber. Bunsen-Ges.* **1998**, *102*, 1718.
[8] B. Luerßen, S. Günther, H. Marbach, M. Kiskinova, J. Janek, R. Imbihl, *Chem. Phys. Lett.* **2000**, *316*, 331–335.
[9] C. G. Vayenas, D. Archonta, D. Tsiplakides, *J. Electroanal. Chem.* **2003**, *554–555*, 301–306.
[10] M. Makri, C. G. Vayenas, S. Bebelis, K. H. Besocke, C. Cavalca, *Surf. Sci.* **1996**, *369*, 351–359.
[11] R. M. Lambert, A. Palermo, J. W. Federico, M. S. Tikhov, *Solid State Ionics* **2000**, *136–137*, 677–685.
[12] B. Luerßen, H. Fischer, S. Günther, J. Janek in *Solid State Ionics: Science and Technology of Ions in Motion* (Eds.: B. V. R. Chowdari, H.-I. Yoo, G. M. Choi, I.-H. Lee), *Proc. of Asian Conf. Solid State Ionics* **2004**, *9*, 139–149.
[13] M. Kiskinova, E. Di Fabrizio, M. Gentili, M. Marsi, *Surf. Rev. Lett.* **2000**, *7*, 265–286.

 © 2006 Wiley-VCH Verlag GmbH & Co. KGaA, Weinheim

[14] J. Janek, M. Rohnke, B. Luerßen, R. Imbihl, *Phys. Chem. Chem. Phys.* **2000**, *2*, 1935 – 1941.
[15] R. B. Banks, *Growth and Diffusion Phenomena*, Springer, Berlin, **1994**, pp. 341 – 343.
[16] J. V. Barth, *Surf. Sci. Rep.* **2000**, 40 – 75.

 © 2006 Wiley-VCH Verlag GmbH & Co. KGaA, Weinheim

Aluminum Clusters

DOI: 10.1002/anie.200502957

The Chlorination of the $[Al_{13}]^-$ Cluster and the Stepwise Formation of Its Intermediate Products, $[Al_{11}]^-$, $[Al_9]^-$, and $[Al_7]^-$: A Model Reaction for the Oxidation of Metals?**

Ralf Burgert, Hansgeorg Schnöckel, Matthias Olzmann, and Kit H. Bowen, Jr.*

By allowing chlorine gas to flow over solid aluminum at temperatures above 100 °C and under standard pressure conditions, gaseous $AlCl_3$ is formed: $Al_{(s)} + {}^3/_2\,Cl_2 \rightarrow AlCl_{3(g)}$. The experimentally determined reaction energy is $-585\ kJ\,mol^{-1}$.[1] To understand the fundamental process of dissolving of a metal in an oxidizing atmosphere—this is analogous to dissolving a metal in aqueous acid—intermediate products of individual reaction steps on the metal surface have to be identified. Because of varying surface properties, however, it is difficult to study local (microscopic) reactivity on macroscopic metal surfaces. "Naked" aluminum (Al_n) clusters, on the other hand, are well-defined molecular model compounds and as such are well-suited for such investigations. Furthermore, the reactions of $[Al_{13}]^-$ with iodine and hydrogen iodide have recently attracted significant interest.[2,3]

[*] R. Burgert, Prof. Dr. H. Schnöckel
Institute of Inorganic Chemistry
University of Karlsruhe (TH)
Engesserstrasse 15, 76128 Karlsruhe (Germany)
Fax: (+49) 721-608-4854
E-mail: schnoeckel@chemie.uni-karlsruhe.de
Prof. Dr. M. Olzmann
Institute of Physical Chemistry
University of Karlsruhe (TH)
Fritz-Haber-Weg 4, 76128 Karlsruhe (Germany)
Prof. Dr. K. H. Bowen, Jr.
Department of Chemistry and Materials Science
Johns Hopkins University
Baltimore, MD 21218 (USA)

[**] This work was financially supported by the Deutsche Forschungsgemeinschaft (Center for Functional Nanostructures, CFN), by the "Fonds der Chemischen Industrie", and by the Air Force Office of Scientific Research (K.B.).

Supporting information for this article is available on the WWW under http://www.angewandte.org or from the author.

Here, we report our Fourier transform ion cyclotron resonance (FT-ICR) mass spectrometric investigations on isolated $[Al_{13}]^-$ clusters and their reactions with chlorine. This is the first time that it has been possible to detect the intermediate products of such reactions, in a time-resolved manner. In particular, single elementary steps of these oxidation processes were identified. Owing to the combination of experimental results and accompanying quantum-chemical calculations, a plausible mechanism for the stepwise reactive decomposition of the $[Al_{13}]^-$ cluster during its reaction with chlorine will be proposed. These elementary steps revealed during the "dissolving" of "naked" metal atom clusters in the gas phase provide topologic and energetic arguments for the understanding of analogous oxidation processes taking place on the bulk metal.

After laser desorption ionization (LDI) of $LiAlH_4$ a homologous series of Al_n^- cluster anions was observed by mass spectrometry. Each of these mass spectra were dominated by an intense signal at m/z 350.8, the mass of $[Al_{13}]^-$. The stability of these icosahedral $[Al_{13}]^-$ ions with their 40 valence electrons has been discussed in the past in terms of the jellium-like shell model.[4] In the experiment described here, $[Al_{13}]^-$ ions were first isolated (stored wave inverse Fourier transformation: SWIFT) in the Penning trap of a FT-ICR mass spectrometer and then cooled using argon as a collision gas.[5,6] Upon exposing these $[Al_{13}]^-$ ions to a chlorine atmosphere of approximately 10^{-8} mbar, new signals, attributed mainly to $[Al_{11}]^-$, $[Al_9]^-$, and $[Al_7]^-$ (Figure 1), were observed after several tens of seconds. Thus, the $[Al_{13}]^-$ cluster was decomposed in a stepwise manner to smaller aluminium clusters according to the reaction sequence (1).

$$[Al_{13}]^- \xrightarrow[-2\,AlCl]{Cl_2} [Al_{11}]^- \xrightarrow[-2\,AlCl]{Cl_2} [Al_9]^- \xrightarrow[-2\,AlCl]{Cl_2} [Al_7]^- \qquad (1)$$

Figure 2, which is based on our experimental observations and theoretical calculations, summarizes the energetics of the stepwise reactions that form these species. In the first step, oxidation of the $[Al_{13}]^-$ cluster surface proceeds to form the $[Al_{13}Cl_2]^{-*}$ intermediate product. That is during the reaction of a cluster with chlorine, two Al–Cl bonds are formed with the Al atoms of the icosahedral Al_{12} skeleton and the Cl–Cl bond is broken. The resulting reaction energy of this step is around $-450\ kJ\,mol^{-1}$, according to density functional calculations.[7,16–21] This leads to vibrational and rotational excitation energy trapped in the $[Al_{13}Cl_2]^{-*}$ cluster (symbol *) that cannot be removed by collisions at pressures around 10^{-8} mbar [Eq. (2a)]. This, in turn, results in the fragmentation of $[Al_{13}Cl_2]^{-*}$ into $[Al_{12}Cl]^{-*}$ and AlCl in the next step [Eq. (2b)]. Phase space theory[8] predicts a lifetime of several nanoseconds for $[Al_{13}Cl_2]^{-*}$, and as a consequence, $[Al_{13}Cl_2]^-$ is not detected in the experiment. In the next step, $[Al_{12}Cl]^{-*}$

$$[Al_{13}]^-_{(g)} + Cl_2 \rightarrow [Al_{13}Cl_2]^-_{(g)} \qquad \Delta_R H^\circ_{(0\,K)} = -450\ kJ\,mol^{-1} \qquad (2a)$$

$$[Al_{13}Cl_2]^-_{(g)} \rightarrow [Al_{12}Cl]^-_{(g)} + AlCl_{(g)} \qquad \Delta_R H^\circ_{(0\,K)} = +195\ kJ\,mol^{-1} \qquad (2b)$$

InterScience © 2006 Wiley-VCH Verlag GmbH & Co. KGaA, Weinheim

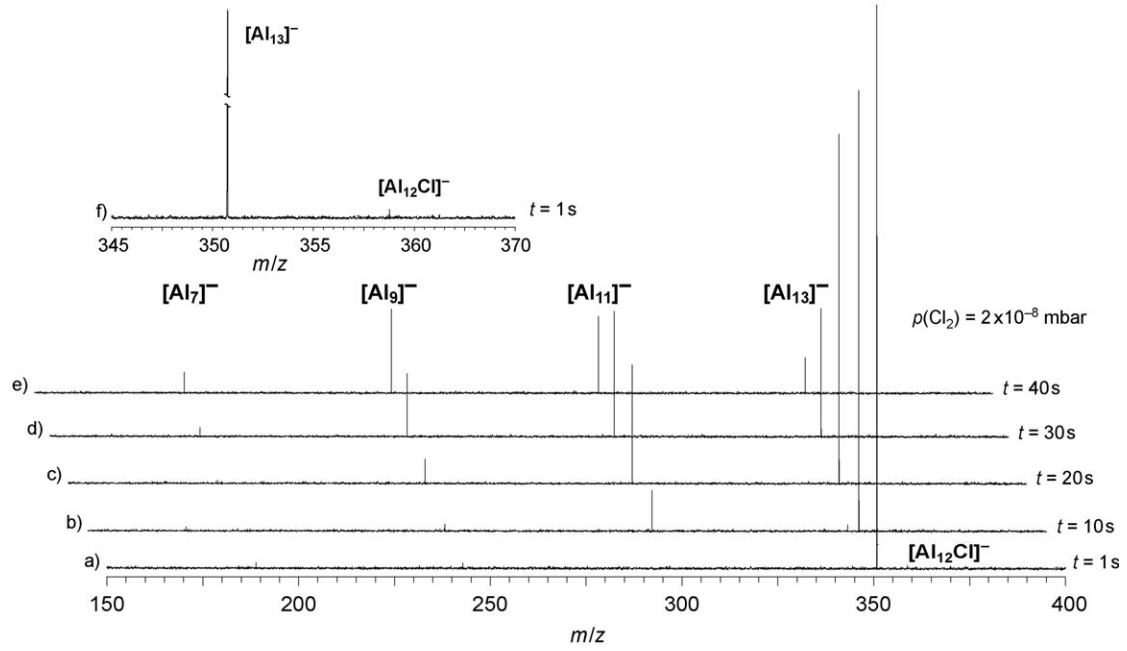


Figure 1. Typical FT-ICR mass spectrum after laser desorption ionization: at $t = 0$ s $[Al_{13}]^-$ is isolated and exposed to a chlorine atmosphere (at 2×10^{-8} mbar). The decay of the $[Al_{13}]^-$ signals in favor of $[Al_{11}]^-$, $[Al_9]^-$, and $[Al_7]^-$ is presented. At $t = 1$ s, $[Al_{12}Cl]^-$ can be detected in small concentrations (a, f). Every spectrum was scaled in such a way that the sum of all (integrated) signals would be 100. For clarity, Cl^- signals are not shown; for further mass spectra see the Supporting Information.

also fragments, ejecting AlCl once again and leaving $[Al_{11}]^-$ [Eq. (2c)]. For this reaction channel the lifetime of $[Al_{12}Cl]^{-*}$

$$[Al_{12}Cl]^-_{(g)} \rightarrow [Al_{11}]^-_{(g)} + AlCl_{(g)} \qquad \Delta_R H^\circ_{(0\,K)} = +203\ \text{kJ mol}^{-1} \qquad (2c)$$

is estimated to be several tenths of a second, and indeed, this anion was observed in small amounts in our experiment (see Figure 1). By performing a double resonant experiment we showed definitively, that this intermediate step takes place, that is, when one continuously removes $[Al_{12}Cl]^-$ by radio frequency (rf) excitation, very few $[Al_{11}]^-$ will be formed.[9,10] The Langevin rate constant k_L for all ion–molecule reactions was determined to be $k_L = 0.09\ s^{-1}$ in the described pressure range.[11,12] As a consequence, an $[Al_n]^-$ cluster molecule collides with a chlorine molecule every 10 s on average, and these will react to form an $[Al_{n-2}]^-$ cluster within another 0.1 s, according to our lifetime estimations. A collisionally induced dissociation of $[Al_{13}]^-$ can be excluded, since corresponding experiments with argon as the collision gas (in the absence of chlorine) showed none of the fragmentation reactions described above.[13]

In summary, the reaction standard energy for the breakdown of $[Al_{13}]^-$ to $[Al_{11}]^-$ due to its reaction with chlorine is $-52\ \text{kJ mol}^{-1}$. In principle, the corresponding reactions of $[Al_{11}]^-$ and $[Al_9]^-$

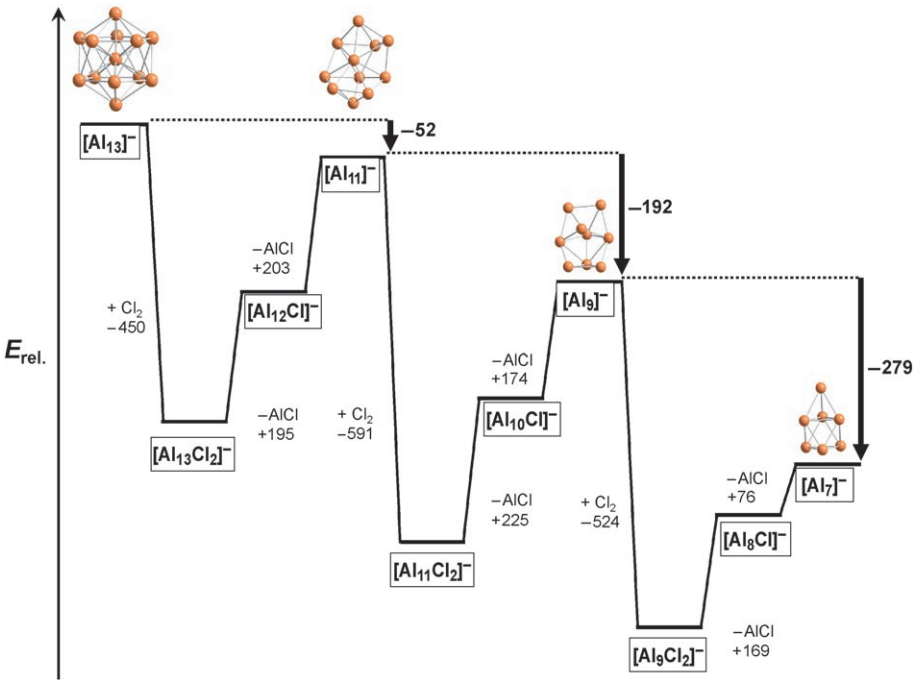


Figure 2. Schematic energy diagram for the breakdown of the cluster; the energy values are given in kJ mol^{-1}. In the first step, chlorine reacts with the surface of the $[Al_{13}]^-$ cluster to form a $[Al_{13}Cl_2]^-$ cluster, which cannot be detected in the experiment because of its short lifetime. In the second step, the spontaneous fragmentation of $[Al_{13}Cl_2]^-$ leads to the release of AlCl and the formation of $[Al_{12}Cl]^{-*}$. Subsequent release of AlCl, leads to $[Al_{11}]^-$. The breakdown of $[Al_{11}]^-$ and $[Al_9]^-$ proceeds in the same manner.

© 2006 Wiley-VCH Verlag GmbH & Co. KGaA, Weinheim

take place in the same way, but are significantly more exothermic than for $[Al_{13}]^-$ with energies of $-192\ kJ\,mol^{-1}$ and $-279\ kJ\,mol^{-1}$, respectively. Figure 2 summarizes all of the pertinent energy balances.

In addition to the reaction products described up to now, Cl^- was always observed, even at the earliest reaction times. This was especially the case at long reaction times, and by 60 s (at a chlorine pressure of 10^{-8} mbar), Cl^- was the only reaction product detected. By determining the intensities of the $[Al_{13}]^-$, $[Al_{11}]^-$, $[Al_9]^-$, $[Al_7]^-$, and Cl^- signals at different times, and thus their concentrations, one can calculate the reaction rates for the individual steps in Equation (1). The exact quantitative description of the chlorination reactions of $[Al_{13}]^-$, including all subsequent and side reactions, is very complex, and it will be presented in a separate publication.[14] Here, we want to restrict ourselves to a qualitative description: essentially $[Al_n]^-$ clusters react with chlorine to give $[Al_{n-2}]^-$ at the same time releasing two AlCl molecules, that is, the resulting cluster has two less aluminum atoms. Also, in a competing reaction channel the $[Al_n]^-$ are oxidized, and Cl^- is formed. Thus, on the one hand, there is the reaction progression in which $[Al_n]^-$ clusters are broken down into smaller units, while on the other hand, there are parallel oxidizing reactions of $[Al_n]^-$ clusters taking place. These latter reactions result in the formation of Cl^- to one extent or another, depending on their different electron affinities.[7]

The reaction path presented here for the reactions of $[Al_n]^-$ cluster ions with chlorine, which results in the release of AlCl as the main product, is a plausible model for the corresponding reaction of bulk aluminum metal and chlorine. This conclusion is in accordance with other experiments as well: The chlorination of aluminum in matrix isolation experiments as well as in experiments on a synthetic scale showed the formation of AlCl at low chlorine pressures.[15] The reaction paths deduced from mass spectrometric investigations with $[Al_n]^-$ clusters provide a reasonable model for the primary steps during the oxidation of bulk aluminum. Below, we want to clarify this idea by a Gedanken experiment with topologic and thermodynamic arguments.

Since the topology of the $[Al_{13}]^-$ cluster with one central Al atom surrounded by twelve other Al atoms is similar to the closest packing of Al atoms in the bulk metal, this cluster is also similar with regard to its energetic behavior: To remove two Al atoms from the closest packing of bulk aluminum [Eq. (3a)] requires 654 $kJ\,mol^{-1}$, that is, double the sublimation energy. According to density functional calculations the analogous reactions of anionic and neutral Al_{13} clusters [Eq. (3b) and (3c)] will require 698 and 638 $kJ\,mol^{-1}$, respectively. Although the difference in energy (60 $kJ\,mol^{-1}$) is not surprising with regard to the usual error ranges for density functional calculations (ca. 10%), the special stability of the $[Al_{13}]^-$ cluster is made clear by the significantly higher energy value for its fragmentation.

$$2\,Al_{(f)} \rightarrow 2\,Al_{(g)} \qquad \Delta_R H^\circ_{(0\,K)} = +654 \pm 8\ kJ\,mol^{-1} \tag{3a}$$

$$[Al_{13}]^-_{(g)} \rightarrow [Al_{11}]^-_{(g)} + 2\,Al_{(g)} \qquad \Delta_R H^\circ_{(0\,K)} = +698\ KJ\,mol^{-1} \tag{3b}$$

$$Al_{13(g)} \rightarrow Al_{11(g)} + 2\,Al_{(g)} \qquad \Delta_R H^\circ_{(0\,K)} = +638\ KJ\,mol^{-1} \tag{3c}$$

These similarities between the bulk metal and Al_{13} clusters for the removal of two Al atoms [Eq. (3a–c)] are also consequently reflected by the corresponding chlorination reactions [Eq. (4a–c)]. The neutral as well as the investigated anionic $[Al_{13}]^-$ cluster can be considered as a well-matched model compound for investigations of primary reactions on the surface of bulk aluminum.

$$[Al_{13}]^-_{(g)} + Cl_2 \rightarrow [Al_{11}]^-_{(g)} + 2\,AlCl_{(g)} \qquad \Delta_R H^\circ_{(0\,K)} = -52\ kJ\,mol^{-1} \tag{4a}$$

$$2\,Al_{(f)} + Cl_2 \rightarrow 2\,AlCl_{(g)} \qquad \Delta_R H^\circ_{(0\,K)} = -103 \pm 12\ kJ\,mol^{-1}\ [1] \tag{4b}$$

$$Al_{13(g)} + Cl_2 \rightarrow Al_{11(g)} + 2\,AlCl_{(g)} \qquad \Delta_R H^\circ_{(0\,K)} = -113\ kJ\,mol^{-1} \tag{4c}$$

When there is a high excess of chlorine, the AlCl primary product will continue to react and form $AlCl_3$. The formation of this final product of chlorination is a very exothermic reaction: ($AlCl_{(g)} + Cl_2 \rightarrow AlCl_{3(g)}$, $\Delta_R H^\circ = -534\ kJ\,mol^{-1}$ [1]). Thus, the chlorination of the bulk metal aluminum must also proceed primarily by the addition of chlorine and the release of AlCl. Then, the subsequent reaction of AlCl to give $AlCl_3$ will take place with the release of reaction energy that is ten times higher ($-534\ kJ\,mol^{-1}$). Consequently, the cumulative reactions [Eq. (5a–c)], which produce $AlCl_3$ as the final product, reflect the character of $[Al_{13}]^-$ as a molecular model for the bulk metal.

$$[Al_{13}]^-_{(g)} + 3\,Cl_2 \rightarrow [Al_{11}]^-_{(g)} + 2\,AlCl_{3(g)} \qquad \Delta_R H^\circ_{(0\,K)} = -1084\ kJ\,mol^{-1} \tag{5a}$$

$$2\,Al_{(f)} + 3\,Cl_2 \rightarrow 2\,AlCl_{3(g)} \qquad \Delta_R H^\circ_{(0\,K)} -1166 \pm 6\ kJ\,mol^{-1}\ [1] \tag{5b}$$

$$Al_{13(g)} + 3\,Cl_2 \rightarrow Al_{11(g)} + 2\,AlCl_{3(g)} \qquad \Delta_R H^\circ_{(0\,K)} = -1145\ kJ\,mol^{-1} \tag{5c}$$

In addition to the central breakdown reactions of $[Al_{13}]^-$ clusters to $[Al_{11}]^-$ and two AlCl, the reverse steps illustrated in Equation (6) are also relevant for understanding the formation of metalloid clusters on a preparative scale. Therefore Equation (6) can be considered as a simplified model for a single step disproportionation, for example, of AlCl solutions ($3\,AlCl \rightarrow 2\,Al + AlCl_3$), in which metalloid $Al_n(AlR)_m$ clusters are formed as intermediates on the way finally to metallic aluminum. This consideration (in the sense of a retrosynthesis, that is, a reverse of the reaction course in Figure 2) appears to be plausible, because in contrast to the presented mass spectrometric experiments in the gas phase,

$$3\,AlCl + [Al_{11}]^- \rightarrow [Al_{13}]^- + AlCl_3 \tag{6}$$

 © 2006 Wiley-VCH Verlag GmbH & Co. KGaA, Weinheim

the concentration of AlCl is high in synthetically prepared AlCl solutions.[15] Here, indeed individual steps can proceed analogously to Equation (6), since this reaction is exothermic by $-467\ kJ\,mol^{-1}$.

Experimental Section

The experiments were performed with an ULTIMA FT-ICR mass spectrometer (Ionspec, MALDI source), equipped with a 7.0-T magnet and a nitrogen laser (Spectra Physics, $\lambda = 337.1$ nm). Selected ions were isolated (SWIFT) and cooled down to room temperature by using argon as collision gas.[5] For the reactions, chlorine was introduced into the ICR cell with a leak valve. This typically raised the pressure from 10^{-10} mbar to 10^{-8} mbar. The reaction time was varied between 2 and 70 s.

The density functional calculations were carried out with the TURBOMOLE[16] program package, using the Becke-Perdew-86 functional (BP86).[17,18] Coulomb interactions were treated within the RI (resolution of the identity) approximation.[19,20] The grids required for the numerical integration of exchange and correlation contributions were of medium coarseness (m3[20]). The basis set was of split valence plus polarization (SVP) type.[21] To check whether the computational methods were suited for our tasks, we compared the following reactions: $AlCl_{(g)} + Cl_2 \rightarrow AlCl_{3(g)}$. The calculated reaction energy was determined to be $\Delta_R H^\circ(\text{calcd}) = -516\ kJ\,mol^{-1}$. The experimental value for the reaction energy is $\Delta_R H^\circ(\text{exp}) = -534 \pm 9\ kJ\,mol^{-1}$. In the past, these methods were used in a density functional study of aluminum clusters.[22] To estimate the lifetimes of the intermediate steps $[Al_{13}Cl_2]^{-*}$ and $[Al_{12}Cl]^{-*}$, phase space theory (PST) was applied.[8]

Received: August 19, 2005
Published online: January 30, 2006

Keywords: aluminium · chlorine · cluster compounds · density functional calculations · mass spectrometry

[1] "NIST-JANAF Thermochemical Tables, 4th ed.": M. W. Chase, *J. Phys. Chem. Ref. Data Monogr.* **1998**, *9*, 1–1951.
[2] D. E. Bergeron, A. W. Castleman, Jr., T. Morisato, S. N. Khanna, *J. Chem. Phys.* **2004**, *121*, 10456.
[3] D. E. Bergeron, A. W. Castleman, Jr., T. Morisato, S. N. Khanna, *Science* **2004**, *304*, 84.
[4] W. D. Knight, K. Clemenger, W. A. De Heer, W. A. Saunders, M. Y. Chou, M. L. Cohen, *Phys. Rev. Lett.* **1984**, *52*, 2141.
[5] X. G. Gong, D. Y. Sun, X.-Q. Wang, *Phys. Rev. B* **2000**, *62*, 15413.
[6] A. G. Marshall, T. C. L. Wang, T. L. Ricca, *J. Am. Chem. Soc.* **1985**, *107*, 7893.
[7] All energy balances, structural parameters of starting materials and intermediate products, as well as for the key electron affinities are listed in the Supporting Information.
[8] T. Baer, W. Hase, *Unimolecular Reaction Dynamics*, Oxford University Press, New York, **1996**.
[9] L. R. Anders, J. L. Beauchamp, R. C. Dunbar, J. D. Baldeschwieler, *J. Chem. Phys.* **1966**, *45*, 1062.
[10] M. B. Comisarow, V. Grassi, G. Parisod, *Chem. Phys. Lett.* **1978**, *57*, 413–416.
[11] P. M. Langevin, *Ann. Chim. Phys.* **1905**, *5*, 245.
[12] J. I. Steinfeld, J. S. Francisco, W. L. Hase, *Chemical Kinetics and Dynamics*, Prentice Hall, Englewood Cliffs, **1989**.
[13] Forcing a collisionally induced dissociation by external rf excitation (SORI-CAD experiments) will result in a totally different fragmentation pattern.
[14] M. Olzmann, R. Burgert, H. Schnöckel, unpublished results.
[15] C. Dohmeier, D. Loos, H. Schnöckel, *Angew. Chem.* **1996**, *108*, 141–161; *Angew. Chem. Int. Ed. Engl.* **1996**, *35*, 129–149; Schnepf, H. Schnöckel, *Angew. Chem.* **2002**, *114*, 3682–3704; *Angew. Chem. Int. Ed.* **2002**, *41*, 3533–3554; H. Schnöckel, *Dalton Trans.* **2005**, 3131.
[16] O. Treutler, R. Ahlrichs, *J. Chem. Phys.* **1995**, *102*, 346.
[17] A. D. Becke, *Phys. Rev. A* **1988**, *38*, 3098.
[18] J. P. Perdew, *Phys. Rev. B* **1986**, 8822.
[19] K. Eichkorn, O. Treutler, H. Oehm, M. Haeser, R. Ahlrichs, *Chem. Phys. Lett.* **1995**, *240*, 283.
[20] K. Eichkorn, F. Weigend, O. Treutler, R. Ahlrichs, *Theor. Chem. Acc.* **1997**, *97*, 119.
[21] A. Schaefer, H. Horn, R. Ahlrichs, *J. Chem. Phys.* **1992**, *97*, 2571.
[22] R. Ahlrichs, S. D. Elliott, *Phys. Chem. Chem. Phys.* **1999**, *1*, 13.

 © 2006 Wiley-VCH Verlag GmbH & Co. KGaA, Weinheim